Hip joint forces

Hip joint forces of 40 to 60 year old normal and total hip replacement subjects during walking and stair, ramp and camber negotiation.

Benedict William Stansfield, BA, MSc, MPhil

PhD Thesis

2000

Bioengineering Unit, University of Strathclyde, Glasgow

Acknowledgements

Josie, Daniel and Clare for sacrifice beyond the call of duty.

Sandy Nicol for allowing me to go my own way.

Prof. Paul for putting me right in all the fine detail.

Robert Hay for equipment construction.

The Medical Research Council for funding.

Contents

Abstract

To design and test hip joint prosthesis it is essential to know the magnitude and character of forces that may be applied to them in-vivo. For this thesis the hip joint forces of 40 to 60 year old subjects (five male and six female normal subjects and five male hip replacement) were studied.

To allow the calculation of hip joint forces data from three-dimensional motion analysis and force plates were applied to a model of the lower limb. The model included the hip, knee and talocrural joints with 3 hip, 8 knee and 8 ankle joint forces, 4 knee ligaments and 47 muscle elements. A double linear optimisation technique (first minimising the maximum muscle stress then minimising the sum of the forces in the force bearing structures) was applied to solve the redundancy problem of force distribution in the muscles.

Walking and stair, ramp and camber negotiation were characterised.

Ground reaction forces, joint angles, intersegmental forces and moments, joint and ligament forces and muscle forces are presented.

Muscle forces predictions were in general agreement with those in the literature, although the model was not capable of correctly distributing forces in the vasti or in the ankle only muscles as patella and talocalcaneonavicular joint equilibria were not included.

In general, hip replacement subjects demonstrated lower hip joint forces than normal subjects. The range of maximum resultant hip joint forces for all activities was 3.04 to 11.85 for male normal subjects, 4.18 to 11.50 for female normal subjects, 3.73 to 6.81 and 2.21 to 8.77 for male hip replacement subjects for their natural and replaced sides respectively.

The results presented define in three dimensions the hip joint forces in both pelvic and femoral axes systems and thus characterise the probable in-vivo requirements of hip joint prostheses during performance of the activities studied.

Glossary of terms

Co-ordinate system axes (X, Y, Z right handed orthogonal sets):

XP,	YP,	ZP	proximal segment axes	(Figure 3.16)
XD,	YD,	ZD	distal segment axes	(Figure 3.16)
XPA,	YPA,	ZPA	pelvic anatomical:	(Figure 3.4)
XPM,	YPM,	ZPM	pelvic moving:	(Figure 3.6)
XPB,	YPB,	ZPB	pelvic Brand's	(Figure 3.2)
XFA,	YFA,	ZFA	thigh (femur) anatomical	(Figure 3.4)
XFM,	YFM,	ZFM	thigh (femur) moving	(Figure 3.6)
XFB,	YFB,	ZFB	thigh (femur) Brand's	(Figure 3.4/3.5)
XTM,	YTM,	ZTM	shank (tibia) moving	(Figure 3.6)
XTB,	YTB,	ZTB	shank (tibia) Brand's	(Figure 3.2)
XKA,	YKA,	ZKA	knee anatomical	(Figure 3.7)
XFA,	YFA,	ZFA	foot anatomical	(Figure 3.12/13)
XAA,	YAA,	ZAA	ankle anatomical	(Figure 3.13/14)

KCA	knee centre (for definition of shank anatomical axes)	(Figure 3.5)
ACA	ankle centre (for definition of shank anatomical axes)	(Figure 3.5)

Dimensions used in definition of shank anatomical axes (Figure 3.5)

a	distance along XTA from YTA axis to tibial tuberosity marker
b	distance along ZTA from plane of XTA and YTA to fibular head marker
c	distance from lateral malleolus marker to ACA
d	distance from intersection of XTA and YTA to KCA

Dimensions used in definition of location of knee centre in shank anatomical axes (Figure 3.7)

e	distance from tibial tuberosity to front of tibial plateau along YTA
f	distance from tibial tuberosity to front of tibial plateau along XTA
g	distance from front of tibial plateau to centre of contact between femur and tibia along XTA
h	distance from front of tibial plateau to centre of contact between femur and tibia along YTA

Parameters used in the definition of the knee model (Figure 3.8)

α	angle between tibial long axis YTA and femoral long axis YFA	
β	angle between patella ligament and tibial plateau (XKA)	
θ_{MUS}	angle of quadriceps muscle to femoral long axis (YFA)	(Figure 3.11)
θ_{TP} (8.2°)	inclination of tibial plateau to long axis of tibia (YTA)	(Figure 3.7)
C	distance along tibial plateau from front of tibial plateau to contact centre	
Fq	force in quadriceps muscle (patella tendon)	
Fp	force in patella ligament	
MCLo, MCLi	origin and insertion points of the medial collateral ligament	(Figure 3.10)
LCLo, LCLi	origin and insertion points of the lateral collateral ligament	(Figure 3.10)

Knee joint force definition parameters (Figure 3.9)

L	distance to femur contact point on tibia from knee anatomical axes origin
ϕ	knee rotation angle offset (knee rotation angle – static trial knee rotation angle).
ACL, PCL	anterior and posterior cruciate ligaments respectively
MCL, LCL	medial and lateral collateral ligaments respectively
KJC1, KJC2	contact points of femur on tibia.
KJY1, KJY2	tibio-femoral contact forces
KJX1, KJX2	rotation forces (not representative of anatomical structures)
KJX3, KJX4	supplementary anterior-posterior forces (not representative of anatomical structures)
KJZ1, KJZ4	medio-lateral forces (not representative of anatomical structures)

(KJZ2, KJZ3 not used)

Ankle joint model parameters (Figure 3.15)

θ_{AA} (15.5°)	angle between the inter malleolar line and ZFA	(Figure 3.12)
θ_{TF}	angle between XTA and XFA	(Figure 3.12)
q	distance to the ankle joint force centres from the ankle anatomical centre along ZAA	
AJC1, AJC2	Ankle joint force centres.	
AJY1, AJY2	ankle joint forces in the YAA direction	
AJX1, AJX2, AJX3, AJX4	ankle joint forces in the XAA direction	
AJZ1, AJZ2	ankle joint forces in the ZAA direction	

Cardan angles (Figure 3.16)

θ_1 flexion/extension angle

θ_2 adduction/abduction angle

θ_3 internal/external rotation angle

Resultant hip joint force femoral angles (Figure 3.17A)

FHYXANG angle between the resultant hip joint force and the YFA axis in the plane of the YFA and XFA axes

FHYZANG angle between the resultant hip joint force and the YFA axis in the plane of the YFA and ZFA axes

FHXZANG angle between the resultant hip joint force and the XFA axis in the plane of the XFA and ZFA axes

Resultant hip joint force pelvic angles (Figure 3.17B)

HJYXANG angle between the resultant hip joint force and the YPA axis in the plane of the YPA and XPA axes

HJYZANG angle between the resultant hip joint force and the YPA axis in the plane of the YPA and ZPA axes

HJXZANG angle between the resultant hip joint force and the XPA axis in the plane of the XPA and ZPA axes

Figure and table lists

List of figures

Appendix figures

A list of figures in each appendix is included at the beginning of the relevant appendix.

List of tables

Chapter 1 Introduction

Knowledge of the magnitude of hip joint forces provides information that is essential for the successful design of hip joint replacements. It is necessary to have knowledge of the forces at the joints of both normal subjects and hip joint replacement subjects. The normal subjects provide an indication of the potential requirements of the hip joint prosthesis and the hip joint replacement subjects would provide examples of the actual use of the prostheses. Hip joint replacement often occurs before 60 years of age. It is possible that these 'young' subjects place greater demands on their prostheses than do older subjects. The age range of 40 to 60 years old was selected for this thesis to represent young hip replacement subjects. The cyclical activities of walking and stair, slope and camber negotiation were studied. Information on the hip joint forces developed during these activities provides suitable specifications for prosthesis testing.

It is possible to study the forces at the hip joint in a number of ways. In vitro analysis has been performed. Typically isolated cadaver samples are instrumented and subjected to a system of forces that mimic those associated with the activity under consideration. This method could be applied to both normal and hip joint replacement conditions. These studies are limited by the fact that they require knowledge of the forces in the structures of the limb, which would have been derived by previous modelling results or limited in-vivo testing. Direct in-vivo examination of hip joint forces has been achieved using instrumented hip joint replacements (Rydell [1966], English & Kilvington [1979], Davy et al [1988], Kotzar et al [1991,1995], Bergmann et al [1993, 1995, 1995B], Graichen et al [1991], Brand et al [1994], Hodge et al [1989], Givens-Heiss et al [1992], Bassey et al [1997], Lu et al [1997, 1998]). The limitations of these studies are that they cannot be used for normal subjects and that only a small number of subjects can be fitted with the prostheses. To test a relatively large number of both normal and hip replacement subjects without invasive surgery and with no assumption of forces in structures it is necessary to adopt another approach. Three dimensional motion analysis of the lower limb with the simultaneous recording of the forces applied to the foot provides the information necessary to calculate the forces at the hip. Knowledge of the location of the internal structures of the lower limbs allows a set of equilibrium equations to be established the solution of which provides information on the development of hip joint forces. This method has been applied by a number of authors (e.g. Seireg & Arvikar [1973, 1975], Crowninshield [1978], Crowninshield & Brand [1981], Pederson et al [1997], Lu et al [1998]). This thesis uses this method adopting a particular implementation to provide information on the development of hip joint forces for both normal and hip joint replacement subjects during a range of locomotion activities.

1.1 Thesis overview

Throughout the thesis, where appropriate, reference has been made to the literature. Basic anatomy related to the implementation of the theory used in this thesis is detailed (Chapter 2). The description of the method of motion analysis employed (Chapter 3) includes details of the equipment used and the marker placement protocol. Descriptive data of the 5 normal male, 6 normal female and 5 male hip replaced subjects are given (Section 3.3). Extensive details of the model of the lower limb are given (Section 3.5) including muscle origins and insertions and joint forces. The optimisation method used to determine the distribution of the forces within the muscles is described (Section 3.6). A marker correction routine was employed to correct for movement of the skin relative to the underlying bones (Section 3.7.2). An attempt was made to determine the three-dimensional position of the hip joint centre of individuals (Section 3.7.4).

Results are presented of the ground reaction forces, joint angles, intersegmental joint forces and moments, muscle forces and joint forces for the hip, knee and ankle (Chapter 4) for walking and stair, slope and camber negotiation. Forces at the hip are given in both thigh and pelvic reference frames. Normal male and female and male total hip replacement hip joint forces are presented. Errors associated with the analysis are discussed.

Discussion of the results incorporates validation against literature references including basic joint angles and hip joint forces (Chapter 5).

Conclusions are drawn (Chapter 6) and recommendations made for further studies in this area of biomechanics (Chapter 7).

Hip joint forces are calculated and presented for a range of locomotion activities in normal and total hip replaced subjects in the 40 to 60 year old age range.

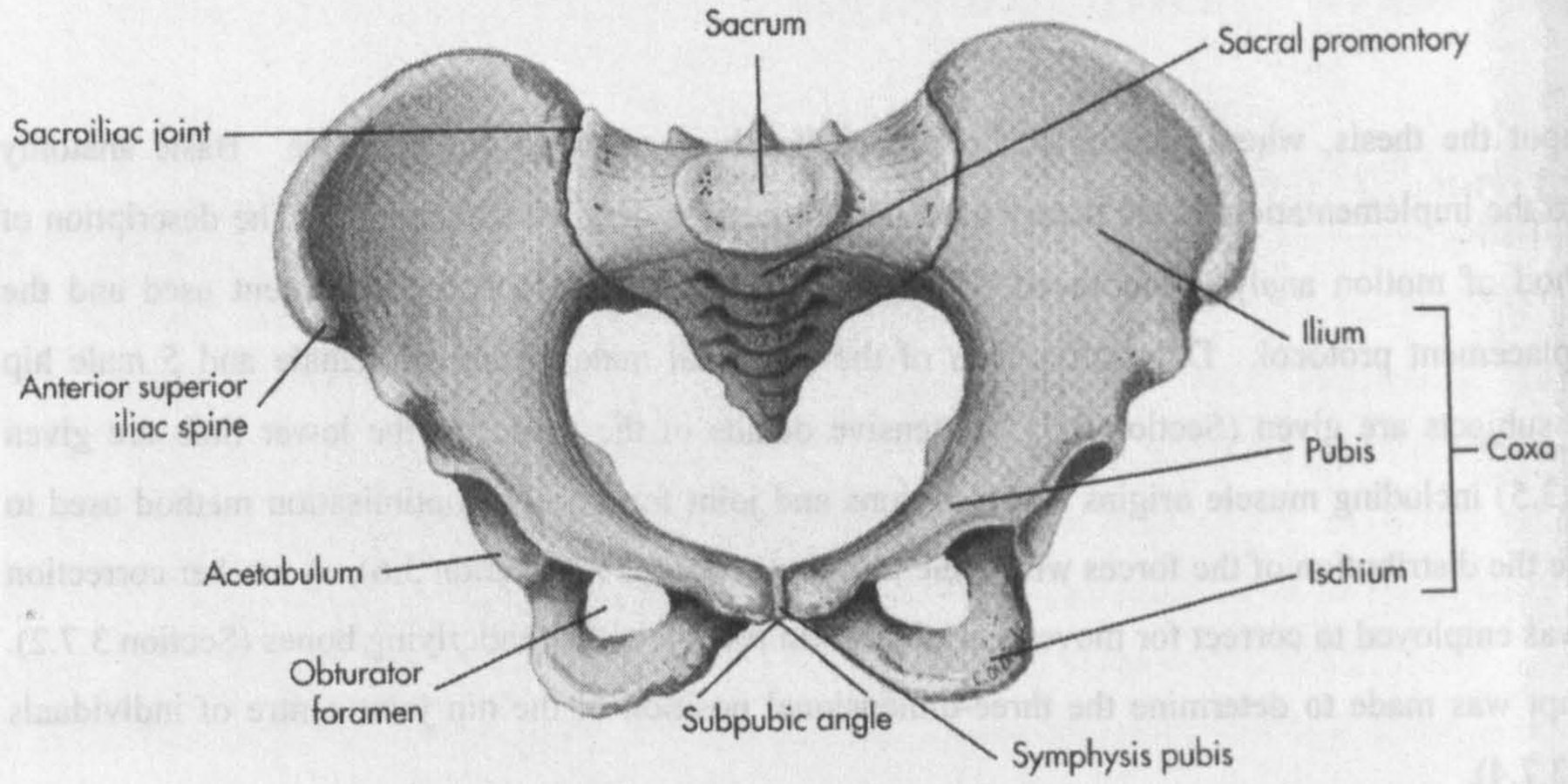

Figure 2.1 The pelvic girdle, anterior view (Seeley et al [1995])

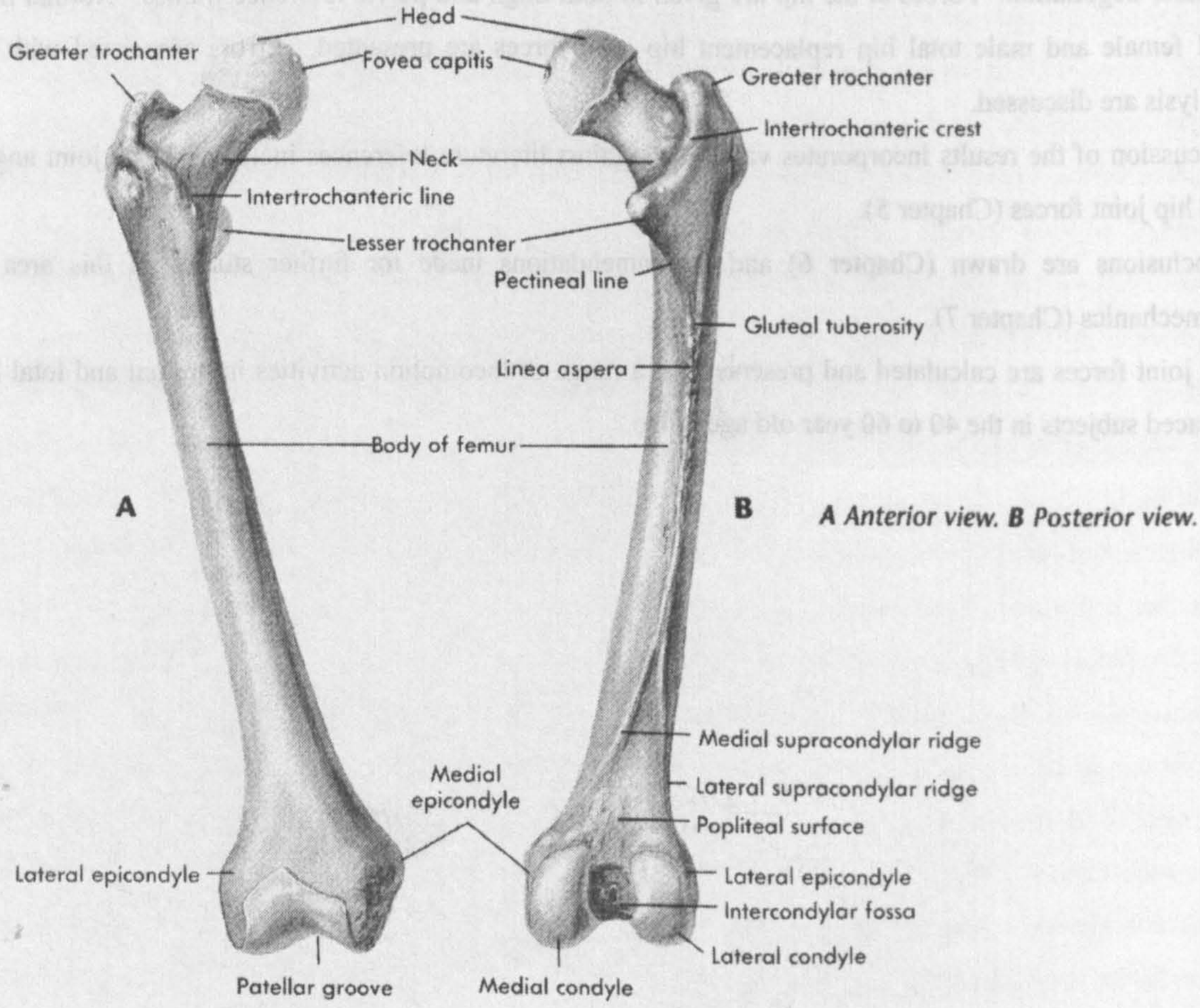

Figure 2.2 The right femur (Seeley et al [1995])

Chapter 2 Anatomy

2.1 Introduction

The elements of the lower limbs anatomy that contribute the most to joint force and moment equilibrium will are described. These include bones, muscles, ligaments and joint structures. Contributions to load bearing would also be made by other soft tissues in the limbs, e.g. skin, nerves, blood vessels and fat deposits, although during normal activity these would have only a small impact on overall joint equilibrium.

This chapter is divided into three sections; skeletal, muscular and joint anatomies. Several texts have been used as reference material. (Seeley et al [1995], Grant's [1991], Joseph [1982])

2.2 Skeletal Anatomy

The bones of the lower limb will be examined from the hip distally with particular reference to the joint anatomy.

2.2.1 The Pelvic Girdle

The sacrum, coccyx and "pelvic" bones constitute the pelvic girdle (Figure 2.1). The ilium contributes the superior portion of the bone with a large face bounded by the iliac crest with anterior and posterior superior spines and its junction with the ischium and pubis at the acetabulum. Inferiorly the ischium forms the ischial tuberosity the bony prominence, which bears weight when the body is in a seated position.

Various features of the bone have been named, facilitating description of muscle attachment and other soft tissue positioning (for full details of these features see for example Palastanga et al [1994]. Lines on the internal and external aspects of the bone are evident. In several cases these border muscle attachments.

Palpable landmarks include the anterior and posterior iliac spines, the iliac crest, the pubic symphysis, ischial tuberosity and various parts of the sacrum.

2.2.2 The Femur

The femur consists of a shaft with two articular ends (Figure 2.2). At the proximal end the femur consists of a head, neck and a greater and lesser trochanter. The head forms slightly more than a half sphere upon which the articular cartilage is found. The neck and trochanteric area of the femur has several features associated with muscle and joint capsule attachment. The shaft has clear demarcations; principally the pectineal line and the linear aspera, splitting into the supracondylar lines distally.

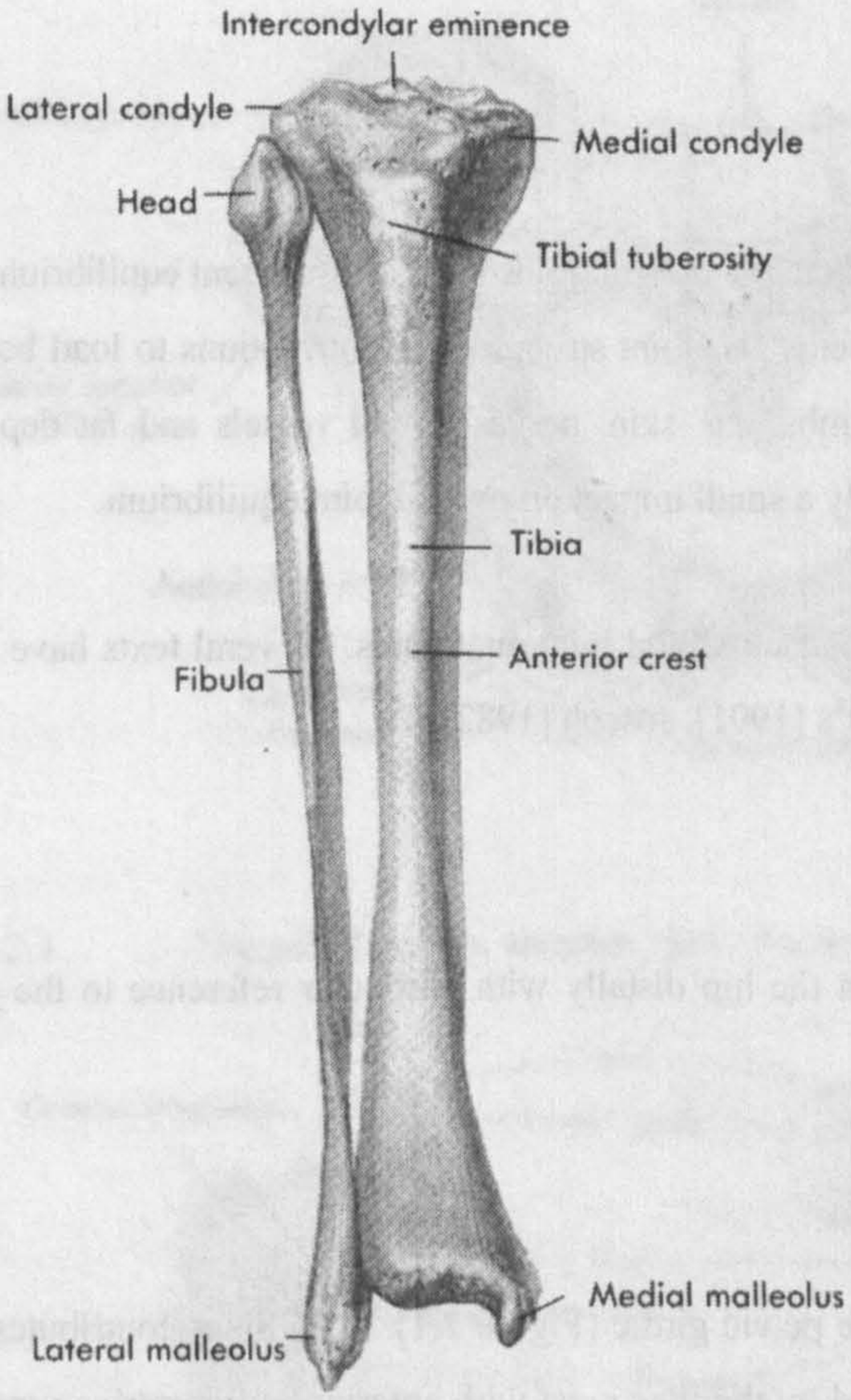

Figure 2.3 Right tibia and fibula, anterior view (Seeley et al [1995])

At its distal end the femur has adaptations for articulation with the tibia. These surfaces are on the medial and lateral condyles separated by the intercondylar fossa. They are principally on the distal and distal posterior surfaces allowing flexion but not extension from the anatomical position. On the anterior side of the distal femur is the patella surface, which articulates with the patella.

Palpable landmarks of the femur are the greater trochanter proximally and the medial and lateral epicondyles distally.

2.2.3 The Tibia and Fibula

The tibia and fibula constitute the skeleton of the shank of the leg, the fibula lying laterally to the tibia (Figure 2.3). At the knee the tibia articulates with the femur on medial and lateral condyles, separated by the intercondylar eminence. The tibial shaft is demarked anteriorly into surfaces, i.e. the medial and lateral, by the anterior border below its tuberosity. Posteriorly the soleal line is present. At its distal end the tibia forms an articulating surface with the talus bone of the foot. The medial malleolus of the tibia forms one side of the "ankle joint". The tibia is the weight-bearing component of the shank with the fibula acting as an additional area for muscle attachment and contributing to stability at the ankle.

The fibula head articulates with the lateral side of the tibia. Its shaft is separated into a number of different surfaces providing specific sites for muscle attachment. At its distal end the fibula forms the lateral malleolus of the ankle, the medial side of which forms part of the ankles articulating surface (with the talus). The role of the patella will be discussed in the examination of joints, Section 2.4.2. Palpable bony landmarks of the shank include the tibia medial condyle, fibula head, tibial shaft anterior crest, tibial medial malleolus and fibula lateral malleolus.

2.2.4 The Foot

Figure 2.4 show the bones of the foot. The talus, tibia and fibula form the ankle joint. The talus is supported inferiorly and posteriorly by the calcaneus. Distally (anteriorly) the navicular (medially), cuboid (laterally) and cuneiform bones transfer load to the metatarsals and on to the phalanges (three for each toe except the big toe or hallus which has two). Beneath the medial metatarsal's distal end are the sesamoid bones. There are numerous features on the dorsum of the foot, which may be palpated.

2.3 Myology

2.3.1 Introduction

The details of muscle anatomy given here will extend to insertions, origins and routing. In most anatomical texts muscles are detailed according to their articulating function. In order to do this the limb must be

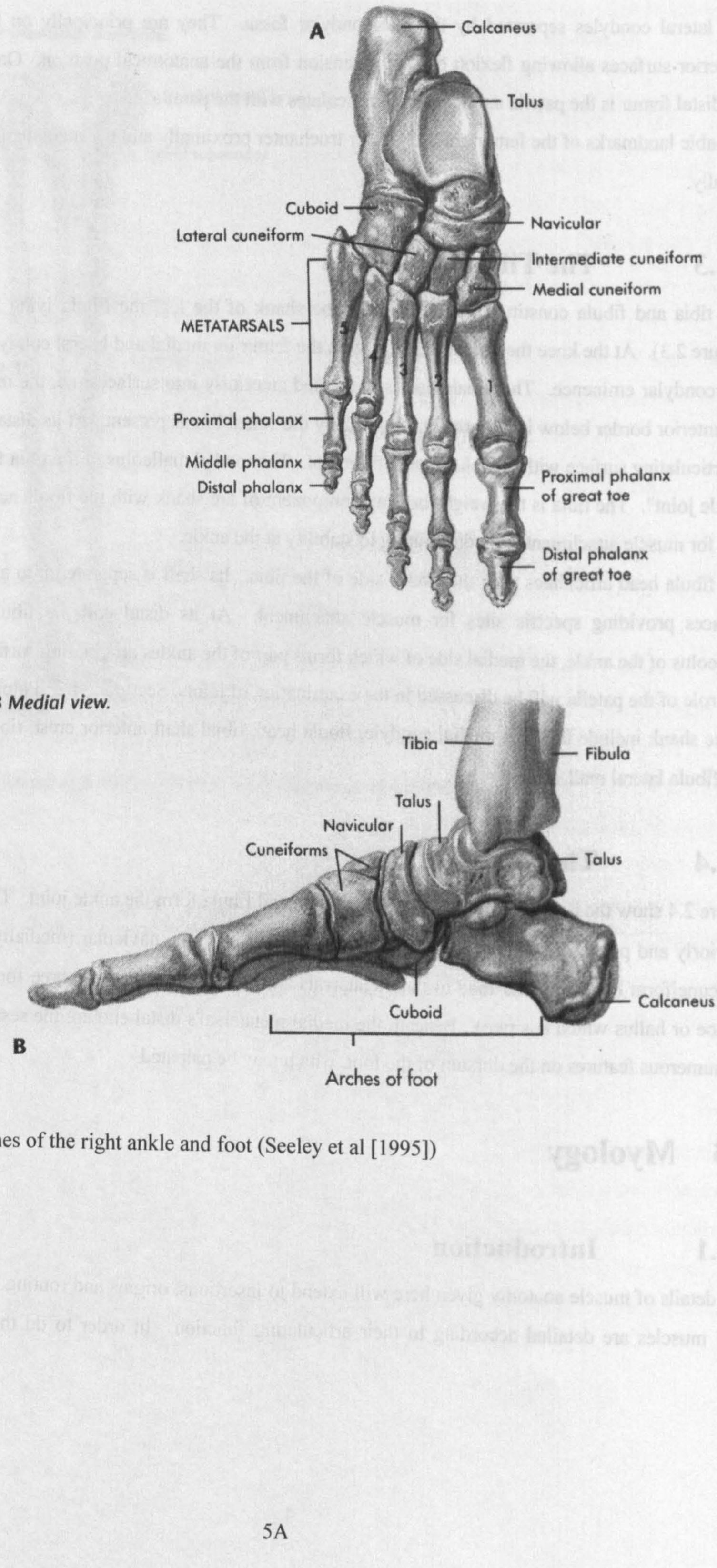

***A** Dorsal view. **B** Medial view.*

Figure 2.4 Bones of the right ankle and foot (Seeley et al [1995])

examined in a set position. Muscles can be classified under their primary, secondary and tertiary role, e.g. flexion/extension, abduction/adduction, internal/external rotation. It should be emphasised that this method of muscle classification is position dependent and that muscle's lines of action change with respect to joint centres during lower limb joint articulation. Strictly it is unnecessary to classify muscles with respect to flexion/extension, abduction/adduction, internal/external rotation for the calculation of the forces. When examining patients, it is, however, necessary to have a frame of reference within which muscle force contributions to joint stability can be defined.

For simplicity muscles are detailed following anatomical location and not by action. Details of origin and insertion are illustrated. It should be noted that location of origin and insertion can vary between individuals, so that illustrations will not be general but specific to the specimen studied.

To characterise the muscles with respect to joint mechanics the following designations have been used:

H- acts at the hip joint

K- acts at the knee joint

A- acts at the ankle joint

m- consists of more than one part or must be considered to consist of more than one part in order to provide a full functional description.

*- those muscles included in the model of the lower limb used in this thesis.

The lower limb has been treated as four sections; hip, thigh, shank and foot, with three associated joints. An attempt has been made to include details of all muscles contributing to lower limb equilibrium. (A comprehensive pictorial description of the lower limb muscles may be found in Palastanga et al [1994])

2.3.2 Muscles of the anterior aspect of the thigh

Iliopsoas (H*)

Figure 2.5 illustrates the two muscles, the iliacus and the psoas major, which constitute the iliopsoas. These muscles are routed so that hip joint extension will cause them to wrap around the pelvic bone across the iliopubic eminence. Their moment arm about the hip joint centre will therefore depend either upon the skeletal dimensions at this point or, if the thigh is in flexion, upon the distance between the direct path between origin and insertion and the joint centre.

Pectineus (H*)

The pectineus travels around the superior ramus of the pubis from its origin linearly to its insertion, thus its effective origin in terms of its line of action is the superior ramus of the pubis.

Psoas Minor (-)

The psoas minor has no resultant effect on the hip joint moment and is not considered in this thesis.

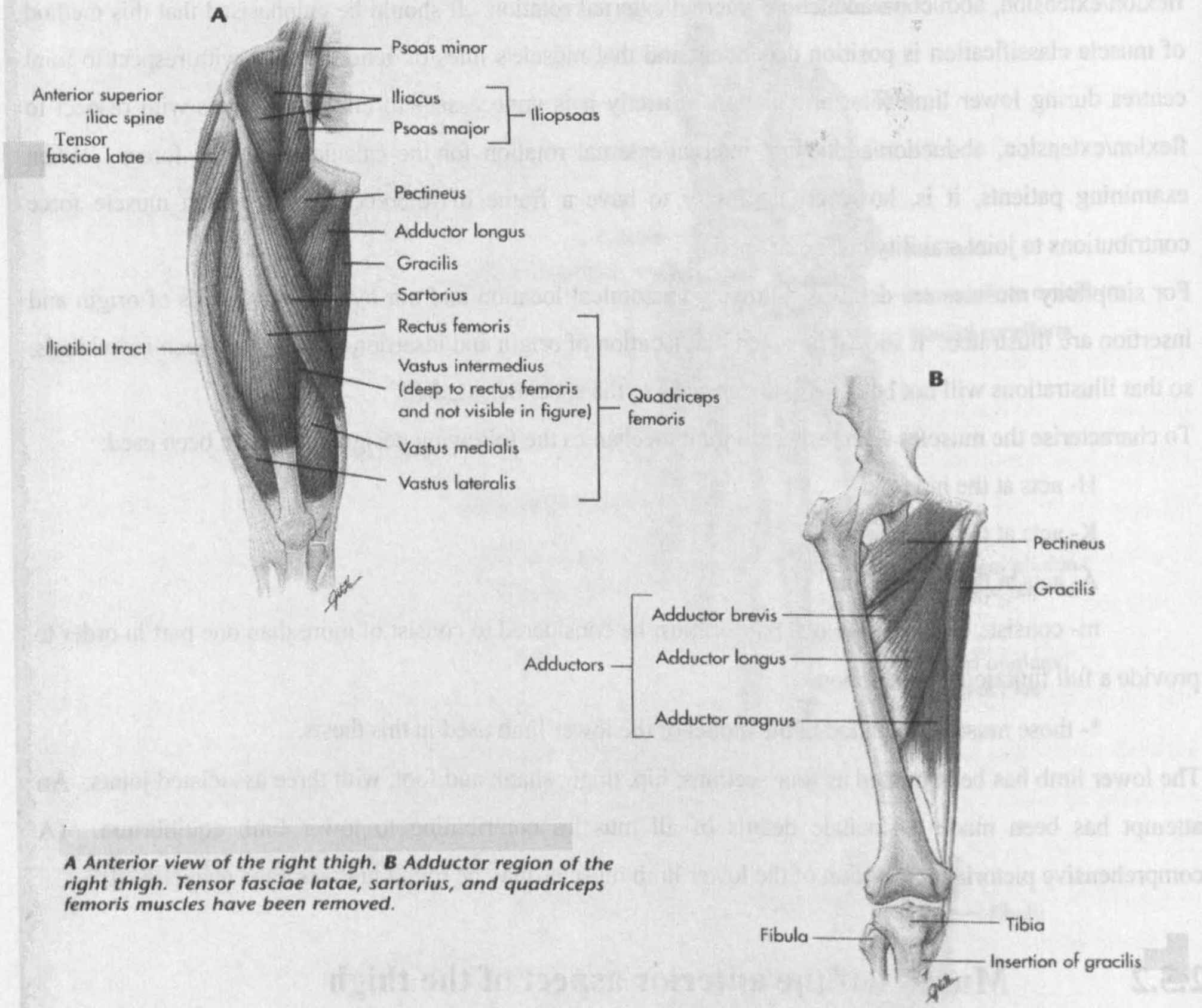

***A** Anterior view of the right thigh. **B** Adductor region of the right thigh. Tensor fasciae latae, sartorius, and quadriceps femoris muscles have been removed.*

Figure 2.5 Muscles of the anterior thigh (Seeley et al [1995])

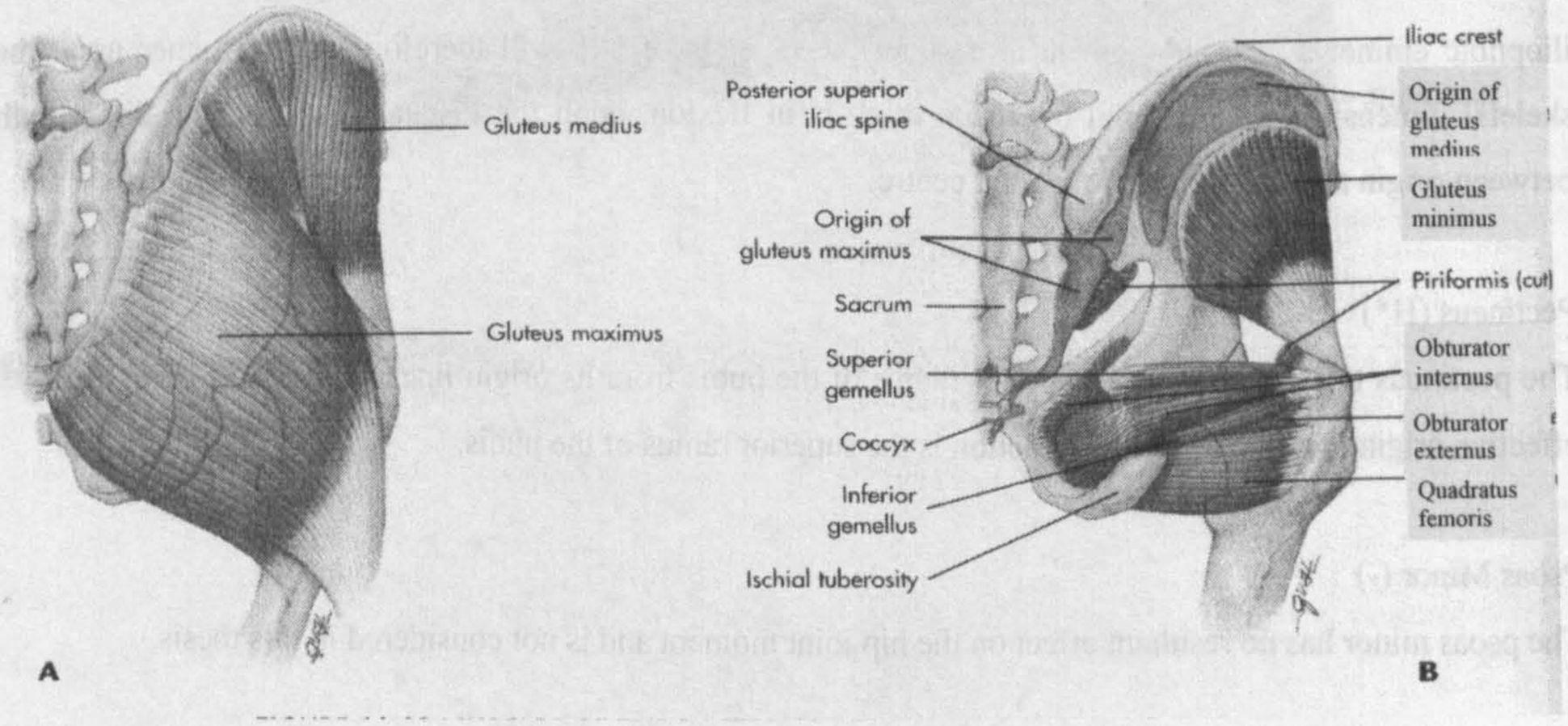

Figure 2.6A Muscles of the posterior hip. **A** Posterior view of the right hip, superficial. **B** Posterior view of the right hip, deep. Gluteus maximus and medius have been removed to reveal deeper muscles. The piriformis has been cut. (Seeley et al [1995])

Quadriceps Femoris:

Rectus Femoris, Vastus Lateralis, Vastus Medialis, Vastus Intermedius (H K *)

The quadriceps femoris consist of the rectus femoris and the vastus muscles; intermedius (deep to the rectus femoris), lateralis and medialis. Figures 2.12 A show these muscle's insertions and their interaction with the patella and its ligaments.

The rectus femoris crosses both hip and knee joints. Its line of action would therefore have to account for diversion around the hip joint at large extensions and also around the knee joint when if becomes flexed. Vastus intermedius is the deepest muscle of the group and along with the lateralis and medialis originates on the femur, thus acting only on the knee joint. Intermedius has a diverse insertion. Medialis and lateralis have thin linear origins on the posterior aspect of the femur before travelling anteriorly. This fact means that their lines of action are complex and must be carefully defined across the knee joint where they act through the patella.

Sartorius (H K *)

The sartorius muscle is the most superficial of the thigh (Figure 2.5). It traverses both hip and knee joints. Its path is determined to a large extent by underlying soft tissues. Changes in hip and knee flexion will alter its lever arm. It is named after cross-legged tailors.

Tensor fasciae latae (H K *)

This muscle's insertion into the iliotibial tract gives it action about both the hip and knee. Its action about the hip is governed by the distance between the greater trochanter and the hip centre. At the knee its action is governed by the action of the iliotibial tract. It has multiple insertions in the iliotibial tract.

Adductor Longus, Adductor Brevis, Adductor Magnus (H m *)

The adductor group consists of adductor brevis, longus and magnus and gracilis. The obturator externus is also included here. Figure 2.5 illustrates the relative positions of these muscles. Both brevis and longus adductors have lines of action that pass directly from origin to insertion. Adductor magnus is an expansive muscle, which has several distinct muscular segments. To examine its mechanical effect it is, therefore, necessary to treat it as several muscular bundles.

The gracilis (H K *) muscle acts in a straight line from its origin to its insertion. The obturator externus (H*) muscle travels around the posterior of the head of the femur below the acetabulum. Its path is, therefore determined by femur-pelvis positioning. Its lever arm would not vary extensively as it is principally determined by the dimension of the femoral head.

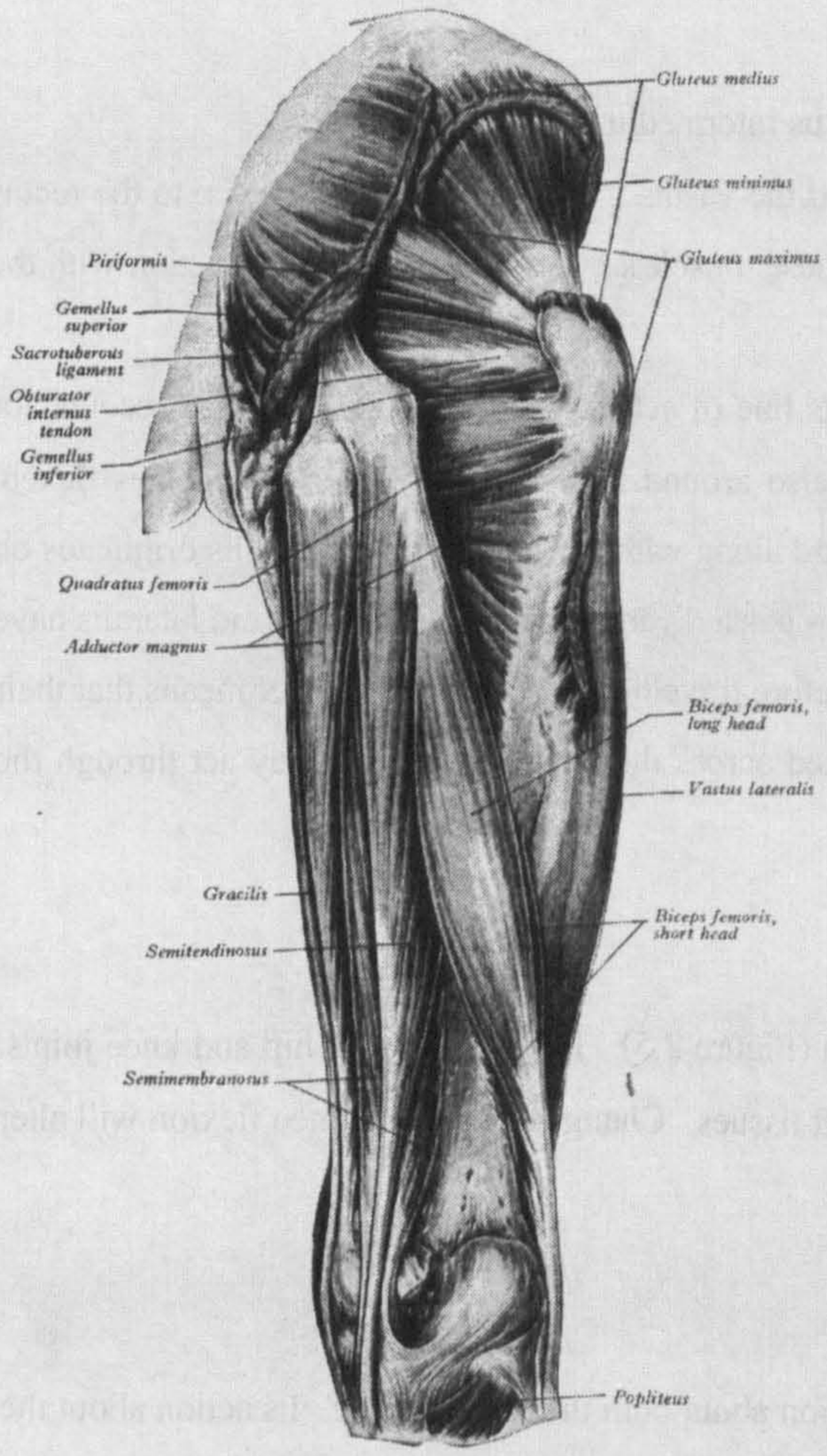

Figure 2.6B
Muscles of the posterior hip. Gluteal muscles. (Gray's Anatomy [1980])

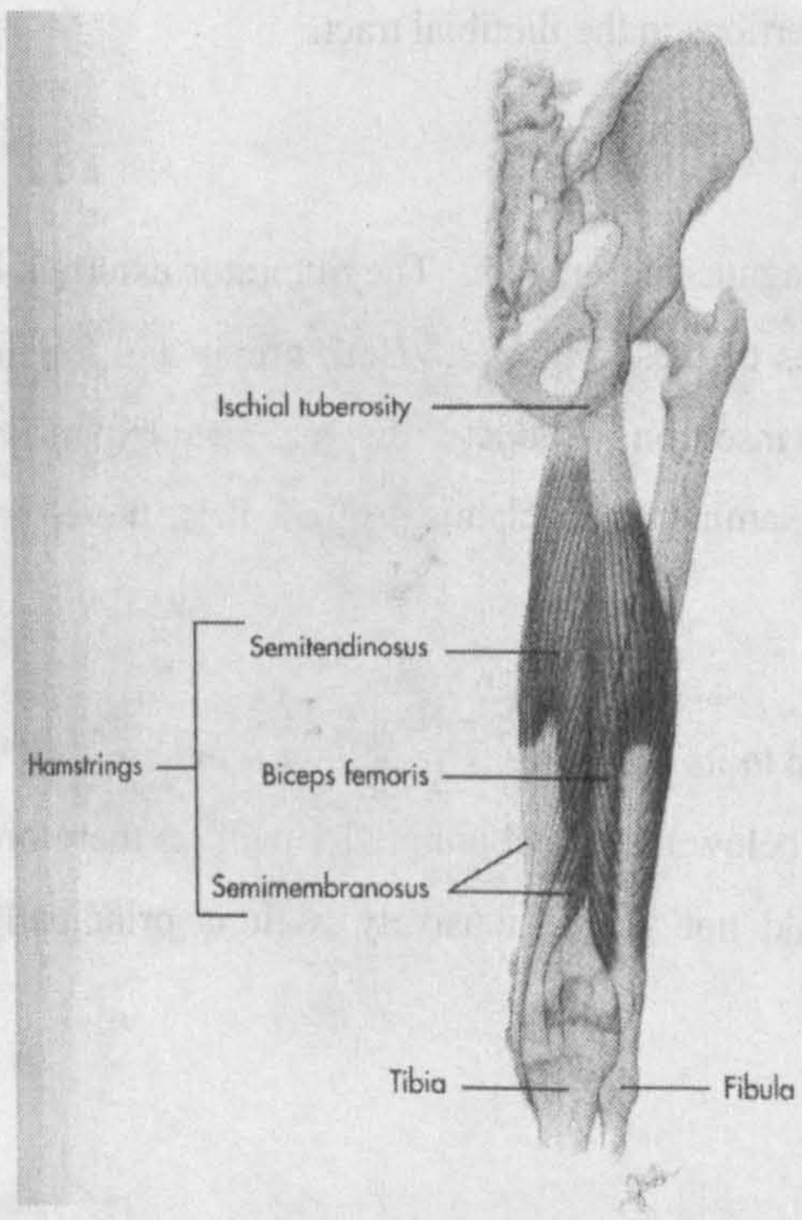

Figure 2.7
Posterior muscles of the right thigh, hip muscles have been removed. (Seeley et al [1995])

2.3.3 Buttock region

Gluteal Muscles:

Gluteus Maximus, Gluteus Medius, Gluteus Minimus (H m *)

The gluteal muscles, i.e. the gluteus maximus, medius and minimus contribute the majority of the buttock region muscle volume. They are all large triangular muscles.

The gluteus maximus is shown in Figures 2.6A and B. It can be seen that its action is complex due to its triangular shape. In order to describe its action it is, therefore, necessary to divide the muscle, treating it as several discrete elements. The action of the forces in each element of the muscle could be considered to act directly from origin to insertion. However, as with most other muscles the change in its course upon contraction may alter its effective distance from the centre of rotation of the hip joint. Part of the gluteus maximus inserts on the tensor fascia lata. This part of the gluteus maximus would therefore also produce some effect at the knee joint.

The gluteus medius (Figure 2.6) is deep to the maximus and anterior to it. Again it is a triangular muscle as is the gluteus minimus. Both of these two muscles would, therefore, be described in multiple parts even though they show no anatomical divide.

Inferior Gemellus, Obturator Internus, Superior Gemellus (H *)

These three muscles are intimately joined (Figure 2.6A and B). They lie deep to the gluteus maximus and piriformis. Their action is predominantly from origin to insertion due to their linear nature. On severe internal rotation of the hip joint these muscles may deviate around the femoral head/neck.

Piriformis (H *)

This muscle, deep to the gluteus maximus, follows a linear route from origin to insertion. On severe internal rotation of the hip joint these muscles may deviate around the femoral head/neck.

Quadratus Femoris (H *)

This muscle has an action along the line between its origin and insertion, a possible deviation from this could occur on severe internal rotation.

2.3.4 Posterior thigh

Biceps Femoris, Semimembranosus, Semitendonosus (H K *)

Figure 2.7 illustrates the relative positioning of the posterior thigh muscles. It can be seen that all have action at both the hip and knee joints. Consideration of knee joint geometry would have to be taken when determining the lines of action of these muscles.

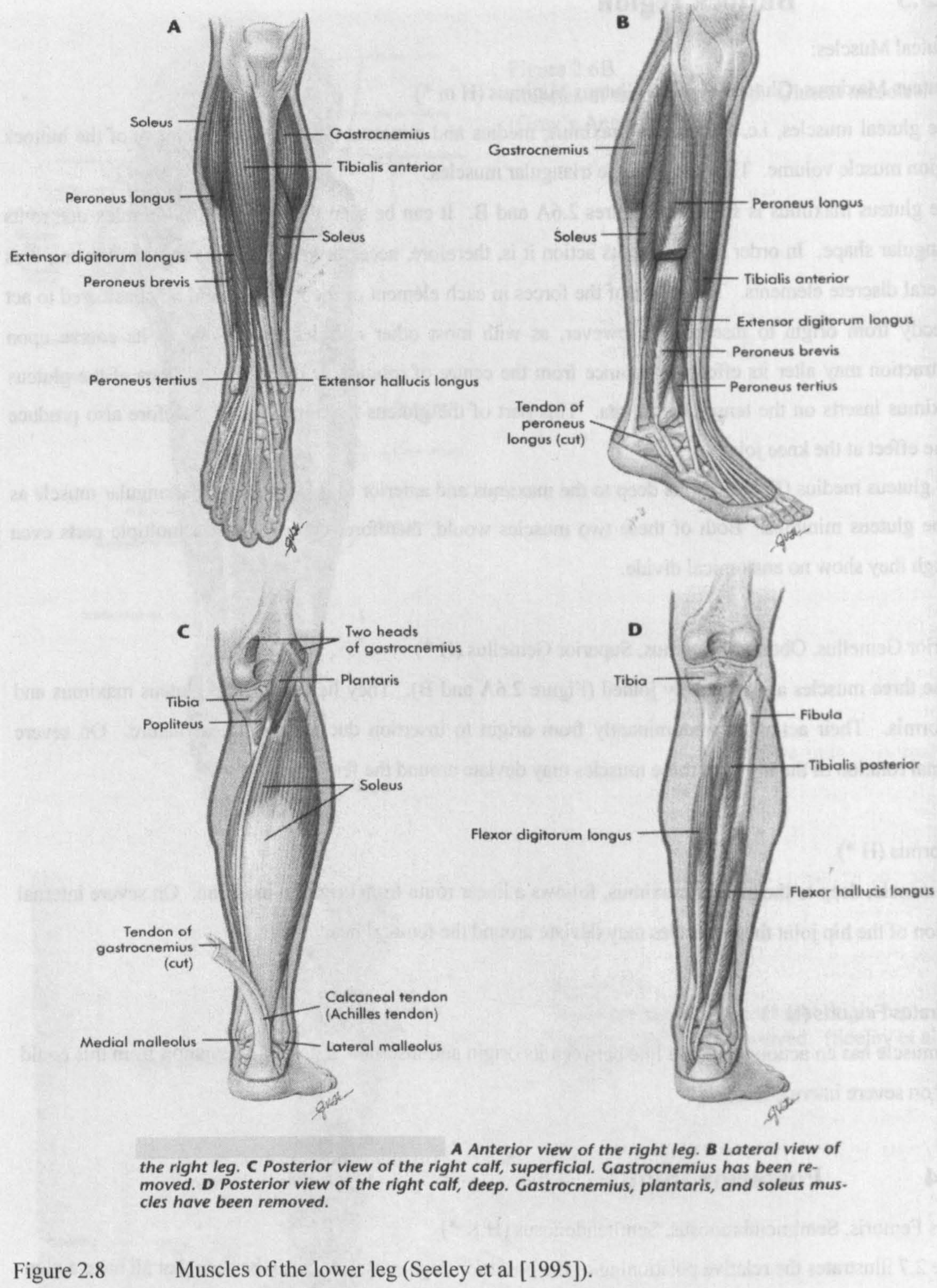

***A** Anterior view of the right leg. **B** Lateral view of the right leg. **C** Posterior view of the right calf, superficial. Gastrocnemius has been removed. **D** Posterior view of the right calf, deep. Gastrocnemius, plantaris, and soleus muscles have been removed.*

Figure 2.8 Muscles of the lower leg (Seeley et al [1995]).

The biceps femoris has a long and short head. The short head only acts across the knee joint, whereas the long acts across both knee and hip.

All these muscles have a small cross-section compared to length except for the short head of the biceps. In general, therefore, they could be considered to have a single line of action.

2.3.5 Calf muscles - superficial

Gastrocnemius (K A m *), Plantaris (K A), Soleus (A *)

Figure 2.8 includes the positioning of the gastrocnemius, plantaris and soleus. Both gastrocnemius and plantaris cross both the knee and ankle joints, the soleus crosses only the ankle joint. The gastrocnemius has two heads originating on the femur. When modelling the gastrocnemius it should, therefore, be treated as two muscle elements. Soleus has origins on both the tibia and fibula. This fact makes modelling of the soleus complicated. It must either be modelled as two elements or as one with an average origin location.

All muscles would have a line of action straight from origin to insertion. This may be slightly altered at origin for gastrocnemius and plantaris at full knee extension due to deviation about the condyles of the femur.

2.3.6 Calf muscles - deep

Flexor digitorum longus, Flexor Hallucis Longus, Tibialis Posterior (A *)

The origins of these three muscles are illustrated in Figure 2.8 with routing at the ankle shown in Figure 2.9 It can be seen that all have a similar relationship to the ankle joint being restrained by retinacula. The action of the tibialis posterior is principally at the tibio-talar joint where as the flexors also influence motion at the metatarsal and phalangeal joints. Their moment arm about the "ankle" joint would remain approximately the same during ankle movement due to restraint from the flexor retinaculum.

Popliteus (K)

The popliteus acts at the knee (Figure 2.8) and passes around the lateral side of the knee joint to attach to the posterior of the tibia. Its line of action is thus complex in its relation to the knee joint and will change significantly with knee flexion.

2.3.7 Lateral muscles of the calf

Peroneus Brevis, Peroneus Longus (A *)

Both of these muscles (Figure 2.8) originate on the fibula and act at the ankle joint. Their insertions can be seen in Figure 2.10. They are restrained at the ankle by the peroneal retinacula. Their line of action would follow the routing of the tendons around the ankle.

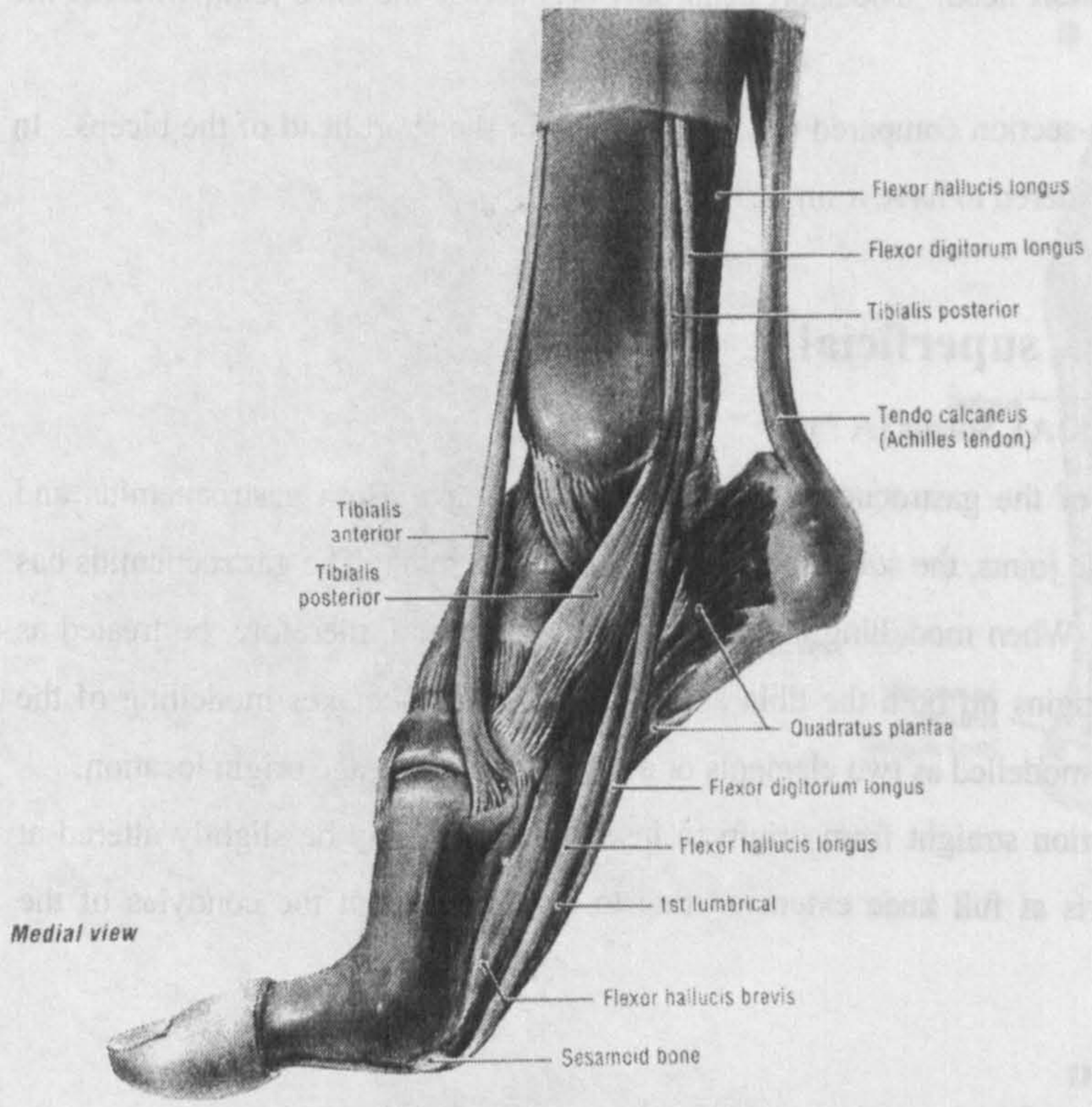

Figure 2.9 Medial view of routing of ankle muscles (Seeley et al [1995])

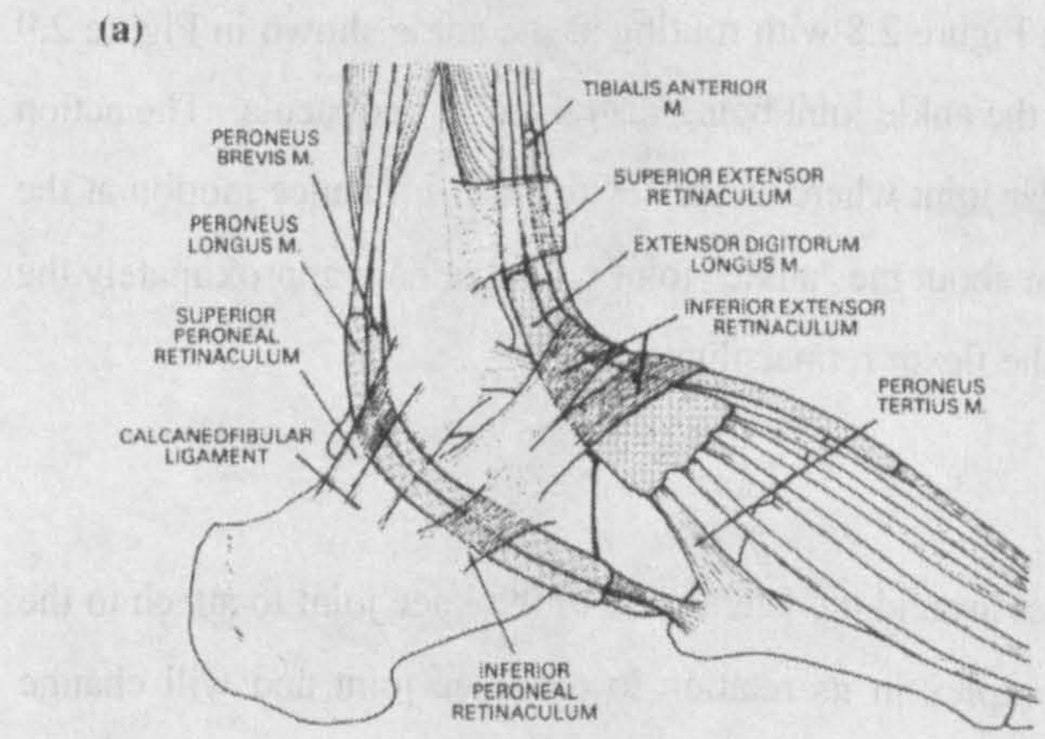

Figure 2.10 The retinacula and synovial sheaths of the ankle: (a) lateral; (b) medial (Joseph [1982]).

2.3.8 Anterior muscles

Extensor Digitorum Longus, Extensor Hallucis Longus, Peroneus Tertius, Tibialis Anterior (A *)

These muscles are shown in Figure 2.8. Their restraint at the ankle is shown in Figure 2.10. It can be seen from these diagrams that all have a single line of action at the ankle but that they may have multiple insertions on the foot. All the muscles would be restrained by the extensor retinacula.

2.3.9 Muscles of the foot

The model of the lower limb used in this thesis does not include equilibrium of structures within the foot, therefore no details of foot only muscles are given.

2.4 The joints

The structures that provide limitations on joint movement are detailed, including ligaments and other capsular fibres. This provides insight into the mechanisms that prevent excessive joint articulation during strenuous activity (Seeley et al [1995] and Grant's [1991] have been used as reference sources).

2.4.1 The hip joint

The hip joint capsular ligaments are illustrated in Figure 2.11. They are the iliofemoral, pubofemoral and ischiofemoral ligaments. It would seem that their principal function is in the limiting of joint articulation, i.e. that they become taut at the extremes of possible movement. Ligaments are elastic in nature, as are the elements of cartilage on the femur and acetabular surfaces. These structures do not therefore provide completely rigid restriction of movement patterns.

The extent of articular cartilage is illustrated in Figure 2.11. This shows the predominance of cartilage on the superior portion of the acetabulum where load bearing for ambulation is the highest. Also illustrated is the acetabular fossa an area of relatively thin bone with no articular cartilage. This area is associated with the supply of nutrients to the femoral head, via the ligamentum teres to the fovea capitalis of the femur.

2.4.2 The knee joint

The knee joint consists of three articulating pairs of surfaces, namely the two tibio-femoral junctions at the condyles and the femoral-patellar junction.

The articular surfaces of the femur, tibia and patella are shown in Figure 2.12. The lateral and medial surfaces of the femur and tibia do not have the same curvature, which indicates that a complex relationship of movement exists between the of the two bones. The intercondylar eminence is not a consistent feature of the tibia. It must, therefore, only be one factor in the pivot mechanism between the femur and tibia. The centre of the contact area of the femur on the tibia (via articular cartilage) moves anteriorly with increasing flexion

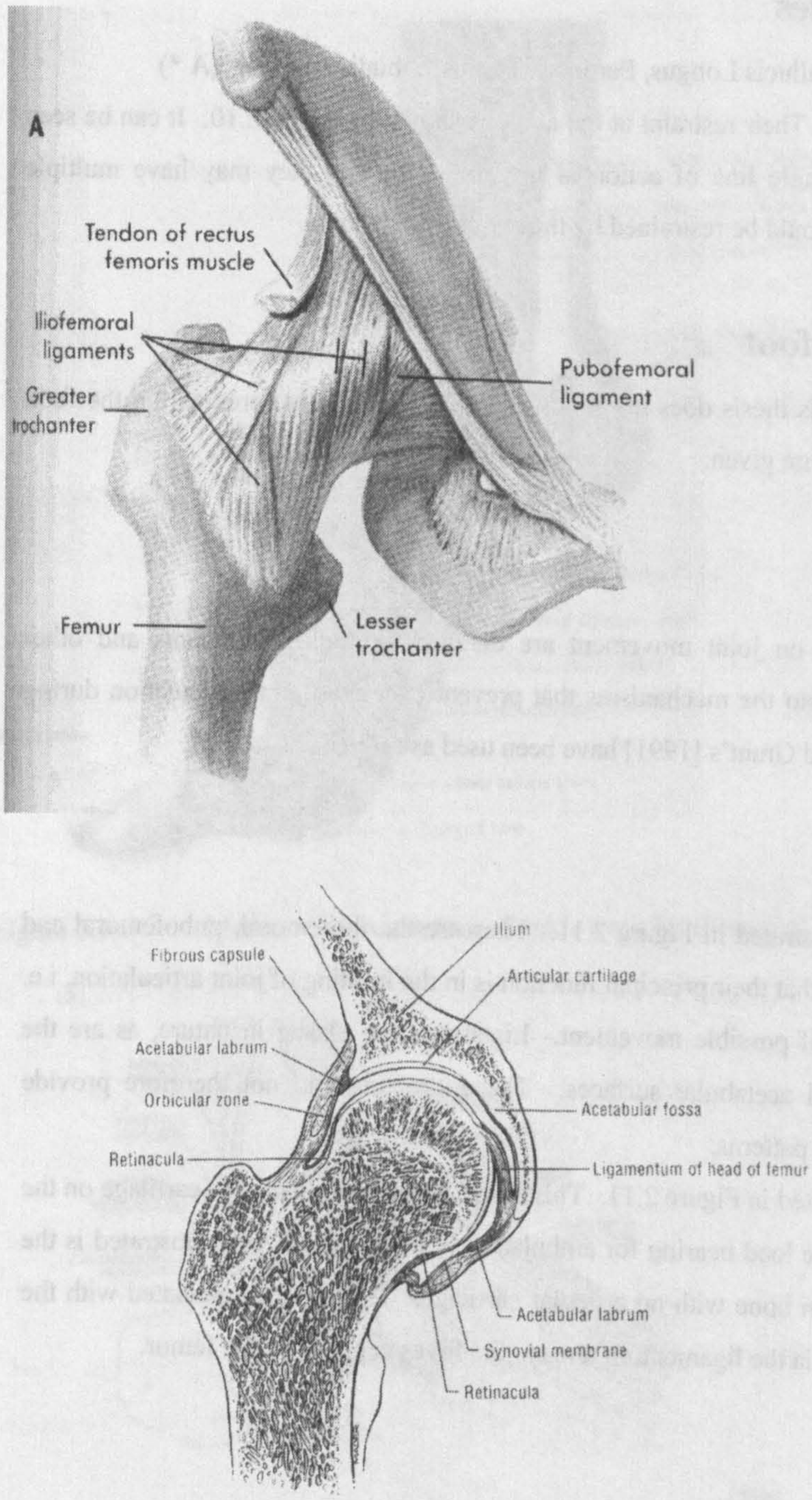

Figure 2.11 The right hip joint. **A** anterior view illustrating ligaments (Seeley et al [1995]). **B** Frontal section (Grant's [1991]).

of the knee. This movement allows the lever arm of the patella ligament about the centre of contact to increase with greater flexion. Soft tissue structures provide limits on the rotation and adduction/abduction that can occur at the knee.

Figure 2.12 shows the attachments of muscles and ligaments on the anterior of the knee. The patella acts as a common attachment for several thigh muscles via the patellar ligament. Interconnection is achieved via the patellar retinacula.

The posterior aspect of the knee can be illustrated in two layers (see Figure 2.12 C and D). In Figure 2.12 D the main collateral ligaments can be seen; the tibial (medial) and fibula (lateral) collateral ligaments. These are complemented by the oblique and arcuate popliteal ligaments. Figure 2.12 D also shows the cruciate ligaments and the interposed menisci of the joint. During rotation of the tibia against the femur these menisci are able to shift with respect to the tibia, thus improving weight bearing characteristics and also allowing more effective utilisation of synovial fluid in joint lubrication. The posterior and anterior cruciate ligaments located within the joint capsule provide resistance against excessive anterior-posterior movement of the tibia with respect to the femur. The ligaments of the knee provide an envelope of allowable relative motion of the femur with respect to the tibia.

2.4.3 The ankle joint

For the purposes of this thesis the ankle joint is considered to consist of the junction between the tibia, fibula and talus. The principal weight bearing surfaces are at the talus-tibia junction. Stability in the medio-lateral direction is maintained by the fibula (providing the lateral malleolar surface) and the tibia (providing the medial malleolar surface).

Figure 2.13 illustrates the principal ligaments at this joint. These ligaments are named following origin and insertion pairs. It can be seen that these ligaments form a comprehensive mesh between the bones of the proximal foot limiting relative movement. These diagrams only show the ligaments superficial to the bone. There are also ligaments interconnecting the bones of the foot between their articulating surfaces.

The articulation of the metatarsals and phalanges is limited by a complex arrangement of ligamentous connections. This is particularly true of the plantar aspect of the foot where multiple layers of ligaments provide limitations to foot arch flattening.

2.5 Summary

The principal components of lower limb anatomy have been detailed. Observations of muscle lines of action have been made as appropriate. Details of foot anatomy have only been given to the extent required for the implementation of the model used in this thesis. Comprehensive muscle anatomy has been documented by Palastanga et al [1994].

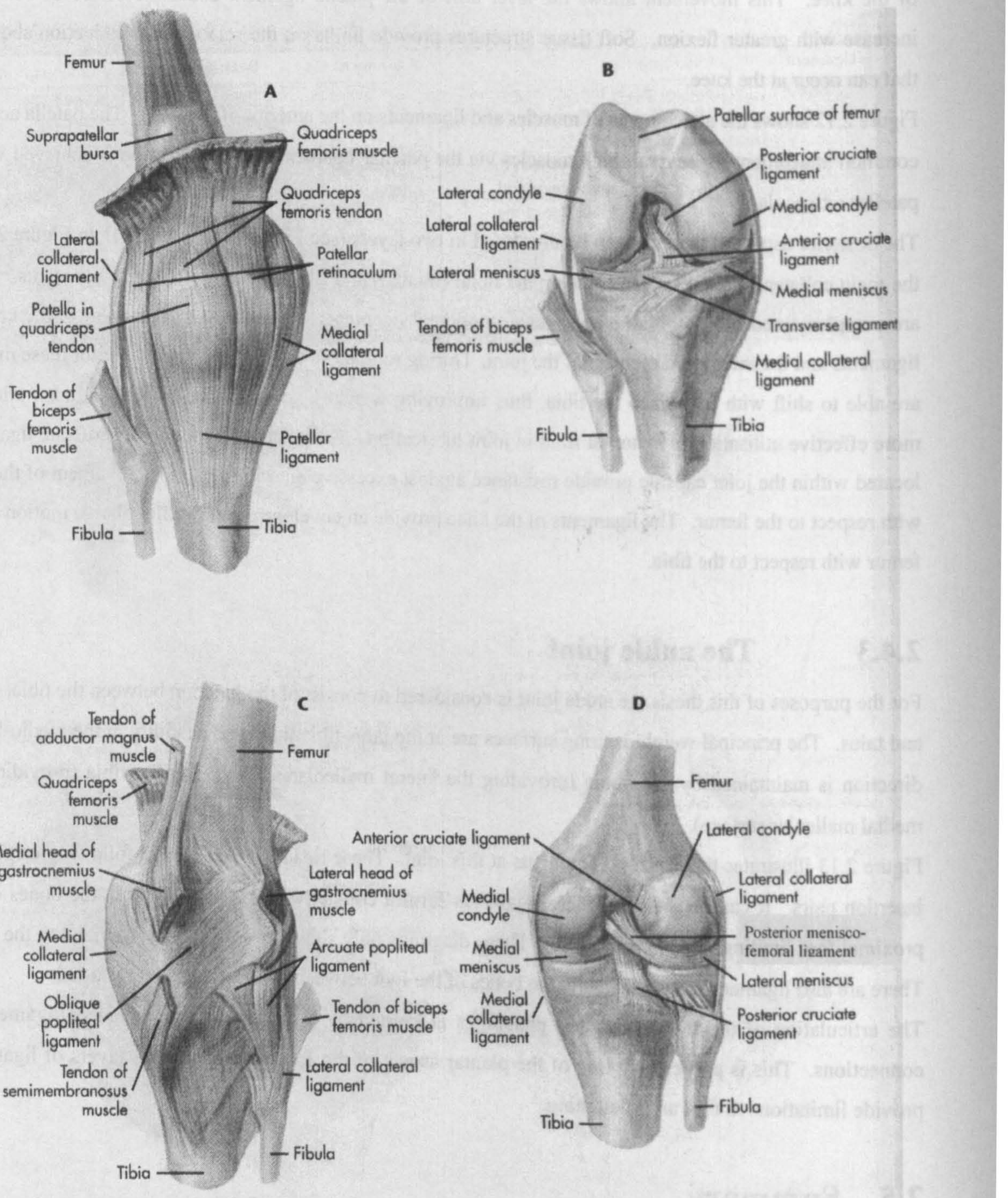

***A** Anterior superficial view. **B** Anterior deep view (knee flexed). **C** Posterior superficial view. **D** Posterior deep view.*

Figure 2.12 Right knee joint (Seeley et al [1995]).

Chapter 3 Methods

3.1 Data collection equipment

Three dimensional motion analysis was performed using a six camera infra-red VICON 370 (Oxford Metrics, Oxford, England) motion analysis system and a Kistler (AG Winterthur, Switzerland) force plate (accuracy ±1%). Retro-reflective markers (25mm diameter) were placed on the subject to identify anatomical features and to allow location of limb segments (the marker set is described in Section 3.5.3). The quoted measure of accuracy for the system, the *residual*, was always less than 0.1% of the largest dimension of the analysed volume, i.e. less than 3mm. The *residual* was calculated during the motion capture system calibration and was defined as the average distance by which rays from a particular camera misplaced the markers of the calibration object. This measure only provided an indication of the accuracy of the system. The error in recording of individual points could have been somewhat higher than this value. Further discussion of the accuracy of the motion analysis system is included in Sections 3.7.2 and 3.7.4.

Calibration of the analysis volume was performed with retro-reflective markers on four hanging poles placed in known locations at the edges of the test volume. The accuracy of the location of the force plate with respect to the calibration poles was ±1mm.

Output from the motion analysis system and force plate was synchronised at 50Hz.

3.2 Test protocol

All subjects were tested following the same protocol. Anatomical measurements were recorded (see Section 3.3.1) before motion analysis began. Subjects wore shorts and T-shirts, which were taped up to allow placement of markers on the skin. Markers were attached using double sided sticky tape. Subjects wore their usual footwear, although low heels were specified. All markers were attached (see section 3.5.3).

A 'static' trial was recorded with the subjects standing with arms folded, standing straight, with legs slightly apart and feet facing forwards. This trial provided information on the relative location of all markers to allow definition of the various segment axes systems and their relative orientation.

Several markers were removed to prevent their interfering with motion during the locomotion activities. Sufficient markers were left on the subject to allow definition of the motion of all limb segments (see Section 3.5.4).

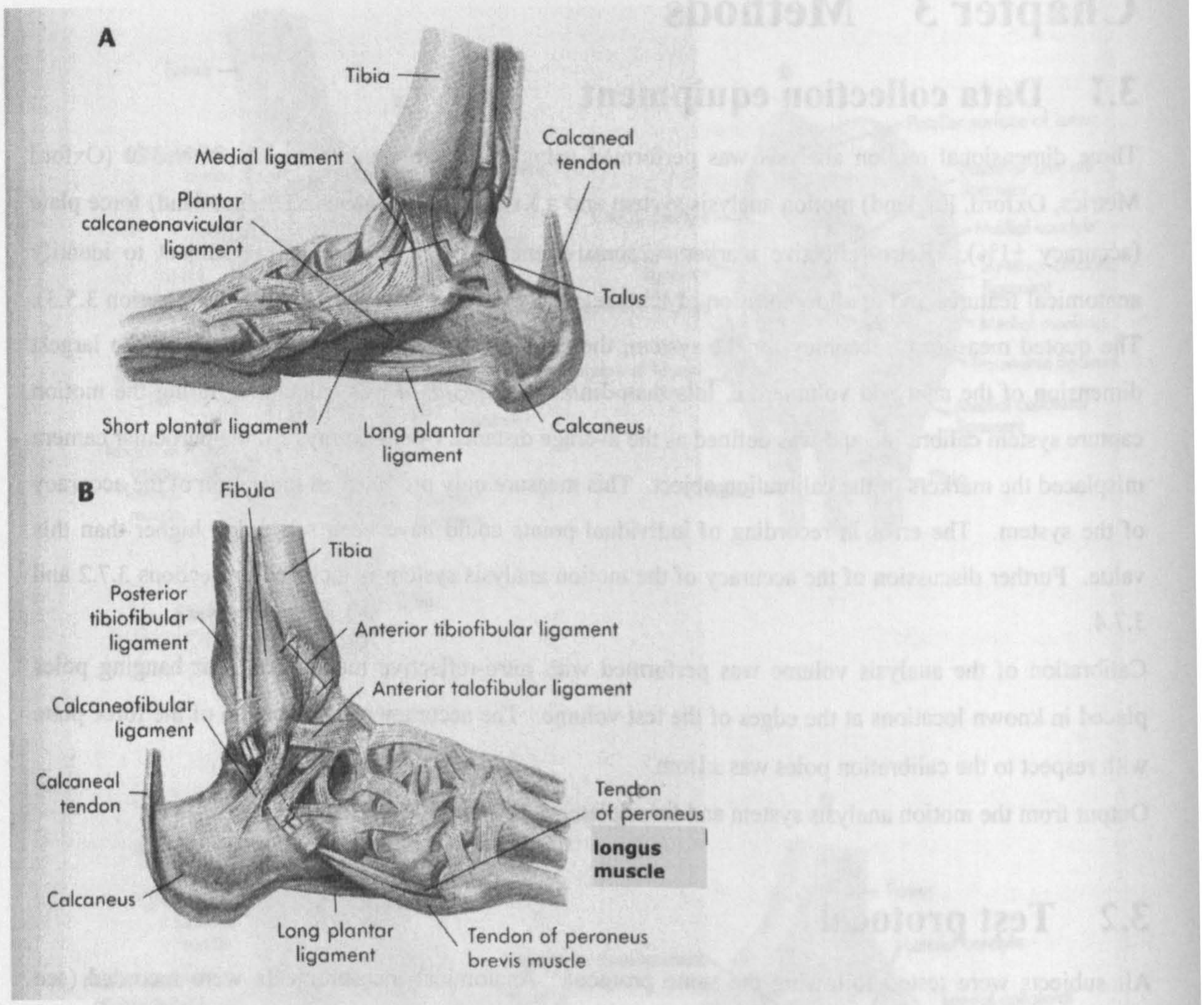

Figure 2.13 Right ankle joint. **A** medial view. **B** Lateral view.

Subjects performed the following activities.

1 Walking

2 Stair ascent, stair descent

3 10° Ramp ascent, ramp descent

4 5° Camber traverse

Before recording of each of the activities the subject was allowed a period of familiarisation with the piece of equipment and an appropriate starting point was determined to allow the subject to perform the activity in a smooth, natural manner. The subjects understood the function of the force plate. All motion trials were observed. Any trials which appeared unnatural, included stumbles or obvious targeting of the force plate were repeated. Each activity was performed five times. Subjects were allowed to rest between each activity whilst the equipment was changed. The total time for testing of each subject was apportioned as follows:

Anatomical measurement	10 minutes
Marker placement	15 minutes
Static trial	15 minutes
Walking trials	10 minutes
Stair trials	20 minutes
Ramp trials	20 minutes
Camber trials	20 minutes
Total time approximately	2 hours

It was possible for subjects to rest seated for a few minutes after each of the activities and at the mid-point of testing during the stair, ramp and camber activities to allow equipment to be changed.

All subjects performed all activities with no signs of physical stress or tiredness.

A walkway of approximately 10m was used for the walking trials allowing several full strides before foot contact with the force plate.

Two steps were allowed before the first foot was placed on the bottom stair for stair ascent. One step on the platform was allowed before stair descent. To allow ascent and descent to be recorded for both feet the force plate section was moved from one side to the other of the second step.

The starting point for the ramp trials was set approximately three steps before the first foot contact with the ramp. Ramp descent trials were started to allow one step on the platform before first foot contact on the ramped section. All subjects performed at least one full stride on the ramped section before foot contact with the force plate section in both ascent and descent. The subjects walked on the ramp off centre to allow either left or right leg contact with the force plate section.

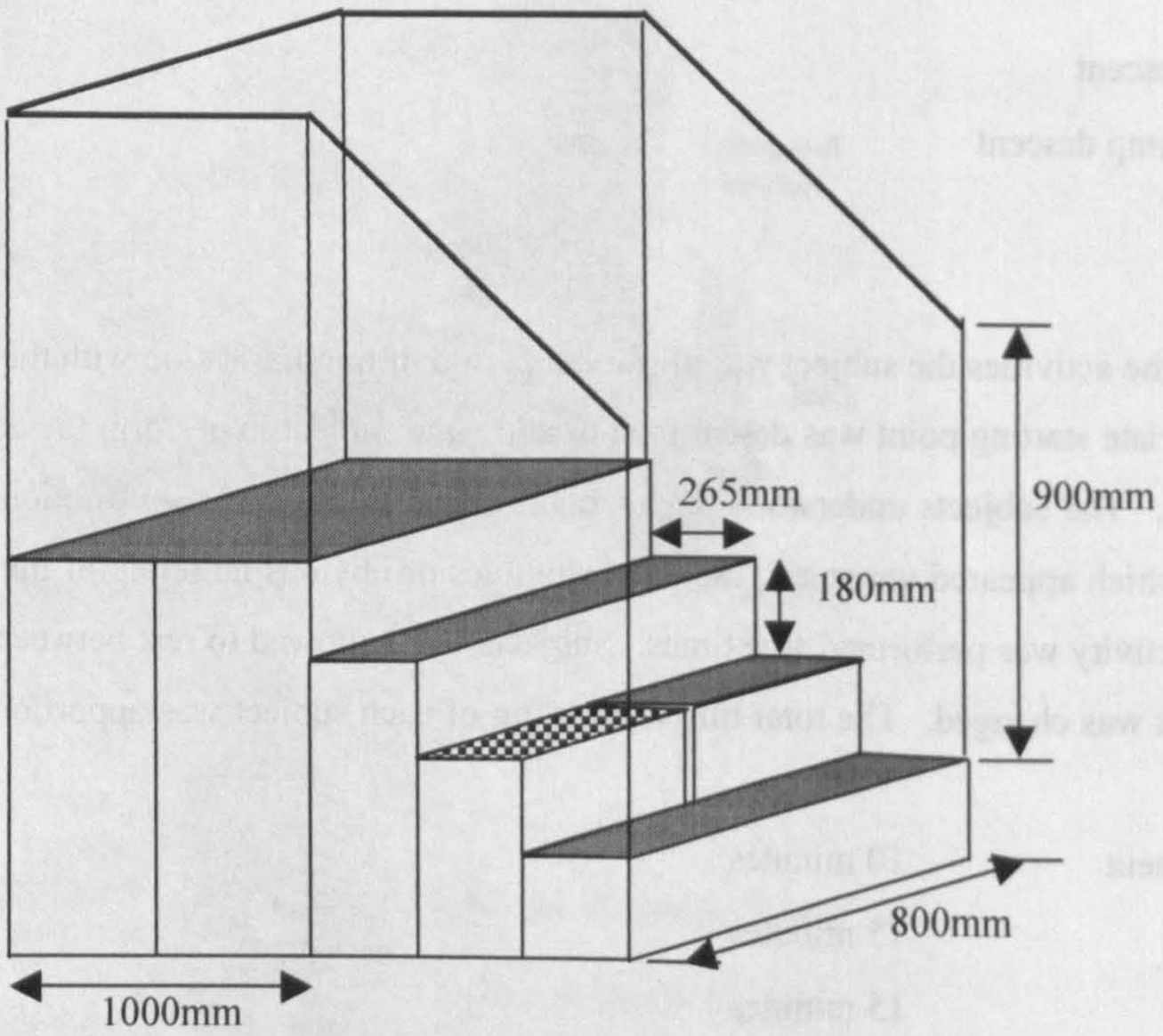

Staircase

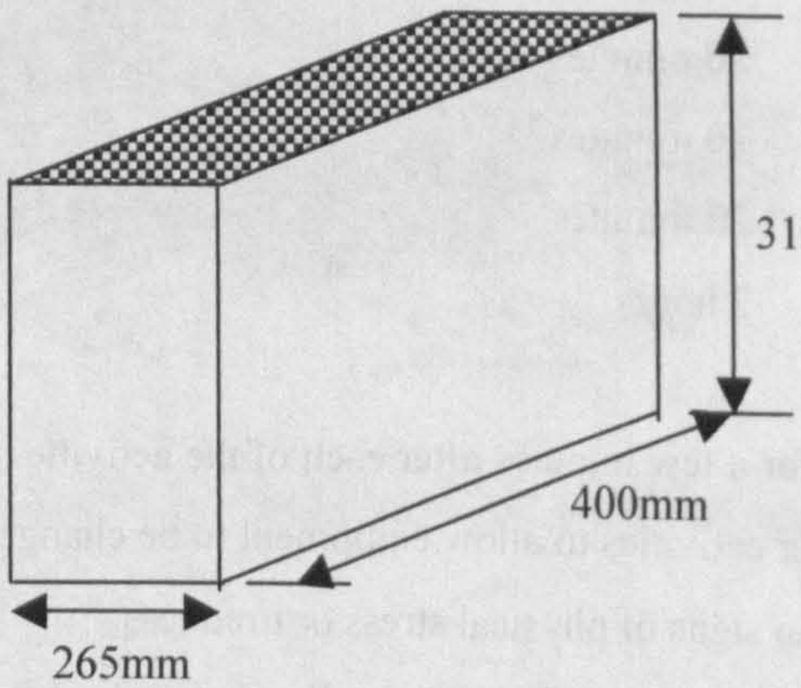

Force plate section

Figure 3.1A Equipment diagram: Stairs

All steps in the camber trials were performed on the camber sections. This gave a camber-way of 7.3m in length, allowing several full strides before foot contact with the force plate section. Subjects were asked to walk either along the lower section or upper section of the camber to ensure that either left or right foot made contact with the force plate section.

3.3 Subjects

The aim of this thesis was to analyse the hip joint forces in 40 to 60 year old subjects. 5 normal male and 6 normal female volunteers were recruited. 5 male subjects with hip replacements were also recruited. Subject details are recorded in Appendix I. Selection of subjects with hip joint replacements was based on a number of criteria. Only those subjects with total hip joint replacements due to osteoarthritis were selected. They were all able to perform all activities comfortably including cyclical (one foot on each step only) stair climbing. None had any secondary illness or disease that significantly affected locomotion. The use of hand-rails and walking stick by subject 27 was the only support used by any of the subjects. All other subjects, normal and with hip replacements, were able to perform all activities with no requirement for additional support.

Ethical approval was obtained for normal and hip joint replacement subjects. Informed consent was obtained on the day of the testing.

3.3.1 Anatomical measurements

To apply the muscle model to the subjects of this study and to scale the joint structures of the leg model it was necessary to measure a number of anatomical dimensions for each individual. These measures were taken using callipers or a rule as appropriate. Anatomical features were palpated. Accuracy of measures was approximately ±5mm, this being the error associated with feature identification through the skin. The following measures were made:

-Inter anterior superior iliac spines distance, measured between the most prominent points of the iliac spines.

-Anterior-posterior distance from the line between the anterior superior iliac spines to the midpoint between the posterior superior iliac spines.

-The vertical distance from the ischial tuberosity to the iliac crest.

-The distance between the most lateral points of the right and left greater trochanters.

-The width of the femoral epicondyles at the widest point.

-The width of the tibial condyles at the widest point.

-The vertical distance from the tibial tuberosity to the tibial plateau.

-The largest medio-lateral dimension of the malleoli.

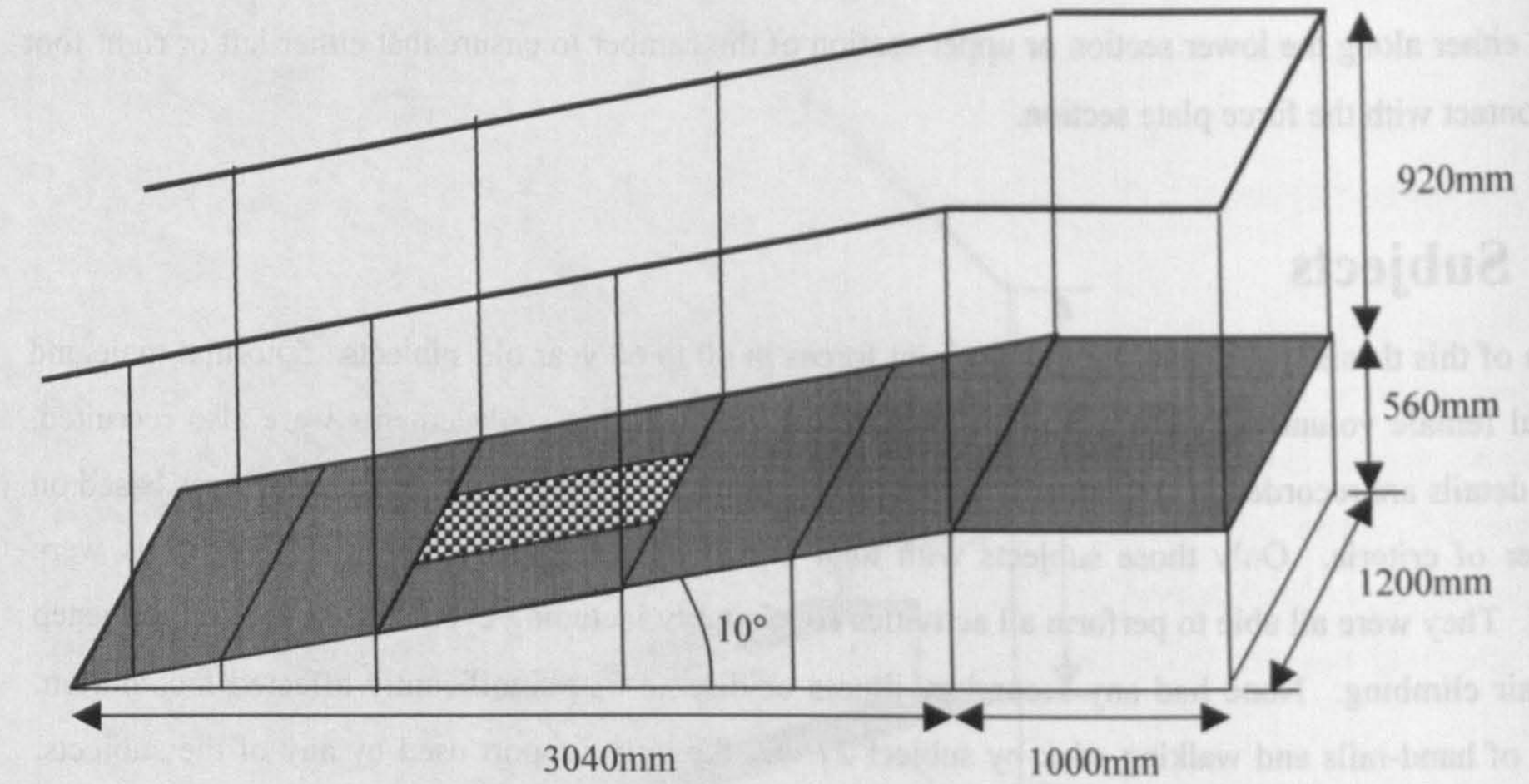

10° ramp

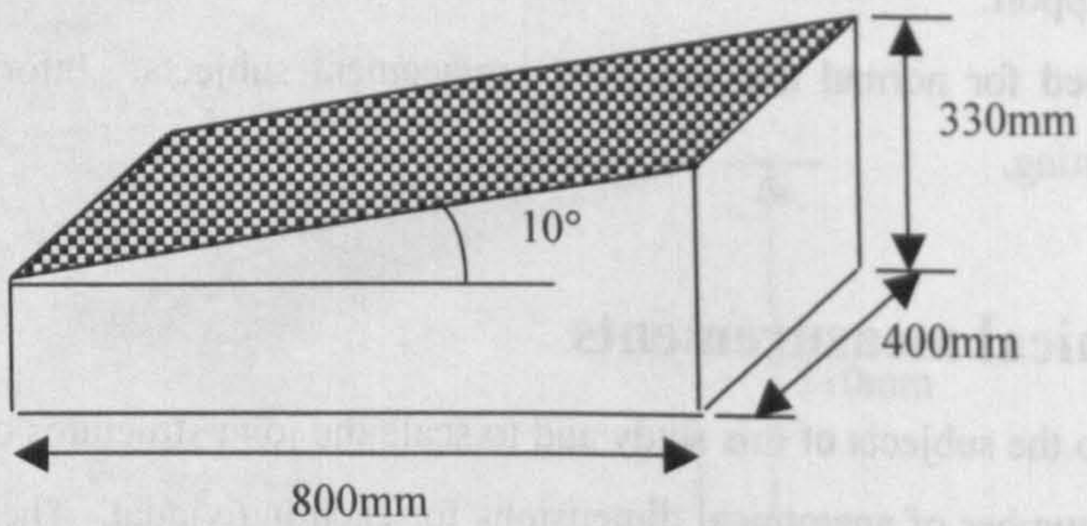

Force plate section

Figure 3.1B Equipment diagram: 10° Ramp

These measurements were corrected for skin cover, to give dimensions which included bone and underlying soft tissue (e.g. joint capsule, ligaments etc.).

3.4 Test equipment

To perform the stair, ramp and camber tests it was necessary to use pieces of equipment designed to integrate with the force plate. In each of these activities a force plate section was bolted via a rigid force plate attachment (Figure 3.1D) onto the force plate. Force application to the section was, therefore recorded by the force plate. Figures 3.1A to 3.1C illustrate the stair, ramp and camber equipment. The force plate attachment (Figure 3.1D) had six 120mm square 10mm thick plates welded to the underside which were machined to lie flush with the surface of the force plate to prevent distortion of the force plate when the bolts were tightened. Each of the force plate sections was precisely machined to allow bolting on top of the force plate attachment. The frame of the stairs, ramp and all force plate sections were made out of 25mm square metal tube. ¾ inch plywood was used for all flooring. 3mm thick ribbed rubber matting covered all sections of flooring to provide friction. Each of the force plate sections illustrated (Figures 3.1A to 3.1C) had a 25mm metal tube frame around the floored area but no other reinforcement under the plywood. There would have been some deformation of the flooring on loading. For the walking trials no attachment to the force plate was required, as the force plate was flush with the floor of the laboratory.

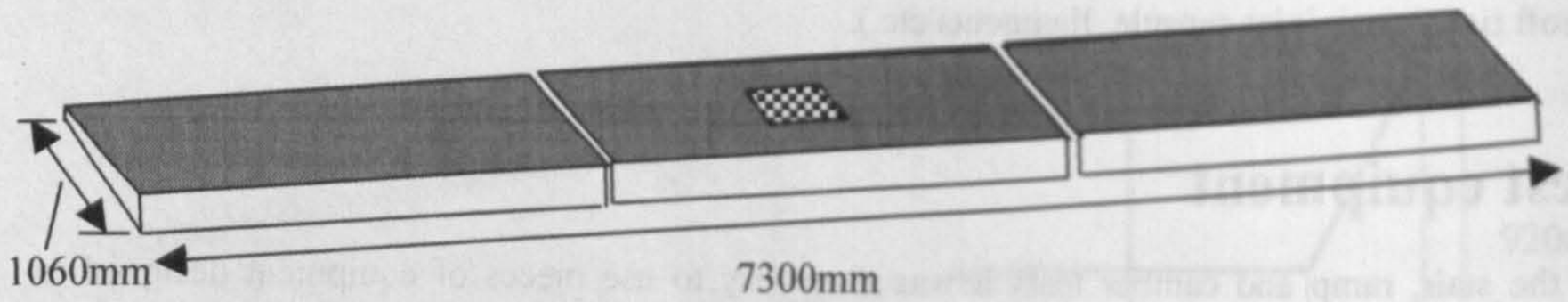

5° cambered section

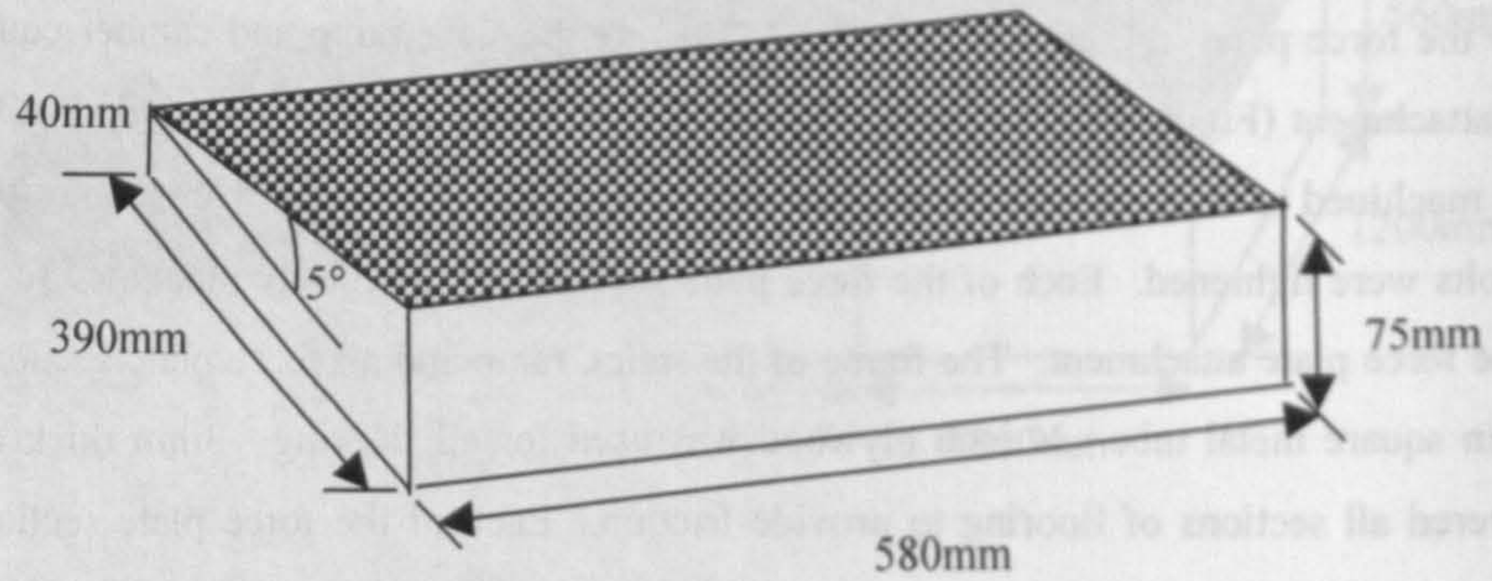

Force plate section

Figure 3.1C Equipment diagram: 5° Cambered section

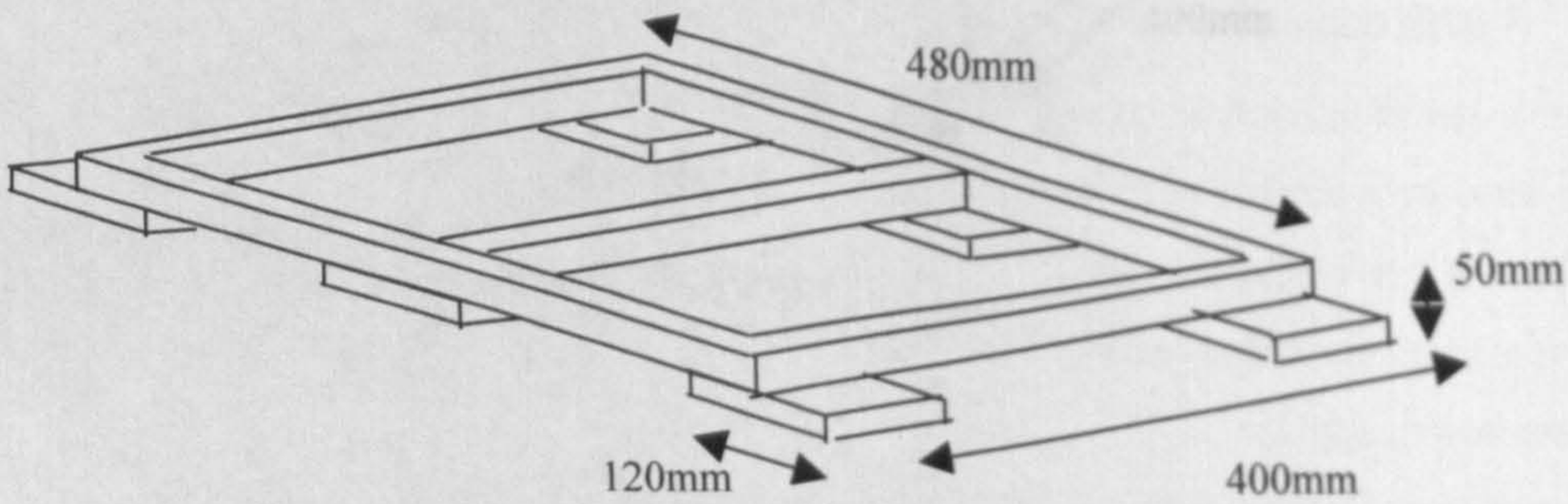

square plate (60mm overhang)

Figure 3.1D Force plate attachment

3.5 Three-dimension modelling of the lower limb

3.5.1 Introduction

To calculate the forces at the hip joint using only external information required the development of a three dimensional model of the lower limb. This required knowledge of the location of force carrying structures such as bones, muscles and other soft tissues and their relative location to external landmarks. Details of the origin and insertion of muscles (Section 3.5.2), the definition of segment and joint axes systems (Section 3.5.4) and a description of joint structures (Section 3.5.5) are given.

3.5.2 Muscle model

The model of muscular anatomy used in this study was based on that of Brand et al [1982]. Several modifications were made to allow Brand's data to be integrated into the model. 47 muscular elements were used. These consisted of 24 hip only, 7 hip and knee, 4 knee only, 2 knee and ankle and 10 ankle only muscles elements. Several muscles at the hip were divided into parts to allow the full action of the muscle to be described.

3.5.2.1 Muscle origin and insertion data

Muscle origins and insertions were defined after Brand et al [1982]. Appendix II gives both unscaled and scaled data from Brand. These data were defined in terms of co-ordinates in the appropriate bone axes system. Three sets of right-handed orthogonal axes were used (pelvic, femoral (thigh) and tibial (shank) as illustrated in Figure 3.2). The pelvic co-ordinate system had its origin at the femoral head centre (hip joint centre) with axes directions defined by

YPB=PP3-PP2

XPB=YPB × (PP1-PP2)

ZPB=XPB × YPB

where PP1 was the right anterior superior iliac spine, PP2 was the midpoint of the pubic tubercles and PP3 was the midpoint between the anterior superior iliac spines. The vector cross product is represented by '×'. The femoral co-ordinate system had its origin at the midpoint of the epicondyles and had axes directions defined by

YFB=PF3-PF2

XFB=YFB × (PF1-PF2)

ZFB=XFB × YFB

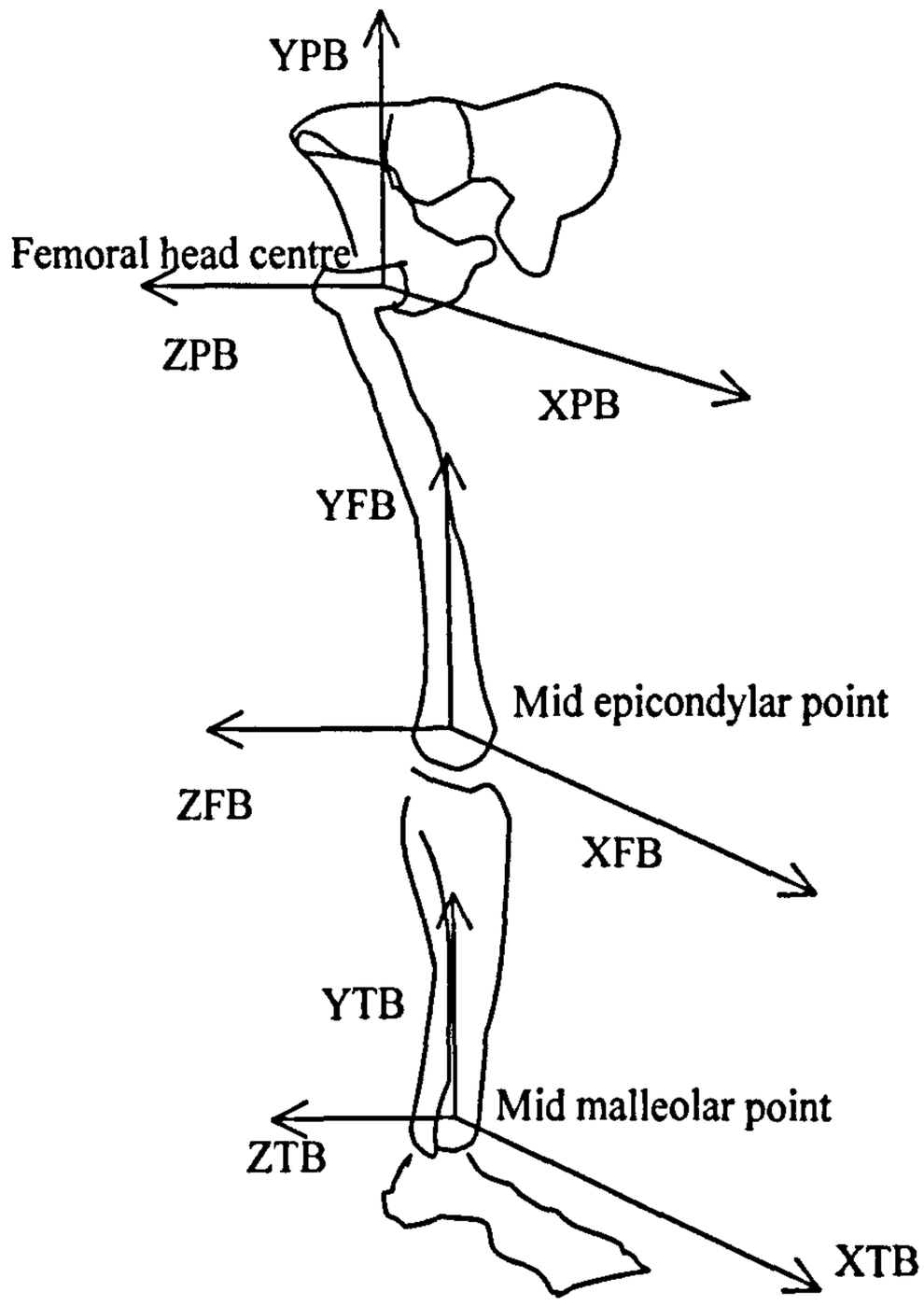

Figure 3.2 Segment axes after Brand at al [1982]. (See Section 3.5.2.1)

where PF1 was the lateral epicondyle, PF2 the midpoint of the epicondyles and PF3 the femoral head centre. The tibial co-ordinate system had its origin at the midpoint of the medial and lateral malleoli with its axes directions defined by

YTB=PT3-PT2

XTB=YTB × (PT1-PT2)

ZTB=XTB × YTB

where PT1 was the lateral malleolus, PT2 the midpoint of the malleoli and PT3 the tibial tuberosity.

3.5.2.2 Factors

Brand presented two sets of data on the origins and insertions of muscles of the lower limb. The first set of data was the actual values of muscle origin and insertion points in metres from the origin of the appropriate coordinate system. The second set of data was a set of origin and insertion points in dimensionless units which required the application of particular factors to arrive at the actual values of origin and insertion locations in metres. It is the second set of values that have been used for this thesis. To obtain the actual value of muscle origin or insertion in metres the following procedure was followed:

Origin or insertion position (m) = Brand's scaled origin or insertion data (dimensionless)
× Brand's factor (m)

The average values of Brand's muscle origin and insertion data from cadaver studies in metres are detailed in Table A-II.1/2, in Appendix II as 'Actual Origins' and 'Actual Insertions'. Brand's dimensionless values of the origin and insertion points are detailed in these tables under the headings of 'Scaled Origins' and 'Scaled Insertions'. Brand's factors are detailed in Table 3.1 and are based on anatomical measurements from the subjects. The average values of Brand's factors were calculated using the two sets of data,.'Actual' and 'Scaled' for each of the co-ordinate systems and in each of the axis directions. These average values are detailed in Table 3.1. A factor was associated with each axis of each of the segment co-ordinate systems as defined by Brand.

Brand's factors were anatomical measurements derived from three cadavers (one female and two male) of average height 1727mm. The average height of the subjects in this study was 1706mm, with approximately the same ratio of female to male subjects, 6:10, as that of Brand. No age of the cadaver specimens was given in Brand et al [1982]. It was assumed that Brand's insertion and origin data could be used for the subjects studied for this thesis. It was necessary to modify a number of the factors used by Brand as it was not possible to obtain radiographs of subjects to allow measurement of bony dimensions.

Table 3.1 Muscle origin and insertion factors

Brand's co-ordinate system and axis direction	Brand's factor (m)	Brand's factor average value (m)	Factor used for this thesis (incorporating multipliers were appropriate) (m)
Pelvic			
X	Anterior-posterior distance from pelvic frontal plane to the top of the sciatic notch	0.0673	(Anterior-posterior distance from mid posterior superior iliac spines to the inter anterior superior iliac spines line) × 0.427
Y	Vertical distance of iliac crest above ischial tuberosity	0.1985	(Vertical distance of iliac crest above ischial tuberosity) × 0.888
+Z	Anterior-superior iliac spine to hip joint centre medio-lateral distance	0.0330	(Inter anterior superior iliac spine distance) × 0.1341
-Z	Ischial tuberosity to hip joint centre medio-lateral distance	0.0792	(Femoral head centre to mid anterior superior iliac spines medial distance) × 0.893
Thigh			
X	Femoral epicondylar width	0.0803	(Femoral epicondylar width) × 0.765
Y	Femoral head centre to mid epicondylar distance	0.3950	Femoral head centre to mid epicondylar distance
Z (gastroc)	Femoral epicondylar width (gastrocnemius only)	0.0800	(Femoral epicondylar width) × 0.765
Z (not gastroc)	Lateral distance from the femoral head centre to the top of the greater trochanter (all other muscles)	0.0531	(Lateral distance from femoral head centre to the most lateral point of the greater trochanter) × 0.621
Shank			
X	Tibial plateau width	0.0638	(Tibial condylar width) × 0.644
Y	Tibial tuberosity to mid malleolar distance	0.3097	Tibial tuberosity to mid malleolar distance
Z	Tibial plateau width	0.0631	(Tibial condylar width) × 0.644

Where necessary allowances for soft tissue cover were calculated based on the average of subject measures for this thesis as compared to those of Brand.

The origin or insertion points were therefore calculated as follows:

Origin or insertion position (m) = Brand's scaled origin or insertion data (dimensionless)
× (factor used in this thesis (incorporating multiplier where appropriate)) (m)

For the two sets of factors to be equivalent it was assumed that the following was true:

Brand's factor average value (m) = (average factor used in this thesis) (m)

The factors used in this thesis were also based on anatomical dimensions and are detailed below and in Table 3.1. Where different anatomical dimensions were used a multiplier was incorporated to ensure that the average factor for the subjects studied for this thesis was the same as that of Brand.

3.5.2.2.1 Pelvic factors

X (applied to all X co-ordinate dimensions)

It was not possible to ascertain accurately the position of the top of the sciatic notch in the anterior posterior direction. The alternative measure of the anterior posterior distance from the mid-posterior superior iliac spines to the inter-anterior superior iliac spines line was used. A multiplier of 0.427 based on the average of Brand's factor and that of the distance measured in the subjects studied was used. It was assumed that the sciatic notch maintained the same relative position between the anterior and posterior aspects of the pelvis.

Y (applied to all Y co-ordinate dimensions)

The measure of the ischial tuberosity to iliac crest taken from the subjects included substantial soft tissue thickness. To compensate for this soft tissue cover a multiplier of 0.888 was applied to the measured value of ischial tuberosity to iliac crest to ensure that the average of the subject's measures corresponded to that of Brand's factor. The use of this factor assumed the same ratio of soft tissue cover to bony dimension for all subjects.

+Z (applied to all +Z co-ordinate dimensions)

The value of this factor as recorded by Brand was approximately 33mm. To reduce the sensitivity of this measure to errors in the location of the hip joint and the anterior superior iliac spines a factor equal to the

inter-anterior superior iliac spine distance was used. To make this factor equivalent to Brand's it was multiplied by 0.1341. This modification made the assumption that the hip joint centre was always placed at a fixed proportion of the anterior-posterior distance between mid anterior superior iliac spines and the anterior superior spines.

-Z (applied to all –Z co-ordinate dimensions)

It was not possible to accurately locate the position of the ischial tuberosity in the medio-lateral direction. The medio-lateral distance from the hip joint centre to the mid-anterior superior iliac spines was therefore used. A multiplier of 0.893 was used to ensure that the average measure of this study was the same as that of Brand.

Summary of pelvic factors

It was necessary to modify significantly the factors used by Brand. The modified factors were chosen to use measures along the same co-ordinate axis with account being taken of soft tissue where appropriate. The factors were derived based on the average of Brand's factors for all muscles and on the average of the measures in the study population. Thus all individuals were considered to be scalable in the same manner. No distinction was made between male and female subjects although it is acknowledged that there are differences between the relative proportions of the male and female pelvis. The muscle model used was derived from one female and two males and, therefore, was a compromise between the two different anatomies.

3.5.2.2.2 Thigh factors

X (applied to all X co-ordinate dimensions)

The femoral epicondylar measure of Brand was 0.765 times that of the average of the subjects studied for this thesis. It would appear that Brand's measure did not include any soft tissue and although a correction for skin thickness was made to the measures in this study that it was not sufficient to take into account the underlying soft tissues. It was also possible that Brand's specimens did not have as wide epicondyles as those of the present study. It was likely that both of these factors affected the relative values, although if Brand's specimens and the subjects studied in the present study were representative of the same population then a multiplier of 0.765 would have been appropriate. This was assumed to be the case.

Y (applied to all Y co-ordinate dimensions)

The thigh Y factor used was the same as that used by Brand, i.e. the distance from the mid femoral epicondylar point to the centre of the femoral head (hip joint centre). This factor relied on the calculation of the location of the femoral head. The standard hip joint centre location was used as more direct measures (e.g. X-ray) were not available.

Z (applied to Z co-ordinate dimensions of the gastrocnemius origin)

The same factor as use for the thigh X co-ordinates was used, i.e. 0.765 times the femoral epicondylar width.

Z (applied to Z co-ordinate dimensions of all muscles except the gastrocnemius)

It was not possible to locate the medio-lateral position of the top of the greater trochanter as no X-rays (or similar) of the subjects were available. It was, therefore, necessary to use a different factor. The distance from the hip joint centre to the most lateral greater trochanter was used as it was hoped that this would be representative of dimensions in the medio-lateral direction. The standard hip joint centre location was used in this factor. A multiplier of 0.621 was used to ensure that the average of Brand's factor values was the same as that for the subjects studied in for this thesis.

Summary of thigh factors

As with the pelvic factors it was necessary to make assumptions about the relative dimensions of various aspects of the femur. The lack of access to X-ray data of the subjects prevented the use of Brand's factors. Dimensions at the hip were considered to be more appropriate for use in most of the factors than for example the femoral condylar width as Brand's factors were based on dimensions at the hip. Factors were determined based on the assumption that Brand's specimens were of the same relative dimensions as those of the subjects studied for this thesis. This was necessary to ensure that the dimensions of underlying soft tissue structures could be taken into account.

3.5.2.2.3 Shank factors

X (applied to all X co-ordinate dimensions)

Tibial condylar width was used instead of tibial plateau width for the tibial X factor. The edges of the tibial plateau were difficult to locate accurately so the alternative of the tibial condylar width was used. A multiplier of 0.644 was used to ensure that the average factors remained the same. This multiplier would have taken into account soft tissue cover of the bones.

Y (applied to all Y co-ordinate dimensions)

The same factor use by Brand was used, i.e. the distance from the tibial tuberosity to the mid malleolar point.

Z (applied to all Z co-ordinate dimensions)

This factor was identical to that of the shank X factor.

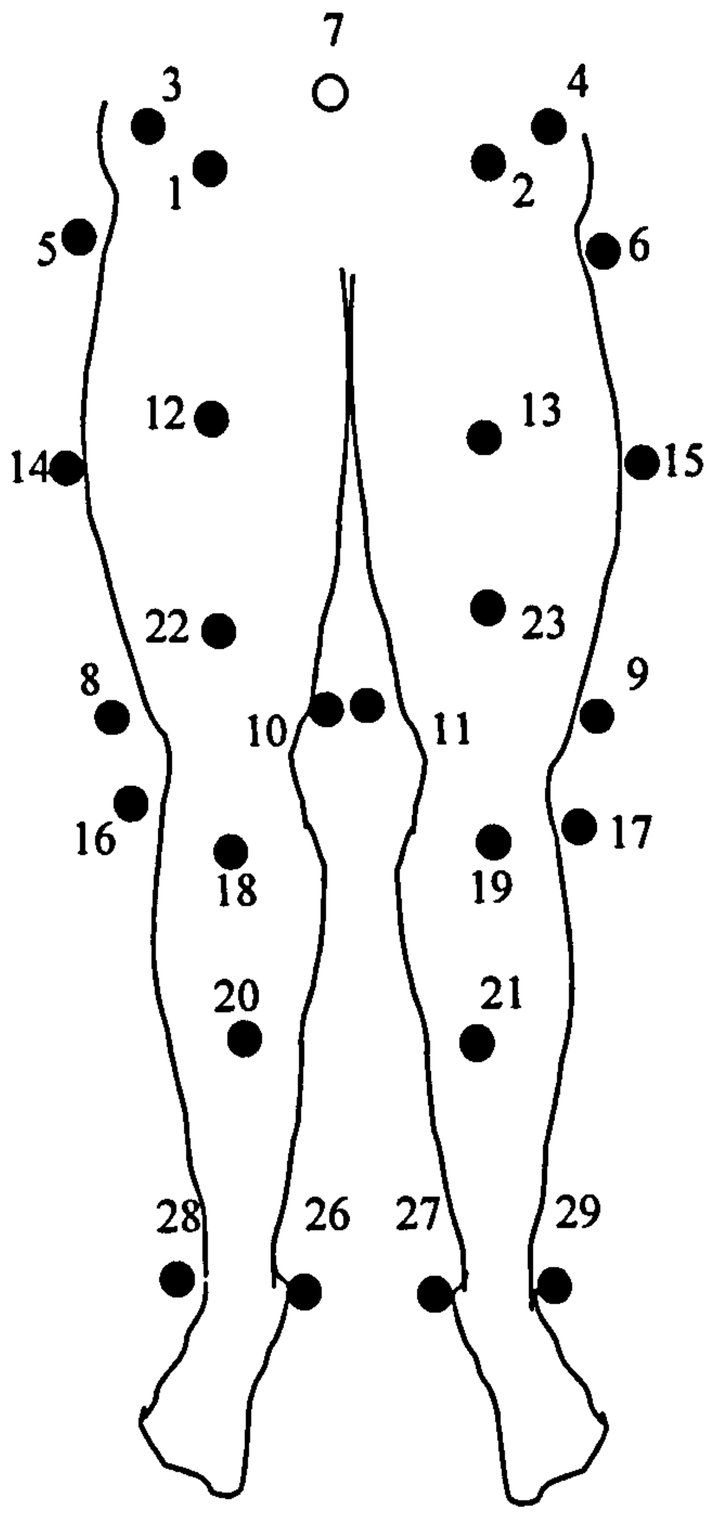

Figure 3.3 External marker set

Marker locations

1 right anterior superior iliac spine (A)
2 left anterior superior iliac spine (A)
3 a point on right iliac crest
4 a point on left iliac crest
5 right most lateral greater trochanter (A)
6 left most lateral greater trochanter (A)
7 mid point of posterior superior iliac spines
8 right lateral femoral epicondyle (A)
9 left lateral femoral epicondyle (A)
10 right medial femoral epicondyle (A)
11 left medial femoral epicondyle (A)
12 right front of thigh mid femur
13 left front of thigh mid femur
14 right lateral thigh mid femur
15 left lateral thigh mid femur
16 right fibular head (A)
17 left fibular head (A)
18 right most prominent tibial tuberosity
19 left most prominent tibial tuberosity
20 right front of tibial (medial face)
21 left front of tibia (medial face)
22 right lower front of thigh
23 left lower front of thigh
24 not used
25 not used
26 right medial malleolus (most medial part) (A)
27 left medial malleolus (most medial part) (A)
28 right lateral malleolus (most lateral part)
29 left lateral malleolus (most lateral part)

(A)=Used in static trial only to define anatomical feature locations.

3.5.2.2.4 Summary of muscle factors

Significant modifications were made to Brand's factors. These were necessary for a number of reasons. It was not possible to obtain radiographs of the subjects, so several of the factors had to be modified to use measurable dimensions of the subjects. A number of Brand's factors were based on measures that included bone only whereas the measures taken of the subjects for this thesis included soft tissue. Brand's factors were adapted appropriately. The use of modified factors could have introduced errors into the location of muscle's origins and insertions. The modified factors were chosen with the aim of minimising any additional errors to those already implicit within Brand's scheme.

3.5.2.3 Modification of pelvic muscle origins

To implement the muscle model of Brand it was necessary to apply a modification to Brand's pelvic axes set. The definition of Brand's pelvic co-ordinate system used the midpoint between the pubic tubercles. It was not possible to palpate this point accurately so an alternative axes set had to be used. The conversion from Brand's axes set to that used for implementation of the muscle model in this study was based on Fitzsimmon's [1995] dry bone study. A rotation of 9.87 degrees about Brand's ZPB axis was required to allow the XPB axis to become parallel to the line joining the mid points of the anterior and posterior superior iliac spines. Thus it was necessary to rotate by 9.87 degrees both the YPB and XPB axes of Brand around Brand's ZPB axis.

3.5.3 External Markers

The motion of the subjects was tracked using markers attached to the skin. A marker set was chosen which allowed the location of all segments of the lower limb. It is possible to supplement markers with points determined using a pointing stick (Cappozzo et al [1995]). This technique was not used as it was possible to define the location of a suitable set of points using skin attached markers only.

The position and number of external retro-reflective markers used in the motion analysis were chosen to provide an accurate representation of the subject's movement. Cappozzo et al [1995] suggests a set of marker locations that could be used in movement analysis. This is only one of the marker configurations suggested in the literature. Common to all marker sets is the need to place markers over readily identifiable anatomical landmarks to allow accurate location of the underlying bony structures. For this thesis a set of markers was used that satisfied the goals of the analysis:

From the external markers the underlying bony structures needed to be identified.

During the moving trials the location of each segment of the lower limb had to be identified.

It was not necessary to use the same set of markers to achieve both of these gaols. If a relationship between the positions of the two sets of markers were established then it would have been possible to establish the position of underlying structures from either of the two sets of markers.

To allow the location of underlying bony structures (and therefore muscle and ligament locations) the following set of markers were used: Three markers were used per segment (pelvis, thigh and shank) to allow three dimensional position and orientation of the segment to be established. Markers were placed so as to allow observation by video cameras during all activities being studied. The marker set used is illustrated in Figure 3.3. Pelvic markers (1 to 4 and 7) were placed on bony landmarks. Markers 3 and 4 were placed on the lateral aspect of the iliac crests to allow observation from both behind and in front of the subjects. 12 to 15 and 22 and 23 were placed on the thigh at convenient locations at approximately mid-thigh (12 to 15) and three-quarters thigh length from the hip joint. 8 to 11 and 16 to 19 were placed on bony landmarks. 20 and 21 were placed on the bony medial side of the tibia at about mid shank. 26 to 29 were placed on the most medial or lateral aspects of the malleoli as appropriate.

The pelvic segment was used to define the location of the hip joint centre and the tibial segment was used to define the location of both the knee and ankle joint centres.

3.5.4 Definition of segment co-ordinate systems

For implementation of the muscle and joint models it was necessary to establish fixed reference frames within each segment of the lower limb. It was necessary to be able to relate these axes to the external markers used to record subject motion. Initially two sets of axes were established for each segment. These were the segment anatomical axes and the segment moving axes.

The segment anatomical axes were defined using anatomical features of the bones of each of the segments. The location of joint structures and muscle origins and insertions could be defined within the anatomical co-ordinate system. The anatomical co-ordinate system was defined using a set of external markers placed over the appropriate bony landmarks (see Section 3.5.4.1 below). It was not possible, however, to use this set of markers during the dynamic trials, as can be seen from the marker location diagram (Figure 3.3). Some of the markers would have obstructed movement, e.g. the medial malleolus marker. To over come this difficulty a set of axes called the segment moving axes were defined based on markers used during the dynamic tests (see Section 3.5.4.2 below).

During the dynamic trials only the segment moving axes were defined. It was therefore necessary to find a way of relating this information to the location of underlying bony and soft tissue structures. This was achieved using a static trial. During the static trial the subject stood still with legs straight and slightly apart and with feet pointing forwards. During this trial all markers were used; both anatomical and moving axes marker sets (as illustrated in Figure 3.3). It was therefore possible to define the relationship between these two sets of axes. Thus from one set of axes the other could be defined.

Each of the relationships between axes sets consisted of two parts a rotation and a translation between origins.

From the static trial the following relationships could be established :

Ground axes to anatomical axes :

$$[P_A] = [R_{GtoA}][P_G - OA_G]$$

Ground axes to moving axes :

$$[P_M] = [R_{GtoM}][P_G - OM_G]$$

And therefore moving axes to anatomical axes :

$$[P_A] = [R_{MtoA}][P_M - OA_M]$$

Where :

$$[R_{MtoA}] = [R_{GtoM}]^{-1}[R_{GtoA}]$$

$[P_A]$ = 1×3 position matrix of a point in anatomical co - ordinates

$[R_{GtoA}]$ = 3×3 rotation matrix from ground to anatomical axes

OA_M = 1×3 position matrix of the origin of the anatomical axes system in moving axes co - ordinates

Similar terms were defined using the following subscripts :

G = ground axes system

A = anatomical axes system

M = moving axes system

From each of the dynamic trials the following relationships could be established :

Ground axes to moving axes

$$[P_M] = [R_{GtoM}][P_G - OM_G]$$

And therefore moving to anatomical, using the relationship derived in the static trial.

$$[P_A] = [R_{MtoA}][P_M - OA_M]$$

From the Anatomical axes the locations of joints, muscles and ligaments were defined.

Each of the rotation matrices was defined as follows :

$$[R_{GtoA}] = \begin{bmatrix} X_1 & Y_1 & Z_1 \\ X_2 & Y_2 & Z_2 \\ X_3 & Y_3 & Z_3 \end{bmatrix} = [P_X \quad P_Y \quad P_Z]$$

Where :

P_X = equivalent in Anatomical co - ordinates of a unit X direction vector in Ground co - ordinates .

Details of the right limb axes sets will now be given.

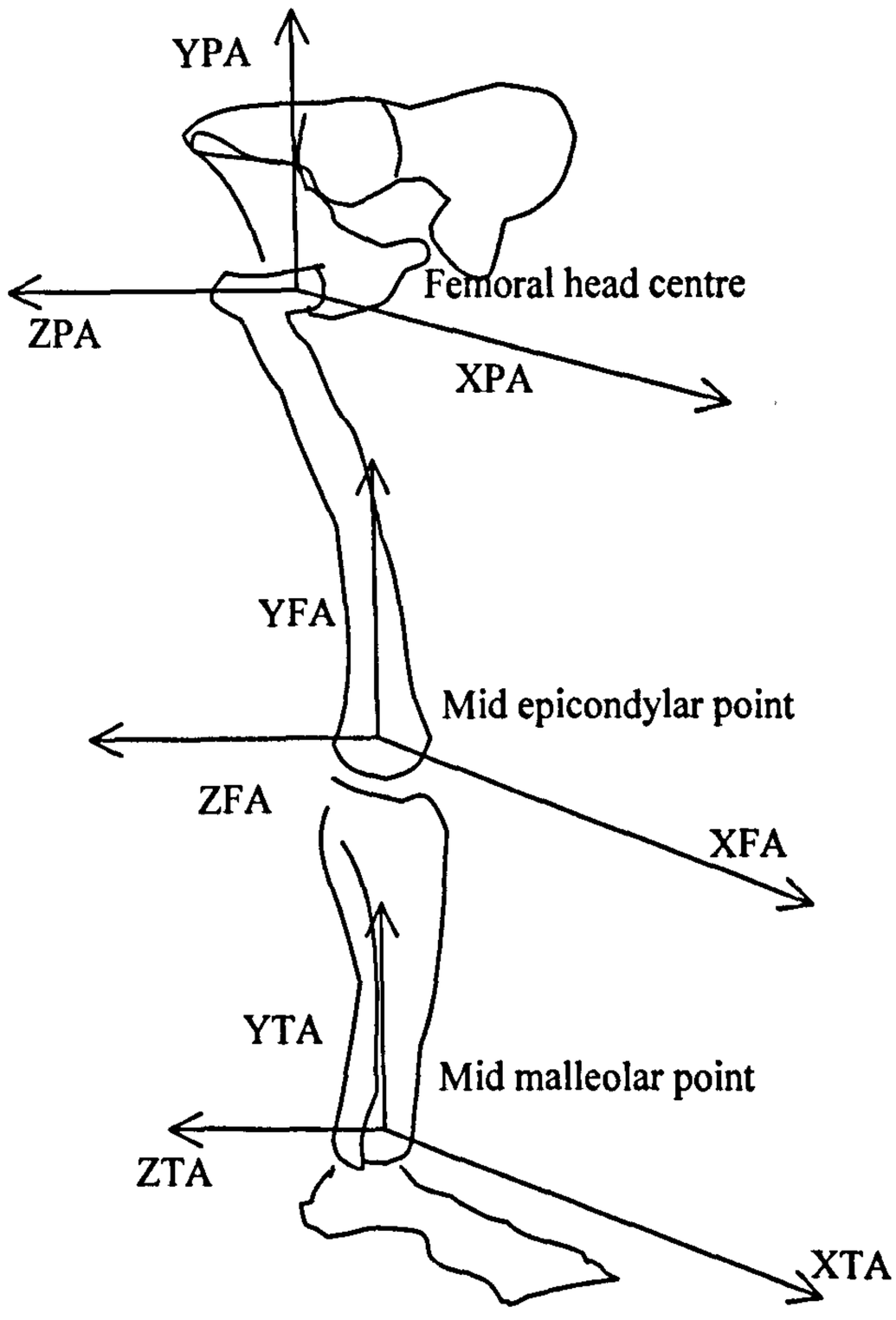

Figure 3.4 Segment anatomical axes (See Section 3.5.4.1)

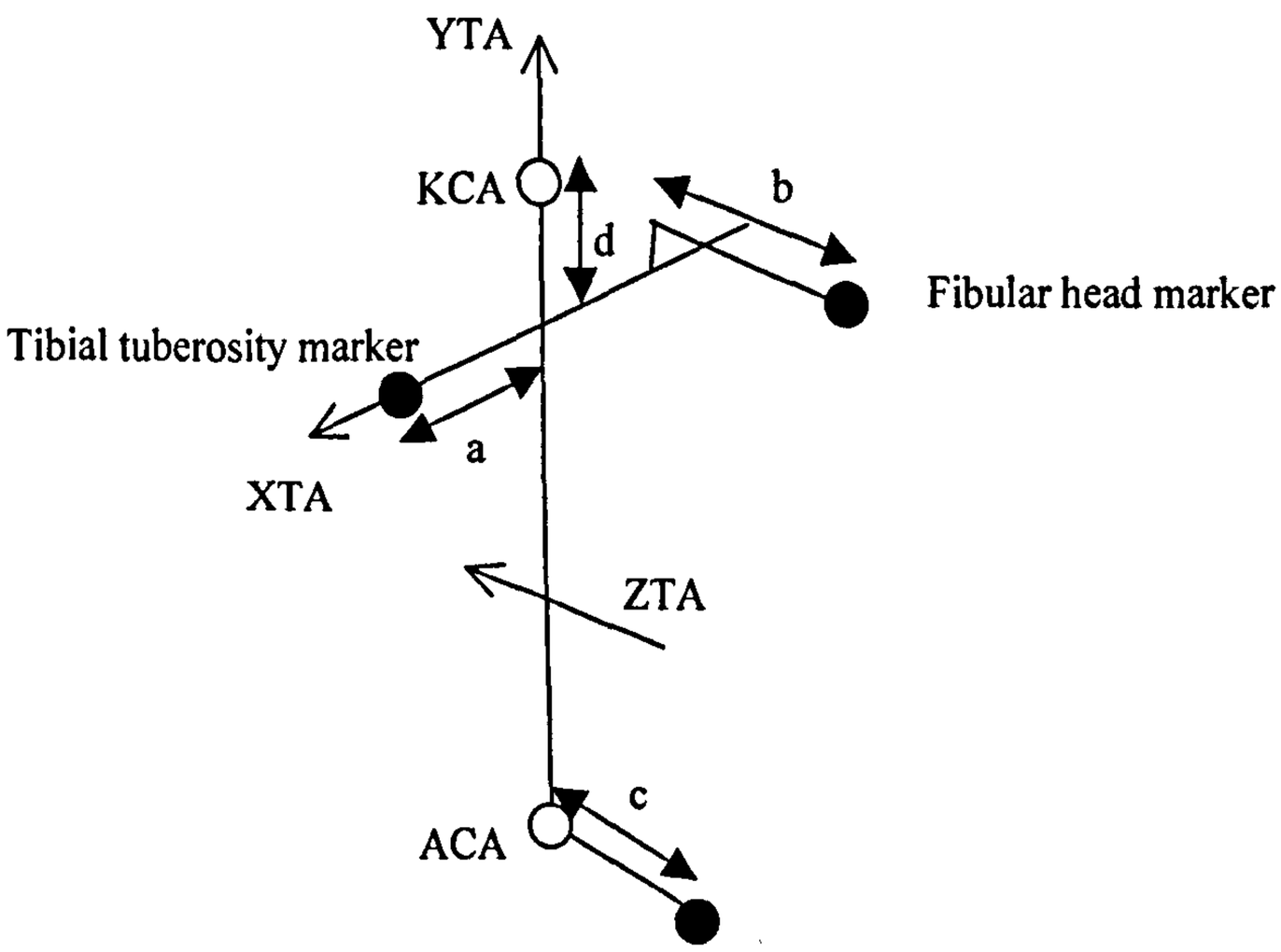

Figure 3.5 Shank segment anatomical axes definition
KCA = knee centre shank anatomical system
ACA = ankle centre shank anatomical system

3.5.4.1 Segment anatomical axes

The segment anatomical axes were defined as follows:

The pelvic axes set for each leg had its origin at the femoral head centre. All axes directions were based on a right-handed orthogonal set (see Figure 3.4).

ZPA = right anterior superior iliac spine – left anterior superior iliac spine

YPA = perpendicular to the plane containing the mid-posterior superior iliac spines and the right and left anterior superior iliac spines.

XPA = perpendicular to both YPA and ZPA pointing anteriorly

The thigh (femur) segment anatomical axes set had its origin at the mid point of the lateral and medial epicondyles with

YFA = femoral head centre – mid epicondyles

XFA = perpendicular to both the YFA and a line joining the epicondyle markers pointing anteriorly

ZFA = perpendicular to both the XFA and YFA axes.

The axes of the shank (tibial) segment anatomical co-ordinate system were fitted to ensure that the XTA axis passed through the midpoint of the tibial plateau at the level of the fibular head marker. This is illustrated in Figure 3.5. The shank YTA axis was fitted to pass through the mid malleoli point and to pass at a certain distance 'a' from the tibial tuberosity. The shank ZTA axis was perpendicular to XTA and YTA.

The dimensions 'a' to 'd' were defined as follows (in units of mm)

$a = (8.2 + 0.5 \times 47.1) \times [(\text{medio-lateral distance between tibial condyles})/97.6]$

b = [(fibular head to medial tibial condyle distance) - (medio-lateral distance between tibial condyles)] + (medio-lateral distance between tibial condyles)/2 + marker base to marker centre distance

c = (medio-lateral distance between malleoli)/2 + marker base to marker centre distance

$d = 25 \times [(\text{medio-lateral distance between tibial condyles})/97.6]$

The dimension 'a' was defined so that the YTA axis passed through the mid-anterior-posterior aspect of the tibial plateau. The dimension 8.2mm was that of the average distance between the tibial tuberosity and the front of the tibial plateau perpendicular to the long axis of the tibia as recorded by Nisell et al [1985]. Nisell recorded 7.2mm for women and 9.2mm for men. The value 47.1mm was the average depth of the medial and lateral tibial plateau for women and men combined taken from the results of Mensch & Amstutz [1975]. 97.6mm was the average of the medio-lateral distance between tibial condyles of the subject studied for this thesis. Thus the dimension 'a' was taken as the average value expected from

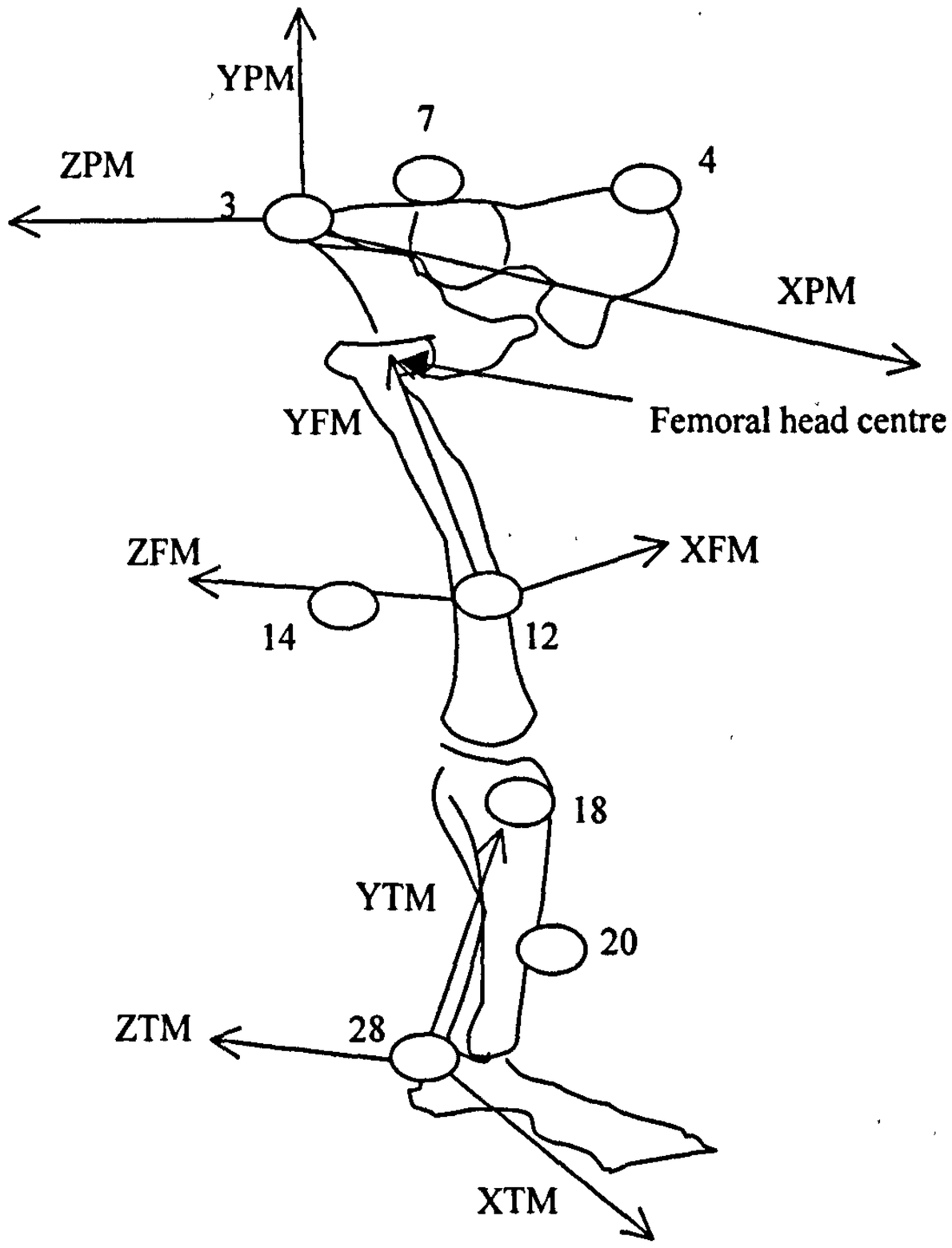

Figure 3.6 Segment moving axes (right leg illustrated). (See Section 3.5.4.2)
(Marker numbers after Figure 3.3)

subjects in this study based on the data of Nisell et al [1985] and Mensch & Amstutz [1975] scaled by the medio-lateral dimension of the tibial condyles. Implicit within the use of this scaling factor was the assumption that Nisell's and Mensch's subjects represented the same population as that of the subjects from this study and that the medio-lateral and anterior-posterior dimensions scaled equally. It was necessary to choose a dimension in the medio-lateral direction as it was not possible to measure accurately anterior-posterior dimensions at the knee.

The definition of dimension 'b' was made based on individual subject's measurements. The aim was to make the YTA axis pass through the mid-medio-lateral aspect of the tibial plateau.

Dimension 'c' used measures of individual subjects to make the YTA axis pass through the mid-medio-lateral aspect of the ankle.

The location of the knee joint centre, KCA, defined by dimension 'd' was used to provide an approximate location of the actual knee joint centre for placement of the shank (tibial) anatomical axes and for definition of joint angles (see Section 3.5.8). This dimension was taken from Ishai [1975] and scaled by the medio-lateral tibial condylar distance assuming that 25mm was the average value for the subjects (97.6mm being the average medio-lateral tibial condylar width). The position of the knee joint centre using this method provided a fixed location. The knee joint centre is in fact not fixed thus this definition was an approximation only, used for convenience to allow joint angle calculation.

The definition of the shank axes used a number of sources for approximation of knee dimensions. The assumption was made that the values taken from the references were suitable to represent the study population. It was also assumed that the knee joints scaled in the same ratio in the medio-lateral and anterio-posterior directions. The shank axes were defined so that the YTA axis coincided with the long axis of the tibia. This was done to ensure that the knee joint centre was above the middle of the tibial plateau.

3.5.4.2 Segment moving axes

The segment moving axes were defined so that they could be derived from marker positions during the activities being studied. During the activities it was not possible to use all of the markers illustrated in Figure 3.3. It was necessary to remove several markers to allow free movement during all activities. Those marked (A) were used only in the static trial and were removed prior to motion analysis. It was, therefore, necessary to use a different set of segment reference axes during the moving trials. These were defined for each segment as follows

The pelvic moving axes set had its origin at the iliac crest marker (see Figure 3.6).

ZMP = right – left iliac crest marker

YMP = perpendicular to the plane containing the mid posterior superior iliac spine marker and those on the right and left iliac crests pointing proximally

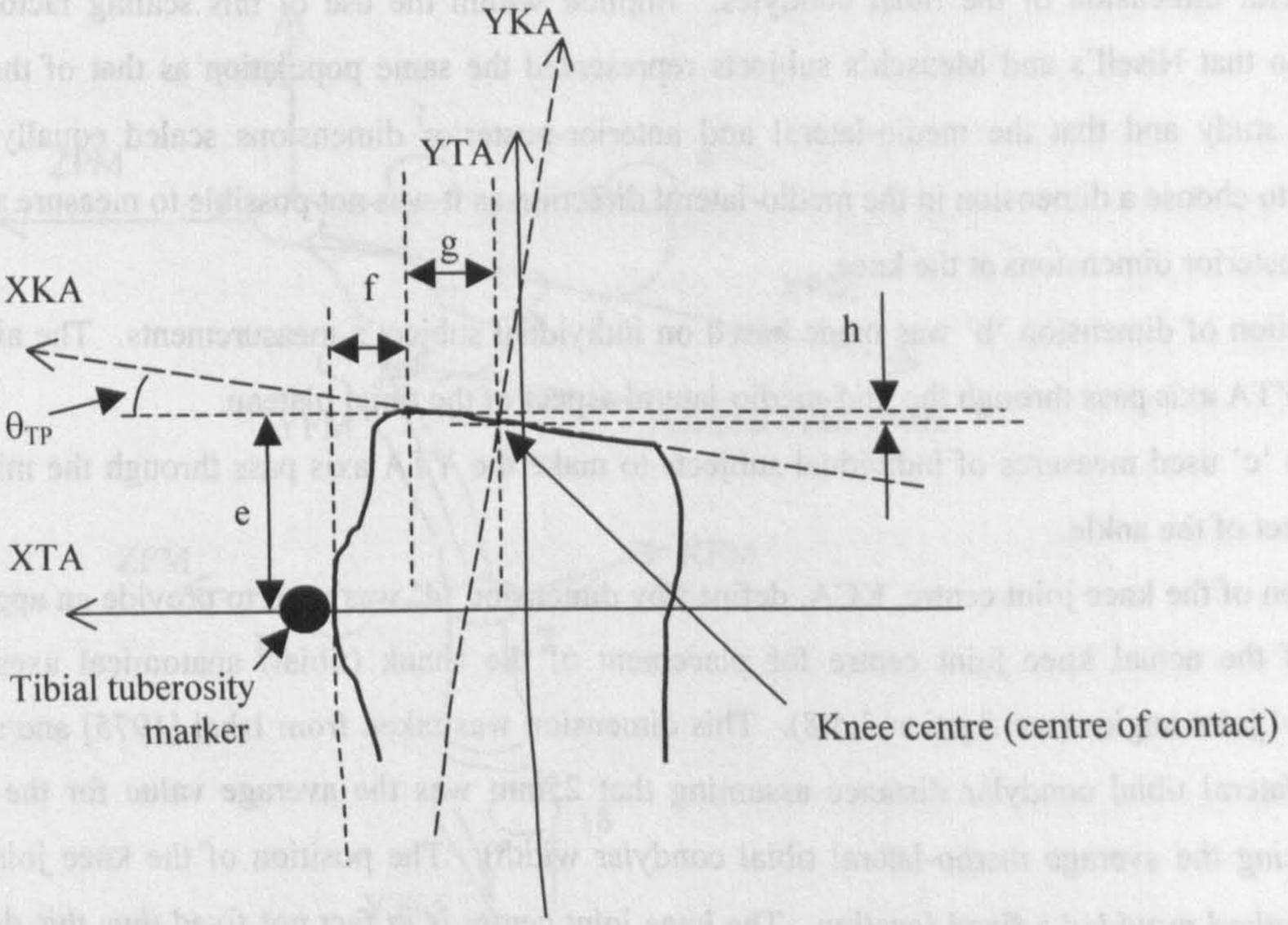

Figure 3.7A Location of the centre of contact of the femur on the tibia in the sagittal plane.
Knee joint anatomical axes. (See text for explanation of symbols and axis labels)

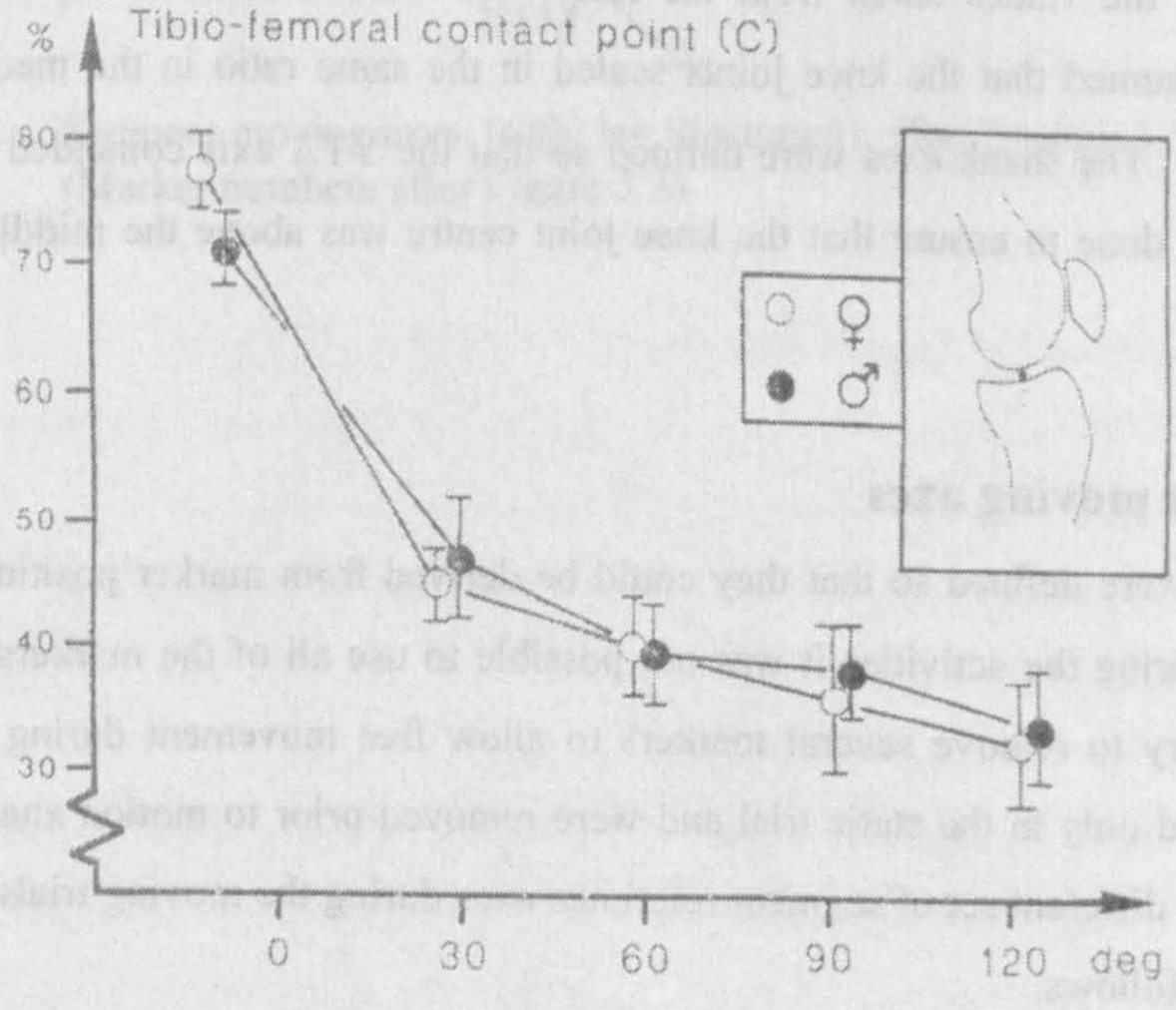

Figure 3.7B Location of the tibio-femoral contact point centre at various knee flexion angles.
From Nisell et al [1985].
95% confidence intervals of the means are indicated. Y-axis shows the displacement in % of the sagittal tibial plateau length. 100% equals the anterior border of the plateau.
(See Figure 3.8 for definition of parameter)

XMP = perpendicular to both ZMP and YMP pointing anteriorly

The femoral moving axes had their origin at the front of mid thigh marker, 12. The hip joint centre and thigh markers were used to define the axes as follows

YFM = femoral head centre (hip joint centre) – front of mid thigh marker 12

XFM = perpendicular to the plane containing the hip joint centre and the lateral and front mid thigh markers (12 and 14)

ZFM = perpendicular to both YFM and XFM

The shank moving axes had their origin at the lateral malleolus marker (28). The tibial tuberosity (18) and medial face of the tibia at mid shank (20) were used to define the axes set.

YTM = tibial tuberosity (marker 18) – lateral malleolus (marker 28)

XTM = perpendicular to the plane containing the tibial tuberosity (18), lateral malleolus (28) and medial face of the tibia at mid shank (20) pointing in an anterior direction

ZTM = perpendicular to the XTM and YTM axes pointing in a medial direction

3.5.4.3 Summary of segment axes definitions

Two sets of axes have been detailed, the anatomical set based on anatomical features and the moving set based on markers that were not necessarily directly located to underlying structures. The relationship between the axes sets was established in a static trial. This allowed the removal of certain markers that would have inhibited motion whilst still allowing the positions of underlying structures to be derived. To allow calculation of muscle origin and insertion locations it was necessary to calculate also the relative location of the segment axes as defined by Brand et al [1982] (see Section 3.5.2.1). It was possible to perform this directly for the femoral and shank co-ordinate systems as the appropriate bony landmarks were identified by markers. It was not possible, however, for the pelvic reference frame. Brand's frame had to be rotated by 9.87 degrees about the commonly defined ZP axis in a negative sense following the right hand convention for positive rotations about axes (after Fitzsimmons [1995] based on dry bone cadaver studies).

Translations between the segment axes sets were defined in three dimensions. These were used to allow conversion of muscle origin and insertion data to different co-ordinate systems and to allow the external forces to be integrated into the leg model.

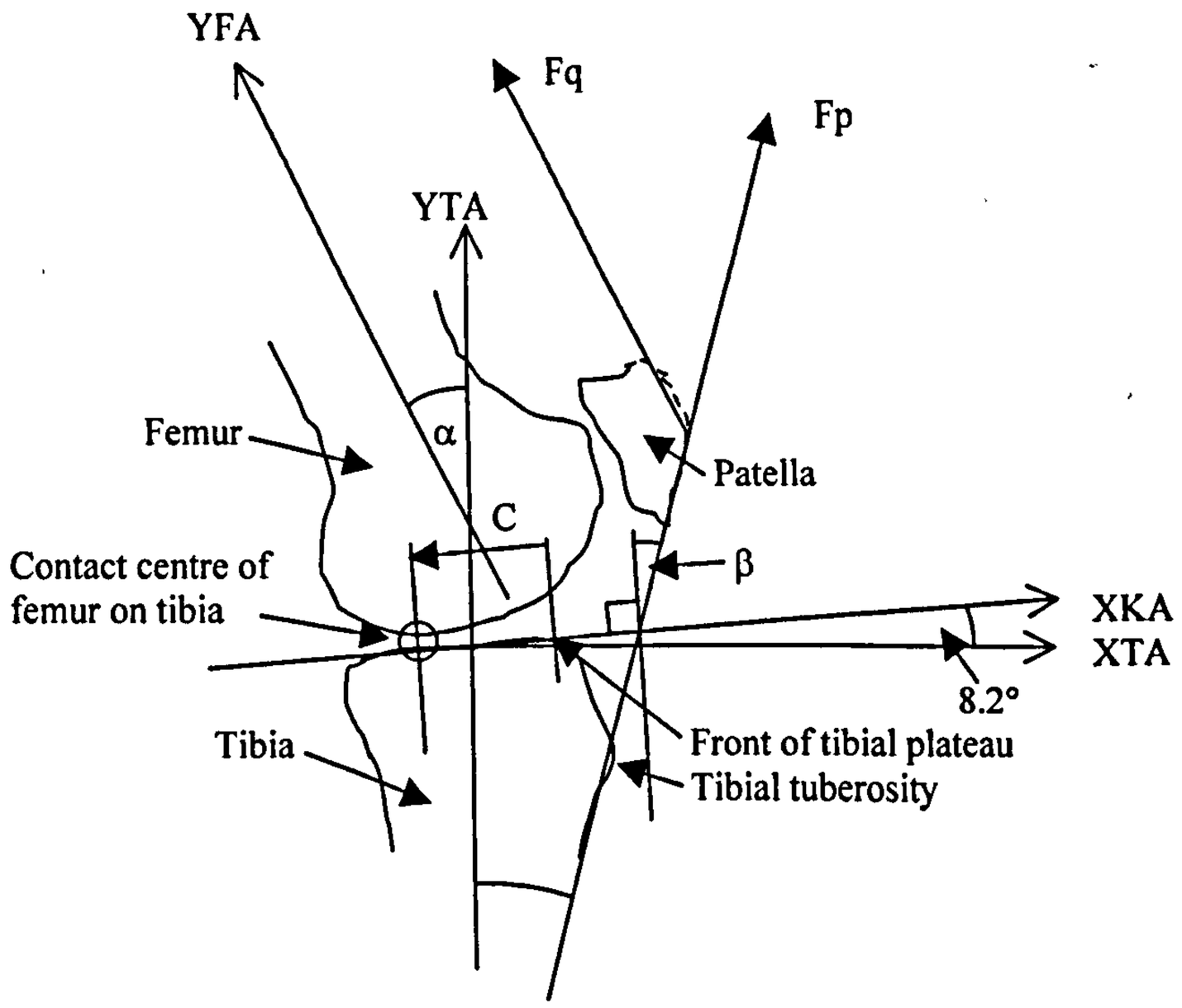

Figure 3.8 Definition of knee joint sagittal plane parameters after Nisell et al [1985].
α = angle between tibial long axis YTA and femoral long axis YFA.
β = angle between patella ligament and tibial plateau (knee anatomical X-axis, XKA).
C = distance along tibial plateau from front of tibial plateau to contact centre.
Fq = Force in quadriceps muscles (patella tendon).
Fp = Force in patella ligament.

3.5.5 Joint models

3.5.5.1 Hip joint

The hip joint was considered to be a ball and socket joint. The activities being studied did not require the use of the extreme range of motion of the hip joint. The joint capsule and ligamentous structures at the hip were, therefore, not included in the model. It is possible that ligament forces at the highest degrees of extension during walking may provide resistance against further extension. For the purposes of this study, however, this action was assumed to be insignificant in comparison with muscle forces. It was assumed that interactions between the rim of the acetabulum and femoral neck did not occur within the range of motion used by the subjects. The forces in the hip joint were considered to act through the centre of the femoral head (hip joint centre). The components of the hip joint force were defined in both femoral anatomical and pelvic anatomical co-ordinate systems.

3.5.5.2 Knee joint

The knee joint does not have a fixed axis of rotation. It must be considered as a joint with a moving axis of rotation, which depends on the angle of joint flexion and rotation for its location. For this thesis the joint was described only from the tibial side with the location of ligamentous and tendinous structures and bony contacts depending on the joint angle of flexion and rotation. A detailed description of the knee model used follows.

To describe the force carrying structures at the knee joint required knowledge of the location of bony contacts as well as soft tissue, such as ligaments, tendons and muscles. The joint contact points at the knee between the tibia and the femur move over the tibial surface during flexion of the knee joint. This movement has been described [Nisell et al, 1985, Dragonich et al, 1987]. Nisell et al examined 10 male and 10 female subjects using X-ray methods. They determined the point at which there was the smallest distance between the femur and tibia in the sagittal plane for a range of joint angles with subjects standing on the leg being examined. Dragonich et al used 6 cadaver specimens and applied a load of 200N through the patellar tendon to simulate joint loading. The point of centre of pressure was defined to be midway between the centre of peak pressure (as measured using pressure sensitive film) and the centre of the contact area. There was general agreement between these two publications with the derived locations being a maximum of 3mm different over the 0 to 90 degree knee flexion range when converted to represent the same average tibial plateau depth. The results of Nisell were chosen to describe the movement of the tibio-femoral contact point in the sagittal plane as they were based on more relevant experimental conditions.

The knee model developed was based on the average dimensions of the tibia as defined by Mensch & Amstutz [1975]. These were calculated as average tibial bony width of 74.9mm and tibial plateau average

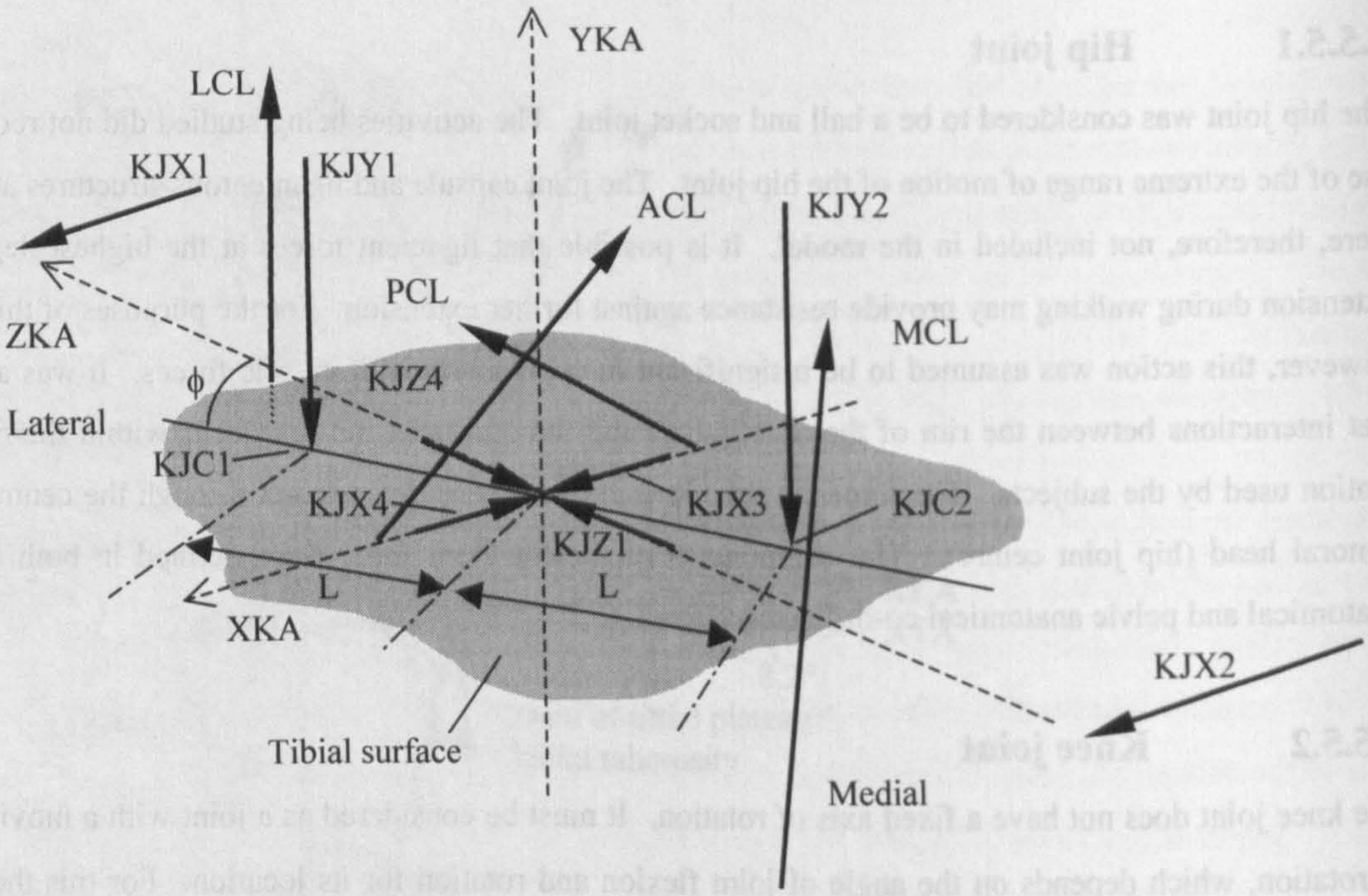

Figure 3.9A Knee joint force bearing structures (muscles not shown). Right knee illustrated.
L = distance to femur contact point on tibia from knee anatomical axes origin
ϕ = knee rotation angle offset (knee rotation angle – static trial knee rotation angle).
ACL, PCL = anterior and posterior cruciate ligaments respectively.
MCL, LCL = medial and lateral collateral ligaments respectively.
KJC1, KJC2 = contact points of femur on tibia.
KJY1, KJY2 = tibio-femoral contact forces.
KJX1, KJX2 = rotation forces (not representative of anatomical structures).
KJX3, KJX4 = supplementary anterior-posterior forces (not representative of anatomical structures).
KJZ1, KJZ4 = medio-lateral forces (not representative of anatomical structures).
(KJZ2, KJZ3 = not used)

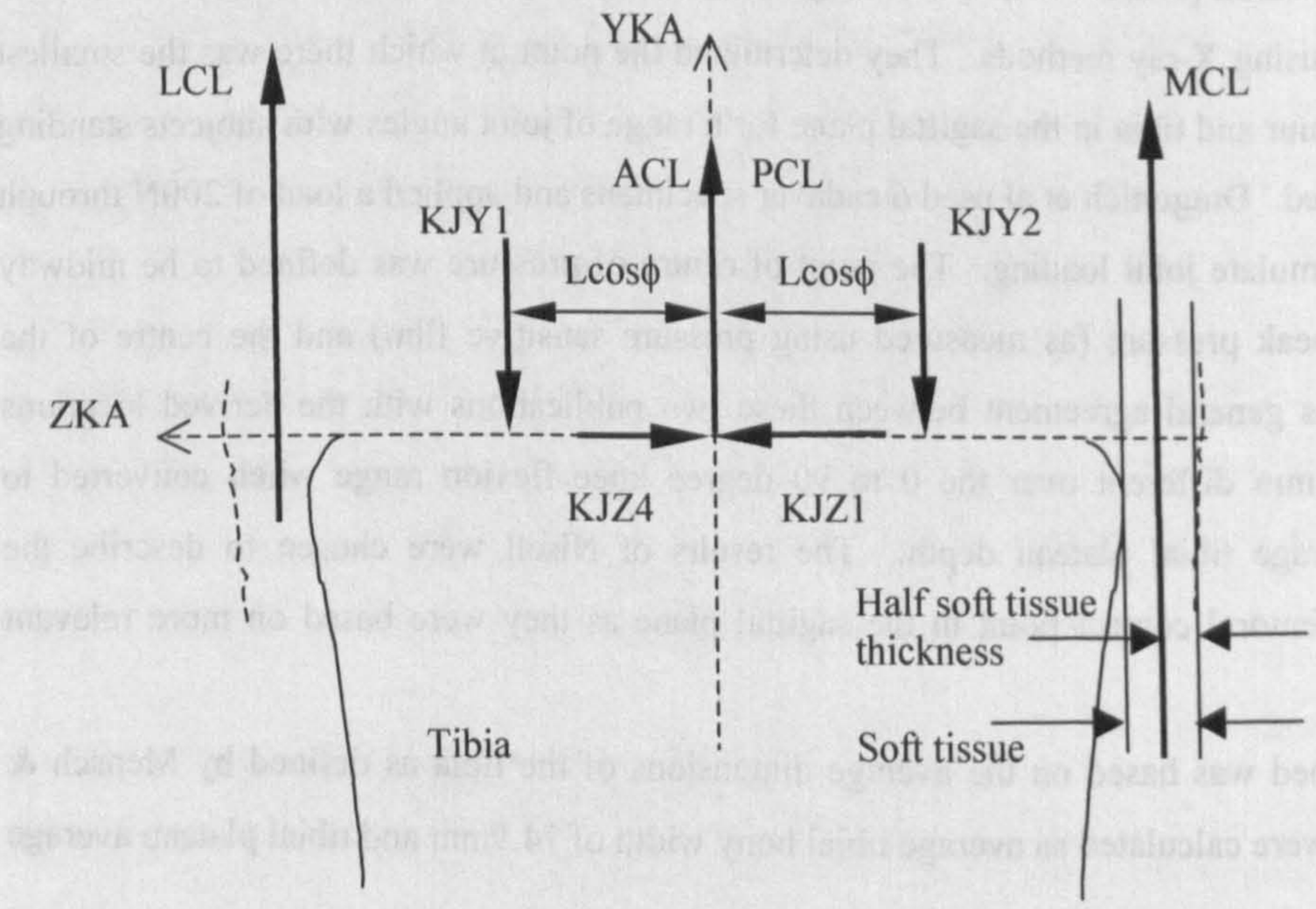

Figure 3.9B Knee joint force bearing structures (muscles not shown) in the plane of YKA and ZKA. Note that the lateral collateral ligament was positioned as the medial collateral ligament at half soft tissue thickness from the tibial condyle border.

depth of 47.1mm. It was assumed that these dimensions were equivalent to the average dimensions of the subjects studied for this thesis. The tibial width measure, which included soft tissue, of 97.6mm, calculated as the average for the subjects of this study, was assumed to correspond to a bony dimension of 74.9mm. This assumption was necessary as there was an unknown thickness of soft tissue included within the tibial width measure. There was soft tissue cover on the tibia that could not be measured, although an average of 11mm of soft tissue on each side of the tibia appeared to be an over estimate. It is possible, therefore, that the use of the average of Mensch's data could have resulted in the model of the tibia being slightly smaller than it actually was. This could have reduced the lever arms of force carrying structures about the 'joint centre', which may have led to higher forces to maintain moment values.

The following description of the knee joint illustrates all dimensions as average values. All dimensions were scaled by the ratio of the subject's actual tibial condylar width (including soft tissue) to that of the average tibial condylar width (including soft tissue). This average value was 97.6mm. I.e. it was assumed that the tibial width dimension as measured externally on the subjects was proportional to both anterior-posterior and medio-lateral dimensions, with the average of the study population being the same as that of all literature sources.

The knee joint model was defined in three-dimensions. A number of elements of the model were, however, defined only in the sagittal plane of the knee. The knee model did not, therefore represent all of the structures at the knee in an anatomically correct way. To minimise the effect of simplifications used a number of 'free' forces were introduced to prevent the distribution of forces being restricted by the shortcomings of the model. Justification of the assumptions is made at appropriate points in the following description of the knee model.

It was assumed that there were two distinct contact points between the femur and the tibia, one on the medial and one on the lateral tibial plateau. It was assumed that these contact points could be represented by point forces acting perpendicular to the tibial plateau. The location of the average contact point in the sagittal plane (containing the YTA and XTA axes) was based on the work of Nisell et al [1985]. This point was used to represent the average position of the medial and lateral contact forces in the XTA direction. The XTA location of the medial and lateral contact points relative to this average point was determined by the rotation of the tibia with respect to the femur. The neutral, or zero rotation position, was taken as that of the static trial. The difference of the angle of rotation at the knee during the dynamic trial to that during the static trial was taken to represent the rotation of the contact points about the average contact location. To define all aspects of the knee model a set of co-ordinates was defined located on the tibial plateau. These axes, the knee anatomical axes, had their origin at the centre of the contact point in the plane of the tibial anatomical Y and X axes. The knee anatomical X axis, XKA, was defined along the tibial plateau as illustrated in Figure 3.7A and the knee anatomical Y axis, YKA, was defined

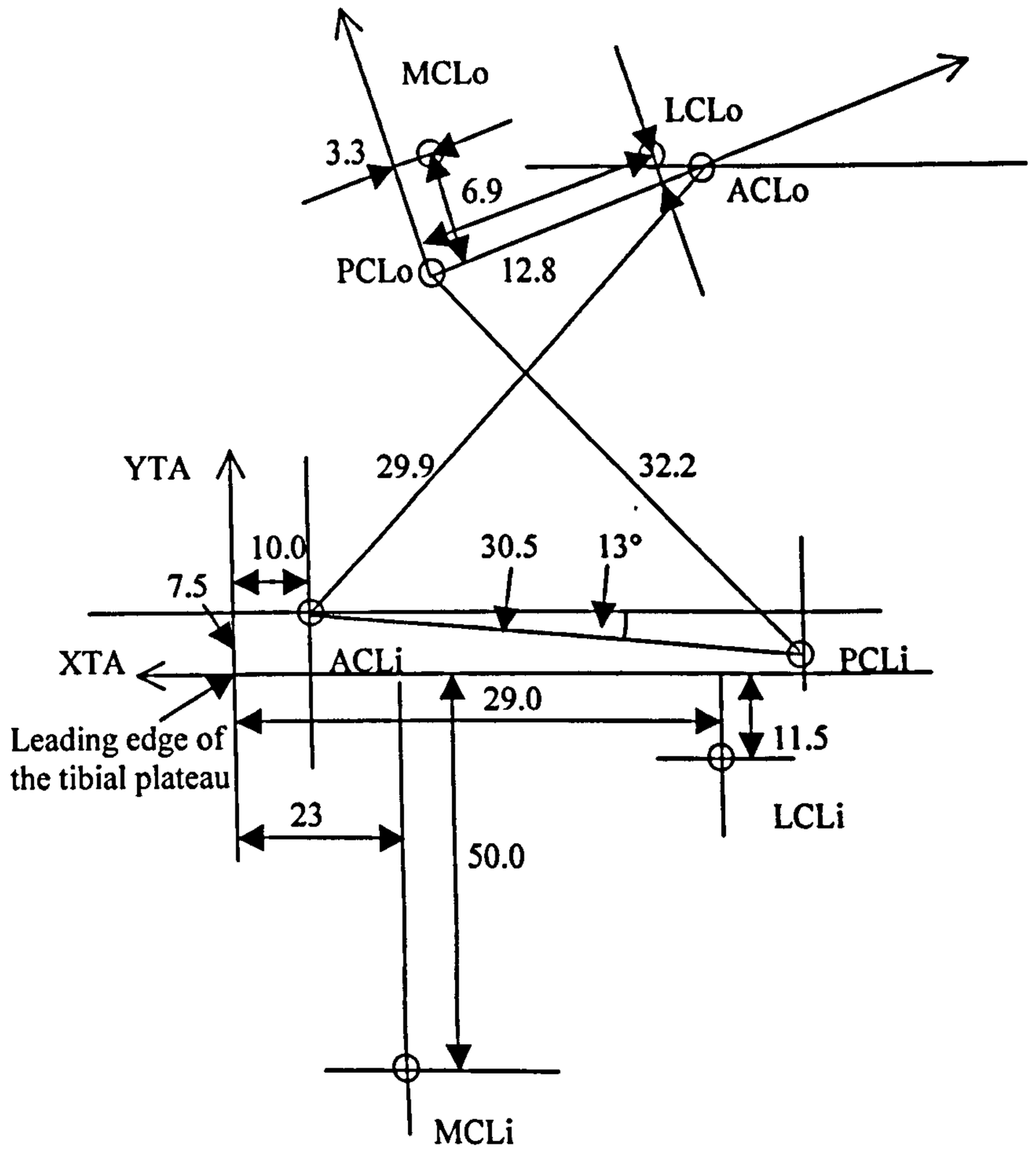

Figure 3.10 Sagittal plane definition of cruciate and collateral ligaments.
(after O'Connor et al [1990]). All measurements in mm. Note that the dimensions in this diagram are for an average tibial plateau depth of 45mm.
ACLo, ACLi = origin and insertion points of the anterior cruciate ligament
PCLo, PCLi = origin and insertion points of the posterior cruciate ligament
MCLo, MCLi = origin and insertion points of the medial collateral ligament
LCLo, LCLi = origin and insertion points of the lateral collateral ligament

perpendicular to the tibial plateau. The axes were used to define the location of all knee force bearing structures. Equilibrium at the knee was specified about these axes.

Figure 3.7A illustrates the dimensions in the sagittal plane that were used to define the centre of contact of the femur on the tibia.

Dimension 'e' was measured on the subjects as the distance in the direction of the long axis of the tibia between the tibial tuberosity and the tibial plateau. 'f' was the average dimension from Nisell et al [1985] of 8.2mm.

'g' and 'h' were related by the angle θ_{TP} (the angle of the tibial plateau to the perpendicular to the long axis of the tibia in the sagittal plane) and defined the location of the centre of femur contact on the tibia. The angle θ_{TP} was taken as the average of male (9.2°) and female (7.2°) values from Nisell et al [1985] as 8.2°. The average of Nisell's male and female contact centres on the tibia was calculated and used to define the sagittal plane location of the point of contact for this study. The calculation of the contact point location was based on an average tibial plateau depth of 47.1mm. Nisell's data (see Figure 3.7B) was interpolated based on a hand fitted smooth curve between recorded points to allow location of the contact centre over the range of flexion angles from -10° to 120°. The values of 'g' are presented in Appendix III. Nisell's data was not continuous, but recorded at discrete intervals of knee flexion. Thus implicit within the use of interpolation is the assumption that the trends in data were consistent between each of the recorded points. This assumption is based on the observation that all recorded points did appear to follow a consistent trend. It is possible, however, that there were deviations from the observed trend. It was not possible to take this fact into account. Nisell's data was interpreted as a representation of a consistent trend. Figure 3.8 illustrates further parameters used to define the knee model. Note that the length 'C' was the distance along the tibial plateau, as compared to 'g' and 'h', which were defined along and perpendicular to the long axis of the tibia.

The locations of the two femoral contact points on the tibia were defined as being at equal distances from the mid-line of the tibial plateau. This distance ('L' in Figure 3.9A) was set based on an illustration in Dragonich et al [1987] at 20mm for the average model with tibial plateau width of 74.1mm. The results of Dragonich were consistent with those of Nisell in terms of the placement of the contact point between femur and tibia in the sagittal plane. The use of the medio-lateral placement as defined by Dragonich was, therefore, considered to be reasonable. Dragonich's results were, however, based on cadaver specimens with very basic loading conditions. To take into account the effects of knee joint rotation on the location of the contact points it was necessary to modify the joint contact locations. Figure 3.9A illustrates the use of the knee rotation angle to provide an offset. The angle of offset was defined as the difference between the static trial rotation angle and that of the instant at which the limb was observed. The static trial value of knee rotation was used to reduce the effect of any misalignment of the segment axes systems.

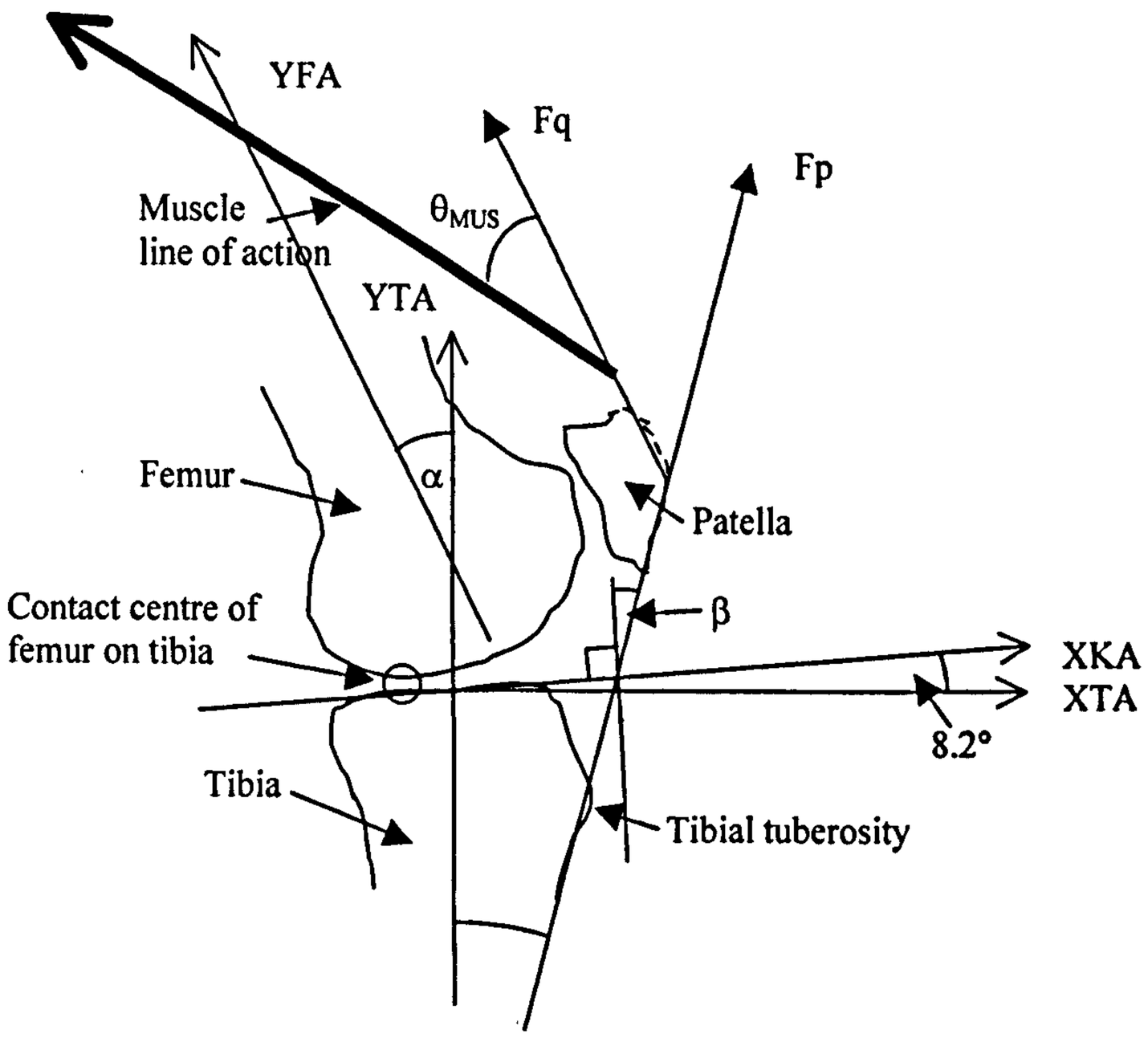

Figure 3.11 The patella mechanism [Nisell et al, 1985].
α = angle between tibial long axis YTA (tibial anatomical axis set) and femoral long axis YFA (femoral anatomical axis set).
β = angle between patella ligament and tibial plateau (knee anatomical X-axis, XKA).
Fq = Force in quadriceps muscles (patella tendon).
Fp = Force in patella ligament.
θ_{MUS} = angle of muscle to femoral long axis (YFA)

The model included the medial and lateral collateral ligaments and the anterior and posterior cruciate ligaments. These ligaments were represented by one linear element defined in the sagittal plane of the knee anatomical axes (Figure 3.9B). This representation did not take into account the action of the ligaments in the other planes or the fact that the ligaments were composed of many fibres. The locations of ligament origins and insertions were taken from O'Connor et al [1990] and are illustrated in Figure 3.10 for a standard tibial plateau depth of 45mm. To ensure that dimensions were compatible with the work of Nisell an average tibial plateau depth of 47.1mm was used for this study. O'Connor et al's data was, therefore scaled appropriately. The anterior and posterior cruciate ligaments were defined to act in the plane of the YKA and XKA axes and to have their origins and insertions in this plane. The medial and lateral collateral ligaments were defined to act in the plane of the YKA and XKA axes but to have their origins and insertions in a plane located at half the soft tissue thickness either side of the bony tibial condyles (Figure 3.9B). The orientation of the ligaments was, therefore, idealised and assumed to be in the sagittal plane. To overcome these simplifications in a manner that would have made the model significantly more accurate would have required the treatment of the ligaments as multi-elemented and to act out of the sagittal plane of the knee joint. The model was intentionally kept simple to reduce the solution complexity (and thus computing time) whilst ensuring that all major force carrying structures were modelled. Due to the simplifications used in the knee model it was necessary to introduce several other forces to ensure that realistic forces in the muscles and joints resulted.

The solution method chosen incorporated force and moment balances at the knee. It was, therefore, necessary to ensure that there were elements of force in all directions and about all axes to provide equilibrium at the knee joint. To prevent unrealistic loading of the 'real' structures which were include in the model a set of extra forces was introduced which represented all other force bearing structures at the knee. These elements are illustrated in Figure 3.9A. The equilibrium of forces in each of the directions and of moments about each of the knee anatomical axes was considered as follows.

YKA forces

KJY1 and KJY2 were considered to be the main contributors to force equilibrium in the YKA direction. These forces would have countered muscle forces and any forces in the collateral and cruciate ligaments and patellar ligament. There would not have been any other soft tissue structures that would have been able to provide YKA forces of comparable magnitude to the modelled structures. Therefore no additional forces in this direction were included.

ZKA forces

Resistance to medio-lateral force at the knee could have arisen due to the interaction between the tibia and femur. The femoral condyles rest in depressions on the surface of the tibia and are separated by the

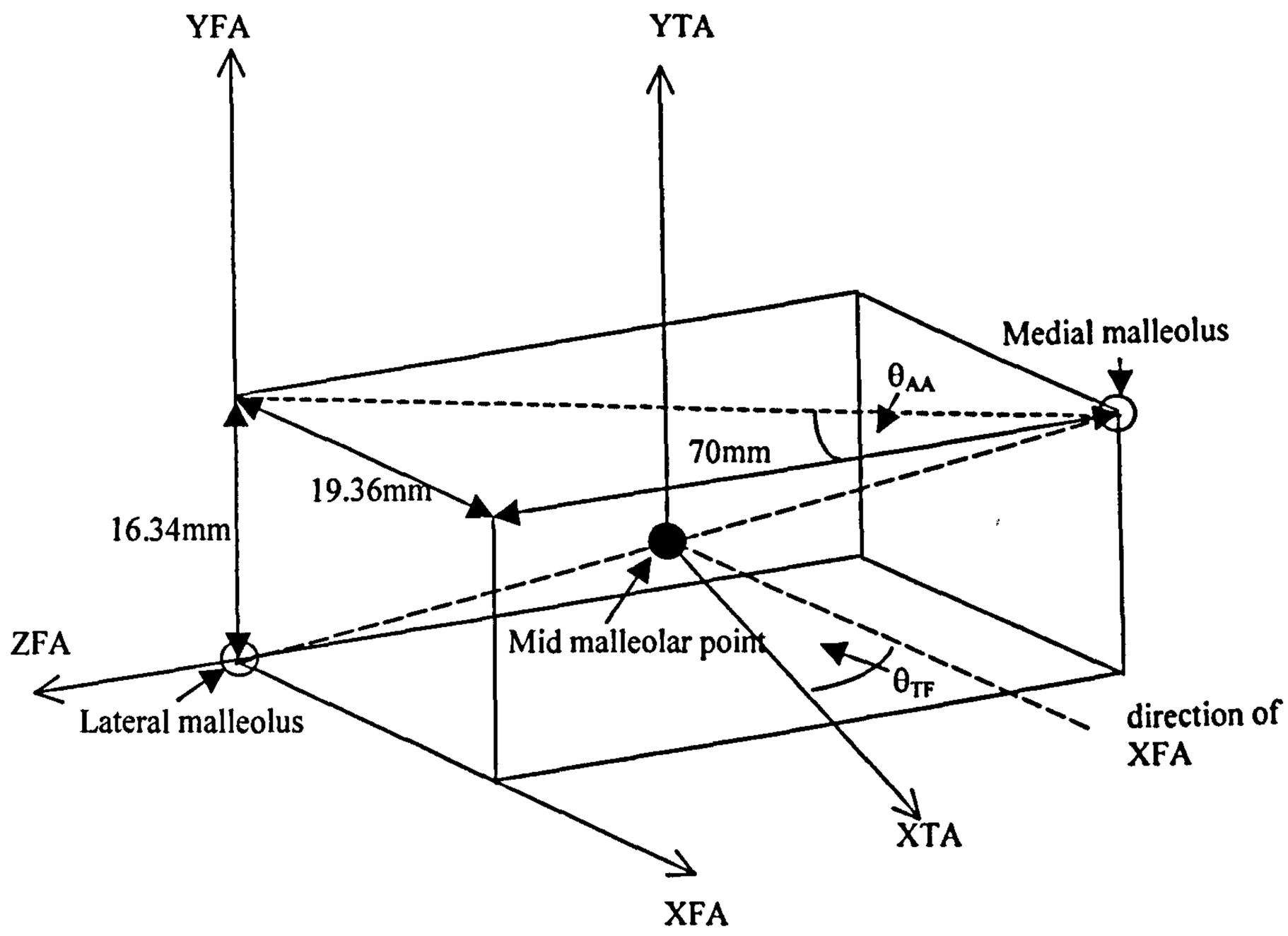

Figure 3.12 Foot anatomical axes defined relative to tibial anatomical axes.
Dimensions shown for average ankle of 74mm malleolar width (including 2mm soft tissue both sides)
θ_{AA} = 15.5° for all ankles.
θ_{TF} = angle between the tibial anatomical X-axis (XTA) and foot anatomical X-axis (XFA)

intercondylar eminence. Intersegmental medio-lateral force would have been resisted by reactions of the femoral condyles against the raised parts of the tibial plateau. To allow for this effect a pair of forces was specified, KJZ1 and KJZ4, which would provide a means of balancing these forces. They were specified as acting through the knee anatomical axes origin.

XKA forces

The main force balancing structures in the XKA direction were the cruciate ligaments, with a small contribution from the collateral ligaments. Preliminary examination of results with only these structures indicated that the cruciate ligaments developed unrealistically high forces. To overcome this KJX3 and KJX4 were introduced. It is possible that the requirement for these forces to ensure realistic solutions in the cruciates indicated that the soft tissues at the knee joint were providing a significant contribution to equilibrium in the XKA direction. The joint capsule and interaction of internal knee joint soft tissue with the joint capsule could have given rise to these forces.

XKA moments

No supplementary forces were required about the XKA axis as the contact forces between femur and tibia and collateral ligaments would have provided a more significant effect than any other soft tissues.

ZKA moments

Equilibrium about the ZKA axis was primarily satisfied by muscle forces. A small contribution from the rotated contact forces would also have been present. No other effects were considered significant, therefore no additional forces were specified.

YKA moments

As discussed for ZKA force balance it was necessary to introduce forces to counter the reaction against rotations by the femoral condyles on the tibial eminence. In a moment sense this required forces with lever arms about the knee anatomical joint axes origin. These were provided by KJX1 and KJX2. These forces were not allowed to contribute to force equilibrium in the XKA direction and, therefore acted only as a moment balance.

3.5.5.2.1 Patella mechanism

The effect of the quadriceps muscles on knee joint equilibrium was taken into account via the patella mechanism. For this thesis the effect of the patella mechanism was incorporated by modification of the force in the patella ligament based on ratios of muscle force and angles reported by Nisell et al [1985]. Movement of the patella itself was not incorporated as the knee model included equilibrium at the level of the tibial plateau only. Nisell provided information on the ratio of the forces in the patella tendon (Fq) to

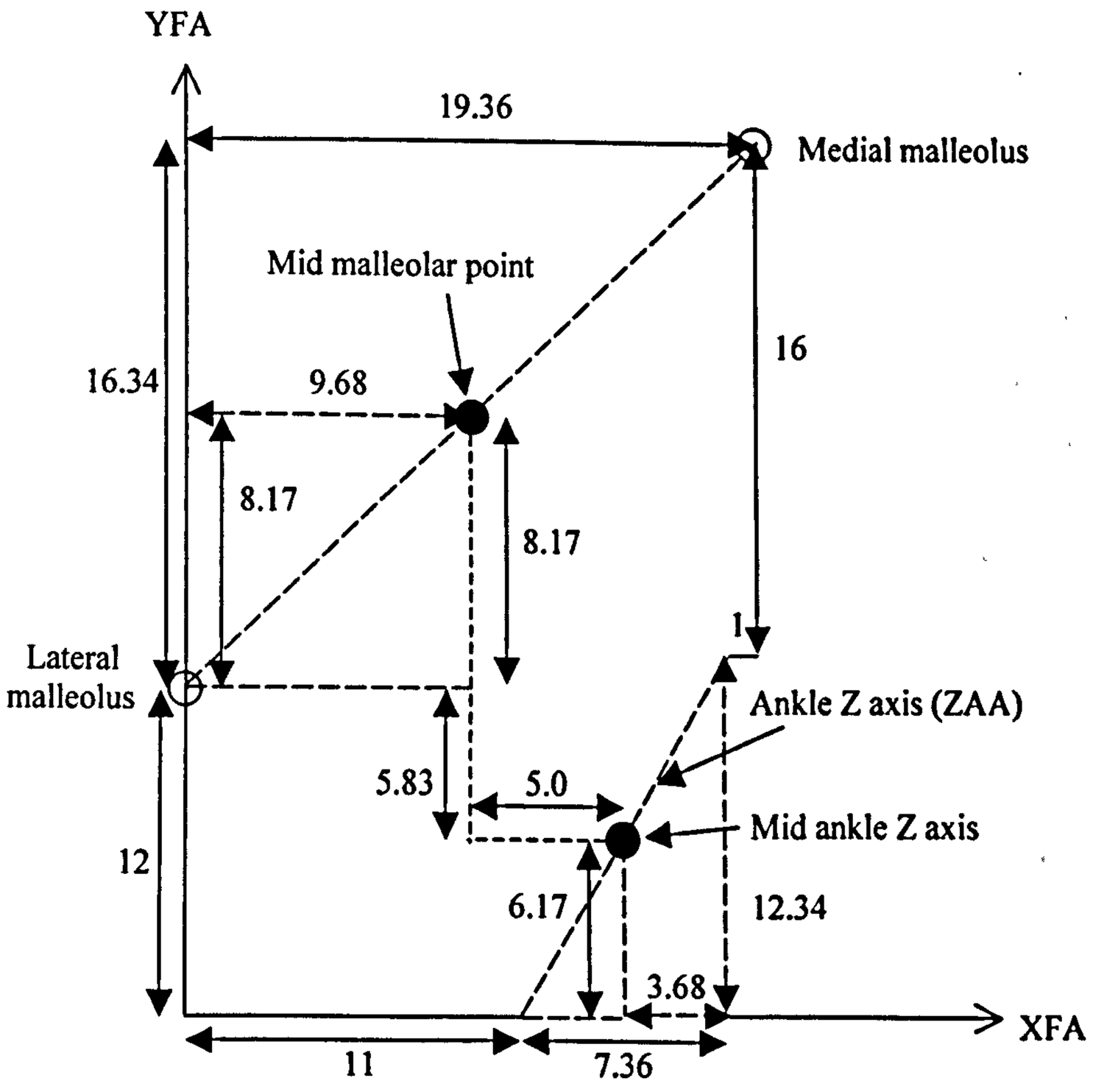

Figure 3.13 Location of the ankle centre in the foot anatomical co-ordinate system's sagittal plane (containing XFA and YFA). (modified from Isman & Inman [1968])

that of the patella ligament (Fp). The ratio Fp/Fq was specified. The average of Nisell's data is reported in Appendix III. These data were extended to cover the full range of –20° to 120° of knee flexion (see Appendix III). Figure 3.11 illustrates the patella mechanism. The contribution of the quadriceps muscles (vasti and rectus femoris) to the patella ligament force was calculated using two factors.

First the force was multiplied by the cosine of the angle θ_{MUS} between the muscle's line of action and the femoral long axis in the plane of the YFA and the XFA axes. The result of this was the component of the muscle force in the direction of Fq specified by Nisell. The force was then multiplied by the ratio Fp/Fq for the appropriate knee flexion angle. The resulting force was that transmitted to the patella ligament and thus to the tibial tuberosity. The angle of the patella ligament to the tibial plateau (i.e. the XKA axis) was taken from Nisell as the angle β (tabulated in Appendix III). The patella ligament was assumed to act in the sagittal plane of the knee anatomical axes, i.e. in the plane of the XKA and YKA axes.

The following formulation was used to calculate the effective lever arm of the quadriceps muscles at the knee:

$$\text{Effective lever arm of quadriceps muscle at knee} = L_{PL} \times \frac{F_P}{F_Q} \times \cos\theta_{MUS}$$

Where :

L_{PL} = lever arm of the patella ligament at the knee

$\frac{F_P}{F_Q}$ = ratio of the force in the patella ligament to that in the patella tendon

θ_{MUS} = angle between the muscle's line of action and the femoral long axis

3.5.5.2.1 Summary of the knee joint model

Force bearing structures in the knee joint model consisted of:

-Two contacts between femur and tibia.

-Medial and lateral collateral ligaments.

-Anterior and posterior cruciate ligaments.

-Patella ligament.

-Two XKA forces to provide 'soft tissue' force balance in the XKA axis direction.

-Two ZKA forces to provide 'soft tissue' force balance in the ZKA axis direction.

-Two XKA forces to provide 'soft tissue' moment balance about the YKA axis.

The model was based on a number of literature sources. It was assumed that the parameters recorded in the literature were compatible, i.e. that they could be combined based on scaling given dimensions to the

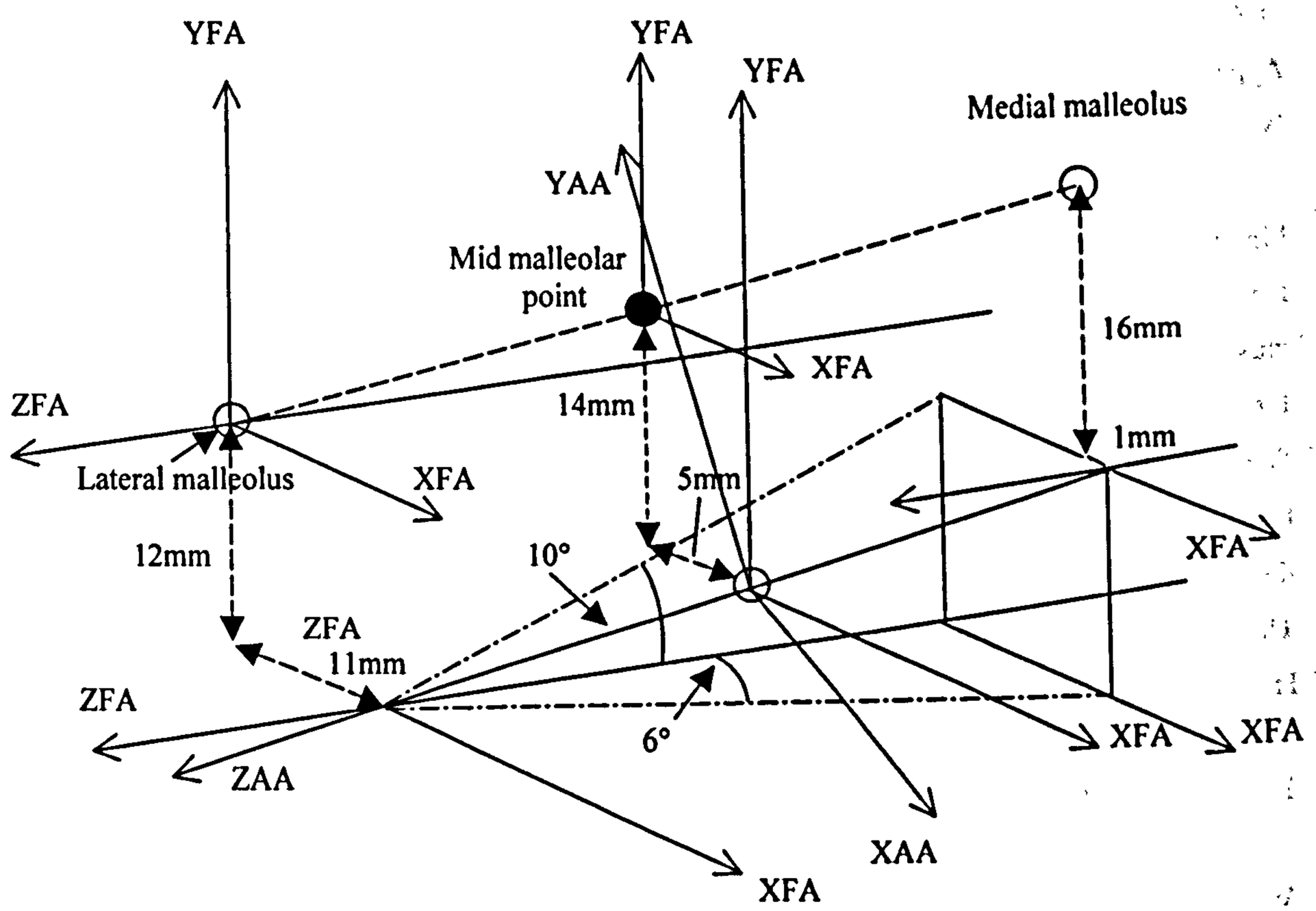

Figure 3.14 Ankle anatomical axes definitions relative to foot anatomical axes (after Isman & Inman [1968]). Note YAA in the plane of ZAA and YFA. Dimensions shown for average ankle joint.

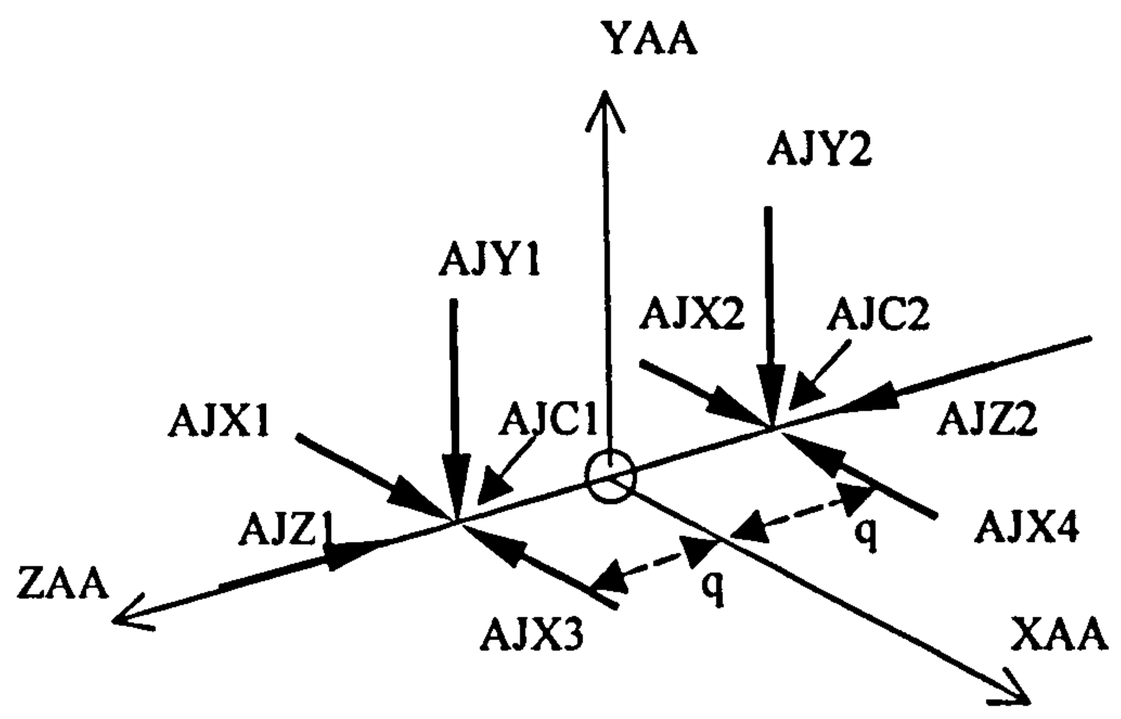

Figure 3.15 Ankle joint forces.
q = distance to the ankle joint force centres from the ankle anatomical centre along the ZAA axis. (10mm for the average ankle model (after Proctor & Paul [1982])).
AJC1, AJC2 = Ankle joint force centres.
AJY1, AJY2 = ankle joint forces in the YAA direction
AJX1, AJX2, AJX3, AJX4 = ankle joint forces in the XAA direction
AJZ1, AJZ2 = ankle joint forces in the ZAA direction

average model used. It was assumed that all the subjects studied for this thesis had tibial dimensions in equal ratios to their tibial condylar width measures.

The knee model was by necessity a compromise between simplicity and the need to include all significant force bearing structures. The knee model provided means for force and moment balance in all dimensions.

3.5.5.3 Ankle joint

The ankle joint was modelled as a single axis hinge joint. The talocrural joint was modelled to allow the inclusion of the main component of dorsiflexion / plantarflexion equilibrium in the model. The talocalcaneonavicular joint was not modelled. To specify the location of the talocrural ankle joint two sets of axes were defined. First the foot anatomical axes were defined in relation to the tibial anatomical axes, then the ankle anatomical axes were defined relative to the foot anatomical axes.

The foot anatomical axes were defined from the tibial anatomical axes (Figure 3.12). The foot anatomical Y axis (YFA) was aligned with the tibial anatomical Y axis (YTA). The foot anatomical X and Z axes were defined relative to the inter-malleoli line by the data of Isman & Inman [1968]. Figure 3.12 illustrates the angle θ_{AA} , defined using the data of Isman (Figure 3.13) and an assumed inter-malleoli distance of 74mm (including 2mm of soft tissue on each malleolus). Isman did not record a malleolar width measure. This inter-malleoli distance was the average of the measurements of the subjects studied for this thesis. It was assumed that the data of Isman represented an individual of the same dimensions as the average of those studied for this thesis. The angle θ_{AA} was calculated as 15.5°. The foot anatomical axes were defined in such a way as to ensure that the angle was maintained at this value.

The ankle anatomical axes were defined based on dimensions and orientations from Isman & Inman, [1968]. Using the angles of alignment and the assumed average malleolar width it was possible to calculate the position of the mid-point of the ankle Z-axis as illustrated in Figure 3.13. This mid point was designated as the origin of the ankle anatomical axes, with the ankle anatomical Z axis as defined by Isman and the ankle anatomical Y axis (YAA) in the plane of ZAA and YFA with the ankle X axis (XAA) perpendicular to the two (Figure 3.14).

3.5.5.3.1 Ankle joint forces

The forces at the modelled talocrural joint (see Figure 3.15) were specified to provide means of opposing all forces and moments except rotation moment about the ZAA axis. I.e. the balance of moments about the ZAA axis was achieved using muscle forces only and not joint forces. AJZ1 and AJZ2 provided reaction against forces along the ZAA axis equivalent to the action of the lateral and medial malleoli in restraining the talus. AJX1 to AJX4 provided reactions against twisting actions about the YAA axis or forces along the XAA axis. AJY1 and AJY2 provided compressive joint forces. These forces were

located at two points equidistant from the ankle anatomical axis origin. The distance 'q' was defined after Proctor & Paul [1982] as 10mm, but scaled by the malleoli width of the subject compared to the mean value of all the subjects (i.e. 74mm).

The joint force at the ankle is spread over an area of contact as illustrated by Calhoun et al [1994] and Kimizuka et al [1980] using pressure sensitive film. It was not possible to model a distributed force without considerably increasing the complexity of the model. The forces used allowed a range of force combinations that effectively allowed the centre of joint force to move between the two joint 'contact' points, approximately the range illustrated by both Calhoun and Kimizuka.

No ligamentous structures were modelled at the ankle joint as it was assumed that the forces in them would not be significant as compared to the bony contact forces and muscle forces.

3.5.5.3.2 Summary of the ankle joint model

The ankle joint model was modelled only at the level of the talocrural joint. Joint forces were idealised to act at two points equidistant from the ankle anatomical Z axis mid point. No joint forces were specified to provide moment about the ZAA axis. The following joint forces were used:

-Two joint forces acted along the ZAA axis modelling the restraining effect of the malleoli.

-Four joint forces acted in the XAA direction modelling aspects of contact between the tibia and talus.

-Two joint forces acted in the YAA direction modelling the main components of the ankle joint force.

The ankle joint anatomical axes were located based on the work of Isman & Inman [1968]. It was assumed that all data could be applied to the same average model, which was scaled to the individual based on their malleolar width.

3.5.6 Muscle lines of action and lever arms

Forces in the muscles and ligaments and joint forces had the effect of both linear force and moment about the joints. To incorporate these two effects into the model it was necessary to know not only the origin and insertion points of the muscles but also the line of action of the muscle. A number of muscles, especially at the hip joint, would not have followed the direct path from their bony origin to insertion. Although Brand's data incorporated some degree of compensation for this fact by using effective origins and insertions, it was still possible that during the activities performed, the direct line from Brand's origin to insertion would have passed through underlying structures. Muscle wrapping procedures of Fitzsimmons [1995] were adopted to reduce the inaccuracies that would have arisen from the use of the direct line between origin and insertion. These procedures were applied to the following muscles at the hip joint: Gluteus maximus, Iliacus, Psoas, Rectus femoris, Obturator internus, Piriformis, Gluteus minimus (lower part), Gemelli.

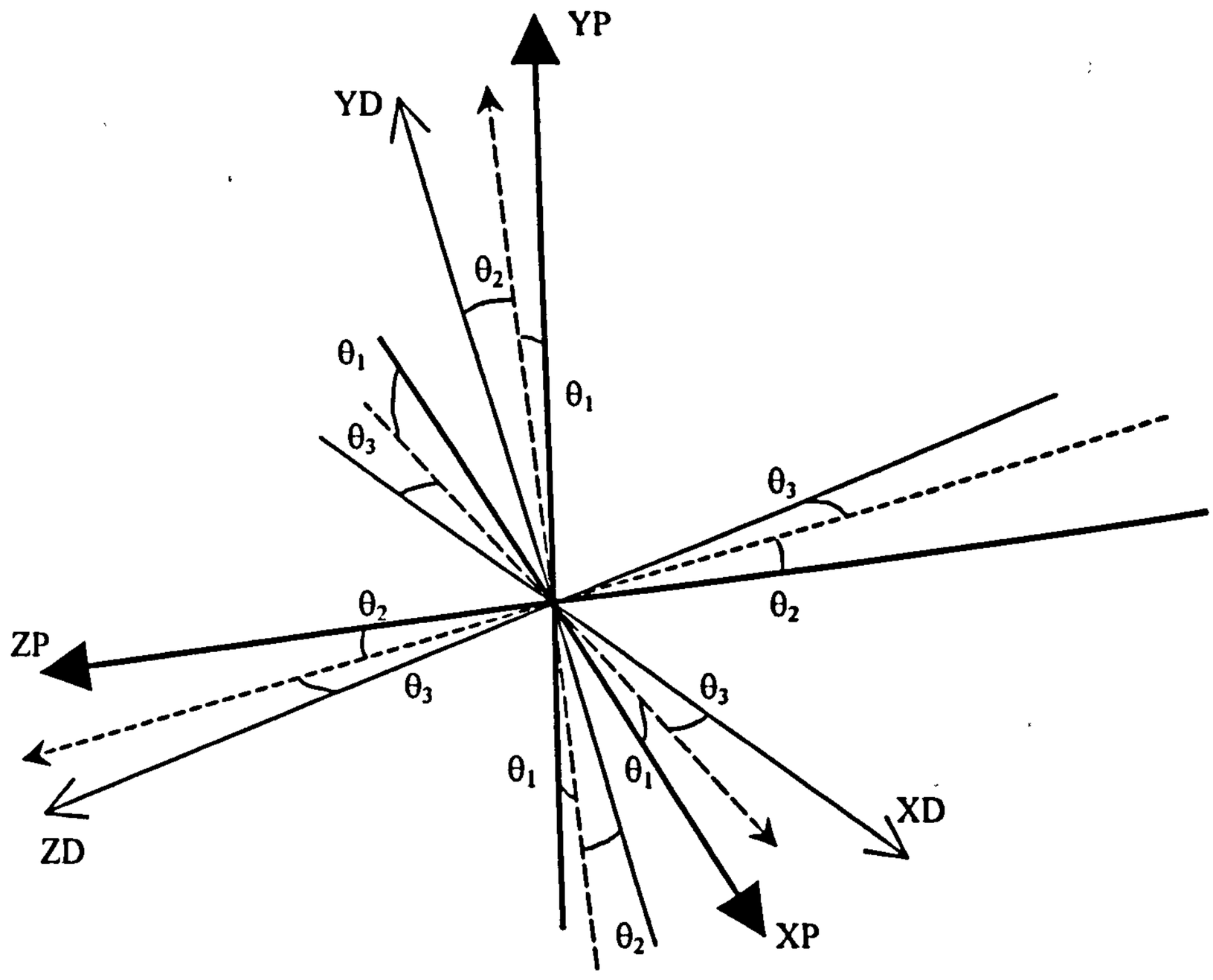

Figure 3.16 Joint angle definitions. Ordered sequence of rotations: θ_1, θ_2, θ_3.
θ_1= flexion/extension angle
θ_2= adduction/abduction angle
θ_3= internal/external rotation angle
XP, YP, ZP = proximal segment axes
XD, YD, ZD = distal segment axes

A full description of the procedures used can be found in Fitzsimmons [1995]. A brief summary is included here.

The obturator internus, piriformis, gemelli and the lower part of the gluteus minimus were observed to interact with the posterior surface of the hip joint beyond approximately 20° of internal rotation. A spherical hip joint of radius 25mm was assumed and the muscles assigned an appropriate effective origin or insertion if the straight line from origin to insertion passed within this sphere.

The lower two elements of the gluteus maximus muscle were found to deviate from their straight paths beyond a certain angle of hip flexion. The lowest element of the gluteus maximus (gluteus max 3) interacted with the ischial tuberosity or the pelvic region between the ischial tuberosity and the hip joint centre during hip flexion. The pelvic region concerned was modelled as a 20mm diameter cylinder, the long axis running between the ischial tuberosity and the hip joint centre. The muscle element was wrapped around this cylinder where appropriate.

The middle element of the gluteus maximus (gluteus max 2) interacted with the underlying lateral rotator muscles beyond 45° of hip flexion. The primary interaction was observed to be with the gemellus inferior. The element of gluteus maximus was wrapped around the gemellus inferior with a clearance of the sum of half the thickness of each muscle (taken to be 10mm).

The highest element of the gluteus maximus (gluteus maximus 1) was found to insert deep to the gluteus medius. To adjust this a total thickness of 9mm was assumed to separate the two muscles, with the gluteus maximus insertion lying outside that of the gluteus medius.

The iliacus and psoas were observed to interact with the front of the hip joint during hip flexion. This was adjusted for with suitable effective origins and insertions being defined.

After wrapping, all muscles were then defined by an effective origin and insertion. These points were then used to describe the muscle's line of action, with the assumption that the line of action was along the line joining the effective origin and insertion. The effective origin and insertion points were calculated in the appropriate joint co-ordinate system so that the lever arm of each muscle could be calculated about the joint axes.

3.5.7 Muscle physiological cross sectional area

Each muscle specified in the model was of a certain size. Its size determined to a certain extent its capacity for supporting load. It was, therefore, necessary to incorporate a means of describing the relative ability of a muscle to support load. This was achieved by incorporating the physiological cross sectional area of each muscle into the model. The data of Freiderich & Brand [1990] were used in this study and are reproduced in Appendix IV. This data was based on a 37 year old, 183cm, 91 kg male subject. The values of physiological cross sectional area calculated as the ratio of the muscle volume to the muscle

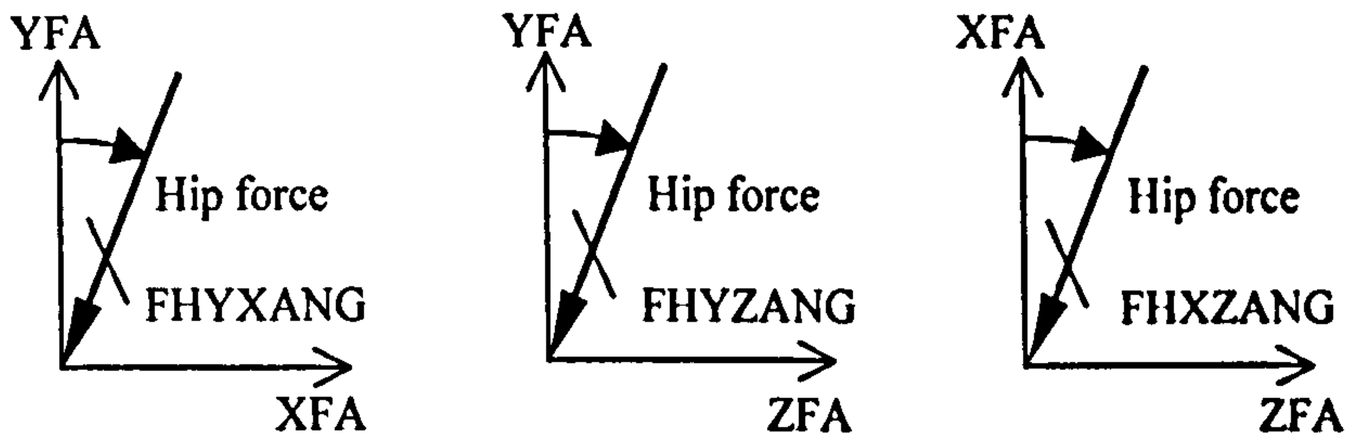

Figure 3.17A Definition of the angles between the resultant force on the femoral head and the femoral anatomical axes.
FHYXANG = angle between the resultant hip joint force and the YFA axis in the plane of the YFA and XFA axes
FHYZANG = angle between the resultant hip joint force and the YFA axis in the plane of the YFA and ZFA axes
FHXZANG = angle between the resultant hip joint force and the XFA axis in the plane of the XFA and ZFA axes

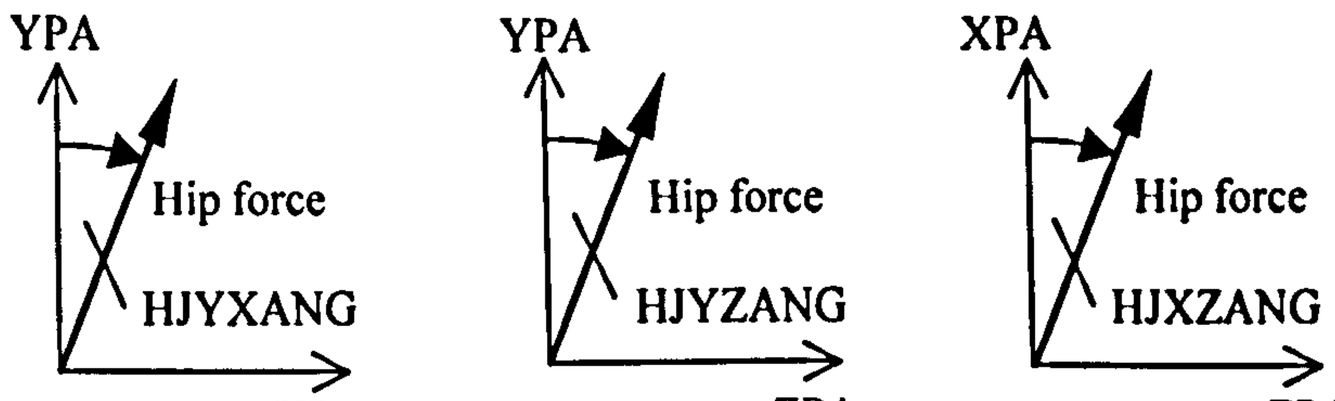

Figure 3.17B Definition of the angles between the resultant force on the acetabulum and the pelvic anatomical axes.
HJYXANG = angle between the resultant hip joint force and the YPA axis in the plane of the YPA and XPA axes
HJYZANG = angle between the resultant hip joint force and the YPA axis in the plane of the YPA and ZPA axes
HJXZANG = angle between the resultant hip joint force and the XPA axis in the plane of the XPA and ZPA axes

fibre length were used in this thesis to indicate the relative capability of muscles to support load. They were not scaled to the individual being modelled. It was assumed that all individuals had the same distribution of muscular tissue in the lower limb as those of the individual studied by Friederich. It was necessary to make this assumption as no scaling factors were presented by Freiderich and no alternative literature references were available.

3.5.8 Joint angles

The calculation of joint angles was performed to allow the knee joint model to be fully described and to provide general information on the orientation of the segments. An implementation of the Cardan angle method was used after Grood & Suntay [1983]. This involved the calculation of joint angles as an ordered set of rotations which allowed the proximal axes set to be rotated to the orientation of the distal set (see Figure 3.16). Although this method of calculation did not provide information of individual joint angles that could be easily related to the change between axes sets (all three angles of rotation at a joint having to be considered at once) it did provide a description of the joint angles in three dimensions. The method was implemented by applying rotations about axes as follows:

Flexion/extension about the proximal segment's Z-axis.

Adduction/abduction about the rotated proximal segment's X-axis.

Internal/external rotation about the distal segment's Y-axis.

To calculate the angles a rotation matrix was established, which represented the transformation from the proximal co-ordinate system to the distal system. This rotation matrix was equated with that which represented the three ordered rotations as above. Comparison of elements in the matrix allowed the derivation of the three angles of flexion/extension, adduction/abduction and internal/external rotation.

Joint angles were calculated at the hip and knee based on the pelvic, thigh and shank anatomical axes systems.

3.5.9 Resultant hip joint force orientation

The inclination of the hip joint force to the pelvic anatomical axes and femoral anatomical axes was calculated and described by three angles in each case. These are illustrated in Figures 3.17A and B. The angles used provide a three dimensional description of the resultant hip joint force orientation in the two co-ordinate systems.

3.5.10 Implementation for the left side

All methods were implemented for the right side. Left limb data was reflected so that it could be treated as right limb data.

3.5.11 Summary of limb model

The limb model was described in relation to palpable bony landmarks

The model included the pelvic, thigh and shank segments. The foot was not included explicitly. Muscles of all joints were included giving a total of 47 muscle elements. Muscle physiological cross-sectional area was incorporated.

The hip, knee and ankle joints were modelled as contact between the pelvis and femur, femur and tibia and tibia and talus respectively. Joint forces were specified at these joints to model all major force carrying structures. At the knee cruciate, collateral and patella ligaments were modelled. No ligamentous structures were modelled at the hip or ankle.

Joint axes systems were set up in such a way as to allow equilibrium equations to be established.

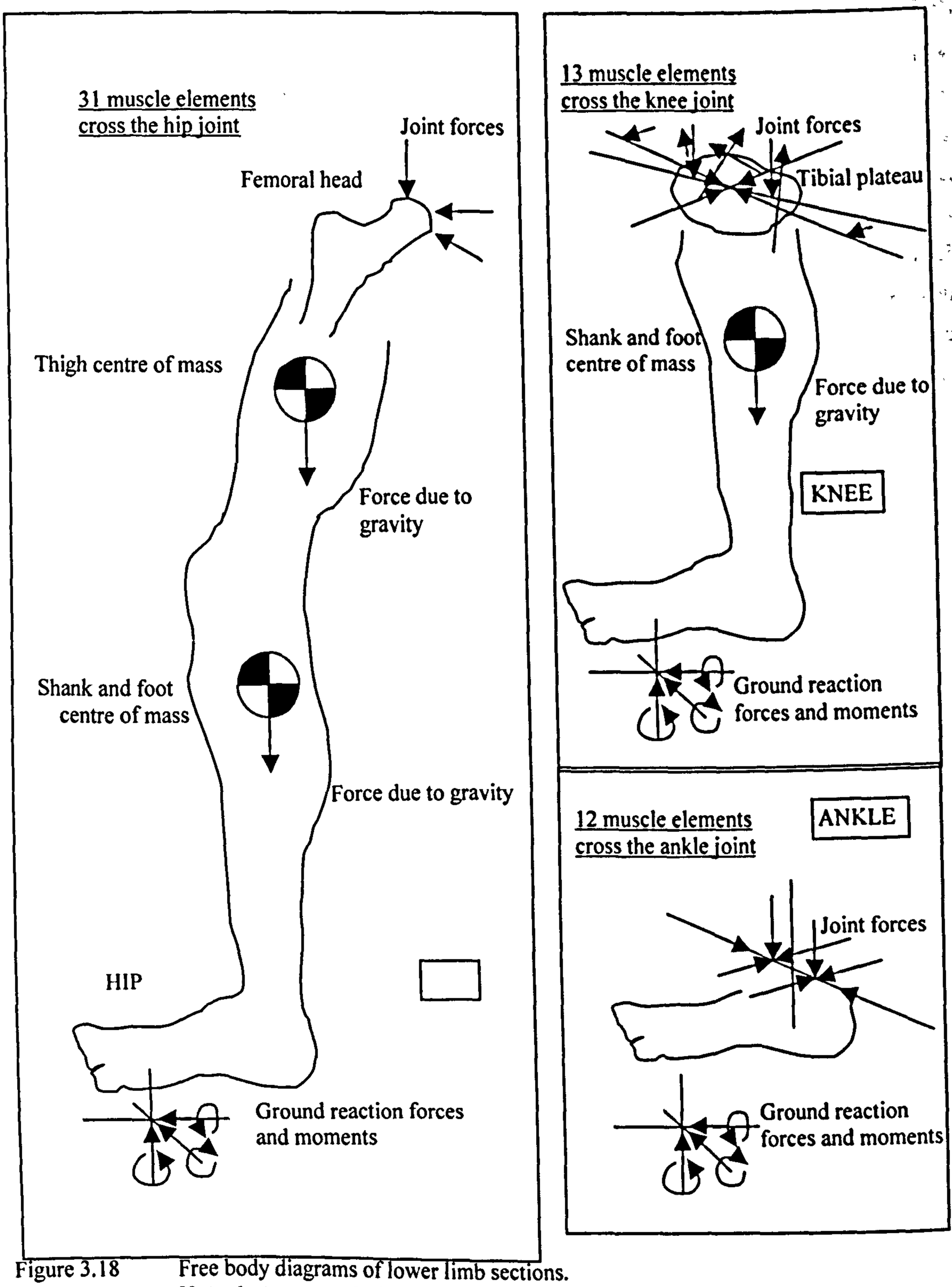

Figure 3.18 Free body diagrams of lower limb sections.
Note that no muscle forces are illustrated.
Three orthogonal components of the hip joint force are illustrated.
See Figure 3.9A for the definition of the knee joint forces.
See Figure 3.15 for the definition of the ankle joint forces.
Three orthogonal components of the ground reaction forces and moments are illustrated.

3.6 Determination of force distribution

3.6.1 Establishing the equilibrium equations

The method used to determine the forces in the leg's force bearing structures was to consider equilibrium in three dimensions at the hip, knee and ankle about the joint's anatomical axes. At each of the joints the following forces acting on the distal limb were included:

Ground reaction forces and moments

Gravitational forces

Joint forces

Ligament forces (at the knee)

Muscle forces

Free body diagrams are illustrated in Figure 3.18. Note that for clarity the muscle forces have not been included in these diagrams. For joint and ligament force definitions reference must be made to the relevant diagrams. Ground reaction forces along and moments about three orthogonal axes are illustrated.

Joint friction was considered to be negligible, it being assumed that joint lubrication prevented significant resistance to relative motion between the bones.

Mass related force actions were considered to be negligible and not included in the analysis. It is typically stated in the literature that mass related load actions account for only approximately 10% of hip joint moment.

Segment mass and location of segment centre of mass were defined after Contini & Drillis [1966].

As no foot markers were used it was not possible to accurately locate the foot centre of mass, therefore for the purposes of gravitational forces the foot and shank were lumped as one.

It was possible to establish 15 equilibrium equations that could be used in the analysis to establish the hip joint forces:

3 hip moments

3 knee moments

3 knee forces

3 ankle moments

3 ankle forces

The intersegmental forces and moments would have been in equilibrium with all internal joint forces and moments. If all of the forces and moments were summed in one direction or about one axis then they would have summed to zero at every time during the activity being performed.

It was assumed that there was a quasi-static equilibrium during all activities and, therefore each frame of data could be treated separately. The equilibrium equations for all of these moments and forces contained a large number of unknown quantities.

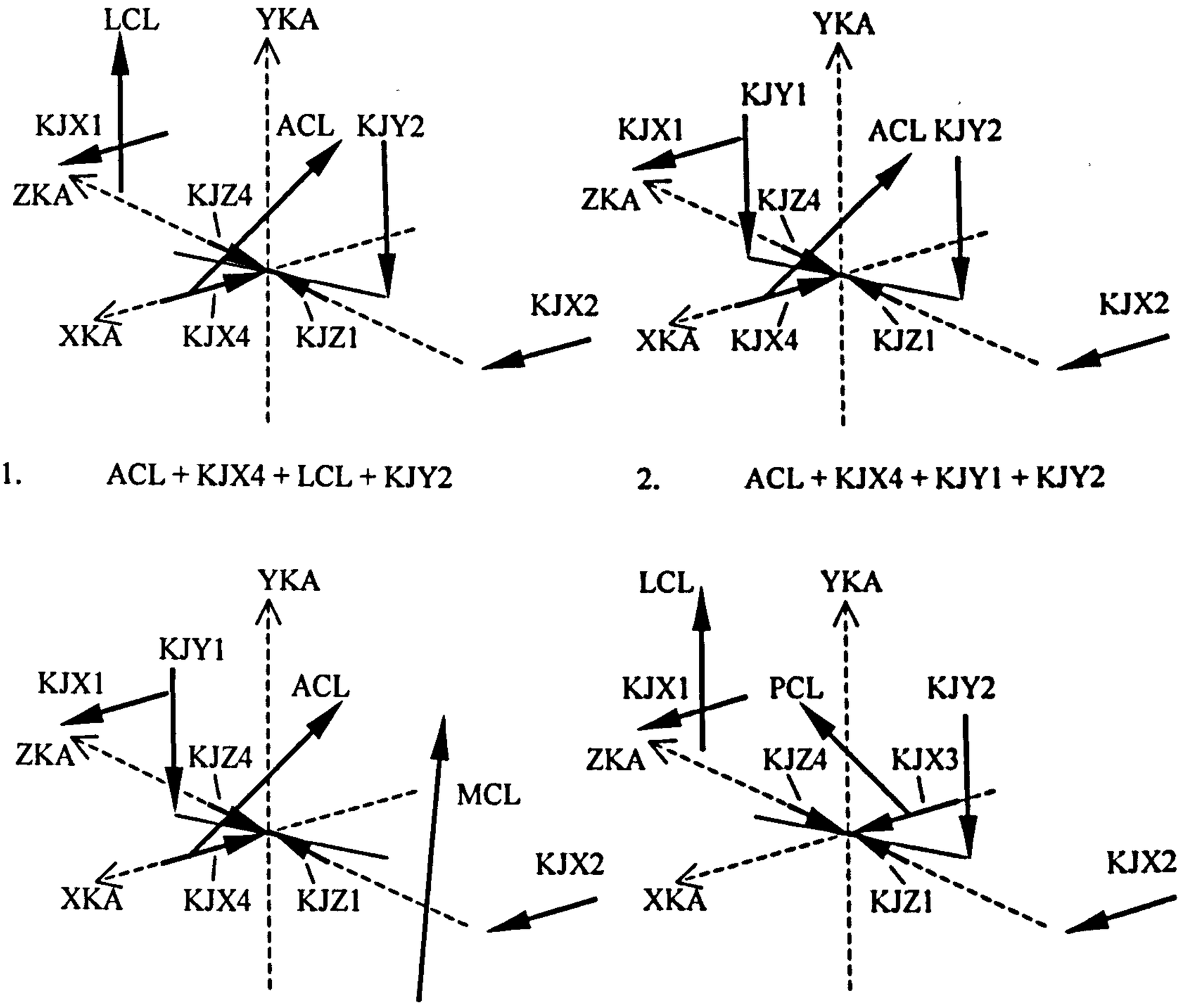

1. ACL + KJX4 + LCL + KJY2

2. ACL + KJX4 + KJY1 + KJY2

3. ACL + KJX4 + KJY1 + MCL

4. PCL + KJX3 + LCL + KJY2

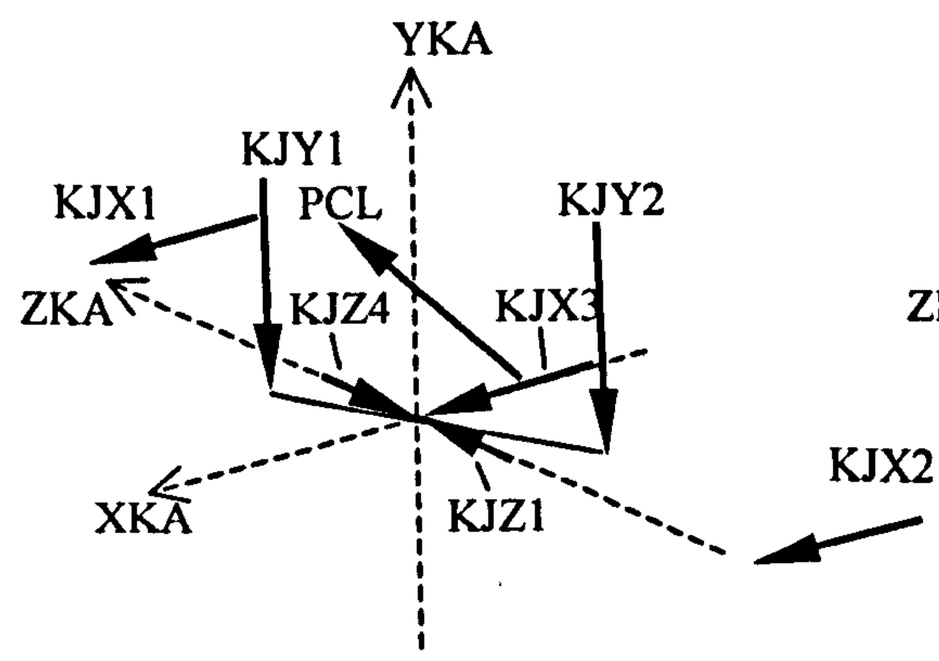

5. PCL + KJX3 + KJY1 + KJY2

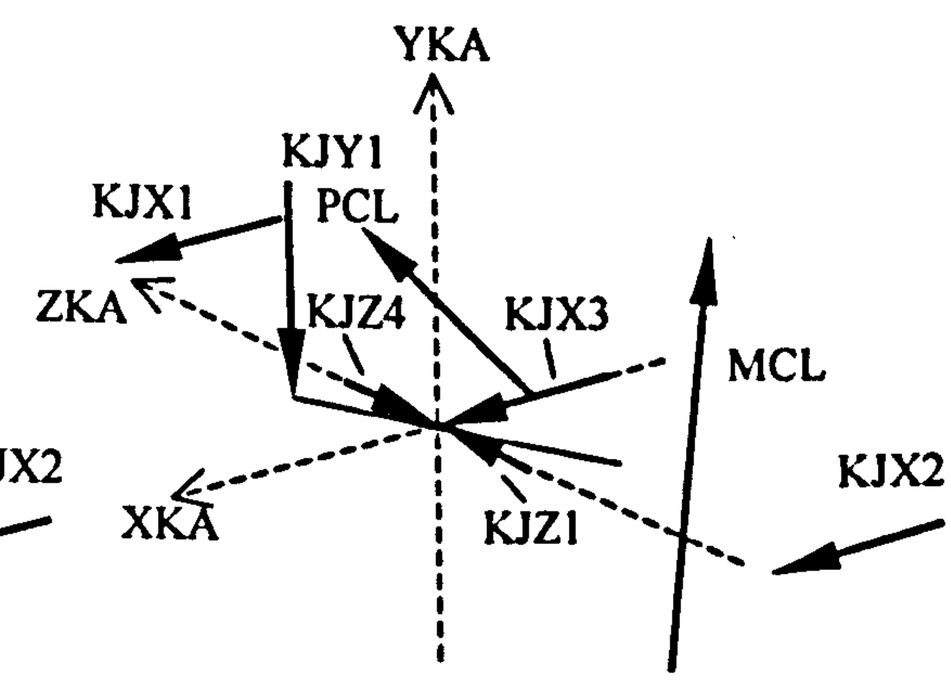

6. PCL + KJX3 + KJY1 + MCL

Figure 3.19 Allowable combinations of active components at the knee joint. Note that KJX1, KJX2, KJZ1 and KJZ4 were always allowed to act.

3.6.2 Unknowns

Within the equilibrium equations for each side of the lower limb model there were 67 unknown quantities:

47 muscle forces

16 joint forces (8 at both knee and ankle)

4 ligament forces (at the knee)

3.6.3 Equilibrium problem solution method

Once the set of equilibrium equations had been formulated it was necessary to decide on a method by which they could be solved for all of the unknown quantities.

The number of equilibrium equations was not sufficient to reduce the solution to a determinate problem. It was necessary to make additional assumptions to distribute the forces among the structures. The solution method chosen was to use a linear optimisation technique (an implementation of the simplex method after Press et al [1989]). This technique set up a matrix form of the equilibrium equations and manipulated this matrix, following a set of rules, to minimise a particular quantity. This solution method allowed the choice of minimum quantity on which to distribute the forces among the load bearing structures. The double linear optimisation method as described by Bean & Chaffin [1988] was implemented. This involved two stages:

During stage one the solution with the lowest maximum stress in any of the muscles was found. Stress was measured as the muscle force divided by the muscle physiological cross-sectional area.

During stage two, the solution (constrained by the maximum stress found in stage one) that minimised the sum of the muscle, joint and ligament forces, was found.

This solution method was based on the assumption that the most important aspect of force distribution was to minimise the maximum level of stress in any of the muscles. This is only one of the criteria that could have been used to allow distribution of the forces in the muscles. It was considered to be reasonable, however, as the activities being performed were not extreme and, therefore, no muscles should have been excessively loaded. Also this approach allowed sharing of force between several muscles. This seemed to be a more reasonable solution than assuming that there were the minimum possible number of muscles working at any point in time.

It is unlikely that the approach employed led to the lowest possible joint forces. Lower joint forces would probably have been achieved using fewer active muscles with higher forces. That method might, however, have led to unrealistic loading of particular muscles.

The criteria of minimum maximum muscle stress did not directly take into account muscle fatigue or energy consumption. The solution method was based on a frame-by-frame analysis with no reference to total cycle consumption of energy or muscle fatigue.

The second part of the optimisation was necessary to ensure that a single solution could be defined. Thus this part of the optimisation was essentially of a mathematical nature. This second part did, however, place a limit on antagonistic activity.

The solution was constrained to prevent overloading of any particular muscle and to prevent unnecessary antagonistic activity by ensuring that the sum of forces was minimised.

3.6.4 Constraint of the solution

The ligaments at the knee joint were included in the model in the same manner as the muscles. If unconstrained they could have acted as 'active' components in the equilibrium of the joint. To restrict the force of the ligaments and to ensure a physiologically reasonable solution it was necessary to place constraints on the number of structures that could carry load at any one time. Only certain combinations of force were allowed in the cruciate ligaments (ACL and PCL), collateral ligaments (MCL and LCL) and joint forces (KJX3, KJX4, KJY1 and KJY2). The allowable combinations of load bearing components were as follows (see Figure 3.19):

1. ACL + KJX4 + LCL + KJY2
2. ACL + KJX4 + KJY1 + KJY2
3. ACL + KJX4 + KJY1 + MCL
4. PCL + KJX3 + LCL + KJY2
5. PCL + KJX3 + KJY1 + KJY2
6. PCL + KJX3 + KJY1 + MCL

No restrictions were placed on the other knee joint forces (KJX1, KJX2, KJZ1 and KJZ4).

Each of these combinations was tested and the one that resulted in the lowest muscle stress was chosen. It was, therefore necessary to perform the first stage of the optimisation (Section 3.6.3) seven times, once for each allowable solution and then to repeat the solutions with the lowest maximum stress value. This was then followed by the second stage optimisation giving a total of eight optimisations.

3.7 Data processing

Force plate and motion analysis data were recorded at 50Hz extending for not less than 10 frames of data before and after foot contact with the force plate or force plate section. From the five trials recorded for each activity for each subject, three were selected. The first three trials with no gaps in marker trajectories were chosen. If there were not three trials with no gaps then the trials with the smallest gaps were chosen. For some subjects fewer than three trials were used for some of the activities due to large gaps in marker trajectories.

3.7.1 Pre-processing

Raw data from the motion analysis system output contained a number of gaps and would have included noise due to skin movement or inaccuracies in the location of markers by the motion analysis system. It was necessary, therefore to process the data in such a way as to reduce these effects. Interpolation of marker location was performed to fill gaps in marker trajectories due to markers being obscured during testing. Both marker location and force plate data were filtered to remove any noise. Further processing involved the application of a marker correction routine to the data in an attempt to reduce skin movement effects.

3.7.1.1 Data Interpolation

There were no gaps in recorded force plate data. There were, however, often numerous gaps in recorded motion analysis data. Whilst the trials that were most significantly affected were simply eliminated from the analysis it was possible to interpolate short gaps in marker trajectories. The results of each trial were examined for accuracy in terms of the location of markers in space. Trials with gaps in marker trajectories were only included if these gaps did not occur at times when the motion was changing direction, i.e. when the end of the marker trajectory before the gap was following a significantly different path from that at the start after the gap. It was also observed that the last recorded location before a gap and the first recorded location after a gap often did not follow the general trend of marker location.

The interpolator used was of a cubic spline type [Press et al, 1989], which was significantly affected by the few points either side of a gap. Therefore, if a gap coincided with a change in direction it would have been unlikely that the interpolation would have calculated the correct trajectory. Due to the sensitivity of the interpolation method to the location of the points either side of the gap it was also necessary to extend the gap by one frame of data either side of any recorded gaps. This reduced the effect of poor marker detection at the edge of gaps.

The cubic spline interpolation method fitted a cubic curve between each of the known points with first and second derivatives of the curves being identical at each of those points. Thus the curve fitted to any particular gap would have been of a cubic nature and heavily affected by locations of recorded points both before and after the gap.

To define fully the cubic spline it was necessary to specify the gradient at the beginning and end of the data. This was achieved at the start of the data by determining the first two sequentially recorded marker locations, calculating the gradient between then and then using the second of the points as the first point in the interpolation procedure. A similar method was used at the end of the data.

3.7.1.2 Data Filtering

Movement of soft tissues over the underlying structures and inaccuracies in the motion capture equipment would both have produced errors in marker location that were out of the frequency range of the activities studied for this thesis. To reduce these and other random errors a filter was applied to both force plate output data and motion analysis data. A low pass non-recursive FIR filter was used [Stewart, 1995] with a cosine window based on up to 20 points before and 20 points after the point at which it was applied. This acted as a low pass filter. A cut off frequency of 10Hz was used.

The use of a cosine window with a maximum width of ±20 samples was a compromise between accuracy and computing time. For the data collected, only 10 frames of data before foot contact and 10 frames after foot off were specified. Thus the full width of the filter would not have always been applied for the first and last 10 frames of foot contact on the force plate section.

3.7.2 Marker correction routine

The location of markers with respect to the underlying bones incorporated a number of errors. Filtering of data was used to eliminate random noise. This, however, would not have removed any systematic error associated with skin movement relative to the underlying bones. An attempt was made to remove this source of error. The relationship between the position of markers within each of the limb segments was established. It was assumed that this was fixed, i.e. that the limb segments could be represented as rigid bodies. This relative positioning of the markers within the limb segments was imposed on all trials. To further enhance this representation a hip joint centre location was established which was considered to maintain a fixed position within the pelvic segment's anatomical co-ordinate system. This fixed hip joint centre location then provided a rotation point of relative movement between pelvic and thigh segments. Thus within segment marker correction could be used to mimic a consistent rigid body with the additional constraint of a fixed hip joint centre. To implement this method of marker correction it was necessary to establish an initial formation of markers for each segment and to establish the location of the hip joint

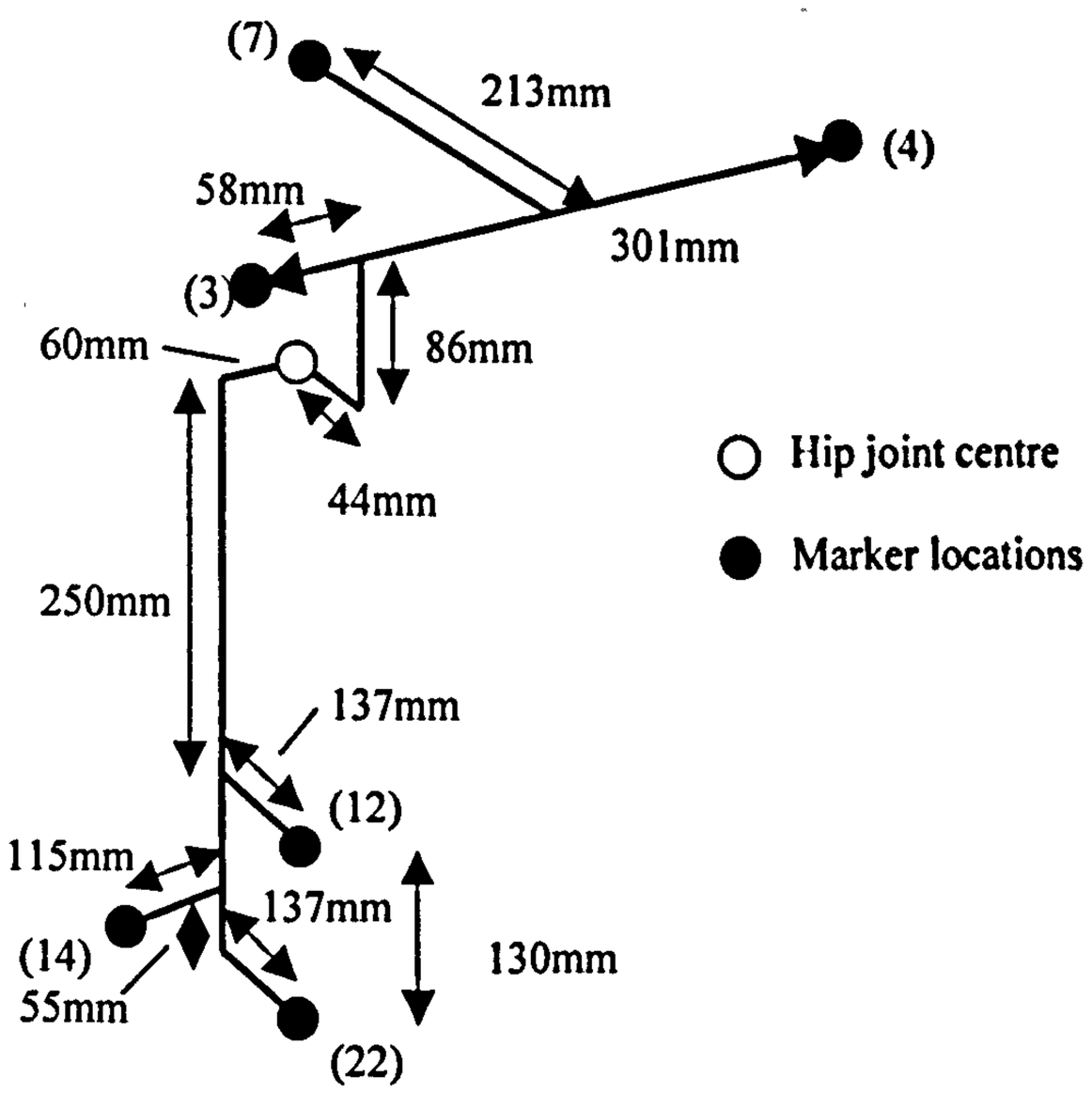

Figure 3.20 Hip joint model.
The markers used represented the following positions:
(3) = Right anterior superior iliac spine, (4) = Left anterior superior iliac spine
(7) = mid-posterior superior iliac spines, (12) = Right upper front of thigh
(14) = Right lateral thigh, (22) = Right lower front of thigh

centre with respect to the pelvic marker set. The first of these two requirements was achieved by the static trial. With the individual standing with legs straight, feet slightly apart and facing forwards, the relative position of all markers of each segment was established. The within segment positions of markers during the dynamic trials were then corrected using the methods of Spoor & Veldpaus [1980] and Veldpaus et al [1988]. A least squares correction was applied to ensure that the within segment markers maintained the same relative positions as in the static trial. The differences between each of the corrected marker positions for a segment and those detected by the motion analysis system were squared and summed. The corrected positions were calculated so as to minimise this sum. Possible corrected positions of the markers were calculated by the rotation and translation of the static markers within a segment, thus maintaining the relative positions of markers.

There are numerous empirical methods of hip joint centre location detailed in the literature [e.g. Andriacchi et al 1980, Seidel et al 1995]. That of Bell et al [1990] was chosen for implementation in this thesis.

For the right leg from the right anterior superior illiac spine the hip joint centre was defined as :
HJC_X = aligned with the greater trochanter
$HJC_Y = -30\% \times \text{interASIS}$
$HJC_Z = -14\% \times \text{interASIS}$
Where :
HJC = hip joint centre co - ordinates based on the pelvic anatomical co - ordinate system
interASIS = inter anterior superior illiac spines distance

The hip joint centre was defined with respect to the anterior superior iliac spine in pelvic anatomical co-ordinates as 14% of the inter anterior superior iliac spine distance medial (-ve ZPA) and 30% distal (-ve YPA) and being aligned with the greater trochanter in the anterior-posterior direction (-ve XPA). This definition was used as it was possible to implement in a reliable and repeatable way from the external features identified on the subjects. It did not require the use of internal imaging techniques, e.g. X-ray. The quoted accuracy for the location of the hip joint centre using this technique in a group of seven male subjects was given as 1.07cm. An accuracy of 0.79cm in the frontal plane (containing axes YPAand ZPA) and 0.73cm in the anterior posterior direction (XPA) are quoted. As this definition was derived using male subjects, it is possible that it would not have identified the hip joint centres of females with the same degree of accuracy.

An alternative method of finding the hip joint centre location was also implemented. This second method was applied to a model of the hip joint to assess the level of accuracy that could be achieved. The model used, as illustrated in Figure 3.20, had a fixed hip joint centre location. The relative location of markers

within each of the pelvic and thigh segments was established from a static trial. The model hip was then rotated using motion similar to that which might have been achieved by one of the subjects studied. The hip joint centre was calculated using a least squares sum of corrections needed to ensure the thigh segment moved about a fixed point with respect to the pelvic segment. This analysis required the implementation of the methods as detailed in Holzreiter [1991]. This information was supplemented by an expansion of the details of the method by Benjes [1996]. Section 3.7.4 details the development of the methods used in the implementation of this theory.

The results of this thesis were calculated using the fixed hip joint centre as defined by Bell et al [1990] as the second method detailed above could not provide an accurate hip joint centre location.

In summary the marker correction procedure involved the following steps for each frame of all dynamic trials:
Correct within pelvic and shank segment marker positions to be the same as the static trial.
Calculate the hip joint centre position
Correct the thigh markers' locations to ensure that they had the same relative position as in the static trial and that they were constrained to move by rotation only about the fixed hip joint centre.

3.7.3 Post processing

3.7.3.1 Data Normalisation

To allow comparison between individuals all results were normalised. Two normalisations were used. The first was to reduce the data to 100 points of the stance phase of the activity being considered. This was achieve by fitting a cubic spline [Press et al, 1989] to all recorded points and then using the spline as an interpolator to calculate all required values.
The second was to normalise the results by subject's weight or mass to allow comparison between the subjects. Normalisation was applied to the following quantities:
Forces: force/body weight = N/body weight
Moments: moment/mass = Nm/body mass

It should be noted that the quantity of normalised moment used was not fully dimensionless. Moment (Nm) divided by the product of body weight (N), acceleration due to gravity (m/s^2) and height (m) (or leg length) of the subject would have provided a fully dimensionless quantity. It is typical in the literature, however, to present moments in terms of Nm/body mass. If the height of the individuals being compared does not vary greatly then this quantity is appropriate. This quantity was used in this thesis to allow comparison of the results with those found in the literature.

3.7.4 Evaluation of a method of Hip Joint Centre Location

The following section provides details of an attempt to develop a method of accurately locating the hip joint centre. This section is self-contained, with methods, results, discussions and conclusions. This method was not implemented in the model of the limb used in this thesis, but is included to demonstrate the levels of accuracy that were attained.

3.7.4.1 Introduction

To find the location of the hip joint centre a method was attempted which it was hoped would provide a more accurate point than that which could be derived using standard definitions as found in the literature. The use of a subject specific hip joint centre location would have eliminated the errors associated with the use of a standard definition from the literature. The examination of the motion of an individual's thigh about their pelvis provides information regarding the location of the hip joint centre. The accuracy of this information as recorded by a motion analysis system would determine the potential for it to be used to identify the actual hip joint centre. Following is a description of a method to calculate the hip joint centre location from motion analysis data. Initially this method was applied to a model of the hip joint (Figure 3.20). This application is described.

3.7.4.2 Method

The model consisted of a pelvic and a thigh segment, each of which had three markers attached (see Figure 3.20). The dimensions of the model were estimated from a 30 year old male. The model was intended to demonstrate the potential of the method not to exactly represent an individual. The model was made of metal tubing which was considered to be rigid. The same motion analysis system and retro-reflective markers, 25mm in diameter, were used in this analysis as in the subject testing. The hip joint was modelled as a fixed centre ball and socket joint.

The method of analysis involved the use of two trials. For the first trial, a static trial, the model was held still in a position in the test volume equivalent to that which would have been taken up by the subjects. This provided a set of data relating the pelvic markers to the thigh markers. For the second trial, a waggle trial, the model hip joint was articulated, moving the pelvic and thigh segments in such a way as to mimic the range of motion that a subject with a hip joint replacement might have achieved.

It was hypothesised that the most accurate calculation of the hip joint centre location could be made by means of the least squares correction of marker locations and that this would overcome the errors associated with motion analysis location of markers in space. The following steps were used:

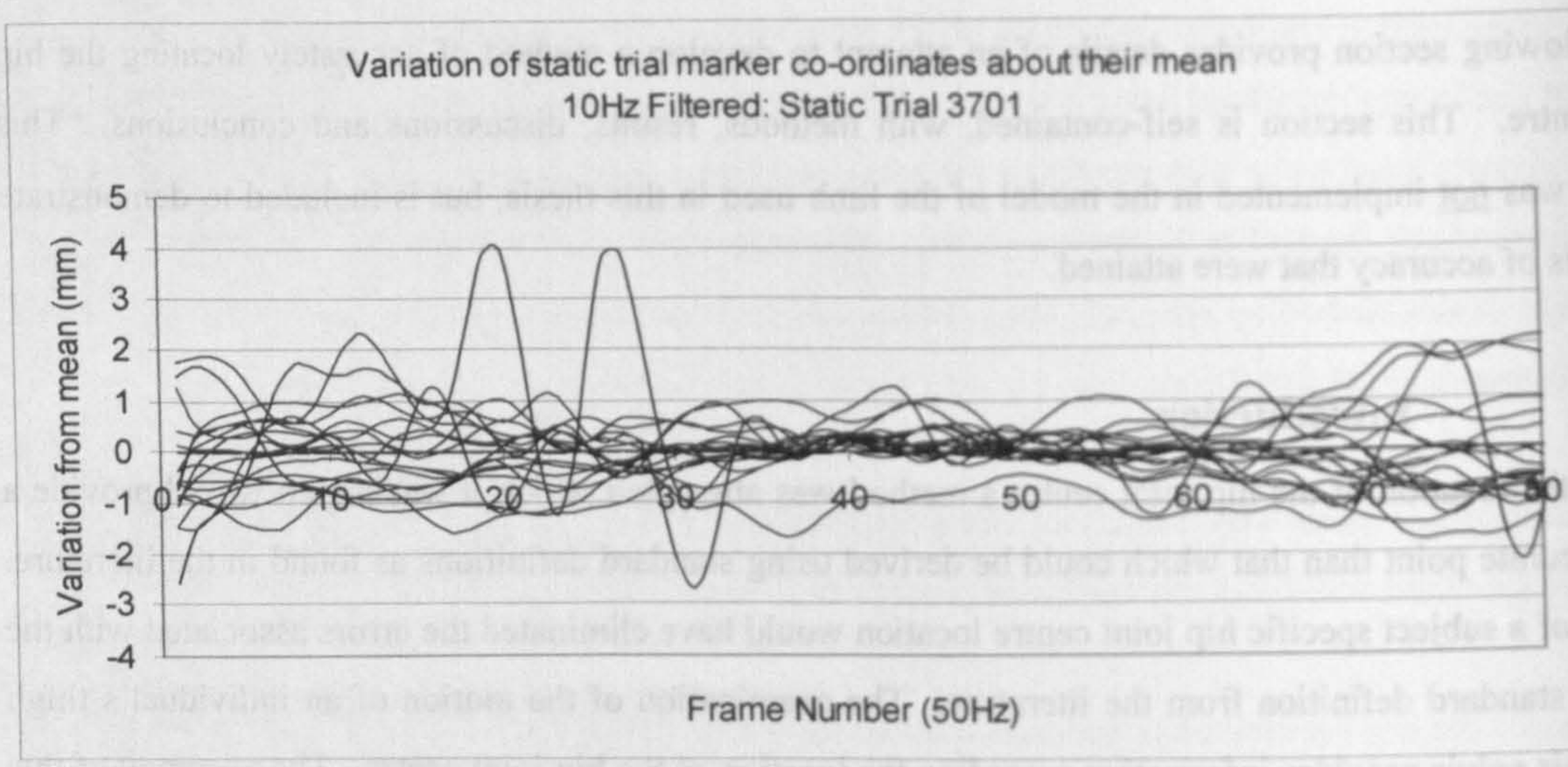

Figure 3.21 Variation of marker co-ordinates about their mean values. (Static trial 3701)

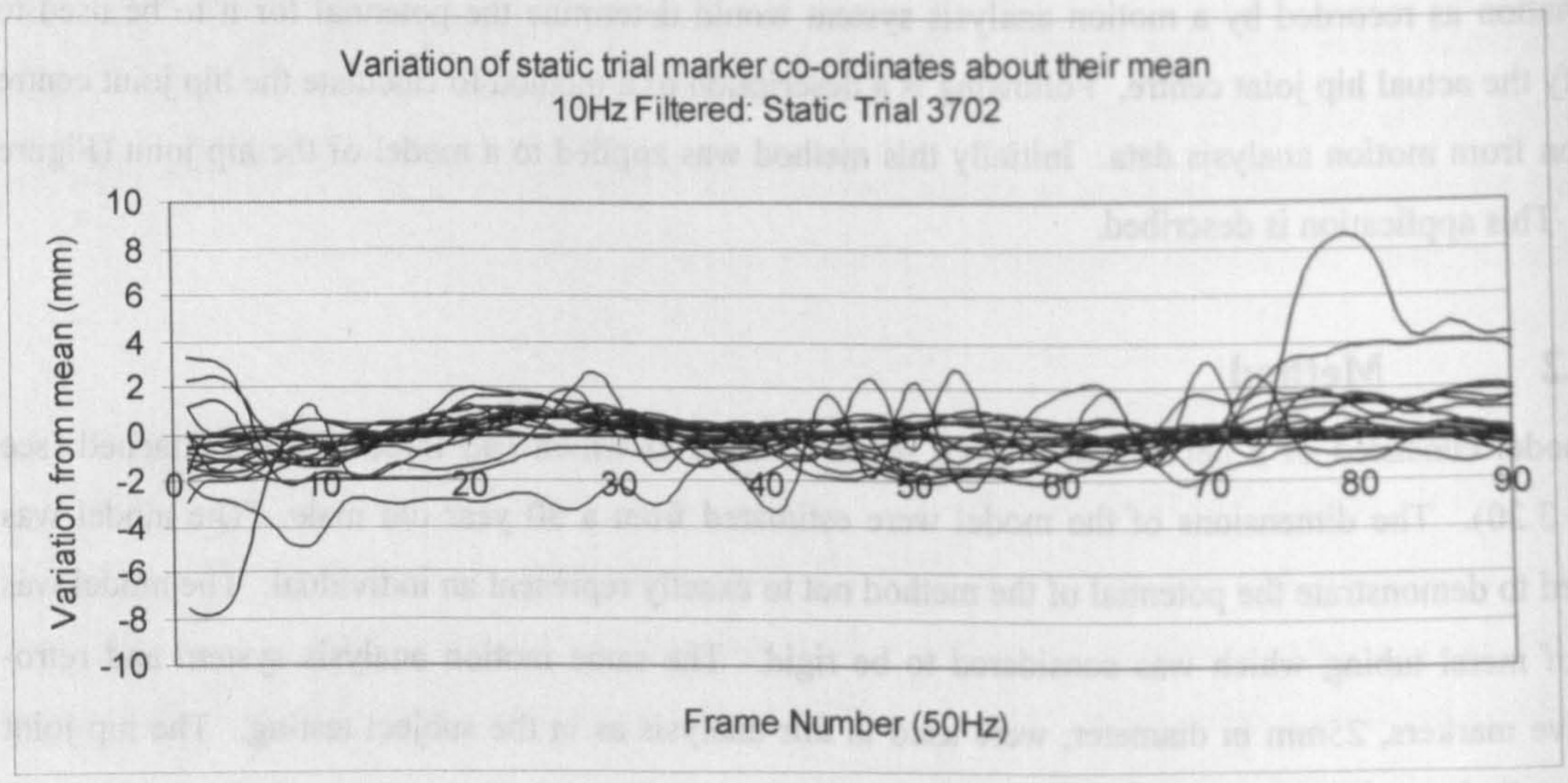

Figure 3.22 Variation of marker co-ordinates about their mean values. (Static trial 3702)

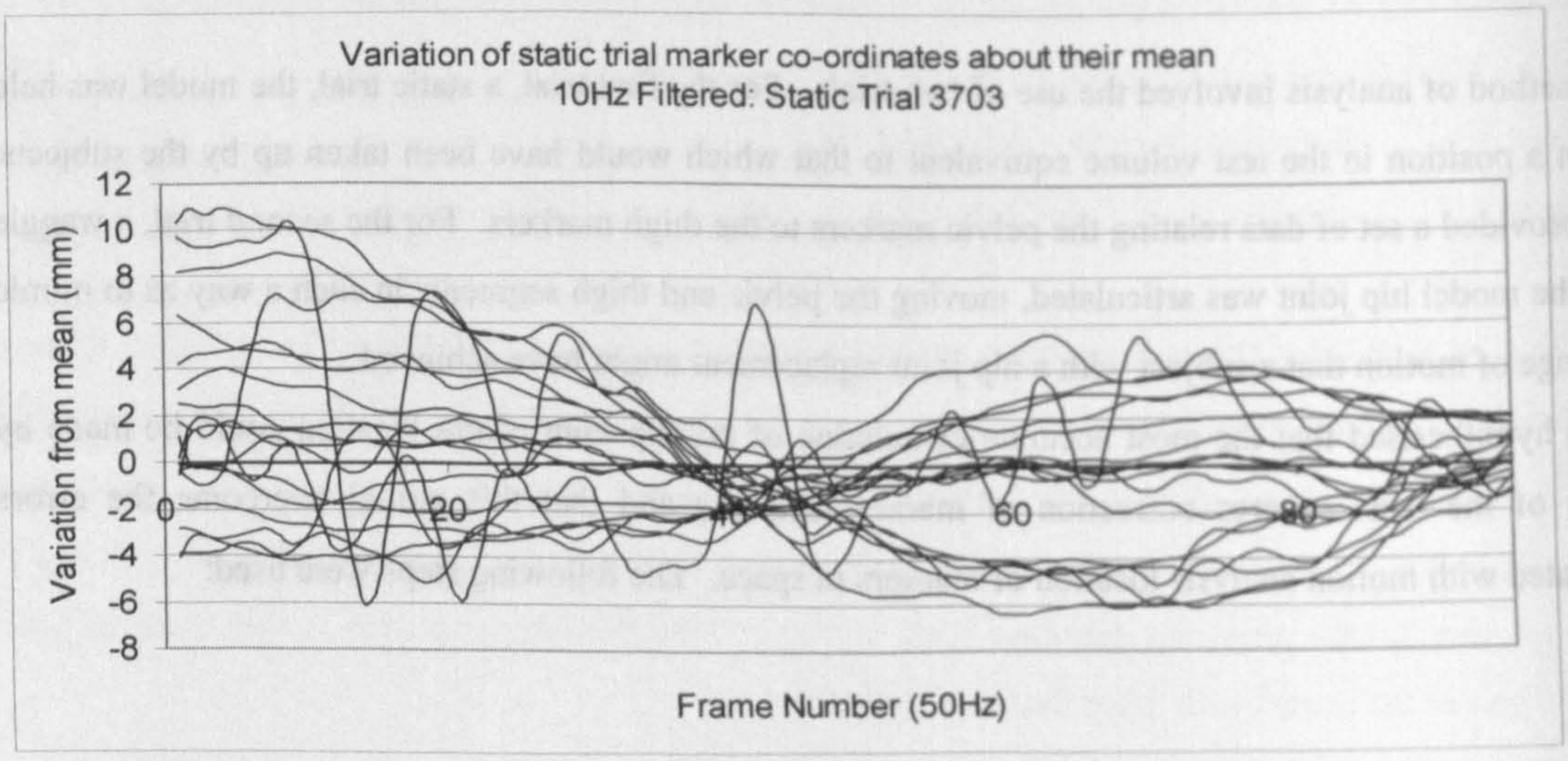

Figure 3.23 Variation of marker co-ordinates about their mean values. (Static trial 3703)

1. Using a least squares error method [Spoor & Veldpaus, 1980 and Veldpaus et al, 1988] the pelvic markers' co-ordinates were corrected for each frame of data of the waggle trial, such that they had the same relationship to each other as in the static trial.
2. It was assumed that the thigh markers moved in such a way as to be rotations of the static trial thigh marker set about some hip joint centre location fixed with respect to the corrected pelvic marker set.
3. The motion of the waggle trial thigh markers about the corrected pelvic marker set was used to calculate the hip joint centre location by assuming that the sum of the squares of the correction needed for the thigh markers was minimised [Holzreiter, 1991].

To provide an indication of the accuracy of this solution method two tests were performed. The first was a test of the mathematical integrity of the method. This involved using the static data as a template from which, using a known hip joint centre location, new positions of the thigh markers were derived by rotations about three orthogonal axes fixed at the hip joint centre. The new trial derived in this manner was used to test the algorithm. As expected the error in hip joint centre location using this method was, to two decimal places, equal to zero mm. This accuracy was maintained with even a very small number of frames (as few as five) with small angles of rotation (less than 5°).

The second phase of testing was to introduce errors associated with the motion capture system. This was achieved by using the model leg. Three static trials and 5 waggle trials were performed using this model. The results presented the opportunity to test each static trial against each of the five waggle trials, thus 15 hip joint centre calculations were performed.

Five different methods of implementation were followed in an attempt to provide an accurate means of identifying the hip joint centre. Common to all of these methods was that only static and waggle trial frames of data that were complete were used, i.e. no interpolated values were used.

3.7.4.2.1 Method 1

The first method used the full static trial's duration, approximately 100 frames or two seconds of data. The average marker positions over all the static trial frames were used. It was hoped that this would reduce any errors associated with noise in the data. The static trial data were 10Hz low pass filtered using the same filter as detailed in Section 3.7.1.2. The waggle trial data were unfiltered.

3.7.4.2.2 Method 2

As an extension of method one and in an attempt to improve the accuracy of the solution, restrictions were placed on the frames of the waggle trial data that were incorporated into the calculation algorithm. The

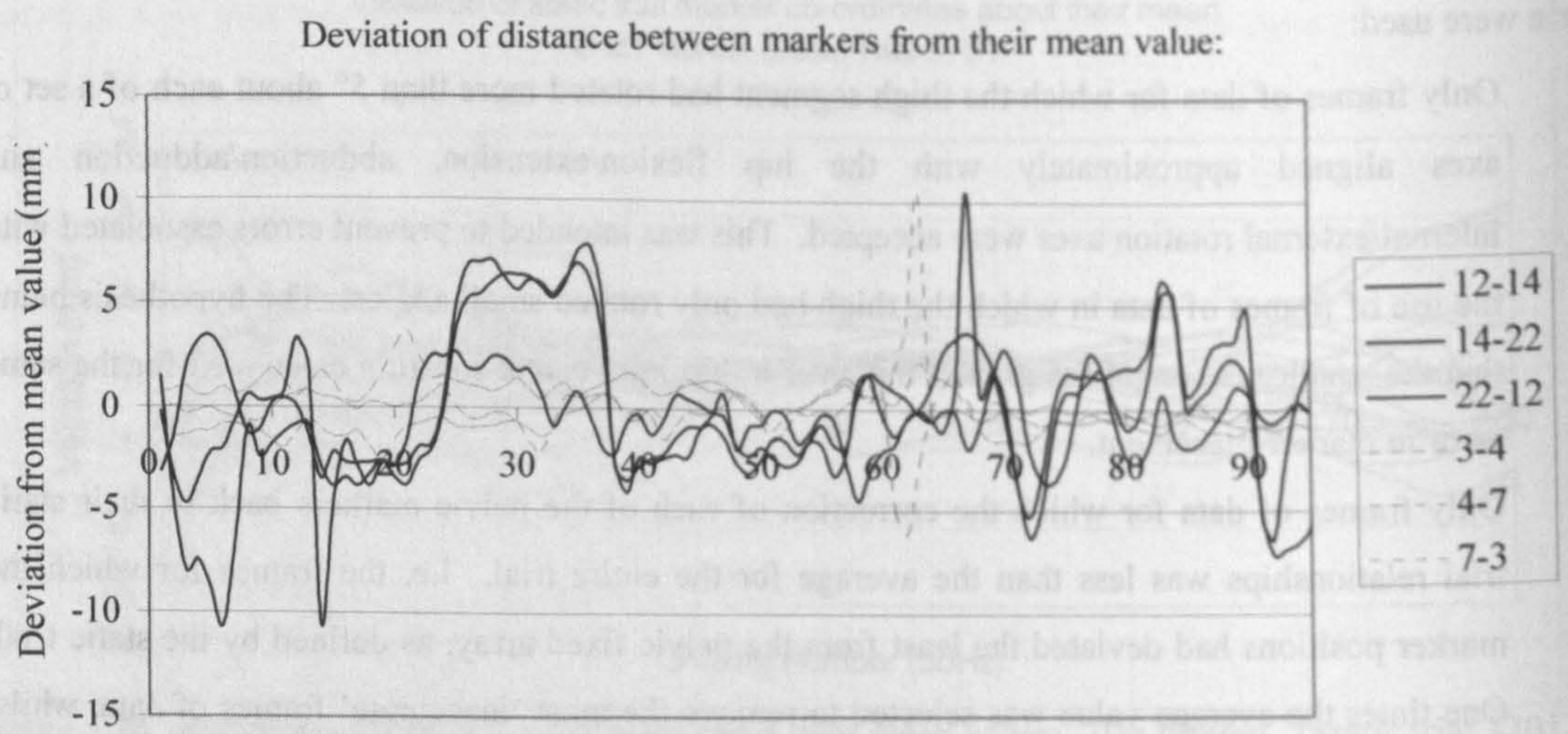

Figure 3.26 Deviation of the distance between markers from the mean value (waggle trial 3704).

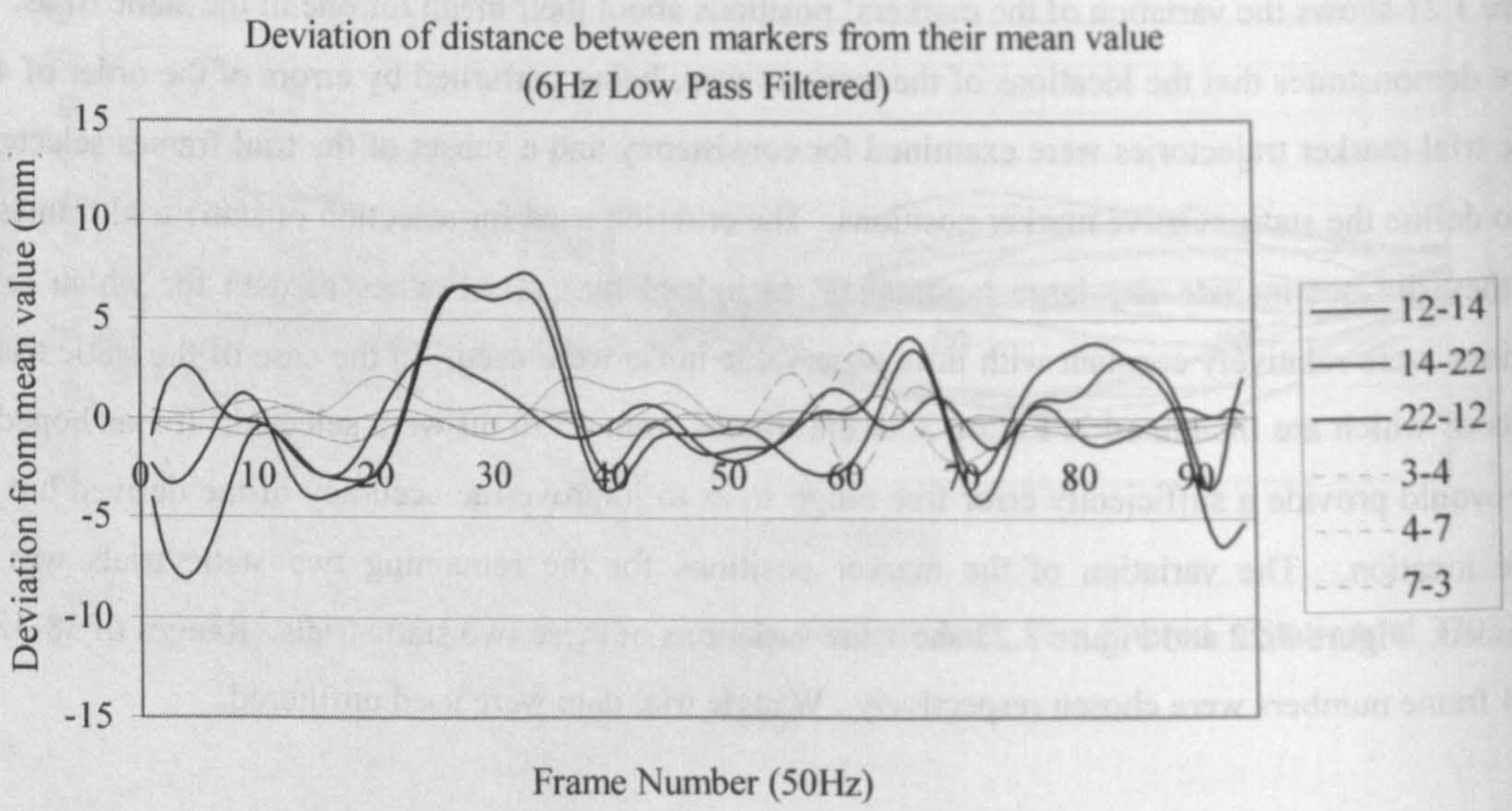

Figure 3.27 Deviation of the distance between markers from the mean value. 6Hz low pass filtered. (waggle trial 3704)

intention being that only the frames of data associated with the lowest errors would be included. Two criteria were used:

1. Only frames of data for which the thigh segment had rotated more than 5° about each of a set of axes aligned approximately with the hip flexion/extension, abduction/adduction and internal/external rotation axes were accepted. This was intended to prevent errors associated with the use of frames of data in which the thigh had only rotated small angles. The hypothesis being that the smaller the angle the greater the error in hip joint centre location calculated for the same error in marker placement.
2. Only frames of data for which the correction of each of the pelvic markers back to their static trial relationships was less than the average for the entire trial. I.e. the frames for which the marker positions had deviated the least from the pelvic fixed array, as defined by the static trial. One times the average value was selected to remove the most 'inaccurate' frames of data, whilst still ensuring that there were sufficient numbers of frames to provide a range of motion.

3.7.4.2.3 Method 3

Figure 3.21 shows the variation of the markers' positions about their mean for one of the static trials. This figure demonstrates that the locations of the markers were being perturbed by errors of the order of 4mm. Static trial marker trajectories were examined for consistency and a subset of the trial frames selected for use to define the static relative marker positions. The criterion used for selection of static trial frames was that they did not include any large 'anomalies' as judged by eye. Frames of data for which marker positions were relatively constant with little observable noise were used. In the case of the static trial the results of which are illustrated in Figure 3.21 the frames from 35 to 60 were selected. It was hoped that these would provide a sufficiently error free range so as to improve the accuracy of the derived hip joint centre location. The variation of the marker positions for the remaining two static trials was also examined. Figure 3.22 and Figure 3.23 show the variations of these two static trials. Ranges of 38-42 and 80-84 frame numbers were chosen respectively. Waggle trial data were used unfiltered.

3.7.4.2.4 Method 4

Examination of the static trials showed that there was considerable noise even after 10Hz low pass filtering. In order to try to remove this noise the static trial was filtered severely using a 2Hz low pass filter. The resulting variations about the means are illustrated by Figures 3.24 and 3.25. It can be seen that the use of a 2Hz filter removed all 'anomalies' from the data. It was assumed that the waggle trial data would also contain noise associated with the motion capture system. A filter of 6Hz was applied to the waggle trial data.

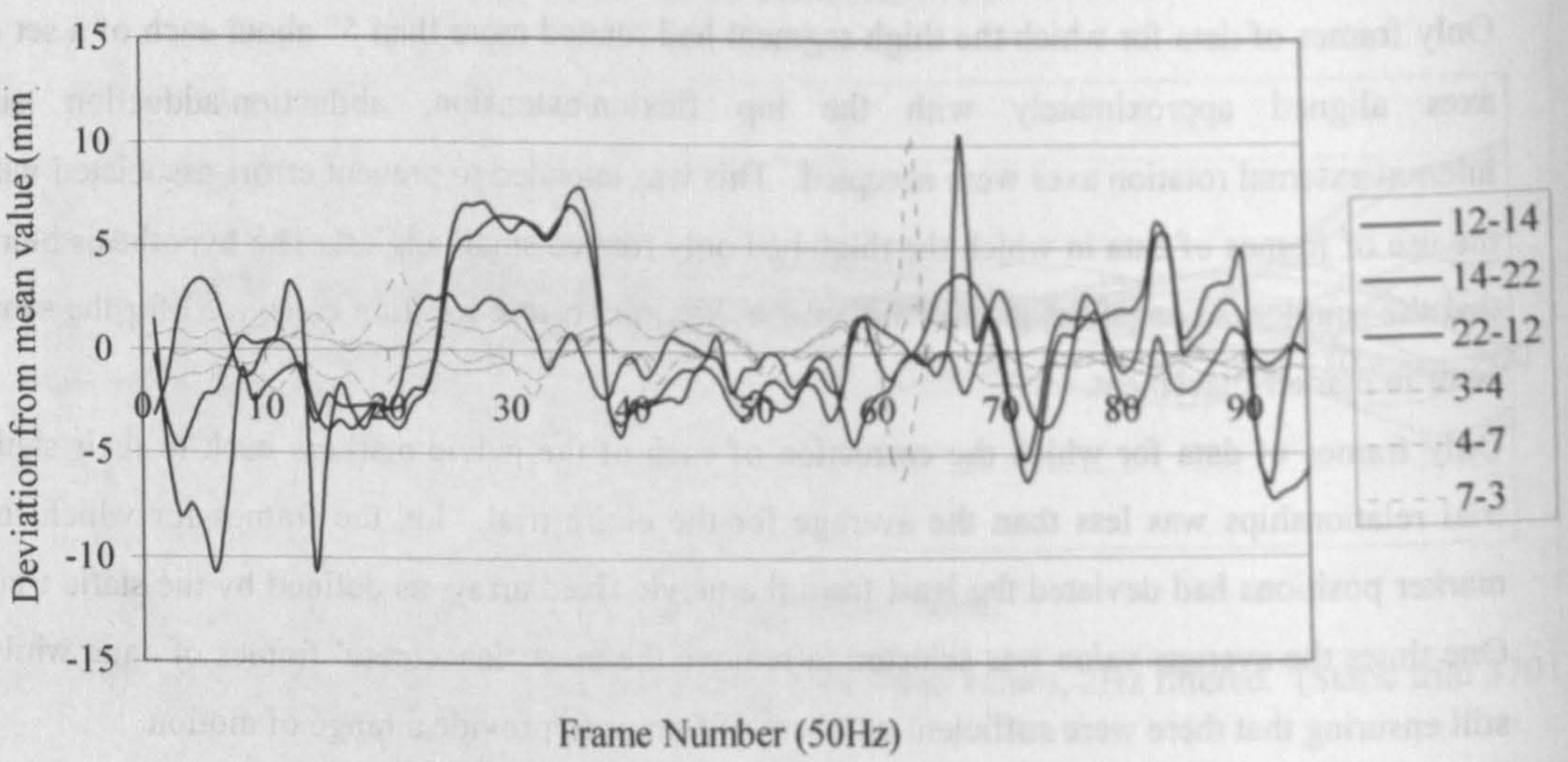

Figure 3.26 Deviation of the distance between markers from the mean value (waggle trial 3704).

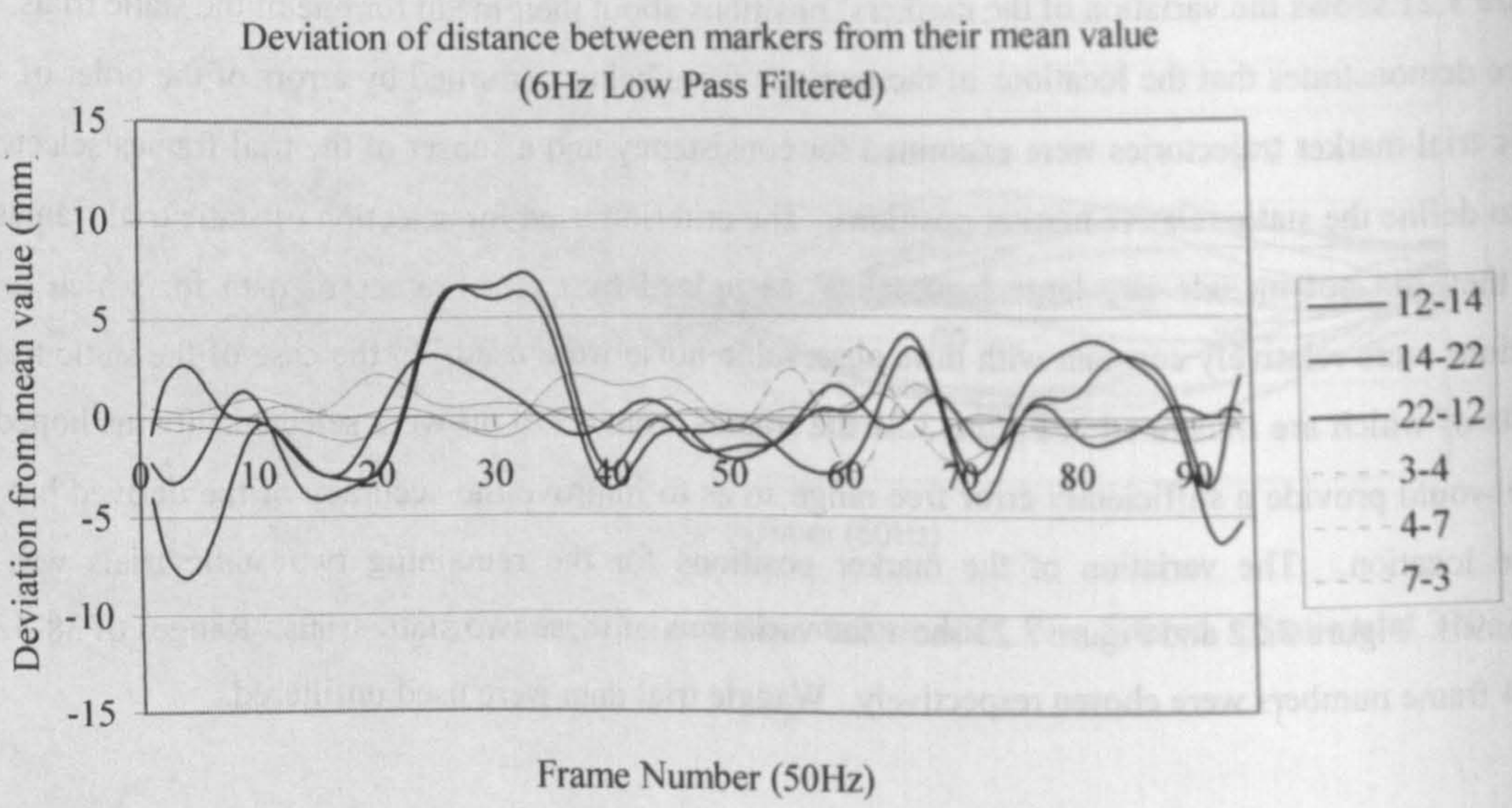

Figure 3.27 Deviation of the distance between markers from the mean value. 6Hz low pass filtered. (waggle trial 3704)

3.7.4.2.5 Method 5

Severe filtering of the static trial with a 2Hz low pass filter and the waggle trial with a 6Hz low pass filter was applied in conjunction with a selection of static trial frames as detailed in method 3.

3.7.4.3 Results

The results of methods 1 to 5 are given in Appendix V. The methods yielded results that were very varied between the different combinations of static and waggle trials.

3.7.4.4 Discussion

Method 1 was not able to calculate the hip joint centre as accurately as might have been expected for a rigid structure. Selection of waggle trial frames as implemented in method 2 did not improve the accuracy of the resulting hip joint centre location. This indicated that it was unlikely that the errors were associated with the inclusion of frames of data where the angle of thigh rotation was small, or due to inclusion of frames of data with relatively large deviations in the pelvic marker set locations. Selection of static trial frames for inclusion in the analysis as illustrated by method 3 produced a small improvement in hip joint centre location. There was, however, still a 13mm maximum error in location of the hip joint centre. The severe filtering of both the static and waggle trial data as implemented in method 4 did not produce any improvement in the results. Using only a selection of static trials (as described in method 3) in conjunction with severe filtering had equally little impact on the accuracy of the hip joint centre location calculation.

It was observed (Figures 3.25) that for static trial 3703 there was a significant movement of the markers about their mean, indicating that the model leg was not held steadily during the capture of static trial data. This amount of motion, up to 16mm, might easily be expected during a static trial on a human subject. It was noted that the results of the calculations using the third static trial, 3703, were not consistently more inaccurate than those using the other two static trials.

The error in locating the hip joint centre using the method of least squares correction could not be removed by filtering trial data, being selective about the range of motion required for acceptance of a frame or by selection of the seemingly most accurate static trial frames of data. An alternative explanation for the poor performance of this method could have been that there were systematic errors in location of the markers in space. This hypothesis was tested, by examining the distance between adjacent markers as they were displaced within the test volume. Figure 3.26 shows the variation of the distances between the markers during one of the waggle trials (3704). During the waggle trials the thigh markers moved the most with respect to the test volume. If there had been errors associated with a markers particular location

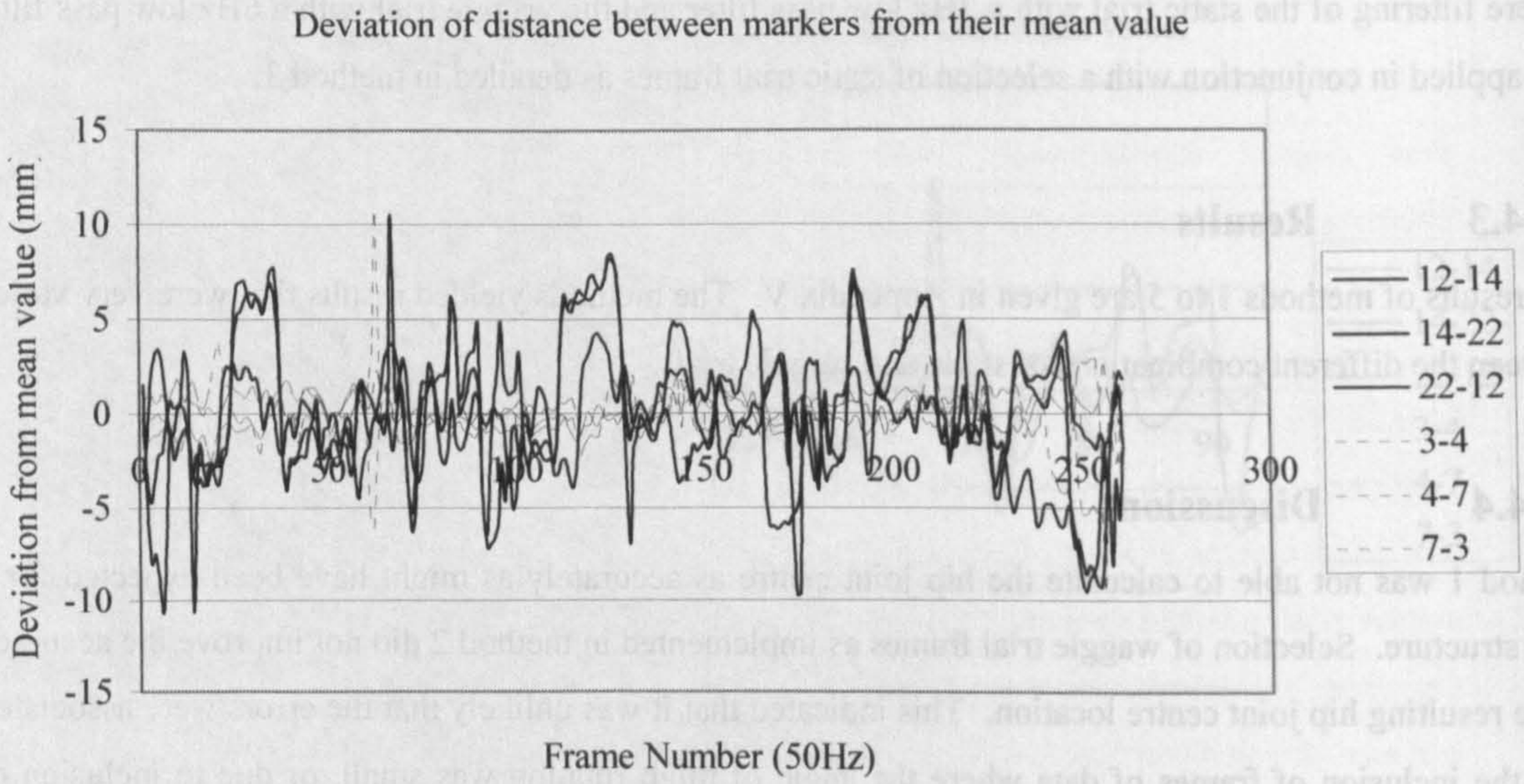

Figure 3.28 Deviation of the distance between markers from their mean value over several rotations of the thigh. (Waggle trial 3704)

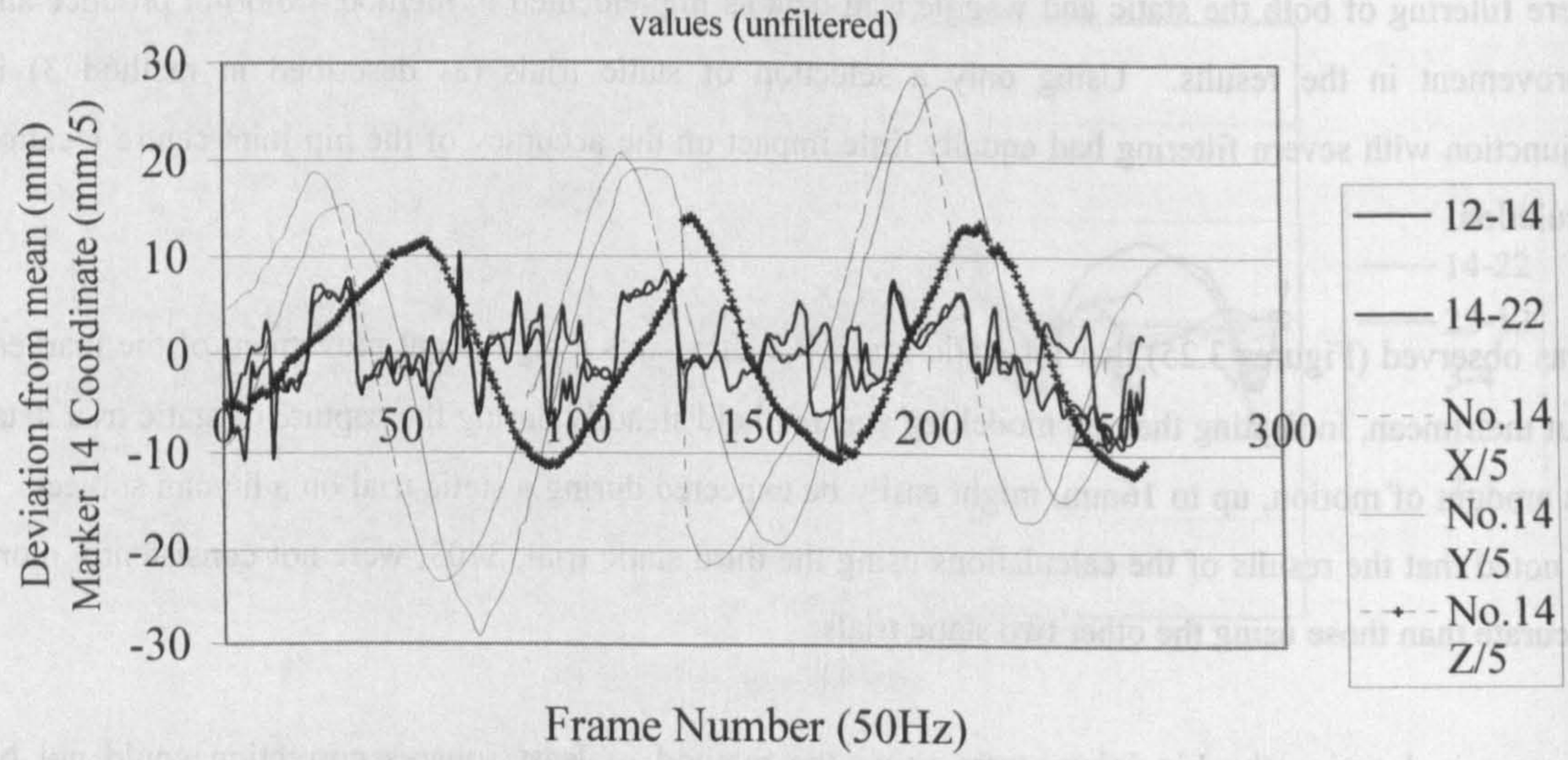

Figure 3.29 Correlation between the deviation of the distance between markers and the movement of marker 14 in the test volume. Unfiltered data shown for waggle trial 3704.

in space, then these would have been most evident in the thigh marker co-ordinates. This is demonstrated in Figure 3.26. The thigh markers were exhibiting deviations from their mean separations of up to 11mm. Once this data had been filtered with a 6Hz low pass filter there were still significant changes in the distances between markers, though they had been reduced to approximately 7mm (Figure 3.27).

The pattern of errors suggested that they were associated with the location of the marker in space, as the large deviations were for several frames of data. Further examination of the full waggle trial (Figure 3.28) showed a repeated pattern of deviation approximately in line with the motion of the artificial model leg. Further evidence of this effect was demonstrated by a plot of the thigh marker number 14's (lateral thigh) co-ordinates alongside the deviations of the distances between marker 14 and 12 and 22. Figure 3.29 shows that the deviations from the mean separation values correlated with motion in the test volume.

The accuracy of the location of markers in space by the motion analysis system depended on how accurately the system could locate the cameras around the test area. Calibration of the system was performed to enable the system to do this. Upon viewing a calibration object, consisting of known marker placements about the test volume, the system located each camera so as to minimise the distance between where all the calibration markers were and where the cameras predicted them to be. The calibration residual, output by the motion analysis system software, provided an estimate of the 'average miss'. The calibration residual was less than 3mm for the work carried out for this thesis. The error in location of the markers within the test area was not, however, so easily defined. Each camera had its own errors for different locations in space. When more than one camera could see a marker, its location was calculated using a number of different factors associated with acceptable limits of marker detection within the system software. The method used was such that the error in location would have been dependent on the error associated with each of the cameras that could see the marker. Jumps in marker location would have been expected when the number of cameras that could see a marker changed. The combination of the effect of changing number of cameras viewing a marker and changing levels of accuracy for each camera within the test volume would have combined to produce unknown, but not necessarily random errors in marker location. These factors could explain the inability of the various methods to reduce the error in hip joint centre location.

The analysis based on a rigid, fixed hip joint centre model did not take into account the systematic errors associated with skin movement with respect to the underlying bone that would have occurred in human subjects. It is difficult to predict the effect of skin movement on the accuracy of this method. To fully test the method's ability to locate the hip joint centre in human subjects it would have been necessary to use X-ray or similar methods. No such method of assessment was possible.

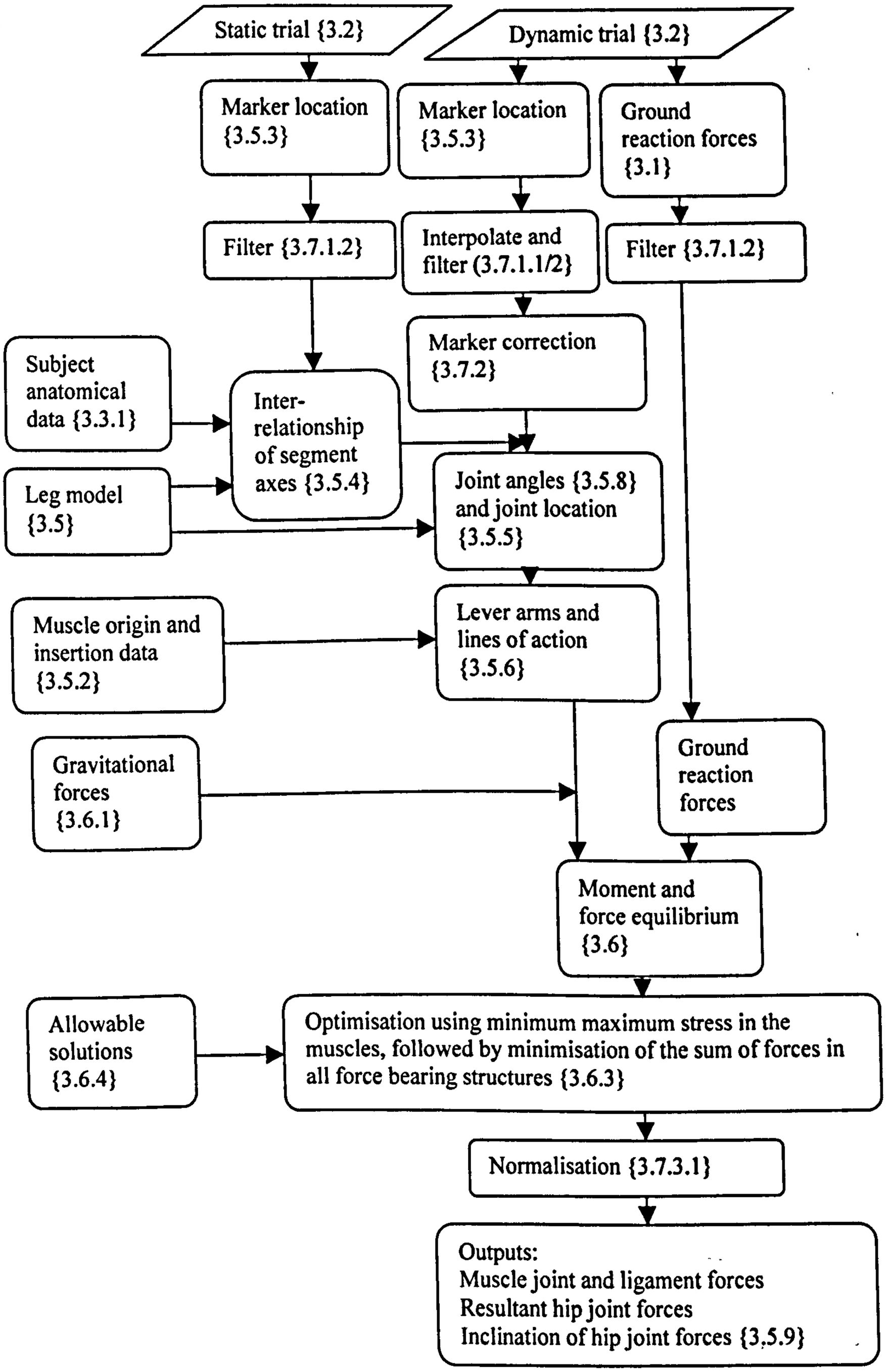

Figure 3.30 Over-view of methods used to calculate hip joint forces from motion analysis data. (brackets, { }, are used to indicate the relevant section of the thesis)

3.7.4.5 Conclusion

No method of improving the results of the hip joint centre algorithm could be found that was reliable or predictable in its improvement of the results over the initial attempts using unfiltered waggle trial data and 100 frames of static trial data filtered at 10Hz.

This method could locate an ideal joint centre to within approximately 15mm of its true location.

The reason for this lack of accuracy was that errors in marker location demonstrated dependence on location within the test volume. These errors may have been associated with a change in the number of cameras that were used to calculate the position of the marker.

This method of hip joint centre location was considered to be too inaccurate for implementation in subjects. It was, therefore discarded in favour of a fixed hip joint centre calculated after Bell et al [1990].

3.8. Software

All methods were implemented using the Turbo Pascal 7.0 programming language (Borland International Inc.).

3.8.1 Flow chart

Figure 3.30 illustrates the order of implementation of the methods described in this chapter for the processing of motion analysis data to obtain hip joint forces.

Table 4.1 Total number of trials per activity per subject subgroup

	Walking	Stair, ascent	Stair, descent	Ramp, ascent	Ramp descent	Camber, up side	Camber, down side
5 Male (5L, 5R)	30	28	24	27	26	25	26
6 Female (6L, 6R)	34	34	35	35	37	35	34
4 HJR, natural side (4R)	12	11	11	12	12	13	12
5 HJR, THR side (5L, 1R)	20	17	12	17	17	20	15

Number of legs in brackets. R = right leg, L = left leg
HJR = subjects with total hip joint replacements
THR side = side of the total hip replacement

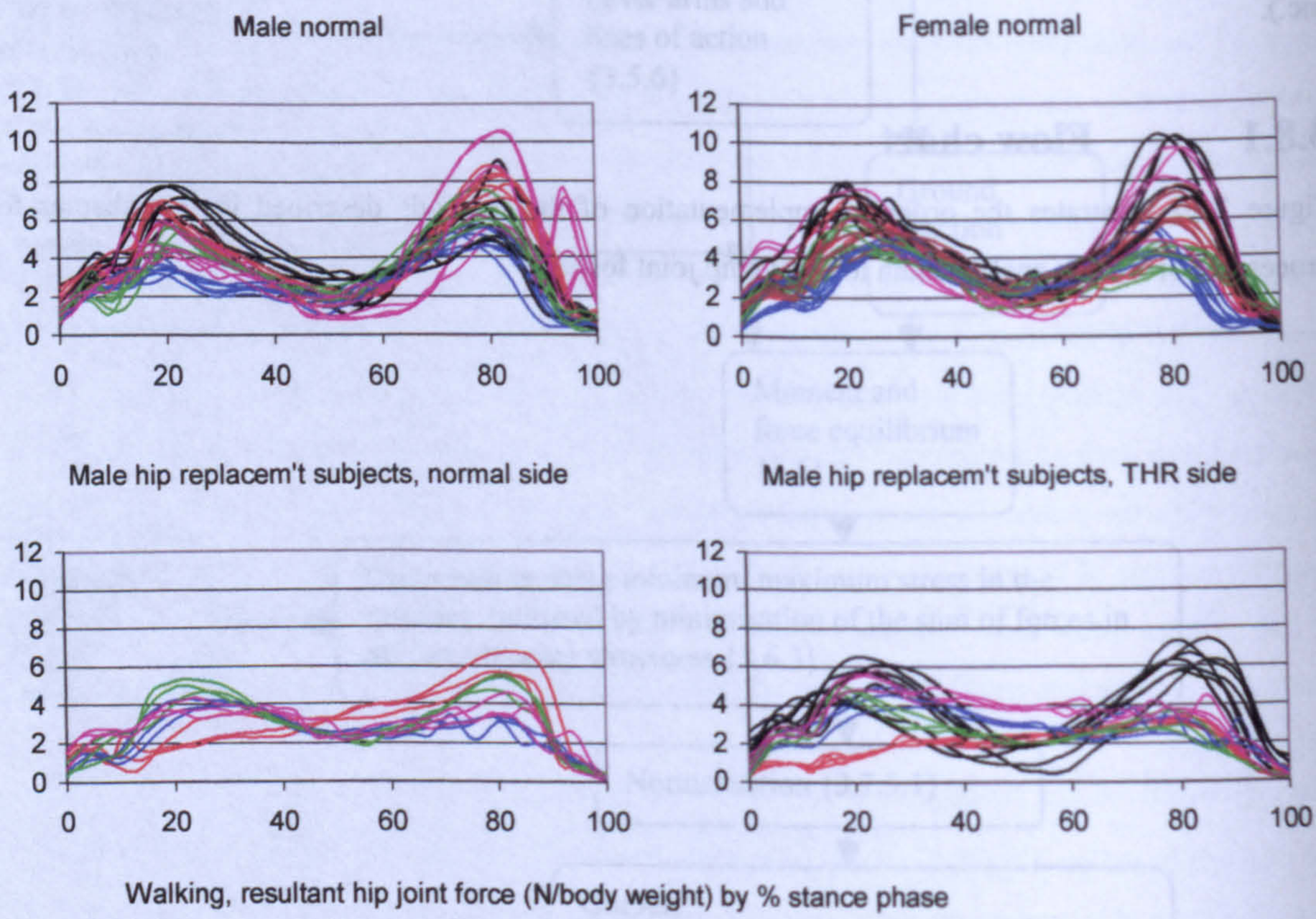

Figure 4.1 Example of results presentation format

Chapter 4 Results

4.1 Introduction

Although it has been possible to include all results on the forces developed at the hip joint only a selection of joint angle, intersegmental joint forces and moments, knee and ankle joint force and muscle force results are presented. These have been selected to provide examples of the results. Where possible both walking and stair ascent results have been included in full to provide an illustration of an activity with small joint range of motion and one with large joint motion range.

All results are included in Appendix VI. A common format has been adopted for the main results presentation. Figure 4.1 provides an illustration of this format. Four graphs are presented. Male and female subjects are presented separately as are the natural and replaced sides of the male hip replacement subjects. All trials successfully recorded are illustrated. Each subject's results have been represented by a particular colour (as indicated in Appendix VI and as illustrated in the fold-out sheet inside the back cover). All scales of the four graphs have been made identical to allow direct comparison between the groups' results. No attempt has been made to make the scales the same for the same variable across activities. Suitable scales have been chosen for each of the variables to allow as much detail as possible to be observed. All X-axes represent 100% of the stance phase. Y-axis variables have been defined in the figure subtitle.

The results are presented in 6 sections:

Appendix VI.3.1 Joint angles

Appendix VI.3.2 Intersegmental joint forces and moments

Appendix VI.3.3 Muscle forces

Appendix VI.3.4 Hip joint forces

Appendix VI.3.5 Knee and ankle joint forces

Appendix VI.3.6 Ground reaction forces

A list of figures has been included at the beginning of each section of the appendix to allow particular results to be located. All appendices have been allocated independent page and figure numbering.

Table 4.1 gives details of the number of trials recorded for each activity by subject sub group. Male, female, hip joint replacement subject's natural sides and replaced sides have been grouped. All left and

right side results have been included together. The number of right and left sides recorded in each subgroup has been indicated. For some of the subjects it was not possible to obtain three satisfactory results for each of the activities. This is reflected in the total number of trials per activity. Where marker detection was particularly trouble free, with no interpolation required, up to four sets of results per subject have been included.

In general the both male and female normal and male hip replacement subjects were able to complete all tasks in a normal manner. In other words with heel strike and toe off in walking and camber. There was, however, variation in the occurrence of heel strike in stair and ramp activities, although none of the subjects had markedly abnormal patterns of movement.

4.2 Cadence, stride length and speed

To characterise further the subjects' movement patterns, cadence, stride length and speed are presented in Appendix VII. Cadence (strides/min) was calculated using timings of the opposite foot initial contacts, one before the beginning of stance of the leg being studied and one towards the end of stance. Speed (m/s) was taken as the average speed of the mid-posterior superior iliac spine marker over approximately two strides of the opposite leg about the period of stance being studied. Stride length (m) was calculated using the cadence and speed measures. For stair ascent and descent cadence only has been presented. Cadence, stride length and speed are also all presented in normalised, dimensionless form (after Hof [1996]). The following definitions of normalised quantities have been used:

Normalised cadence = cadence [strides/s] × {√(height [m] / acceleration due to gravity [m/s^2])}
Normalised stride length = stride length [m] / height [m]
Normalised speed = speed [m/s] / {√(height [m] × acceleration due to gravity [m/s^2])}

The method of normalisation used for these temporal distance parameters allows comparison between individuals and allows two individuals with the same normalised cadence, stride length and speed but of different heights to have dynamically similar patterns of motion.

4.2.1 Walking

All subjects appeared to have a normal walking pattern, with heel strike and toe off. There was a wide variation in the average cadence, stride length and speed of the subjects (Table A-VII.1). Normal male and normal female results were similar. One exception to this was female subject 35 who walked with very high cadence, which resulted in a high normalised speed of 0.49, considerably higher than all other subjects. Male hip replacement subject 27, walked with a lower cadence than all other subjects. This

resulted in a relatively slow normalised speed. Male hip replacement subject 26 walked with a long stride length and high cadence compared to the other hip replacement subjects resulting in a higher normalised speed.

4.2.2 Stair ascent and descent

Males and females demonstrated approximately the same range of cadence for both stair ascent and descent (Table A-VII.2). The exception to this was female subject 35 who demonstrated high cadence in ascent and very high cadence, 89 strides/min, in descent. All hip replacement subjects had lower cadence rates compared to the normal subjects for both ascent and descent. Male hip replacement subjects 26 and 27 both demonstrated particularly low stair ascent and descent cadence.

4.2.3 Ramp ascent

Male and female normal results were approximately the same (Table A-VII.3). Notable exceptions to this were male normal subject 20 who had a relatively long stride length, and female normal subject 35 who exhibited a high cadence compared with all other subjects. Hip replacement subjects tended to ascend at lower cadence and with shorter step lengths than normal subjects. Male hip replacement subject 27, ascended slower than all other subjects.

4.2.4 Ramp descent

Male and female normal results covered similar ranges (Table A-VII.4). Notable exceptions were male normal subject 20, with long normalised stride length and female normal subject 35, who had both a high cadence and long normalised stride length. Male hip replacement subjects had lower cadence than normal subjects, resulting in lower normalised speeds. Subject 27 exhibited particularly low cadence and stride length.

4.2.5 Camber foot up and foot down

The cadence, stride length and speed of the camber foot up and camber foot down were approximately the same for all subjects. Male and female normal subjects exhibited the same range of cadence, stride length and speed. Exceptions to this were male normal subject 20 with high normalised stride length and female normal subject 35, who exhibited very high cadence and high normalised stride length. In general male hip replacement subjects used a lower cadence than normal subjects. Subject 26 had a longer normalised stride length than all other hip replacement subjects and subject 27 had a very low cadence.

4.3 Ground reaction forces

Ground reaction forces on the foot are presented in Appendix VI.6. The forces are reported as three components. These components were calculated in the laboratory co-ordinate system. All activities were performed along approximately the X-axis of the laboratory. The X-axis components are, therefore, approximately the anterior-posterior ground reaction forces, the Y-axis the vertical forces and the Z-axis the medio-lateral forces. The sense of the results has been corrected so that all X-axis forces are presented as anteriorly directed force on the foot as positive and all Z-axis forces are presented as laterally directed forces on the foot.

4.3.1 Walking

Anterior-posterior ground reaction force (Figure A-VI.6.1) demonstrated an initial posteriorly directed peak with reversal to an anteriorly directed peak for all subject groups. In general the peak values of the hip replacement subjects' forces were lower than those of the normal subjects. The notable exception to this was hip replacement subject 26 (black). This subject demonstrated forces of the same magnitude as the normal subjects.

The double peak pattern of the vertical ground reaction force (Figure A-VI.6.2) was present for all subjects. For the hip replacement subjects, however, there were several subject who demonstrated very low peaks as compared to the mid stance trough in the force traces. Female normal subject 35 (pink) demonstrated a particularly low trough value in mid stance accompanied by high peak values. Hip replacement subject 26 (black) demonstrated higher forces than all other high replacement subjects.

Medio-lateral ground reaction forces demonstrated an initial laterally directed peak then two medial peaks. This pattern was not, however, consistent across all the subjects. Female normal subject 19 (red) exhibited particularly low medial forces.

4.3.2 Stair ascent

All groups of subjects demonstrated a peak of posteriorly directed force before 20% of stance (Figure A-VI.6.4). There was, however, a marked difference between the normal and hip replacement subjects in the second half of stance. The normal subjects demonstrated a peak at approximately 90% of stance that was not present in most of the hip replacement subjects' traces.

Hip replacement subjects demonstrated lower vertical ground reaction forces than normal subjects (Figure A-VI.6.5). There were notable differences in the timing of the first peak between the male normal subjects.

All subject groups demonstrated the same patterns of medio-lateral ground reaction forces (Figure A-VI.6.6).

4.3.3 Stair descent

The anterior-posterior forces indicate that there were several different modes of stair descent being employed. Late occurrence of the posteriorly directed peak was observed in one male subject (14, red). This peak did not occur for one female normal subject (35, pink). There was erratic occurrence of a relatively large posteriorly directed force in one of the female normal subjects (33, blue) and two of the male normal subjects (29, green, 38, pink).

The second peak of the vertical ground reaction force was consistently lower than the first peak for all subject groups (Figure A-VI.6.8).

Similar patterns were demonstrated by all subject groups for medio-lateral ground reaction force (Figure A-VI.6.9).

4.3.4 Ramp ascent

The patterns of the subject groups' ramp ascent ground reaction forces were all similar. Female normal subject 35 (pink) demonstrated particularly erratic medio-lateral ground reaction force in the first part of stance (Figure A-VI.6.12).

4.3.5 Ramp descent

Female subject 35 (pink) demonstrated a different pattern of anterior-posterior ground reaction force than the other subjects in the first part of stance (Figure A-VI.6.13), this was accompanied by higher vertical (Figure A-VI.6.14) and medio-lateral forces (Figure A-VI.6.15).

4.3.6 Camber foot up and foot down

There were only minor differences between the ground reaction forces developed during the camber traverse and walking. There were indeed only minor changes between the two sides of the camber (Figures A-VI.6.16-21). One difference was that the medio-lateral ground reaction force on the camber down side was higher than that for either walking or the camber up side.

4.4 Joint angles

Hip and knee joint angles are presented in Appendix VI.3.1. Hip and knee flexion, abduction and rotation angles are presented for walking and stair ascent (Figures A-VI.3.1.1 to 12). Hip and knee flexion angles are presented for all other activities (Figures A-VI.3.1.13 to 21). All results are presented in degrees with angles defined as in Section 3.5.8.

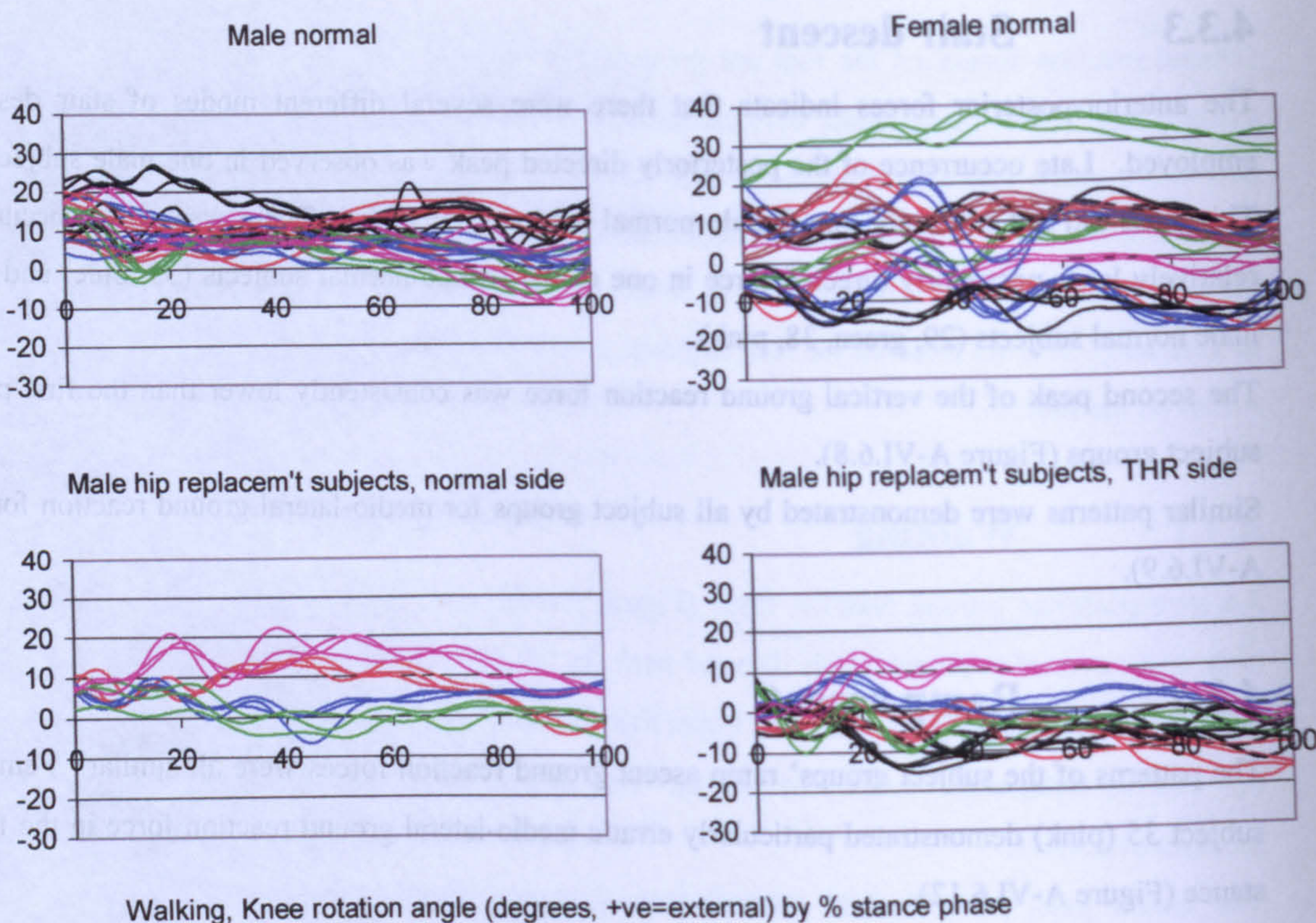

Figure 4.2 Walking, knee rotation angle

4.4.1 Walking

Hip flexion abduction and rotation angles are presented (Figures A-VI.1.1 to 3) followed by knee flexion, abduction and rotation (Figures A-VI.1.4 to 6).

Male and female normal subjects' hip flexion (Figure A-VI.1.1) traces were similar in form. Male subject 20 (pink) exhibited particularly high extension in late stance compared to the other normal subjects. In general the range of the male hip replacement subjects' hip flexion was lower. The exception to this being subject 26 (black) who exhibited a wide range of motion, with relatively high extension in late stance. Normal and replaced sides of the hip replacement subjects were similar except for subject 27 (red), whose replaced side showed a range of motion approximately 10° less than that of their normal side.

The patterns of male and female normal subjects' hip abduction (Figure A-VI.1.2) were different in character. The female traces had a distinct adduction peak at approximately 40% of stance. This was not as distinct in the male subjects. Male hip replacement subjects' abduction covered the same range as the normal subjects. Subject 27 (red) exhibited an unsymmetrical pattern.

Male normal subject's hip rotation angle (Figure A-VI.1.3) fell mainly within the –10 to +10 degrees band. Female normal subject 33 (blue), however, had a hip rotation angle of approximately 0° on one side and 20° on the other. Female subject 19 (red) also appeared to have a difference between sides, this being of approximately 15° in magnitude. Hip replacement subjects 26 (black) and 28 (blue) had approximately the same rotation angle on both sides, however, subjects 27 (red) and 29 (green) had differences of 20° and 15° respectively.

Male and female normal subject's knee flexion angles (Figure A-VI.1.4) were similar in range and pattern. Male hip replacement subjects exhibited the same pattern of knee flexion as normal subjects although asymmetry in subject 27 (red) was observed with the subject's replaced side flexing by approximately 20° less at 30% of stance than his natural side. Subject 26 (black) exhibited a wide range of knee joint motion comparable with the extremes of the normal subjects' range.

Both normal and hip replacement subjects' knee abduction angles (Figure A-VI.1.5) were mostly within the -10° to +10° range. There appeared to be consistency between sides of the normal subjects and the hip replacement subjects' natural and replaced sides.

Knee rotation angle (Figure A-VI.1.6) varied considerable within the female normal subjects (see Figure 4.2). Female normal subject 34 (green) exhibited a particularly high external rotation angle of up to 40°. Asymmetry in subjects 34 (green), 19 (red) and 33 (blue) was also observed. Male normal and hip replacement subjects' results covered approximately the same range of -20° to +20°.

4.4.2 Stair ascent

Stair ascent hip flexion angle (Figure A-VI.1.7) was similar in character and range for all subject sub groups although hip replacement subjects tended to have lower hip flexion in late stance than the normal subjects.

Male normal subject 20 (pink) exhibited high abduction throughout mid to late stance compared to the other male normal subjects. Female normal subjects (Figure A-VI.1.8) had a peak in adduction at approximately 15% of stance that was not as distinct in the male subjects. Male hip joint replacement subject 27 (red) exhibited asymmetry with high abduction in the normal side and adduction in the replaced side in early stance.

The majority of hip rotation angles (Figure A-VI.1.9) were within the range -10° to +20°. Female normal subject 33 (blue), however, exhibited asymmetry and a maximum hip external rotation angle of almost 40°. There was also asymmetry in the hip replacement subjects with approximately 20° difference between natural and replaced sides in subjects 27 (red) and 29 (Green).

The range of normal and hip replacement subject's knee flexion angles (Figure A-VI.1.10) were approximately the same. The exception to this was female normal subject 35 (pink) who maintained relatively high knee flexion throughout late stance.

Knee abduction angles (Figure A-VI.1.11) were similar for all subject groups. Female subject 33 (blue), however, exhibited particularly high abduction throughout stance.

Female normal subjects showed a wide range of knee rotation angles (Figure A-VI.1.12) compared to all other subgroup often with high levels of asymmetry (e.g. subject 34 (green)). Apparently anomalous results appeared in male normal subject 20's (pink) traces at 60% of stance.

4.4.3 Stair descent

Hip flexion in stair descent (Figure A-VI.1.13) followed approximately the same trend for all subjects although there was a 20° range of result magnitudes. Knee flexion angles (Figure A-VI.1.14) patterns were also similar in normal and hip replacement subjects.

4.4.4 Ramp ascent

Hip flexion angles (Figure A-VI.1.15) of normal and hip replacement subjects followed the same pattern, although hip replacement subject 27 (black) exhibited greater extension in late stance than all other subjects. In general the replaced sides of the hip replacement subjects were less flexed during early stance.

Male hip replacement subject 27 (red) exhibited asymmetry with lower knee flexion (Figure A-VI.1.16) in early stance in the replaced side.

4.4.5 Ramp descent

Male normal subject 20 (pink) showed high hip extension (Figure A-VI.1.17) in late stance compared with the other male normal subjects. Male hip replacement subject 27 (red) used only 10 degrees of range of motion in the replaced side compared to 25 degrees in the natural side. Hip replacement subject 26 (black) exhibited high hip extension in late stance.

Knee flexion of normal male subject 20 (pink) was lower than all other normal subjects in mid to late stance. Male hip replacement subject 26 (black) exhibited low flexion in late stance.

4.4.6 Camber foot up and foot down

There were only minor differences in the hip (Figures A-VI.1.19 and 21) and knee (Figures A-VI.1.20 and 22) flexion angles between the camber foot up and camber foot down activities. The most notable was that of hip replacement subject 27's (red) knee flexion during early stance. These two sets of results will therefore be detailed together in this section.

Male normal subject 20 (pink) exhibited high hip extension in late stance as did hip replacement subject 26 (black). Hip replacement subject 27 (red) exhibited low peak hip flexion in early to mid stance on the replaced side.

Male hip replacement subject 26 (black) exhibited a large swing to lower knee flexion in late stance than did the other hip replacement subjects. The initial peak in knee flexion at 30 % of stance was 20° lower for hip replacement subject 27 (red) on the replaced side than on the natural side.

4.5 Intersegmental forces and moments

Intersegmental forces and moments for hip, knee and ankle joints are presented for walking and stair ascent (Appendix VI.2). Camber ankle joint ZAA intersegmental forces have also been presented. Forces and moments have been defined along and about particular axes systems. At the hip the femoral anatomical system has been used. At the knee and the ankle the knee anatomical and ankle anatomical axes systems have been used respectively. Thus when examining these results it must be taken into account that the axes systems would have been moving with the limb and that, therefore the patterns of forces and moment generated would have been affected by limb position in space. In the following sections only those traces that were noticeably different from the others will be detailed. All figures can be found in Appendix VI.2. Forces are presented as force divided by body weight (N/body weight) and moments as Nm divided by body mass (Nm/body mass).

4.5.1 Walking

4.5.1.1 Intersegmental forces

The hip replacement subjects exhibited large variations in XFA force (Figure A-VI.2.1). Subject 26 (black) exhibited large positive and negative values. Subject 27 (red) had an asymmetrical pattern with the replaced side showing very low XFA force.

Female normal subject 35 (pink) had both higher peak values and lower trough values of YFA force (Figure A-VI.2.2) than all other normal subjects. All hip replacement subjects except 26 (black) exhibited smoother traces of YFA force than normal subjects. The trace of subject 27 (red) exhibited little difference between peak and trough values of YFA force.

All normal and hip replacement subjects had the same pattern of ZFA force (Figure A-VI.2.3) although hip replacement subjects 27 (red) and 28 (blue) had relatively lower forces.

All subjects' results followed the same trends of XKA force (Figure A-VI.2.4). Hip replacement subject 27 (red) exhibited a positive XKA force up to mid stance, this was not typical of the other subjects. Hip replacement subject 26 (black) exhibited a more pronounced first negative peak than other hip replacement subjects.

YKA force in all subjects was characterised by a double peak pattern. Female normal subject 35 (pink) and hip replacement subject 26 (black) had higher peak and lower trough values of YKA force than other subjects. Of the hip replacement subjects subject 27 (red) had the least difference between peak and trough values. All hip replacement subjects except subject 26 (black) had less range between peak and trough values than normal subjects.

There was a lot of variation in the patterns of ZKA forces in male and female normal subjects. Male normal subject 8 (black) demonstrated particularly low forces as did female normal subject 33 (blue). Male hip replacement subject 26 (black) exhibited a higher negative peak at 20% of the stance phase than all other subjects.

All normal and hip replacement subjects demonstrated the same pattern of XAA force. The replaced side of hip replacement subjects did, however, not have as distinct a first negative peak (with the exception of subject 26 (black)), subject 27 (red) exhibiting a particularly low value.

YAA force was similar in character to the YKA force pattern. Female normal subject exhibited greater peak to trough range than all other normal subjects. Hip replacement subject had only small differences between peak and trough values (with the exception of subject 26 (black)).

ZAA forces were almost always negative for all subjects. The hip replacement subjects exhibited smaller differences between peak and troughs of the negative profiles (with the exception of subject 26 (black)).

4.5.1.2 Intersegmental moments

Intersegmental hip moments about the XFA axis (Figure A-VI.2.10) followed the same trends in all subjects. The exceptions to this were hip replacement subjects 27 (red) and 28 (blue), who both exhibited smoother patterns than all other subjects. Subject 27 (red) had neither first nor second peaks (at 20 or 80% of the stance phase) and 28 (blue) had no second peak.

The pattern of YFA moment of the hip (Figure A-VI.2.11) replacement subjects was the same as that of the normal subjects, but was in general of a lower magnitude.

Hip replacement subject 27 (red) exhibited a degree of asymmetry in ZFA moment (Figure A-VI.2.12) profile, with the replaced side sustaining moment of smaller magnitude.

Female subject 34 (green) exhibited unsymmetrical knee XKA moment (Figure A-VI.2.13). Female subject 33 (blue) showed a large negative peak in early stance. Hip replacement subject 28 (blue) exhibited high values over most of the stance period.

The YKA moment (Figure A-VI.2.14) profile of male normal subject 8 (black) exhibited a different peak in late stance than all other subjects.

All ZKA moment (Figure A-VI.2.15) traces followed the same general pattern.

Ankle XAA moment (Figure A-VI.2.16) tended to be either predominantly positive or predominantly negative. Male normal subject 8 (black) exhibited a peak in late stance which did not follow the same pattern as any of the other subjects.

Both ankle YAA and ZAA moments (Figures A-VI.2.17 and 18 respectively) followed the same patterns with initial negative peak followed by higher magnitude positive peak at approximately 80% of stance.

4.5.2 Stair ascent

4.5.2.1 Intersegmental forces

Stair ascent intersegmental forces are illustrated in Figures A-VI.2.19 to 27. In general the magnitude of the forces sustained by the hip replacement subjects were lower than those of the normal subjects. Notable features of the traces include the following:

Female subjects exhibited high ZFA forces (Figure A-VI.2.21). Female subject 35 exhibited high second peaks of both knee XKA force (Figure A-VI.2.22) and ankle XAA force (Figure A-VI.2.25). Female subject 34 (green) exhibited positive knee ZKA force (Figure A-VI.2.24) compared to other subjects whose forces were predominantly negative. All subjects exhibited negative ZAA force (Figure A-VI.2.27).

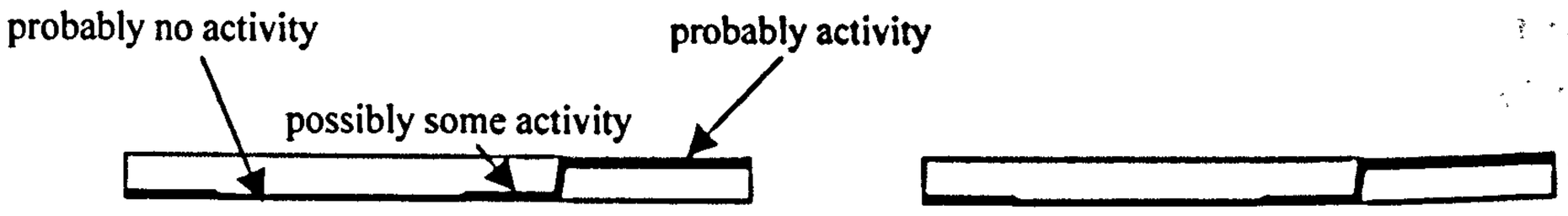

Figure 4.3 Example of emg activity after University of California [1953].

4.5.2.2 Intersegmental moments

Notable features of the intersegmental moments (Figures A-VI.2.28 to 36) follow:

In general the hip joint replacement subjects intersegmental moments were lower in magnitude than those of the normal subjects. Subject 26 (black) was, however, often an exception to this with profiles similar to those of the normal subjects. Hip replacement subject 27 (red) exhibited asymmetry in ZFA, ZKA and YAA moments (Figures A-VI.2.30, 33 and 35 respectively), and exhibited relatively low ZAA moment (Figure A-VI.2.34). Female normal subject 34 (green) showed a large negative XKA (Figure A-VI.2.31) in early stance compared to other subjects. Hip replacement subject 26 (black) exhibited a particularly erratic XKA (Figure A-VI.2.31) profile. In the XAA moment (Figure A-VI.2.34) male normal subject 20 (pink) showed a large positive magnitude for most of stance and female normal subject 34 (green) a large positive value in late stance.

4.5.3 Camber foot up and foot down

ZAA force for both camber foot up and camber foot down was negative for all subjects (Figure A-VI.2.37 and 38). In general camber foot up ZAA force was lower in magnitude than that of camber foot down. This was not, however, true for all subjects. Hip replacement subject 27 (red) exhibited different patterns for replaced and natural sides for both camber up and camber down sides. In general hip replacement subjects exhibited smoother profiles than normal subjects.

4.6 Muscle forces

All muscle forces have been normalised by the subject's body weight to allow comparison between individuals. An additional feature has been included in the muscle force results (Appendix VI.3). To allow comparison with published emg data the results of University of California [1953] have been incorporated. Where appropriate these results have been presented above the relevant muscle force graphs. The information in University of California [1953] did not represent the same muscle set as that used in this study. For comparison with adductor magnus, gluteus maximus, gluteus medius, gluteus minimus and gastrocnemius, represented in this thesis as multi-elemented, the single result of University of California [1953] has been used. Two different activity patterns were presented for adductor magnus and gracilis in University of California [1953]. Both of these have been reproduced above the relevant figures. For all other sets of data the appropriate emg muscle activity pattern has been reproduced twice above the graphs. The emg data has been reduced to three conditions. An example of this is presented in Figure 4.3. The upper level represents the average characteristic patterns as determined by University of

California [1953] and has been used to represent probable muscle activity, the middle level indicates that there was activity in the muscle of one or more of the subjects studied and represents possible activity. The base level has been used to represents no recorded activity and, therefore, probably no muscle activity. When comparing the results of this study with the emg patterns the delay in the development of muscle force following electrical activation must be taken into account. A 0.08 second time-lag between peak electrical activity and peak of maximal tension has been found. This would have been approximately 10% of the stance phase.

Muscle activity patterns are illustrated in terms of their force normalised by body weight. All muscle forces for walking (Appendix VI.3A) and stair ascent (Appendix VI.3B) have been included. Forces in the quadriceps femoris and calf muscles have also been included for all other activities (Appendix VI.3C). The patterns of muscle force development will not be described in detail. Brief details of the comparison between the displayed emg results of University of California [1953] and the patterns calculated for this thesis will be given.

It was observed that there was a variation in the muscle activation patterns chosen between individuals. Also that a number of muscle activation patterns were not smooth in character, but appeared to indicate muscles switching on and off a number of times during stance. There were a number of uncharacteristically large muscle force magnitude spikes. All of these observations will be discussed in the next chapter.

4.6.1 Walking

Muscle patterns of walking are illustrated in Figures A-VI.3A.1 to 47. Only the most significant features of these variables will be detailed.

There was little or no force in a number of muscles. These included adductor brevis (superior and inferior), gemellus inferior and obturator externus and internus. Particularly for the hip joint replacement subjects there were only very small or no forces in the quadratus femoris and the gemellus superior.

Adductor magnus muscle forces elements tended to followed the second emg pattern as described by University of California [1953] rather than the first.

Force was predicted in the gluteus maximus 1 muscle element over a greater range of the tests than was indicated by the emg pattern. The other elements of the muscle force, 2 and 3, however, followed the emg pattern.

The gluteus medius muscle and gluteus minimus elements all followed approximately the same double peak pattern of force, although the third element did not show as distinct a second peak as the first two for the hip replacement subjects.

In general the iliacus force conformed to that indicated by the emg pattern.

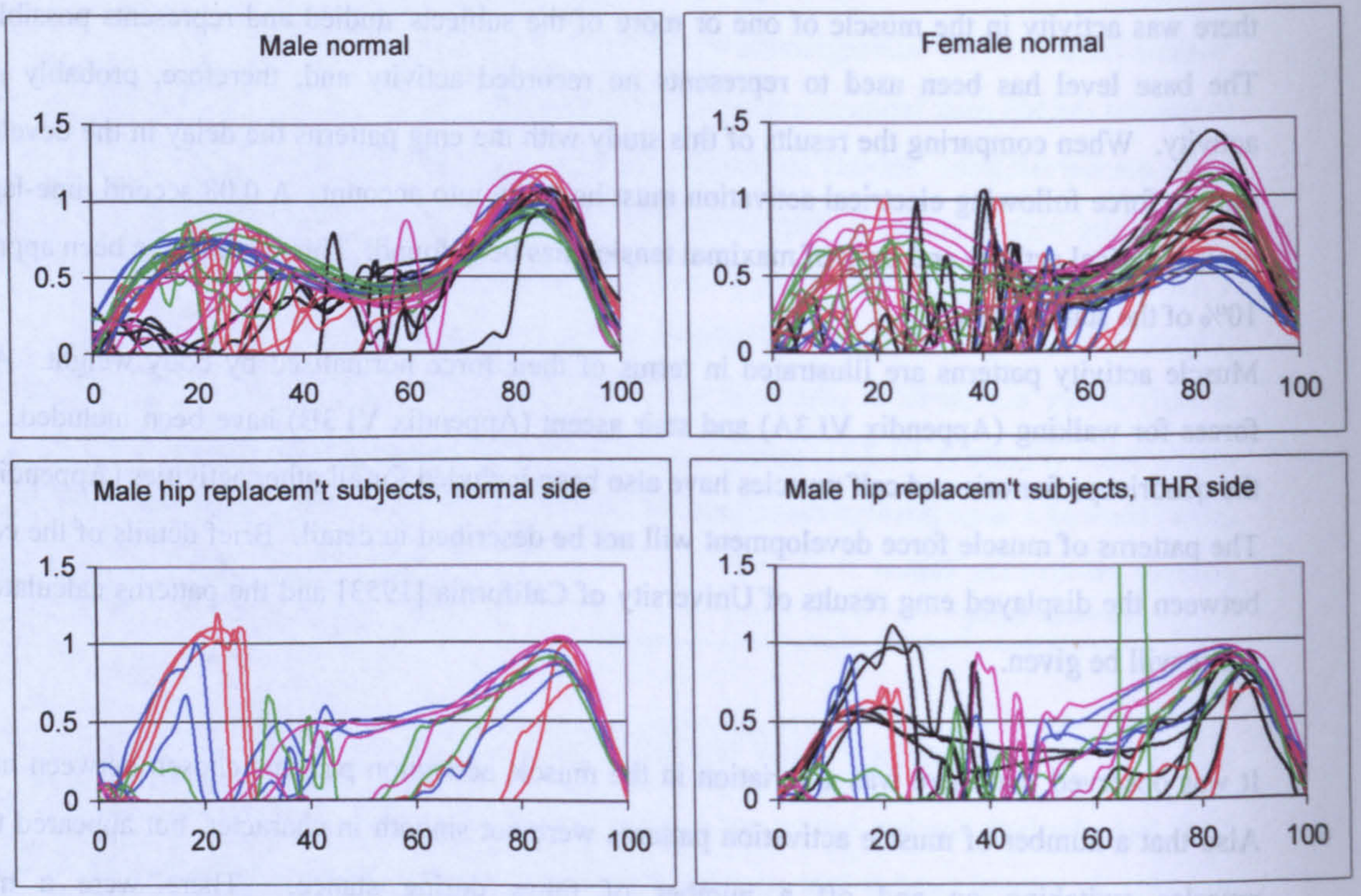

Figure 4.4 Stair ascent muscle force, gastrocnemius (M)

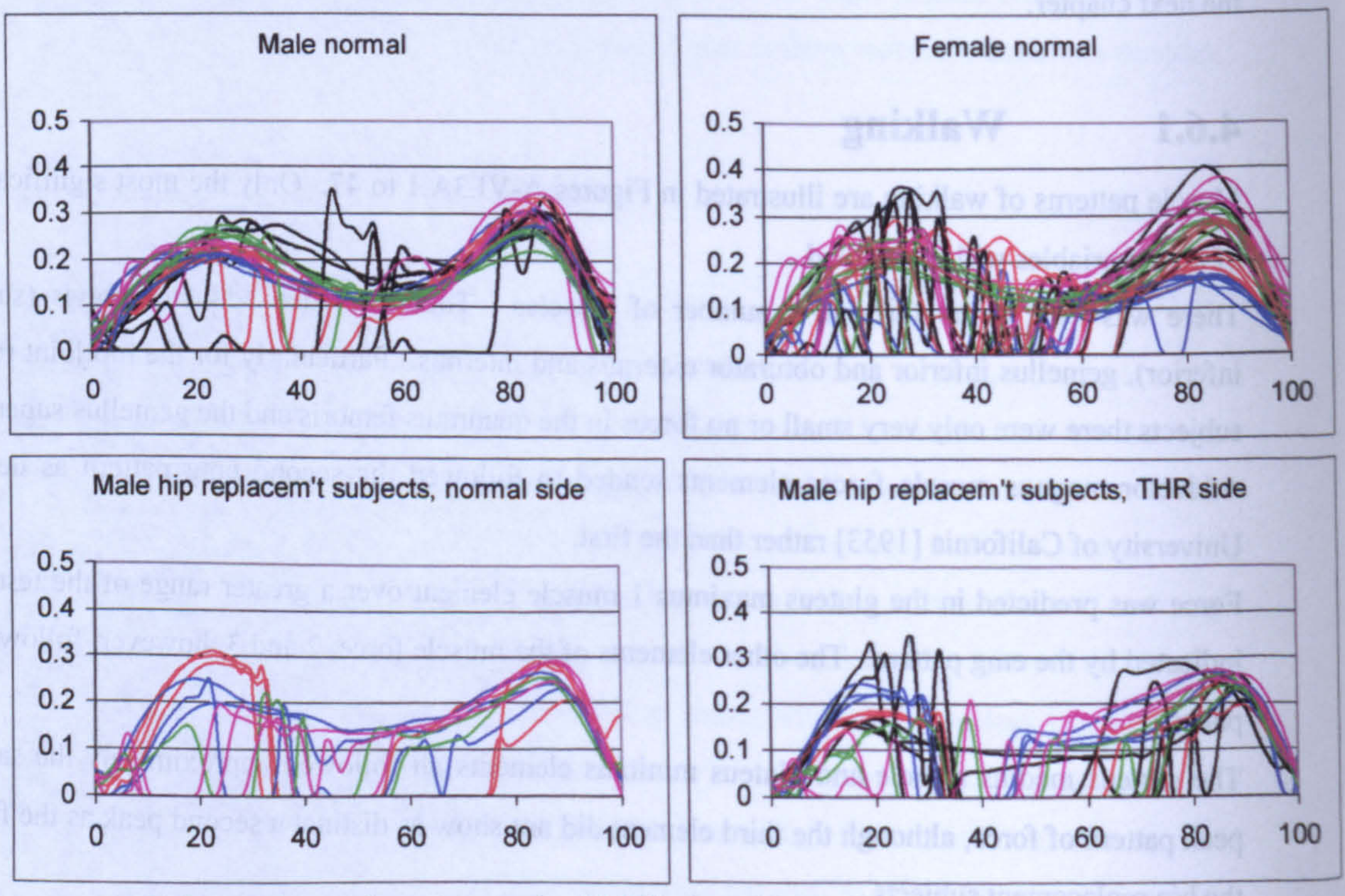

Figure 4.5 Stair ascent muscle force, gastrocnemius (L)

The psoas and pectineus demonstrated late stance force particularly in the normal subjects.

Piriformis force tended to occur in early stance. A notable exception to this was normal female subject 33 (blue) who exhibited a large peak at 75% of stance.

Biceps femoris long head muscle force tended to occur in early stance. Biceps femoris short head force tended to occur in mid to late stance peaking at 80% of stance.

Gracilis had a minor peak in early stance and then a peak at 80% of stance. Hip replacement subjects did not tend to exhibit this second peak.

Rectus femoris (upper part) exhibited a double peak pattern, although this pattern varied between individuals.

Sartorius force occurred immediately after initial foot contact then reduced to zero before rising again to peak first at approximately 20% and then at 80% of stance.

Semimembranosus force was present across the stance phase. This was not indicated by the emg. Hip replacement subjects did not show as much force as normal subjects, indeed subject 27 (red) showed little force at all.

Semitendinosus muscle forces tended to occur over the 0 to 70 and 80 to 100% ranges of stance. Hip replacement subject 38 (pink) demonstrated force over the whole of stance phase.

Tensor fascia lata force was calculated over all of the stance phase from 5%. This tended to form a two peaked pattern.

The gastrocnemius muscle elements demonstrated approximately the same patterns, being active from approximately 30 to 100% of stance. Not all subjects demonstrated force for all of this period, however, with indications of rapid reduction of muscle forces to zero value.

The soleus muscle forces of all subjects followed the same general pattern. There were, however, a number of traces that demonstrated abrupt changes in value. The general force patterns were compatible with the emg profiles.

Vastus intermedius force exhiited an initial large peak at approximately 20% of stance and a minor peak at approximately 95% of stance. This was in agreement with the emg profiles.

There was little force in the vastus lateralis and medialis compared to the intermedius. The force that was calculated was in agreement with the emg data.

Tibialis posterior only showed force in the early part of stance. The emg data suggested that force should be present for a large proportion of stance, this was not calculated.

Flexor digitorum longus force was only predicted for a small proportion of stance for a few subjects. This was not in agreement with the emg data which suggested force across most of the stance phase.

Flexor hallucis longus force tended to occur in the second half of stance. The patterns calculated were not consistent across the subjects. The emg data suggested that a more consistent pattern across the 40 to 90% range might have been expected.

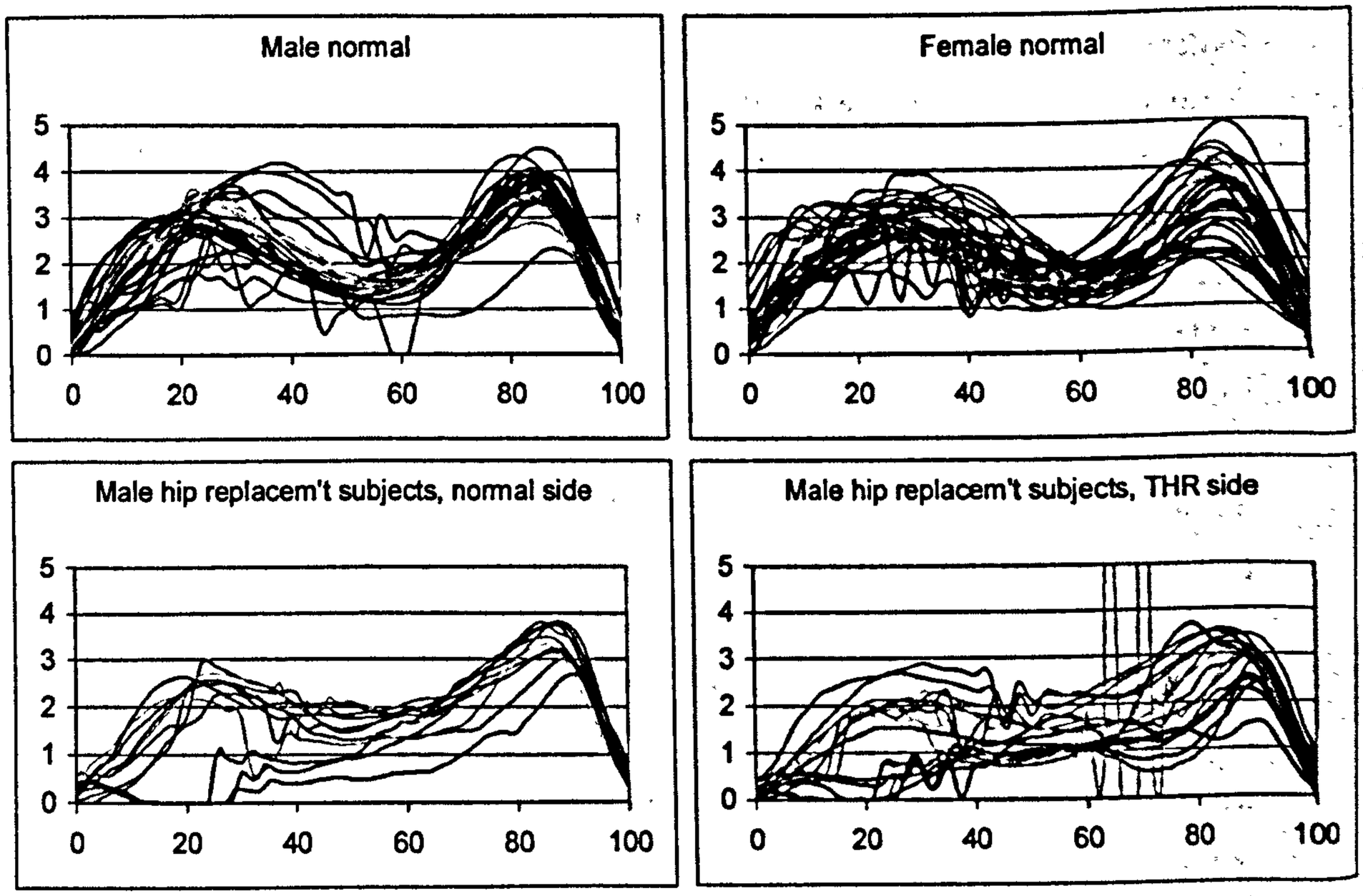

Figure 4.6 Stair ascent muscle force, soleus

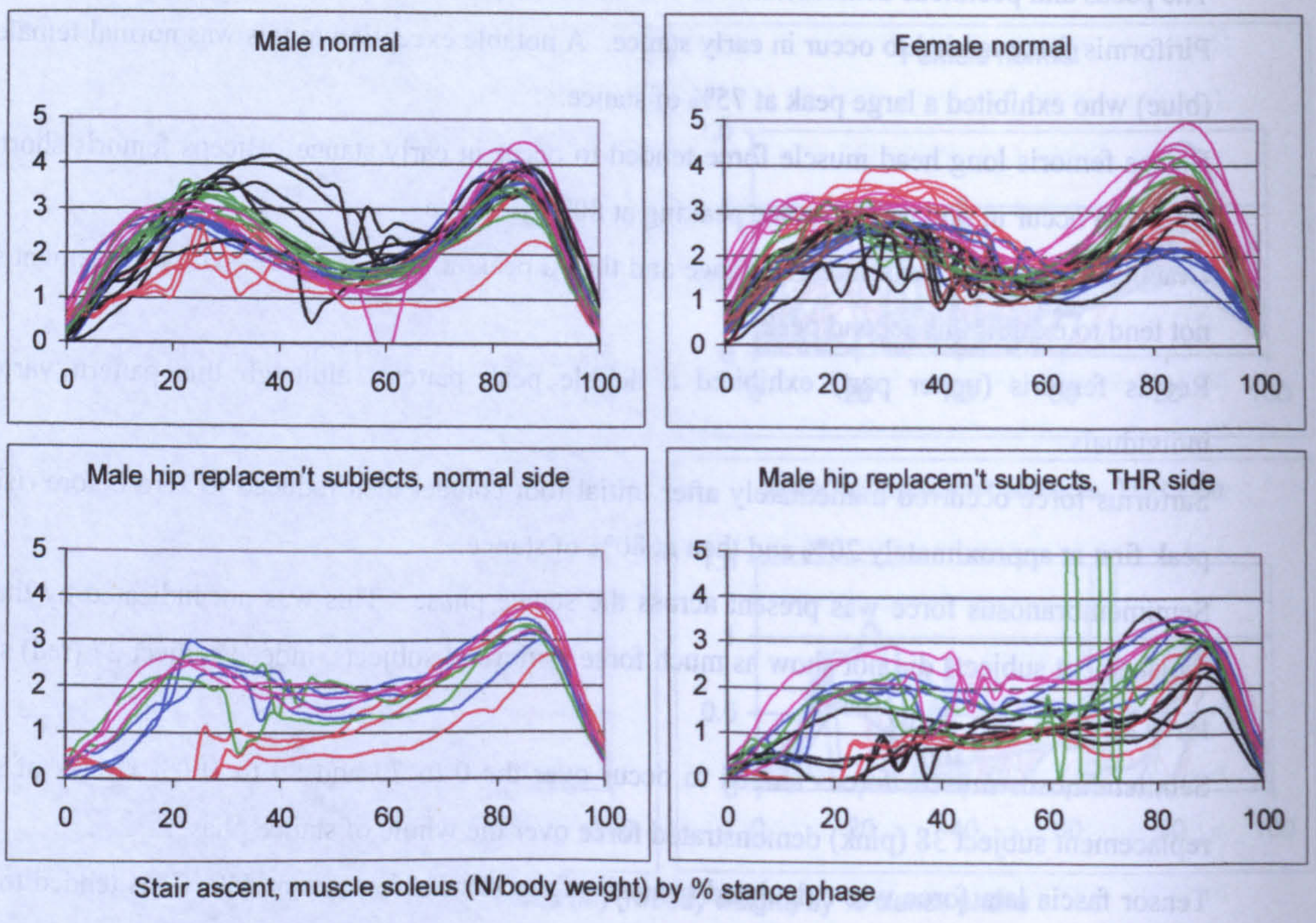

Figure 4.6 Stair ascent muscle force, soleus

Peroneus brevis and longus demonstrated patterns very similar to flexor hallucis longus. These patterns demonstrated less force than indicated by the emg data.

Peroneus tertius, tibialis anterior, extensor digitorum longus and extensor hallucis longus all demonstrated the same general pattern, peaking in early stance then demonstrating no force from approximately 30% of stance. This force was in general agreement with the emg data which showed an initial high activation level.

4.6.2 Stair ascent

Muscle forces calculated by the model for stair ascent are given in Appendix VI.3C. In general the muscle forces associated with stair climbing demonstrated a more varied pattern than those associated with walking. It appeared that there were more sharp changes in the values of muscle forces than for walking. This occurred in a number of muscles.

Several muscles showed little force including; adductor brevis (both superior and inferior heads), adductor longus, pectineus, psoas, obturator externus, gracilis, tibialis posterior, peroneus tertius, tibialis anterior, extensor digitorum longus and extensor hallucis longus.

In general hip replacement subjects exhibited lower muscle force magnitude than normal subjects.

Adductor magnus tended to follow the second of the emg patterns. Elements of gluteus maximus had a two peak pattern compared to the emg data that indicated the most significant force in the first half of stance. Gluteus medius also exhibited a two-peak pattern, this was more consistent with the emg data for this muscle as force across most of stance was indicated. Gluteus minimus exhibited a lot of switching on and off during stance. Iliacus exhibited force in early stance, which was associated with only a low probability of emg. Gemellus inferior force was not consistent across subjects. Obturator internus exhibited some force in normal subjects. In hip replacement subjects there was, however, very little force. Piriformis exhibited higher forces in normal subjects than in hip joint replacement subjects, with a lot of variation in pattern between subjects. Gemellus superior showed large changes in value over short periods of time. Biceps femoris long head exhibited force throughout most of stance extending its major force to a greater extent than indicated in the emg patterns. Biceps femoris short head showed force in rough agreement with emg. Rectus femoris force was variable with sharp changes evident particularly in normal females. Semimembranosus and semitendinosus were also variable in pattern. Tensor facia lata force covered most of the stance phase in agreement with the emg data. Forces in the gastocnemius medial and lateral elements and the soleus approximately followed the emg patterns. There was, however, considerable switching on and off of the muscles, which appeared to be inter-related (see Figures 4.4 to 4.6 – reproduced from Appendix A-VI.3B). Vastus intermedius force appeared to be in agreement with the emg profile. Force in the vastus lateralis and vastus medialis was, in general, over a smaller range of the stance phase than the emg pattern

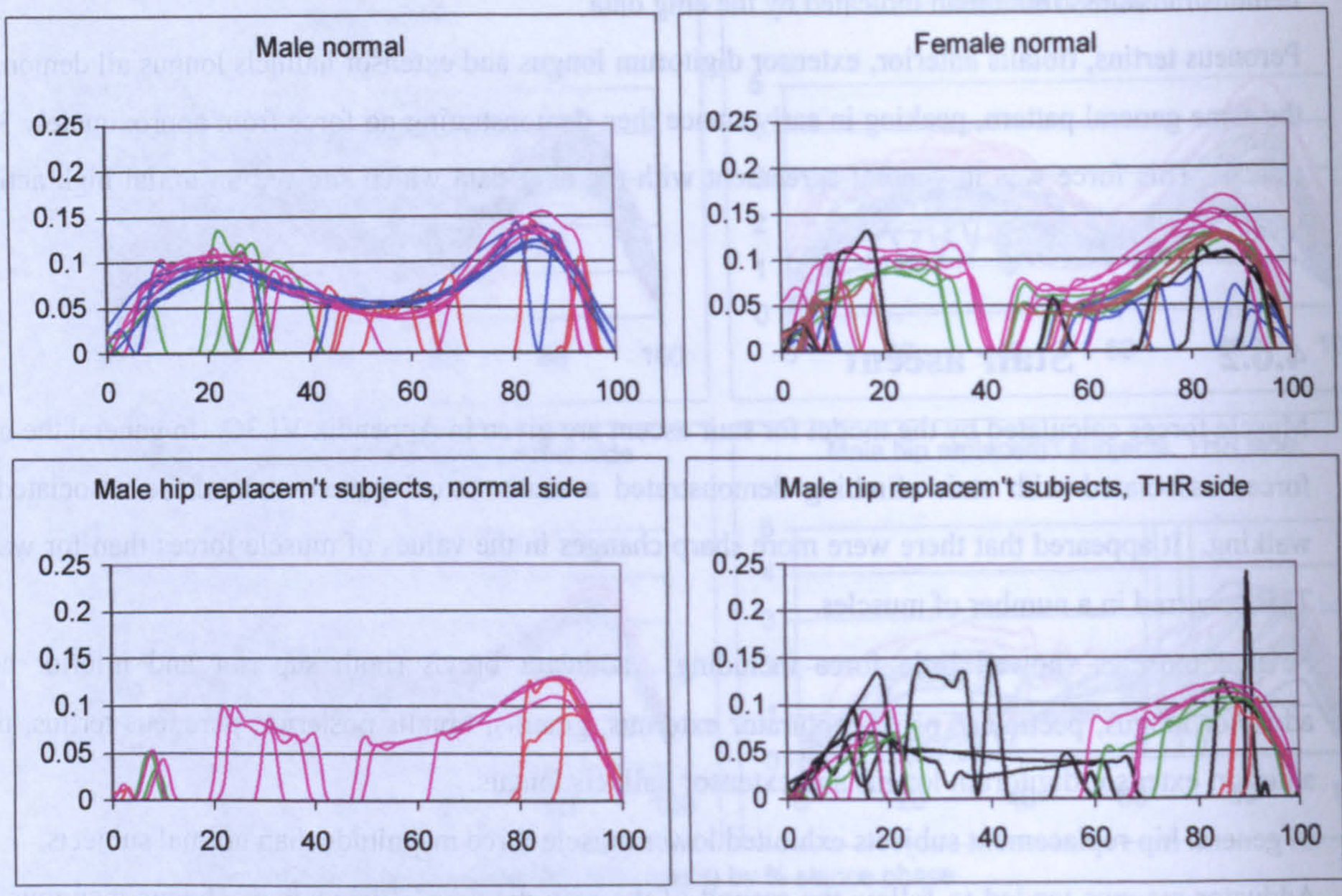

Figure 4.7 Stair ascent muscle force, flexor digitorum longus

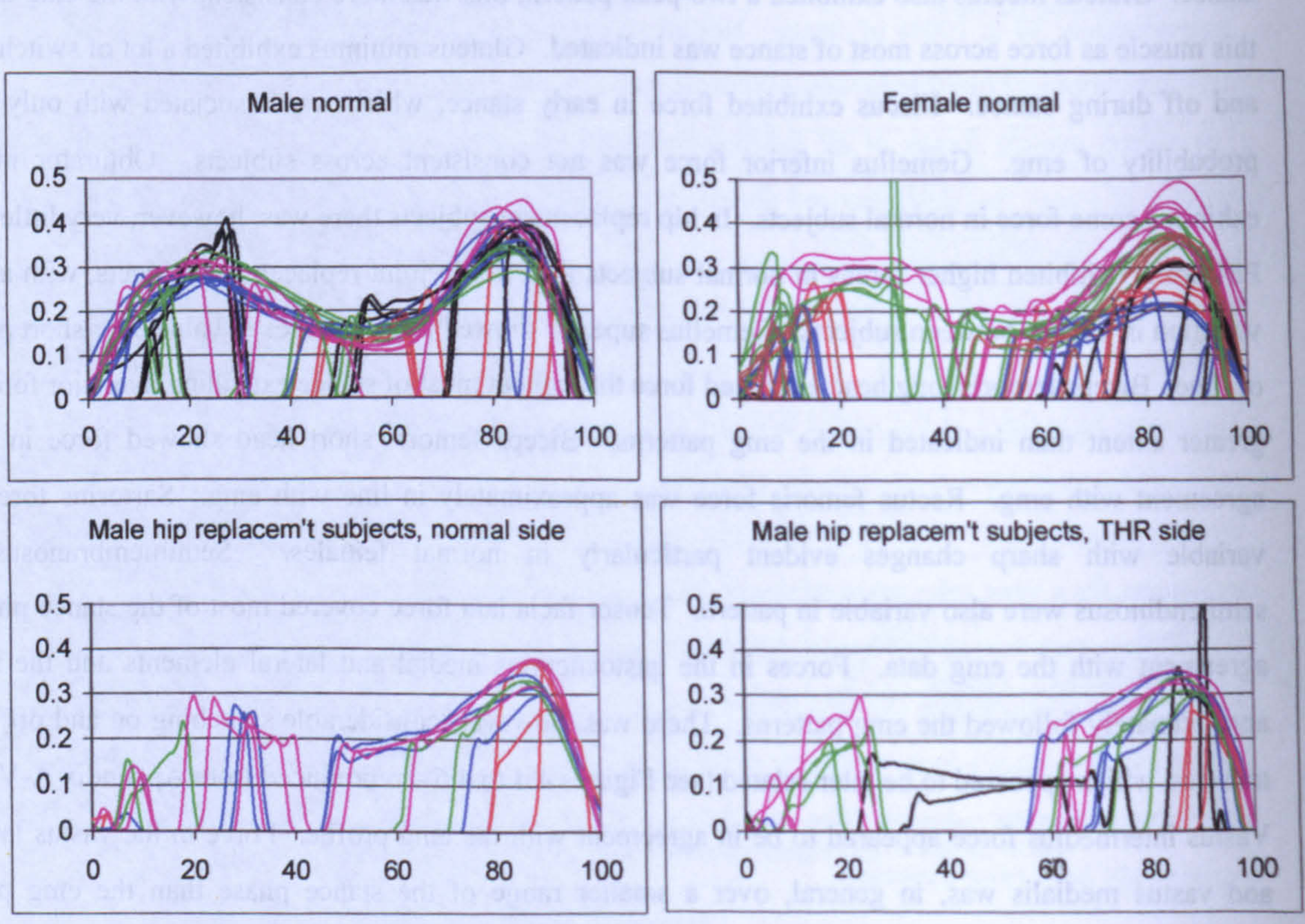

Figure 4.8 Stair ascent muscle force, flexor hallucis longus

suggested. Flexor digitorum longus, flexor hallucis longus, peroneus brevis and peroneus longus all exhibited forces traces which included rapid transitions from force to no force (see Figures 4.7 to 4.10 – reproduced from Appendix A-VI.3B). When there was force there appeared to be a common magnitude between individuals.

4.6.3 Quadriceps femoris and calf muscles force

Appendix VI.3C gives the force profiles of the quadriceps and calf muscle for all other activities. These results have been included to indicate the ability of the model to distribute the forces in the muscles. Comparison with emg profiles is made.

4.6.3.1 Stair descent

Rectus femoris and vastus intermedius forces were approximately in agreement with the emg profiles. The hip replacement subjects' vastus lateralis and medialis were less active than the emg patterns suggested.

There was in general more force in the gastrocnemius elements than indicated by the emg. Soleus force was approximately in agreement with the emg.

4.6.3.2 Ramp ascent and descent

Ramp ascent

The muscle forces of the vasti were in approximate agreement with emg. The rectus femoris muscle, however, was more active in early to mid stance than might have been expected from the emg profile. There was good agreement between the gastrocnemius and soleus and the emg data. There were, however, a lot of rapid changes in muscle force values.

Ramp descent

The rectus femoris appeared to be more active than indicated by the emg profile. Vastus intermedius was in general agreement with the emg profile. Vastus lateralis and medialis were in general less active than the emg profile suggested. Force of the gastrocnemius and soleus were erratic, but in general agreement with the emg profiles.

4.6.3.3 Camber foot up and camber foot down

Camber foot up and camber foot down results exhibited approximately the same patterns of quandriceps and calf muscle force. Of the vasti the intermedius was the most active in both cases. There was a lot of rapid switching between force values in the gastrocnemius and soleus profiles.

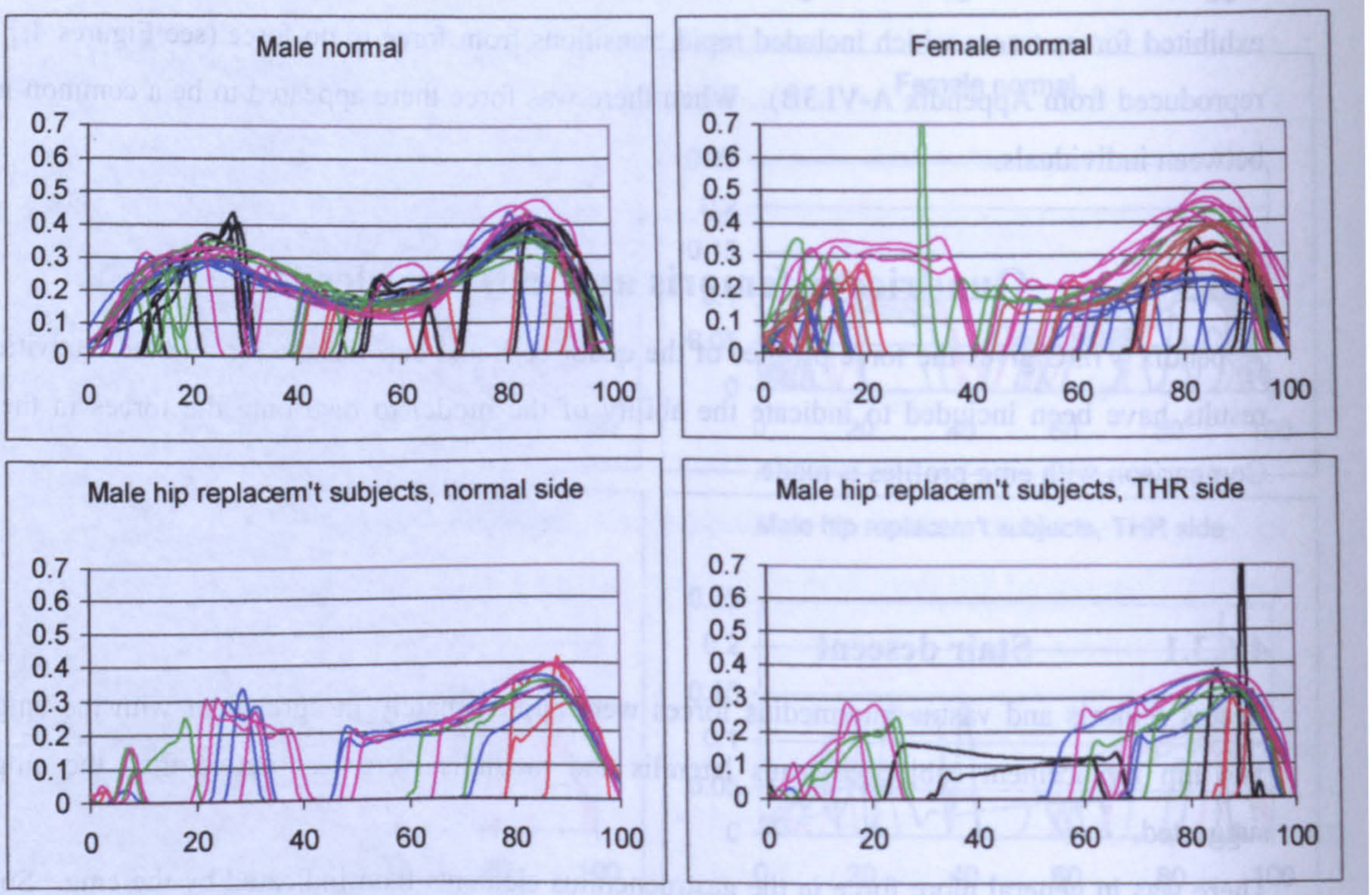

Figure 4.9 Stair ascent muscle force, peroneus brevis

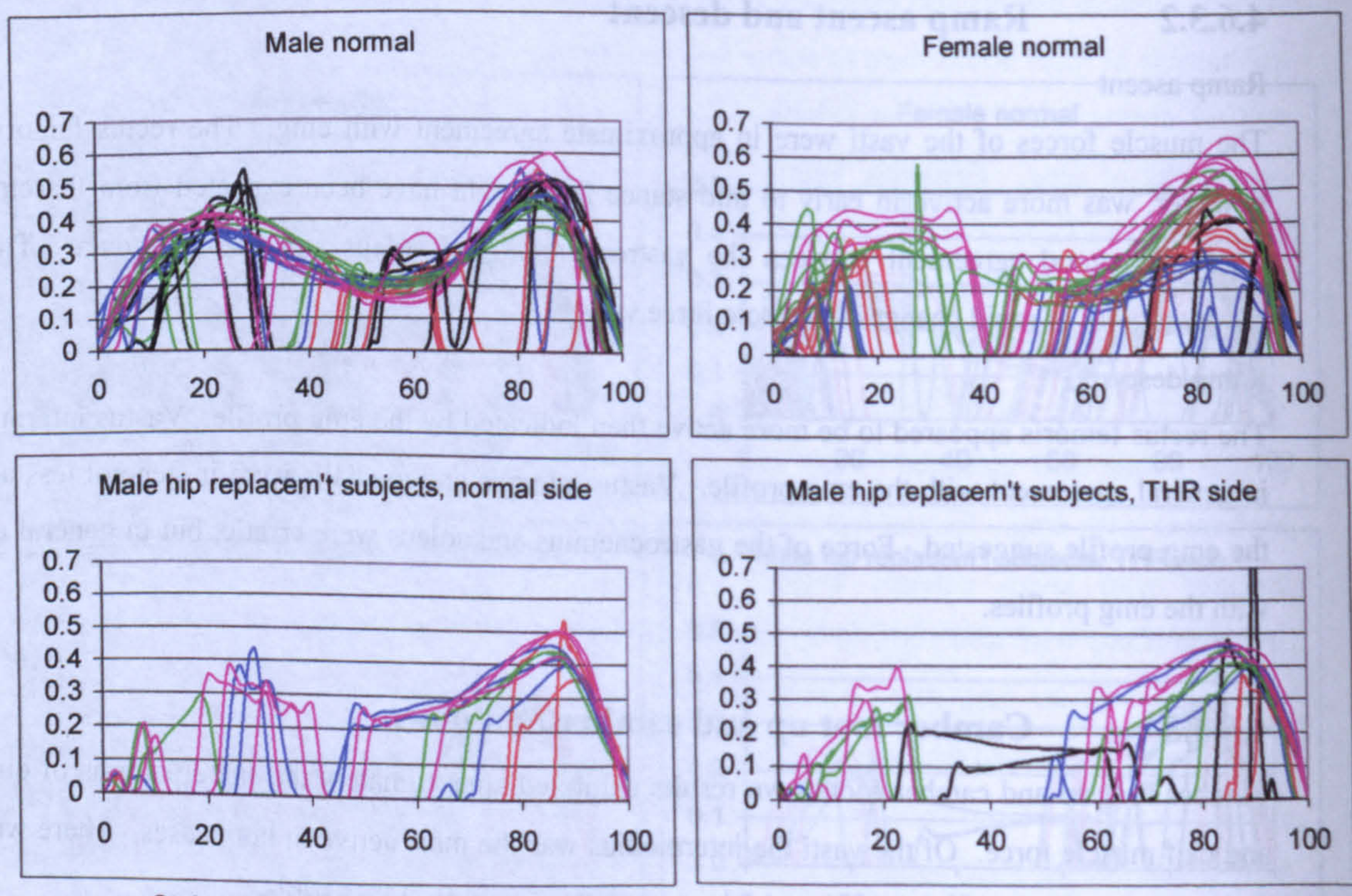

Figure 4.10 Stair ascent muscle force, peroneus longus

4.7 Hip joint forces

All hip joint forces are presented in multiples of body weight (Appendix VI.4). Hip joint forces are presented in two co-ordinate systems. Results in both the femur based co-ordinate system (femoral (thigh) anatomical axes) and pelvic based co-ordinate system (pelvic anatomical axes) are presented.

The total resultant force is presented followed by XFA, YFA and ZFA forces, and then XPA, YPA and ZPA forces. To provide an indication of the orientation of the resultant force pelvic and femoral co-ordinate systems the angles of the force to the pelvic and femoral anatomical axes are presented (as described in Section 3.5.9).

Hip joint force results are presented for each of the activities in turn.

4.7.1 Walking

All normal subjects' resultant hip joint forces followed a double peak pattern. The magnitude of peak values varied considerably between subjects, between approximately 4 and 10 times body weight. There was evidence of an extra peak in the profile of male normal subject 20 (pink) just before the end of stance. All hip replacement subjects had resultant hip joint forces to the lower end of the range of results. Hip replacement subject 27 (red) exhibited an asymmetric pattern (see Figure 4.11 – reproduction from Appendix A-VI.4).

There was a negative peak in XFA force at the hip joint at approximately 20% of stance for all subjects. There was a variation in the pattern of XFA force in late stance, however, with some subjects demonstrating a positive force and some a negative force.

All YFA forces were negative. There was a large amount of variation in magnitude of values between individuals.

ZFA forces were almost always positive and followed a double peak pattern. Notable exceptions to this were hip replacement subject 28 (blue) who exhibited no second peak and hip replacement subject 27 (red) who showed no first peak.

FHYXANG followed approximately the same trend for all subjects. Hip replacement subjects tended to have a lower first peak in early stance.

FHYZANG was predominantly between –10 and -20°. There was considerable variation at the end of stance (see Figure 4.12 – reproduced from Appendix A-VI.4).

There was variation in FHXZANG in the second half of stance between subjects especially the normal males. Hip replacement subjects exhibited a negative peak in late stance.

Pelvic XPA forces exhibited a negative peak at approximately 20% of stance. This was of varying magnitude. Hip replacement subject 27 (red) exhibited a particularly low force value, especially on the replaced side.

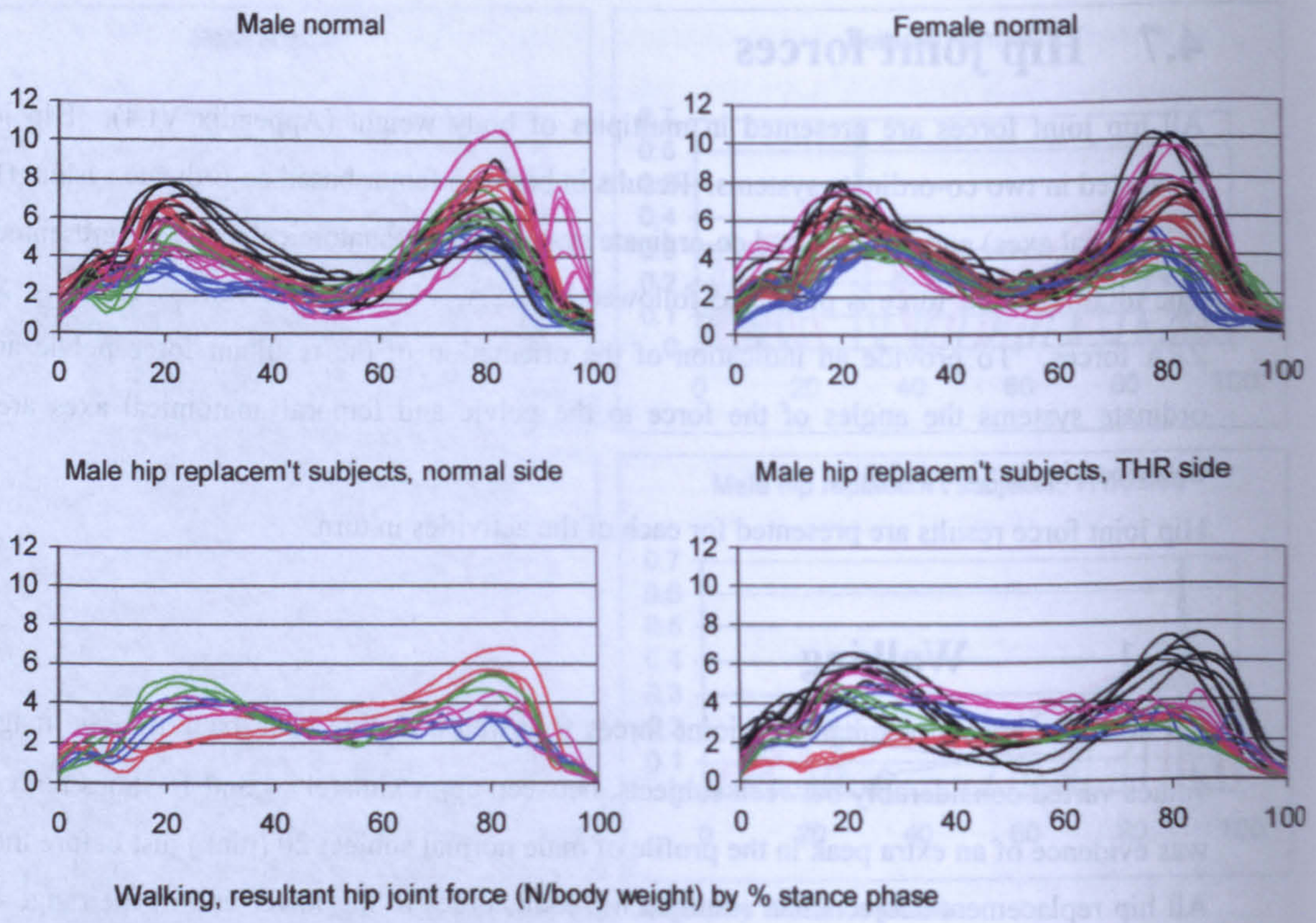

Figure 4.11 Walking, resultant hip joint force

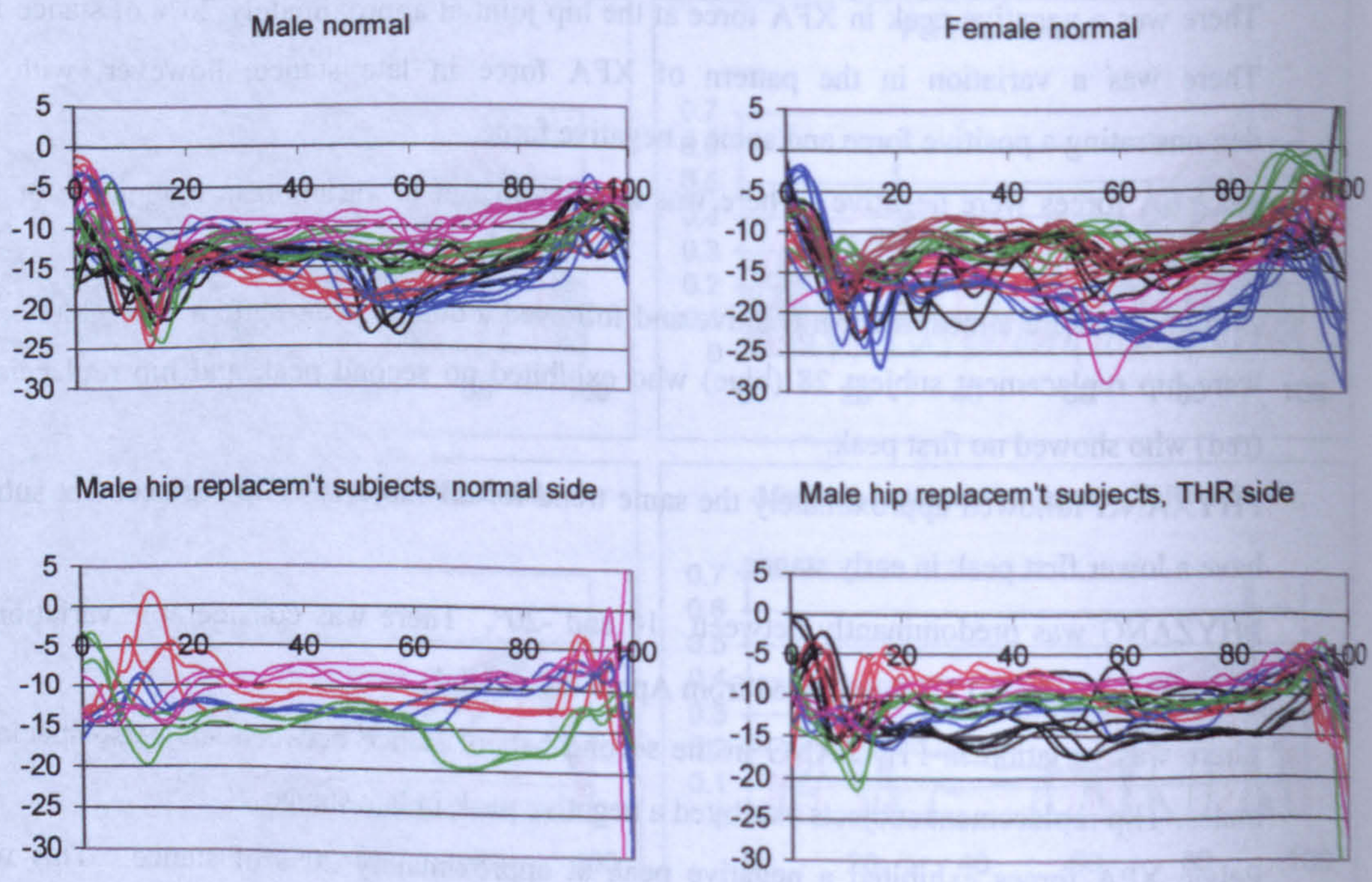

Figure 4.12 Walking, FHYZANG resultant hip joint force femoral angle

Normal subjects YPA force patterns followed a double peak profile. The profiles of the hip replacement subjects had only a relatively small variation between peak and trough values in their double peak patterns and in some cases there was no second peak at all. Subject 26 (black) was the exception to this, with force profiles similar to the normal subjects (see Figure 4.13 – reproduced from Appendix A-VI.4).

ZPA forces varied between subjects, but were in general negative throughout stance. Hip replacement subject 27 (red) exhibited an asymmetric pattern.

HJYXANG followed approximately the same trend for all subjects. There were, however, difference of up to 20° between individuals across stance.

There was only a small range in HJYZANG from approximately 0 to 30°. For some individuals the angle became very large in magnitude at the end of stance.

HJXZANG changed by up to 150° over the stance phase. There was considerable variation in the angle in late stance for some of the female subjects.

4.7.2 Stair ascent

The resultant hip joint force during the activity of stair ascent was in general characterised by a double peak pattern. The second peak tended to be lower than the first. Hip replacement subjects exhibited lower forces than normal subjects. Male normal subject 6 (black) exhibited a late peak at 40% of stance.

XFA force exhibited a negative peak at approximately 20% of stance. There was variation in the magnitude of this peak between subjects.

YFA force followed a double peak pattern with a lower magnitude of second peak as compared to first peak. The second peak was hardly present in a number of subjects.

The ZFA force was always positive. Profiles followed a double peak pattern with a relatively low second peak. Hip replacement subjects force magnitudes were in general lower than those of the normal subjects.

FHYXANG exhibited consistent trends across the subject sub groups. Female subject 35 (pink) exhibited high values throughout stance.

FHYZANG was confined within the 0 to -20° band for all of stance after approximately the 30% point.

There was considerable variation (80°) in FHXZANG between individuals in the second half of stance.

All XPA forces followed the same pattern with a peak in the negative direction at approximately 20% of stance. The timing of this peak varied for the female normal subjects.

YPA force followed, in general, a double peak pattern. There were a number of deviations from this however, with a large variation in the relative magnitude of the second peak.

The negative peak in ZPA force in early stance of hip replacement subject 28 (blue) was larger in magnitude than that of all the other subjects. Male normal subject 14 (red) exhibited high values in the second half of stance.

All subjects' HJYXANG angles followed the same trend although values differed by up to 35°.

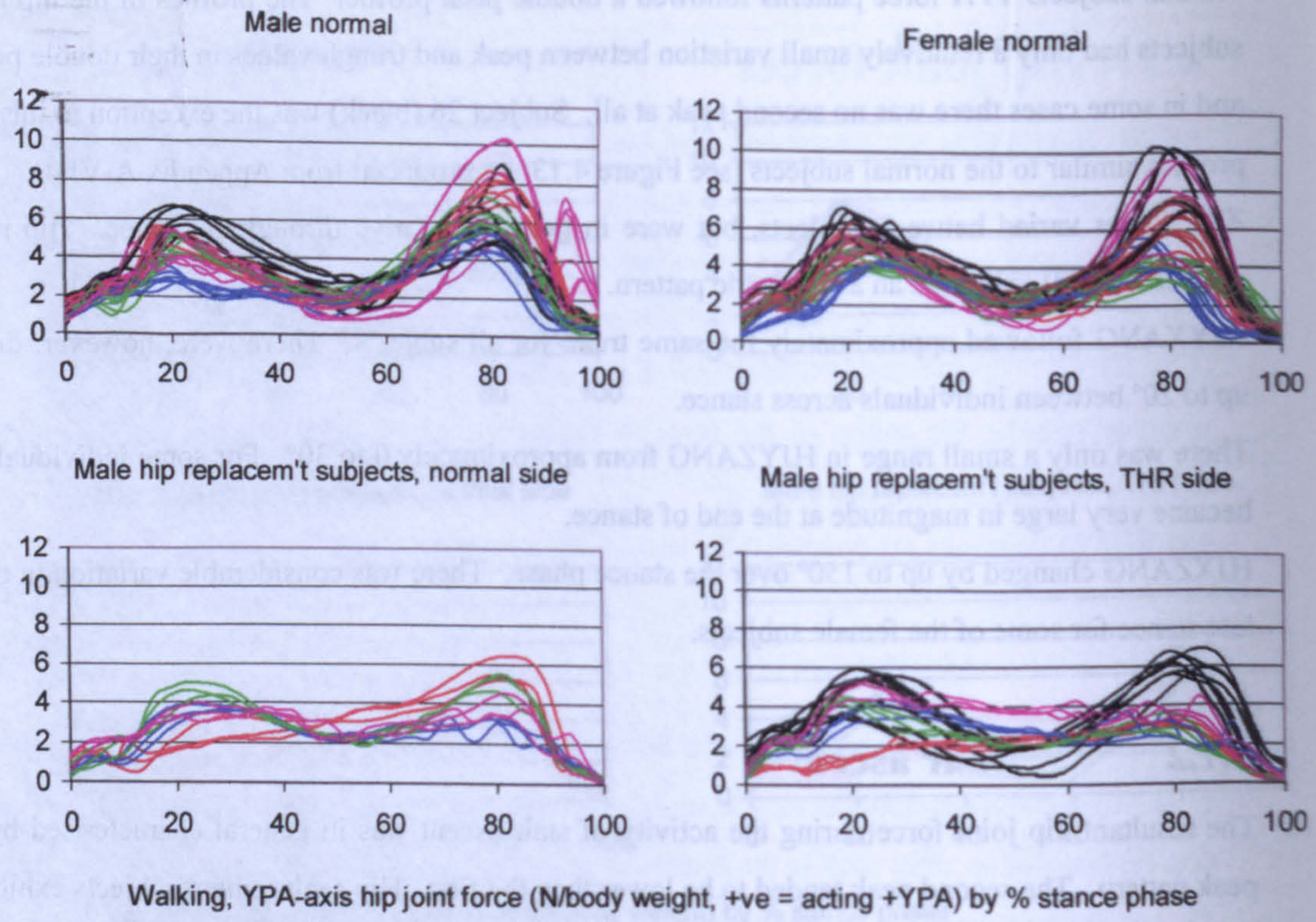

Figure 4.13 Walking, YPA hip joint force

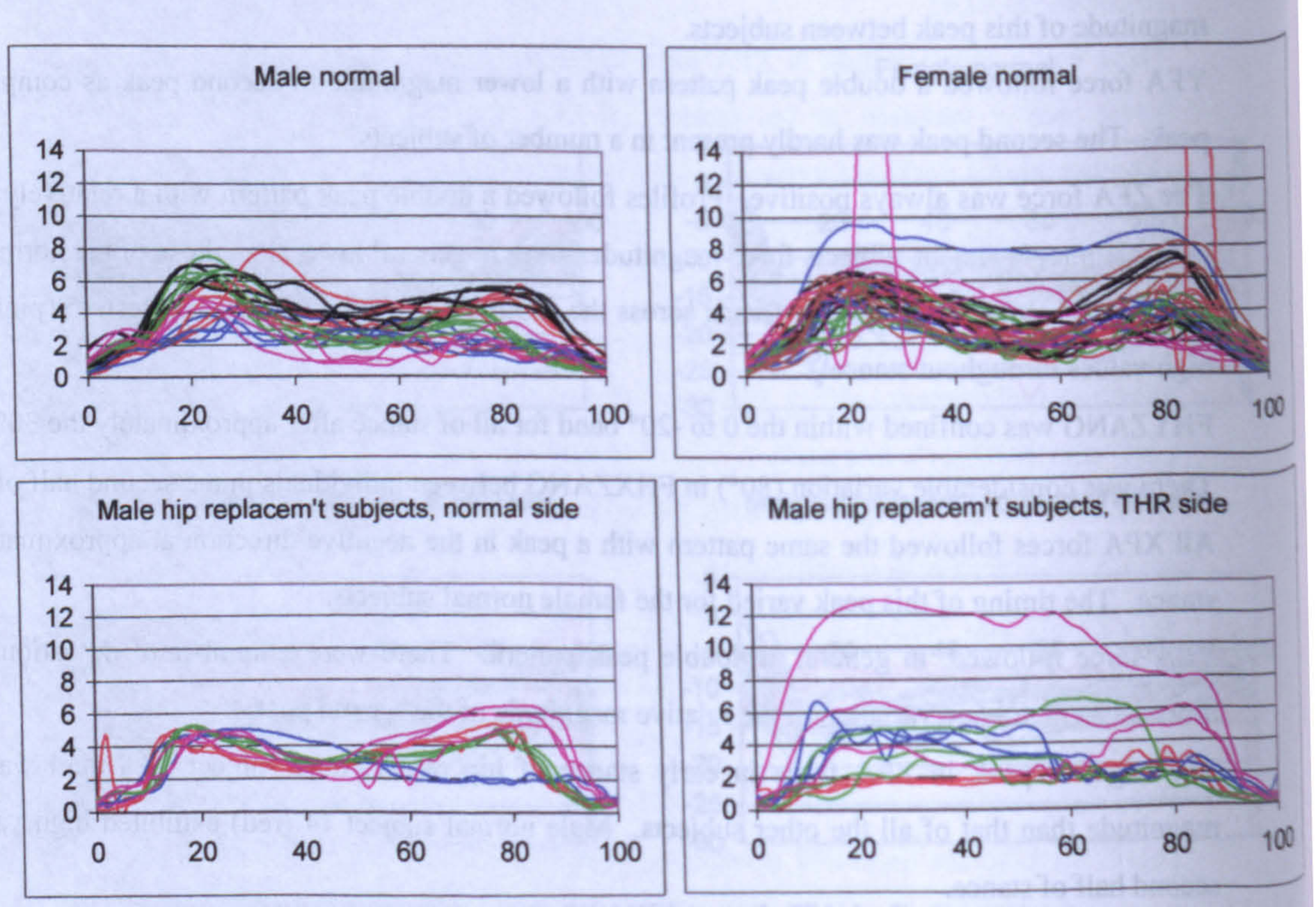

Figure 4.14 Stair descent, resultant hip joint force

Angle HJYZANG was almost always negative. The angle reduced in magnitude initially after foot contact before becoming relatively stable after 40% of stance.

For all subjects HJXZANG increased in magnitude initially up to 20% of stance then became lower in magnitude. There was a greater variation in the hip joint replacement subjects than in the normal subjects.

4.7.3 Stair descent

Stair descent resultant hip joint force varied in magnitude and form between individuals. Almost all subjects exhibited a first peak at approximately 20% of stance, but not all demonstrated a second peak at approximately 80%. Hip replacement subject 38 (pink) demonstrated a very high hip joint force across the stance phase (see Figure 4.14 – reproduced from Appendix A-VI.4). This was, however, only evident in one of the subjects' traces.

XFA force demonstrated a range of different patterns. Of note were the large negative forces exhibited by hip replacement subject 38 (pink).

YFA force demonstrated variation in magnitude between individuals. Hip replacement subject 35 (pink) demonstrated high forces across most of stance of one trial.

ZFA forces were all positive. One trial of female subject 33 (blue) was higher in magnitude than all other female trials. One of the trials of hip replacement subject 38 (pink) exhibited high force across most of stance.

FHYXANG increased from approximately 0° to 15° across stance.

FHYZANG was relatively constant over the whole of stance, although small changes of approximately 5° were common in several of the subjects.

FHXZANG followed approximately the same trends for all sub groups. There were several anomalous results.

XPA force was predominantly negative. Hip replacement subject 27 (red) had forces that were very low for both hips for all of stance.

YPA force had the same notable differences in subjects' traces as YFA force and resultant force.

One trial of the replaced sides of each of hip replacement subjects 34 (green) and 35 (pink) showed particularly high magnitudes for ZPA force.

There was a range of resultant angle HJYXANG covering 30°. All results appeared to follow approximately the same trends with a slight decrease in negative value over the 10 to 90% range.

Female normal subjects HJYZANG reduced in magnitude over the first 20% of stance to a greater extent than male subjects. Hip joint replacement subjects exhibited a wide range of results.

There was a large variation in HJXZANG between subjects. Male normal subject 20 (pink) exhibited low negative values compared to other male subjects.

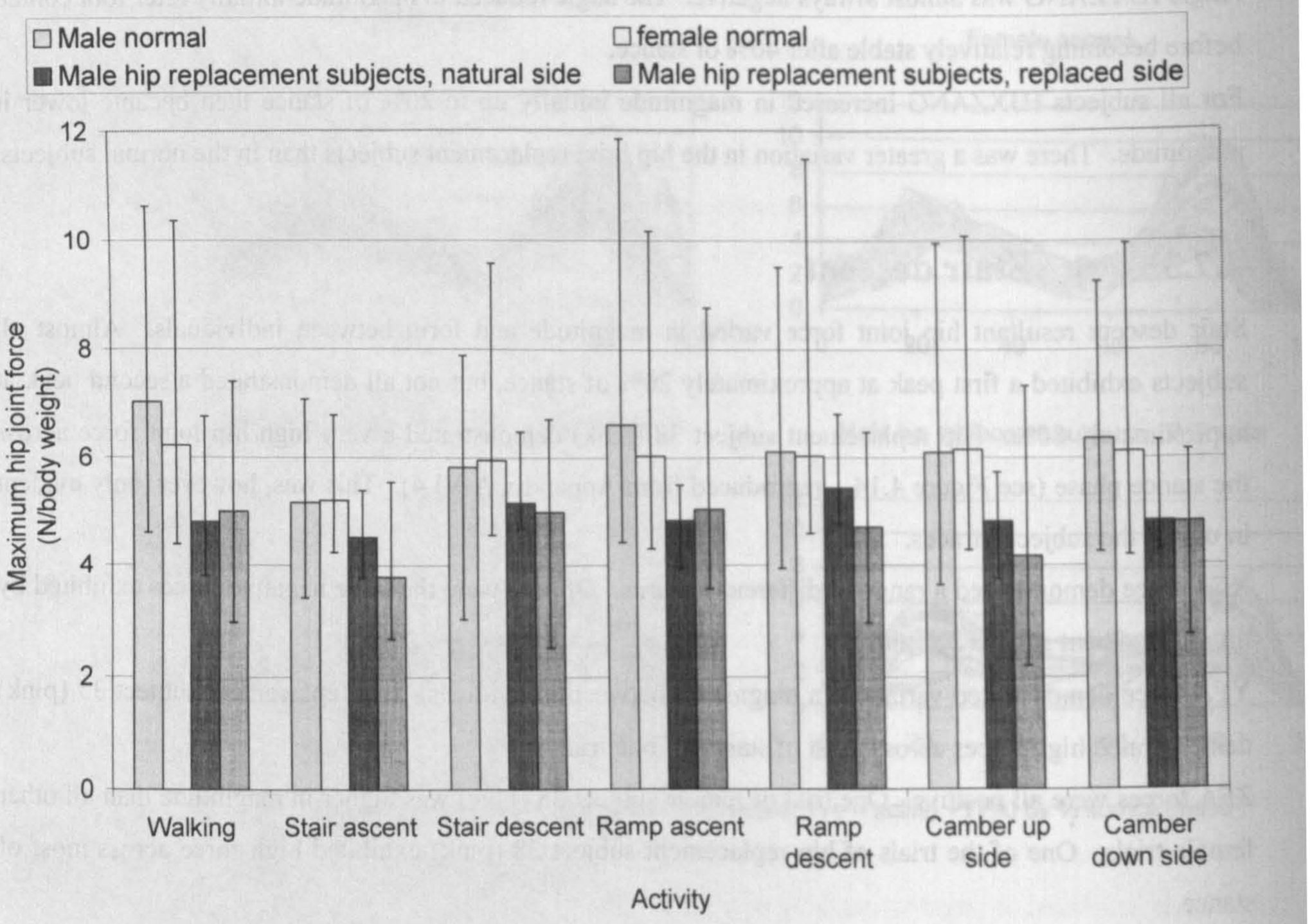

Figure 4.15 Maximum resultant hip joint force (N/body weight) for all activities by subject sub group. Median and range of maximum resultant hip joint force are illustrated.

Table 4.2 Median and range of maximum resultant hip joint forces by activity

Activity	Male normal (N/body weight)	Female normal (N/body weight)	Male hip replacement subjects, natural side (N/body weight)	Male hip replacement subjects, replaced side (N/body weight)
Walking	7.02 (4.60-10.63)	6.22 (4.38-10.36)	4.81 (3.81-6.76)	5.01 (2.97-7.40)
Stair ascent	5.17 (3.42-7.07)	5.21 (4.23-6.78)	4.52 (3.78-5.39)	3.79 (2.69-5.55)
Stair descent	5.83 (3.04-7.89)	5.96 (4.56-9.57)	5.17 (4.69-6.49)	4.99 (2.54-6.72*)
Ramp ascent	6.62 (4.42-11.85)	6.04 (4.30-10.18)	4.83 (3.96-5.50)	5.04 (3.58-8.77)
Ramp descent	6.11 (3.94-9.51)	6.03 (4.58-11.50)	5.43 (4.76-6.81)	4.70 (2.97-6.47)
Camber up side	6.10 (3.64-9.95)	6.15 (4.27-10.08)	4.80 (3.75-5.73)	4.16 (2.21-7.33)
Camber down side	6.36 (4.24-9.25)	6.12 (4.18-9.95)	4.82 (4.28-6.33)	4.80 (2.74-6.15)

* One exceptional case of 13.02

4.7.4 Ramp ascent

Notable individual results in ramp ascent hip joint forces are as follows:

Male subject 20 (pink) exhibited high second peak value in resultant force, YFA and YPA forces.

Hip joint replacement subject 26 (black) exhibited erratic YFA and YPA forces.

There was considerable variation in hip replacement subjects natural side femoral angles. Hip joint replacement subject 27 (red) exhibited a high first negative peak ZPA angle.

There were different patterns in ZPA force, with some subjects exhibiting a peak in force in both early and late stance and others exhibiting only one of these peaks.

There was a large change in hip replacement subject 29 (green) HJXZANG in late stance.

4.7.5 Ramp descent

Ramp descent resultant force varied in magnitude and pattern between subjects. Normal female subject 35 (pink) exhibited a high first peak. These high first peaks were evident in all other force curves.

Female normal subjects 33 (blue) and 35 (pink) FHYZANG's were higher negatively than the other subjects.

Hip replacement subject 27 (red) exhibited XPA forces approaching zero in value across the whole of stance. HJXZANG exhibited large jumps in value for a number of subjects.

4.7.6 Camber foot up and foot down

The following observations were made for both camber foot up and camber foot down. Normal male subject 20 (pink) exhibited a late peak in resultant group reaction force, this was also pronounced in ZPA force. Male normal subject 14 (red) exhibited high force magnitudes in all hip joint forces. In general female normal subject 35 exhibited higher forces at the first peak (20% of stance) than the other females for all forces. In general the forces of the hip replacement subjects were lower in magnitude than the normal subjects. The exception to this was hip replacement subject 26 (black) who exhibited forces of similar magnitudes to the normal subjects.

Normal females' FHYZANGs showed greater differences between individuals than normal males.

HJXZANG of hip replacement subject 26 (black) was lower in magnitude than all other subjects over the second half of stance.

4.7.6 Summary of hip joint force results

Figures 4.15 to 4.17 present summaries of the maximum resultant hip joint forces for each of the activities studied for each of the subject sub groups. Figure 4.15 summarises maximum resultatnt force over the

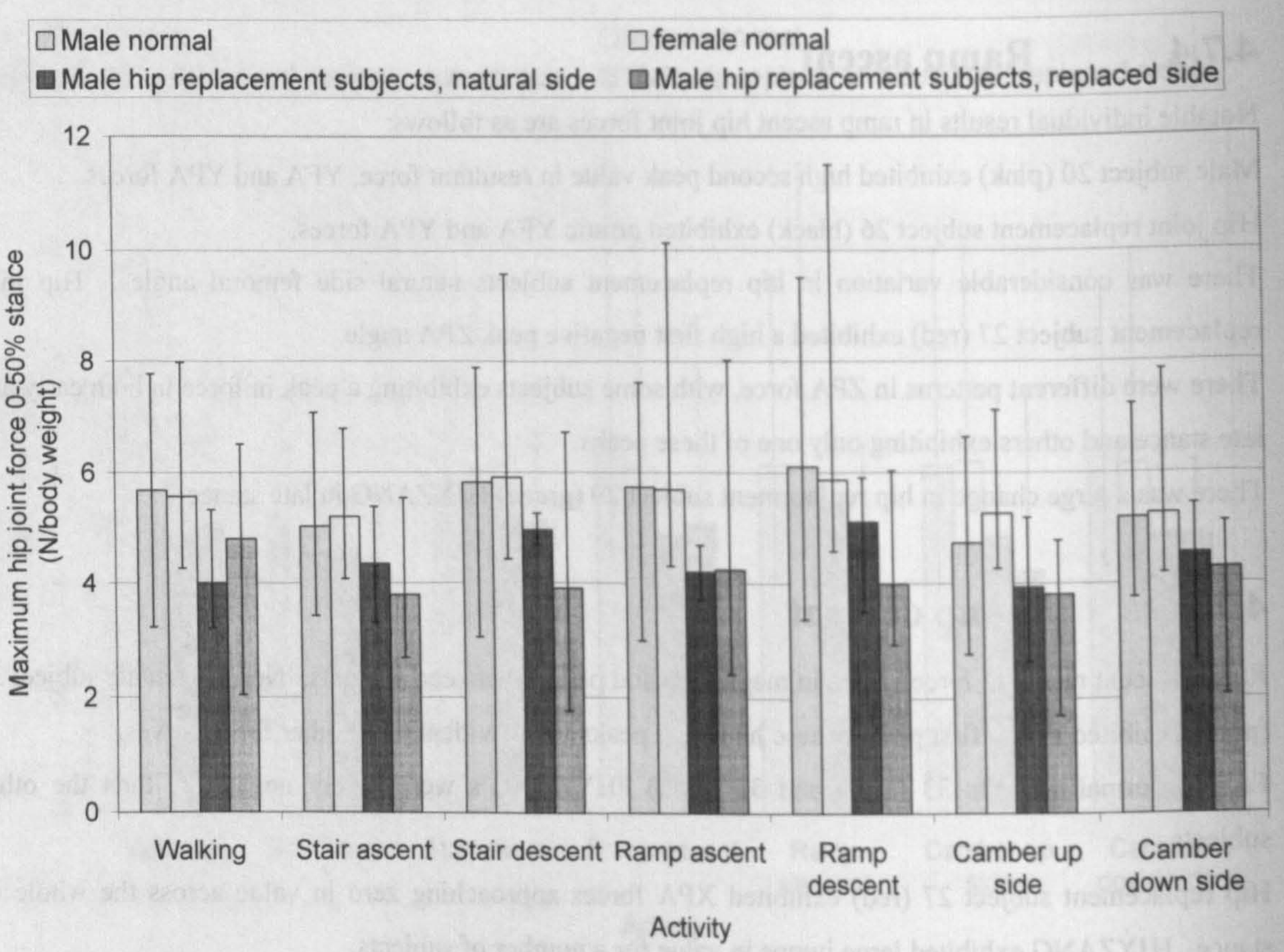

Figure 4.16 Maximum resultant hip joint force (N/body weight) over 0-50% of stance for all activities by subject sub group. Median and range of maximum resultant hip joint force are illustrated.

Table 4.3 Median and range of maximum resultant peak hip joint forces in 0-50% of stance phase by activity.

Activity	Male normal (N/body weight)	Female normal (N/body weight)	Male hip replacement subjects, natural side (N/body weight)	Male hip replacement subjects, replaced side (N/body weight)
Walking	5.69 (3.22-7.77)	5.58 (4.27-7.99)	4.00 (3.20-5.34)	4.81 (2.05-6.51)
Stair ascent	5.04 (3.42-7.07)	5.21 (4.07-6.78)	4.34 (3.30-5.39)	3.79 (2.69-5.55)
Stair descent	5.83 (3.04-7.89)	5.91 (4.42-9.57)	4.96 (4.69-5.27)	3.90 (1.77-6.72)
Ramp ascent	5.74 (2.99-7.62)	5.70 (4.30-10.13)	4.20 (3.72-4.69)	4.24 (2.43-8.03)
Ramp descent	6.11 (3.37-9.51)	5.87 (4.58-11.50)	5.11 (3.50-5.91)	3.99 (2.94-6.04)
Camber up side	4.73 (2.77-6.64)	5.27 (4.27-7.12)	3.93 (2.64-5.19)	3.80 (1.71-4.77)
Camber down side	5.19 (3.75-7.22)	5.27 (4.18-7.85)	4.53 (2.69-5.44)	4.26 (2.06-5.11)

whole of stance and Figures 4.16 and 4.17 include the maximum resultant hip joint forces for 0-50% of stance and 51-100% of stance respectively. Median and range of the maximum forces are indicated. Table 4.2 to 4.4 present summaries of these values. This simple summary of results illustrates that on average the hip replacement subjects had lower maximum hip joint forces than the normal subjects. It also illustrates the large range of maximum forces calculated. There were, however, only minor differences between the different activities. Maximum forces in stair ascent and descent tended to be lower than for the other activities. This was particularly true for the peak values in the second half of stance. Stair ascent forces were, on average, the lowest in the second half of stance.

4.8 Knee and ankle joint forces

Knee and ankle joint forces are presented in Appendix VI.5 in multiples of body weight over the stance phase. All joint forces at the knee and the ankle are presented for walking and stair climbing. Only the two Y direction bone-on-bone forces are presented for the other activities.

4.8.1 Walking

4.8.1.1 Knee joint forces

In general hip replacement subjects had lower KJY1 forces than normal subjects. Several trials of the hip replacement subjects exhibited no KJY1 force for parts of stance. This was reflected in the force of the LCL particularly for subject 28 (blue). Several of the male normal subject trials also exhibited LCL force and no KJY1 force for parts of stance. The KJY2 force was present for almost all subjects for all of stance. MCL force was only calculated in two subjects in isolated trials at low magnitudes. KJY2 was higher in magnitude than KJY1.

Little force was predicted in the ACL, with only hip replacement subject 28 (blue) exhibiting force across a range of stance timings. There was also little force predicted in the PCL.

KJX1 force tended to be present in early and late stance. KJX2 force was calculated for the remainder of stance, being particularly active in mid to late stance.

KJX3 exhibited force between 30 to 50% and 90 to 100% of stance. KJX4 tended to be active in the form of two peaks, one at 15% and one at 80% of stance.

KJZ1 exhibited force for the majority of trials walked for the whole of stance, peaking at approximately 80% of stance. There were, however, a number of trials, which exhibited KJZ2 forces, particularly of the female normal subjects who exhibited force between 20 and 40% of stance. Male normal subject 8 (black) exhibited KJZ2 forces across most of stance. There was very little force in KJZ2 for the hip replacement subjects.

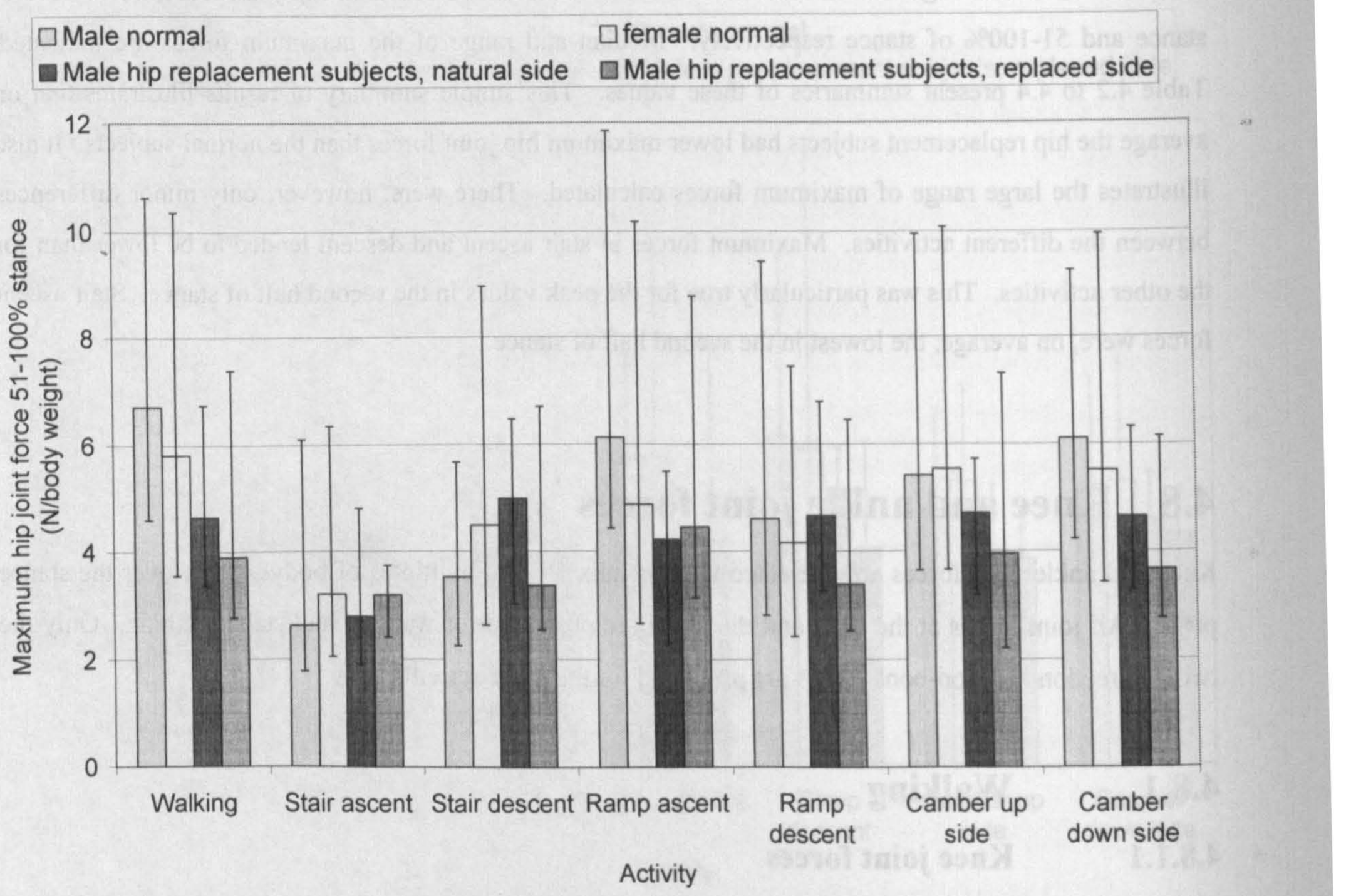

Figure 4.17 Maximum resultant hip joint force (N/body weight) over 51-100% of stance for all activities by subject sub group. Median and range of maximum resultant hip joint force are illustrated.

Table 4.4 Median and range of maximum resultant peak hip joint forces in 51-100% of stance phase by activity.

Activity	Male normal (N/body weight)	Female normal (N/body weight)	Male hip replacement subjects, natural side (N/body weight)	Male hip replacement subjects, replaced side (N/body weight)
Walking	6.73 (4.60-10.63)	5.82 (3.55-10.36)	4.65 (3.37-6.76)	3.90 (2.75-7.40)
Stair ascent	2.61 (1.78-6.11)	3.19 (2.05-6.36)	2.77 (1.92-4.81)	3.18 (2.40-3.73)
Stair descent	3.52 (2.25-5.67)	4.48 (2.62-8.96)	4.99 (3.01-6.49)	3.36 (2.54-6.72)
Ramp ascent	6.14 (4.42-11.85)	4.87 (2.66-10.18)	4.22 (2.32-5.50)	4.45 (3.13-8.77)
Ramp descent	4.60 (2.80-9.42)	4.15 (2.42-7.46)	4.66 (3.26-6.81)	3.38 (2.53-6.47)
Camber up side	5.42 (3.64-9.95)	5.54 (3.66-10.08)	4.71 (3.18-5.73)	3.95 (2.21-7.33)
Camber down side	6.11 (4.22-9.25)	5.51 (3.41-9.95)	4.64 (3.28-6.33)	3.66 (2.74-6.15)

4.8.1.2 Ankle joint forces

AJY1 rose to a peak at 80% of stance. This same pattern was evident in almost all subjects. AJY2, exhibited an initial peak at 10% of stance and then a steady rise to a second peak at approximately 80% of stance. AJY2 force was not always present.

AJX1 tended to exhibited force in the first 40% of stance, with an additional burst of force after 95% in a number of subjects.

AJX2 varied in magnitude between subjects but followed the same general trend, rising to a peak at approximately 80% of stance.

AJX3 followed a similar pattern to AJX2, with force mainly over the 30 to 100% range rising to a peak at approximately 80% before reducing to low levels at foot off.

AJX4 force occurred mainly in early stance, with a very small amount of force also predicted in late stance.

AJZ1 demonstrated no force for all subjects. AJZ2 exhibited force for all subjects for the whole of stance, peaking at approximately 80% of stance.

4.8.2 Stair ascent

4.8.2.1 Knee joint forces

Stair ascent KJY1 forces followed a general pattern of two peaks, one at approximately 20% and one at 85% of stance. There was, however, a lot of variability in the results in terms of minor swings within this overall pattern. Not all trials exhibited KJY1 forces for the whole of stance. This is reflected in the force of the LCL where isolated activation occurred.

KJY2 exhibited force for almost all subjects for all of stance. A pattern of double peak was evident, although within this general pattern there were minor peaks and troughs. Force in the MCL ligament was only observed in isolated cases was expected with the KJY2 force being present for almost all of stance.

There was little force in the ACL. Hip replacement subject 27 (red) exhibited what appeared to be consistent force in the ACL within the first 40 % of stance.

There was virtually no force calculated in the PCL.

KJX1 tended to exhibited force in early and late stance, although some subjects exhibited force for all of the stance phase.

KJX2 force was present mainly between 15 and 95% of stance. This force was, however, varied in pattern between trials.

KJX3 tended to be active over the first 60% of stance, though not for all subjects.

KJX4 tended to be active in the last 60% of stance, although this varied between subjects.

KJZ1 force was present for a number of trials across the whole of stance. KJZ4 force was also evident for some of the normal subjects for the whole of stance. A number of female normal subjects exhibited KJZ1 force for one leg and KJY2 force for the other leg.

4.8.2.2 Ankle joint forces

Ankle joint AJY1 forces followed a double peak pattern, with a positive force for almost all trials for the whole of stance. AJY2 was also active for almost all of stance and exhibited a double peak pattern. Hip replacement subject 27 (red) exhibited particularly low forces on both normal and replaced side.

For normal subjects AJX1 tended to exhibit force in early stance up to 40% of stance. Hip replacement subject 27 (red), exhibited force for all of stance in the replaced side.

AJX2 force was evident for the majority of subjects across the stance phase. There was, however, a considerable variation in the magnitude of the forces of different subjects.

AJX3 followed the same pattern as AJX2.

AJX4 force was evident over early stance and in late stance following the same patterns as AJX1.

No AJZ1force was recorded for any of the subjects. AJZ2 was recorded for all of the trials and followed a double peak pattern. Hip replacement subject 27 (red) exhibited particularly low forces.

4.8.3 Stair descent

Stair descent KJY1 varied in magnitude between subjects. Hip replacement subjects exhibited lower forces than normal subjects. There was also considerable variation in the magnitude of the KJY2 force between subjects. Both of the knee forces approximately followed a double peak pattern.

Male normal subject 17 (blue) exhibited particularly high AJY1 force at 30 % of stance for a number of trials. Female subject 35 (pink) did not exhibit a trough in the AJY1 force at mid-stance as other subjects did.

Female subject 34 (green) exhibited high AJY2 force relative to all other female subjects throughout stance.

4.8.4 Ramp ascent

A two-peaked pattern of KJY1 force for ramp ascent was evident in most of the normal subjects. A number of both normal and hip replacement subjects did not exhibit KJY1 force in mid to late stance. All subjects, however, had KJY2 forces throughout stance, again forming a double peak pattern.

AJY1 forces were present in all subjects for almost all of the stance phase. Male subject 20 (pink) exhibited an element of asymmetry in late stance. AJY2 force peaked at approximately 85% of stance. Male normal subject 20 (pink) exhibited force at this point that was approximately twice as large as any other subject.

4.8.5 Ramp descent-

The first peak of KJY1 force during ramp descent tended to be higher in magnitude than the second. There was, however, a lot of variation in the form of individual traces. Female normal subject 34 (green) exhibited high HJY1 force compared to all other subjects. This was also true for KJY2.

AJY1 force exhibited a peak at approximately 30% of stance and a second higher peak at approximately 85% of stance. The first peak was more evident in the normal subjects than the hip replacement subjects.

AJY2 force exhibited a distinct initial peak before 10% of stance.

4.8.6 Camber foot up

KJY1 force for camber foot up followed approximately a two peak pattern for the normal subjects. The second peak was often not present for the hip replacement subjects, indeed hip replacement subject 28 (blue) did not exhibit any KJY1 force after 40 % of stance.

All subjects exhibited KJY2 forces for most of stance. The pattern followed a double peak. Hip replacement subject 27 (red) did not exhibit the first peak on the replaced side.

All subjects exhibited AJY1 force for all of stance. Female subject 35 (pink) exhibited particularly high force at the peak at 80% of stance. Hip replacement subject 29 (green) exhibited a sharp peak at approximately 90% of stance, which was not evident in other subjects.

An initial peak in AJY2 force was evident in almost all subjects' traces. Not all subjects exhibited AJY2 force up to 60 % of stance. After this, however, all subjects exhibited a peak at approximately 85% of stance.

4.8.7 Camber foot down

KJY1 force followed approximately a double peak pattern in normal subjects, although there was a large variation in magnitudes of the force between subjects. Hip replacement subjects had low force in comparison to the normal subjects.

KJY2 force followed a double peak pattern for most of the subjects. Hip replacement subject 27 (red) did, however, not exhibit a first peak on the replaced side. Male normal subject 20 (pink) demonstrated higher second peak force than all other subjects.

AJY1 for was present in almost all of stance for all subjects. Female subject 35 (pink) exhibited particularly high peak magnitude at approximately 80% of stance compared to all other subjects. AJY2 exhibited a minor peak before 10% of stance, before rising to a second peak at approximately 80% of stance. AJY2 force was evident in almost all subjects for the whole of stance.

Chapter 5 Discussion

5.1 Introduction

The model of the lower limb used in this thesis was based on the model developed by Fitzsimmons [1995]. Indeed the pascal software used by Fitzsimmons was used as the basis for the implementation of software for this thesis. The main aspect of the implementation of Fitzsimmons preserved in this thesis was the wrapping procedures implementation applied to some of the muscles to ensure that they did not pass through underlying structures.

Extensive modifications were implemented including development of the knee and ankle models and the extension of the musculature to cover the whole leg.

All pre-processing including interpolation, filtering and marker correction routines were fully implemented by the author of this thesis. Attempts to determine hip joint centre location using dynamic 'waggle' trials were also fully implemented by the present author.

Errors associated with the analysis are discussed (Section 5.2). Aspects of the model of the lower limb used are discussed (Section 5.4). Comparable results from the literature are included to allow examination of their agreement with the results of this study (Section 5.7).

5.2 Experimental errors

5.2.1 Anatomical measurements

Measurement of distances between anatomical features was to within approximately ±5mm. This error was due to the difficulty in locating the precise location of points under the skin. Skin thickness measures were taken over the appropriate bony points. These measures would have included any underlying soft tissue that was attached immediately below the skin. As discussed in the methods section any additional soft tissues over the bones were accounted for using scaling methods. As there is a natural variation in soft tissue between individuals it is possible that errors may have been introduced due to assuming that all subjects scaled in the same manner.

5.2.2 Ground reaction force measurements

The force plate used for the analysis was accurate to within ±1% of full scale reading. The accuracy of measurement across the surface of the force plate varied. Attachment of sections to the force plate would have changed the characteristics of the force plate. As the force plate was loaded in all directions at once

it is unlikely that an accuracy level of ±1% was achieved. The error was likely to have been higher than this during particular loading combinations. Immediately before each trial the force plate was zeroed to reduce any error associated with offset. The presence of cross-talk between the output channels of the force plate has been demonstrated (Hall et al [1996]). For this thesis no correction for cross-talk was applied. This could have introduced errors into the results of the ground reaction forces and moments, which would have propagated through the model. Although cross-talk errors from one recorded force component to the others are stated to be less than ±2% of recorded values, as indicated by Hall et al [1996] these could have produced relatively large errors, as high 20%, in the values of the medio-lateral ground reaction force componenets.

5.2.3 3D motion analysis

An indication of the motion analysis system accuracy can be gauged by the discussion in Section 3.7.4. Included in that discussion is the observation of the accuracy of the determination of the distance between two points on a rigid frame. It was observed that there was a systematic error in the calculated distance depending on location in space of the markers. This error, of the order of 5mm, could have affected all markers. It must be assumed therefore, that the accuracy of the motion analysis system was at best within 5mm of the actual location of markers within the test volume.

The accuracy of the calibration of the camera system depended on the accuracy in the location of the hanging calibration poles. These were measured to within the nearest mm. These poles, however, only sparsely populated the test volume, leaving the problem of interpolation between the known values. This method of calibration does not use detailed information on the location of markers across the test volume. The recently implemented method of dynamic calibration, uses a stick of known length with attached markers which is waved in the desired calibration volume. This would provide the calibration software with relationships of position across the test volume and would appear to be more reasonable than the hanging poles method used for this thesis. Unfortunately this method was not available for calibration for this thesis.

5.3 Marker correction

In view of the inaccuracies of the motion analysis system's location of markers in space it was essential that some form of marker correction routine be implemented. The method chosen for this thesis required 3 markers on each segment, the minimum for reconstruction of the location of a 3 dimensional segment. The static trial was used as the template for the rigid body representation of all the lower limb segments. The dynamic trials were then corrected back to this template of pelvic, hip joint, thigh and shank segments. It was assumed that a least squares correction would be appropriate for this. The definition of segments using only 3 markers does not provide any detail of changes outside the plane defined by the

markers. If the error of the markers had been out of the plane defined by the original positions of the 3 markers then the routine used would not have provided a suitable correction. The use of 4 non-coplanar markers per segment would have improved the ability of the routine to correct for misplacement. This method was not, however, implemented due to the lack of suitable bony locations on each of the segments. The accuracy of the marker correction routine depended on the accuracy of the static trial. The accuracy of the location of markers in the static trial depended on their location in the test volume and therefore, an element of error was systematically incorporated into the marker correction of each dynamic trial. This, however, was at least consistent between trials.

5.4 Model

5.4.1 Introduction

To model the lower limb as accurately as possible would require the development of a model with all structures included. This model would have to incorporate a description of the mechanical properties of all structures and the method by which each of the active elements was controlled. This ideal model would be extremely complex and would still require the inclusion of numerous assumptions on the activation pattern of muscles and the application of the standard model to individuals. Although the model implemented in this thesis is far from ideal it incorporates most of the force bearing structures and provides a means of calculating the hip joint forces in a range of activities. As indicated in the description of the lower limb model (Section 3.5) numerous assumptions were made in its development. These were made to allow the model to be adapted to the individuals being tested. The following sections discuss the implications of the assumptions made.

5.4.2 Data interpolation and filtering

The interpolation of the three dimensional motion of markers in space presented a number of difficulties. Examination of the marker trajectories near to gaps in the data suggested that marker location at the edge of gaps was in error. It was therefore necessary to effectively increase the gap width. This would have lead to further inaccuracies in the interpolation as the cubic spline used would not have fully characterised the complex motion of the subject. All trials with large gaps in data (greater than 5 frames) were discarded and no attempt at interpolation was made. It is still possible that there were errors introduced due to incorrect interpolation. This may explain some of the apparently erroneous values observed in the results.

A 10Hz low pass filter was used. It is possible that some noise not associated with subject motion was still present in the results of subjects who performed the activities particularly slowly. A more

mathematically correct method of filtering may have been to perform a residual analysis to assess the filter frequency appropriate for each individual trial. The application of a uniform filtering frequency was performed, however, to preserve some consistency between subject analyses.

5.4.3 Muscle model

The same muscle model was applied to all subjects including the hip replacement subjects. It was assumed that the musculature was not changed during surgery and that all muscle elements stayed intact. There are several descriptions of the lower limb musculature available in the literature (e.g. Delp [1990], Delp et al [1990], Dostal & Andrews [1981], Kepple et al [1998], White et al [1989]). These vary in complexity and comprehensiveness. One of the most important aspects of the muscle description is that it takes into account the changes in muscle paths with changes in joint angles. This is achieved in one of two ways. Some of the publications define the path of a muscle as a series of points in the appropriate segment's co-ordinate system. To some extent this description method already takes into account the requirement to not pass through underlying structures as the path of each element can be defined so that this does not occur. Another method is to use effective origin and insertion data. This method defines the origins and insertions of the muscles in such a way as to ensure that they do not pass through underlying structures and that the line of action of the muscle is correct about the appropriate joint centres. This was the case for the muscle model of Brand et al [1982]. This method, however, does not take into account the changes in muscle line of action with changing joint angles. Thus it is possible for the muscles to pass through underlying structures. It is therefore necessary to make modifications to these models to ensure that underlying structures are not crossed. A method commonly known as wrapping is used, where the underlying structures are given appropriate dimensions and the overlying structures routed to ensure that they do not pass through the underlying structures. The model of Brand et al [1982] was modified in this way by Fitzsimmons [1995]. This modified model has been used in this thesis.

The models of muscular anatomy are invariably based on a small number of subjects. It is inevitable, therefore, that a scaling scheme has to be used to apply the model to a subject being studied. The scaling scheme specified by Brand et al [1982] used bony dimensions as scaling factors. Some of the dimensions required would have only been obtainable from X-ray or similar analysis of the subjects, which was not possible for this study. Modification of the scaling factors was therefore necessary. This involved making assumptions about the relationship between various anatomical dimensions. These assumptions will have incorporated errors in the analysis. The scaling scheme adopted was aimed at ensuring that reliable measures and ones that were, where possible, along the same axis as the original factors were used. Within the assumptions made was the fact that the average bony dimensions of subjects studied for this thesis was the same as that of Brand et al's subjects. This was based on the observation that the height of the two groups was approximately equal. It was necessary to make this assumption as it was not possible

to get accurate bony dimensions of the subjects in this study. This assumption could have introduced errors into the analysis especially at the knee. It is not possible, however, to assess the extent of any errors except in that the knee musculature may have been scaled down as compared to its real dimensions.

5.4.3.1 Muscle physiological cross sectional area

The model of the lower limb developed for this thesis used the physiological cross sectional area of muscles from one source [Freiderich & Brand, 1990], which was based on a single cadaver specimen. This publication was used as it provided the values of physiological cross sectional area for all of the muscles of the muscle model. Indeed this work was associated with the same research group. A further publication from this group examined the sensitivity of muscle force predictions to changes in physiological cross-sectional area [Brand et al, 1986]. In light of the influence of assumptions such as using standard physiological cross sectional area data they concluded that "*muscle force solutions are best used to determine relative values (i.e. trends) in parametric studies. On the other hand, the joint force solutions are less sensitive to such variations, and the absolute values are more reliable.*" In other words the values of individual muscle forces may be critically affected by particular values of physiological cross sectional area, but the influence on joint resultant force is less critical. A database of muscle physiological cross sectional area scalable to individuals would have provided a much more satisfactory source, but unfortunately was not available.

5.4.4 The definition of joints and joint structures

5.4.4.1 The hip joint

A method for locating the hip joint centre that would have used dynamic data of individuals was attempted (Section 3.7.4). It was concluded that the motion capture system was not accurate enough to allow the use of this method. A standard method of calculating the hip joint centre was therefore used [Bell et al 1990]. Section 5.4.5 gives details of the deviation in resultant hip joint force arising from a change in hip joint centre position of 10mm in each of the pelvic anatomical axes directions. It was necessary to rely on some form of standard hip joint centre location. This may have introduced errors in the analysis.

No ligaments or other soft tissue structures except muscles were included in the model at the level of the hip joint. It was assumed that the contribution from these structures were negligible. Vrahas et al [1990] estimated that the contribution of the passive structures at the hip is "*usually well less than 10%*" of the total moment during most of the gait cycle and normal stair climbing.

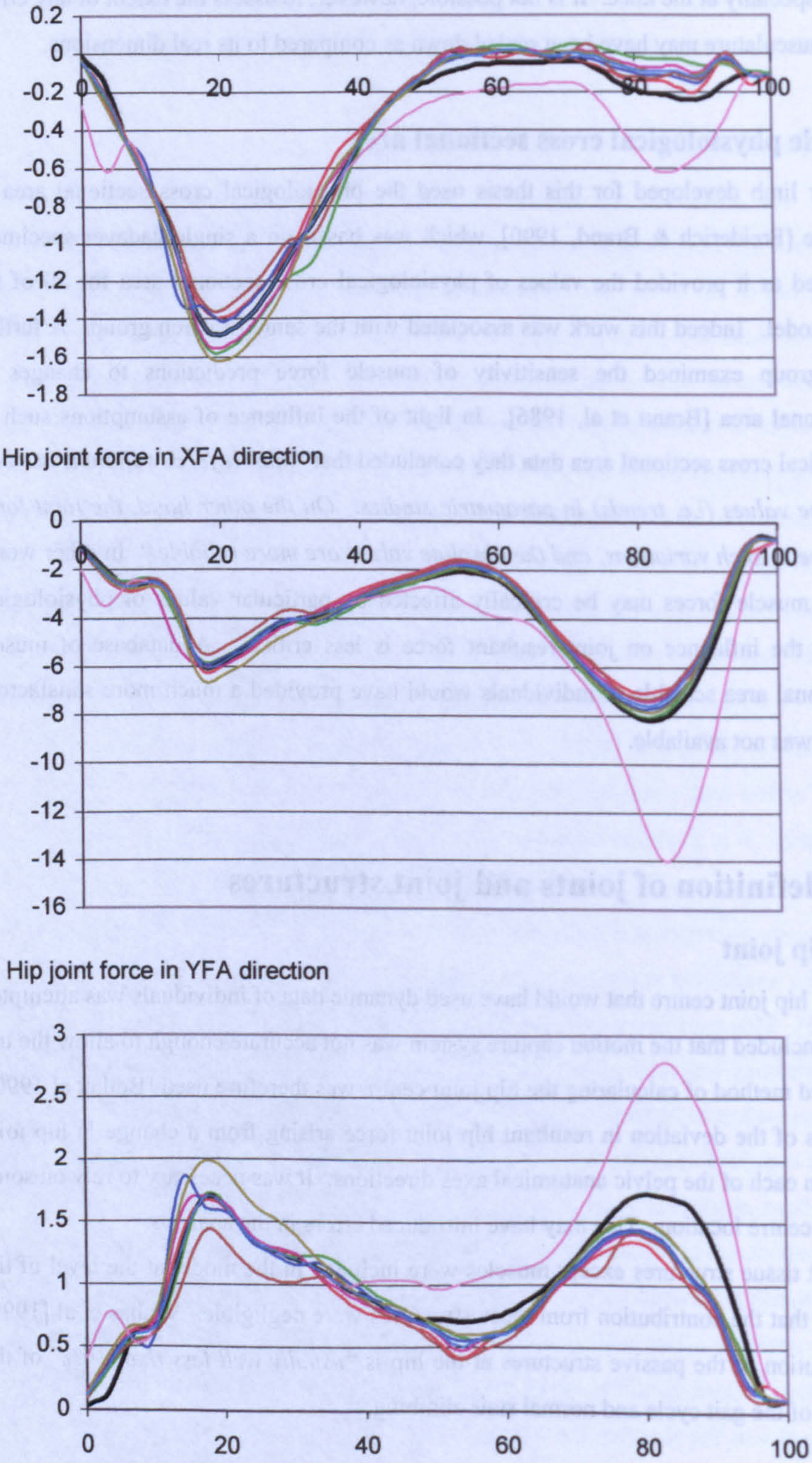

Figure 5.1 Hip joint forces in femoral anatomical co-ordinates resulting from hip and knee centre displacement

5.4.4.2 The knee joint

The knee joint was developed using information from a number of different publications. It was assumed that all these publications were compatible in that data could be scaled using the same average dimensions of the tibial plateau. It was also assumed that the tibial plateau scaled the same in the anterior-posterior and medio-lateral dimensions. These assumptions were necessary as no reliable anterior-posterior dimension could be defined.

The knee joint forces were not completely defined in three dimensions. All elements including bony contact forces and ligaments were defined to act in one of the planes of the knee anatomical axes set. Supplementary forces to act as soft tissue or unknown bony contact forces were introduced to ensure that the model was able to represent the major force carrying structures in a reasonable manner. It was necessary to ensure that the bony contact forces and other major force carrying structures were modelled, and that they were not unrealistically loaded due to shortcomings of the model.

Shank axes alignment

The definition of the shank anatomical axes was used to define the location of the knee joint anatomical axes and therefore the knee joint forces and bony contact points. An attempt was made to define the centre of the tibial plateau as being on the long axis of the tibia which also passed through the mid malleolar point. The definition of the shank axes depended to a great extent on the location of the tibial tuberosity marker with respect to the fibular head marker. It was assumed that the tibial tuberosity marker was located at the mid point of the tibial plateau in the medio-lateral direction. If it was not then the shank axes would have been rotated and the knee centre offset. The use of a medial tibia marker for use in defining the medio-lateral axis of the shank could have overcome any possible error. This was not, however, used due to poor detection of the marker next to the femur medial marker.

Knee ligaments

There are a number of definitions of the locations of the ligaments in the knee. The work of 0'Connor et al [1990] was used as it provided a definition of the ligaments in their simplest form. All ligaments were represented by single elements. They are actually constituted of several different elements. The single element model was used as a compromise between increasing complexity of the model and providing a description of the main force bearing structures.

Knee ligaments were modelled in the same way as other force bearing structures. This meant that additional restraints had to be added to the model to ensure that the ligaments did not act as active structures. It was not possible to completely eliminate the possibility that this would occur, but only to provide additional forces to reduce the likelihood of it occurring. It would appear from the results of knee joint forces (Appendix VI.5) that the anterior and posterior cruciate ligament force was restricted and that the KJX3 and KJX4 forces were used in preference by the minimisation procedure in the force balance.

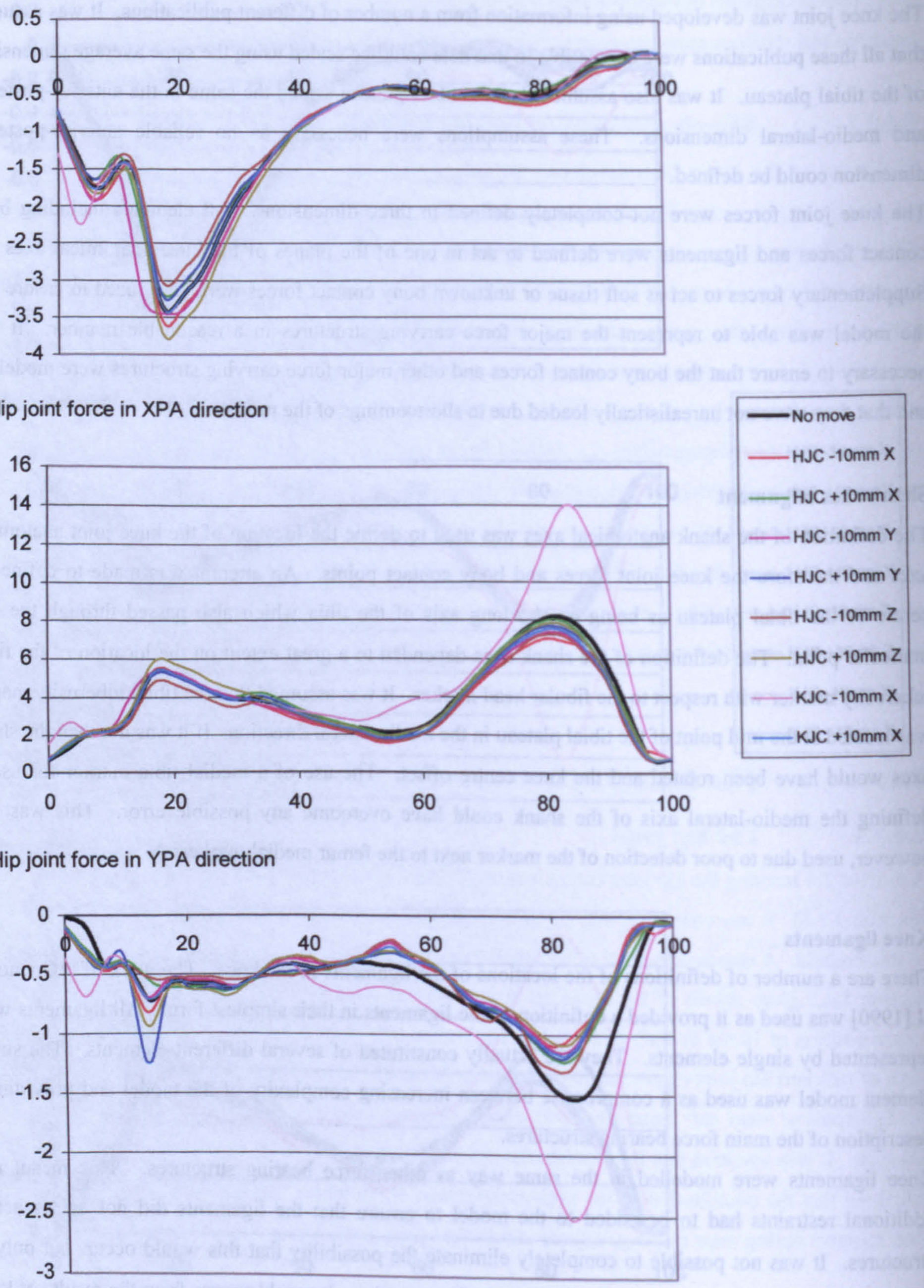

Hip joint forces in pelvic anatomical axes co-ordinates (N/body weight, % stance phase)

Figure 5.2 Hip joint forces in pelvic anatomical co-ordinates resulting from hip and knee centre displacement

This aspect of the knee joint force balance could have lead to reduced requirement of force in other structures than if the cruciate ligaments had been required to take a greater proportion of the anterior posterior knee force.

The medial and lateral collateral ligaments provided a means of balancing high moments about the XKA axis of the knee. Force was recorded in the collaterals for a number of subjects. The restrictions placed on allowable combinations of components of the model bearing force (Section 3.6.4) prevented the collaterals becoming active unless the same side bony joint force had reduced to zero. This restriction could have resulted in less force bearing than actually occurs. This restriction had to be applied, however, to ensure that the collaterals did not act as active components.

Contact forces

The locations of the contact points were taken to be defined after Nisell [1985] with the modification that the location of the points of contact were rotated by the angle of rotation at the knee joint. This modification was incorporated to ensure that the movement of the femur on the tibia was taken into account. The offset in the angle of rotation by the amount of static trial rotation was used to ensure that errors in the alignment of the femoral anatomical axes did not affect the contact point positions too greatly. The contact forces were only defined perpendicular to the tibial surface and would, therefore, not have incorporated forces along the tibial plateau. The additional forces KJZ1 and KJZ4 were used to compensate for this in the ZKA direction.

Nisell [1985] presented a model of the movement of the point at which the tibia and femur came into closest contact. This was defined at discrete intervals of flexion of the knee joint. This information was only two dimensional. It was necessary to make assumptions about the form of the movement of the contact point between Nisell's recorded points. This may have led to errors in the location of the knee contact location. There did not, however, appear to be any more suitable sources of information in the literature. It was considered that Nisell's data provided a reasonable description of the contact point movement and it was therefore used in the model.

5.4.4.3 The ankle joint

Ankle joint forces

The ankle was defined as a single hinge joint at the level of the talo-crural joint. It was defined with eight bony contact forces. No ligaments were incorporated as it was assumed that the force in the ligaments would not have been significant compared to the bony contact and muscle forces. The characterisation of the forces by eight components allowed the effective force to act over a narrow band of the ankle joint. The use of two force centres allowed the effective force to move between the two positions. Had the

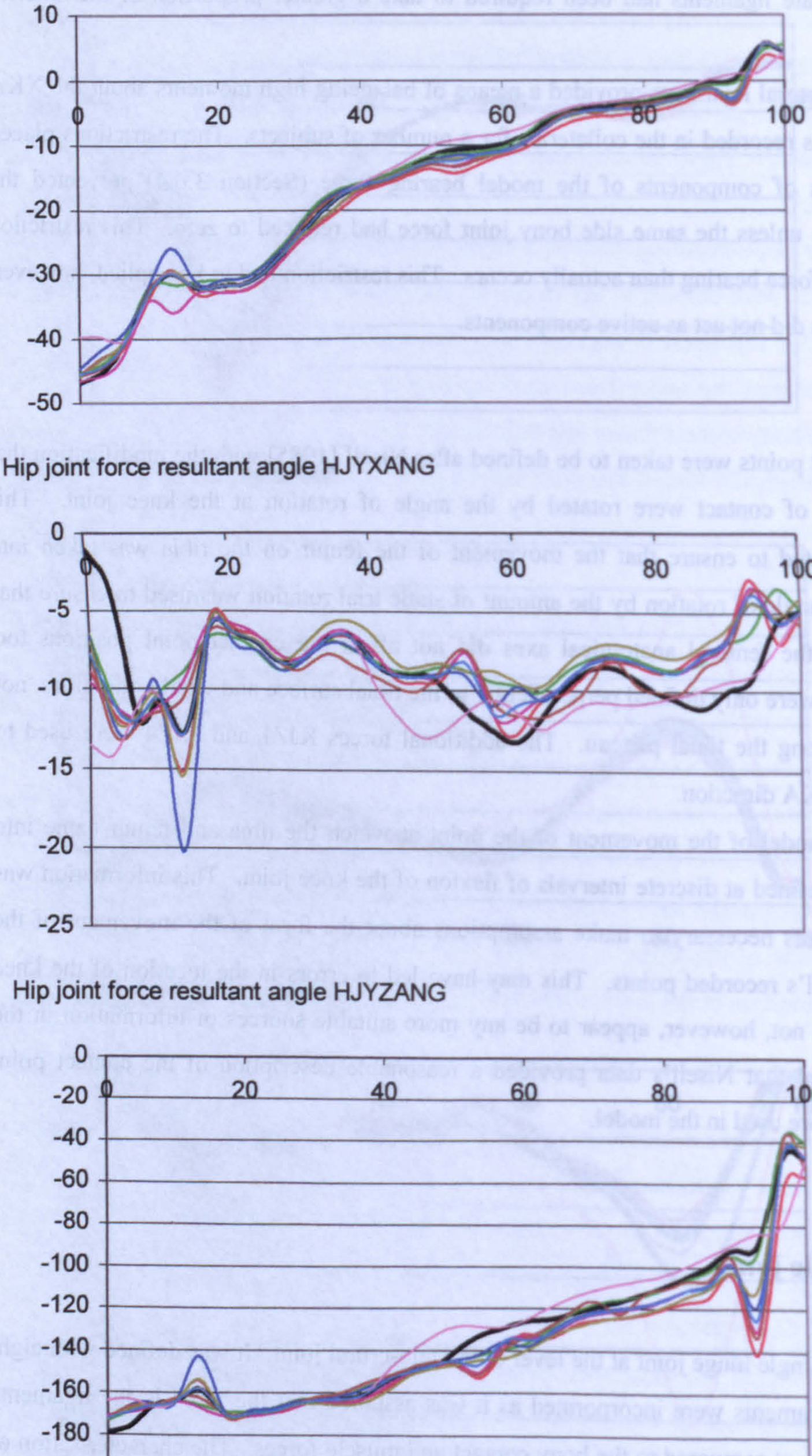

Hip joint force resultant angle HJYXANG

Hip joint force resultant angle HJYZANG

Hip joint force resultant angle HJXZANG

Hip joint force resultant angles to pelvic anatomical axes (degrees, % stance phase)

Figure 5.3 Hip joint force resultant angles to pelvic anatomical co-ordinates resulting from hip and knee centre displacement

forces been defined only at one location then no movement of the resultant force would have been possible.

5.4.4.4 The patella and foot

The model implemented for this thesis did not explicitly include the patella or foot. To completely describe the lower limb it would have been necessary to include these elements. Their inclusion, however, would have increased the complexity of the model. Inclusion of the patella may have allowed a more realistic distribution of the forces in the quadriceps muscle. Inclusion of the foot including the talocalcaneonavicular joint may have improved the ability of the model to distribute the forces in the ankle muscles.

Distribution of the forces in the vasti and ankle muscles would have had only a secondary influence on the hip joint forces calculated using the model described in this thesis. The influence of the vasti muscles on equilibrium was via the patella ligament. Therefore, only the magnitude of the resolved sum of forces in the vasti would have affected knee joint equilibrium and therefore hip joint forces. The only muscle that crossed the knee and ankle was the gastrocnemius. Any further modelling of the ankle or foot complex would have influenced the distribution of forces in the ankle muscles. The model used, however, included the tibio-talar joint and as such included the most significant element of imbalance in the flexion/extension sense at the ankle. The calculated gastrocnemius and soleus forces would, therefore, have already been providing the most significant element of balance force required at the ankle joint. Any balance at the more distal joints of the ankle, including the talocalcaneonavicular joint, would have been provided by the remaining ankle musculature, with only minor changes in the soleus and gastrocnemius forces.

5.4.5 The effect of hip and knee joint location on hip joint forces

The location of the hip joint was determined using a standard definition based on bony dimensions. Any inaccuracy in the location of the hip joint centre may have influenced the results. To provide an indication of the effect of different hip joint centre locations on the model implemented in this thesis the hip joint centre was moved in turn by ±10mm in the XPA, YPA and ZPA directions. The hip joint force components are plotted in Figures 5.1 to 5.3.

The definition of the knee joint centre was based on a number of assumptions regarding its location in the anterior posterior direction. To provide an indication of the effect of change in knee joint centre (the origin of the knee anatomical axes set) it was shifted by 10mm in the anterior and posterior directions from that calculated in the model. The results of this analysis are also included in Figures 5.1 to 5.3.

Figures 5.1 to 5.3 illustrate the effect of moving the hip and knee centres for one trial of one individual. These results are therefore only an indication of the effect that might occur due to changes in hip or knee location. When interpreting the results of this analysis the influence of moving the joint centres on the

model should be understood. Movement of the hip centre would have also moved the majority of structures around the hip joint as they were defined with respect to the hip joint centre location. Also muscle scaling factors would have been changed to accommodate the new hip location. At the knee the centre of the knee anatomical axes was used in the definition of the tibio-femoral contact points and other joint forces. The ligaments, however, were defined in the shank anatomical axes set and so would not have moved with the relocation of the centre of the knee anatomical axes. Thus the influence of movement of the hip and knee centres on the model would not have been simple, but would have been a complex interaction between all components at the joints.

There was little change in the pattern of the XFA force except with a –10mm XKA movement of the knee centre. This introduced a minor peak in early stance and increased the peak magnitude at 85% of stance. Changes in the force with movement of the hip joint were relatively minor. There was a large change in magnitude of peak YFA force with a –10mm shift of the knee joint centre. There were relatively small changes with hip joint centre location. The second peak of ZFA force also increased substantially with a negative 10mm knee joint centre move. There were also changes in the peak at 20 % of stance most notably for shifts of ±10mm of the hip joint centre in the ZPA direction. In pelvic co-ordinates the YPA and ZPA forces exhibited the greatest changes. Again these were in general due to knee joint centre movement in the negative XKA direction. Other notable features included the emergence of a minor peak in ZPA force at approximately 15 % of stance, which had the highest magnitude with hip joint centre movement of +10mm in the YPA direction.

From this one example of the effect of hip and knee centre movement on hip joint forces it would appear that incorrect location of the hip joint centre had a minor effect on the results as compared to errors in the location of the knee joint. The magnitude of the effect could be partly explained by the smaller size of the knee joint and the relatively large shift in position. This analysis does, however, show the critical nature of the correct location of the knee joint centre.

5.5 Solving the redundancy problem

The problem of distributing the forces in the muscle of the lower limb can be solved by one of several methods. The set of equilibrium equations can be reduced to a determinate set (e.g. Paul [1967], Morrison [1970]) or a number of different linear or nonlinear optimisation criteria can be used (a review of optimisation methods is provided by Tsirakos et al [1997]). These methods are often based on physiological considerations such as minimising muscle fatigue or maximising efficiency. It is possible to enhance the solution method with simultaneous recording of emg in an attempt to match muscle force with that actually occurring in the subject. Numerous criteria for the optimal control of lower limb muscles have been proposed.

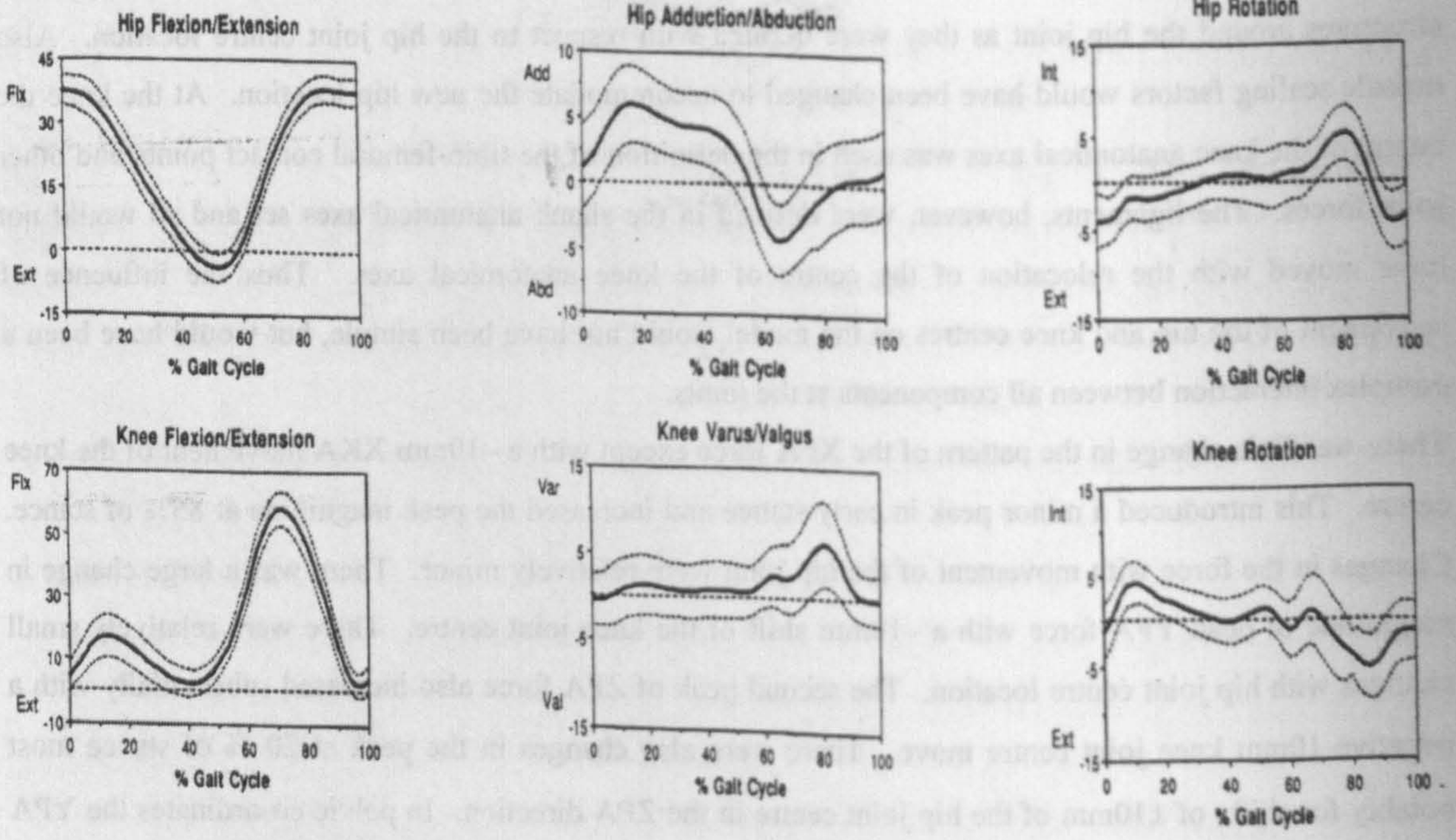

Figure 5.4A Mean and standard deviation of joint angles of normal adults during walking (from Kadaba et al [1990]). Stance forms approximately the first 60% of the gait cycle. Angles are illustrated in degrees during the gait cycle starting from foot contact and ending at next foot contact.

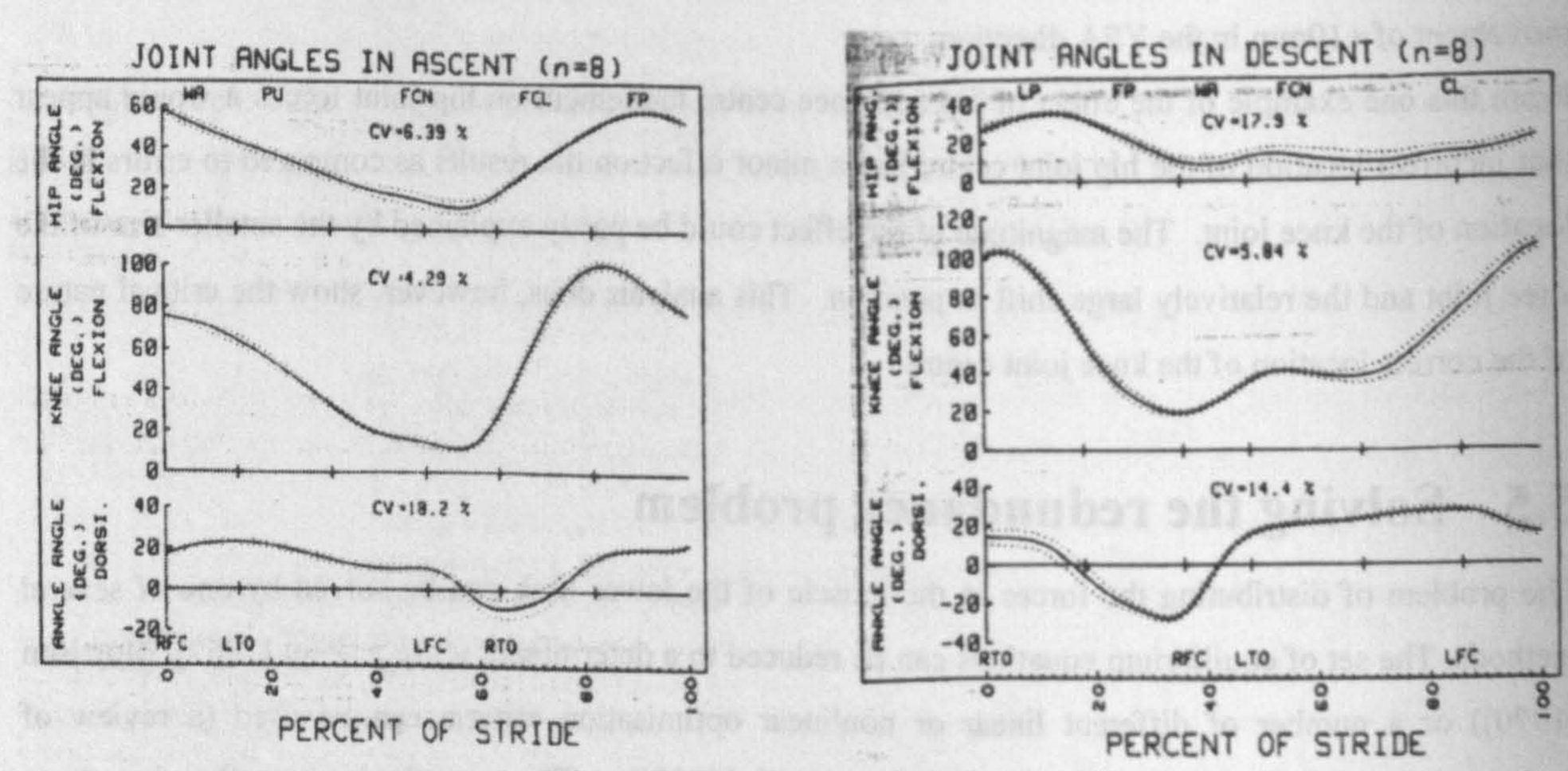

Figure 5.4B Average and standard deviation of joint angles during ascent and descent of stairs (from McFadyen and Winter [1988]).
RFC=right foot contact, LTO=left toe off, LFC=left foot contact, RTO=right toe off. Angles are illustrated in degrees for one stride.

The "*first attempt at a mathematical model of the musculo-skeletal system*" was reported by Seireg & Arvikar [1973]. They developed a model of the lower limb including all major muscle components with simple joint configurations. A linear optimisation technique based on only one of a selection of criteria was used. The results of this study were further reported in Seireg & Arvikar [1975]. Since these publications there have been numerous publications on the solution of the force distribution in the muscles of the lower limb [Tsirakos et al, 1997]. None of these publications has, however, been able to produce the definitive procedure for solving the distribution problem. Indeed Collins [1995] states that it may be "*unreasonable to suppose that the behaviour of the multi-articulated structure of the human body is governed by a unique performance criterion over the entire course of the complex movements involved in level walking*".

The method used for this thesis included first the physiological consideration of minimisation of maximum muscle stress (claimed to be a "*new*" optimisation approach by An et al [1984]). If motion is considered to be quasi-static this may be considered to be a reasonable basis on which the muscles might operate. Secondly the mathematically based criterion of minimisation of the sum of the forces in muscles, ligaments and joints. The two part optimisation formed the double linear approach proposed by Bean & Chaffin [1988]. The combination of the two was necessary to ensure that within the constraint of the first criterion a solution could be defined. The use of a set of linear criteria allowed relatively rapid computation of results for the large number of trials studied. Although this may not be a consideration in future it was for this thesis.

There were limitations to the ability of the optimisation method to distribute the forces in the muscles. Although the criteria of minimisation of maximum muscle stress allowed an increase in the number of active muscles beyond the number of equilibrium equations it still did not distribute the forces in a very physiological way. The muscle element with the maximum stress would have been either a one joint muscle or a two joint muscle and therefore the limiting factor at a maximum of only two joints. The second optimisation criterion, the minimisation of the sum of forces would have been the deciding factor at the other joint. Therefore, the distribution in forces to the muscles exhibited switching in a number of cases. The gastrocnemius and soleus muscles provide examples of the way in which the optimum solution switches between two solutions, with sharp changes in muscle forces. The only way to overcome this problem would have been to link the results of different frames of data and by setting a limit on the rate of change of muscle force. This would have involved a massive increase in the computing time and was not considered appropriate.

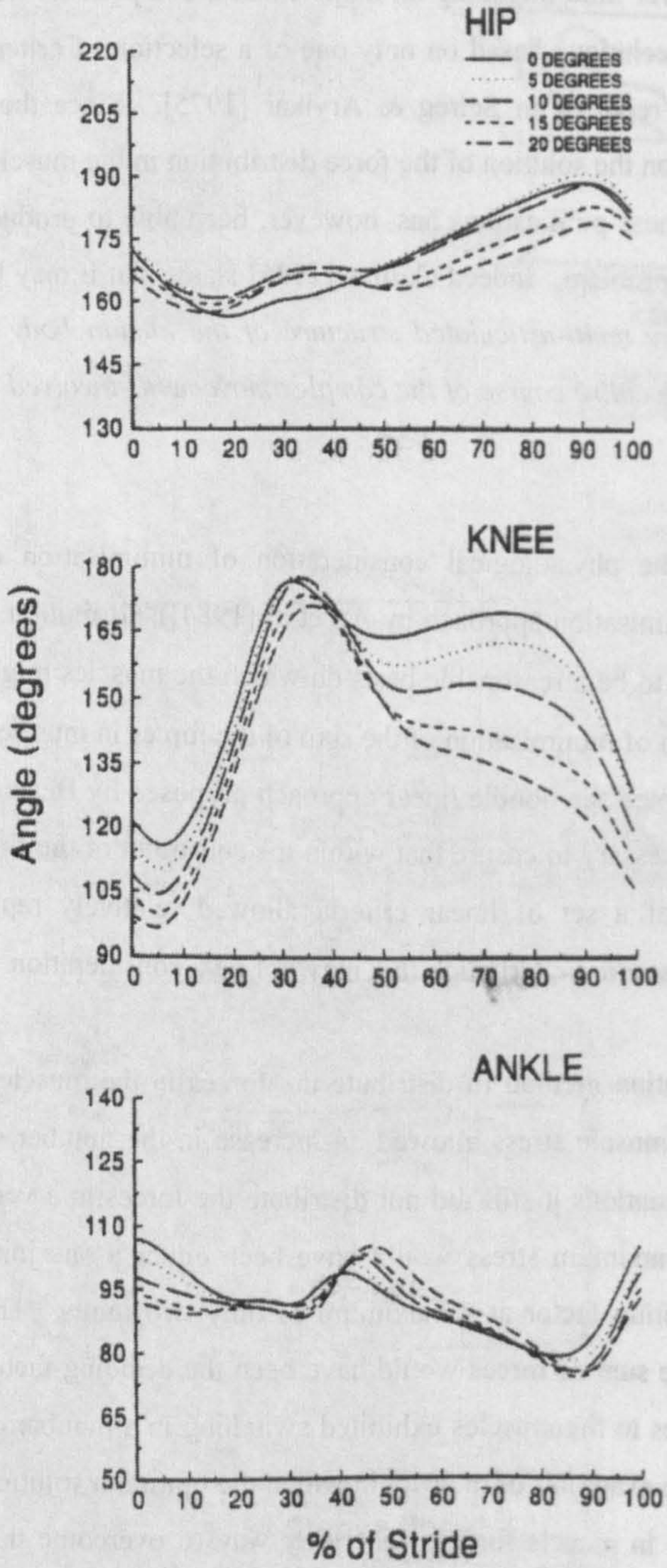

Figure 5.4C Sagittal plane joint angles in ramp descent (from Redfern and DiPasquale [1997]). Mean angles (degrees) are illustrated over the stride from toe-off to toe-off (heel contact at approximately 35% of the stride).

5.6 Inertia

The exclusion of inertial forces from the analysis may have introduced inaccuracies into the force equilibrium equations. Although it has been demonstrated that inertial forces have only a small influence on the results of slow activities such as walking it is still possible that the subjects moving at higher speeds would have developed significant inertial forces. The inclusion of inertial forces requires the double differentiation of motion data, which in itself could have introduced errors into the analysis. No inertial forces were included.

5.7 Comparison of results with others

5.7.1 Joint angles

The definition of joint angles used in this thesis was based on an ordered series of rotations. The joint angles calculated depended on the definition of the segment axes systems. Both these factors must be taken into account when comparing the joint angles presented in this thesis with those of other researchers. It is also possible that small changes in the alignment of the segment axes affected the joint angles due to a degree of cross over from the true flexion/extension, which was a relatively large angle, to the abduction and rotation angles, which were relatively small. The definition of segment axes systems has been performed in numerous ways. There is no definitely correct way of defining joint angles.

Comparing the results of walking joint angles at the hip and knee with those of Kadaba et al [1990] (Figure 5.4A) indicates that there is agreement for hip flexion and abduction and knee flexion and abduction, but not for hip and knee rotation angles. The rotation angles calculated for this thesis covered a wide range of values although in general they were consistent across the stance phase. The differences between the results of this study and those of Kadaba et al [1990] were possibly due to the differences in joint segment axes definitions. The relative segment axes orientations as defined in this study demonstrated large differences between subjects. Knee joint kinematics presented by Chao et al [1983] and Lafortune et al [1992] also agree with the results of this study for knee flexion and abduction angles, but not for the range of knee rotation angles. The patterns of the joint abduction and rotation angles of these three publications did not follow exactly the same trends as each other. It is possible that this was due to the dependence of joint angles on segment axes definitions.

McFadyen & Winter [1988] recorded sagittal plane motion for stair ascent and descent for the second step of a five step set, with a 22cm riser and a 28cm tread (Figure 5.4B). These stair dimensions were slightly higher than the 18cm riser and 26.5cm tread used for this thesis. The results of stair ascent and stair descent, hip and knee flexion angles exhibited similar patterns to those of the results in this thesis. There were, however, a number of subjects who tended to flex the knee joint to a greater degree than McFadyen & Winter's subjects.

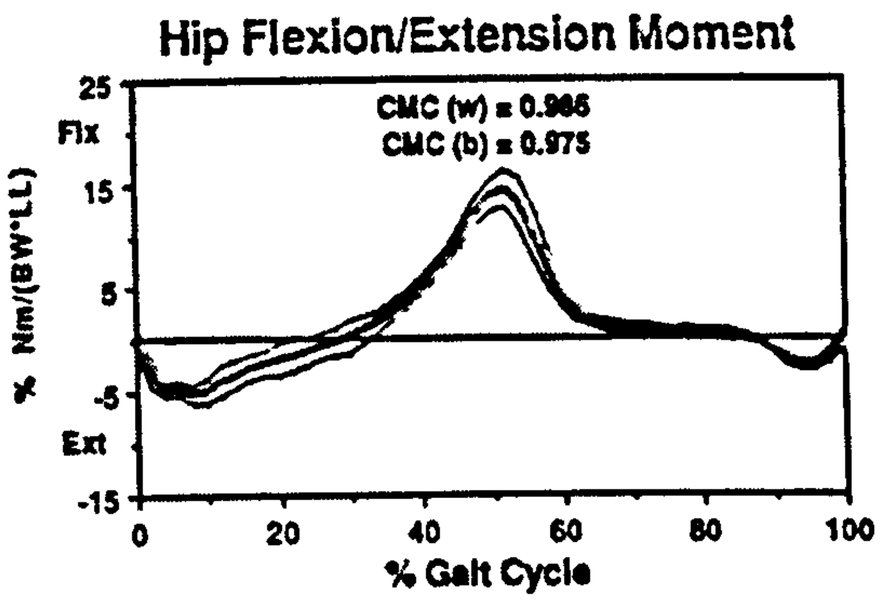

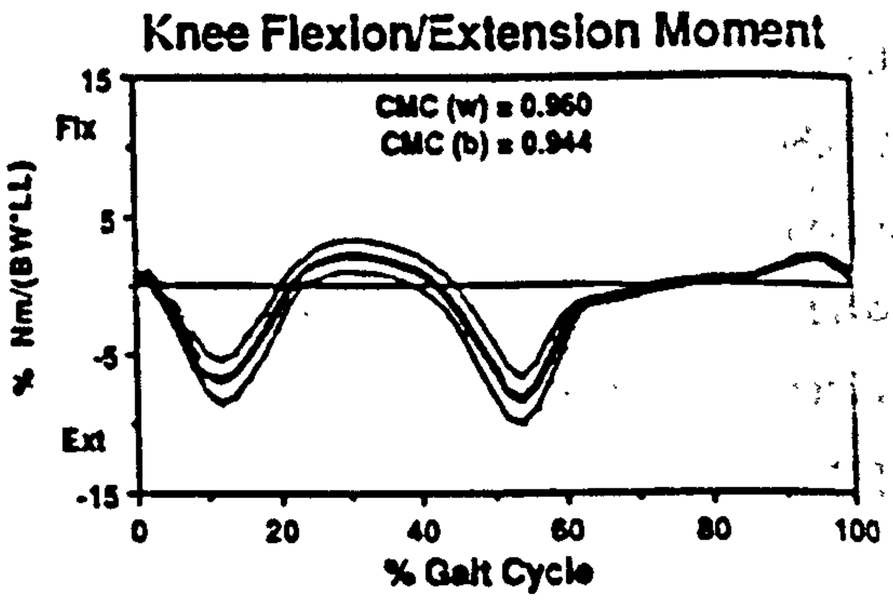

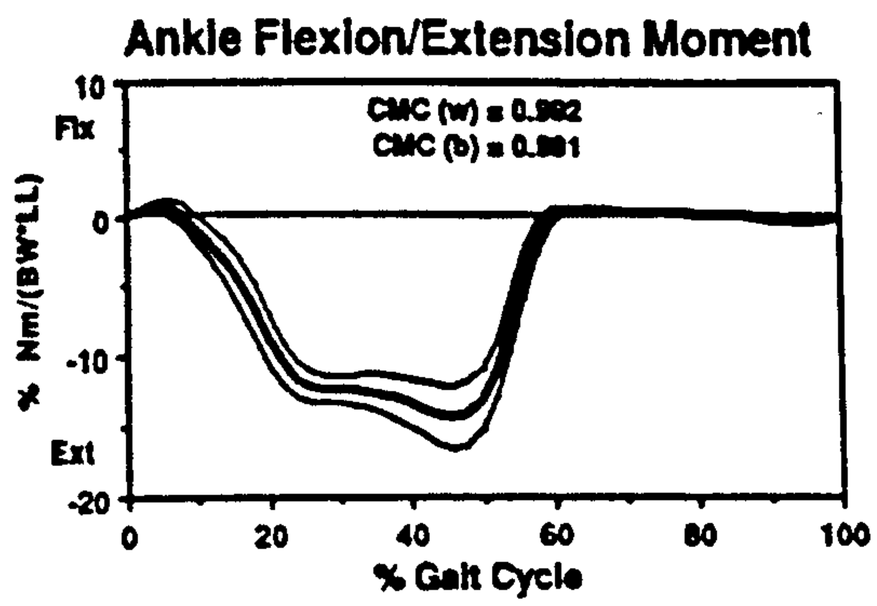

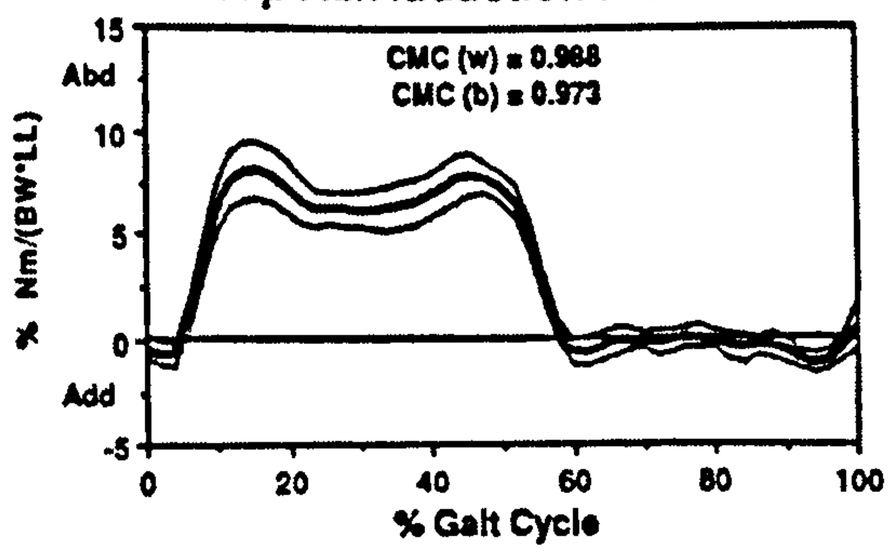

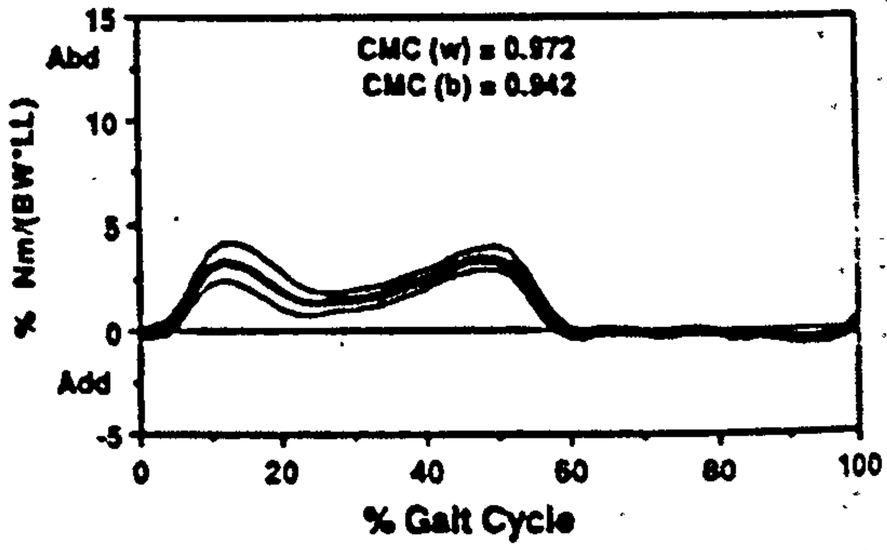

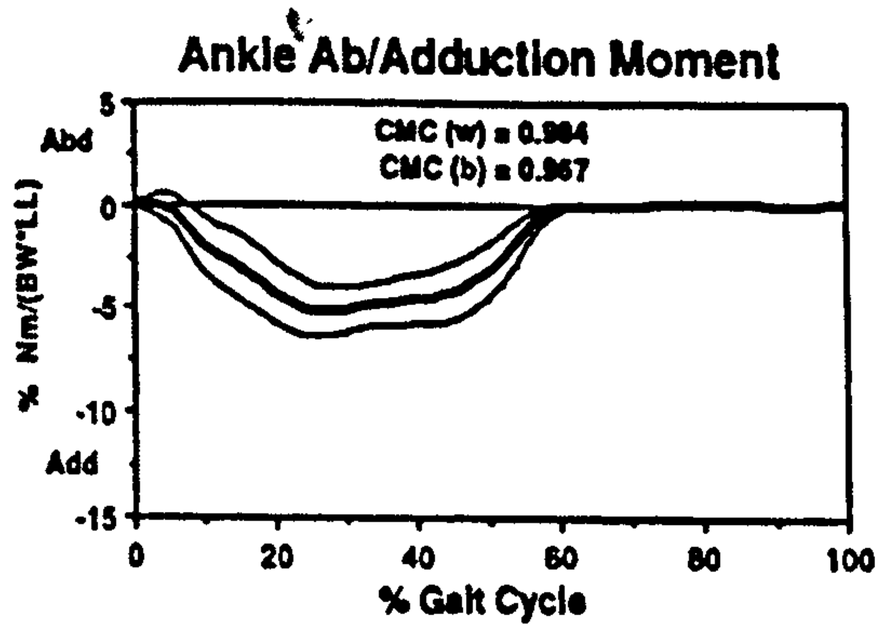

Figure 5.4D-1 Mean and standard deviation of joint intersegmental moments (from Kadaba et al [1989]).
Moments (divided by the product of body weight and leg length) are presented over the gait cycle from foot contact to next same foot contact (stance approximately 61%).

Ramp descent sagittal plane angles have been reported by Redfern & DiPasquale [1997] (Figures 5.4C). The results presented in this thesis are very similar to those presented by Redfern & DiPasquale for a 10° ramp.

The references mentioned above provide evidence that the angle calculations performed in this thesis gave results comparable with other researchers. The exceptions to this were the rotation angles at the hip and knee. These angles exhibited a greater range of values than indicated by the references. The value of the rotation angles was, however, relatively constant over stance for both walking and stair ascent. It is possible that the use of markers attached to the femoral epicondyles to define the direction of the femoral ZFA axis was not reliable. Or that the method used to define the shank segment axes using fibula head and tibial tuberosity markers was not able to accurately determine the tibial ZTA axis. The definition of the orientation of the Z axes of femur and tibia is difficult to achieve in a way that ensures they maintain the 'correct' relative orientations. The method used was aimed at establishing axes based on anatomical points of the relevant segments. A more practical method might have been to link the axes sets of the two segments, using information from both segments to establish the most correct location of their respective Z axes. This, however, was not done as an independent axis system for the two segments was considered to be more appropriate.

5.7.2 Joint intersegmental moments and forces

Ground reaction forces and resulting joint moments are dependent on the velocity at which an activity is performed [Crowinshield et al, 1978]. When comparing the results presented in this thesis with those of other publications the speed of progression (and cadence and step length) (all reported in Appendix VII) must be taken into consideration.

The intersegmental joint forces and moments presented in this thesis are particular to the joint axes systems used in their definition. A brief comparison of joint moments with the literature will, however, be given to provide an indication of the agreement between the results of this thesis and those of other researchers.

For walking, Glitsch & Baumann [1997] present three-dimensional intersegmental moments at the hip, knee and ankle. Their presentation of the moments was, however, based on the pelvic, shank and shank co-ordinate systems for the hip, knee and ankle moments respectively and, therefore the hip and ankle joint moments are not directly comparable. Moment patterns, however, demonstrate general agreement with the results presented in this thesis. The knee joint sagittal moment of Glitsch & Baumann [1997] demonstrated two negative peaks whereas the results of this thesis demonstrated only one, with a late stance switch to positive moment. This difference may be due to the fact that Glitsch & Baumann [1997] used a fixed knee joint centre.

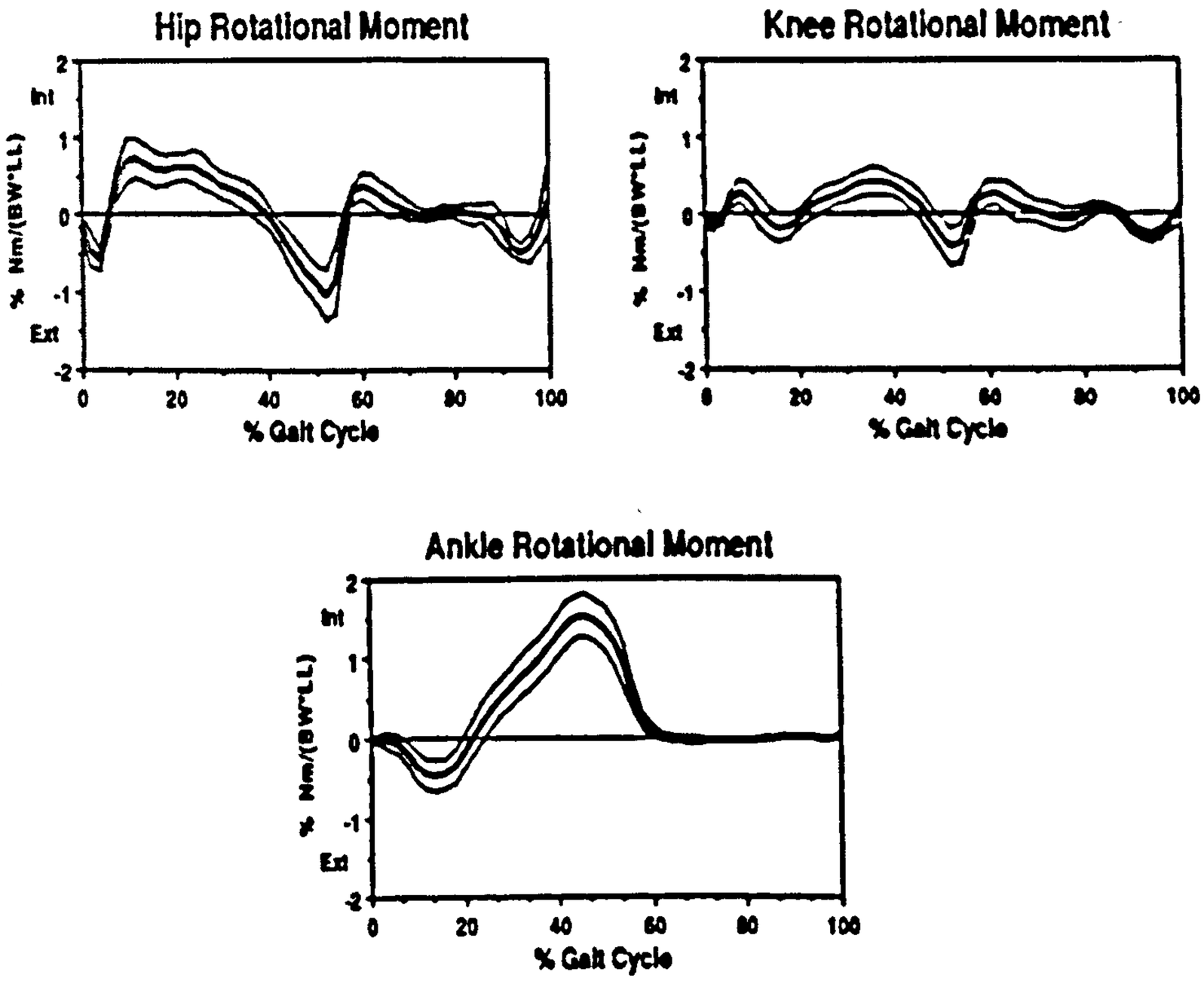

Figure 5.4D-2 Mean and standard deviation of joint intersegmental moments (from Kadaba et al [1989]).
Moments (divided by the product of body weight and leg length) are presented over the gait cycle from foot contact to next same foot contact (stance approximately 61%).

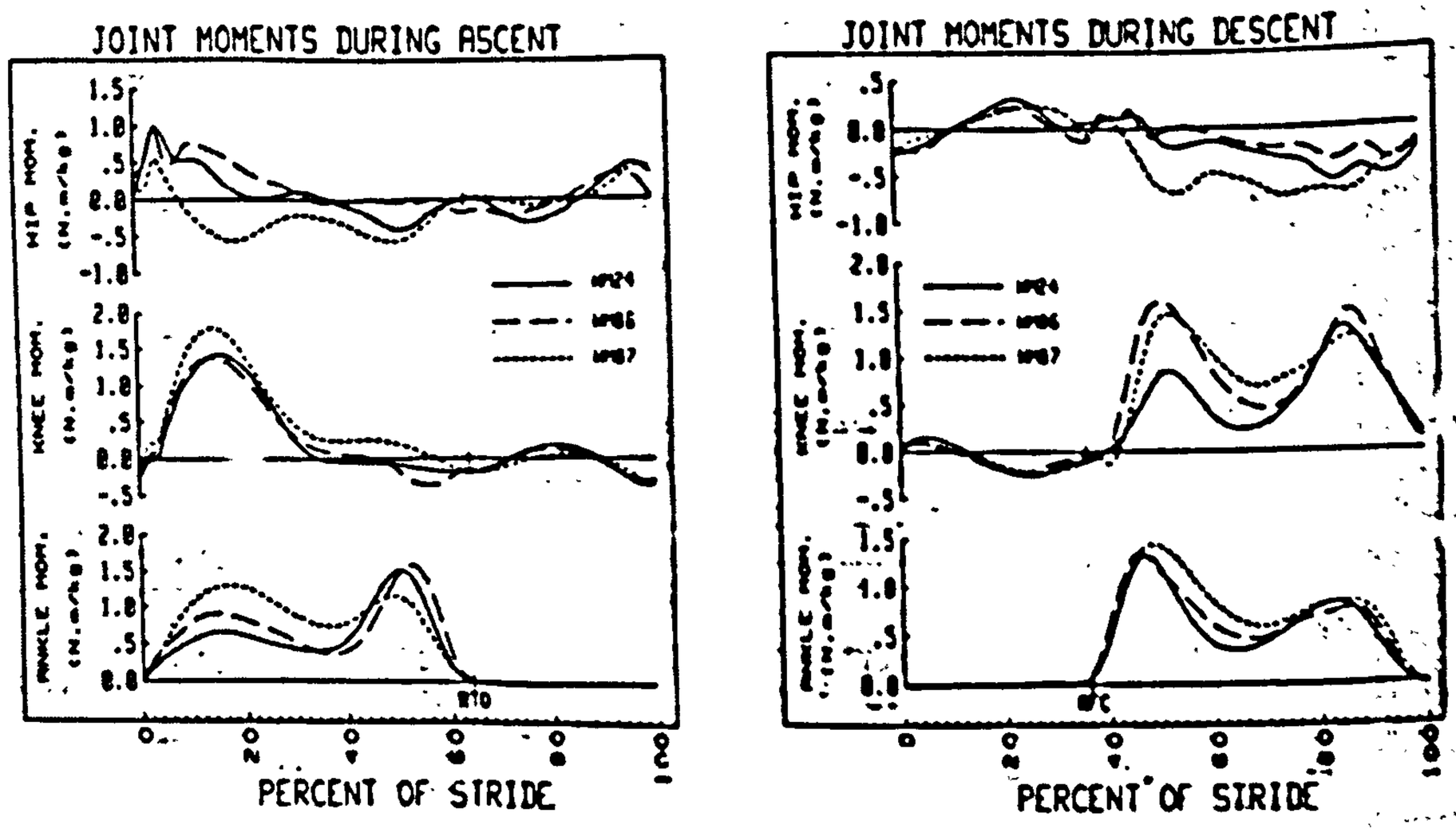

Figure 5.4E Sagittal plane joint moments during stair ascent and descent (from McFadyen and Winter [1988]).
Moments (divided by body mass) are illustrated over one stride. For ascent the stride commences at initial foot contact and for descent at foot off.

Kadaba et al [1989] also present intersegmental moments (Figures 5.4D-1 and 2) at all the joints for walking, but again these were in different co-ordinate systems and about different joint centres. Hip, knee and ankle sagittal and frontal plane moments compare well, with approximately the same patterns, although the knee flexion pattern of Kadaba et al [1989] exhibited the same double peak as that of Glitsch & Baumann [1997]. Transverse or rotation moments were not of similar patterns. This may have been due to the differences in segment axes and joint centre definitions.

McFadyen & Winter [1988] and Kowalk et al [1996] (0.203m riser, 0.254m run) present moments for stair ascent (Figure 5.4D), which demonstrated the same general pattern as those of the present study.

The patterns and magnitudes of the ankle moments reported in the literature were in some cases similar to those of this study. There were, however, differences, which may have been due to the definition of the ankle joint centre and orientation of the axes of the talo-crural joint used in this thesis. The publications reported tended to use the mid malleolar point as the ankle joint centre with a variety of definitions of the ankle medio-lateral axis. The use of the talo-crural axis would have reduced the moment compared to the inter-malleolar axis as the lever arm of the resultant force (usually tending to cause a dorsiflexion moment) would have been reduced. It must be reiterated that the intersegmental moments and forces presented within this thesis are co-ordinate system dependent.

5.7.3 Muscle activation patterns

EMG patterns have been reproduced to provide an indication of the agreement between the muscle activation patterns of this study and the activity indicated by University of California [1953]. The activity as recorded by University of California [1953] varied between subjects, indeed for several muscles two distinct activation patterns were recorded. The emg patterns can only, therefore, be used as a guide to possible muscle force. An additional difficulty in interpreting results arises from the time delay between emg activity and muscle force generation. It is suggested in University of California [1953], that there could be a delay of 0.08s between peak electrical and peak force activity. The muscle force results of walking and stair ascent have been included to provide an indication of the ability of the model to distribute the forces between the muscles. Numerous other authors have provided records of emg activity in the muscles of the lower limb. Examples of these are Arendt-Nielsen et al [1991] who presented walking and ramp emg patterns for treadmill walking and Joseph and Watson [1967] who presented stair ascent and descent emg profiles. Also Kadaba et al [1989] who examined the emg profiles of 40 subjects during walking in a gait laboratory. The results of all of these authors followed the same general patterns as those recorded by University of California [1953].

Table 5.1 Measured in-vivo hip joint forces for walking

Author	Comments	Speed (m/s)	Post op time (weeks)	Max 1 (%body weight)	Max 2 (%body weight)
Rydell [1966]					
	Patient 1	0.89	26	151	159
		1.31	26	182	176
	Patient 2	1.11	26	269	222
		1.39	26	327	222
English & Kilvington [1979]					
		0.444	1.7	287*	
		0.730	6	320*	
Davy [1988]					
		0.5	4.4	264*	
Kotzar et al [1991]					
Patient 1, 67 yrs female	Crutch or parallel bars	0.43-0.50	4.4	230-310*	
Patient 2, 72 yrs male		0.9	8.3	240*	
		1.1	8.3	250*	
		1.3-1.4	8.3	280*	
		1.8	8.3	360*	
Bergmann et al [1993]					
Patient 1 (EB) left		0.28	130	293*	
	53cm length steps	0.83	35?	340*	
	64cm length steps	0.83	35?	357*	
		0.83	130	330*	
		1.39	130	394*	
Patient 1 (EB) right		0.28	130	293*	
	52cm length steps	0.83	35?	405*	
	60cm length steps	0.83	35?	449*	
	70cm length steps	0.83	35?	428*	
		0.83	130	352*	
		1.39	130	471*	
Patient 2 (JB)		0.83	35	464*	
Bergmann et al [1995B]					
Patient 1 (EB) left	bare foot	0.83	30	289*	
	other foot wear	0.83	30	±6	
Brand et al [1994]					
		1.11-1.36	8	200-300	180-330

*=Overall maximum

5.7.3.1 Walking

In general there was good agreement between the emg patterns and the muscle forces. There were, however, several exceptions to this. The force in gluteus maximus 1 covered a wider range of stance than the emg pattern suggested. The other two part of gluteus maximus did, however, conform to the emg, suggesting that the emg profile could have been taken from a less active section of the muscle. Biceps femoris long head force in early stance agreed with the emg profiles, however, force in late stance was not indicated by the emg. Gracilis force was concentrated in the second half of stance and although force was indicated as possible in this part of stance it did not coincide with the peak emg activity. The second peak in rectus femoris force was not indicated by the emg profile although there was possible activity indicated for the whole of stance. Sartorius, semimembranosus and semitendinosus appeared to be more active than suggested by the emg profiles. This might indicate that the model had a tendency to predict higher antagonism than actually occurs in order to satisfy the imposed equilibrium constraints at the knee. Vastus lateralis and vastus medialis were not as active as the emg patterns suggested. This may have indicated that the muscle forces in the vasti were not being distributed correctly. Several of the ankle muscles did not exhibit patterns of force in agreement with the emg profiles. These included: Tibialis posterior, flexor digitorum longus, flexor hallucis longus, peroneus brevis and peroneus longus. It must be concluded from this observation that the forces were not correctly distributed in the ankle muscles. This was most probably due to the modelling of only one of the ankle's two principal joints. Had equilibrium about the talocalcaneonavicular joint been required then the forces in the ankle muscle would have been further constrained.

5.7.3.2 Stair ascent

Stair ascent muscle force patterns followed approximately the trends of the emg patterns. There were, however, several exceptions to this: Iliacus was active for more of the stance phase than indicated by the emg patterns. Gracilis exhibited less force than indicated by the emg profile. Sartorius, semimembranosus and semitendonosus all exhibited force over a wider range of the stance phase than indicated by the emg patterns. Vastus lateralis and medialis tended to exhibit less force in the second half of stance than the emg profiles indicated. Several ankle muscles did not show as much force as suggested by the emg. These included: tibialis posterior, flexor digitorum longus, flexor hallucis longus, peroneus brevis, peroneus longus, tibialis anterior, extensor digitorum longus and extensor hallucis longus. Some of these ankle muscles, exhibited force in agreement with the emg patterns for a small number of subjects. The lack of agreement of the ankle only muscles and the emg patterns suggested that the model was not distributing the forces at the ankle in a physiologically correct manner. As detailed above in the discussion of walking muscle forces it is suggested that the inclusion of the talocalcaneonavicular joint in the model would have forced a more reasonable distribution of muscle forces.

Table 5.2 Measured in-vivo hip joint forces for stair and camber

Author	Comments	Post op time (weeks)	Max 1 (%body weight)	Max 2 (%body weight)
Stair ascent and descent				
Rydell [1966]				
Ascent, subject 1			150*	
Ascent, subject 2			340*	
Davy et al [1988]				
Ascent	Rise 0.17m, tread 0.28m. Using banister	4.5	260*	
Kotzar et al [1991]				
Ascent, patient 1	Banister	4.4	230*	
Ascent, patient 2		8.3	260*	
Bergmann et al [1995]				
Ascent, patient 1 left	Rise 0.17m	61-143	345*	
Descent patient 1 left		61-130	394*	
Ascent, patient 1 right		117-130	356*	
Descent, patient 1 right		117-130	390*	
Ascent, patient 2		35	552*	
Descent, patient 2		35	509*	
Ramp ascent and descent				
Bergmann et al [1993]				
Ramp 15°, patient 1 left		35	Walking +30%	

*=Overall maximum

5.7.3.3 Quadriceps and calf muscle force distribution

The distribution of the forces in the quadriceps and calf muscle provides an indication of the model's ability to distribute the forces in the muscles for the other activities. Several general observations can be made about the results presented in Appendix VI.3C. Firstly vastus lateralis and medialis force was lower than indicated by the emg profiles and secondly there was switching of muscle forces between the soleus and the two elements of the gastrocnemius. These observations indicate an inability of the model to distribute force in the vasti and the tendency of the optimisation to switch between favoured solutions.

5.7.4 Shortcomings in the ability of the model to distribute force

Reasonable agreement between the emg profiles and the muscle force profiles at the hip were obtained for both walking and stair ascent. There was some disagreement between the force indicated by the emg patterns and some of the hip and knee two joint muscles. The semimembranosus, semitendonosus and sartorius force patterns did not match those of the emg profiles. It is possible that the line of action of these muscles were not adequately defined for the full range of motion encountered in these activities.

Distribution of muscle force in the vasti seemed to favour the vastus intermedius. The distribution of forces in the vasti may have been improved if the patella bone equilibrium had been included in the model.

Ankle muscle force distribution was not adequately enforced by the single talo-crural joint. Inclusion of the talocalcaneonavicular joint may have been able to overcome this inability.

5.7.5 Muscle force switching and erroneous results

Within the muscle force results there were numerous indications of switching between muscles to satisfy the two criteria of minimisation of maximum stress and minimisation of the sum of muscle forces. It was hoped that the use of these two criteria would provide a stable solution to the force distribution problem. It would appear, however, that as the model included three joints the solution frequently changed its choice of the optimum combination of muscles. An example of the effect of the switching on and off of a muscle can be seen in peroneus brevis in stair ascent (Figure A-VI.3B.42). It would appear from this figure that there was a level of force common to most subjects, but that this level of force was not always the optimum based on the specified criteria. The muscle was either on or off. This is not a physiological muscle force pattern. Unfortunately the optimisation criteria chosen could not eliminate this effect. Additional constraints such as specifying the maximum change in muscle force with time could have over come this problem but would have increased the computational time enormously.

Table 5.3 Calculated hip joint forces for walking

Author	Comments	Speed (m/s)	Max 1 (%body weight)	Max 2 (%body weight)
Paul [1964]				
	Double '2nd peak'		580	380/470
Paul[1967]				
			425	442
Paul [1975]				
			296	450
		1.11	411	480
		1.47	675	736
		2.00	554	585
Paul & Poulson [1974]				
	Mean range	1.50	298-753	447-697
			687	771
	Mean range	2.06	572-1032	572-1012
			590	582
Brown et al [1984]				
	Normal		417	477
	Patient Charnley		263	329
	Patient Muller		343	440
Seireg & Arvikar [1975]				
			532	464
Crowninshield et al [1978B]				
		0.95-1.05	350-520	190-320
Crowninshield et al [1978]				
	Old person	0.28	331±118*	
	Old person	0.83	381±118*	
	Old person	1.39	442±118*	
	Young person	0.28	344±140*	
	Young person	0.83	429±134*	
	Young person	1.39	585±151*	
Rohrle et al [1984]				
		0.8	290	410
		1.2	430	550
		1.6	570	690
Brand et al [1989]				
			310-500*	
Simonsen et al [1995]				
	Mean	1.43	639*	
Pedersen et al [1997]				
	72yrs male	0.89	251	315
Fitzsimmons [1995]				
	Normal, mean		425	501
	Hip replacement, mean		333	350

*=Overall maximum

The switching of muscle forces affected the hip joint forces, although the effect was smoothed as the hip joint force was the resultant acting against a large number of muscle force components.

A number of the result's graphs include values that are much higher or much lower than the common trend in the data. The majority of these results are in error and in the majority of cases due to one of the following reasons: Poor location of markers in space, large soft tissue movements, poor interpolation, inability of the software to find the correct optimised solution. Grossly different results of individual trials are, therefore likely to be in error and are only included for completeness.

5.7.6 Ankle and knee joint forces

Proctor & Paul [1982] reported ankle joint forces for walking at the talo-crural joint of between 2.91 and 4.67 times body weight. These values are in generally lower than those of the present study (Appendix VI.5). The pattern of ankle joint force, however, followed approximately that of the present study. It is possible that differences in speed of progression of the subjects affected the results. The redundancy problem was solved, by Proctor & Paul [1982], by reducing the problem to a determinate solution. It is possible that this also had a significant impact on the results. Seireg & Arvikar [1975] reported total ankle joint forces of up to 5 times body weight. The resultant force profiles that they calculated were in general agreement with the results of this thesis, although somewhat lower in magnitude. Seireg & Arvikar used only a single joint force in their model.

Knee joint forces have been reported by a number of authors. The value of the total knee force between femur and tibia is reported by Morrison [1970] as being between 2.06 and 4 times body weight, by Paul & Poulson [1974] as an average maximum of 3.70 times body weight, by Harrington [1983] as to average 3.5 times body weight and by Cheng et al [1993] to be a maximum of 4.31 times body weight. Seireg & Arvikar [1975] reported values over 7 times body weight, calculated using a linear optimisation model. The results of this thesis suggest that knee joint forces reach higher values than those demonstrated by the first four publications with the sum of the two components reaching up to 7 times body weight for walking. The pattern of joint force calculated by both Morrison and Harrington were of approximately the same form as that of this study, having two characteristic peaks. Both Morrison and Harrington, however, recorded an initial peak after foot contact that was not always evident in the present study. Both of these two studies use a determinate solution for the calculation of results and only considered the knee joint in isolation. The initial peak observed in the results of these two authors is attributed to hamstring force. It is possible, therefore, as two joint muscles are involved, that the force peak is an artefact of the solution method taking into account only the knee joint and not hip joint equilibrium. The further constraints of hip and ankle joint equilibrium, required for solution in this thesis, were likely to have introduced more

Table 5.4 Calculated hip joint forces for stair and ramp

Author	Comments	Max 1 (%body weight)	Max 2 (%body weight)
Stair ascent and descent			
Paul & Poulson [1974]			
Ascent/descent		300-1050*	
Crowninshield et al [1978]			
Ascent		600-800*	
Descent		300-400*	
Fitzsimmons [1995]			
Ascent	Normal subjects, mean	467	408
	Hip replacement subjects, mean	384	344
Descent	Normal subjects, mean	436	359
	Hip replacement subjects, mean	379	322
Physical model			
Shelley et al [1996]			
Ascent		470*	
Ramp ascent and descent			
Paul & Poulson[1974]			
Ascent	(mean range)	325-769	436-782
Descent	(mean range)	359-790	308-820

*=Overall maximum

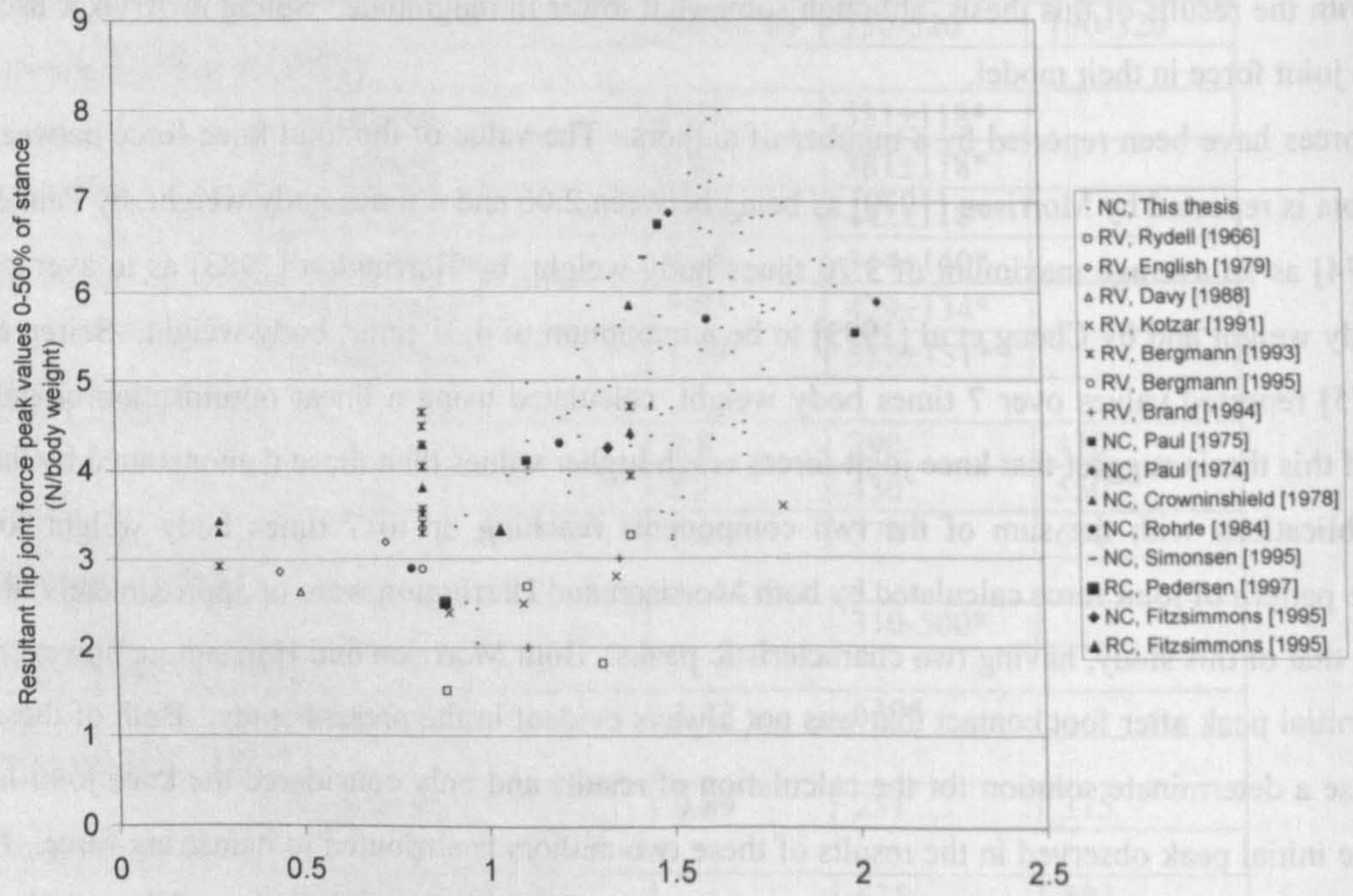

Figure 5.5A Maximum resultant force first peak for this thesis and as reported in the literature (maximum force used if no information on first peak given, see Tables for details). N=normal subject, R=hip replacement subject, V=in-vivo measurement, C=calculated value.

demanding restrictions on the muscle force patterns. This would have lead to higher muscle and joint forces as evident in the results of this thesis. The results of Seireg & Arvikar [1975] were based on a model minimising the sum of muscle forces plus 4 times the sum of moments at all the joints. Their knee joint force was modelled as a single force. The values of peak magnitude calculated for the knee force were in agreement with the forces exhibited by subjects studied for this thesis. The pattern of the forces was, however, more variable with four peaks of force indicated compared to the two major peaks observed in the present work.

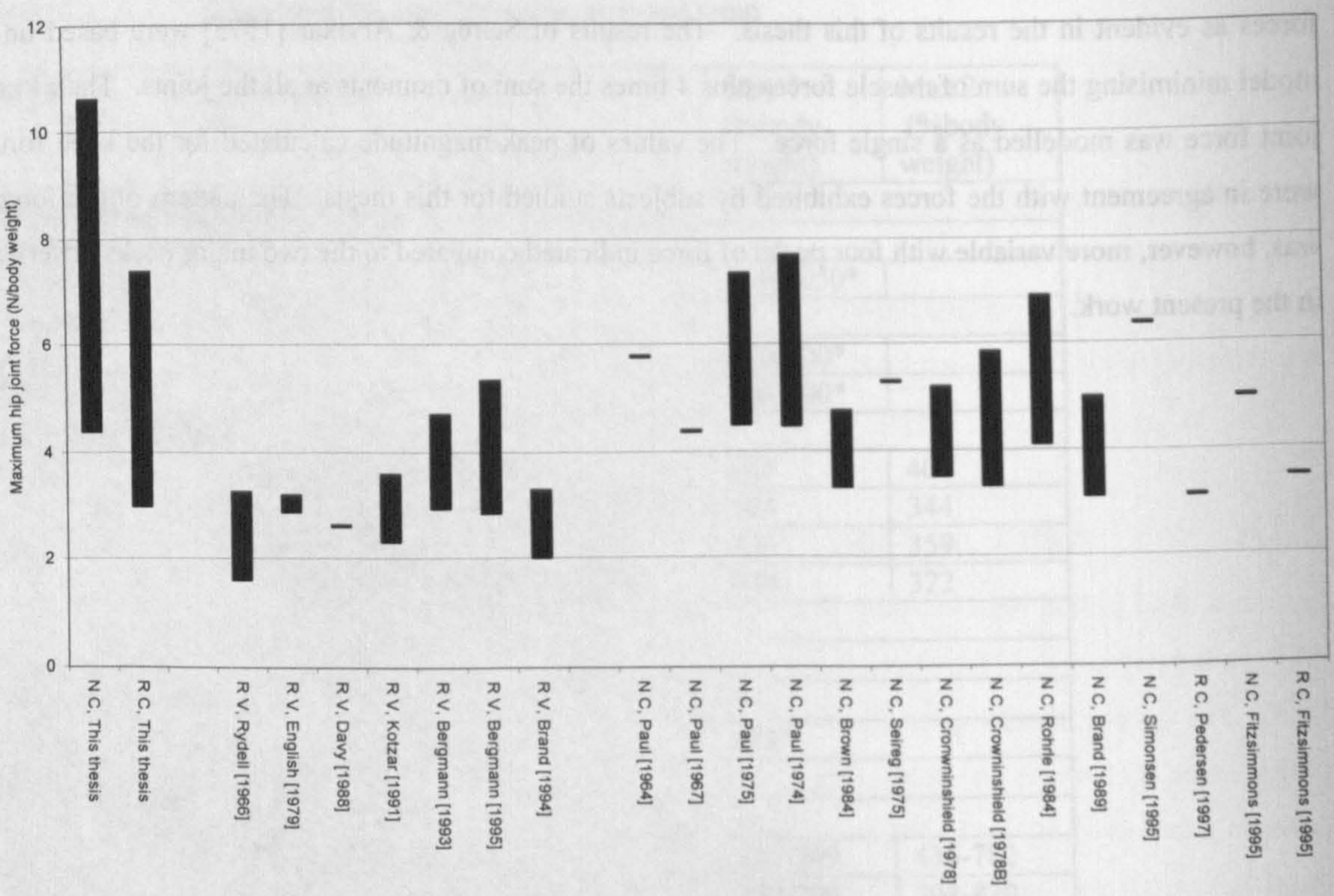

Figure 5.5B Walking. Range of maximum resultant hip joint force, by author. Either range or mean value is illustrated. N=normal subject, R=hip replacement subject, V=in-vivo measurement, C=calculated value.

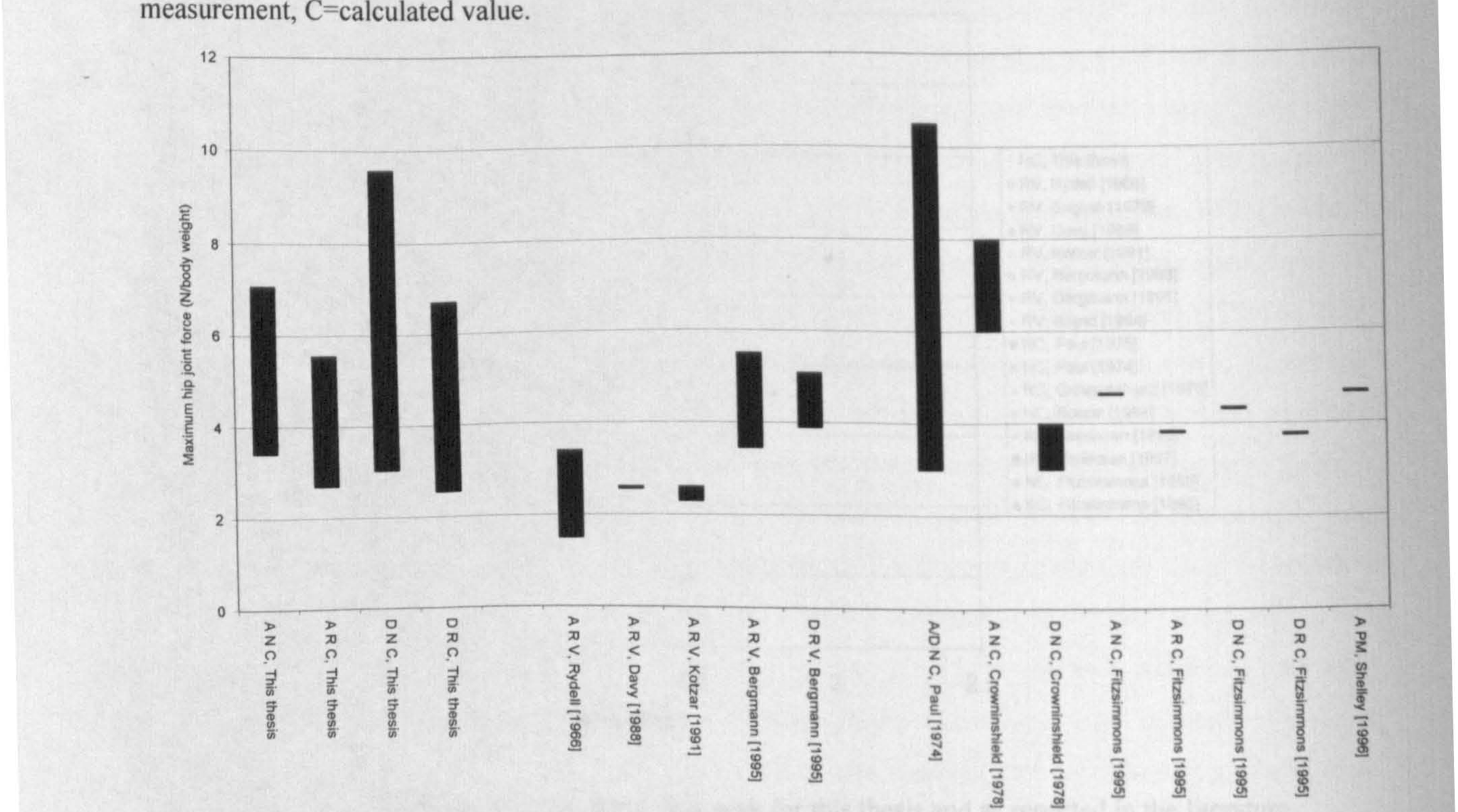

Figure 5.5C Stair ascent and descent. Range of maximum resultant hip joint force, by author. Either range or mean value is illustrated. A=ascent, D=descent, N=normal subject, R=hip replacement subject, V=in-vivo measurement, C=calculated value, PM=physical model.

5.7.7 Hip joint forces

5.7.7.1 Introduction

Hip joint forces are presented in both femoral and pelvic anatomical co-ordinate systems with the angles of the resultant force to each system also given (Appendix VI.4).

Hip joint forces have been reported by a number of authors. Sources are either theoretical or in-vivo. As the effect of differences in speed, cadence and step length on joint kinetics is known to be large (e.g. the effect of speed on calculated joint forces Rohrle et al [1984]) an attempt has been made to indicate these parameters.

Studies of the forces in an instrumented massive femoral implant have been reported in comparison with model calculations (Bassey et al [1997], Lu [1997], Lu et al [1997,1998]). The subjects underwent major alterations to lower limb musculature and, therefore, the results would not be directly comparable with the results presented in this thesis.

Femoral head pressures have been measured using an instrumented endoprosthesis by Hodge et al [1989] (Givens-Heiss et al [1992]). These were not directly comparable with the results of this study and are therefore not discussed.

The following discussion of hip joint forces will concentrate on the components of force as presented in the results. Femoral torque and femoral resultant force angles have not been presented although these may be derived from the results presented.

Bergmann et al [1993] provided a summary of hip joint force measurements and calculations by other authors for comparison with their data of the hip joint forces in two subjects with telemeterised hip replacements. Part of these data have been reproduced in Tables 5.1 to 5.4 with the results of more recent studies and those of Bergmann et al [1993] included.

5.7.7.2 Walking

Peak resultant hip joint forces as demonstrated by prosthetic implants in general increased with increase in speed of walking (Table 5.1). Bergmann et al [1993] demonstrated the variation in resultant hip joint force with changes in step length at the same walking speed. There were changes, but these were not consistent with increasing step length indicating that both step length and cadence may influence hip joint force. In general Bergmann et al's [1993] subjects demonstrated the highest resultant force peaks. Bergmann et al [1993] also report hip joint forces of 720 and 870% body weight in two of their subjects when they stumbled.

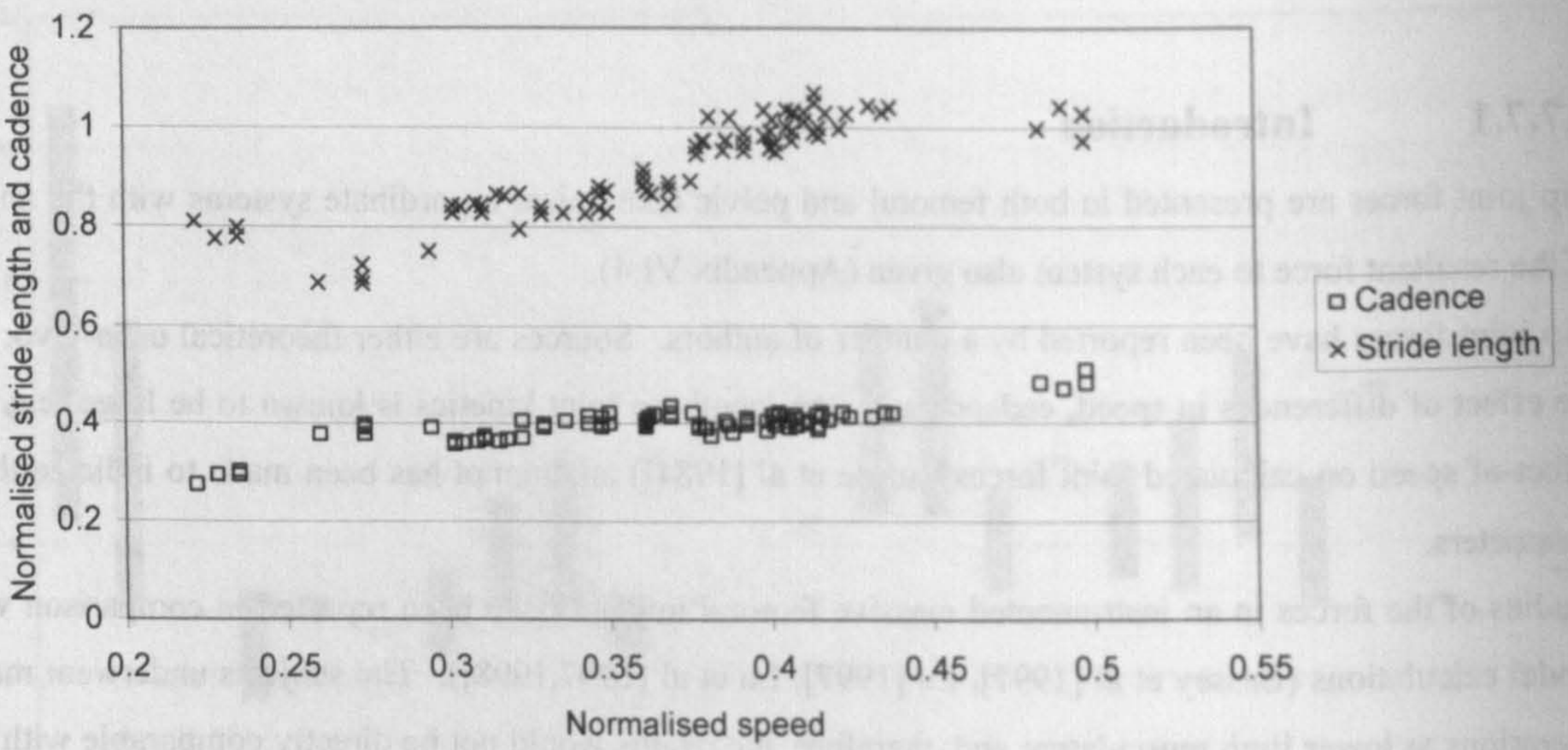

Figure 5.6A Normalised stride length and normalised cadence vs. normalised speed. All walking trials, all subjects.

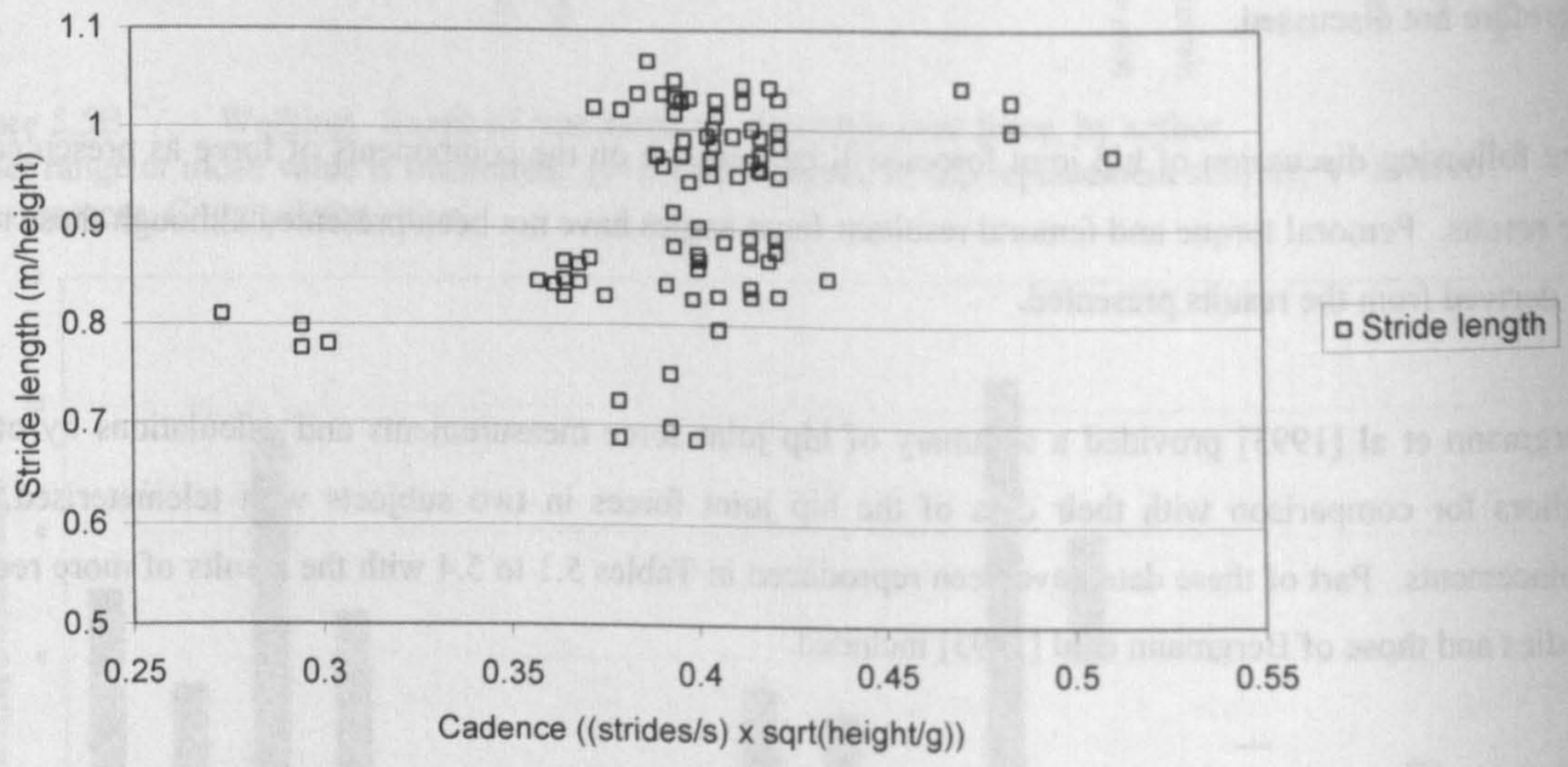

Figure 5.6B Normalised stride length vs. normalised cadence. All walking trials, all subjects.

Figure 5.5A illustrates the comparison between the results of the present study and those reported in the literature. Peak hip joint forces over the first 50% of stance from this study have been plotted against speed (m/s), with literature results superimposed. It should be noted that the results of Bergmann [1993] were controlled for speed whilst different stride lengths were used. Figure 5.5B plots the ranges of results reported in the literature for maximum resultant hip joint force with those from the present study. There was a wide range of values demonstrated The results of Rydell [1966] were particularly low in comparison with all other data sources. These results were, however, recorded only shortly after implantation. Calculated results (using models of the lower limb and assumptions of muscle force distribution) (Table 5.3) were in general higher than those of the in-vivo measures. In general these calculations were based on subjects moving at higher speeds than the in-vivo studies (Figure 5.5A). The peak forces of the calculated results from the literature were of the same order of magnitude as those calculated for the subjects studies for this thesis.

The pattern of the resultant hip joint force was demonstrated to follow a double peak pattern by almost all subjects in all the literature. This was not the case for very early post operative results of English & Kilvington [1979], where the hip joint forces varied in profile with some steps demonstrating single and some double peaks. The relative magnitude of the peaks differed between publications. The subjects studied by Davy et al [1988] and Kotzar et al [1991,1995] demonstrated a lot of variation in the relative magnitude of the two peaks, with no distinct tendency for one or the other to be the largest. Bergmann et al [1993], however, recorded a distinctly larger first peak than second. For calculated forces Crowninshield et al [1978] demonstrated a very large first compared to second peak and Rohrle et al [1984] demonstrated a high second peak compared to first.

It is possible that the differences in resultant joint force profiles calculated using leg models were due to differences in the models used. The differences in in-vivo hip joint force measurements, however, demonstrate the variation in the form of the hip joint force profile. This was reflected in the different magnitudes of resultant joint force calculated in this thesis especially for the hip replacement subjects.

The relative contributions of the components of the hip joint force to the resultant depend on the axes system used in their definition. The femoral anatomical components of the hip joint forces presented in this thesis are in general agreement with those presented in the literature, although the second peak as demonstrated in the ZFA direction was more pronounced in this work than in the literature. Pelvic forces were approximately similar in profile to those of Pedersen et al [1997] although the XPA forces of this thesis did not demonstrate as large a force in the second half of stance.

The resultant hip joint force angles were in general agreement with those in the literature (e.g. Bergmann et al [1993]). The angles of inclination to the defined axes reflect the relative magnitude of the joint force components. As the comparison of the joint force components as given above indicated that

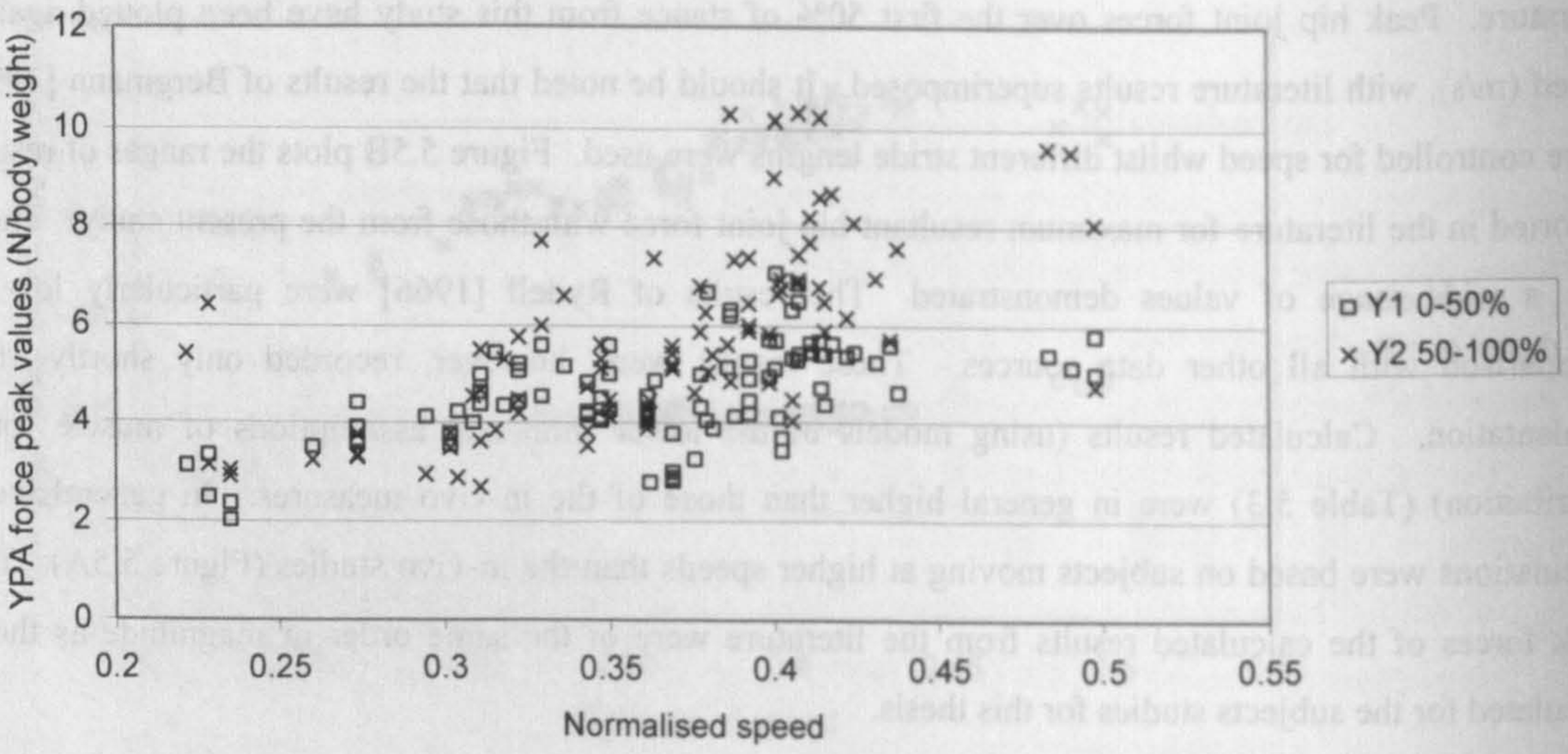

Figure 5.7A YPA hip joint force peak values vs. normalised speed. All walking trials, all subjects.

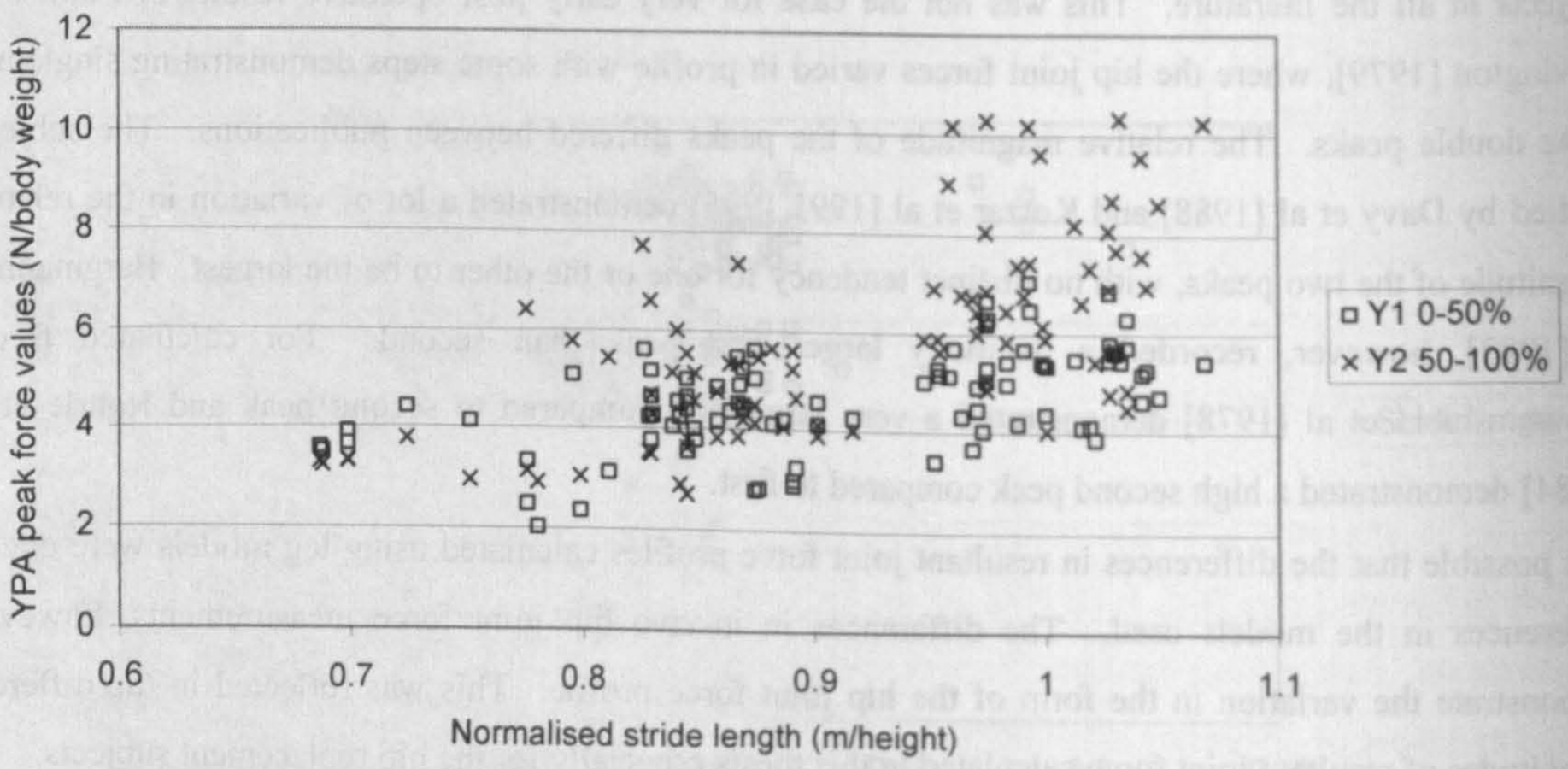

Figure 5.7B YPA hip joint force peak values vs. normalised stride length. All walking trials, all subjects.

approximately the same trends were followed then it was not surprising to find that the hip joint force angles were also similar.

Comparing the results of this thesis with those of others can, at best, only provide an indication of the suitability of the model used. It is likely that a number of factors affect the results including, speed, step length, cadence, age and post op time. The complex interaction between these factors makes direct comparison of all but within subject very difficult.

5.7.7.3 Stair ascent

Stair ascent force resultant exhibited a two peaked profile the second peak of which was lower in magnitude (compared to the walking force profiles with two approximately equal force peaks). This was also the case for the ZFA force.

In general the force magnitudes were lower than those for walking. This could be a reflection of the restricted step length enforced for a set stair tread. The exception to this being the XPA forces, which were in general higher in stair ascent than in walking.

In general the in-vivo peak resultant hip joint forces of stair ascent and descent (Table 5.2) were within the range of those of walking. Bergmann et al's [1993] second subject, however, demonstrated peak forces higher than those in walking. Calculated results presented in Table 5.4 show a wide range, rising to over 10 times body weight [Paul & Poulson, 1974]. Figure 5.5C presents maximum resultant hip joint force values as reported in the literature as compared to the results calculated for this study. This figure demonstrates the similarity in range of maximum values between this study and those of others. In-vivo studies of Rydell [1966] and Davy [1988] demonstrated particularly low forces as compared to Bergmann et al [1995]. Bergmann et al's [1995] results were of similar magnitude to those of the calculated hip joint forces. Trends between the subject sub groups of Fitzsimmons [1995] were the same as those of the present study.

The force profiles of this study were in general agreement with the patterns as demonstrated in Bergmann et al [1993]. This was similarly the case for the joint force resultant angles. The patterns of force demonstrated by Davy et al [1988] and Kotzar et al [1991, 1995] were, however, different reflecting the fact that the orientation of the axes within the femoral head were not the same as those of this study.

5.7.7.4 Stair descent

Stair descent forces differed from those of star ascent in a number of ways: They were more variable. The second peak of resultant force was in some cases more prominent. XFA demonstrated a second peak. XPA forces were lower.

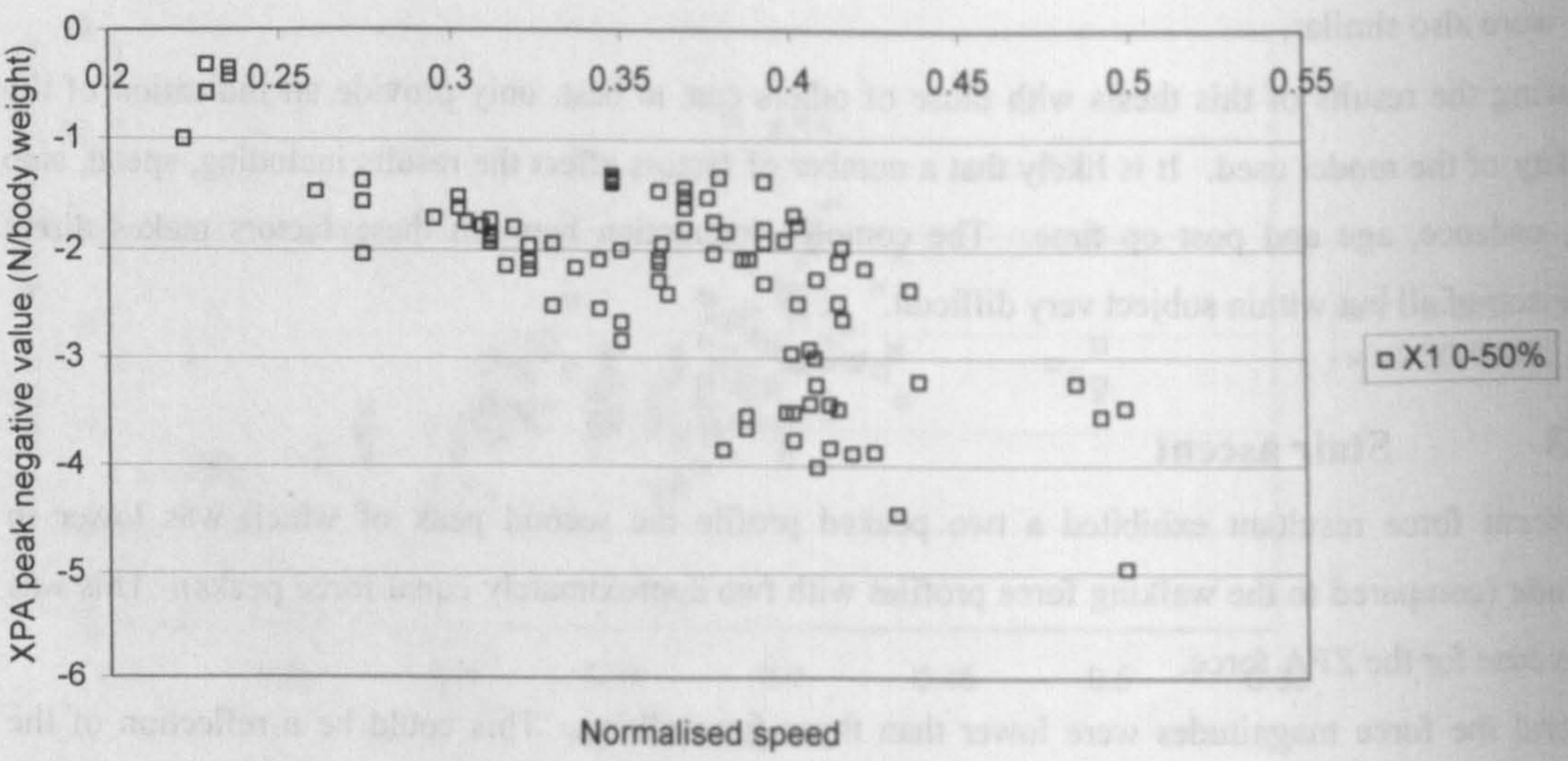

Figure 5.8A XPA hip joint force peak negative value vs. normalised speed. All walking trials, all subjects.

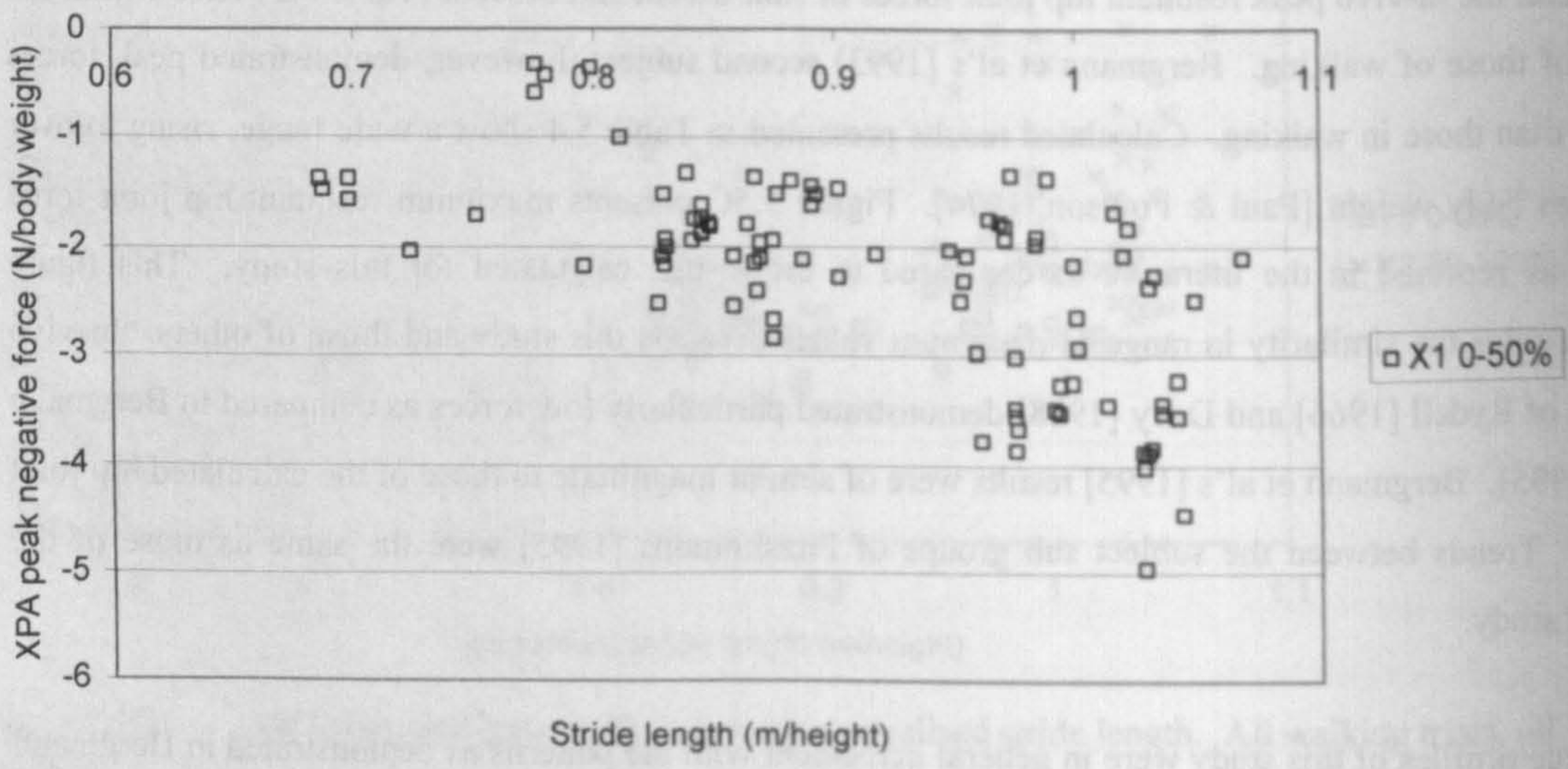

Figure 5.8B XPA hip joint force peak negative value vs. normalised stride length. All walking trials, all subjects.

Bergmann et al [1993] recorded traces for stair descent with variable relative second peak magnitude. With this exception, the general pattern of Bergmann et al's [1993] data followed that of this study. Crowninshield's [1978] calculated data demonstrated the same trend of lower XPA forces for stair descent as compared to ascent as the results presented in this thesis, but also demonstrated large differences in ZPA force component which were not so evident.

5.7.7.5 Ramp ascent

Ramp ascent femoral force components appeared to be comparable in magnitude and pattern with those of walking. XPA ramp ascent force was higher in magnitude than the equivalent walking joint force. There were differences in the other force components within subjects, but these were not consistent between subjects.

Bergmann et al's observation that for a 15° ramp the forces were approximately 30% higher than for walking was not indicated by the results for a 10° slope recorded for this thesis. The ranges of peak resultant hip joint forces as calculated by Paul & Poulson [1974] were of the same approximate magnitude as for the results of the normal subjects studied for this thesis.

5.7.7.6 Ramp descent

Different subjects ramp descent hip joint force profiles differed in different ways from the ramp ascent force profiles. Some hip joint replacement subjects demonstrated higher forces, whilst other subjects (particularly male normal subjects) demonstrated lower second peak values of resultant force. XFA forces tended to be less negative and sometimes positive in stair descent as compared to ascent. ZFA forces were in general lower for ramp descent. XPA and ZPA forces were lower in descent than ascent.

5.7.7.7 Camber foot up and foot down sides

There were only small differences between the hip joint forces in flat walking and camber walking. These tended to be in the Z direction as might be expected. It would appear that the camber slope of 5° was not sufficient to cause large difference in the forces at the hip joint.

5.7.7.8 Summary of hip joint forces.

Results from the model of the lower limb have been presented and compared with data available in the literature. It has been demonstrated that the model implemented was capable of calculating joint forces, which were of the same general form with similar magnitudes as those in the literature.

The hip joint forces of the hip replacement patients were, in general, of lower magnitude than those of the normal subjects, studied for this thesis. This could be explained by the relative speed and stride length of the two groups with normal subjects travelling faster and with longer stride lengths than the hip

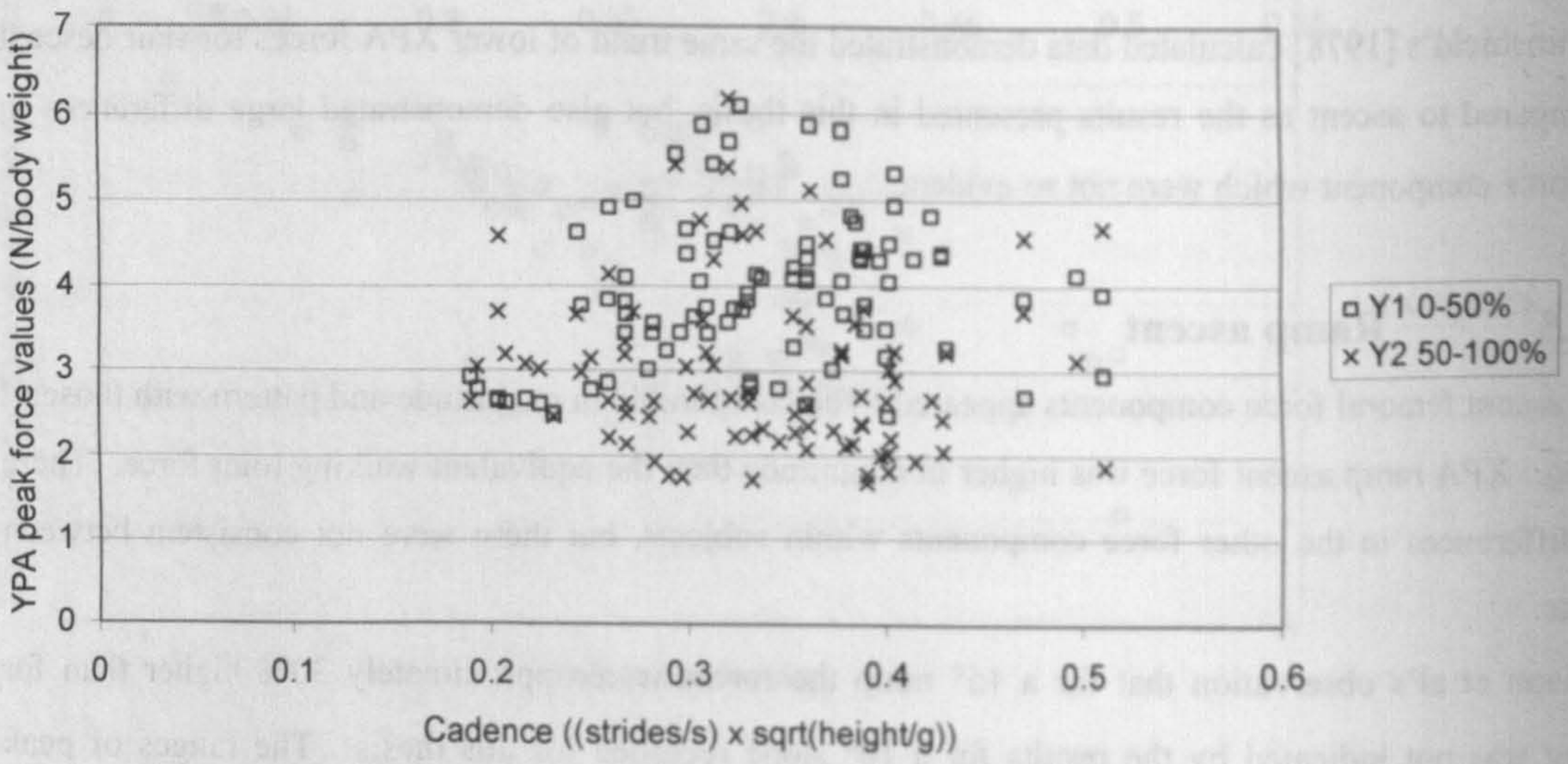

Figure 5.9 YPA hip joint force peak values vs. normalised cadence. All stair ascent trials, all subjects

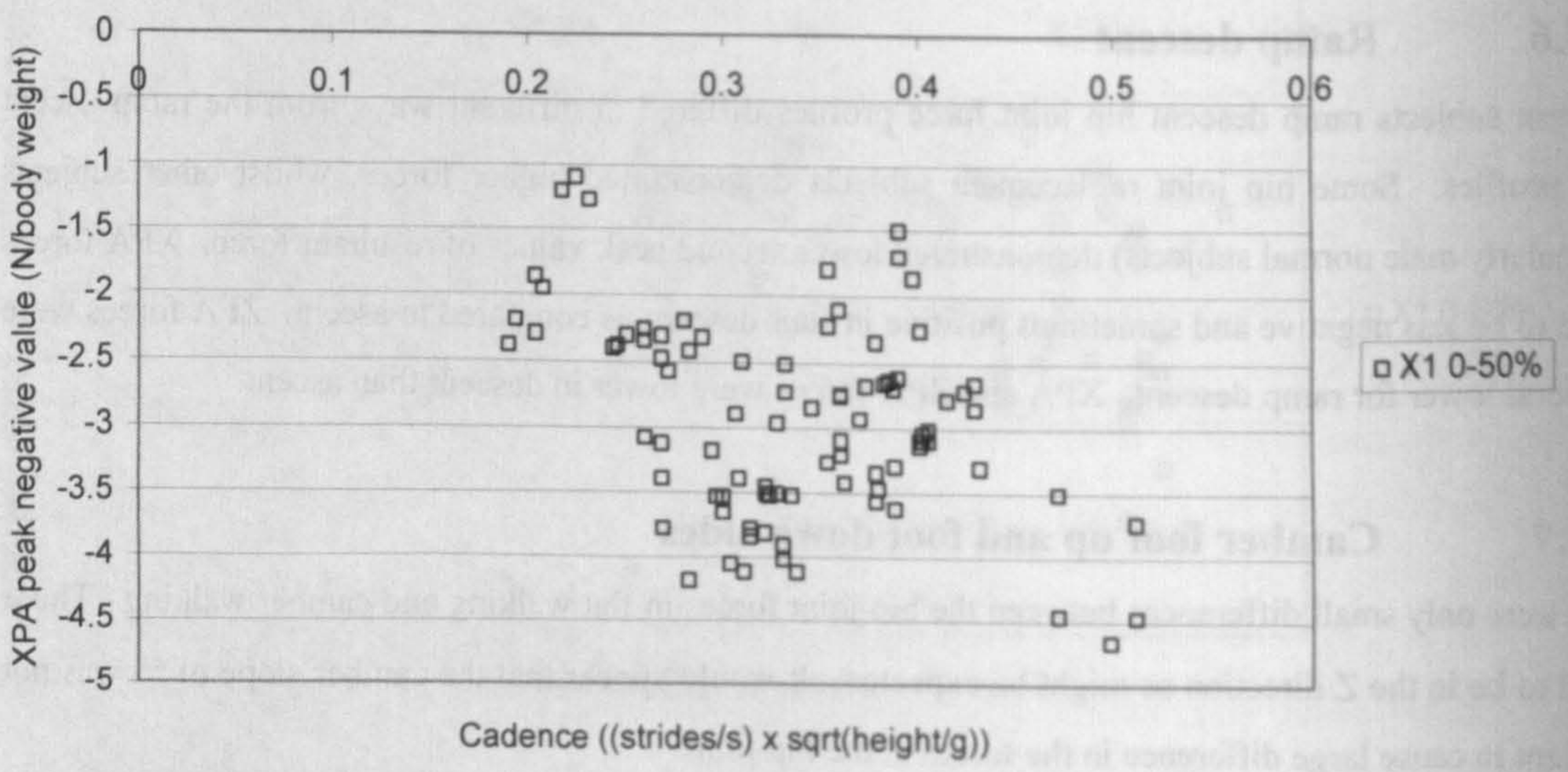

Figure 5.10 XPA hip joint force peak negative value vs. normalised cadence. All stair ascent trials, all subjects.

replacement subjects. Some of the hip replacement patients demonstrated asymmetry in their force profiles, this was, in general, characterised by lower forces on the replaced side. There was considerable variation within the groups of subjects.

Differences in the hip joint force profiles of stair ascent and descent were observed. Also ramp ascent and ramp descent force profiles differed, but those of camber foot up and camber foot down did not.

A summary of the range of the maximum resultant hip joint force for each of the subgroups is presented in Table 4.2. This summary, although easy to read, is difficult to interpret as in a number of cases the top of the range values were individuals who exhibited hip joint forces considerably higher than all others in their subject group. This presentation does, however, highlight the low values of hip joint forces experienced by the hip replacement subjects as compared to the normal subjects.

5.7.9 Speed and stride length effects on hip joint forces

It is recognised that ground reaction forces and joint kinematics are dependent on walking speed (Winter [1991]). It might be expected therefore that hip joint forces are also dependent on the speed at which an activity is executed. Paul [1999] examined the relationship between published hip joint forces and both speed and stride length. Paul [1999] favoured stride length for characterisation of hip joint forces demonstrating that hip joint forces were widely scattered when plotted against speed. To test the relationship between the hip joint forces calculated in this thesis and the speed and stride length of walking all subjects' data for all trials have been collated. To allow the comparison of different subjects' data fully dimensionless quantities of speed, stride length and cadence have been used. These quantities will be referred to as 'normalised'. Normalised stride length increased with normalised speed, but normalised cadence was not so clearly related to normalised speed (Figure 5.7A) although there was a tendency for higher normalised cadence at higher normalised speeds. There was no clear relationship between normalised stride length and normalised cadence (Figure 5.7B). The relationship between normalised speed and normalised stride length suggested that it was likely that characterisation by either of the two variables would produce the same result.

The aspects of the hip joint forces chosen for this analysis were the peak negative value of the XPA component (minimum value in the first half of the stance phase) and the two peak values of the YPA component. The first YPA force peak was calculated as the maximum value of the YPA force in the first half of stance and the second in the second half of stance.

Both of the YPA force component peaks tended to increase in magnitude with increasing normalised speed (Figure 5.8A) and normalised stride length (Figure 5.8B). There was considerable scatter of data when presented against normalised speed and normalised stride length.

There was a tendency for the peak negative value of the XPA component of the hip joint force to become greater in magnitude with increase in normalised speed (Figure 5.8A) and normalised stride length (Figure 5.8B). Neither of the trends was more pronounced than the other.

The data presented in this thesis do not suggest that normalised stride length is a better descriptor of hip joint forces than speed. The two variables appeared to be correlated for the walking tests performed for this thesis. Subjects were walking at self-selected speeds and were not asked to walk particularly quickly or slowly. A wider range of walking speeds and stride lengths may have indicated a more pronounced dependence on one of these variables.

Examination of the changes in stair ascent hip joint forces with normalised cadence, indicated that there was no clear relationship with either of the YPA force component peaks (Figure 5.9), but that there was a tendency for an increase in the XPA force component negative peak magnitude with higher normalised cadence (Figure 5.10). This relationship was, however, not as distinct as those observed in walking with normalised speed and normalised stride length.

In general YPA and XPA force components of the hip joint force increased with both normalised speed and normalised stride length. There was, however, considerable variation in the values of the forces within these general trends.

Chapter 6 Conclusions

Three-dimensional motion analysis with simultaneous recording of ground reaction forces was used to characterise the activities of walking and stair, ramp and camber negotiation.

A method of marker correction was applied to the motion data that preserved the within segment configuration of markers and incorporated a fixed hip joint centre. An attempt to locate the centre of the hip joint using motion of the thigh with respect to the pelvis was not successful due to the inability of the motion capture system to locate markers in space with sufficient accuracy.

A three-dimensional model of the lower limb including hip, tibio-femoral and talocrural joints was developed to facilitate the calculation of the forces at the hip joint. This model incorporated 3 hip, 8 knee and 8 ankle joint forces, 4 knee ligaments and 47 muscle elements. It was applied to five male and six female normal subjects and five male hip replacement subjects all within the 40 to 60 year old age range. To produce a three-dimensional model of the internal structures of the lower limb it was necessary to integrate the results of a number of researchers. Standard models of muscle origin and insertion data and muscle physiological cross sectional area were used. The knee joint model, although three-dimensional was defined based on a two-dimensional definition of contact force location. It is acknowledged that these aspects of the lower limb model would have introduced errors into the analysis.

The double linear optimisation method applied to solve the force distribution problem in the muscles and force bearing structures of the lower limb used first a minimisation of the maximum muscle stress then a minimisation of the sum of forces in the force bearing structures. Muscle and joint force profiles calculated were in agreement with those presented in the literature and demonstrated the ability of the linear optimisation method employed to distribute forces within the force bearing structures. The model of the lower limb used in this thesis was not, however, able to predict force sharing in the vasti or ankle muscle correctly. This was due to the model not including patello-femoral or talocalcaneonavicular joints.

Although the general patterns of activity in the muscles were in agreement with emg activity reported in the literature there was some switching of force between muscles particularly in the calf. It is possible that this was due to a limitation of the optimisation method, in that it was not able to apply effectively the constraint of minimisation of maximum muscle stress across all of the joints as the limiting muscle would have only spanned a maximum of two joints. The second criterion of minimisation of the sum of the forces would have thus had a significant effect at the other (in this case ankle) joint.

In general normal subjects exhibited higher hip joint forces than hip replacement subjects at self selected speeds for all activities. Examination of the calculated hip joint forces during walking suggested that there were trends of both higher anterior-posterior and vertical components of the hip joint forces for walking with higher normalised speed and normalised stride length, although there was considerable variation within this general trend. There was, however, no clear relationship between the hip joint forces during either stair ascent or descent and the stepping rate on the stairs.

The relatively low hip joint forces of the hip replacement subject suggested that even in the age group of 40 to 60 year olds the event of hip replacement is not followed by a return to levels of use equivalent to that of normal subjects. There was one hip replacement subject who did, however, demonstrate hip joint forces in line with those of normal subjects. This subject was the only one with bilateral hip replacements.

The range of maximum resultant hip joint forces for all activities was 3.04 to 11.85 for male normal subjects, 4.18 to 11.50 for female normal subjects, 3.73 to 6.81 and 2.21 to 8.77 for male hip replacement subjects for their natural and replaced sides respectively. These maximum force ranges do not provide a true picture of the differences in hip joint forces calculated for the different groups of subjects and should be interpreted with caution.

Ascent and descent force patterns for a 10° slope were different in character to those of walking, but similar to those of stair ascent and descent. A 5° camber was not sufficient to alter walking patterns to a large degree.

Error analysis suggested that for the three-dimensional model developed the location of the centre of the knee joint was more critical than the location of the hip joint centre. This observation must, however, be qualified by the fact that at the hip numerous structures were located with respect to the hip joint and would therefore have moved with the displaced joint centre. This was not the case for most of the force bearing structures at the knee where all muscular and ligament forces were fixed relative to the tibia and femur.

Ground reaction forces, joint angles, intersegmental forces and moments, muscle forces and knee and ankle joint forces are presented for a selection of the activities performed. Hip joint forces in both pelvic and femoral co-ordinate systems with resultant joint force angles are presented for all subjects for all years. Data on the speed, step length and cadence of the subject has also been included.

The results presented define in three dimensions the hip joint forces in both pelvic and femoral axes systems and thus fully characterise the probable in-vivo requirements of hip joint prosthesis during performance of the activities studied.

Chapter 7 Recommendations for further work

Muscle model

The muscle model used in this thesis was adapted considerably to allow it to be implemented. This would have introduced errors into the analysis which would have been avoided had a more detailed muscle model been available. Kepple et al [1998] have published a database of muscle origin and insertion data based on the study of a number of cadaver specimens that is much more comprehensive than other models. The use of such a model may reduce errors associated with the muscle model definition.

Knee model

The knee model was only partially three-dimensional. Full three-dimensional modelling of the knee would obviously improve the ability of the model to predict realistic forces especially in the ligaments of the knee.

Patello-femoral and talocalcaneonavicular joints

Extension of the model to include the patello-femoral and talocalcaneonavicular joints would enhance its ability to distribute the forces among the vasti and ankle muscles.

Optimisation

There are numerous optimisation methods that can be used. The one used in this thesis was perhaps not ideal for the three joint system modelled. The criteria of minimising the maximum muscle stress may have limited only muscles at one of the joints, leaving the force distribution at the other joints to be achieved by the second criterion the minimisation of muscle forces. This second criterion has a tendency to introduce an element of switching between preferred muscles. To overcome this problem it may be appropriate to link successive frames of data, limiting the allowed difference between muscle forces over time. The use of other optimisation techniques may also be able to overcome these difficulties.

The effect of inertia

The model used for this thesis did not included inertial effects. These effects are often considered to be small in comparison to the effects of ground reaction forces and gravity during stance for relatively slow activities as performed for this thesis. Inclusion of the inertial forces would allow extension to the modelling of swing and allow further testing of the model against data in the literature.

Hip joint centre modelling and marker correction routines

The accurate location of the hip joint centre is an important aspect of the modelling of the lower limb. A more accurate method than using standard definitions should be found to improve the lower limb model. The implementation of this method would require more accurate location of markers in space than was possible using the equipment used for this thesis. Recently Leardini et al [1999] have demonstrated that it is possible to calculate the hip joint position accurately using a functional method as attempted in this thesis. It would appear that there is promise in this method.

References

Andriacchi TP, Andersson GBJ, Fermier RW, Stern D and Galante GO (1980), A study of lower-limb mechanics during stair-climbing, Journal of Bone and Joint Surgery, [Am], 62, 749-757.

Arendt-Nielsen L, Sinkjaer T, Nielsen J, Kallesoe K (1991), Electromyographic patterns and knee joint kinematics during walking at various speeds, Journal of Electromyography and Kinesiology, Vol.1, No.2, pp89-95.

Bassey EJ, Littlewood JJ, Taylor SJG (1997), Relations between compressive axial forces in an instrumented massive femoral implant, ground reaction forces, and integrated electromyographs from vastus lateralis during various 'osteogenic' exercises, Journal of Biomechanics, Vol.30, pp 213-223.

Bean JC, Chaffin DB (1988), Biomechanical model calculation of muscle contraction forces: A double linear programming method, Journal of Biomechanics, Vol 21, No.1, pp59-66.

Bell AL, Brand RA, Pedersen DR (1989), Prediction of hip joint centre location from external landmarks, Human Movement Science, Vol.8, pp3-16.

Bell AL, Pedersen DR, Brand RA (1990), A comparison of the accuracy of several hip centre location prediction methods, Journal of Biomechanics, Vol.23, No.6, pp617-621.

Bergmann G, Graichen F, Rohlmann A (1993), Hip joint loading during walking and running, measured in two patients, Journal of Biomechanics, Vol.26, No.8, pp969-990.

Bergmann G, Graichen F, Rohlmann A (1995), Is staircase walking a risk for the fixation of hip implants, Journal of Biomechanics, Vol.28, No.5, pp535-553.

Bergmann G, Kniggendorf H, Graichen F, Rohlmann A (1995B), Influence of shoes and heel strike on the loading of hip implants, Journal of Biomechanics, Vol.28, pp817-827.

Benjes M (1996), A least-squares Algorithm for the equiform transformation from spatial marker co-ordinates, Veldpaus and Woltring 1988. Specification for the spherical case, Technical University of Darmstadt, Germany, personal communication.

Brand RA, Crowninshield RD, Wittstock CE, Pedersen DR, Clark CR, Van Krieken FM (1982), A model of lower extremity muscular anatomy, Transactions of the ASME, Journal of Biomechanical Engineering, Vol.104, pp304-310.

Brand RA, Pedersen DR, Friederich JA (1986), The sensitivity of muscle force predictions to changes in physiological cross-sectional area, Journal of Biomechanics, Vol.19, No.8, pp589-596.

Brand RA, Pedersen DR, Davy DT, Kotzar GM, Heiple KG, Goldberg VM (1994), Comparison of hip joint force calculations measured in the same patient, Journal of Arthroplasty, Vol.9, pp45-51.

Brown TRM, Nicol AC, Paul JP (1984), Comparison of loads transmitted by Charnley and CAD Muller total hip arthroplasties, Proc. Conf. Engineering and Clinical Aspects of Endoprosthetic Fixation, Institute of Mechanical Engineering, pp63-68.

Calhoun JH, Li F, Ledbetter BR, Viegas SF (1994), A comprehensive study of pressure distribution in the ankle joint with inversion and eversion, Foot and Ankle, Vol.15, pp125-33.

Chao EY, Laughman RK, Schneider E, Stauffer RN (1983), Normative data of knee joint motion and ground reaction forces in adult level walking, Journal of Biomechanics, Vol.16, No.3, pp219-233.

Cheng C-K, Brand RA, Brown TD (1993), Knee joint force distribution in the stance phase of the human gait, Biomedical Engineering – Applications, Basis and Communications, Vol.5, pp806-814.

Collins JJ (1995), The redundant nature of locomotor optimisation laws, Journal of Biomechanics, Vol.28, No.3, pp251-267.

Crowninshield RD (1978), Use of optimisation techniques to predict muscle forces, Journal of Biomechanical Engineering, Vol.100, pp88-92.

Crowninshield RD, Brand RA and Johnston RC (1978), The effects of walking velocity and age on hip kinematics and kinetics, Clinical Orthopaedics and Related Research, Vol.132, pp140-144.

Crowninshield RD, Johnston RC, Andrews JG, Brand RA (1978B), A biomechanical investigation of the human hip, Journal of Biomechanics, Vol.11, pp75-85.

Crowninshield RD, Brand RA (1981), A physiologically based criterion of muscle force prediction in locomotion, Journal of Biomechanics, Vol 14, No.11, pp793-801.

Davy DT, Kotzar GM, Brown RH, Heiple KG, Goldberg VM, Heiple KG (Jr.), Berilla J, Burstein AH (1988), Telemetric force measurements across the hip after total hip arthroplasty, Journal of Bone and Joint Surgery, Vol.70A, No.1, pp45-50.

Delp SL (1990), A computer-graphics system to analyse and design musculoskeletal reconstructions of the lower limb, PhD thesis, Dept. of Mechanical Engineering, Stanford University.

Delp SL, Loan JP, Hoy MG, Zajac FE, Topp EL, Rosen JM (1990), An interactive graphics-based model of the lower extremity to study orthopaedic surgical procedures, IEEE Trans. Biomedical Engineering, Vol.37, No.8, pp757-767.

Dostal WF, Andrews JG (1981), A three-dimensional model of hip musculature, Journal of Biomechanics, Vol.14, No.11, pp803-812.

Draganich LF, Andriacchi TP, Andersson GBJ (1987), Interaction between intrinsic knee mechanics and the knee extensor mechanism, Journal of Orthopaedic Research, Vol.5, pp539-547.

Drillis R, Contini R (1966), Body segment parameters. Technical Report No.1166.03, New York University, School of Engineering and Science, New York, USA.

English TA, Kilvington M (1979), In vivo records of hip loads using a femoral implant with telemetric output (A preliminary report), Journal of Biomedical Engineering, Vol.1, No.2, pp111-115.

Fitzsimmons A (1995), Hip joint forces in hip replacement patients and normal subjects during activities of daily living, PhD, University of Strathclyde, Glasgow.

Friederich JA, Brand RA (1990), Muscle fibre architecture in the human lower limb, Journal of Biomechanics, Vol.23, No.1, pp91-95.

Givens-Heiss DL, Krebs DE, Riley PO, Strickland EM, Fares M, Hodge WA, Mann RW, Oatis CA (1992), In vivo acetabular contact pressures during rehabilitation, Part II: Postacute phase, Physical Therapy, Vol.72, No.10, pp 700-710.

Glitsch U, Baumann W (1997), The three-dimensional determination of internal loads in the lower extremity, Journal of Biomechanics, Vol.30, No.11-12, pp1123-1131.

Graichen F, Bergmann G (1991), Four-channel telemetry system for in vivo measurement of hip joint forces, Journal of Biomedical Engineering, Vol.13, No.5, pp 370-374.

Grant's Atlas of Anatomy (1991), 9th Edition, Ed. Agur AMR, Williams and Wilkins, Baltimore, Maryland, USA.

Grood ES, Suntay WJ (1983), A joint coordinate system for the clinical description of three-dimensional motions: Application to the knee, Transactions of the ASME, Journal of Biomechanical Engineering, Vol.105, pp136-144.

Hall MG, Fleming HE, Dolan MJ, Millbank SFD, Paul JP (1996), Static in situ calibration of force plates, Journal of Biomechanics, Vol.29, No.5, pp659-665.

Harrington IJ (1983), Static and dynamic loading patterns in the knee joints with deformities, Journal of Bone and Joint Surgery, Vol.65-A, No.1, pp247-259.

Hodge WA, Carlson KL, Fijan RS, Burgess RG, Riley PO, Harris WH, Mann RW (1989), Contact pressures from an instrumented hip endoprosthesis, Journal of Bone and Joint Surgery, Vol.71-A, No.9, pp1378-1386.

Hof AL (1996), Scaling gait data to body size, Gait & Posture, Vol.4. pp222-223.

Holzreiter ST (1991), Calculation of the instantaneous centre of rotation for a rigid body, Journal of Biomechanics, Vol 24, No.7, pp643-647.

Ishai GA (1975), Whole body gait kinetics, PhD, University of Strathclyde, Glasgow.

Isman RE, Inman VT (1968), Anthropometric studies of the human foot and ankle, Technical Report 58, Biomechanics Laboratory, University of California, San Francisco, Berkeley.

Joseph J, Watson R (1967), Telemetering electromyography of muscles used in walking up and down stairs, Journal of Bone and Joint Surgery, Vol.49-B, No.4, pp774-780.

Joseph J (1982), A texbook of regional anatomy, MacMillan Press Ltd, London.

Kadaba MP, Ramakrishnan HK, Wootten ME, Gainey J, Gorton G, Cochran GVB (1989), Repeatability of kinematic, kinetic and electromyographic data in normal adult gait, Journal of Orthopaedic Research, Vol.7, No.6, pp849-860.

Kadaba MP, Ramakrishnan HK, Wodtten ME (1990), Measurement of lower extremity kinematics during level walking, Journal of Orthopaedic Research, Vol.8, No.3, pp383-392.

Kepple TM, Sommer III HJ, Siegel KL, Stanhope SJ (1998), A three-dimensional musculoskeletal database for the lower extremities, Journal of Biomechanics, Vol.31, No.1, pp77-80.

Kimizuka M, Kurosawa H, Fukubayashi T (1980), Load-bearing pattern of the ankle joint. Contact area and pressure distribution, Arch Orthop Trauma, Vol.96, pp45-9.

Kotzar GM, Davy DT, Goldberg VM, Heiple KG, Berilla J, Heiple Jr KG, Brown RH, Burstein AH (1991), Telemeterized in vivo hip joint force data: A report on two patients after total hip surgery, Journal of Orthopaedic Research, Vol.9, No.5, pp 621-633.

Kotzar GM, Davy DT, Berilla J, Goldberg VM (1995), Torsional Loads in Early Post Operative Period - a report on 2 patients after total hip surgery, Journal of Orthopaedic Research, Vol.13, No.6, pp945-955.

Lafortune MA, Cavanagh PR, Sommer III HJ, Kalenak A (1992), Three-dimensional kinematics of the human knee during walking, Journal of Biomechanics, Vol.25, No.4, pp347-357.

Leardini A, Cappozzo A, Catani F, Toksvig-Larsen S, Petitto A, Sforza V, Cassanelli G, Giannini S (1999), Validation of a functional method for the estimation of hip joint centre location, Journal of Biomechanics, Vol.32, pp99-103.

Lu TW (1997), Geometric and mechanical modelling of the human locomotor system, PhD Thesis, University of Oxford.

Lu TW, Taylor SJG, O'Connor JJ, Walker PS (1997), Influence of muscle activity on the forces in the femur: an in vivo study, Journal of Biomechanics, Vol.30, No.11-12, pp1101-1106.

Lu TW, O'Connor JJ, Taylor SJG, Walker PS (1998) Validation of a lower limb model with in vivo femoral forces telemetered from two subjects, Journal of Biomechanics, Vol.31, No.1, pp63-69.

McFadyen BJ, Winter DA (1988), An integrated biomechanical analysis of normal stair ascent and descent, Journal of Biomechanics, Vol 21, No.9, pp733-744.

Mensch JS, Amstutz HC (1975), Knee morphology as a guide to knee replacement, Clinical Orthopaedics., Vol.112, pp231-241.

Morrison JB (1967), The forces transmitted by the human knee joint during activity, PhD thesis, University of Strathclyde, Glasgow.

Morrison JB (1970), The mechanics of knee joint in relation to normal walking, Journal of Biomechanics, Vol.3, pp51-61.

Nisell R (1985), Mechanics of the knee - a study of joint and muscle loads with clinical applications, Acta. Orthop. Scand., Vol.57 (Suppl No.216), pp1-42.

O'Connor JJ, Shercliff T, FitzPatrick D, Bradley J, Daniel D, Biden E, Goodfellow H (1990), Geometry of the knee. Chapter 10 In 'Knee ligaments-structure, function, injury, and repair (Eds. Daniel DM, Akeson WH, O'Connor JJ), pp163-200, Raven Press, New York.

Palastanga N, Field D, Soames R (1994), Anatomy and human movement: Structure and function, 2nd Edition, Butterworth - Heinemann Ltd., Oxford.

Paul JP (1967), Forces at the human hip joint, PhD, Glasgow University, Scotland.

Paul JP (1967B), Forces transmitted by joints in the human body, Proceedings of the Institute of Mechanical Engineering, Vol.181, pp8-15.

Paul JP, Poulson J (1974), The analysis of forces transmitted by joints in the human body, Proc. 5th Int. Conf. Stress Analysis, pp3.34-3.42.

Paul JP (1975), Force actions transmitted by joints in the human body, Proc. R. Soc. Med., Vol.192, pp163-172.

Paul JP (1999), Strength requirements for internal and external prostheses, Journal of Biomechanics, Vol.32, pp381-393.

Pedersen DR, Brand RA, Davy DT (1997), Pelvic muscle and acetabular contact forces during gait, Journal of Biomechanics, Vol.30, pp959-965.

Press WH, Flannery BP, Teukolsky SA, Vetterling WT (1989), Numerical recipes in Pascal: The art of scientific computing, Cambridge University Press, Cambridge.

Proctor P, Paul JP (1982), Ankle joint biomechanics, Journal of Biomechanics, Vol.15, No.9, pp627-634.

Rohrle H, Scholten R, Sigolotto C and Sollbach W (1984), Joint forces in the human pelvis-leg skeleton during walking, Journal of Biomechanics, Vol.17, No.6, pp409-424.

Rydell, N (1966), Forces acting on the femoral head prosthesis. A study on strain gauge supplied prostheses in living persons, Acta Orthop. Scan., Suppl.88.

Seeley RR, Stephens TD, Tate P (1995), Anatomy and Physiology, 3rd Edition, Mosby, St Louis, Missouri, USA.

Seidel GK, Marchinda DM, Dijkers M and Soutas-Little RW (1995), Hip joint location from palpable boney landmarks - a cadaver study, Journal of Biomechanics, Vol.28, pp995-998.

Seireg A, Arvikar RJ (1973), A mathematical model for evaluation of forces in lower extremities of the musculo-skeletal system, Journal of Biomechanics, Vol.6, pp313-326.

Seireg A, Arvikar RJ (1975), The prediction of muscular load sharing and joint forces in the lower extremity during walking, Journal of Biomechanics, Vol.8, pp89-102.

Shelley FJ, Anderson DD, Kolar MJ, Millar MC, Rubash HE (1996), Physical modelling of hip joint forces in stair climbing, Journal of Engineering in Medicine, Vol.210H, pp65-68.

Simonsen EB, Dyhre-Poulsen P, Voigt M, Aagaard P, Sjogaard G and Bojsen-Moller F (1995), Bone-on-bone forces during loading and unloaded walking, Acta Anatomica, Vol.152, pp133-142.

Spoor CW, Veldpaus FE (1980), Rigid body motion calculated from spatial co-ordinates of markers, Journal of Biomechanics, Vol.13, pp391-393.

Stewart C (1995), Swing phase and its control in the human trans-femoral amputee, PhD Thesis, University of Strathclyde, Glasgow.

Tsirakos D, Baltzopoulos V, Bartlett R (1997), Inverse optimization: Functional and physiological considerations related to the force-sharing problem. Critical Reviews in Biomedical Engineering, Vol.25, No.4-5, pp371-407.

University of California, Berkeley (1953), The pattern of muscular activity in the lower extremity during walking, Prosthetic Devices Research Project, Inst. of Engineering Research, Series II, Issue 25.

Veldpaus FE, Woltring HJ, and Dortmans LJMG (1988), A least-squares algorithm for the equiform transformation from spatial marker co-ordinates, Journal of Biomechanics, Vol.21, No.1, pp45-54.

Vrahas MS, Brand RA, Brown TD, Andrews JG (1990), Contribution of passive tissues to the intersegmental moments at the hip, Journal of Biomechanics, Vol.23, No.4, pp357-362.

White SC, Yack HJ, Winter DA (1989), A three dimensional musculoskeletal model for gait analysis. Anatomical variability estimates, Journal of Biomechanics, Vol.22, No.8/9, pp885-893.

Winter DA (1991), The biomechanics and motor control of human gait: Normal, elderly and pathological, 2nd Edition, University of Waterloo Press, Waterloo, Canada.

Appendices

Note: All page numbers are prefixed with the appendix number. For example the fourth page of appendix three has been labelled as page A-III.4.

Appendix I Subject Details

Table A-I.1 Normal subject details

Subject Number	Sex	Age (years)	Body mass (kg)	Height (cm)
8	M	52	79	171
14	M	57	69	179
17	M	47	82.75	168.5
18	M	46	80.5	184
20	M	45	81	182
15	F	59	61.5	165
19	F	51	59.5	161
33	F	47	89.3	163
34	F	44	61.85	180.5
35	F	50	51.5	155
36	F	47	56	167

Table A-I.2 Total hip replacement subject details

Subject Number	Sex	Age (years)	THR side	Body mass (kg)	Height (cm)	Months post operative	Comments
26	M	60	Both	88.75	181	20/22	
27	M	43	Left	75.5	174	12	Left leg 1 inch shorter than right. Shoe insert to compensate. Used stick for walking and camber and hand rails for stair and ramp.
28	M	57	Left	73.75	167.5	18	
29	M	53	Left	78.75	164.5	19	
38	M	50	Left	72.4	167	22	

Appendix II Muscle origin and insertion data

After Brand et al [1982]. Co-ordinates are given in the appropriate segment's reference frame.

Table A-II.1 Muscle origin data (after Brand et al [1982])

Brand's muscle origin data						
	Actual Origins (m)			Scaled Origins		
Muscle	X	Y	Z	X	Y	Z
Add brevis (S)	0.0312	-0.0373	-0.0611	0.4611	-0.1927	-0.7865
Add brevis (I)	0.0326	-0.0371	-0.0613	0.4822	-0.1917	-0.7882
Add longus	0.049	-0.0316	-0.061	0.7266	-0.1629	-0.7862
Add magnus 1	-0.0117	-0.0552	-0.0486	-0.181	-0.2785	-0.6454
Add magnus 2	-0.012	-0.0552	-0.0485	-0.1856	-0.2784	-0.6434
Add magnus 3	-0.012	-0.0551	-0.0486	-0.185	-0.2776	-0.6447
Gluteus max 1	-0.0338	0.1288	-0.0275	-0.4892	0.6544	-0.3505
Gluteus max 2	-0.0652	0.0842	-0.0429	-0.9664	0.4315	-0.5495
Gluteus max 3	-0.0747	0.0127	-0.0709	-1.0937	0.0682	-0.9122
Gluteus med 1	0.0168	0.0905	0.0356	0.2462	0.4556	1.0205
Gluteus med 2	-0.0239	0.109	0.0054	-0.3523	0.547	0.2392
Gluteus med 3	-0.0546	0.0721	-0.0257	-0.8096	0.3584	-0.3306
Gluteus min 1	0.0236	0.0611	0.0305	0.3508	0.3079	0.8956
Gluteus min 2	-0.0084	0.0648	0.013	-0.1228	0.3265	0.3571
Gluteus min 3	-0.0293	0.0423	-0.0053	-0.4348	0.2092	-0.0657
iliacus	0.0199	0.0493	0.0025	0.3022	0.235	0.1228
iliopsoas	0.0315	0.0111	-0.0102	0.4675	0.0567	-0.1279
Inf gemelli	-0.0426	-0.0165	-0.0095	-0.6331	-0.0811	-0.1172
Obturator ext	0.0057	-0.028	-0.0415	0.0821	-0.1419	-0.532
Obturator int	-0.0488	-0.0091	-0.0135	-0.7265	-0.0444	-0.1603
Pectineus	0.0318	-0.0096	-0.0299	0.4725	-0.0501	-0.3798
Piriformis	-0.0559	0.0562	-0.0404	-0.8331	0.2902	-0.4803
Quad femoris	-0.0319	-0.0479	-0.0231	-0.4774	-0.2364	-0.291
Sup gemelli	-0.0435	0.0009	-0.0201	-0.6465	0.0043	-0.2423
Biceps femoris	-0.0414	-0.0474	-0.0146	-0.6206	-0.237	-0.1888
Gracilis	0.0303	-0.0441	-0.0691	0.4481	-0.2262	-0.8847
Rectus Femoris	0.0326	0.0323	0.0174	0.4852	0.1638	0.4944
Sartorius	0.0488	0.0649	0.0438	0.7252	0.3231	1.0923
Semimembranos	-0.0382	-0.0448	-0.0143	-0.5668	-0.2246	-0.1614
Semitendinosus	-0.0457	-0.0446	-0.0125	-0.6844	-0.2235	-0.1595
Ten Fas Latae	0.0327	0.0882	0.0547	0.4819	0.4429	1.3515
Gastroc (M)	-0.0204	0.0077	-0.0157	-0.2635	0.0186	-0.192
Gastroc (L)	-0.0198	0.0048	0.0226	-0.2475	0.0116	0.2887
Biceps Fem (S)	-0.0007	0.1784	0.0144	-0.0086	0.4563	0.2832
Vastus interm	0.0232	0.2067	0.0176	0.2888	0.5253	0.3578
Vastus lateral	0.001	0.2127	0.0365	0.0148	0.5392	0.6861
Vastus medial	0.0043	0.188	0.0088	0.0483	0.4779	0.173
Tibialis anter	-0.0067	0.2397	0.0132	-0.0973	0.7615	0.2126
Ext dig comm	-0.0228	0.259	0.028	-0.3591	0.8243	0.4561
Ext hall long	-0.0155	0.2175	0.0134	-0.2396	0.6934	0.2295
Flexor dig	-0.0246	0.1996	0.0016	-0.3865	0.6326	0.0266
Flexor hall long	-0.0266	0.166	0.0204	-0.4108	0.5243	0.3386
Peroneus brev	-0.0226	0.1364	0.0253	-0.348	0.4334	0.3857
Peroneus long	-0.0268	0.2419	0.0356	-0.4132	0.7766	0.5755
Peroneus tert	-0.0099	0.1202	0.021	-0.1441	0.3854	0.3319
Tibialis poste	-0.0128	0.1786	0.0137	-0.1921	0.5748	0.2222
Soleus	-0.0292	0.2467	0.0006	-0.459	0.7831	0.01

Table A-II.2 Muscle insertion data (after Brand et al [1982])

Brand's muscle insertion data						
	Actual Insertions (m)			Scaled Insertions		
Muscle	X	Y	Z	X	Y	Z
Add brevis (S)	-0.0082	0.2828	0.0215	-0.1126	0.7174	0.4125
Add brevis (I)	-0.0112	0.2534	0.0211	-0.1451	0.6477	0.4068
Add longus	-0.0031	0.1924	0.0134	-0.0407	0.4858	0.2591
Add magnus 1	-0.0122	0.2758	0.029	-0.1542	0.6961	0.5411
Add magnus 2	-0.0036	0.174	0.0163	-0.0463	0.4351	0.3034
Add magnus 3	-0.0064	0.0166	-0.0297	-0.0768	0.0419	-0.5723
Gluteus max 1	-0.0158	0.4055	0.035	-0.2023	1.0407	0.7167
Gluteus max 2	-0.0158	0.3609	0.035	-0.2023	0.9262	0.7167
Gluteus max 3	-0.0158	0.2894	0.035	-0.2023	0.7427	0.7167
Gluteus med 1	-0.0195	0.3899	0.0598	-0.2329	0.9971	1.0869
Gluteus med 2	-0.0197	0.3902	0.0597	-0.2336	0.9977	1.0857
Gluteus med 3	-0.0195	0.3901	0.0596	-0.2325	0.9976	1.0846
Gluteus min 1	-0.0073	0.381	0.0572	-0.0853	0.9658	1.0814
Gluteus min 2	-0.0072	0.381	0.0571	-0.0842	0.9658	1.0801
Gluteus min 3	-0.0073	0.381	0.0572	-0.0851	0.9659	1.0818
iliacus	-0.0179	0.335	0.0116	-0.22	0.8544	0.207
iliopsoas	-0.018	0.3352	0.0116	-0.2207	0.8548	0.2061
Inf gemelli	-0.0113	0.3949	0.0448	-0.1298	0.9975	0.8385
Obturator ext	-0.0242	0.3821	0.0415	-0.2963	0.9662	0.7647
Obturator int	-0.0113	0.3947	0.0446	-0.1307	0.9969	0.8348
Pectineus	-0.0109	0.3146	0.0248	-0.1501	0.7985	0.4674
Piriformis	-0.0132	0.3983	0.0484	-0.1829	1.0039	0.9366
Quad femoris	-0.0164	0.3446	0.0329	-0.2205	0.8766	0.6147
Sup gemelli	-0.0113	0.3947	0.0445	-0.1304	0.9971	0.8321
Biceps femoris	-0.0383	0.3321	0.0431	-0.5884	1.0742	0.6863
Gracilis	-0.0586	0.3426	-0.0095	-0.9692	1.0923	-0.1333
Rectus Femoris	0.0041	0.4084	-0.0006	0.0591	1.3037	-0.0084
Sartorius	-0.0515	0.3478	-0.0205	-0.8524	1.1075	-0.324
Semimembranos	-0.0564	0.3297	-0.0072	-0.9018	1.0521	-0.0886
Semitendinosus	-0.0542	0.3369	-0.0058	-0.9478	1.0917	-0.0682
Ten Fas Latae	-0.0099	0.3504	0.0292	-0.1587	1.1039	0.4869
Gastroc (M)	-0.0368	-0.0429	0.0028	-0.5649	-0.1371	0.0603
Gastroc (L)	-0.0369	-0.043	0.0028	-0.5667	-0.1372	0.0594
Biceps Fem (S)	-0.0384	0.3323	0.0433	-0.5897	1.0746	0.6888
Vastus interm	-0.0018	0.411	0.0006	-0.0339	1.312	0.0085
Vastus lateral	0.0089	0.405	0.0151	0.1375	1.2927	0.2423
Vastus medial	-0.0079	0.3996	-0.0137	-0.1321	1.2751	-0.2238
Tibialis anter	0.0221	0.0132	-0.0194	0.3548	0.0429	-0.3123
Ext dig comm	0.0253	0.0116	-0.0021	0.4058	0.0375	-0.0375
Ext hall long	0.0259	0.0117	-0.0093	0.4156	0.0378	-0.151
Flexor dig	-0.007	-0.0024	-0.0222	-0.1095	-0.0086	-0.3427
Flexor hall long	-0.0092	-0.0065	-0.0159	-0.146	-0.0232	-0.2367
Peroneus brev	-0.0081	-0.0058	0.0273	-0.1111	-0.0193	0.4159
Peroneus long	-0.0094	-0.0076	0.024	-0.1329	-0.0245	0.3641
Peroneus tert	0.0205	0.0032	0.0097	0.325	0.0105	0.1446
Tibialis poste	-0.0023	0.0023	-0.0276	-0.0425	0.0075	-0.4294
Soleus	-0.0365	-0.0428	0.0056	-0.5563	-0.1389	0.1038

Appendix III Knee joint parameters

For definitions of α, g, Fp/Fq and β see Figures 3.7 and 3.8.
acl ang = anterior cruciate ligament angle to tibial plateau.
pcl ang = posterior cruciate ligament angle to tibial plateau.
mclo = medial collateral ligament origin in knee anatomical (axes x and y co-ordinates).
lclo = lateral collateral ligament origin in knee anatomical axes (axes x and y co-ordinates).
(Cruciate ligament angles and collateral ligament origins and insertions are illustrated in Figures 3.9 and 3.10)

Notes:
The data of Nisell et al [1985] used to calculate g, Fp/Fq and β only extended to $\alpha = -10°$ (i.e. 10° of extension). Data out with this range was extrapolated based on the following assumptions:
g was maintained at the same value as at $\alpha = -10°$ throughout the $-11°$ to $-20°$ range as it was felt appropriate to limit the progression of the centre of contact on the tibia to the maximum anterior position recorded by Nisell. Similarly with Fp/Fq the same value was used for the whole of the extrapolated range from $\alpha = -11°$ to $-20°$ to maintain the extreme value. For the angle β, however, an extended range was considered possible, so the values were incremented by 0.2° per degree of extension to follow approximately the same pattern as for the range $\alpha = -1°$ to $-10°$.

All ligament angles and origin and insertion point data was derived from O'Connor et al [1990].

Table A-III.1 Knee joint model parameters

α	g	Fp/Fq	β	acl ang	pcl ang	mclo x	mclo y	lclo x	lclo y
(degrees)	(mm)	(N/N)	(degrees)	(degrees)	(degrees)	(mm)	(mm)	(mm)	(mm)
-20	12.3	1.019	30.25	74.9	45.4	-10.39	27.20	-15.69	34.73
-19	12.3	1.019	30.05	74.5	45.3	-10.42	27.28	-15.85	34.72
-18	12.3	1.019	29.85	74.1	45.3	-10.45	27.36	-16.01	34.70
-17	12.3	1.019	29.65	73.8	45.2	-10.49	27.44	-16.17	34.69
-16	12.3	1.019	29.45	73.4	45.1	-10.52	27.52	-16.34	34.67
-15	12.3	1.019	29.25	73.0	45.0	-10.57	27.61	-16.51	34.65
-14	12.3	1.019	29.05	72.6	45.0	-10.62	27.69	-16.68	34.63
-13	12.3	1.019	28.85	72.2	44.9	-10.67	27.77	-16.85	34.61
-12	12.3	1.019	28.65	71.8	44.8	-10.72	27.86	-17.02	34.58
-11	12.3	1.019	28.45	71.4	44.8	-10.78	27.94	-17.20	34.56
-10	12.3	1.019	28.25	71.0	44.7	-10.84	28.03	-17.37	34.53
-9	12.7	1.018	28.05	70.6	44.7	-10.91	28.12	-17.55	34.50
-8	13.0	1.017	27.86	70.2	44.7	-10.98	28.20	-17.73	34.47
-7	13.4	1.016	27.67	69.8	44.6	-11.06	28.29	-17.92	34.44
-6	13.7	1.015	27.47	69.4	44.6	-11.14	28.38	-18.10	34.41
-5	14.1	1.014	27.28	69.0	44.6	-11.22	28.47	-18.29	34.37
-4	14.5	1.013	27.09	68.5	44.5	-11.30	28.55	-18.47	34.33
-3	14.8	1.012	26.90	68.1	44.5	-11.39	28.64	-18.66	34.29
-2	15.3	1.011	26.68	67.7	44.5	-11.48	28.73	-18.85	34.25
-1	15.7	1.011	26.47	67.3	44.5	-11.58	28.82	-19.04	34.21
0	16.0	1.010	26.25	66.9	44.5	-11.68	28.91	-19.23	34.17
1	16.4	1.010	26.02	66.4	44.5	-11.77	28.99	-19.42	34.12

α	g	Fp/Fq	β	acl ang	pcl ang	mclo x	mclo y	lclo x	lclo y
(degrees)	(mm)	(N/N)	(degrees)	(degrees)	(degrees)	(mm)	(mm)	(mm)	(mm)
2	16.8	1.010	25.77	66.0	44.5	-11.88	29.08	-19.62	34.08
3	17.2	1.010	25.52	65.6	44.5	-11.99	29.17	-19.81	34.03
4	17.6	1.011	25.25	65.1	44.5	-12.09	29.25	-20.00	33.98
5	18.0	1.011	25.00	64.7	44.6	-12.21	29.34	-20.20	33.93
6	18.4	1.011	24.71	64.3	44.6	-12.33	29.43	-20.40	33.88
7	18.7	1.012	24.45	63.8	44.6	-12.44	29.51	-20.59	33.82
8	19.1	1.012	24.21	63.4	44.6	-12.57	29.60	-20.79	33.77
9	19.5	1.011	23.96	62.9	44.7	-12.69	29.68	-20.98	33.70
10	19.8	1.011	23.75	62.5	44.7	-12.82	29.77	-21.18	33.65
11	20.2	1.010	23.55	62.1	44.8	-12.96	29.86	-21.38	33.59
12	20.4	1.009	23.35	61.6	44.8	-13.08	29.94	-21.57	33.52
13	20.7	1.008	23.17	61.2	44.8	-13.23	30.03	-21.77	33.46
14	21.0	1.007	23.00	60.7	44.9	-13.36	30.11	-21.97	33.39
15	21.3	1.005	22.84	60.3	44.9	-13.50	30.20	-22.17	33.33
16	21.6	1.004	22.68	59.9	45.0	-13.65	30.28	-22.37	33.26
17	21.8	1.002	22.52	59.4	45.1	-13.79	30.36	-22.56	33.18
18	22.1	1.000	22.35	59.0	45.2	-13.95	30.45	-22.76	33.12
19	22.4	0.998	22.18	58.5	45.2	-14.09	30.52	-22.95	33.04
20	22.6	0.996	22.00	58.1	45.3	-14.25	30.60	-23.16	32.97
21	22.8	0.994	21.82	57.7	45.4	-14.41	30.69	-23.36	32.90
22	23.2	0.991	21.62	57.2	45.4	-14.57	30.76	-23.55	32.81
23	23.5	0.989	21.43	56.8	45.6	-14.73	30.84	-23.75	32.74
24	23.7	0.986	21.24	56.4	45.7	-14.90	30.93	-23.95	32.66
25	24.1	0.984	21.04	55.9	45.7	-15.06	30.99	-24.13	32.57
26	24.3	0.981	20.85	55.5	45.8	-15.23	31.07	-24.33	32.49
27	24.6	0.977	20.64	55.0	45.9	-15.39	31.14	-24.52	32.40
28	24.9	0.973	20.43	54.6	46.0	-15.57	31.22	-24.72	32.32
29	25.2	0.969	20.21	54.2	46.2	-15.75	31.30	-24.92	32.24
30	25.4	0.965	20.00	53.7	46.3	-15.92	31.36	-25.10	32.14
31	25.6	0.960	19.76	53.3	46.4	-16.10	31.43	-25.29	32.05
32	25.8	0.955	19.51	52.9	46.5	-16.29	31.51	-25.49	31.97
33	25.9	0.949	19.25	52.5	46.7	-16.48	31.58	-25.68	31.88
34	26.1	0.943	19.00	52.0	46.8	-16.65	31.64	-25.86	31.78
35	26.2	0.937	18.71	51.6	46.9	-16.84	31.71	-26.05	31.69
36	26.4	0.931	18.45	51.2	47.0	-17.03	31.78	-26.24	31.60
37	26.5	0.924	18.19	50.8	47.2	-17.23	31.85	-26.43	31.51
38	26.6	0.917	17.94	50.6	47.5	-17.47	31.96	-26.67	31.45
39	26.7	0.911	17.70	49.9	47.5	-17.60	31.97	-26.79	31.30
40	26.8	0.904	17.50	49.5	47.6	-17.80	32.03	-26.98	31.21
41	26.9	0.897	17.31	49.1	47.8	-18.00	32.10	-27.16	31.11
42	27.0	0.890	17.14	48.7	47.9	-18.21	32.16	-27.35	31.01
43	27.1	0.882	17.01	48.3	48.1	-18.41	32.22	-27.53	30.92
44	27.2	0.874	16.87	47.9	48.3	-18.62	32.28	-27.71	30.82
45	27.3	0.867	16.75	47.4	48.4	-18.80	32.32	-27.87	30.69
46	27.4	0.859	16.63	47.0	48.6	-19.01	32.37	-28.04	30.59

α	g	Fp/Fq	β	acl ang	pcl ang	mclo x	mclo y	lclo x	lclo y
(degrees)	(mm)	(N/N)	(degrees)	(degrees)	(degrees)	(mm)	(mm)	(mm)	(mm)
47	27.4	0.852	16.49	46.6	48.8	-19.21	32.43	-28.22	30.49
48	27.5	0.845	16.35	46.2	48.9	-19.42	32.48	-28.39	30.38
49	27.6	0.838	16.19	45.8	49.1	-19.63	32.53	-28.57	30.28
50	27.6	0.831	16.00	45.4	49.3	-19.84	32.58	-28.74	30.17
51	27.7	0.823	15.80	45.1	49.6	-20.08	32.65	-28.93	30.09
52	27.7	0.818	15.55	44.7	49.7	-20.29	32.69	-29.10	29.98
53	27.8	0.812	15.33	44.3	49.9	-20.51	32.74	-29.26	29.87
54	27.9	0.806	15.08	43.9	50.1	-20.72	32.78	-29.42	29.76
55	27.9	0.801	14.83	43.5	50.3	-20.94	32.82	-29.58	29.65
56	28.0	0.796	14.57	43.1	50.5	-21.15	32.86	-29.74	29.53
57	28.1	0.791	14.30	42.8	50.8	-21.39	32.92	-29.93	29.44
58	28.2	0.786	14.04	42.4	51.0	-21.61	32.95	-30.08	29.33
59	28.2	0.781	13.76	42.0	51.2	-21.82	32.98	-30.23	29.21
60	28.3	0.777	13.50	41.6	51.4	-22.04	33.01	-30.38	29.10
61	28.4	0.774	13.24	41.3	51.7	-22.28	33.06	-30.55	29.00
62	28.5	0.771	12.98	40.9	51.9	-22.50	33.09	-30.70	28.89
63	28.6	0.768	12.70	40.6	52.1	-22.75	33.13	-30.87	28.79
64	28.7	0.766	12.46	40.2	52.3	-22.96	33.16	-31.01	28.67
65	28.8	0.764	12.18	39.9	52.6	-23.21	33.20	-31.18	28.57
66	28.9	0.762	11.91	39.5	52.8	-23.42	33.22	-31.31	28.45
67	29.0	0.760	11.62	39.2	53.1	-23.67	33.25	-31.47	28.35
68	29.1	0.758	11.34	38.8	53.3	-23.89	33.27	-31.60	28.23
69	29.1	0.757	11.05	38.5	53.6	-24.13	33.30	-31.76	28.13
70	29.2	0.755	10.75	38.2	53.9	-24.38	33.33	-31.91	28.03
71	29.3	0.753	10.41	37.8	54.1	-24.59	33.34	-32.03	27.90
72	29.3	0.750	10.09	37.5	54.4	-24.84	33.36	-32.18	27.80
73	29.3	0.748	9.73	37.2	54.7	-25.09	33.39	-32.33	27.70
74	29.3	0.746	9.38	36.9	55.0	-25.33	33.41	-32.48	27.60
75	29.3	0.744	9.01	36.5	55.2	-25.54	33.41	-32.58	27.47
76	29.3	0.742	8.66	36.2	55.5	-25.79	33.43	-32.72	27.37
77	29.4	0.740	8.30	35.9	55.8	-26.03	33.44	-32.86	27.26
78	29.4	0.738	7.93	35.6	56.1	-26.27	33.45	-33.00	27.16
79	29.4	0.737	7.59	35.3	56.3	-26.52	33.47	-33.13	27.05
80	29.4	0.735	7.25	35.0	56.6	-26.76	33.47	-33.26	26.94
81	29.4	0.733	6.92	34.7	56.9	-27.00	33.48	-33.38	26.84
82	29.5	0.731	6.63	34.4	57.2	-27.24	33.48	-33.50	26.73
83	29.5	0.730	6.33	34.1	57.5	-27.48	33.48	-33.62	26.62
84	29.5	0.728	6.03	33.9	57.9	-27.76	33.51	-33.78	26.54
85	29.5	0.726	5.74	33.6	58.2	-27.99	33.50	-33.90	26.43
86	29.6	0.725	5.45	33.3	58.5	-28.23	33.50	-34.01	26.32
87	29.6	0.724	5.16	33.0	58.8	-28.46	33.49	-34.11	26.21
88	29.6	0.722	4.86	32.8	59.1	-28.74	33.50	-34.26	26.13
89	29.7	0.721	4.55	32.5	59.4	-28.97	33.48	-34.36	26.02
90	29.7	0.721	4.25	32.3	59.8	-29.24	33.49	-34.51	25.94
91	29.7	0.720	3.92	32.0	60.1	-29.47	33.47	-34.60	25.82

α	g	Fp/Fq	β	acl ang	pcl ang	mclo x	mclo y	lclo x	lclo y
(degrees)	(mm)	(N/N)	(degrees)	(degrees)	(degrees)	(mm)	(mm)	(mm)	(mm)
92	29.8	0.720	3.58	31.7	60.4	-29.69	33.45	-34.69	25.71
93	29.8	0.719	3.22	31.5	60.8	-29.96	33.45	-34.82	25.63
94	29.8	0.719	2.87	31.3	61.1	-30.23	33.45	-34.95	25.54
95	29.9	0.719	2.53	31.0	61.4	-30.44	33.42	-35.03	25.43
96	29.9	0.719	2.15	30.8	61.8	-30.71	33.41	-35.16	25.34
97	29.9	0.720	1.80	30.6	62.2	-30.97	33.40	-35.28	25.26
98	30.0	0.720	1.44	30.3	62.4	-31.18	33.36	-35.34	25.14
99	30.0	0.720	1.10	30.1	62.8	-31.44	33.34	-35.46	25.06
100	30.1	0.721	0.75	29.9	63.2	-31.70	33.33	-35.57	24.97
101	30.2	0.722	0.41	29.7	63.5	-31.95	33.30	-35.68	24.88
102	30.3	0.722	0.08	29.5	63.9	-32.20	33.28	-35.78	24.79
103	30.4	0.723	-0.25	29.3	64.3	-32.45	33.25	-35.88	24.70
104	30.5	0.724	-0.58	29.1	64.6	-32.70	33.22	-35.98	24.62
105	30.6	0.725	-0.90	28.9	65.0	-32.95	33.19	-36.08	24.53
106	30.7	0.726	-1.23	28.7	65.4	-33.19	33.16	-36.17	24.44
107	30.8	0.727	-1.54	28.5	65.7	-33.43	33.12	-36.25	24.35
108	30.9	0.728	-1.87	28.3	66.1	-33.66	33.08	-36.33	24.26
109	31.0	0.729	-2.20	28.1	66.4	-33.89	33.03	-36.41	24.17
110	31.1	0.731	-2.50	27.9	66.8	-34.12	32.99	-36.49	24.08
111	31.2	0.732	-2.85	27.8	67.2	-34.41	32.96	-36.62	24.02
112	31.2	0.733	-3.15	27.6	67.6	-34.63	32.91	-36.68	23.93
113	31.3	0.734	-3.50	27.4	67.9	-34.85	32.86	-36.74	23.84
114	31.3	0.735	-3.80	27.3	68.4	-35.13	32.83	-36.87	23.78
115	31.4	0.736	-4.12	27.1	68.7	-35.34	32.77	-36.92	23.69
116	31.4	0.737	-4.46	27.0	69.2	-35.61	32.73	-37.03	23.63
117	31.5	0.738	-4.78	26.8	69.5	-35.82	32.66	-37.08	23.54
118	31.5	0.739	-5.11	26.7	69.9	-36.08	32.62	-37.18	23.47
119	31.6	0.740	-5.42	26.6	70.4	-36.35	32.57	-37.29	23.41
120	31.6	0.741	-5.75	26.4	70.7	-36.53	32.50	-37.31	23.32

Appendix IV Muscle physiological cross-sectional areas.

After Freiderich &Brand [1990]
Physiological cross-sectional area (PCSA) = muscle volume/muscle fibre length

Table A-IV.1 Muscle physiological cross sectional area

	PCSA (cm^2)		Muscle	PCSA (cm^2)
Add brevis (S)	11.52		Biceps femoris	27.34
Add brevis (I)	5.34		Gracilis	3.74
Add longus	22.73		Rectus Femoris	42.96
Add magnus 1	25.52		Sartorius	2.90
Add magnus 2	18.35		Semimembranos	46.33
Add magnus 3	16.95		Semitendinosus	23.27
Gluteus max 1	20.20		Ten Fas Latae	8.00
Gluteus max 2	19.59		Gastroc (M)	50.60
Gluteus max 3	20.00		Gastroc (L)	14.30
Gluteus med 1	25.00		Biceps Fem (S)	8.14
Gluteus med 2	16.21		Vastus interm	82.00
Gluteus med 3	21.21		Vastus lateral	64.41
Gluteus min 1	6.76		Vastus medial	66.87
Gluteus min 2	8.20		Tibialis anter	16.88
Gluteus min 3	11.98		Ext dig comm	7.46
iliacus	23.33		Ext hall long	6.49
iliopsoas	25.70		Flexor dig	6.40
Inf gemelli	4.33		Flexor hall long	18.52
Obturator ext	2.71		Peroneus brev	19.61
Obturator int	9.07		Peroneus long	24.65
Pectineus	9.03		Peroneus tert	4.14
Piriformis	20.54		Tibialis poste	26.27
Quad femoris	21.00		Soleus	186.69
Sup gemelli	2.13			

Appendix V Hip joint centre location errors (Section 3.7.4)

Note that the static and waggle trial number prefix of '37' has been omitted from the following table.

Table A-V.1 Method 1: All static trial frames used, no other conditions

Static,Waggle Trial No.s	X-Coordinate (mm)	Y-Coordinate (mm)	Z-Coordinate (mm)	Error (mm)
01,04	-46.32	-87.06	-62.18	4.90
01,05	-37.56	-81.11	-59.05	8.15
01,06	-41.04	-92.63	-53.57	8.51
01,07	-41.63	-85.45	-58.45	2.47
01,08	-42.02	-80.28	-62.16	7.34
02,04	-44.29	-92.71	-65.25	9.88
02,05	-35.99	-88.46	-65.90	11.51
02,06	-38.11	-94.71	-64.54	12.38
02,07	-40.70	-94.06	-65.84	11.72
02,08	-42.45	-95.92	-62.24	10.90
03,04	-45.08	-100.34	-61.63	14.83
03,05	-32.07	-86.04	-61.86	12.54
03,06	-33.68	-91.49	-61.36	12.16
03,07	-35.45	-89.63	-62.78	10.45
03,08	-38.36	-92.16	-59.78	8.54
Actual	**-44**	**-86**	**-58**	**0.00**
Average	-39.65	-90.14	-61.77	9.75
Minimum	-46.32	-100.34	-65.90	2.47
Maximum	-32.07	-80.28	-53.57	14.83

Table A-V.2 Method 2: No angles less than 5°, frames requiring least pelvic correction

Static,Waggle Trial No.s	X-Coordinate (mm)	Y-Coordinate (mm)	Z-Coordinate (mm)	Error (mm)
01,04	-48.74	-92.86	-62.57	9.51
01,05	-35.98	-79.81	-59.45	10.23
01,06	-39.77	-99.39	-51.02	15.68
01,07	-43.03	-89.42	-56.88	3.73
01,08	-42.83	-79.27	-61.00	7.46
02,04	-43.24	-96.15	-62.66	11.19
02,05	-38.06	-90.92	-66.61	11.56
02,06	-37.98	-97.58	-63.12	14.02
02,07	-40.86	-95.22	-66.00	12.60
02,08	-41.22	-95.45	-62.34	10.76
03,04	-46.94	-103.63	-57.70	17.88
03,05	-33.06	-86.81	-62.51	11.86
03,06	-34.81	-91.18	-62.50	11.47
03,07	-34.81	-91.18	-62.50	11.47
03,08	-38.15	-90.28	-60.05	7.53
Actual	**-44**	**-86**	**-58**	**0.00**
Average	-39.97	-91.94	-61.13	11.13
Minimum	-48.74	-103.63	-66.61	3.73
Maximum	-33.06	-79.27	-51.02	17.88

Table A-V.3 Method 3: Selected static trial frames

Static,Waggle Trial No.s	X-Coordinate (mm)	Y-Coordinate (mm)	Z-Coordinate (mm)	Error (mm)
01,04	-46.06	-83.51	-63.18	6.11
01,05	-39.16	-80.74	-59.38	7.28
01,06	-43.44	-93.76	-53.17	9.16
01,07	-44.08	-86.03	-58.38	0.39
01,08	-42.61	-78.67	-63.30	9.15
02,04	-43.73	-84.15	-66.44	8.64
02,05	-39.80	-87.49	-65.45	8.68
02,06	-46.05	-95.15	-64.74	11.55
02,07	-46.05	-95.15	-64.74	11.55
02,08	-44.30	-92.69	-63.46	8.64
03,04	-45.83	-88.50	-65.07	7.72
03,05	-40.84	-90.45	-62.91	7.34
03,06	-43.39	-98.54	-61.37	13.00
03,07	-46.41	-97.78	-62.78	12.94
03,08	-46.80	-97.09	-60.36	11.68
Actual	**-44**	**-86**	**-58**	**0.00**
Average	-43.90	-89.98	-62.32	8.92
Minimum	-46.80	-98.54	-66.44	0.39
Maximum	-39.16	-78.67	-53.17	13.00

Table A-V.4 Method 4: Static trial 2Hz and waggle trial 6Hz low pass filtered

Static,Waggle Trial No.s	X-Coordinate (mm)	Y-Coordinate (mm)	Z-Coordinate (mm)	Error (mm)
01,04	-47.83	-88.43	-63.10	6.83
01,05	-42.05	-84.51	-61.83	4.55
01,06	-38.47	-78.32	-57.79	9.47
01,07	-45.07	-96.11	-55.36	10.50
01,08	-38.83	-78.09	-59.26	9.53
02,04	-44.85	-92.10	-64.26	8.78
02,05	-39.08	-89.93	-68.25	12.03
02,06	-34.74	-87.81	-61.60	10.10
02,07	-38.56	-99.49	-59.37	14.61
02,08	-38.30	-94.02	-62.88	10.98
03,04	-46.27	-100.93	-60.81	15.36
03,05	-36.21	-93.46	-64.21	12.45
03,06	-34.74	-87.81	-61.60	10.10
03,07	-38.56	-99.49	-59.37	14.61
03,08	-32.24	-90.53	-60.36	12.82
Actual	**-44**	**-86**	**-58**	**0.00**
Average	-39.72	-90.74	-61.34	10.85
Minimum	-47.83	-100.93	-68.25	4.55
Maximum	-32.24	-78.09	-55.36	15.36

Table A-V.5 Method 5: Static trial 2Hz and waggle trial 6Hz low pass filtered using selected static trial frames

Static,Waggle Trial No.s	X-Coordinate (mm)	Y-Coordinate (mm)	Z-Coordinate (mm)	Error (mm)
01,04	-47.79	-84.61	-64.38	7.55
01,05	-43.73	-81.68	-61.76	5.73
01,06	-40.39	-76.10	-57.20	10.57
01,07	-47.77	-97.63	-54.32	12.77
01,08	-40.73	-74.05	-59.80	12.52
02,04	-44.26	-87.17	-64.91	7.01
02,05	-40.80	-86.68	-68.05	10.57
02,06	-40.84	-89.10	-64.88	8.18
02,07	-46.12	-106.51	-61.07	20.85
02,08	-40.48	-91.76	-63.18	8.51
03,04	-45.50	-91.53	-63.23	7.76
03,05	-41.19	-89.82	-65.24	8.65
03,06	-40.29	-89.78	-62.49	6.94
03,07	-44.35	-107.16	-58.88	21.18
03,08	-39.03	-90.84	-61.29	7.68
Actual	**-44**	**-86**	**-58**	**0.00**
Average	-42.88	-89.63	-62.05	10.43
Minimum	-47.79	-107.16	-68.05	5.73
Maximum	-39.03	-74.05	-54.32	21.18

Appendix VI Results

This appendix has been divided into the following parts:

The results are presented in a common format. This consists of four graphs per variable. Each graph represents one of the groups; male, female, male hip replacement subject's normal side or male hip replacement subject's replaced side. There has been no attempt to allow the values of individual traces to be measured from the graphs although this is possible in some figures. Different colours have been used to define each individual. Individual's left and right sides are included without distinction. The figure below defines the colours assigned to individuals.

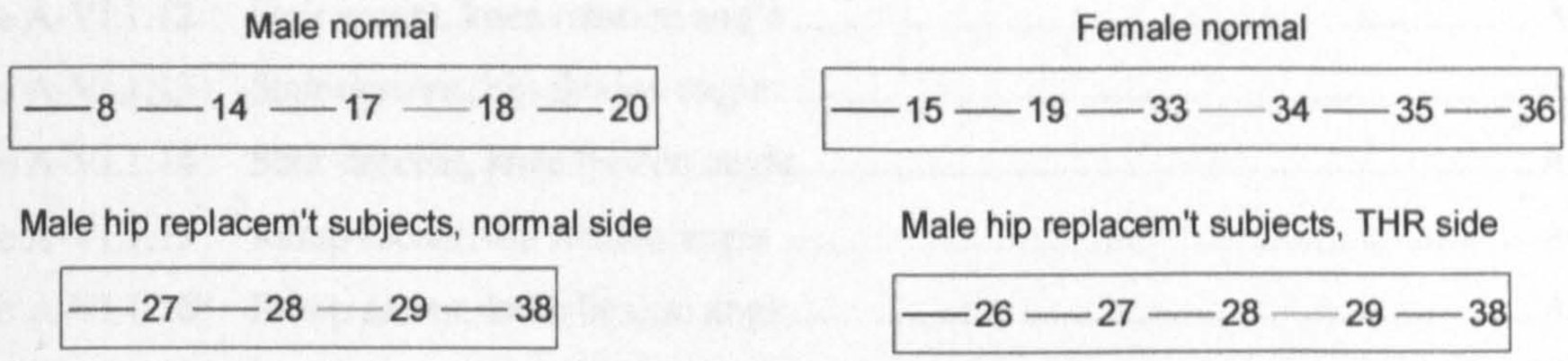

Pages and figures have been numbered by section of this Appendix. Thus all figures in section 3 are prefixed with A-VI.3 as are all page numbers.

Section A-V1.3 contains indications of muscle emg activity after University of California [1953]. The following example illustrates the levels of activity expected:

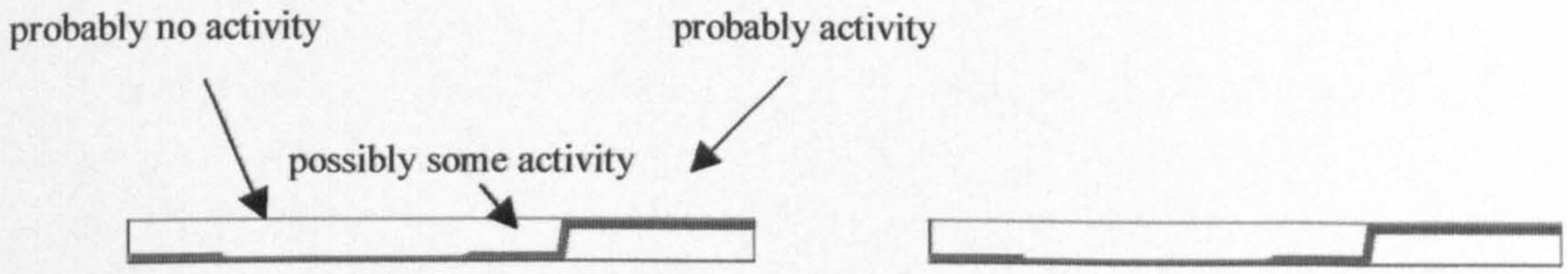

A-VI.1 Joint angles

List of figures

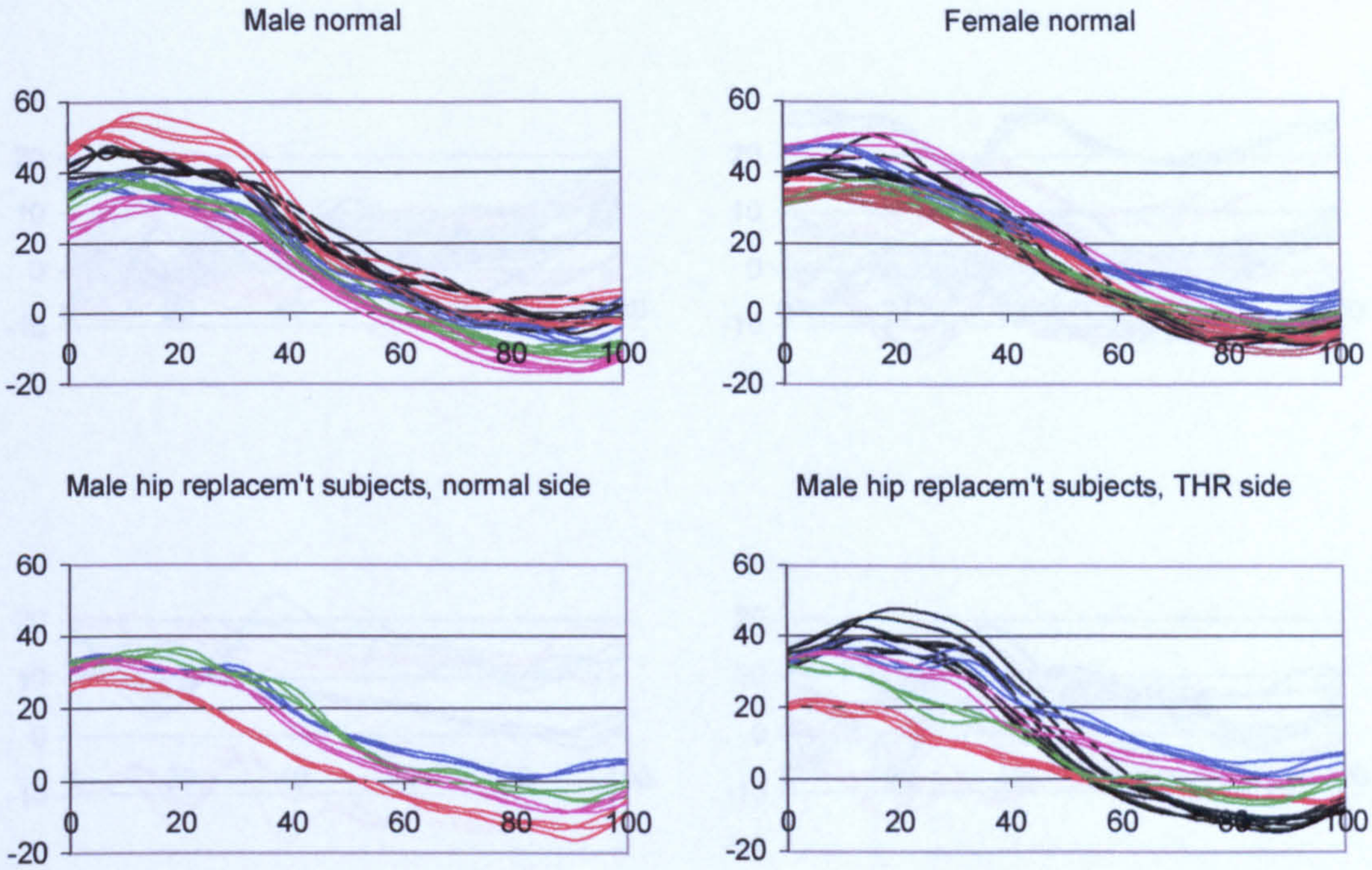

Figure A-VI.1.1 Walking, hip flexion angle

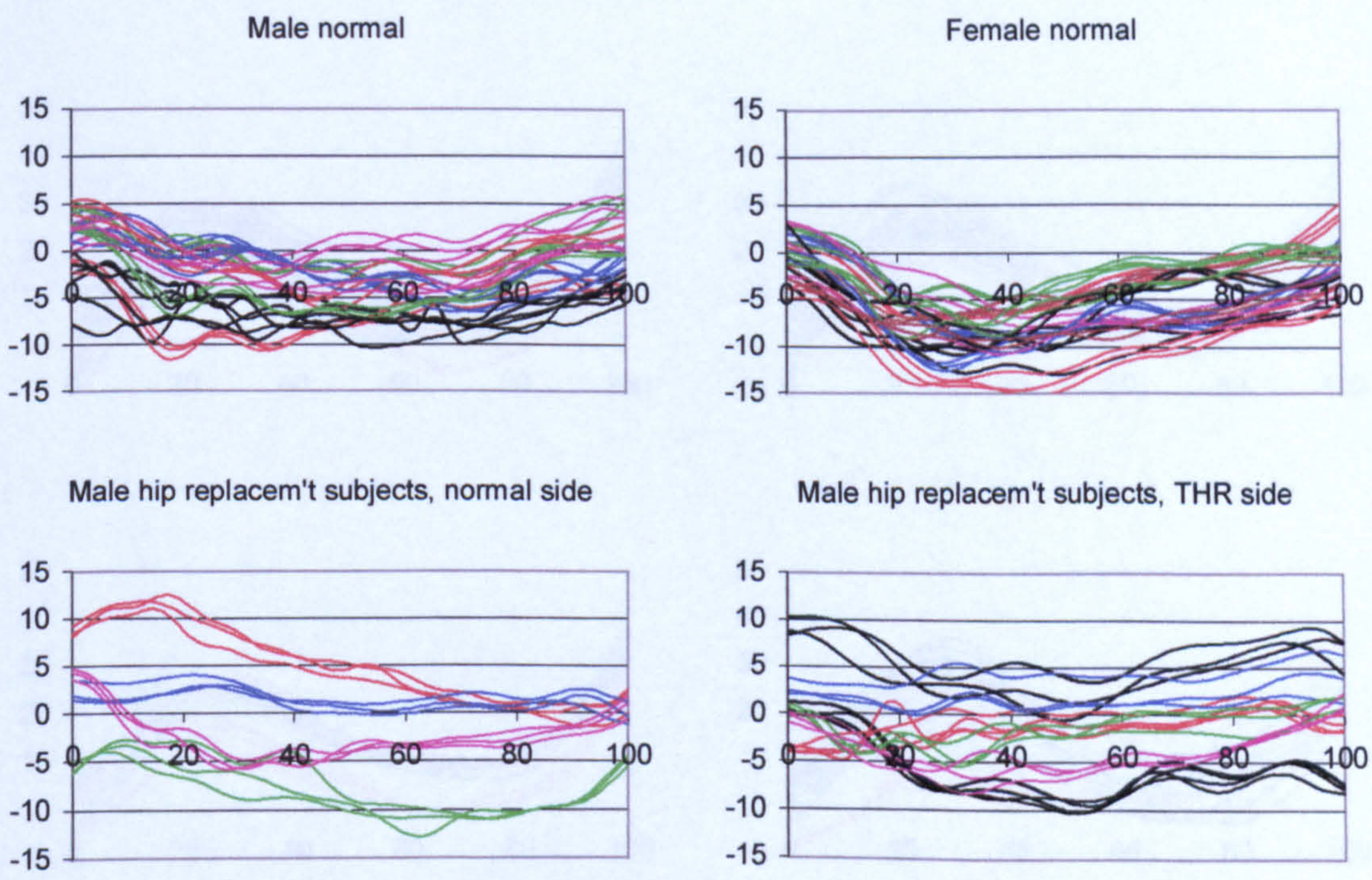

Figure A-VI.1.2 Walking, hip abduction angle

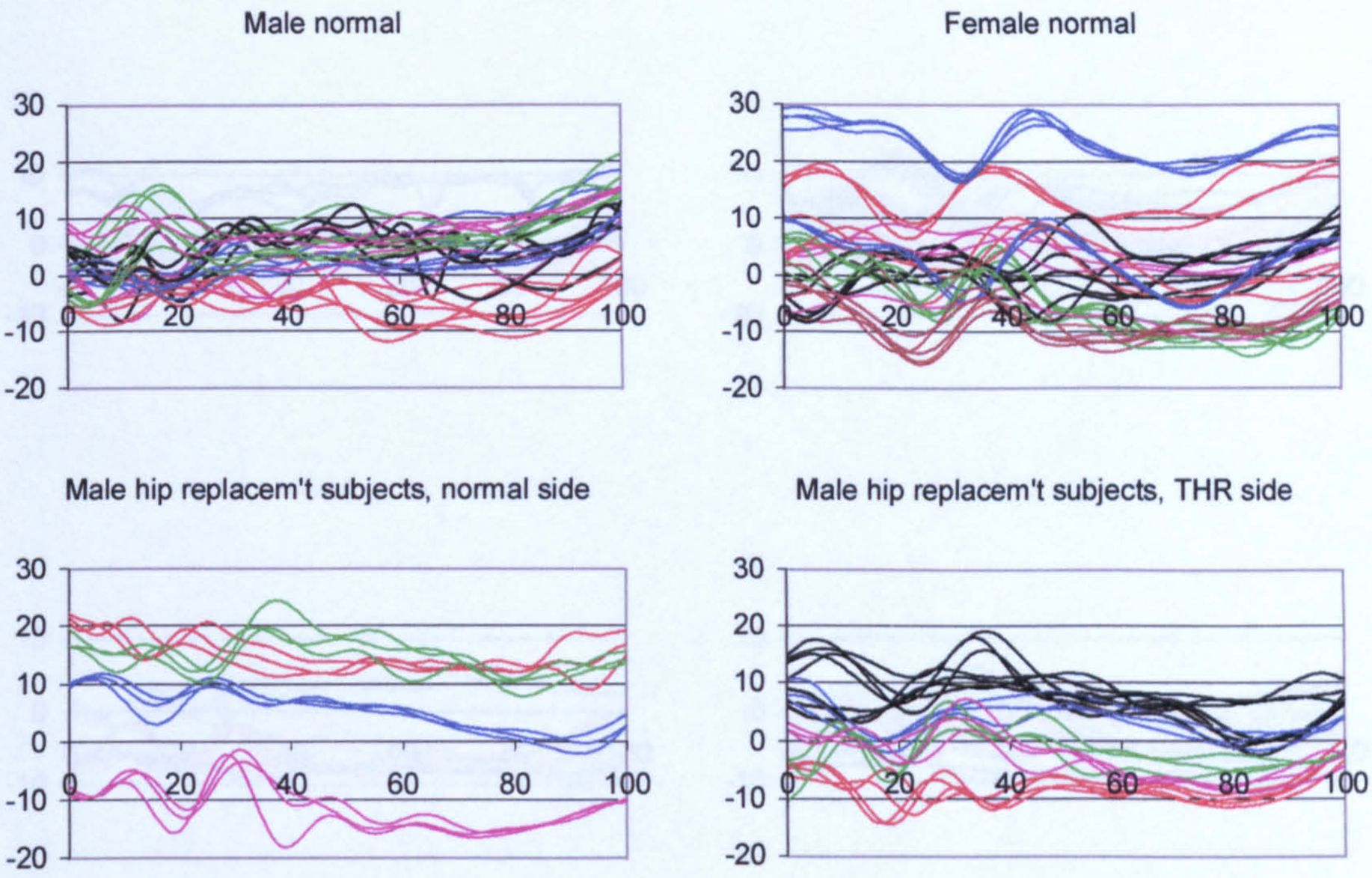

Figure A-VI.1.3 Walking, hip rotation angle

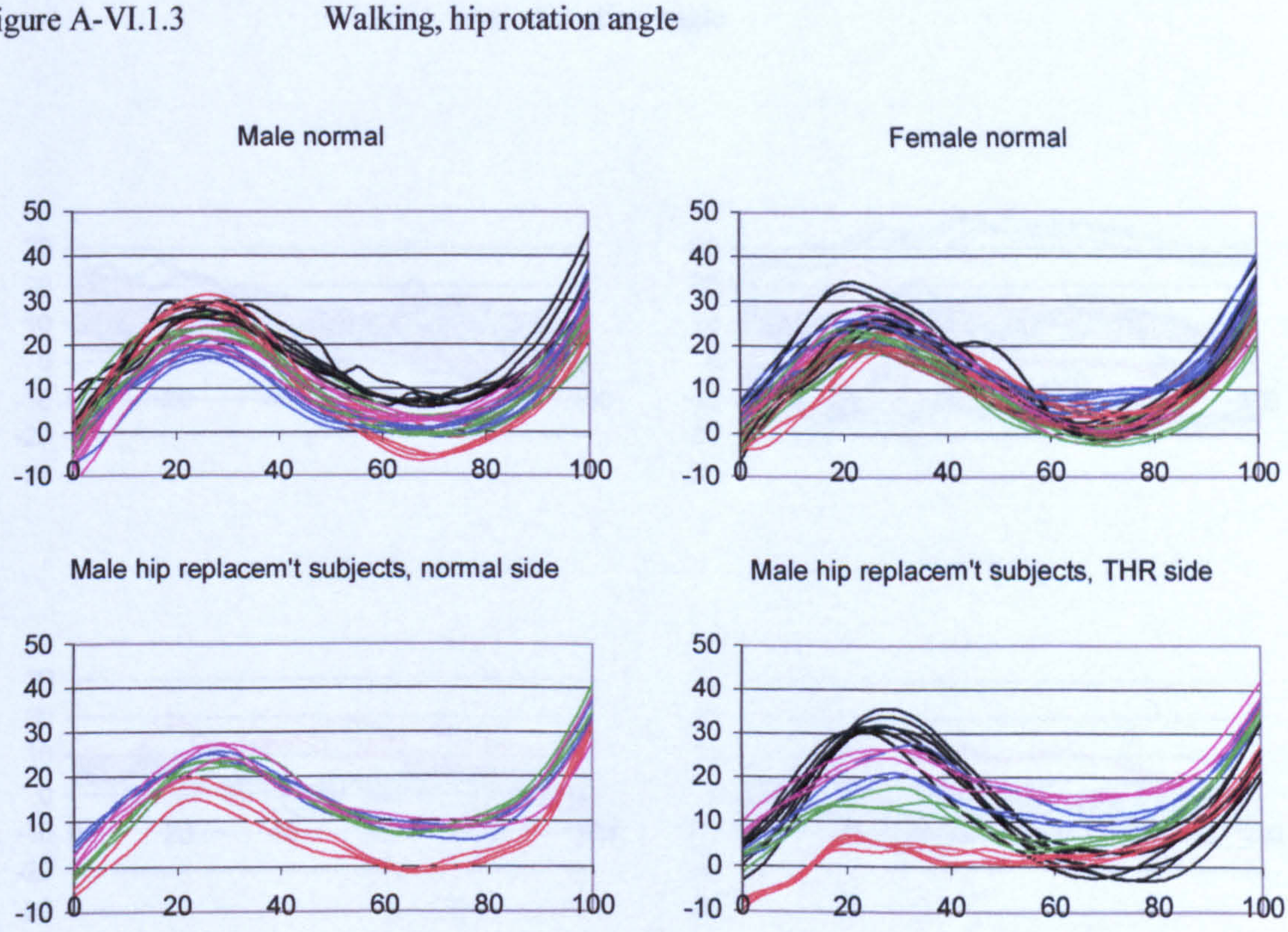

Figure A-VI.1.4 Walking, knee flexion angle

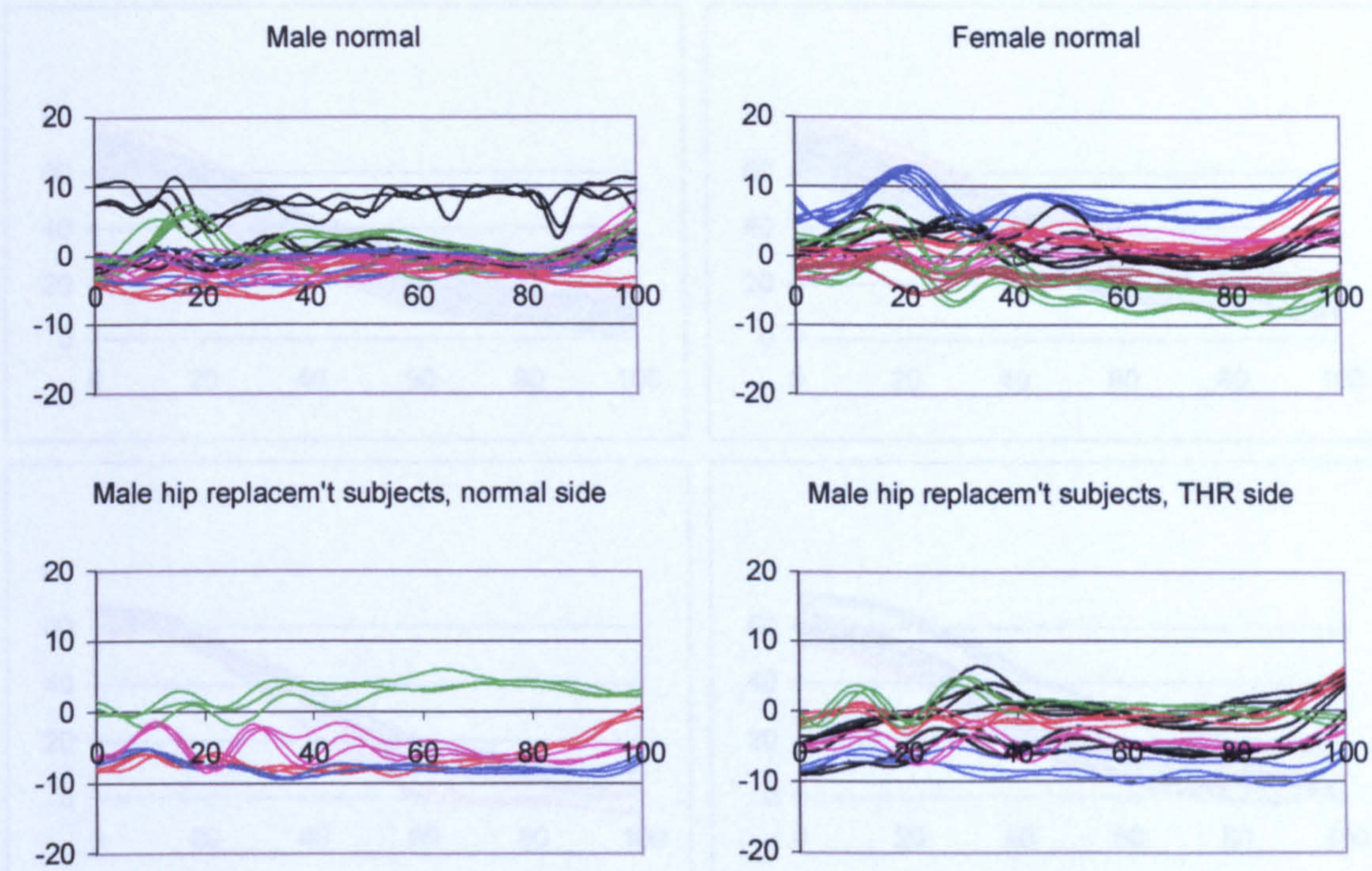

Figure A-VI.1.5 Walking, knee abduction angle

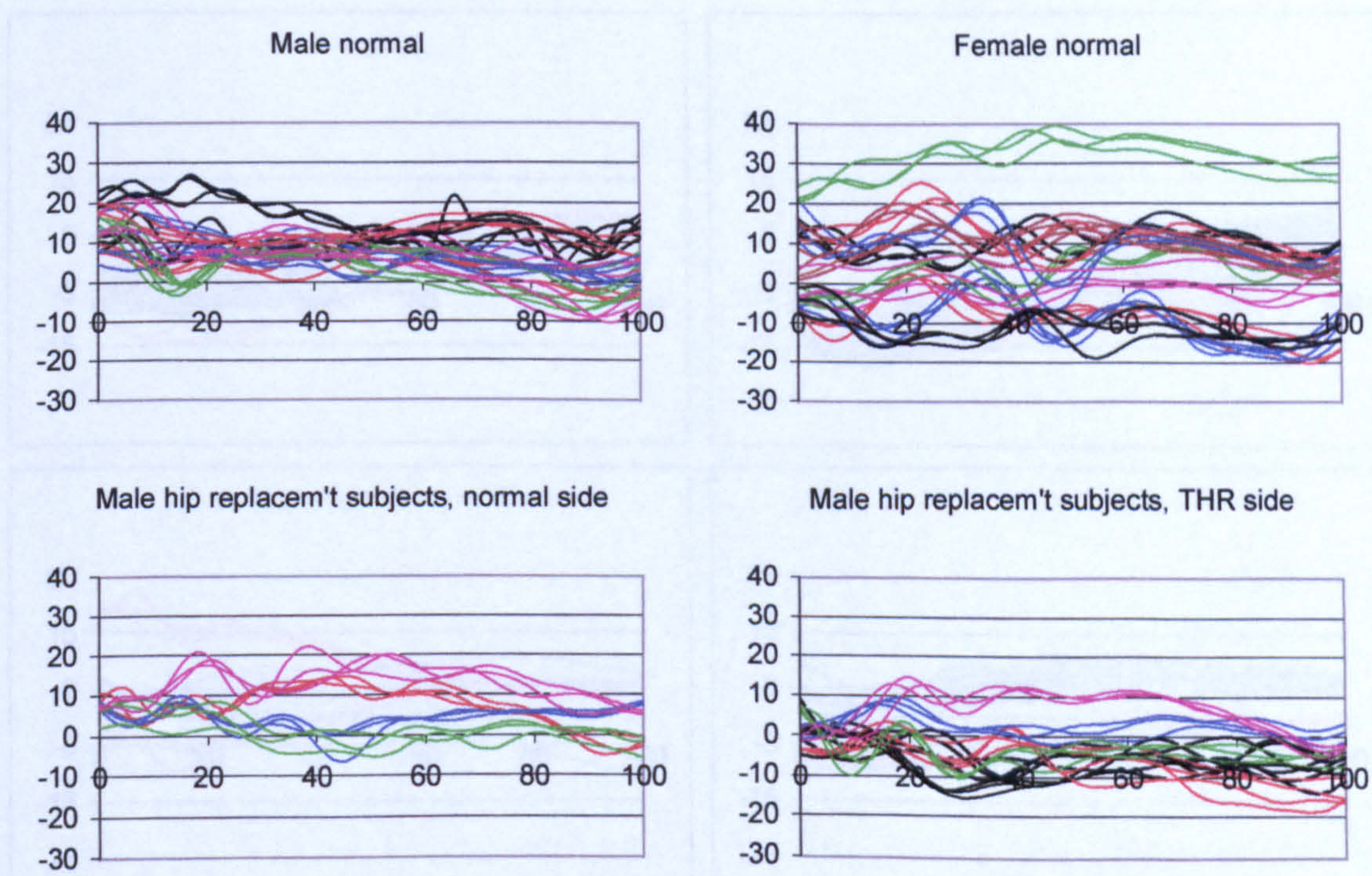

Figure A-VI.1.6 Walking, knee rotation angle

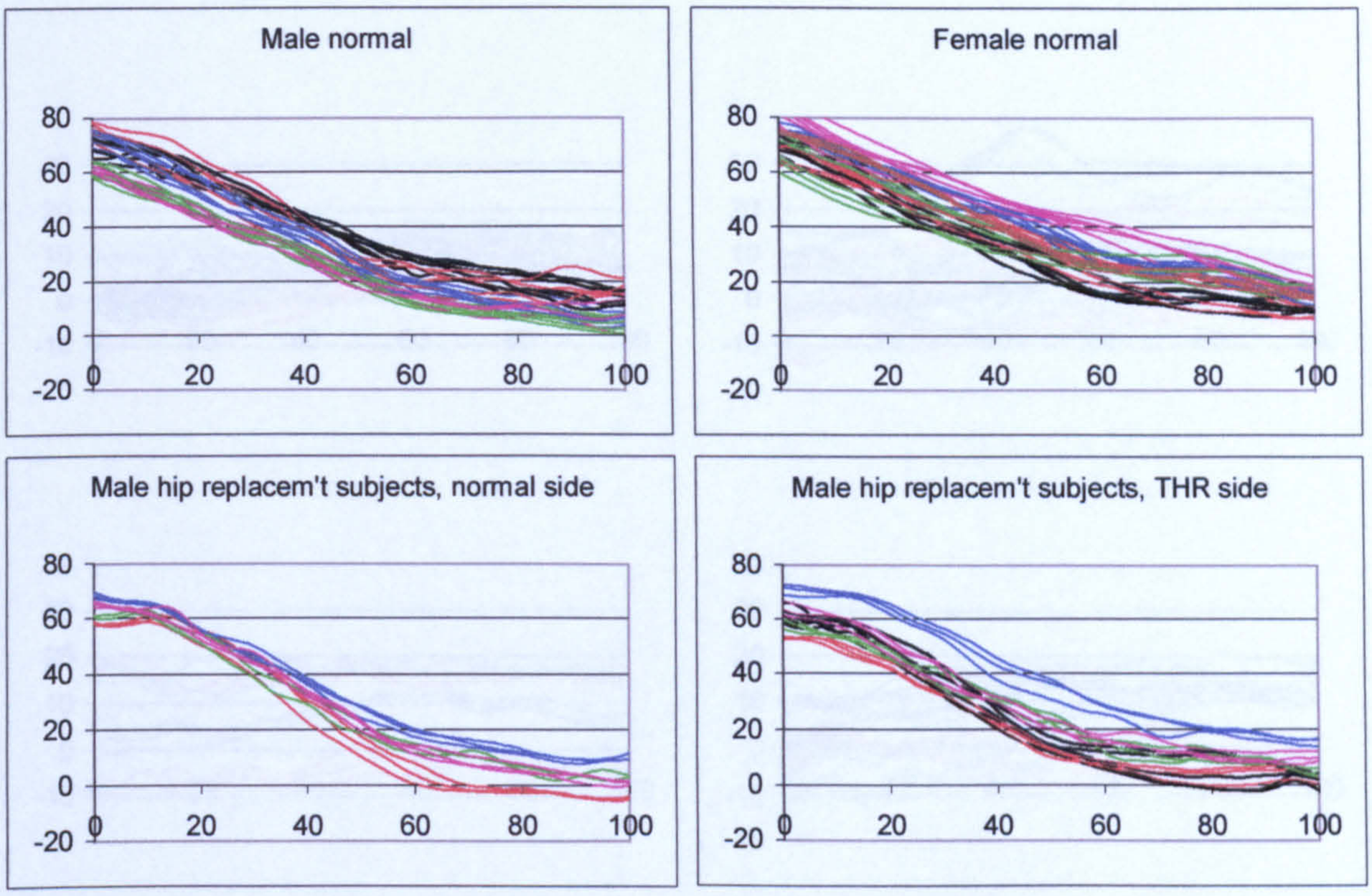

Figure A-VI.1.7 Stair ascent, hip flexion angle

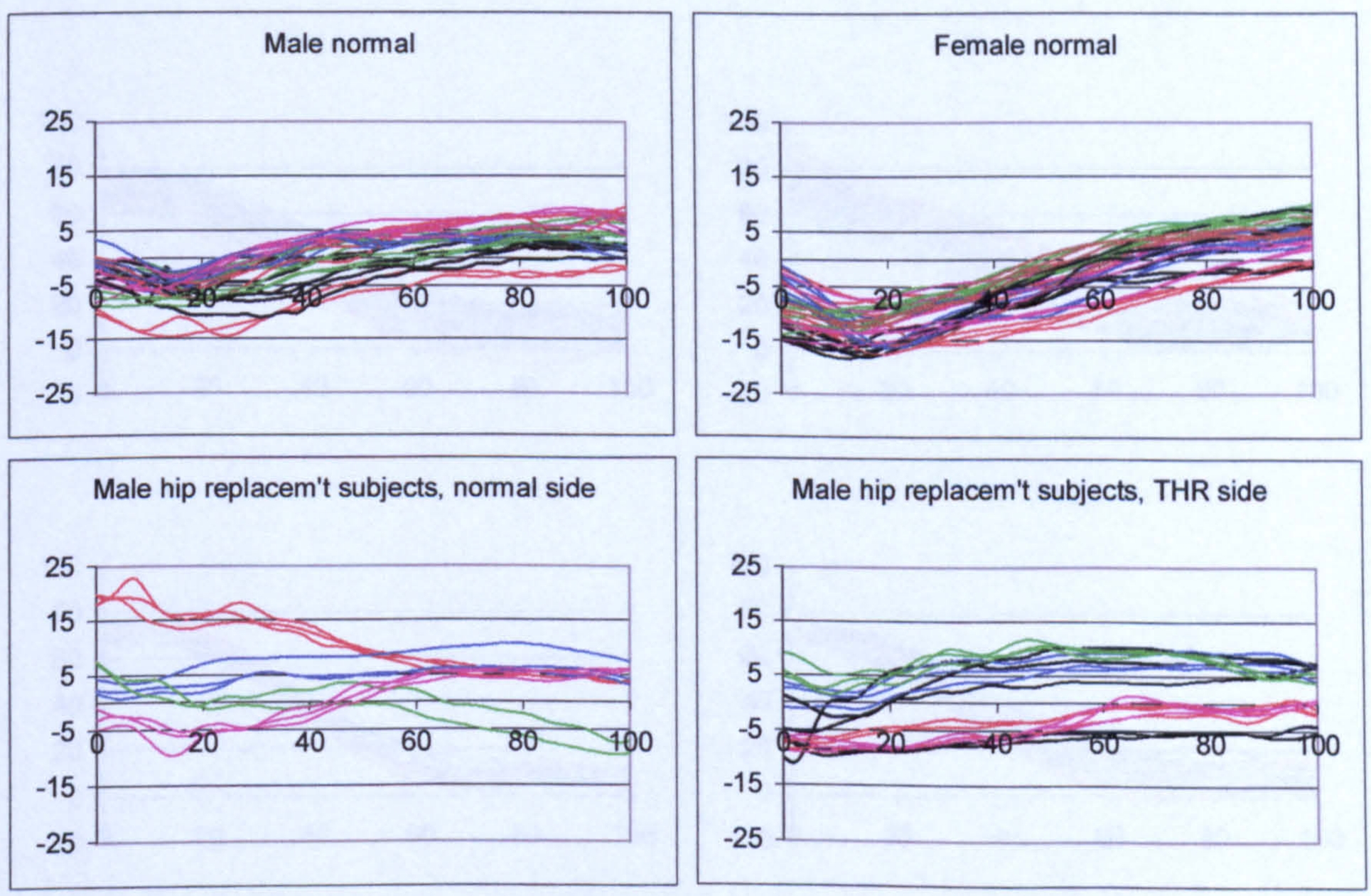

Figure A-VI.1.8 Stair ascent, hip abduction angle

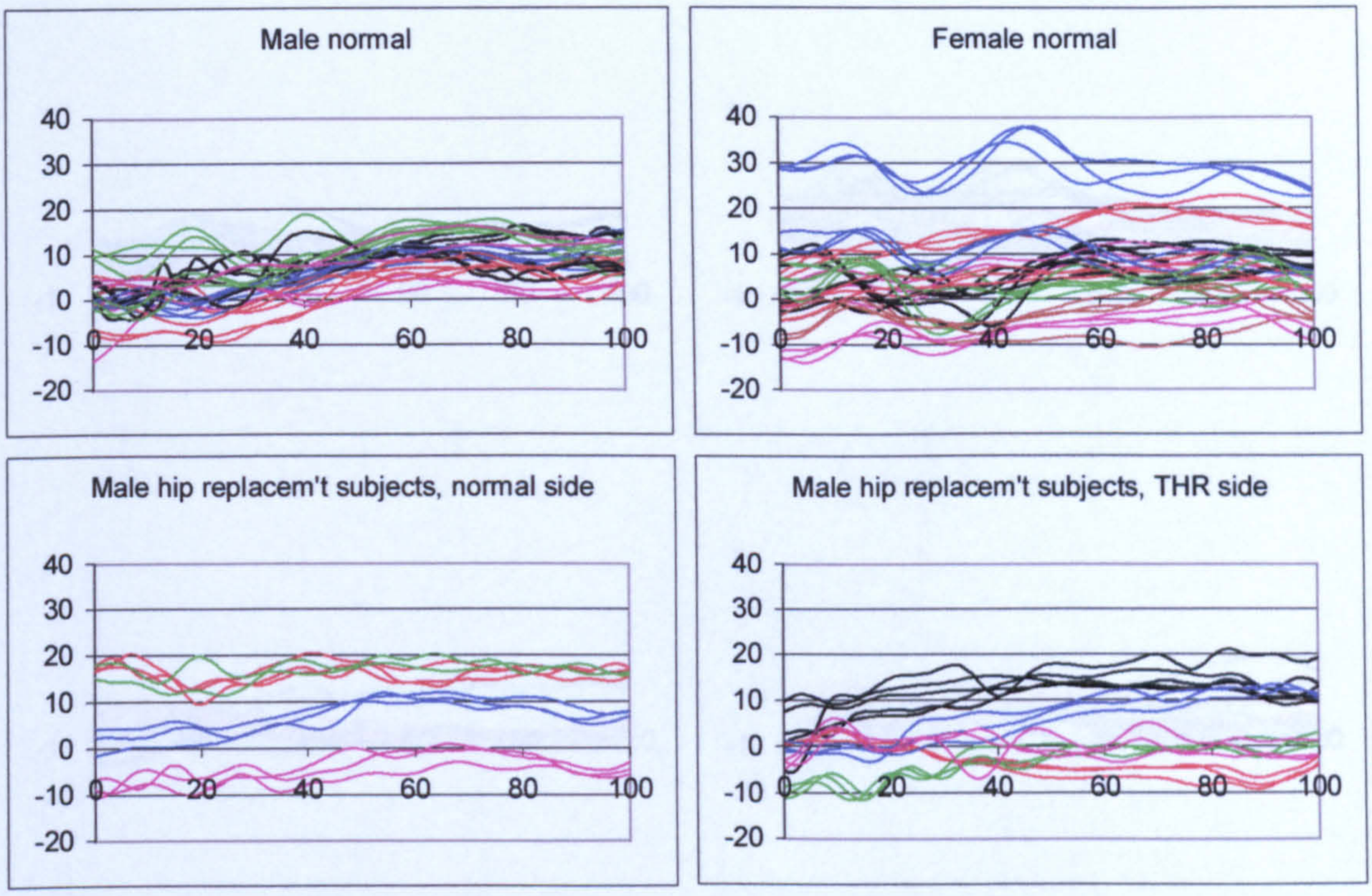

Stair ascent, hip rotation angle (degrees, +ve=external) by % stance phase

Figure A-VI.1.9 Stair ascent, hip rotation angle

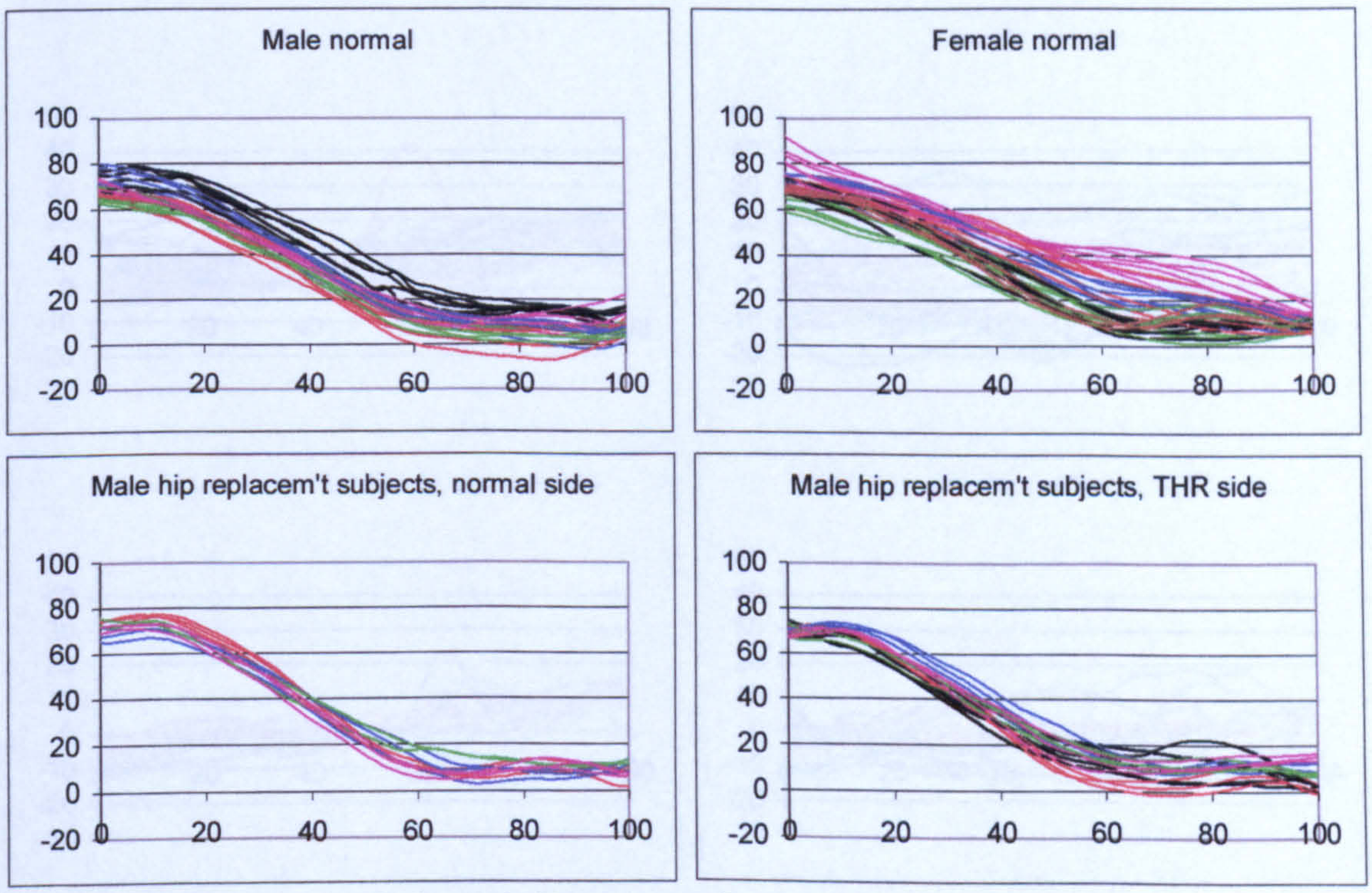

Stair ascent, knee flexion angle (degrees, +ve=flexion) by % stance phase

Figure A-VI.1.10 Stair ascent, knee flexion angle

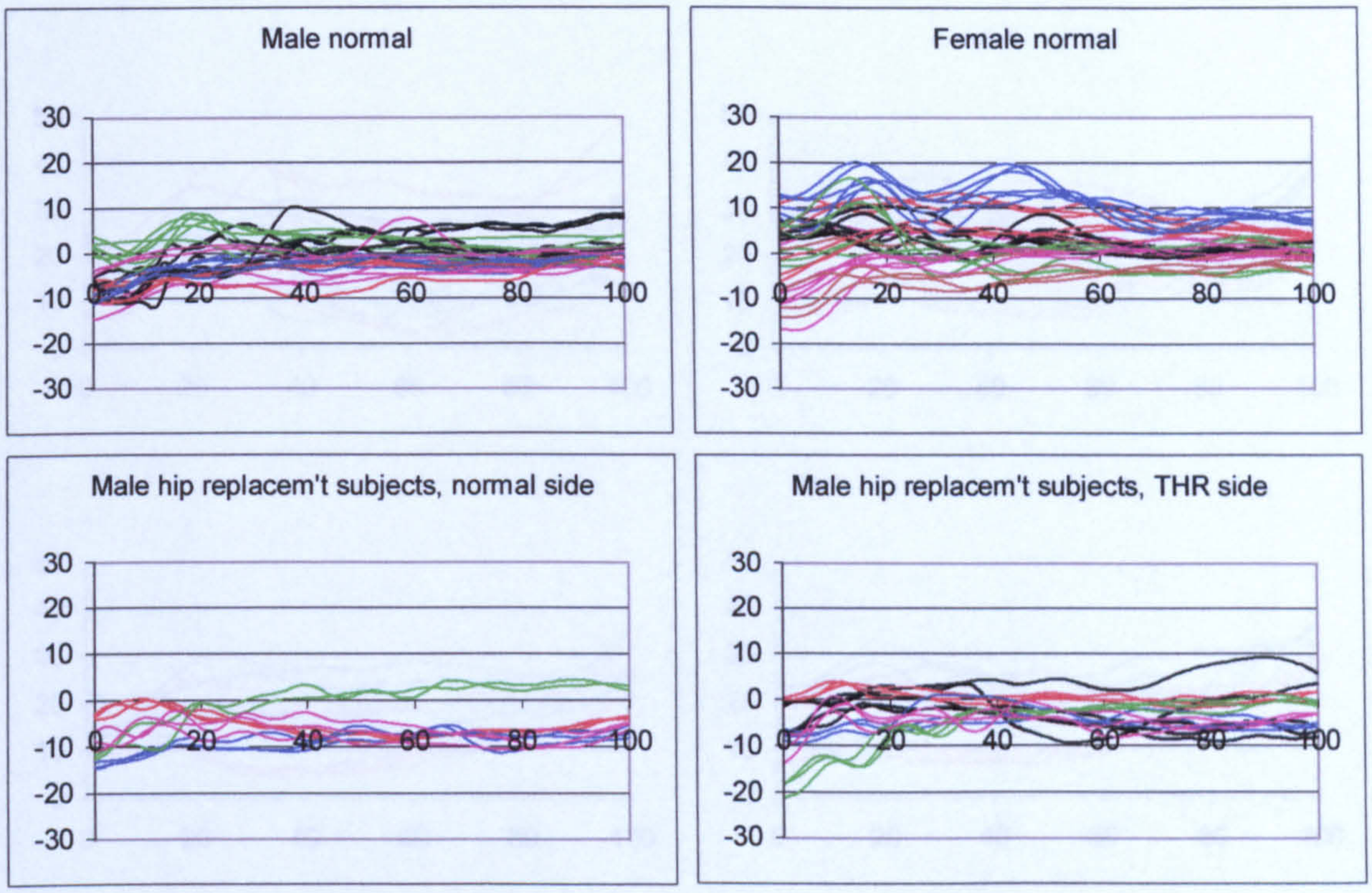

Figure A-VI.1.11 Stair ascent, knee abduction angle

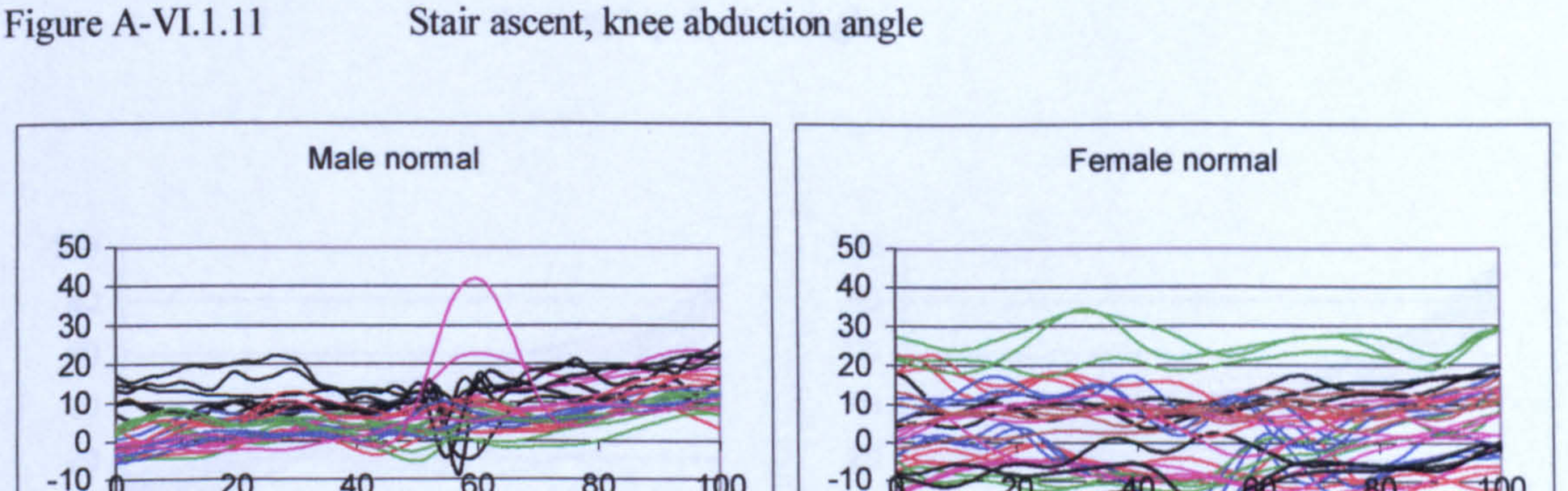

Figure A-VI.1.12 Stair ascent, knee rotation angle

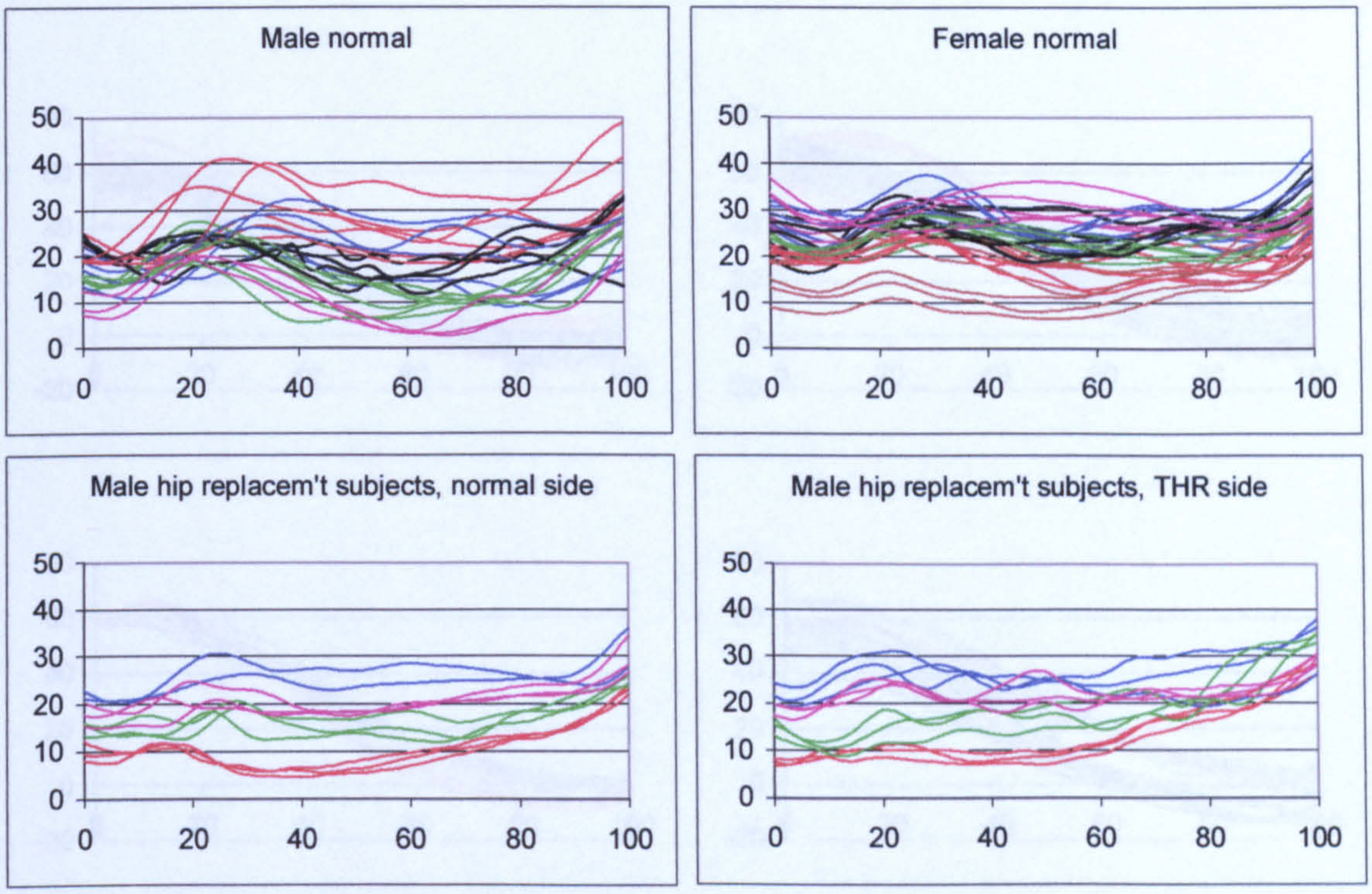

Stair descent, hip flexion angle (degrees, +ve=flexion) by % stance phase

Figure A-VI.1.13 Stair descent, hip flexion angle

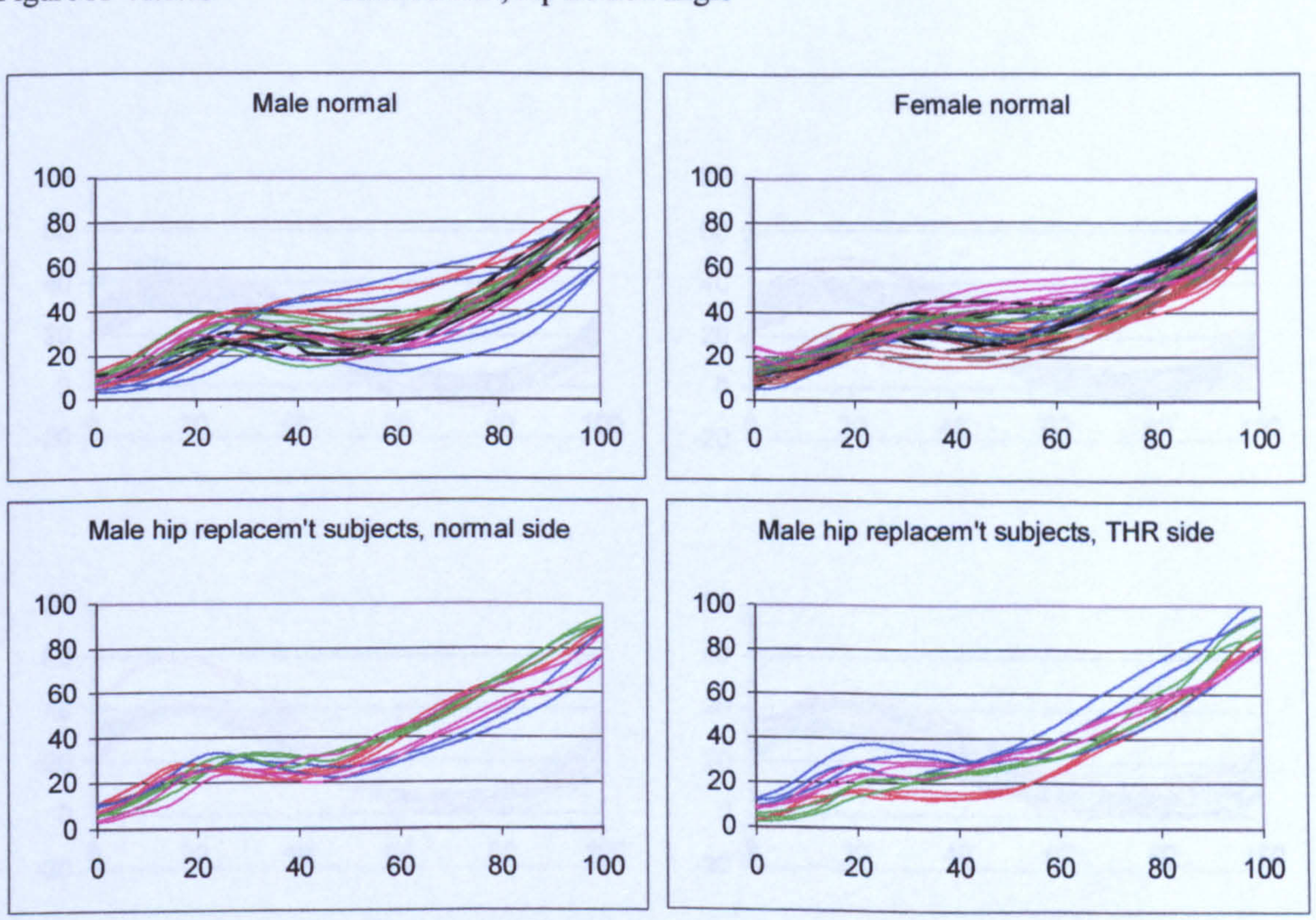

Stair descent, knee flexion angle (degrees, +ve=flexion) by % stance phase

Figure A-VI.1.14 Stair descent, knee flexion angle

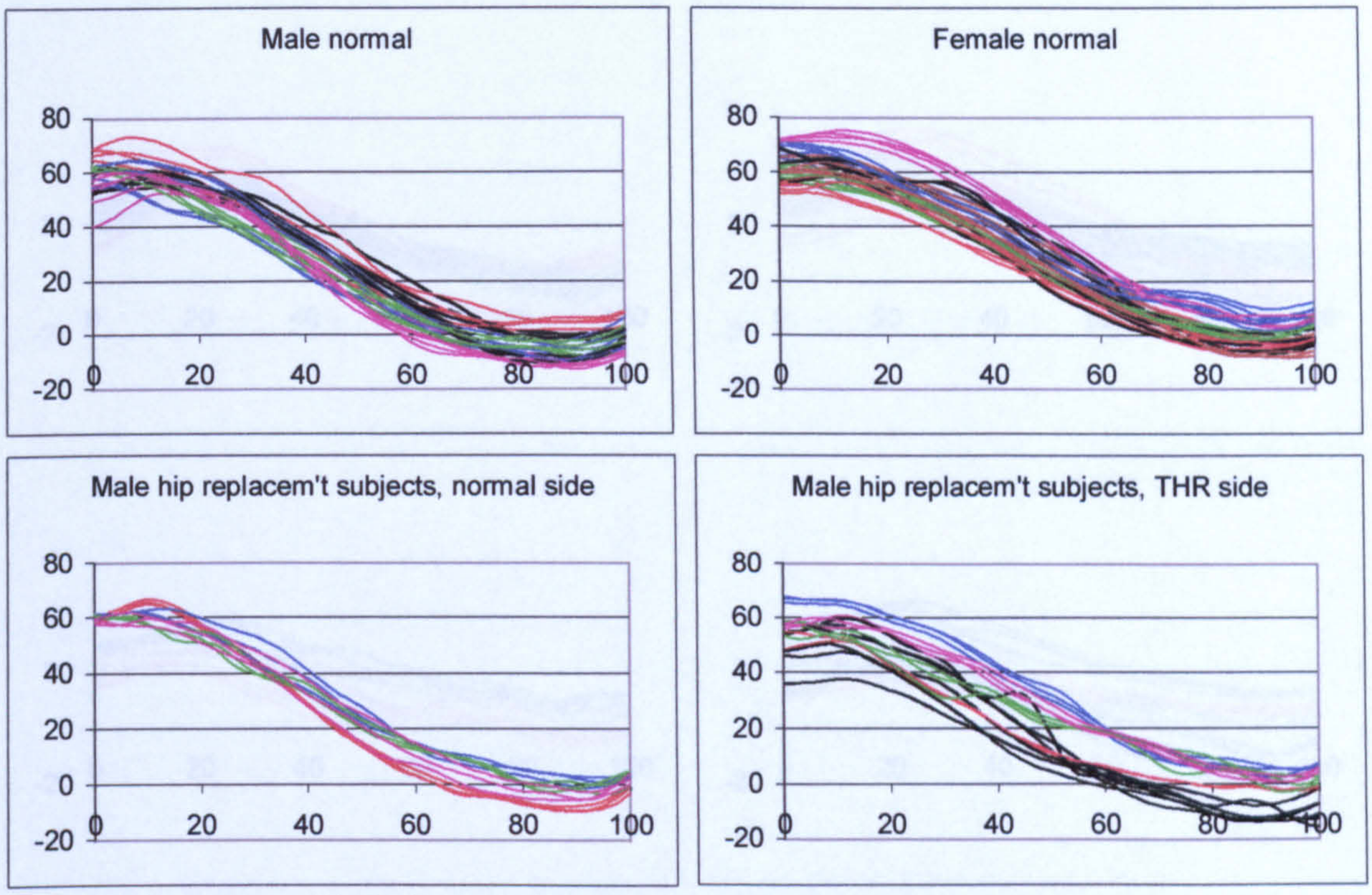

Figure A-VI.1.15 Ramp ascent, hip flexion angle

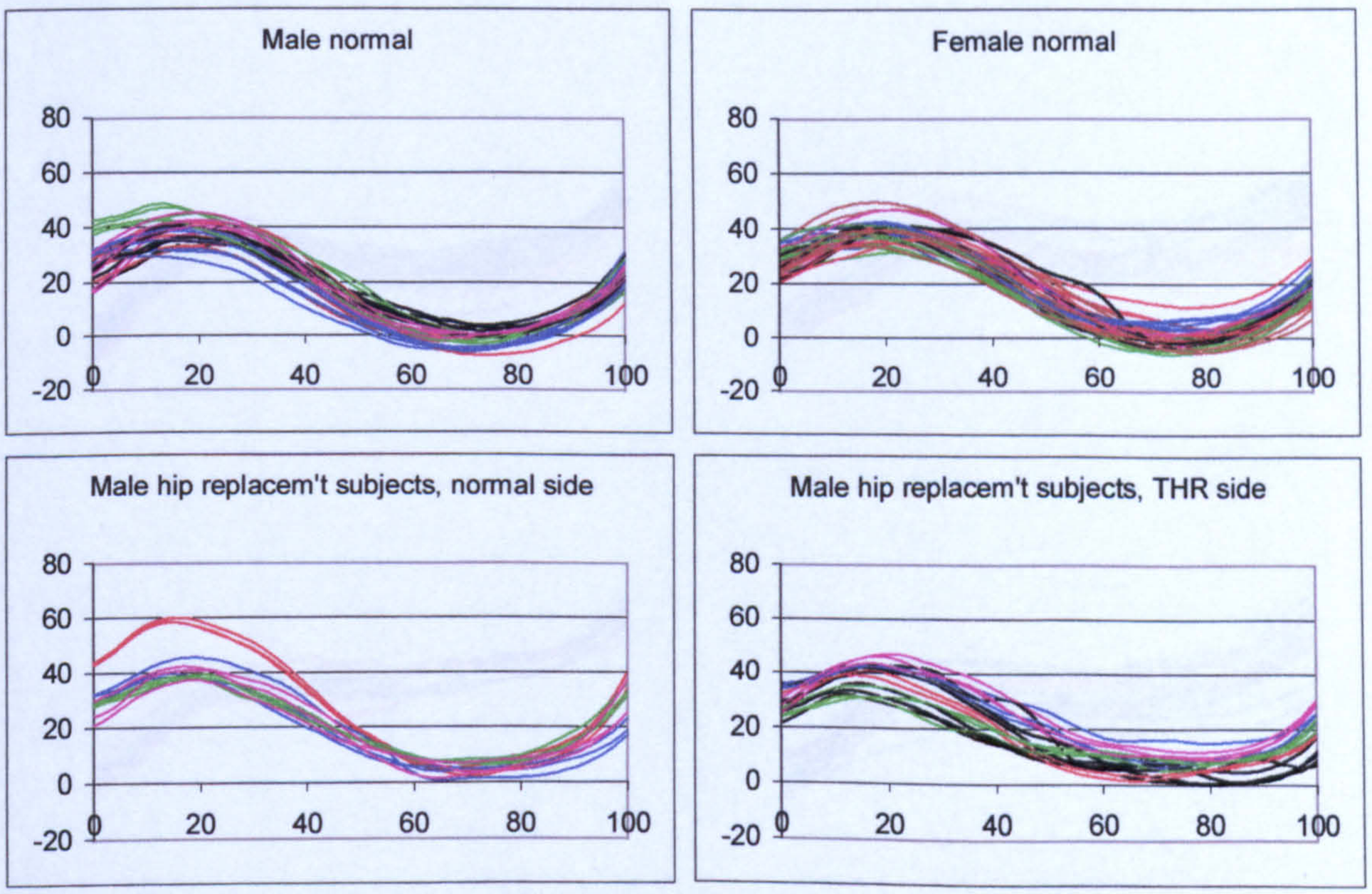

Figure A-VI.1.16 Ramp ascent, knee flexion angle

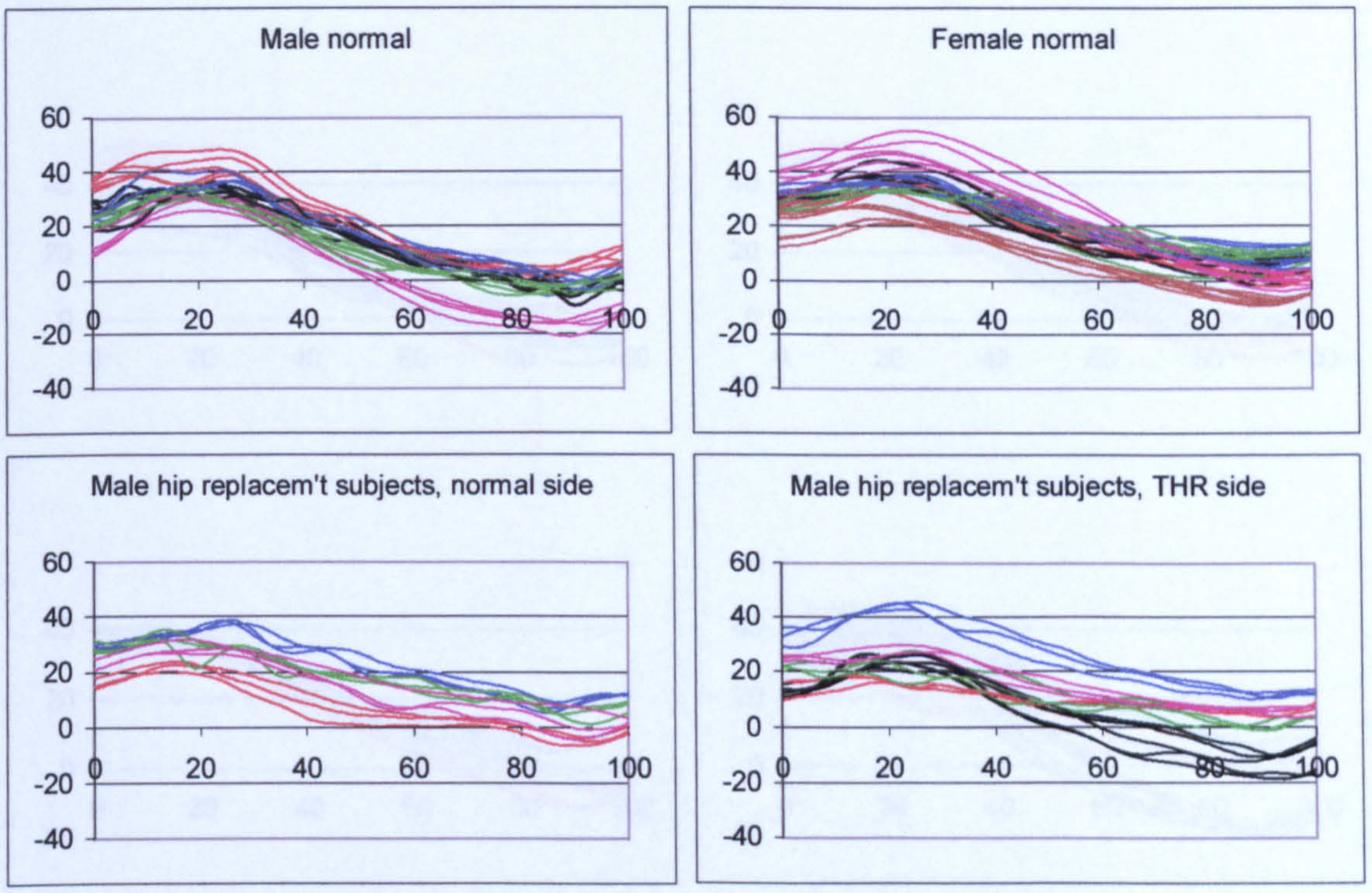

Figure A-VI.1.17 Ramp descent, hip flexion angle

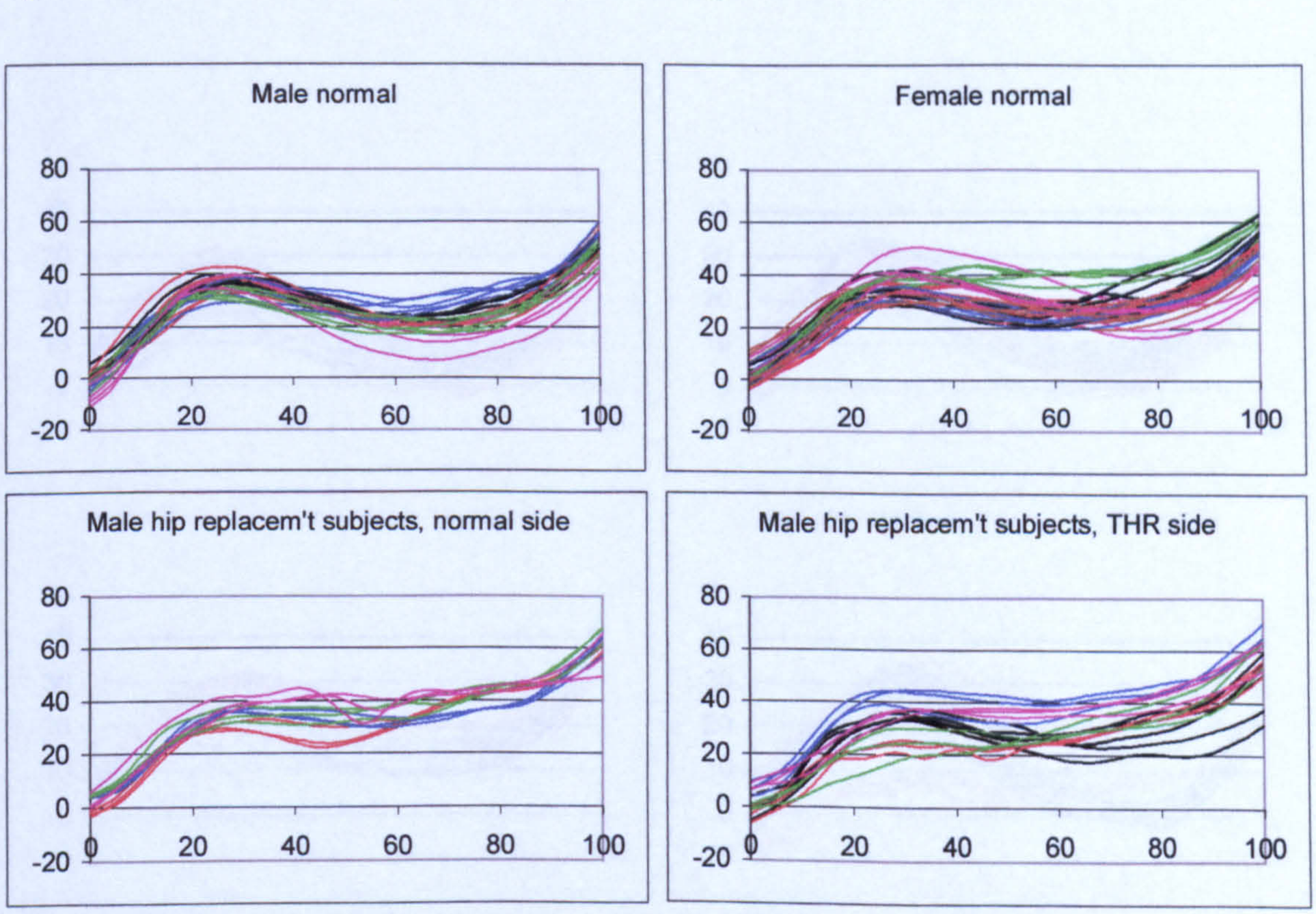

Figure A-VI.1.18 Ramp descent, knee flexion angle

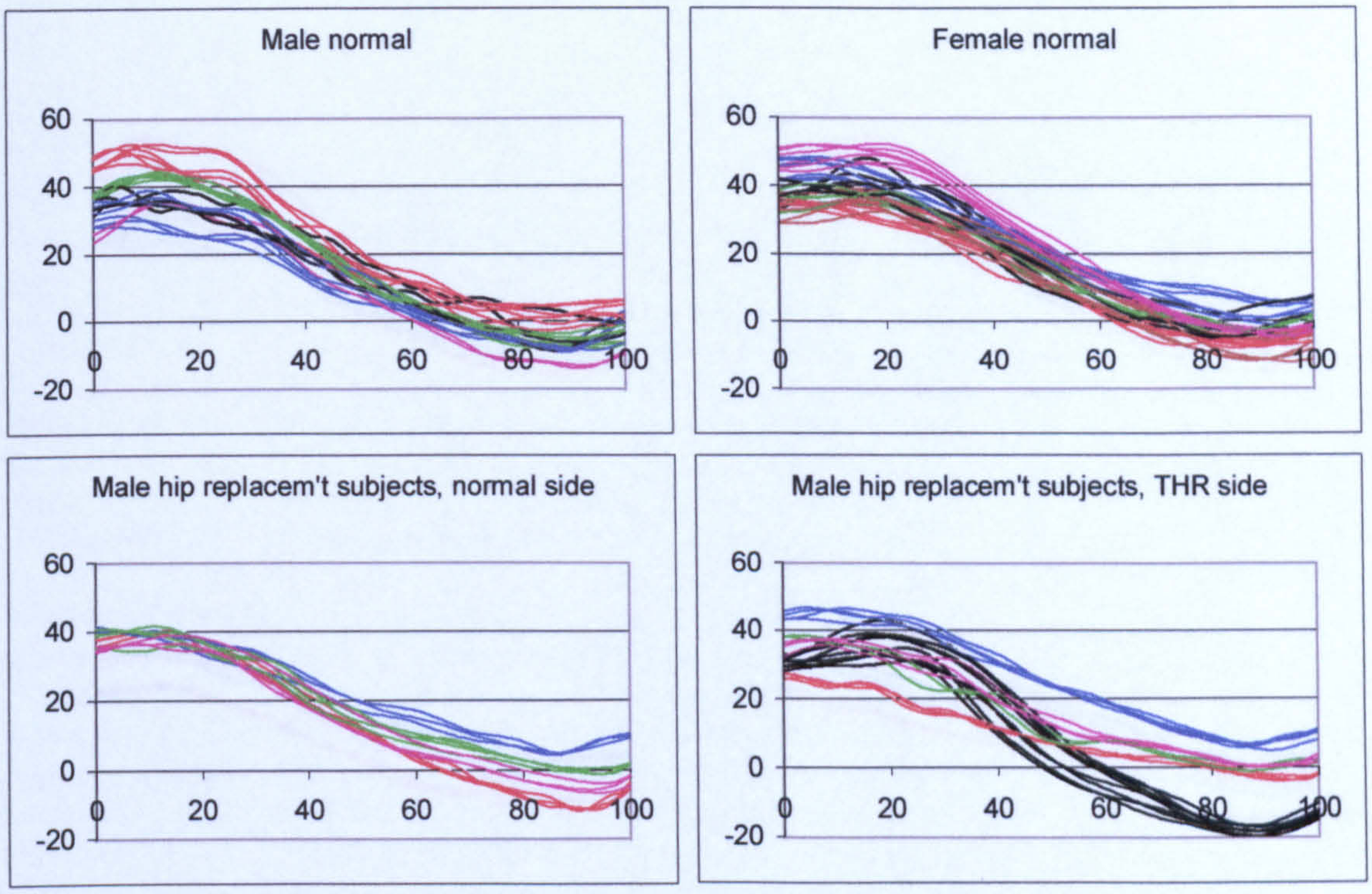

Camber up side foot, hip flexion angle (degrees, +ve=flexion) by % stance phase

Figure A-VI.1.19 Camber up side foot, hip flexion angle

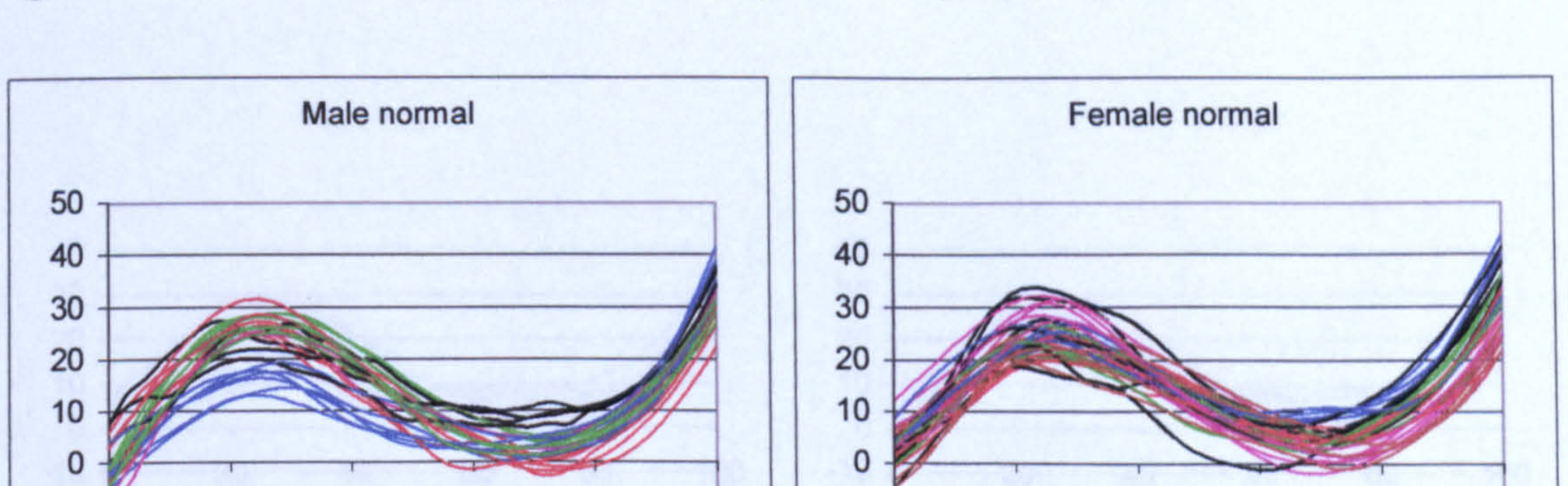

Camber up side foot, knee flexion angle (degrees, +ve=flexion) by % stance phase

Figure A-VI.1.20 Camber up side foot, knee flexion angle

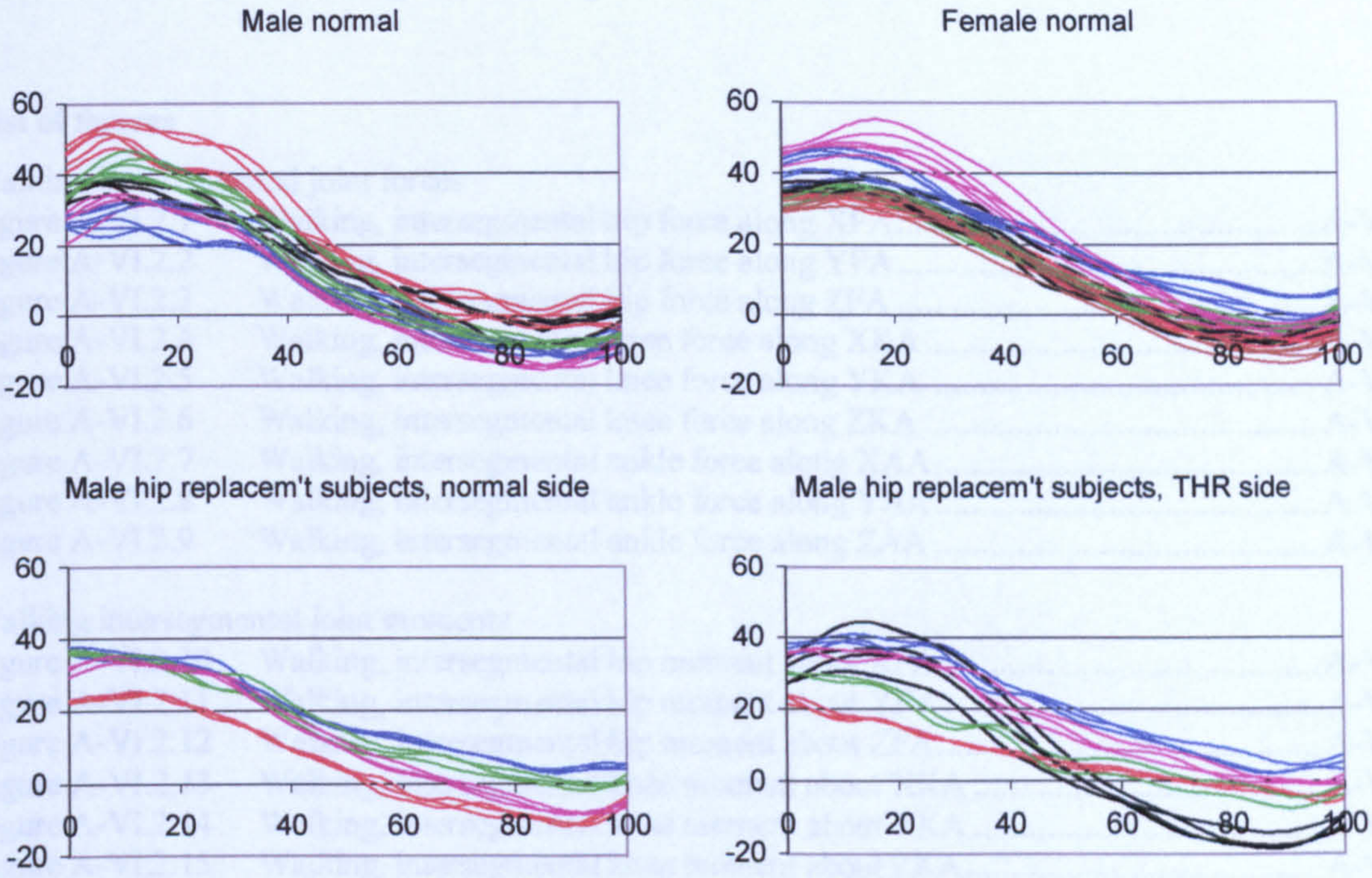

Figure A-VI.1.21 Camber down side foot, hip flexion angle

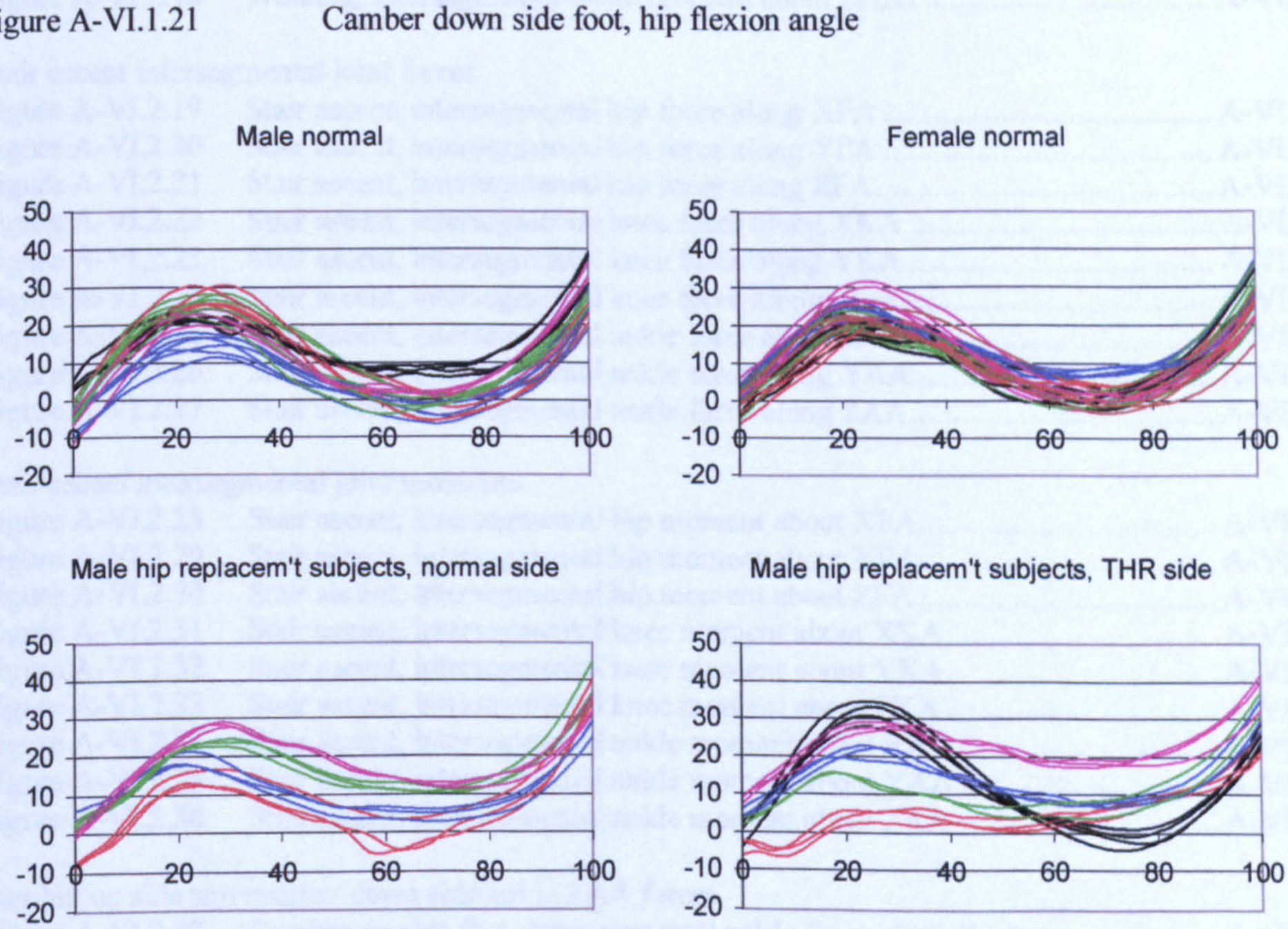

Figure A-VI.1.22 Camber down side foot, knee flexion angle

A-VI.2 Intersegmental joint forces and moments

List of figures

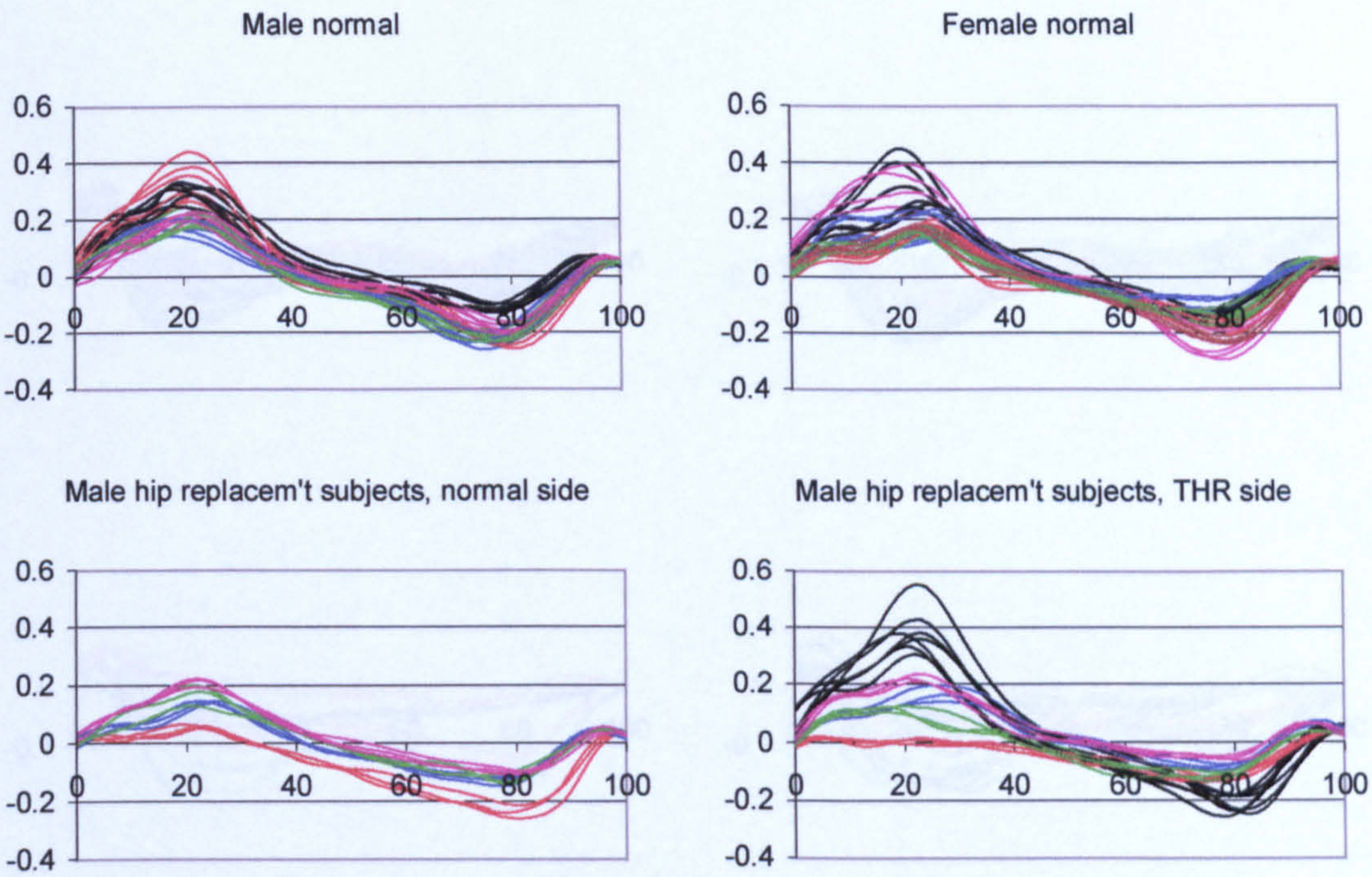

Figure A-VI.2.1 Walking, intersegmental hip force along XFA

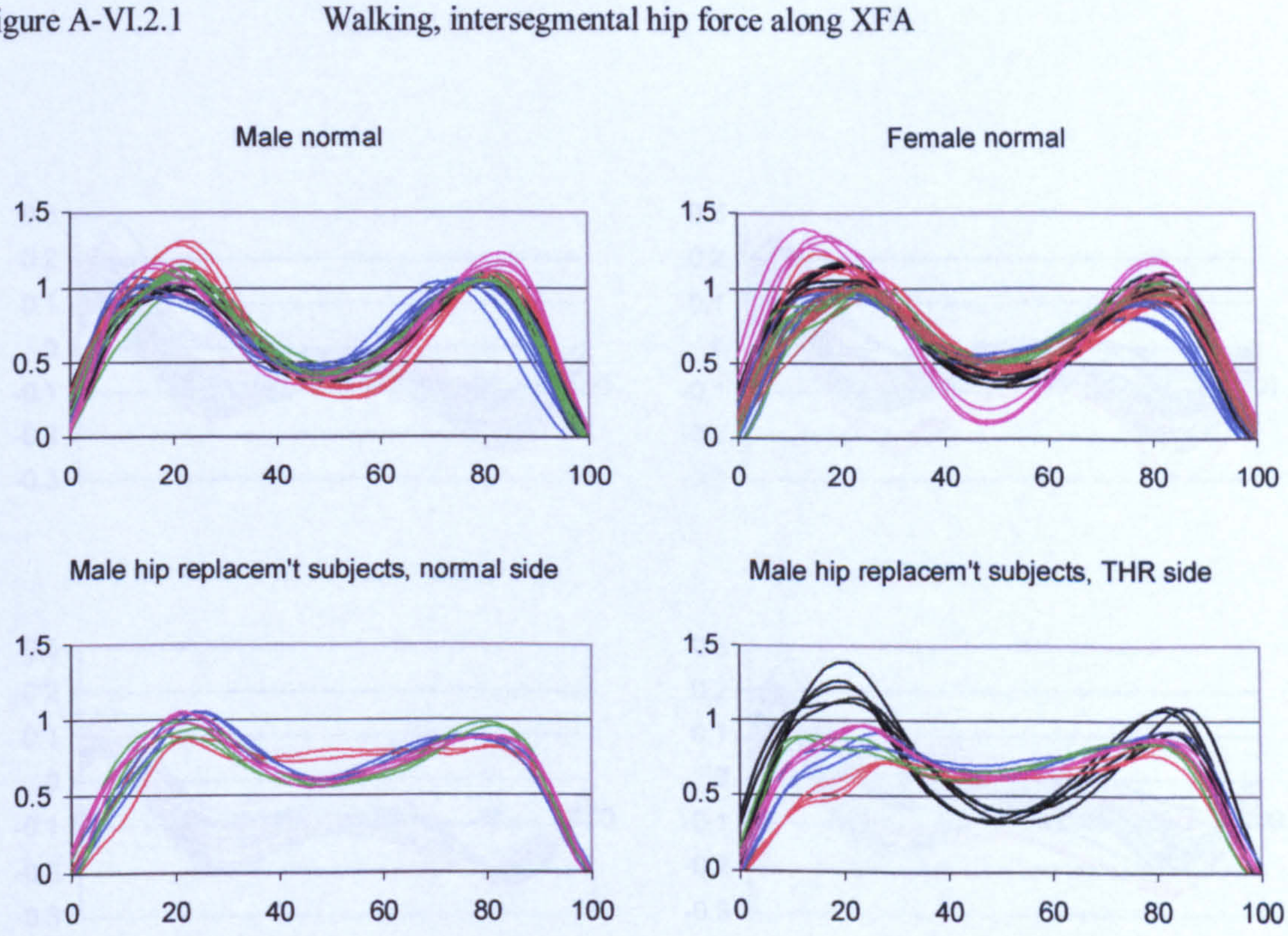

Figure A-VI.2.2 Walking, intersegmental hip force along YFA

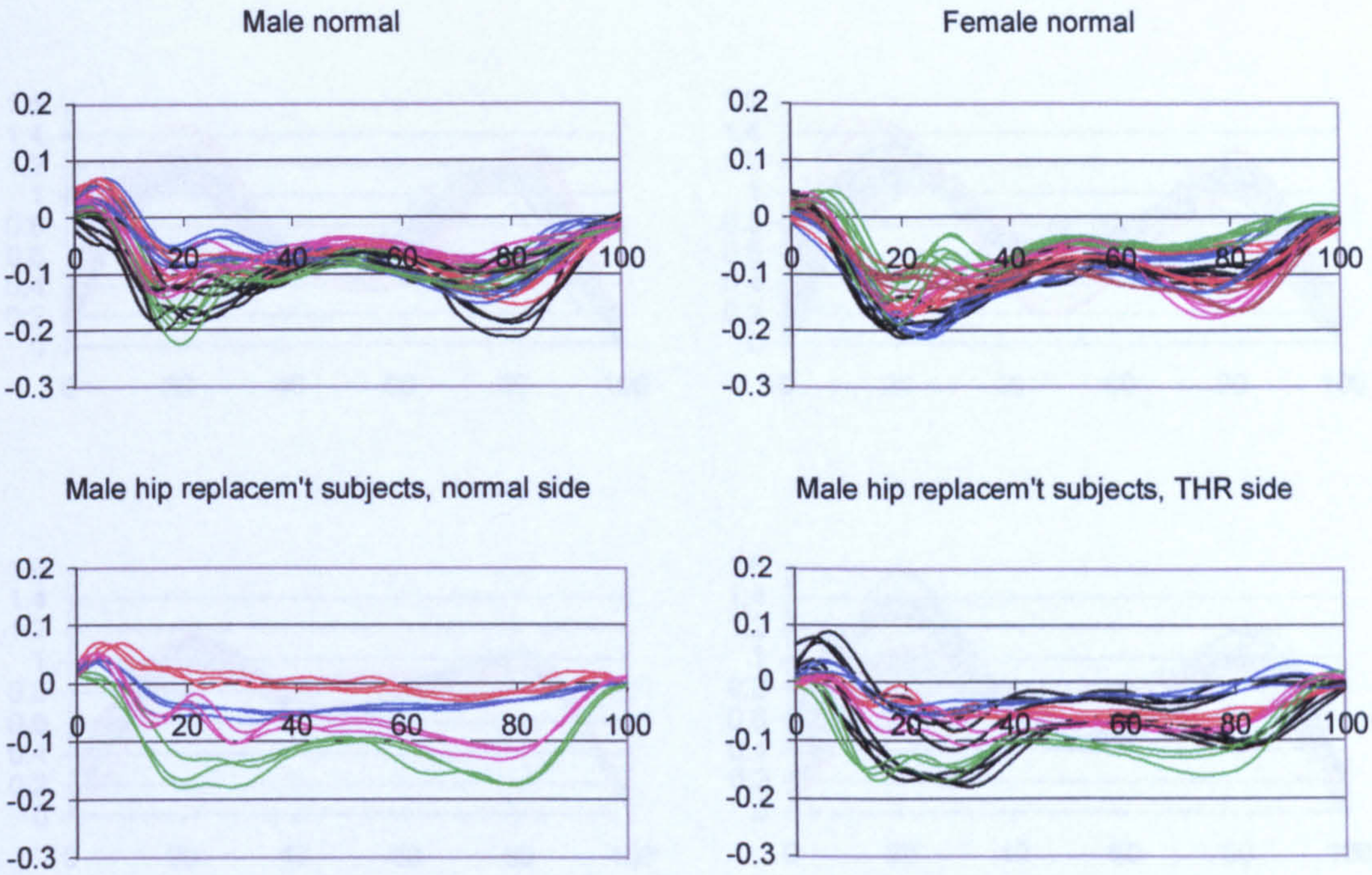

Figure A-VI.2.3 Walking, intersegmental hip force along ZFA

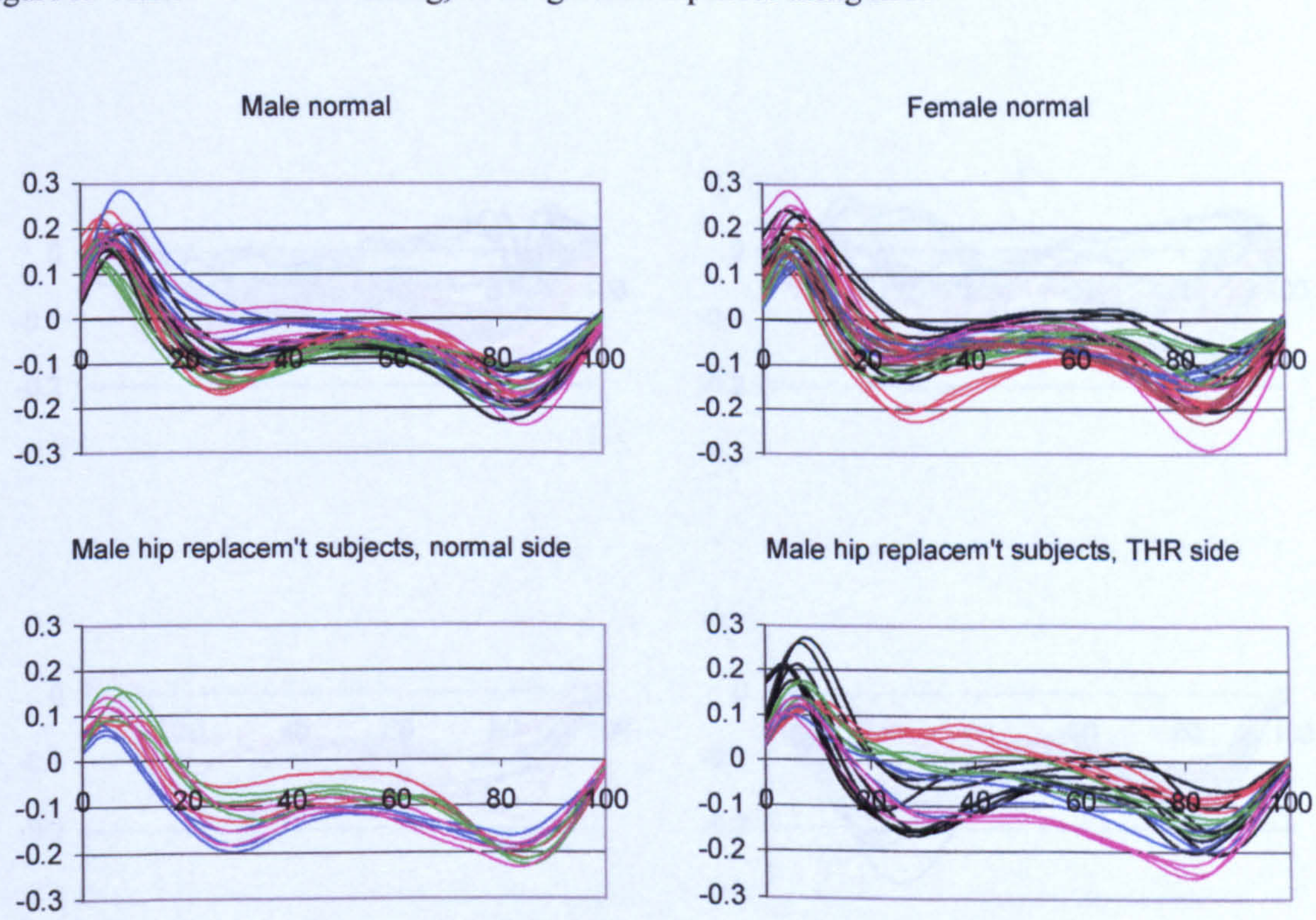

Figure A-VI.2.4 Walking, intersegmental knee force along XKA

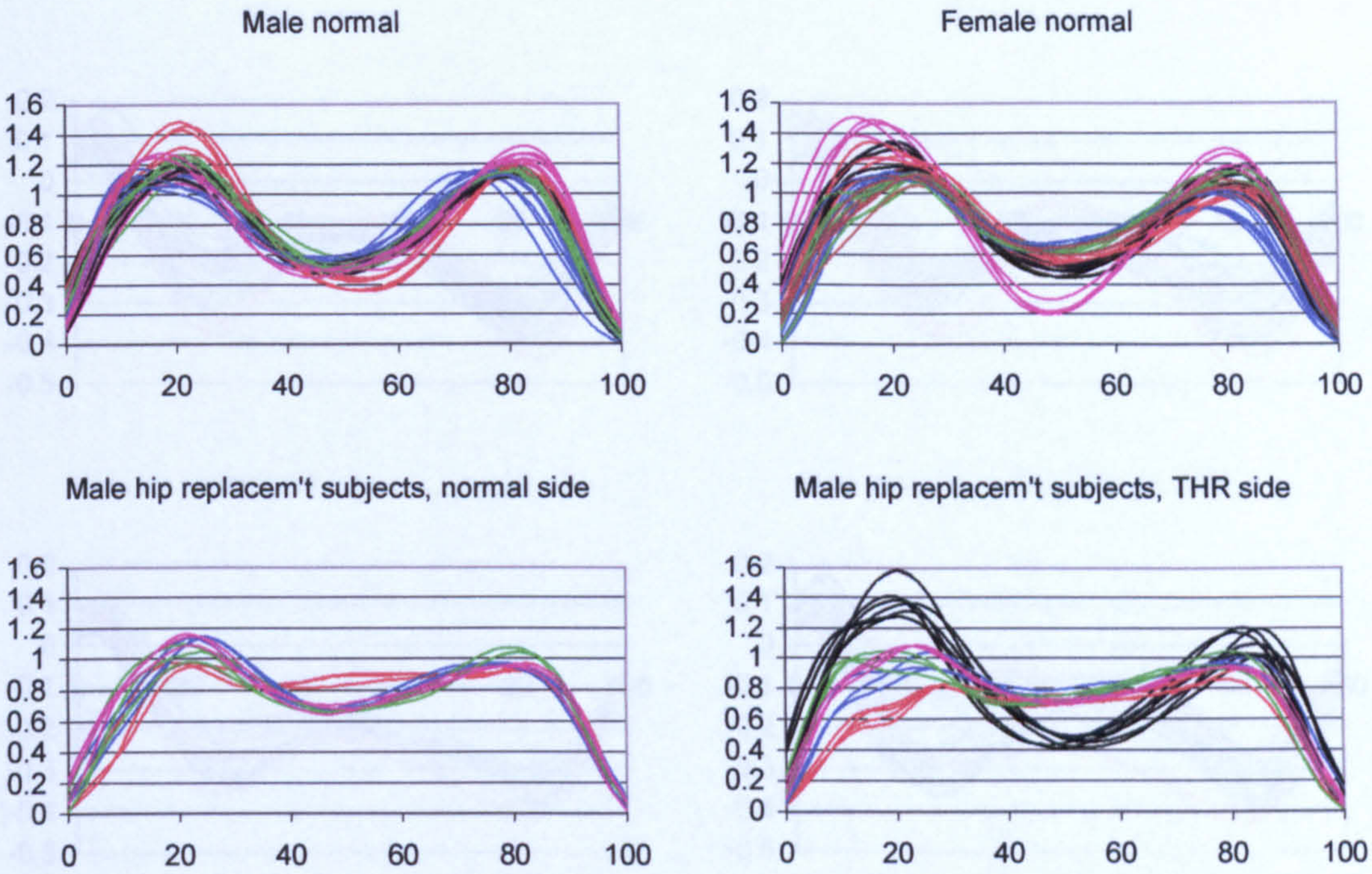

Figure A-VI.2.5 Walking, intersegmental knee force along YKA

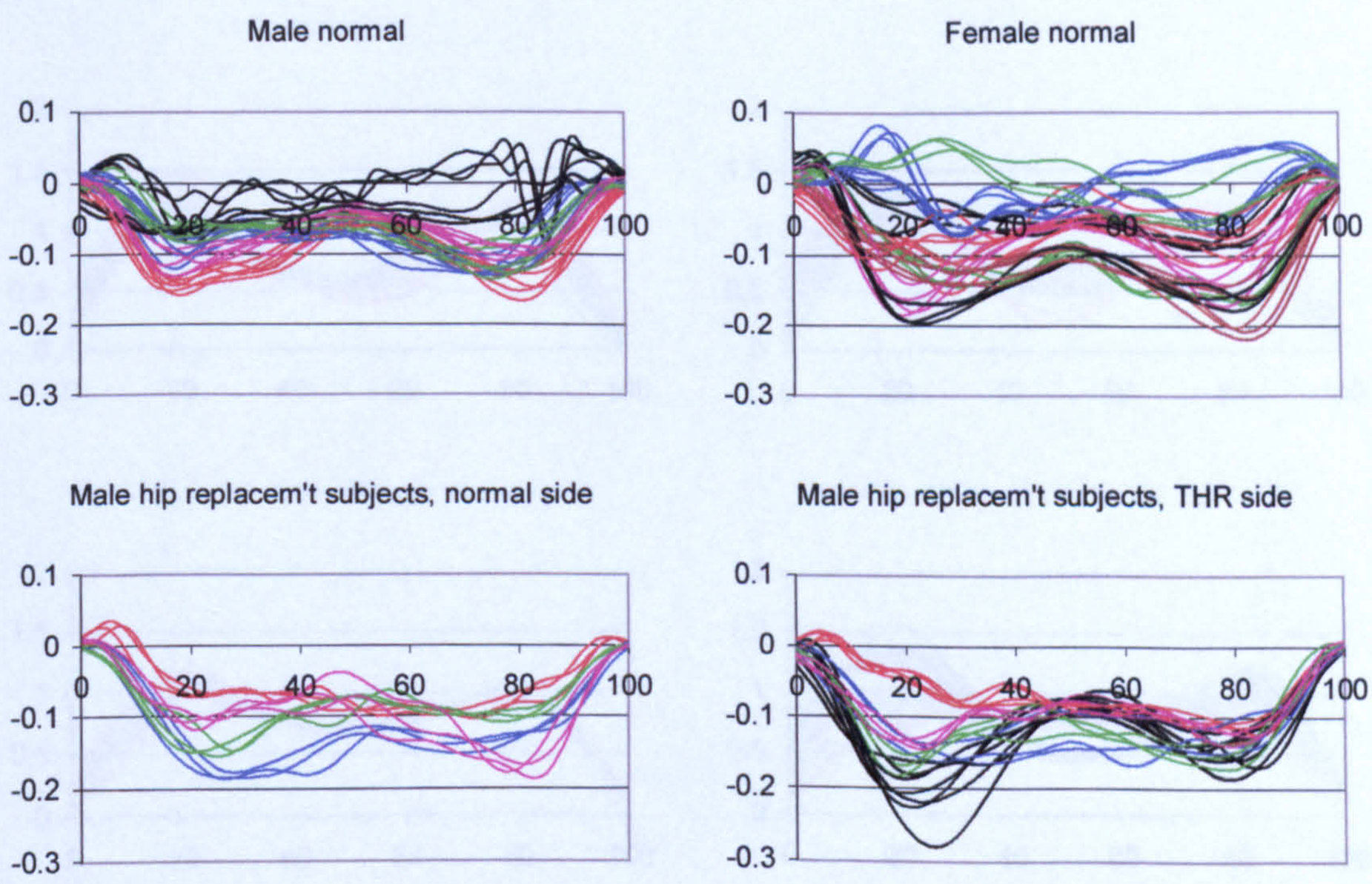

Figure A-VI.2.6 Walking, intersegmental knee force along ZKA

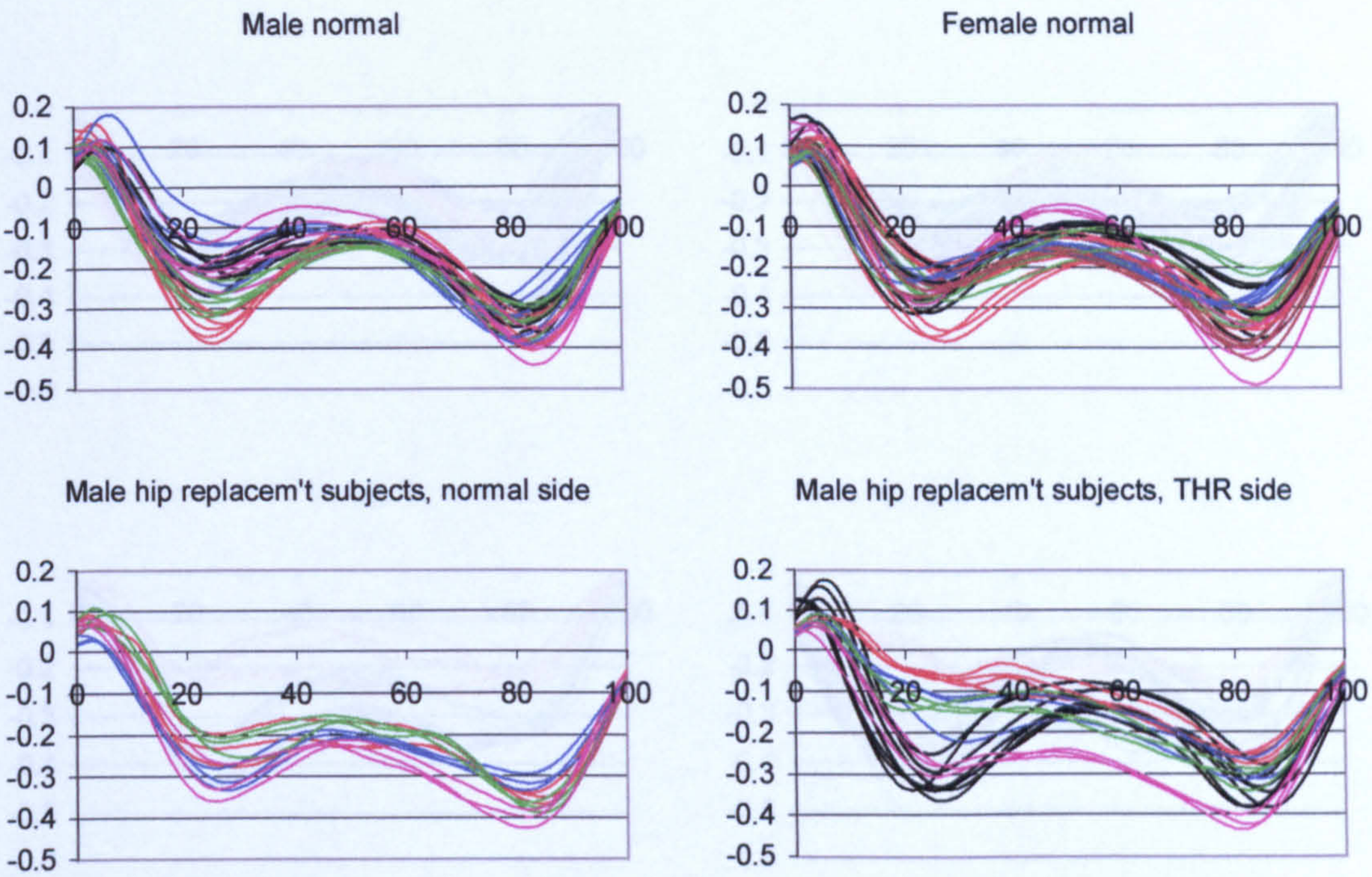

Figure A-VI.2.7 Walking, intersegmental ankle force along XAA

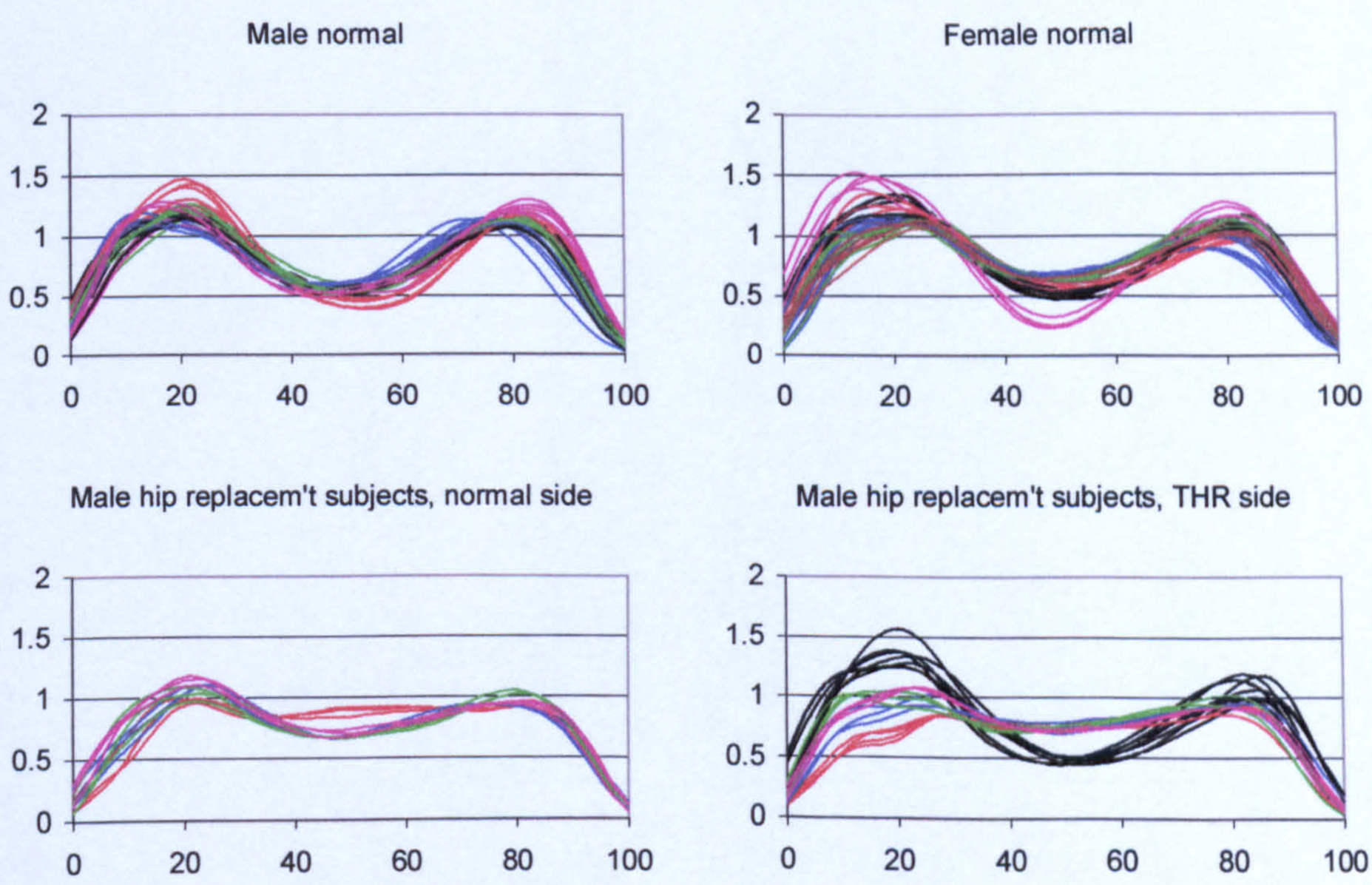

Figure A-VI.2.8 Walking, intersegmental ankle force along YAA

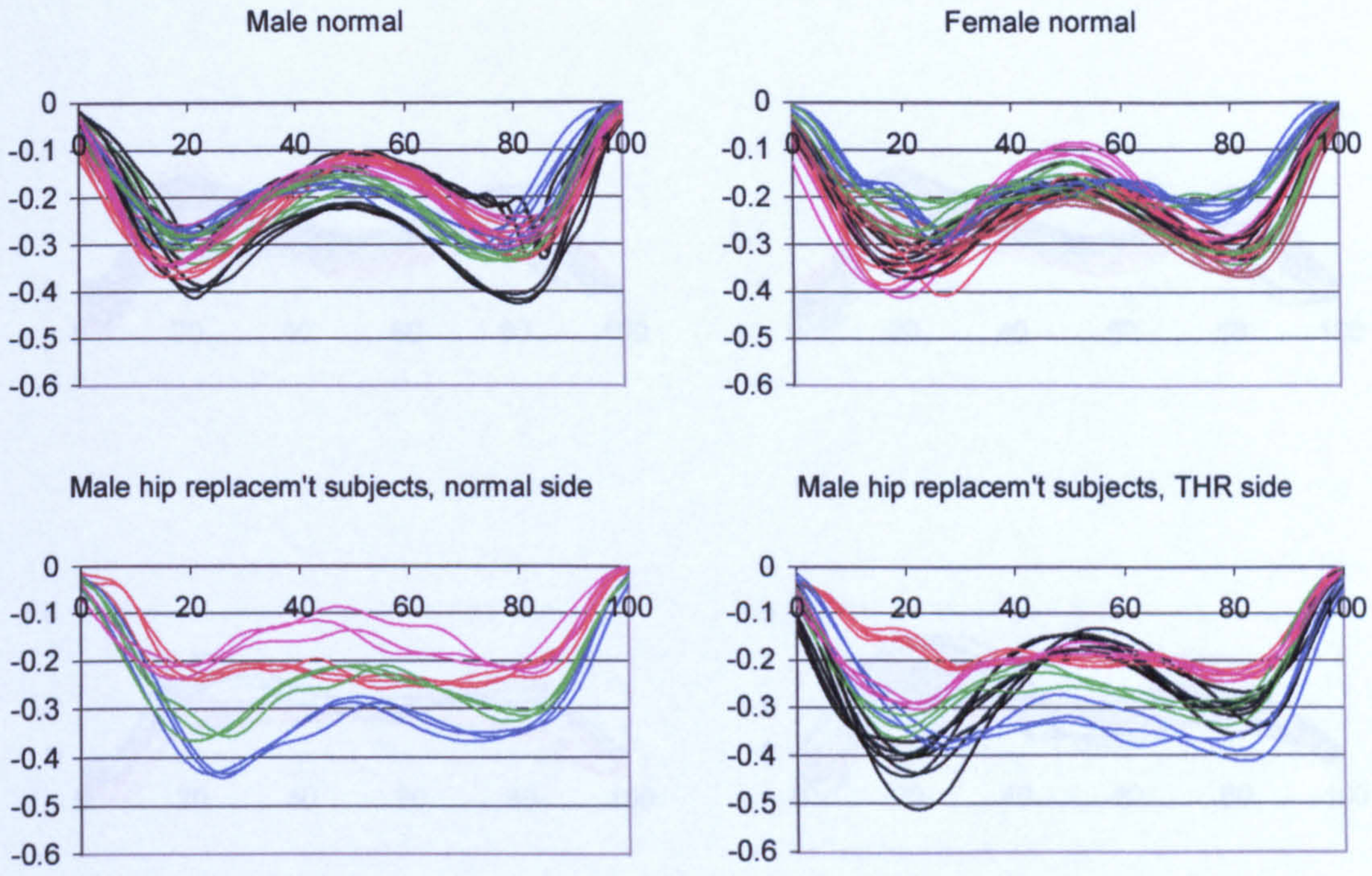

Figure A-VI.2.9 Walking, intersegmental ankle force along ZAA

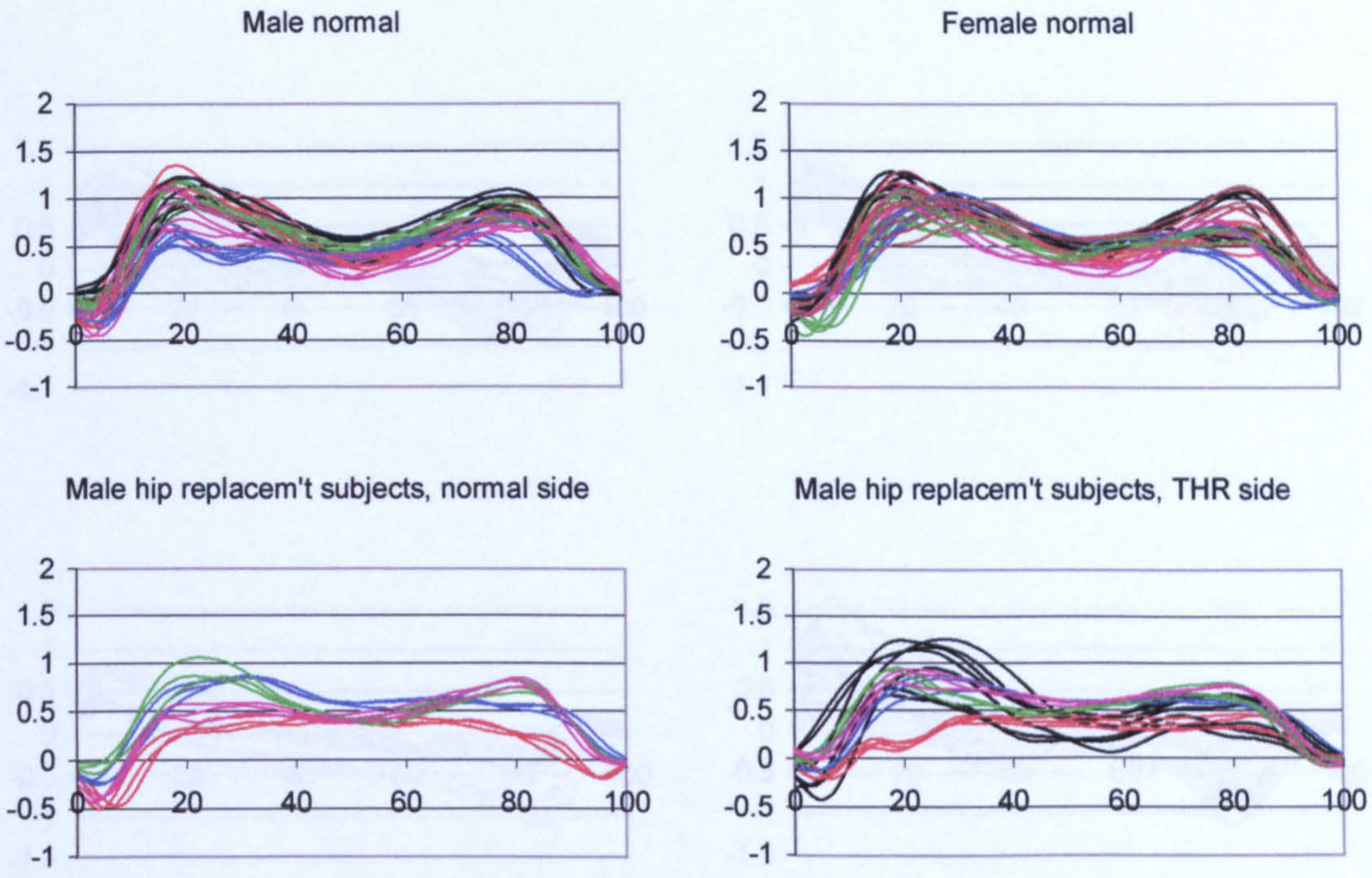

Figure A-VI.2.10 Walking, intersegmental hip moment about XFA

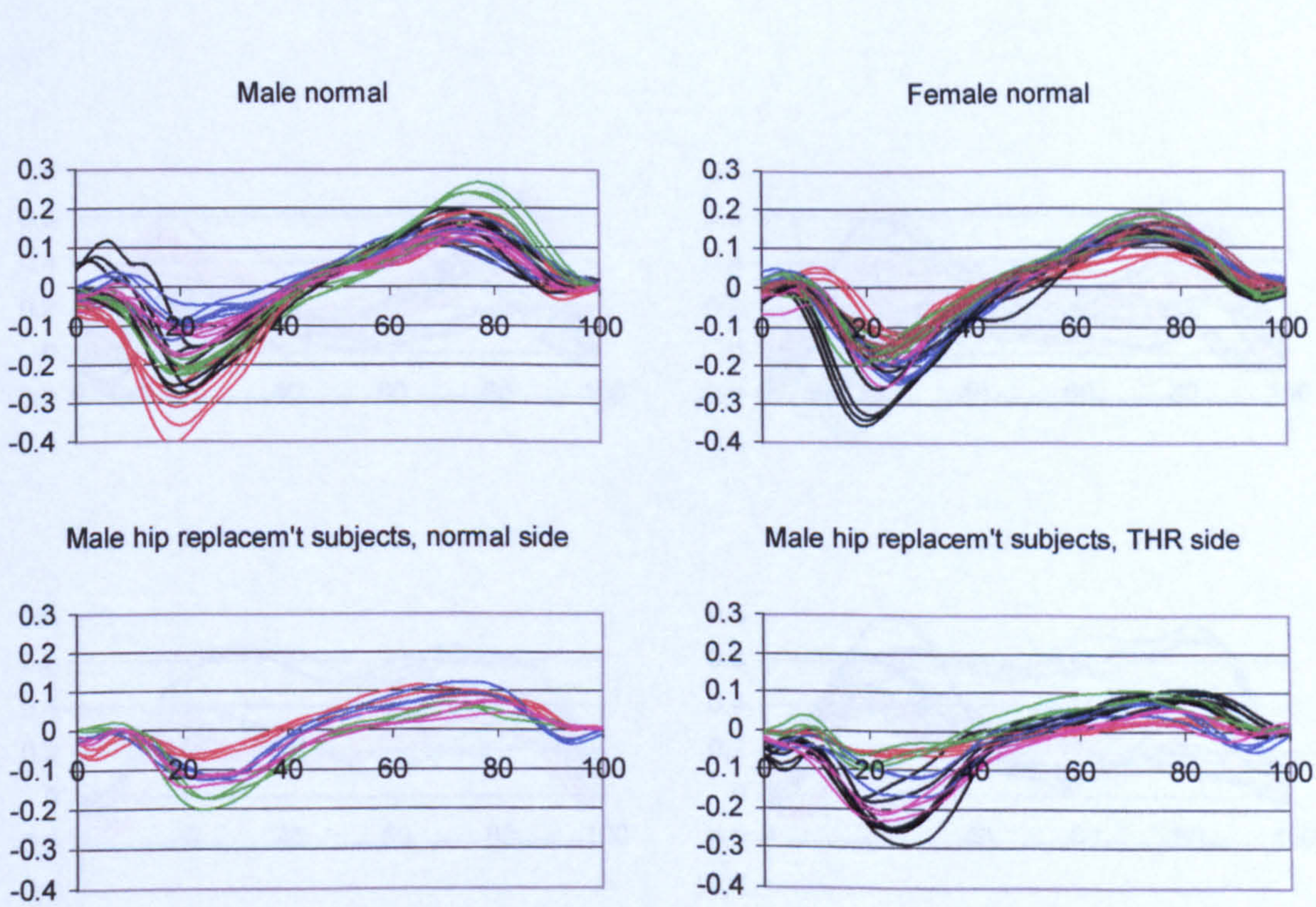

Figure A-VI.2.11 Walking, intersegmental hip moment about YFA

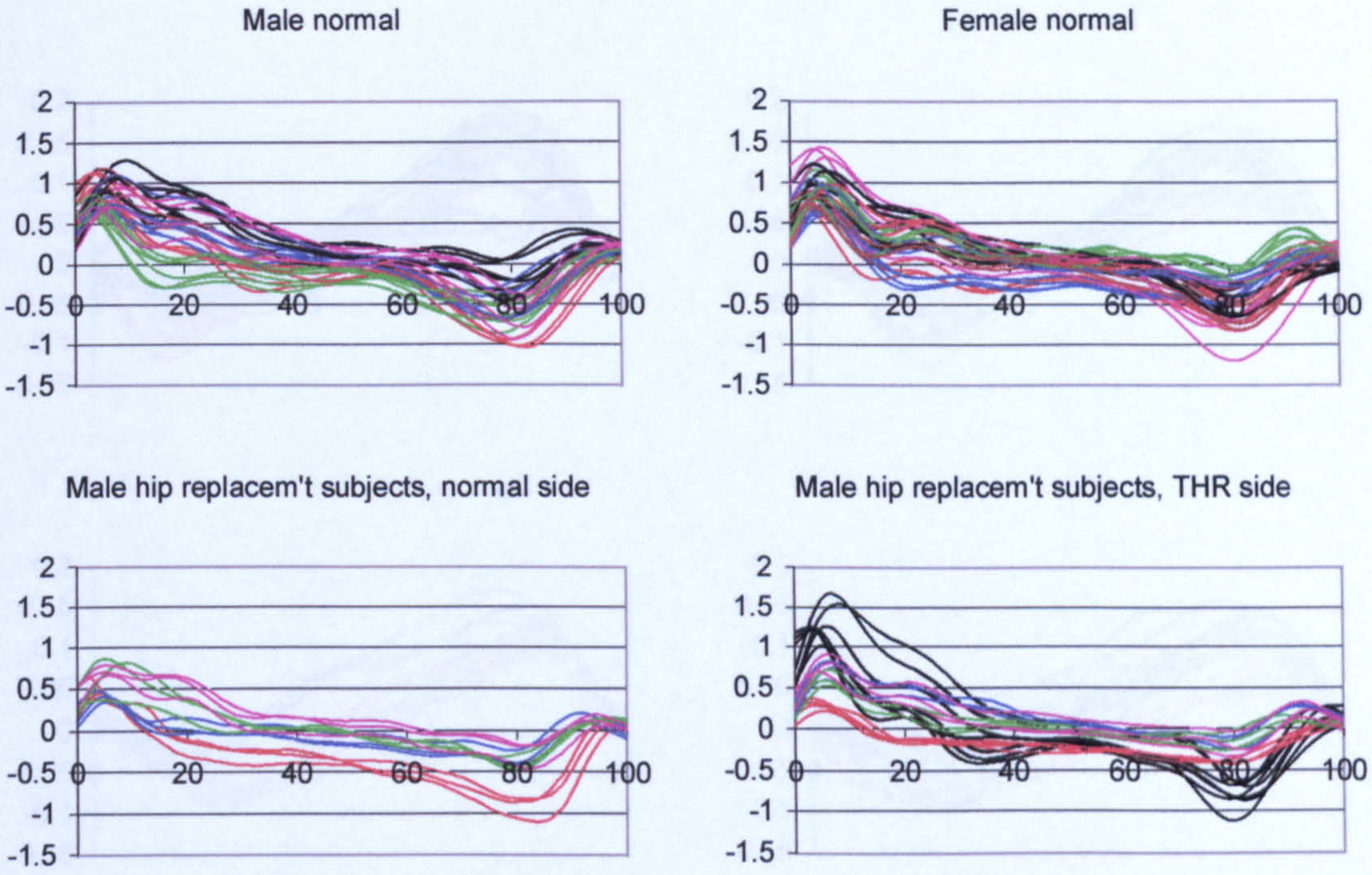

Figure A-VI.2.12 Walking, intersegmental hip moment about ZFA

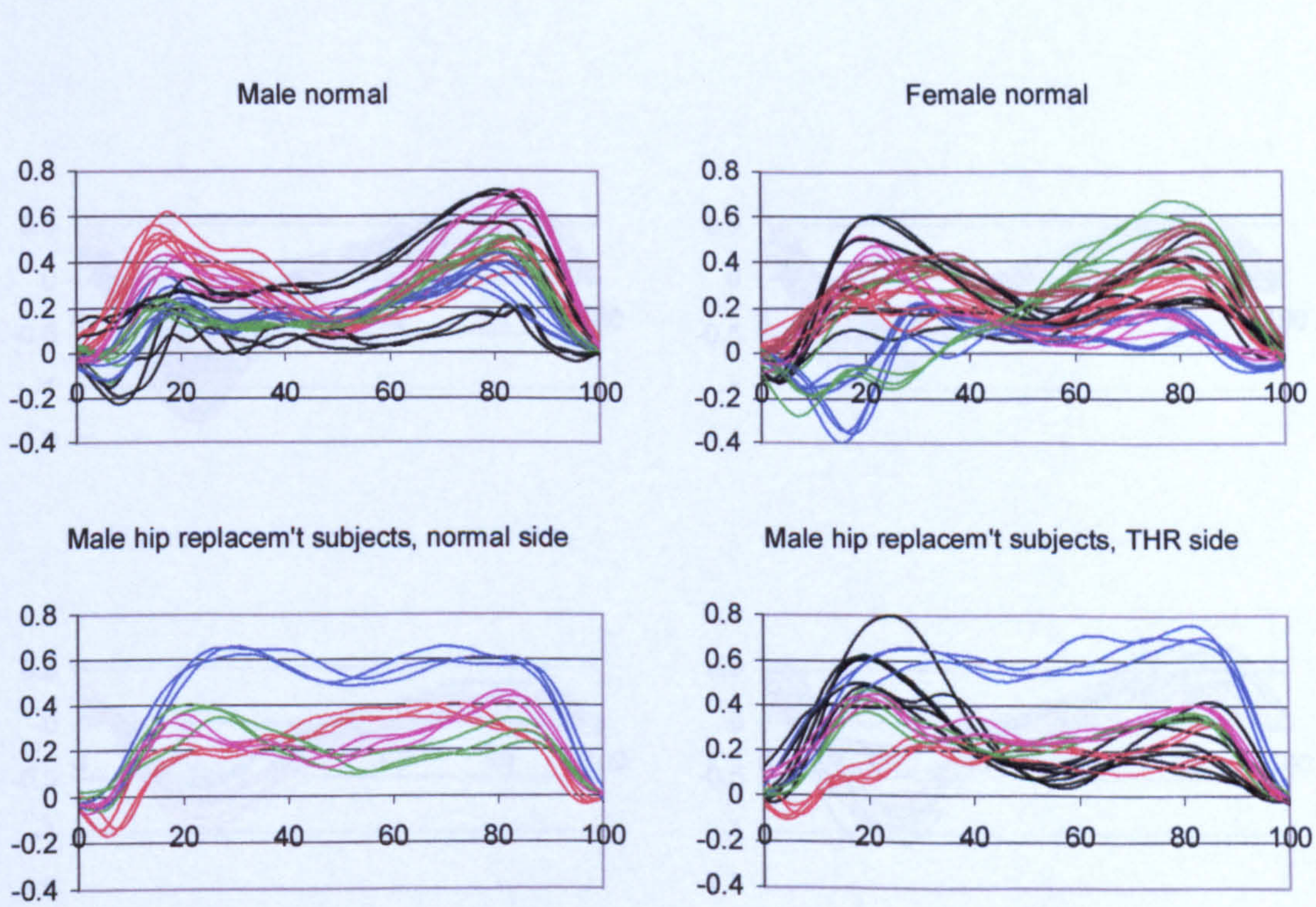

Figure A-VI.2.13 Walking, intersegmental knee moment about XKA

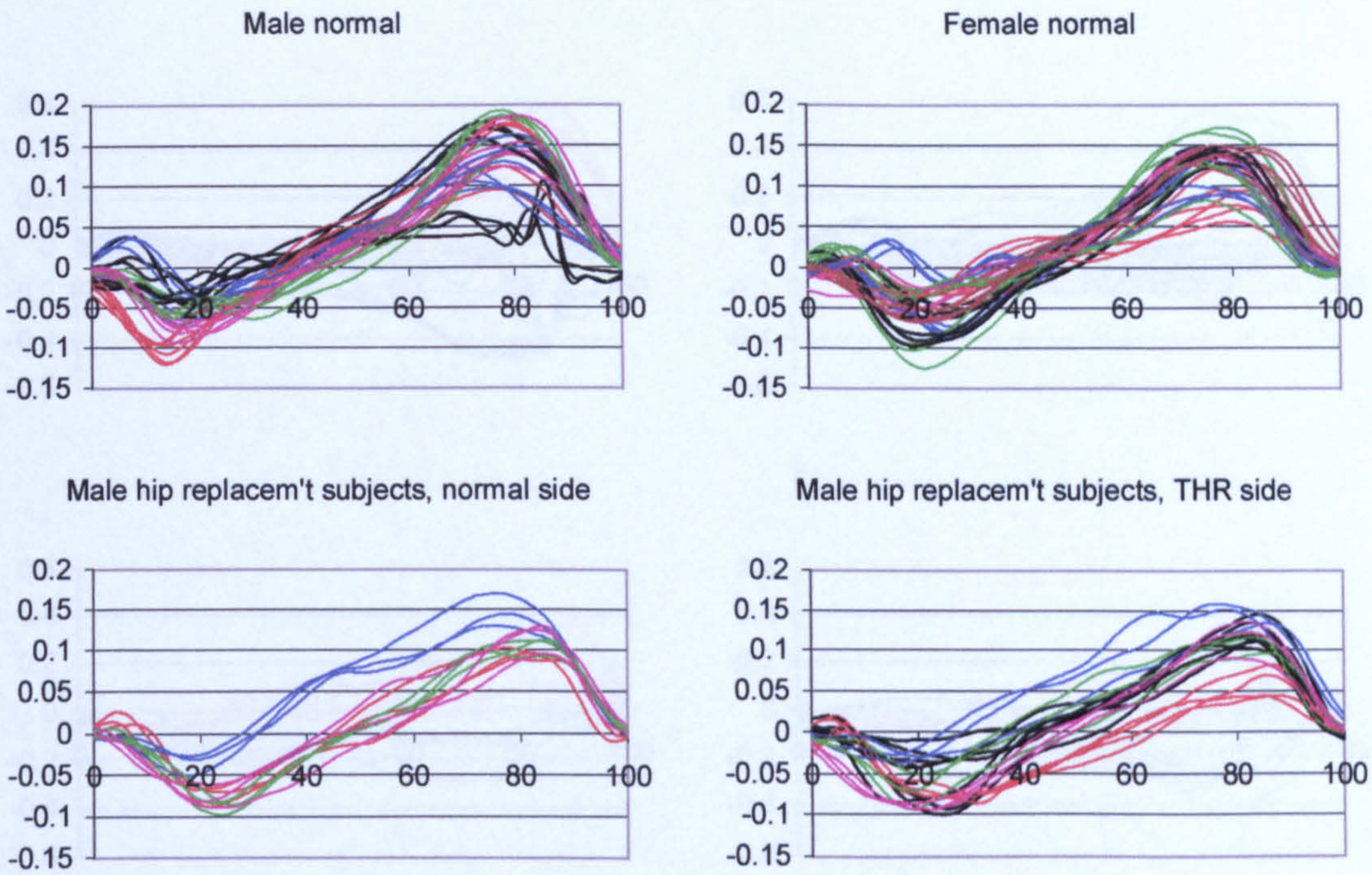

Walking, knee moment YKA (Nm/body mass, +ve = clockwise along axis) by % stance phase

Figure A-VI.2.14 Walking, intersegmental knee moment about YKA

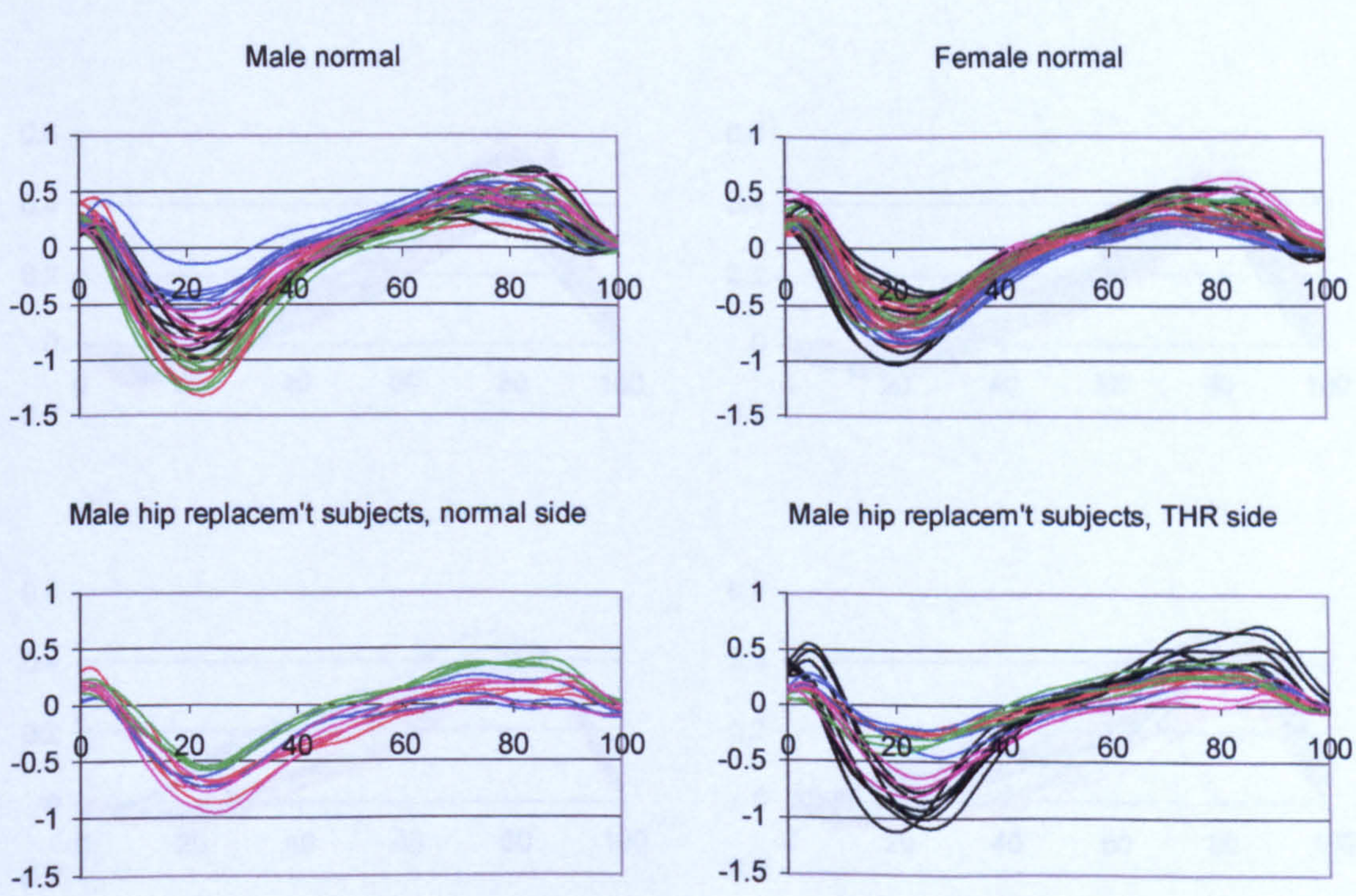

Walking, knee moment ZKA (Nm/body mass, +ve = clockwise along axis) by % stance phase

Figure A-VI.2.15 Walking, intersegmental knee moment about ZKA

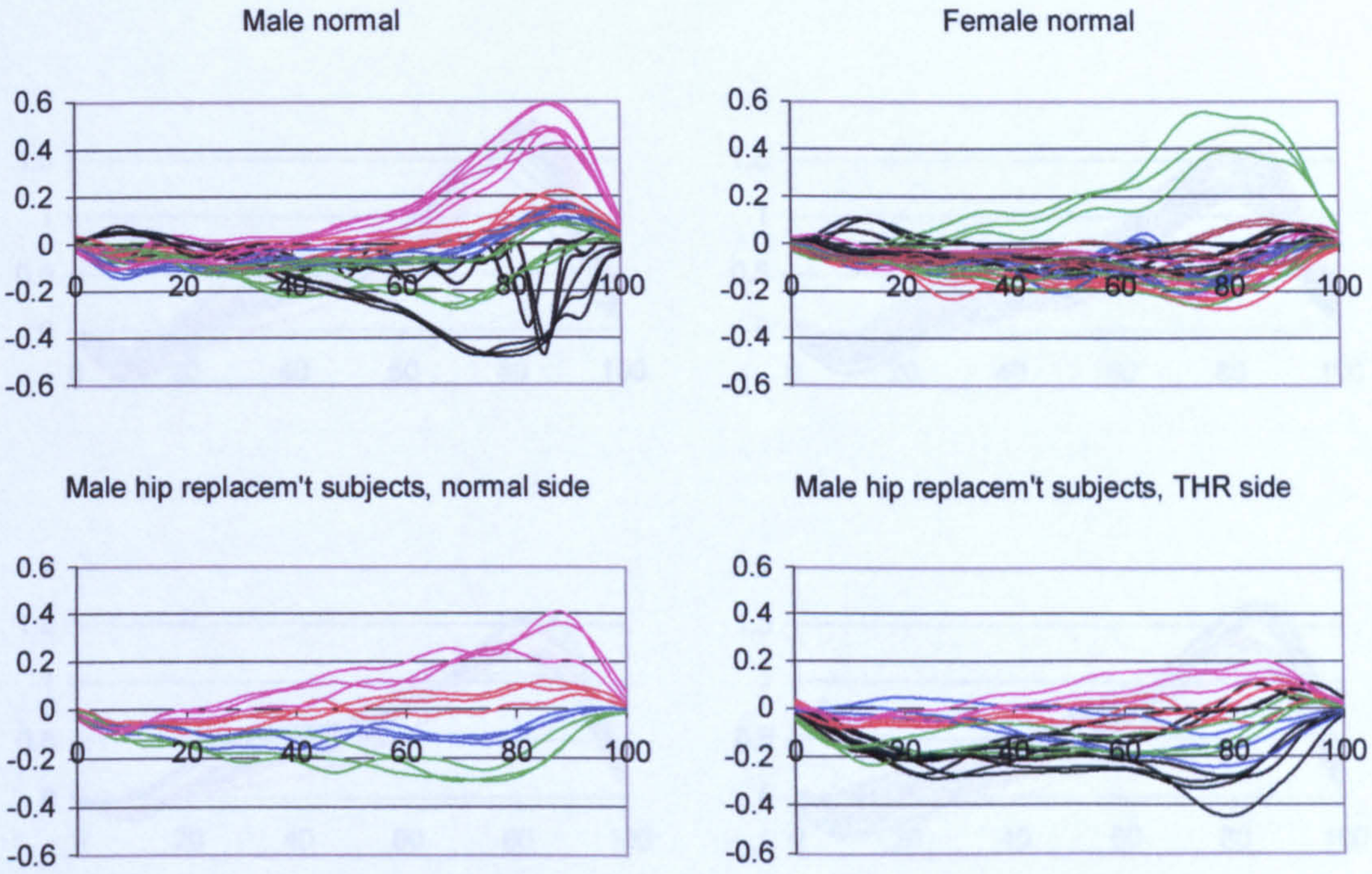

Figure A-VI.2.16 Walking, intersegmental ankle moment about XAA

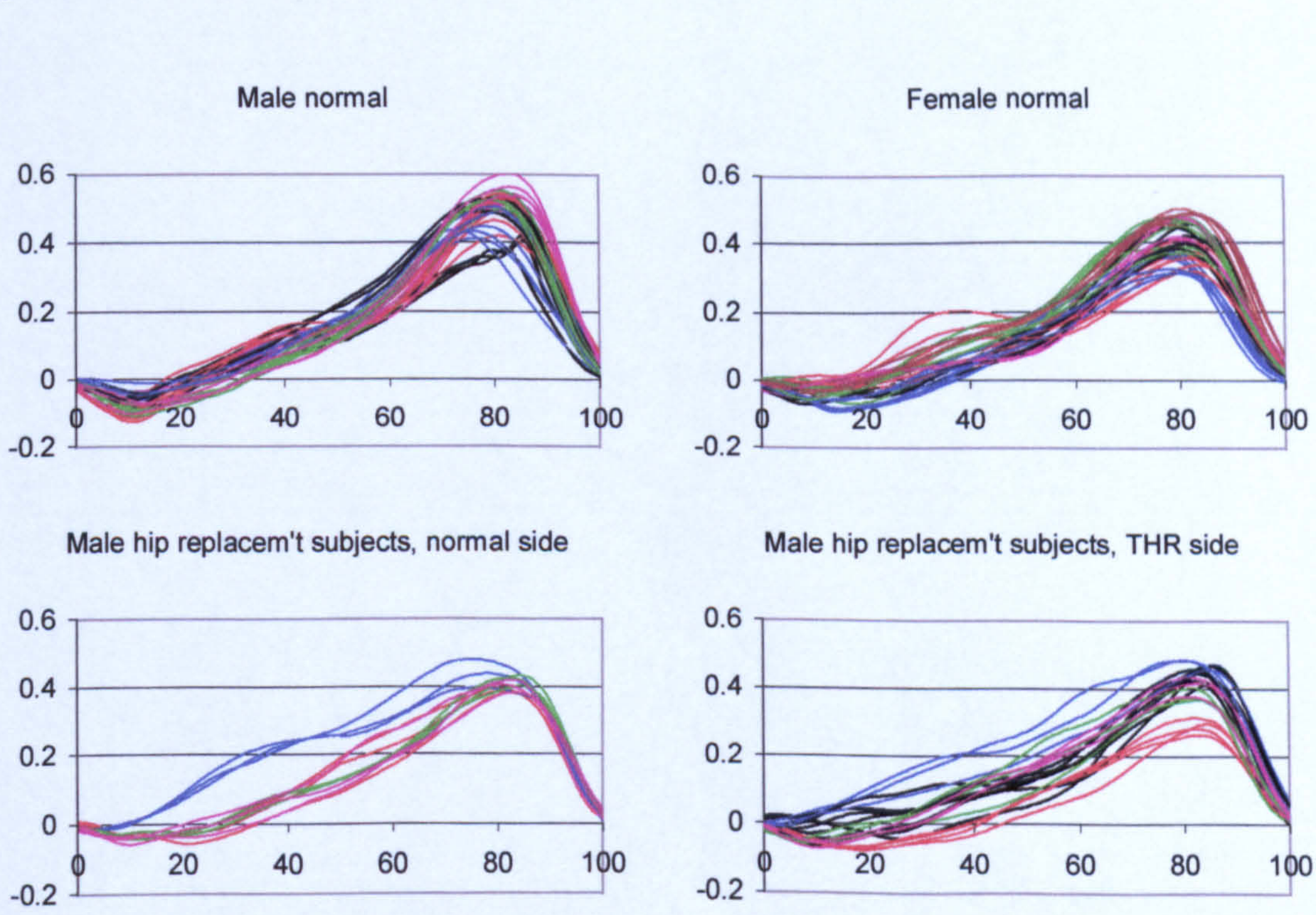

Figure A-VI.2.17 Walking, intersegmental ankle moment about YAA

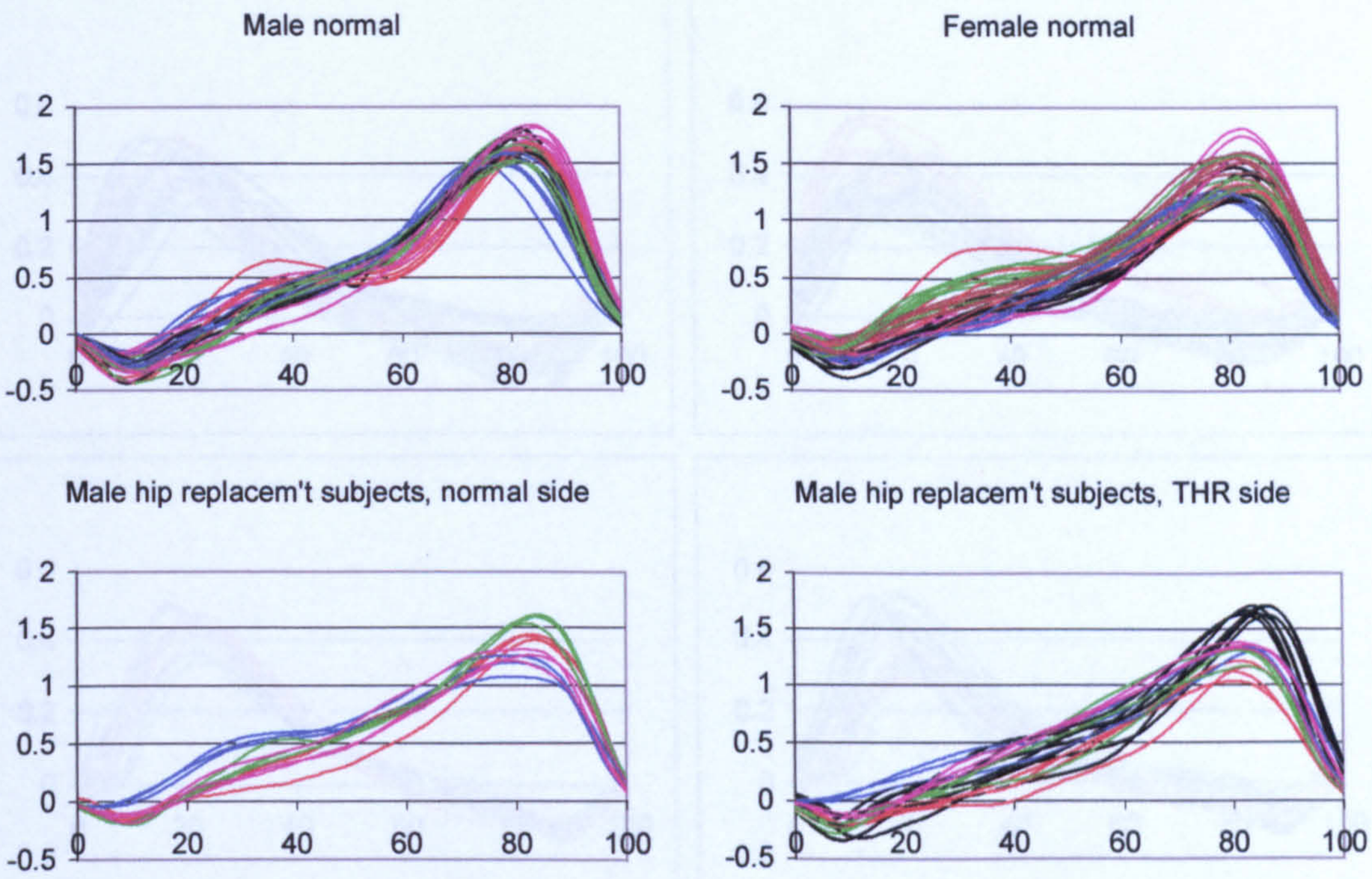

Figure A-VI.2.18 Walking, intersegmental ankle moment about ZAA

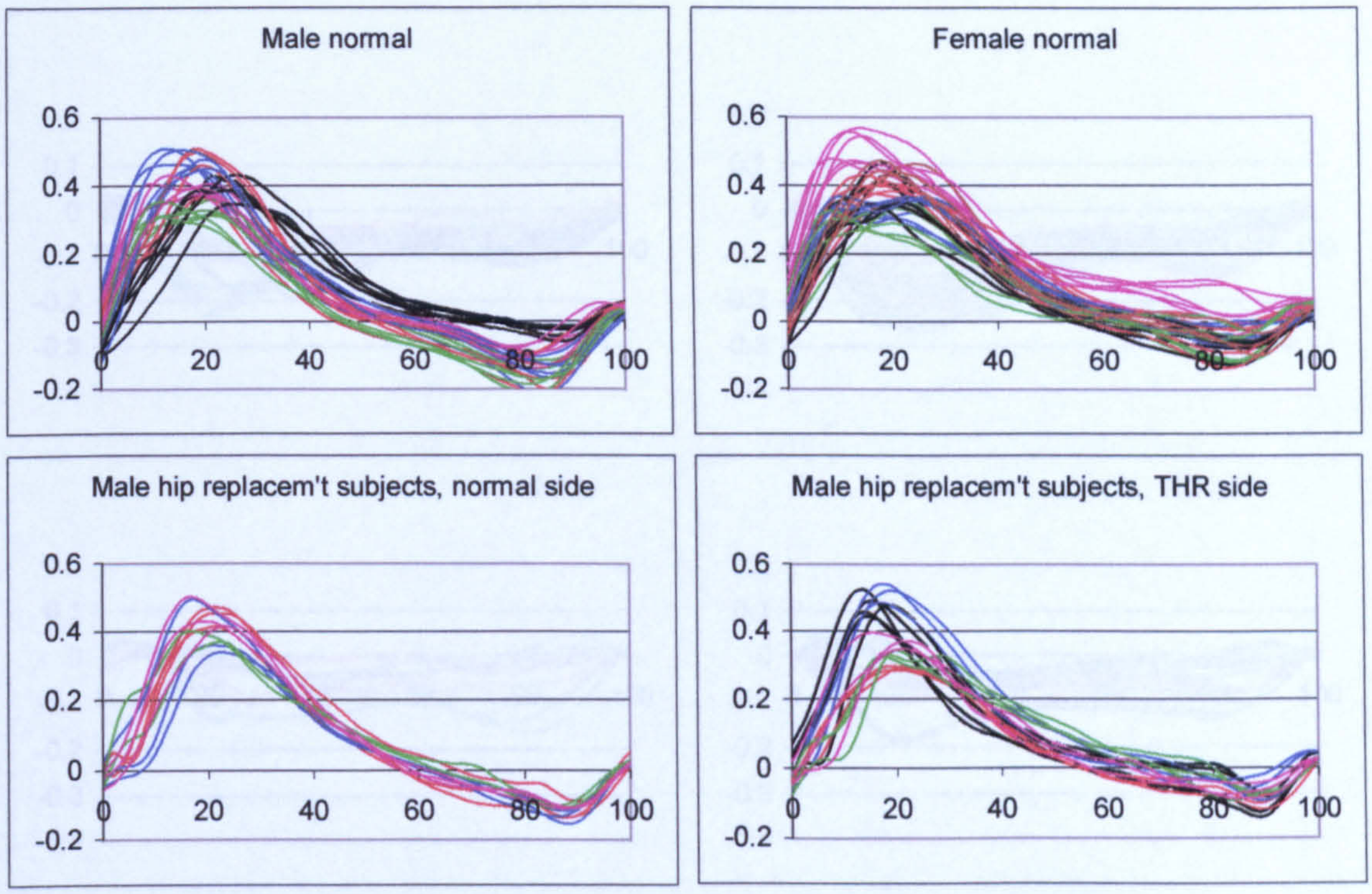

Figure A-VI.2.19 Stair ascent, intersegmental hip force along XFA

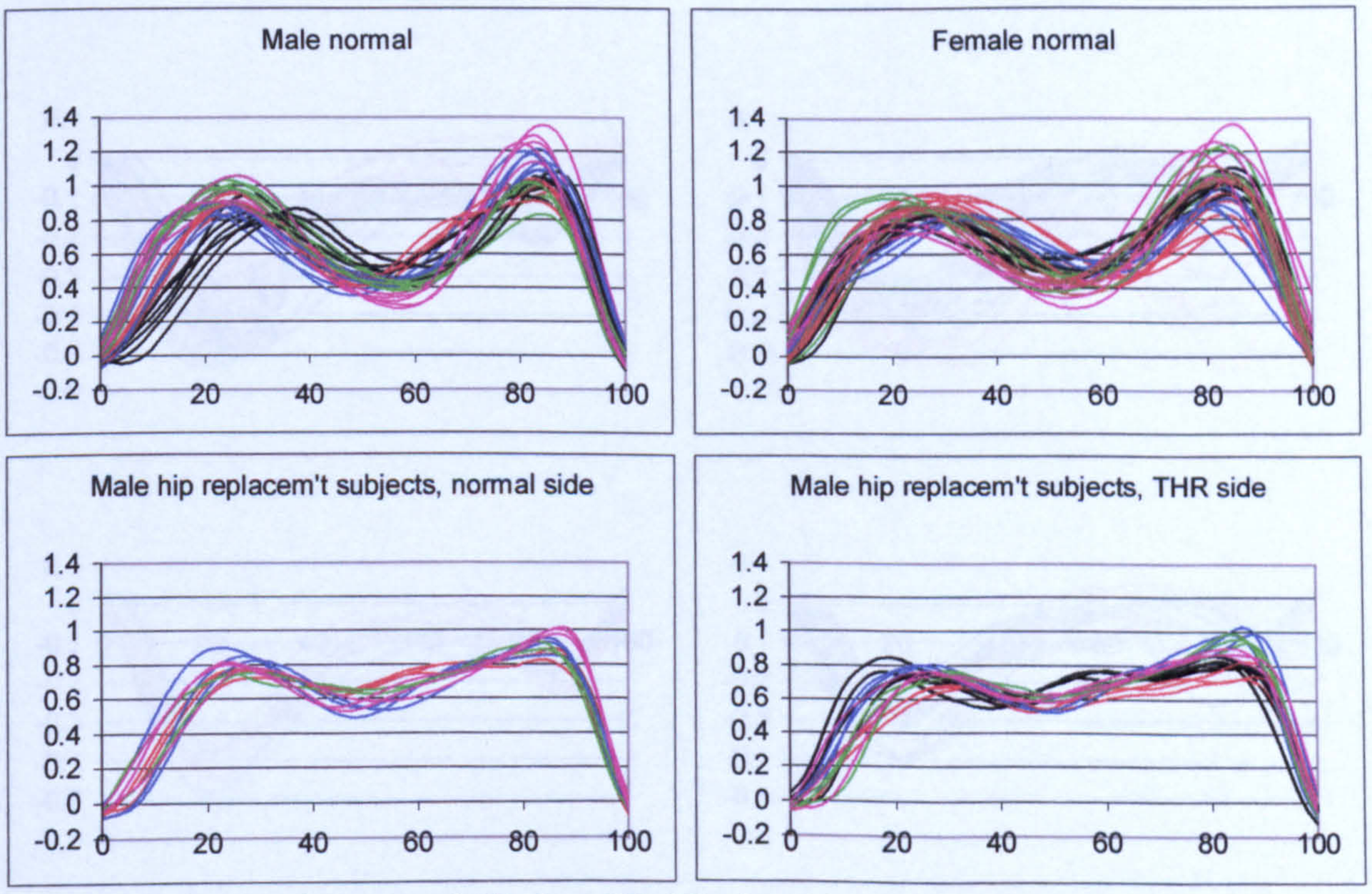

Figure A-VI.2.20 Stair ascent, intersegmental hip force along YFA

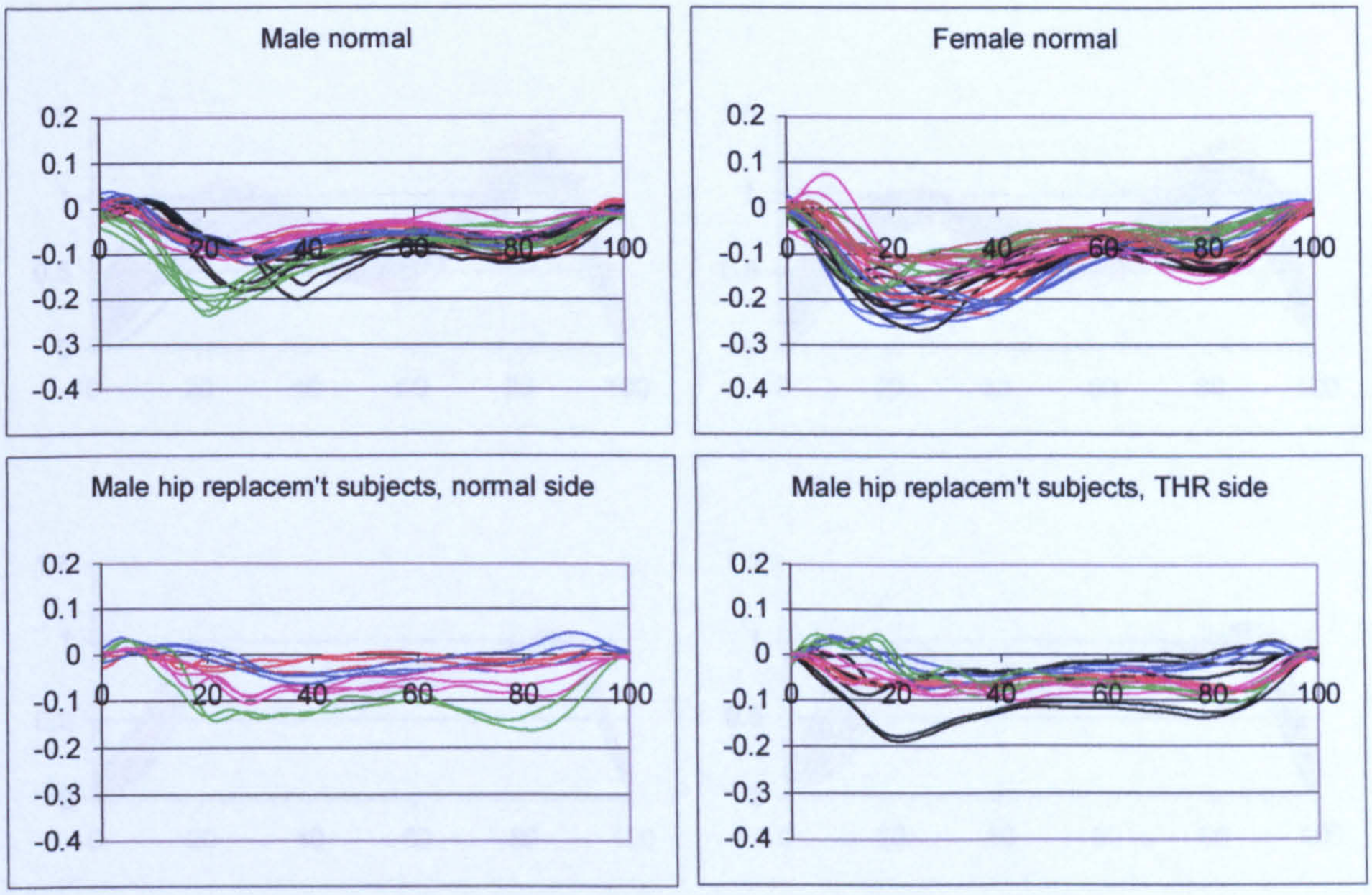

Figure A-VI.2.21 Stair ascent, intersegmental hip force along ZFA

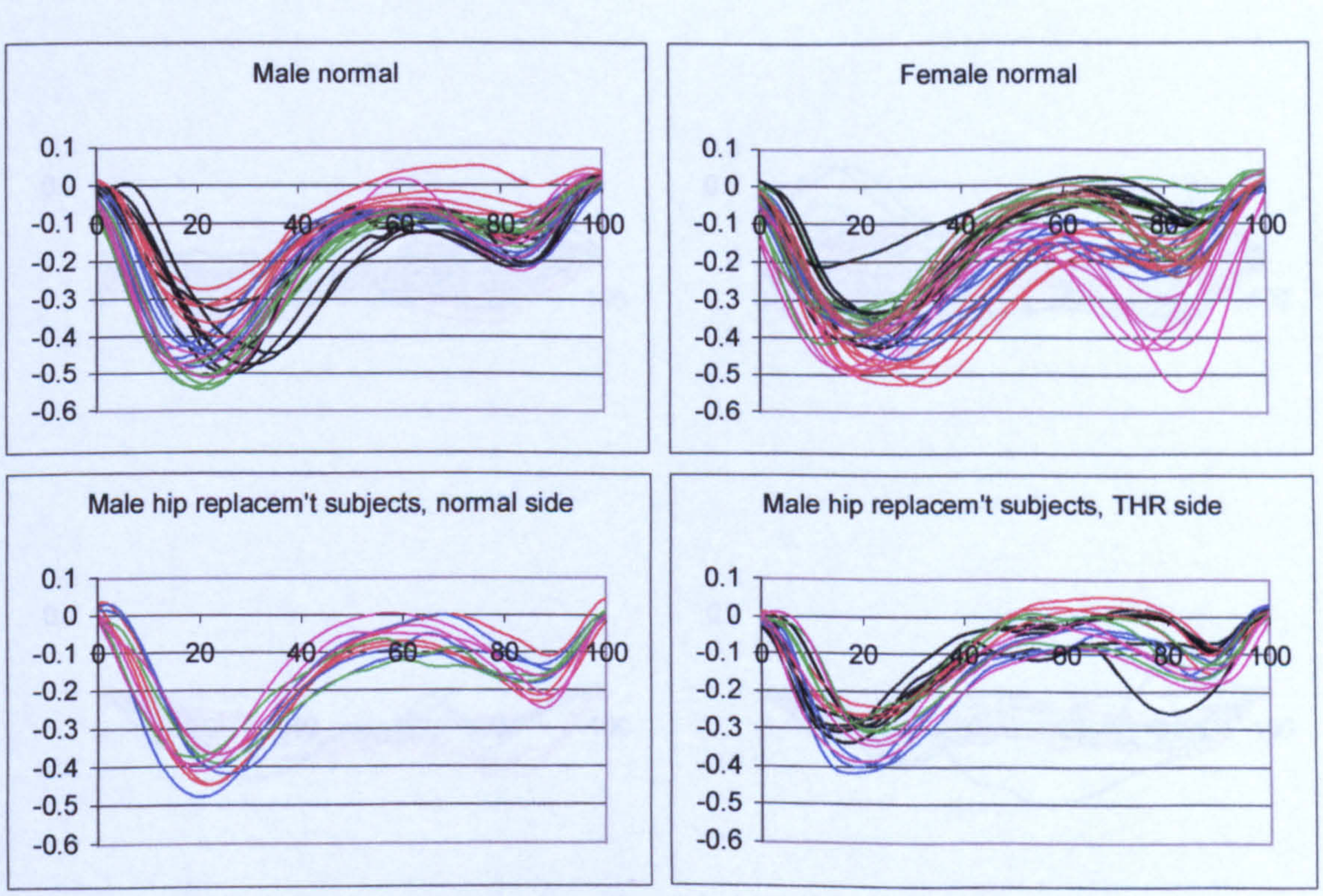

Figure A-VI.2.22 Stair ascent, intersegmental knee force along XKA

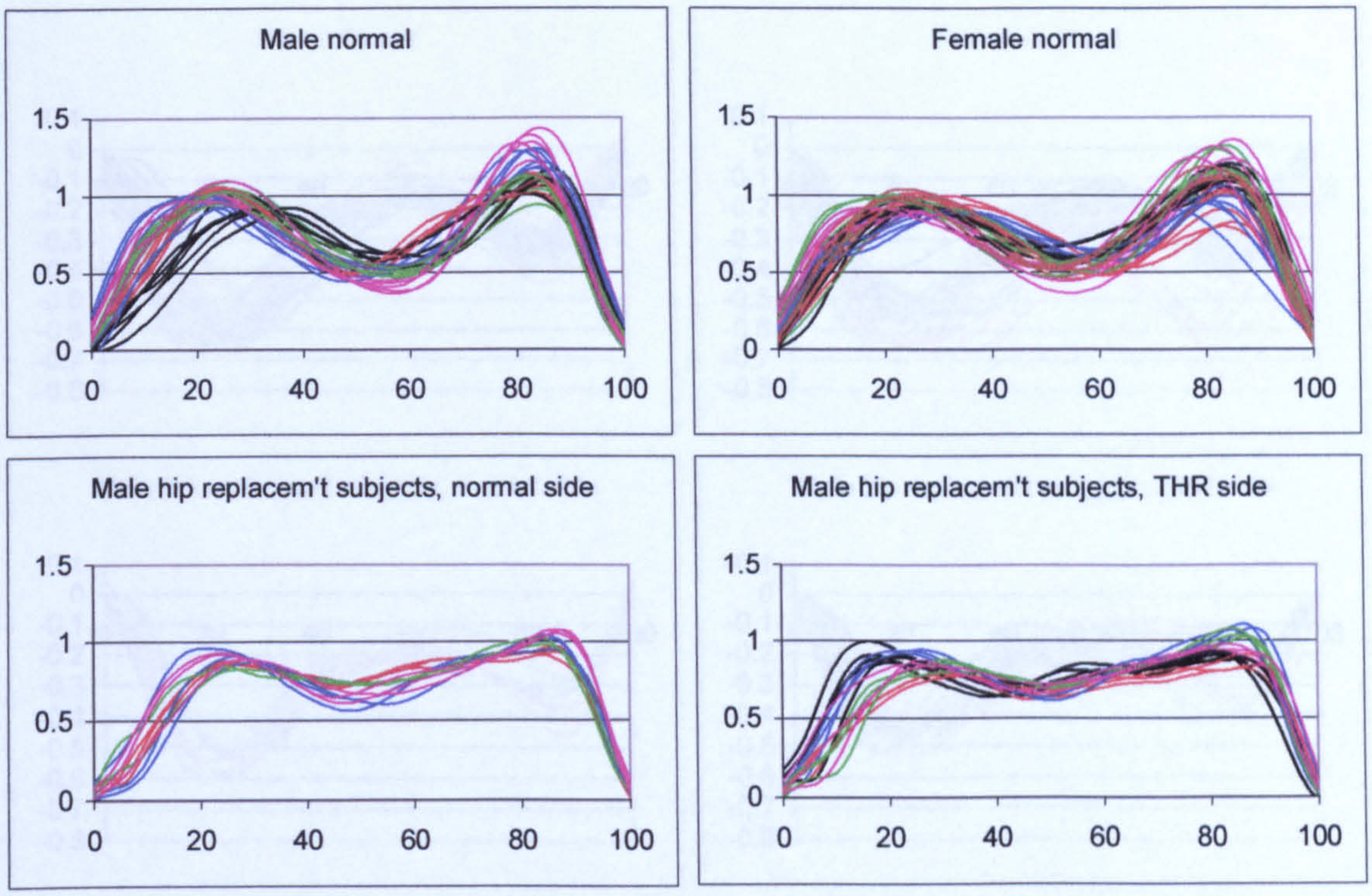

Figure A-VI.2.23 Stair ascent, intersegmental knee force along YKA

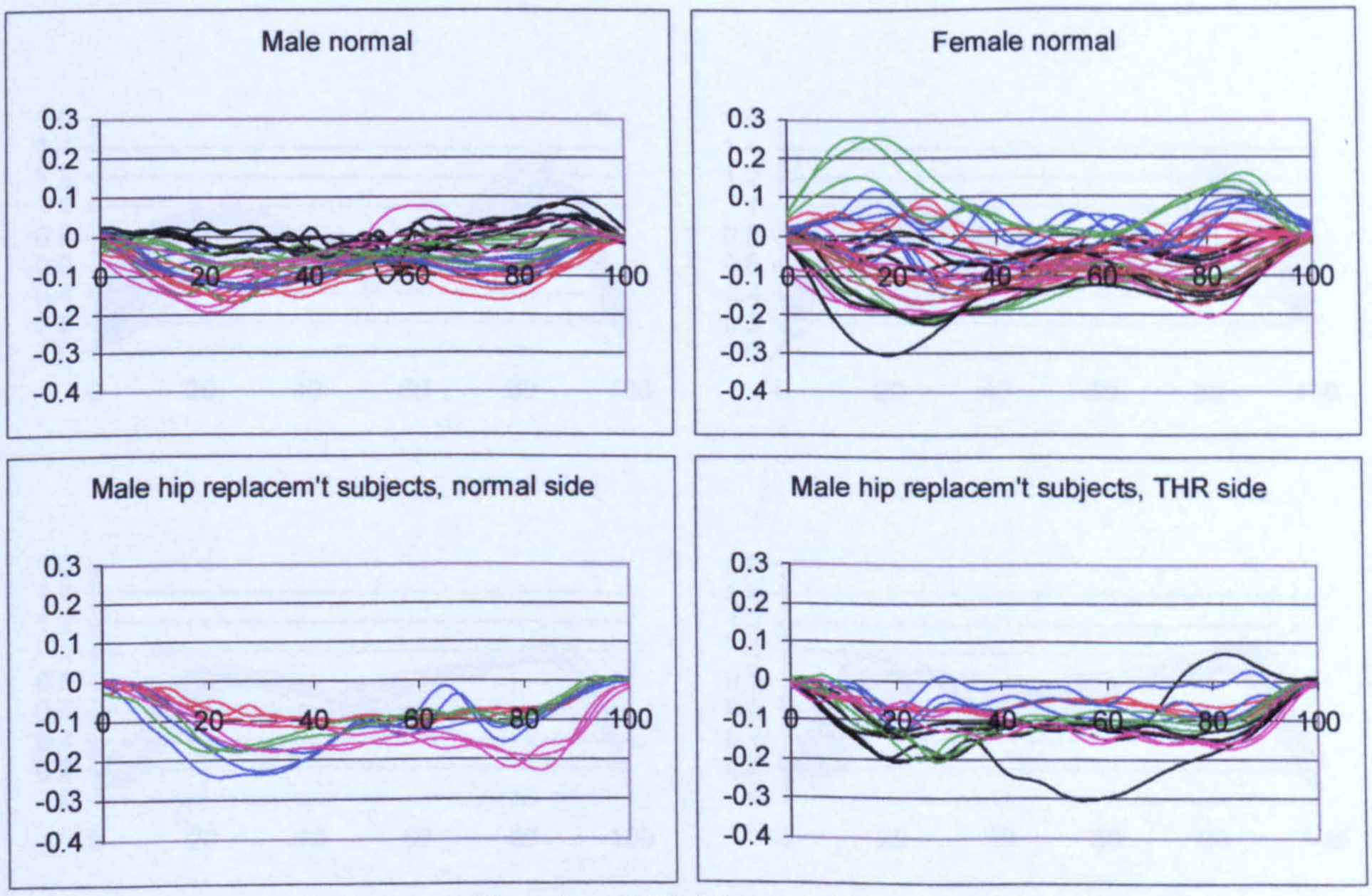

Figure A-VI.2.24 Stair ascent, intersegmental knee force along ZKA

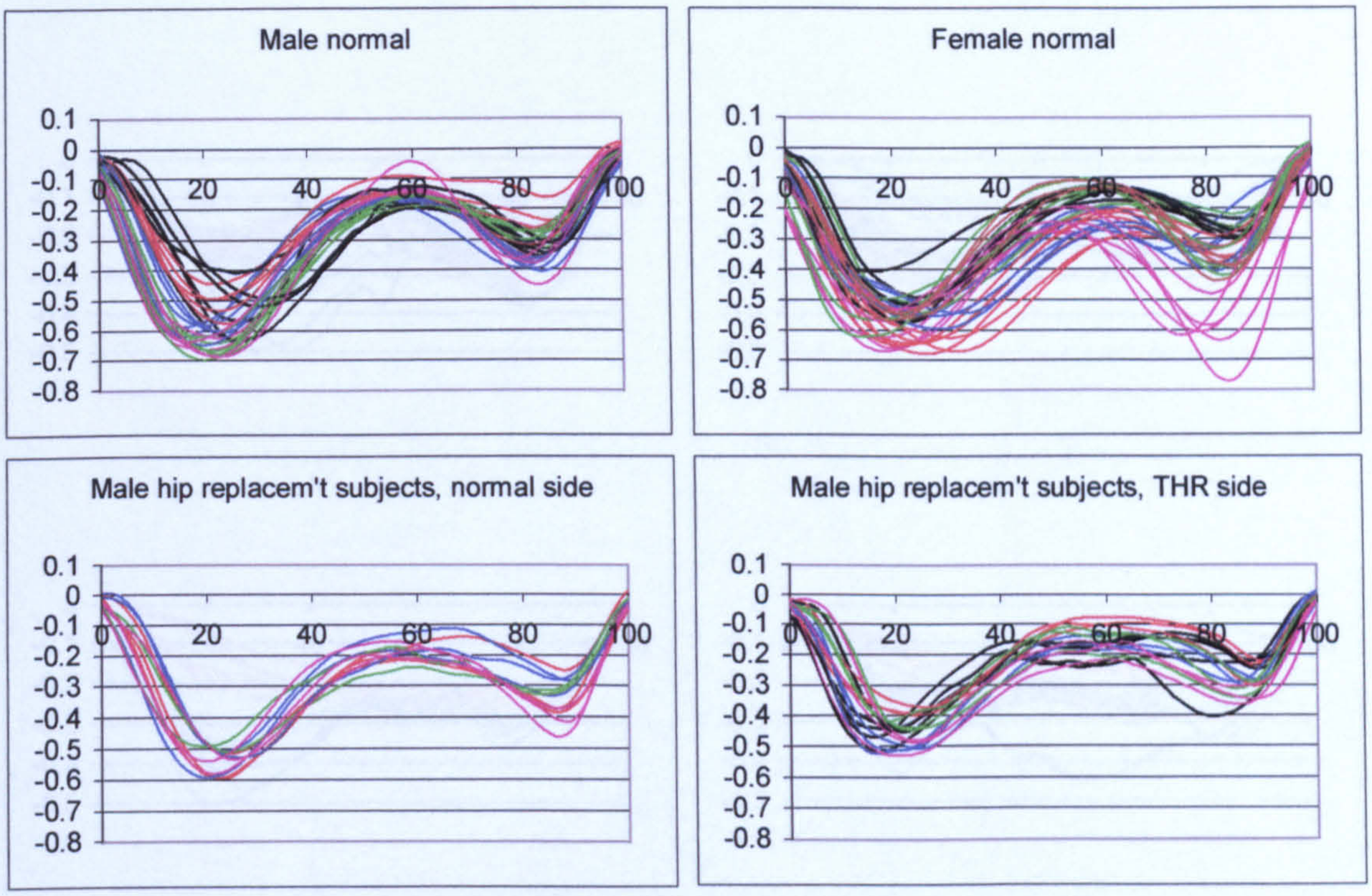

Figure A-VI.2.25 Stair ascent, intersegmental ankle force along XAA

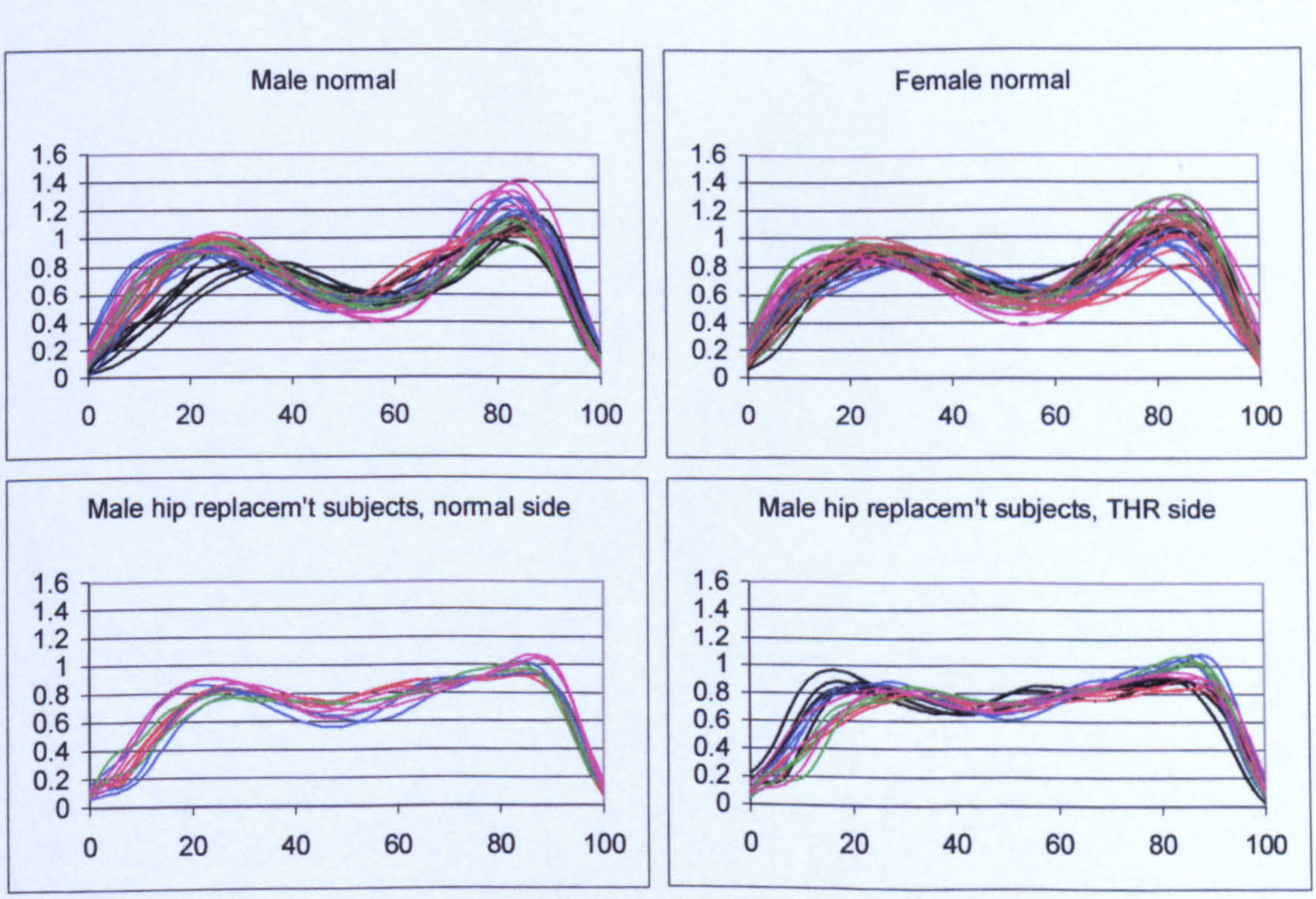

Figure A-VI.2.26 Stair ascent, intersegmental ankle force along YAA

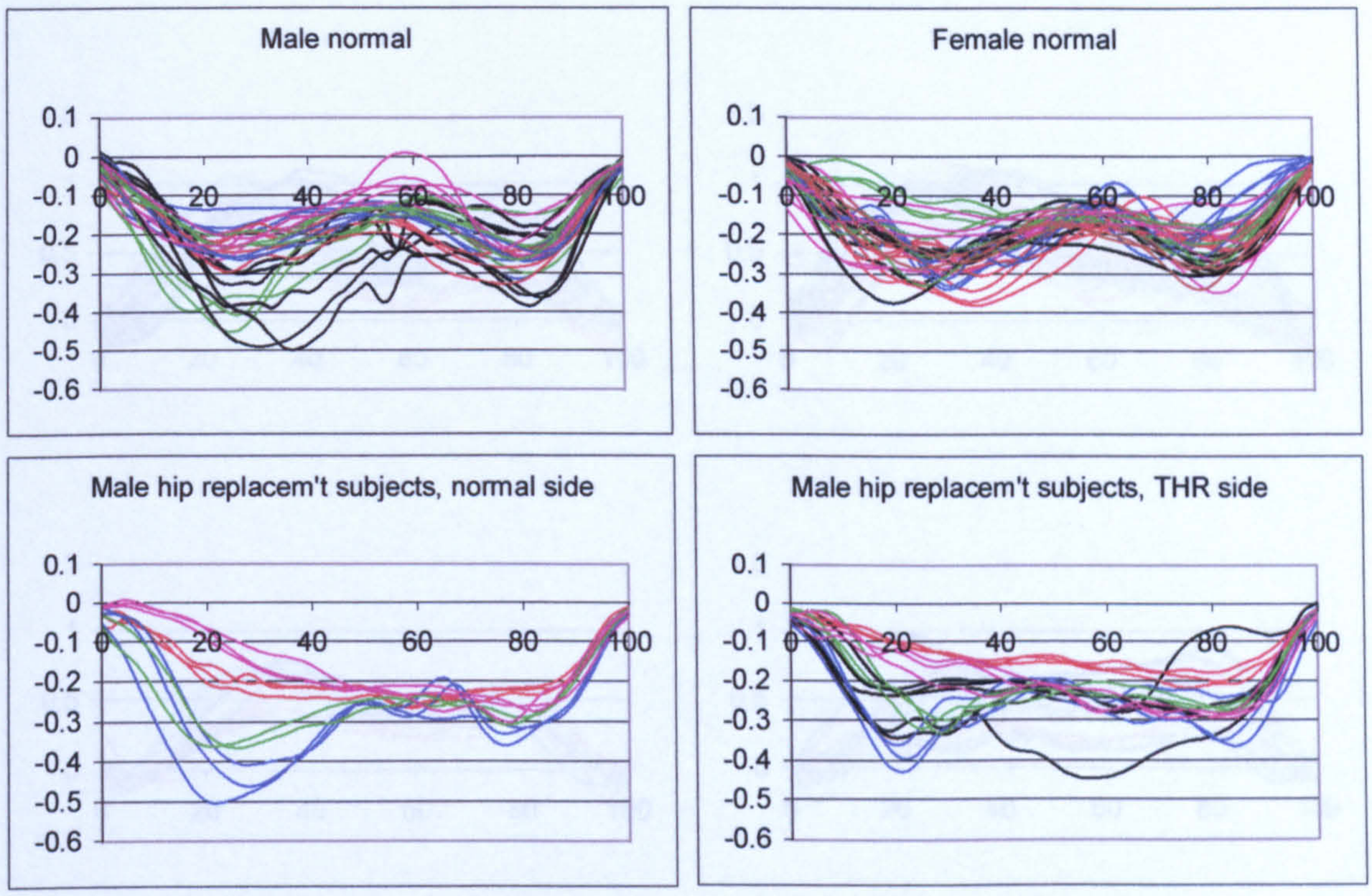

Figure A-VI.2.27 Stair ascent, intersegmental ankle force along ZAA

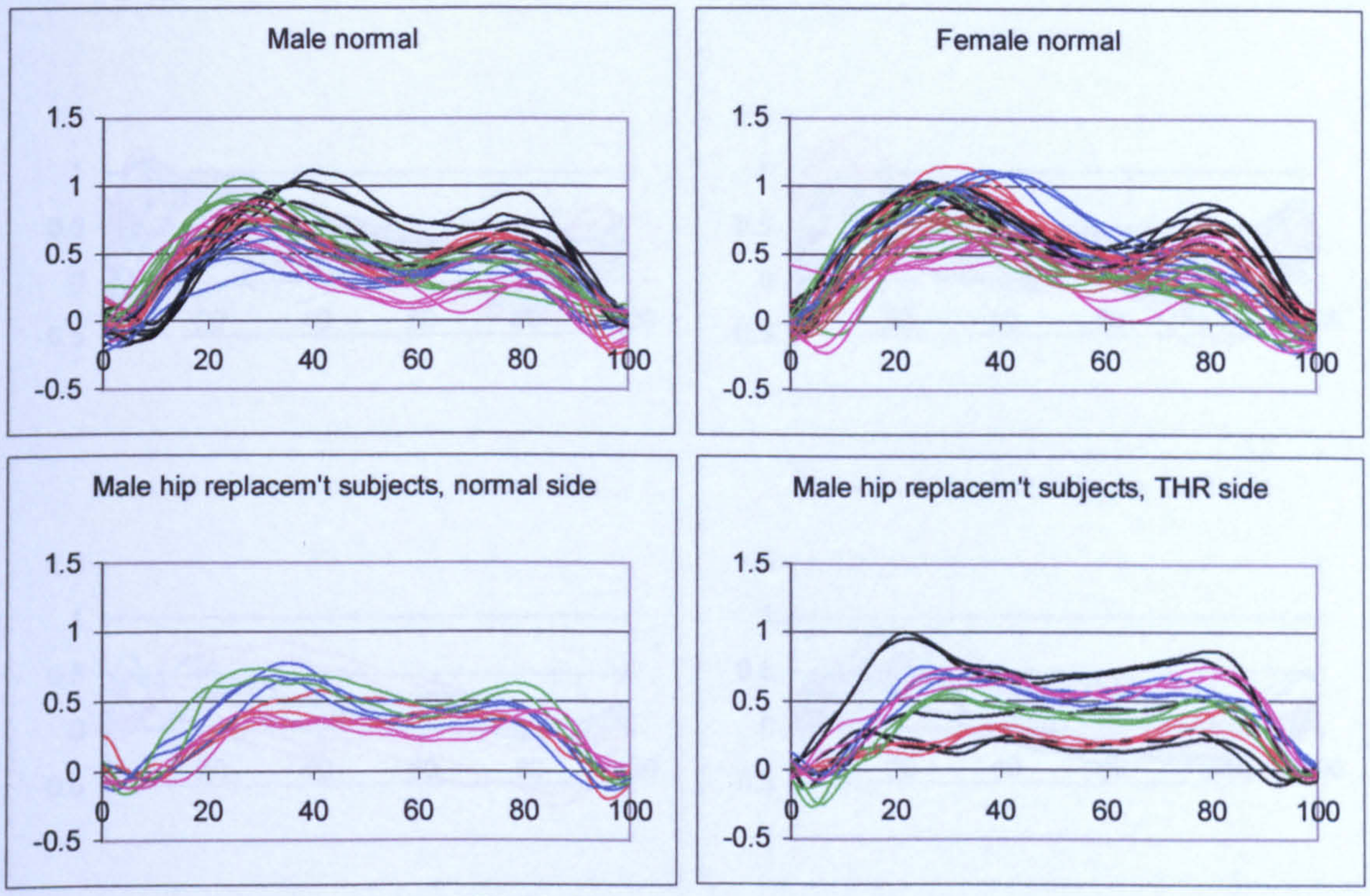

Figure A-VI.2.28 Stair ascent, intersegmental hip moment about XFA

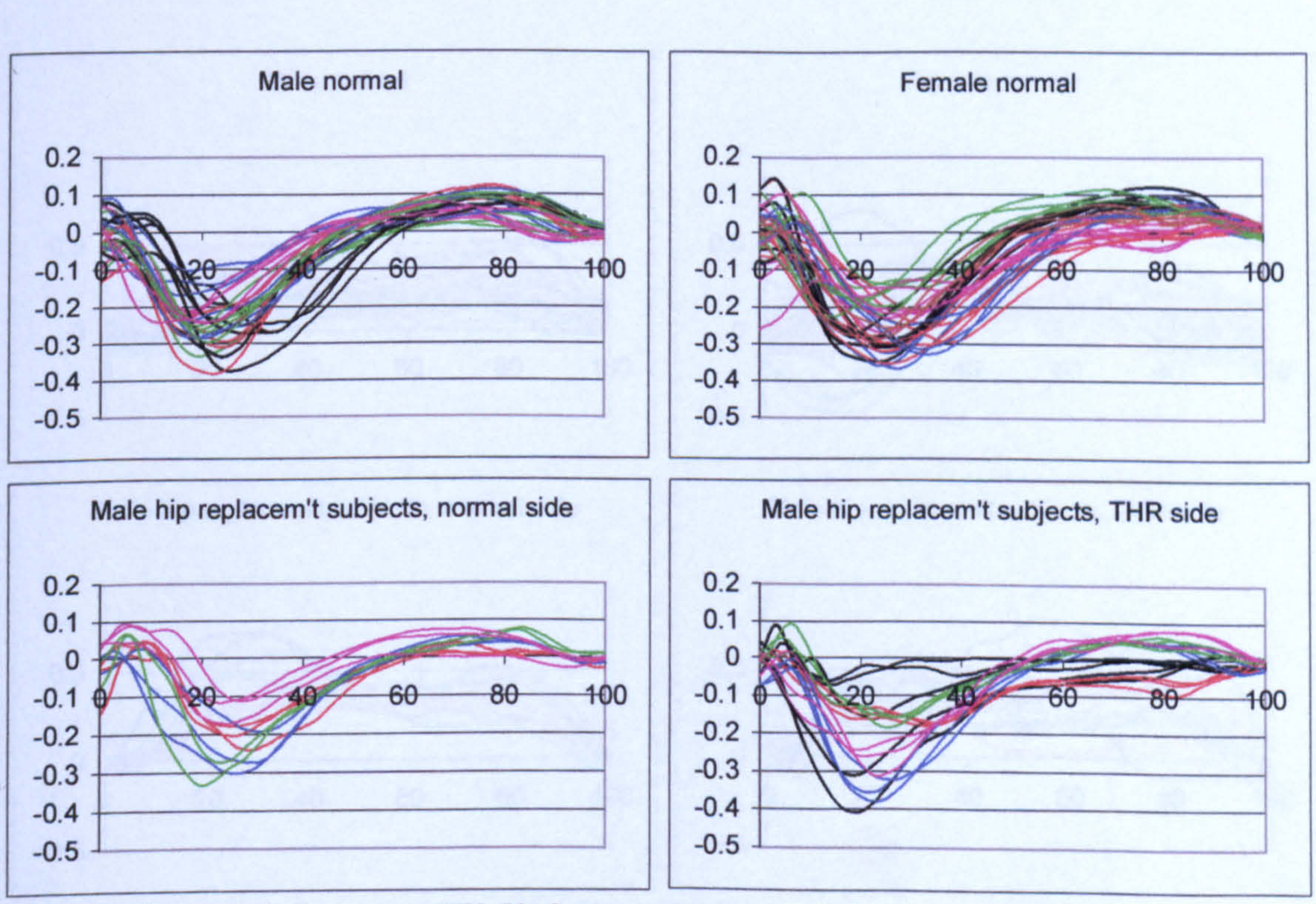

Figure A-VI.2.29 Stair ascent, intersegmental hip moment about YFA

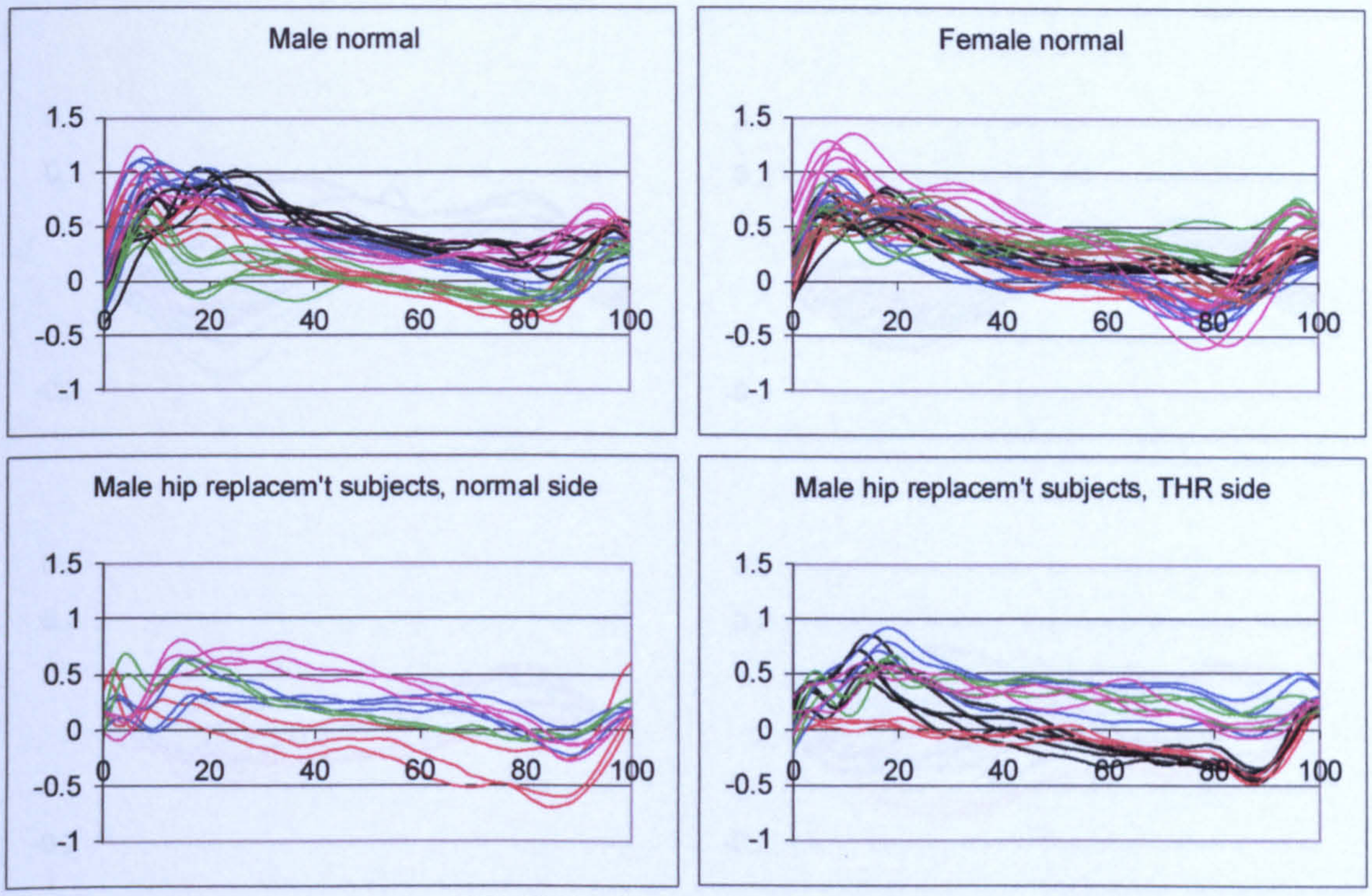

Figure A-VI.2.30 Stair ascent, intersegmental hip moment about ZFA

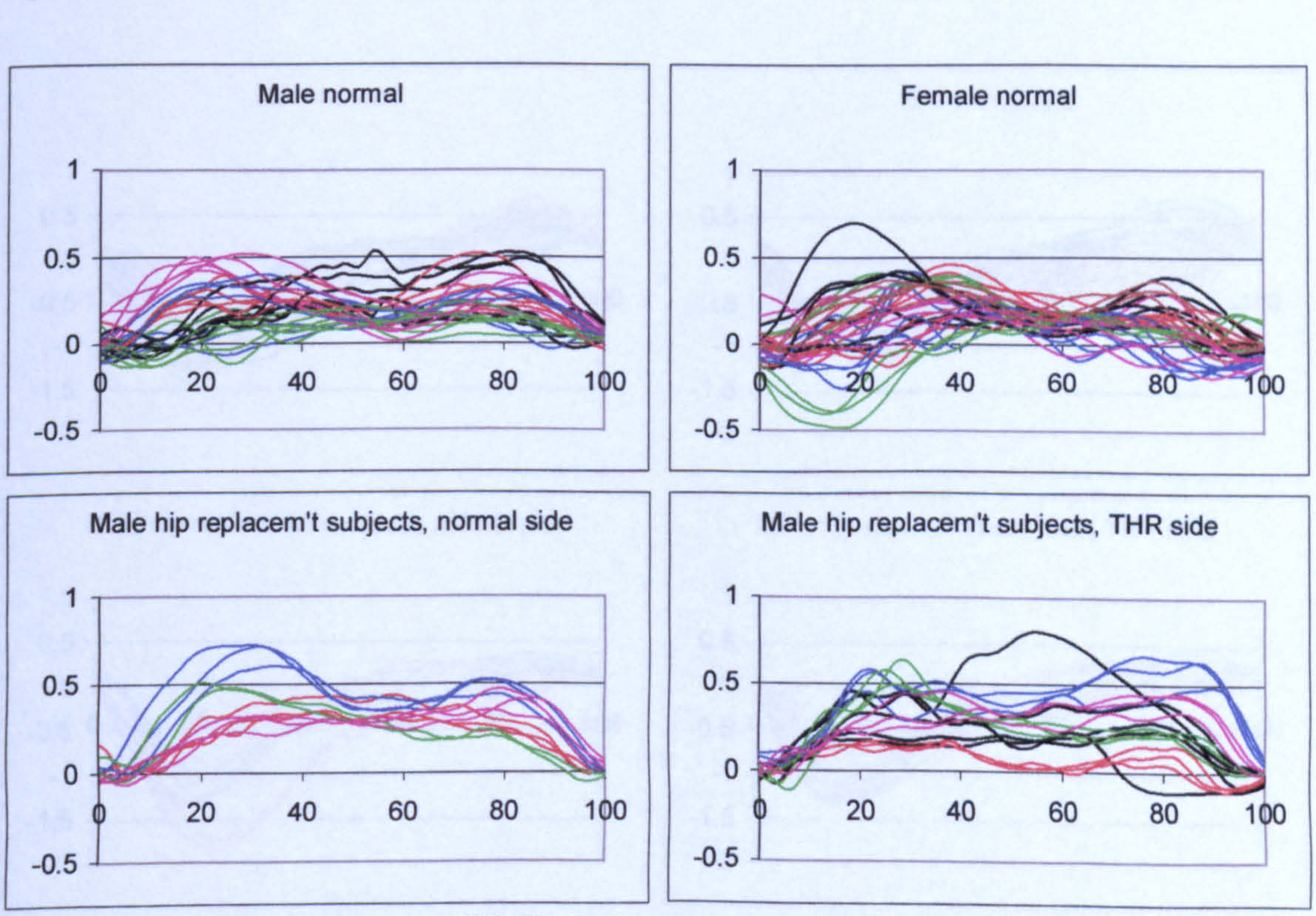

Figure A-VI.2.31 Stair ascent, intersegmental knee moment about XKA

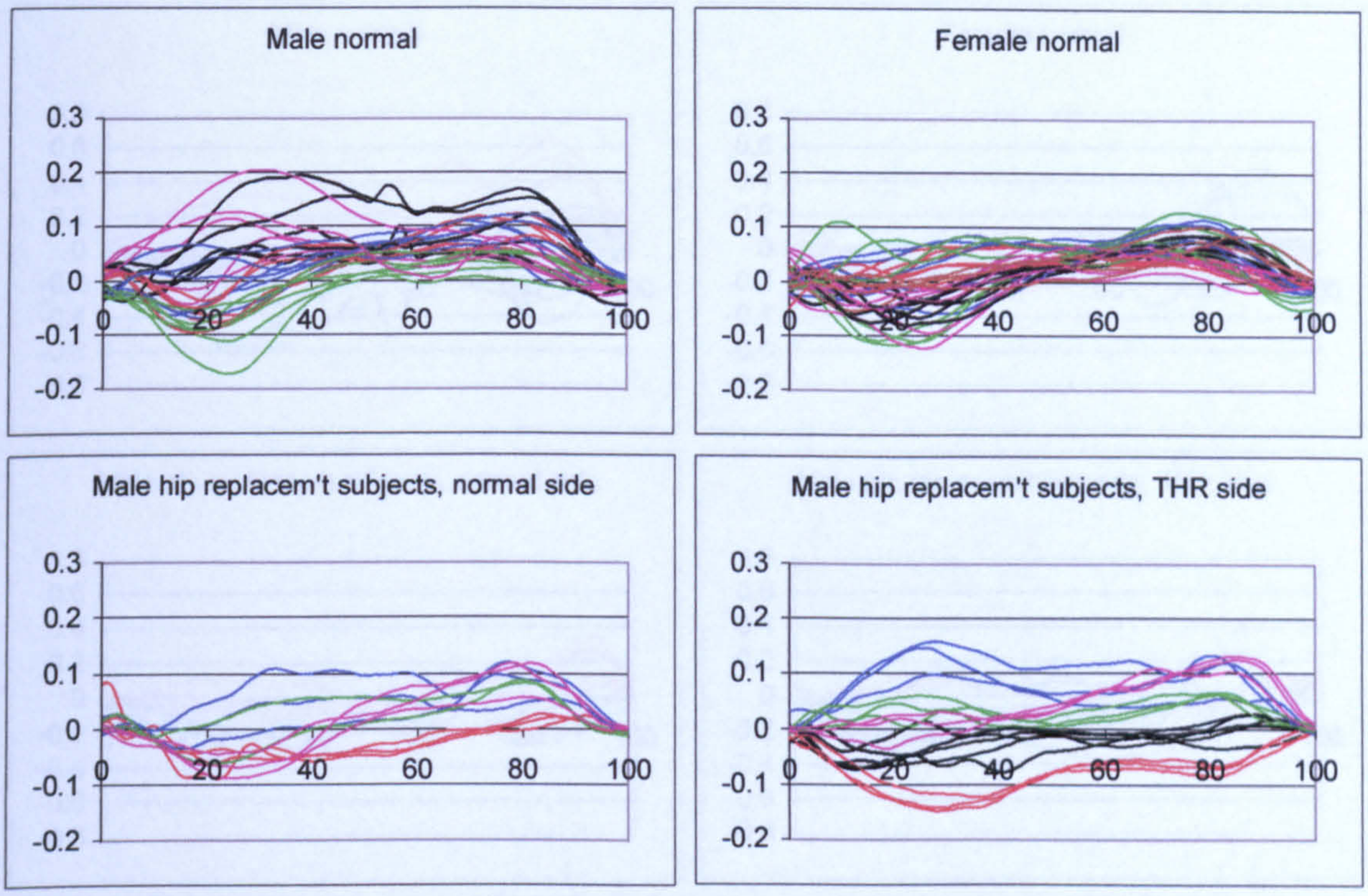

Stair ascent, knee moment YKA (Nm/body mass, +ve = clockwise along axis) by % stance phase

Figure A-VI.2.32 Stair ascent, intersegmental knee moment about YKA

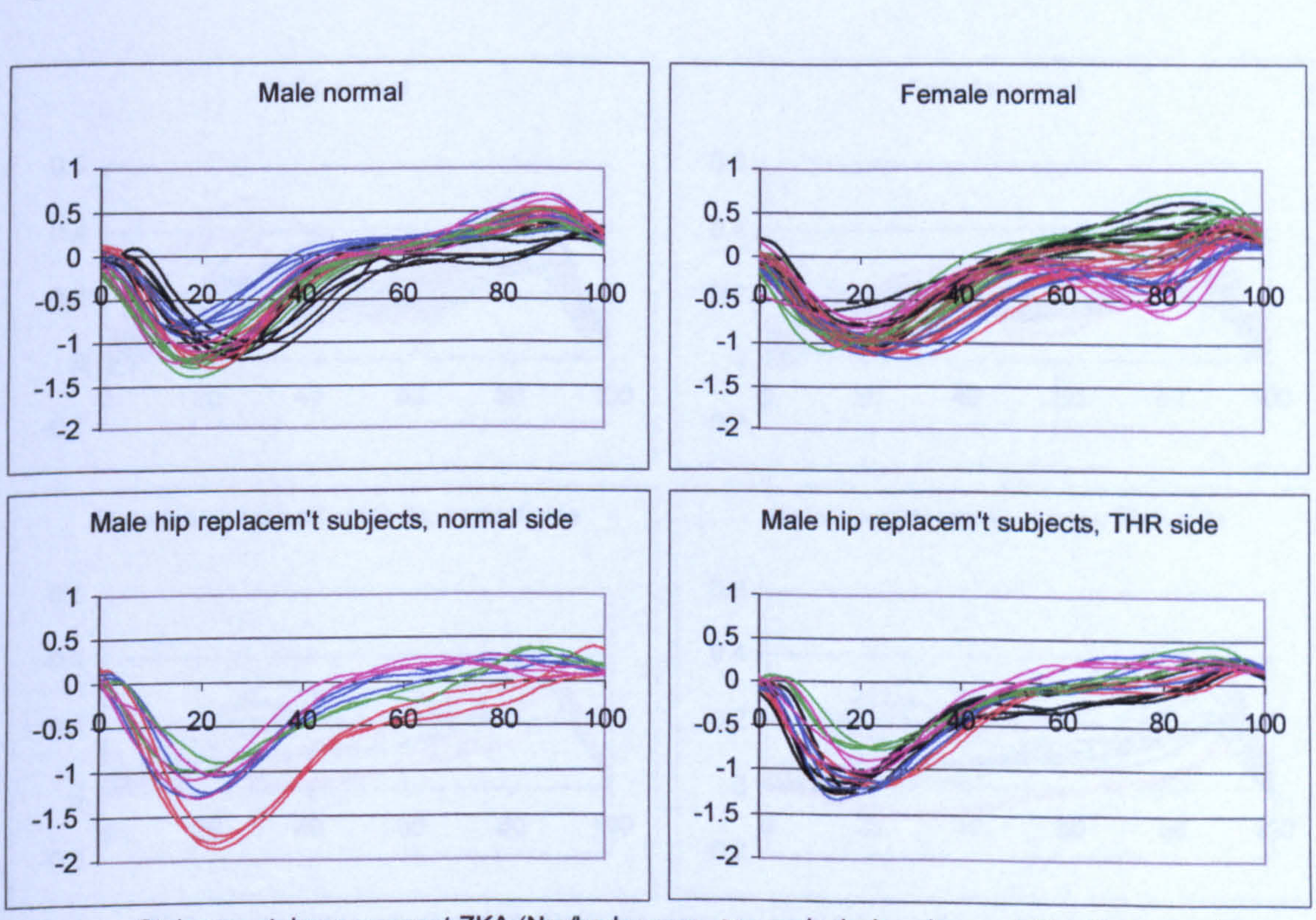

Stair ascent, knee moment ZKA (Nm/body mass, +ve = clockwise along axis) by % stance phase

Figure A-VI.2.33 Stair ascent, intersegmental knee moment about ZKA

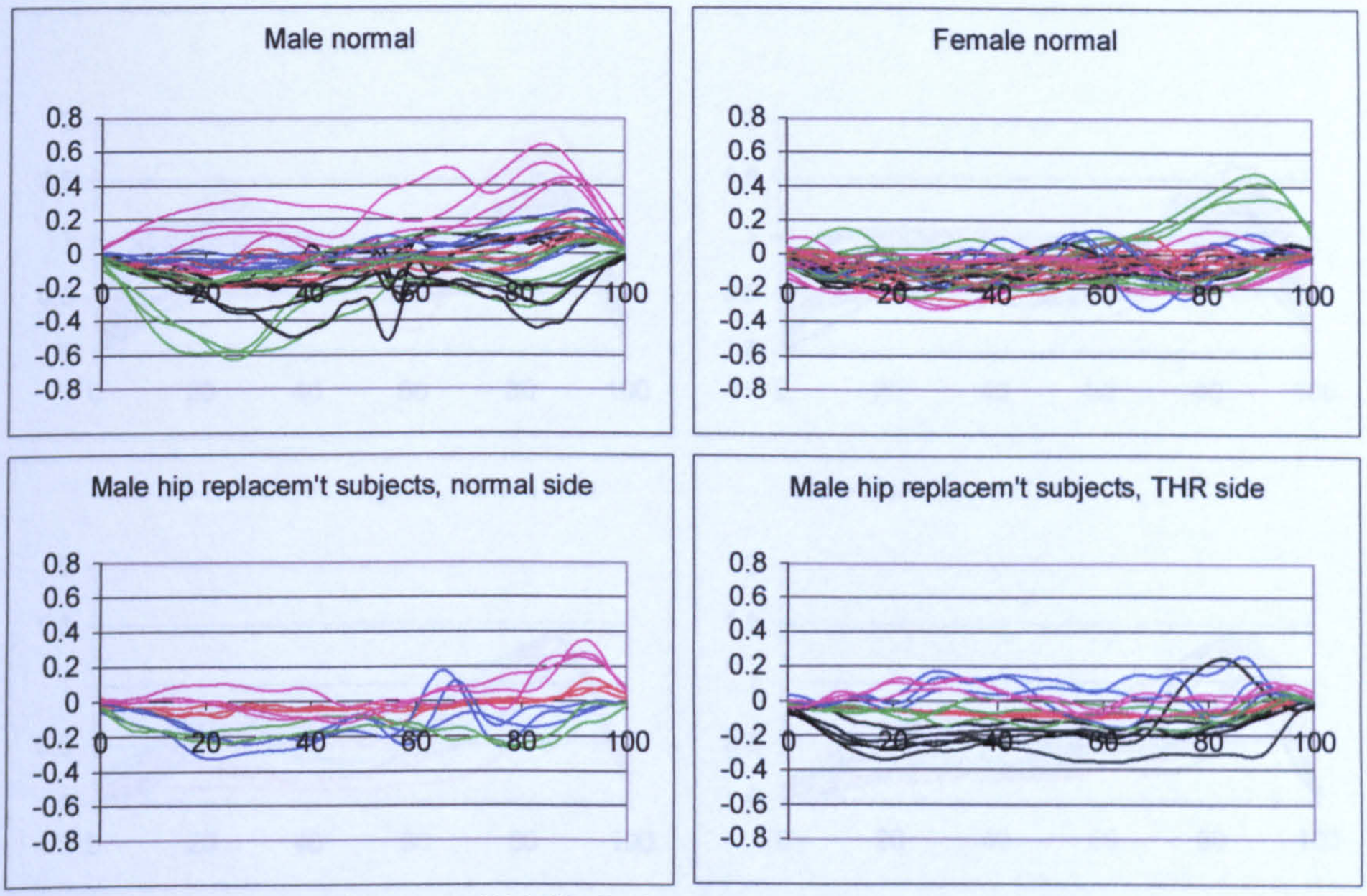

Figure A-VI.2.34 Stair ascent, intersegmental ankle moment about XAA

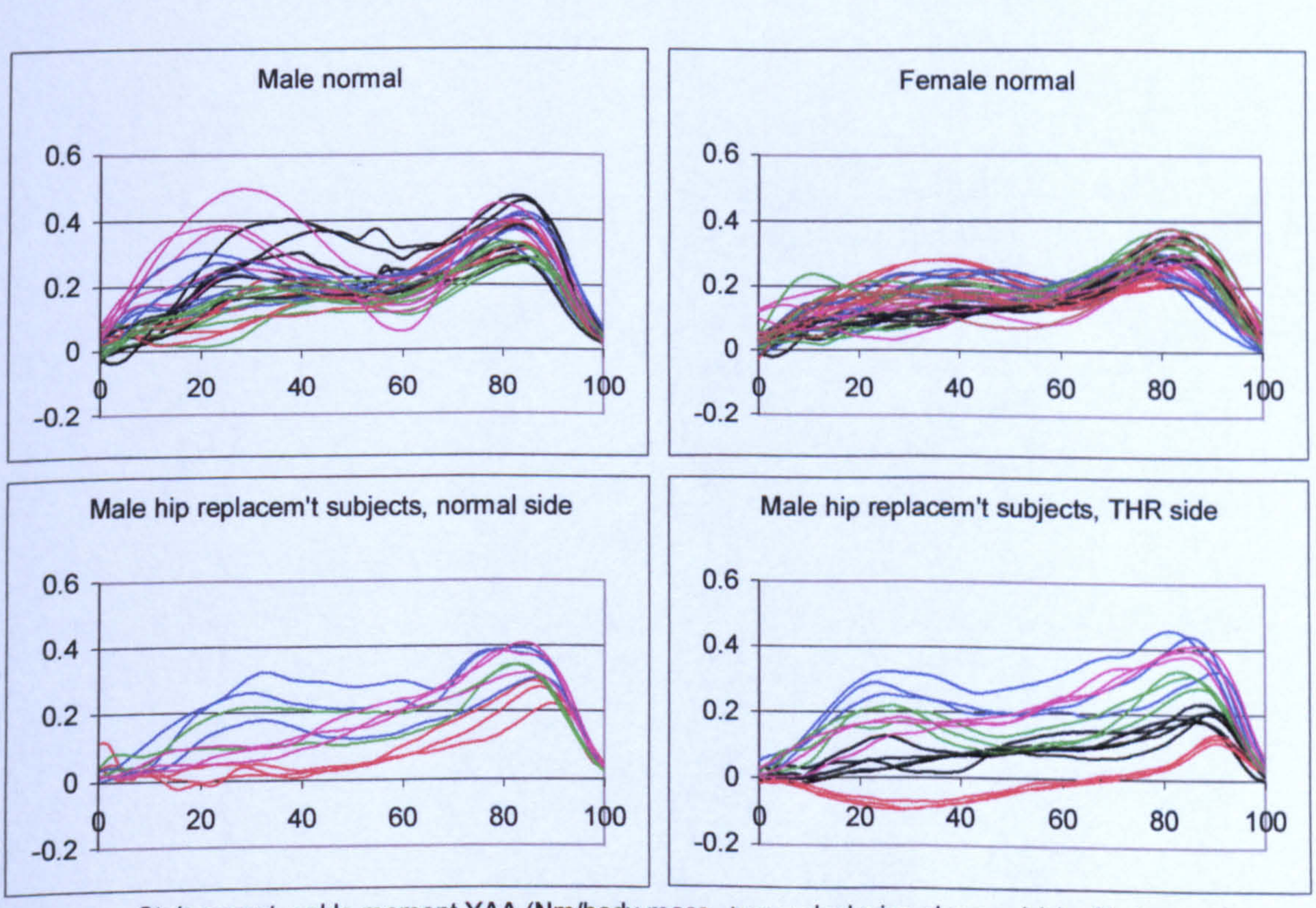

Figure A-VI.2.35 Stair ascent, intersegmental ankle moment about YAA

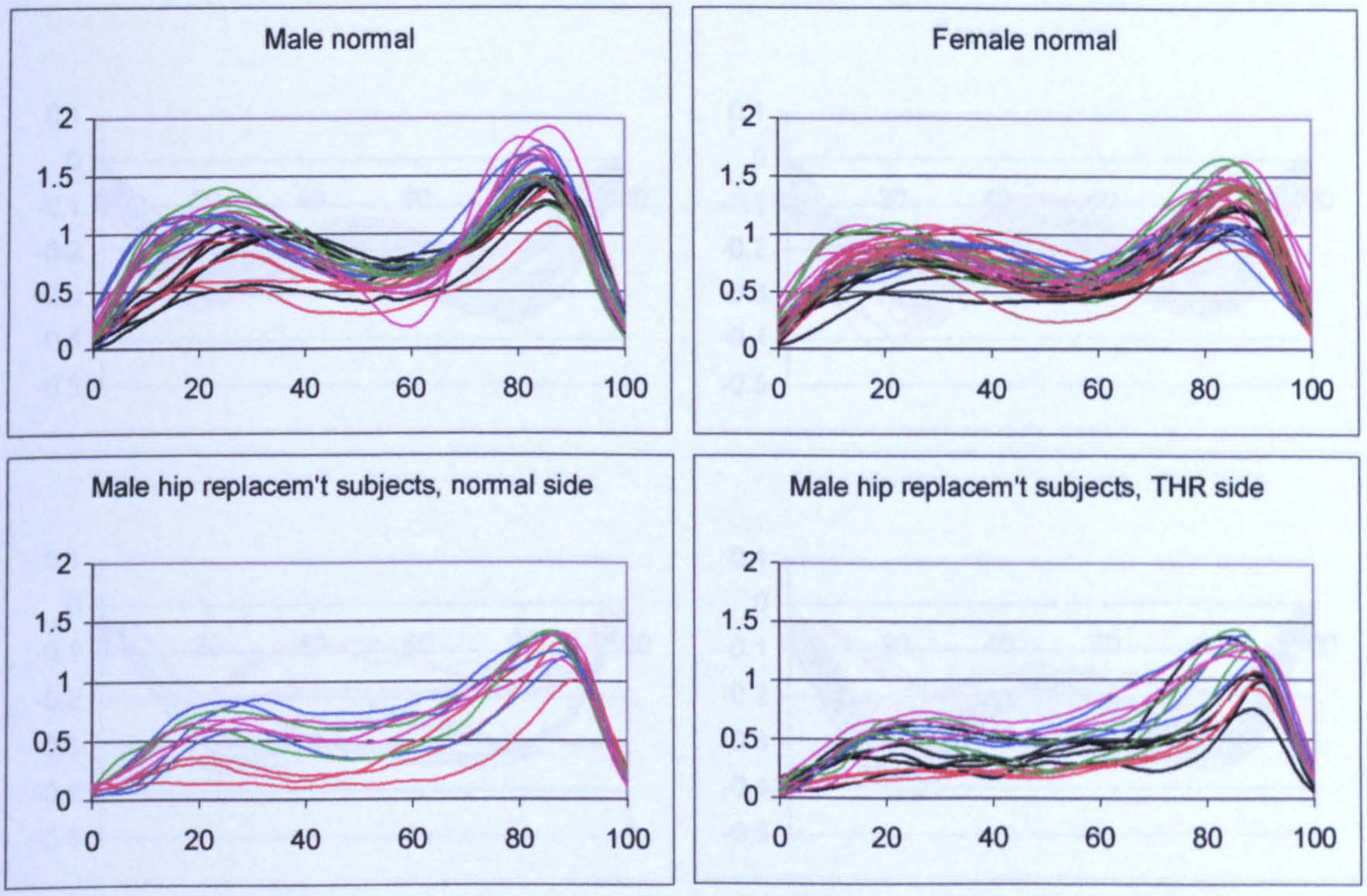

Figure A-VI.2.36 Stair ascent, intersegmental ankle moment about ZAA

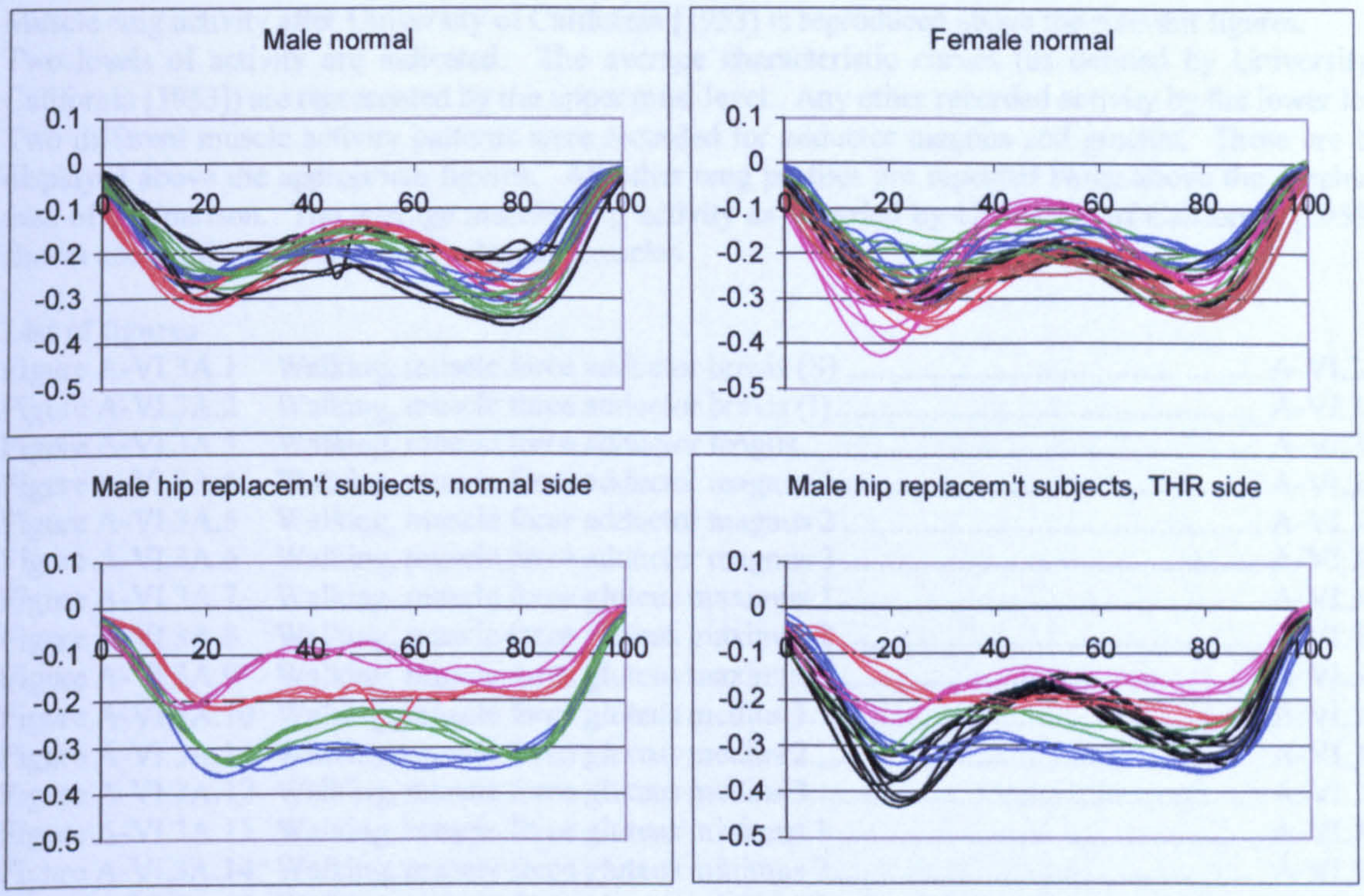

Figure A-VI.2.37 Camber up side foot, intersegmental ankle force along ZAA

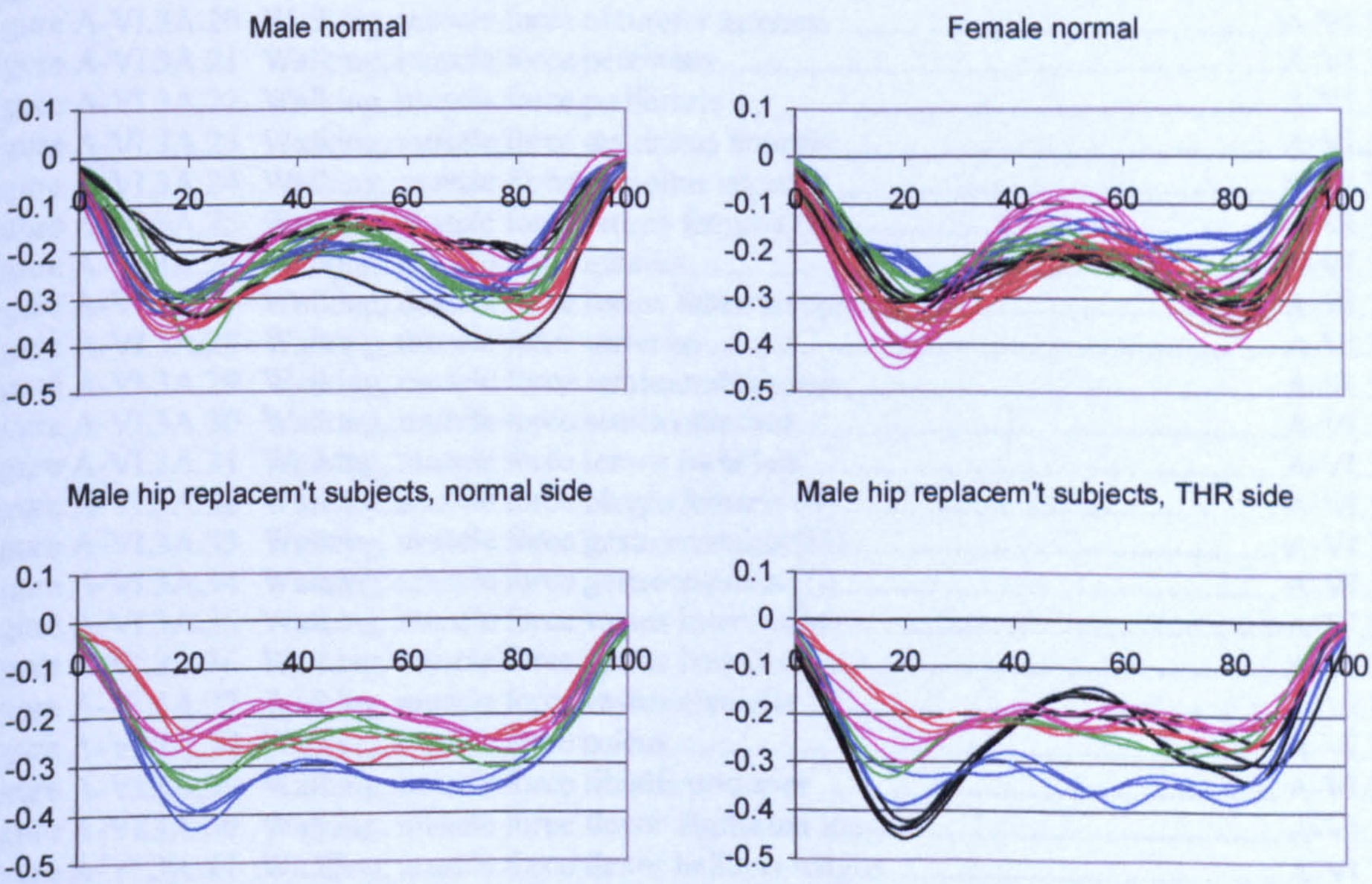

Figure A-VI.2.38 Camber down side foot, intersegmental ankle force along ZAA

A-VI.3A Muscle forces, walking

Muscle emg activity after University of California [1953] is reproduced above the relevant figures.
Two levels of activity are indicated. The average characteristic curves (as defined by University of California [1953]) are represented by the upper most level. Any other recorded activity by the lower level
Two different muscle activity patterns were recorded for adductor magnus and gracilis. These are both displayed above the appropriate figures. All other emg profiles are repeated twice above the graphs for ease of comparison. The average muscle emg activity as recorded by University of California [1953] is shown above all parts of the multi-element muscles.

List of figures

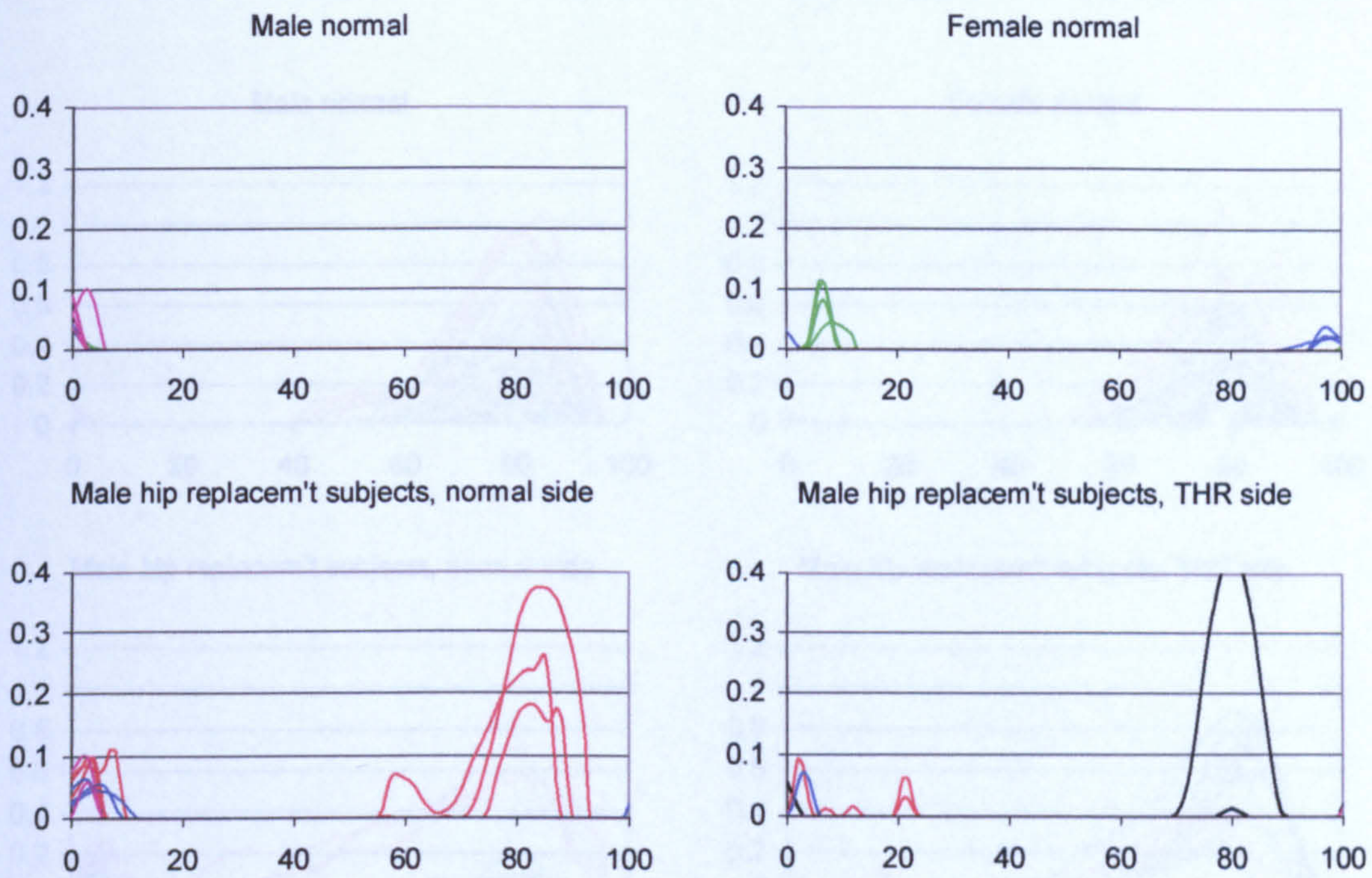

Figure A-VI.3A.1 Walking, muscle force adductor brevis (S)

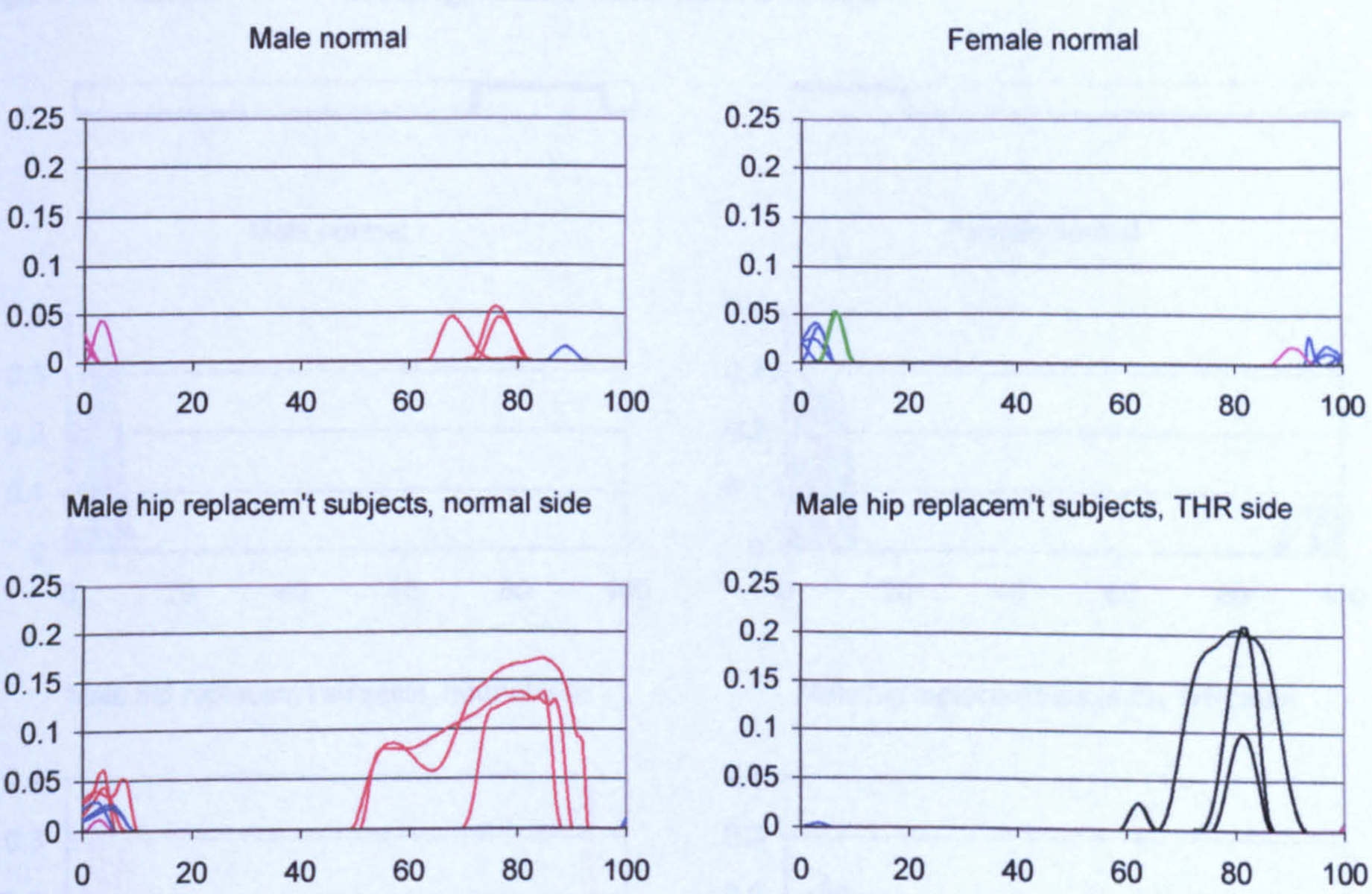

Figure A-VI.3A.2 Walking, muscle force adductor brevis (I)

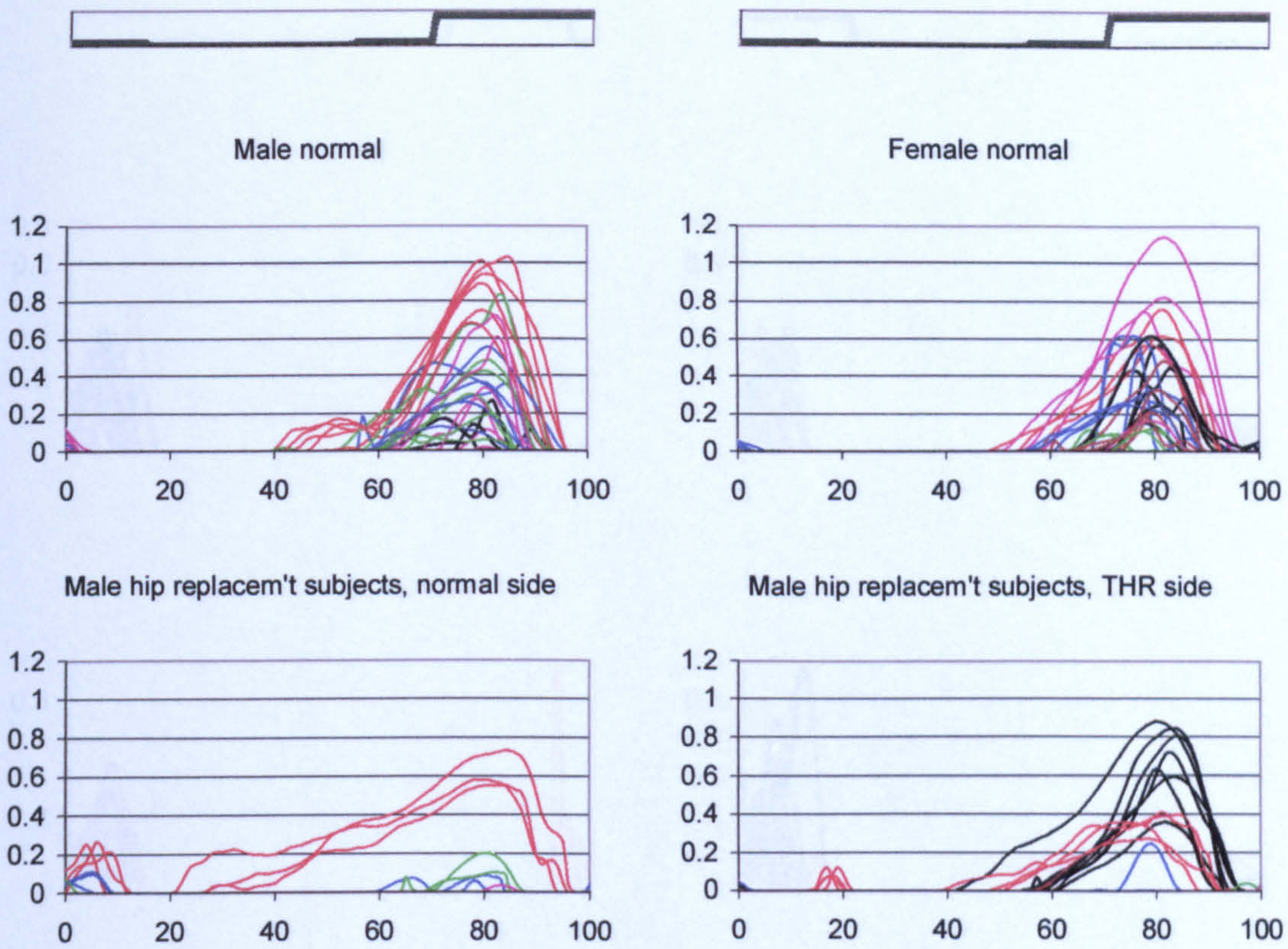

Figure A-VI.3A.3 Walking, muscle force adductor longus

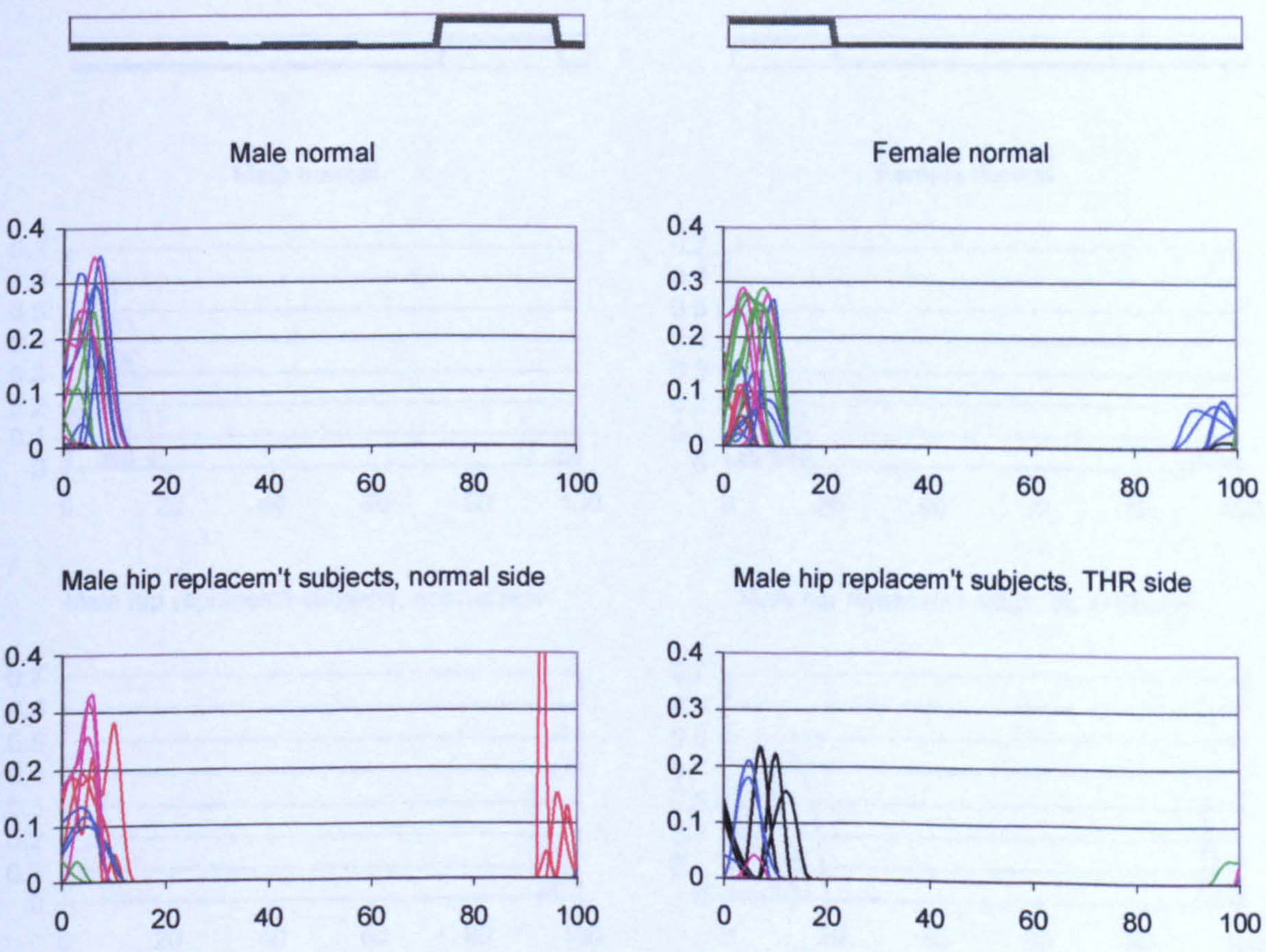

Figure A-VI.3A.4 Walking, muscle force adductor magnus 1

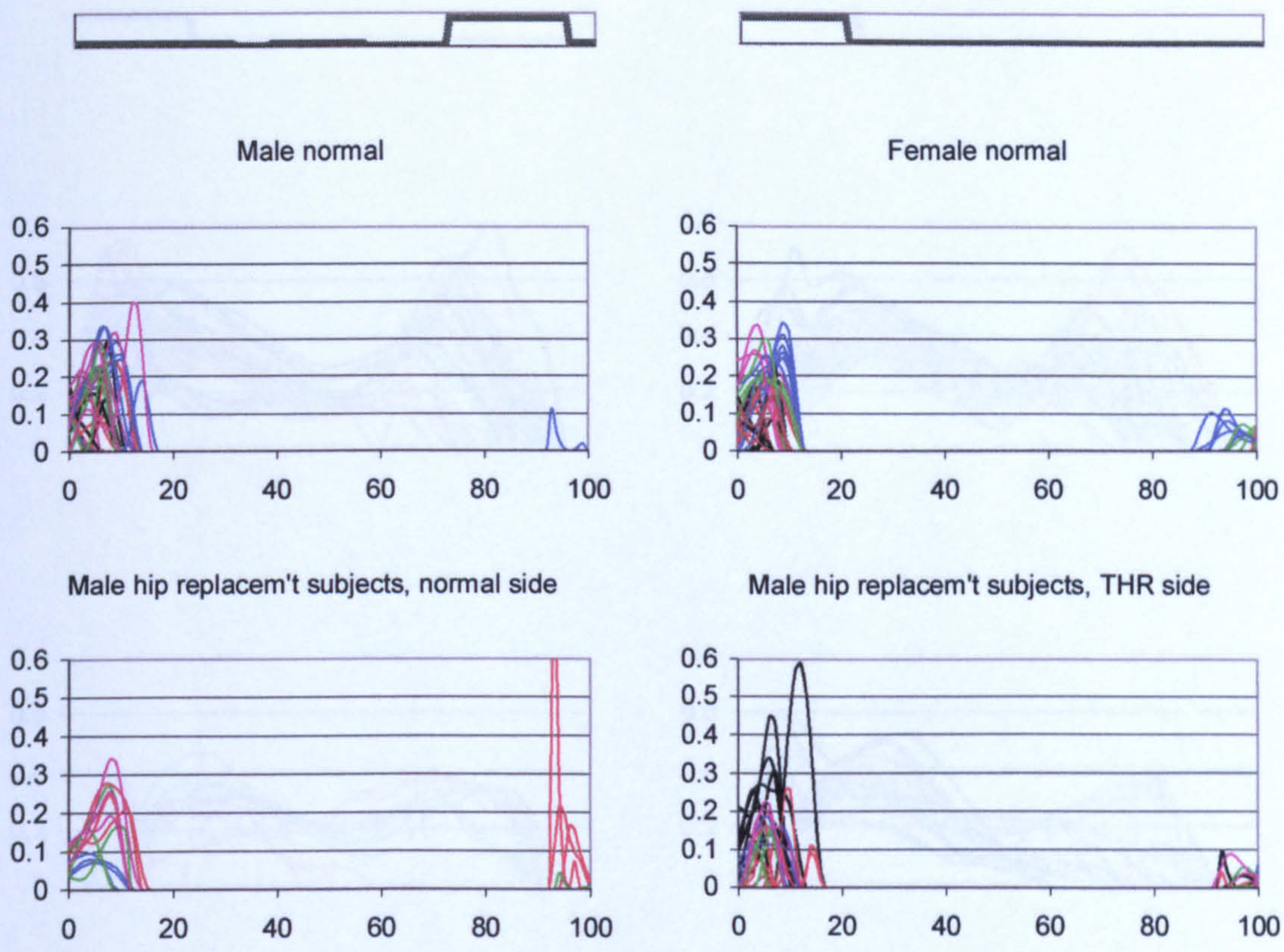

Figure A-VI.3A.5 Walking, muscle force adductor magnus 2

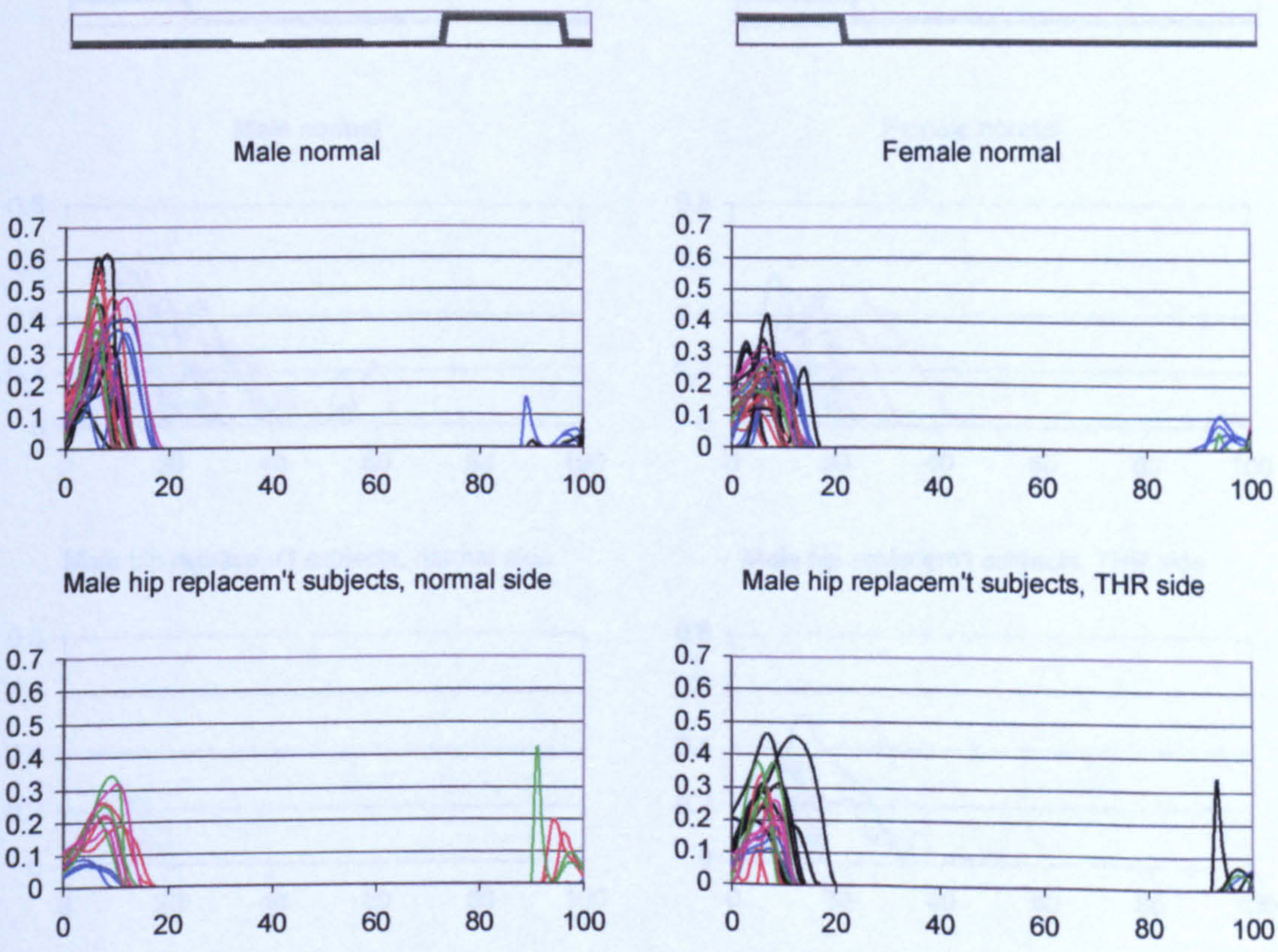

Figure A-VI.3A.6 Walking, muscle force adductor magnus 3

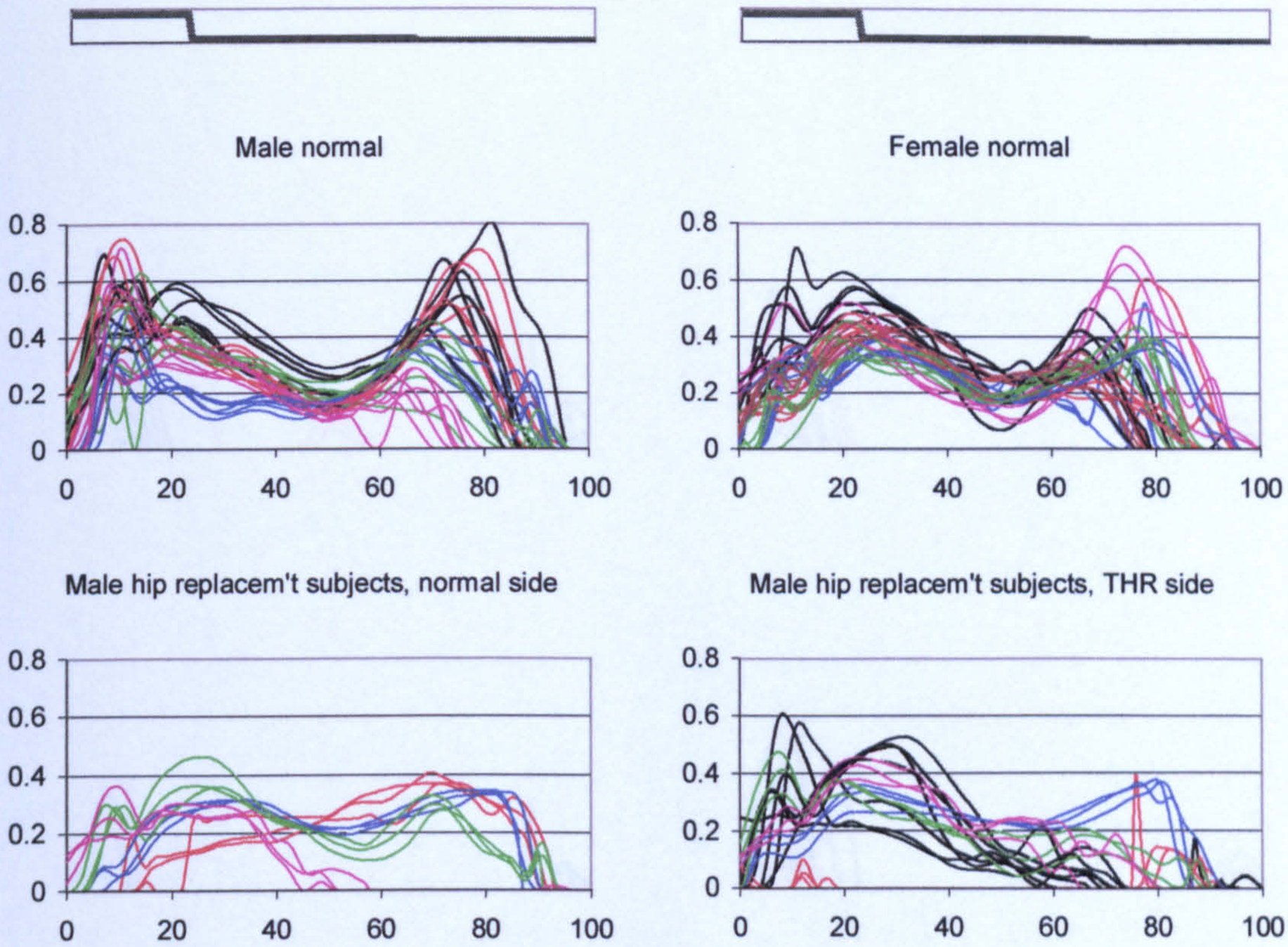

Figure A-VI.3A.7 Walking, muscle force gluteus maximus 1

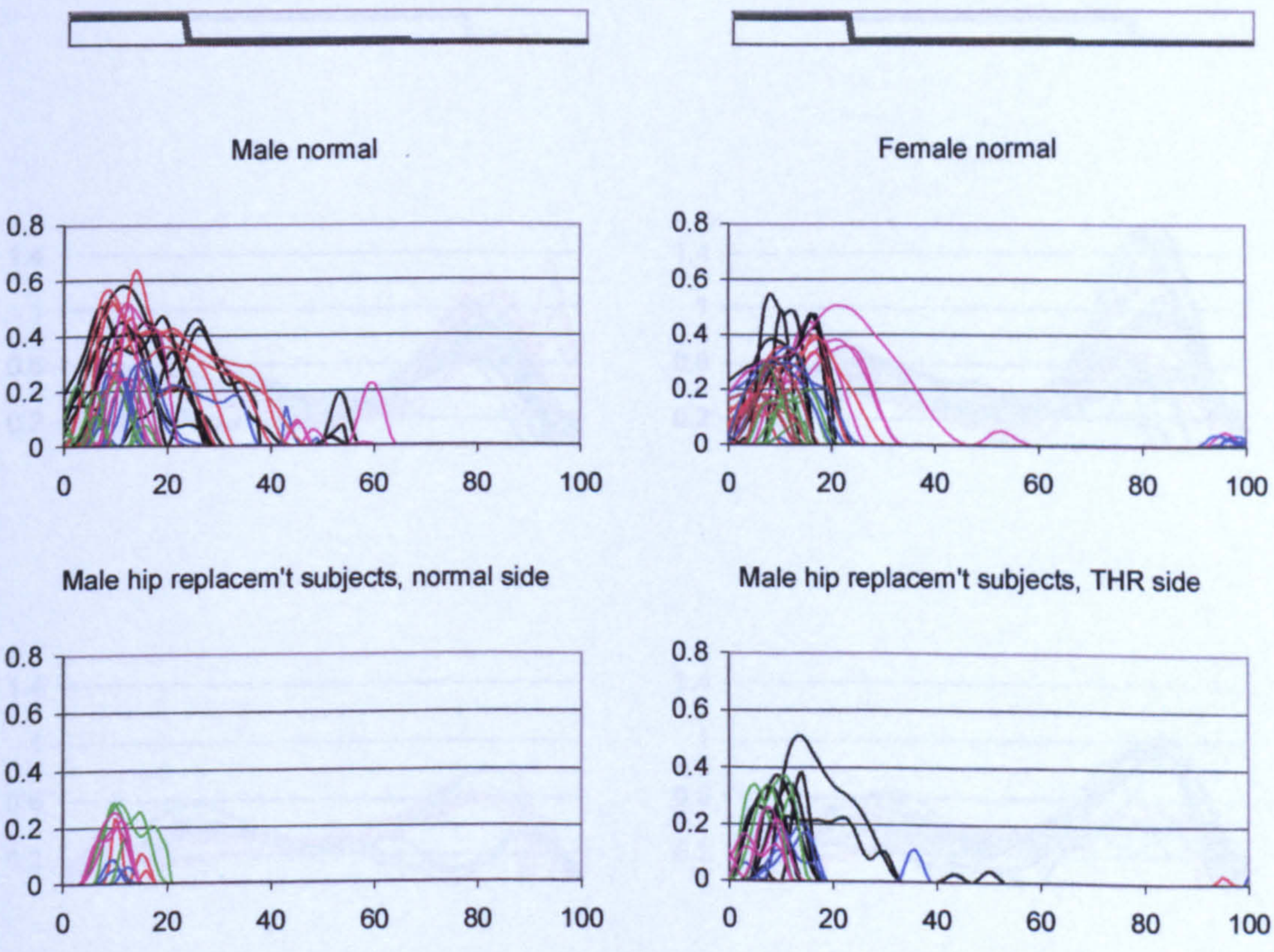

Figure A-VI.3A.8 Walking, muscle force gluteus maximus 2

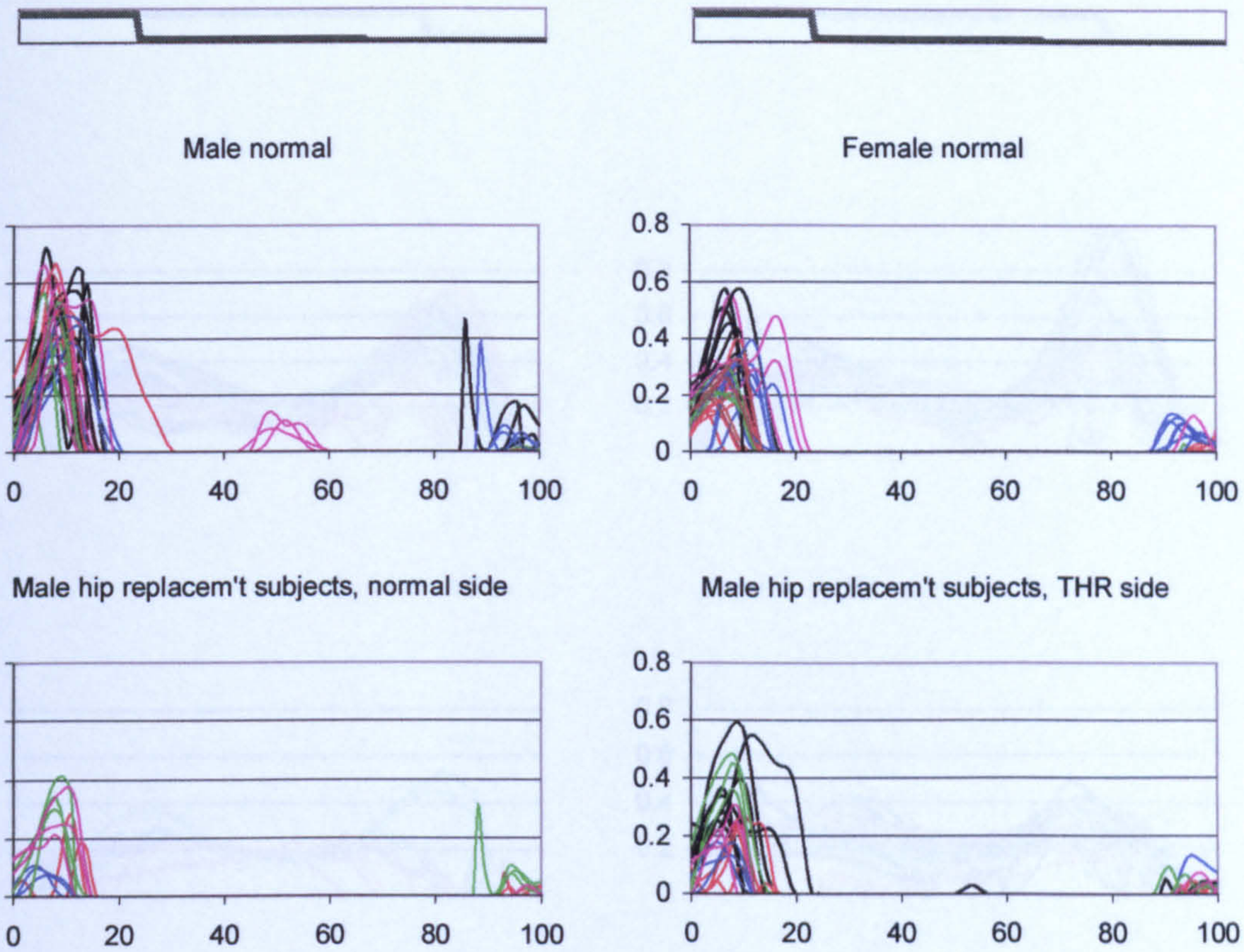

Figure A-VI.3A.9 Walking, muscle force gluteus maximus 3

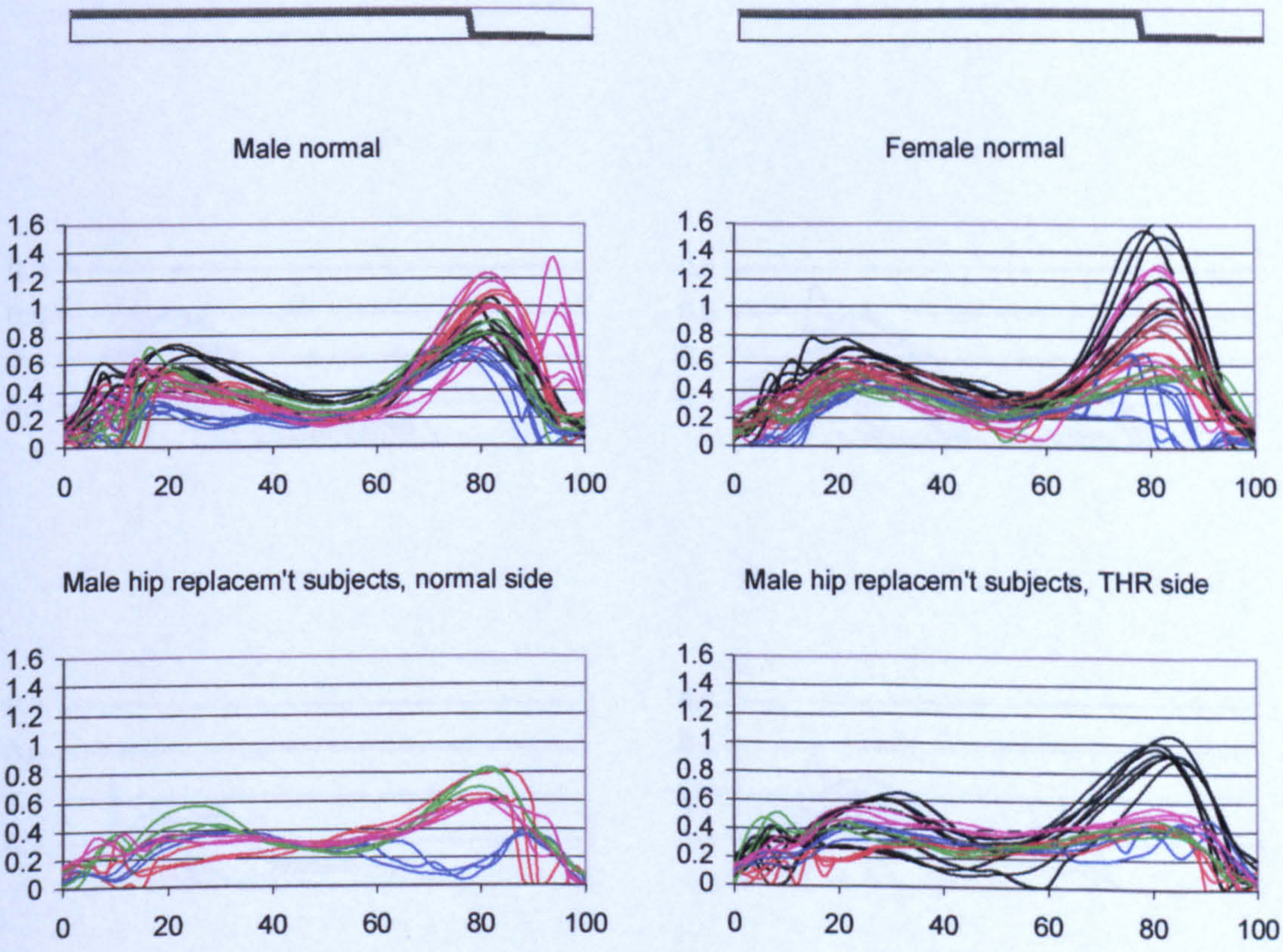

Figure A-VI.3A.10 Walking, muscle force gluteus medius 1

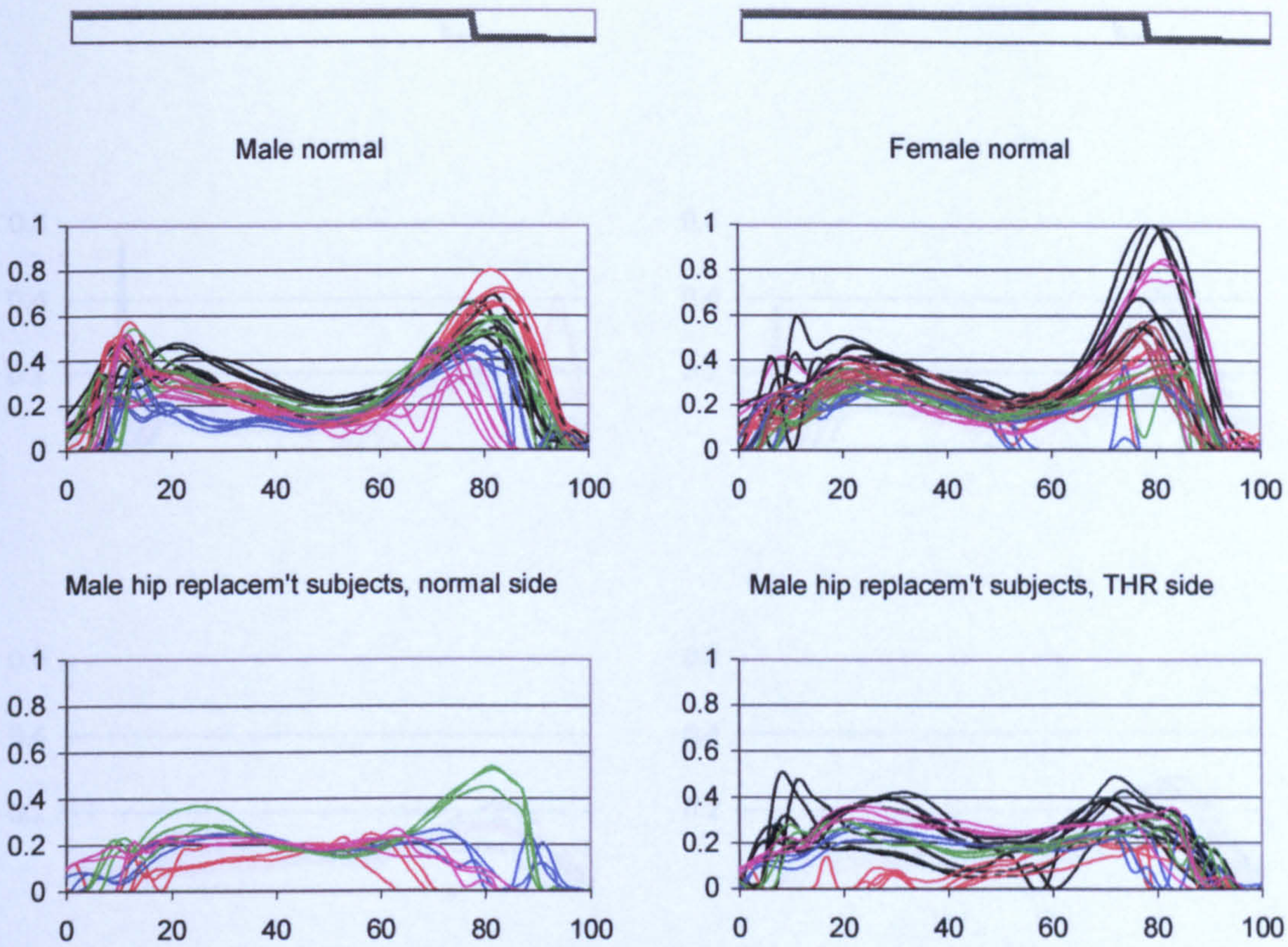

Figure A-VI.3A.11 Walking, muscle force gluteus medius 2

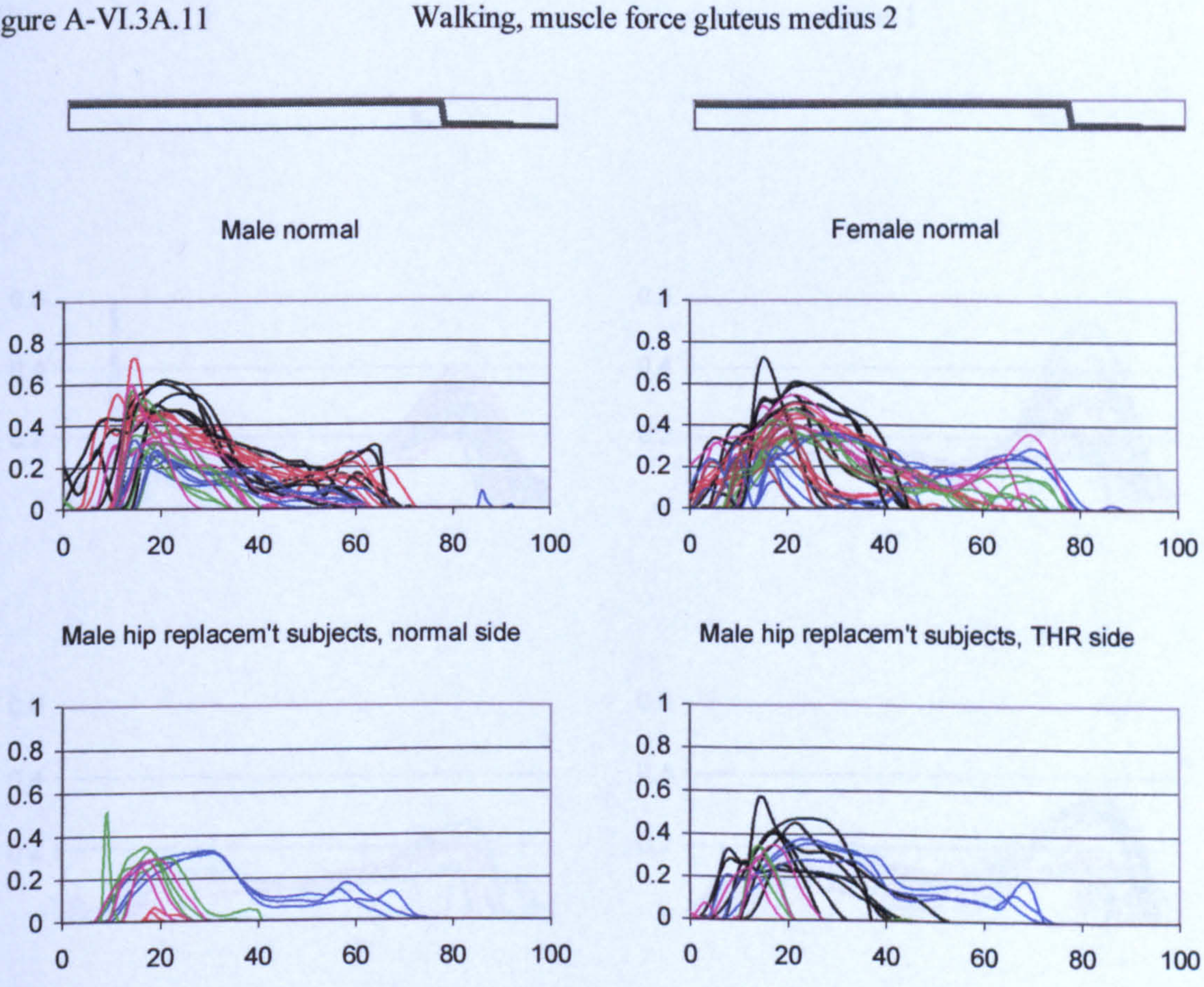

Figure A-VI.3A.12 Walking, muscle force gluteus medius 3

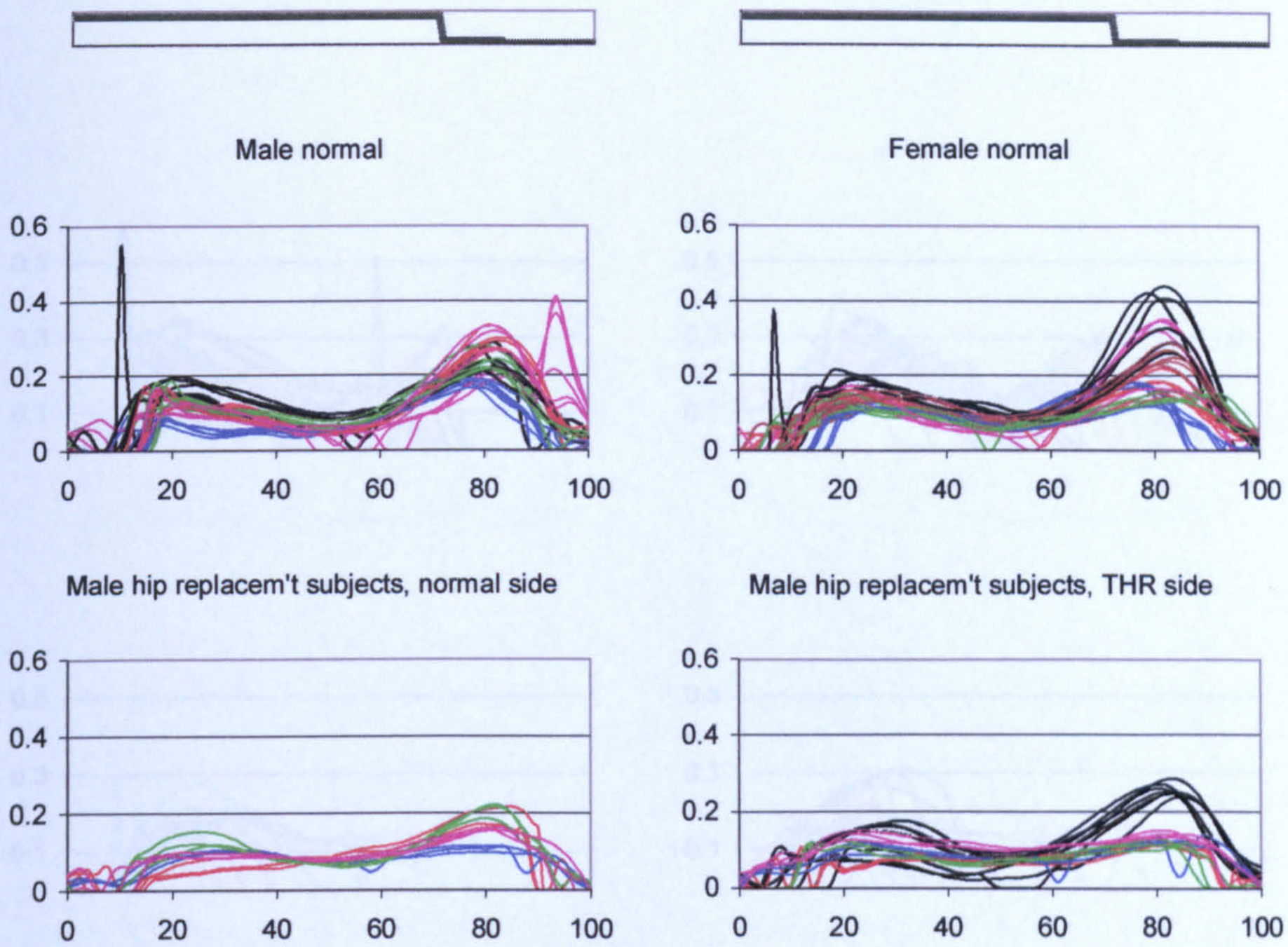

Figure A-VI.3A.13 Walking, muscle force gluteus minimus 1

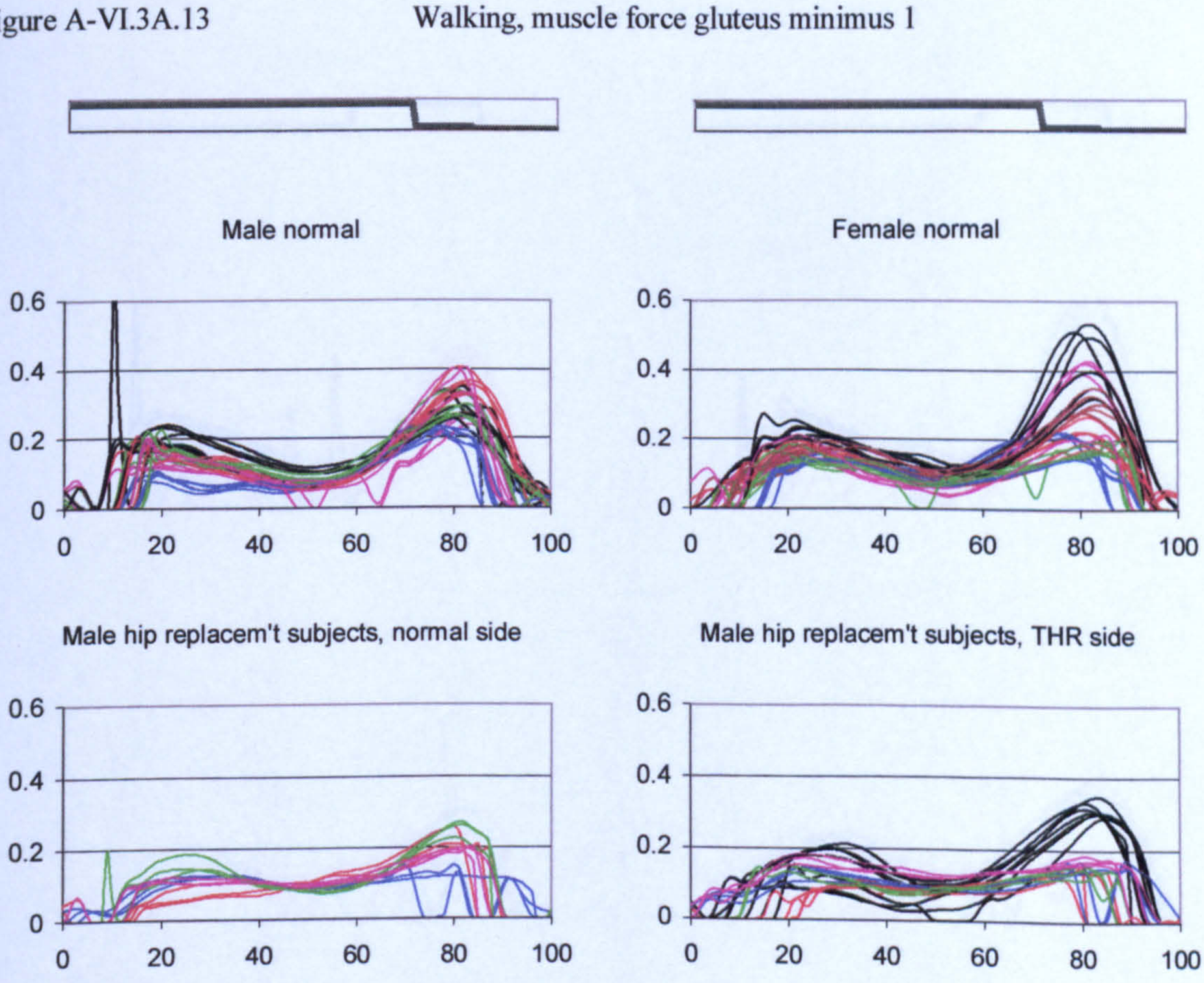

Figure A-VI.3A.14 Walking, muscle force gluteus minimus 2

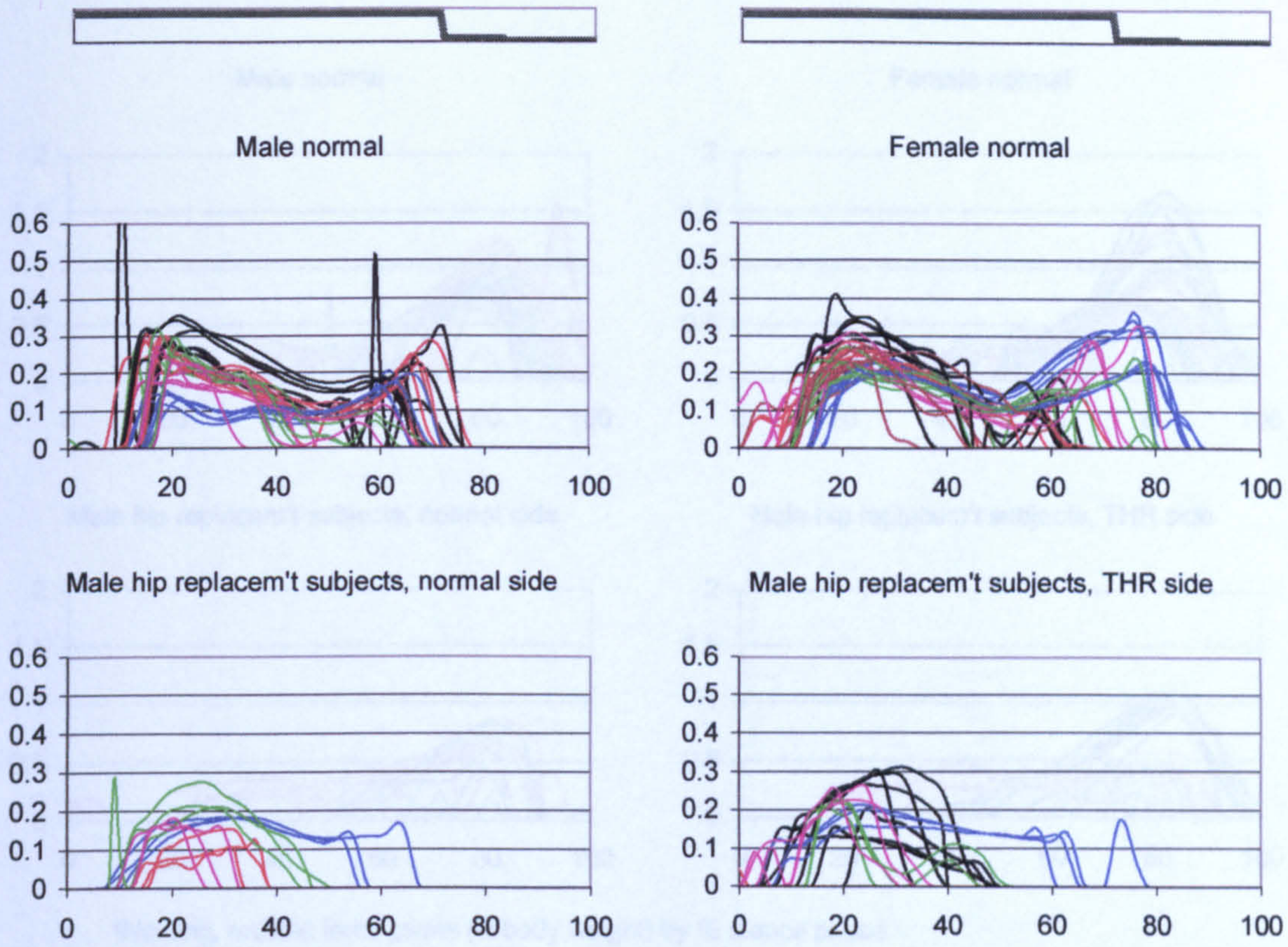

Figure A-VI.3A.15 Walking, muscle force gluteus minimus 3

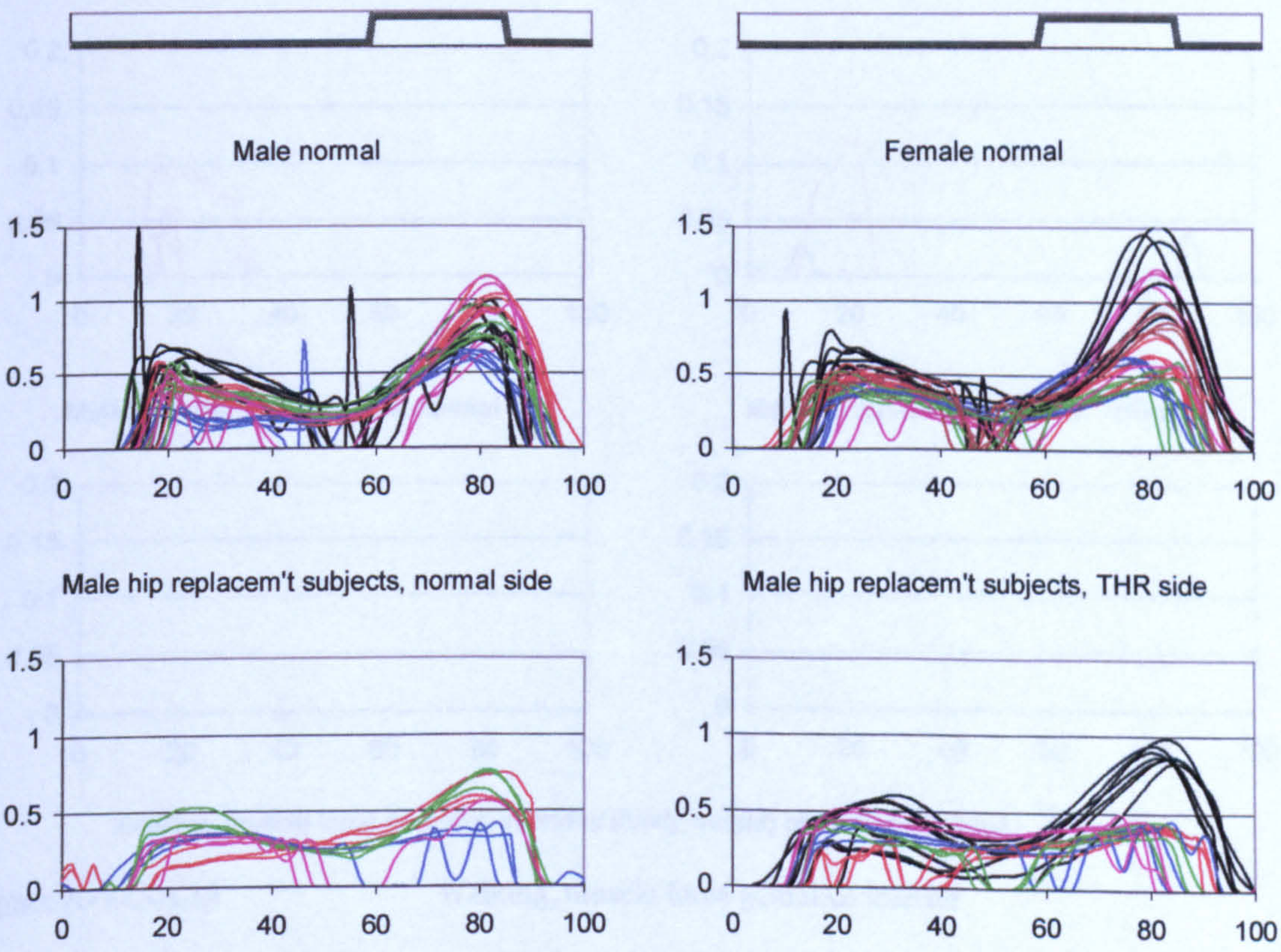

Figure A-VI.3A.16 Walking, muscle force iliacus

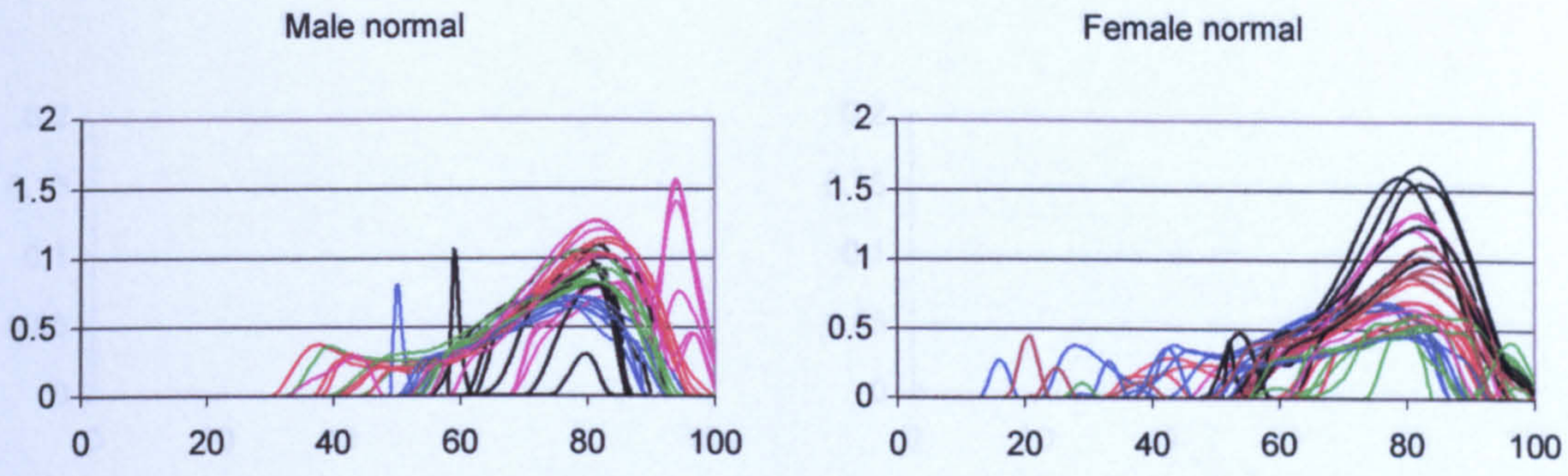

Figure A-VI.3A.17 Walking, muscle force psoas

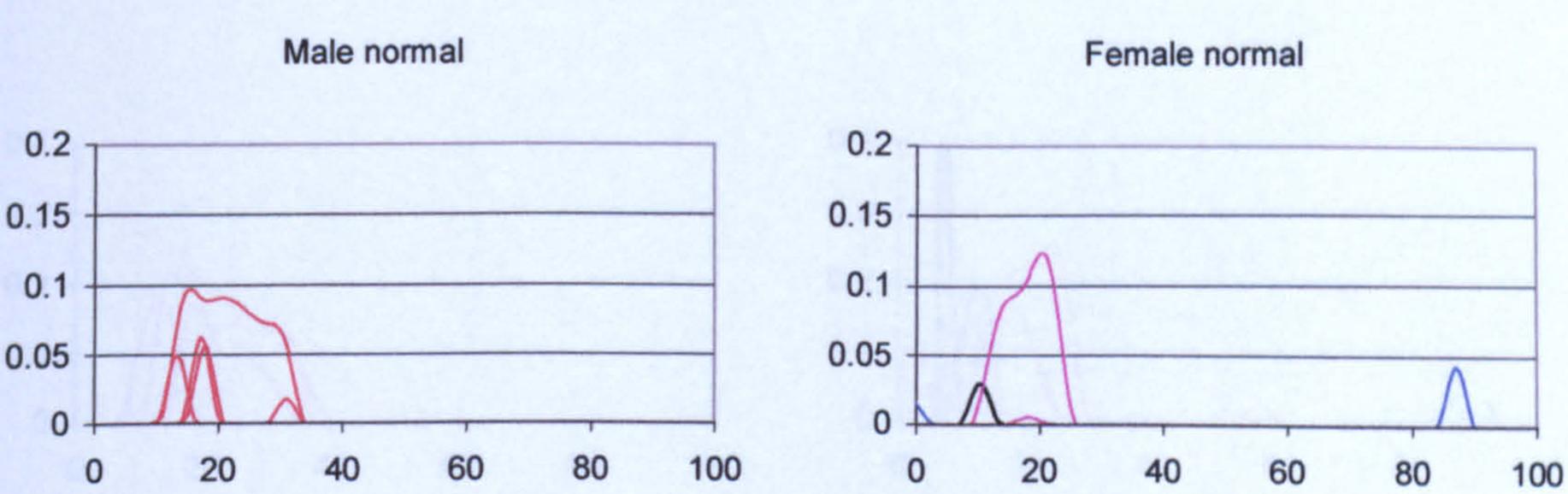

Figure A-VI.3A.18 Walking, muscle force gemellus inferior

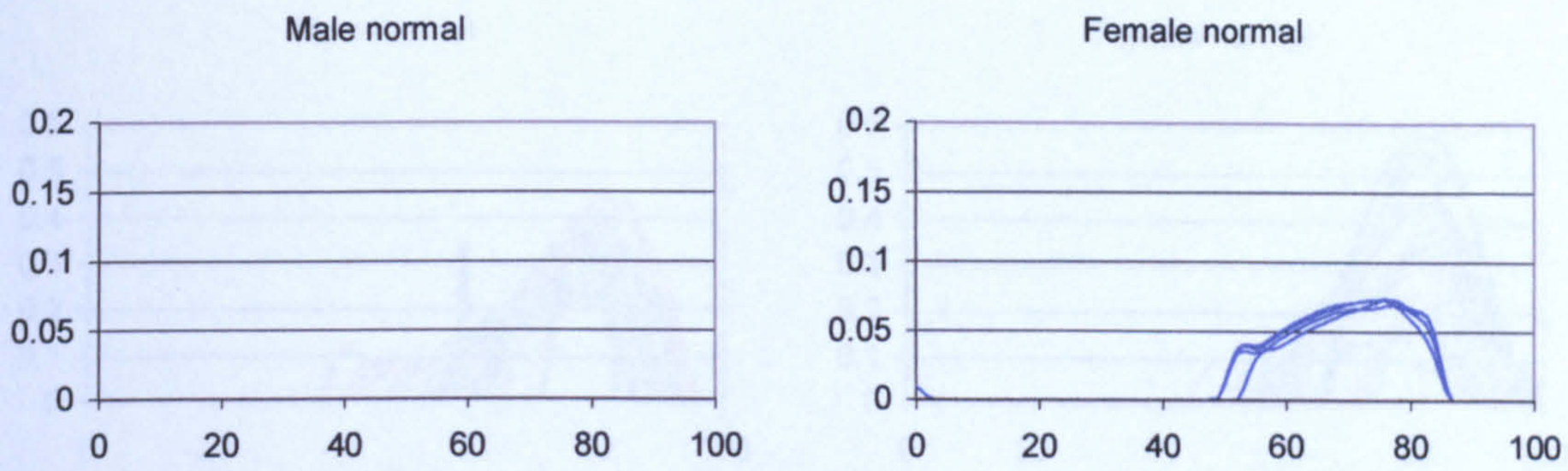

Figure A-VI.3A.19 Walking, muscle force obturator externus

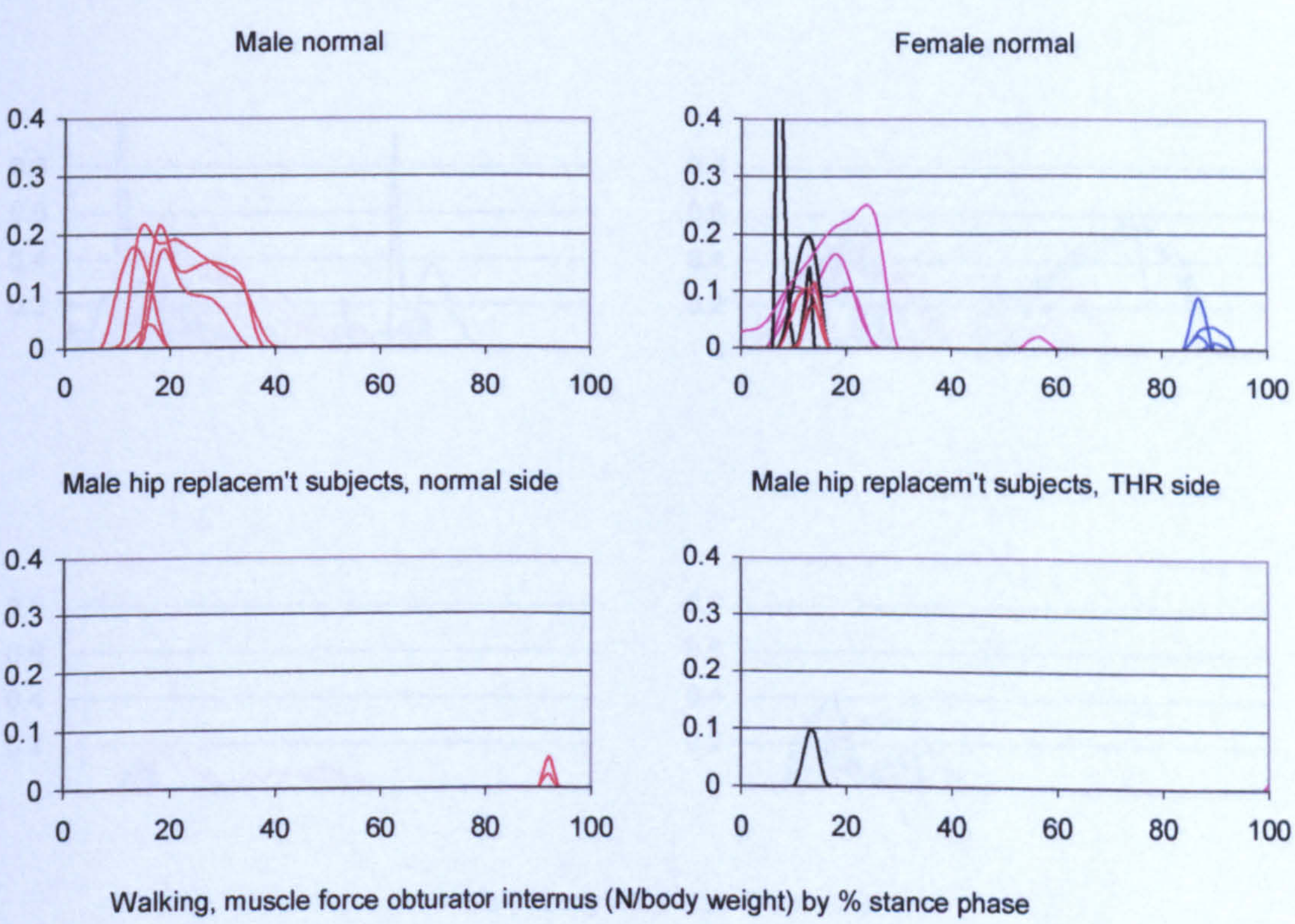

Figure A-VI.3A.20 Walking, muscle force obturator internus

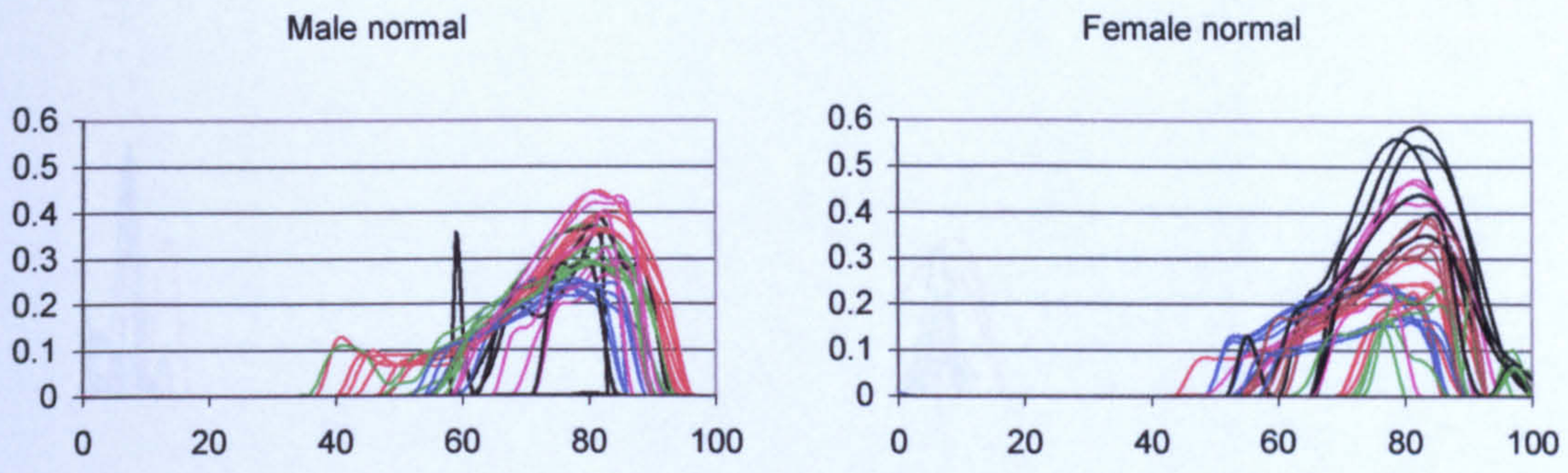

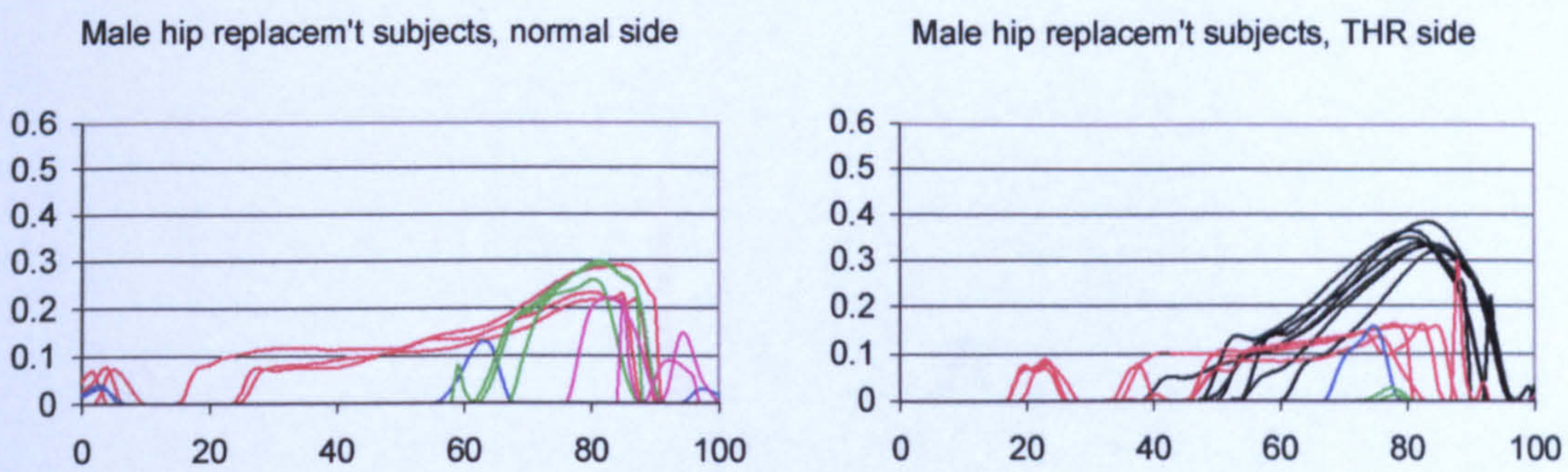

Figure A-VI.3A.21 Walking, muscle force pectineus

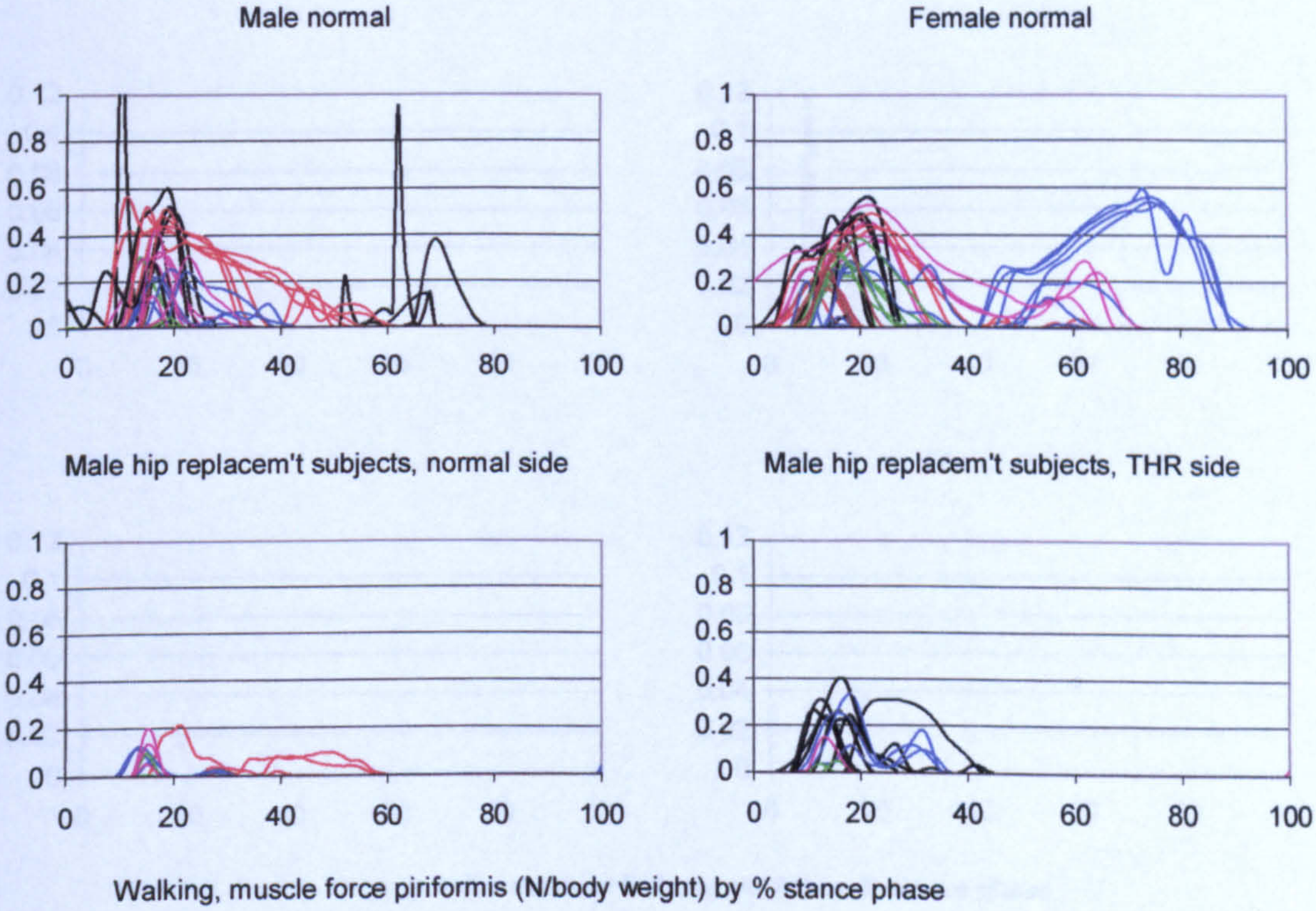

Figure A-VI.3A.22 Walking, muscle force piriformis

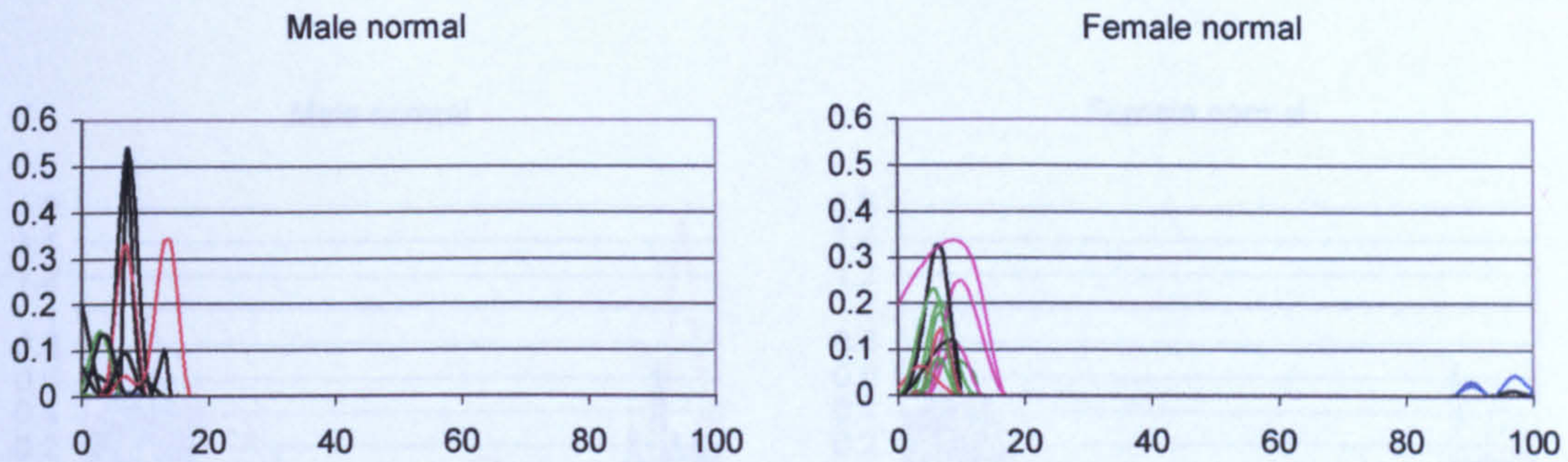

Figure A-VI.3A.23 Walking, muscle force quadratus femoris

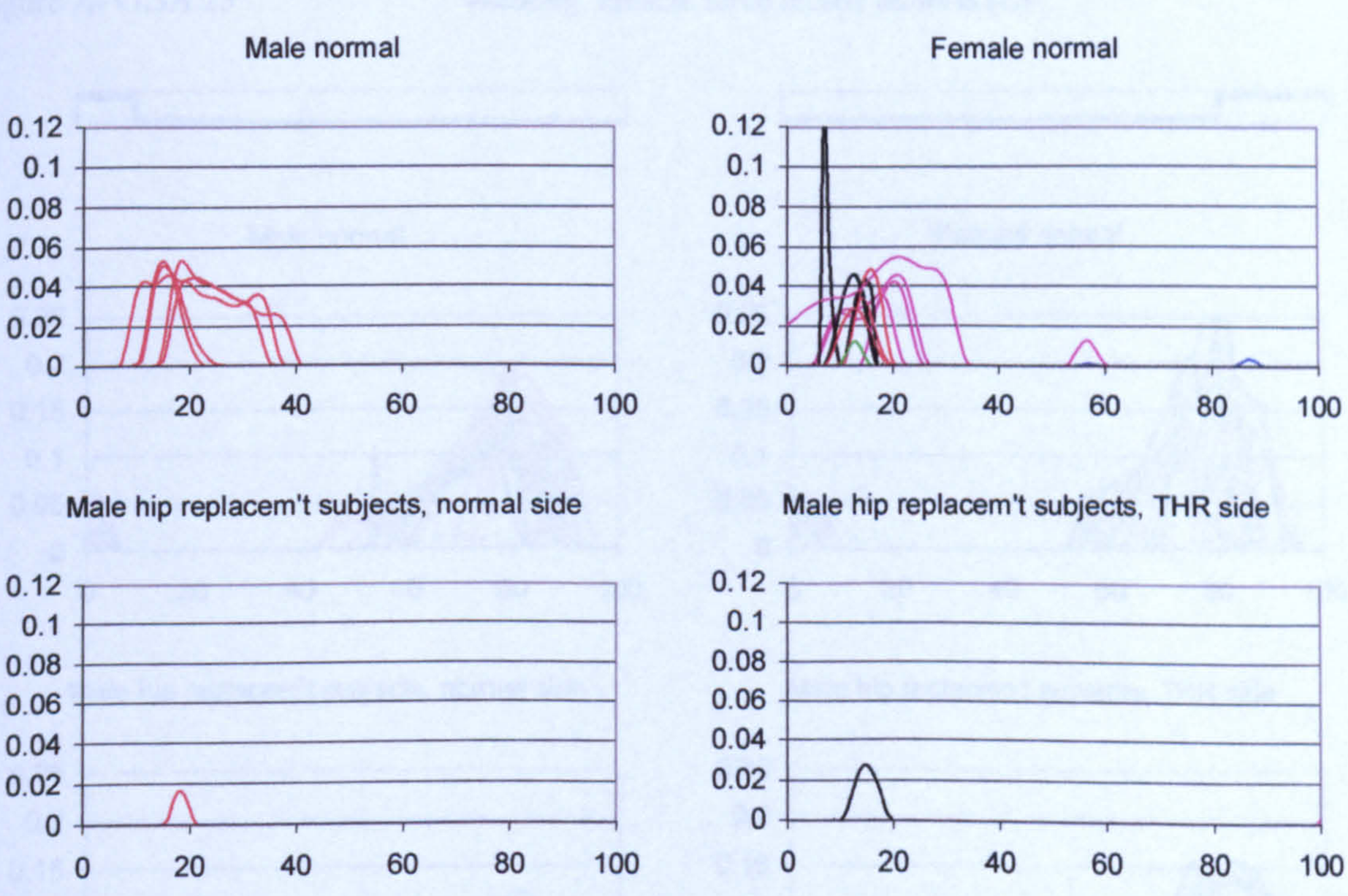

Figure A-VI.3A.24 Walking, muscle force gemellus superior

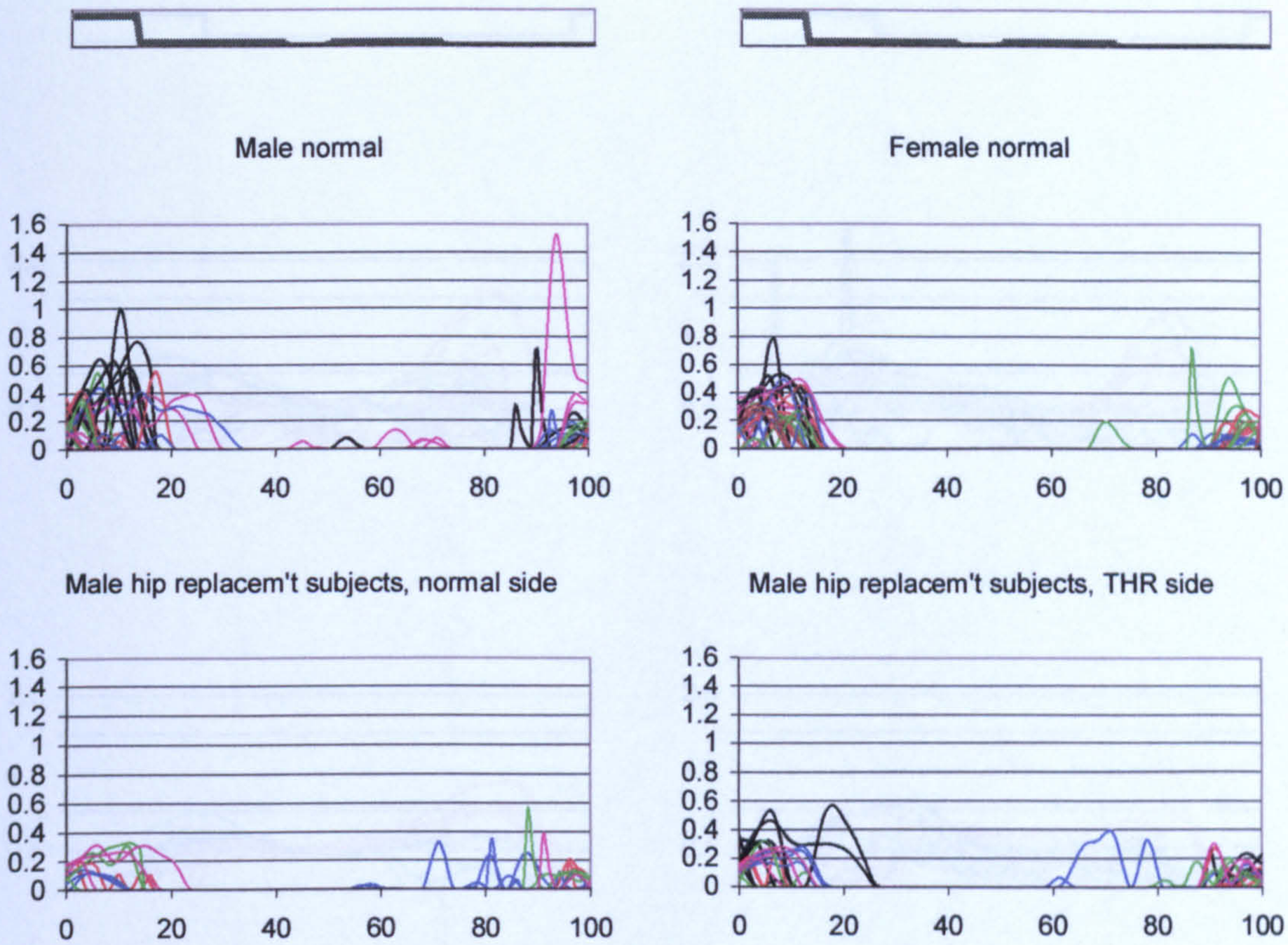

Walking, muscle force biceps femoris (L) (N/body weight) by % stance phase

Figure A-VI.3A.25 Walking, muscle force biceps femoris (L)

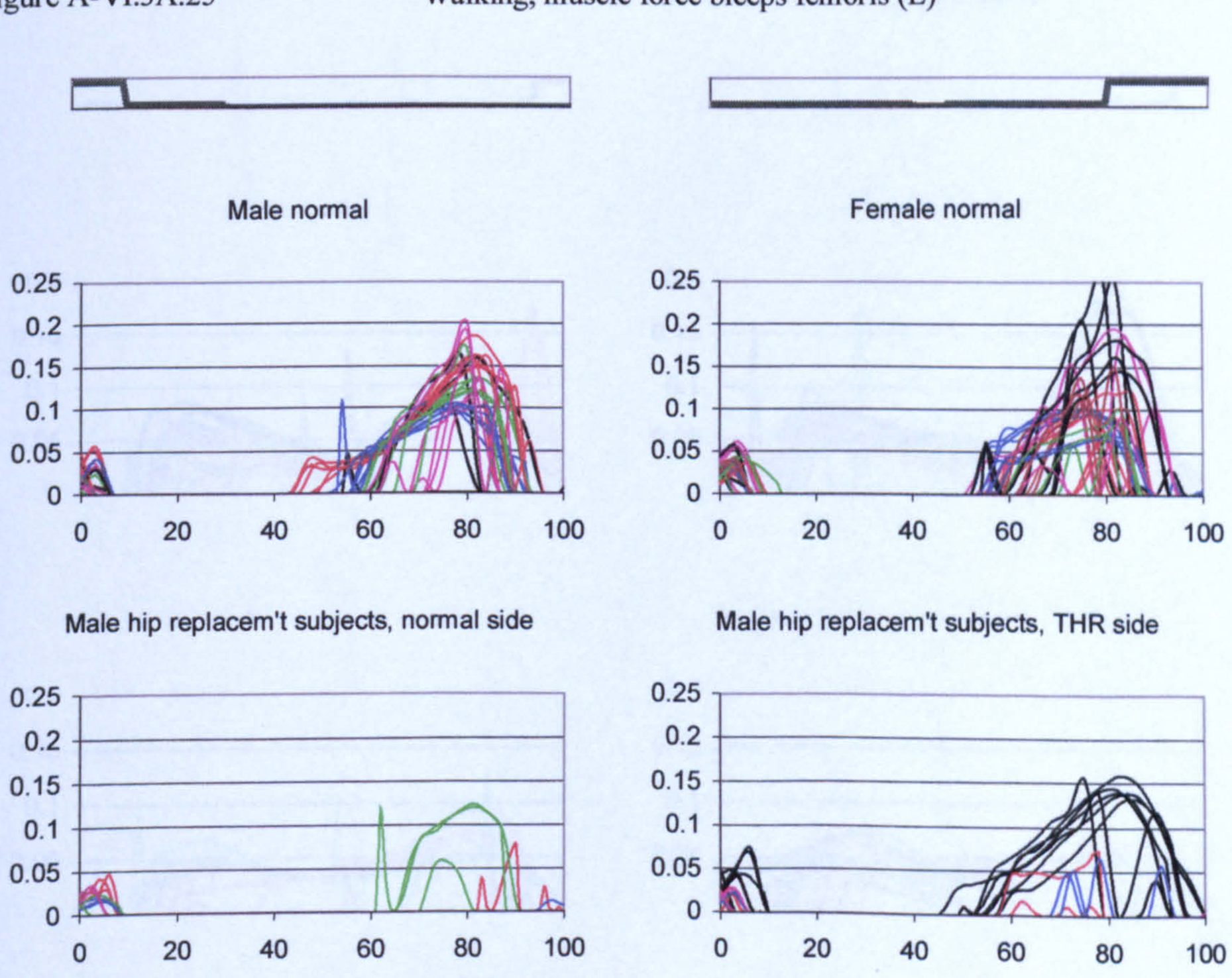

Walking, muscle force gracilis (N/body weight) by % stance phase

Figure A-VI.3A.26 Walking, muscle force gracilis

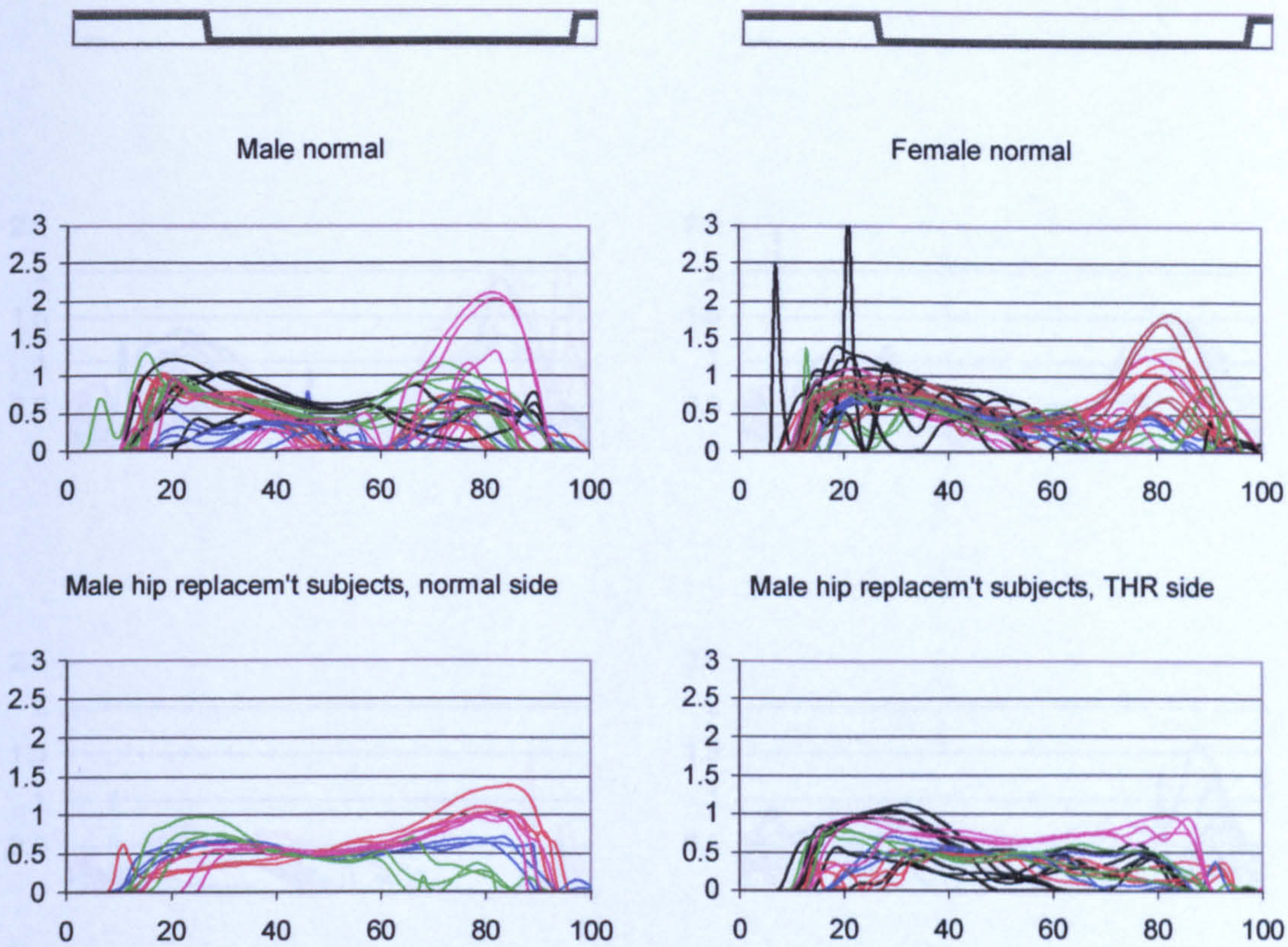

Walking, muscle force rectus femoris (upper part) (N/body weight) by % stance phase

Figure A-VI.3A.27 Walking, muscle force rectus femoris (upper part)

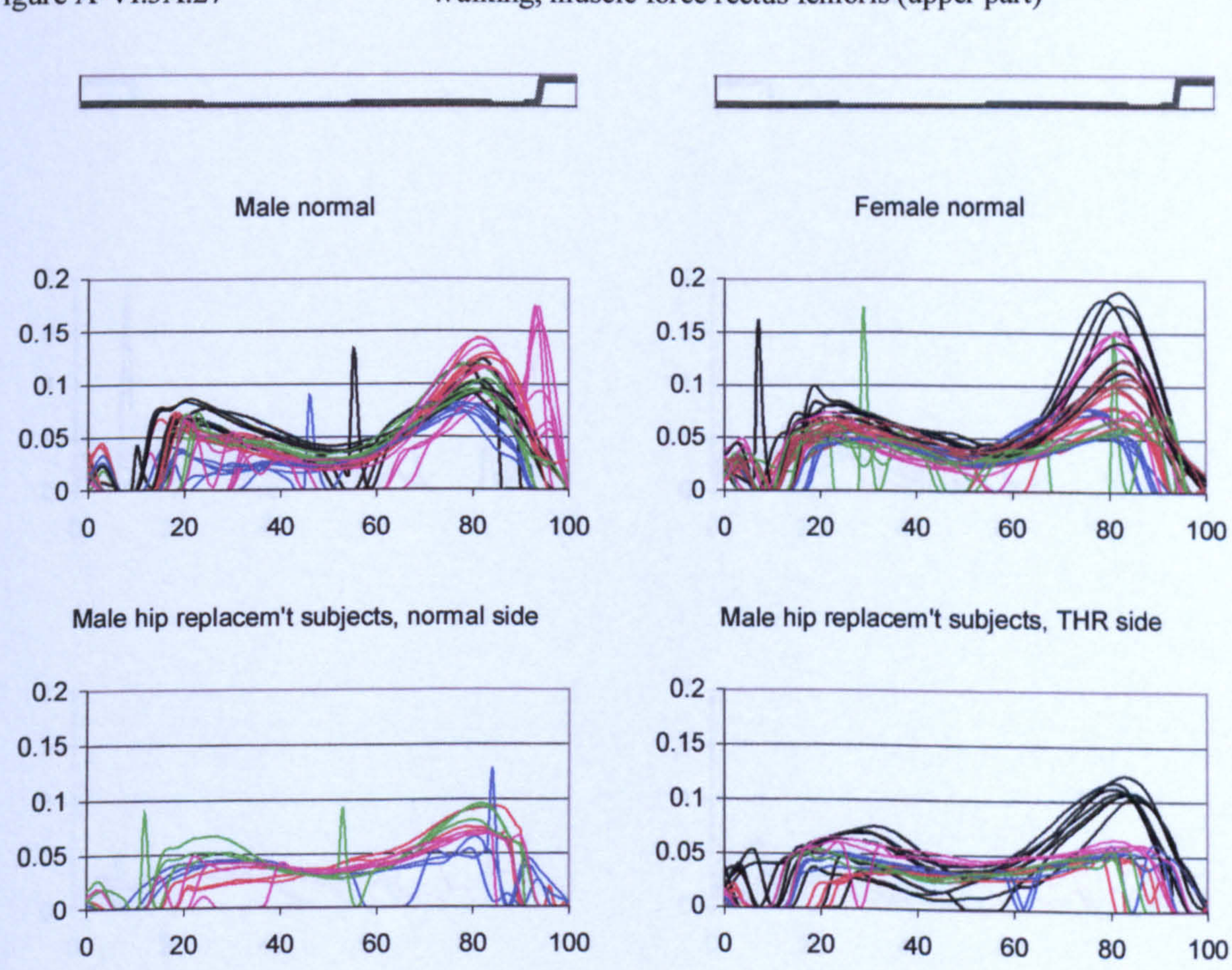

Walking, muscle force sartorius (N/body weight) by % stance phase

Figure A-VI.3A.28 Walking, muscle force sartorius

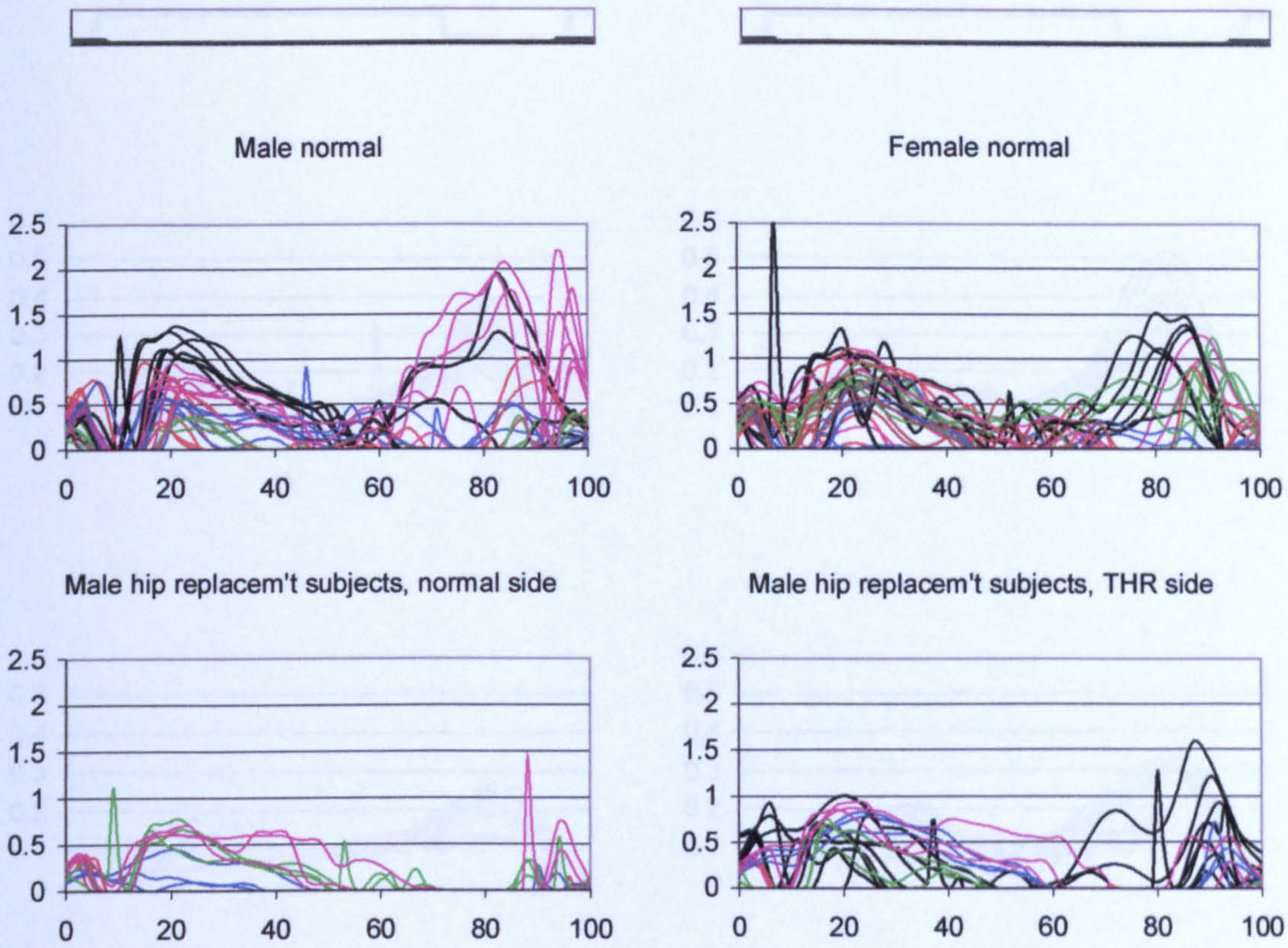

Figure A-VI.3A.29 Walking, muscle force semimembranosus

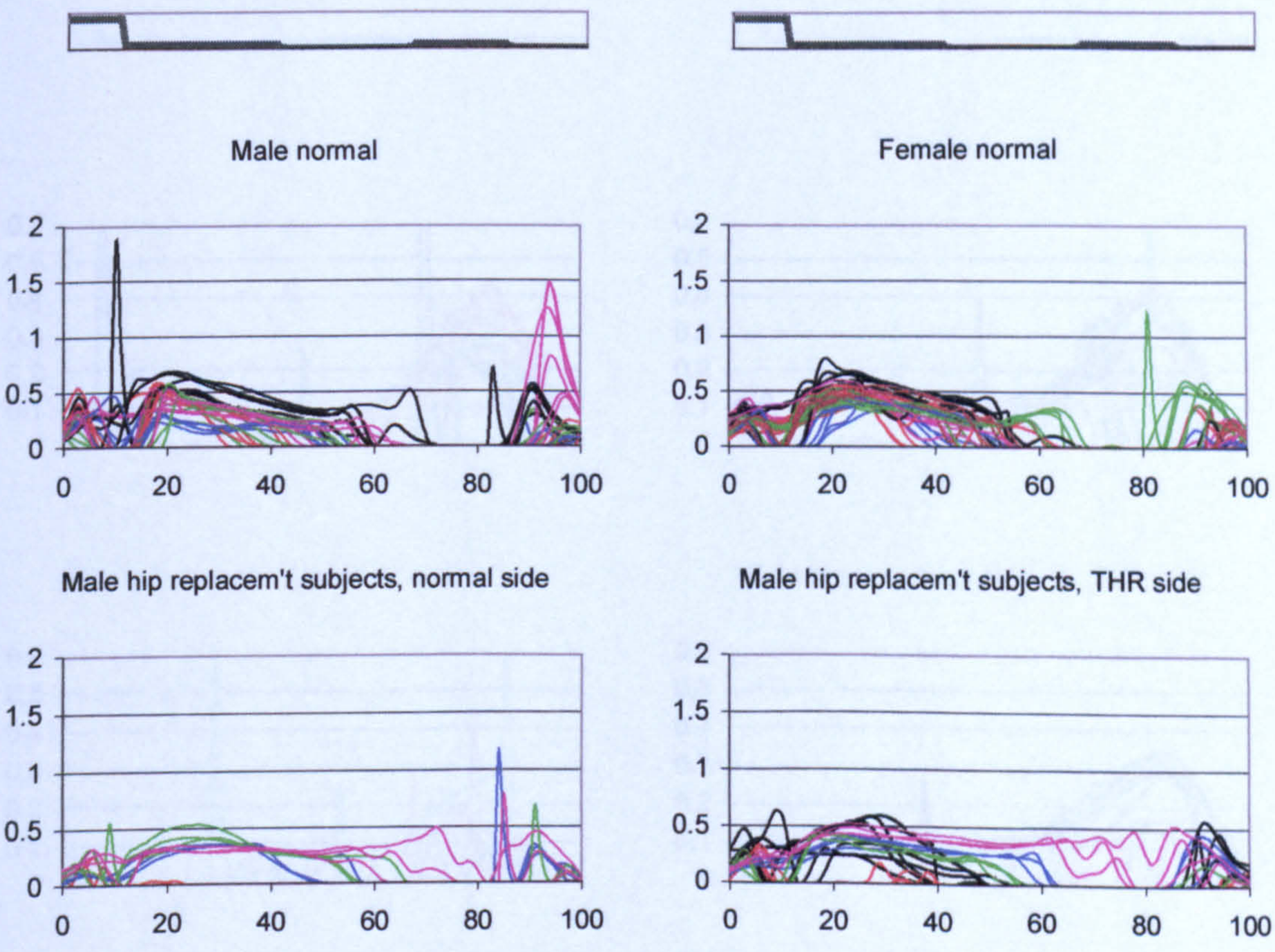

Figure A-VI.3A.30 Walking, muscle force semitendinosus

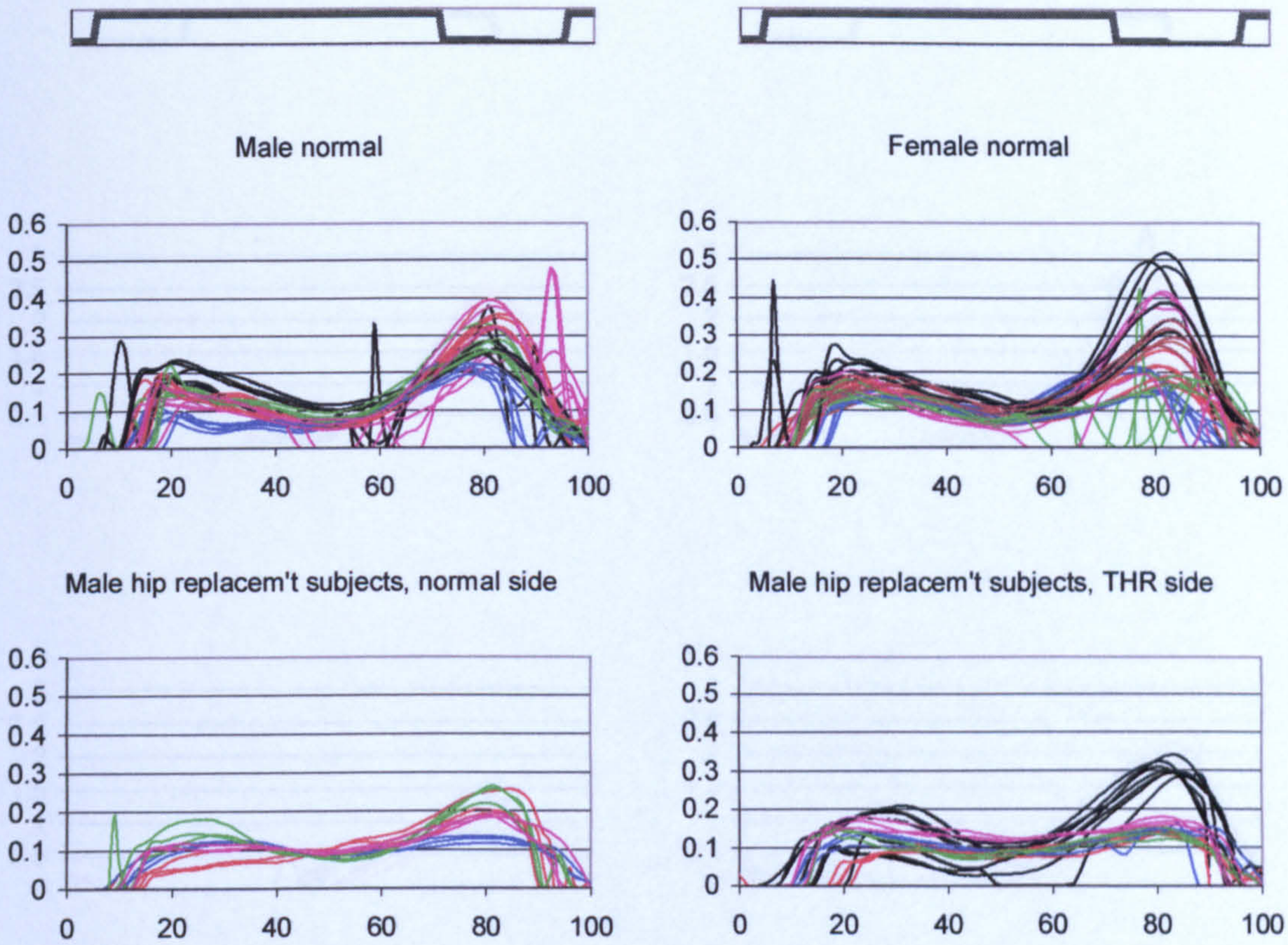

Figure A-VI.3A.31 Walking, muscle force tensor facia lata

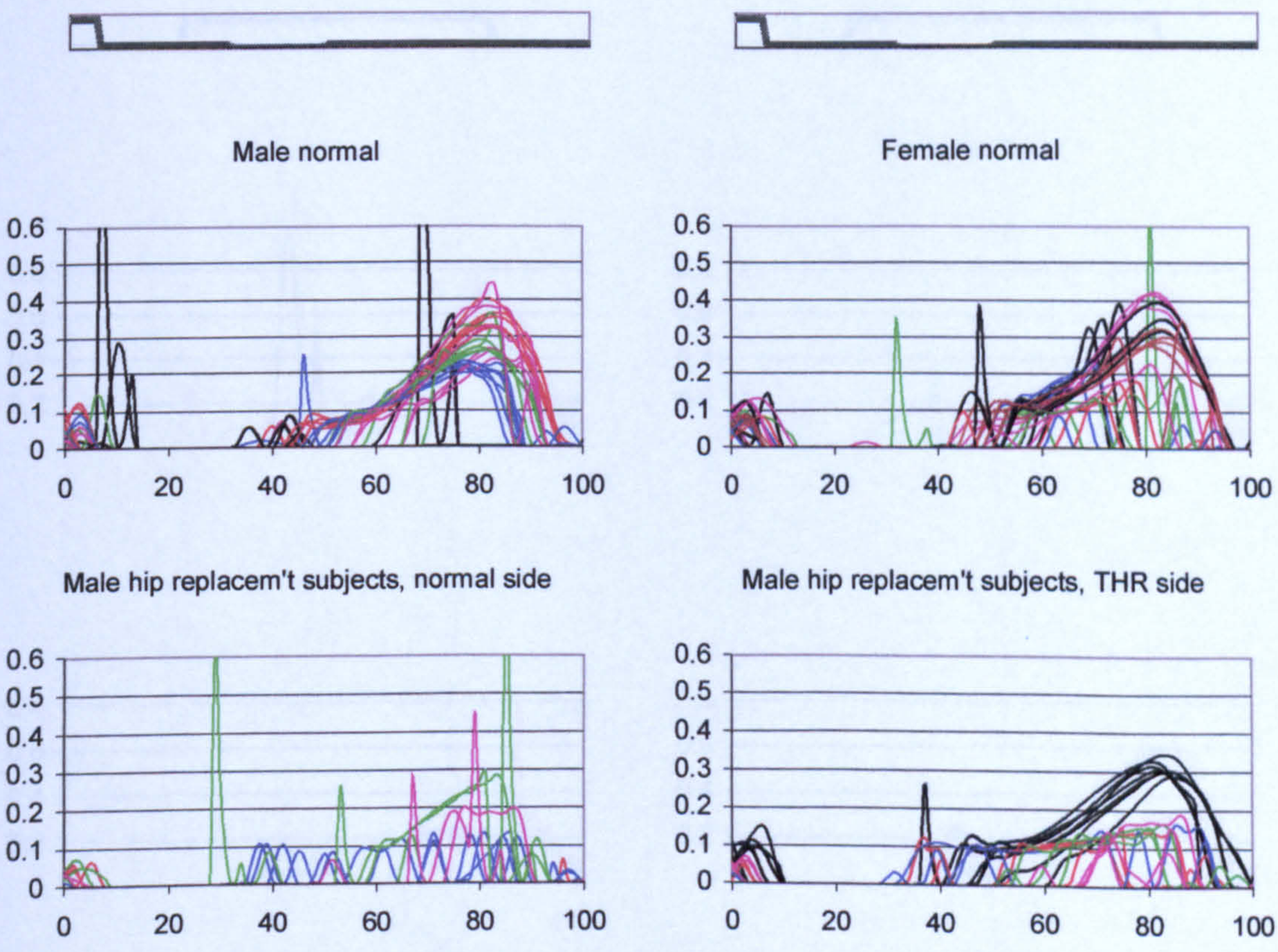

Figure A-VI.3A.32 Walking, muscle force biceps femoris (S)

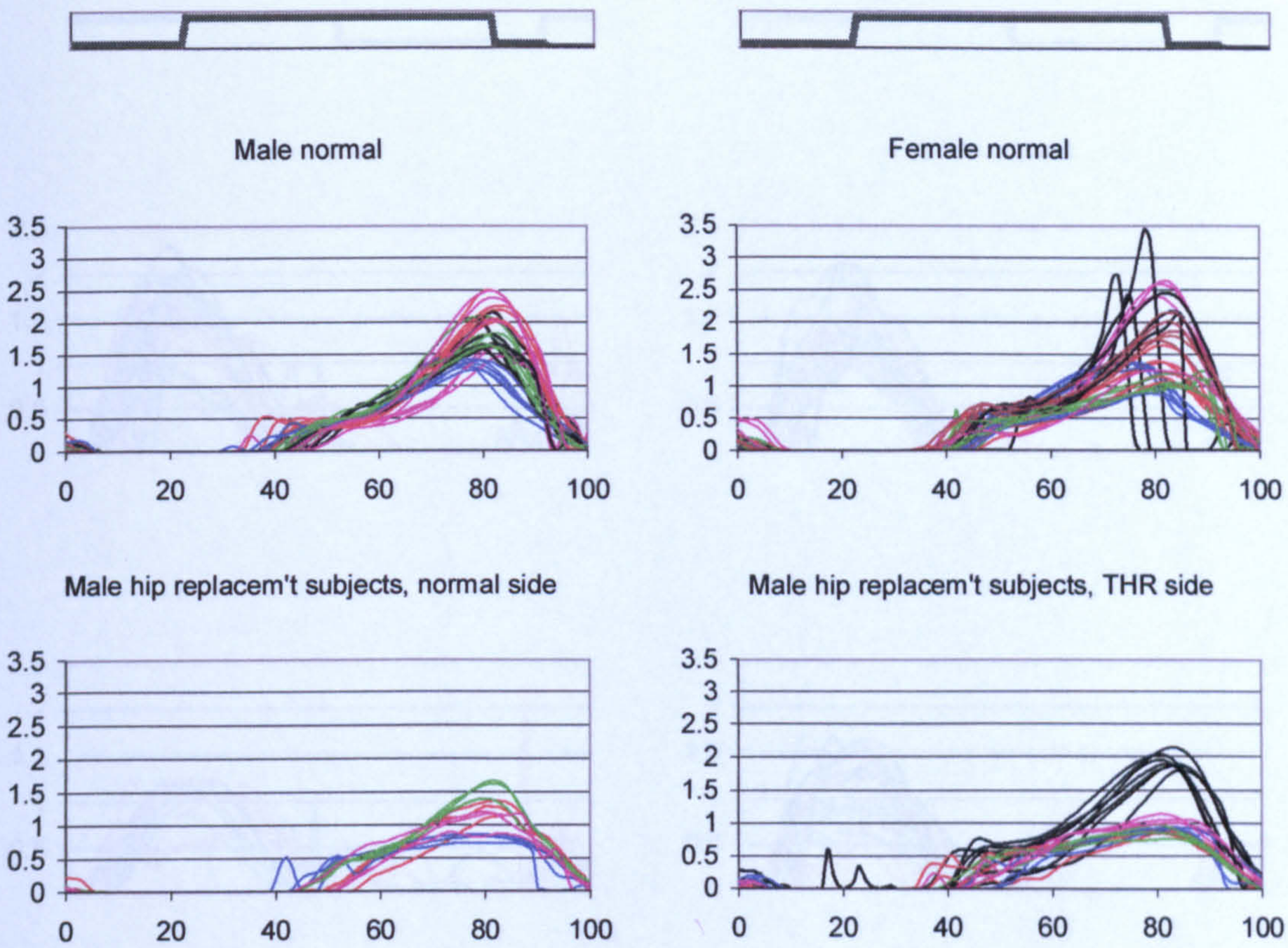

Figure A-VI.3A.33 Walking, muscle force gastrocnemius (M)

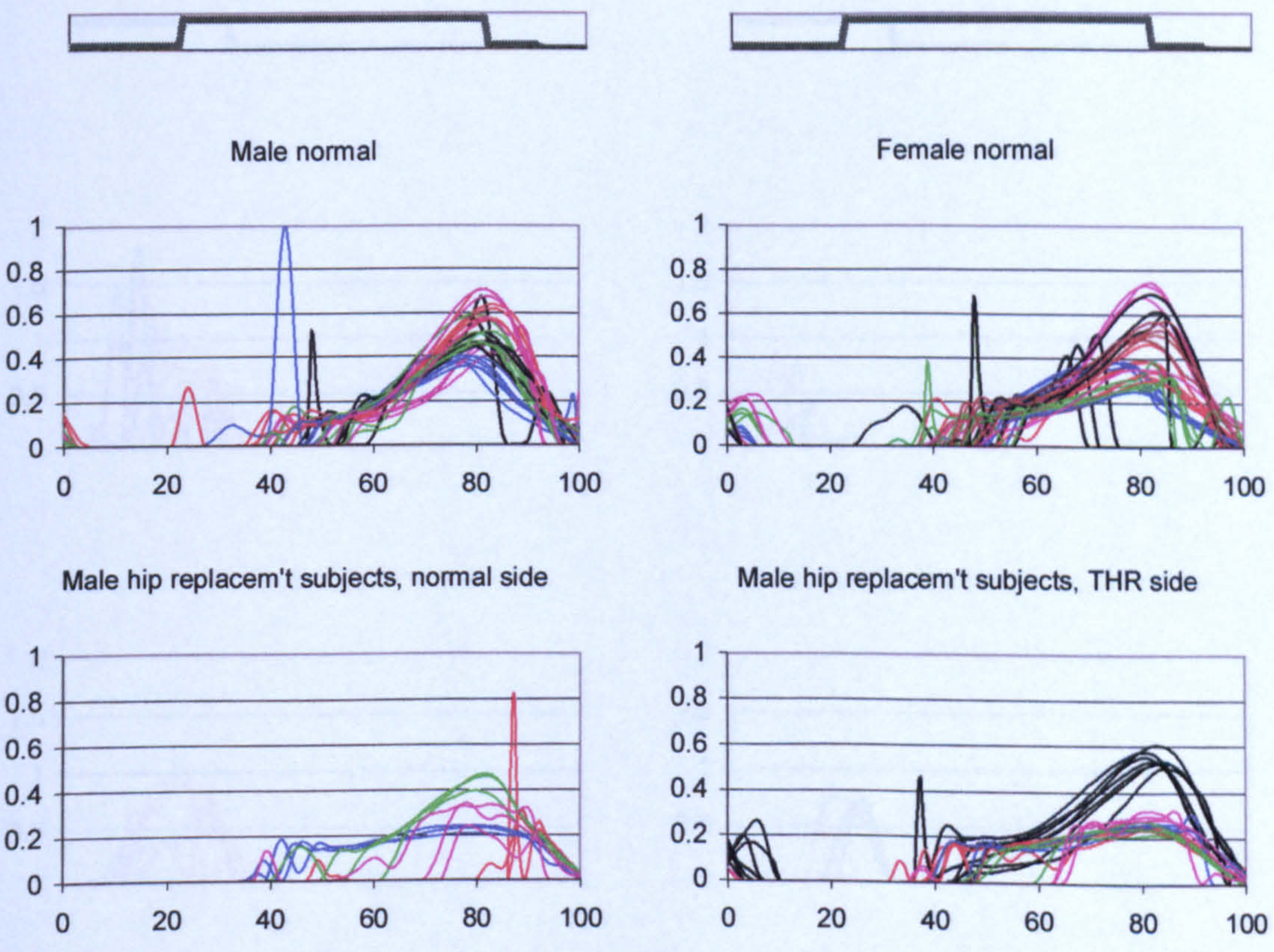

Figure A-VI.3A.34 Walking, muscle force gastrocnemius (L)

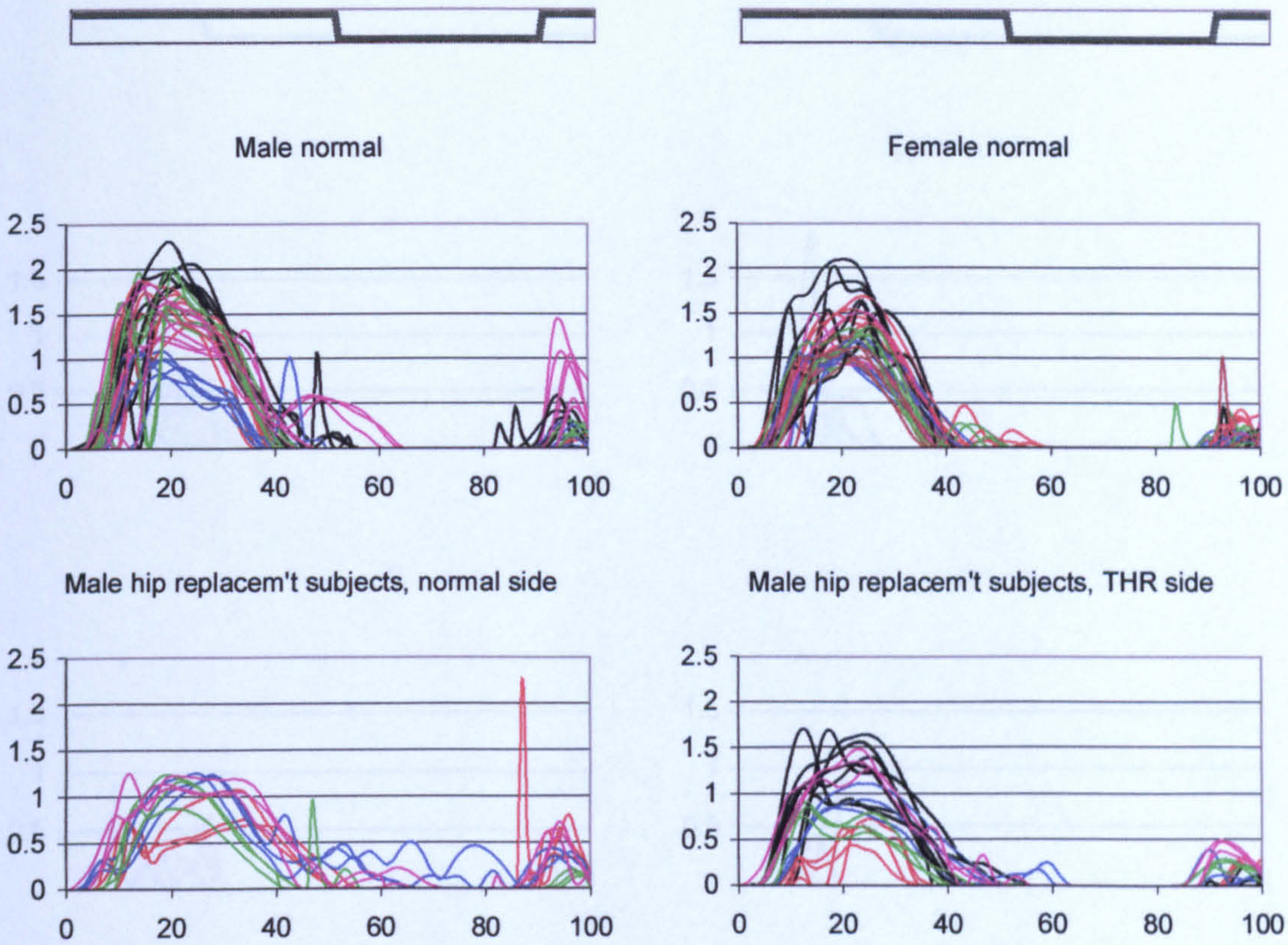

Walking, muscle force vastus intermedius (N/body weight) by % stance phase

Figure A-VI.3A.35 Walking, muscle force vastus intermedius

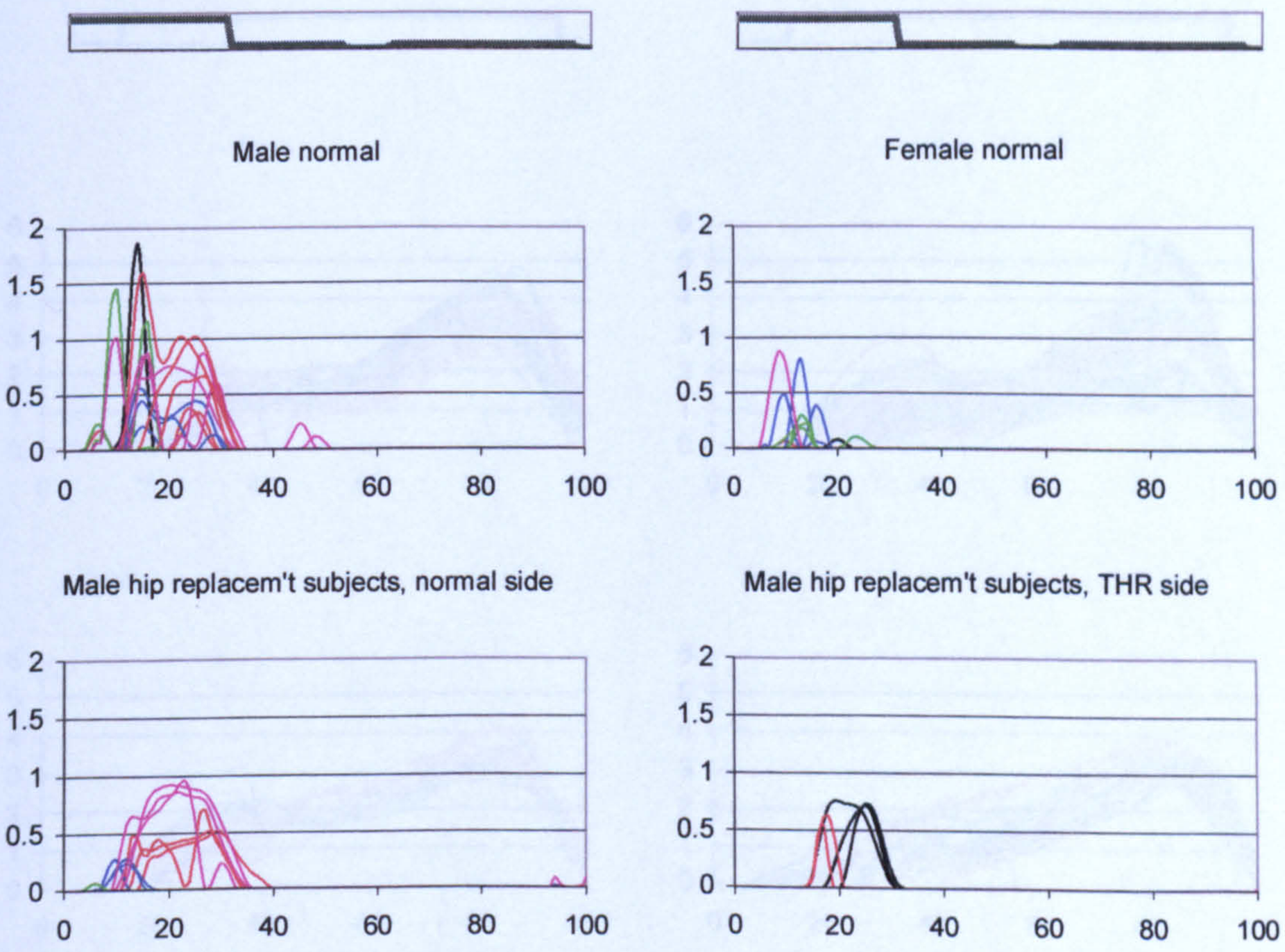

Walking, muscle force vastus lateralis (N/body weight) by % stance phase

Figure A-VI.3A.36 Walking, muscle force vastus lateralis

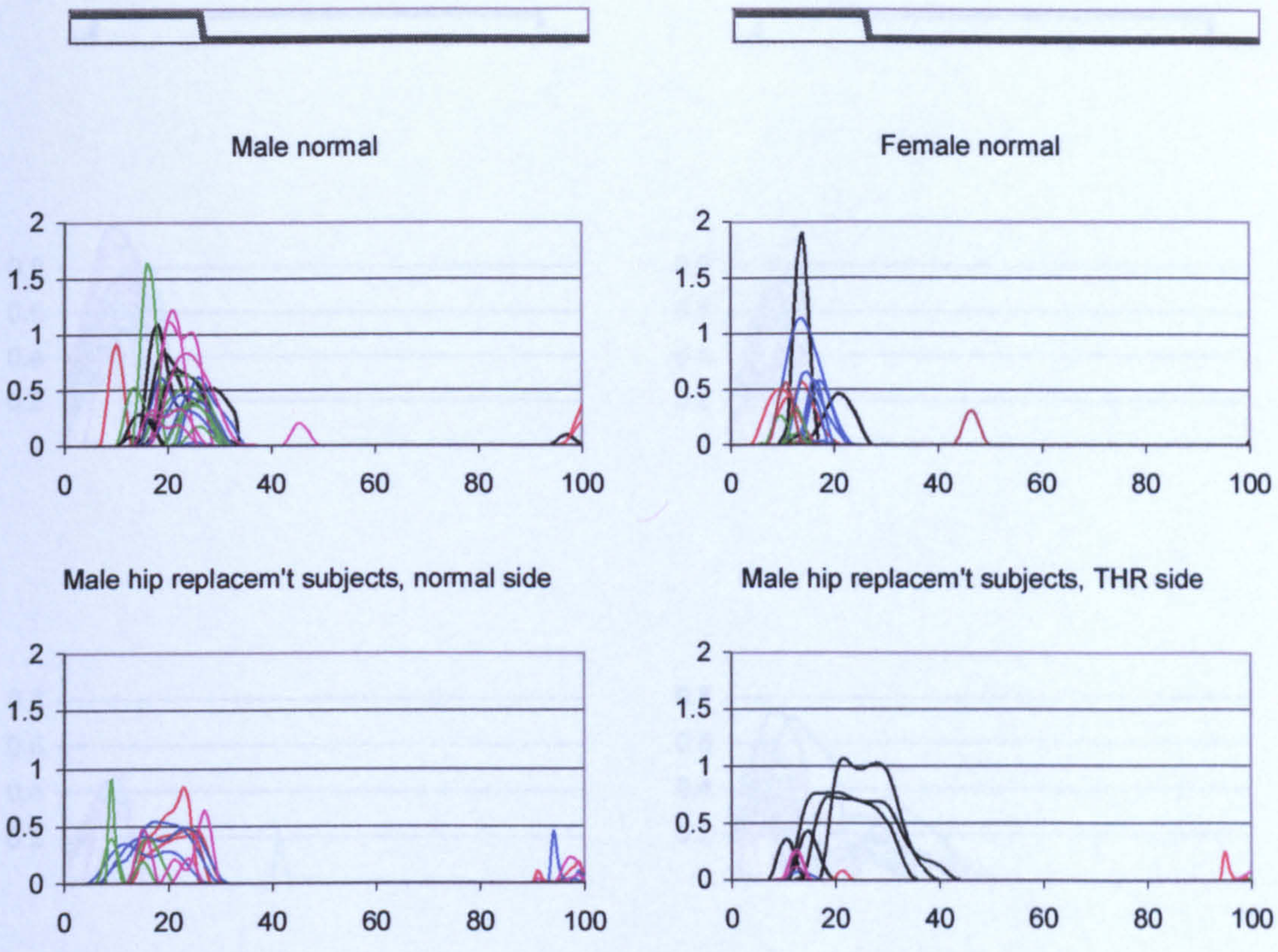

Figure A-VI.3A.37 Walking, muscle force vastus medialis

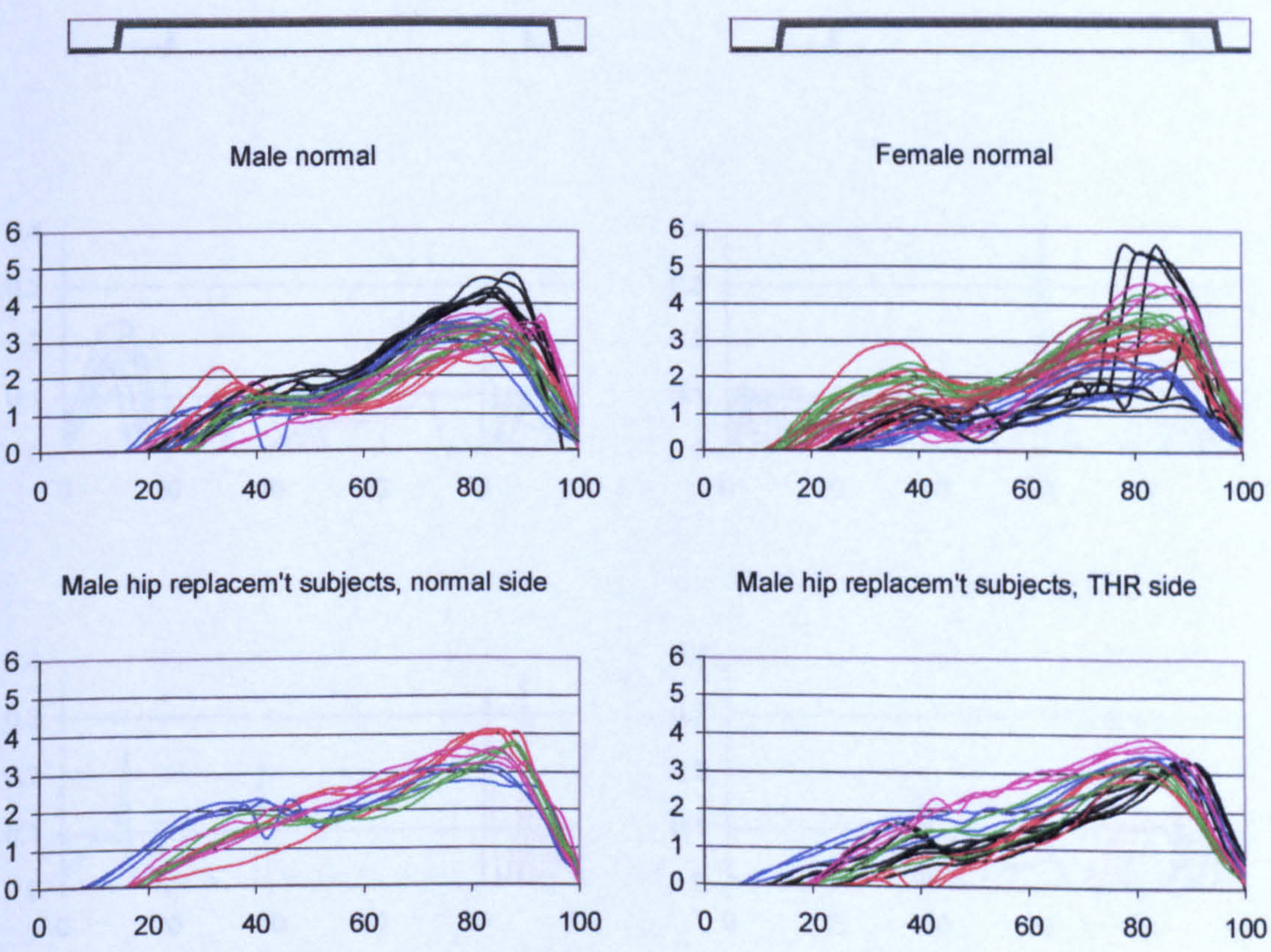

Figure A-VI.3A.38 Walking, muscle force soleus

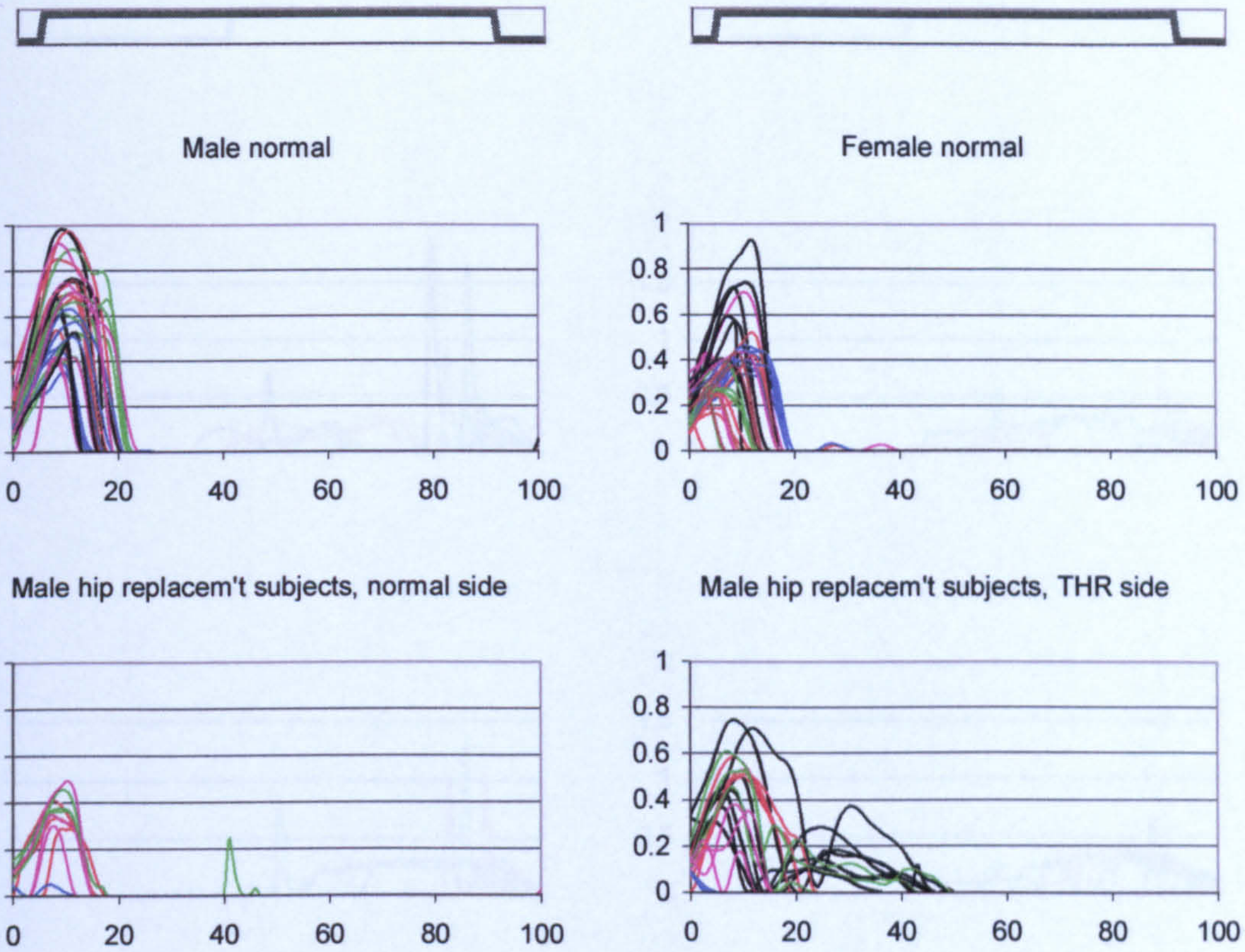

Figure A-VI.3A.39 Walking, muscle force tibialis posterior

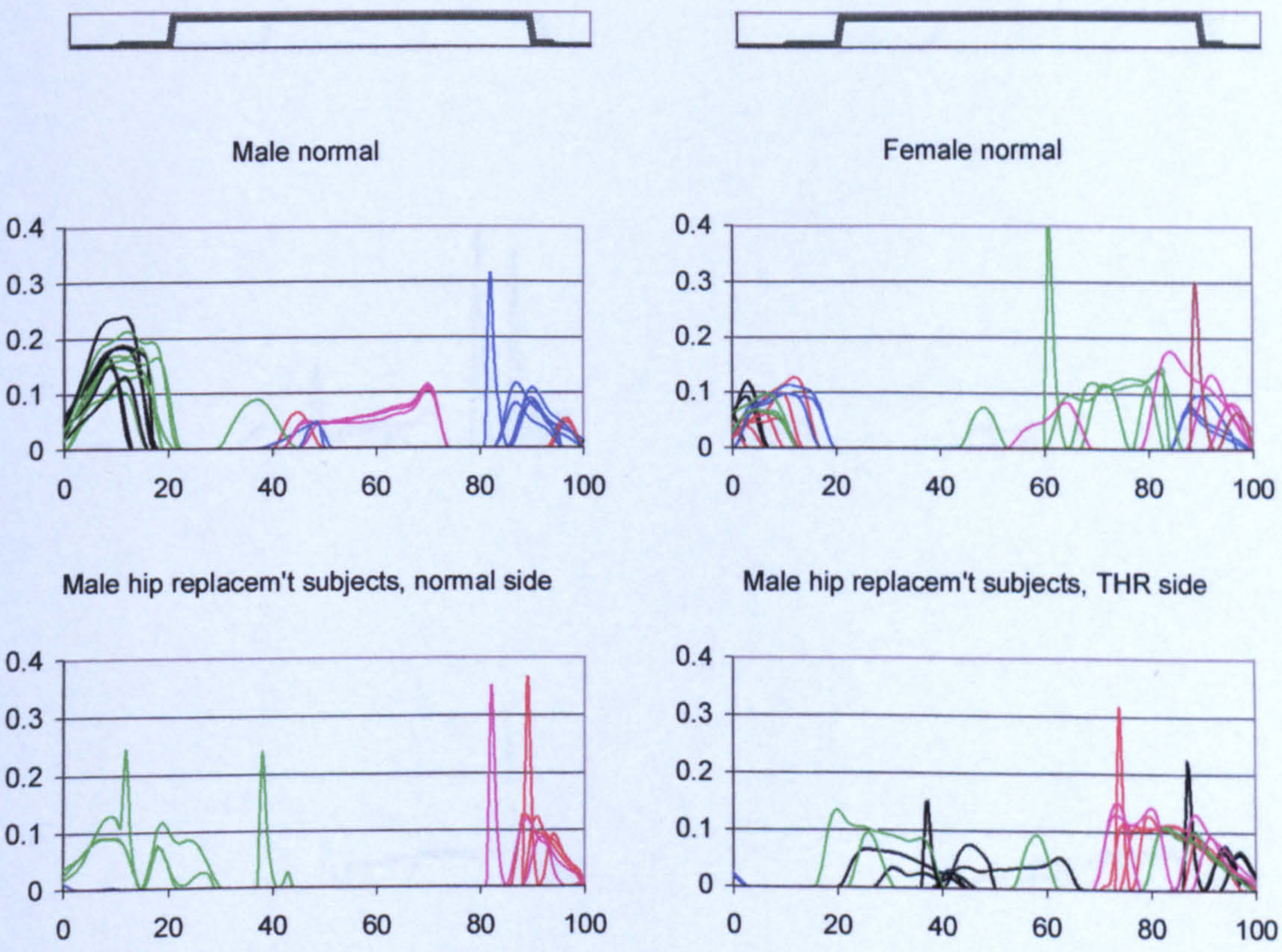

Figure A-VI.3A.40 Walking, muscle force flexor digitorum longus

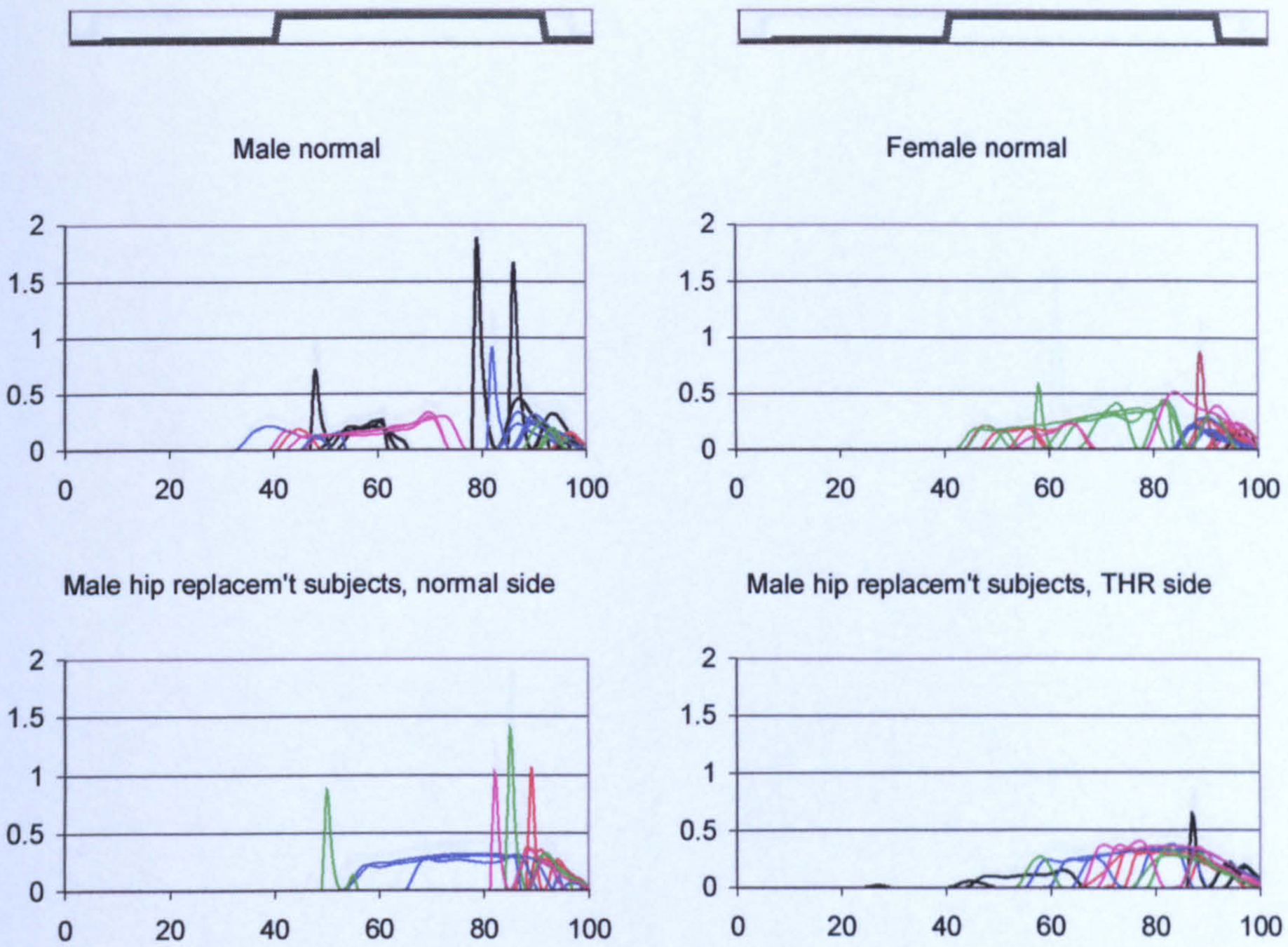

Figure A-VI.3A.41 Walking, muscle force flexor hallucis longus

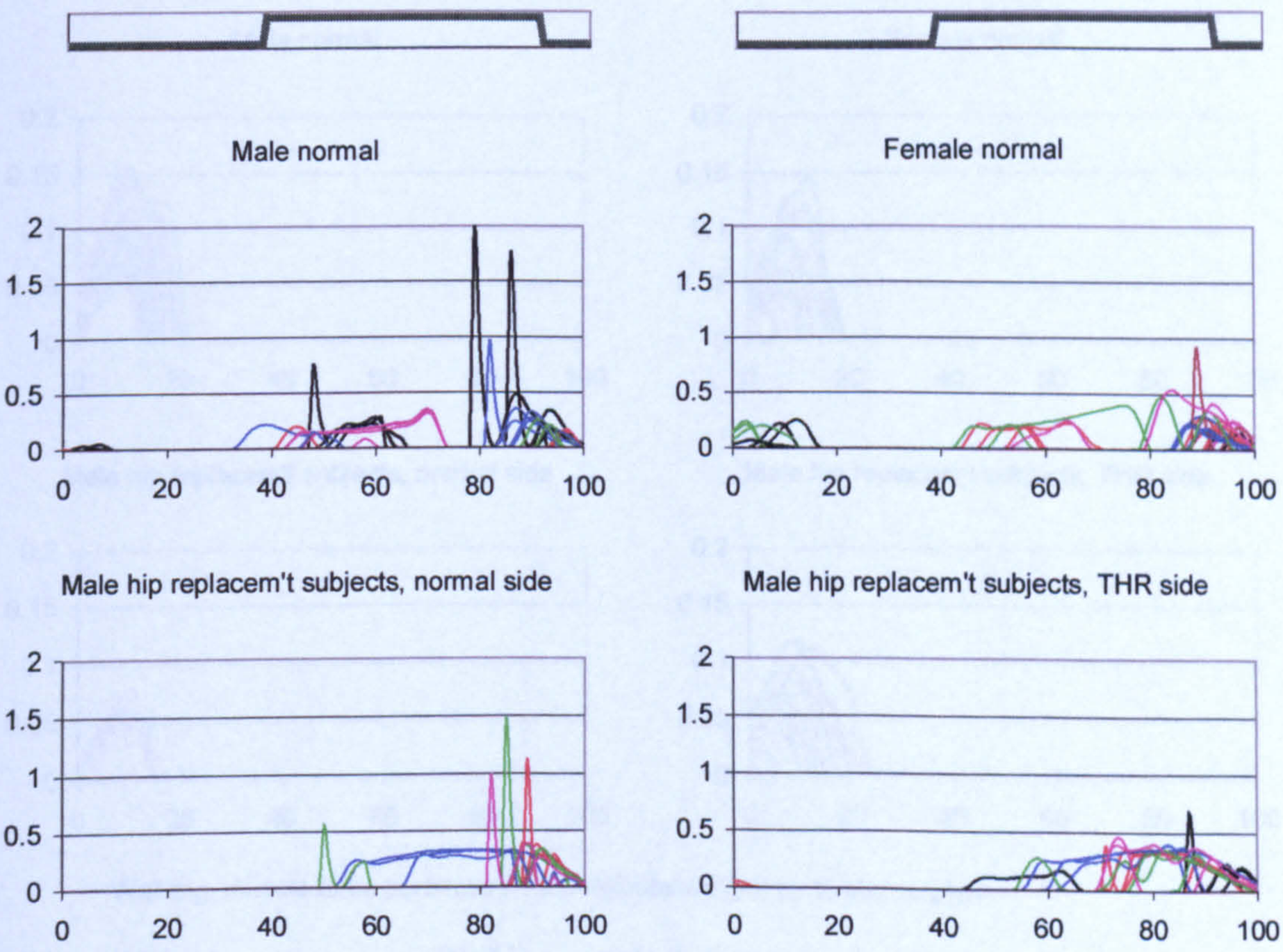

Figure A-VI.3A.42 Walking, muscle force peroneus brevis

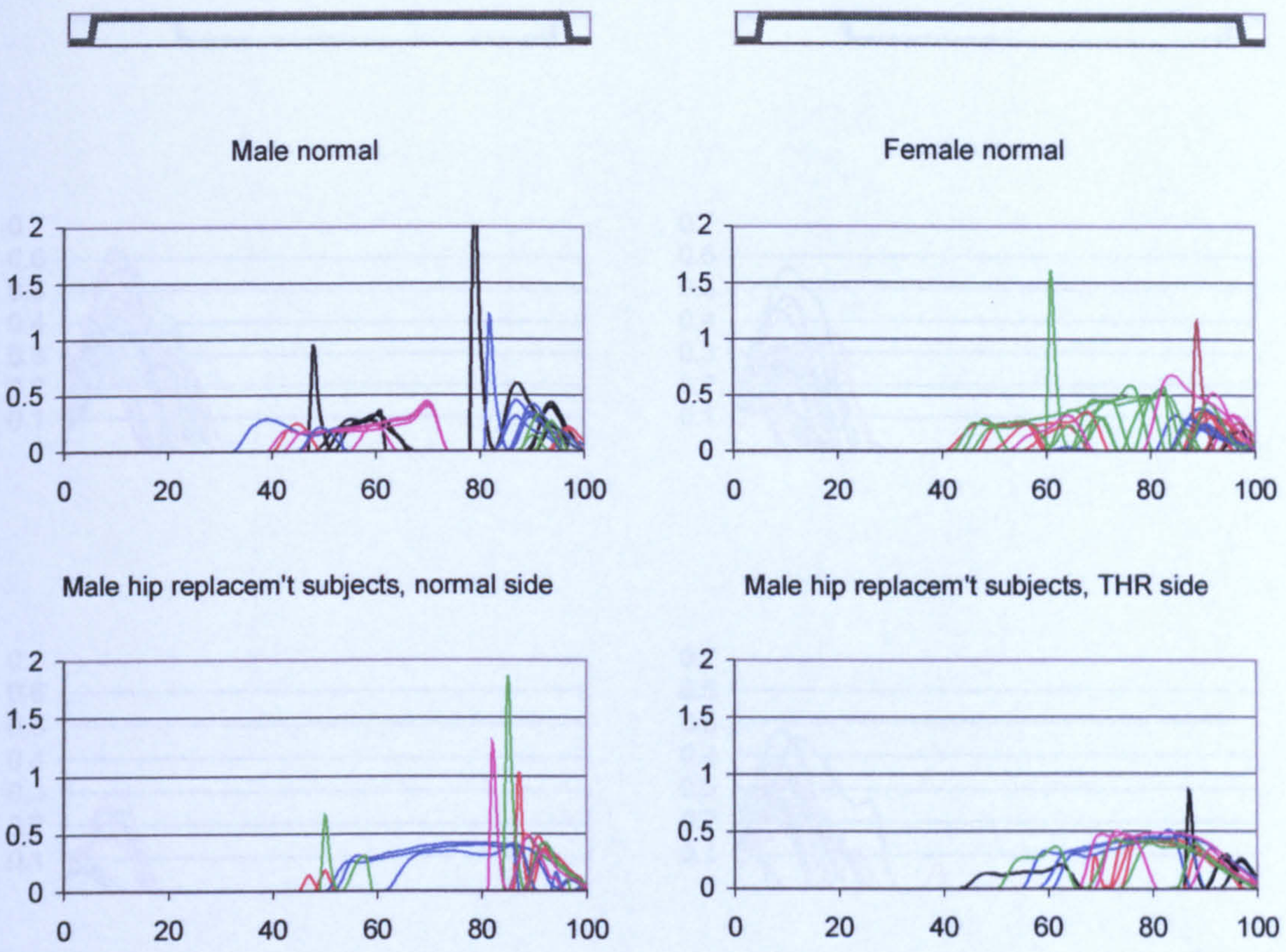

Figure A-VI.3A.43 Walking, muscle force peroneus longus

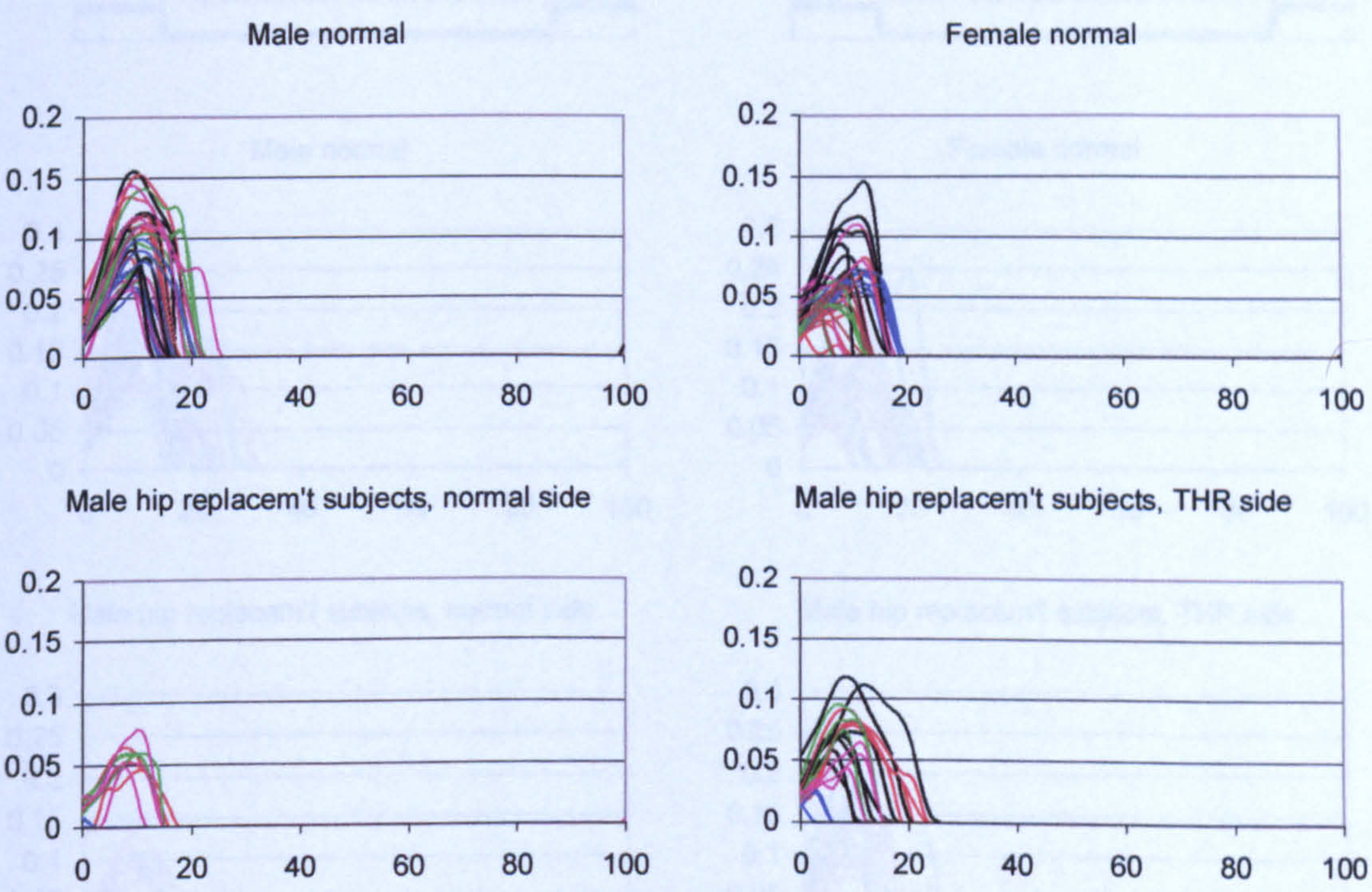

Figure A-VI.3A.44 Walking, muscle force peroneus tertius

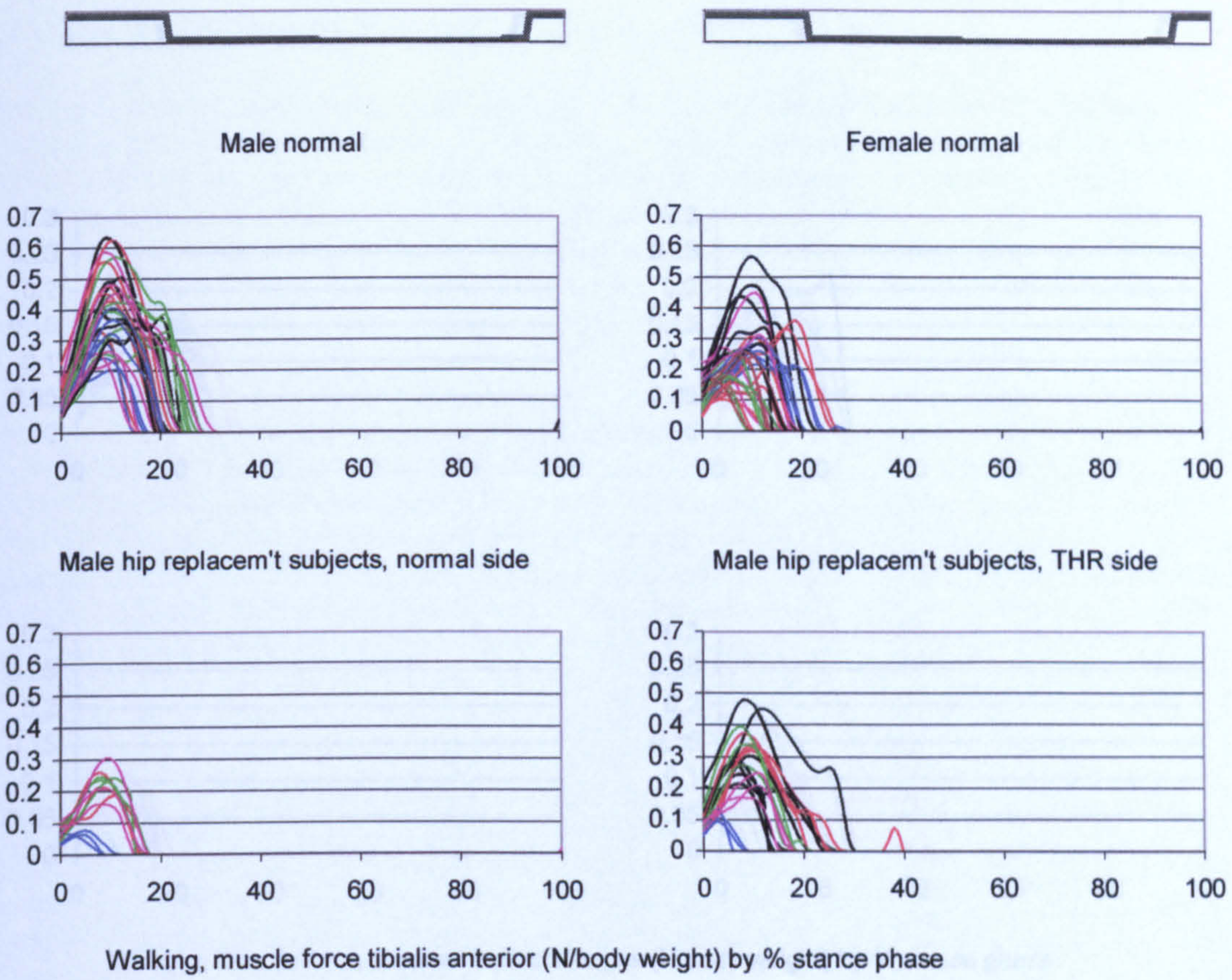

Figure A-VI.3A.45 Walking, muscle force tibialis anterior

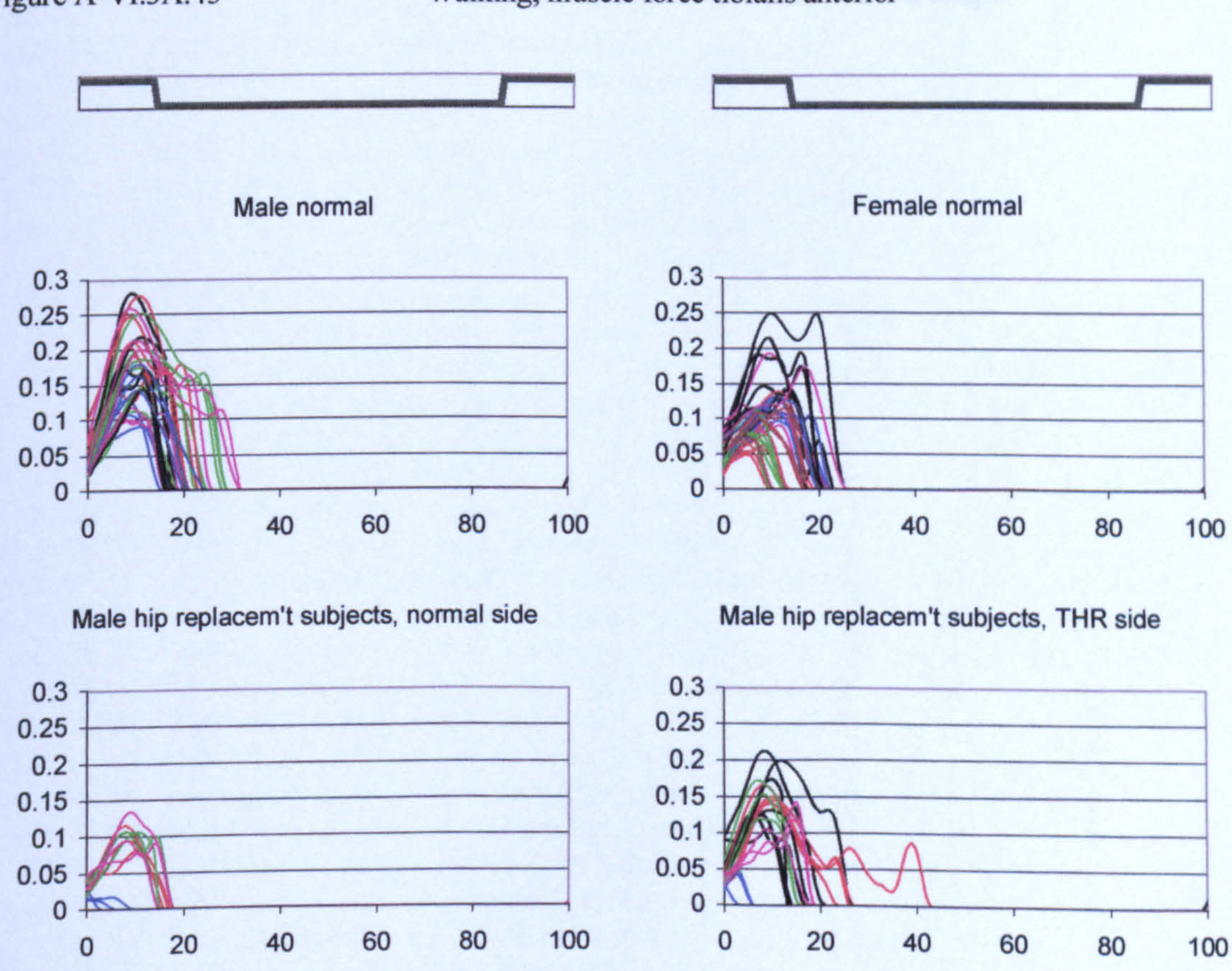

Figure A-VI.3A.46 Walking, muscle force extensor digitorum longus

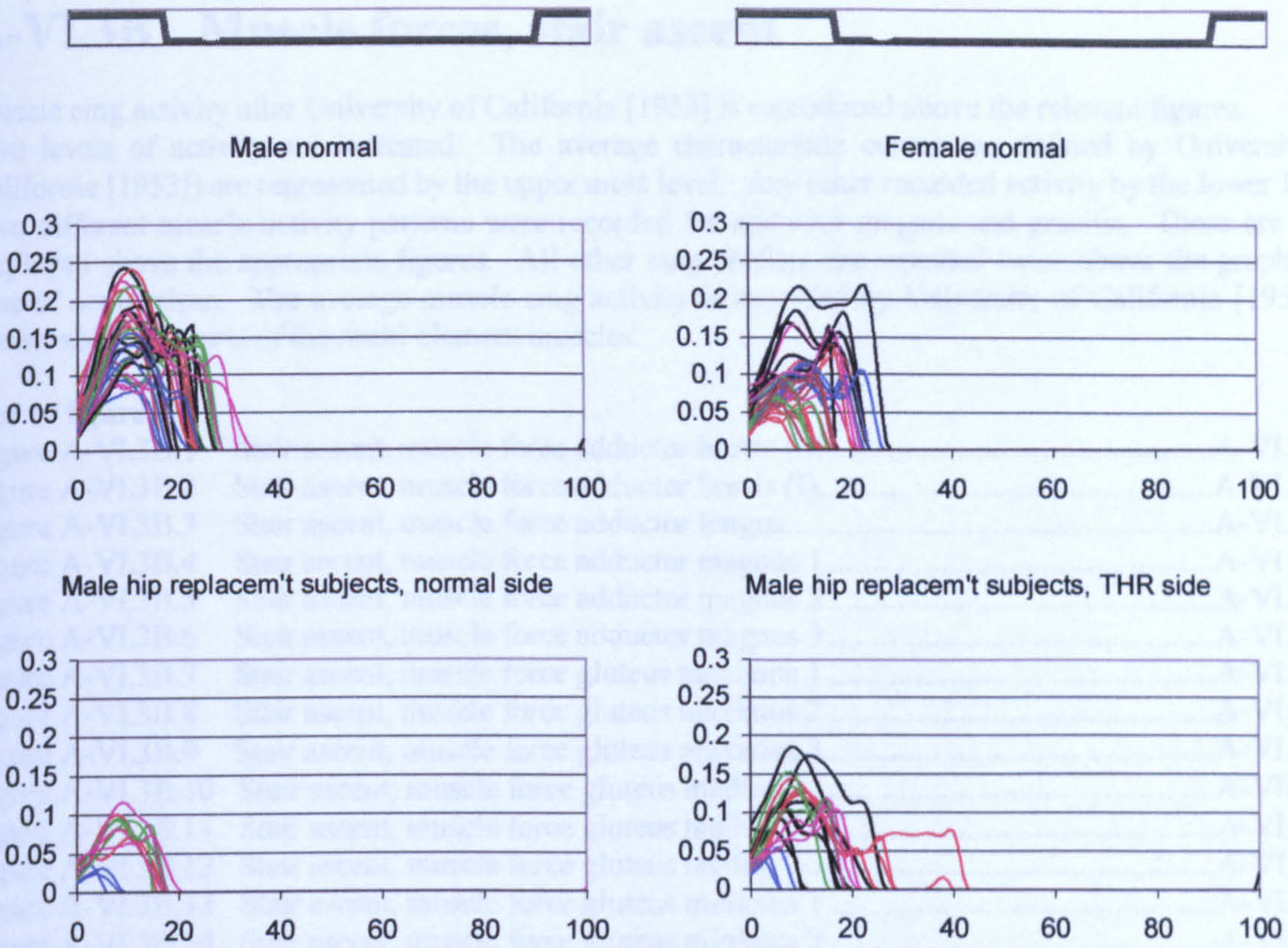

Figure A-VI.3A.47 Walking, muscle force extensor hallucis longus

A-VI.3B Muscle forces, stair ascent

Muscle emg activity after University of California [1953] is reproduced above the relevant figures. Two levels of activity are indicated. The average characteristic curves (as defined by University of California [1953]) are represented by the upper most level. Any other recorded activity by the lower level Two different muscle activity patterns were recorded for adductor magnus and gracilis. These are both displayed above the appropriate figures. All other emg profiles are repeated twice above the graphs for ease of comparison. The average muscle emg activity as recorded by University of California [1953] is shown above all parts of the multi-element muscles.

List of figures

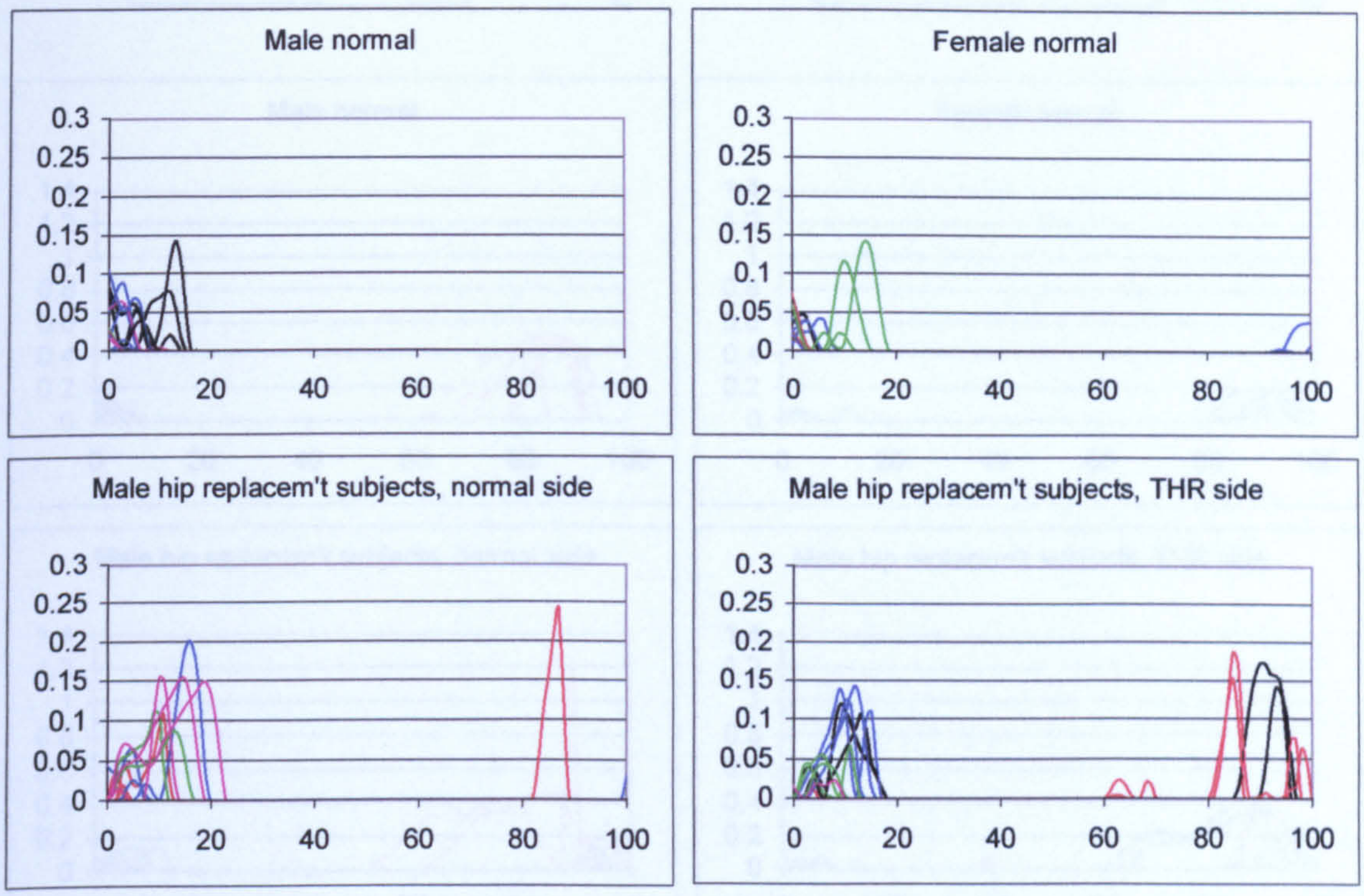

Stair ascent, muscle force adductor brevis (S) (N/body weight) by % stance phase

Figure A-VI.3B.1 Stair ascent, muscle force adductor brevis (S)

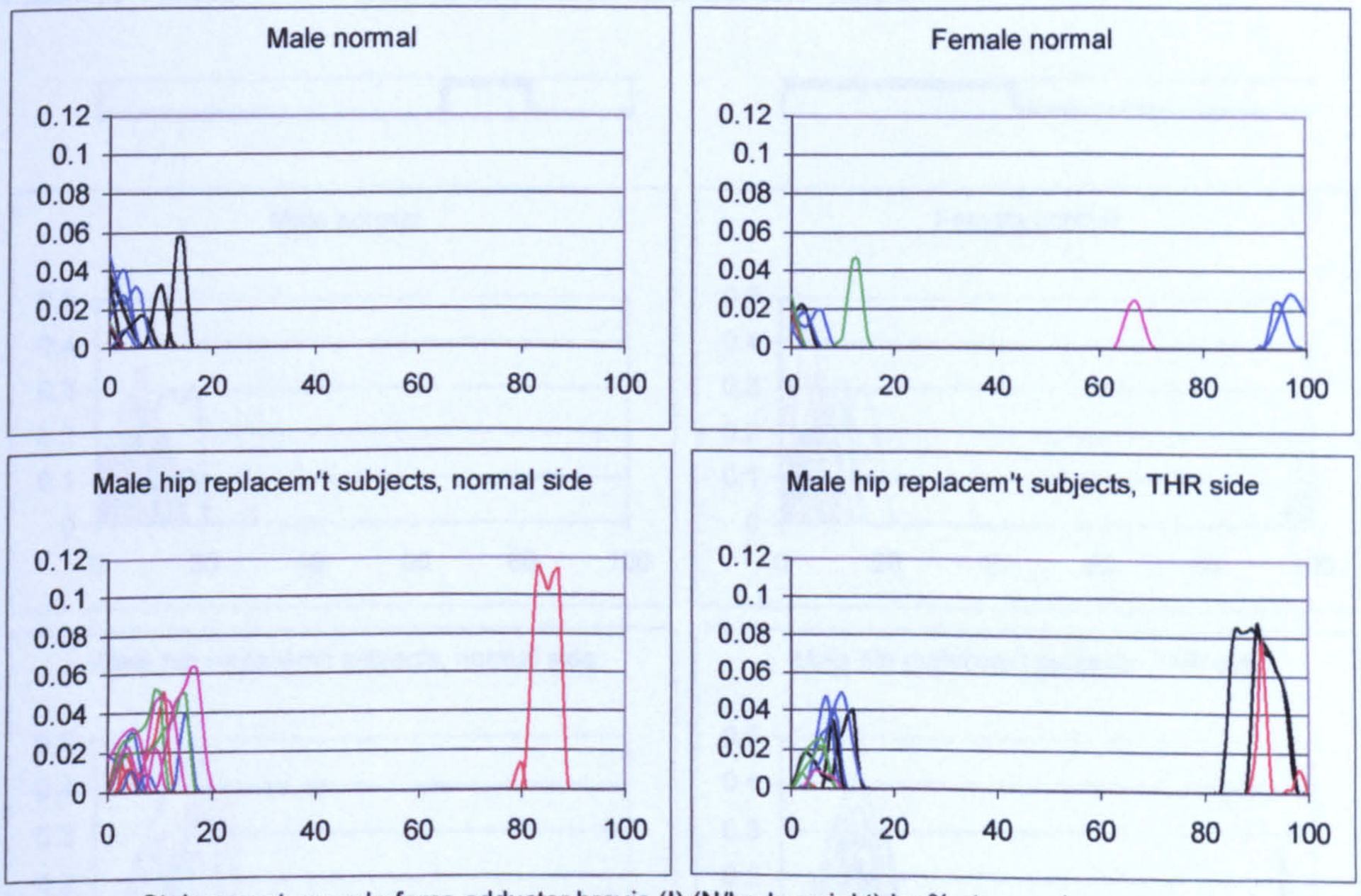

Stair ascent, muscle force adductor brevis (I) (N/body weight) by % stance phase

Figure A-VI.3B.2 Stair ascent, muscle force adductor brevis (I)

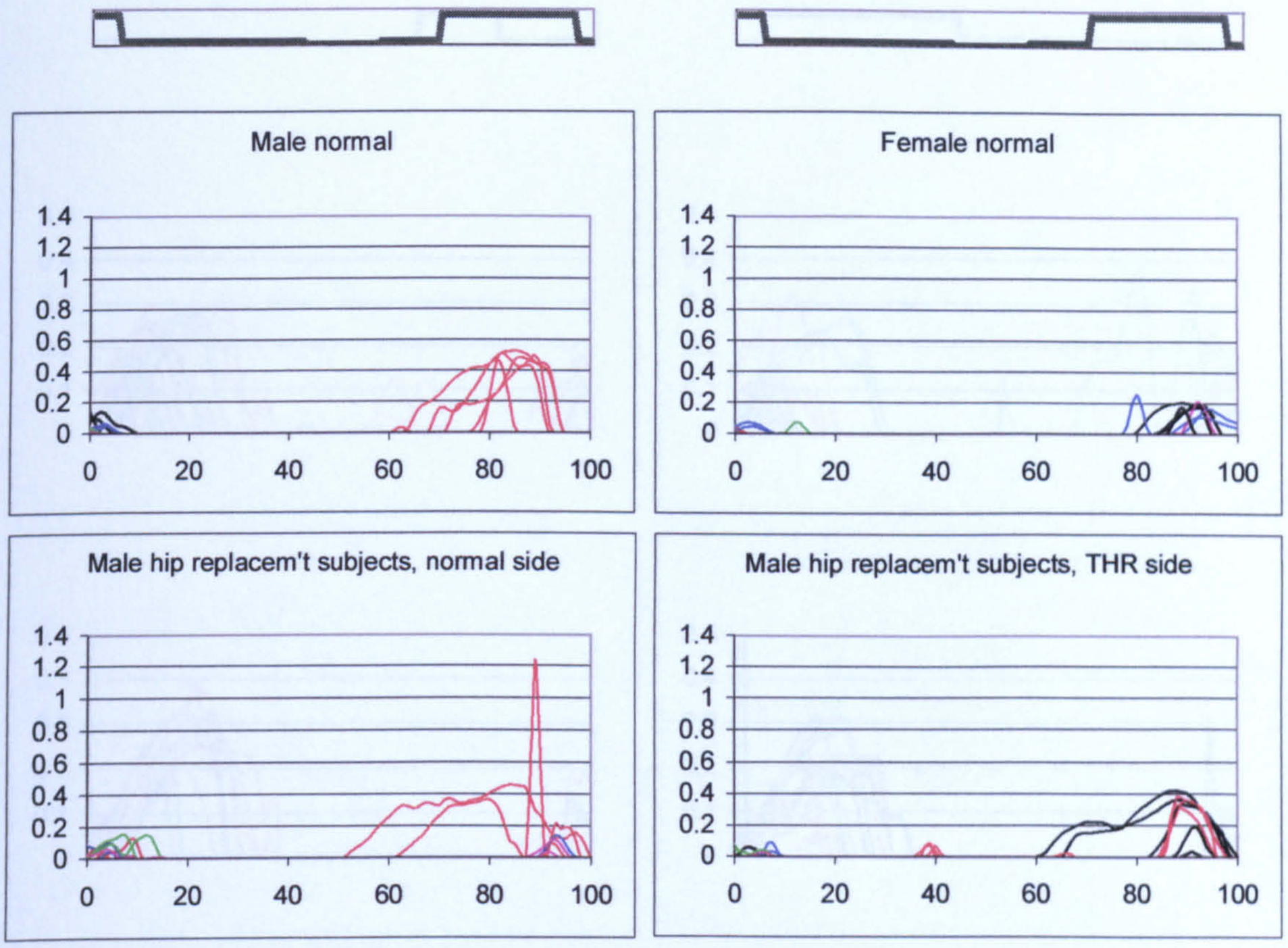

Stair ascent, muscle force adductor longus (N/body weight) by % stance phase

Figure A-VI.3B.3 Stair ascent, muscle force adductor longus

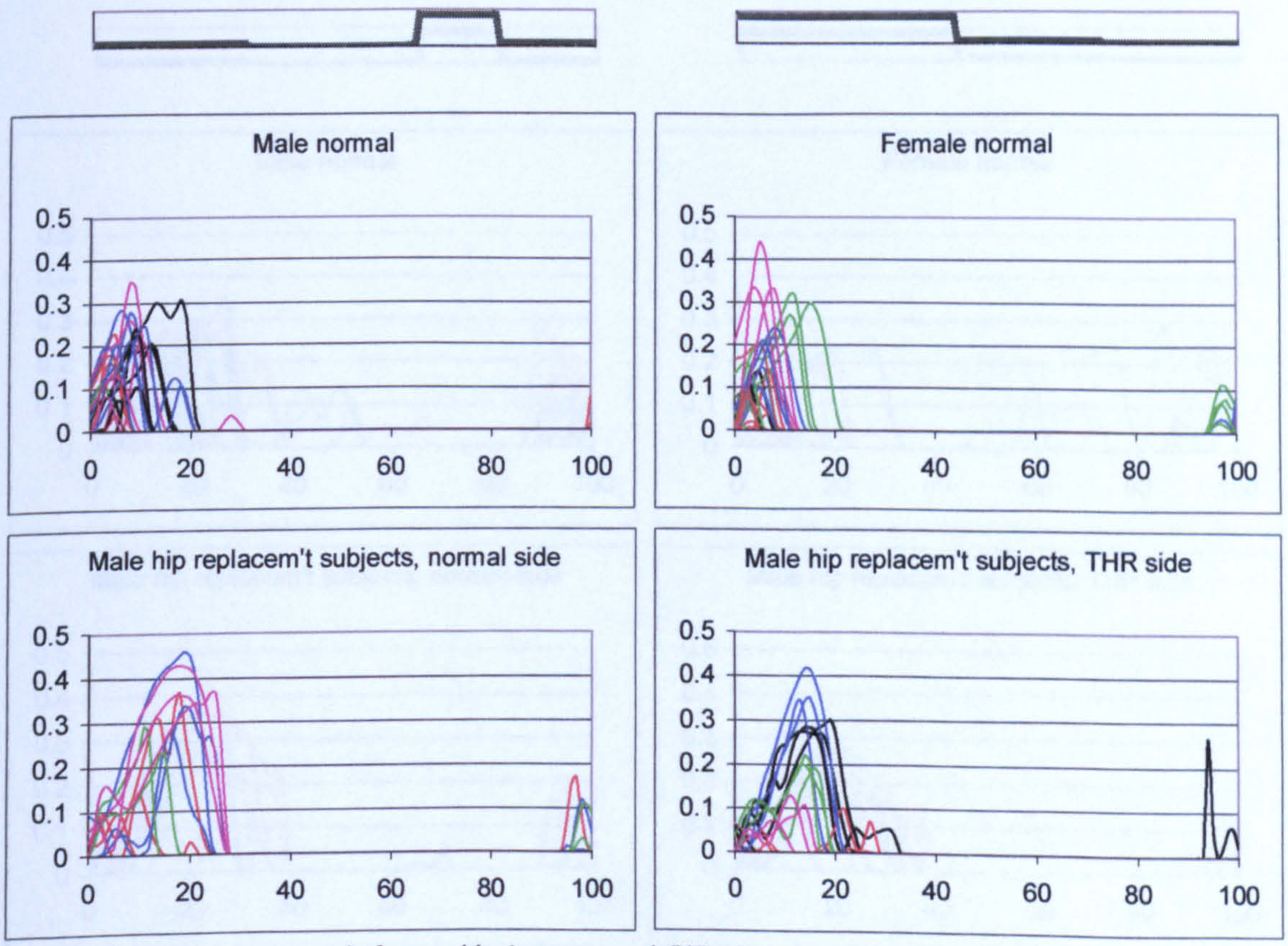

Stair ascent, muscle force adductor magnus 1 (N/body weight) by % stance phase

Figure A-VI.3B.4 Stair ascent, muscle force adductor magnus 1

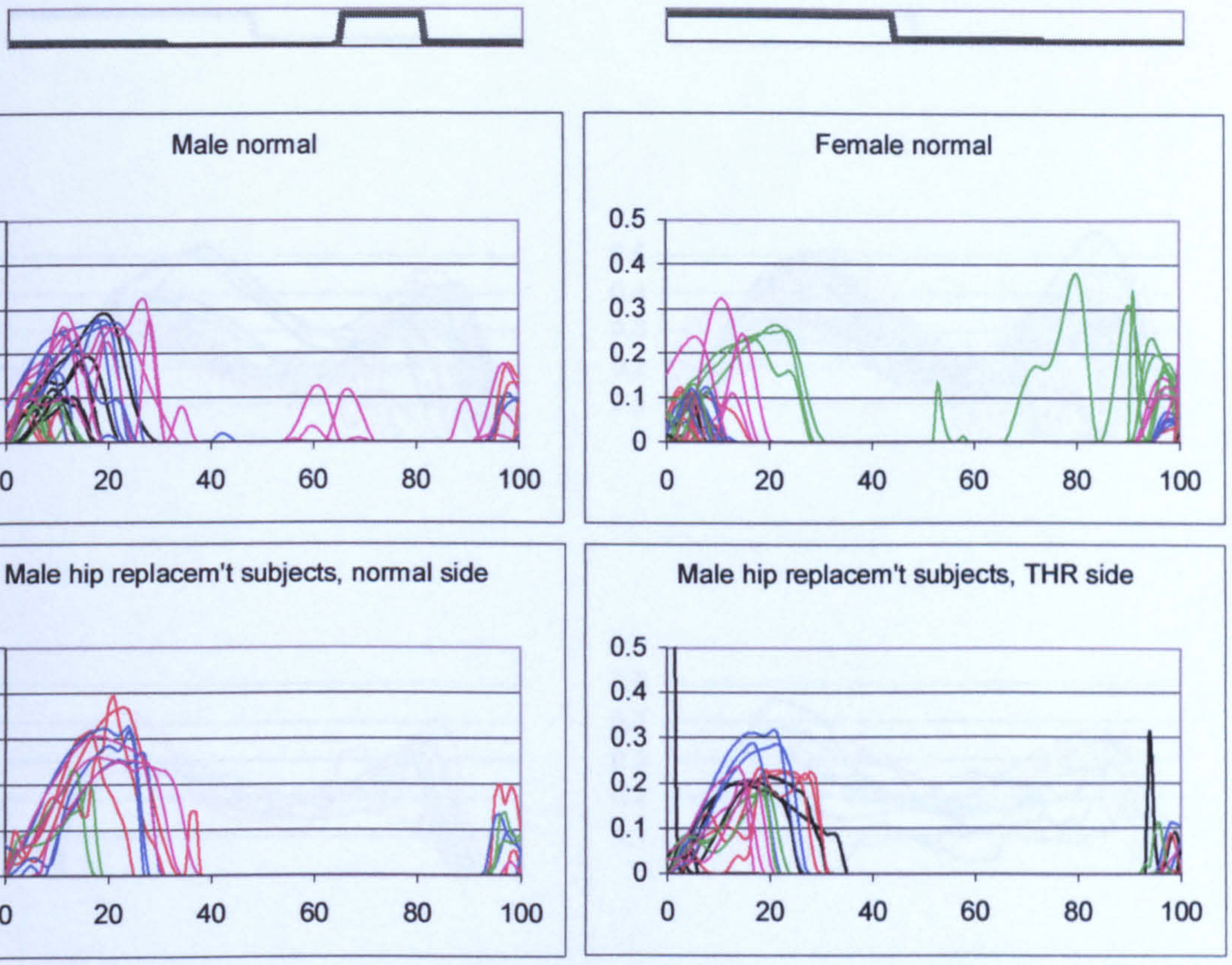

Stair ascent, muscle force adductor magnus 2 (N/body weight) by % stance phase

Figure A-VI.3B.5 Stair ascent, muscle force adductor magnus 2

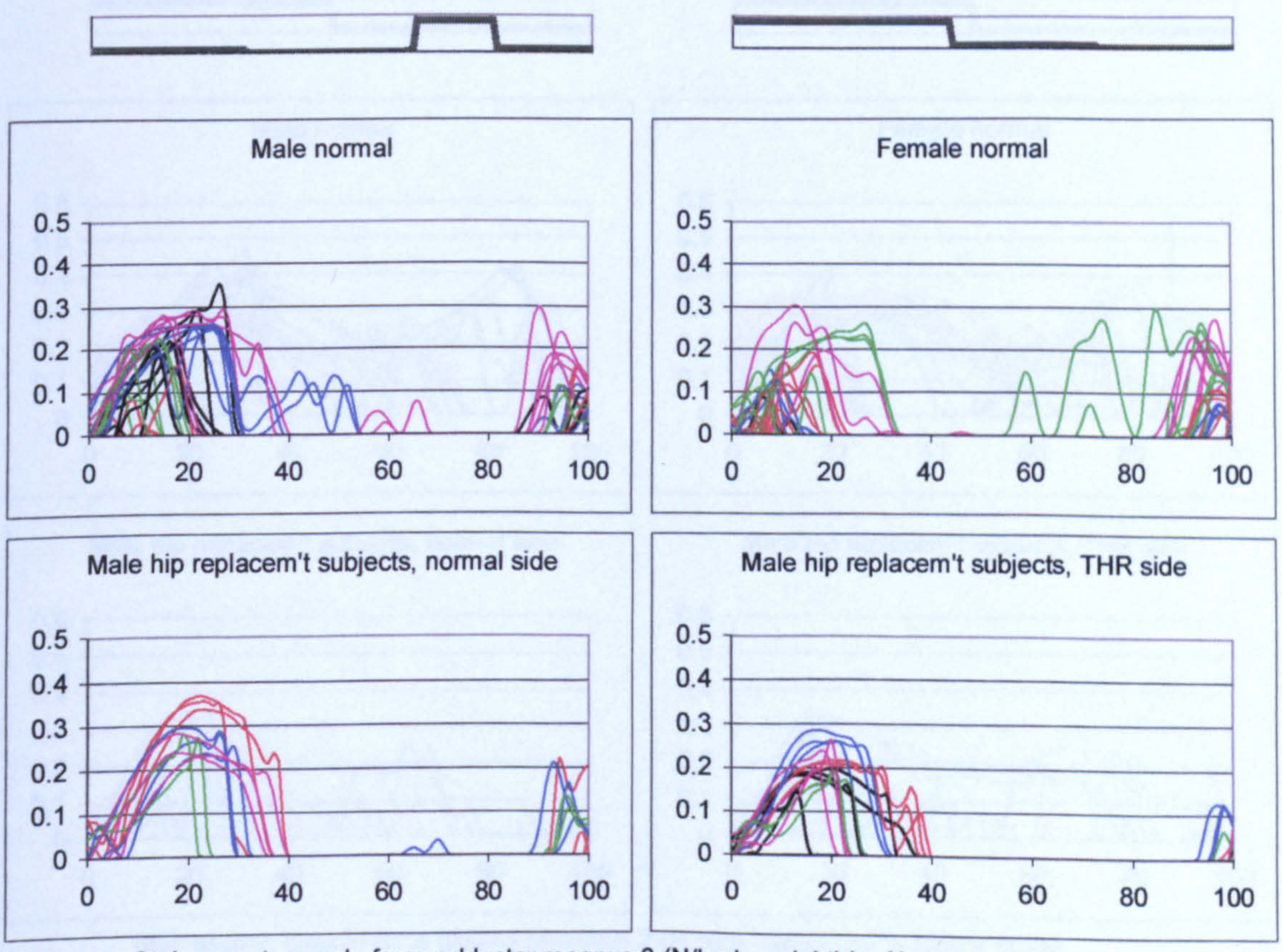

Stair ascent, muscle force adductor magnus 3 (N/body weight) by % stance phase

Figure A-VI.3B.6 Stair ascent, muscle force adductor magnus 3

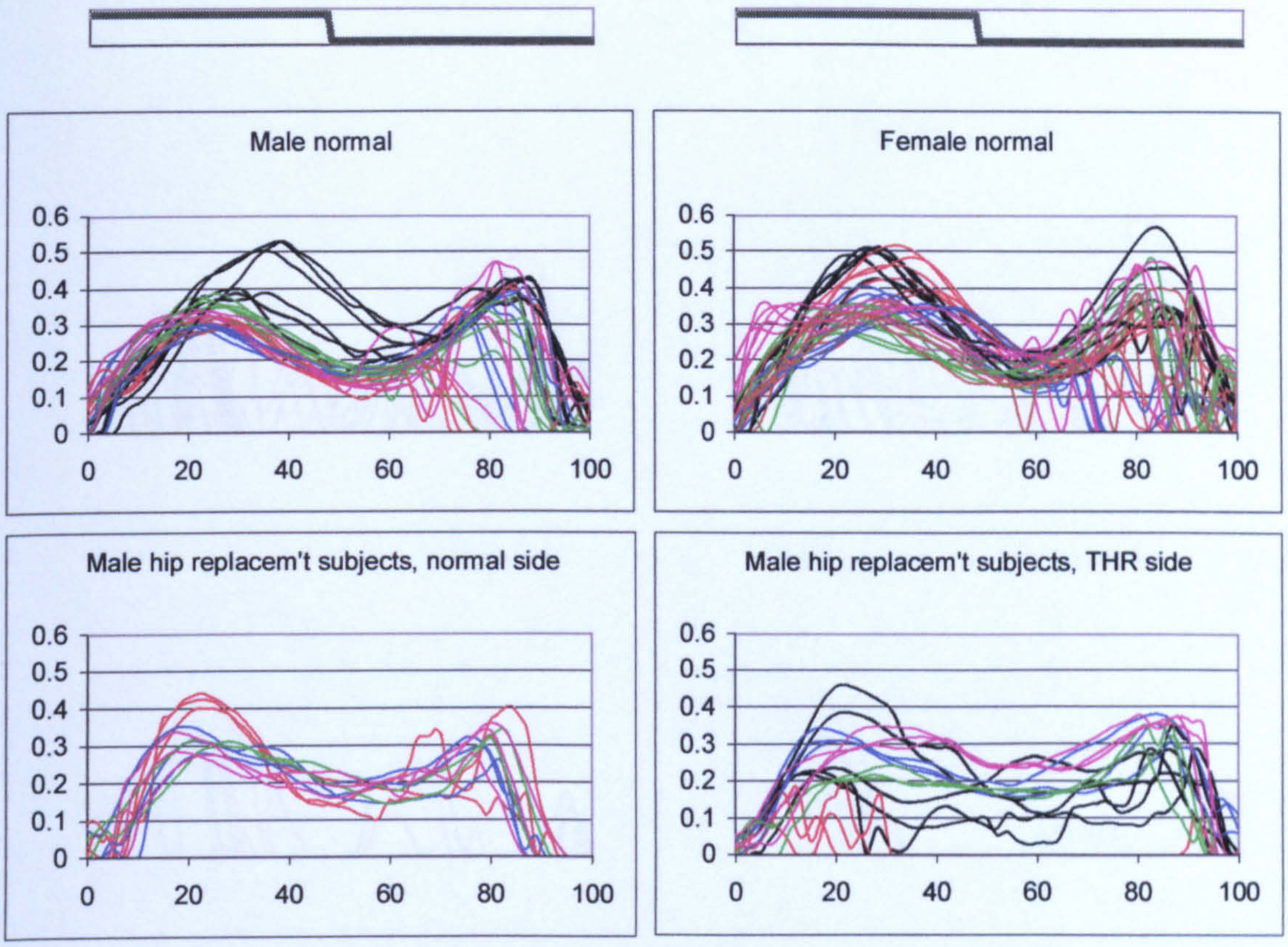

Stair ascent, muscle force gluteus maximus 1 (N/body weight) by % stance phase

Figure A-VI.3B.7 Stair ascent, muscle force gluteus maximus 1

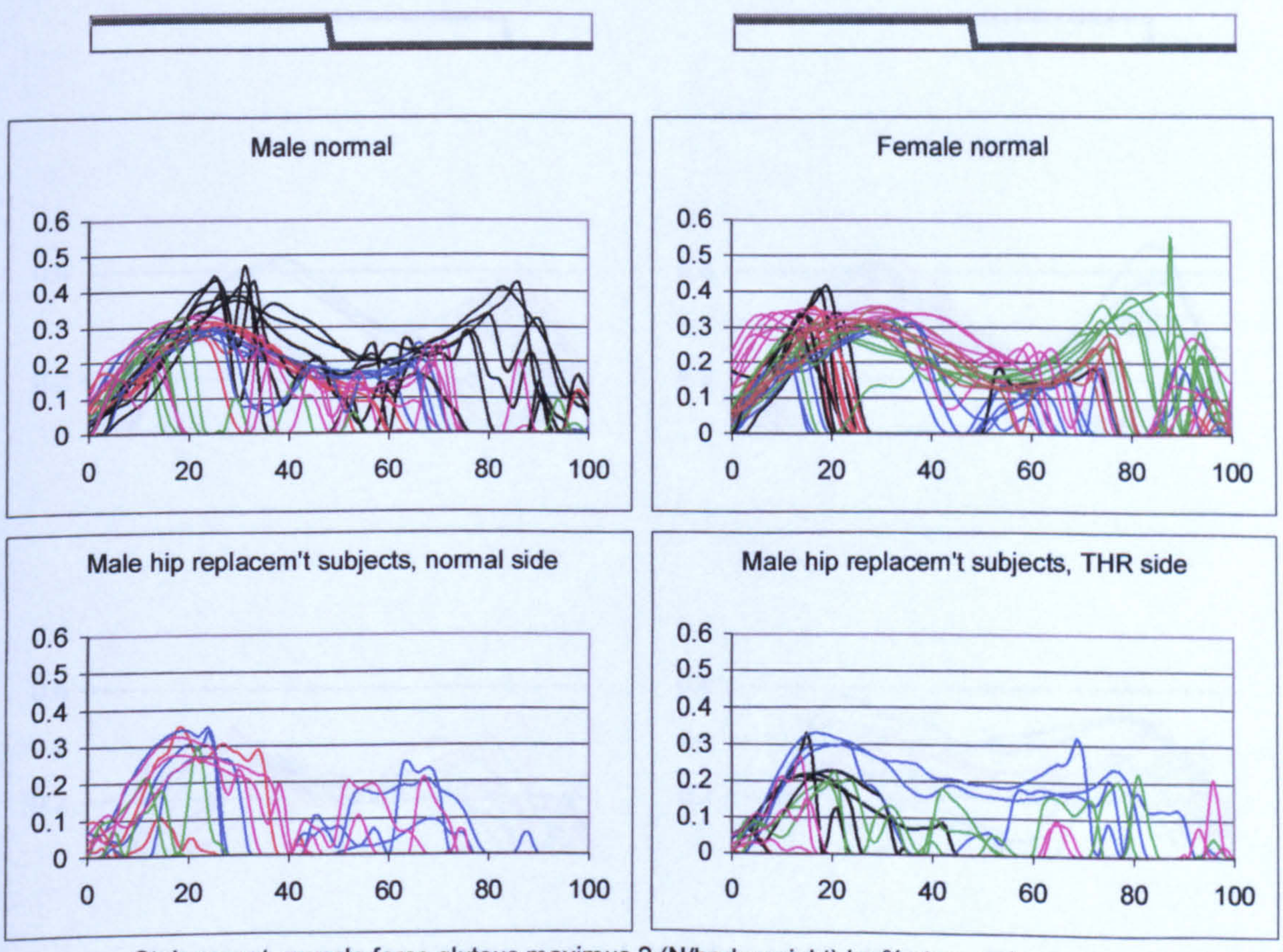

Stair ascent, muscle force gluteus maximus 2 (N/body weight) by % stance phase

Figure A-VI.3B.8 Stair ascent, muscle force gluteus maximus 2

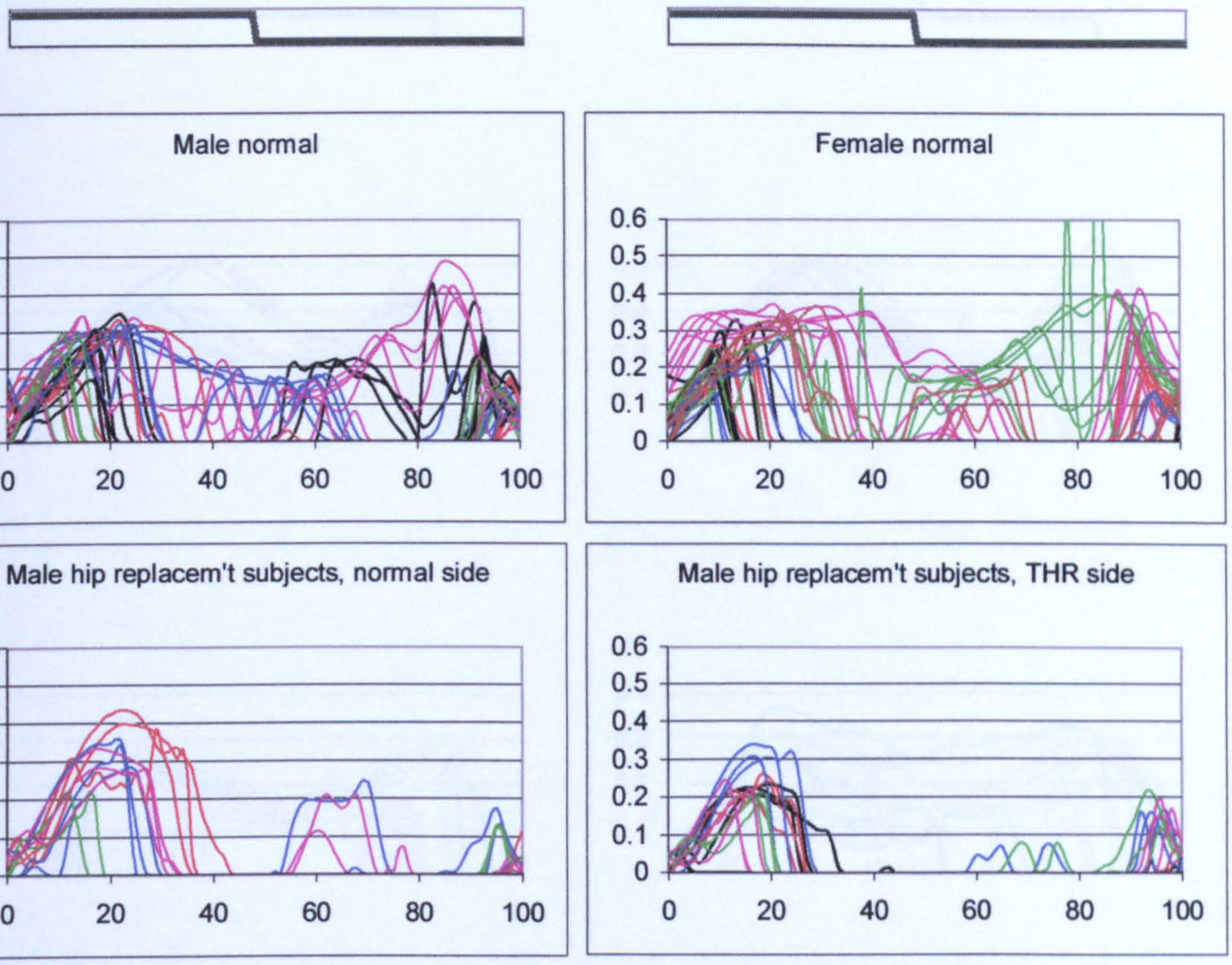

Stair ascent, muscle force gluteus maximus 3 (N/body weight) by % stance phase

Figure A-VI.3B.9 Stair ascent, muscle force gluteus maximus 3

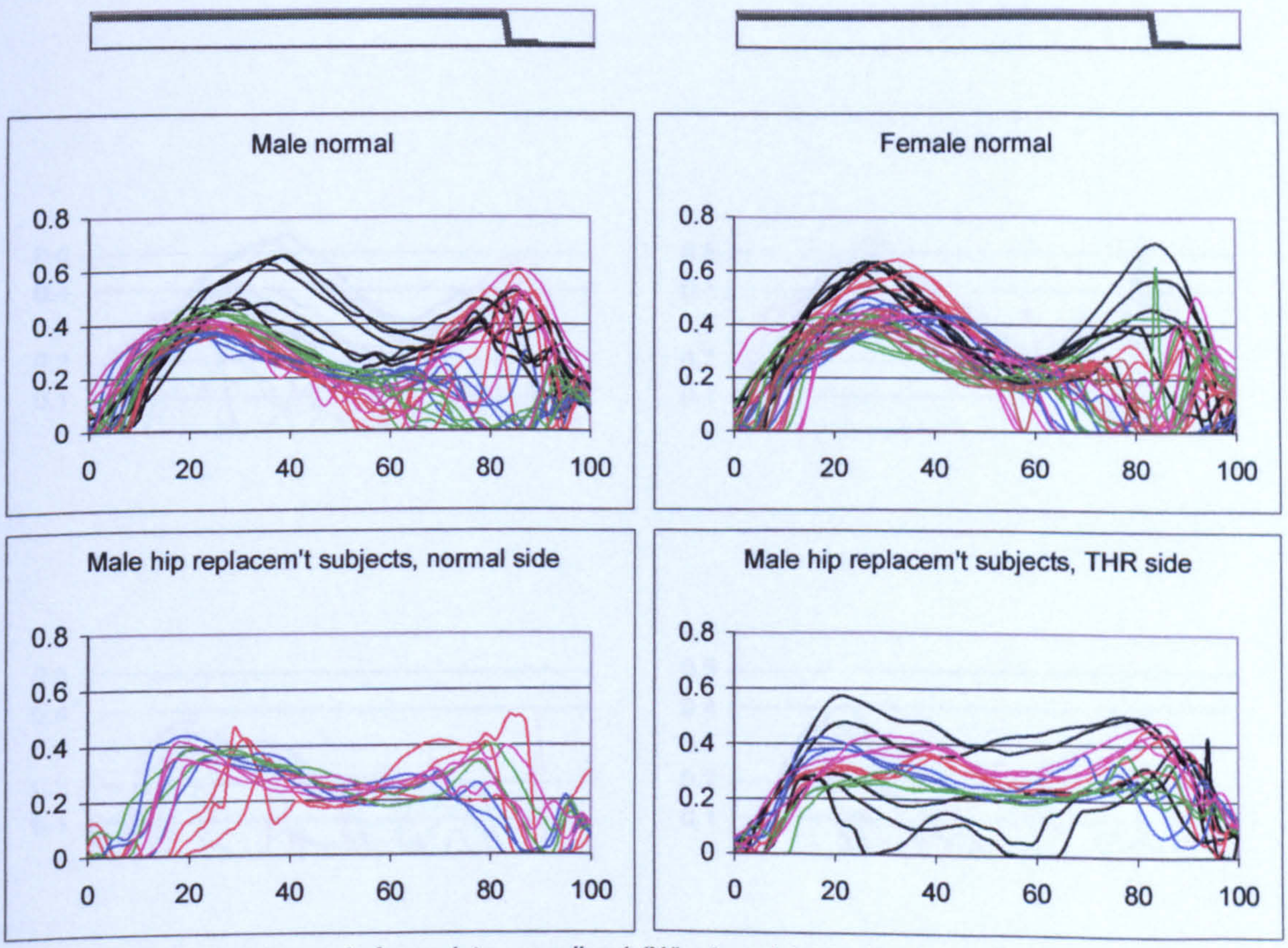

Stair ascent, muscle force gluteus medius 1 (N/body weight) by % stance phase

Figure A-VI.3B.10 Stair ascent, muscle force gluteus medius 1

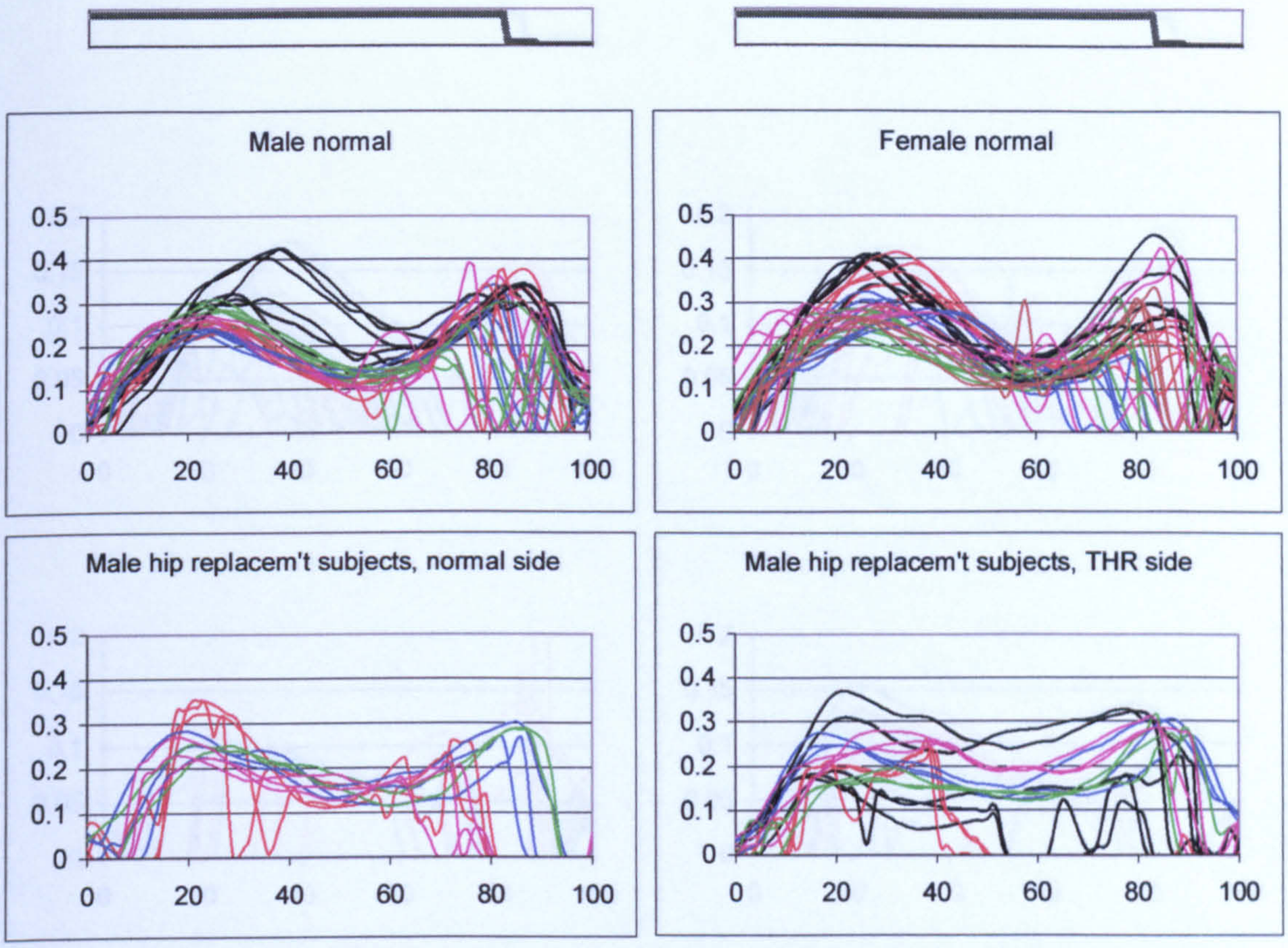

Stair ascent, muscle force gluteus medius 2 (N/body weight) by % stance phase

Figure A-VI.3B.11 Stair ascent, muscle force gluteus medius 2

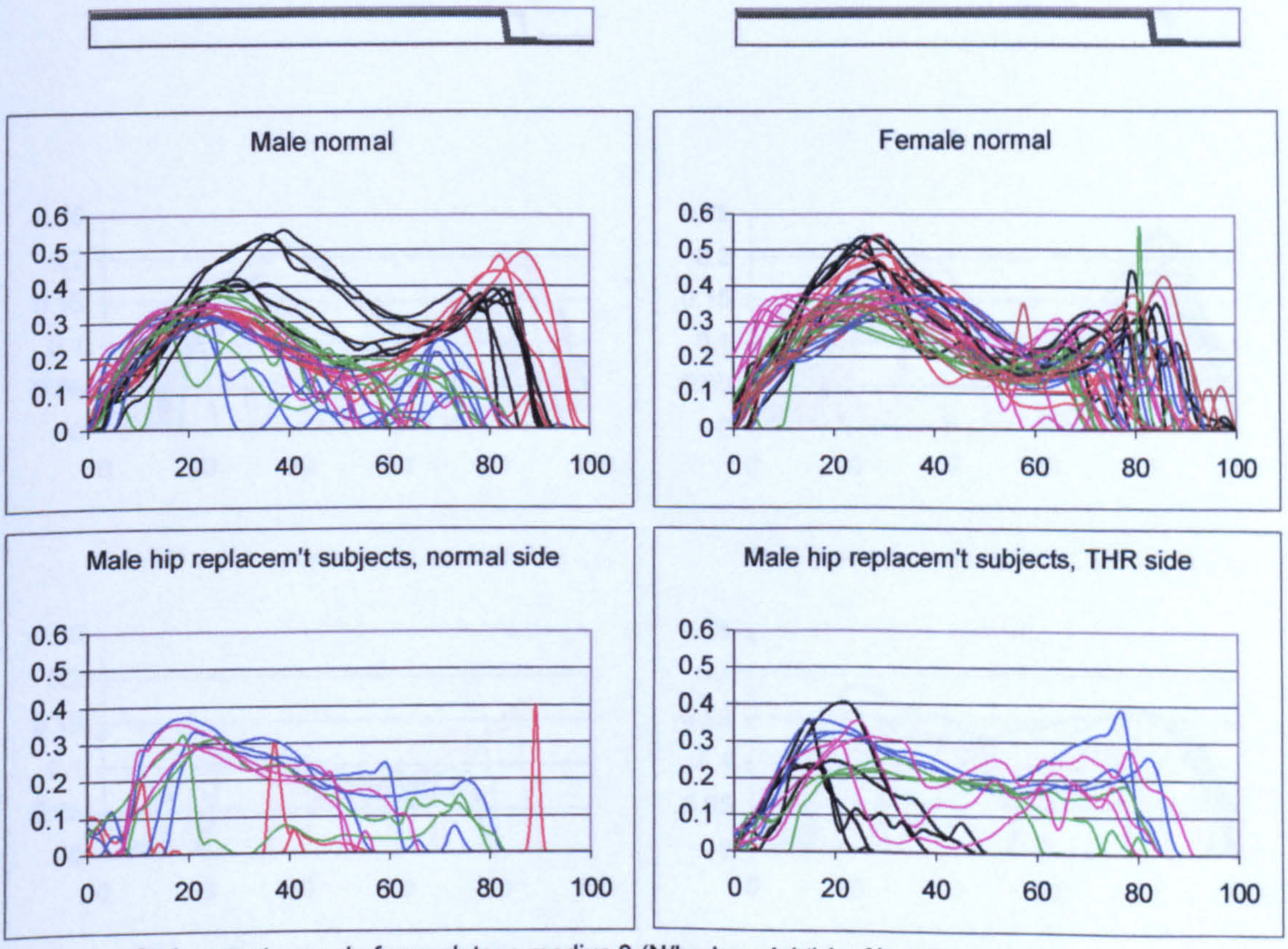

Stair ascent, muscle force gluteus medius 3 (N/body weight) by % stance phase

Figure A-VI.3B.12 Stair ascent, muscle force gluteus medius 3

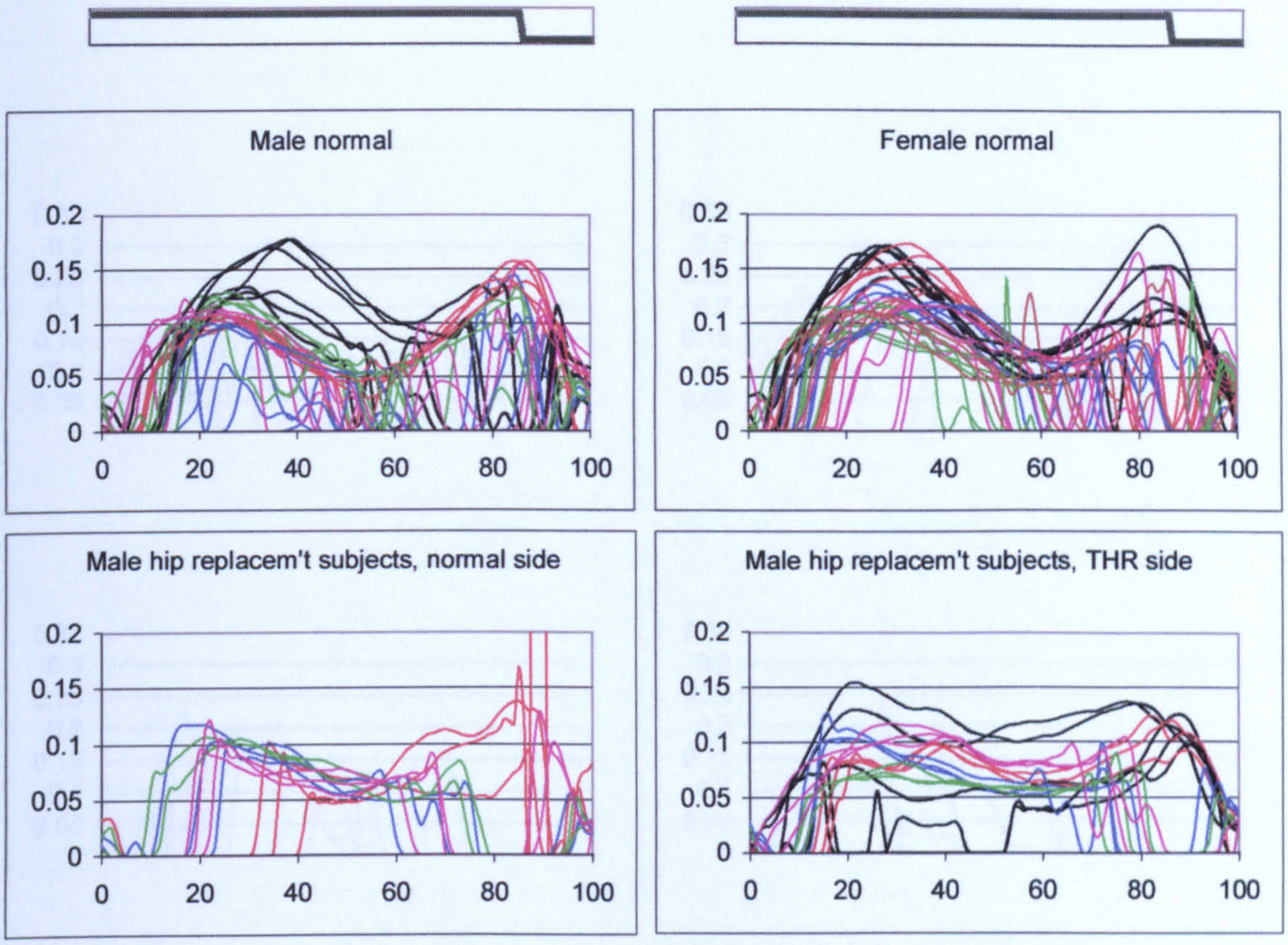

Stair ascent, muscle force gluteus minimus 1 (N/body weight) by % stance phase

Figure A-VI.3B.13 Stair ascent, muscle force gluteus minimus 1

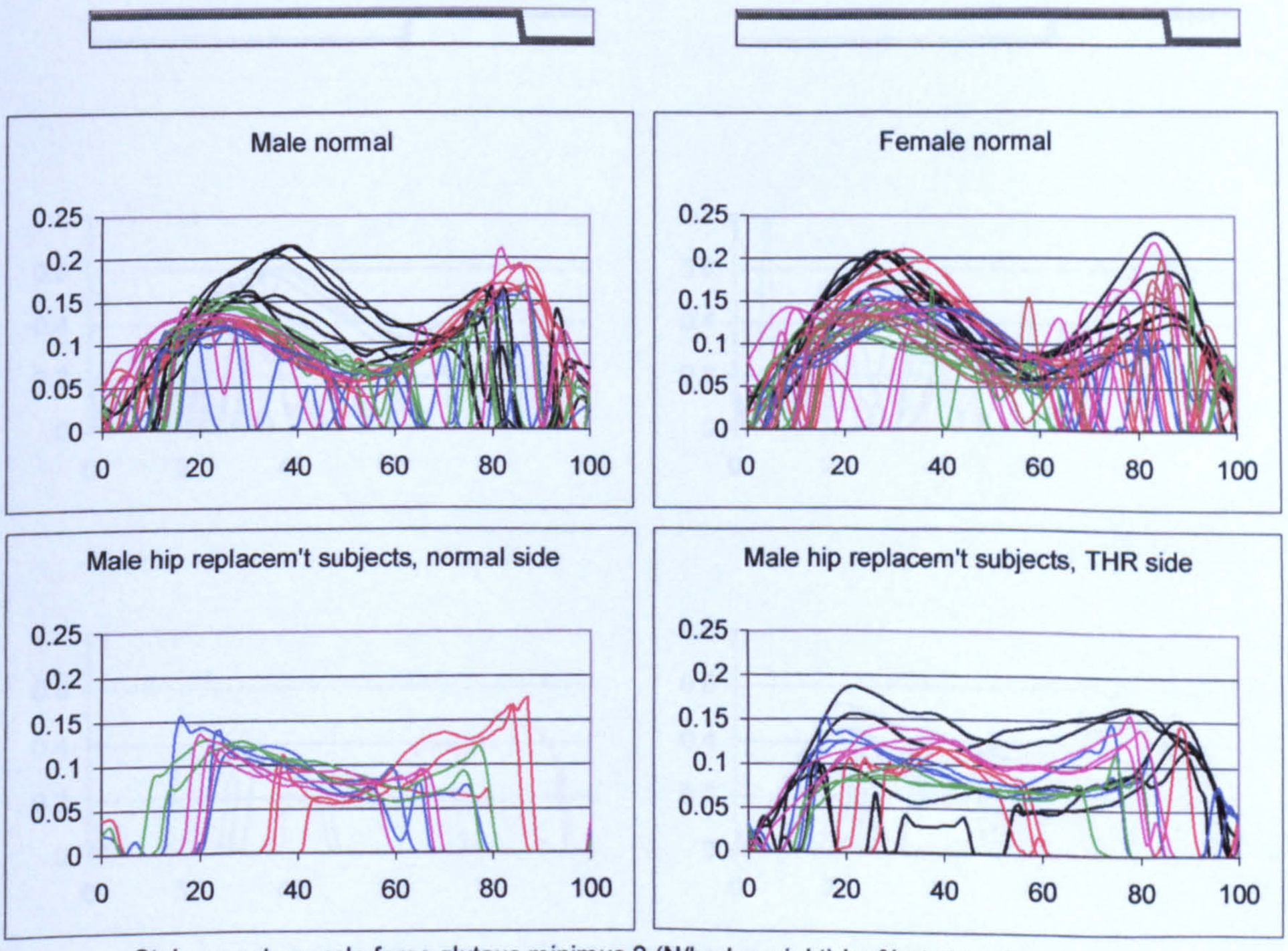

Stair ascent, muscle force gluteus minimus 2 (N/body weight) by % stance phase

Figure A-VI.3B.14 Stair ascent, muscle force gluteus minimus 2

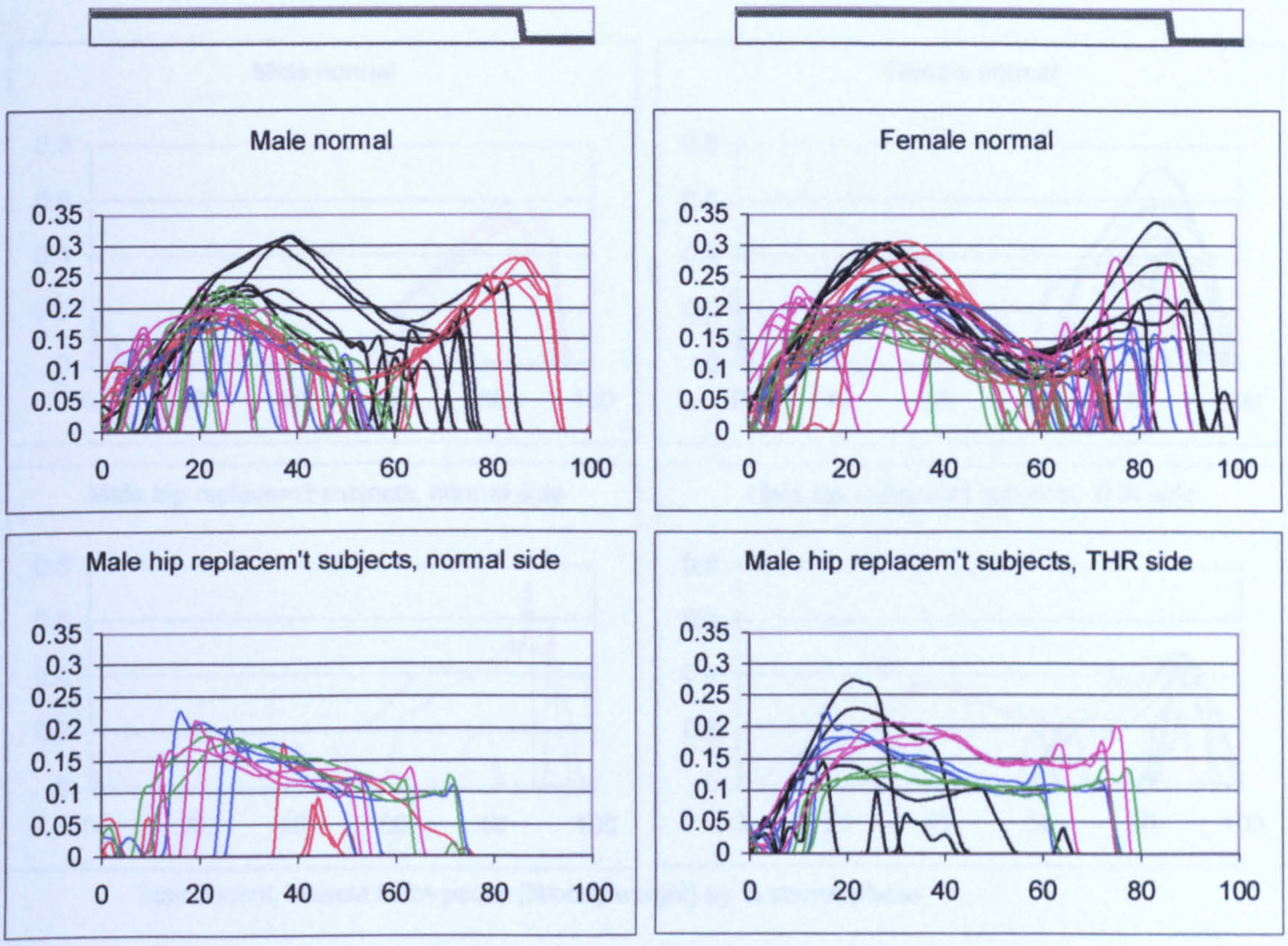

Stair ascent, muscle force gluteus minimus 3 (N/body weight) by % stance phase

Figure A-VI.3B.15 Stair ascent, muscle force gluteus minimus 3

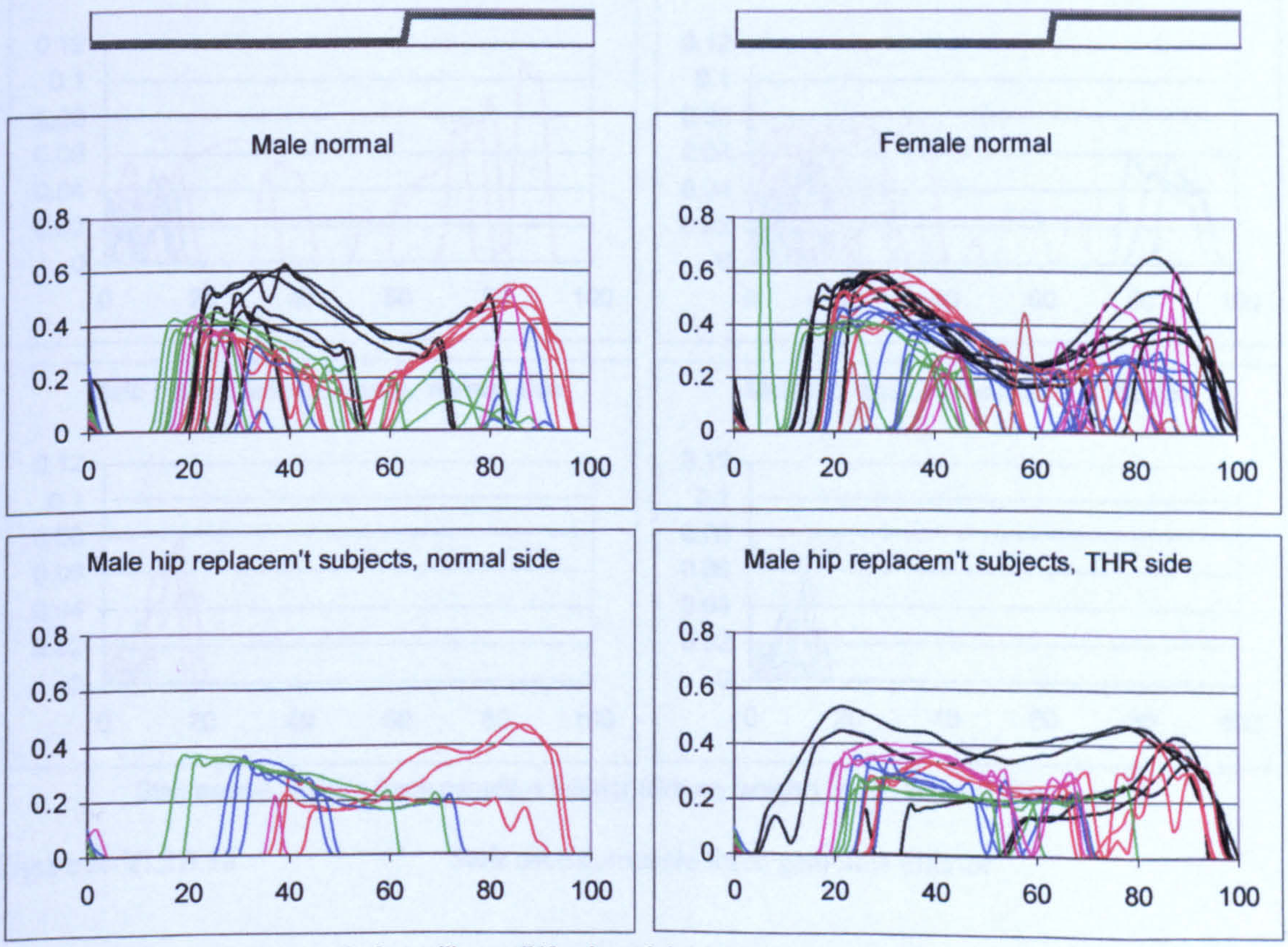

Stair ascent, muscle force iliacus (N/body weight) by % stance phase

Figure A-VI.3B.16 Stair ascent, muscle force iliacus

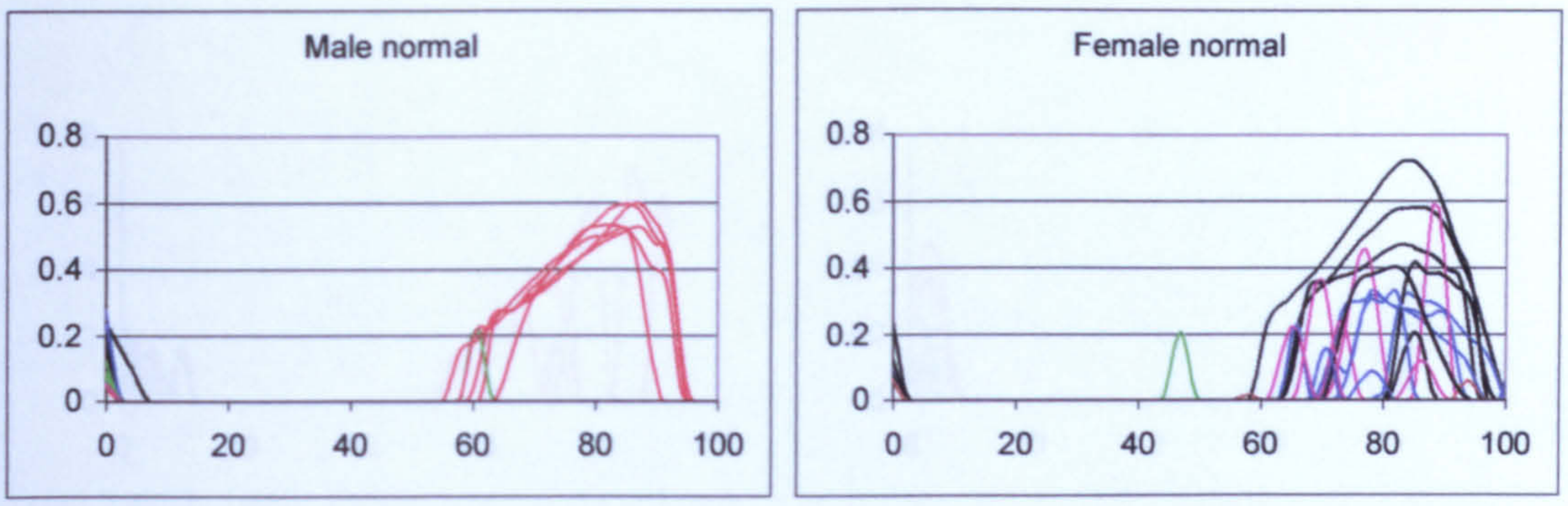

Stair ascent, muscle force psoas (N/body weight) by % stance phase

Figure A-VI.3B.17 Stair ascent, muscle force psoas

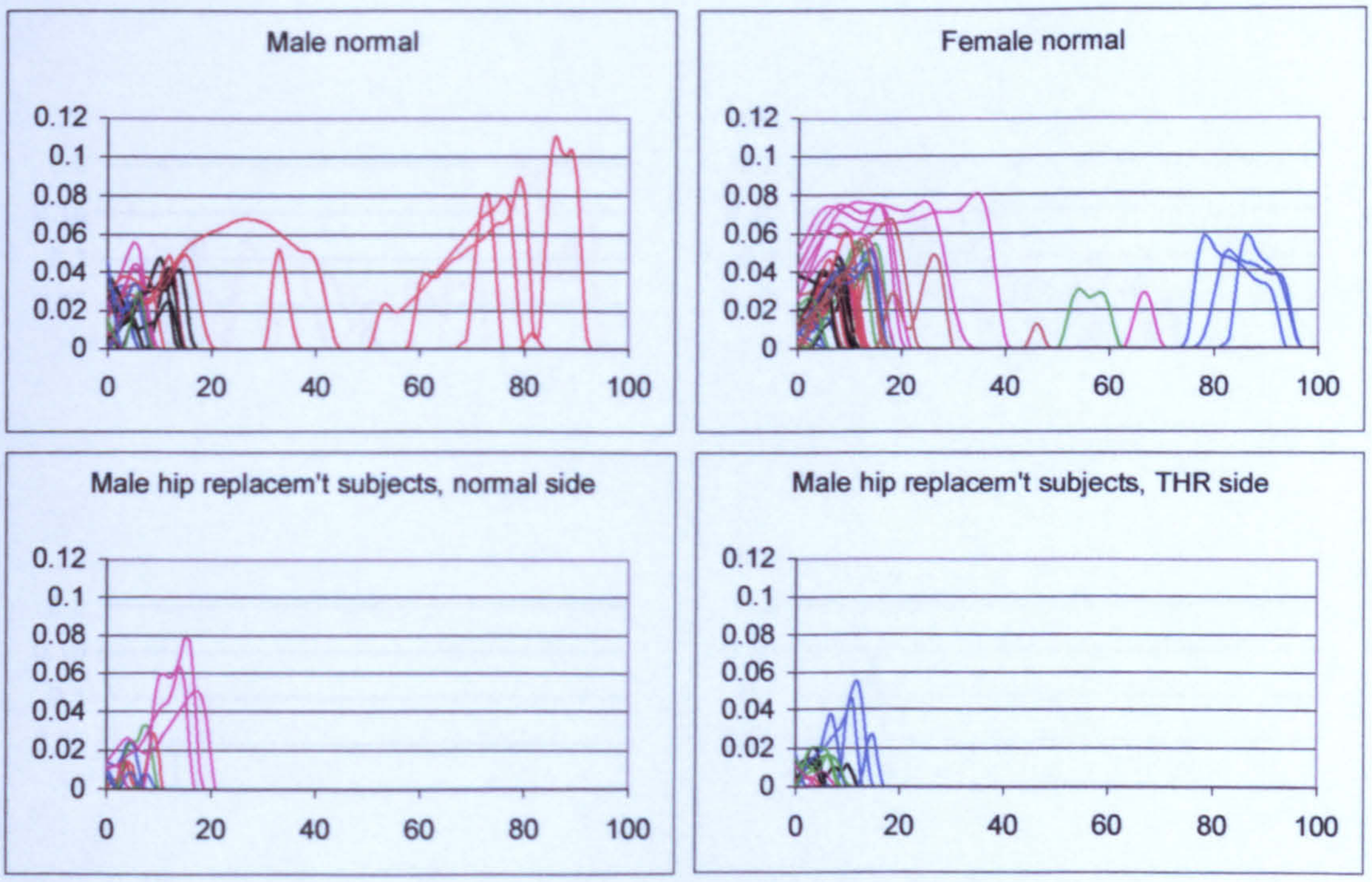

Stair ascent, muscle force gemellus inferior (N/body weight) by % stance phase

Figure A-VI.3B.18 Stair ascent, muscle force gemellus inferior

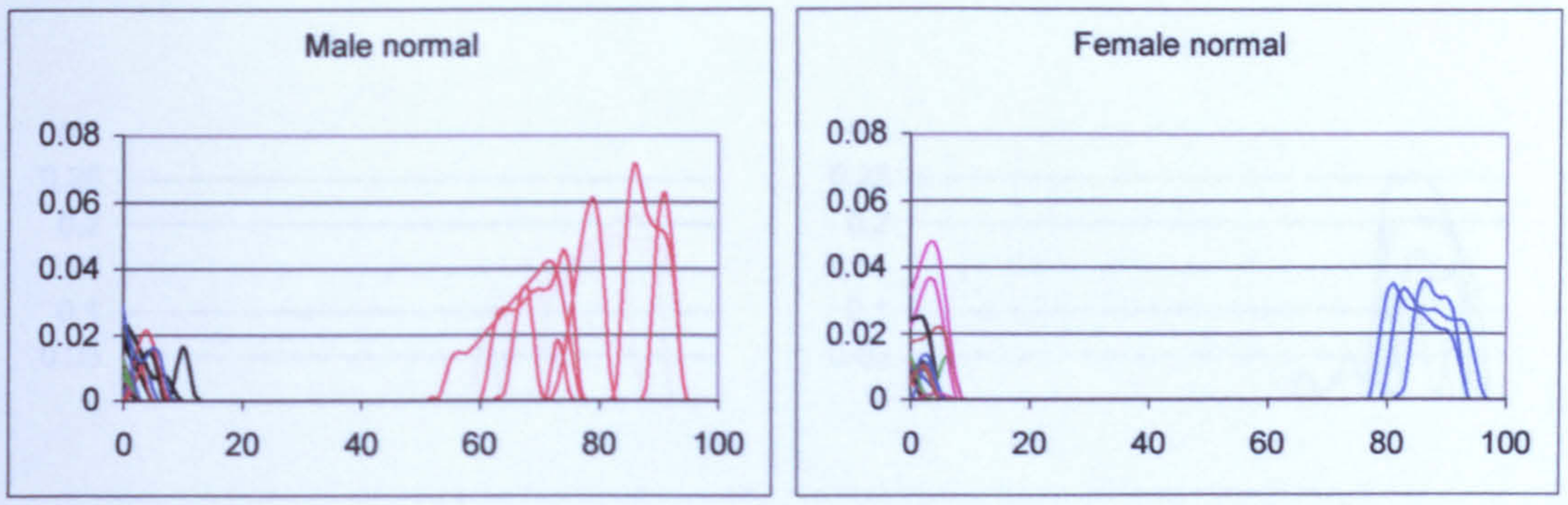

Stair ascent, muscle force obturator externus(N/body weight) by % stance phase

Figure A-VI.3B.19 Stair ascent, muscle force obturator externus

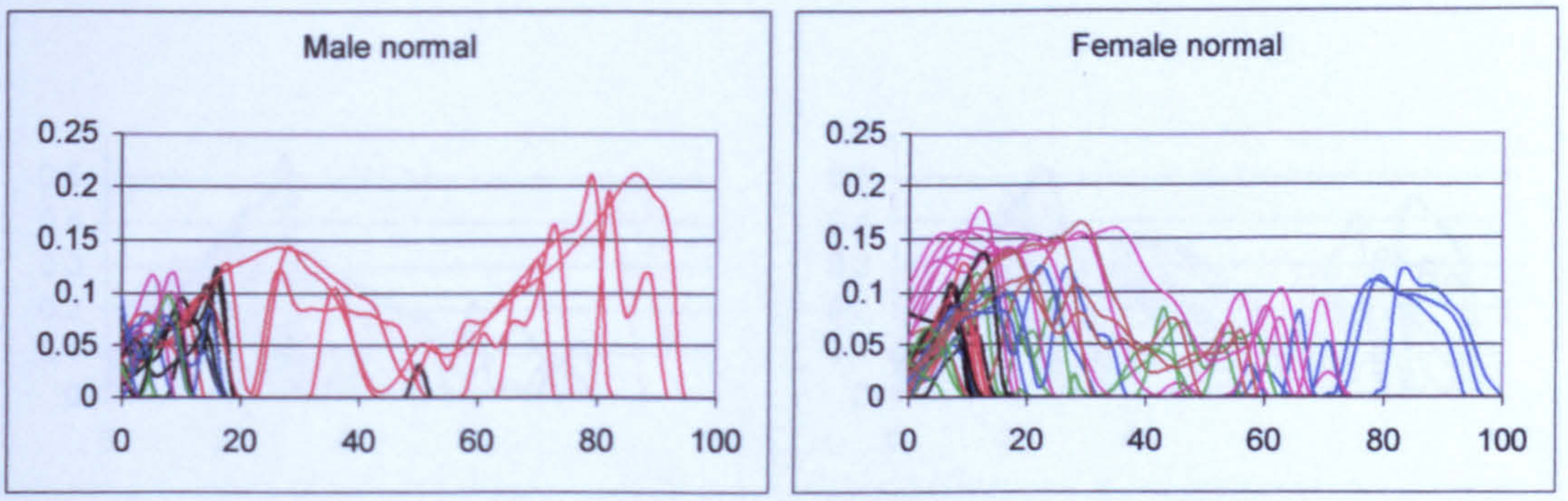

Stair ascent, muscle force obturator internus(N/body weight) by % stance phase

Figure A-VI.3B.20 Stair ascent, muscle force obturator internus

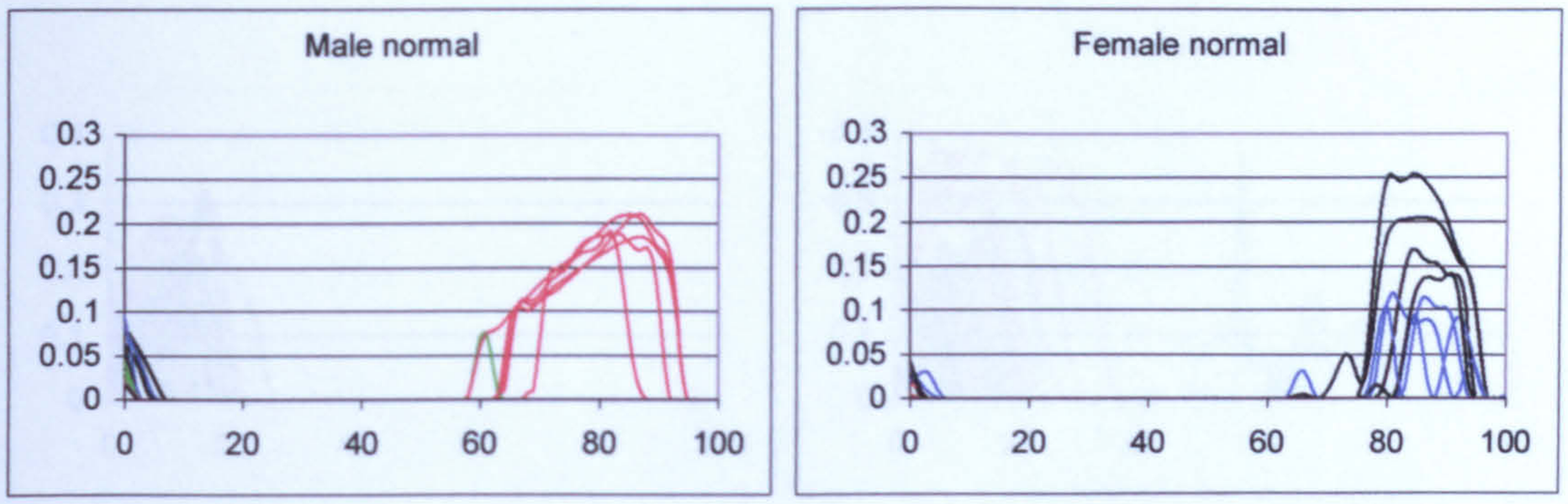

Stair ascent, muscle force pectineus (N/body weight) by % stance phase

Figure A-VI.3B.21 Stair ascent, muscle force pectineus

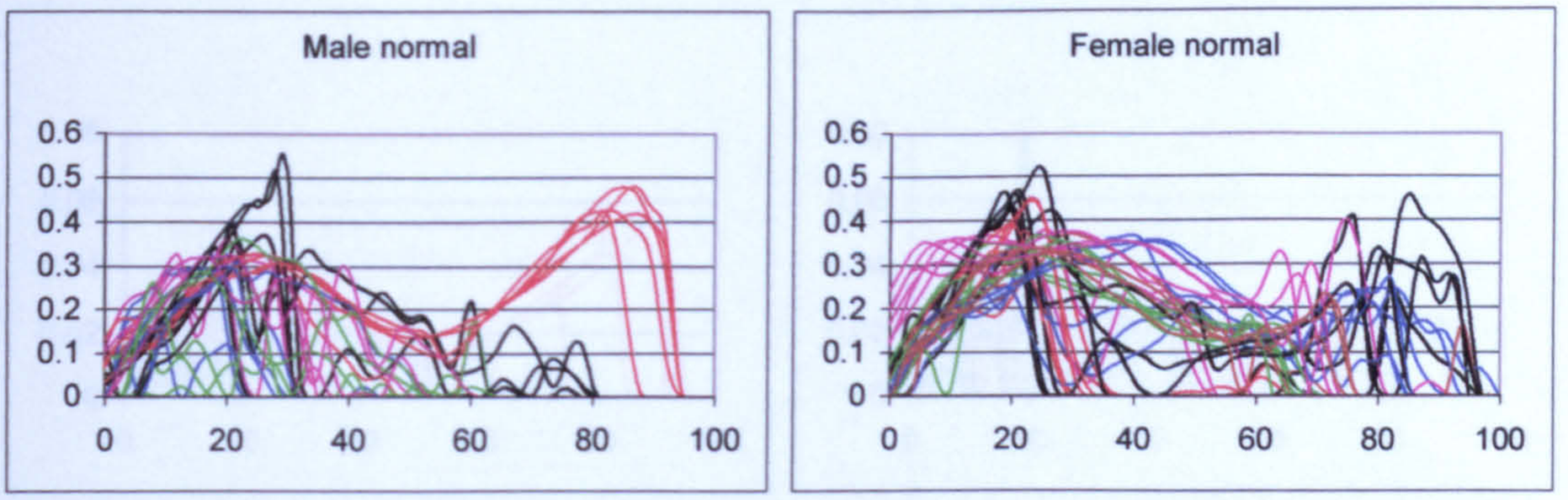

Stair ascent, muscle force piriformis (N/body weight) by % stance phase

Figure A-VI.3B.22 Stair ascent, muscle force piriformis

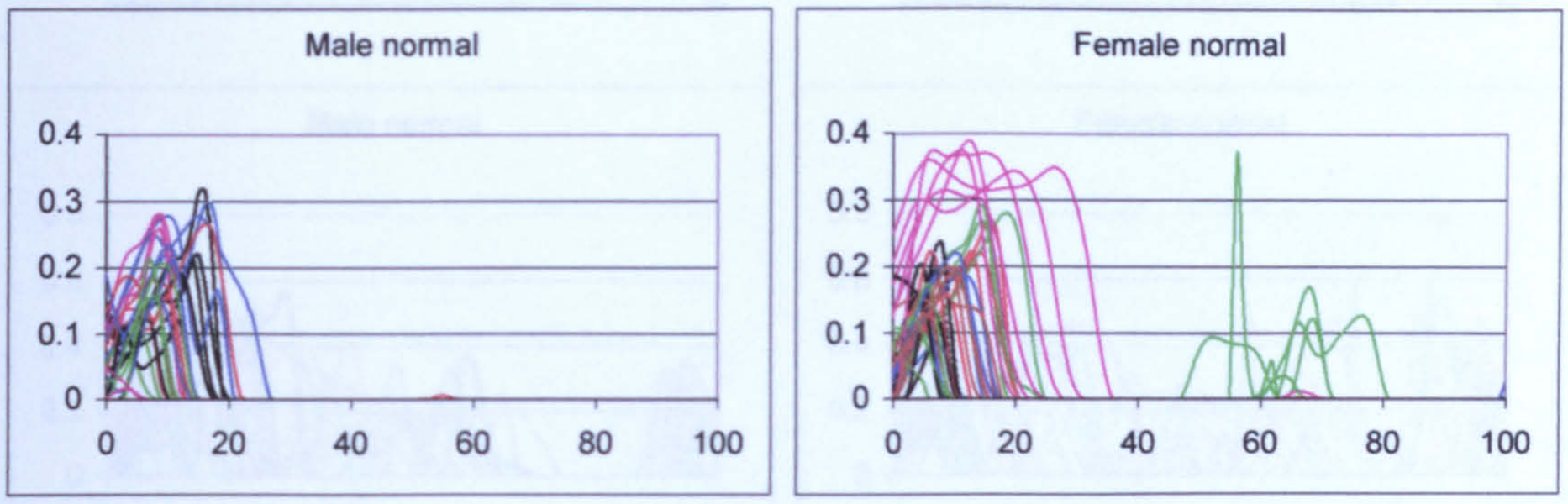

Stair ascent, muscle force quadratus femoris (N/body weight) by % stance phase

Figure A-VI.3B.23 Stair ascent, muscle force quadratus femoris

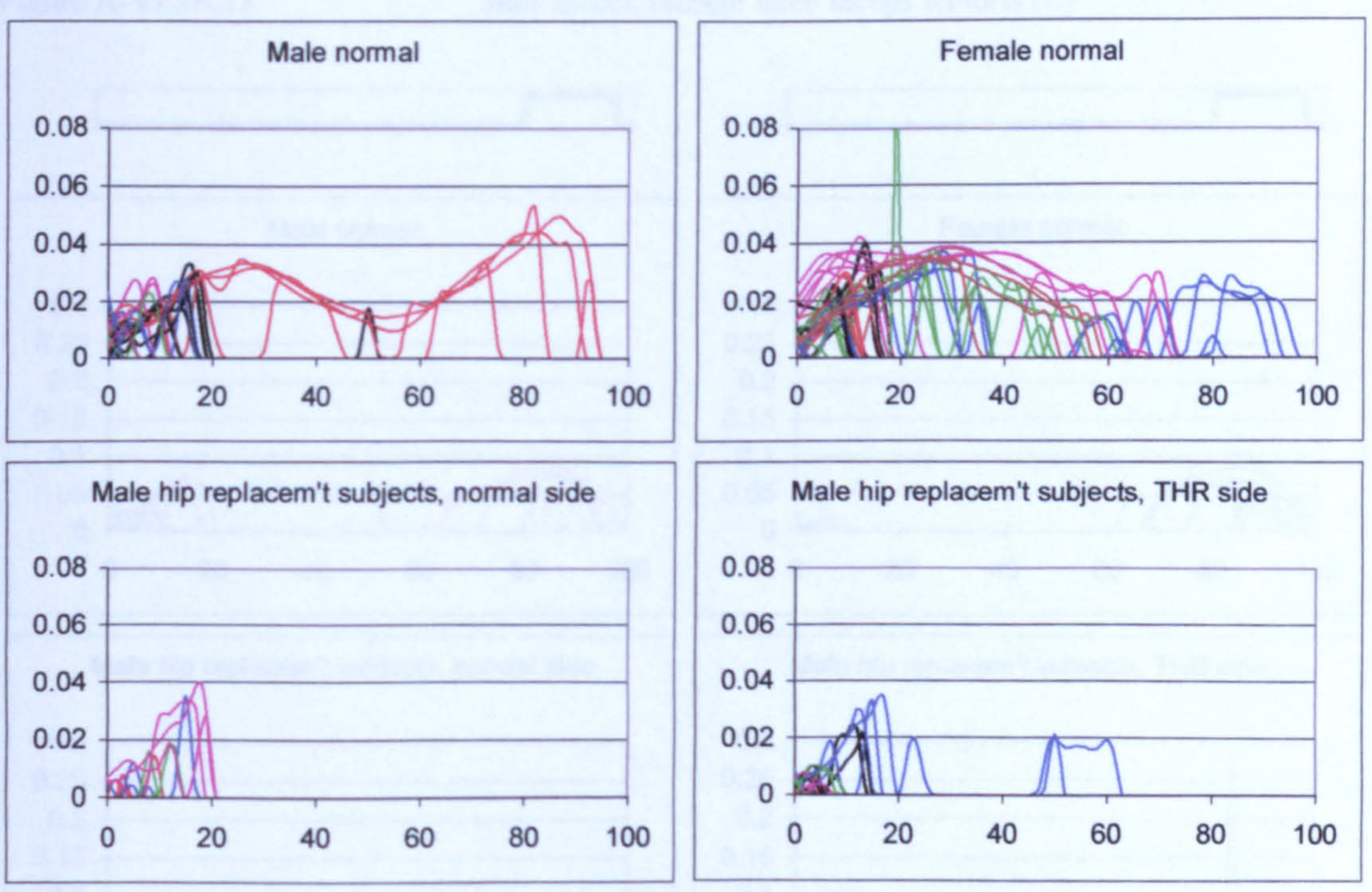

Stair ascent, muscle force gemellus superior (N/body weight) by % stance phase

Figure A-VI.3B.24 Stair ascent, muscle force gemellus superior

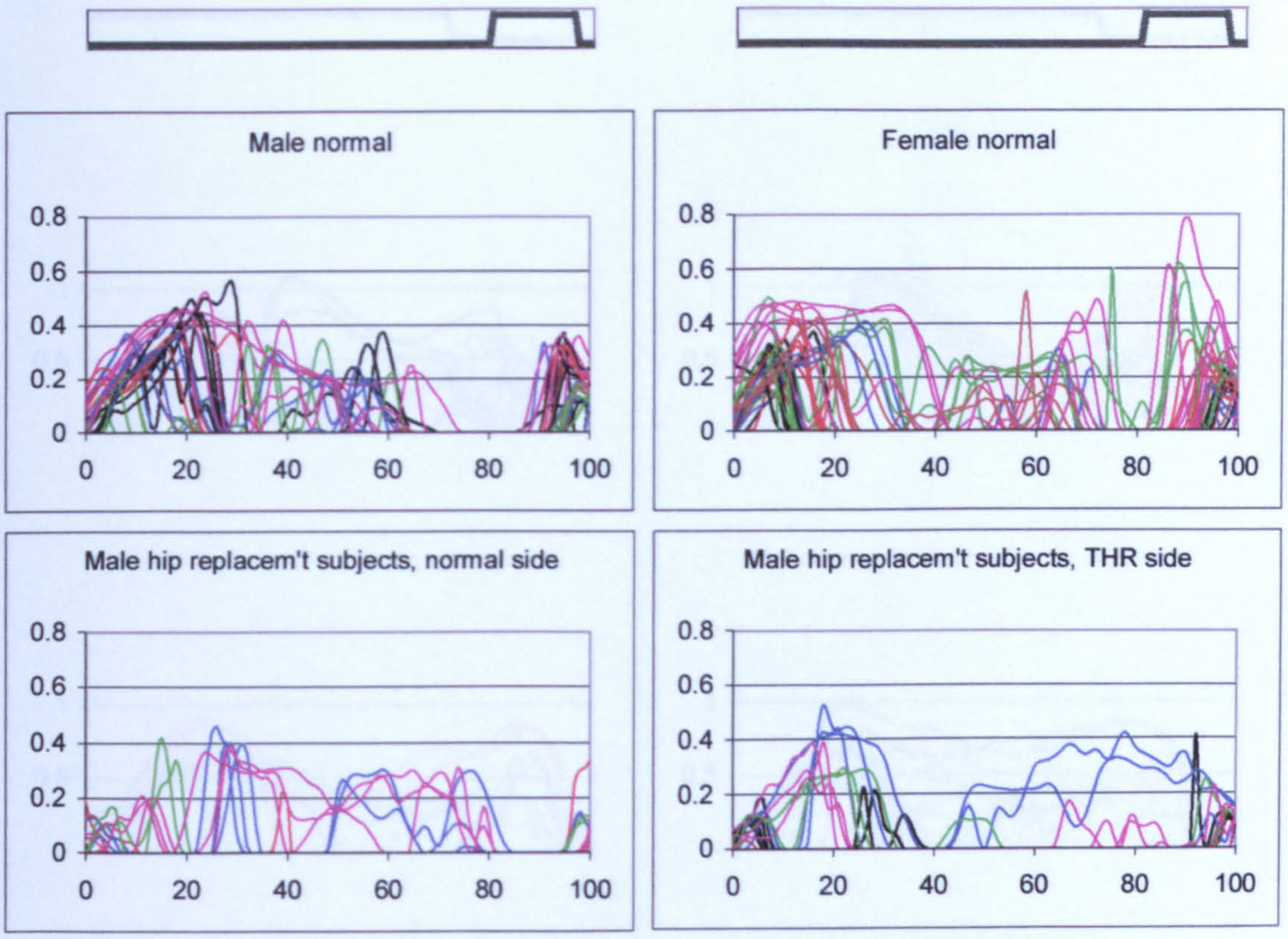

Stair ascent, muscle force biceps femoris (L) (N/body weight) by % stance phase

Figure A-VI.3B.25 Stair ascent, muscle force biceps femoris (L)

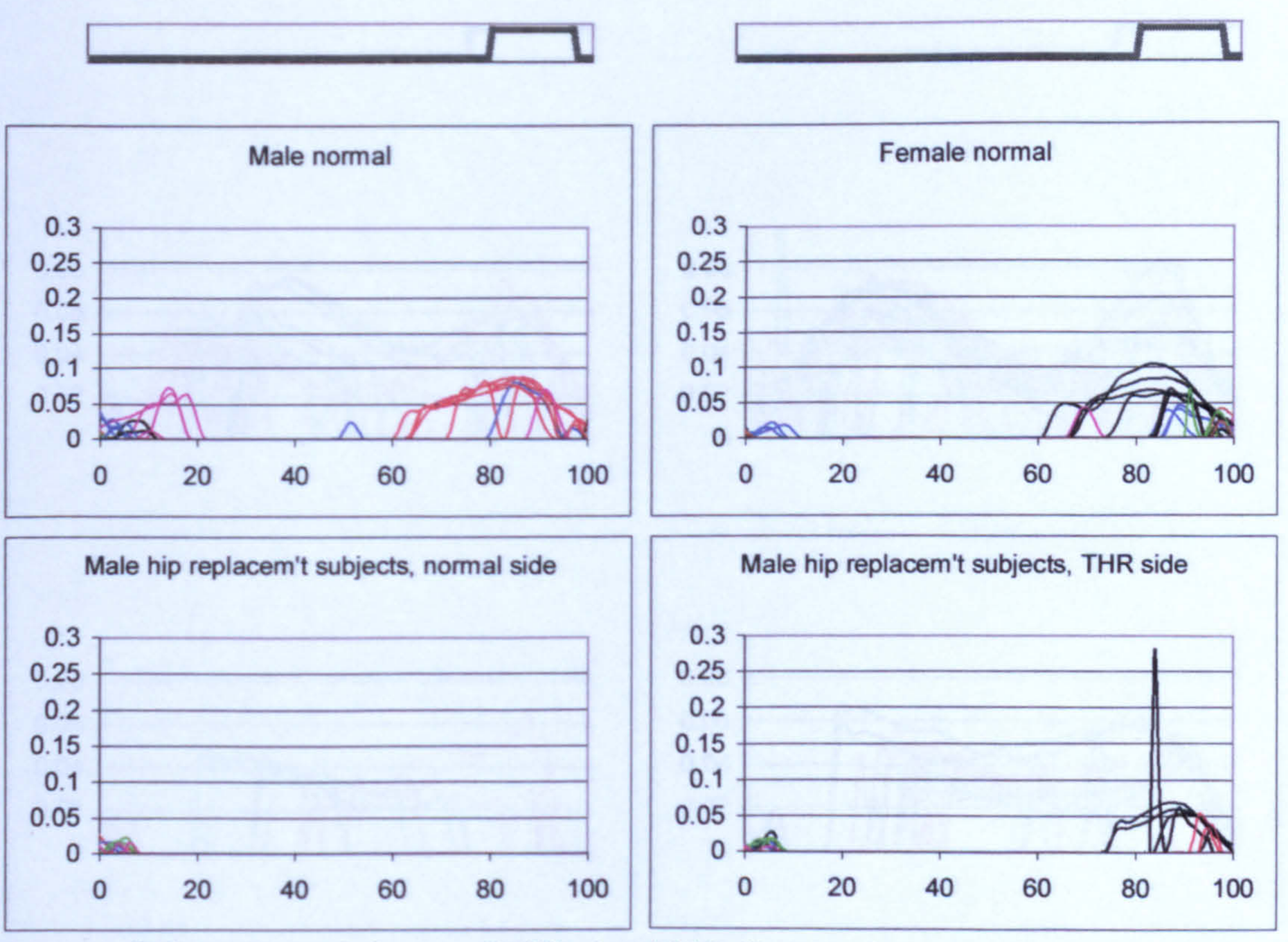

Stair ascent, muscle force gracilis (N/body weight) by % stance phase

Figure A-VI.3B.26 Stair ascent, muscle force gracilis

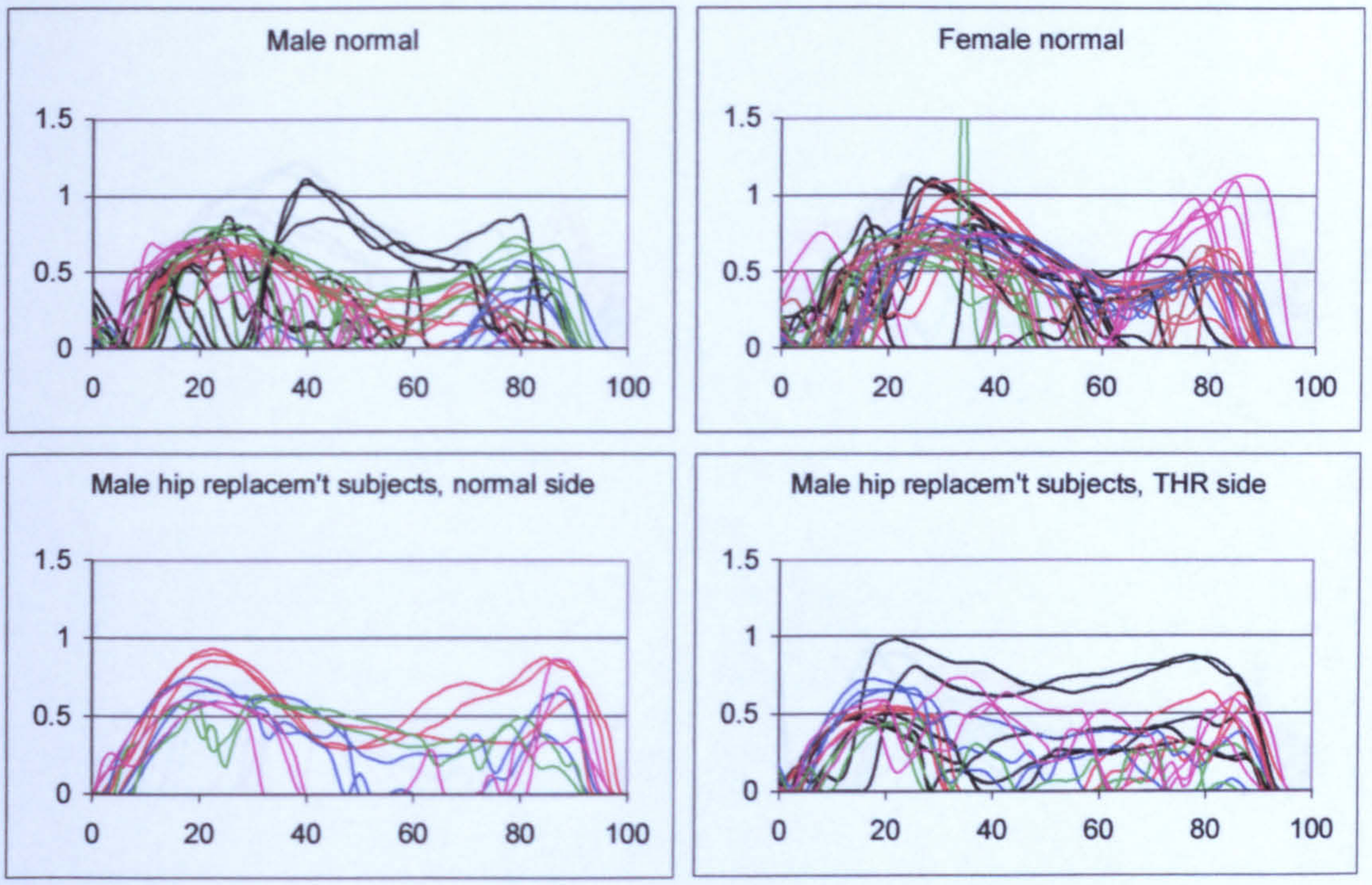

Stair ascent, muscle rectus femoris (upper part) (N/body weight) by % stance phase

Figure A-VI.3B.27 Stair ascent, muscle force rectus femoris (upper part)

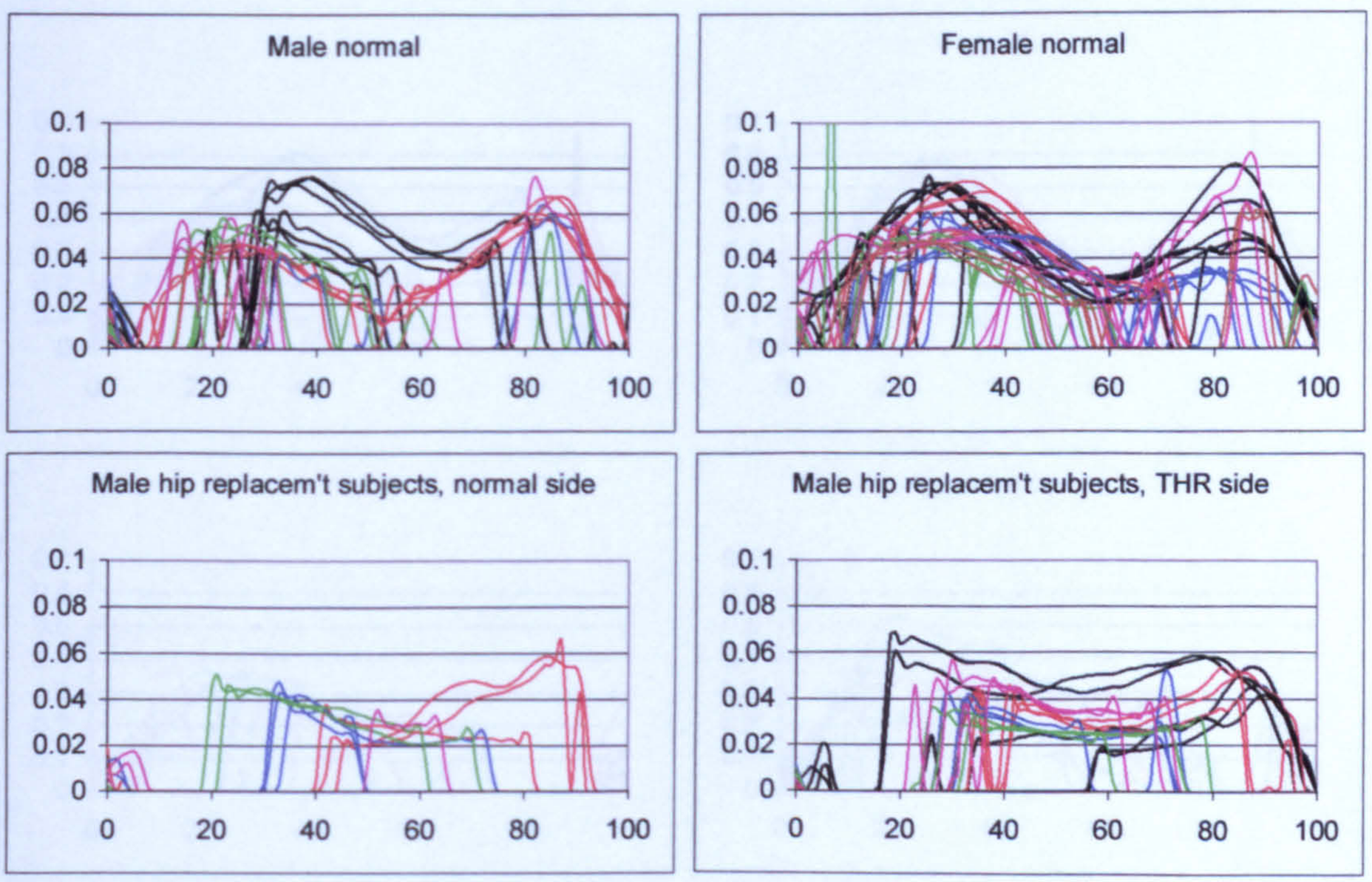

Stair ascent, muscle sartorius (N/body weight) by % stance phase

Figure A-VI.3B.28 Stair ascent, muscle force sartorius

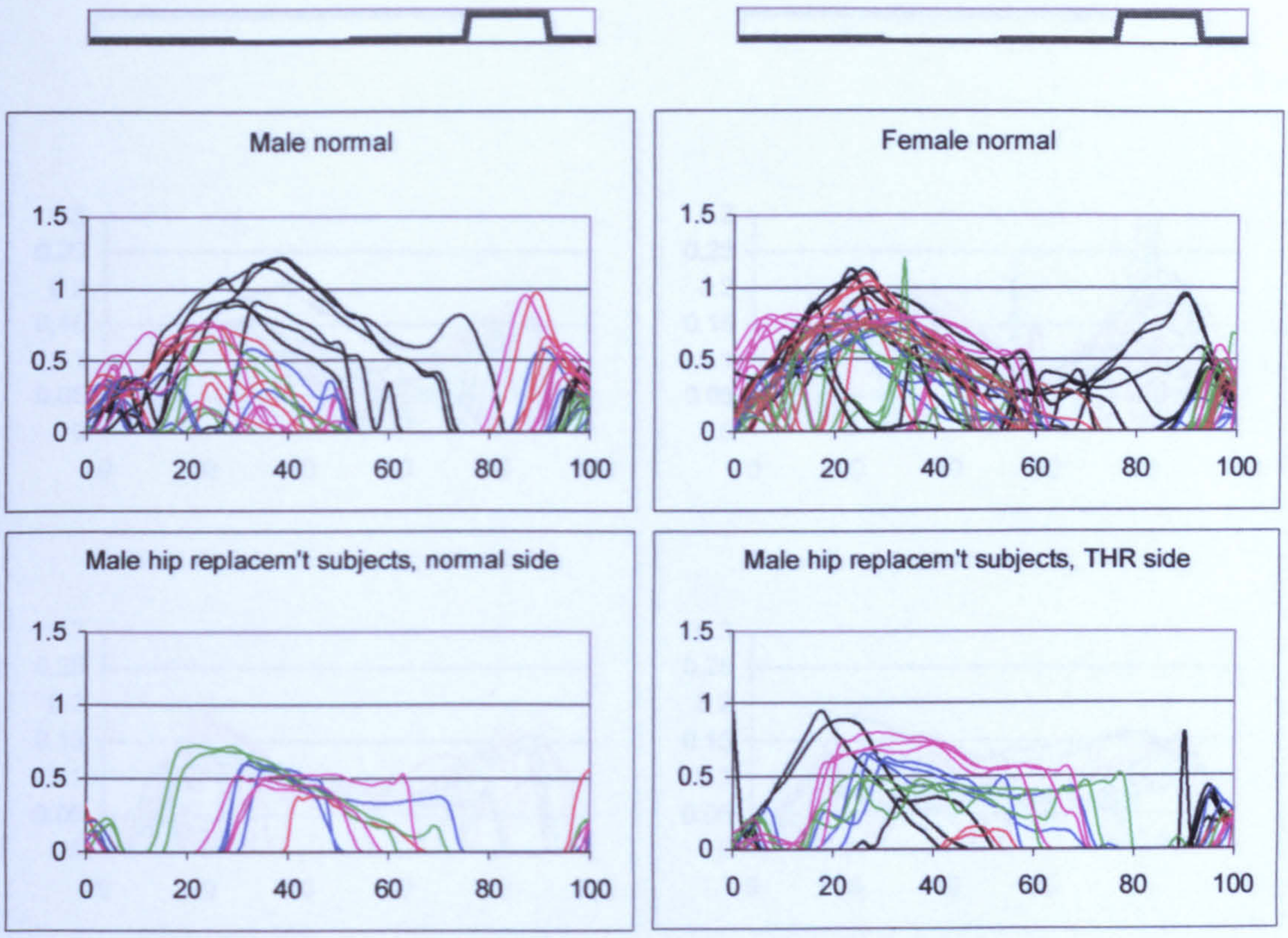

Stair ascent, muscle sartorius (N/body weight) by % stance phase

Figure A-VI.3B.29 Stair ascent, muscle force semimembranosus

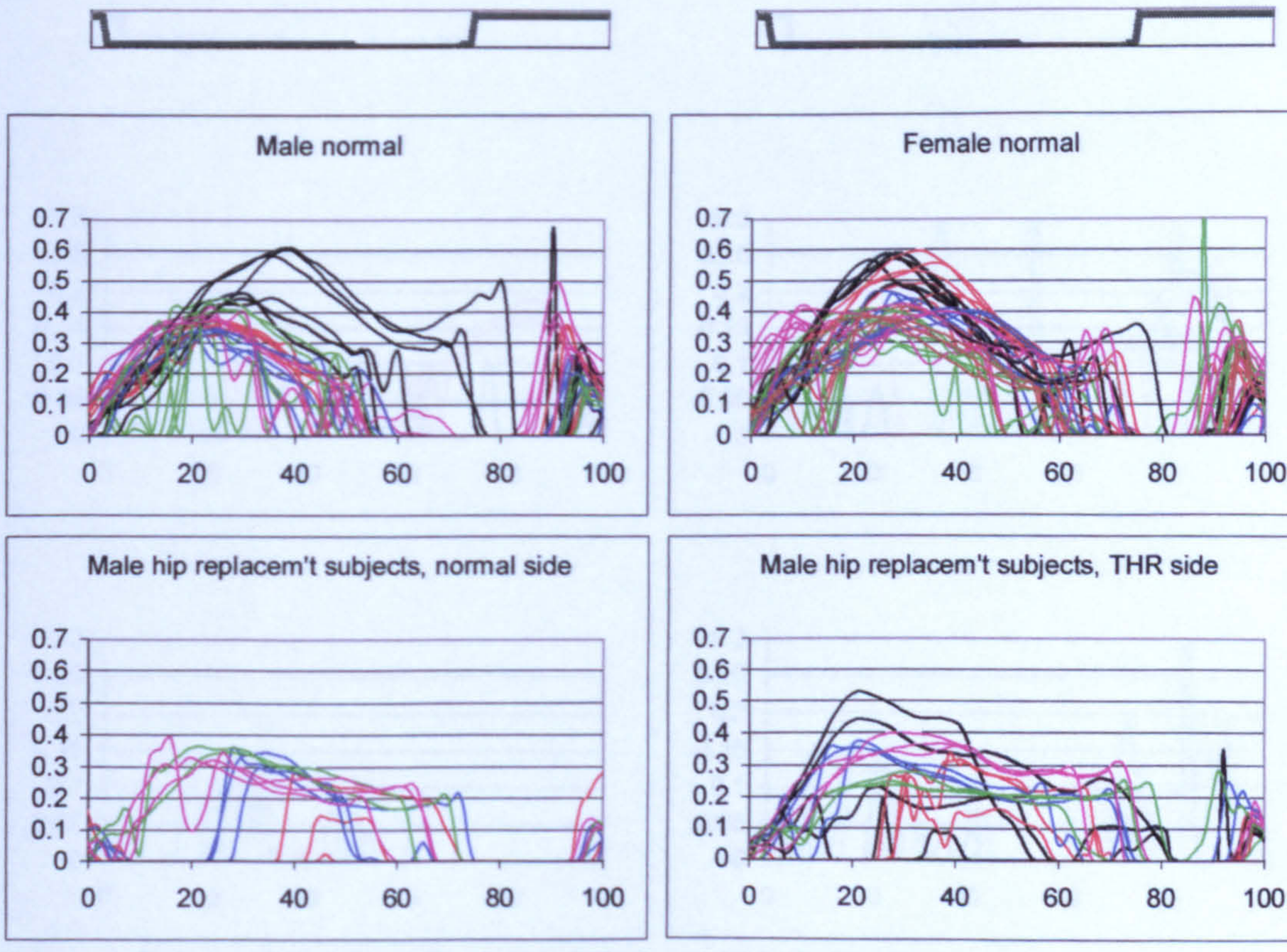

Stair ascent, muscle semitendinosus (N/body weight) by % stance phase

Figure A-VI.3B.30 Stair ascent, muscle force semitendinosus

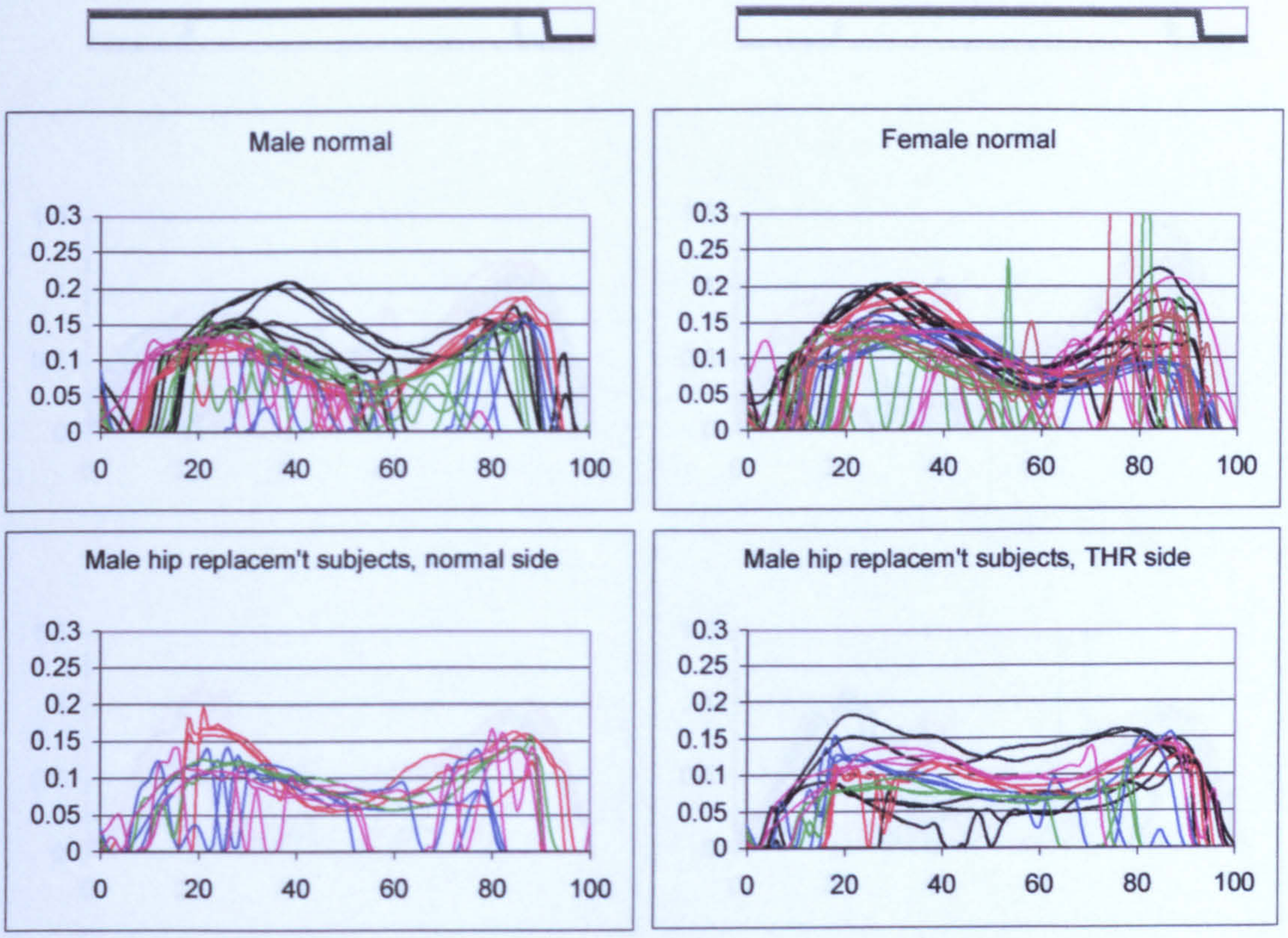

Stair ascent, muscle tensor fascia lata (N/body weight) by % stance phase

Figure A-VI.3B.31 Stair ascent, muscle force tensor facia lata

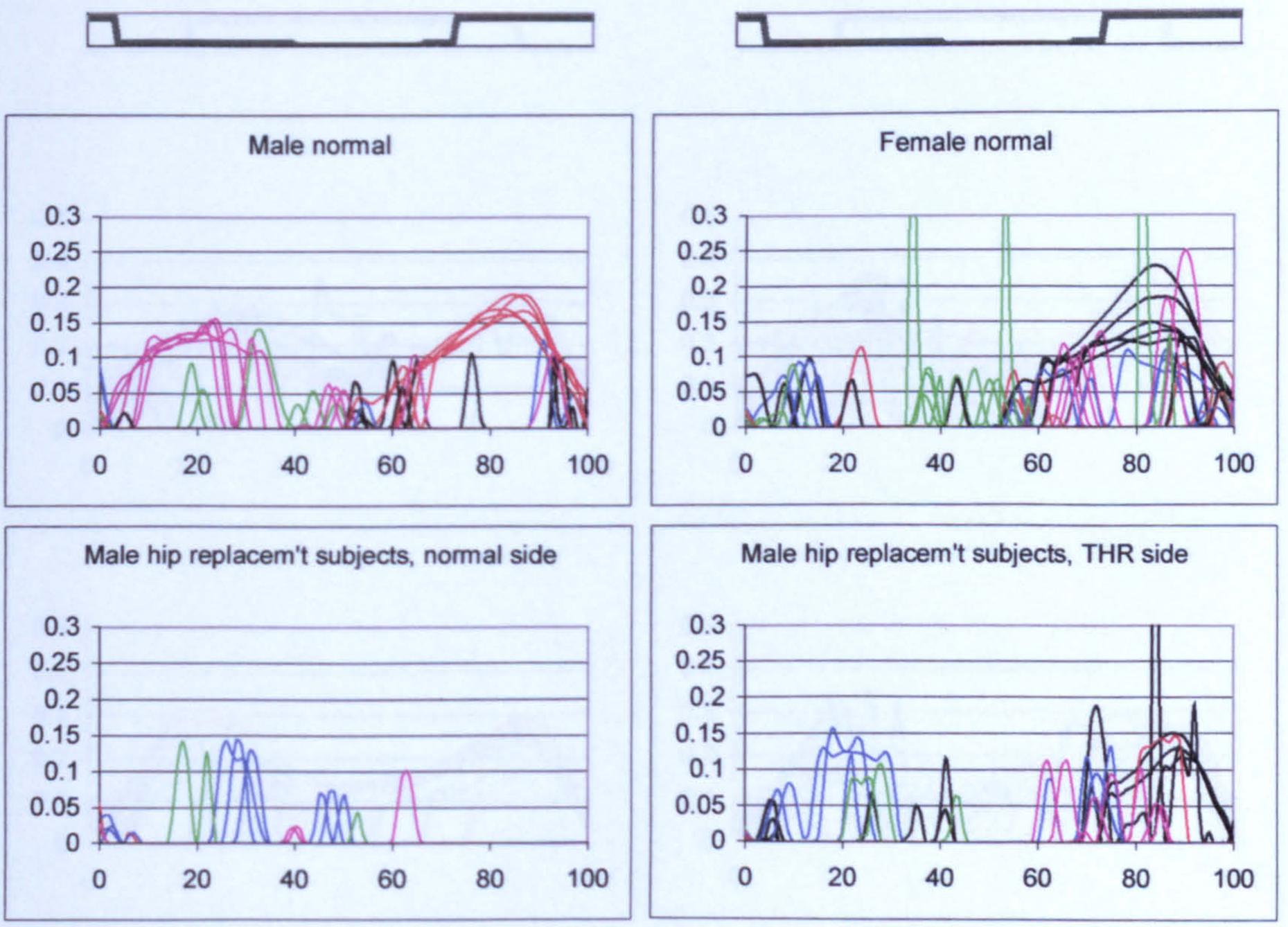

Stair ascent, muscle biceps femoris (S) (N/body weight) by % stance phase

Figure A-VI.3B.32 Stair ascent, muscle force biceps femoris (S)

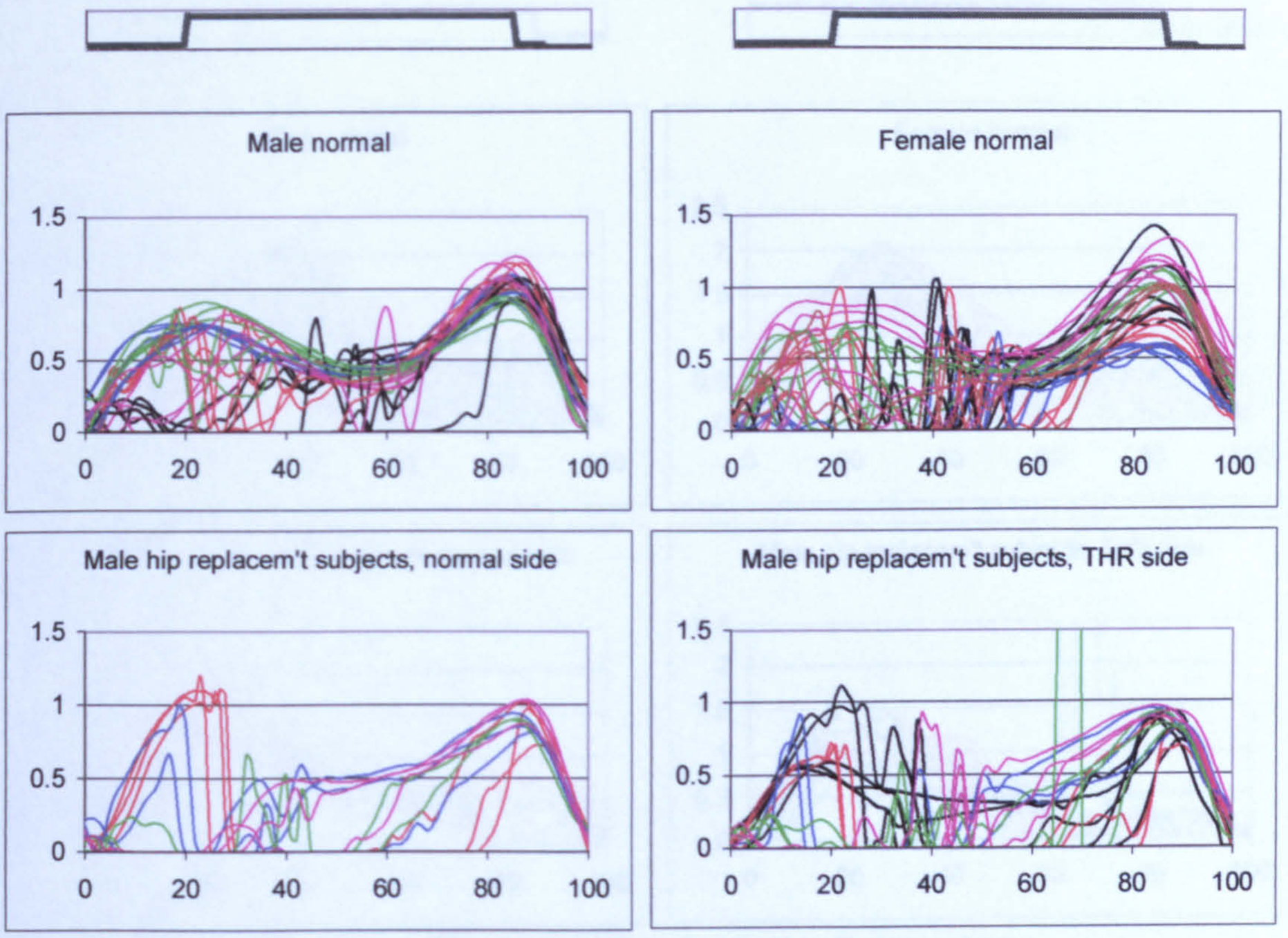

Stair ascent, muscle gastrocnemius (M) (N/body weight) by % stance phase

Figure A-VI.3B.33 Stair ascent, muscle force gastrocnemius (M)

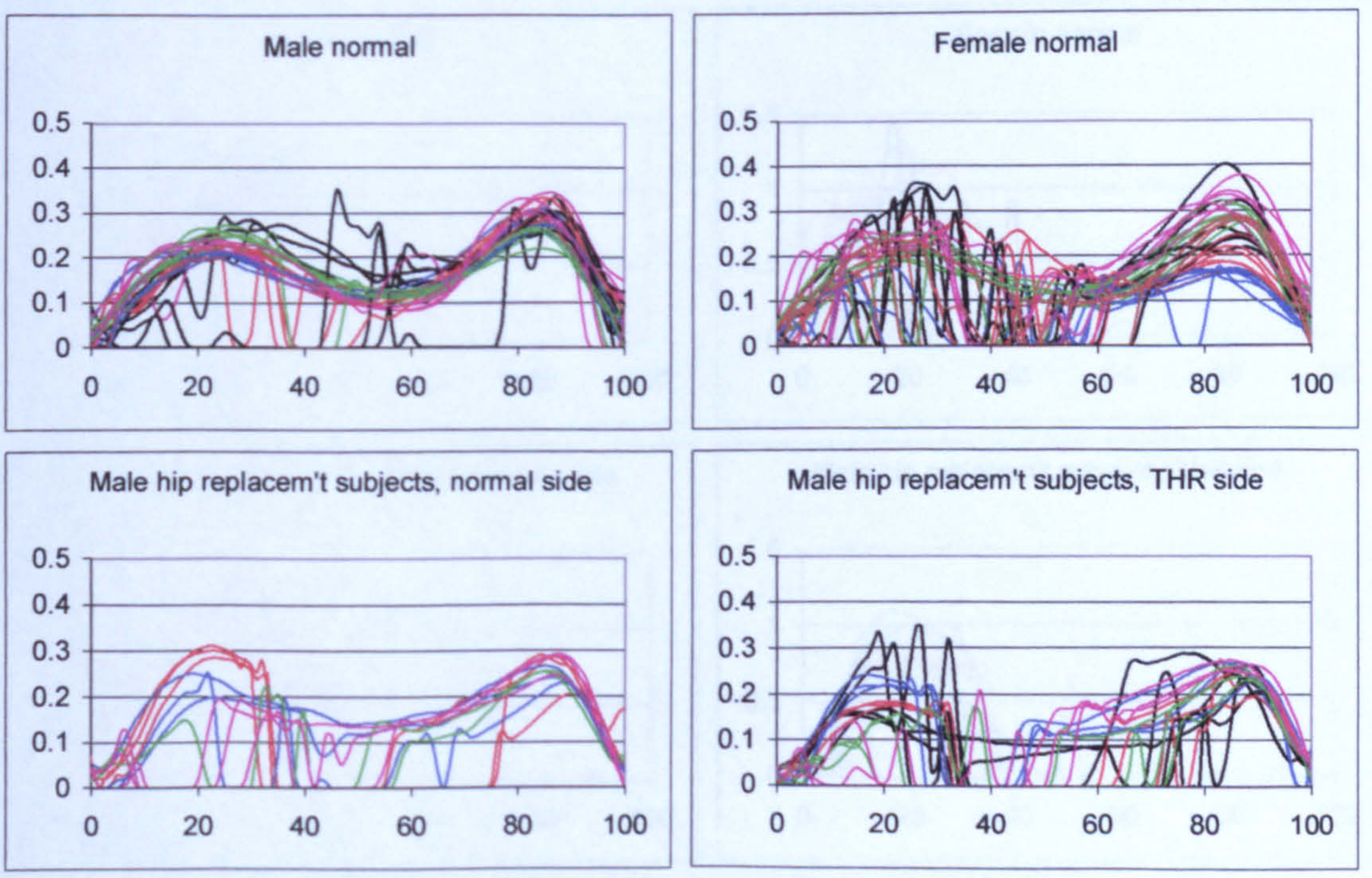

Stair ascent, muscle gastrocnemius (L) (N/body weight) by % stance phase

Figure A-VI.3B.34 Stair ascent, muscle force gastrocnemius (L)

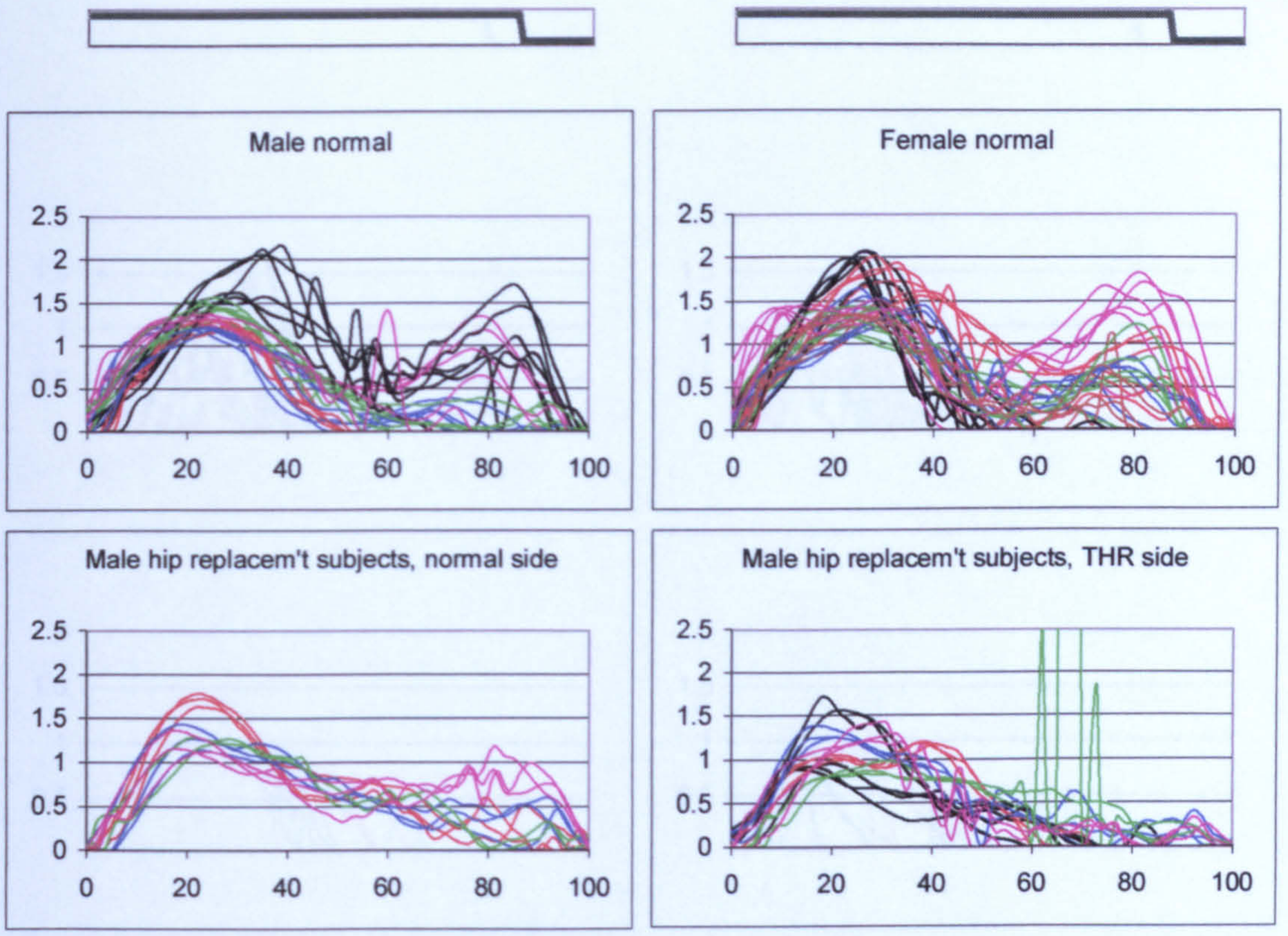

Stair ascent, muscle vastus intermedius (N/body weight) by % stance phase

Figure A-VI.3B.35 Stair ascent, muscle force vastus intermedius

Stair ascent, muscle vastus lateralis (N/body weight) by % stance phase

Figure A-VI.3B.36 Stair ascent, muscle force vastus lateralis

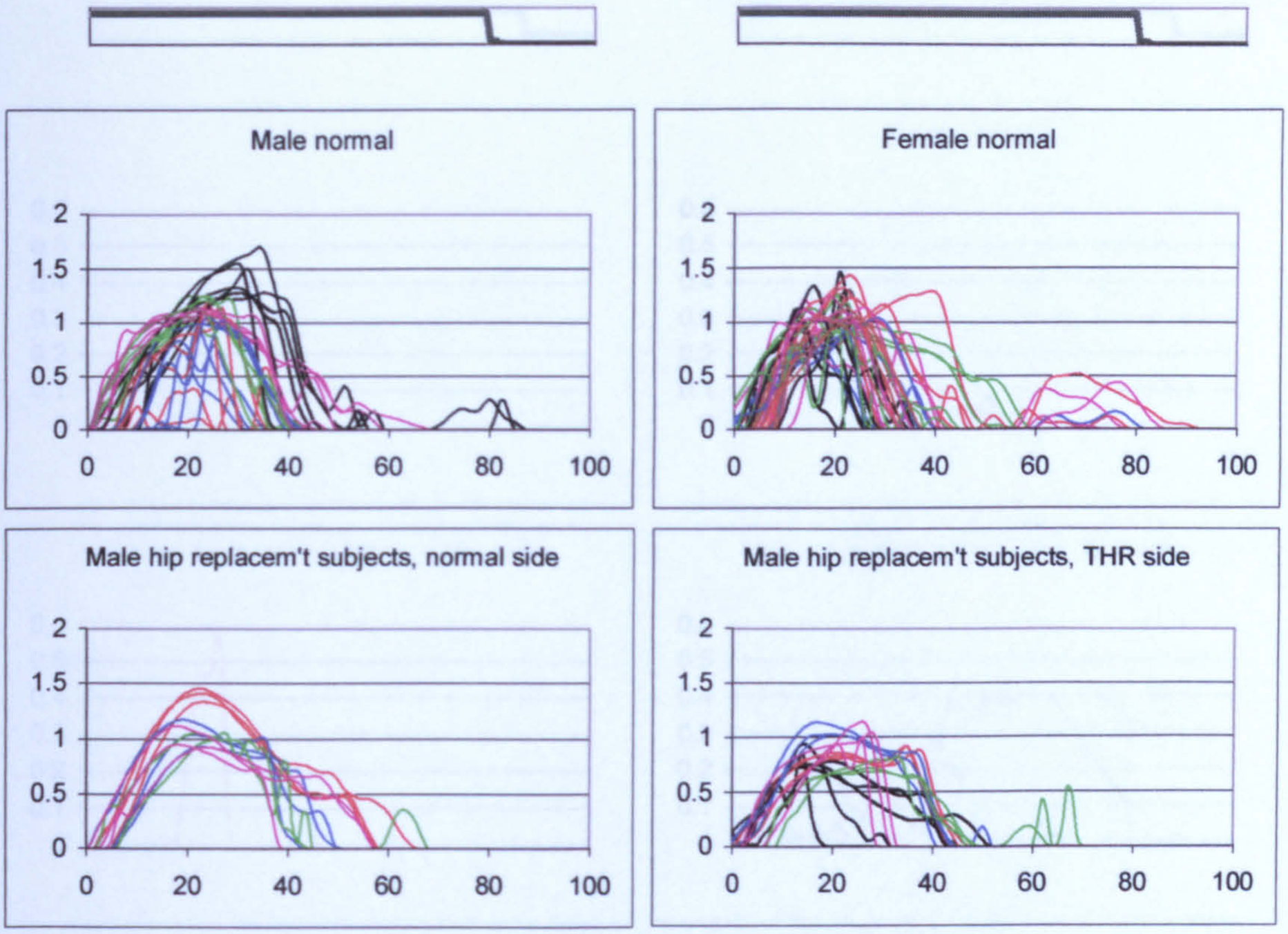

Stair ascent, muscle vastus medialis (N/body weight) by % stance phase

Figure A-VI.3B.37 Stair ascent, muscle force vastus medialis

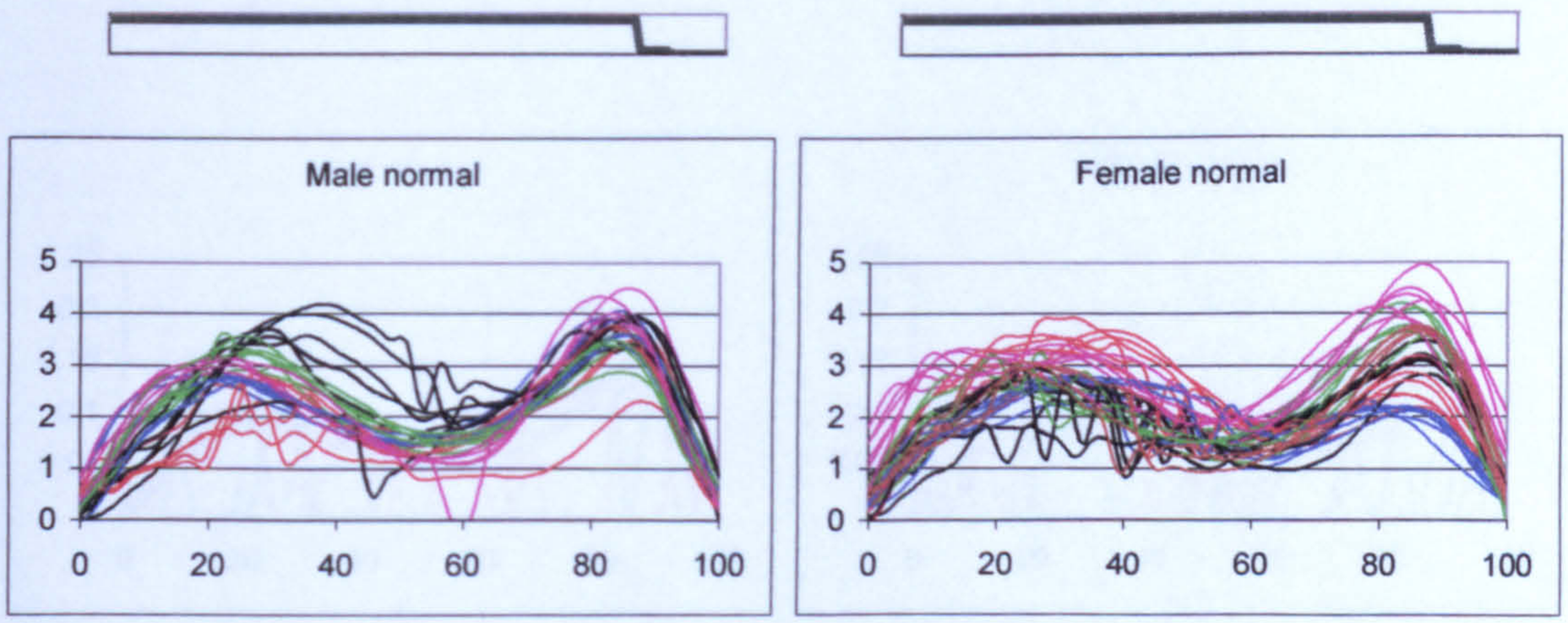

Stair ascent, muscle soleus (N/body weight) by % stance phase

Figure A-VI.3B.38 Stair ascent, muscle force soleus

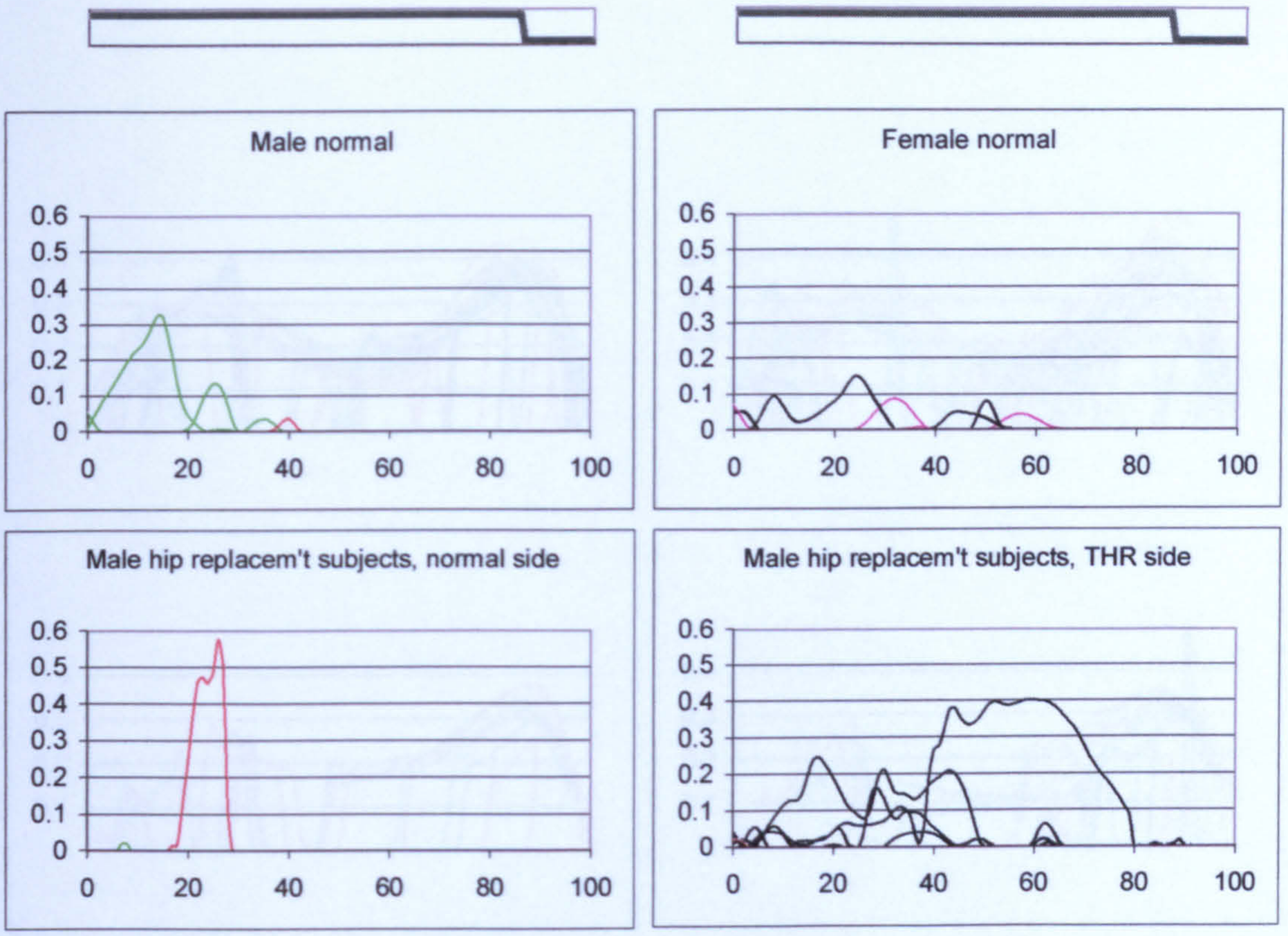

Stair ascent, muscle tibialis posterior (N/body weight) by % stance phase

Figure A-VI.3B.39 Stair ascent, muscle force tibialis posterior

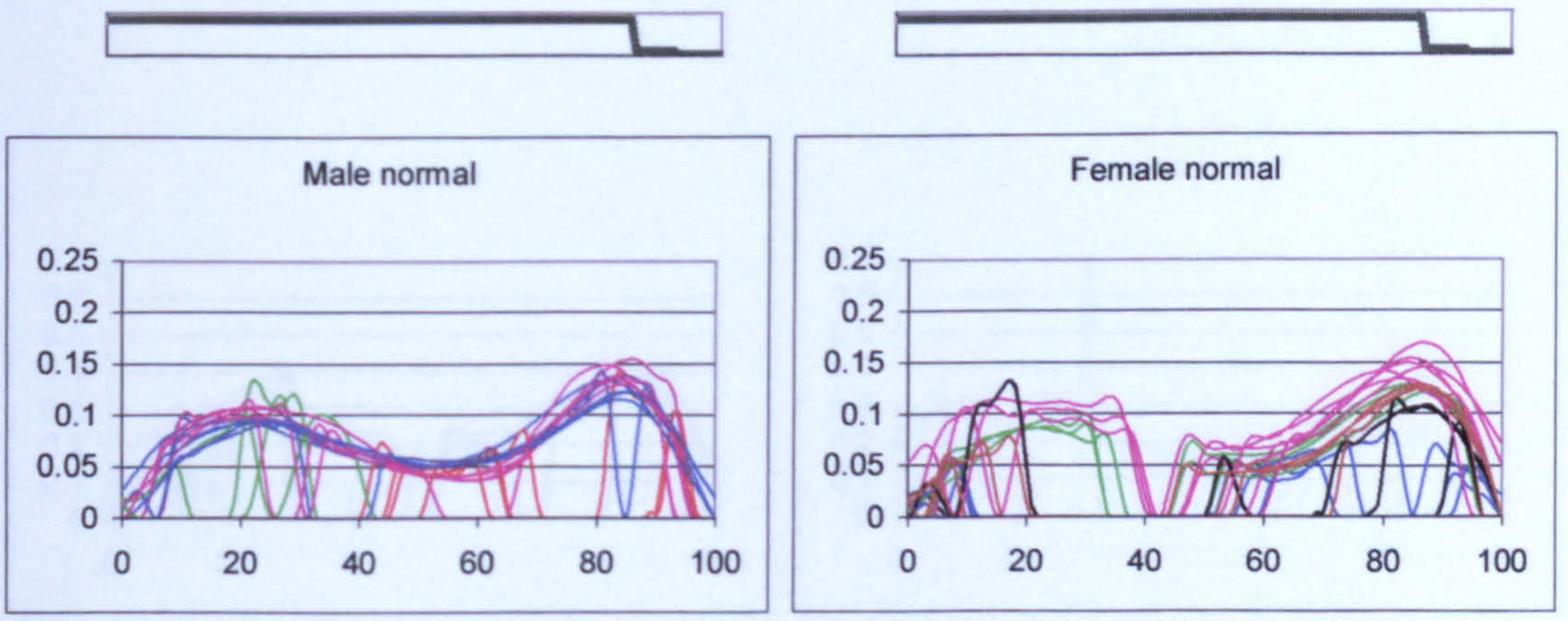

Stair ascent, muscle flexor digitorum longus (N/body weight) by % stance phase

Figure A-VI.3B.40 Stair ascent, muscle force flexor digitorum longus

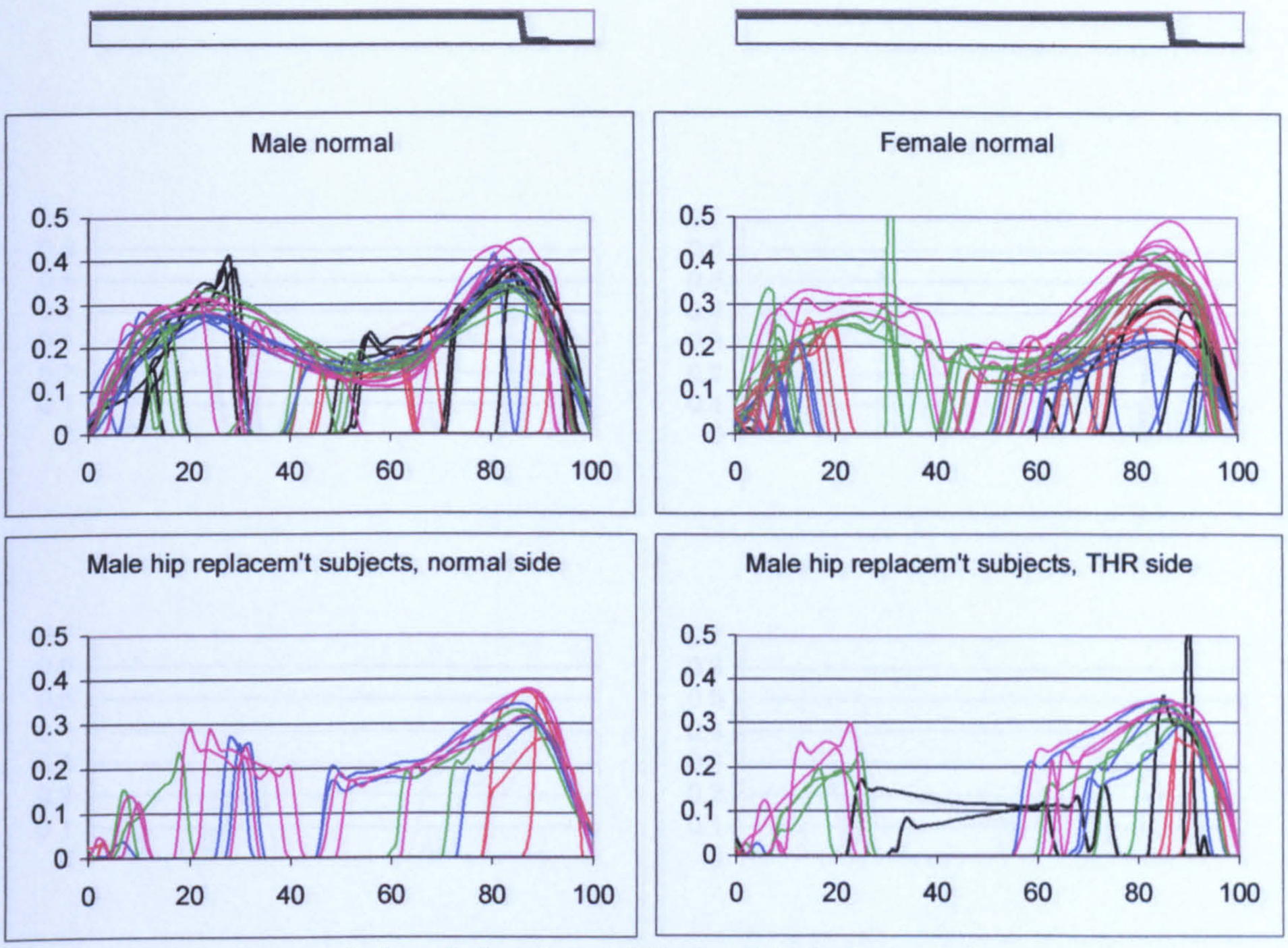

Stair ascent, muscle flexor hallucis longus (N/body weight) by % stance phase

Figure A-VI.3B.41 Stair ascent, muscle force flexor hallucis longus

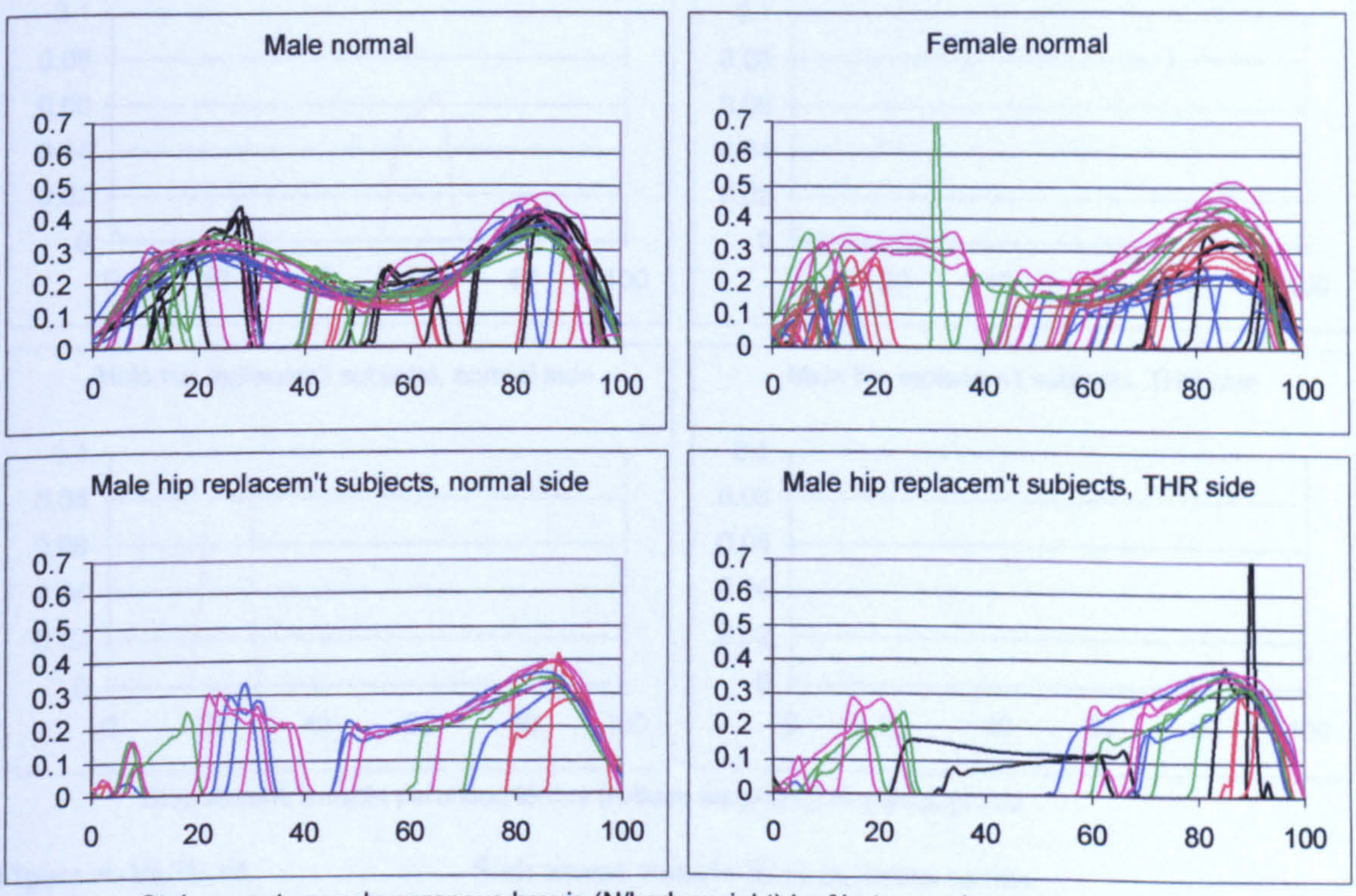

Stair ascent, muscle peroneus brevis (N/body weight) by % stance phase

Figure A-VI.3B.42 Stair ascent, muscle force peroneus brevis

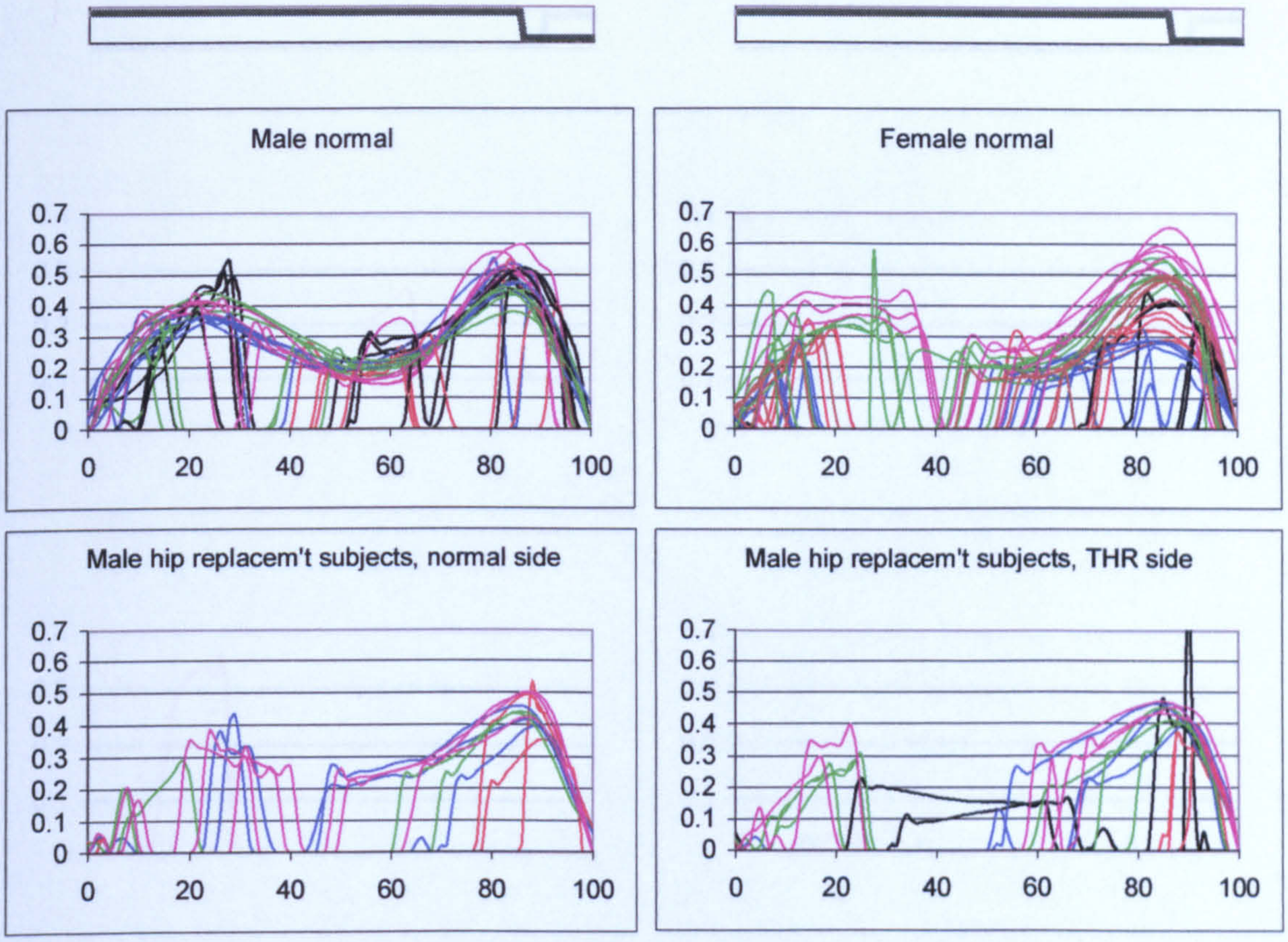

Stair ascent, muscle peroneus longus (N/body weight) by % stance phase

Figure A-VI.3B.43 Stair ascent, muscle force peroneus longus

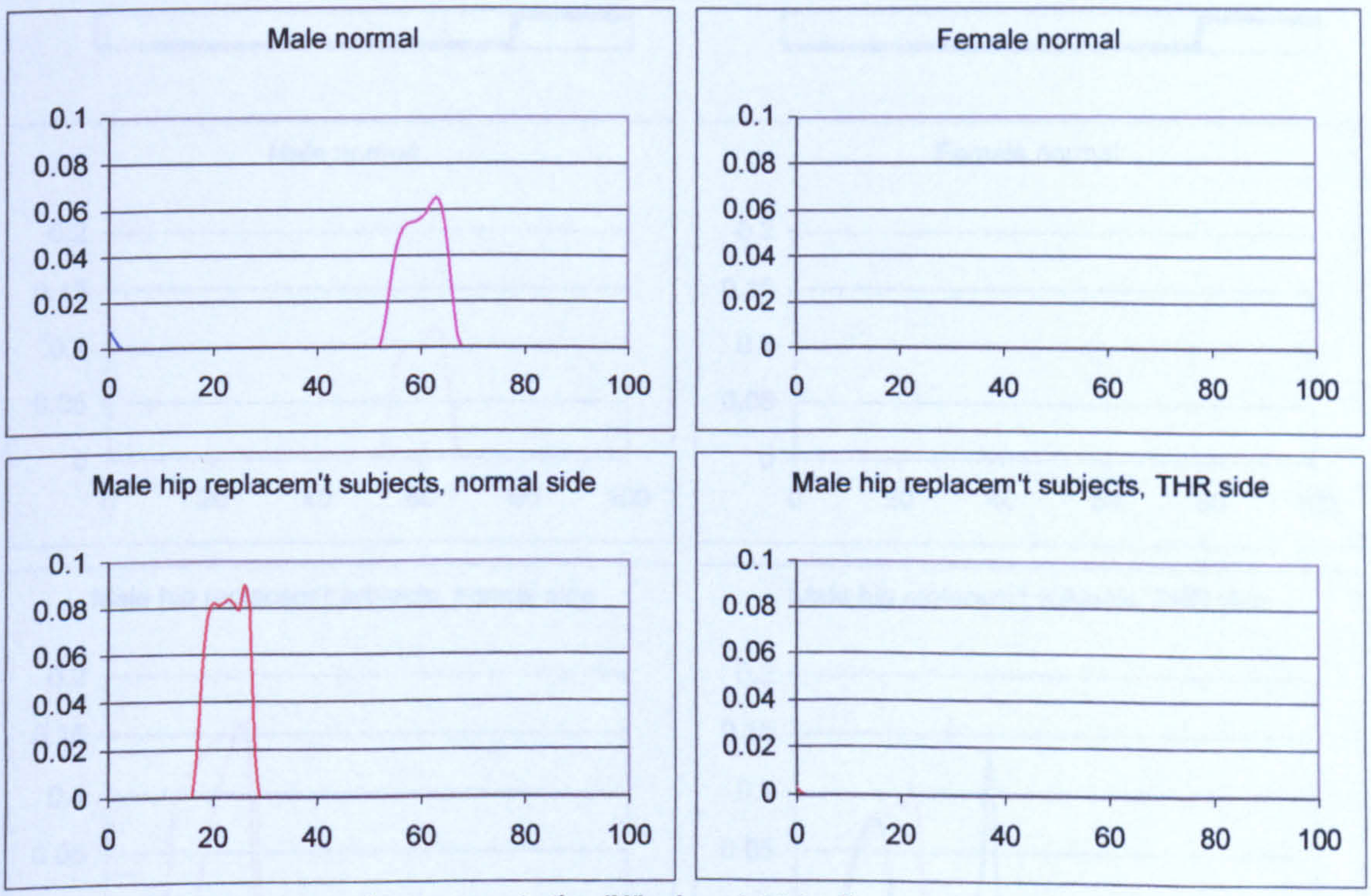

Stair ascent, muscle peroneus tertius (N/body weight) by % stance phase

Figure A-VI.3B.44 Stair ascent, muscle force peroneus tertius

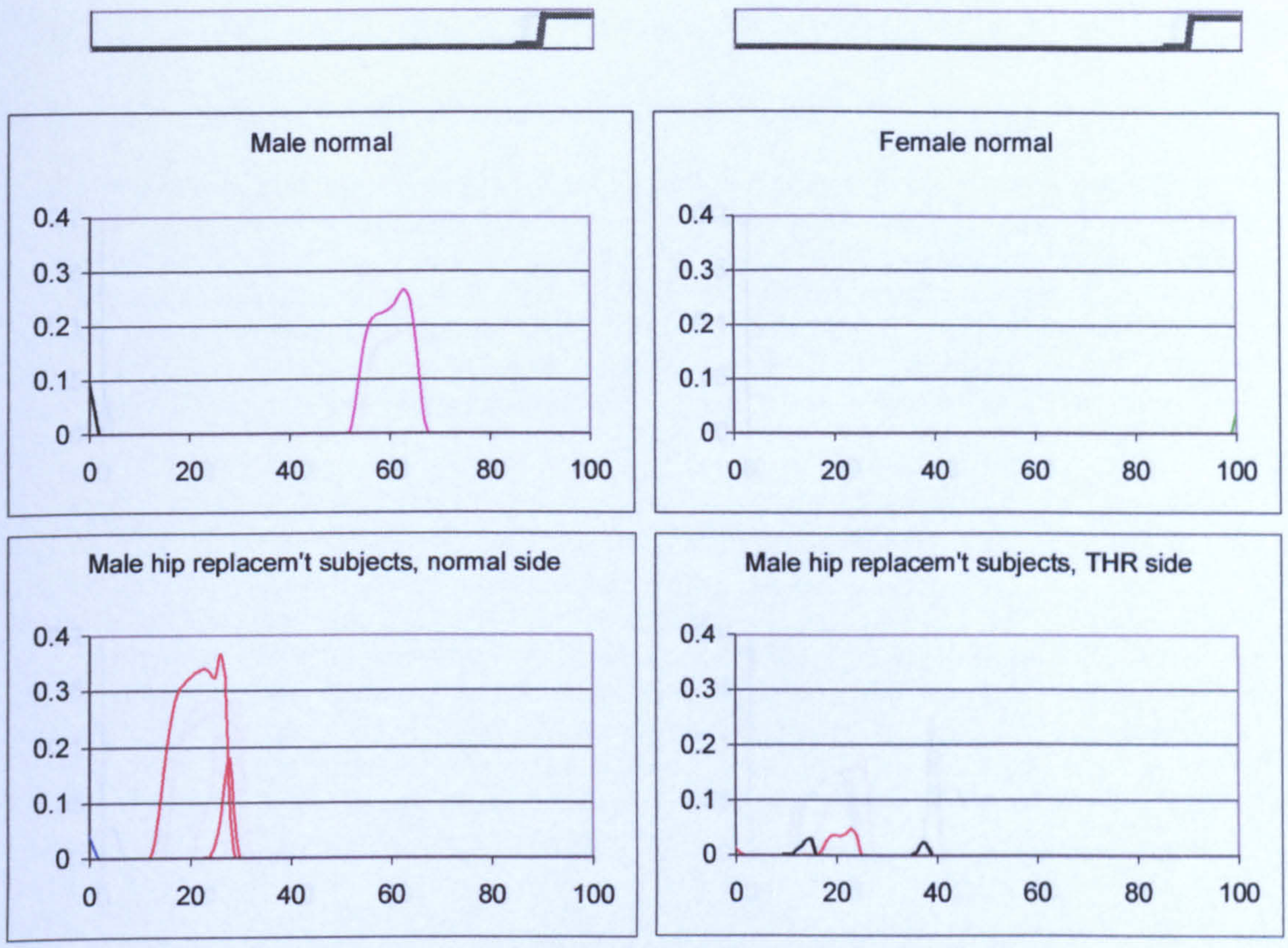

Stair ascent, muscle tibialis anterior (N/body weight) by % stance phase

Figure A-VI.3B.45 Stair ascent, muscle force tibialis anterior

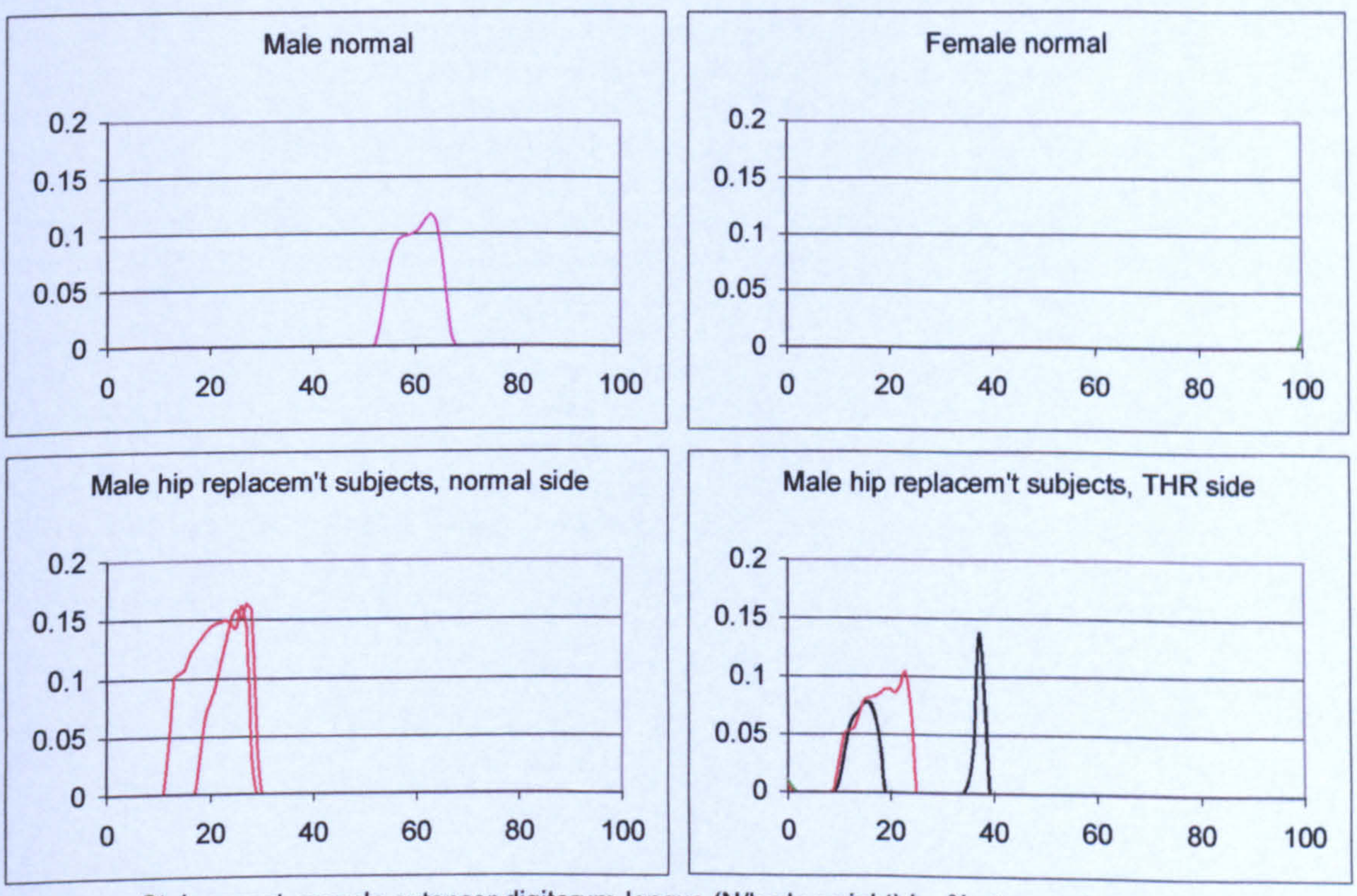

Stair ascent, muscle extensor digitorum longus (N/body weight) by % stance phase

Figure A-VI.3B.46 Stair ascent, muscle force extensor digitorum longus

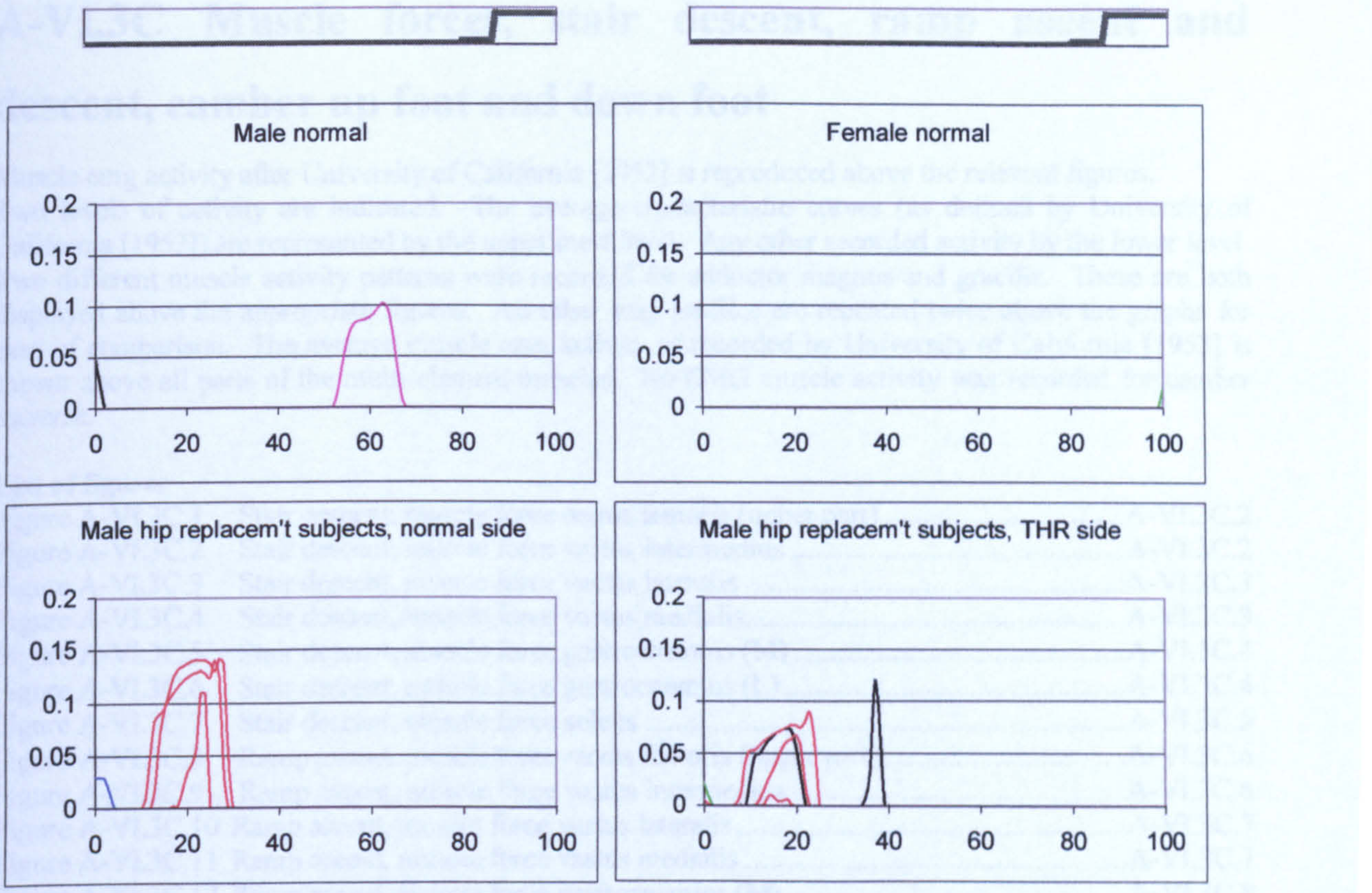

Figure A-VI.3B.47 Stair ascent, muscle force extensor hallucis longus

A-VI.3C Muscle forces, stair descent, ramp ascent and descent, camber up foot and down foot

Muscle emg activity after University of California [1953] is reproduced above the relevant figures. Two levels of activity are indicated. The average characteristic curves (as defined by University of California [1953]) are represented by the upper most level. Any other recorded activity by the lower level Two different muscle activity patterns were recorded for adductor magnus and gracilis. These are both displayed above the appropriate figures. All other emg profiles are repeated twice above the graphs for ease of comparison. The average muscle emg activity as recorded by University of California [1953] is shown above all parts of the multi-element muscles. No EMG muscle activity was recorded for camber traverse.

List of figures

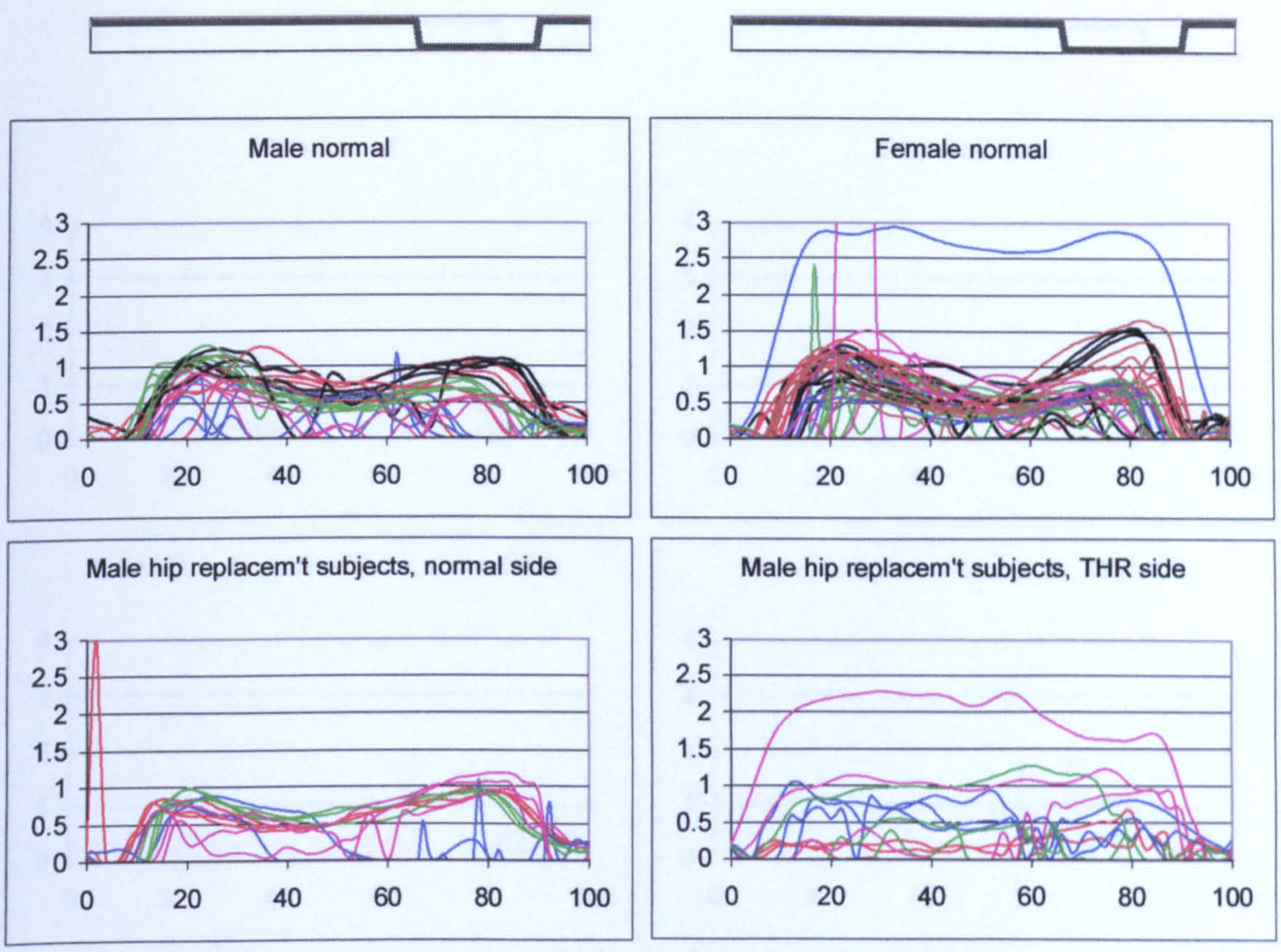

Stair descent, muscle force rectus femoris (N/body weight) by % stance phase

Figure A-VI.3C.1 Stair descent, muscle force rectus femoris (upper part)

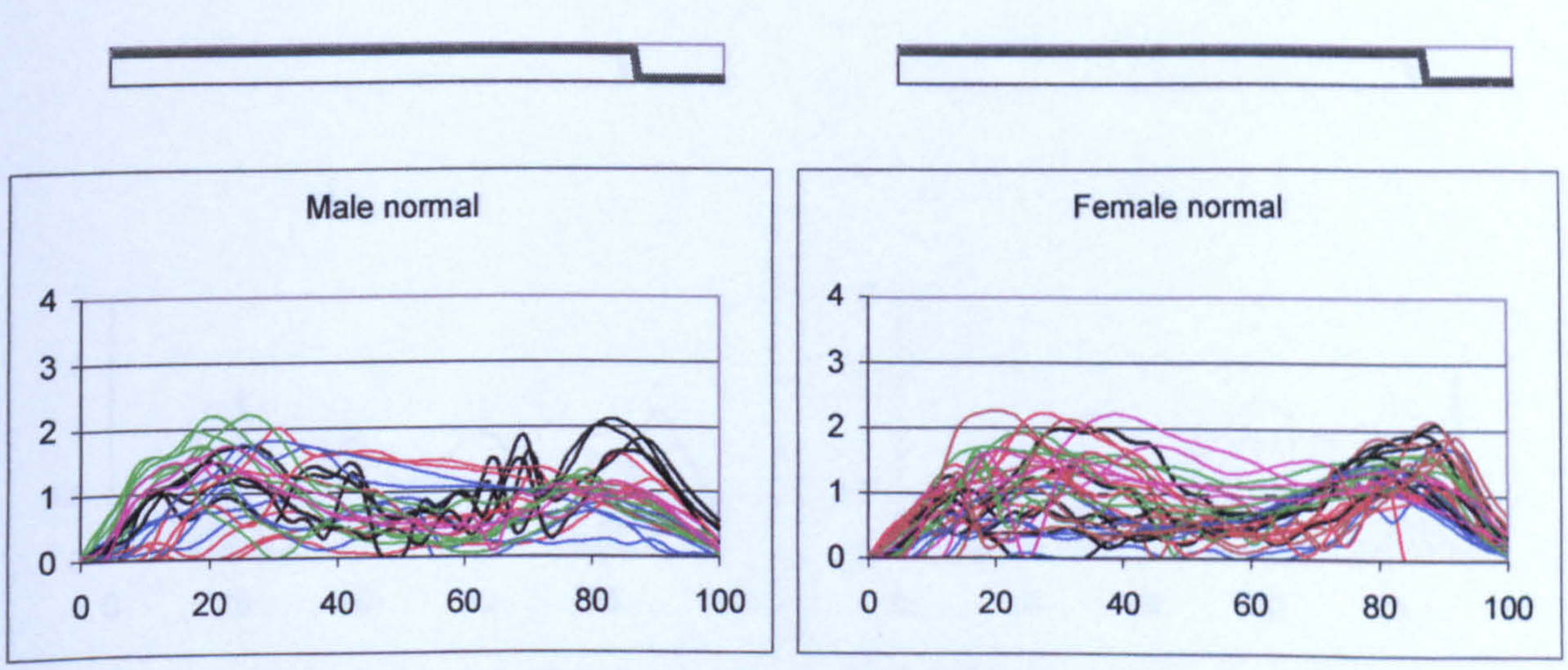

Stair descent, muscle force vastus intermedius (N/body weight) by % stance phase

Figure A-VI.3C.2 Stair descent, muscle force vastus intermedius

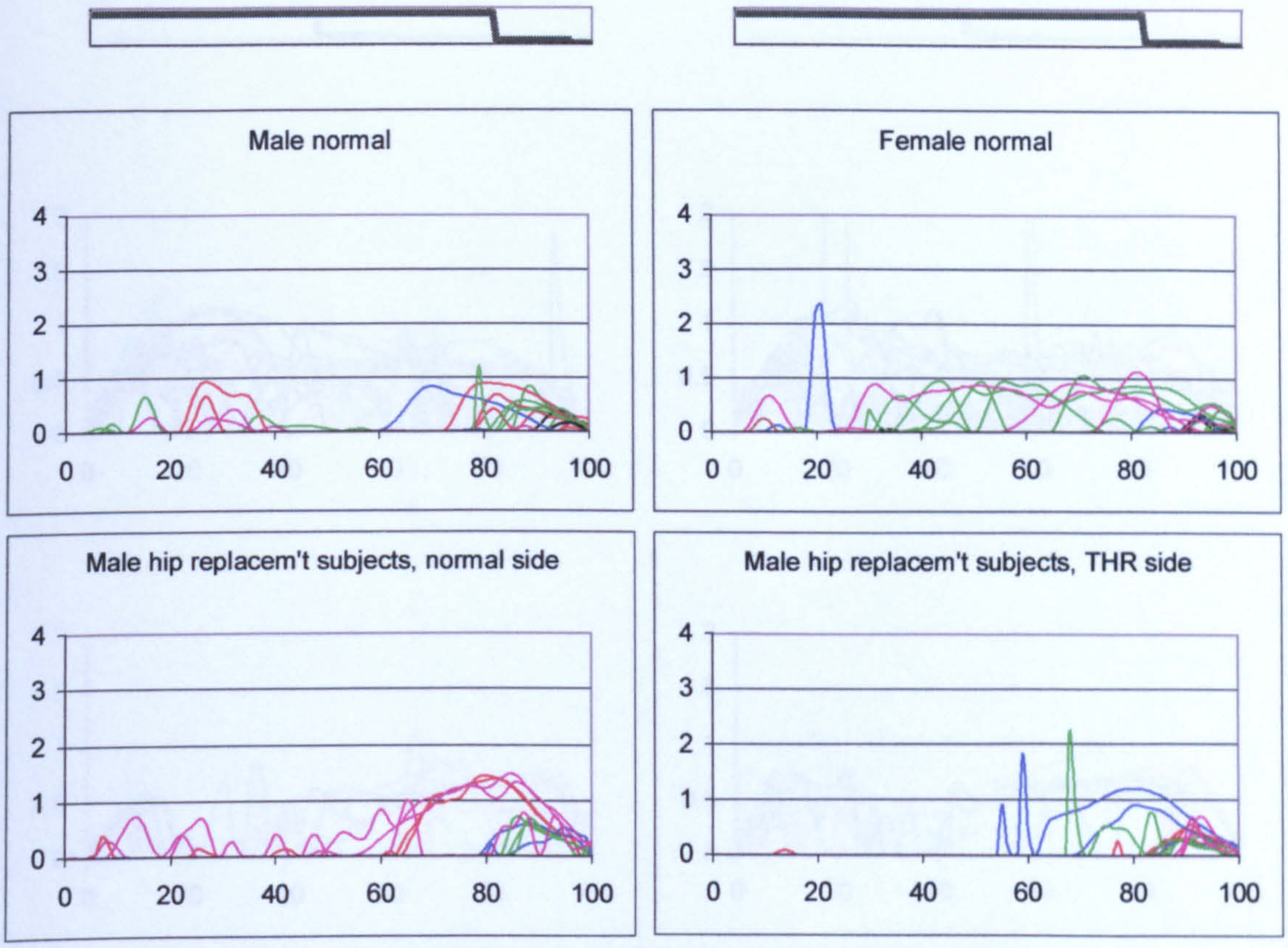

Stair descent, muscle force vastus lateralis (N/body weight) by % stance phase

Figure A-VI.3C.3 Stair descent, muscle force vastus lateralis

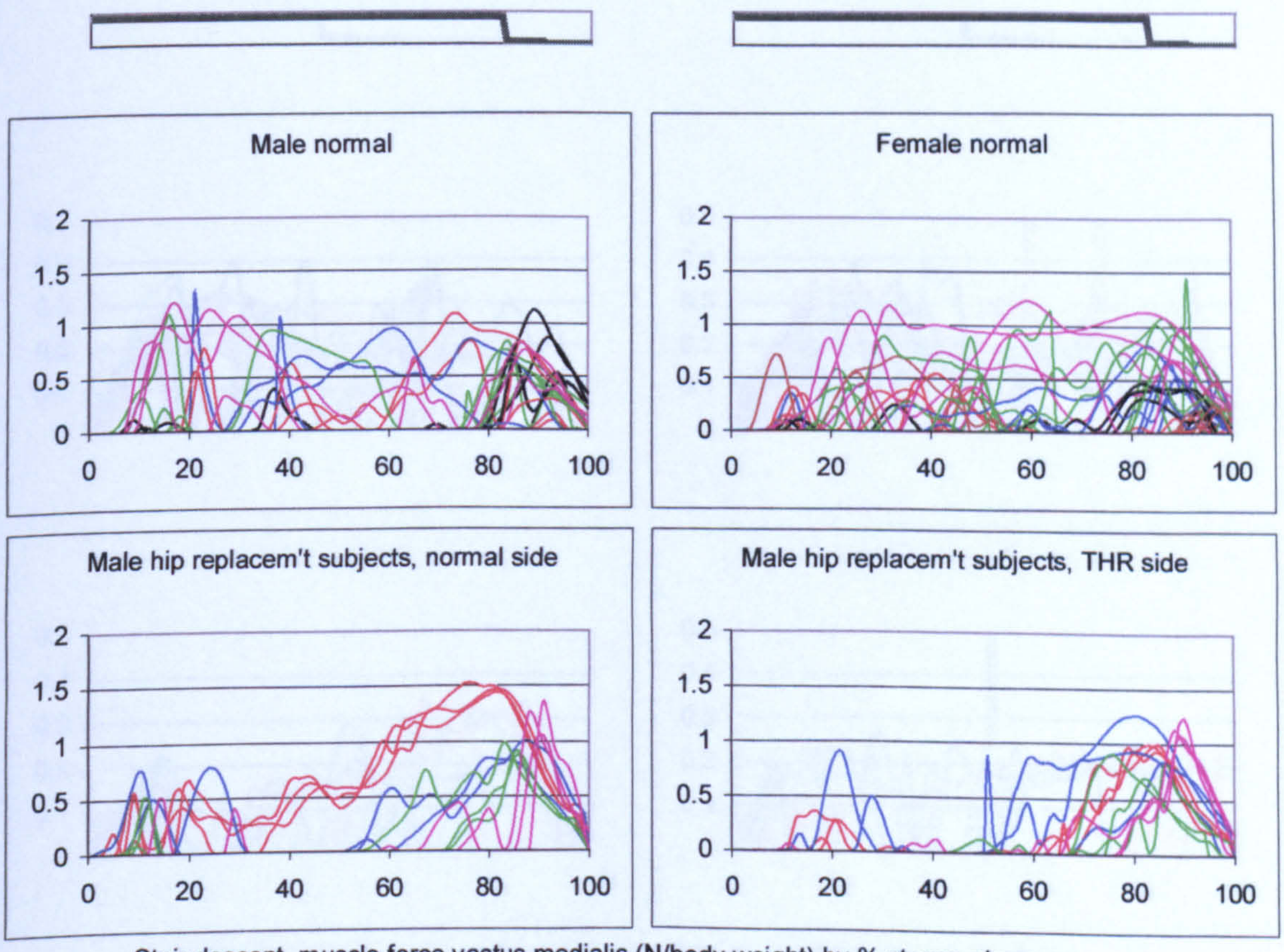

Stair descent, muscle force vastus medialis (N/body weight) by % stance phase

Figure A-VI.3C.4 Stair descent, muscle force vastus medialis

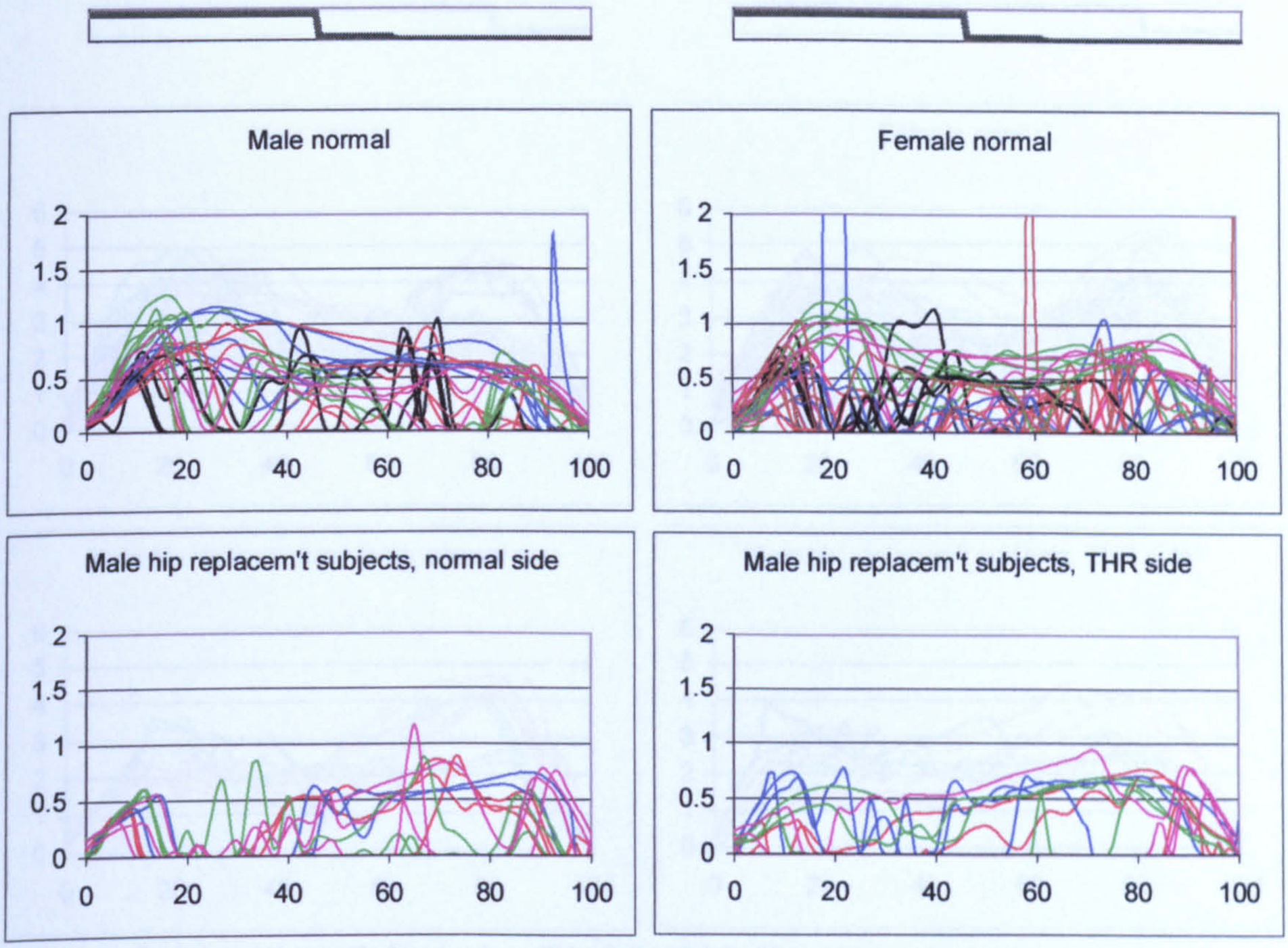

Stair descent, muscle force gastrocnemius (M) (N/body weight) by % stance phase

Figure A-VI.3C.5 Stair descent, muscle force gastrocnemius (M)

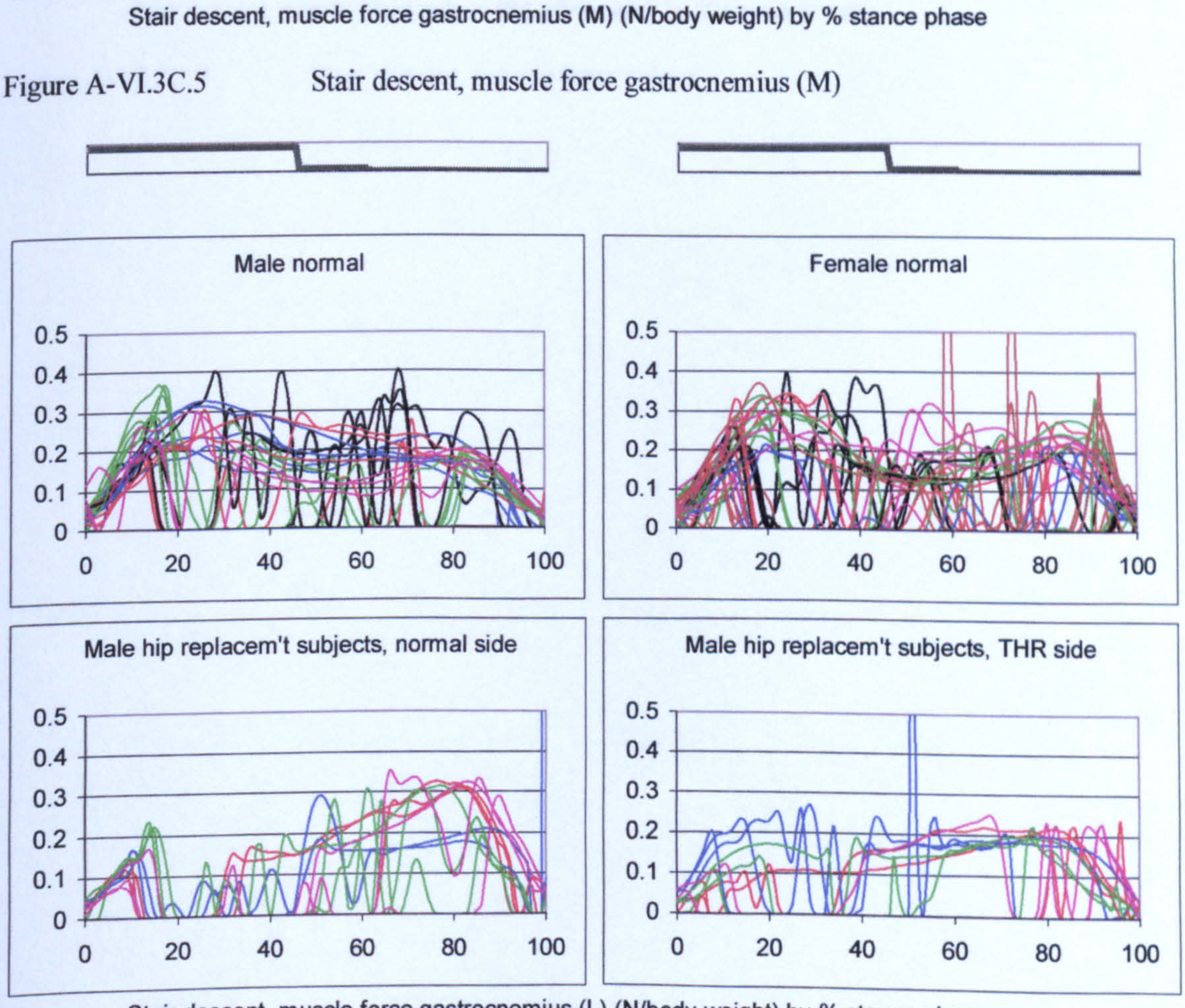

Stair descent, muscle force gastrocnemius (L) (N/body weight) by % stance phase

Figure A-VI.3C.6 Stair descent, muscle force gastrocnemius (L)

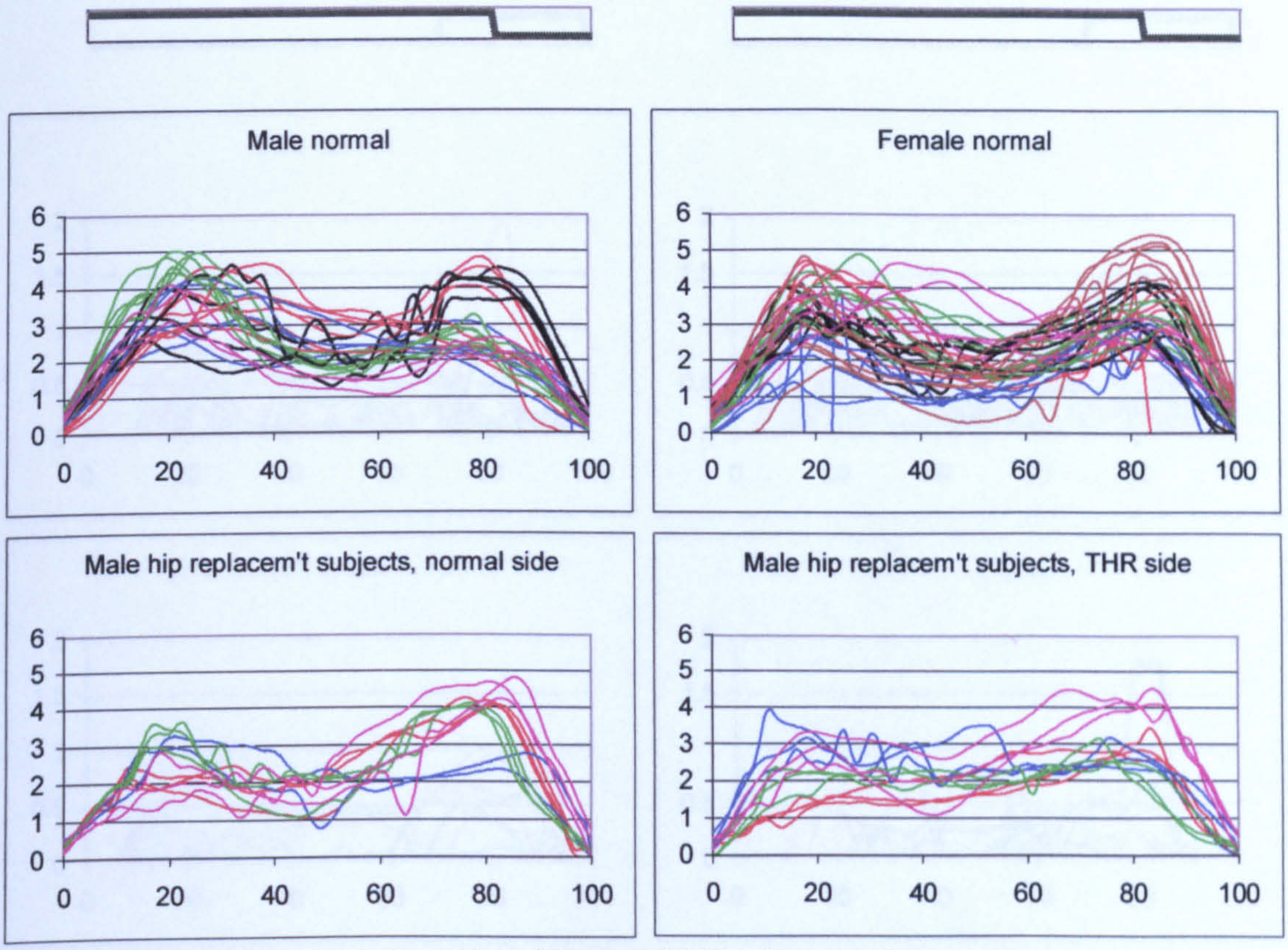

Figure A-VI.3C.7 Stair descent, muscle force soleus

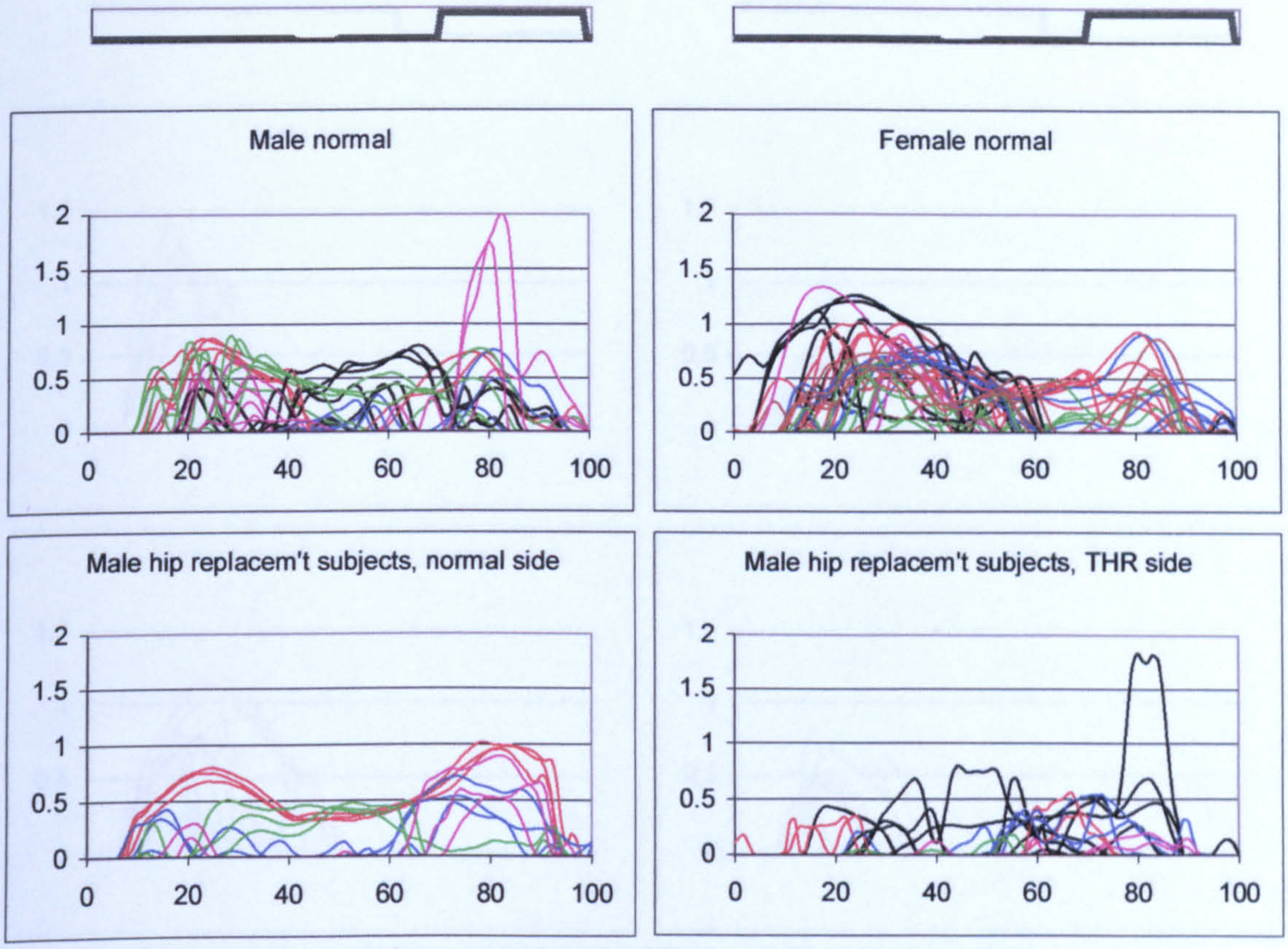

Ramp ascent, muscle force rectus femoris (N/body weight) by % stance phase

Figure A-VI.3C.8 Ramp ascent, muscle force rectus femoris (upper part)

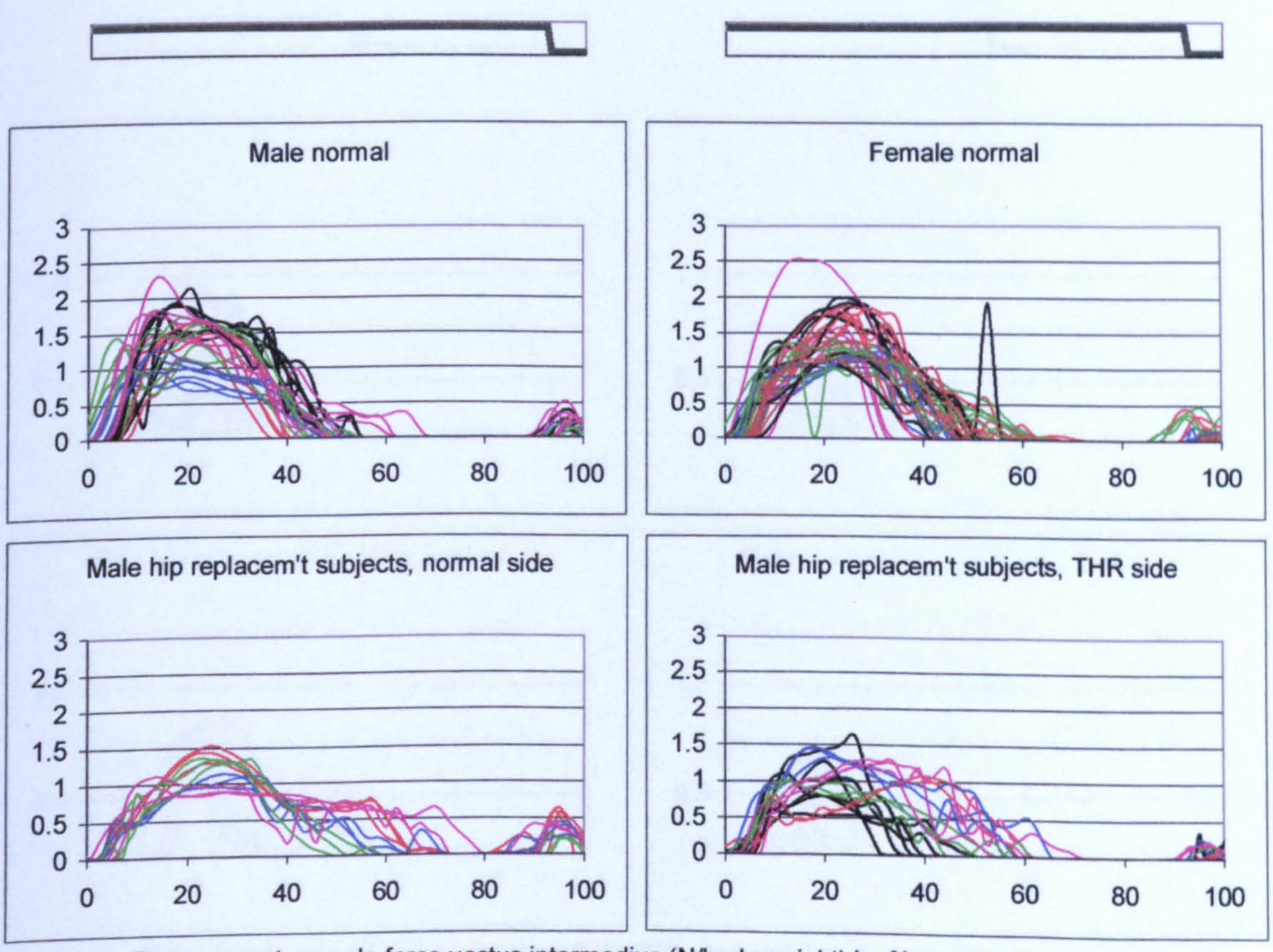

Ramp ascent, muscle force vastus intermedius (N/body weight) by % stance phase

Figure A-VI.3C.9 Ramp ascent, muscle force vastus intermedius

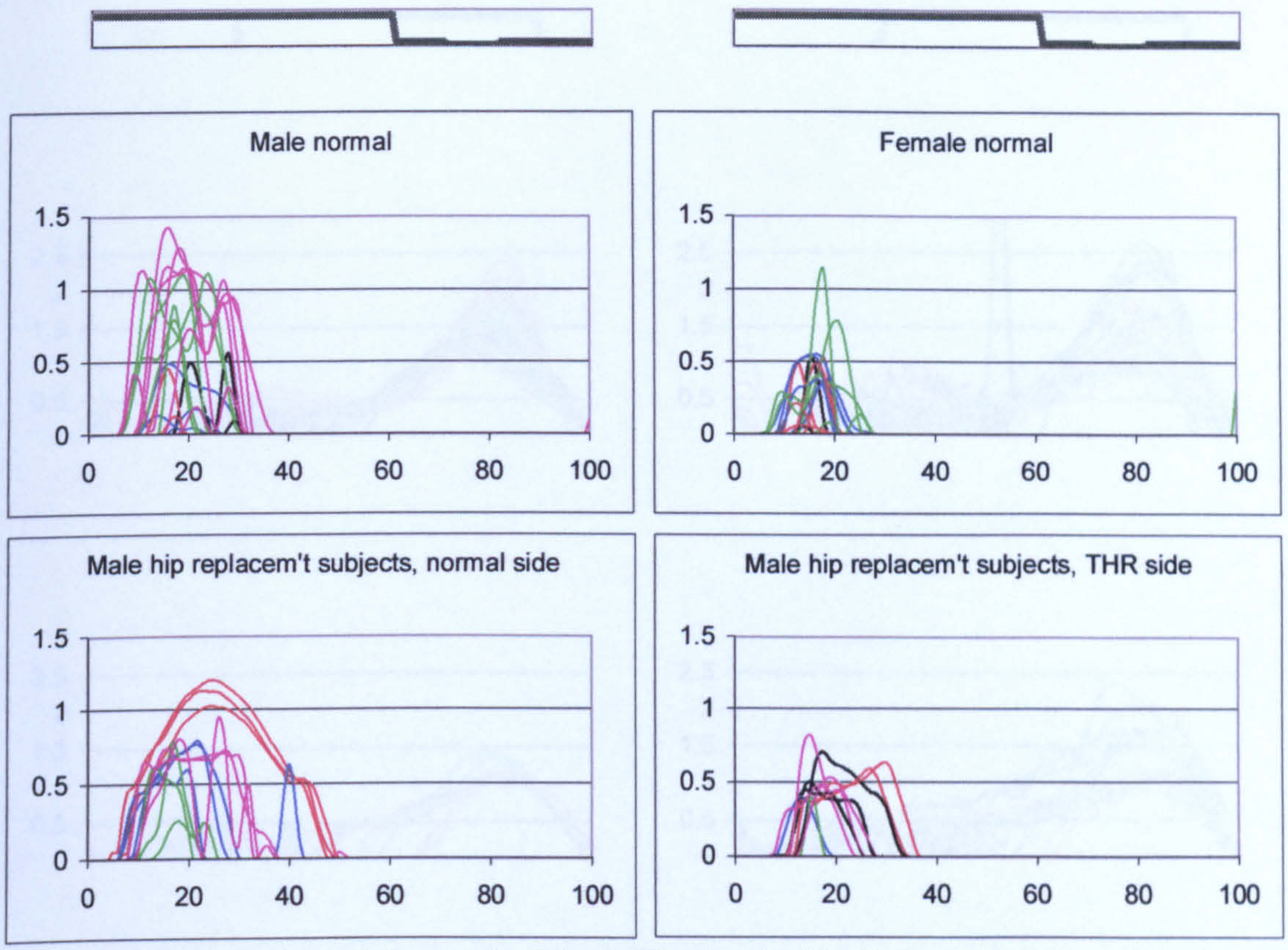

Ramp ascent, muscle force vastus lateralis (N/body weight) by % stance phase

Figure A-VI.3C.10 Ramp ascent, muscle force vastus lateralis

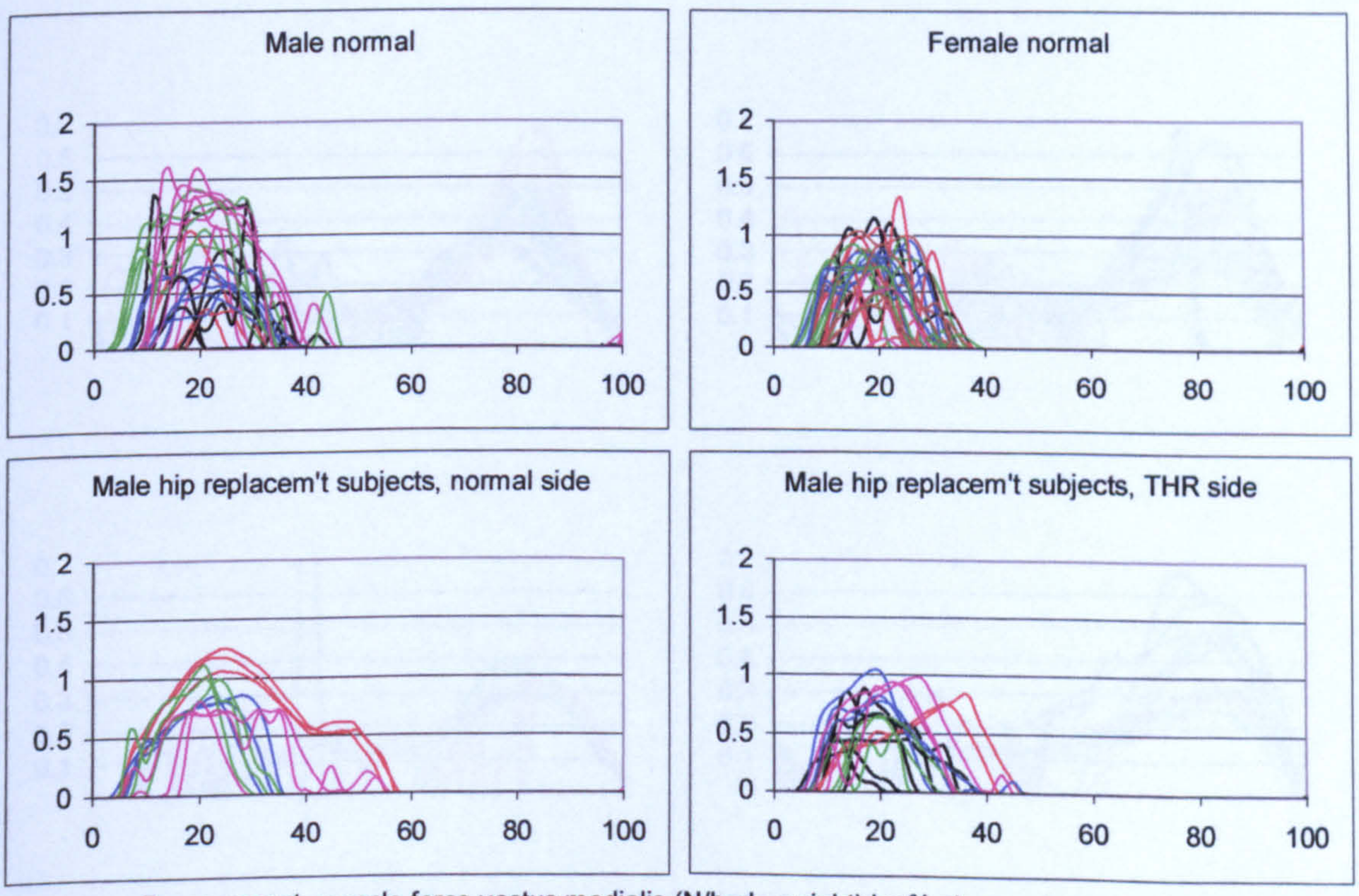

Ramp ascent, muscle force vastus medialis (N/body weight) by % stance phase

Figure A-VI.3C.11 Ramp ascent, muscle force vastus medialis

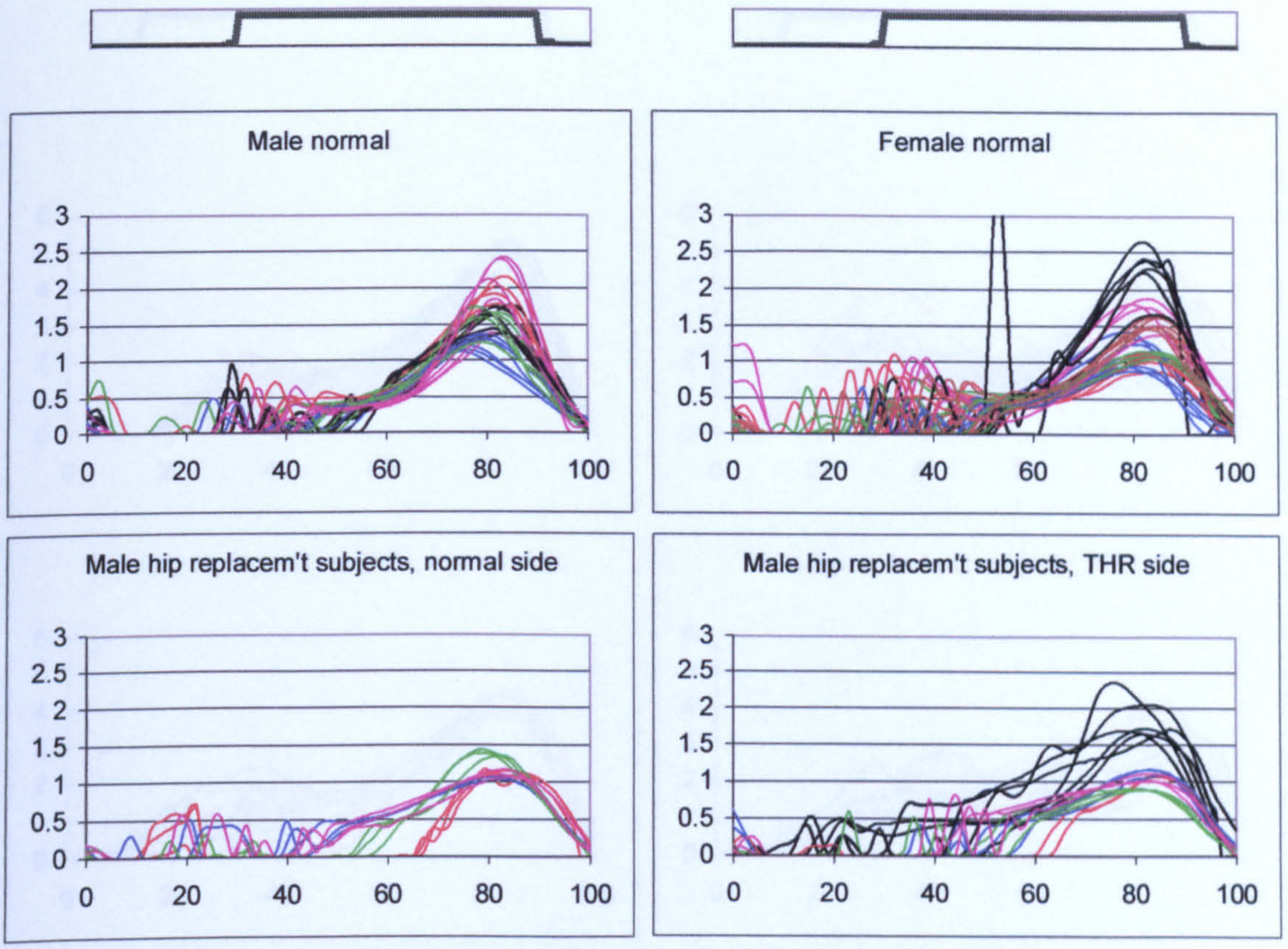

Ramp ascent, muscle force gastrocnemius (M) (N/body weight) by % stance phase

Figure A-VI.3C.12 Ramp ascent, muscle force gastrocnemius (M)

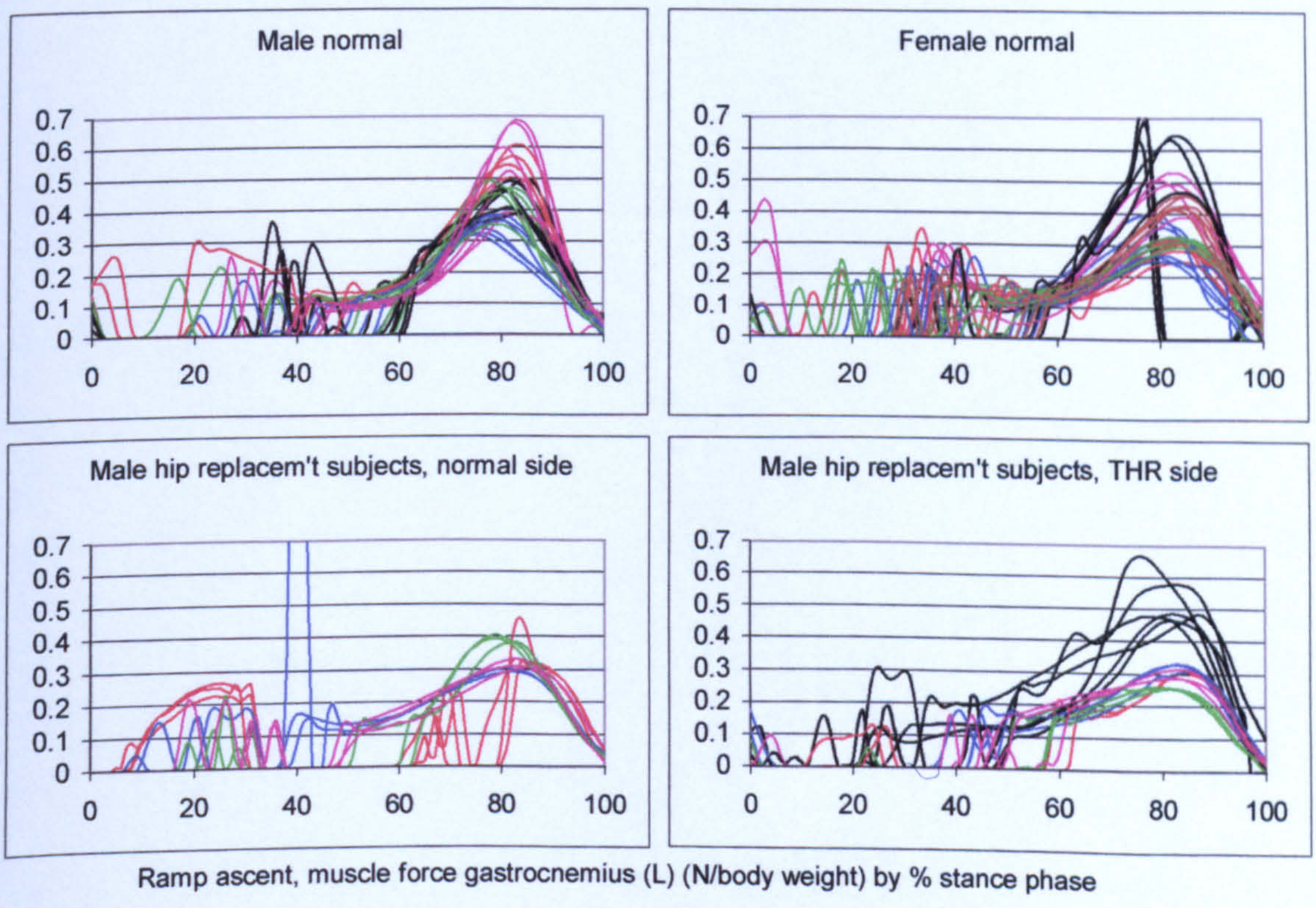

Ramp ascent, muscle force gastrocnemius (L) (N/body weight) by % stance phase

Figure A-VI.3C.13 Ramp ascent, muscle force gastrocnemius (L)

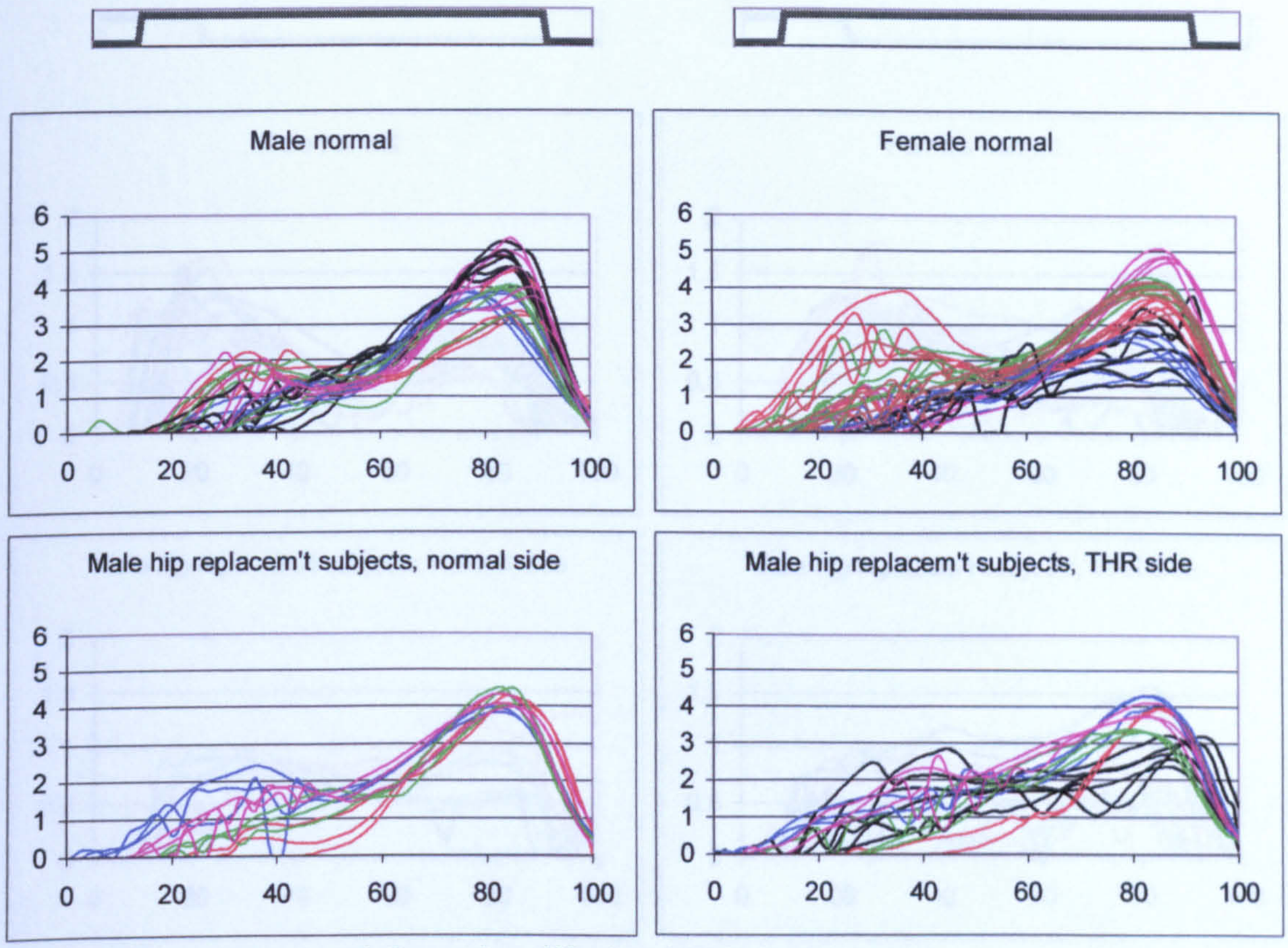

Figure A-VI.3C.14 Ramp ascent, muscle force soleus

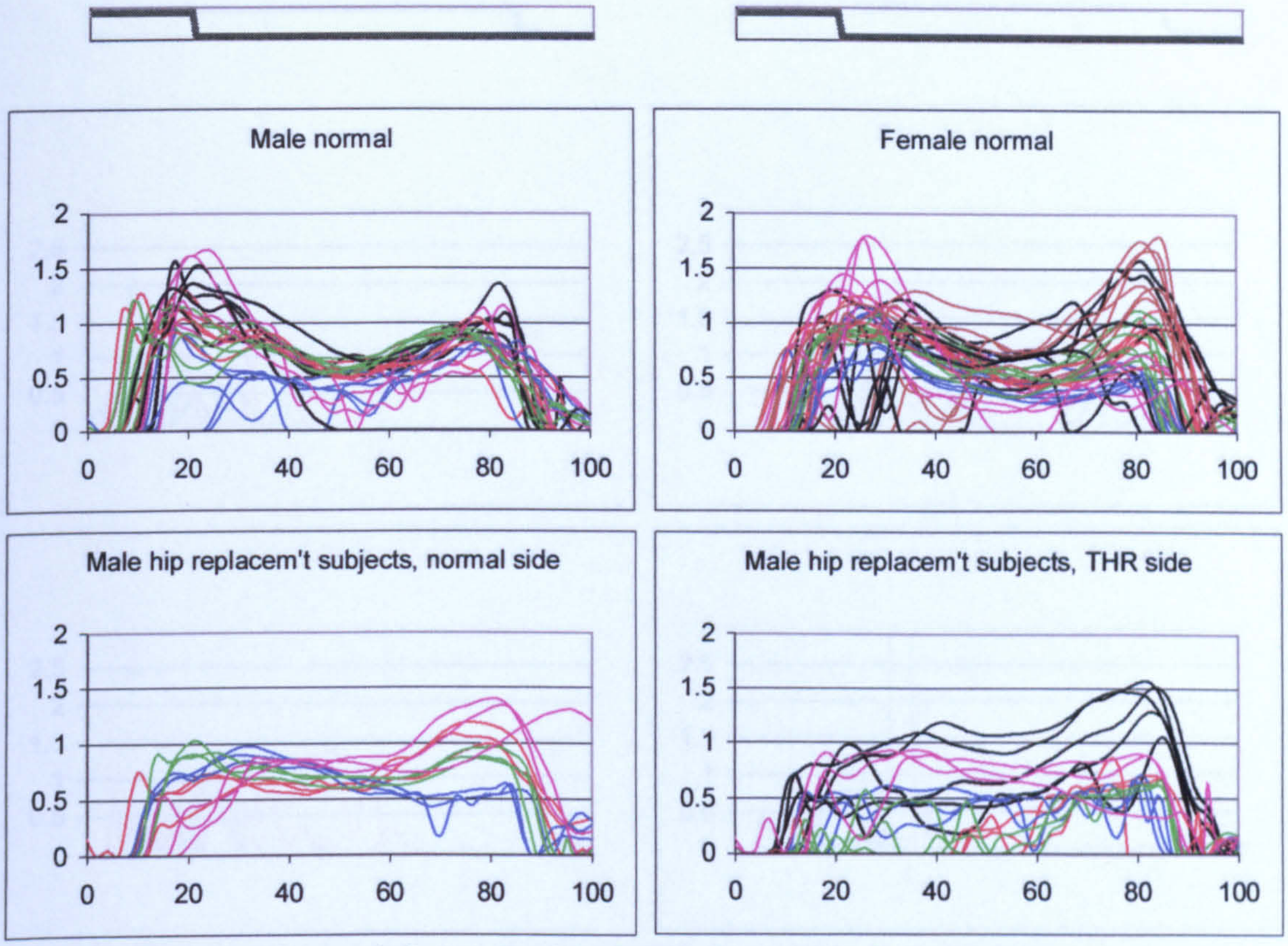

Ramp descent, muscle force rectus femoris (upper part) (N/body weight) by % stance phase

Figure A-VI.3C.15 Ramp descent, muscle force rectus femoris (upper part)

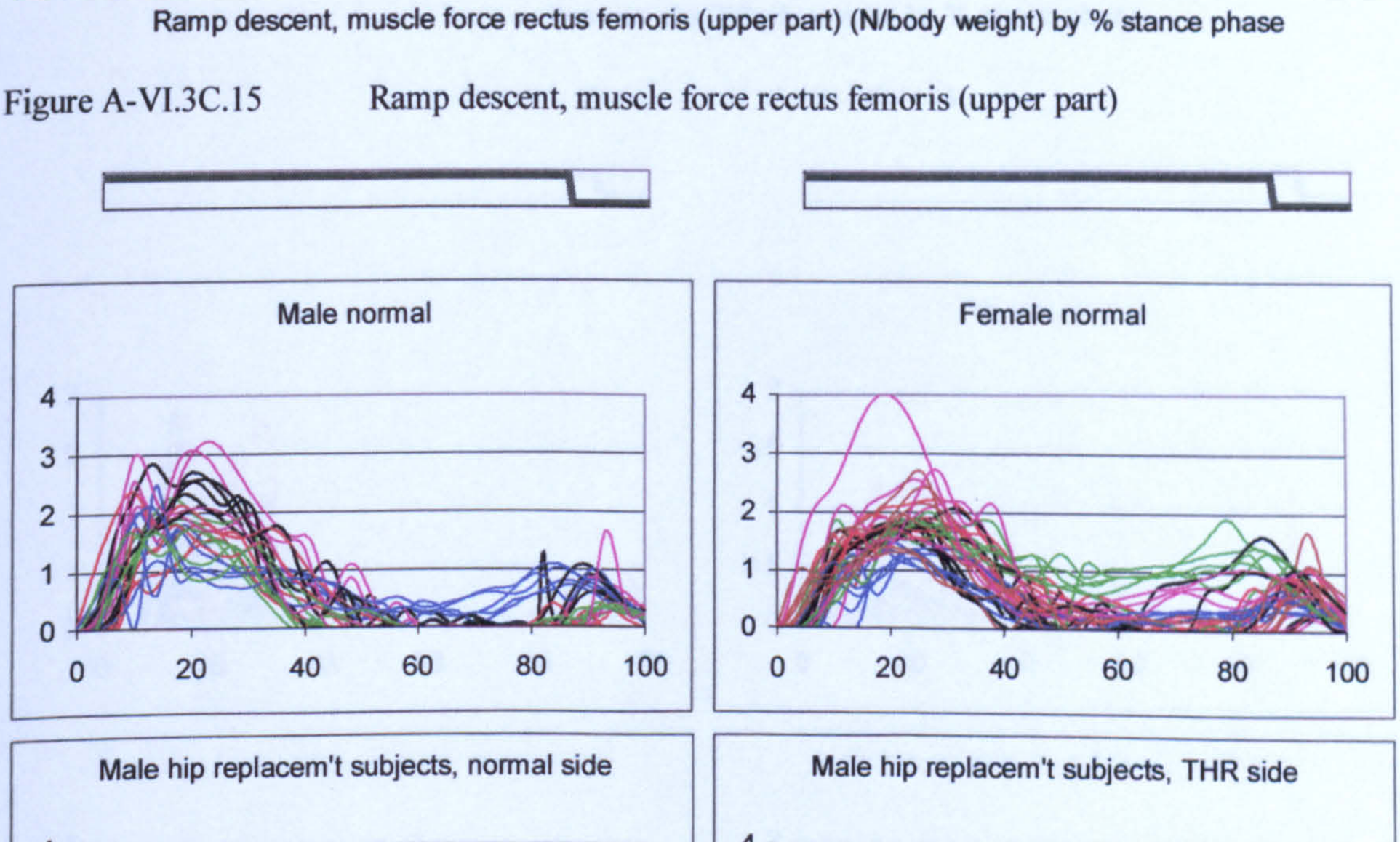

Ramp descent, muscle force vastus intermedius (N/body weight) by % stance phase

Figure A-VI.3C.16 Ramp descent, muscle force vastus intermedius

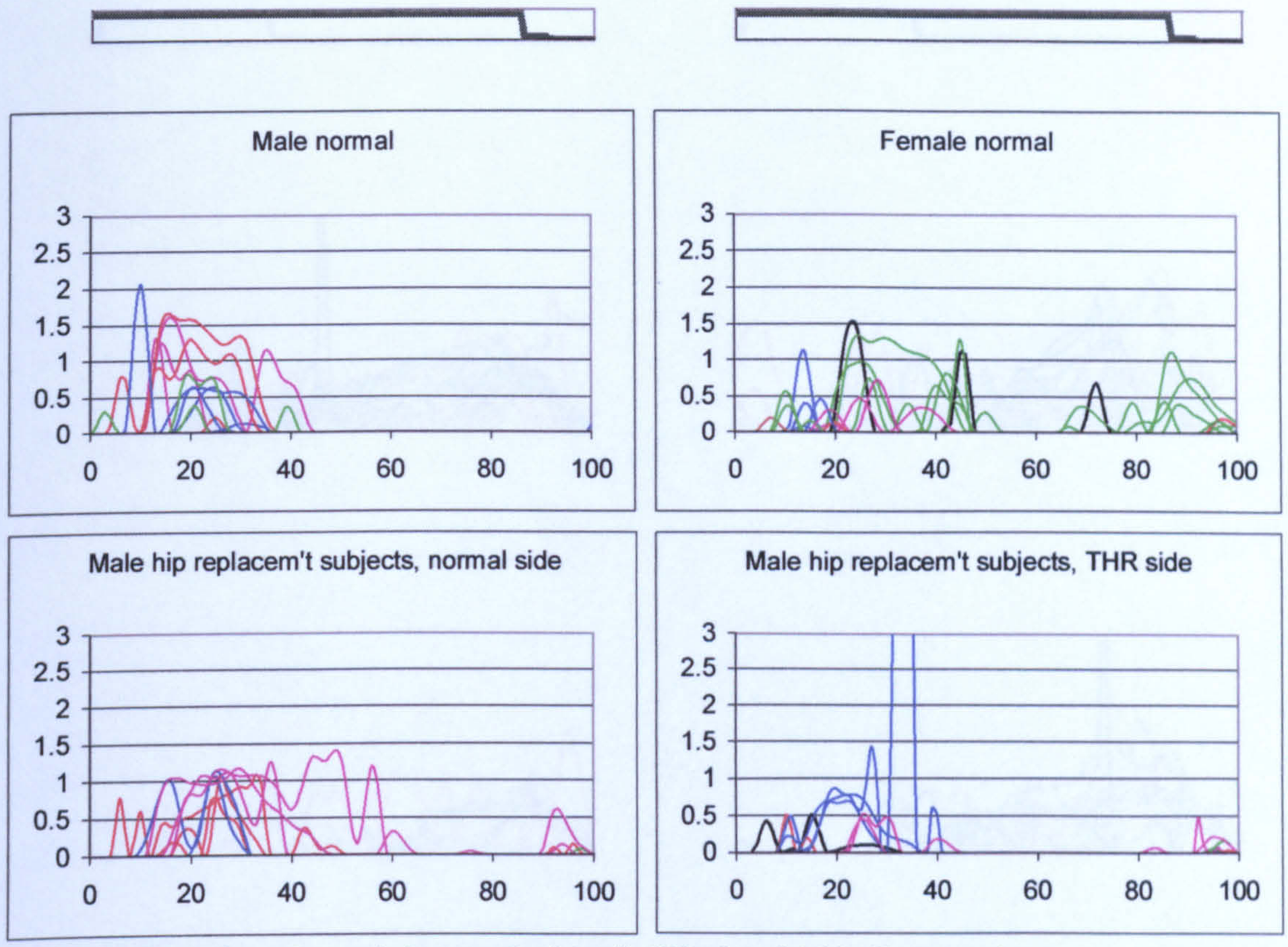

Ramp descent, muscle force vastus lateralis (N/body weight) by % stance phase

Figure A-VI.3C.17 Ramp descent, muscle force vastus lateralis

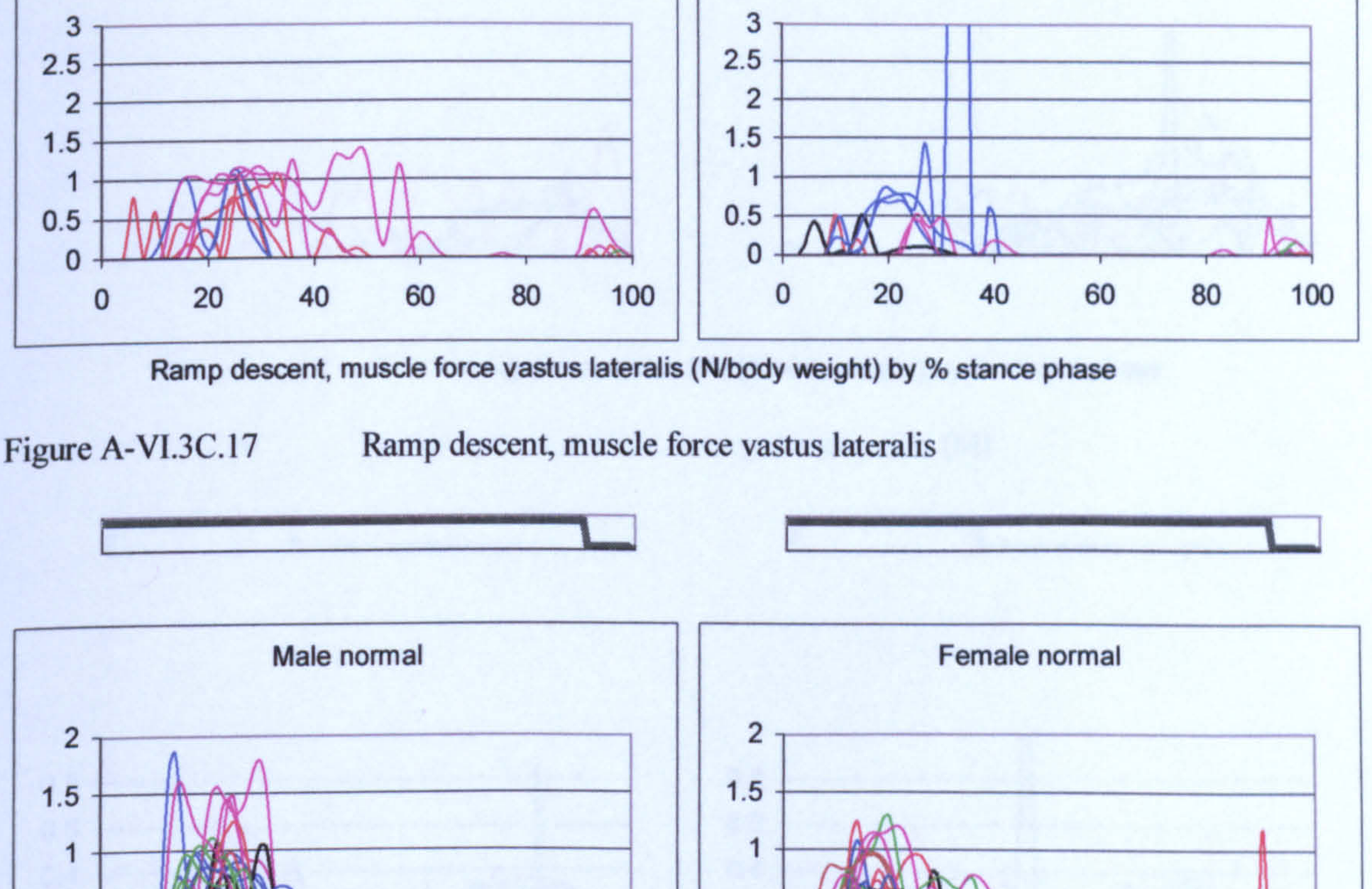

Ramp descent, muscle force vastus medialis (N/body weight) by % stance phase

Figure A-VI.3C.18 Ramp descent, muscle force vastus medialis

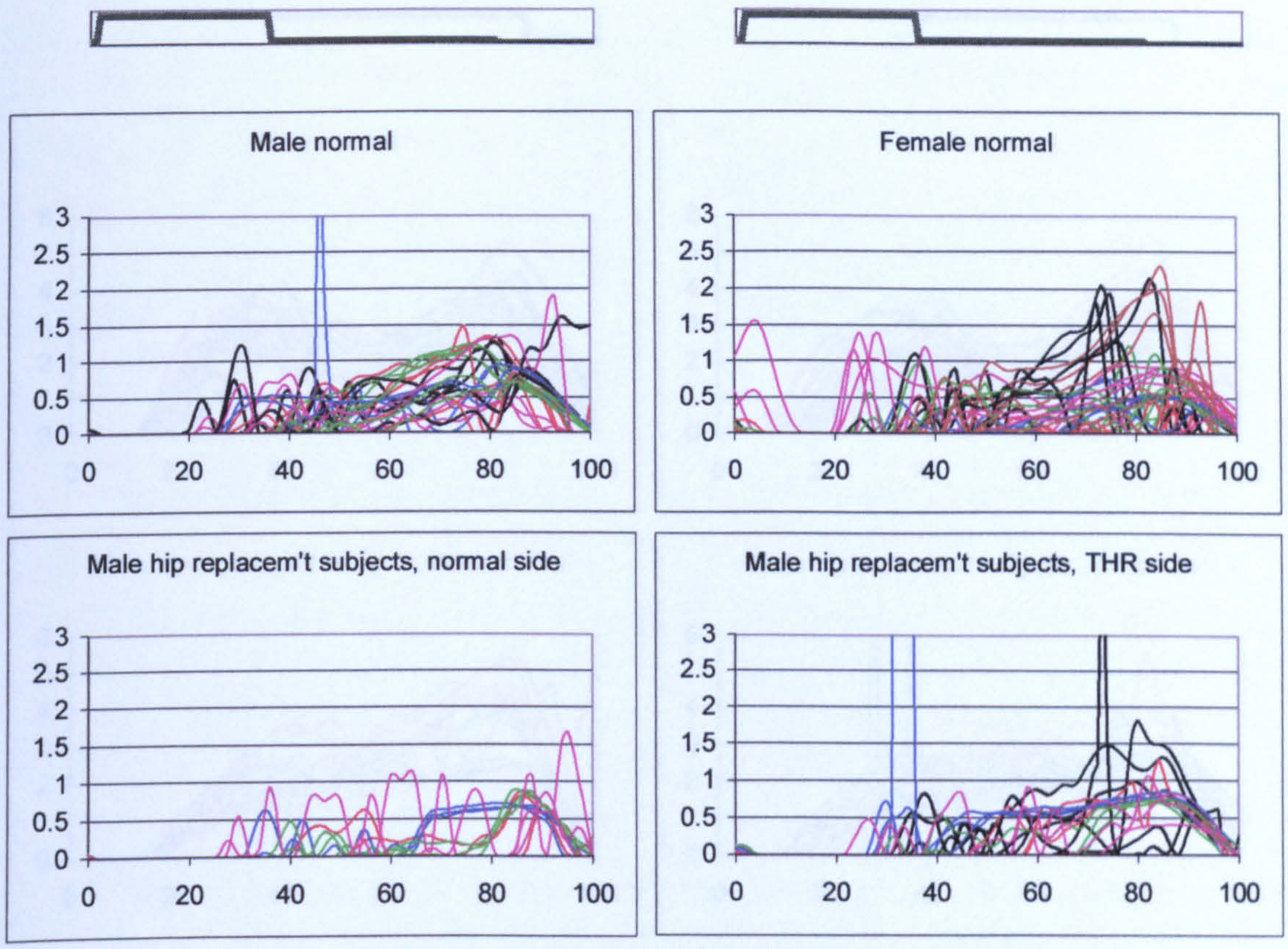

Ramp descent, muscle force gastrocnemius (M) (N/body weight) by % stance phase

Figure A-VI.3C.19 Ramp descent, muscle force gastrocnemius (M)

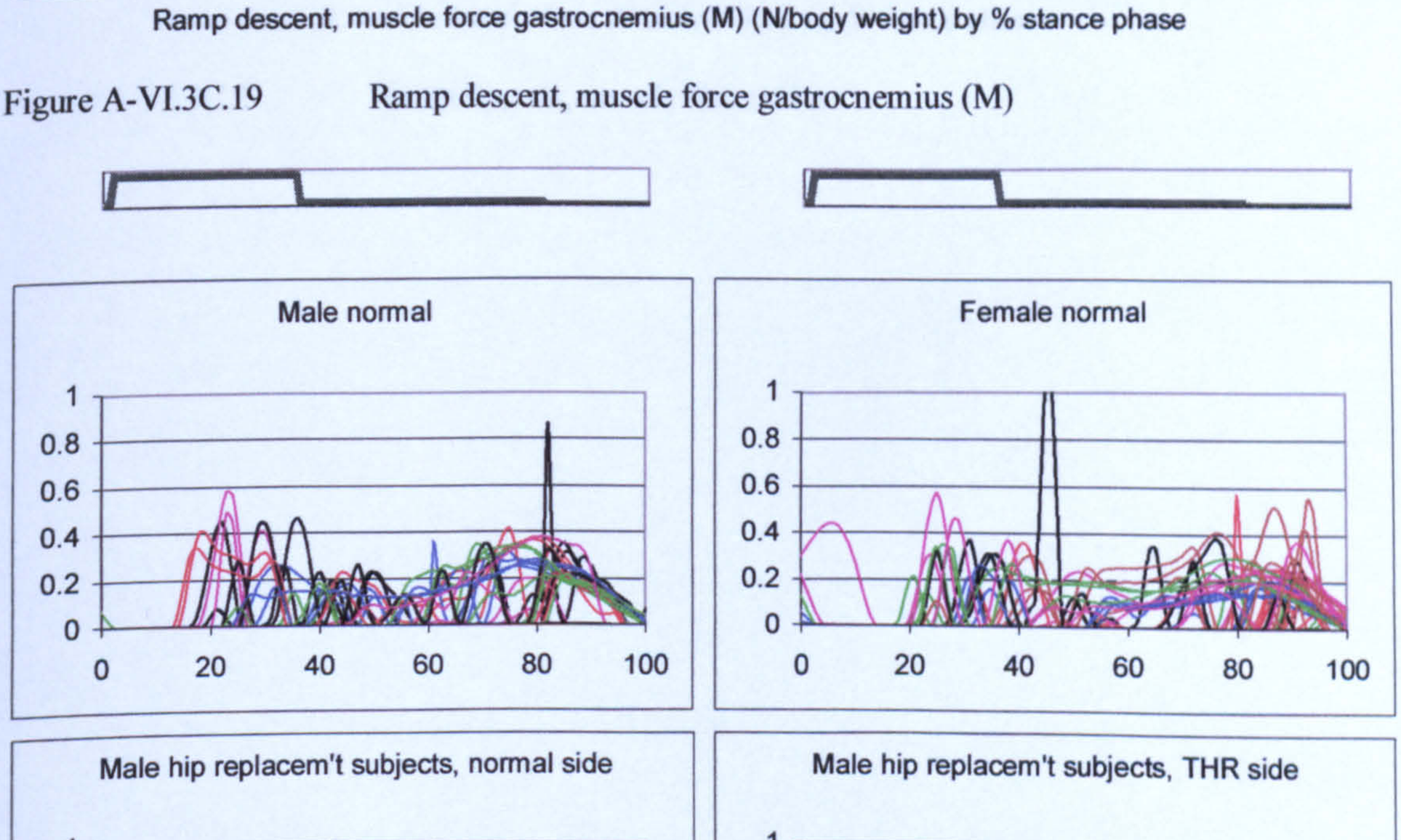

Ramp descent, muscle force gastrocnemius (L) (N/body weight) by % stance phase

Figure A-VI.3C.20 Ramp descent, muscle force gastrocnemius (L)

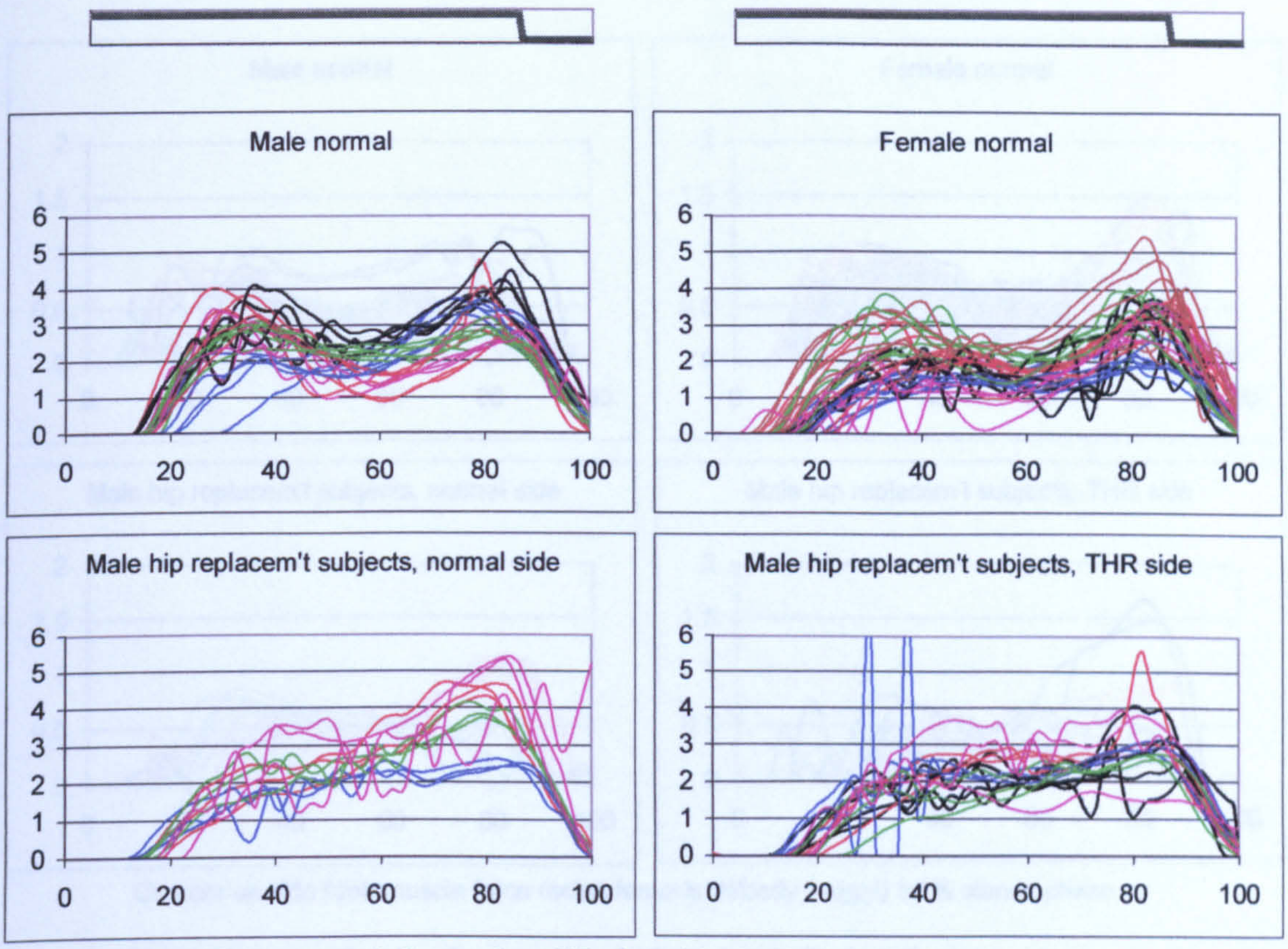

Figure A-VI.3C.21 Ramp descent, muscle force soleus

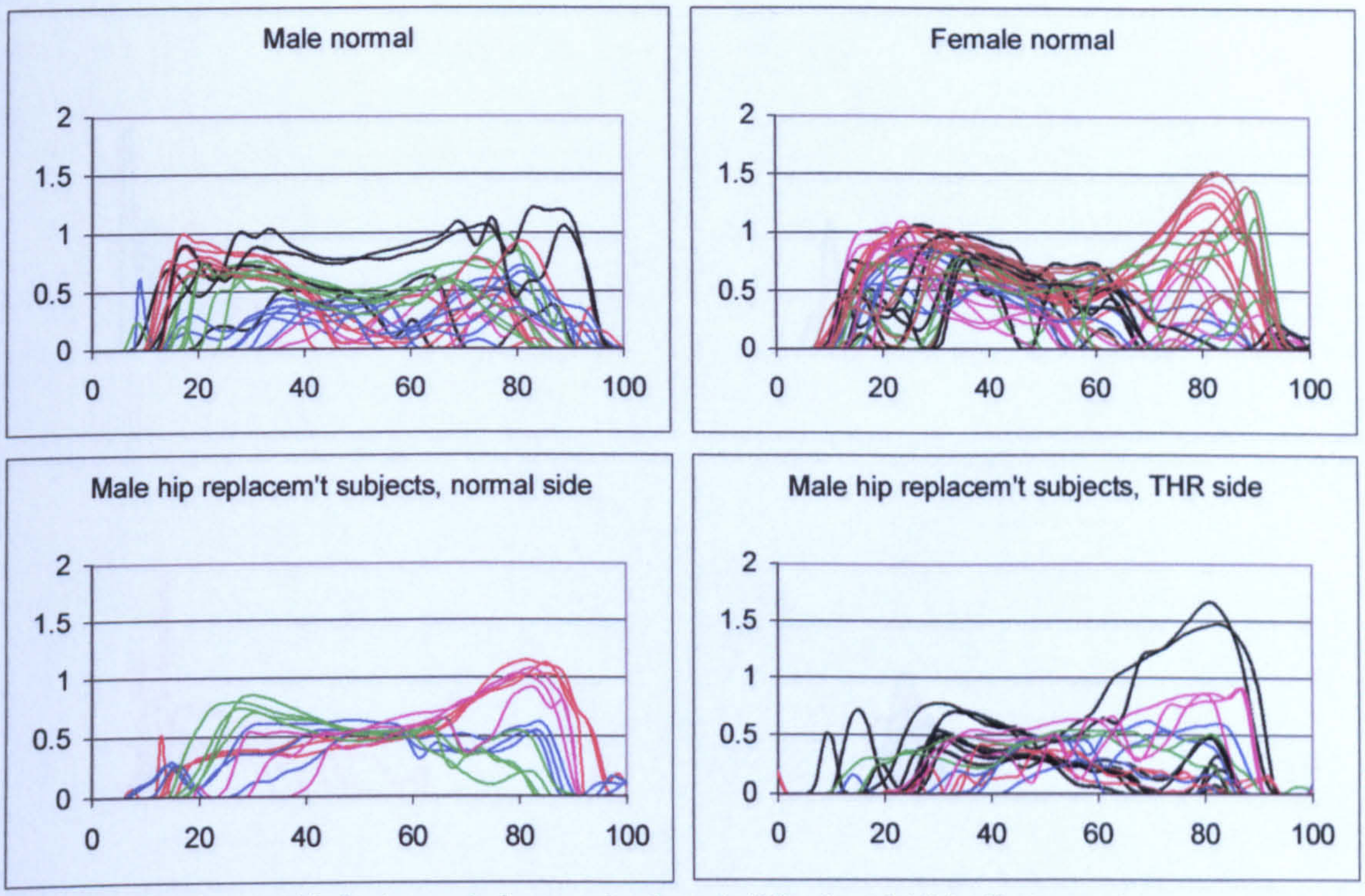

Figure A-VI.3C.22 Camber foot up, muscle force rectus femoris (upper part)

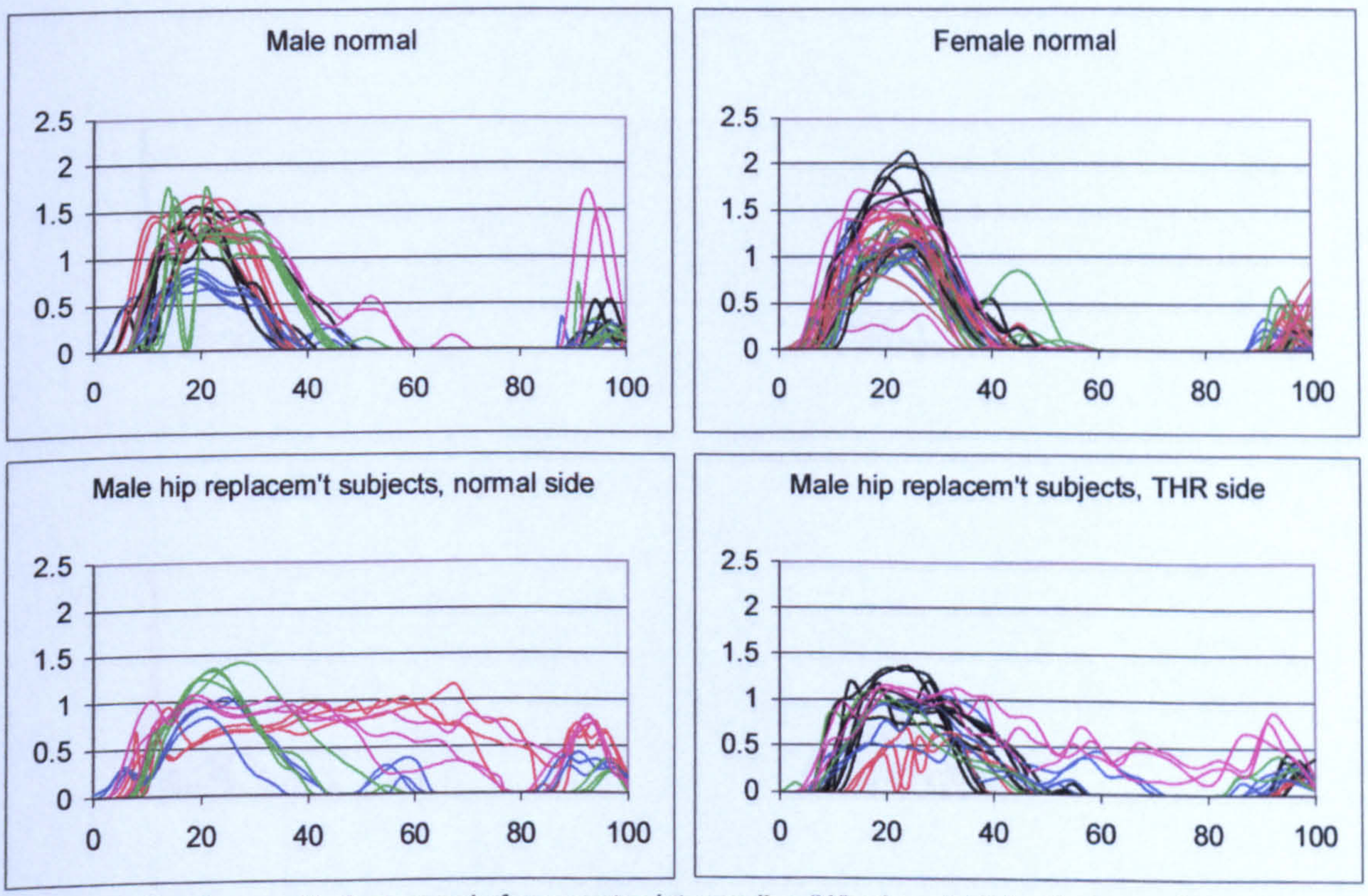

Figure A-VI.3C.23 Camber foot up, muscle force vastus intermedius

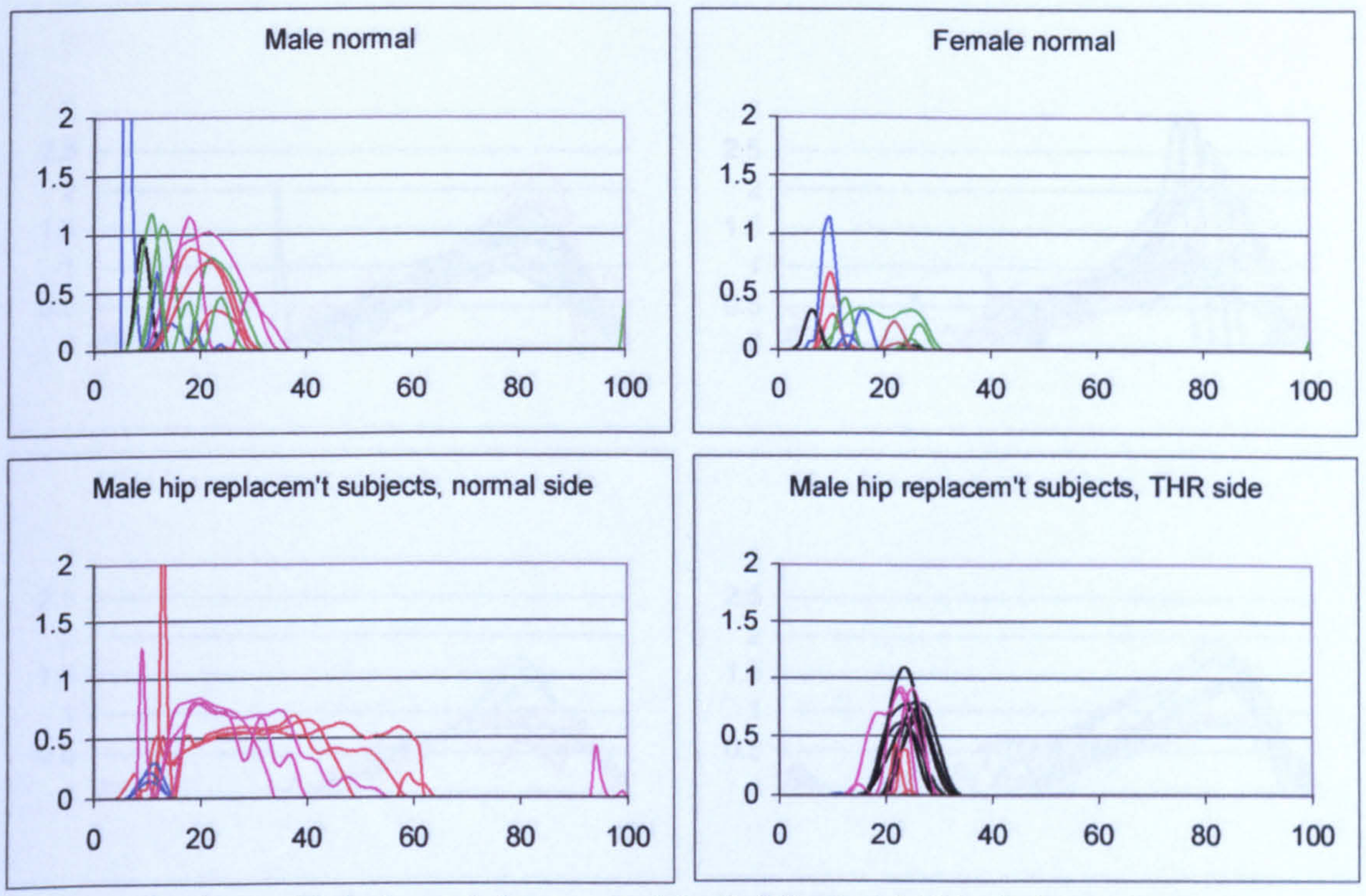

Camber up side foot, muscle force vastus lateralis (N/body weight) by % stance phase

Figure A-VI.3C.24 Camber foot up, muscle force vastus lateralis

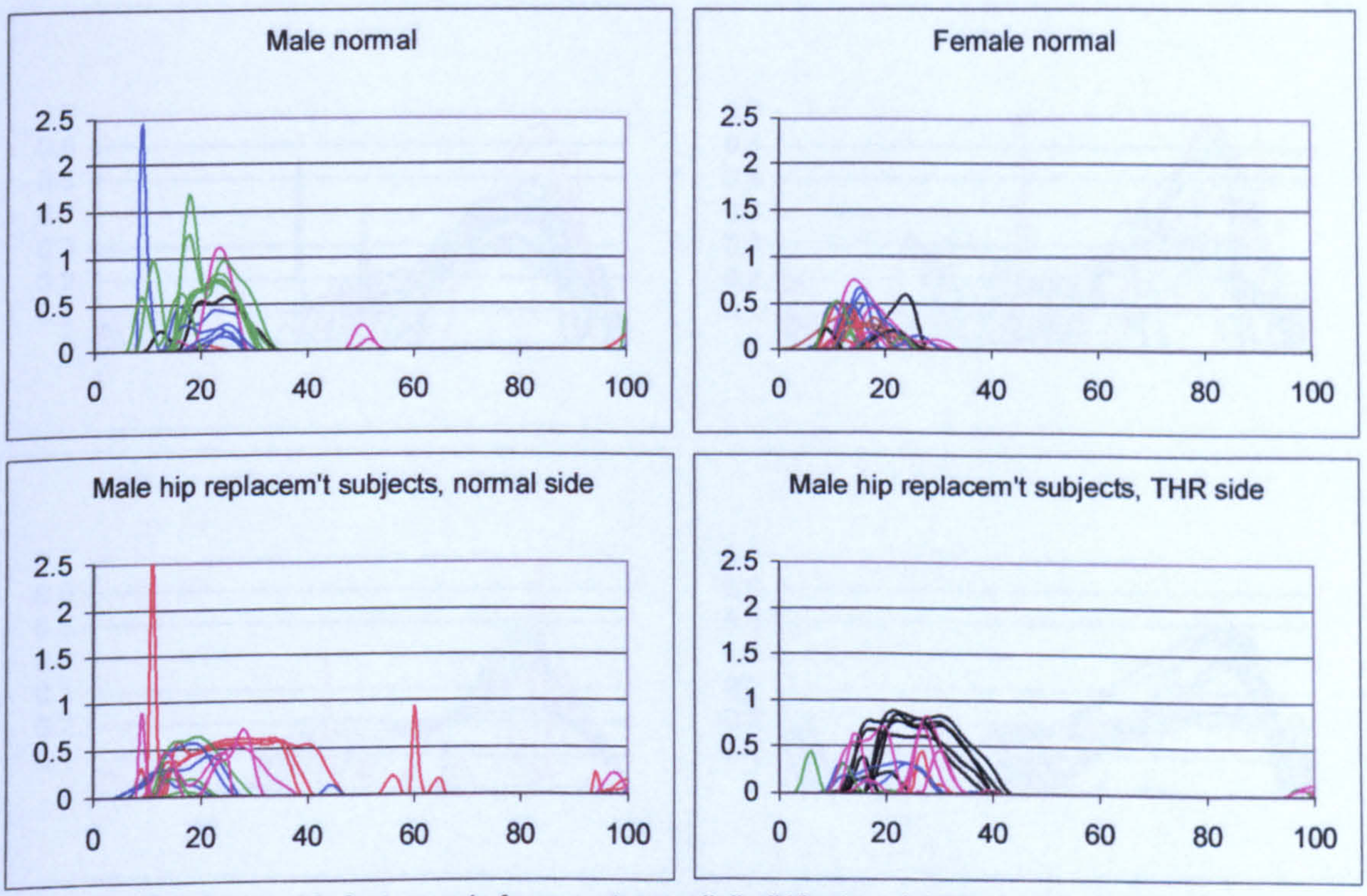

Camber up side foot, muscle force vastus medialis (N/body weight) by % stance phase

Figure A-VI.3C.25 Camber foot up, muscle force vastus medialis

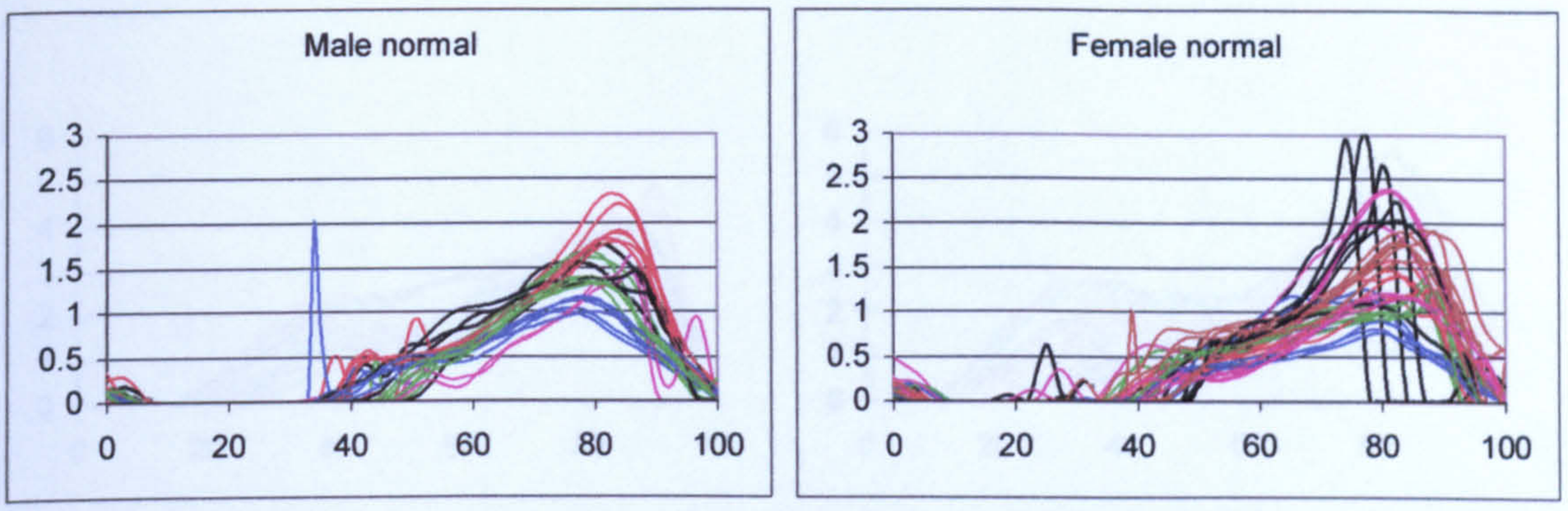

Figure A-VI.3C.26 Camber foot up, muscle force gastrocnemius (M)

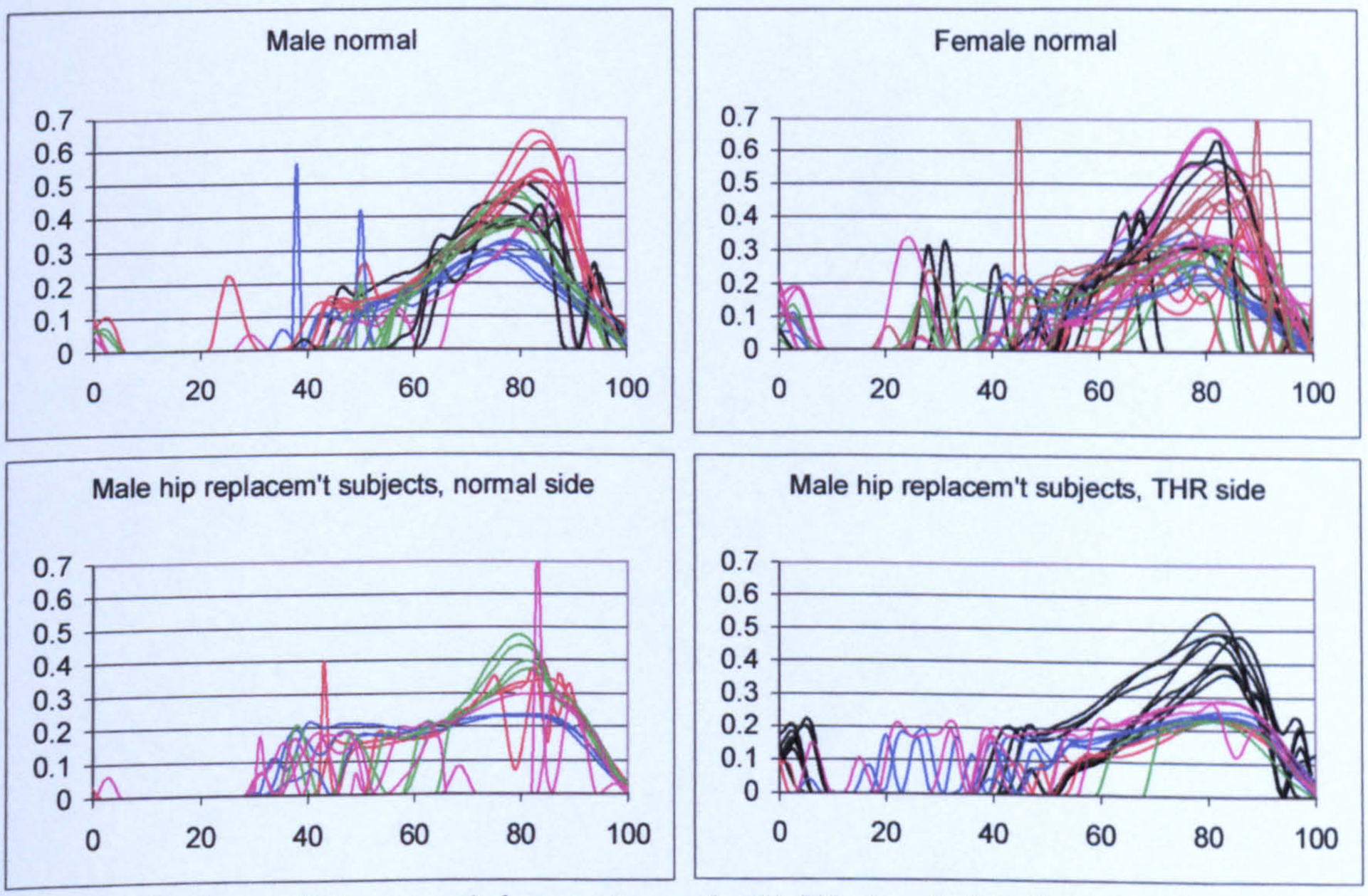

Figure A-VI.3C.27 Camber foot up, muscle force gastrocnemius (L)

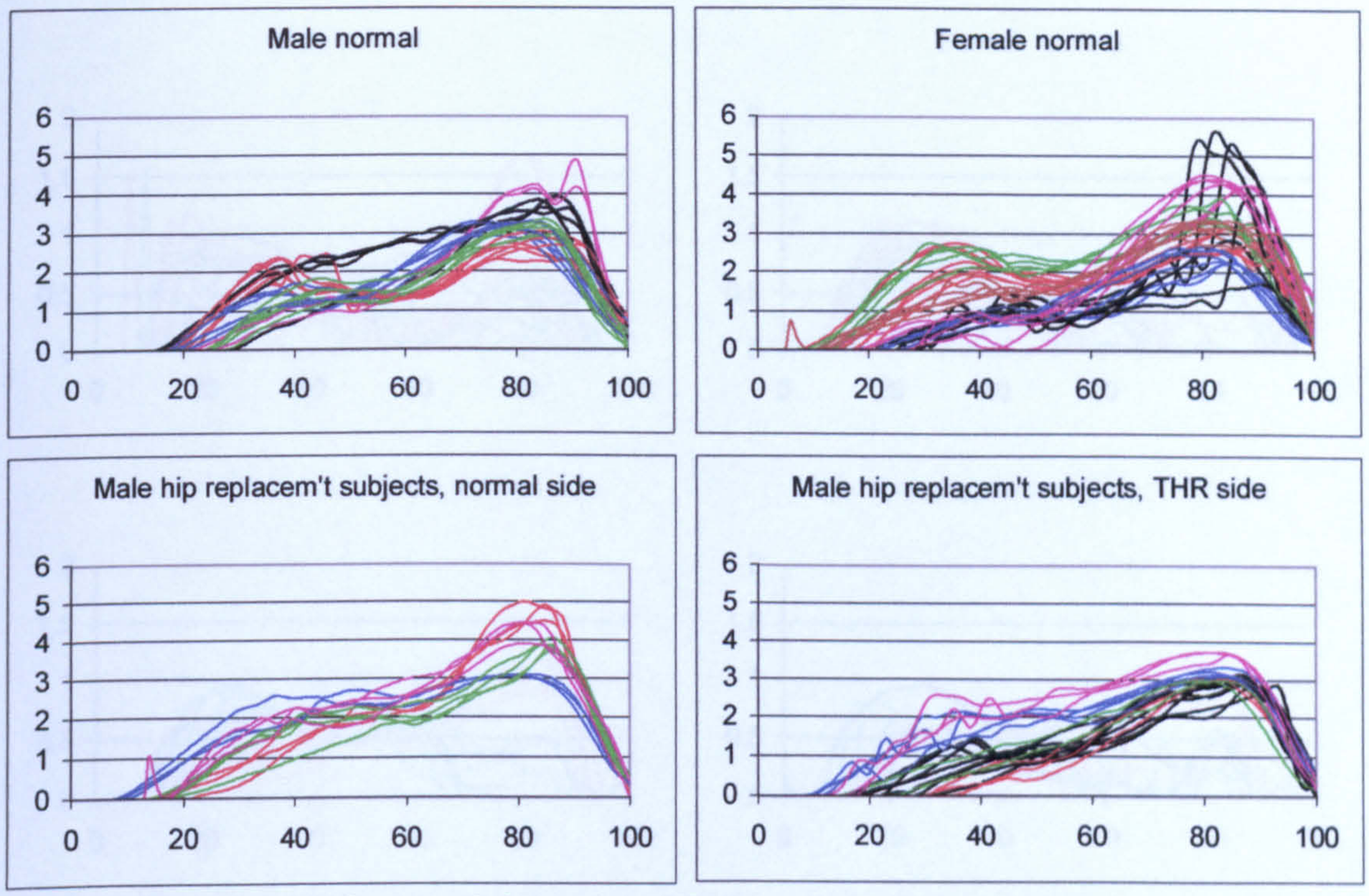

Figure A-VI.3C.28 Camber foot up, muscle force soleus

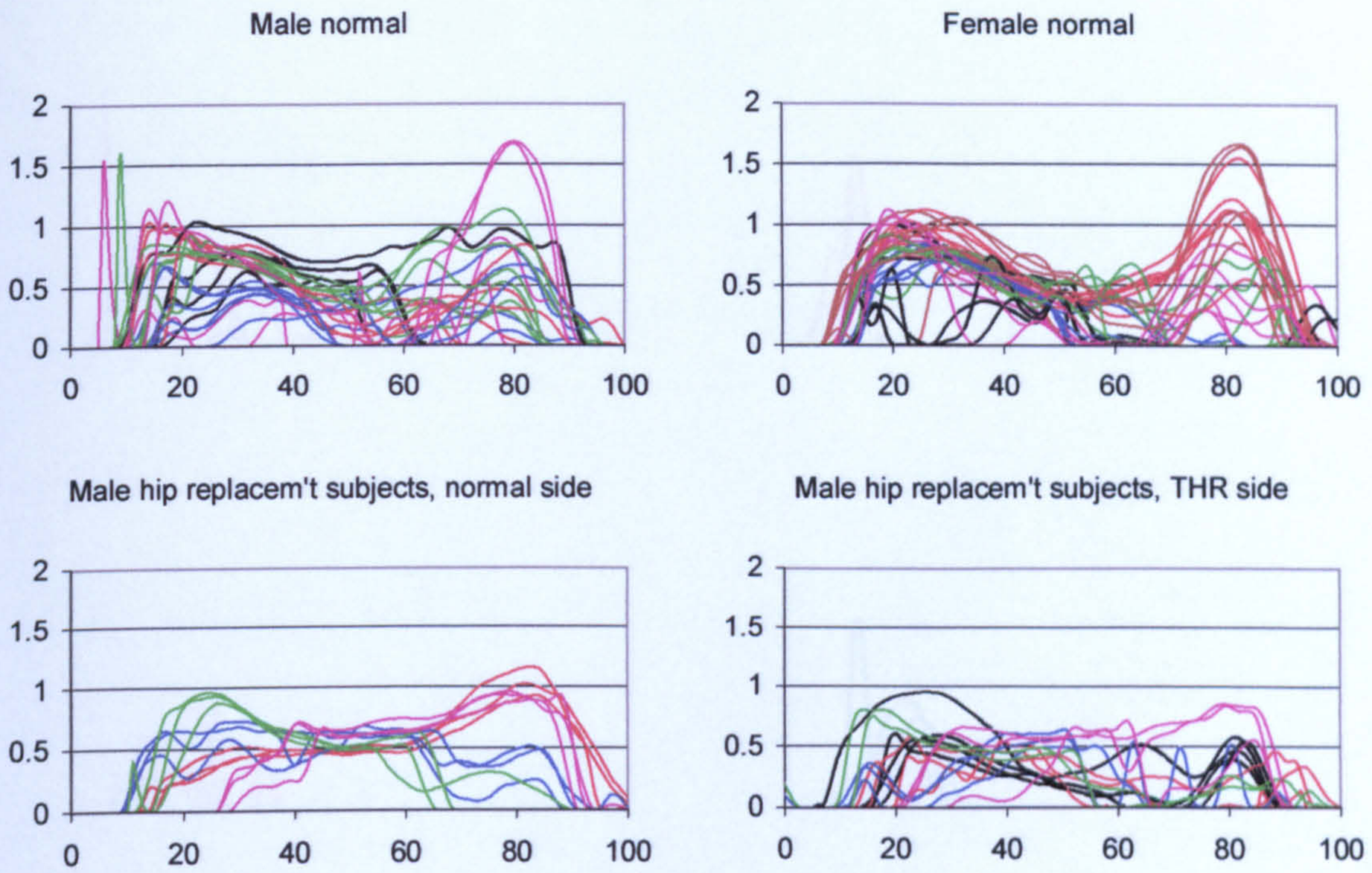

Camber foot down, muscle force rectus femoris (N/body weight) by % stance phase

Figure A-VI.3C.29 Camber foot down, muscle force rectus femoris (upper part)

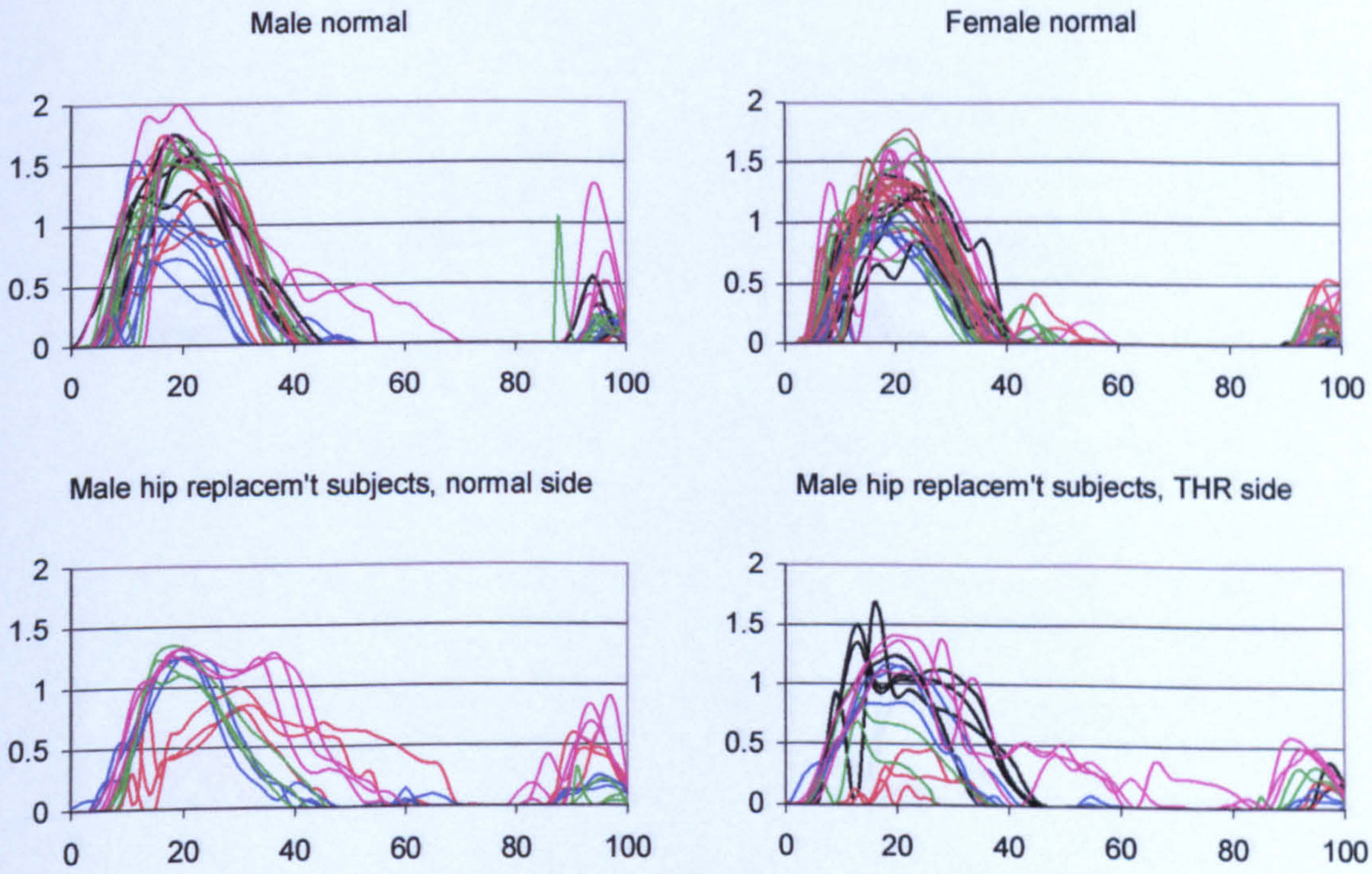

Camber foot down, muscle force vastus intermedius (N/body weight) by % stance phase

Figure A-VI.3C.30 Camber foot down, muscle force vastus intermedius

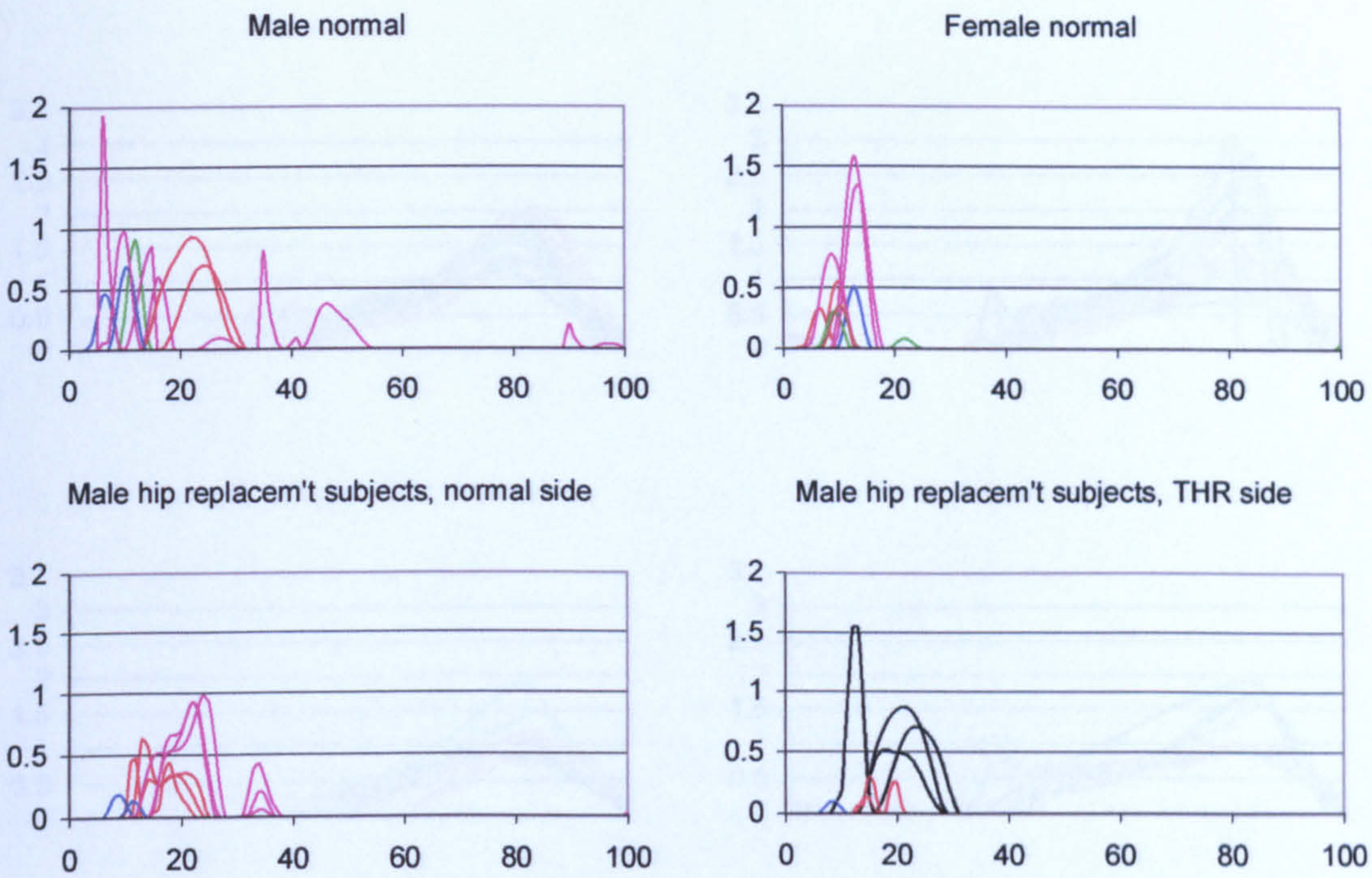

Camber foot down, muscle force vastus lateralis (N/body weight) by % stance phase

Figure A-VI.3C.31 Camber foot down, muscle force vastus lateralis

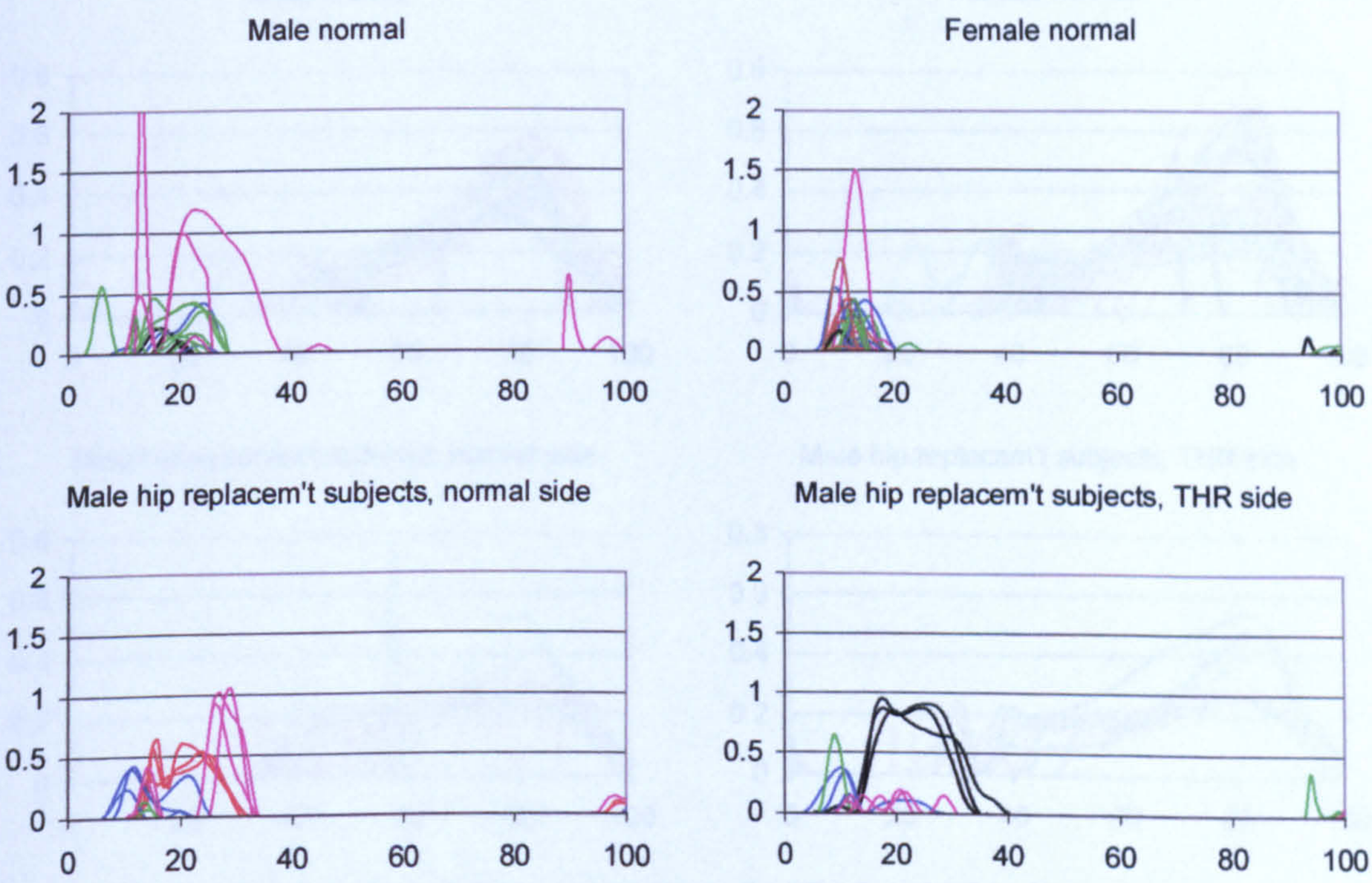

Camber foot down, muscle force vastus medialis (N/body weight) by % stance phase

Figure A-VI.3C.32 Camber foot down, muscle force vastus medialis

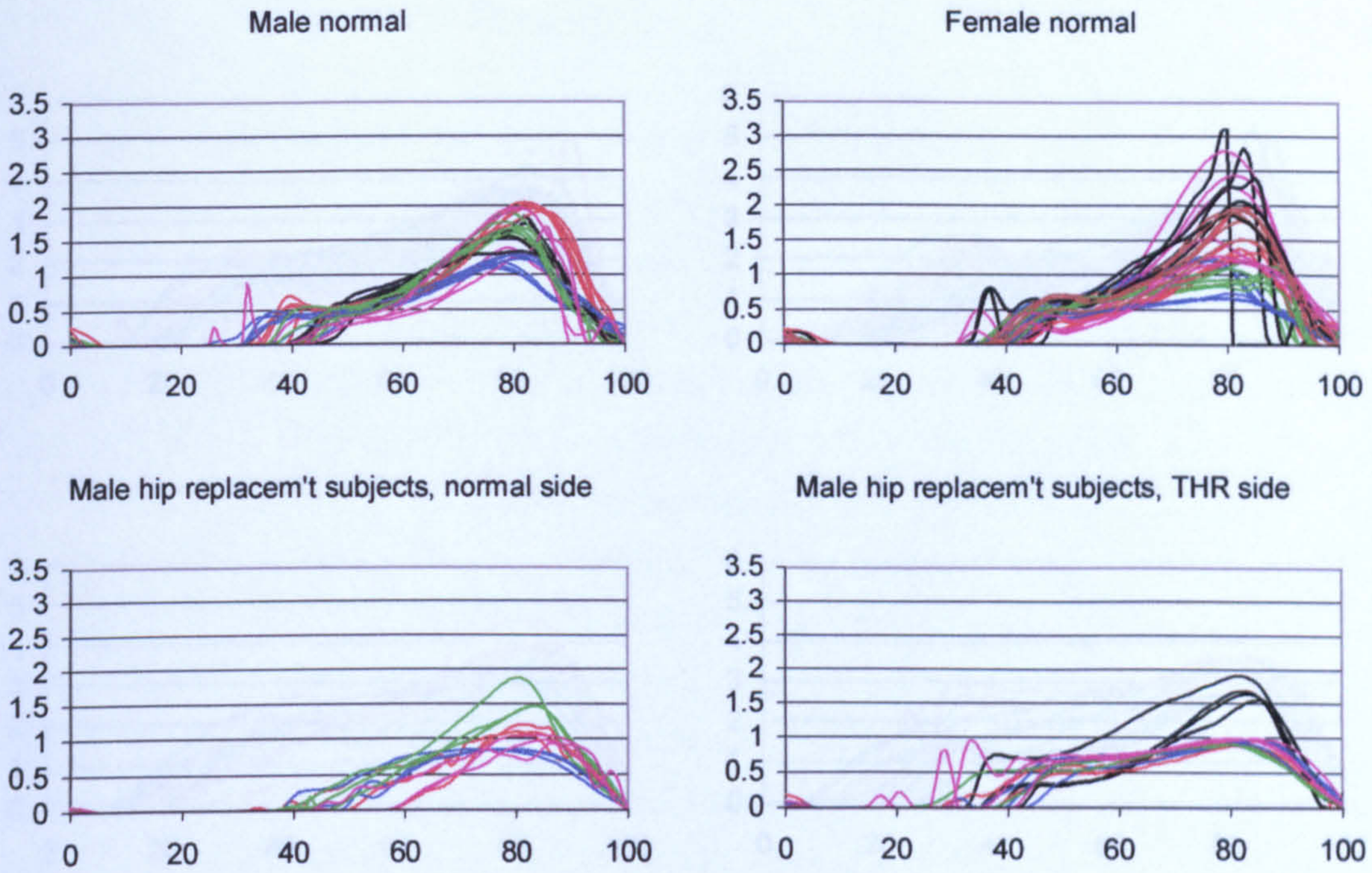

Figure A-VI.3C.33 Camber foot down, muscle force gastrocnemius (M)

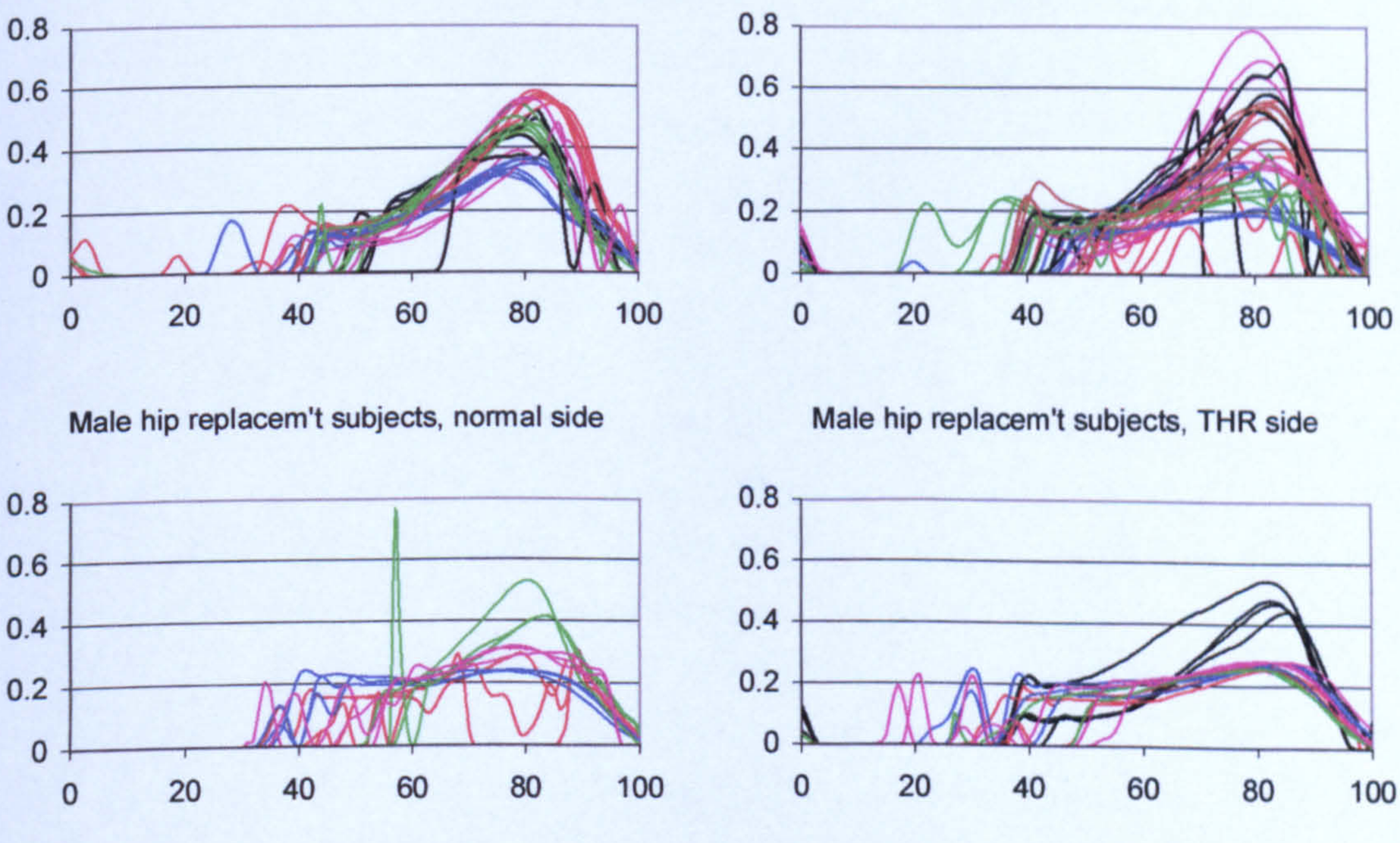

Figure A-VI.3C.34 Camber foot down, muscle force gastrocnemius (L)

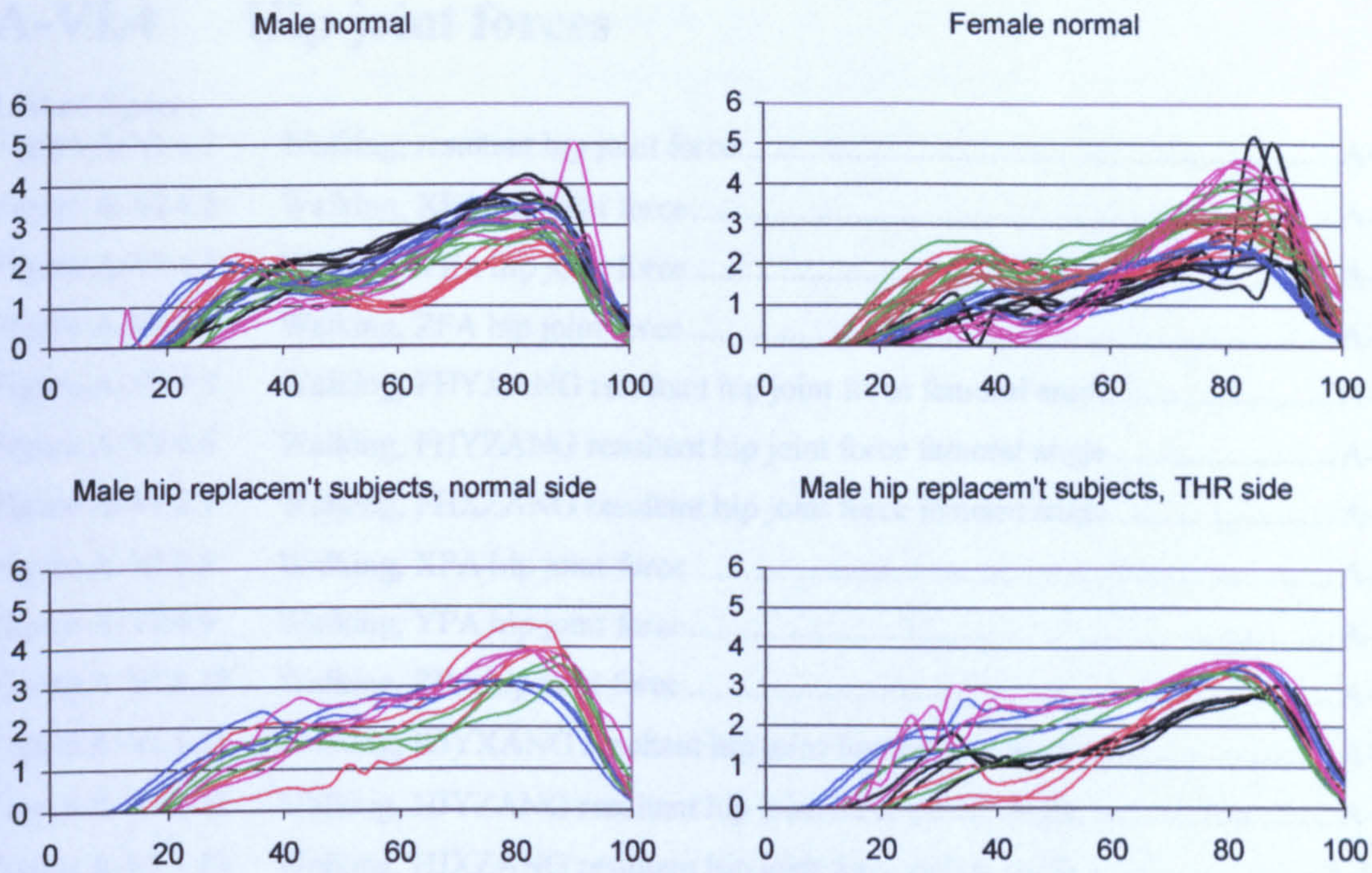

Figure A-VI.3C.35 Camber foot down, muscle force soleus

A-VI.4 Hip joint forces

List of figures

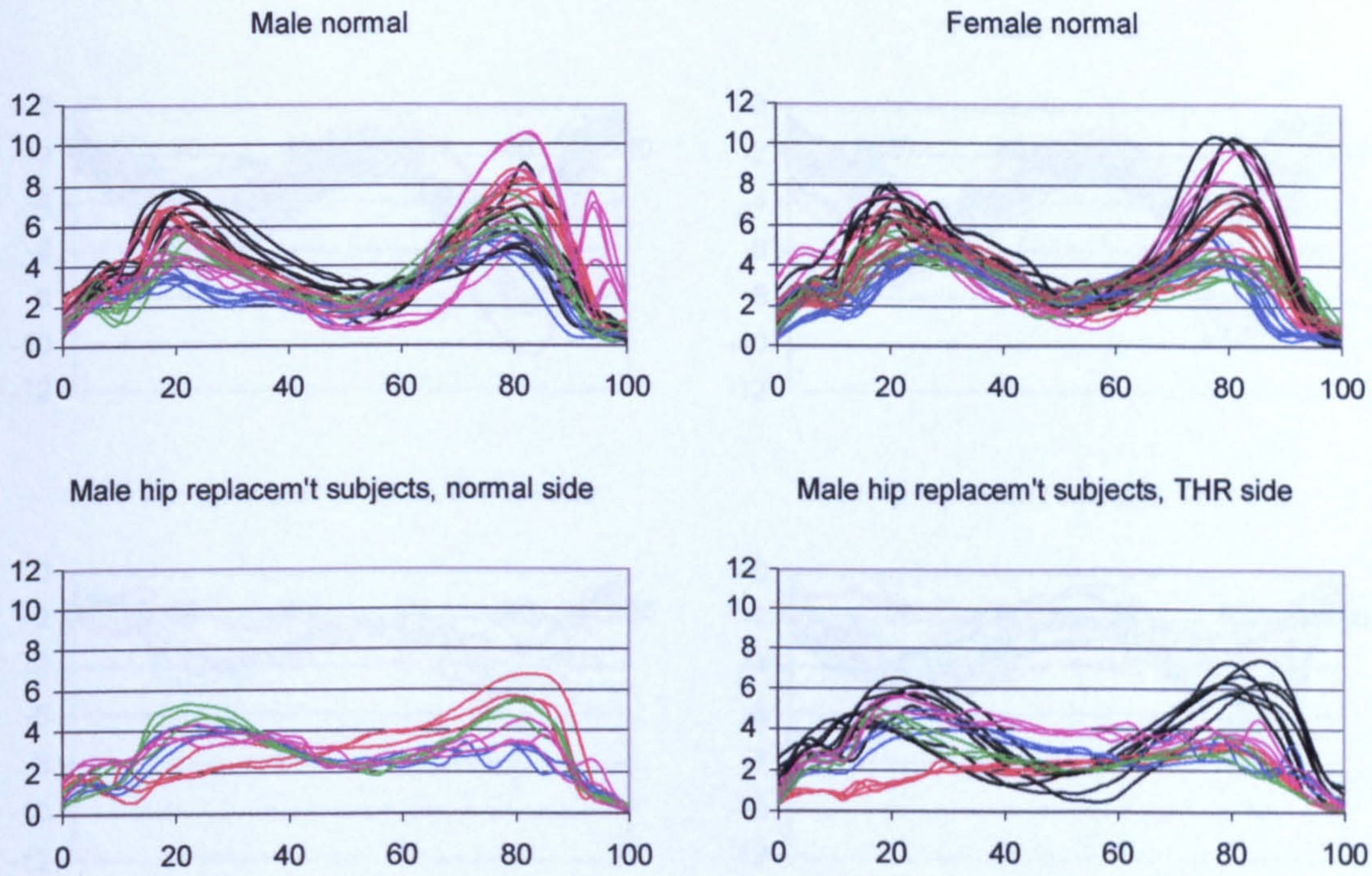

Figure A-VI.4.1 Walking, resultant hip joint force

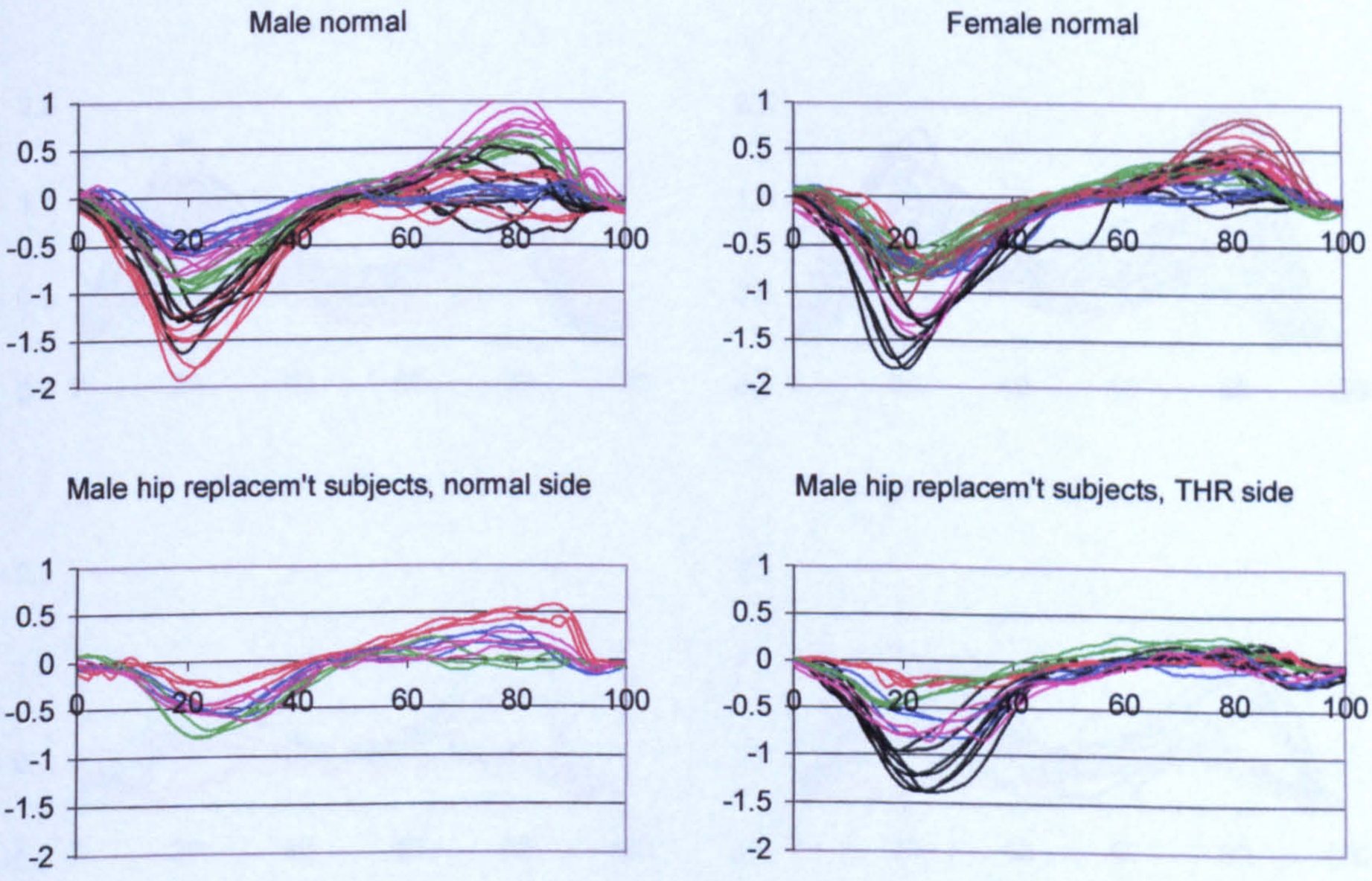

Figure A-VI.4.2 Walking, XFA hip joint force

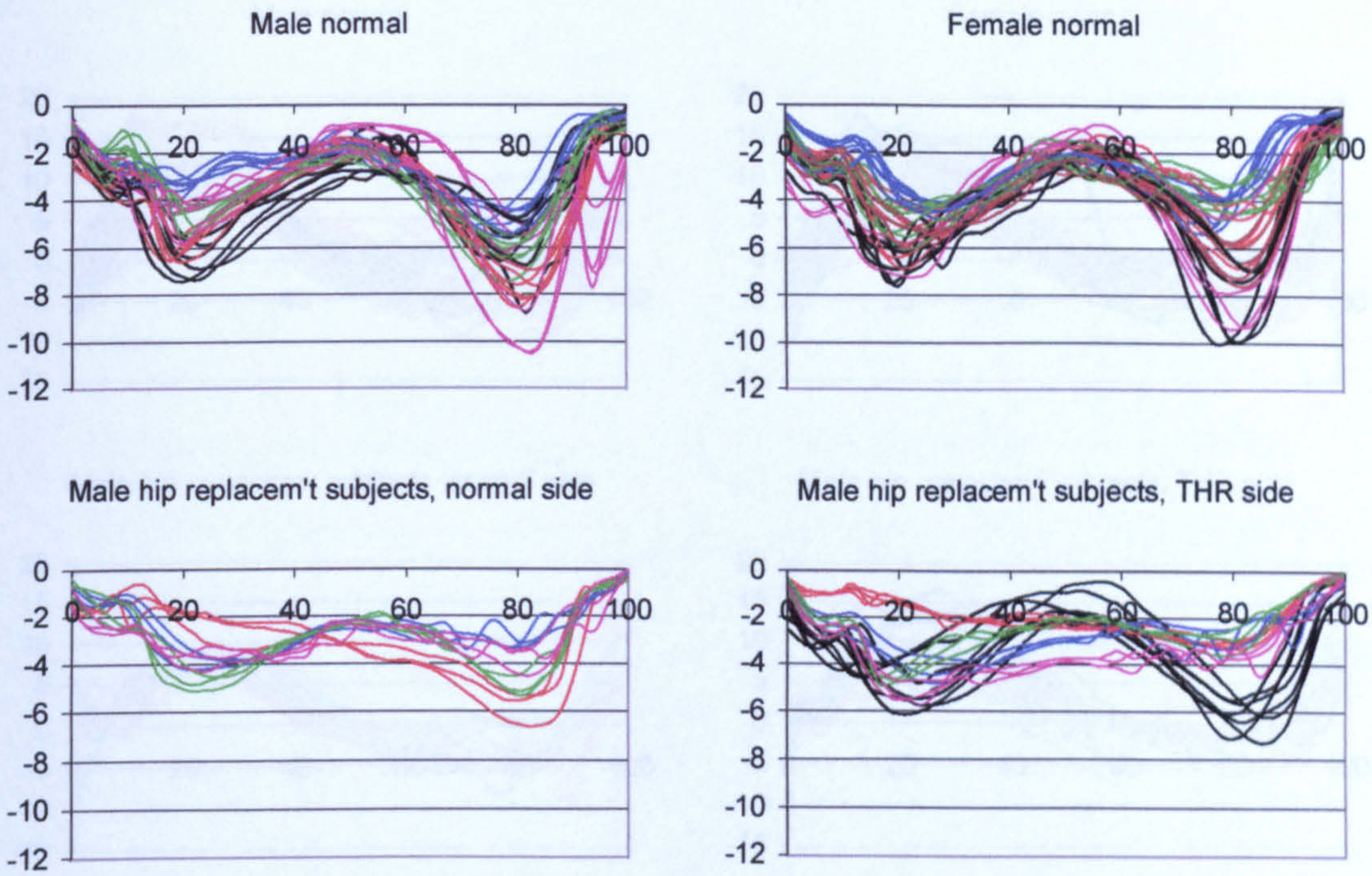

Figure A-VI.4.3 Walking, YFA hip joint force

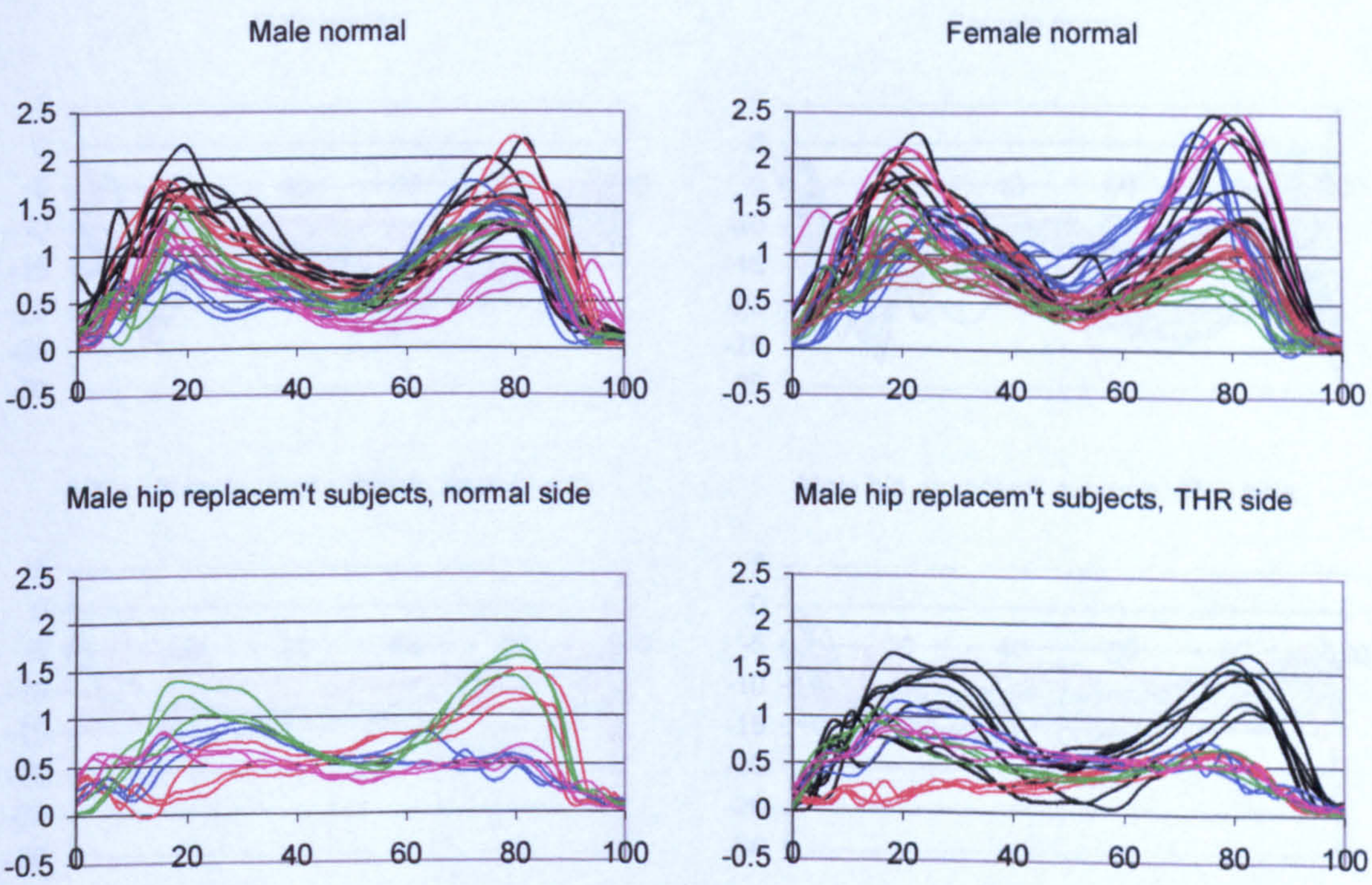

Figure A-VI.4.4 Walking, ZFA hip joint force

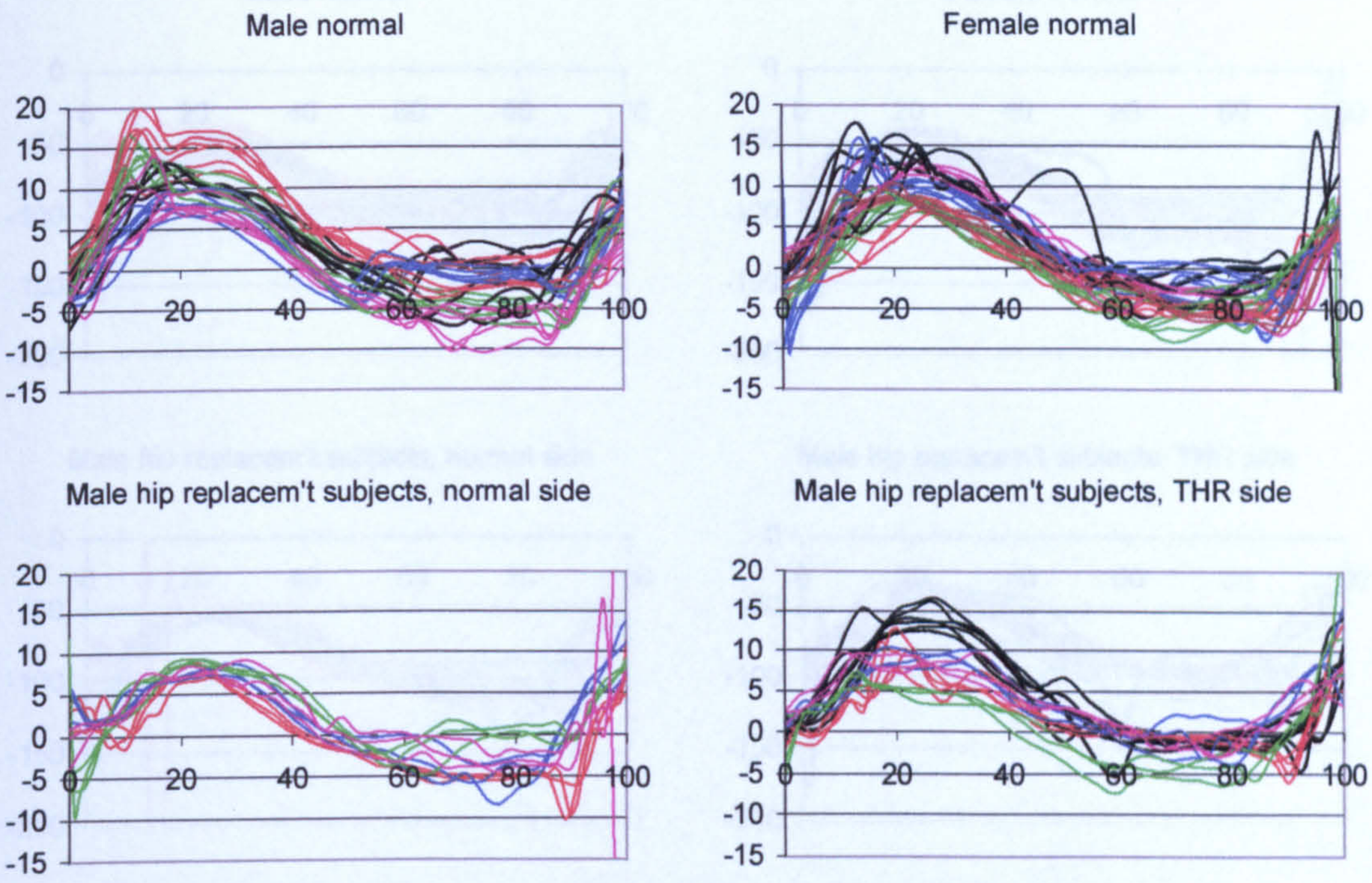

Figure A-VI.4.5 Walking, FHYXANG resultant hip joint force femoral angle

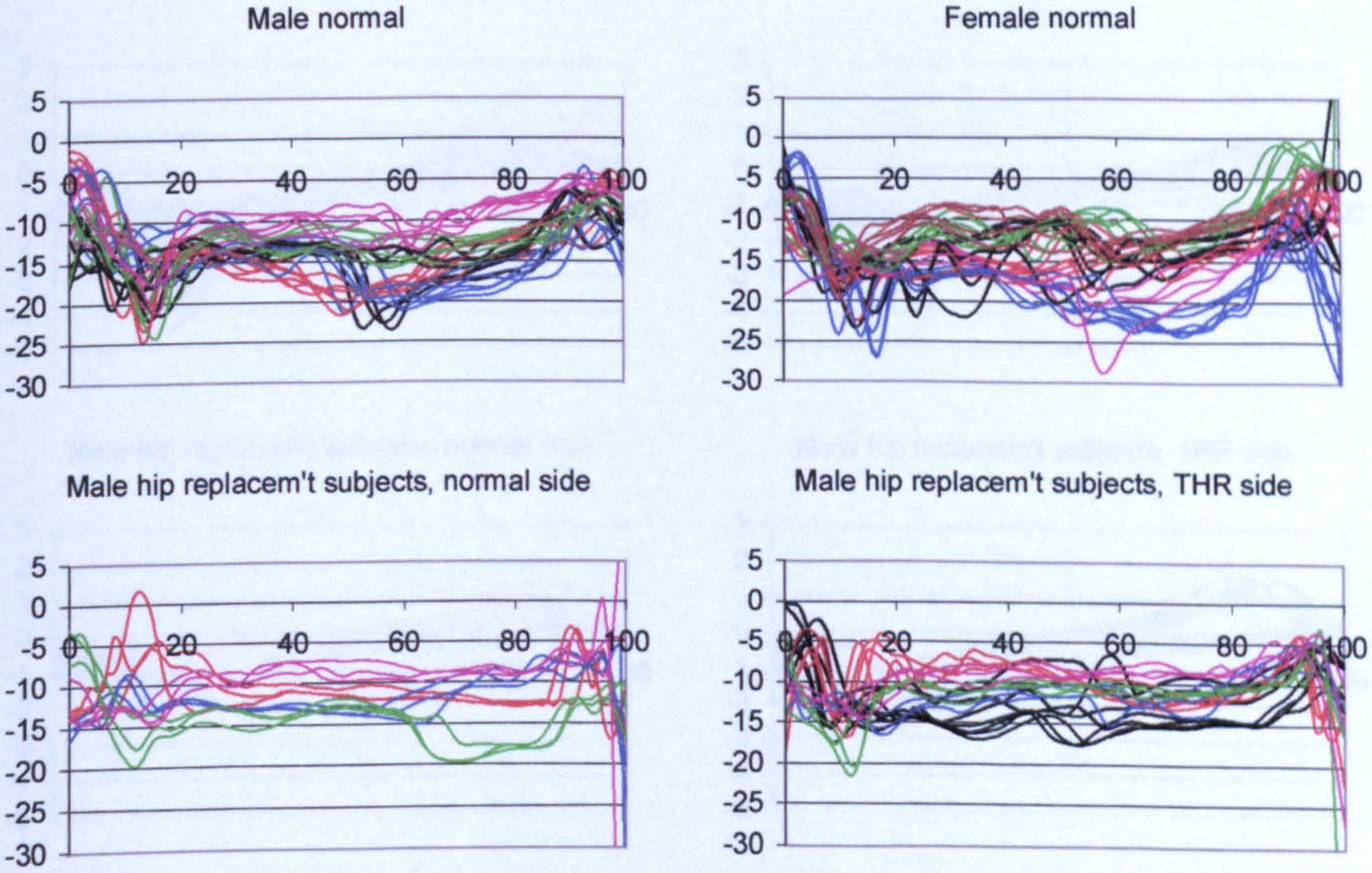

Figure A-VI.4.6 Walking, FHYZANG resultant hip joint force femoral angle

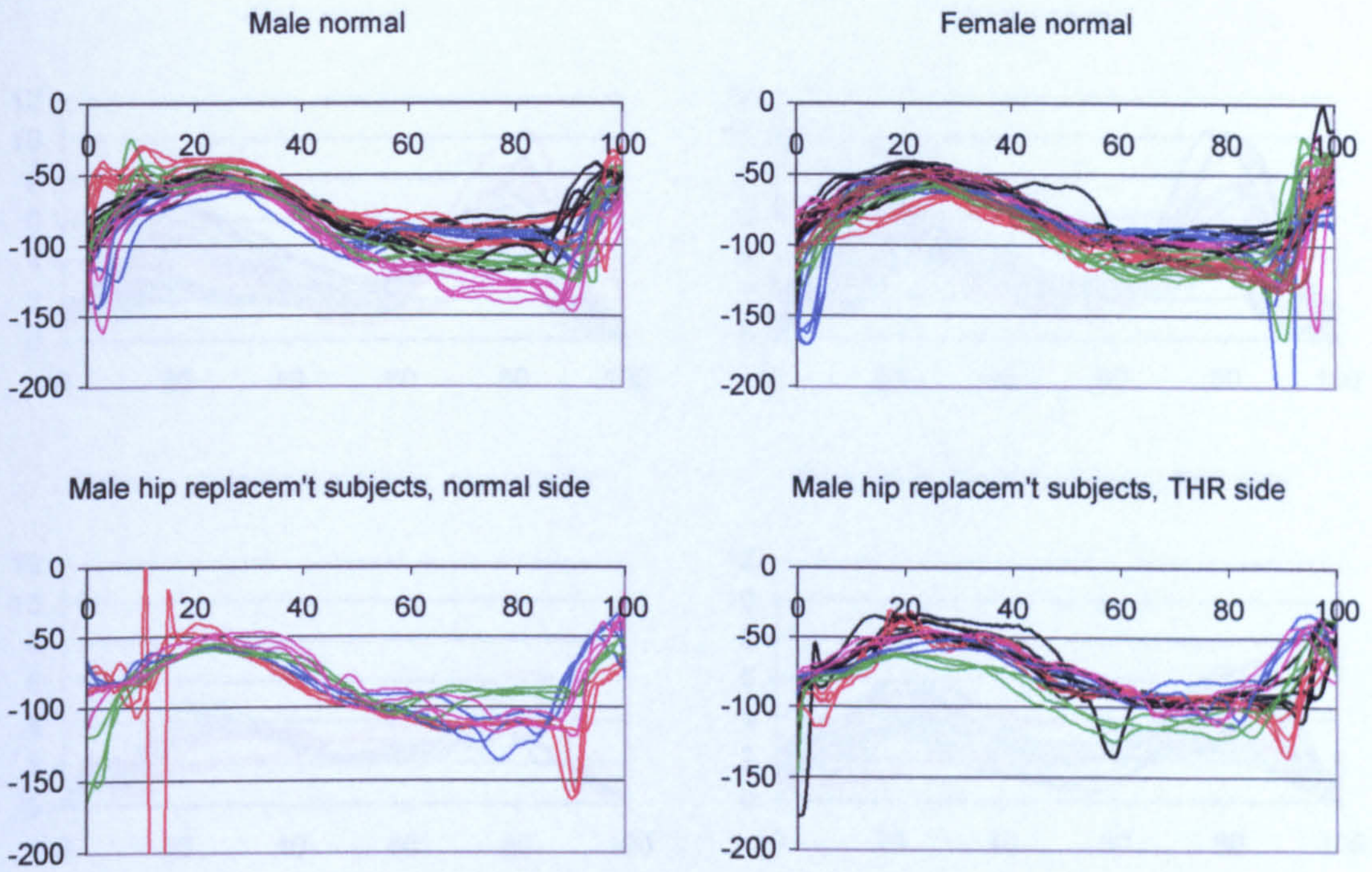

Figure A-VI.4.7 Walking, FHXZANG resultant hip joint force femoral angle

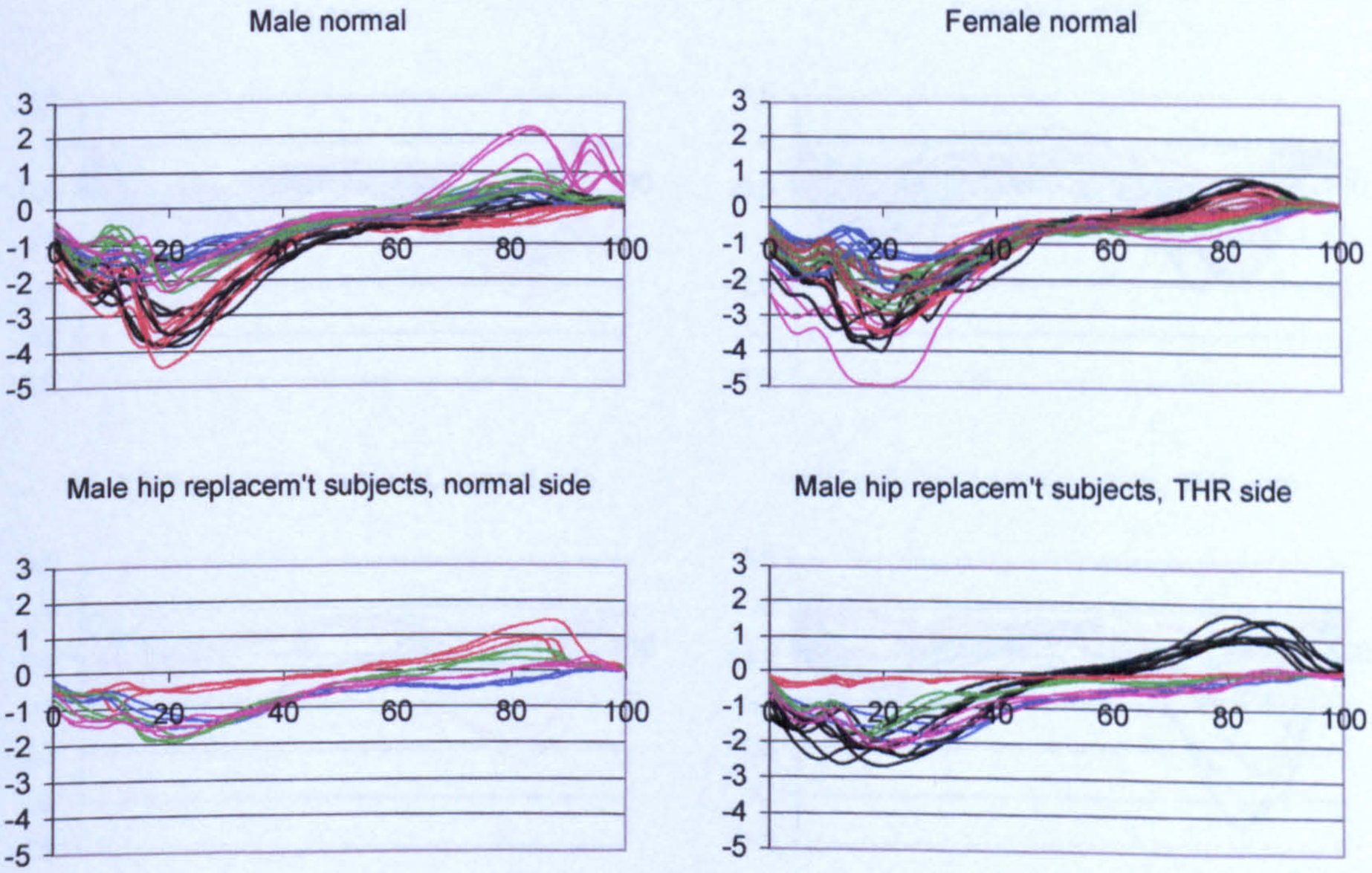

Figure A-VI.4.8 Walking, XPA hip joint force

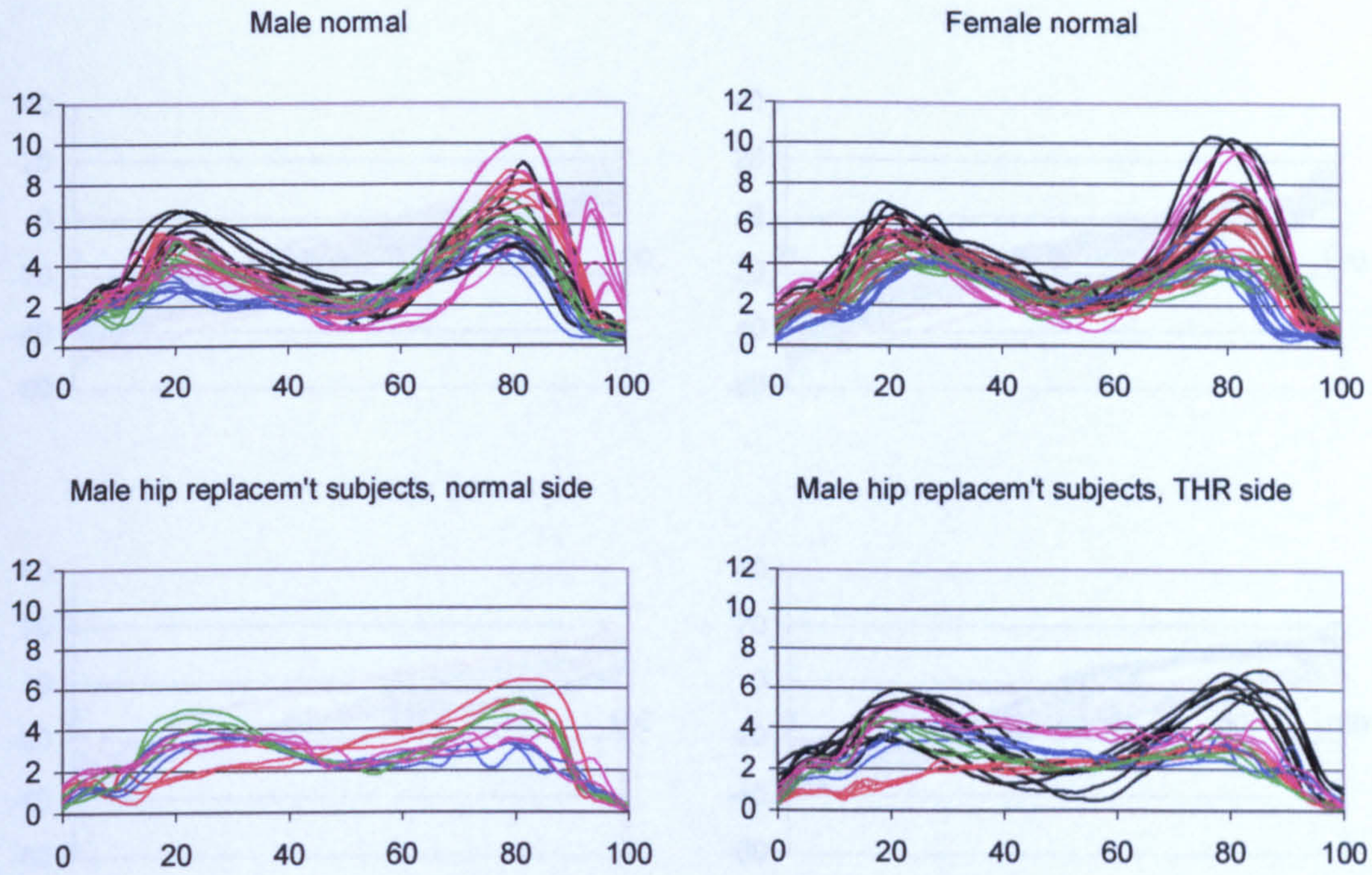

Walking, YPA-axis hip joint force (N/body weight, +ve = acting +YPA) by % stance phase

Figure A-VI.4.9 Walking, YPA hip joint force

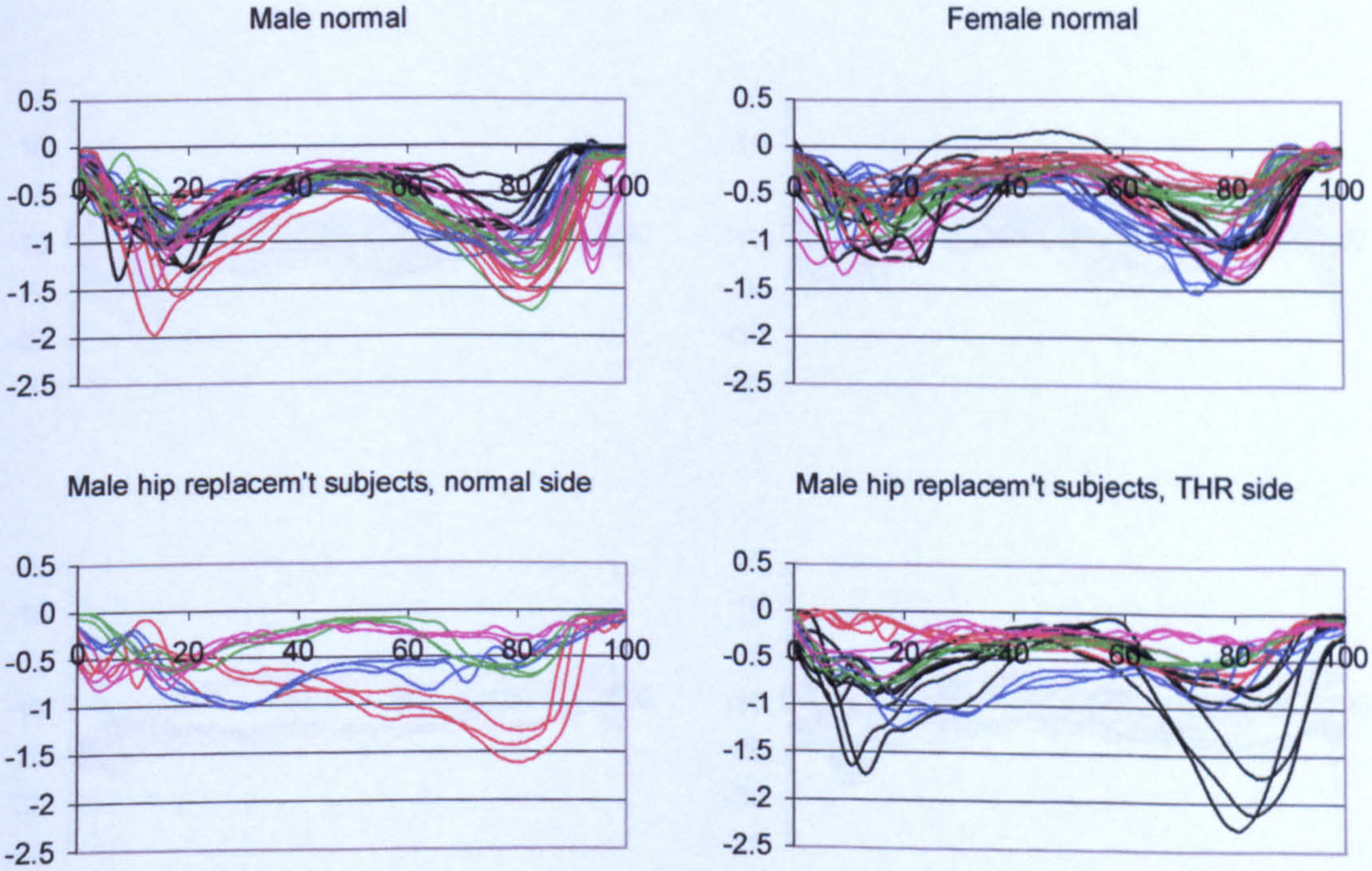

Walking, ZPA-axis hip joint force (N/body weight, +ve = acting +ZPA) by % stance phase

Figure A-VI.4.10 Walking, ZPA hip joint force

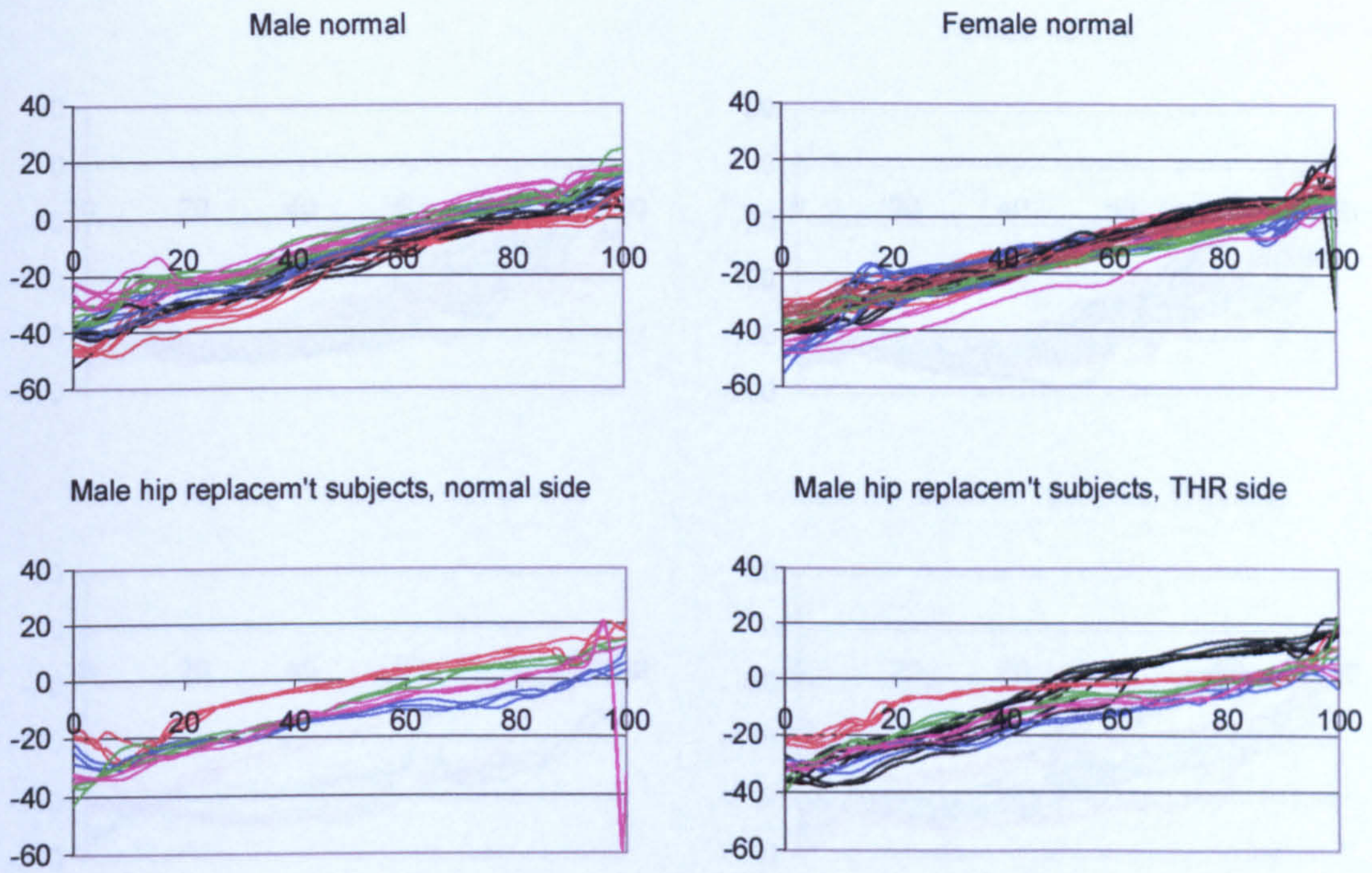

Walking, HJYXANG (degrees, +ve = from YPA towards XPA) by % stance phase

Figure A-VI.4.11 Walking, HJYXANG resultant hip joint force pelvic angle

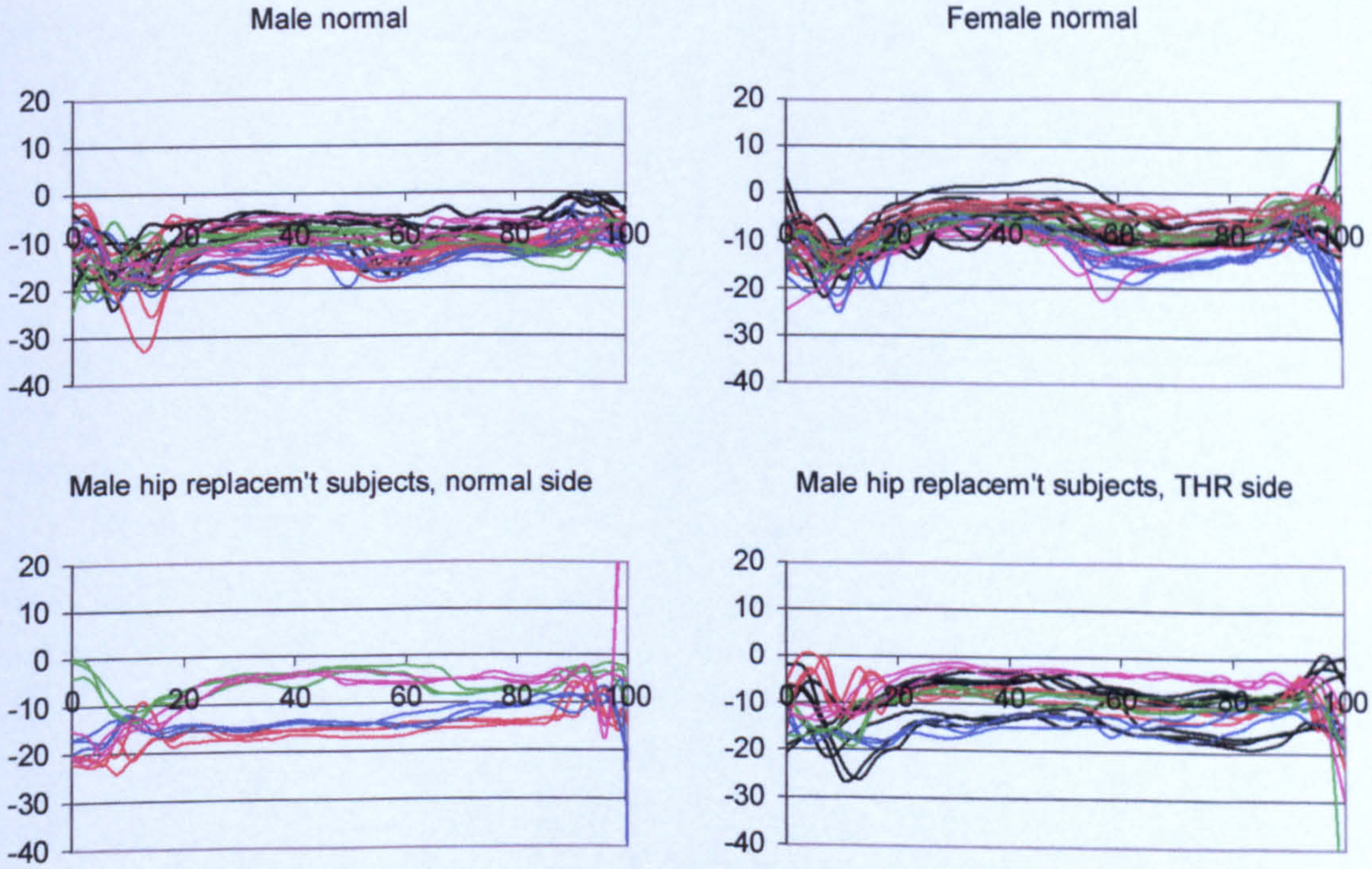

Walking, HJYZANG (degrees, +ve = from YPA towards ZPA) by % stance phase

Figure A-VI.4.12 Walking, HJYZANG resultant hip joint force pelvic angle

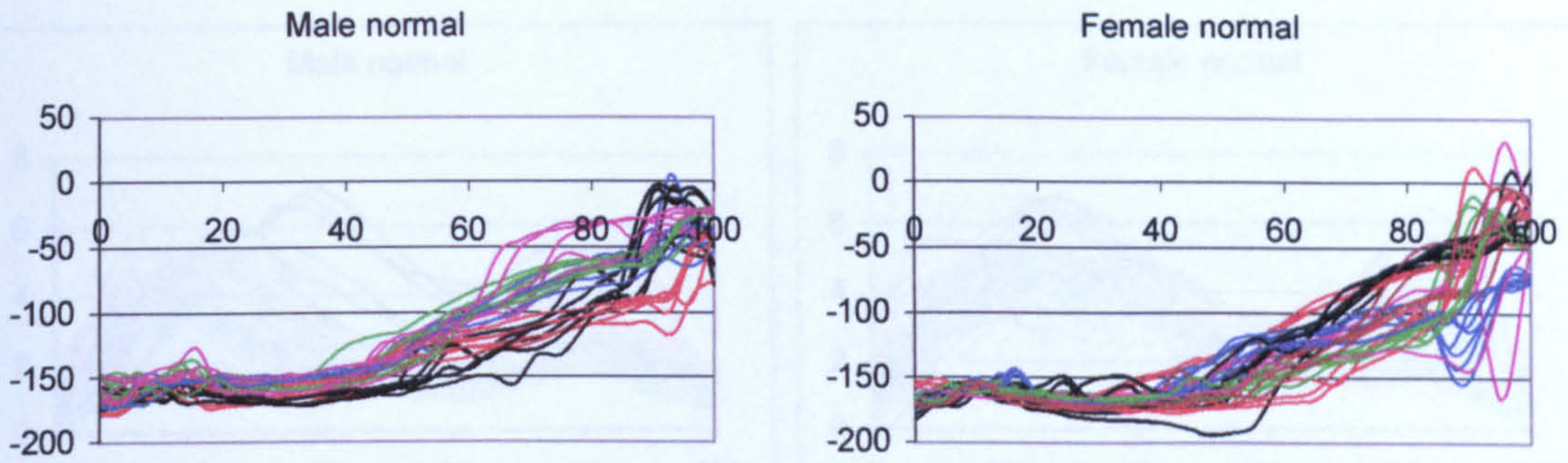

Figure A-VI.4.13 Walking, HJXZANG resultant hip joint force pelvic angle

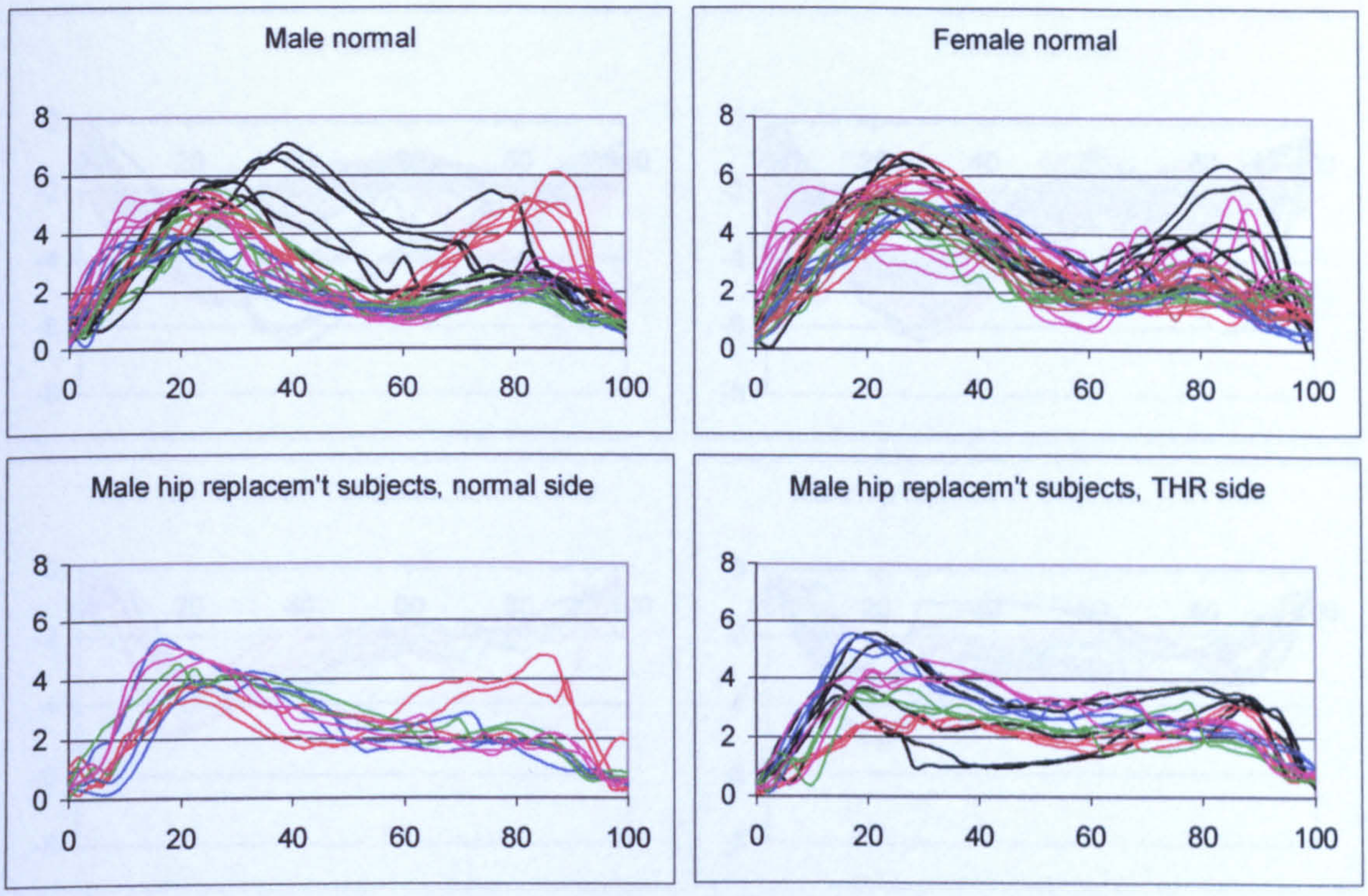

Stair ascent, resultant hip joint force (N/body weight) by % stance phase

Figure A-VI.4.14 Stair ascent, resultant hip joint force

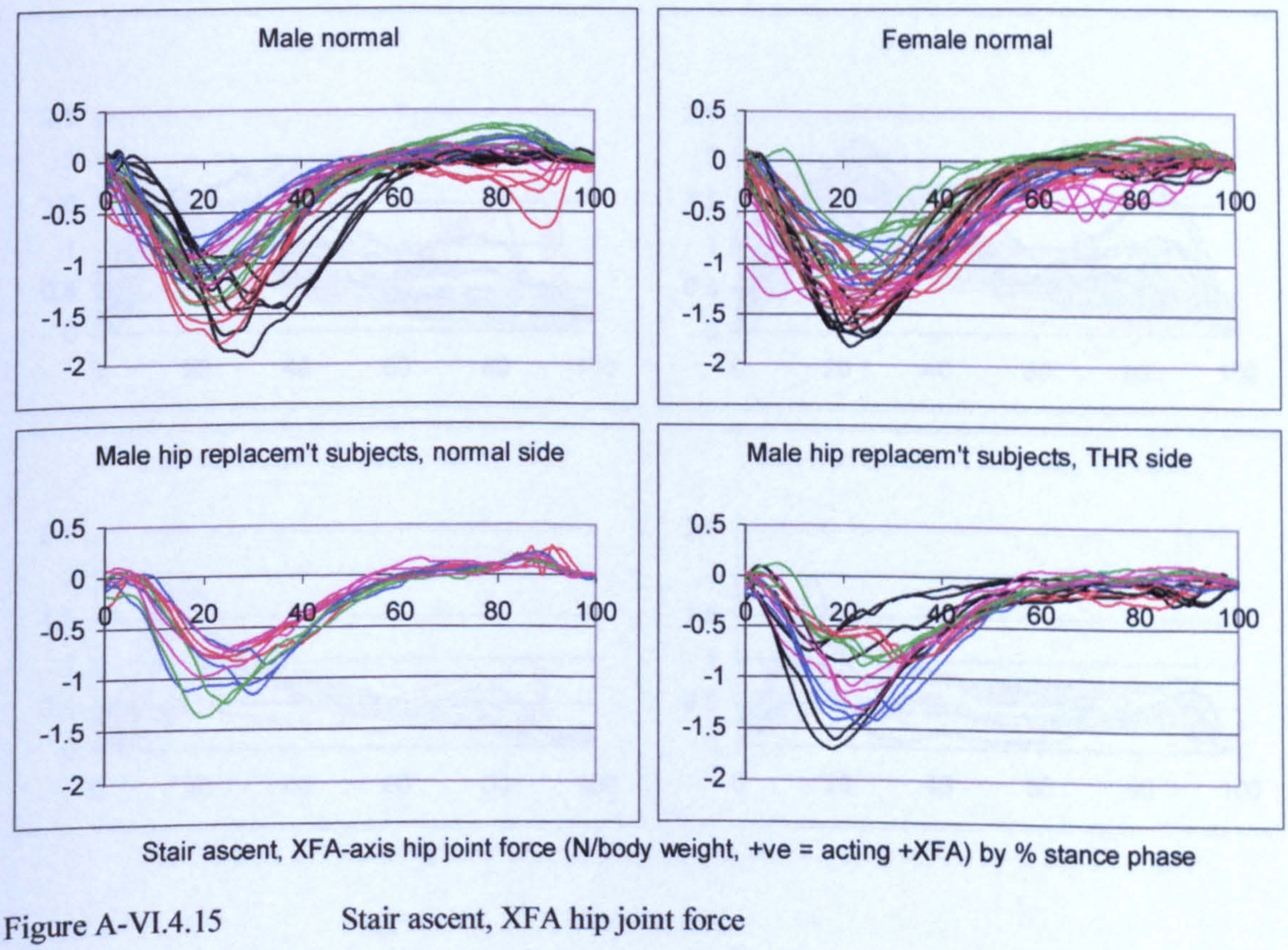

Stair ascent, XFA-axis hip joint force (N/body weight, +ve = acting +XFA) by % stance phase

Figure A-VI.4.15 Stair ascent, XFA hip joint force

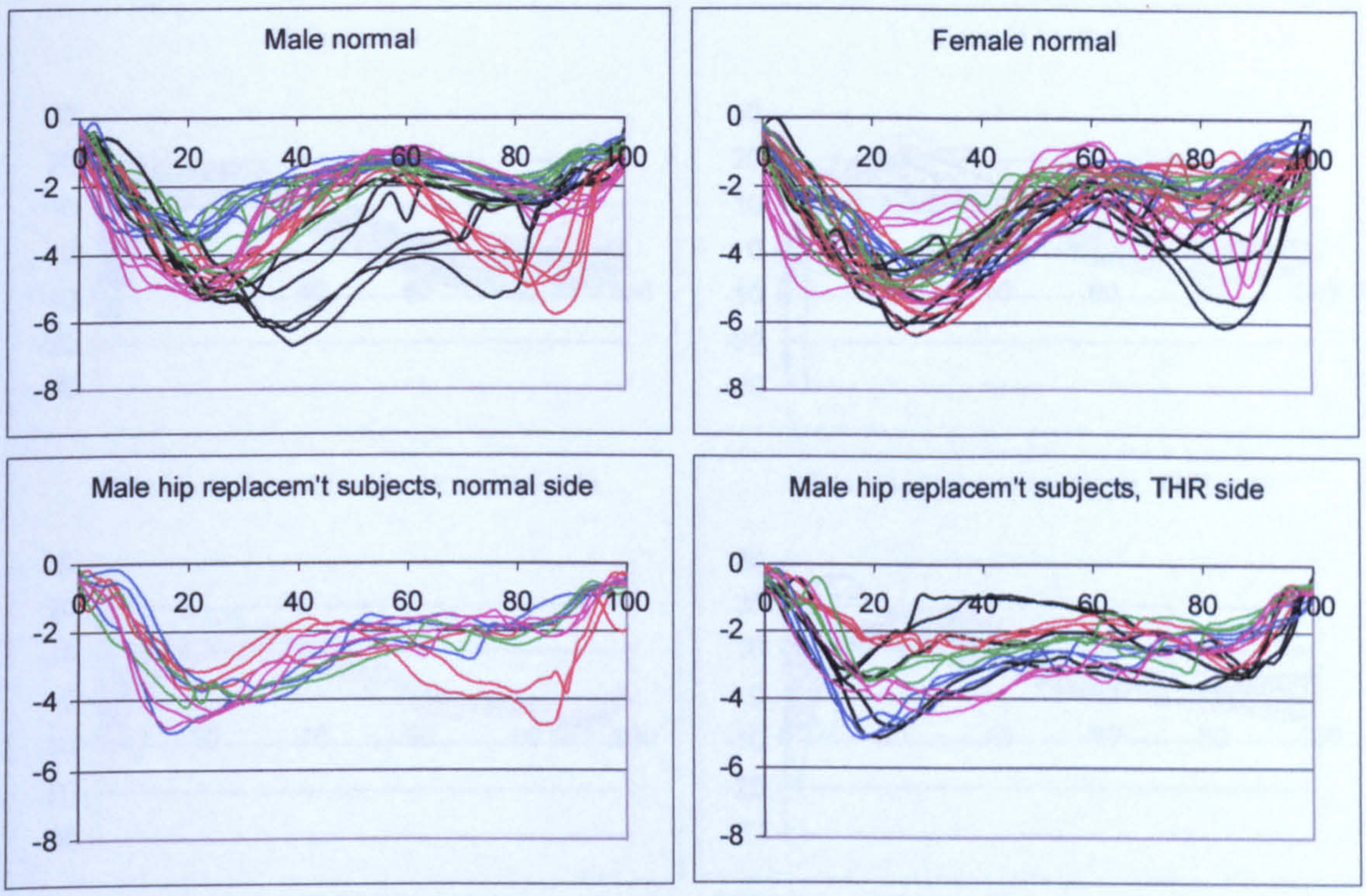

Stair ascent, YFA-axis hip joint force (N/body weight, +ve = acting +YFA) by % stance phase

Figure A-VI.4.16 Stair ascent, YFA hip joint force

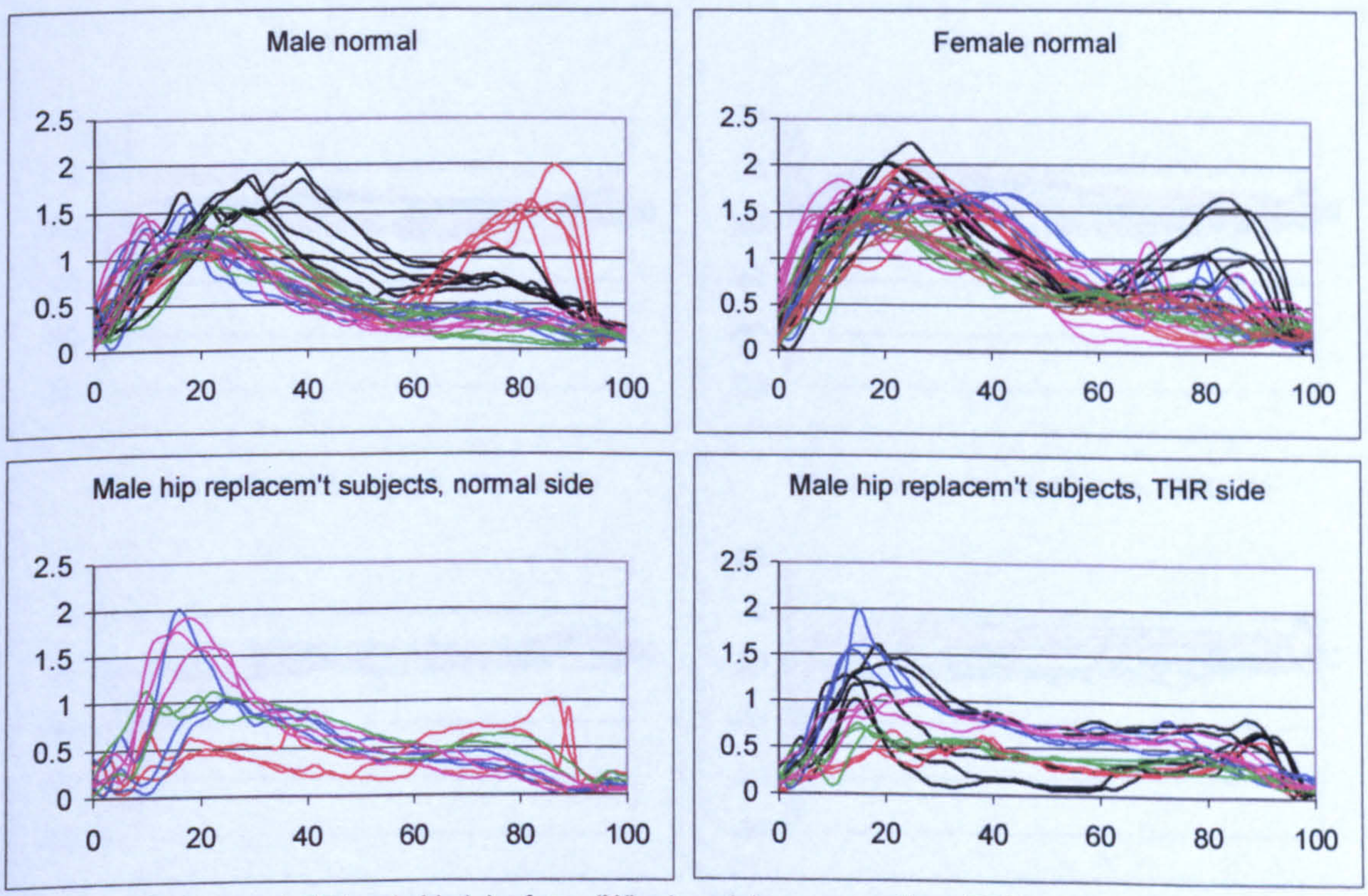

Stair ascent, ZFA-axis hip joint force (N/body weight, +ve = acting +ZFA) by % stance phase

Figure A-VI.4.17 Stair ascent, ZFA hip joint force

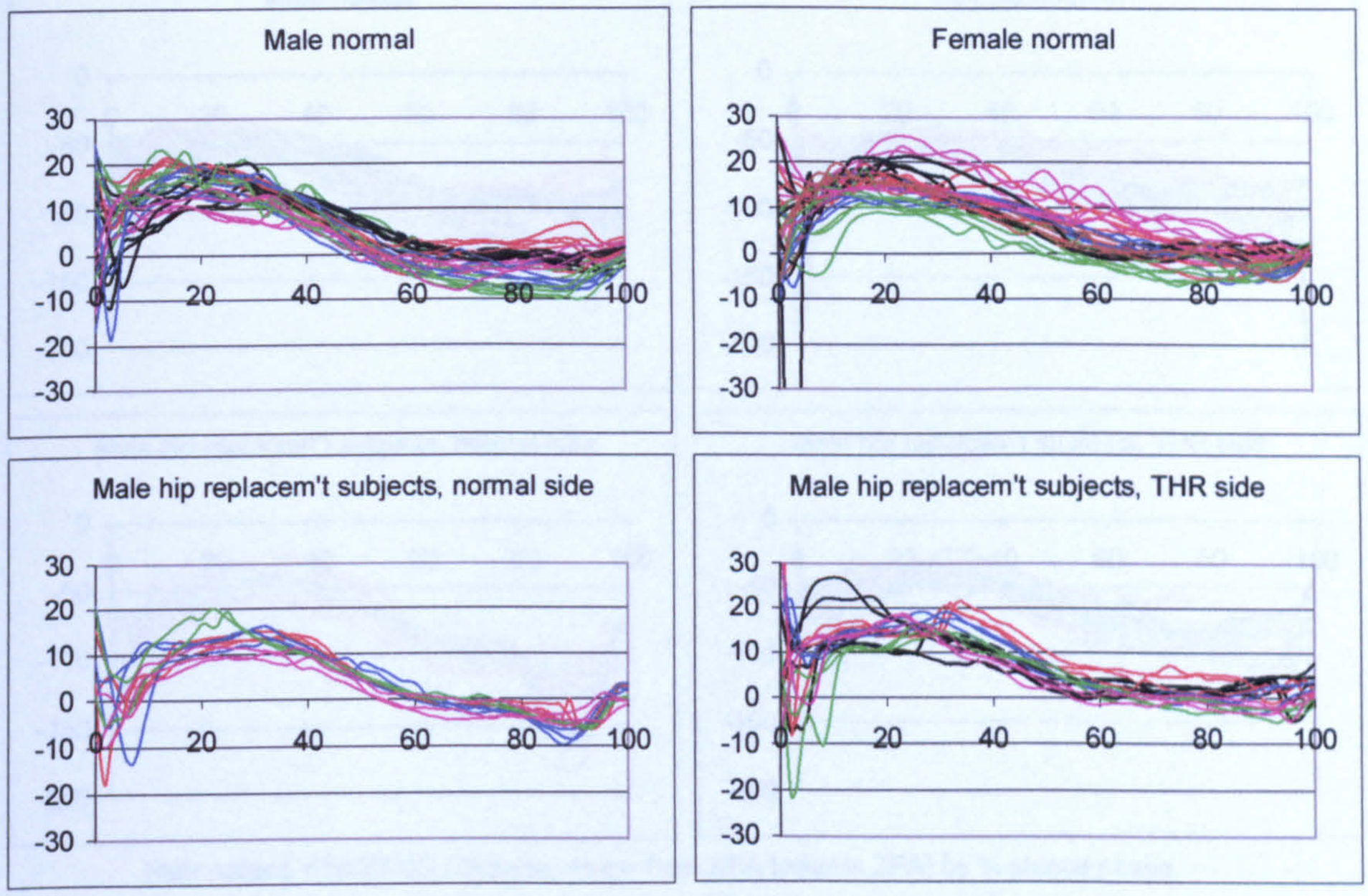

Stair ascent, FHYXANG (degrees, +ve = from YFA towards XFA) by % stance phase

Figure A-VI.4.18 Stair ascent, FHYXANG resultant hip joint force femoral angle

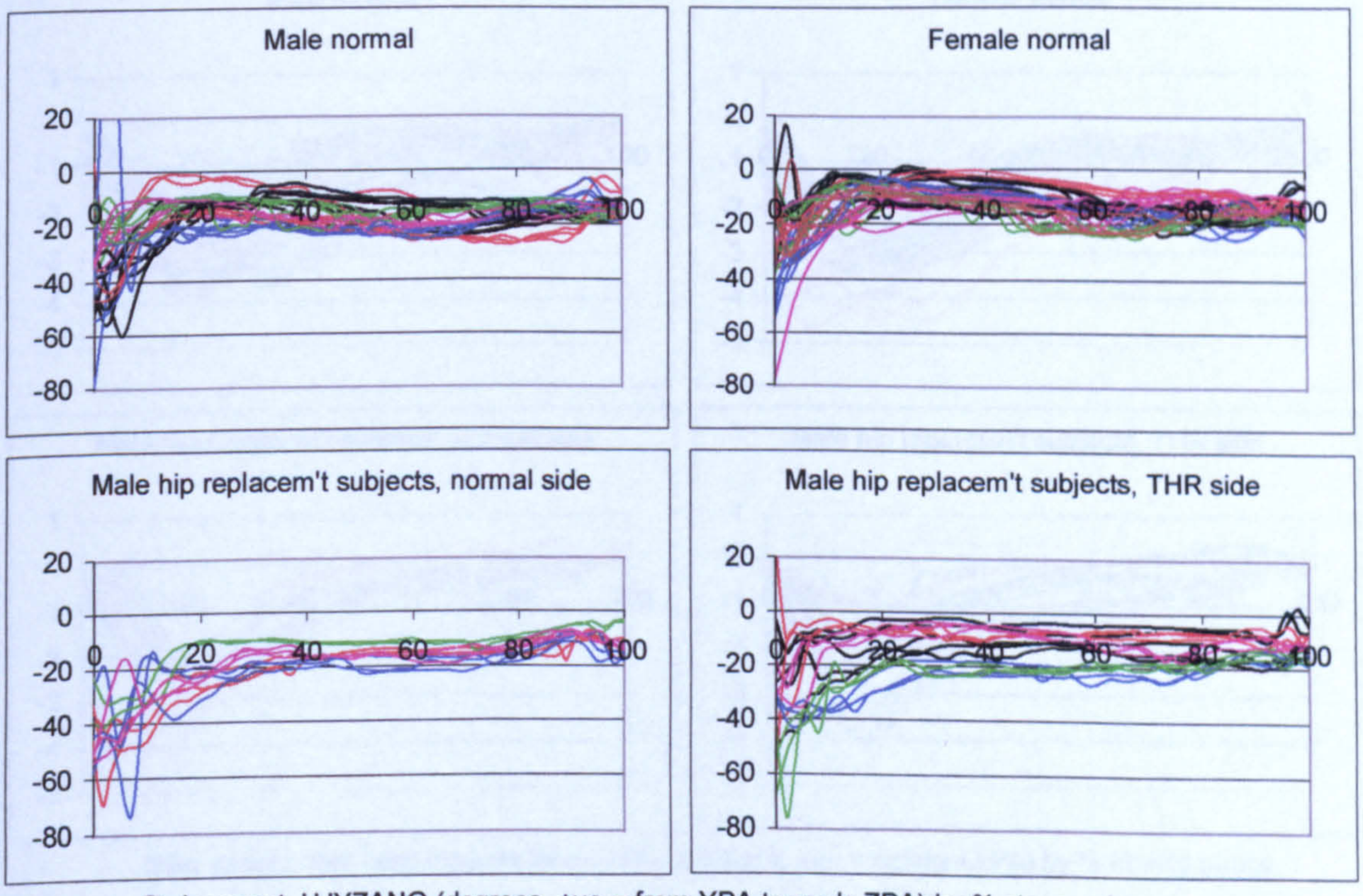

Stair ascent, HJYZANG (degrees, +ve = from YPA towards ZPA) by % stance phase

Figure A-VI.4.19 Stair ascent, FHYZANG resultant hip joint force femoral angle

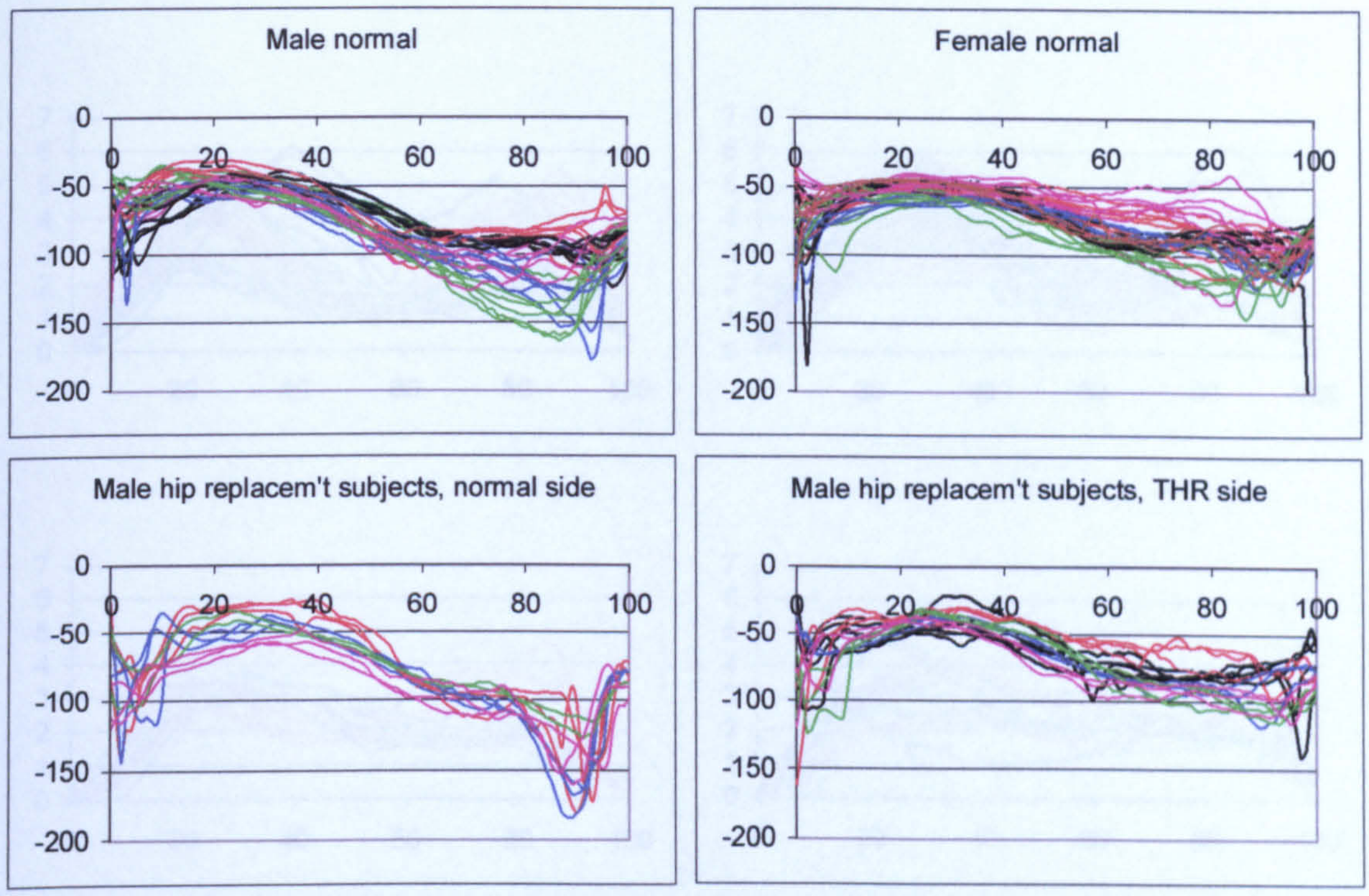

Figure A-VI.4.20 Stair ascent, FHXZANG resultant hip joint force femoral angle

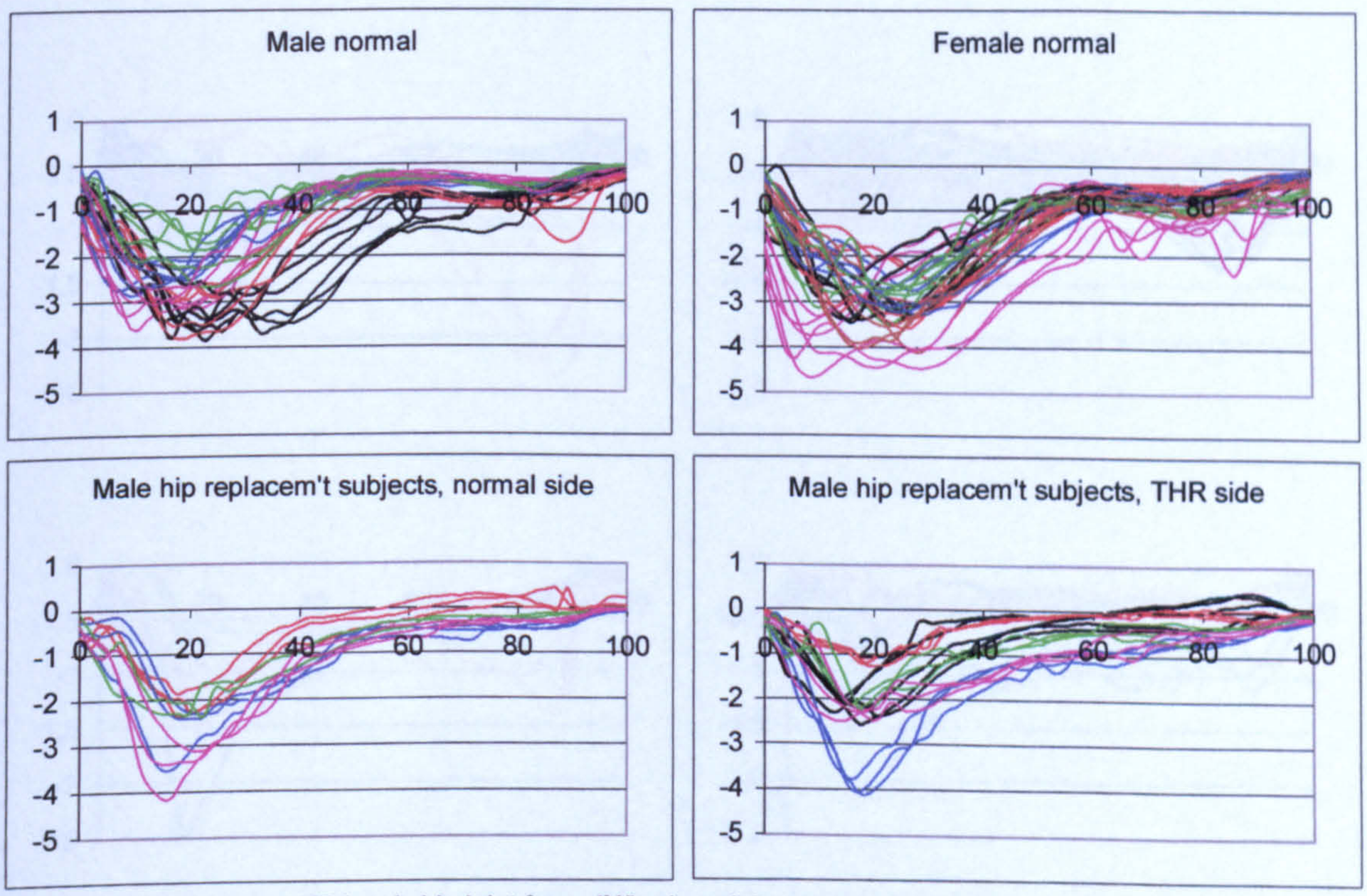

Figure A-VI.4.21 Stair ascent, XPA hip joint force

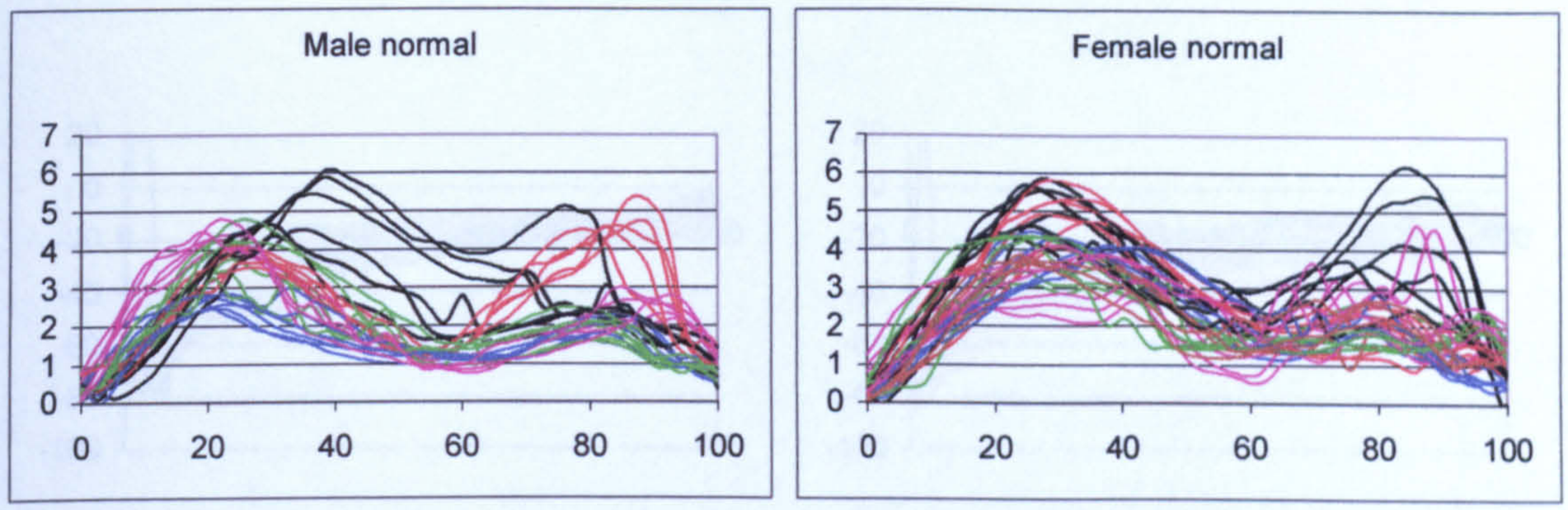

Stair ascent, YPA-axis hip joint force (N/body weight, +ve = acting +YPA) by % stance phase

Figure A-VI.4.22 Stair ascent, YPA hip joint force

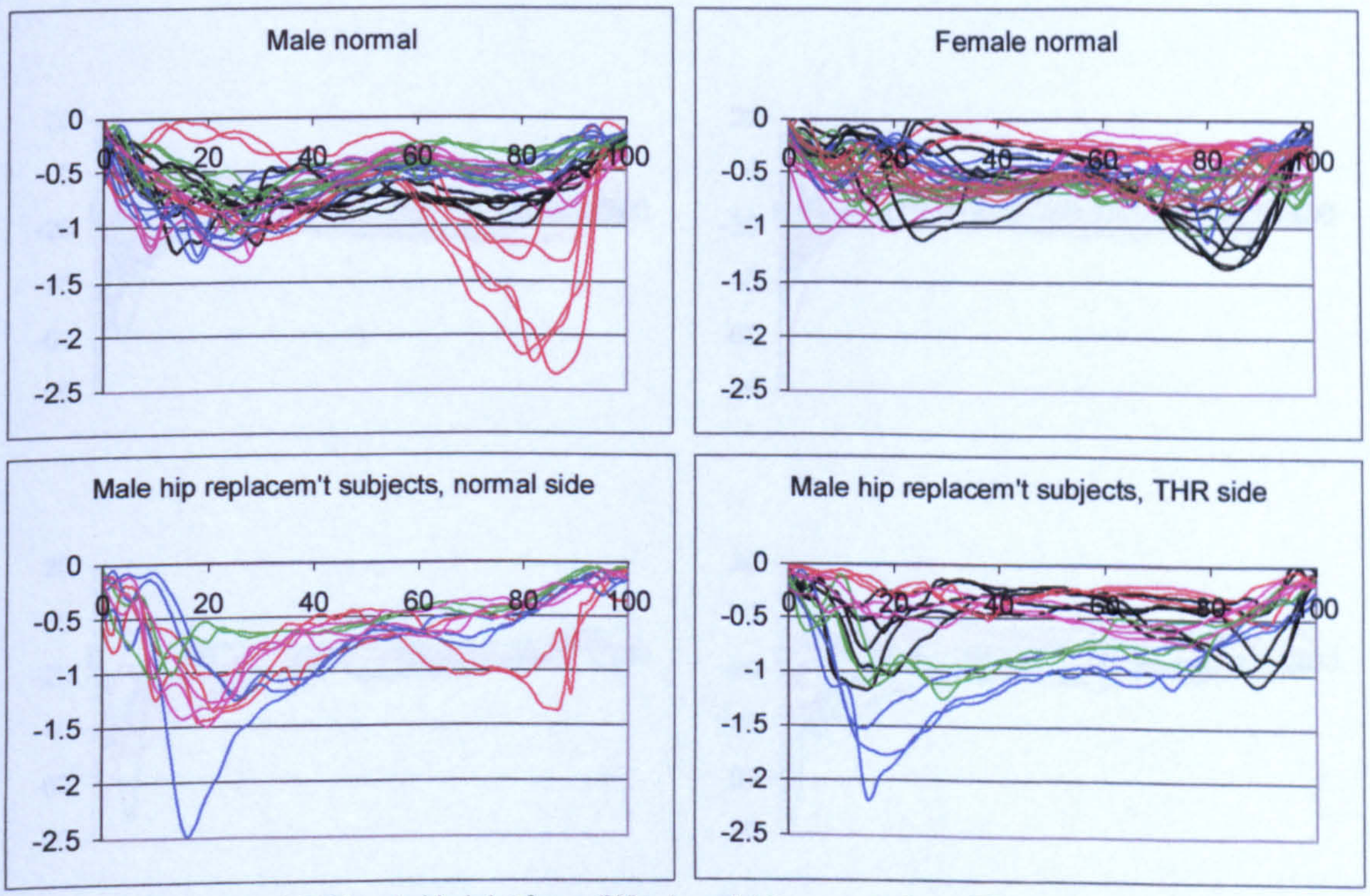

Stair ascent, ZPA-axis hip joint force (N/body weight, +ve = acting +ZPA) by % stance phase

Figure A-VI.4.23 Stair ascent, ZPA hip joint force

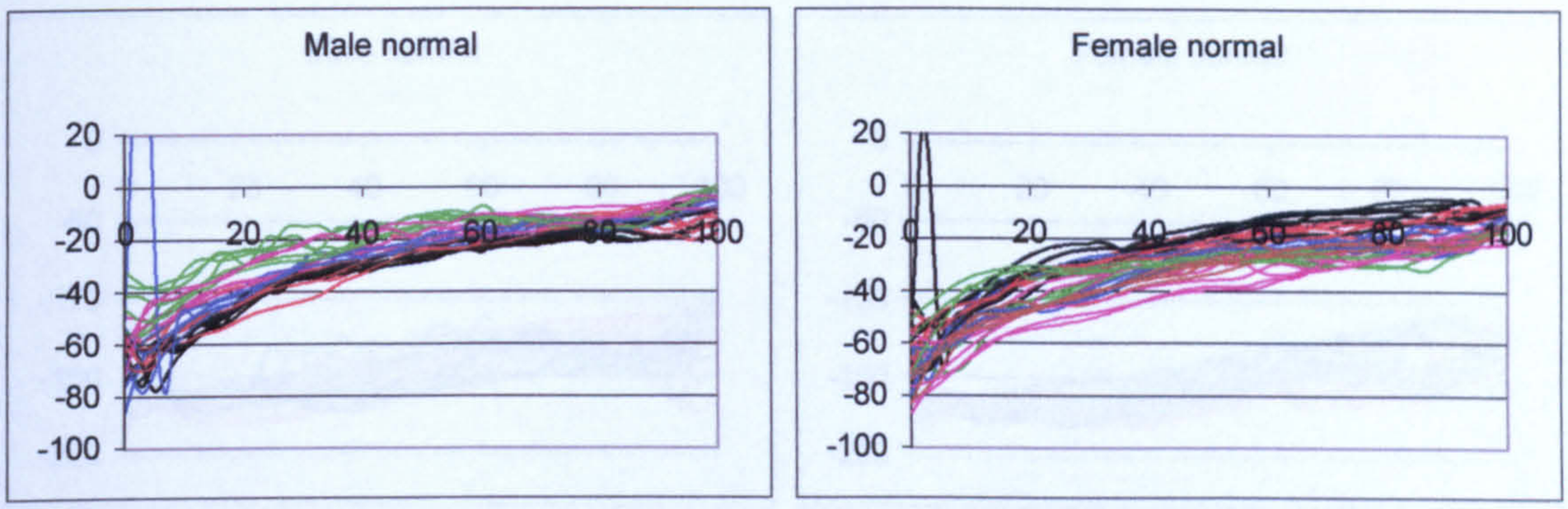

Figure A-VI.4.24 Stair ascent, HJYXANG resultant hip joint force pelvic angle

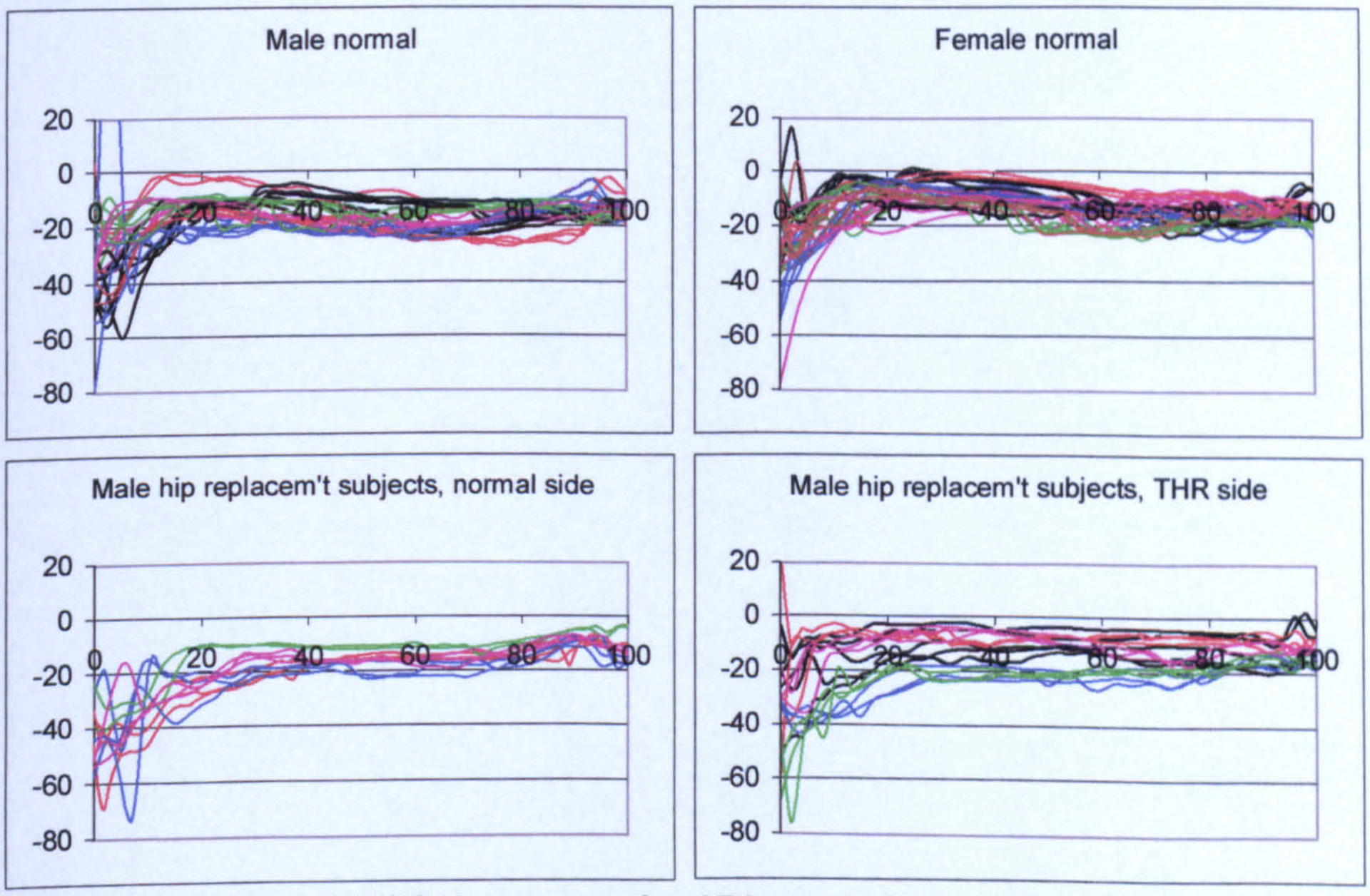

Figure A-VI.4.25 Stair ascent, HJYZANG resultant hip joint force pelvic angle

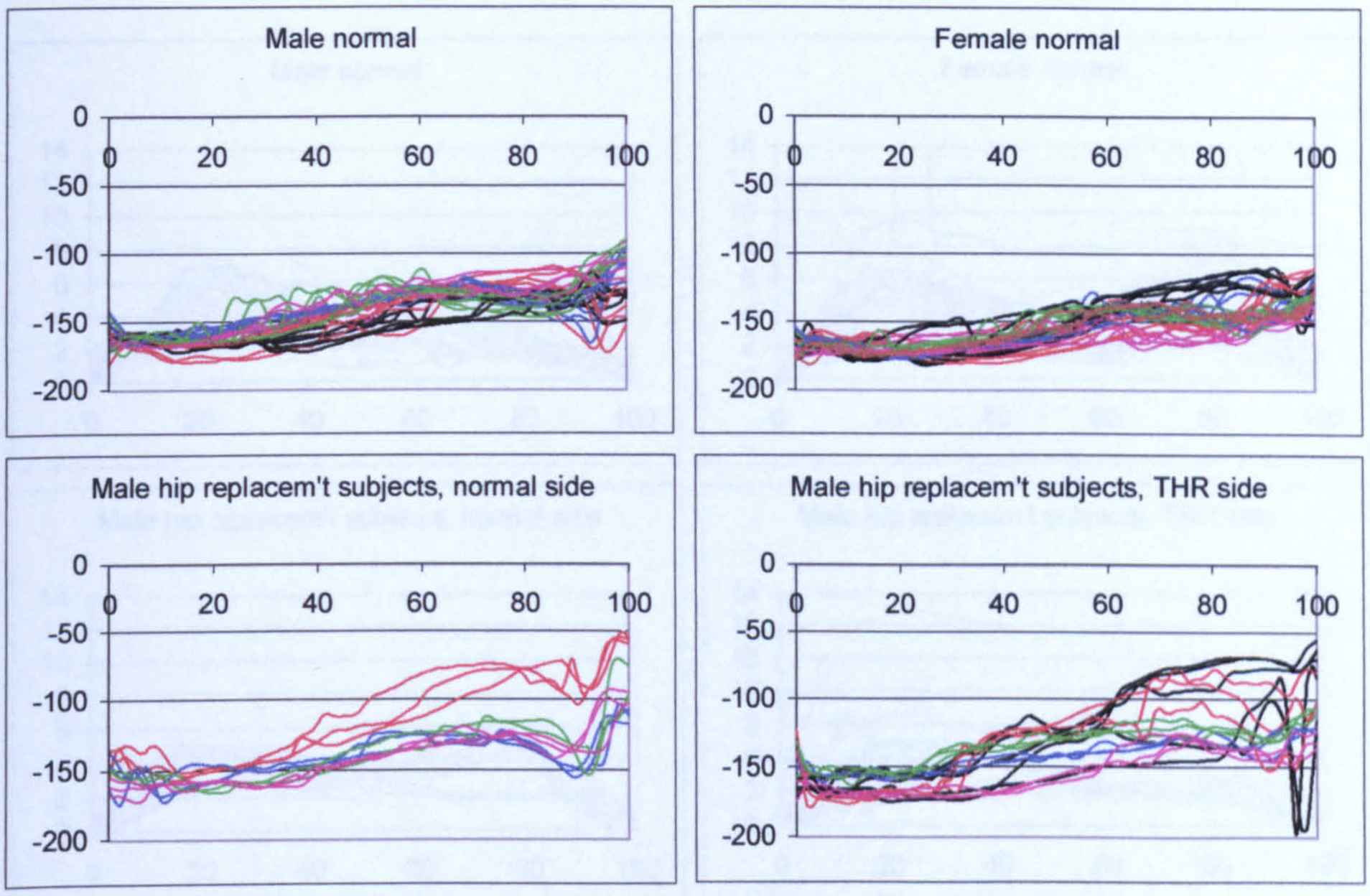

Figure A-VI.4.26 Stair ascent, HJXZANG resultant hip joint force pelvic angle

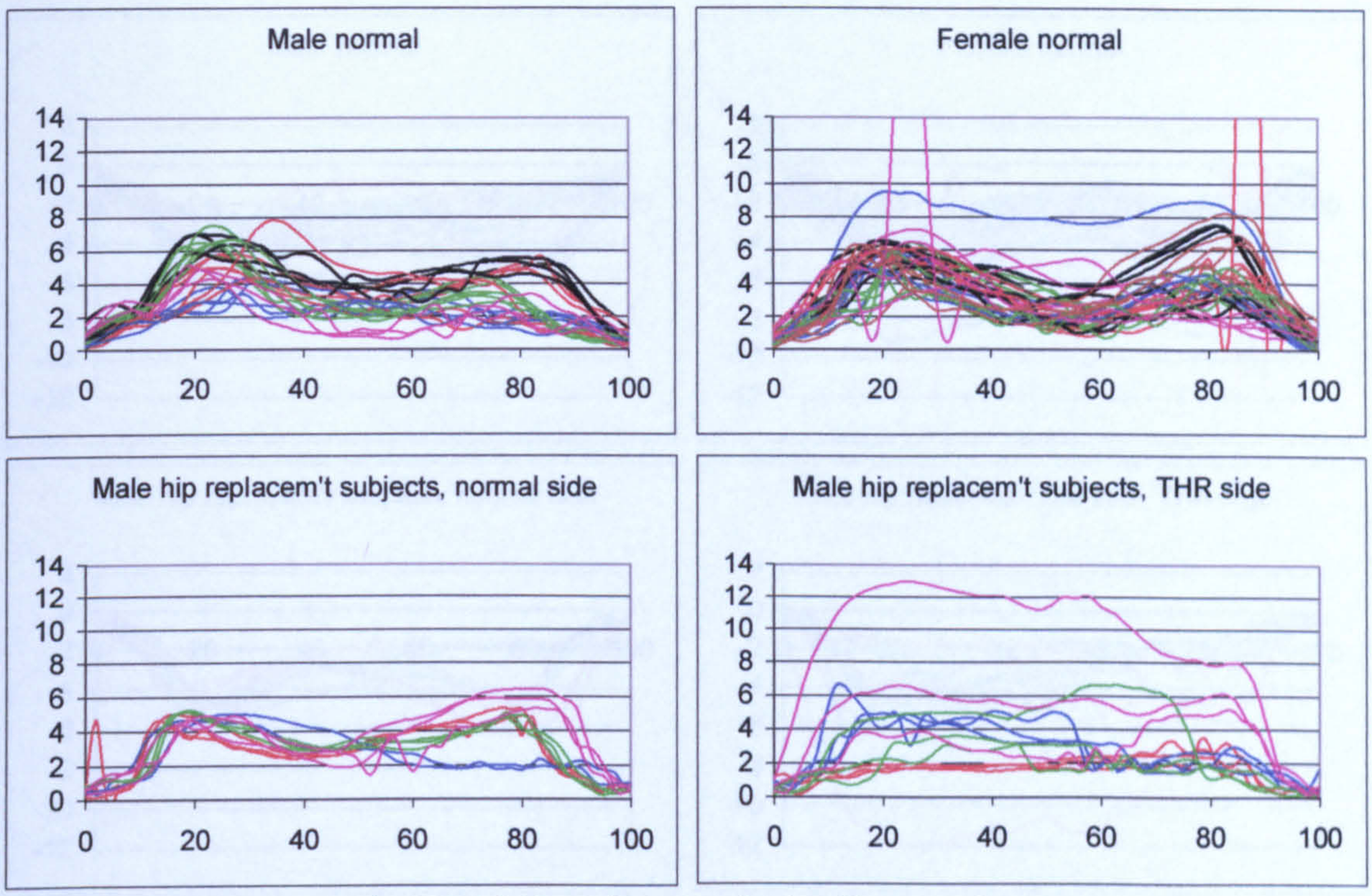

Figure A-VI.4.27 Stair descent, resultant hip joint force

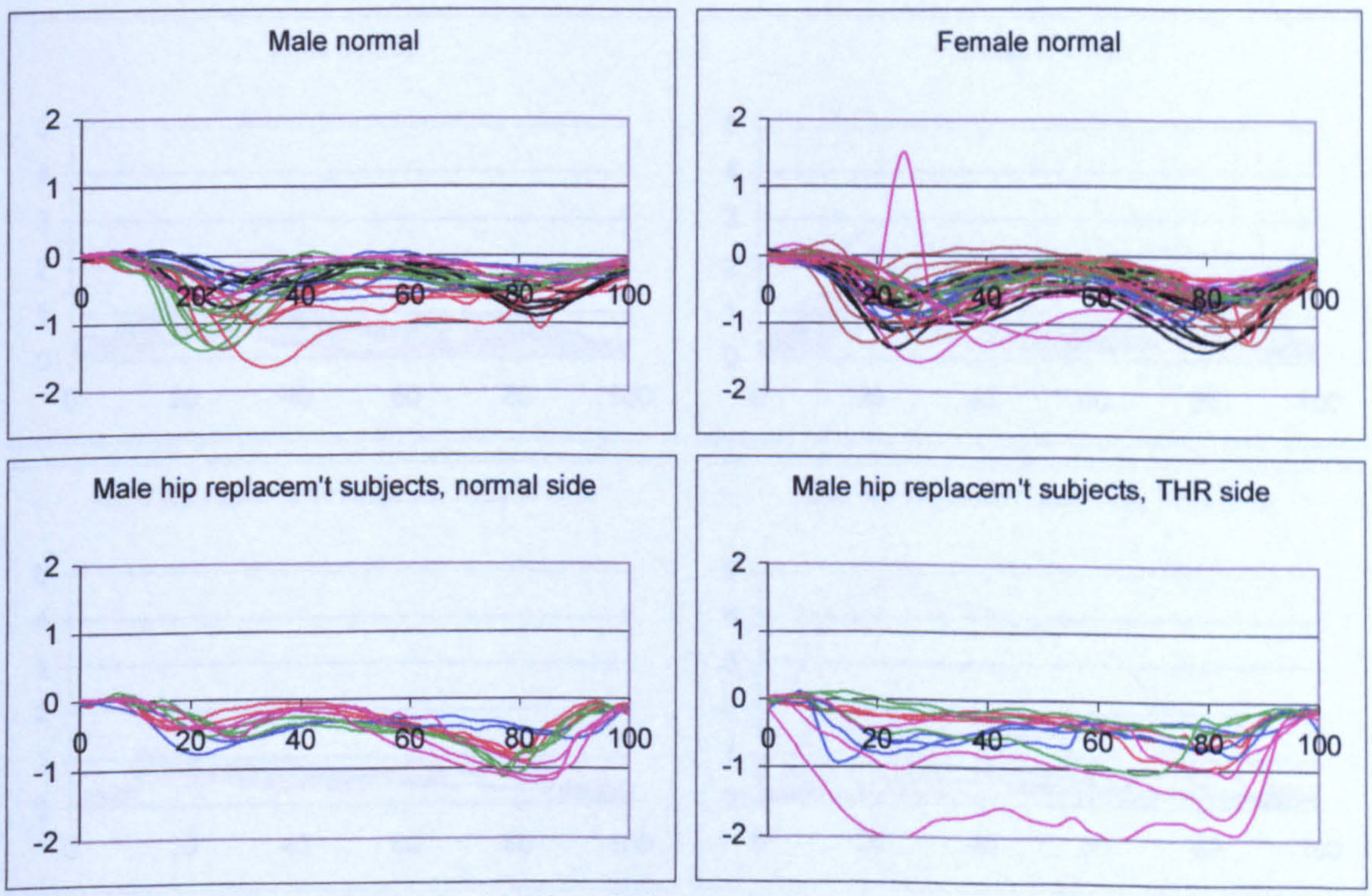

Figure A-VI.4.28 Stair descent, XFA hip joint force

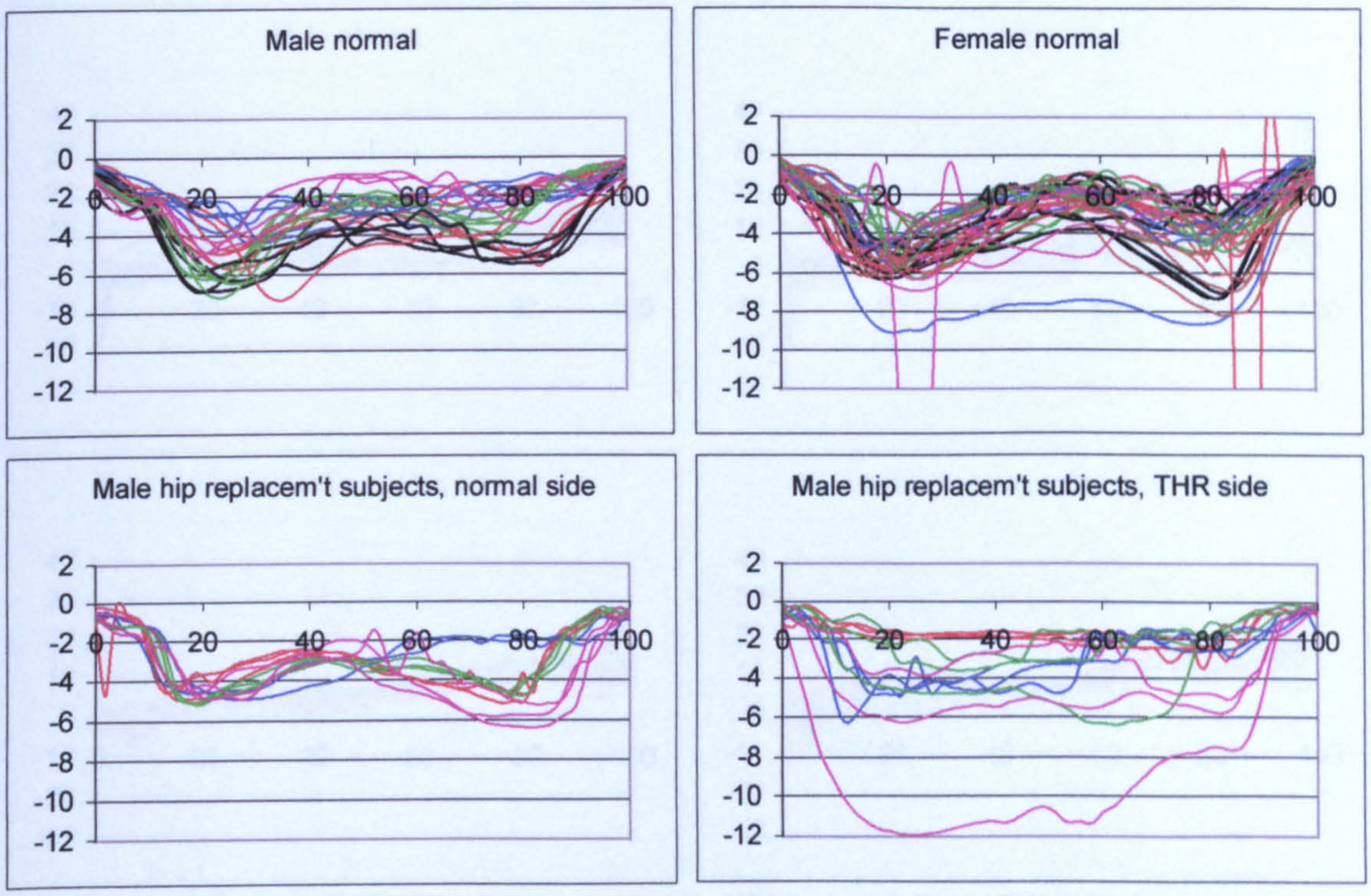

Stair descent, YFA-axis hip joint force (N/body weight, +ve = acting +YFA) by % stance phase

Figure A-VI.4.29 Stair descent, YFA hip joint force

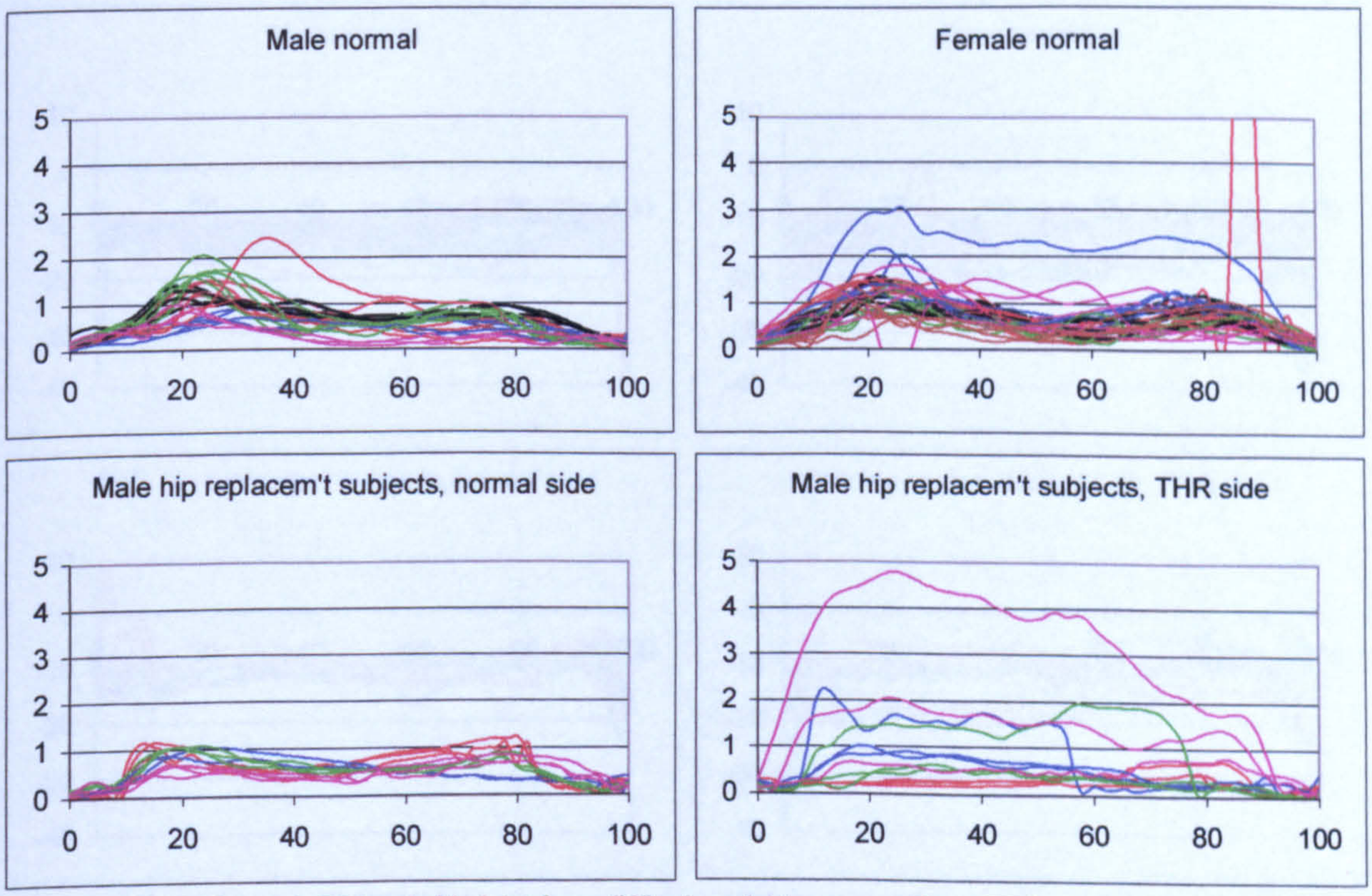

Stair descent, ZFA-axis hip joint force (N/body weight, +ve = acting +ZFA) by % stance phase

Figure A-VI.4.30 Stair descent, ZFA hip joint force

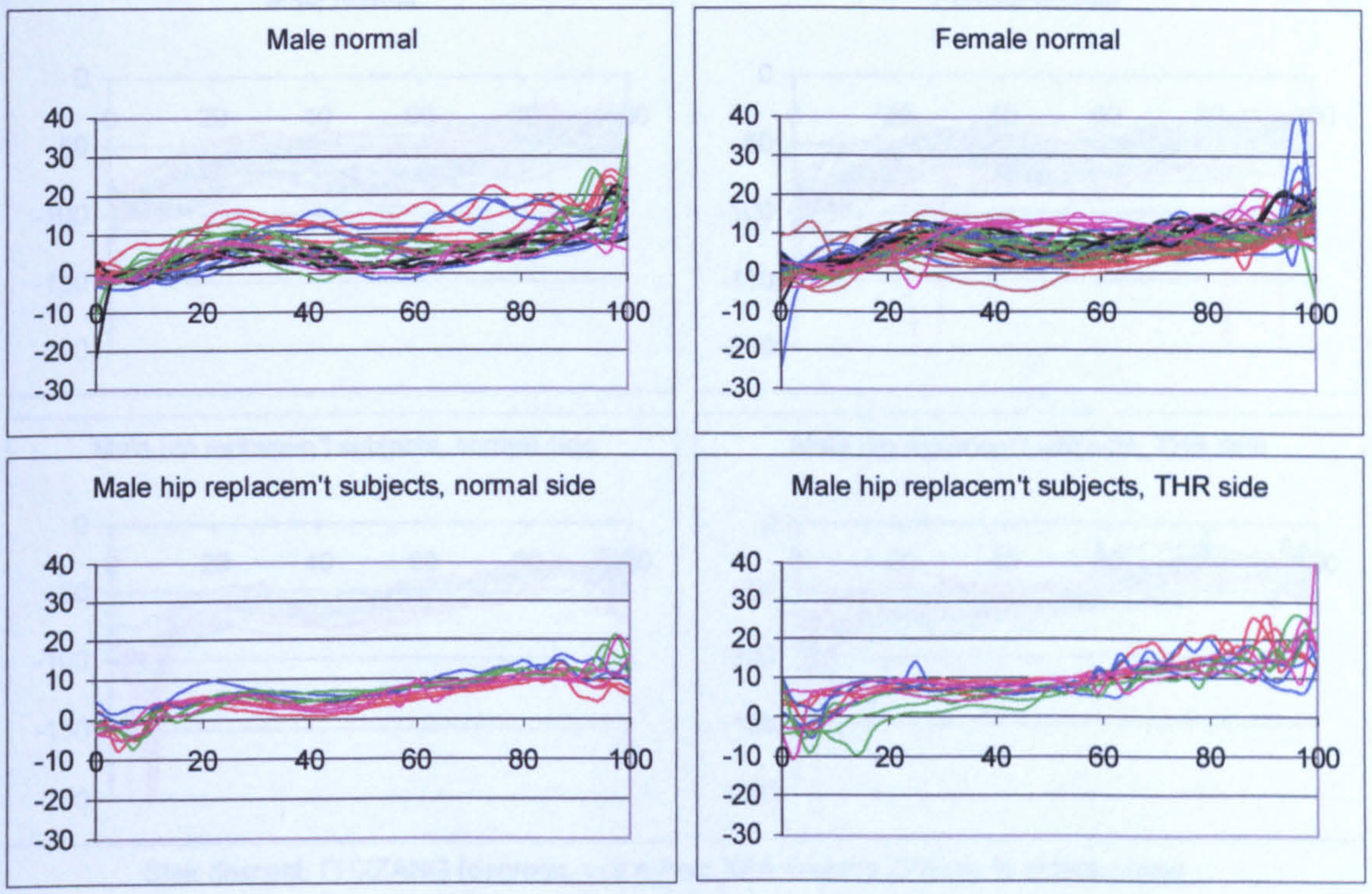

Figure A-VI.4.31 Stair descent, FHYXANG resultant hip joint force femoral angle

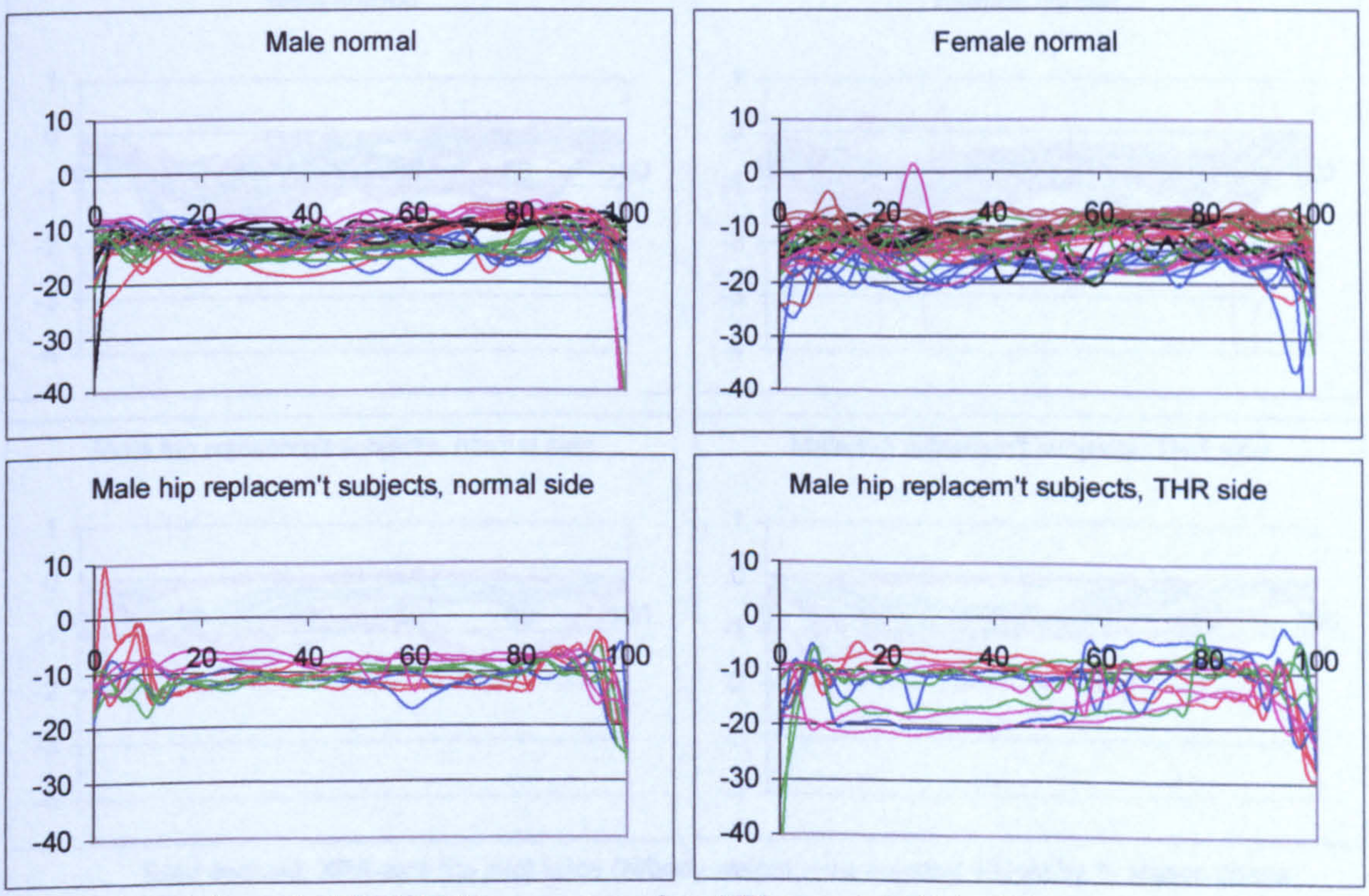

Figure A-VI.4.32 Stair descent, FHYZANG resultant hip joint force femoral angle

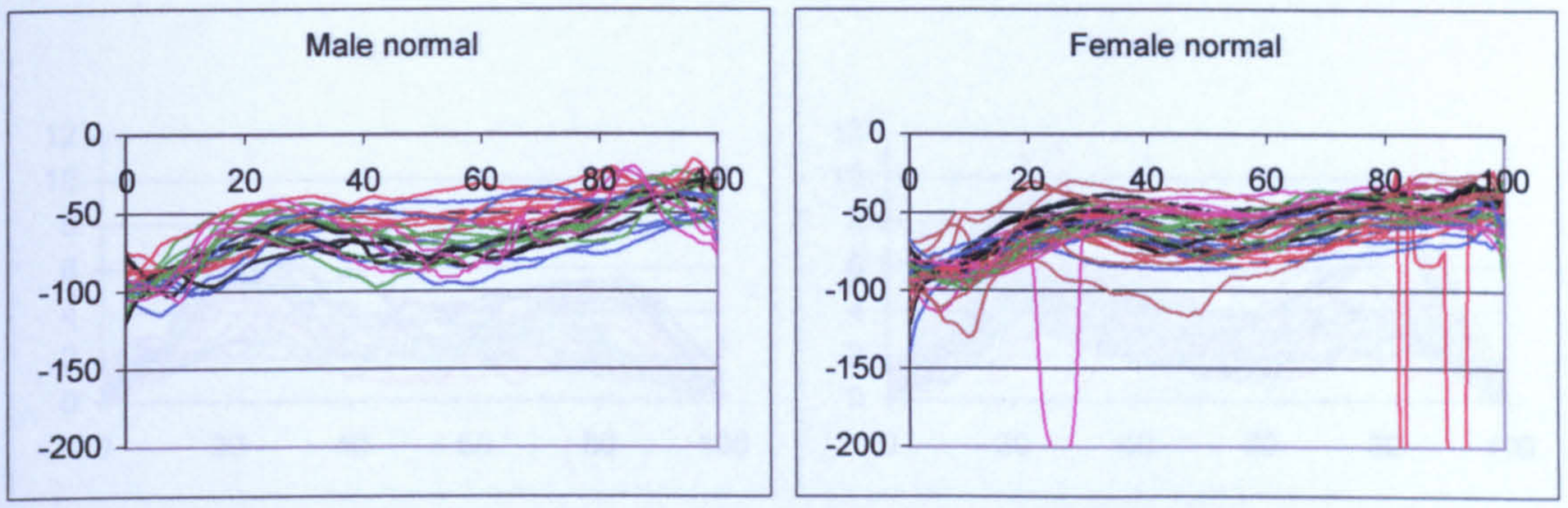

Figure A-VI.4.33 Stair descent, FHXZANG resultant hip joint force femoral angle

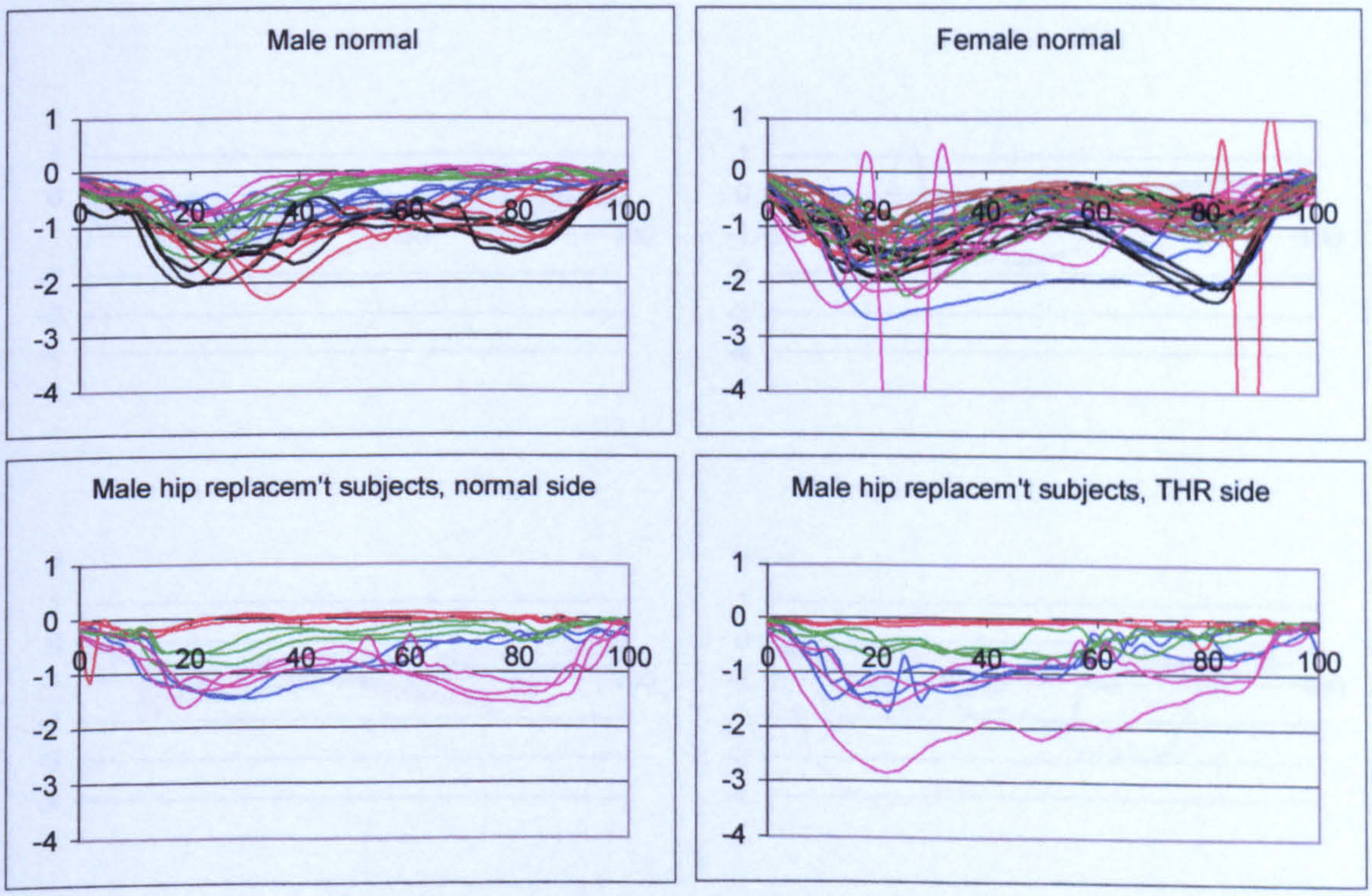

Figure A-VI.4.34 Stair descent, XPA hip joint force

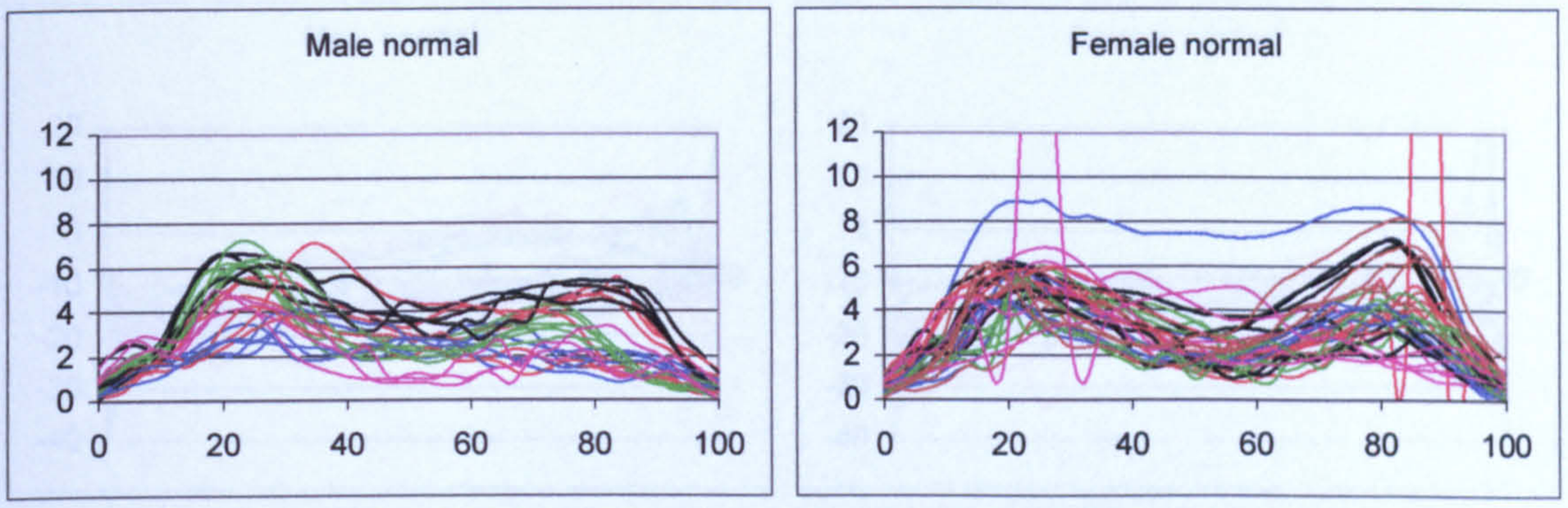

Stair descent, YPA-axis hip joint force (N/body weight, +ve = acting +YPA) by % stance phase

Figure A-VI.4.35 Stair descent, YPA hip joint force

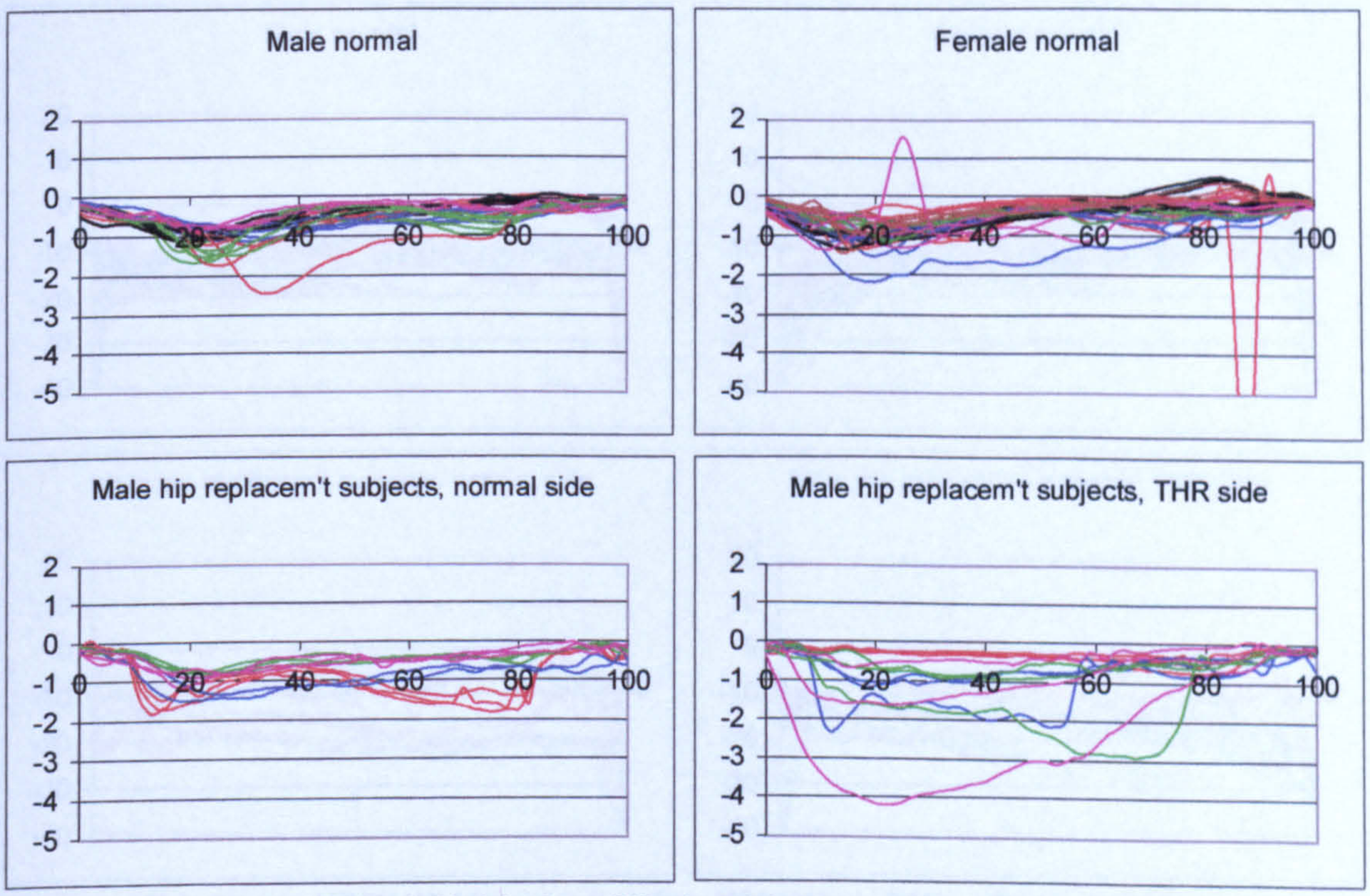

Stair descent, ZPA-axis hip joint force (N/body weight, +ve = acting +ZPA) by % stance phase

Figure A-VI.4.36 Stair descent, ZPA hip joint force

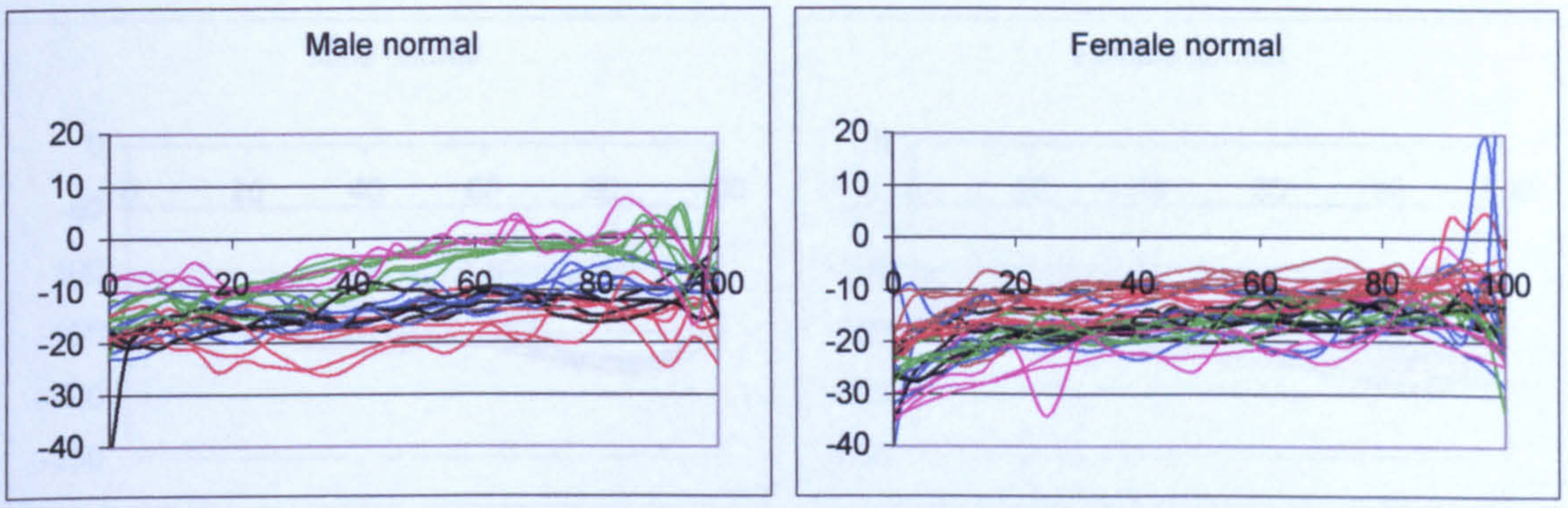

Figure A-VI.4.37 Stair descent, HJYXANG resultant hip joint force pelvic angle

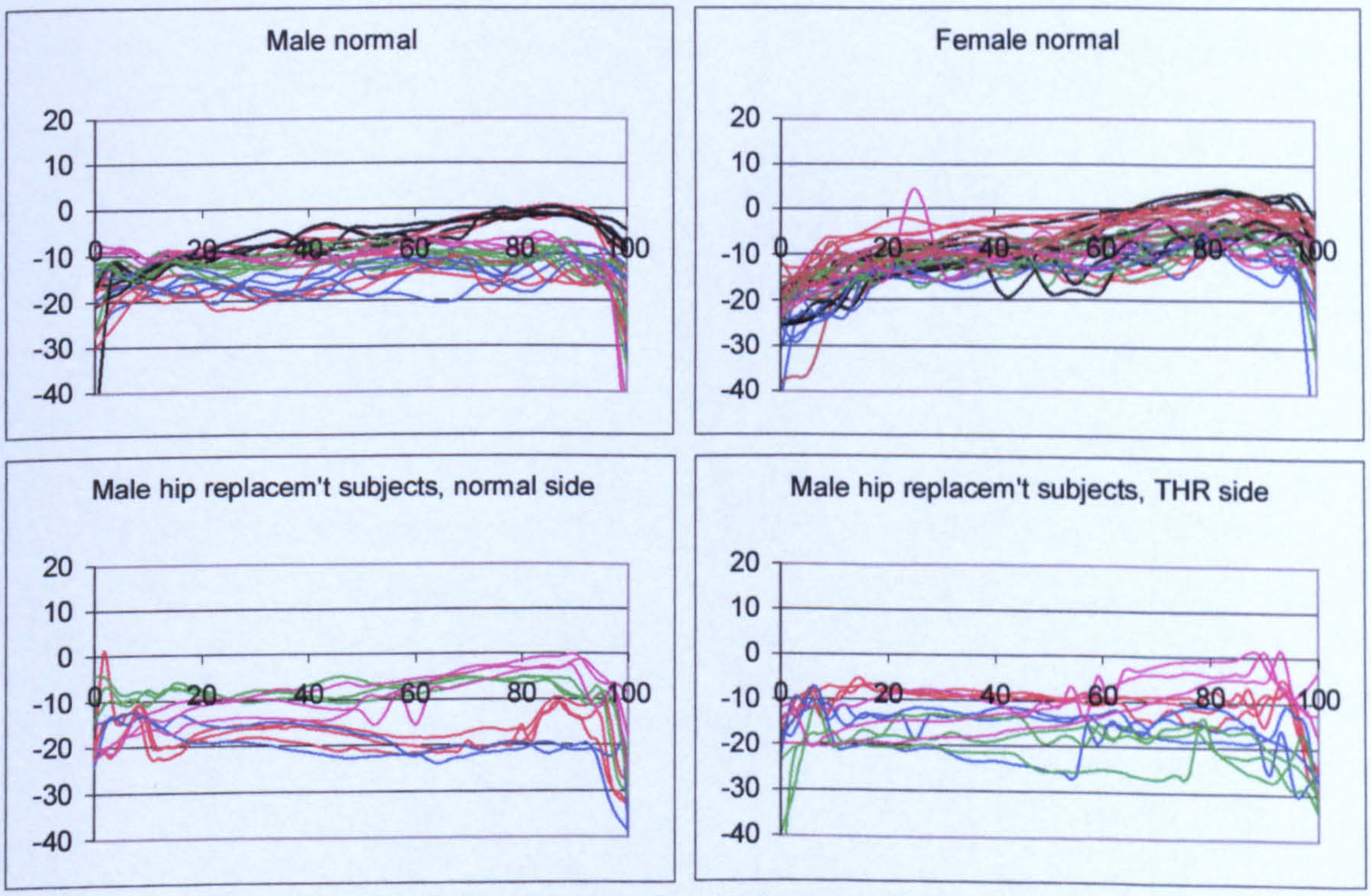

Figure A-VI.4.38 Stair descent, HJYZANG resultant hip joint force pelvic angle

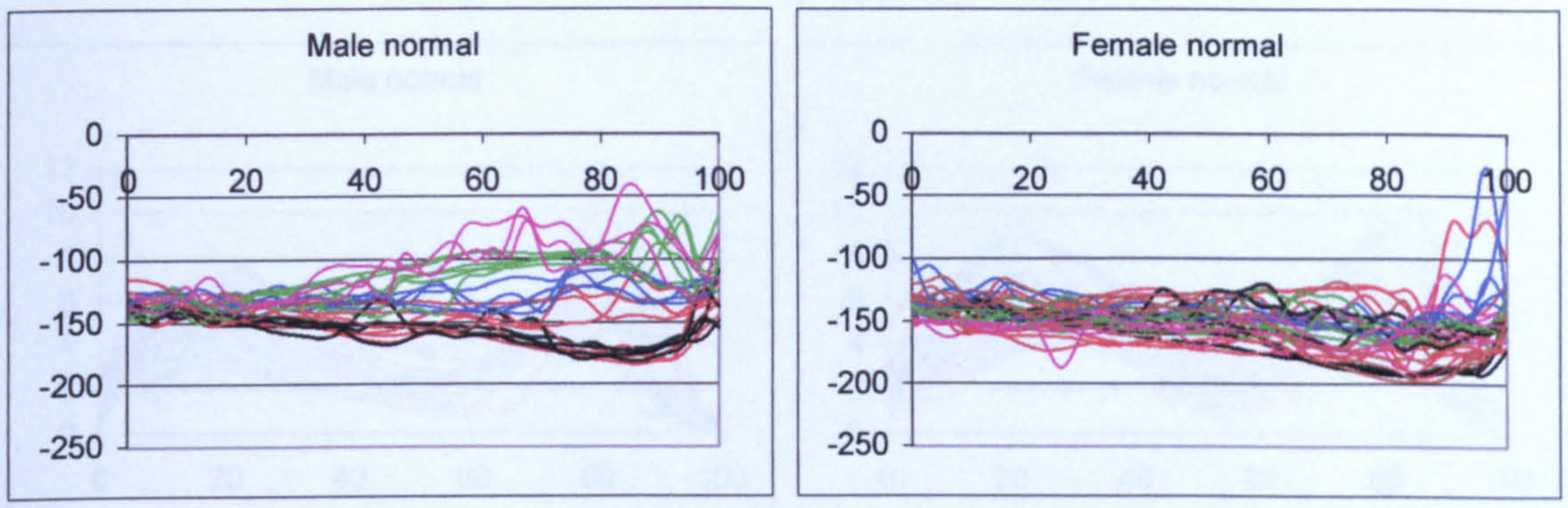

Figure A-VI.4.39 Stair descent, HJXZANG resultant hip joint force pelvic angle

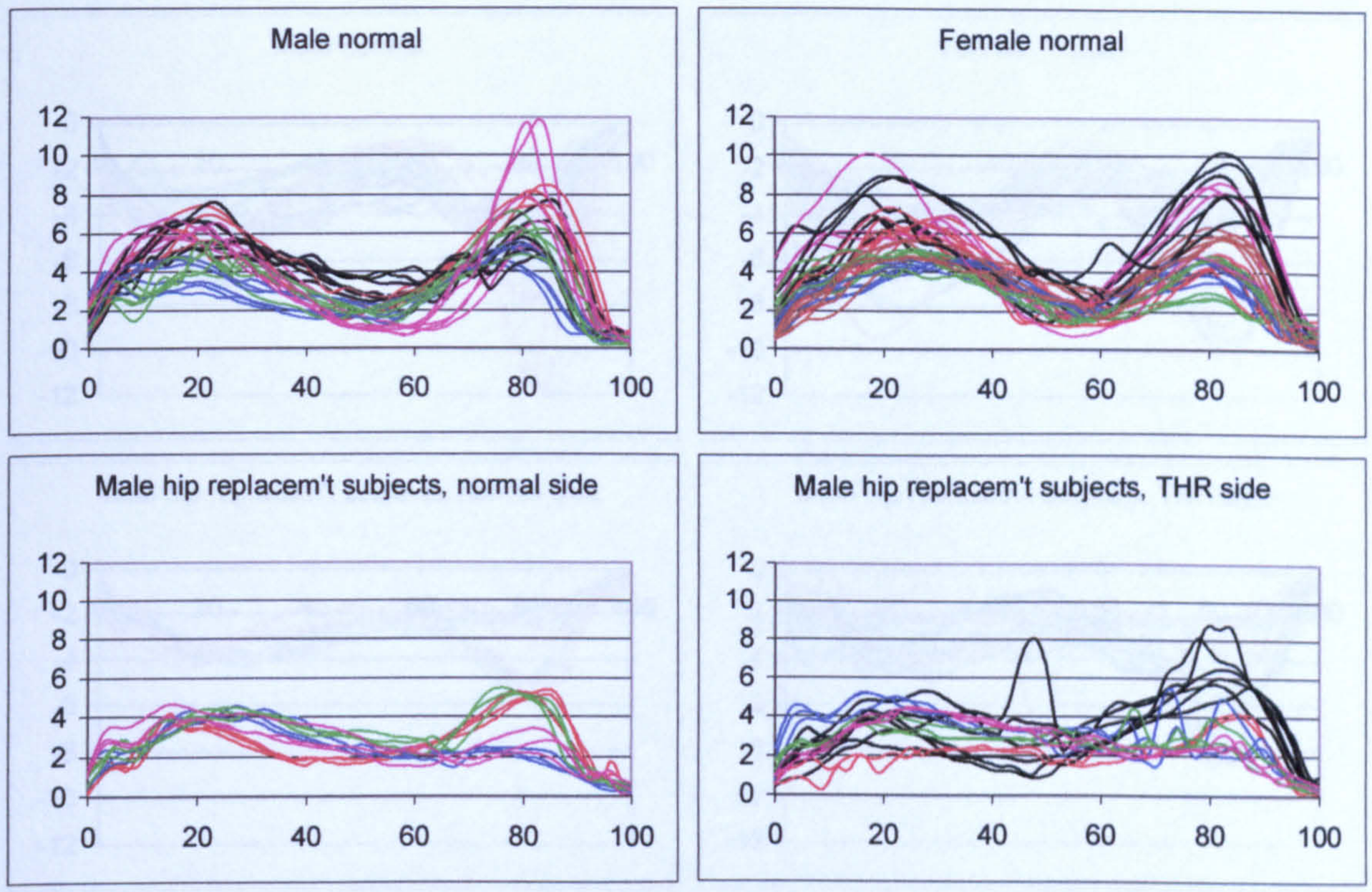

Figure A-VI.4.40 Ramp ascent, resultant hip joint force

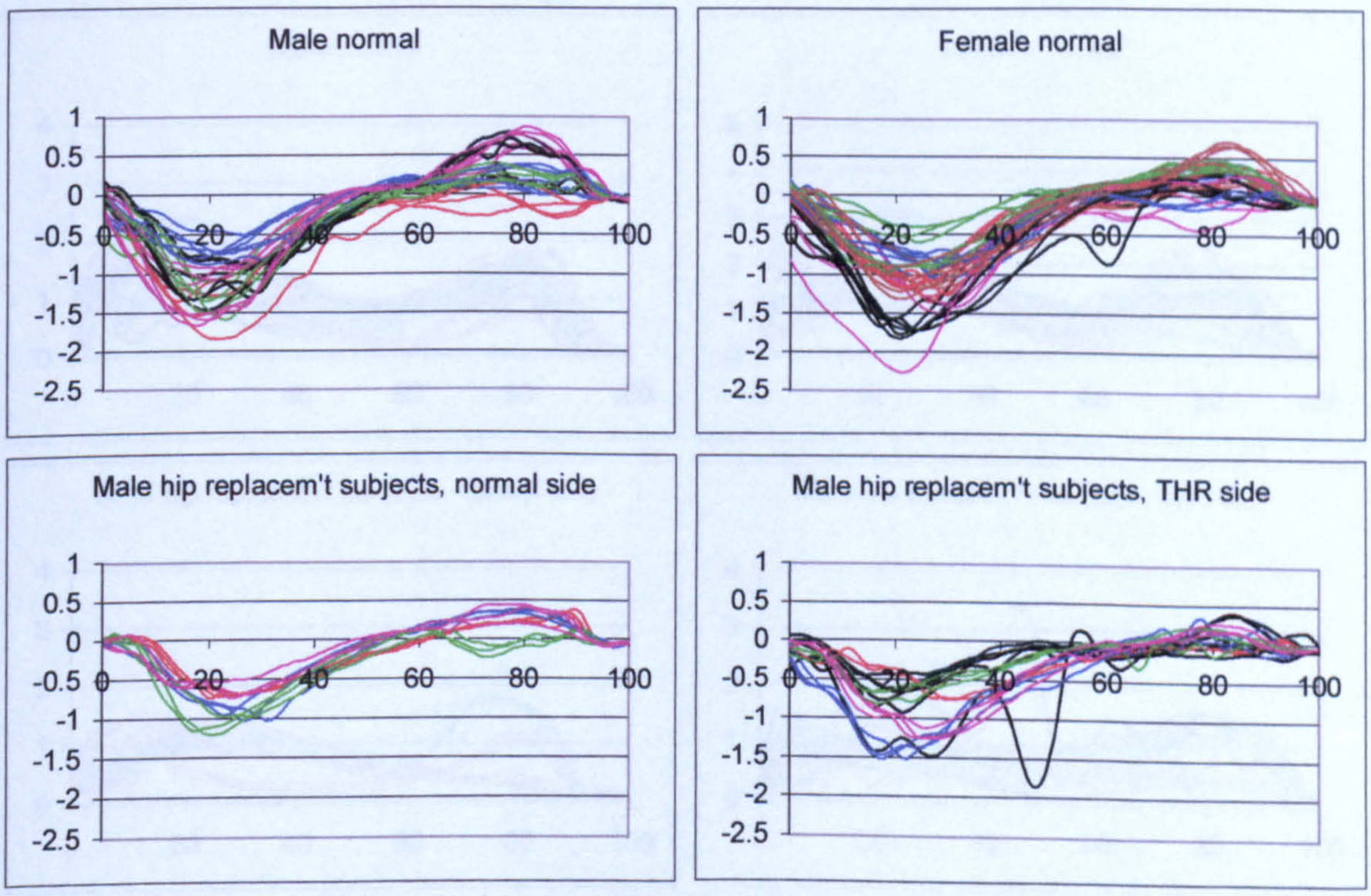

Figure A-VI.4.41 Ramp ascent, XFA hip joint force

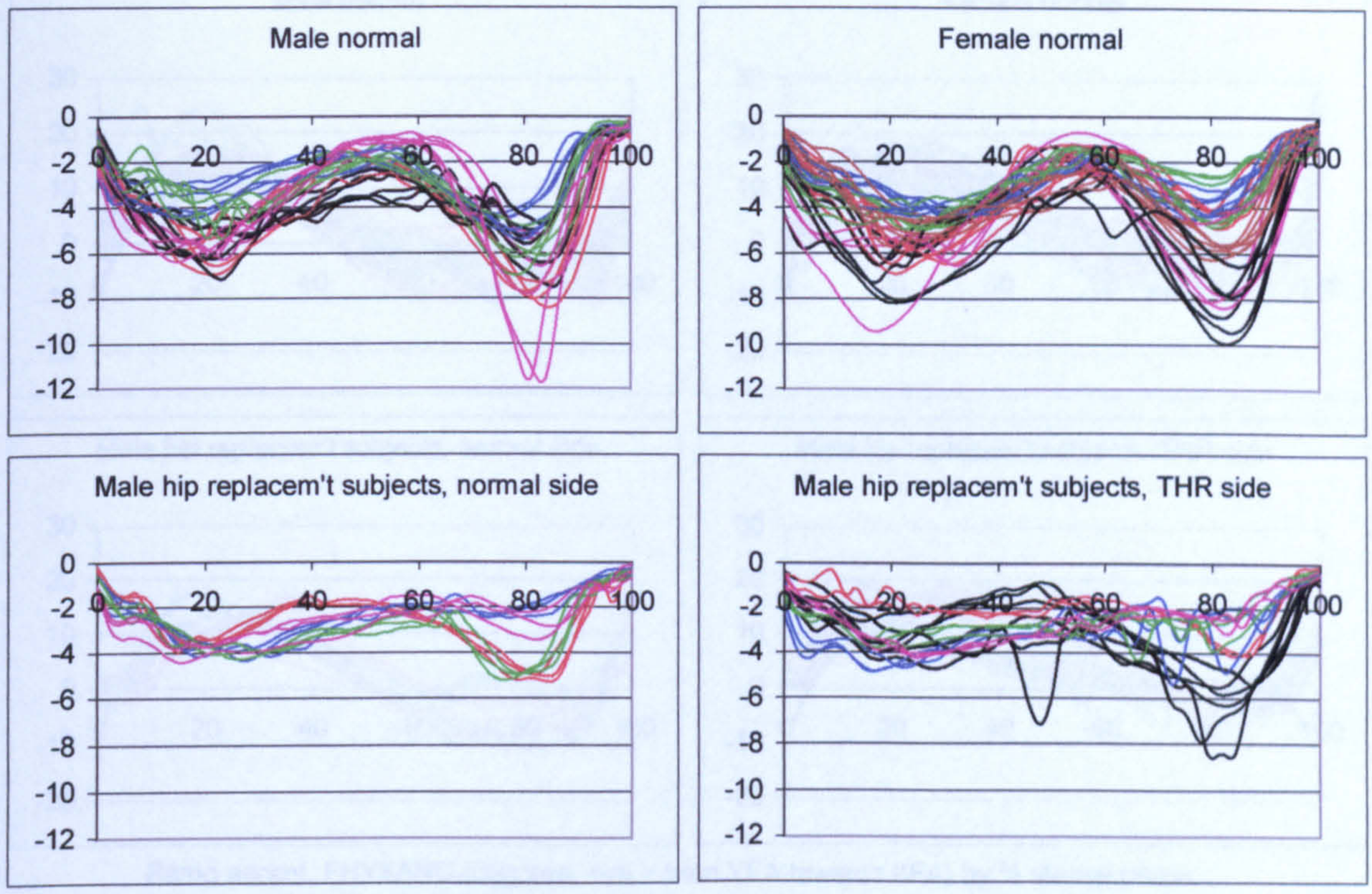

Ramp ascent, YFA-axis hip joint force (N/body weight, +ve = acting +YFA) by % stance phase

Figure A-VI.4.42 Ramp ascent, YFA hip joint force

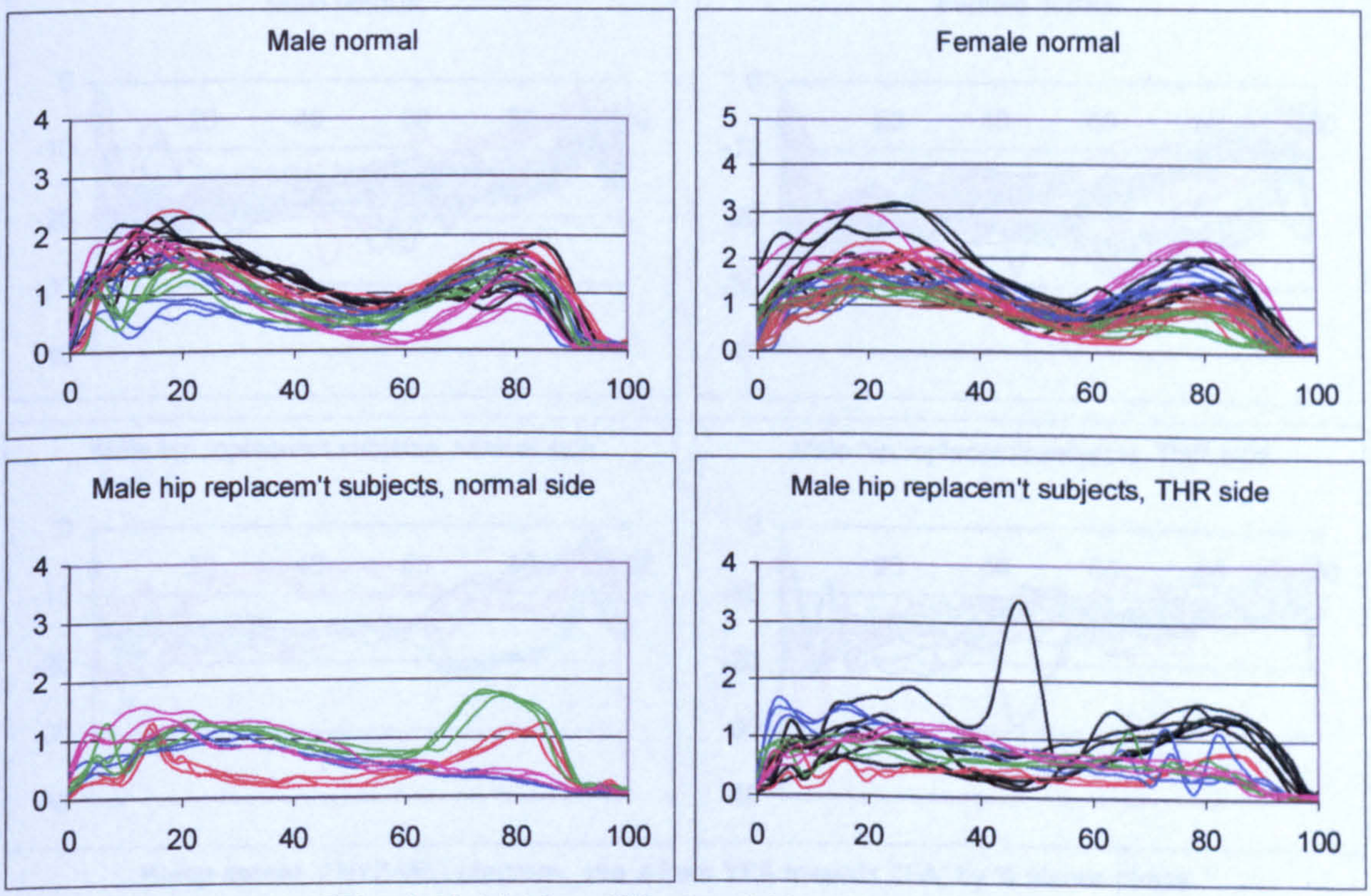

Ramp ascent, ZFA-axis hip joint force (N/body weight, +ve = acting +ZFA) by % stance phase

Figure A-VI.4.43 Ramp ascent, ZFA hip joint force

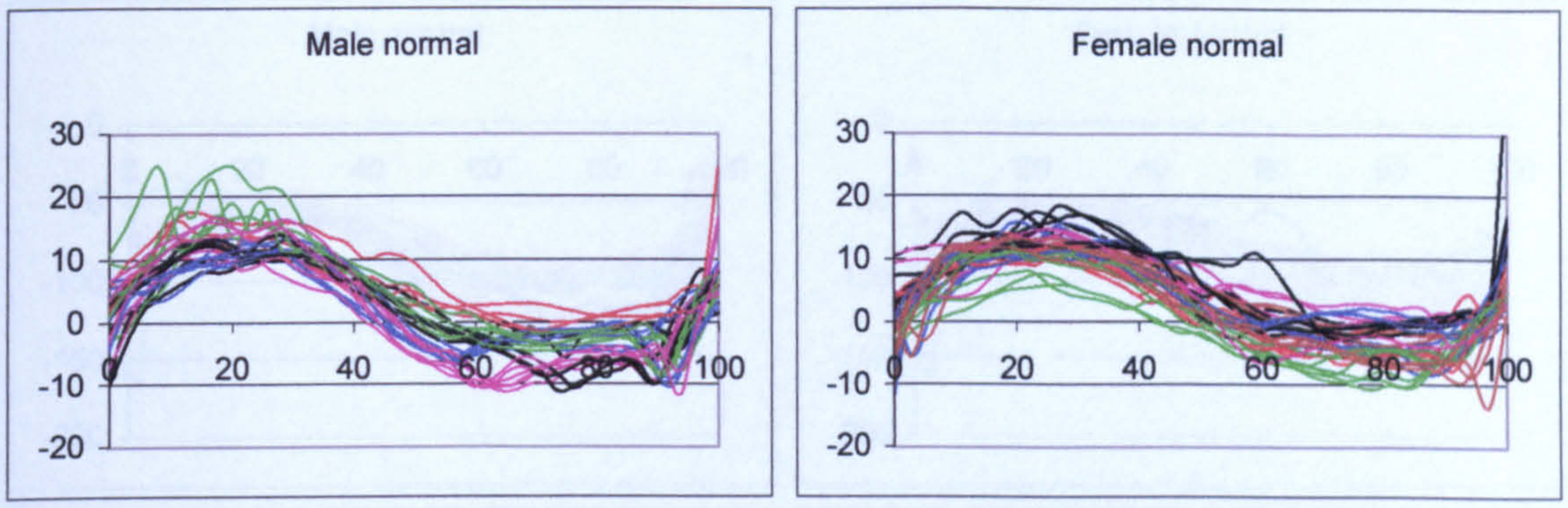

Ramp ascent, FHYXANG (degrees, +ve = from YFA towards XFA) by % stance phase

Figure A-VI.4.44 Ramp ascent, FHYXANG resultant hip joint force femoral angle

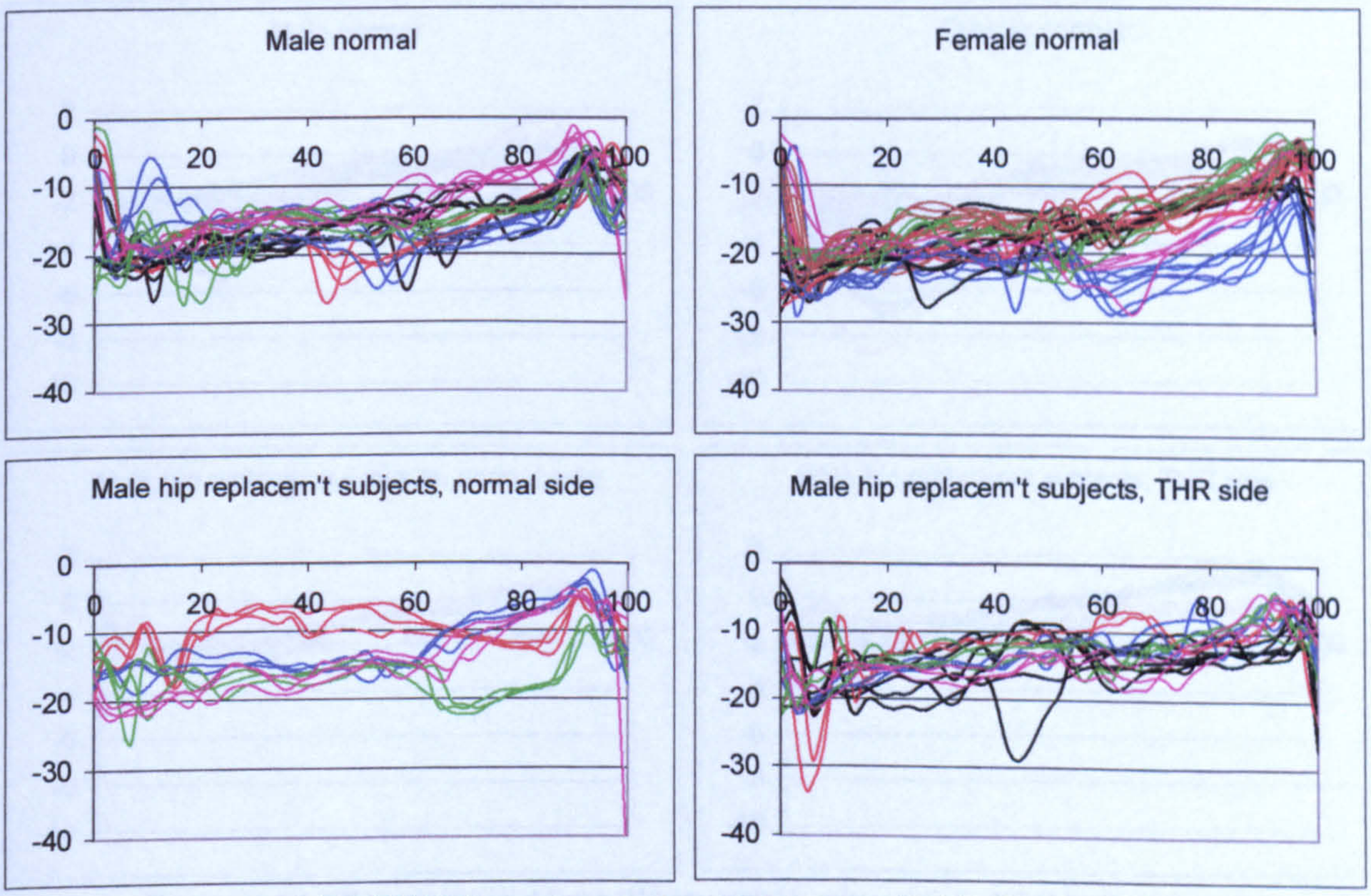

Ramp ascent, FHYZANG (degrees, +ve = from YFA towards ZFA) by % stance phase

Figure A-VI.4.45 Ramp ascent, FHYZANG resultant hip joint force femoral angle

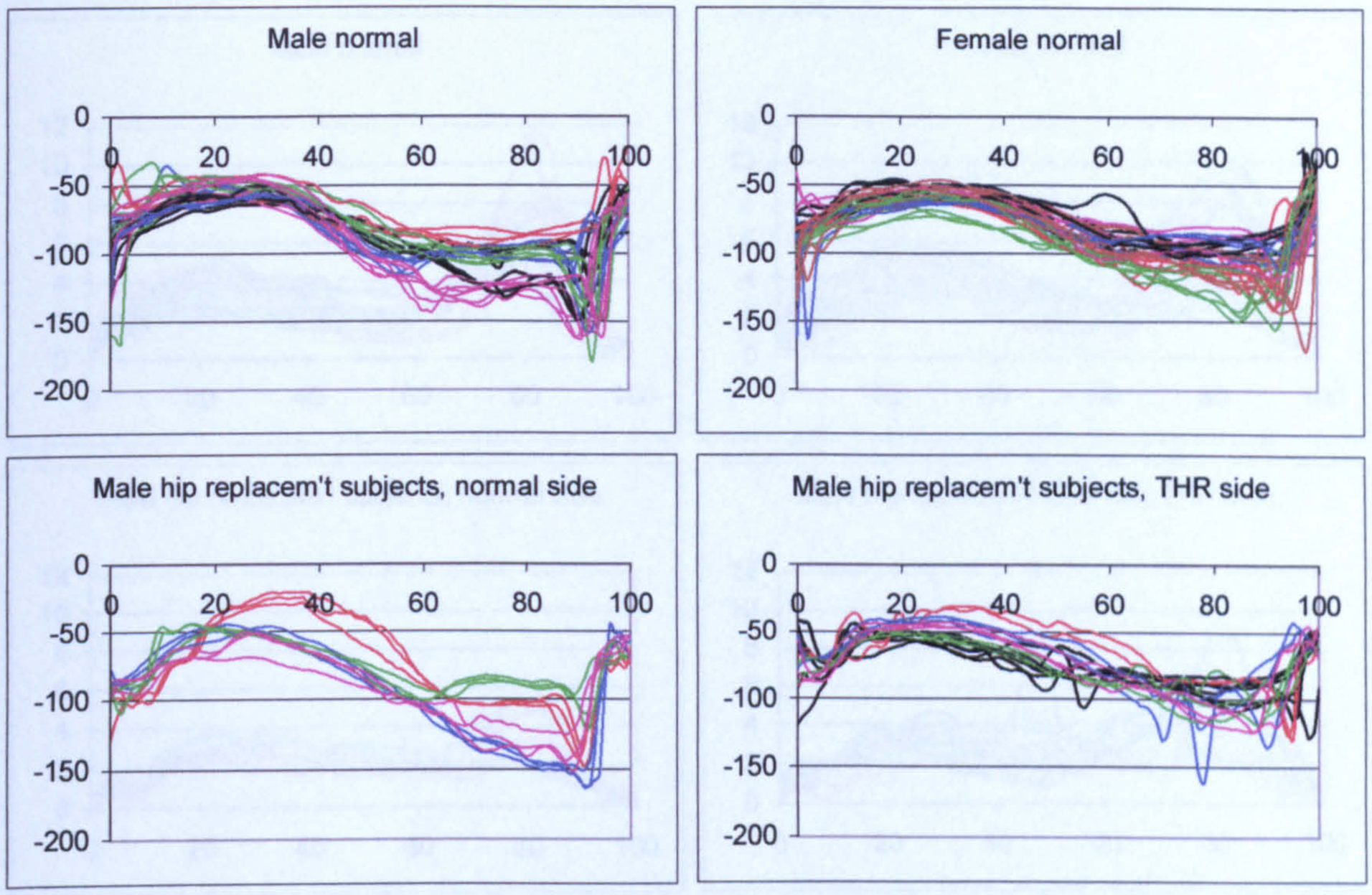

Figure A-VI.4.46 Ramp ascent, FHXZANG resultant hip joint force femoral angle

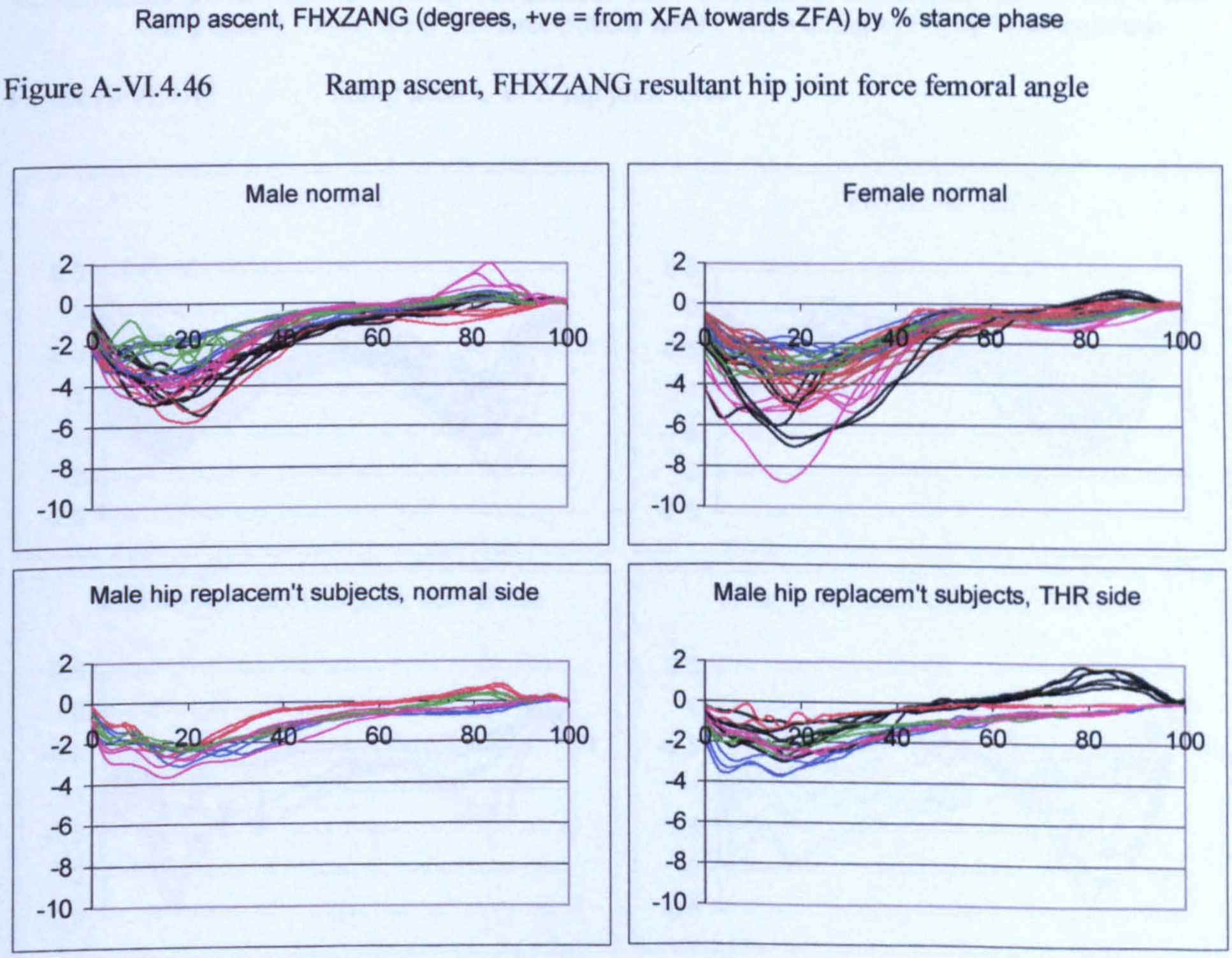

Figure A-VI.4.47 Ramp ascent, XPA hip joint force

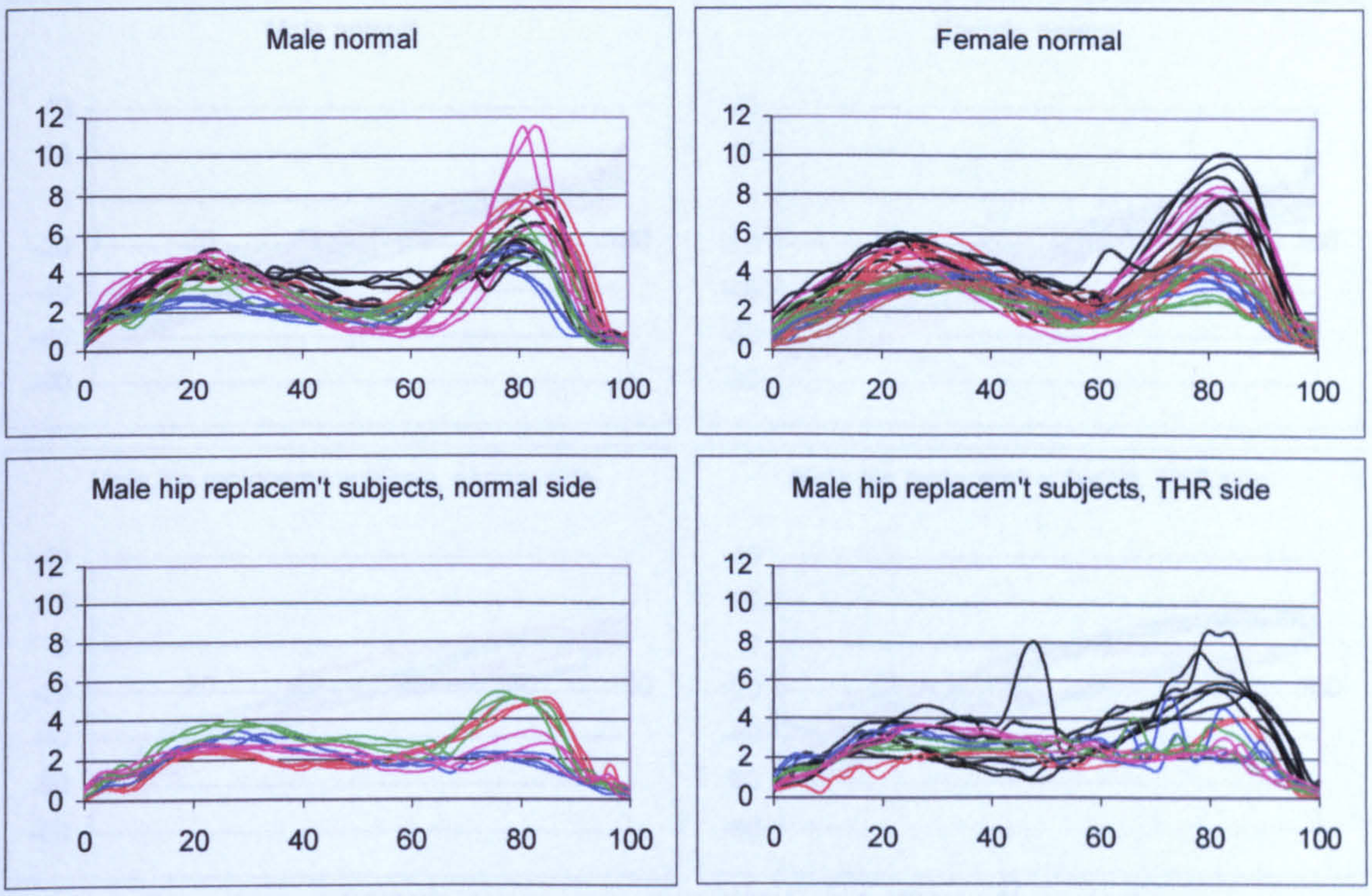

Ramp ascent, YPA-axis hip joint force (N/body weight, +ve = acting +YPA) by % stance phase

Figure A-VI.4.48 Ramp ascent, YPA hip joint force

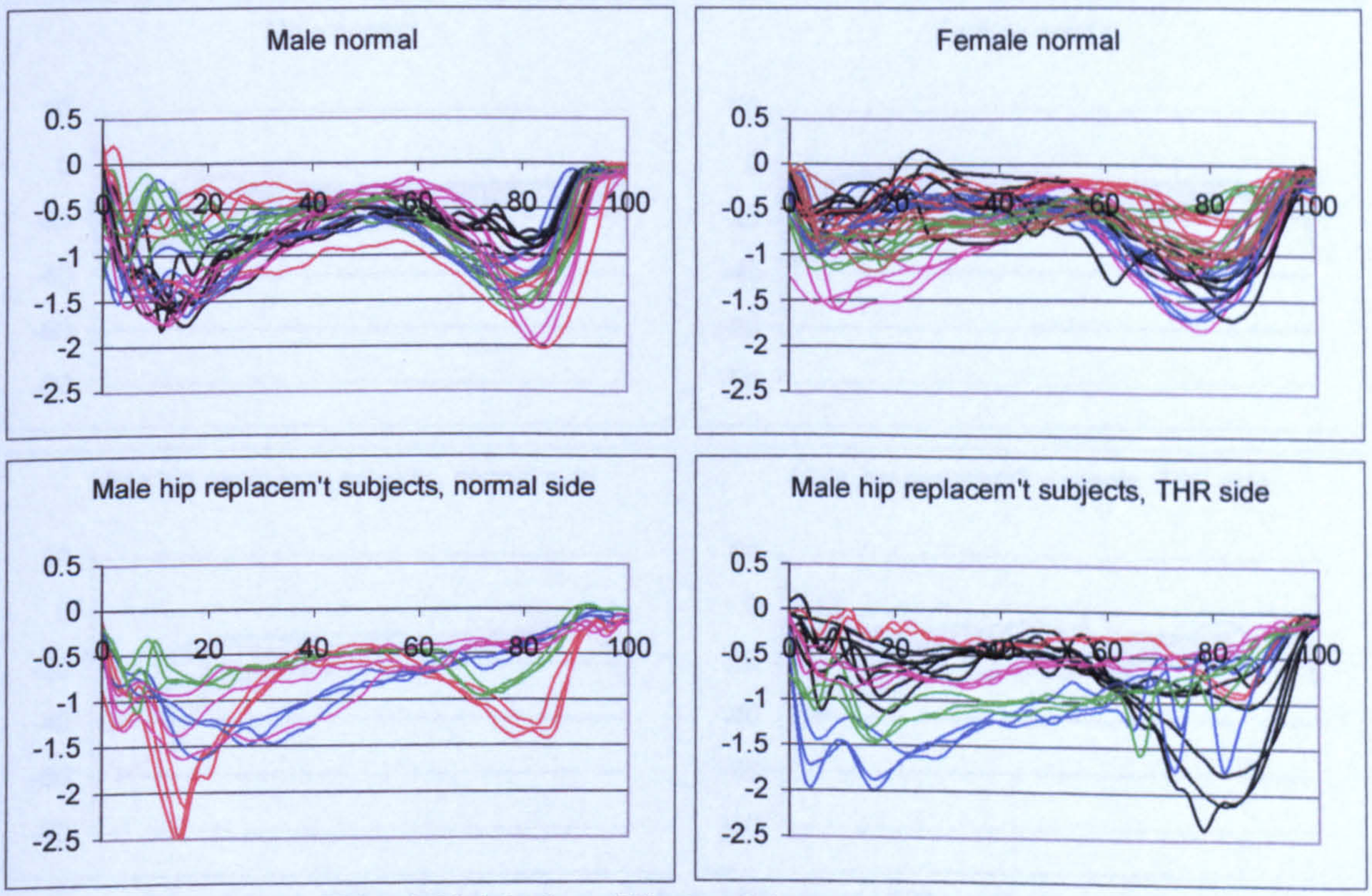

Ramp ascent, ZPA-axis hip joint force (N/body weight, +ve = acting +ZPA) by % stance phase

Figure A-VI.4.49 Ramp ascent, ZPA hip joint force

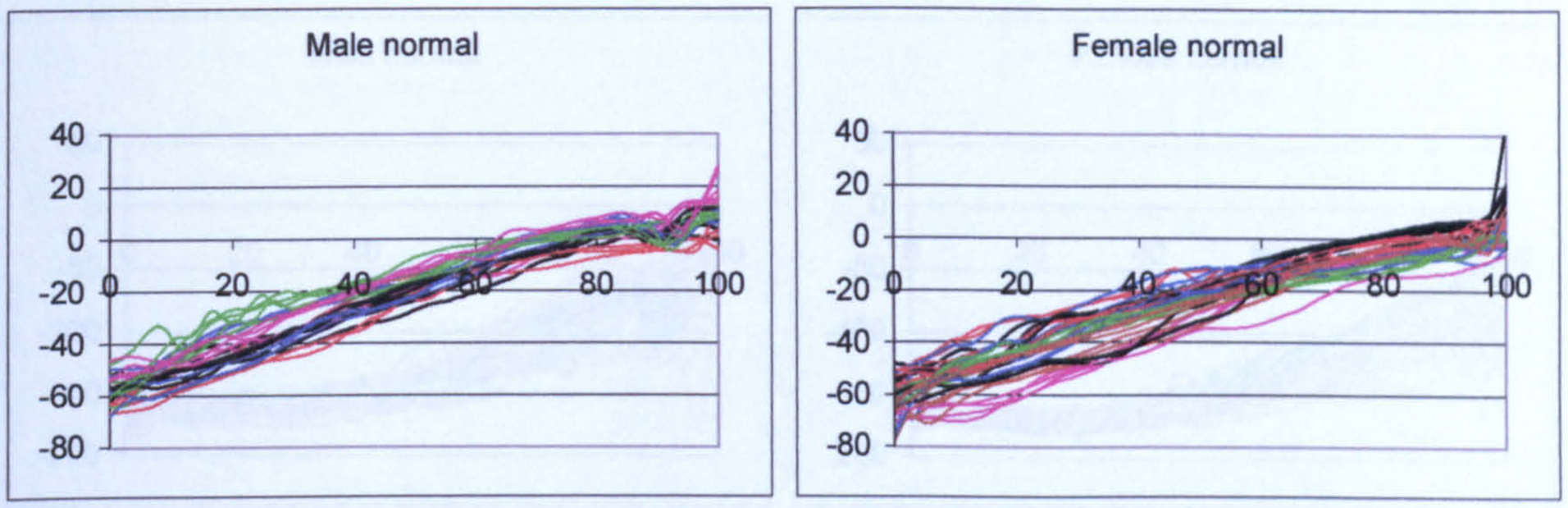

Ramp ascent, HJYXANG (degrees, +ve = from YPA towards XPA) by % stance phase

Figure A-VI.4.50 Ramp ascent, HJYXANG resultant hip joint force pelvic angle

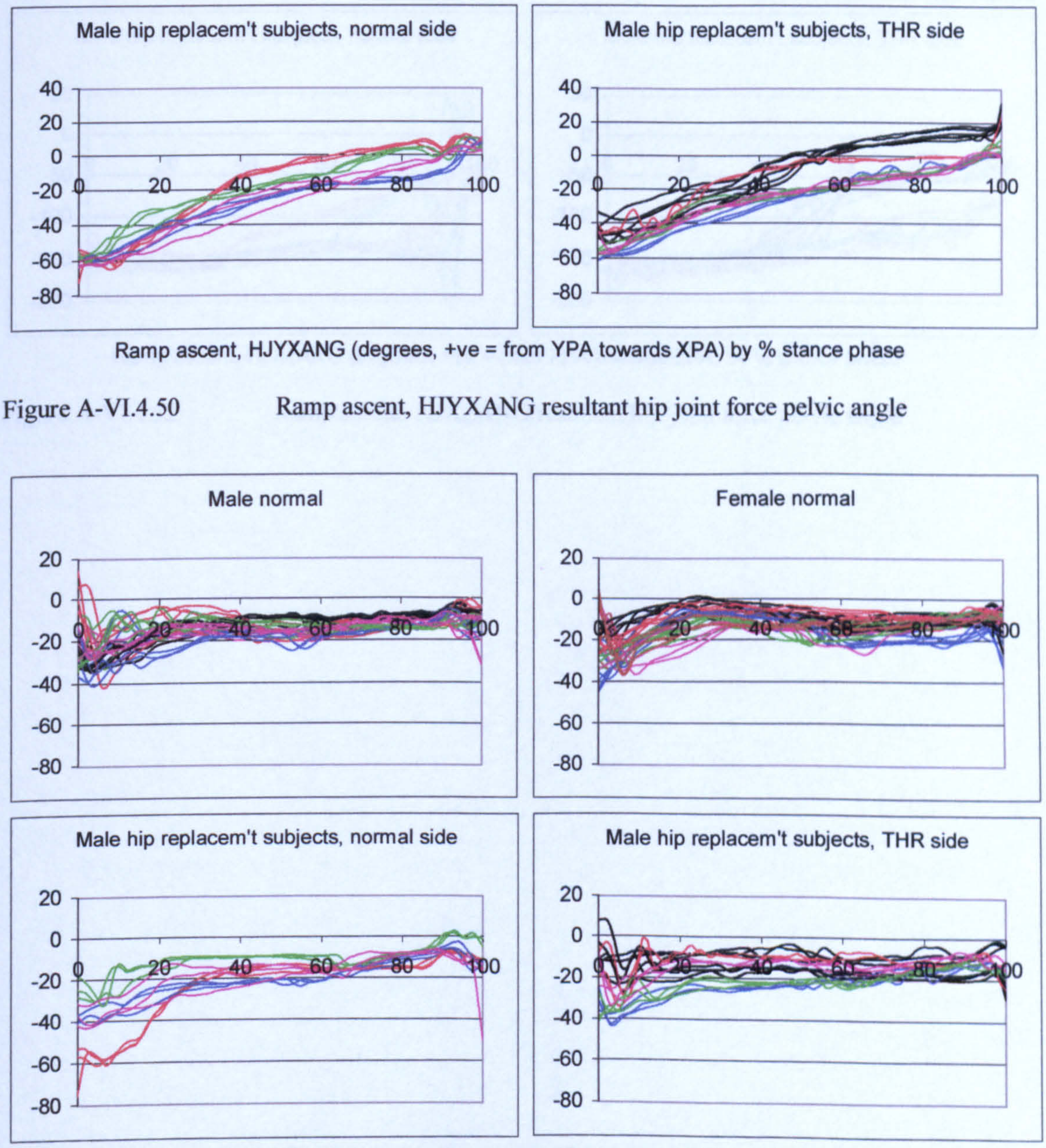

Ramp ascent, HJYZANG (degrees, +ve = from YPA towards ZPA) by % stance phase

Figure A-VI.4.51 Ramp ascent, HJYZANG resultant hip joint force pelvic angle

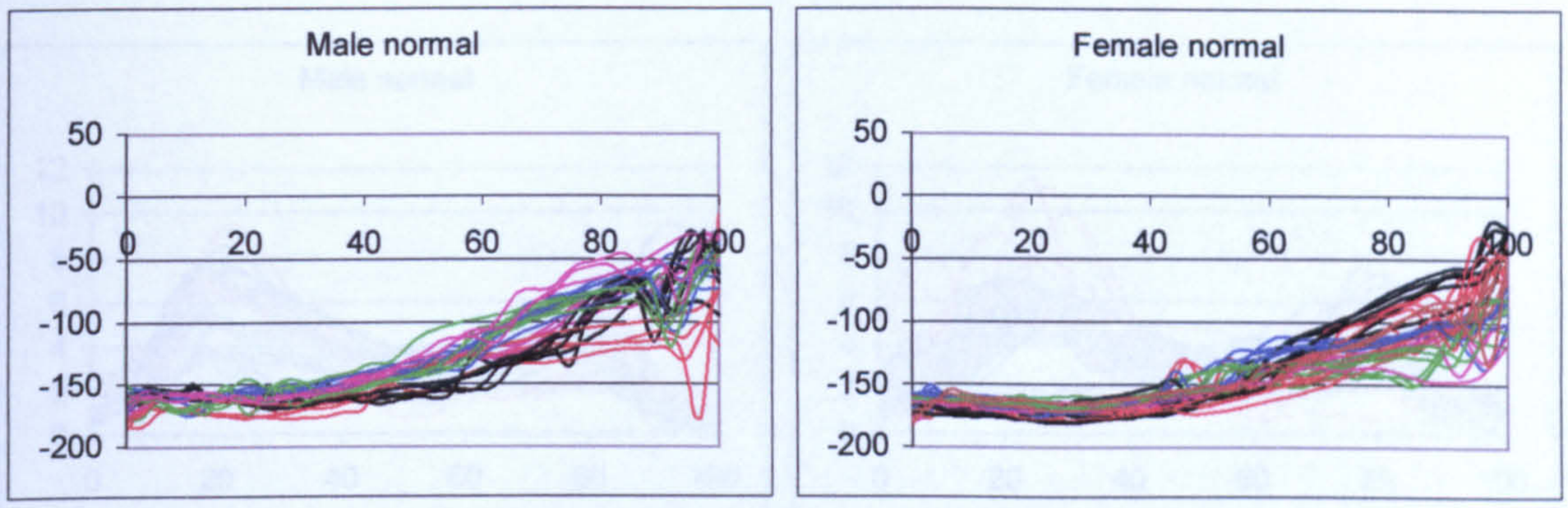

Figure A-VI.4.52 Ramp ascent, HJXZANG resultant hip joint force pelvic angle

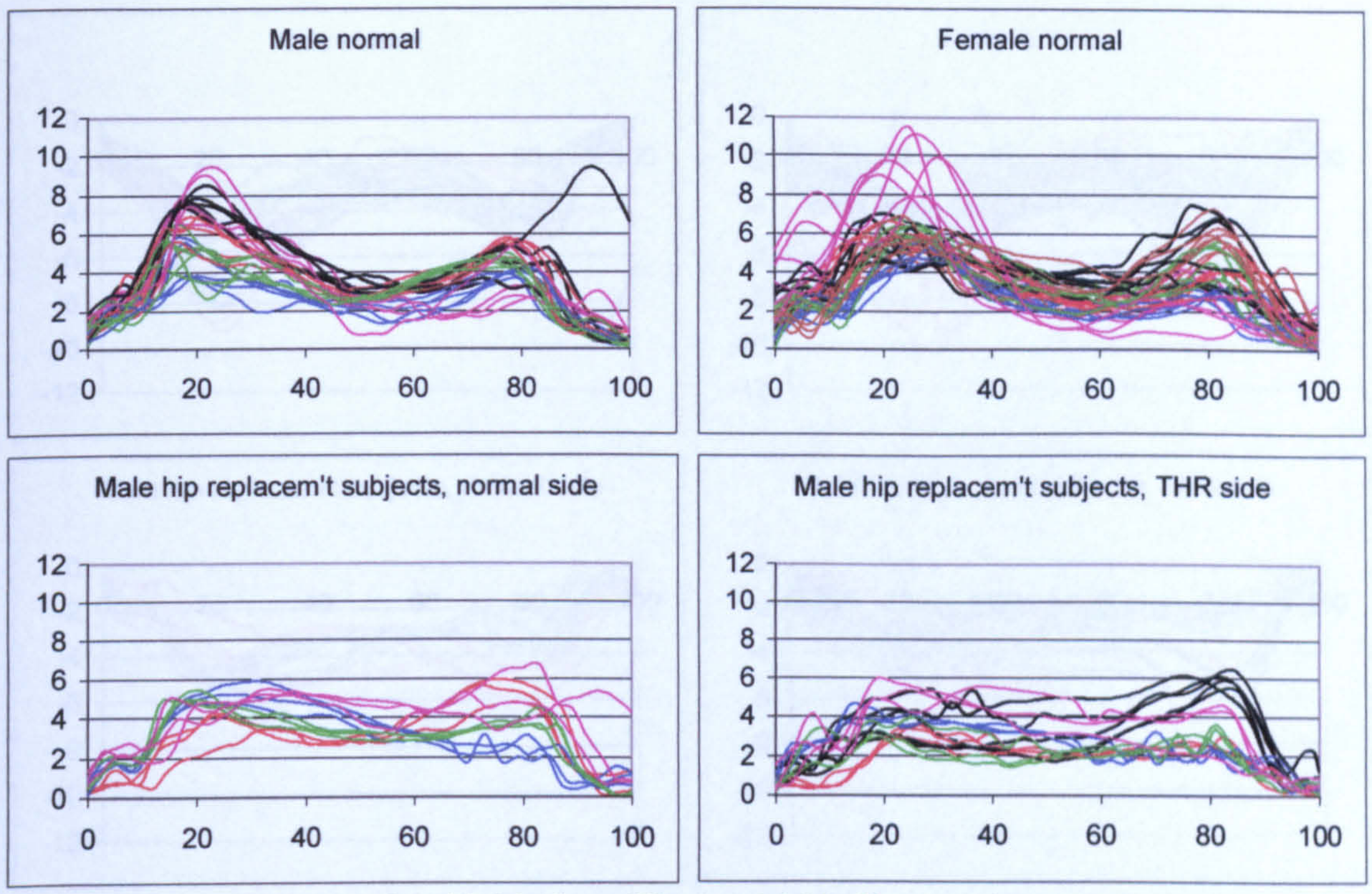

Ramp descent, resultant hip joint force (N/body weight) by % stance phase

Figure A-VI.4.53 Ramp descent, resultant hip joint force

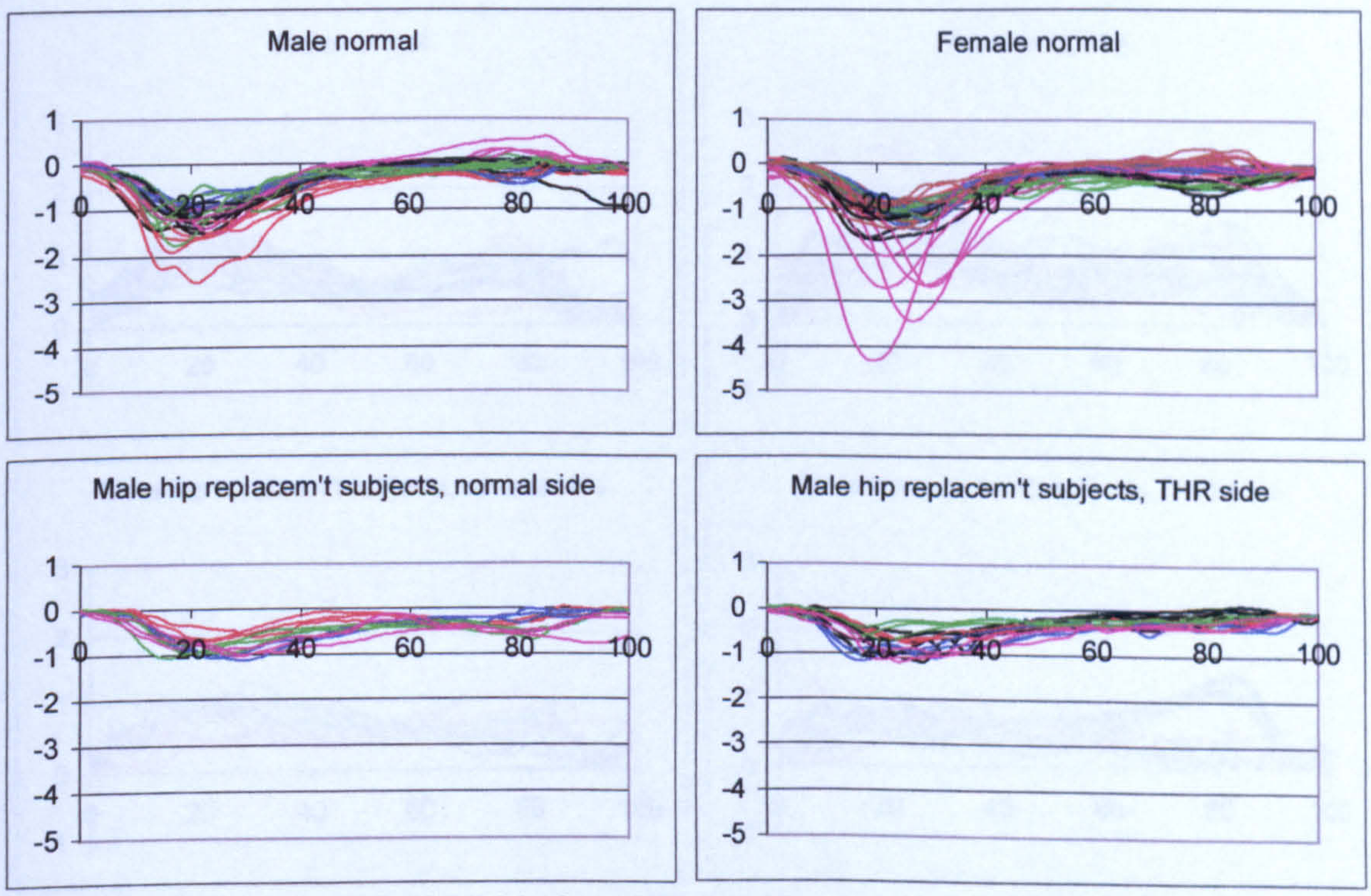

Ramp descent, XFA-axis hip joint force (N/body weight, +ve = acting +XFA) by % stance phase

Figure A-VI.4.54 Ramp descent, XFA hip joint force

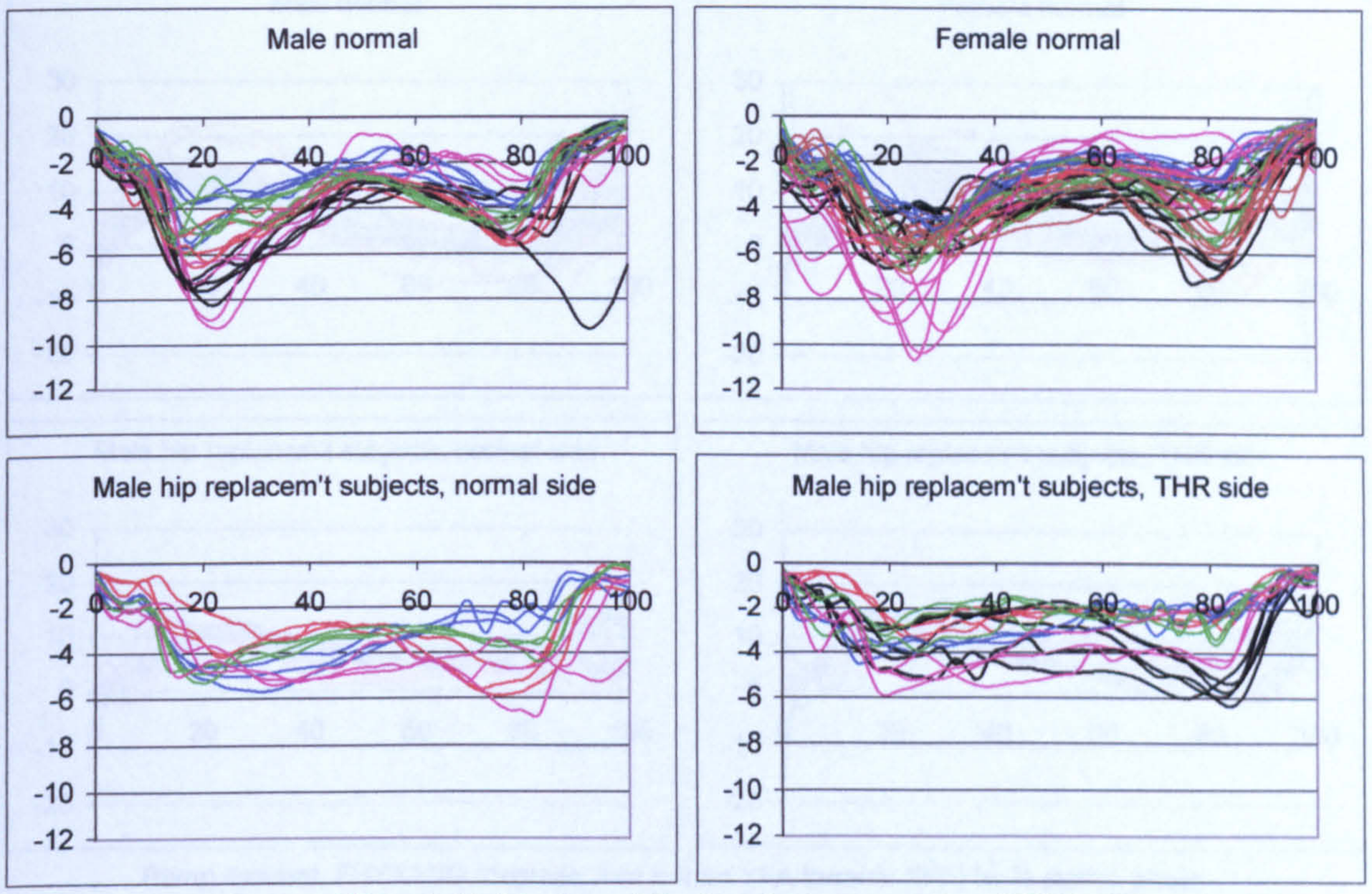

Ramp descent, YFA-axis hip joint force (N/body weight, +ve = acting +YFA) by % stance phase

Figure A-VI.4.55 Ramp descent, YFA hip joint force

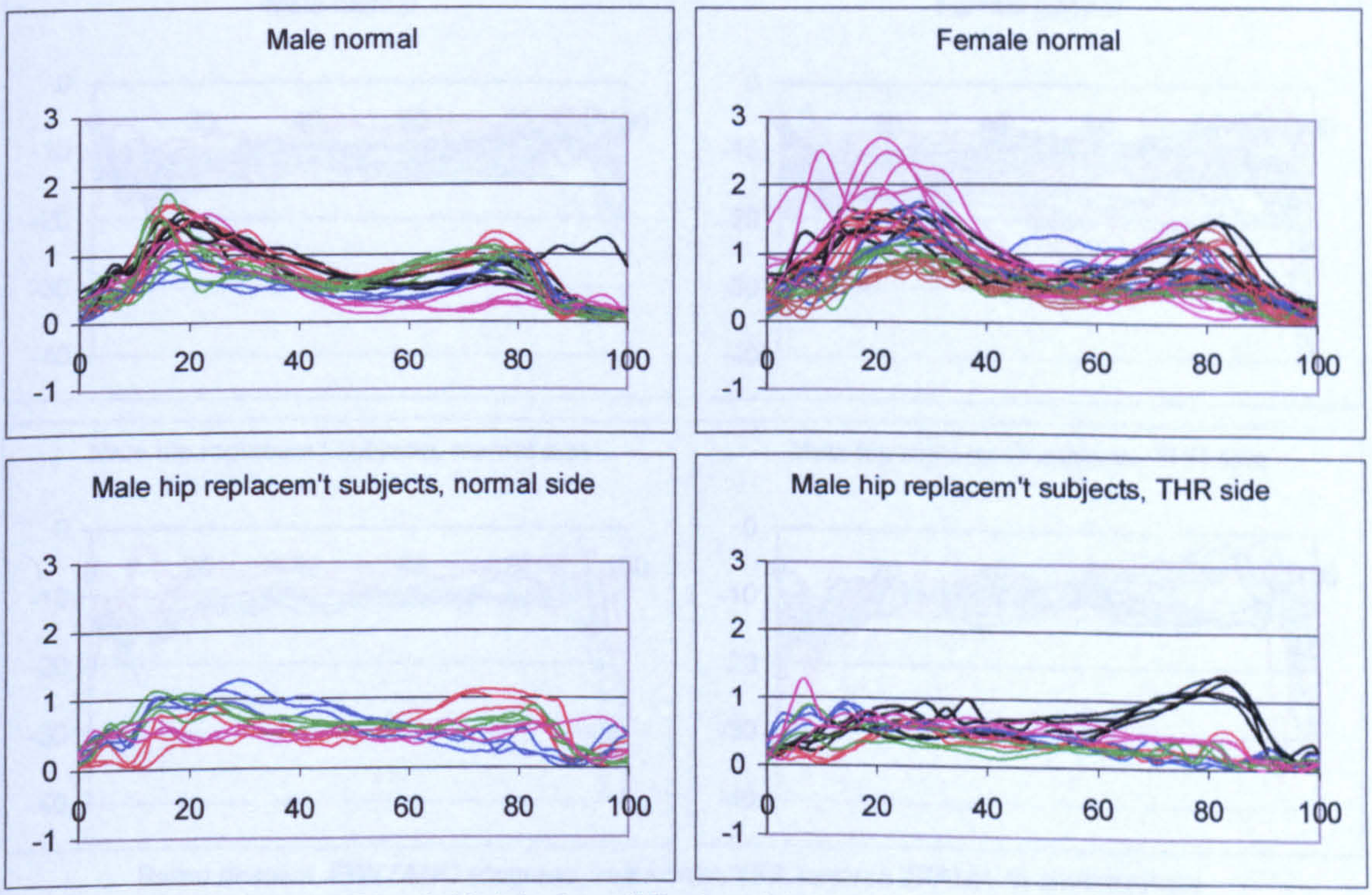

Ramp descent, ZFA-axis hip joint force (N/body weight, +ve = acting +ZFA) by % stance phase

Figure A-VI.4.56 Ramp descent, ZFA hip joint force

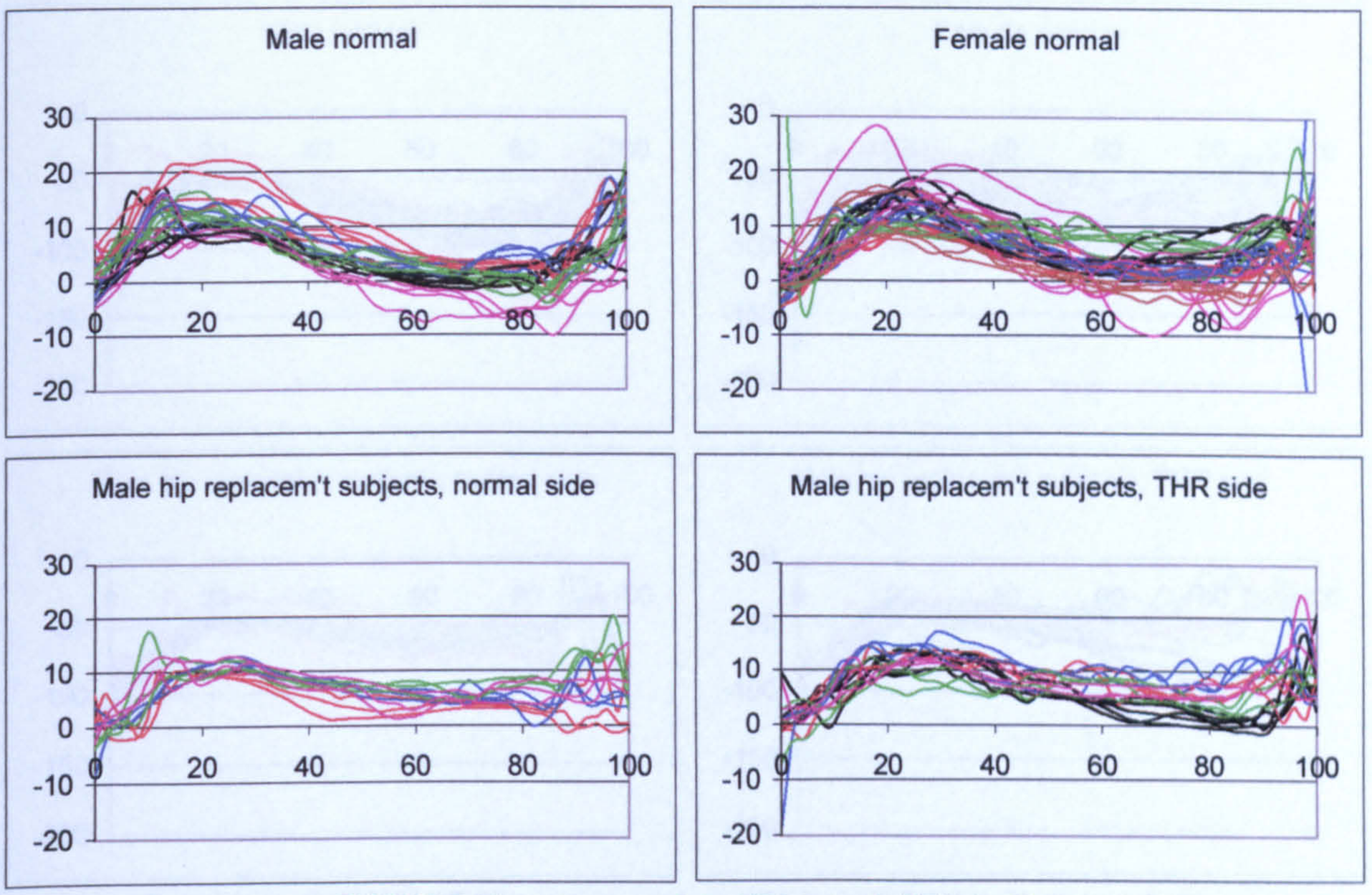

Ramp descent, FHYXANG (degrees, +ve = from YFA towards XFA) by % stance phase

Figure A-VI.4.57 Ramp descent, FHYXANG resultant hip joint force femoral angle

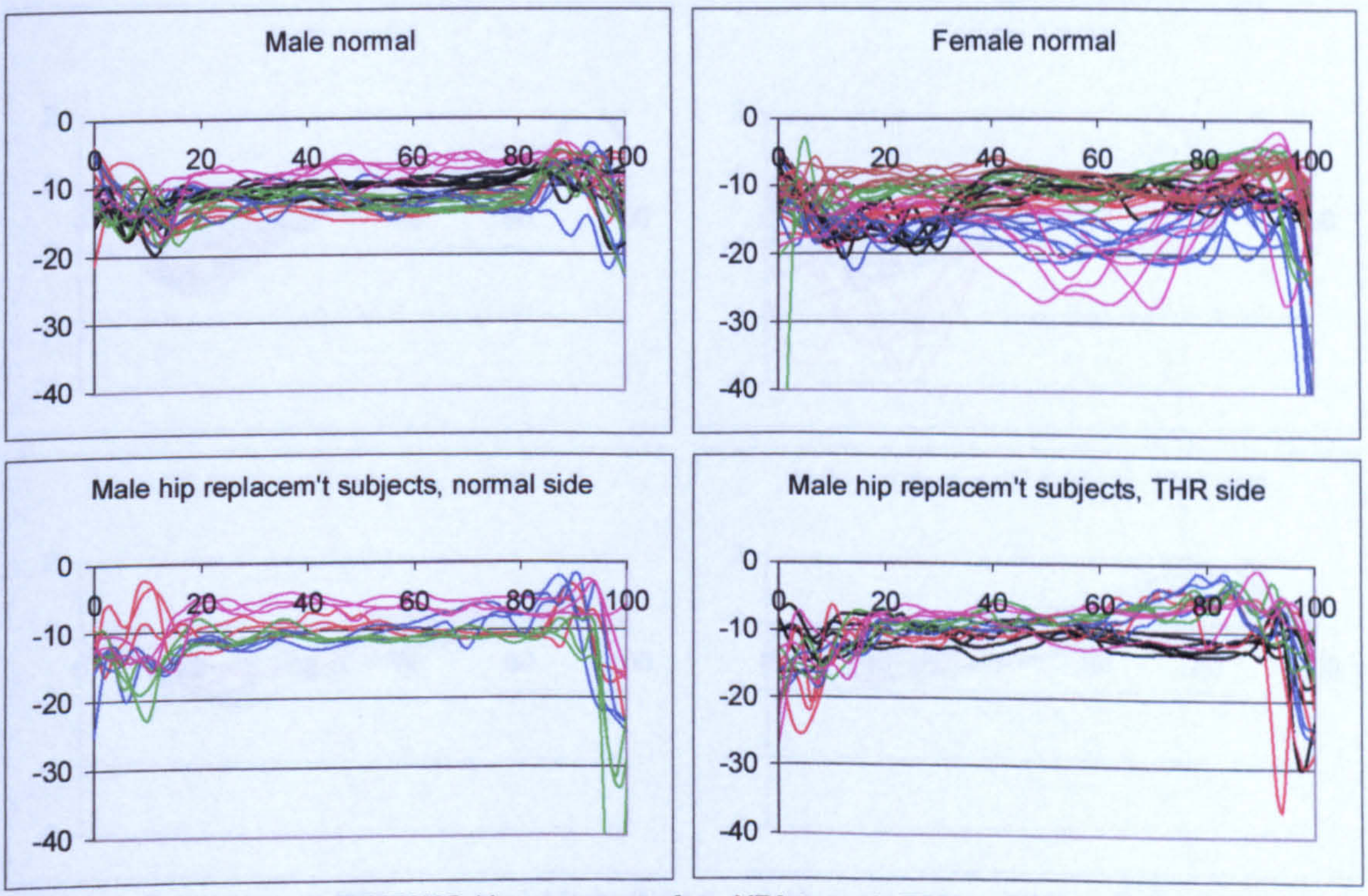

Ramp descent, FHYZANG (degrees, +ve = from YFA towards ZFA) by % stance phase

Figure A-VI.4.58 Ramp descent, FHYZANG resultant hip joint force femoral angle

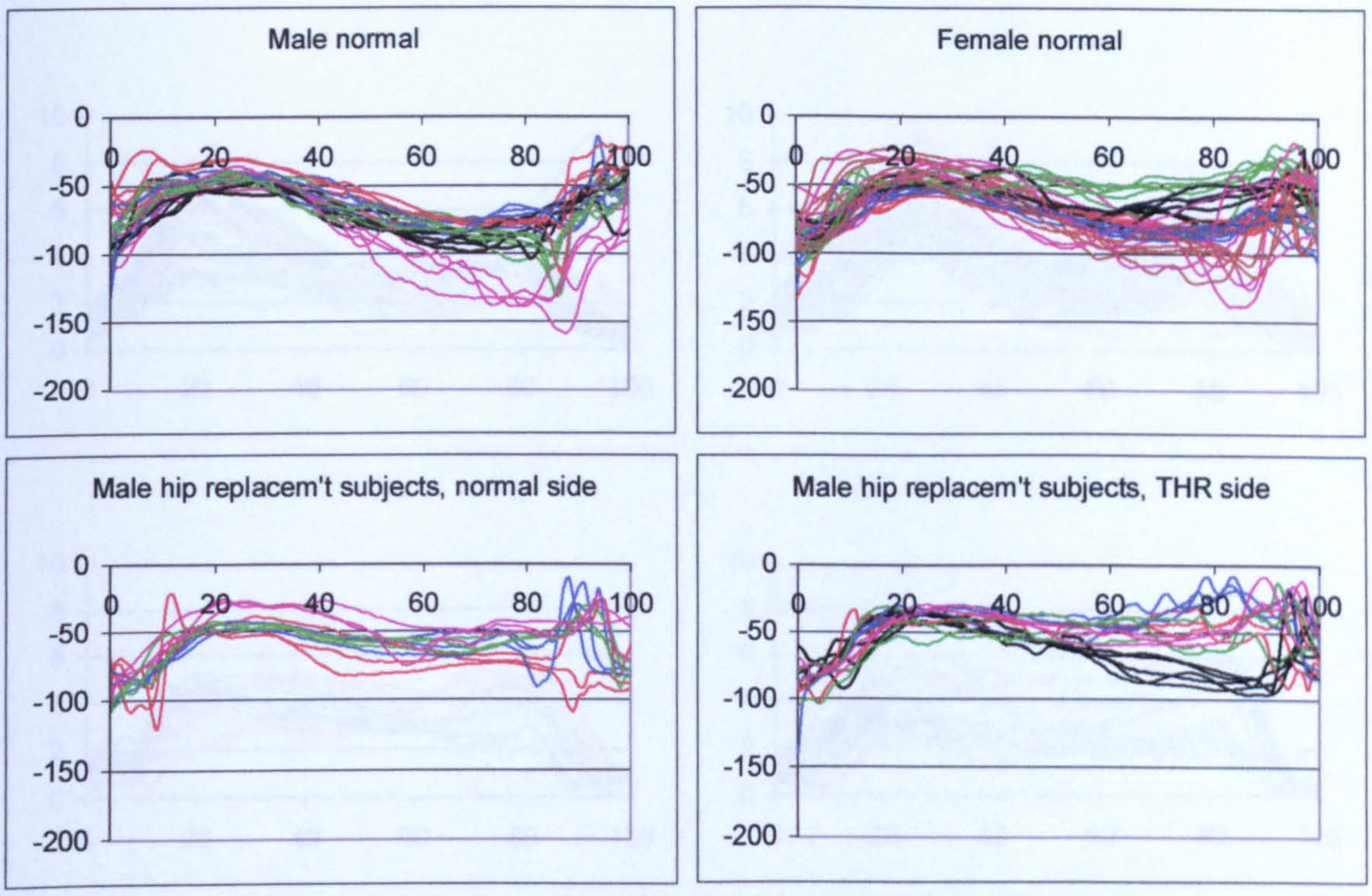

Figure A-VI.4.59 Ramp descent, FHXZANG resultant hip joint force femoral angle

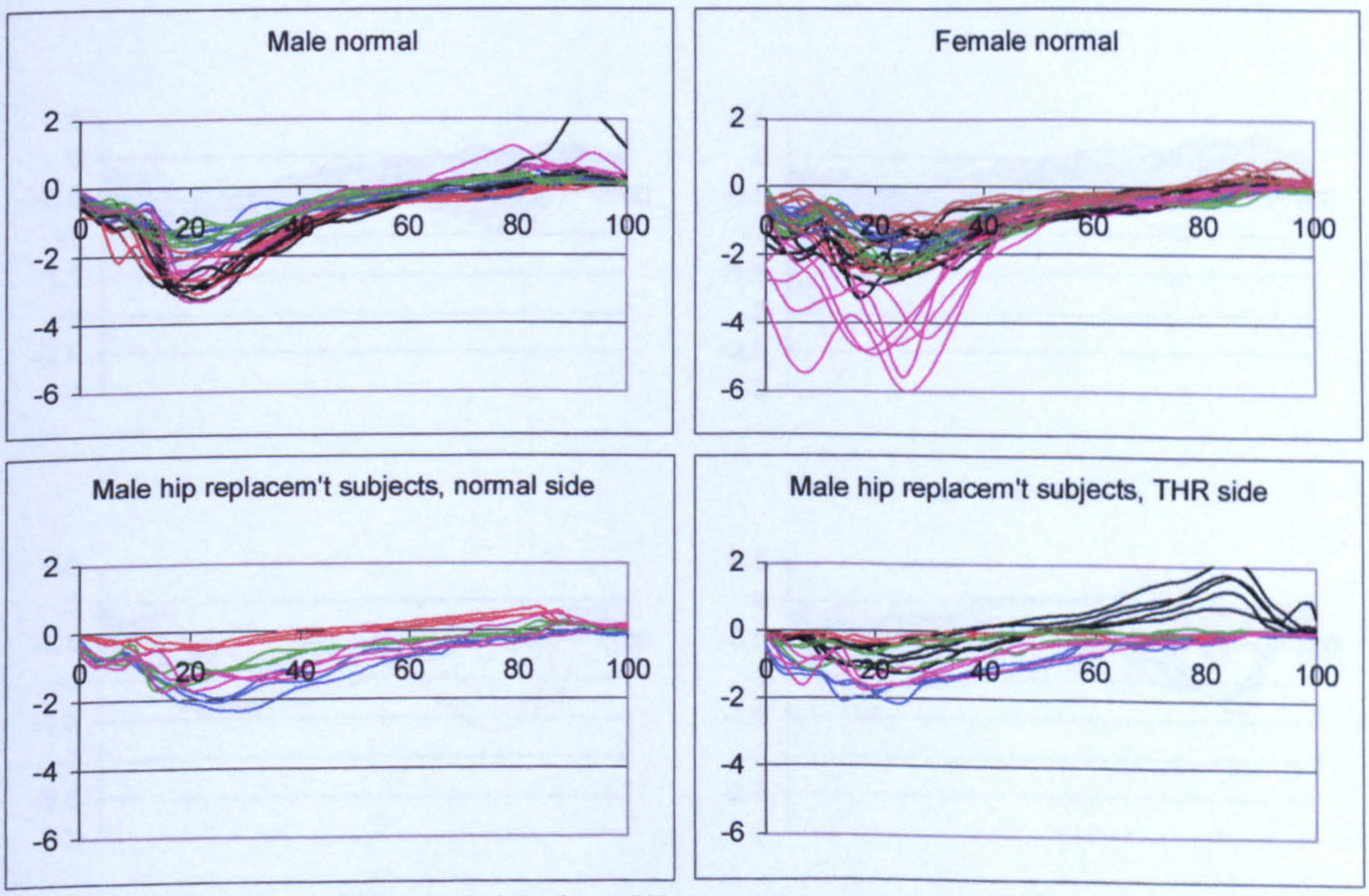

Figure A-VI.4.60 Ramp descent, XPA hip joint force

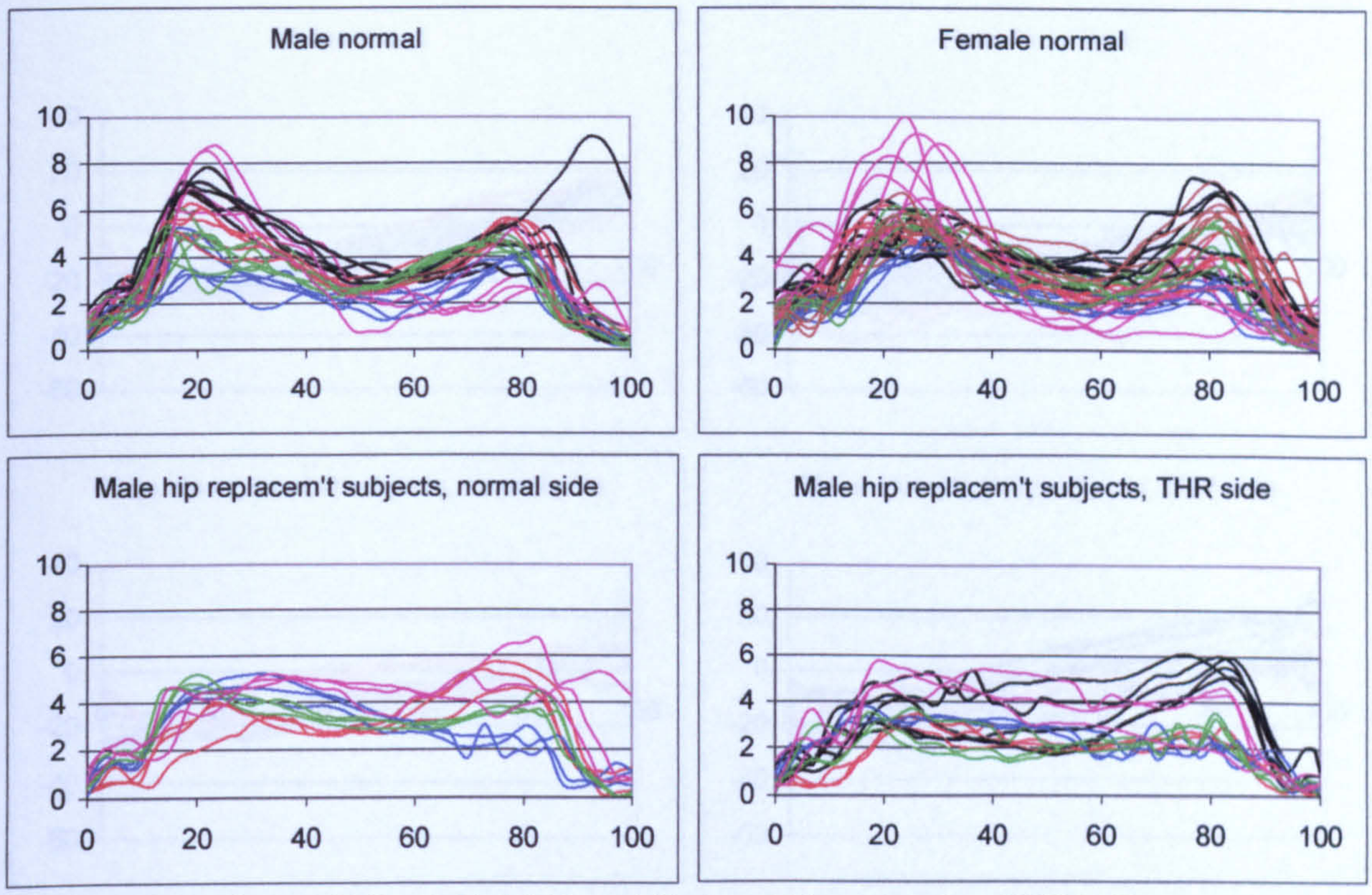

Ramp descent, YPA-axis hip joint force (N/body weight, +ve = acting +YPA) by % stance phase

Figure A-VI.4.61 Ramp descent, YPA hip joint force

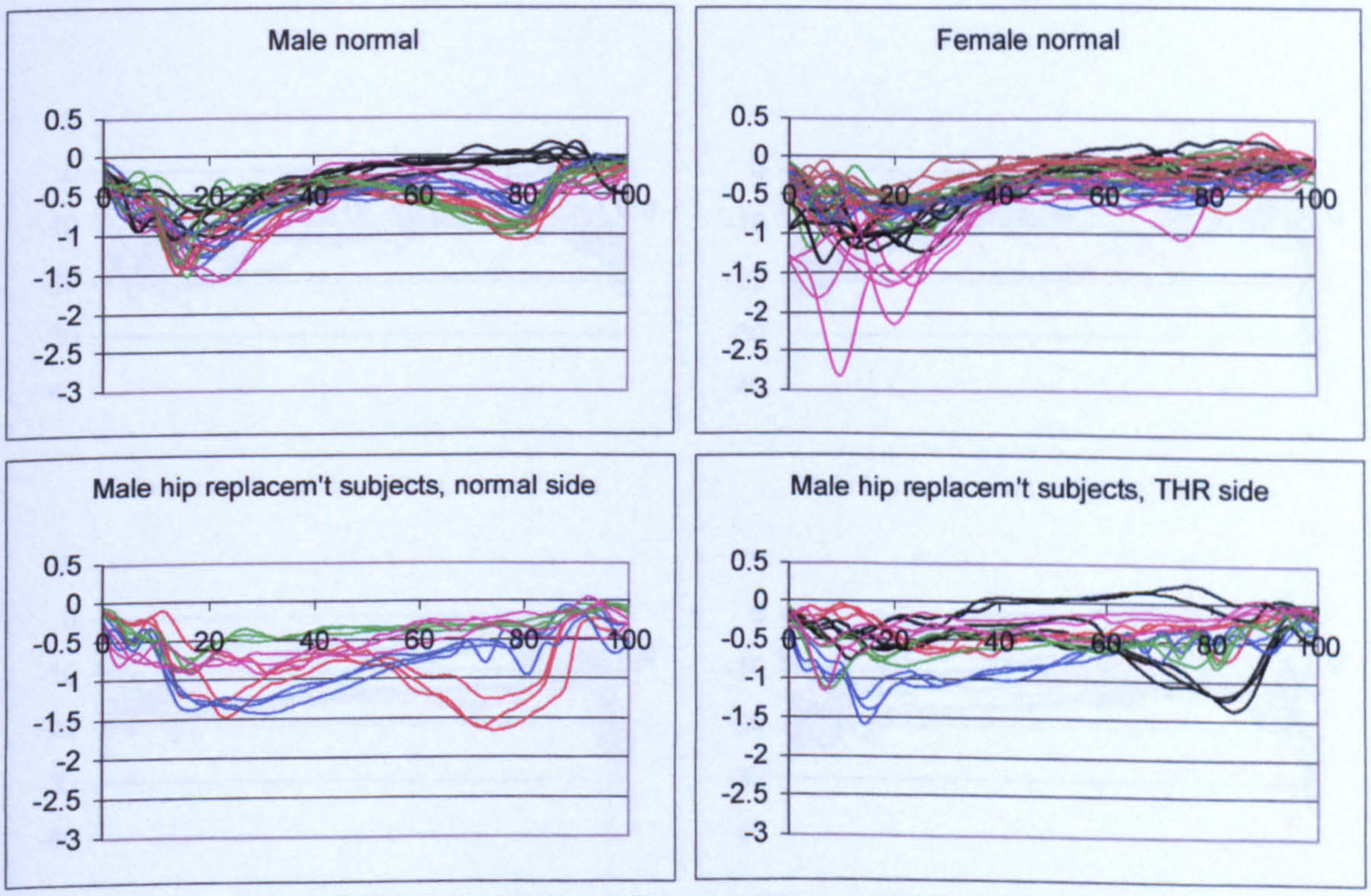

Ramp descent, ZPA-axis hip joint force (N/body weight, +ve = acting +ZPA) by % stance phase

Figure A-VI.4.62 Ramp descent, ZPA hip joint force

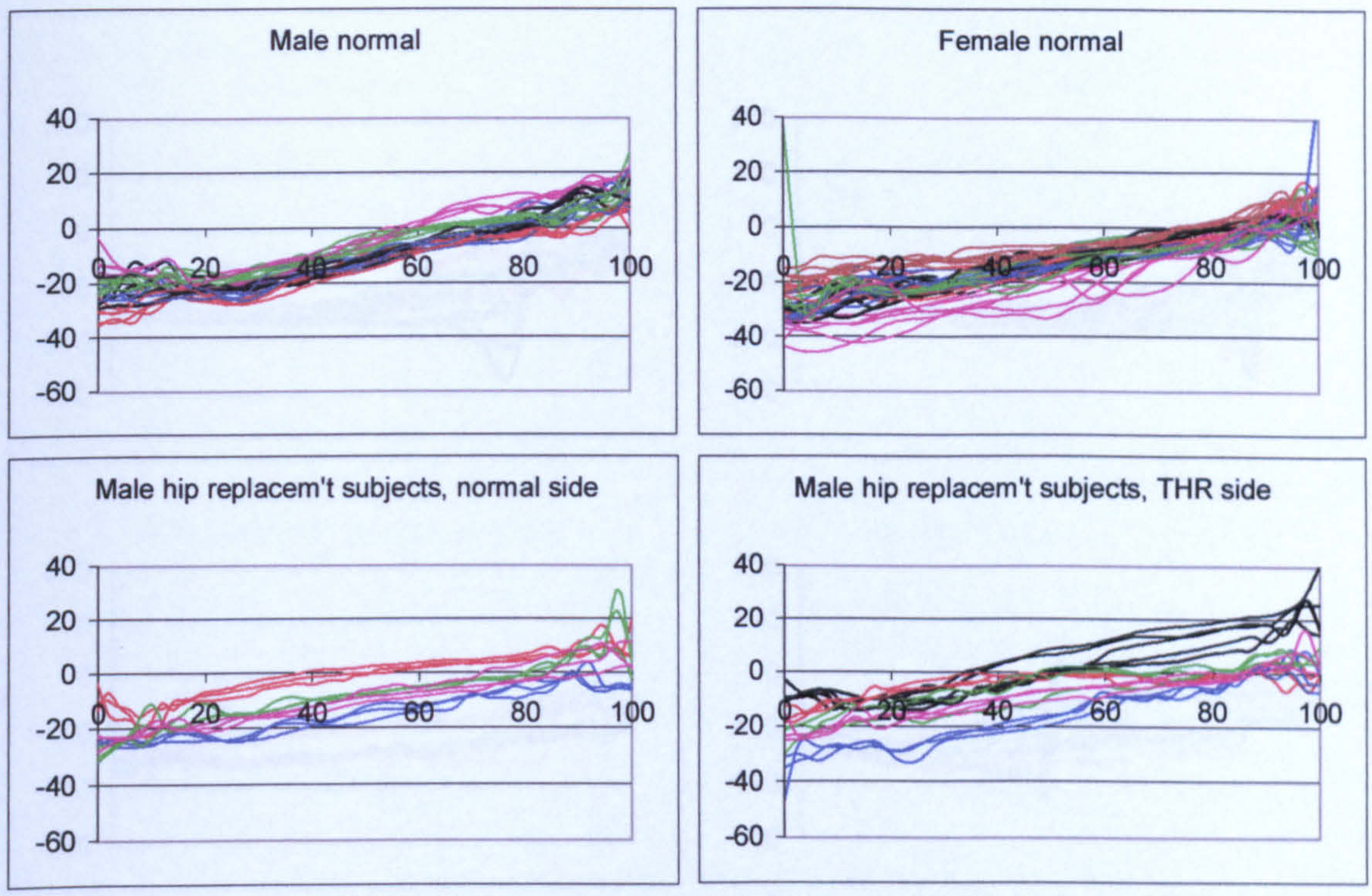

Ramp descent, HJYXANG (degrees, +ve = from YPA towards XPA) by % stance phase

Figure A-VI.4.63 Ramp descent, HJYXANG resultant hip joint force pelvic angle

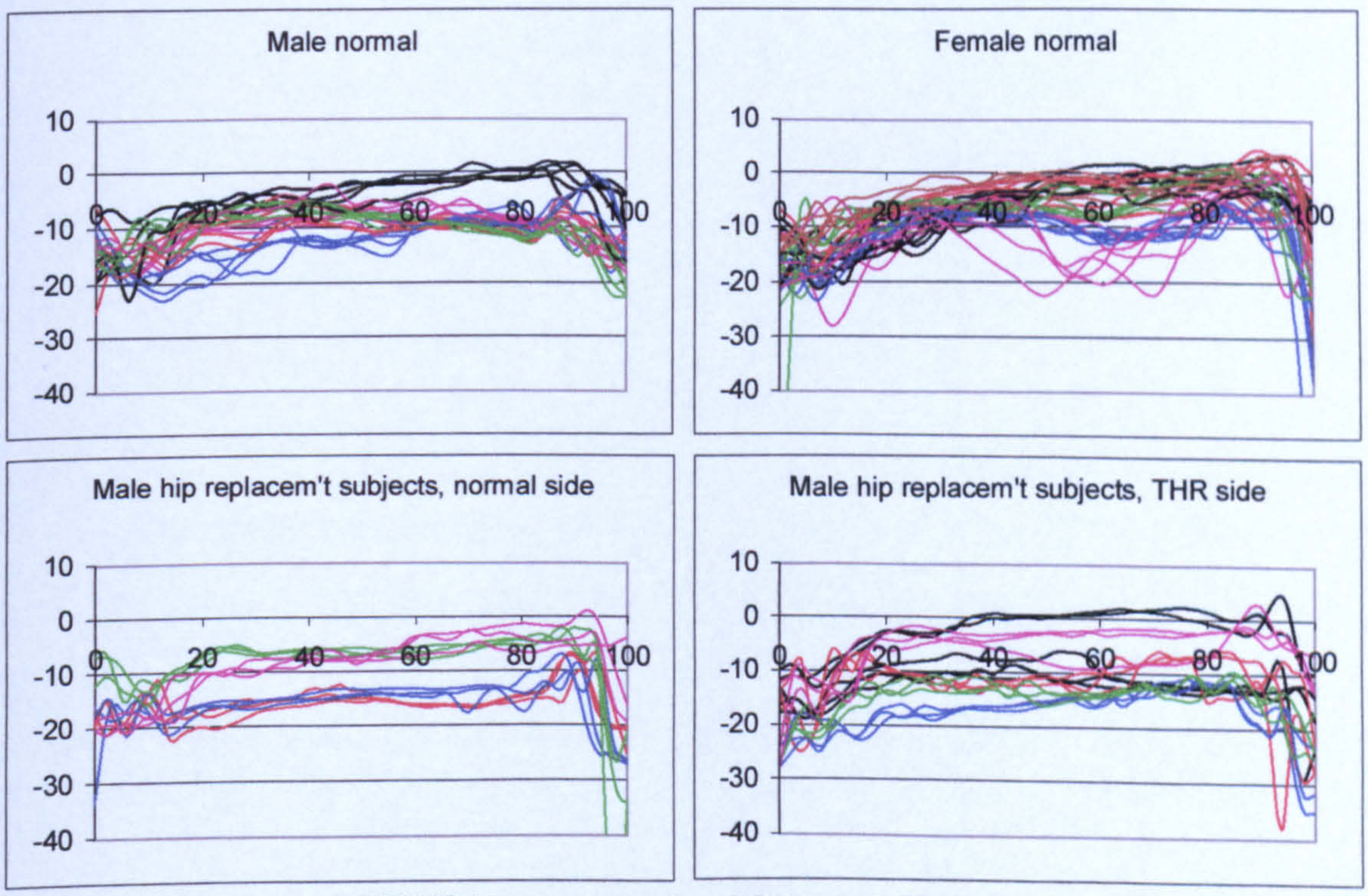

Ramp descent, HJYZANG (degrees, +ve = from YPA towards ZPA) by % stance phase

Figure A-VI.4.64 Ramp descent, HJYZANG resultant hip joint force pelvic angle

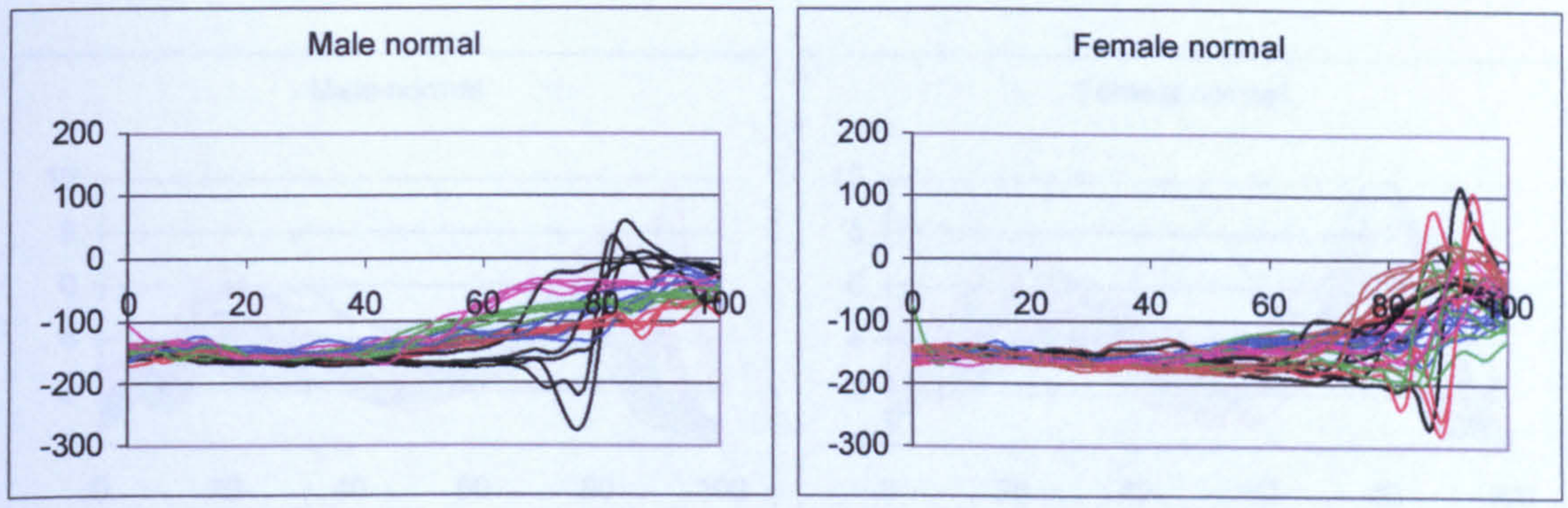

Figure A-VI.4.65 Ramp descent, HJXZANG resultant hip joint force pelvic angle

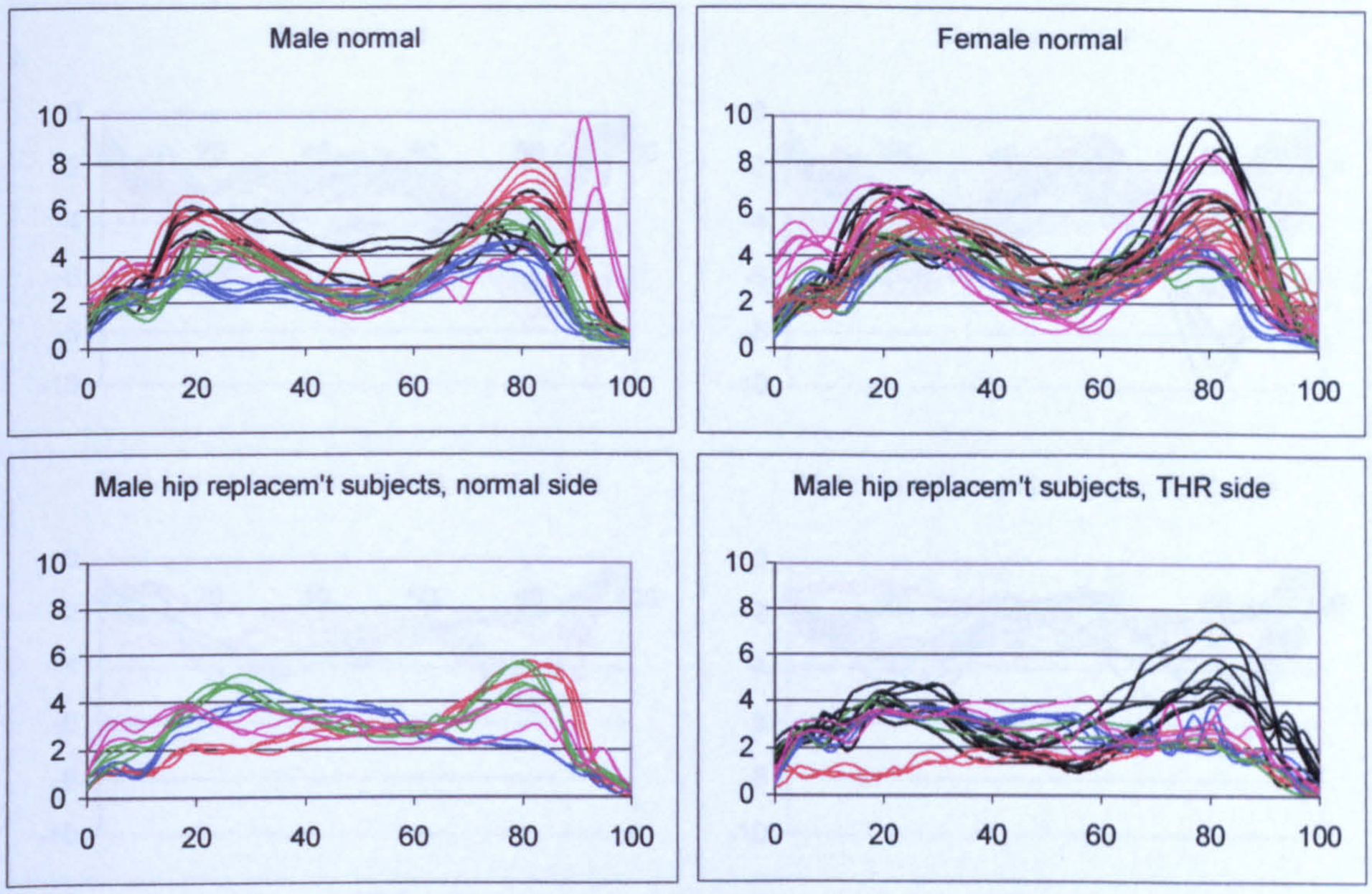

Figure A-VI.4.66 Camber foot up, resultant hip joint force

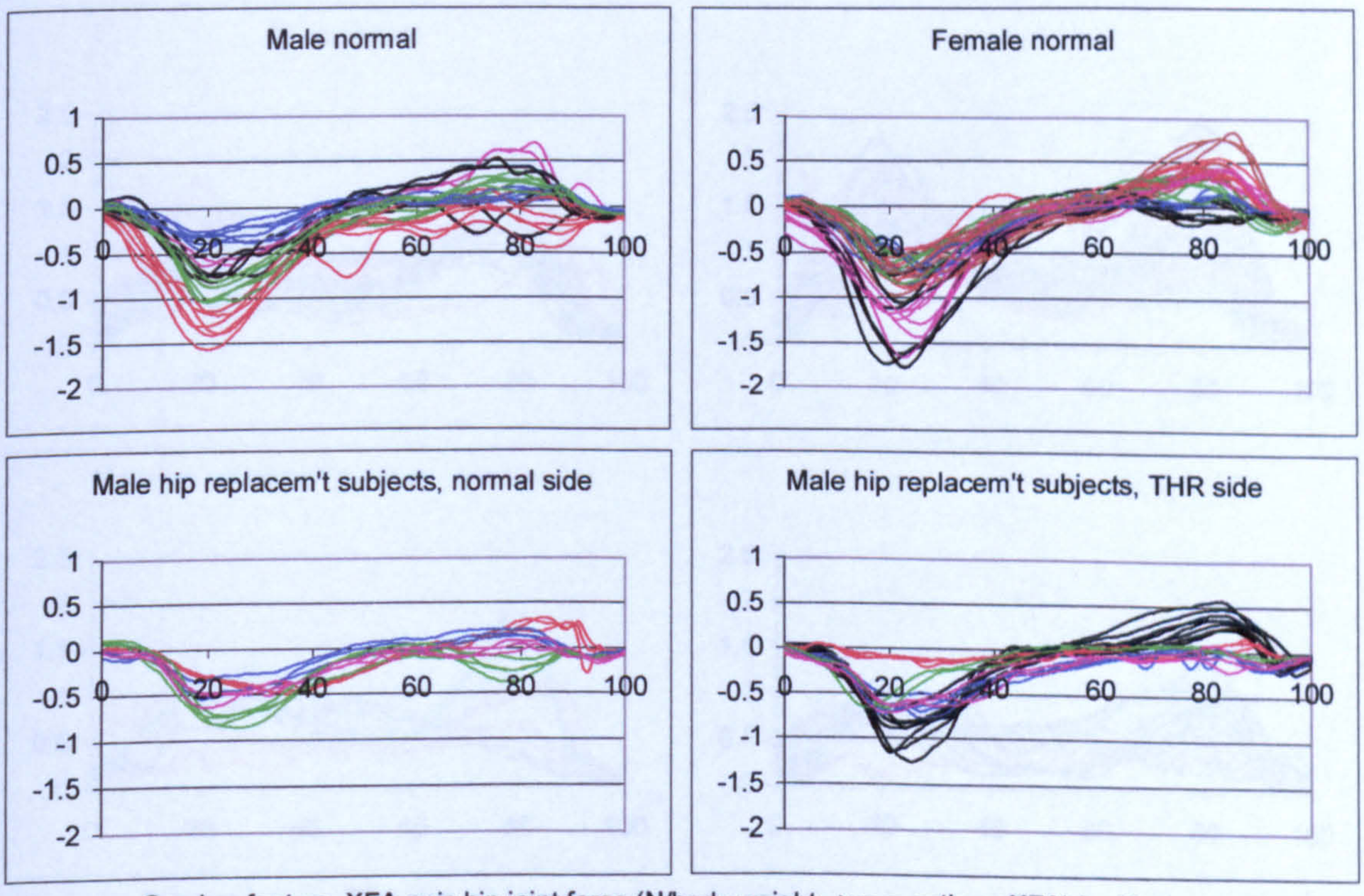

Figure A-VI.4.67 Camber foot up, XFA hip joint force

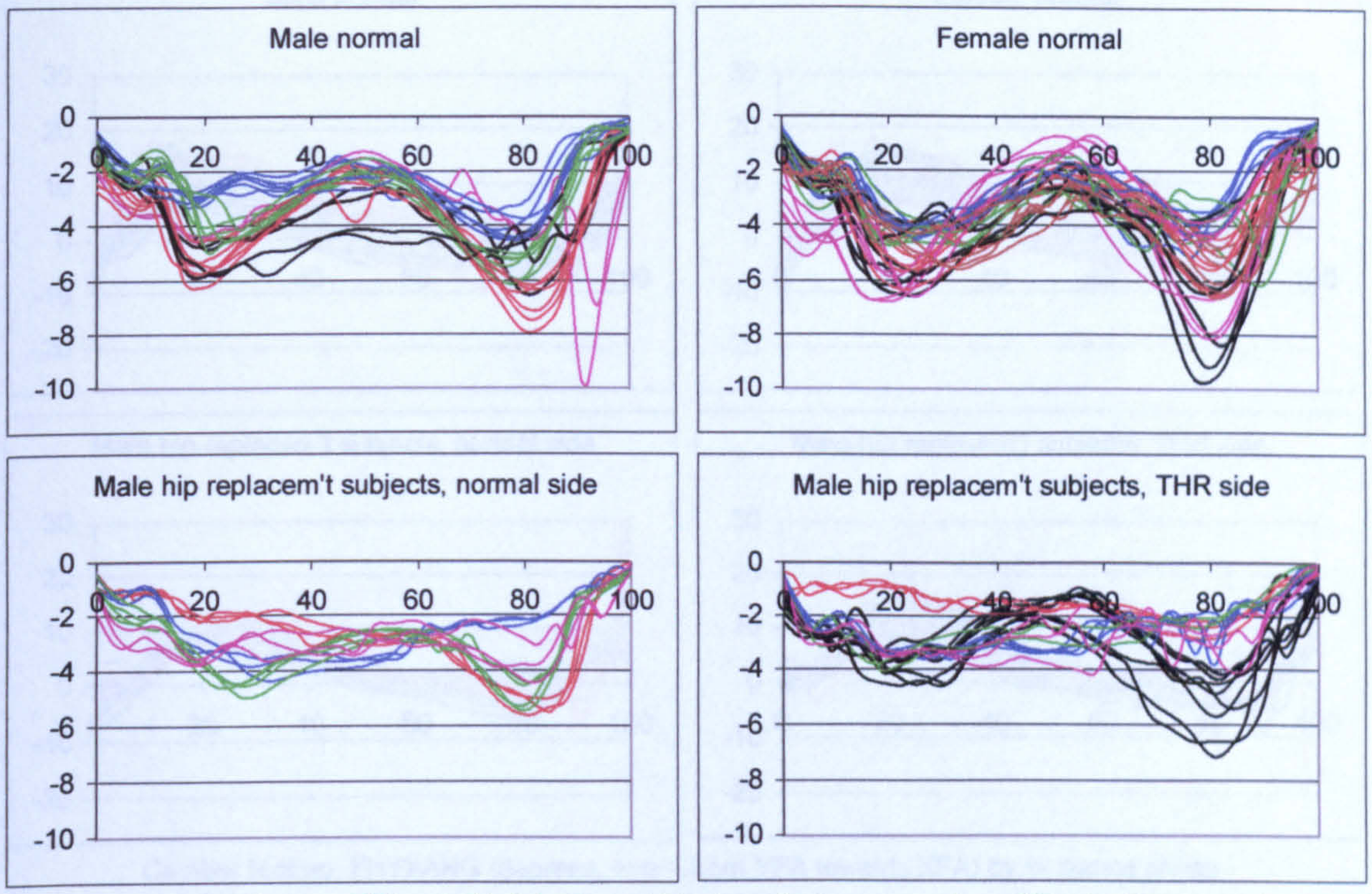

Figure A-VI.4.68 Camber foot up, YFA hip joint force

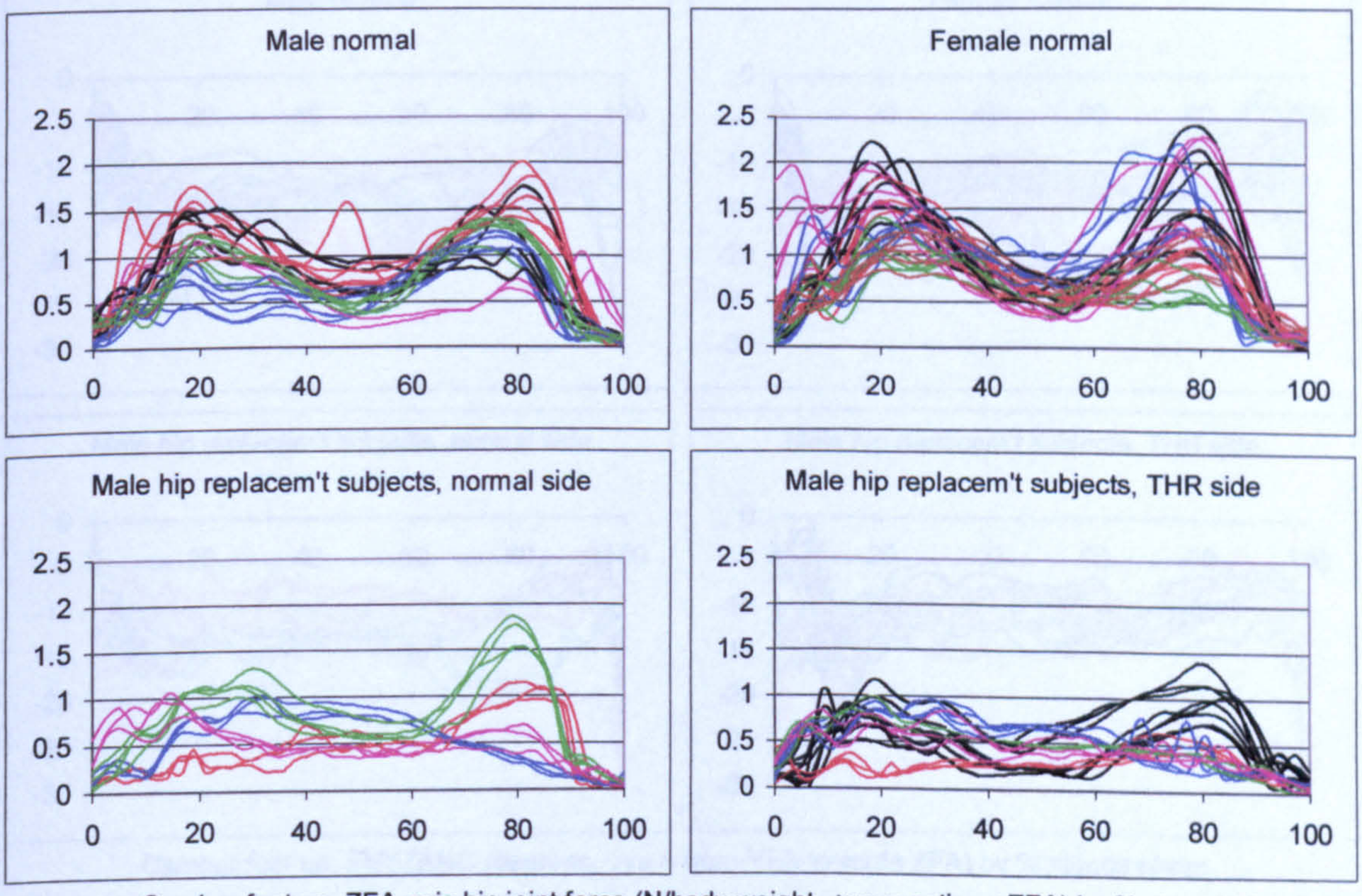

Figure A-VI.4.69 Camber foot up, ZFA hip joint force

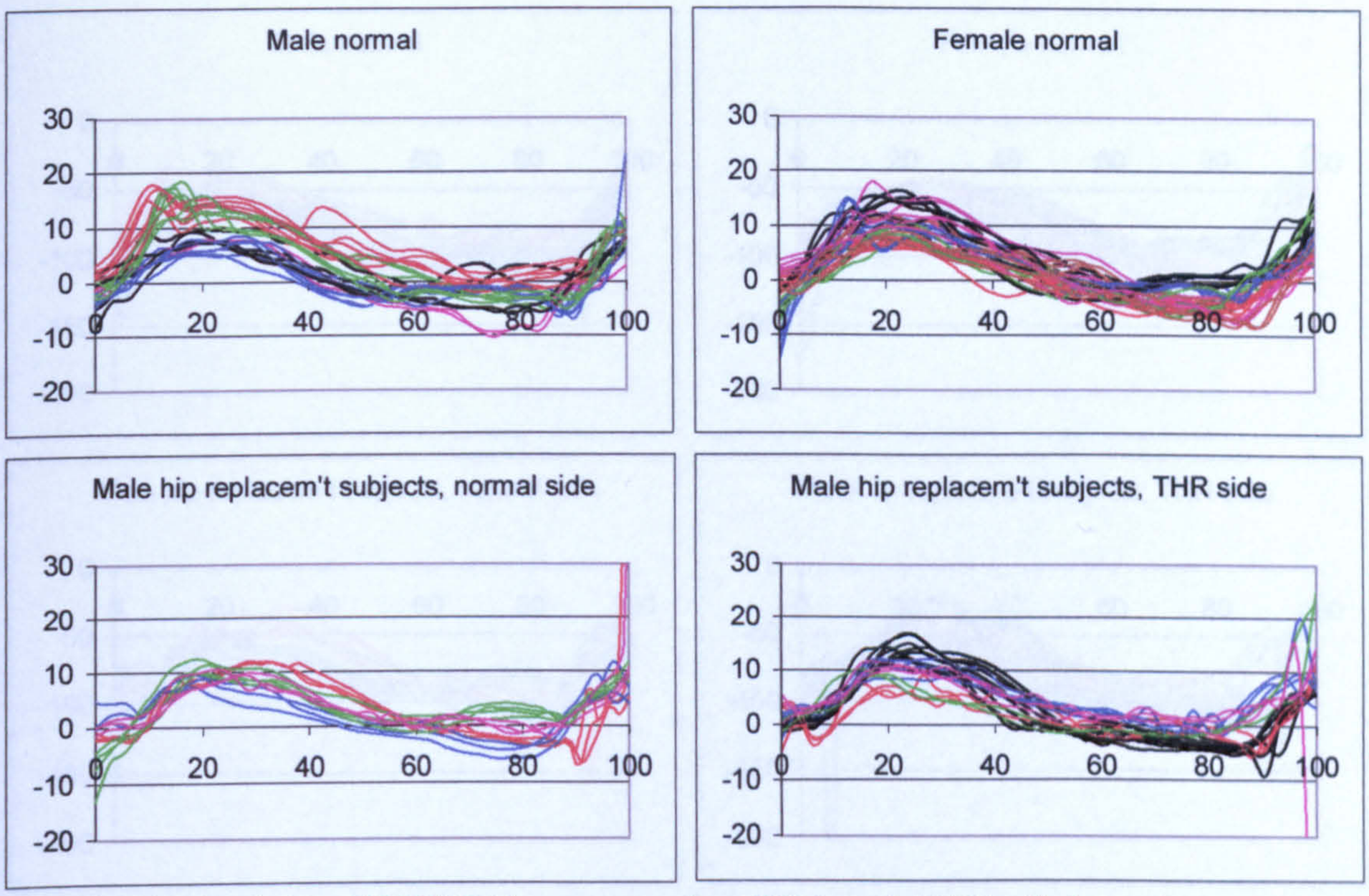

Camber foot up, FHYXANG (degrees, +ve = from YFA towards XFA) by % stance phase

Figure A-VI.4.70 Camber foot up, FHYXANG resultant hip joint force femoral angle

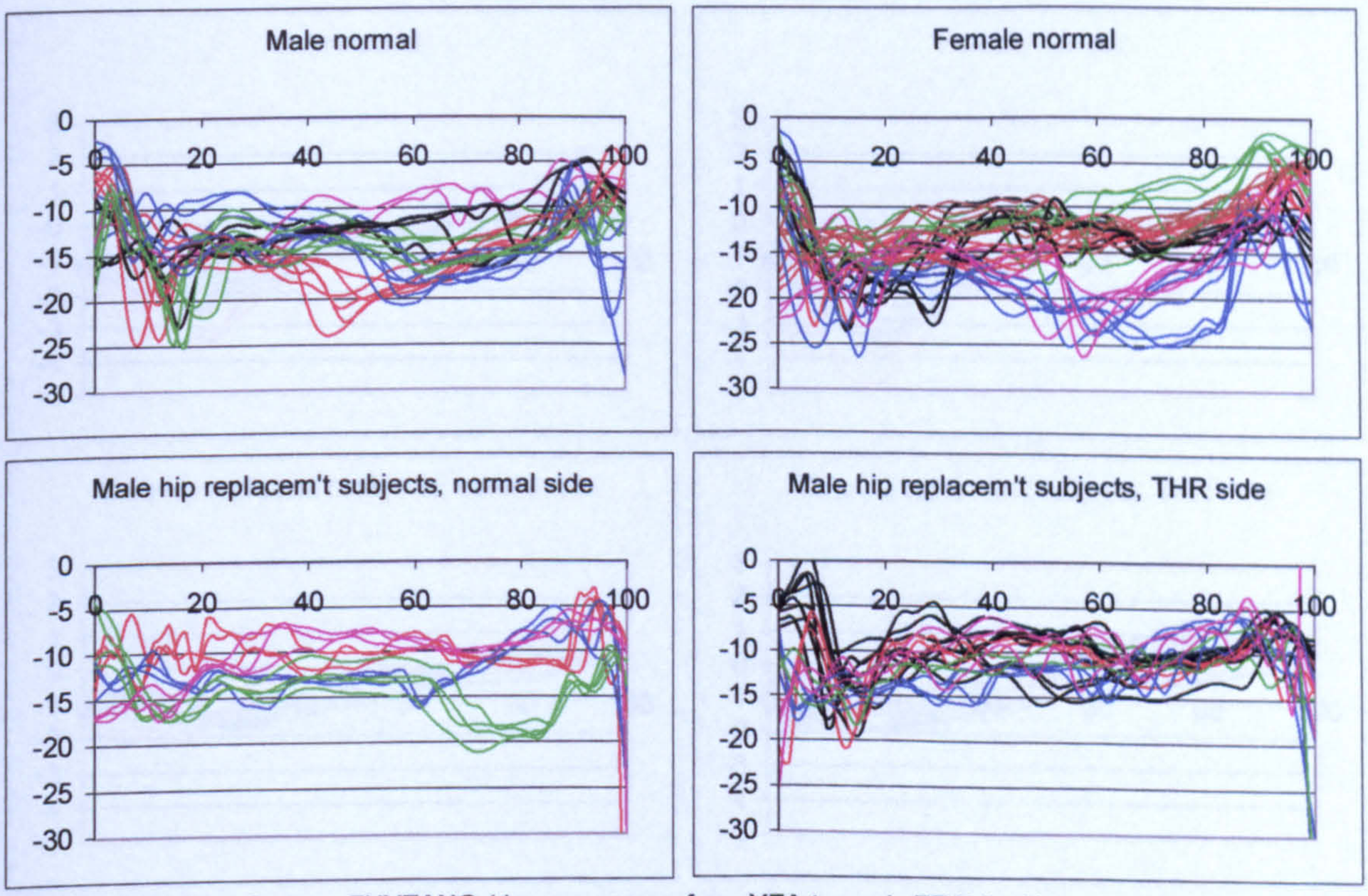

Camber foot up, FHYZANG (degrees, +ve = from YFA towards ZFA) by % stance phase

Figure A-VI.4.71 Camber foot up, FHYZANG resultant hip joint force femoral angle

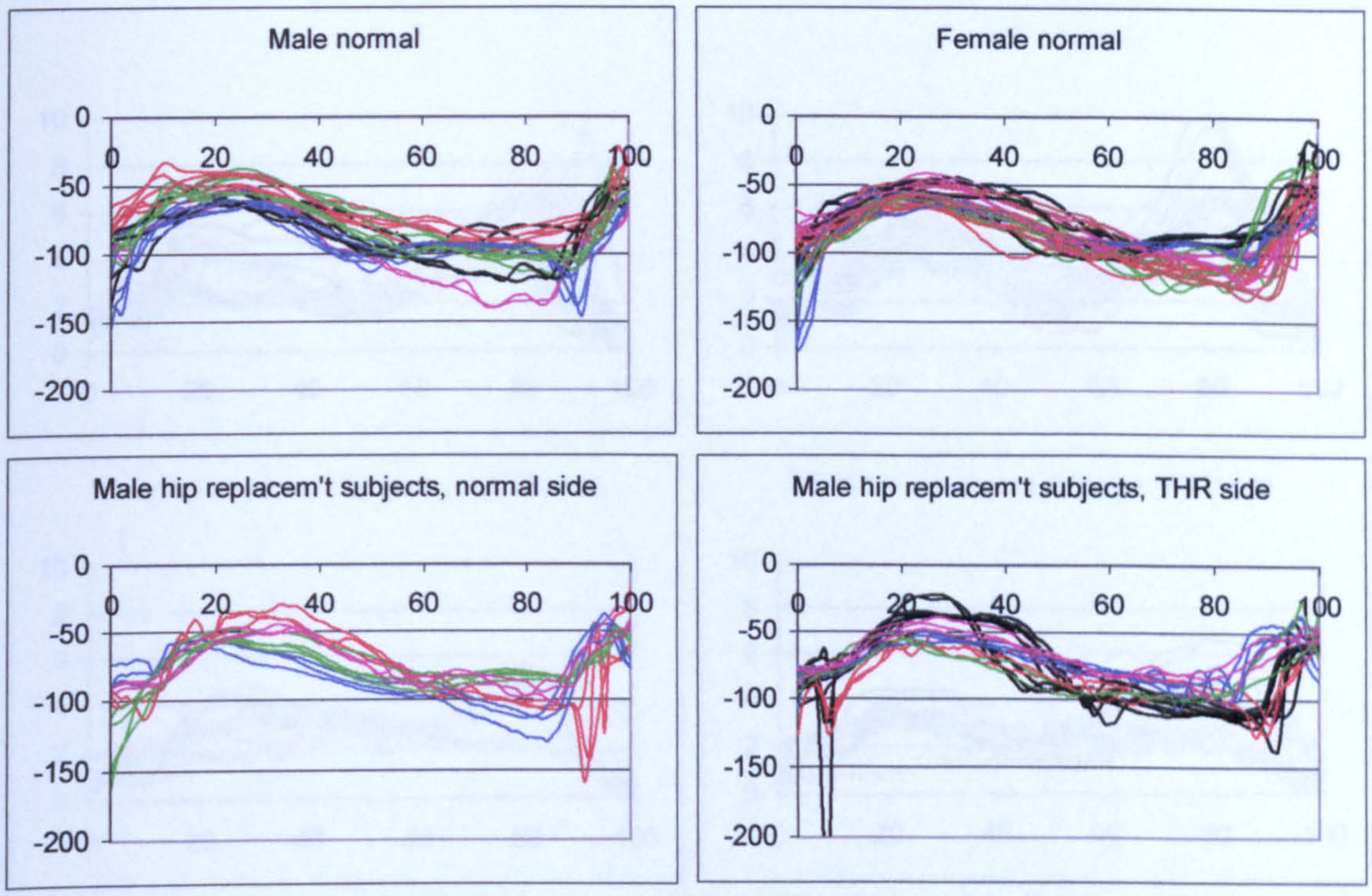

Figure A-VI.4.72 Camber foot up, FHXZANG resultant hip joint force femoral angle

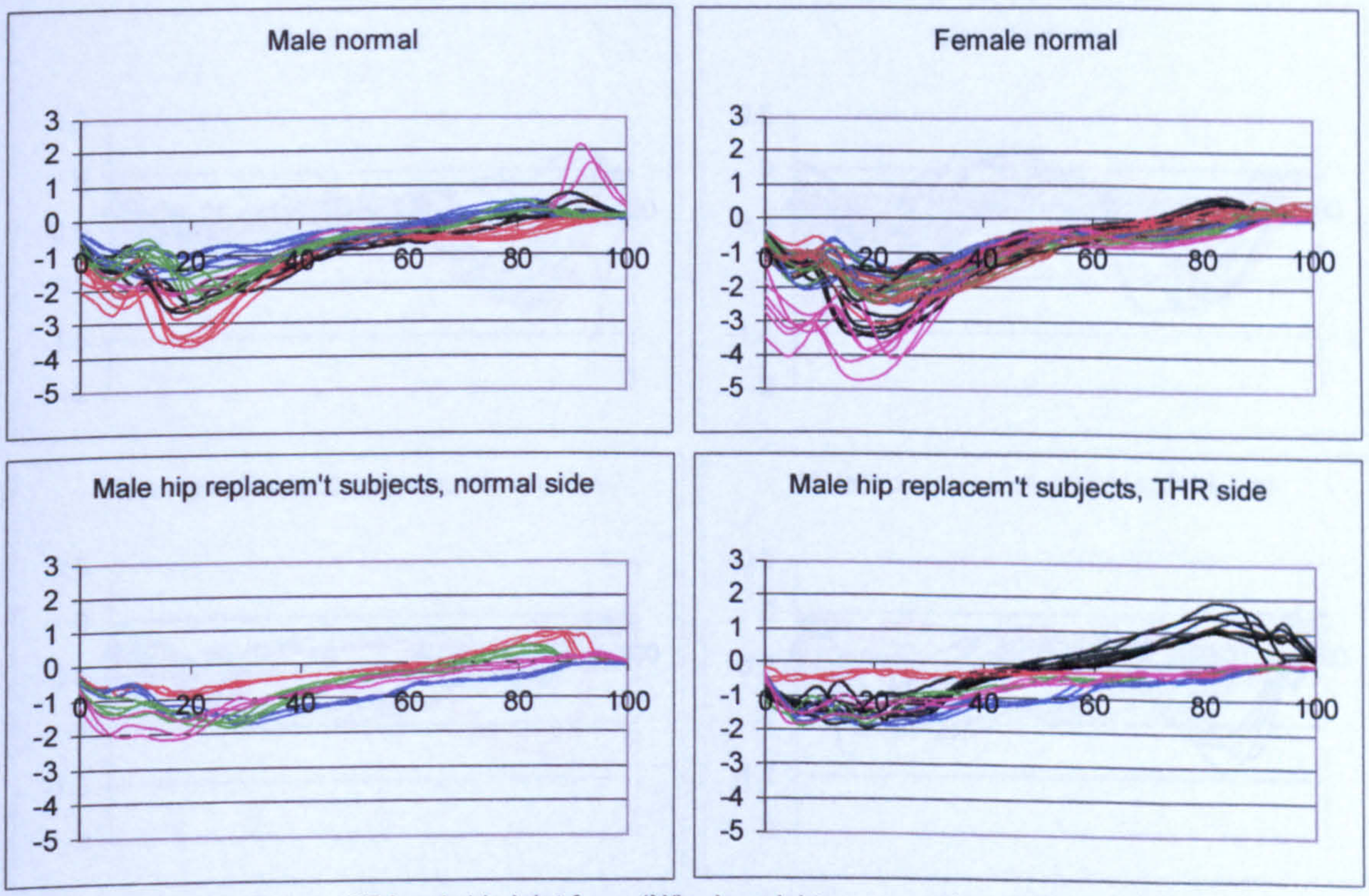

Figure A-VI.4.73 Camber foot up, XPA hip joint force

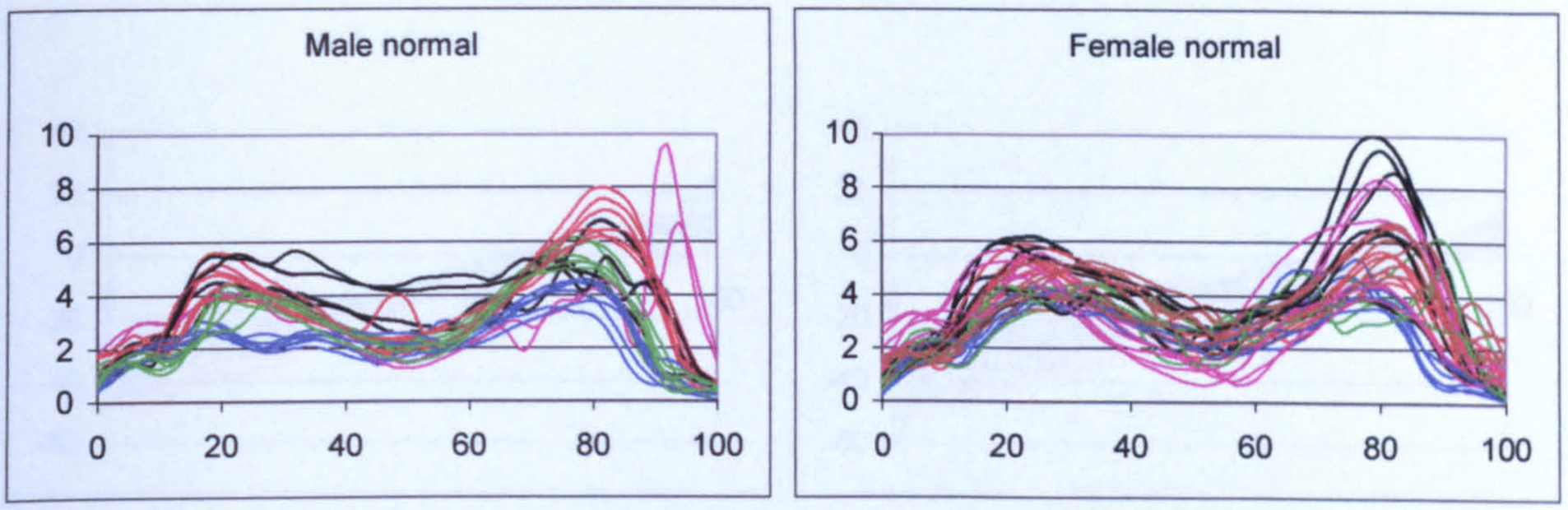

Camber foot up, YPA-axis hip joint force (N/body weight, +ve = acting +YPA) by % stance phase

Figure A-VI.4.74 Camber foot up, YPA hip joint force

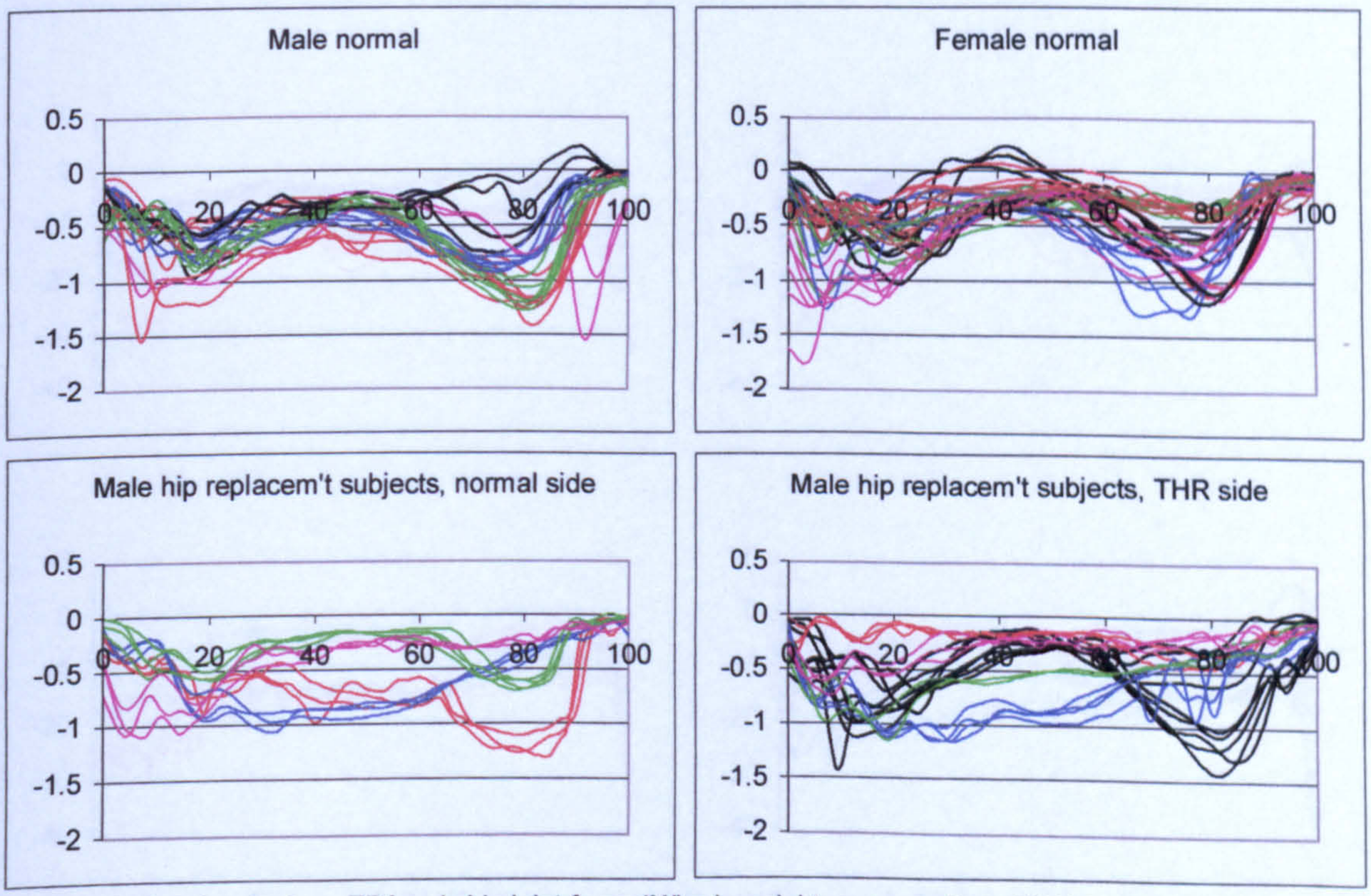

Camber foot up, ZPA-axis hip joint force (N/body weight, +ve = acting +ZPA) by % stance phase

Figure A-VI.4.75 Camber foot up, ZPA hip joint force

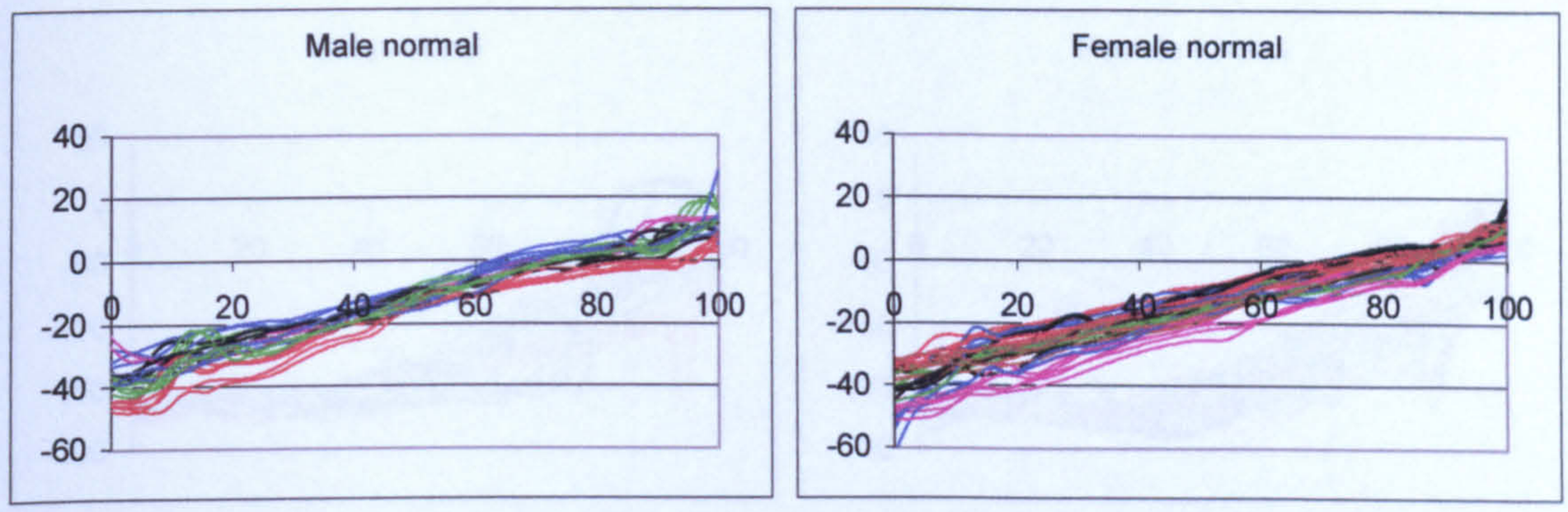

Figure A-VI.4.76 Camber foot up, HJYXANG resultant hip joint force pelvic angle

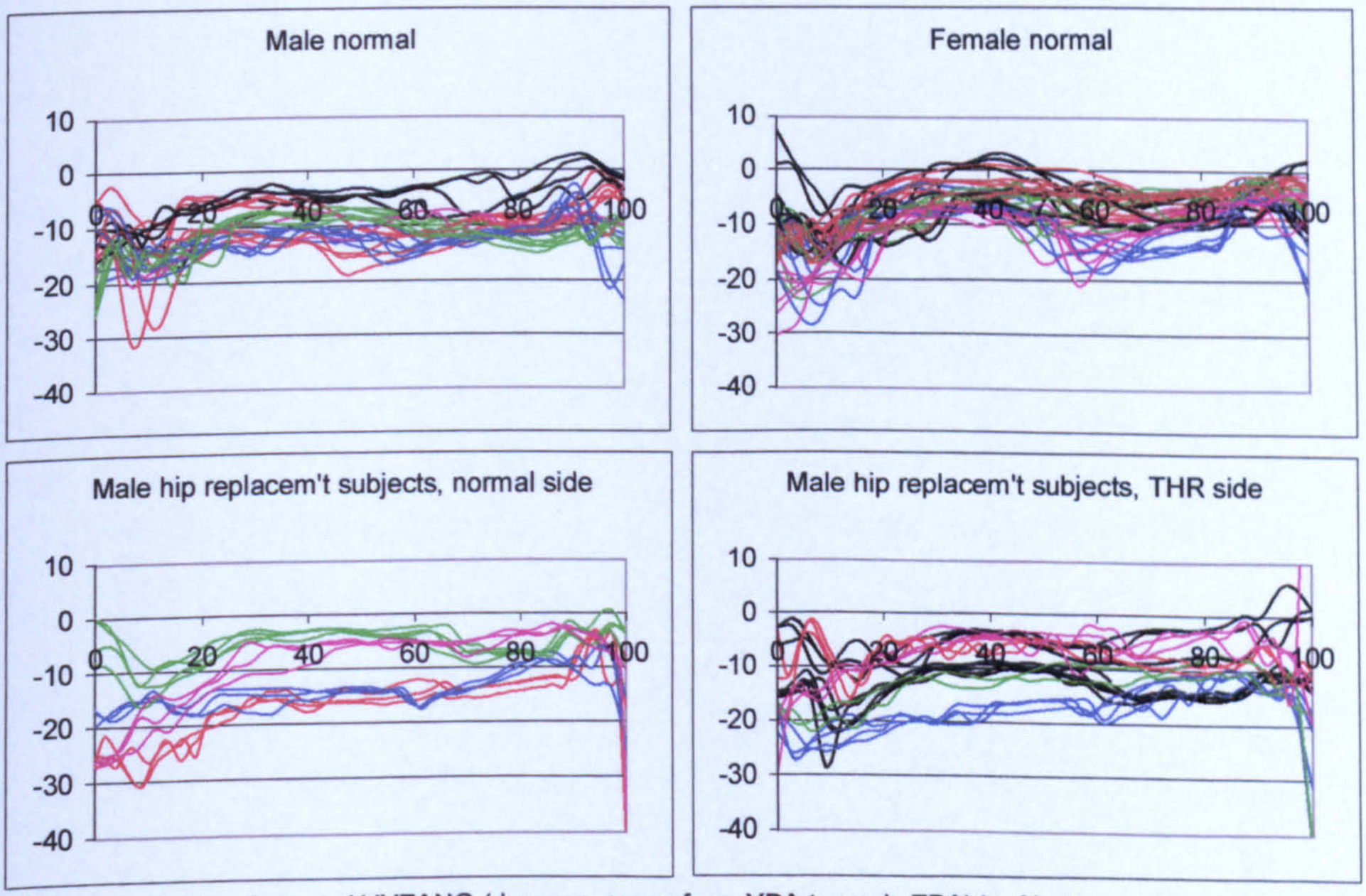

Figure A-VI.4.77 Camber foot up, HJYZANG resultant hip joint force pelvic angle

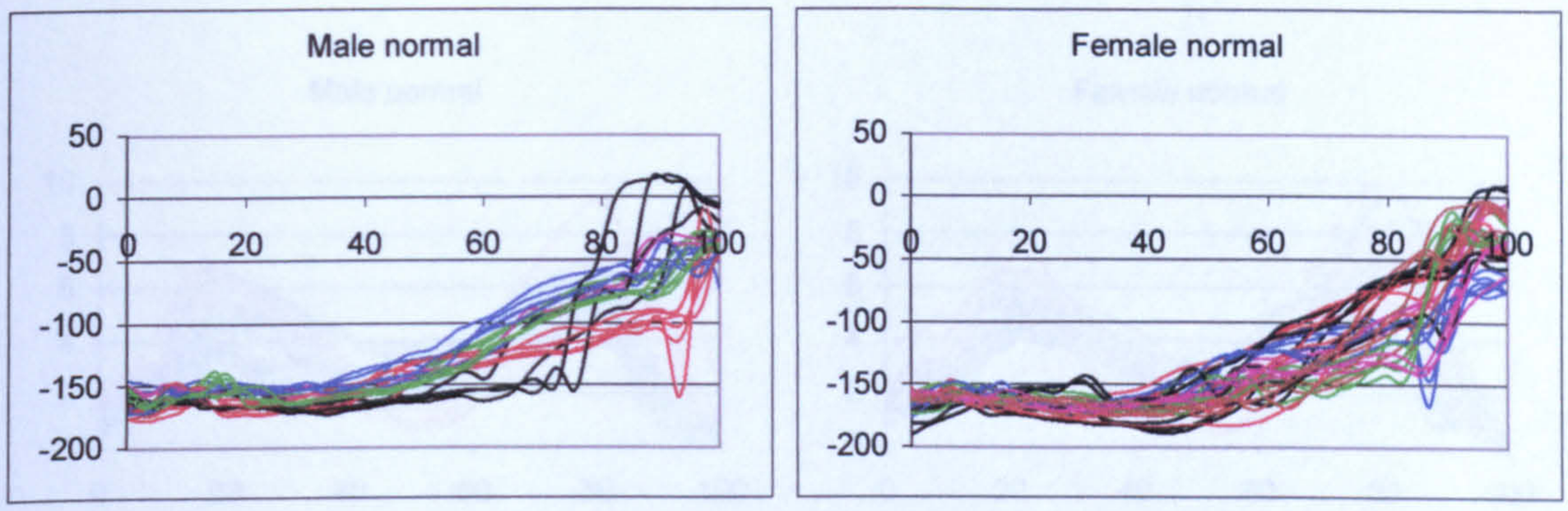

Figure A-VI.4.78 Camber foot up, HJXZANG resultant hip joint force pelvic angle

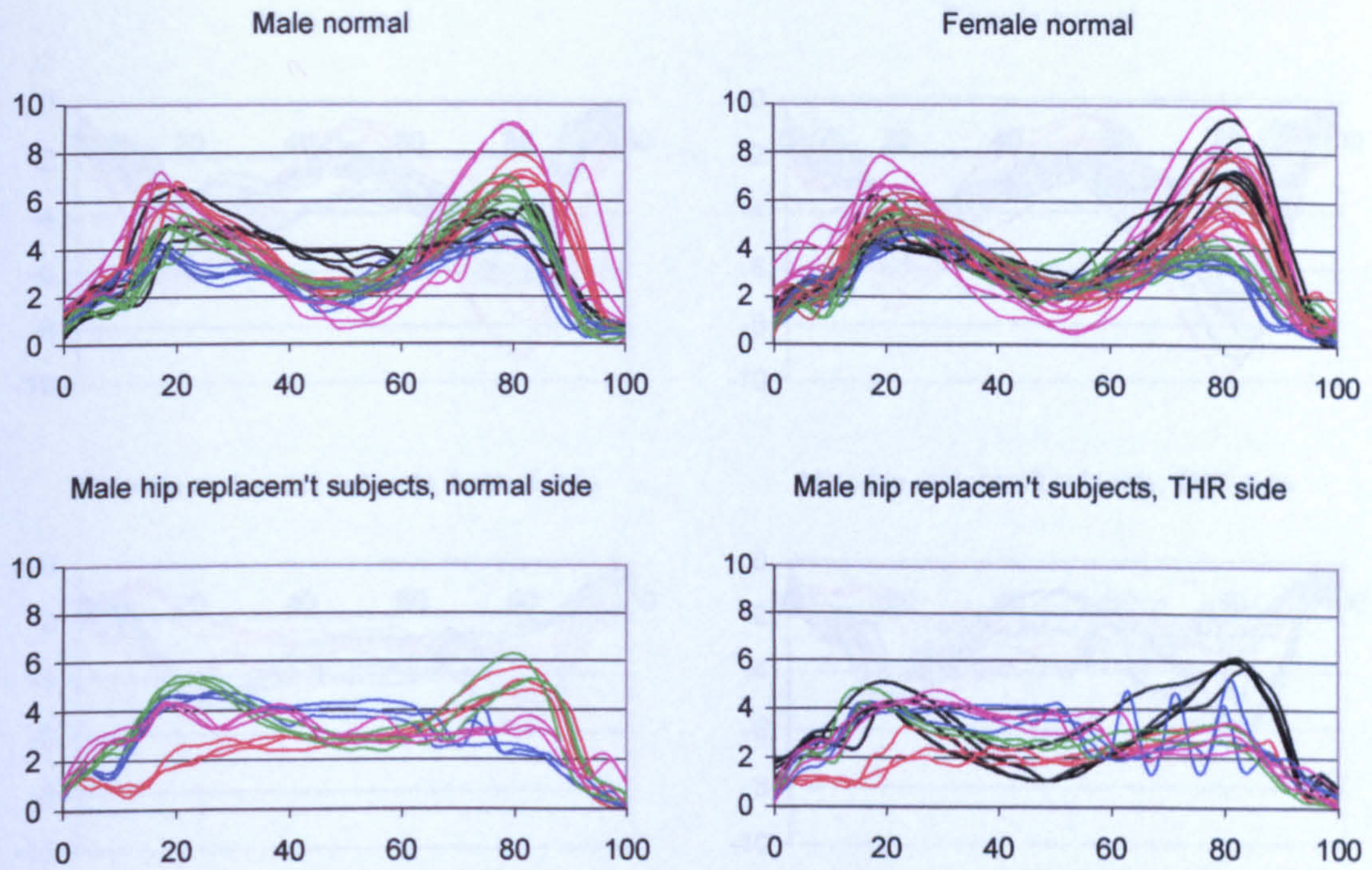

Figure A-VI.4.79 Camber foot down, resultant hip joint force

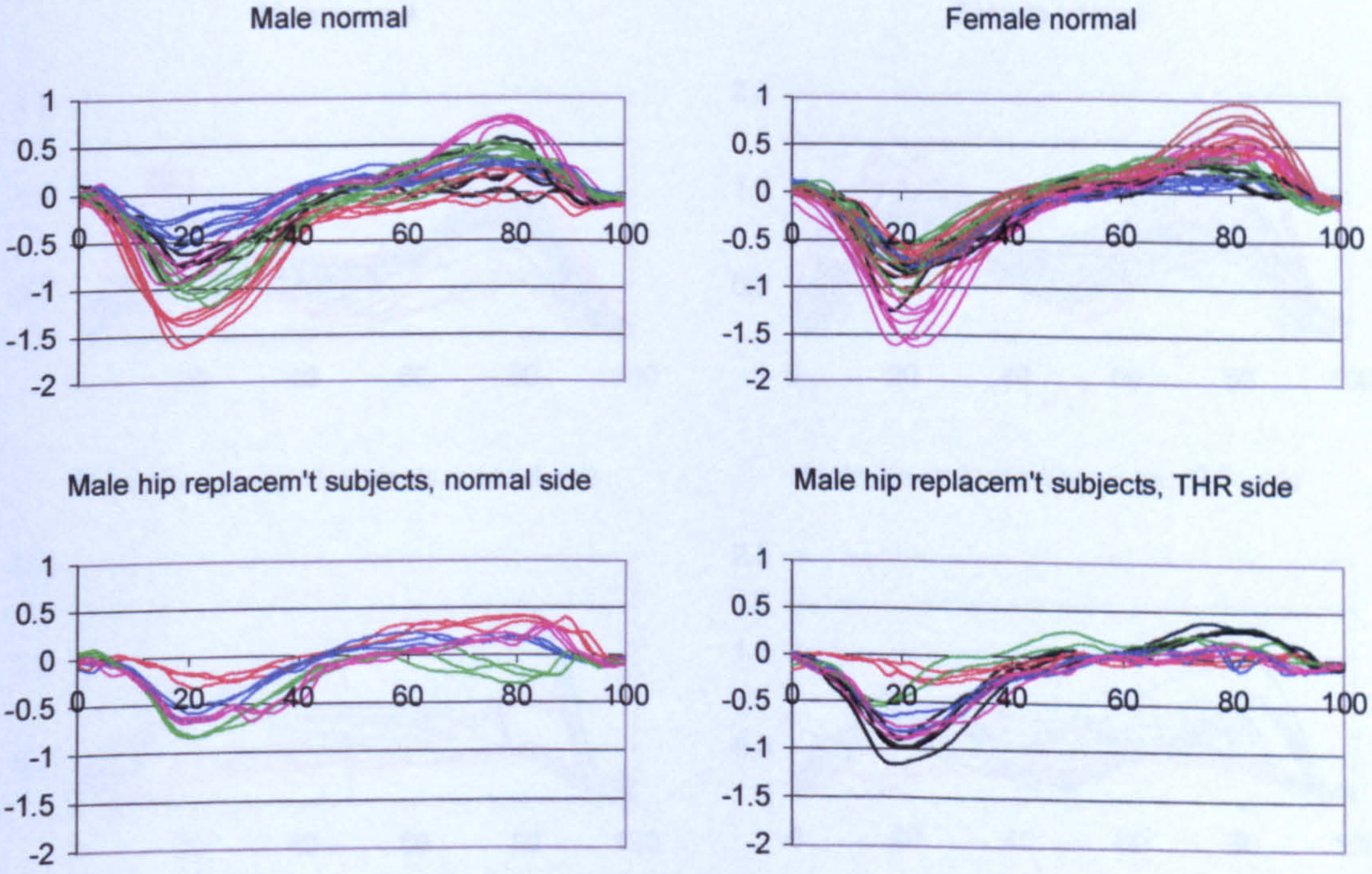

Figure A-VI.4.80 Camber foot down, XFA hip joint force

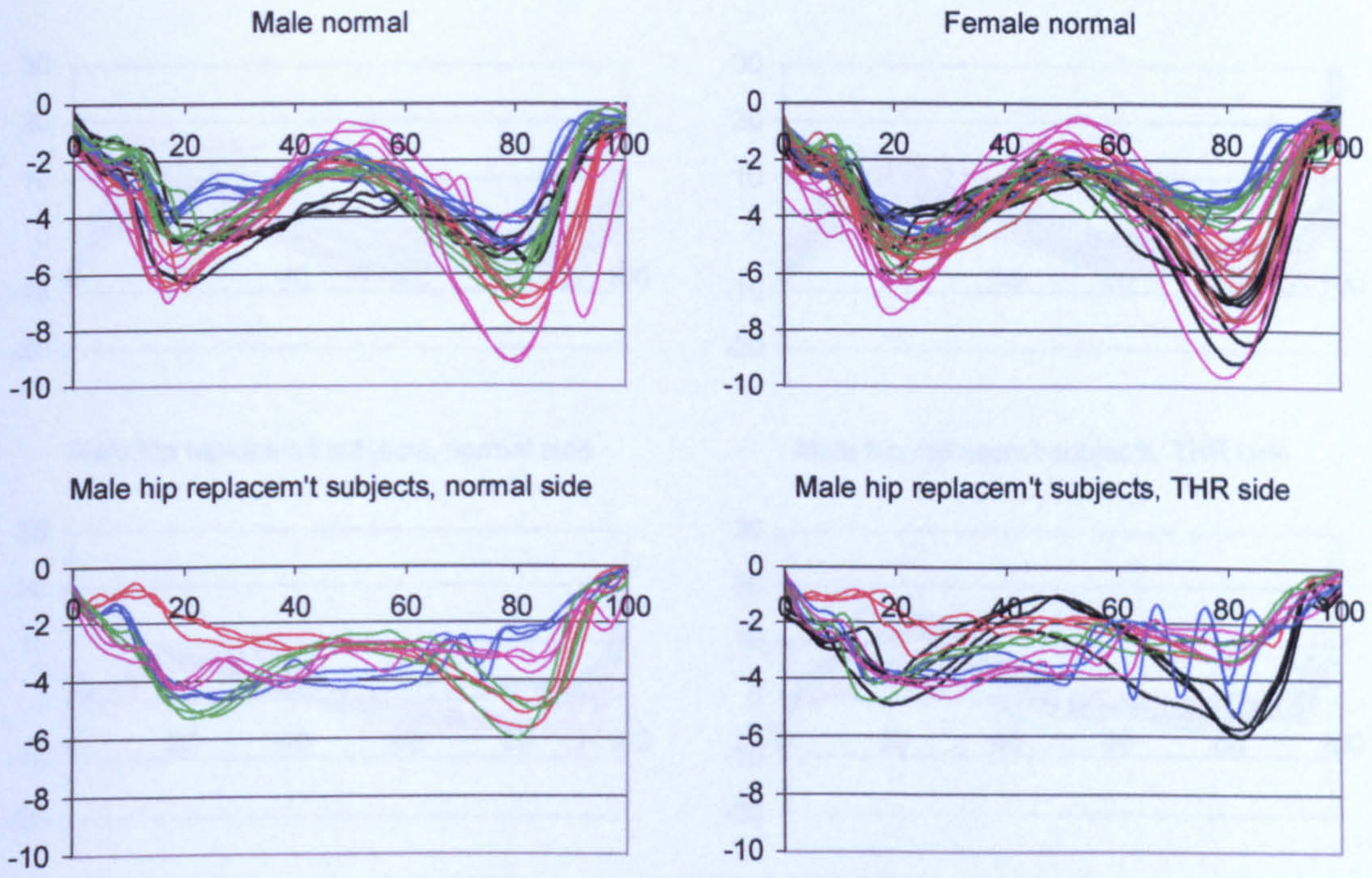

Figure A-VI.4.81 Camber foot down, YFA hip joint force

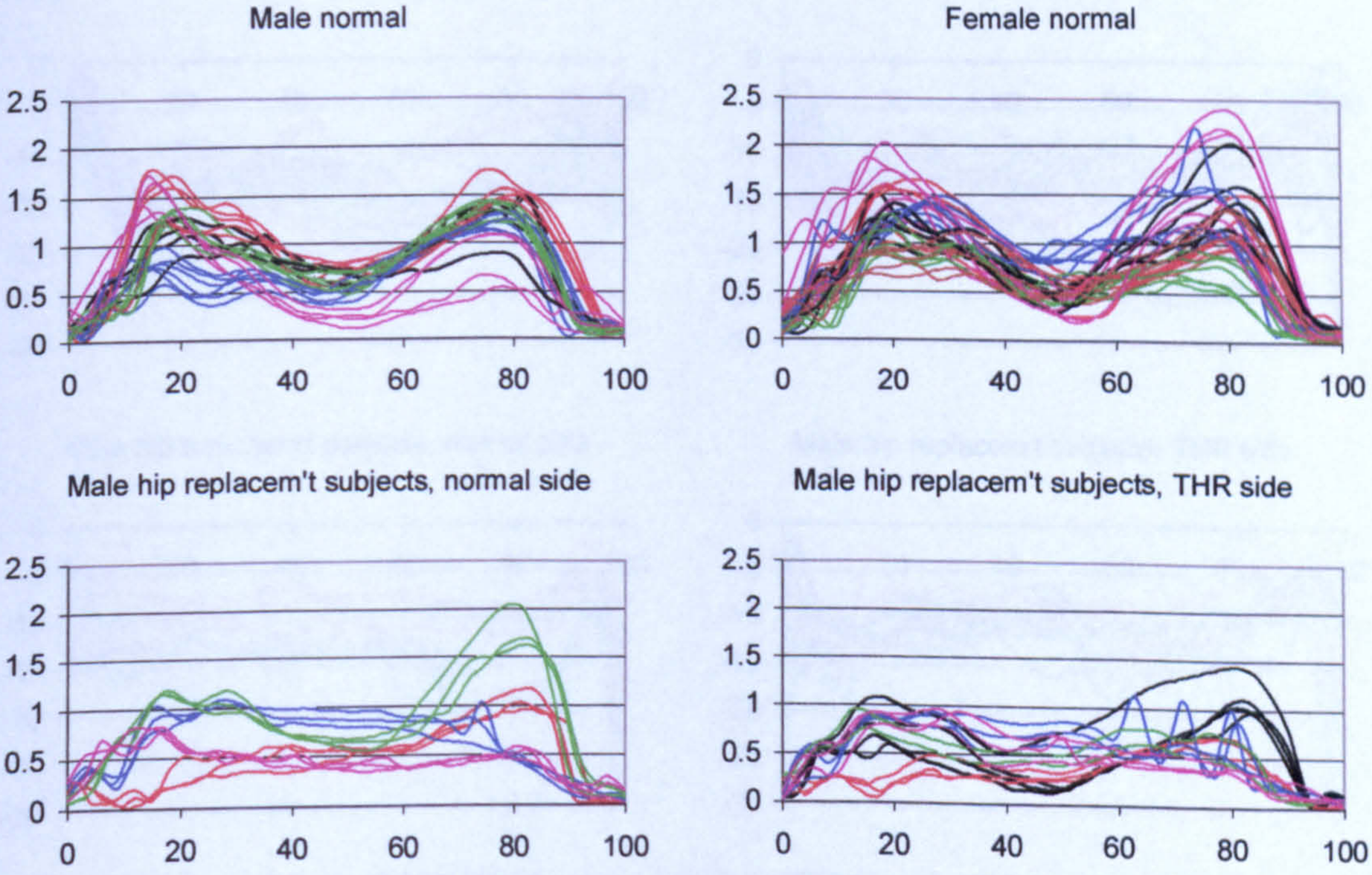

Figure A-VI.4.82 Camber foot down, ZFA hip joint force

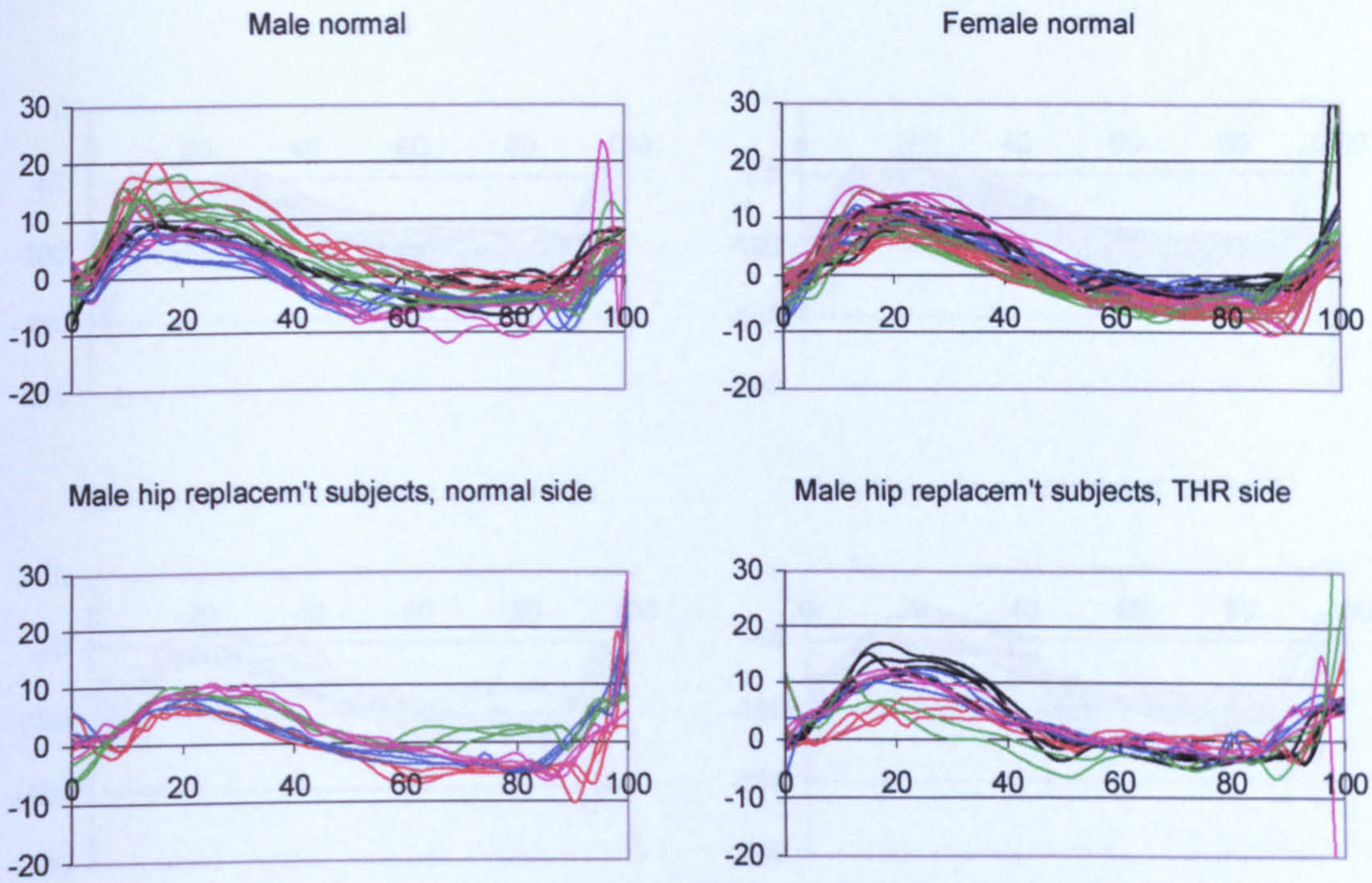

Camber foot down, FHYXANG (degrees, +ve = from YFA towards XFA) by % stance phase

Figure A-VI.4.83 Camber foot down, FHYXANG resultant hip joint force femoral angle

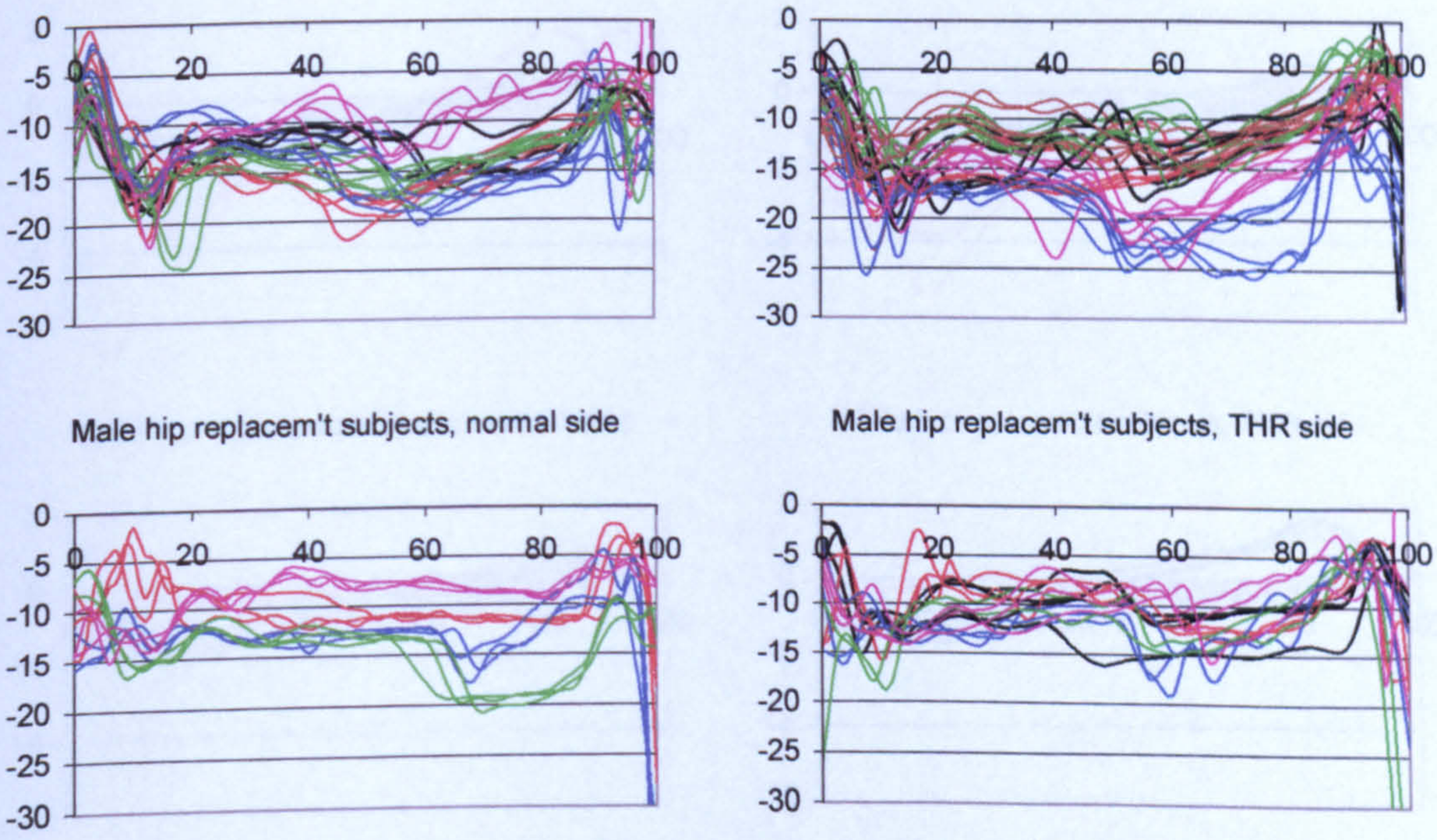

Camber foot down, FHYZANG (degrees, +ve = from YFA towards ZFA) by % stance phase

Figure A-VI.4.84 Camber foot down, FHYZANG resultant hip joint force femoral angle

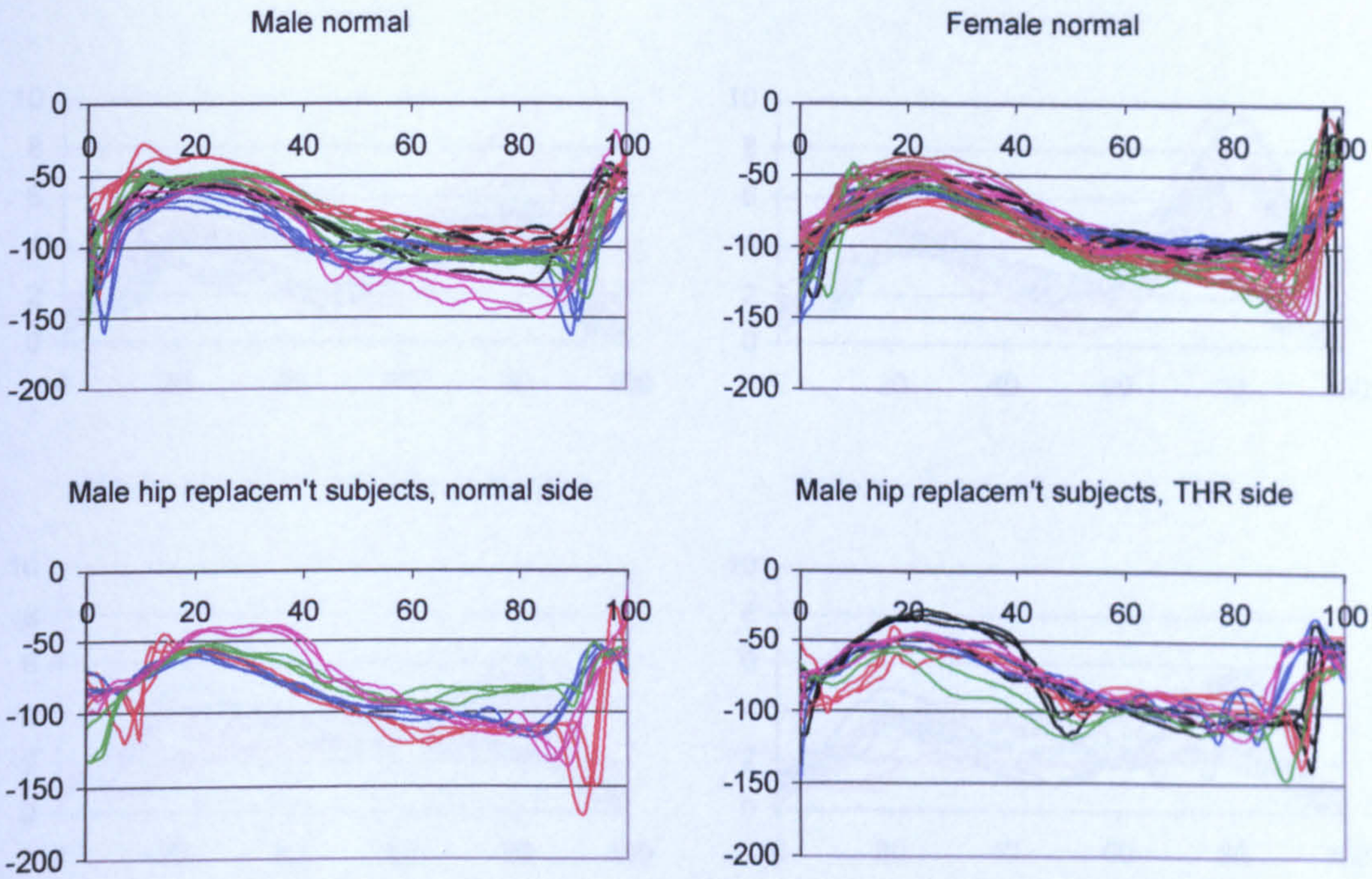

Figure A-VI.4.85 Camber foot down, FHXZANG resultant hip joint force femoral angle

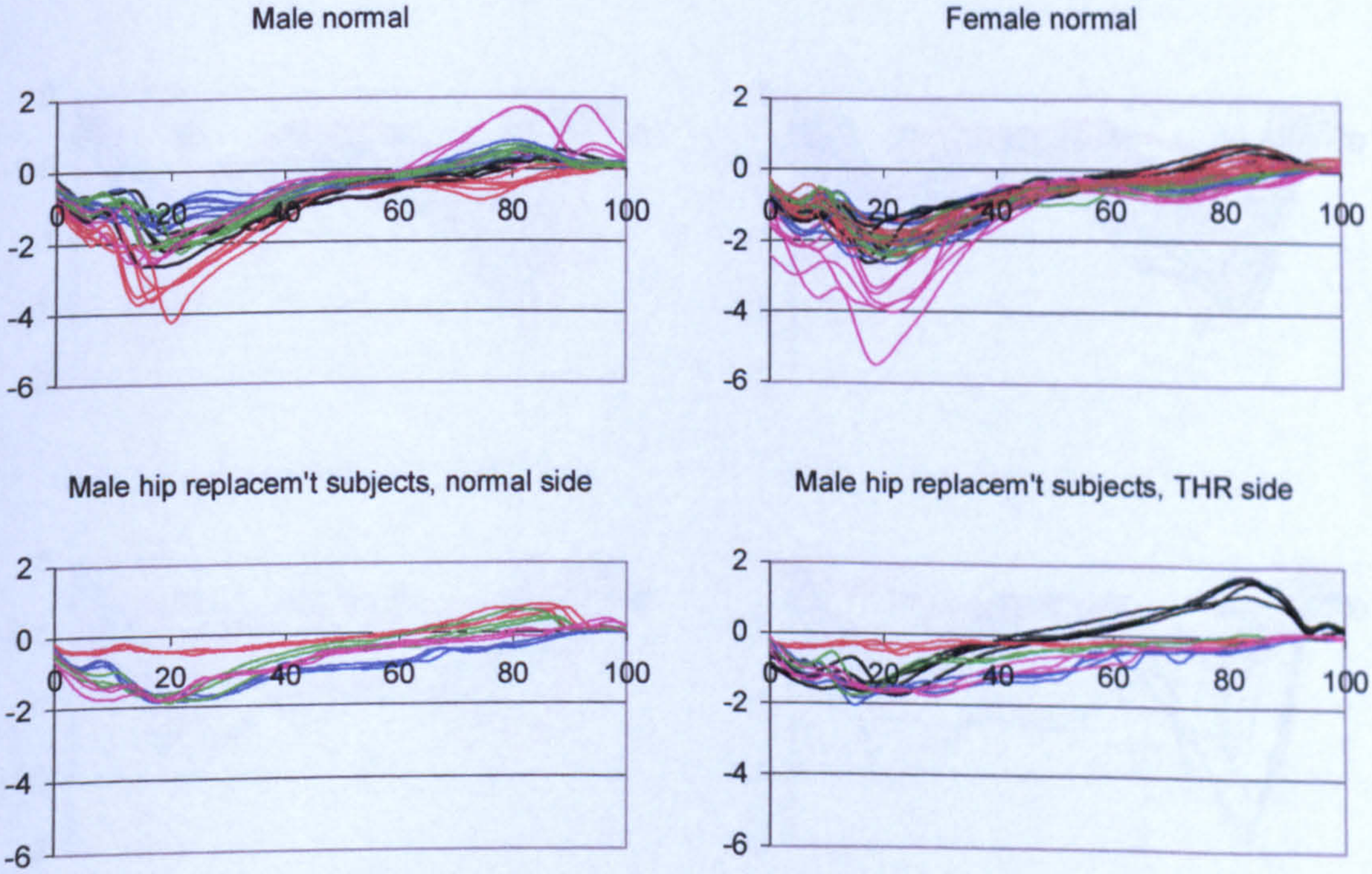

Figure A-VI.4.86 Camber foot down, XPA hip joint force

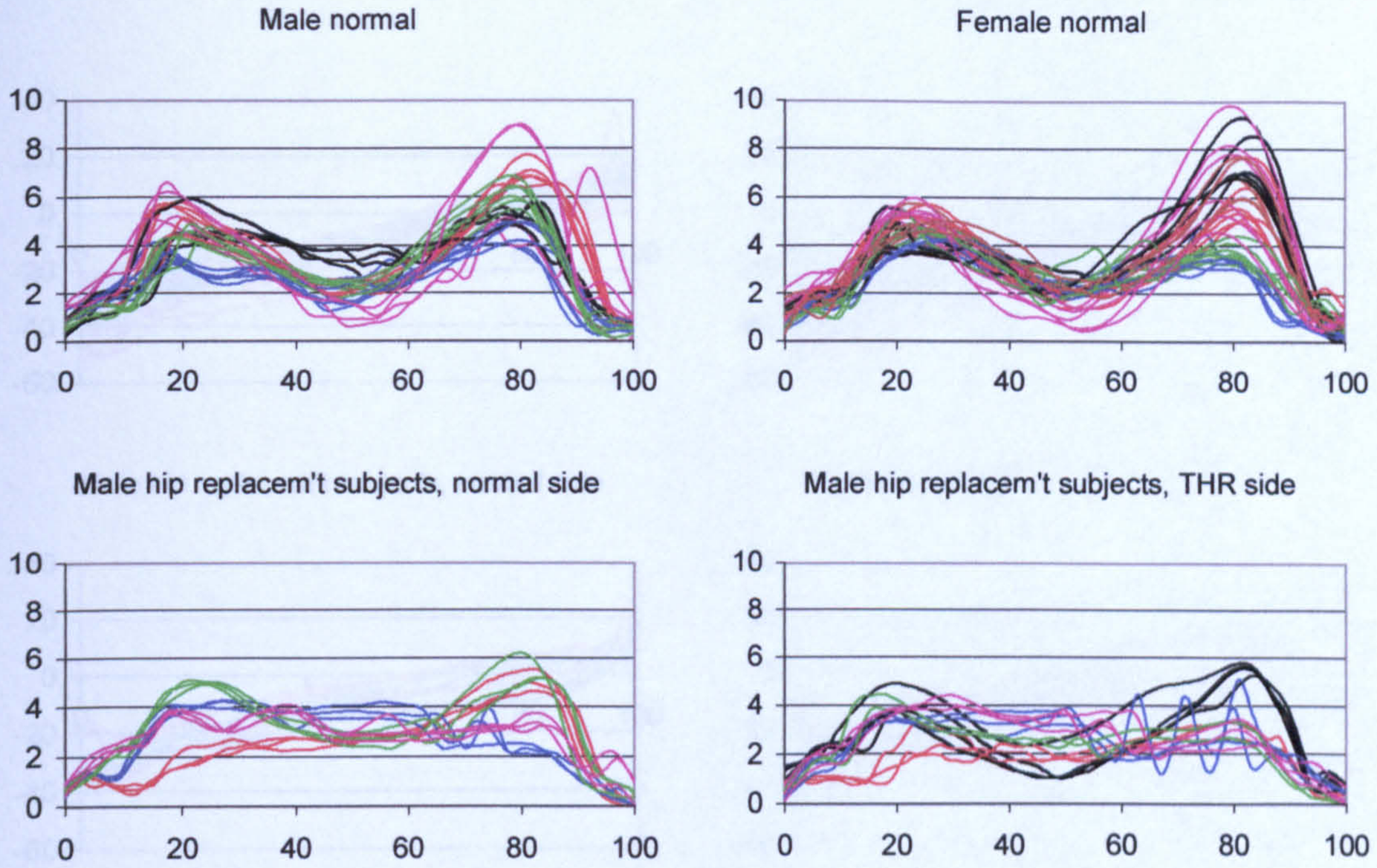

Figure A-VI.4.87 Camber foot down, YPA hip joint force

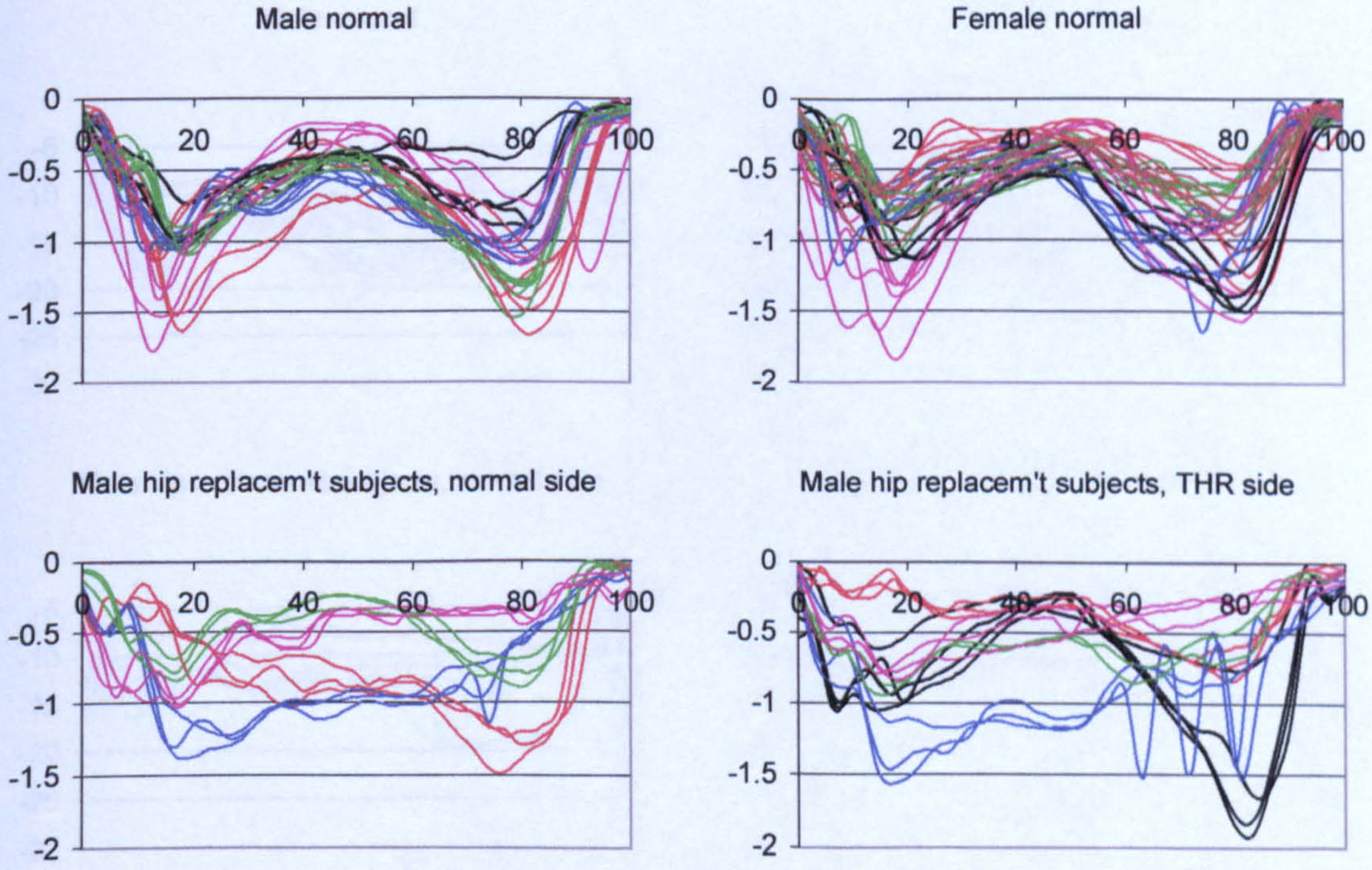

Figure A-VI.4.88 Camber foot down, ZPA hip joint force

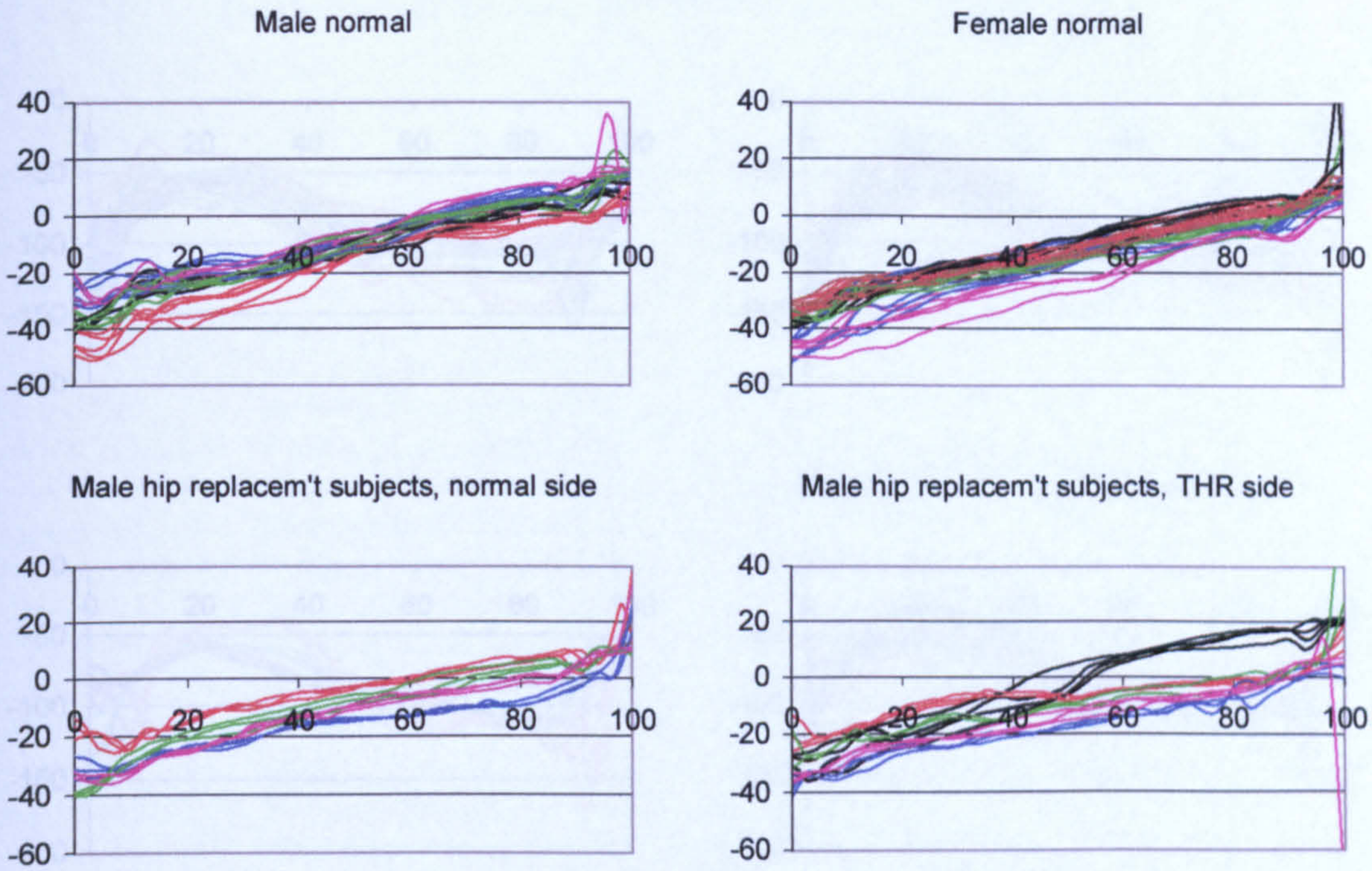

Camber foot down, HJYXANG (degrees, +ve = from YPA towards XPA) by % stance phase

Figure A-VI.4.89 Camber foot down, HJYXANG resultant hip joint force pelvic angle

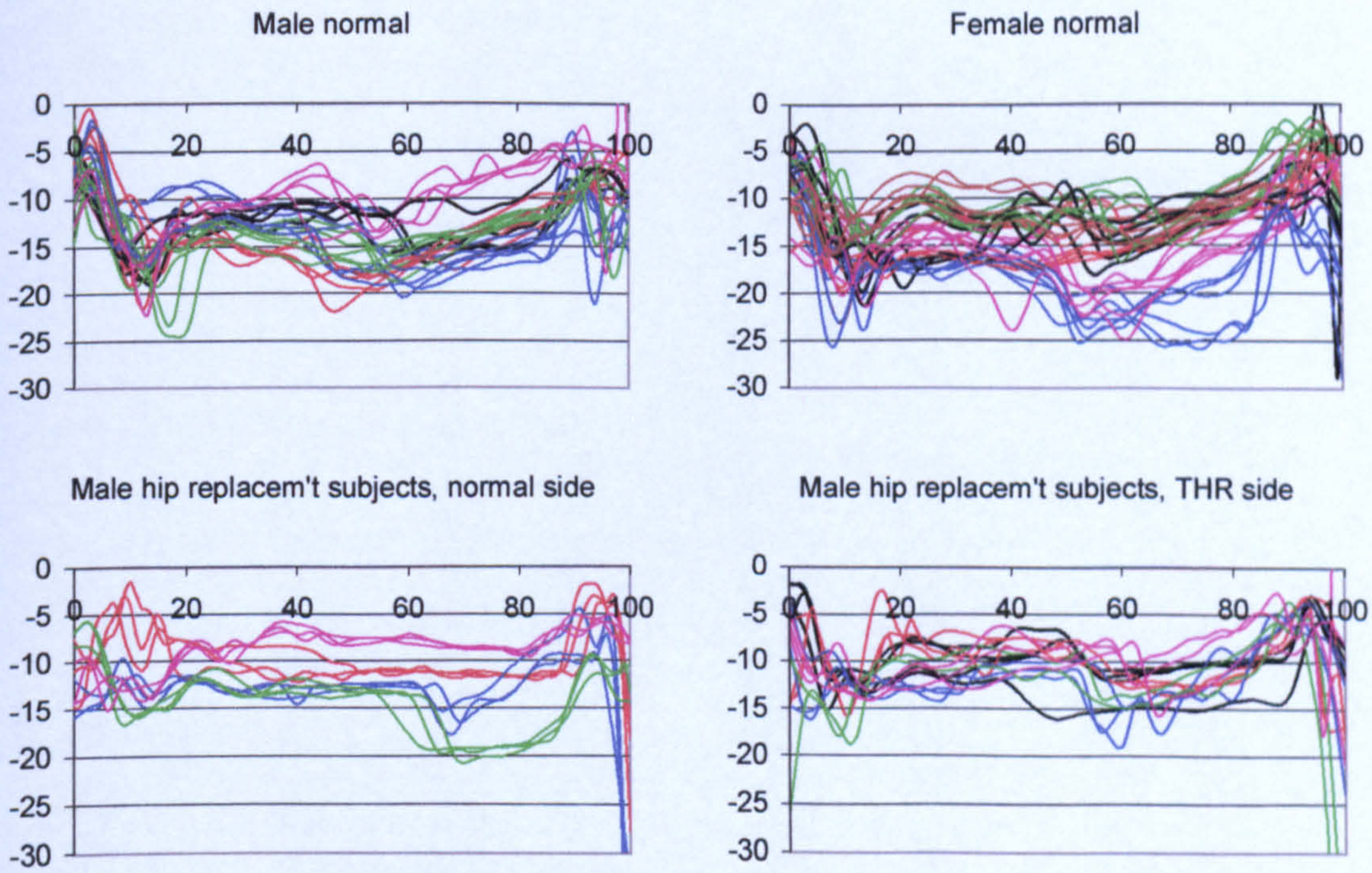

Camber foot down, FHYZANG (degrees, +ve = from YFA towards ZFA) by % stance phase

Figure A-VI.4.90 Camber foot down, HJYZANG resultant hip joint force pelvic angle

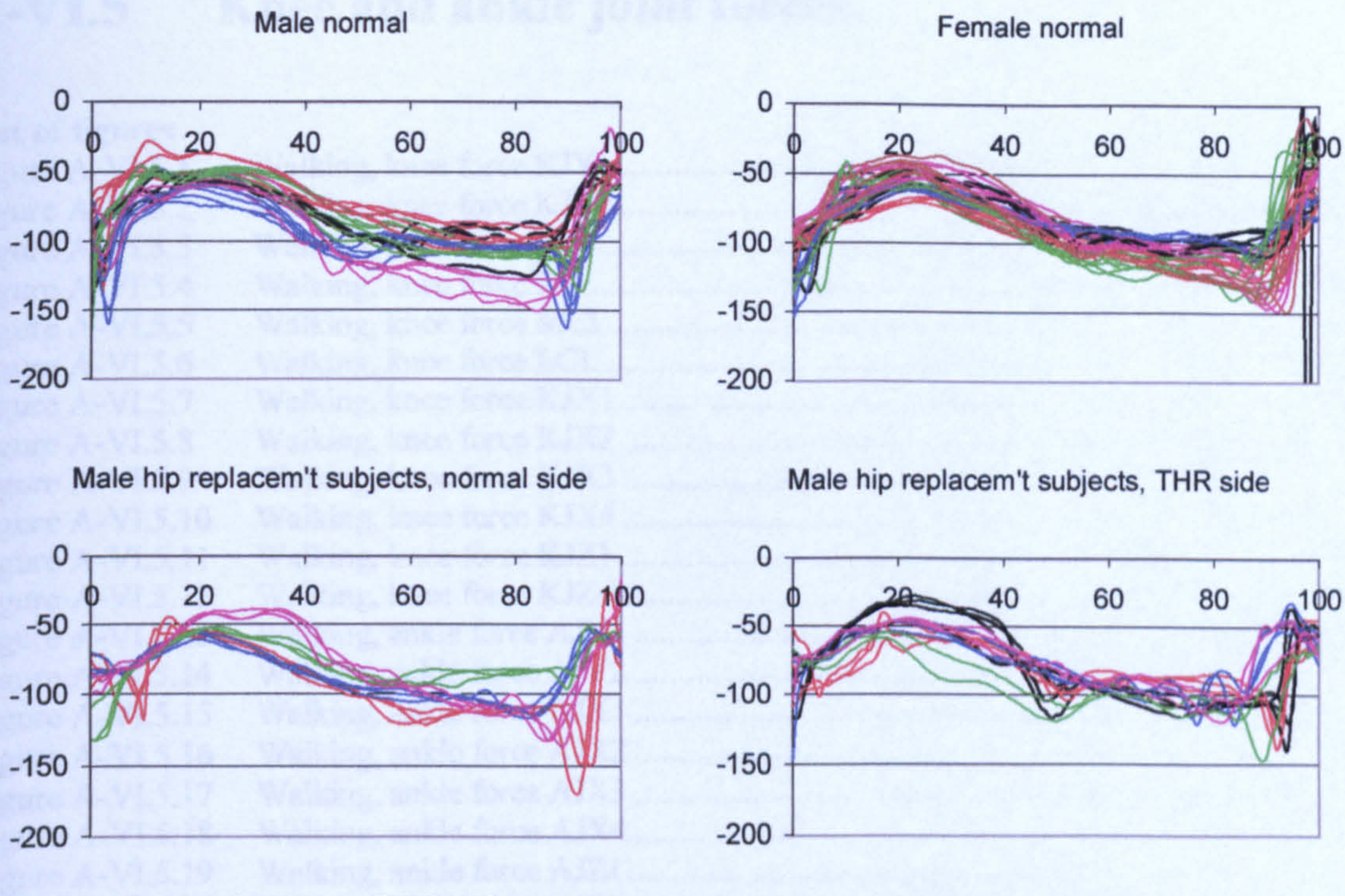

Figure A-VI.4.91 Camber foot down, HJXZANG resultant hip joint force pelvic angle

A-VI.5 Knee and ankle joint forces

List of figures

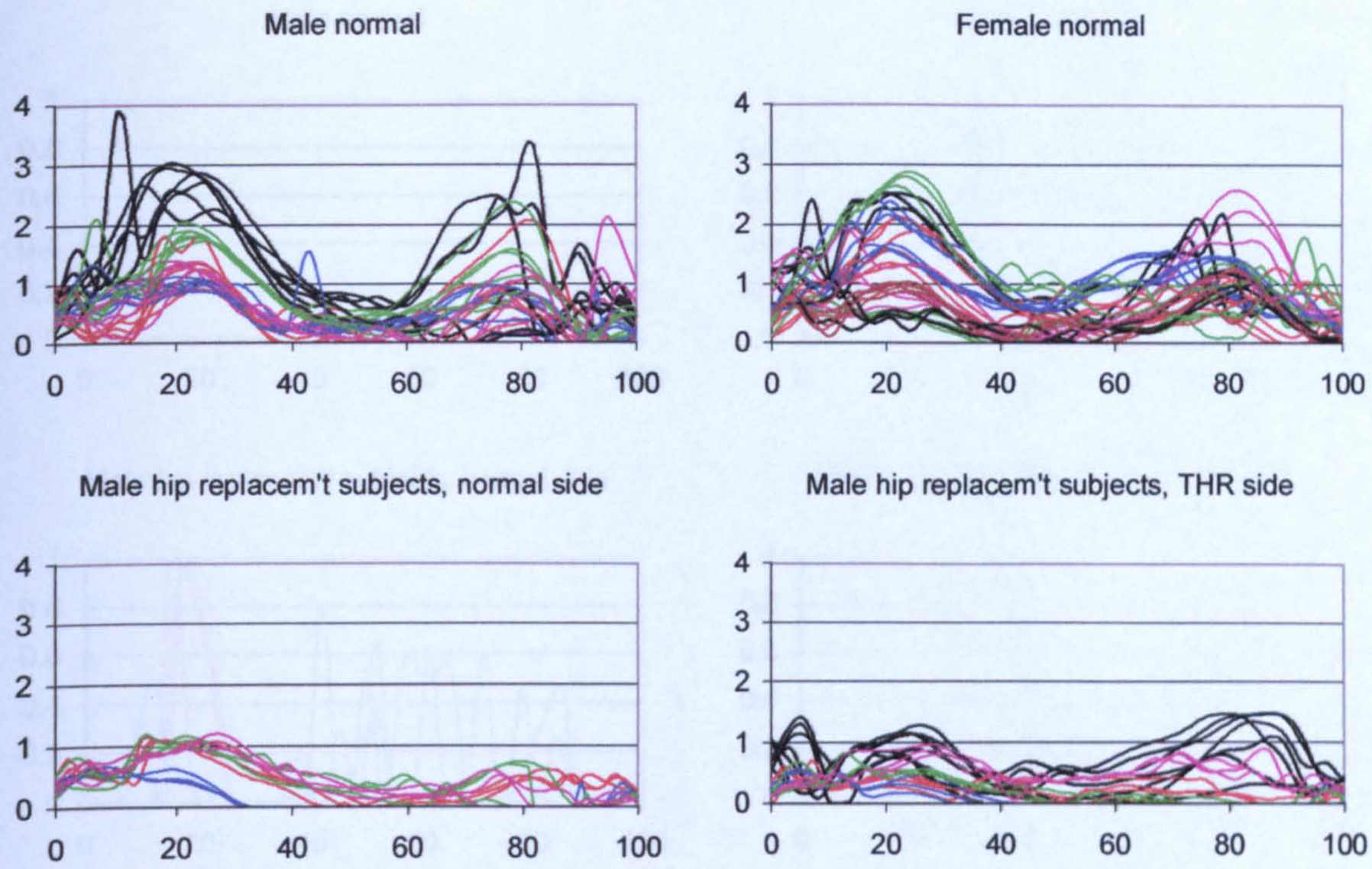

Figure A-VI.5.1 Walking, knee force KJY1

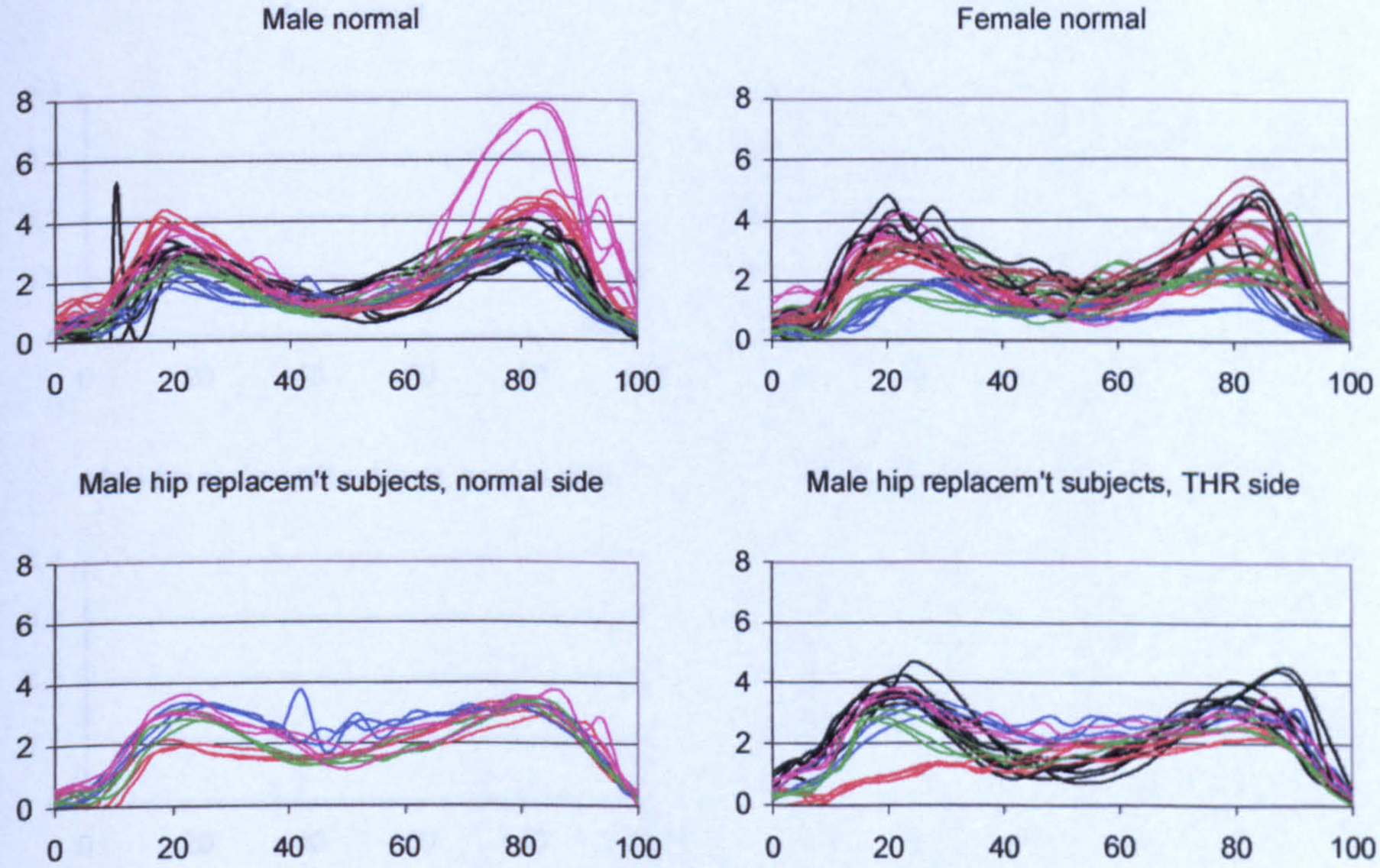

Figure A-VI.5.2 Walking, knee force KJY2

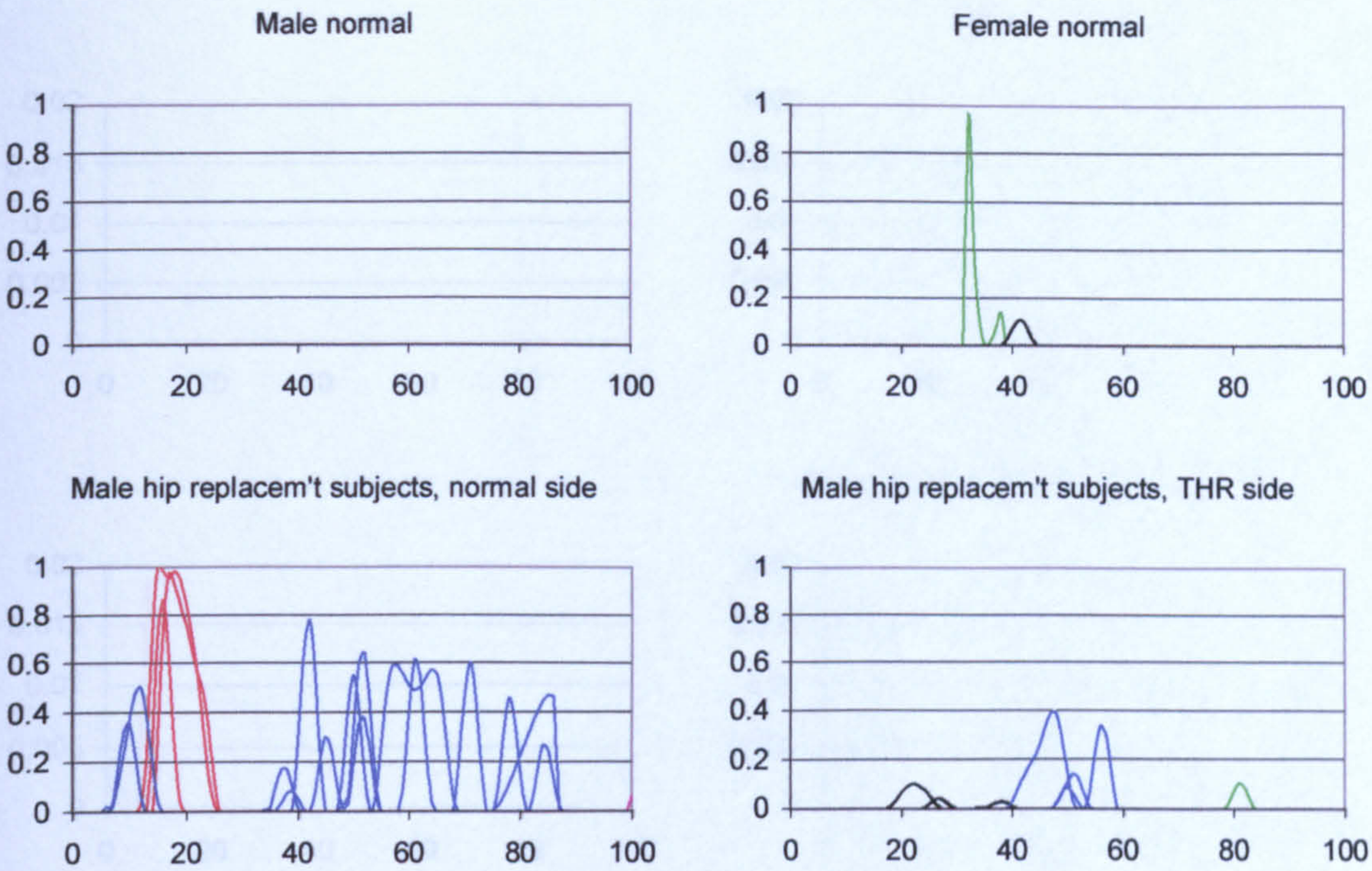

Figure A-VI.5.3 Walking, knee force ACL

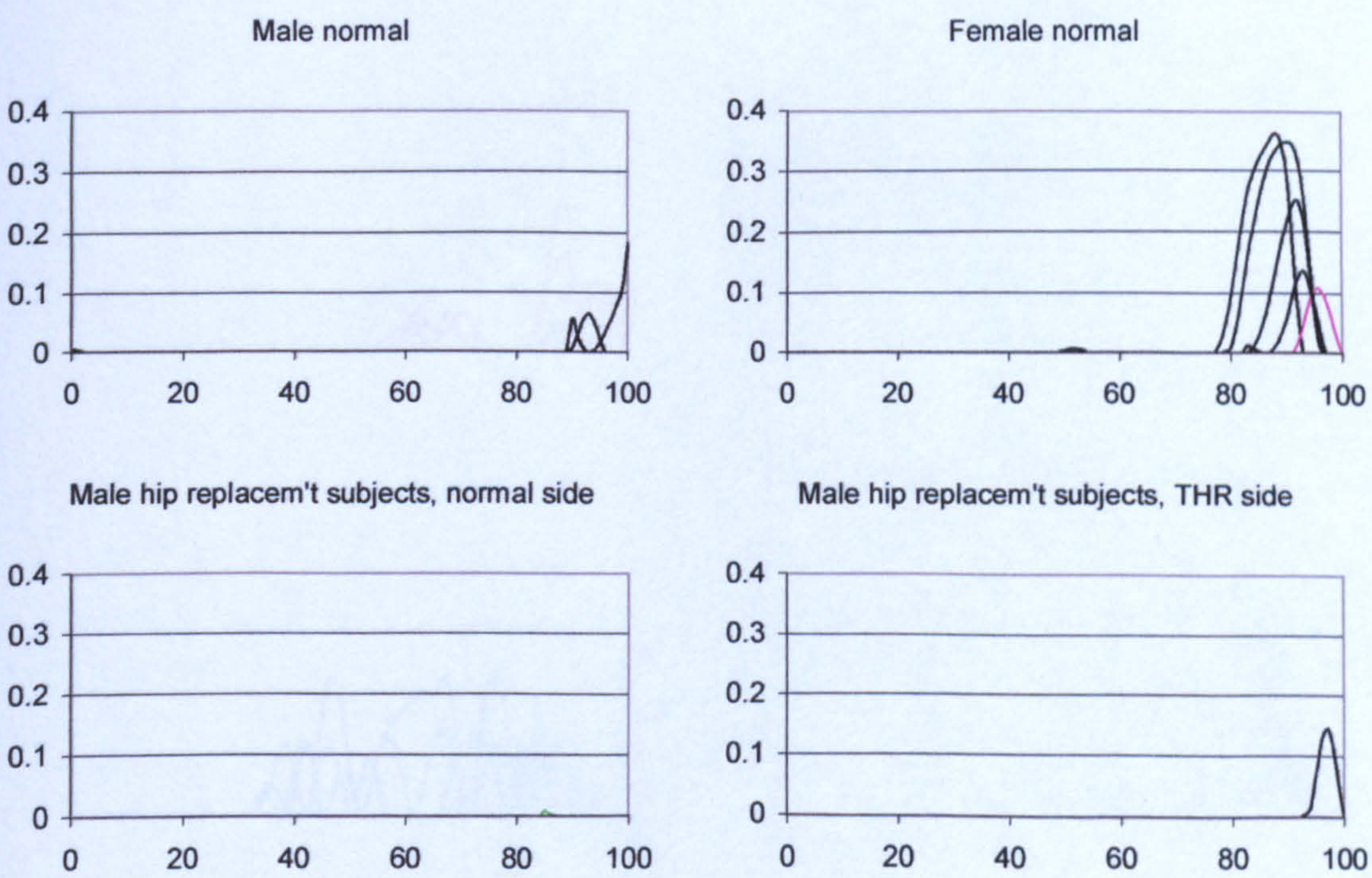

Figure A-VI.5.4 Walking, knee force PCL

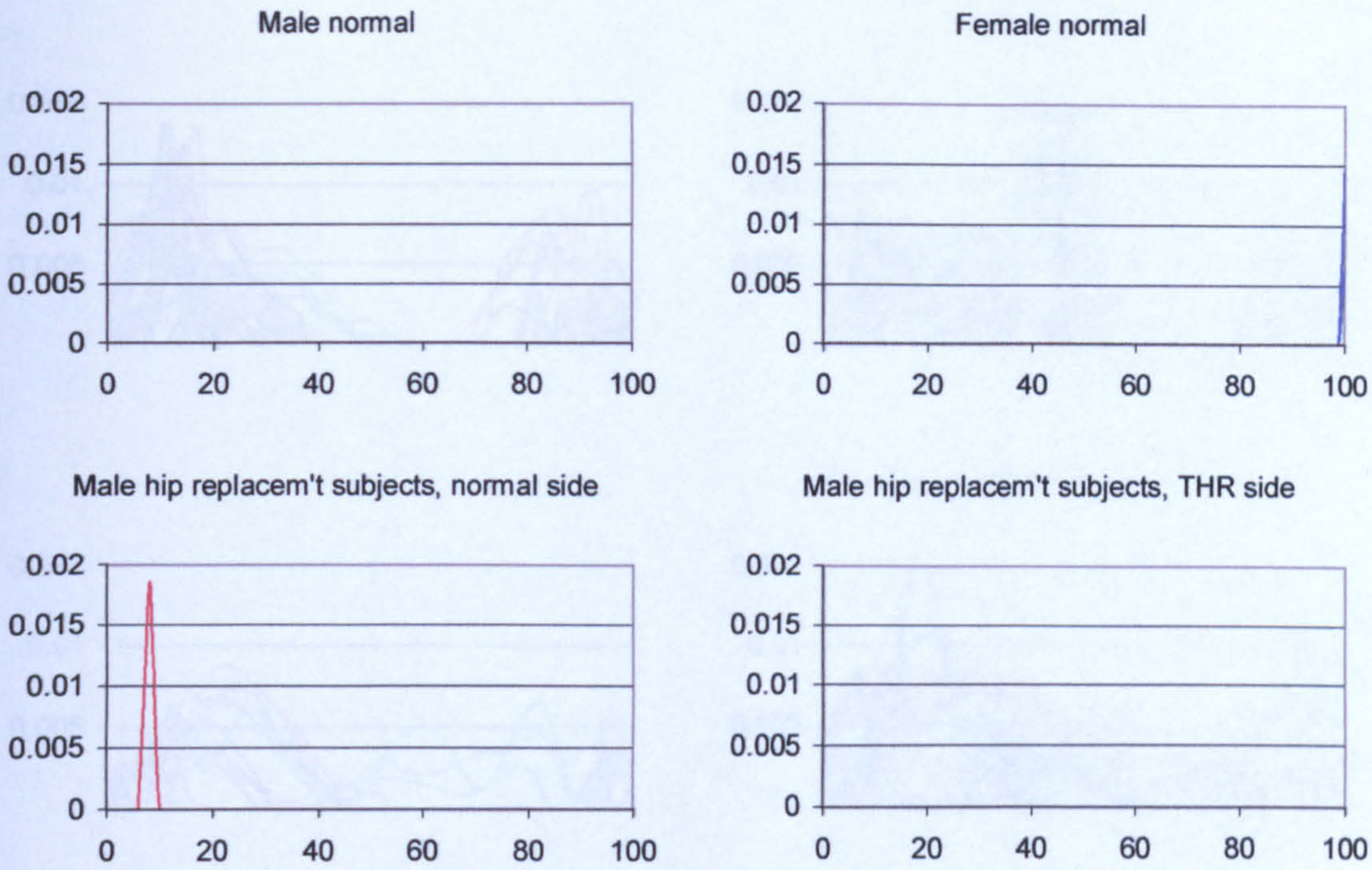

Figure A-VI.5.5 Walking, knee force MCL

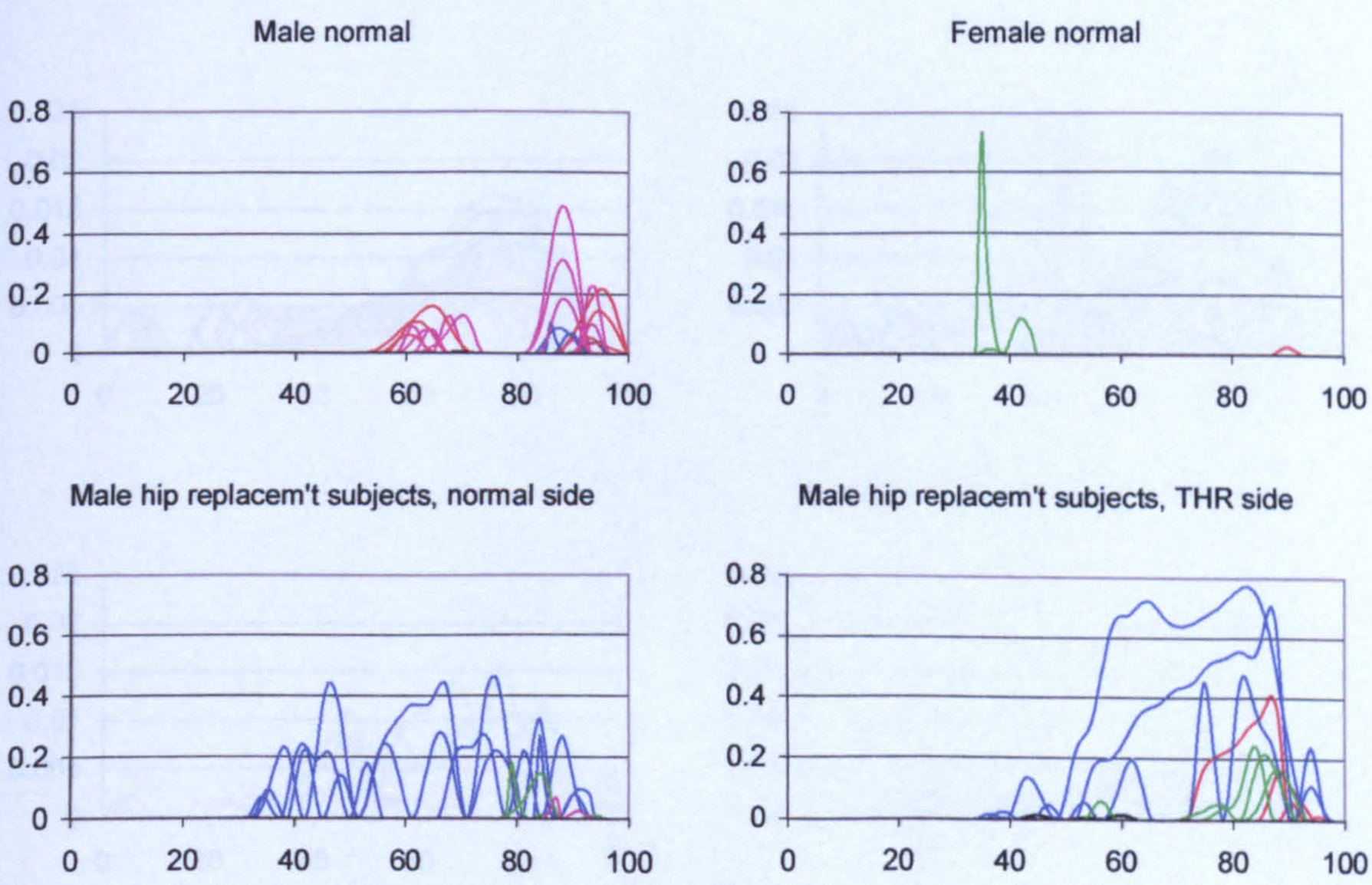

Figure A-VI.5.6 Walking, knee force LCL

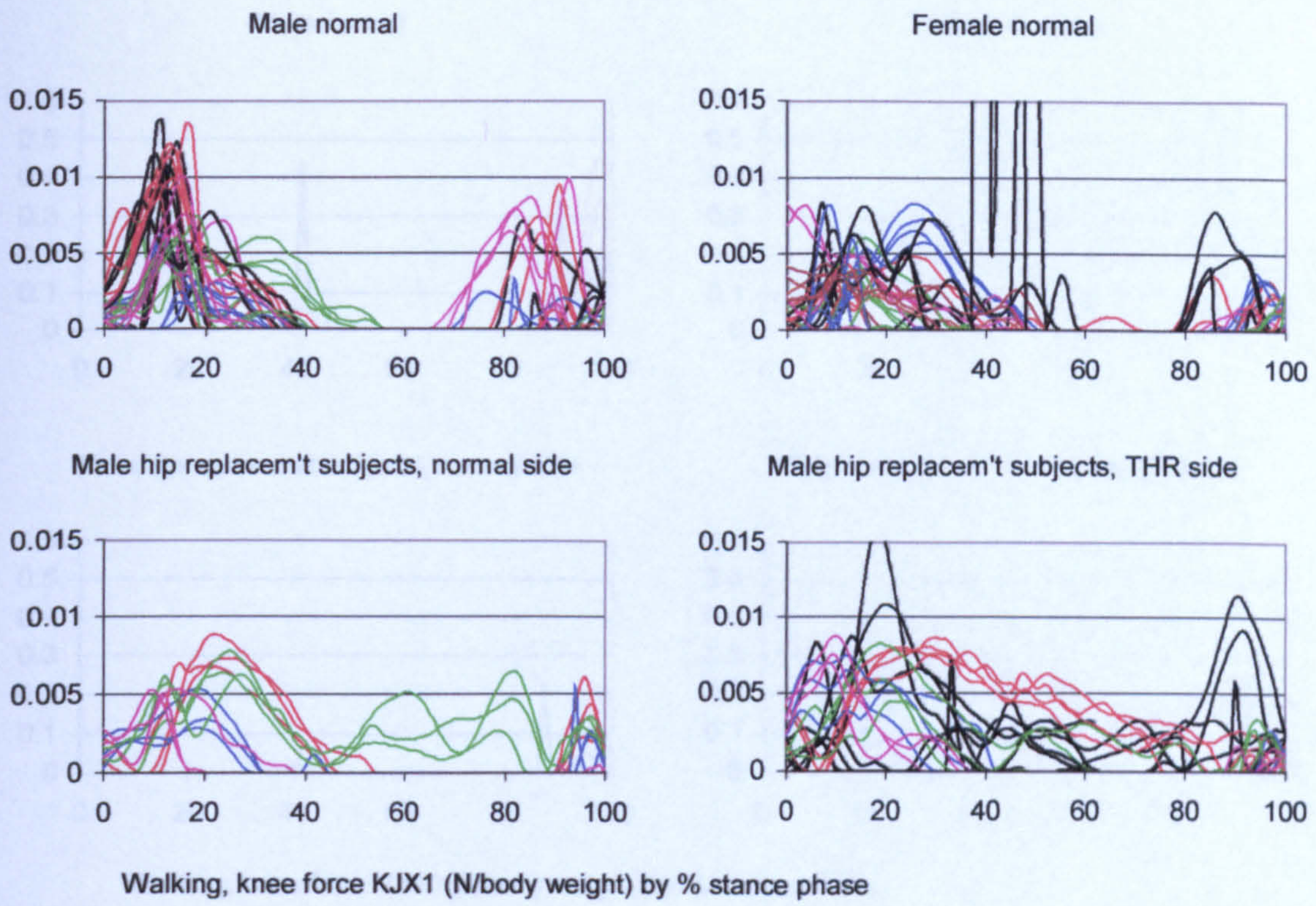

Figure A-VI.5.7 Walking, knee force KJX1

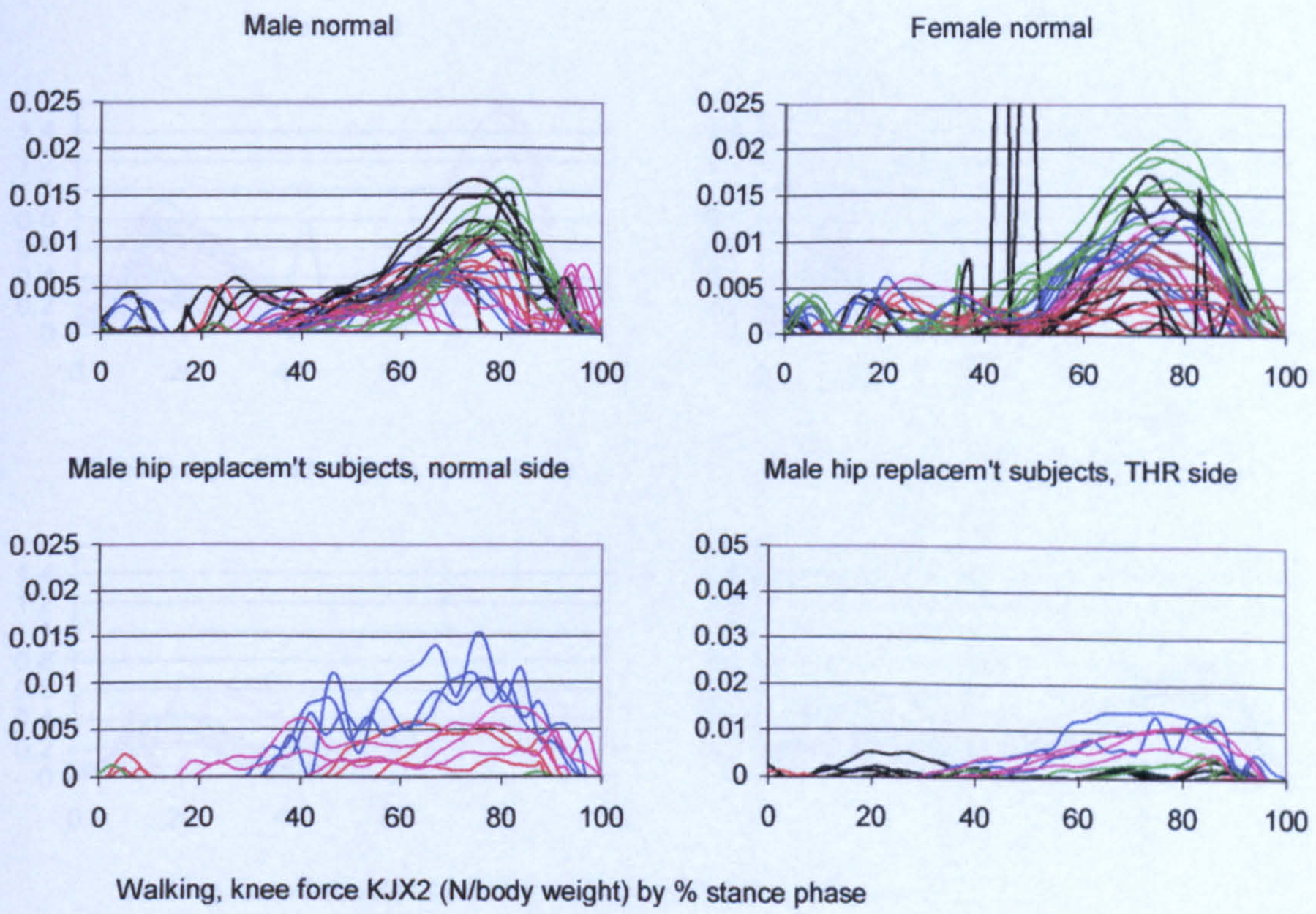

Figure A-VI.5.8 Walking, knee force KJX2

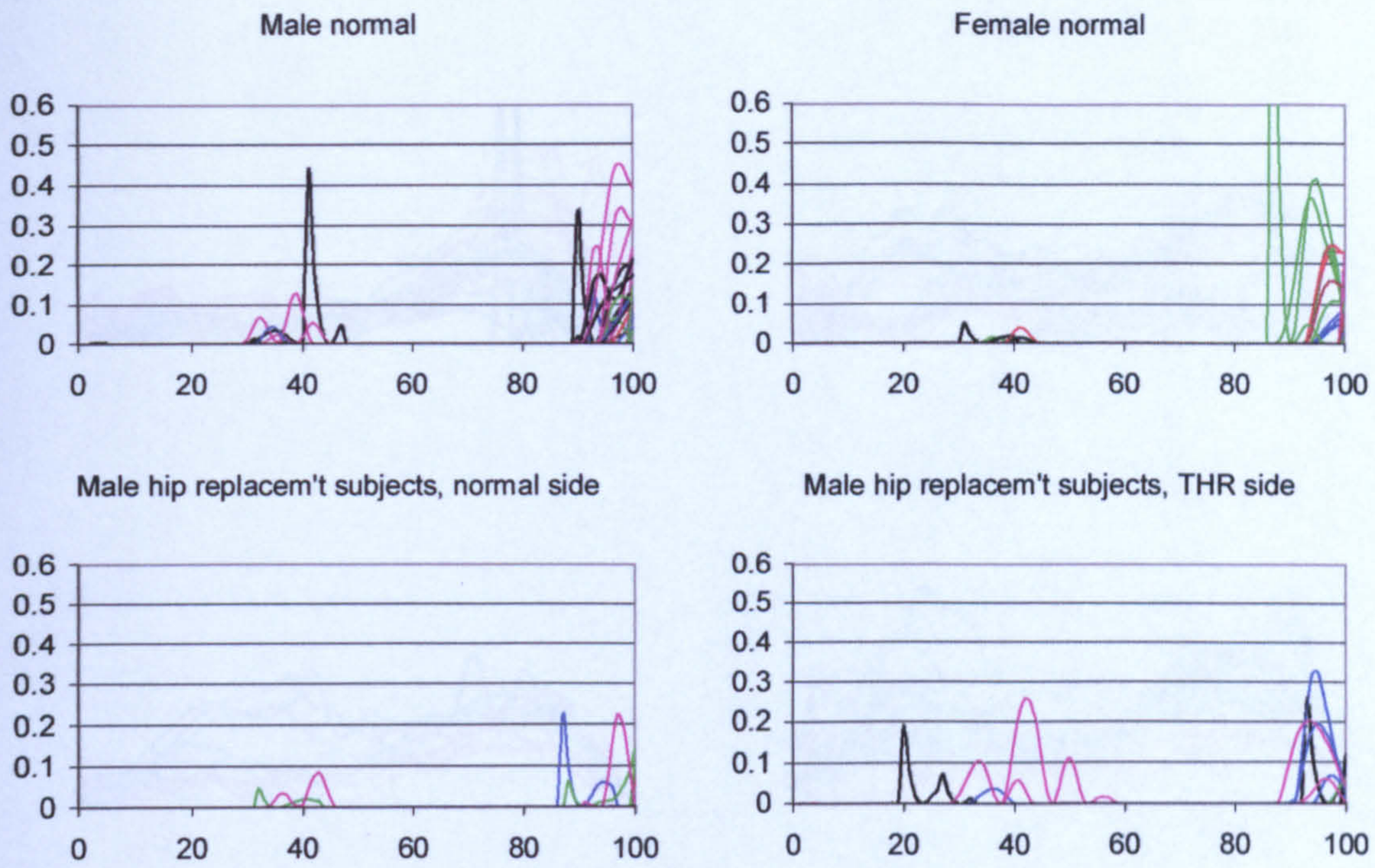

Figure A-VI.5.9 Walking, knee force KJX3

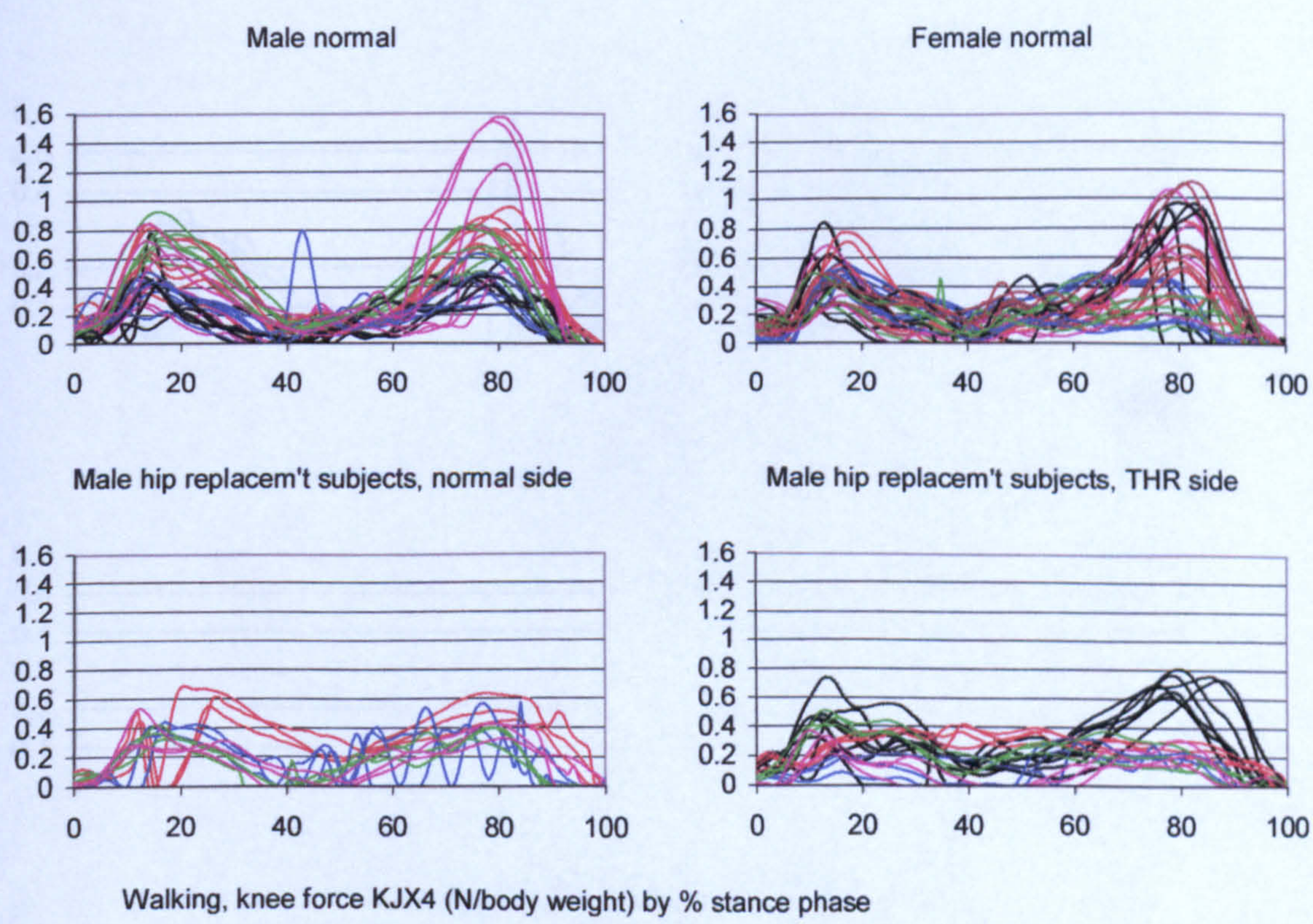

Figure A-VI.5.10 Walking, knee force KJX4

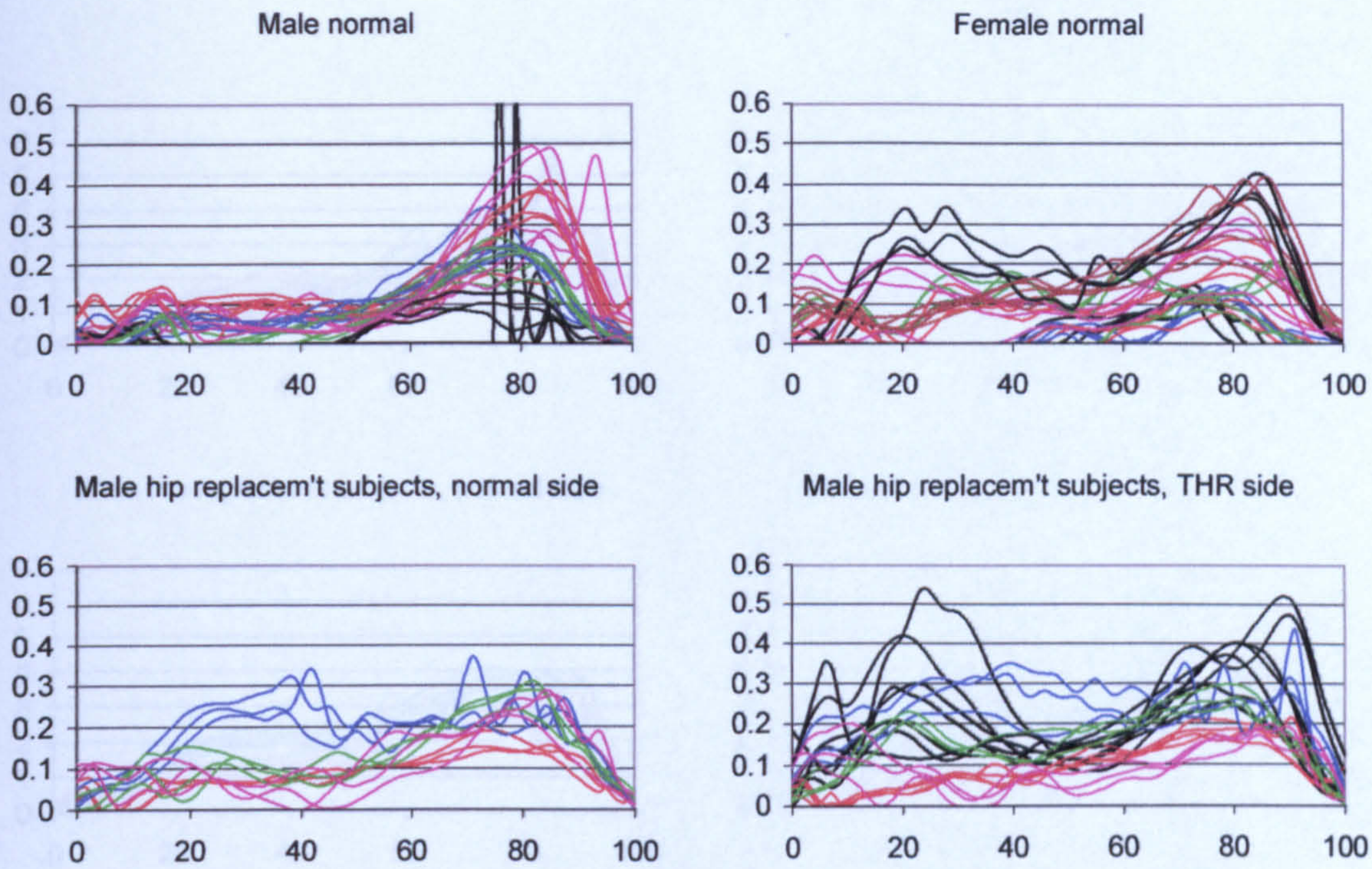

Figure A-VI.5.11 Walking, knee force KJZ1

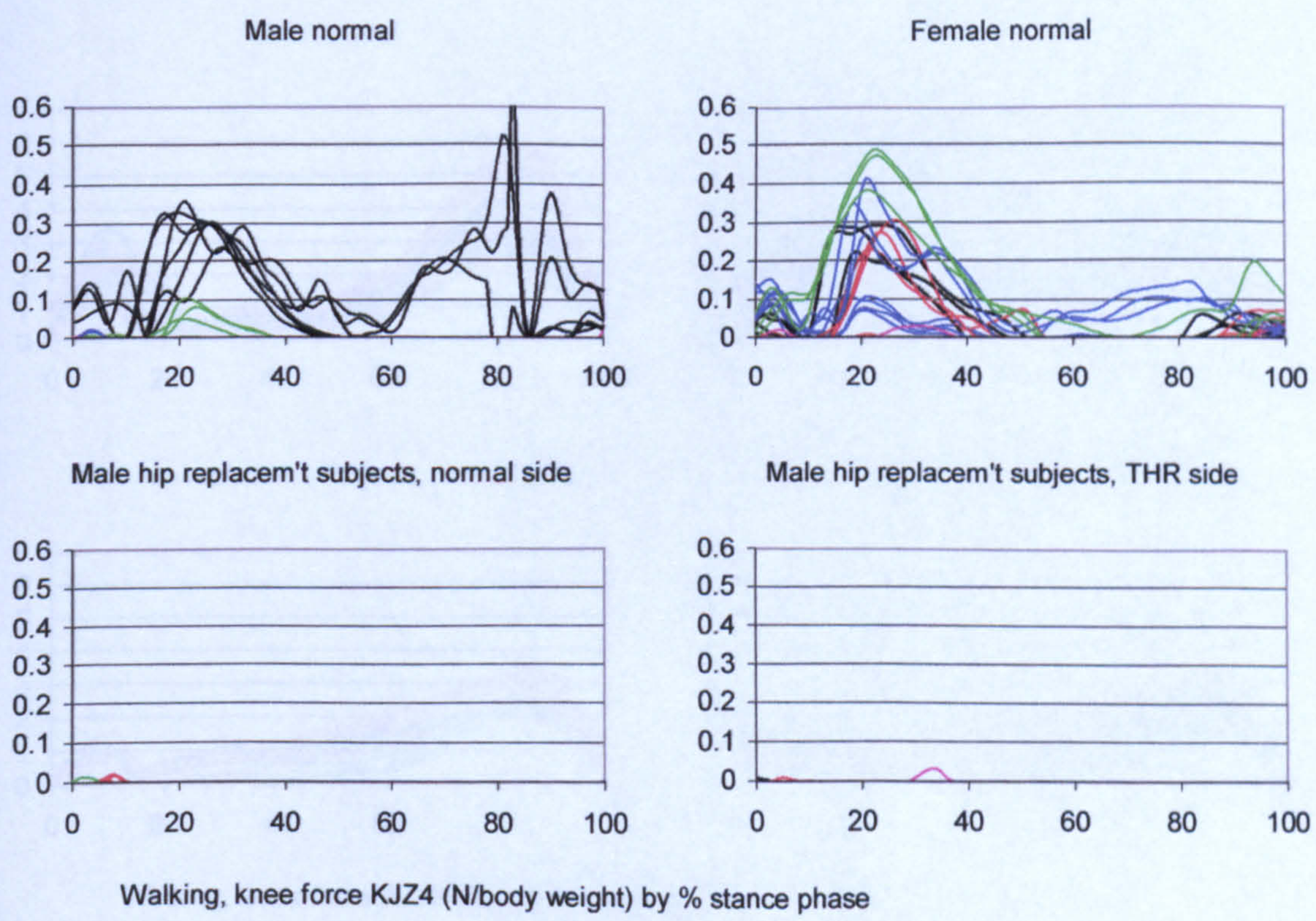

Figure A-VI.5.12 Walking, knee force KJZ4

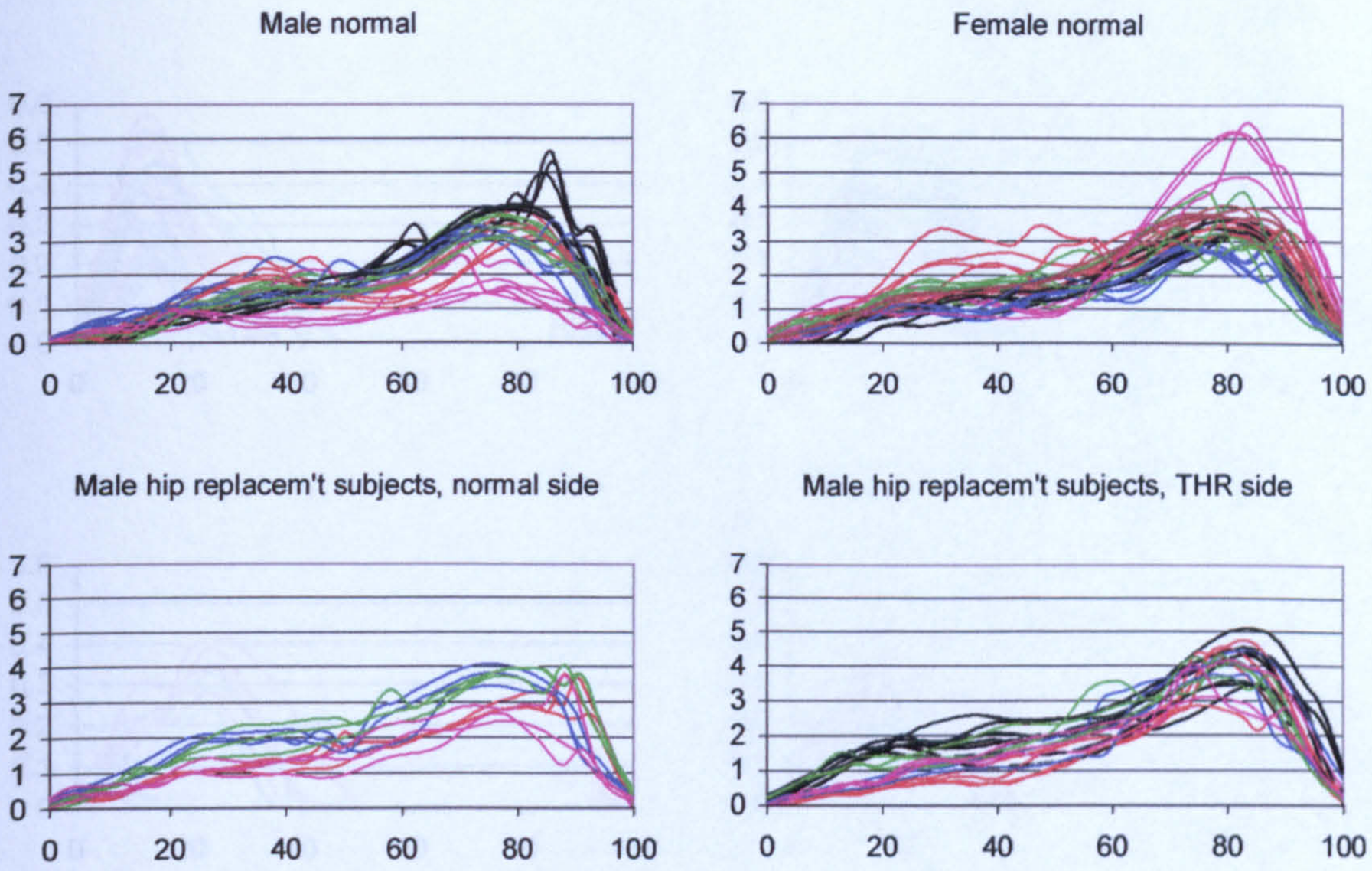

Figure A-VI.5.13 Walking, ankle force AJY1

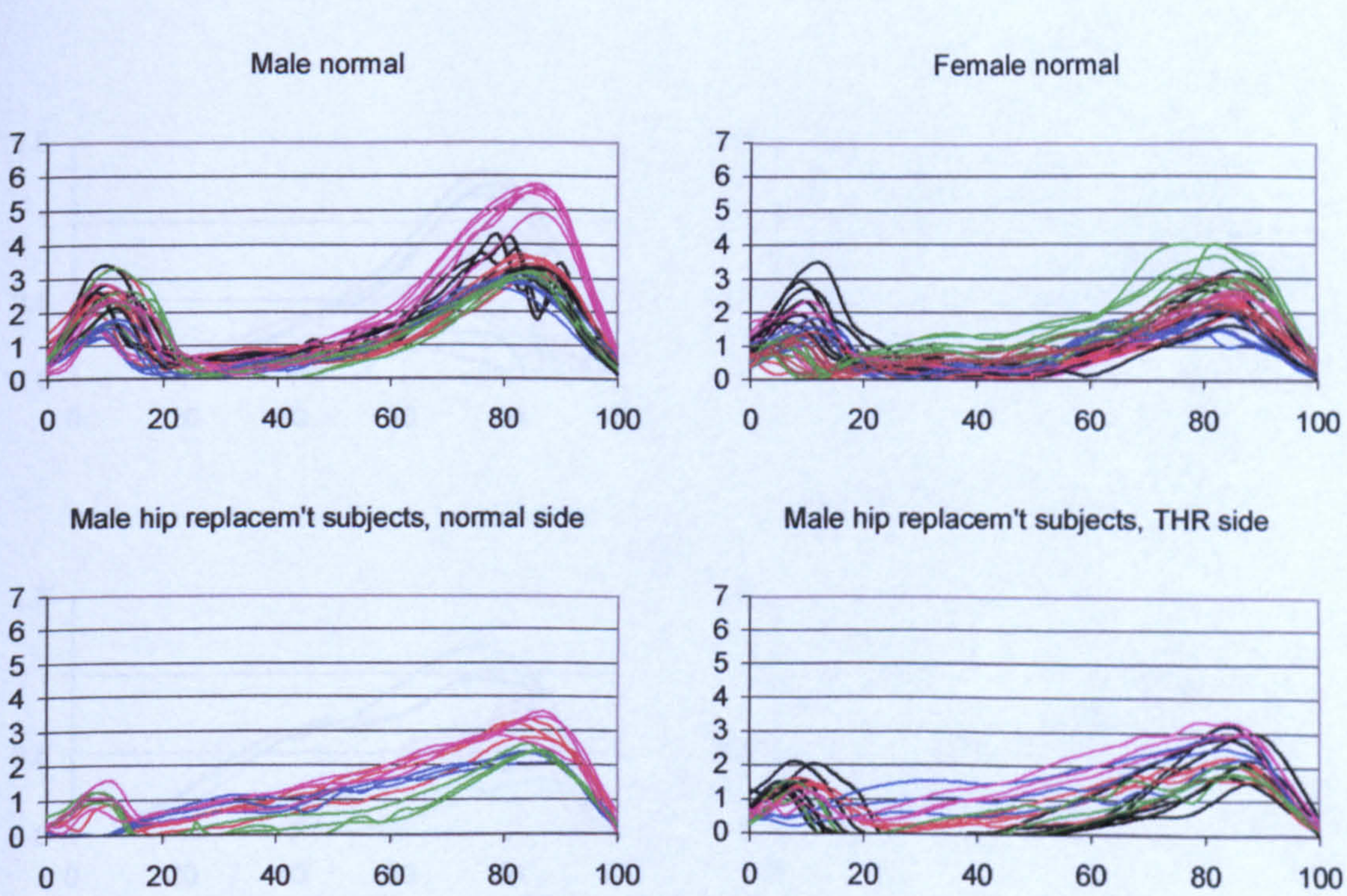

Figure A-VI.5.14 Walking, ankle force AJY2

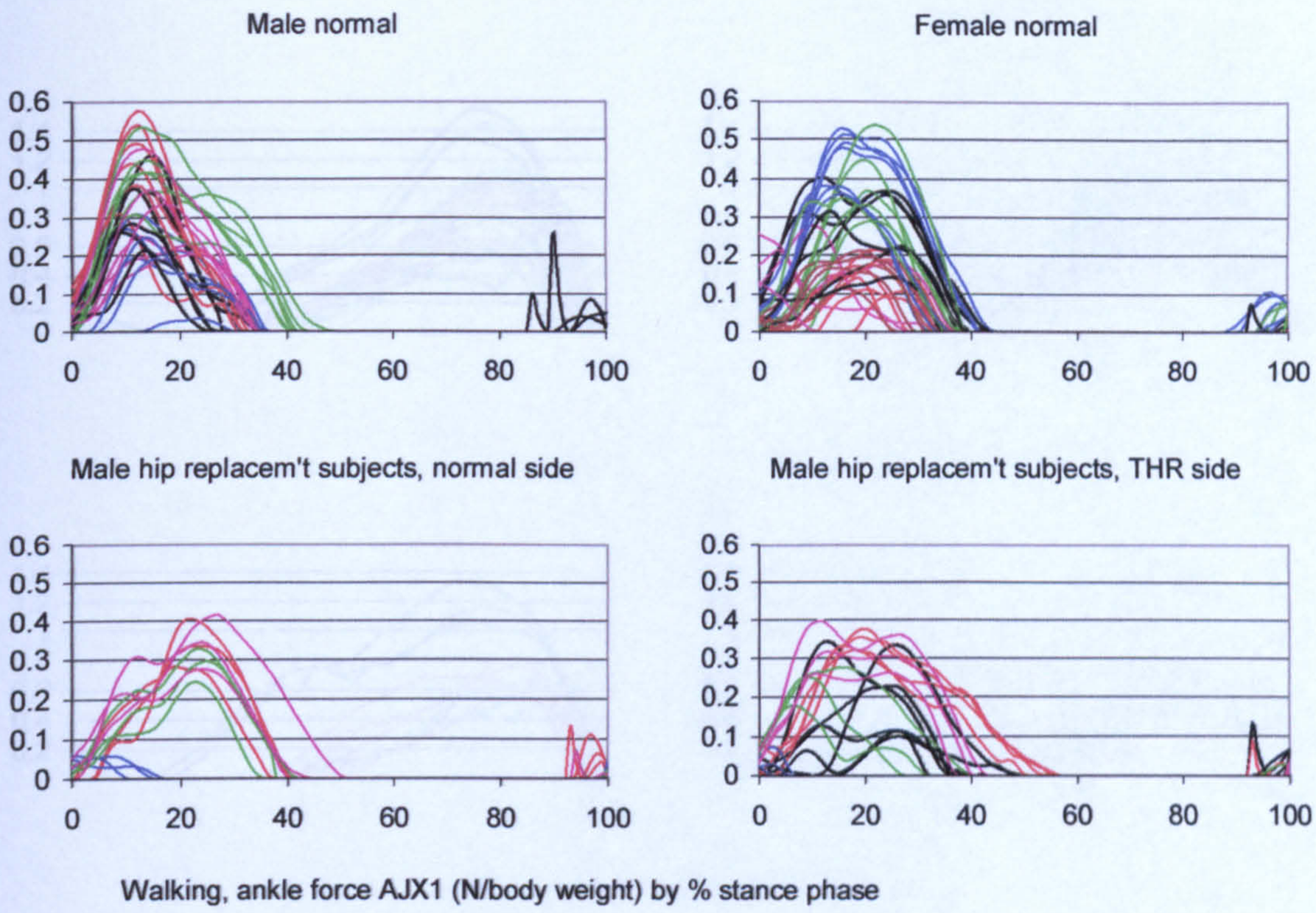

Figure A-VI.5.15 Walking, ankle force AJX1

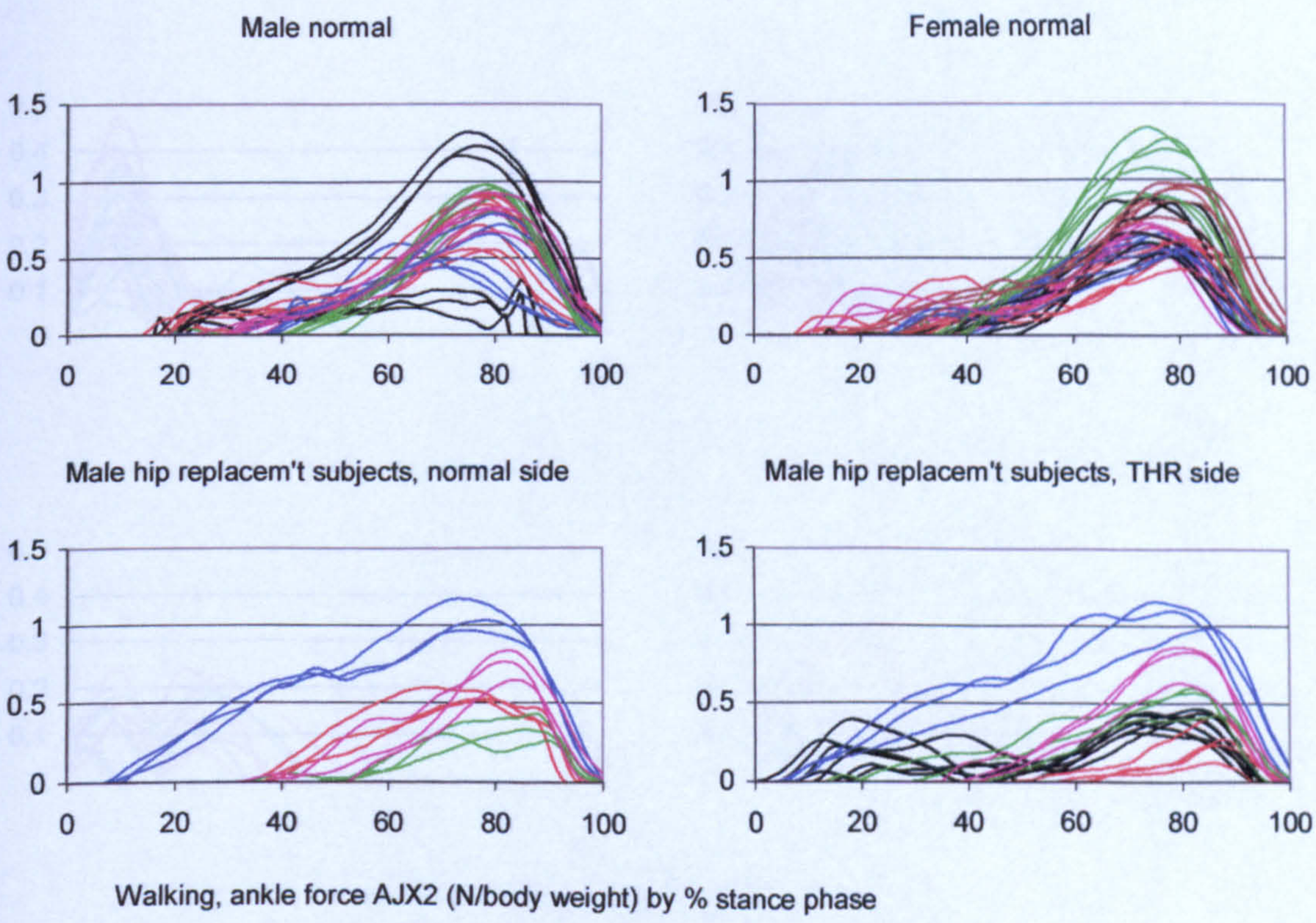

Figure A-VI.5.16 Walking, ankle force AJX2

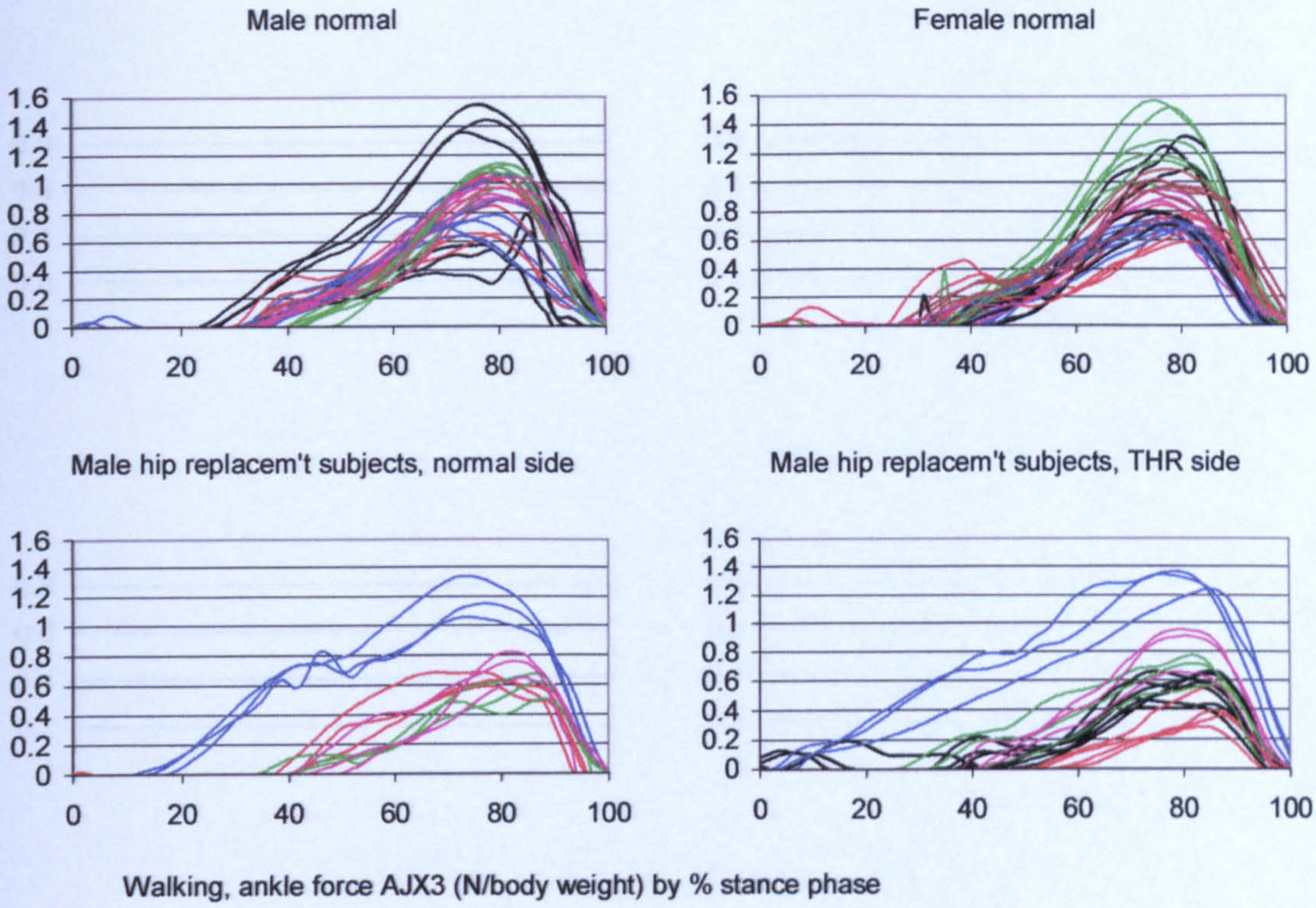

Figure A-VI.5.17 Walking, ankle force AJX3

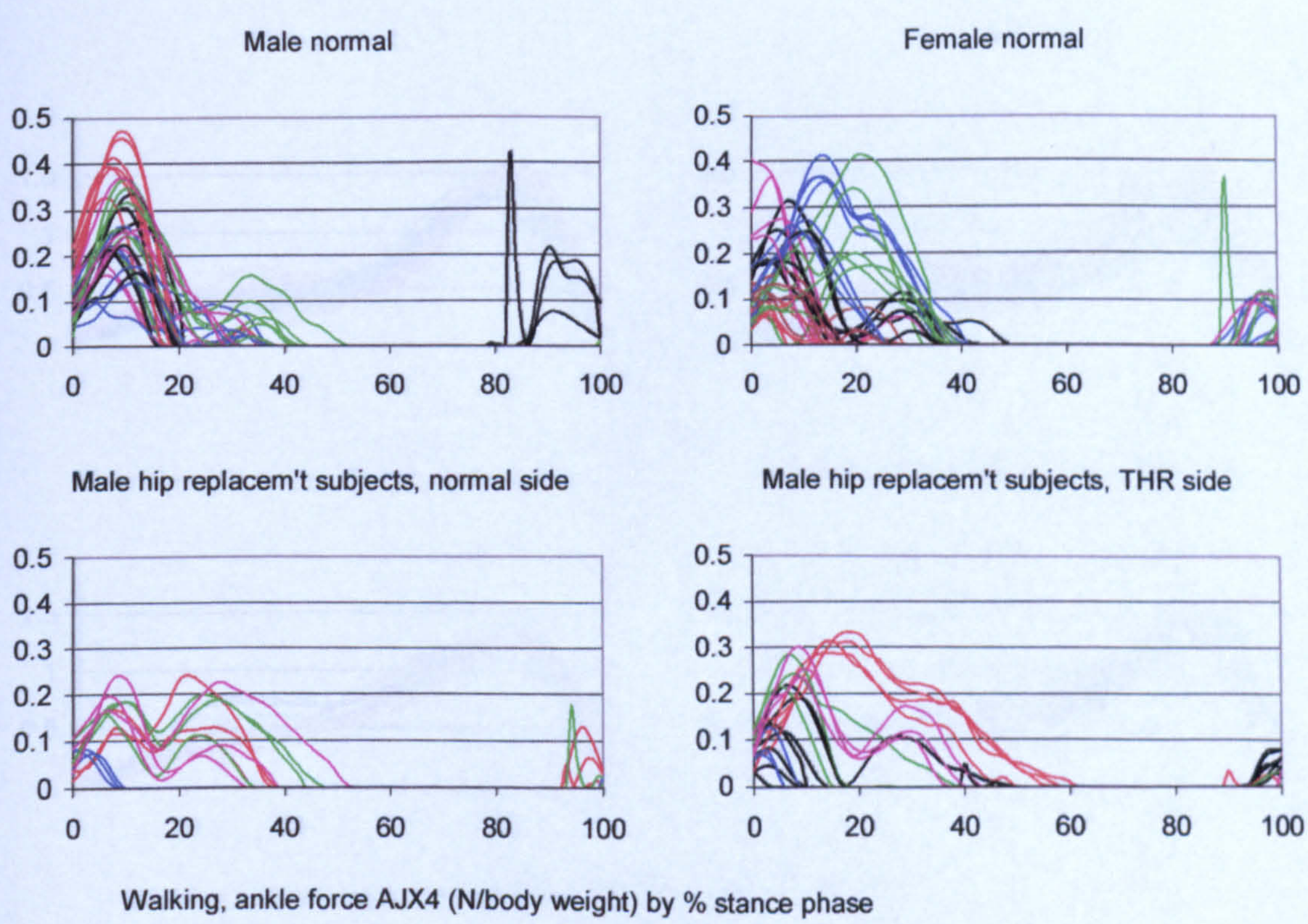

Figure A-VI.5.18 Walking, ankle force AJX4

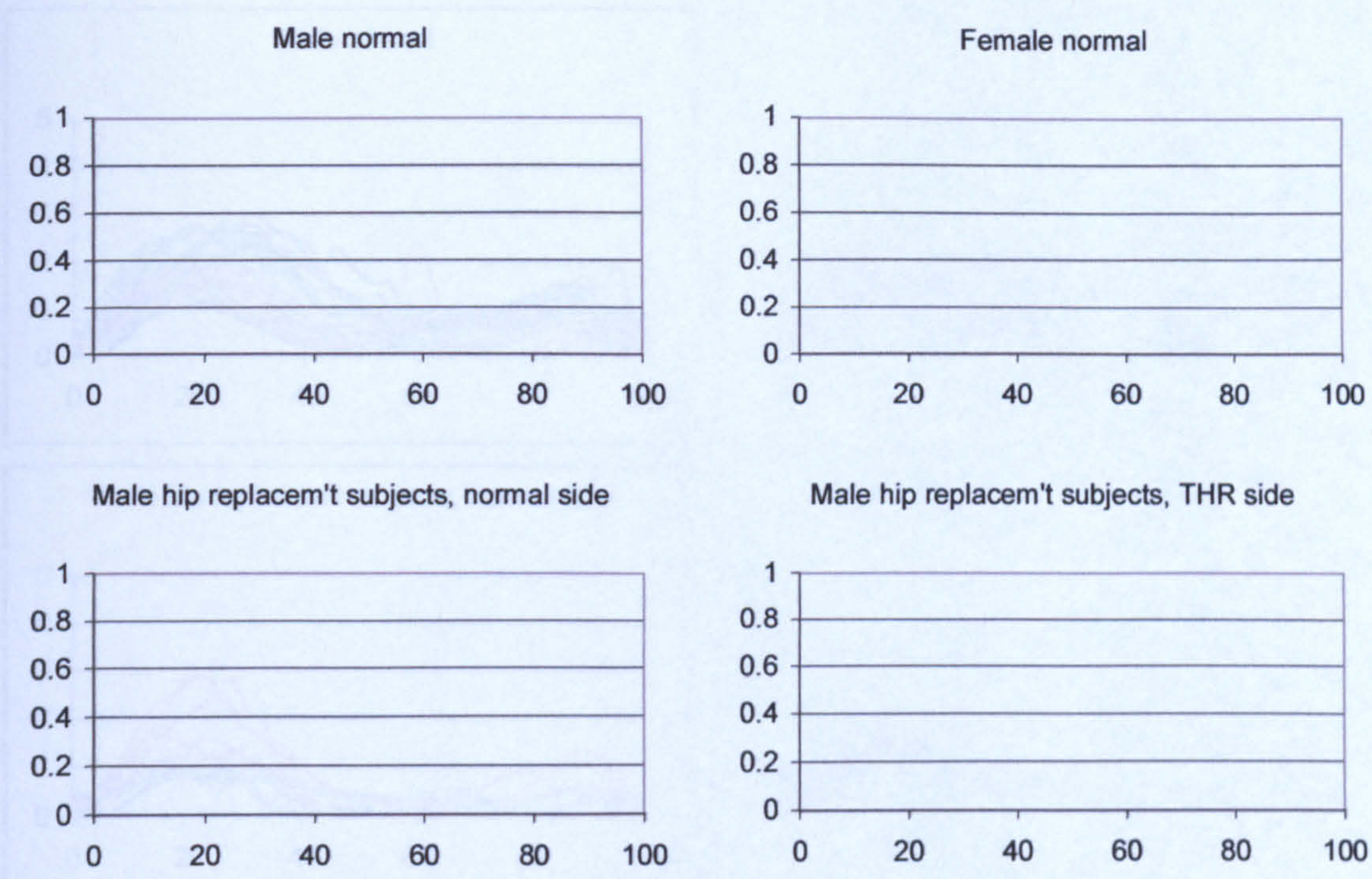

Figure A-VI.5.19 Walking, ankle force AJZ1

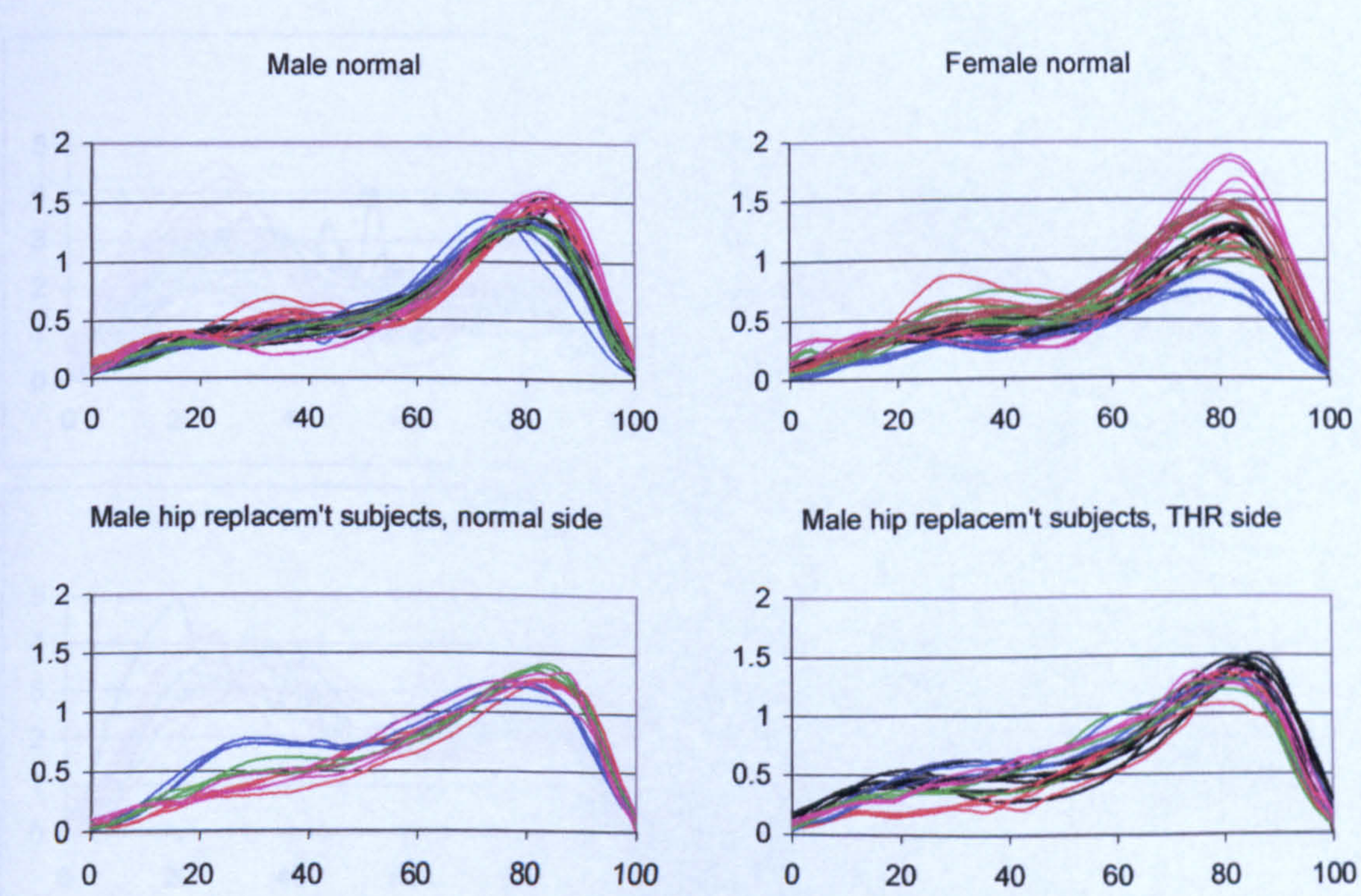

Figure A-VI.5.20 Walking, ankle force AJZ2

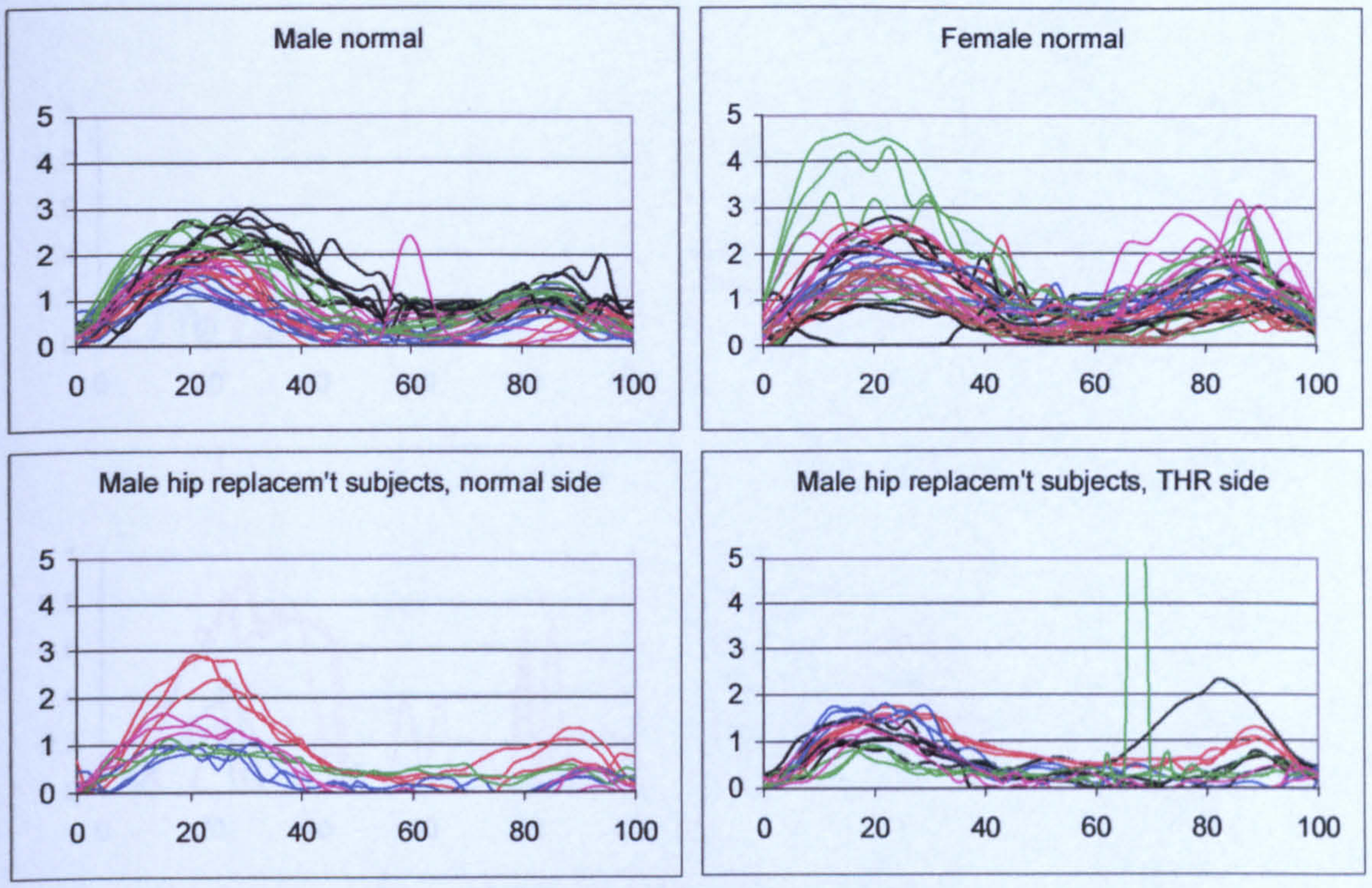

Stair ascent, knee force KJY1 (N/body weight) by % stance phase

Figure A-VI.5.21 Stair ascent, knee force KJY1

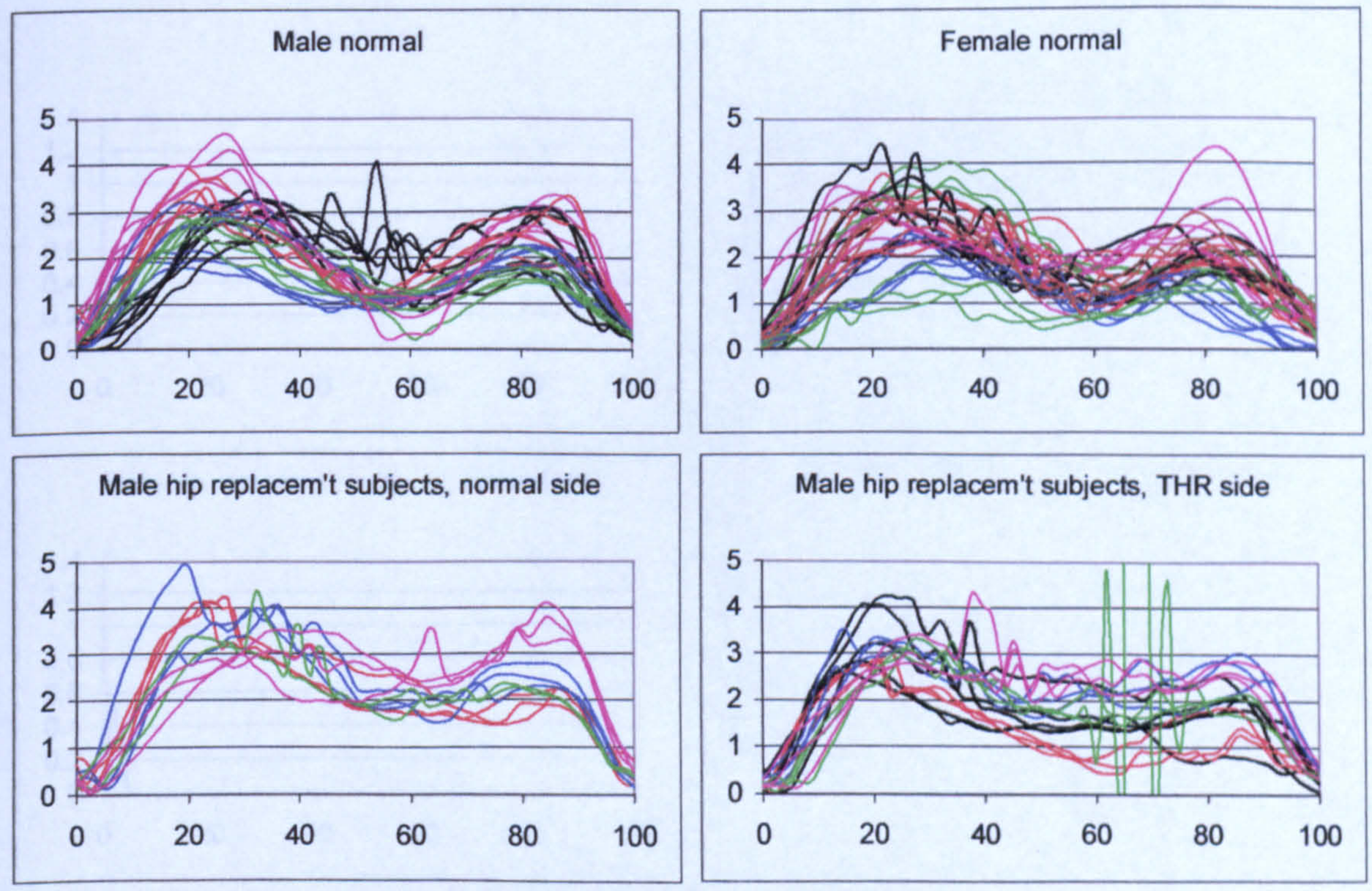

Stair ascent, knee force KJY2 (N/body weight) by % stance phase

Figure A-VI.5.22 Stair ascent, knee force KJY2

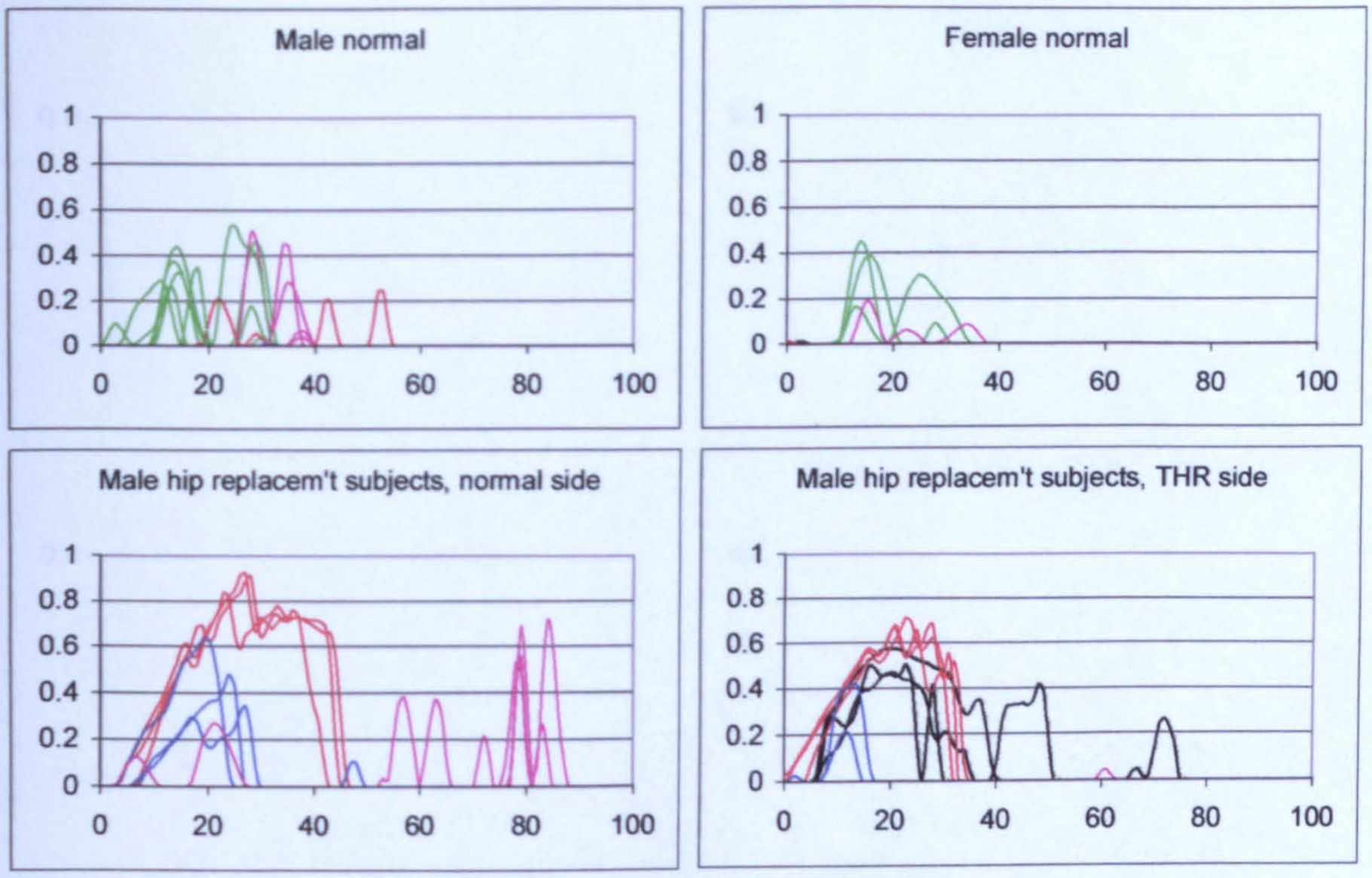

Stair ascent, knee force ACL (N/body weight) by % stance phase

Figure A-VI.5.23 Stair ascent, knee force ACL

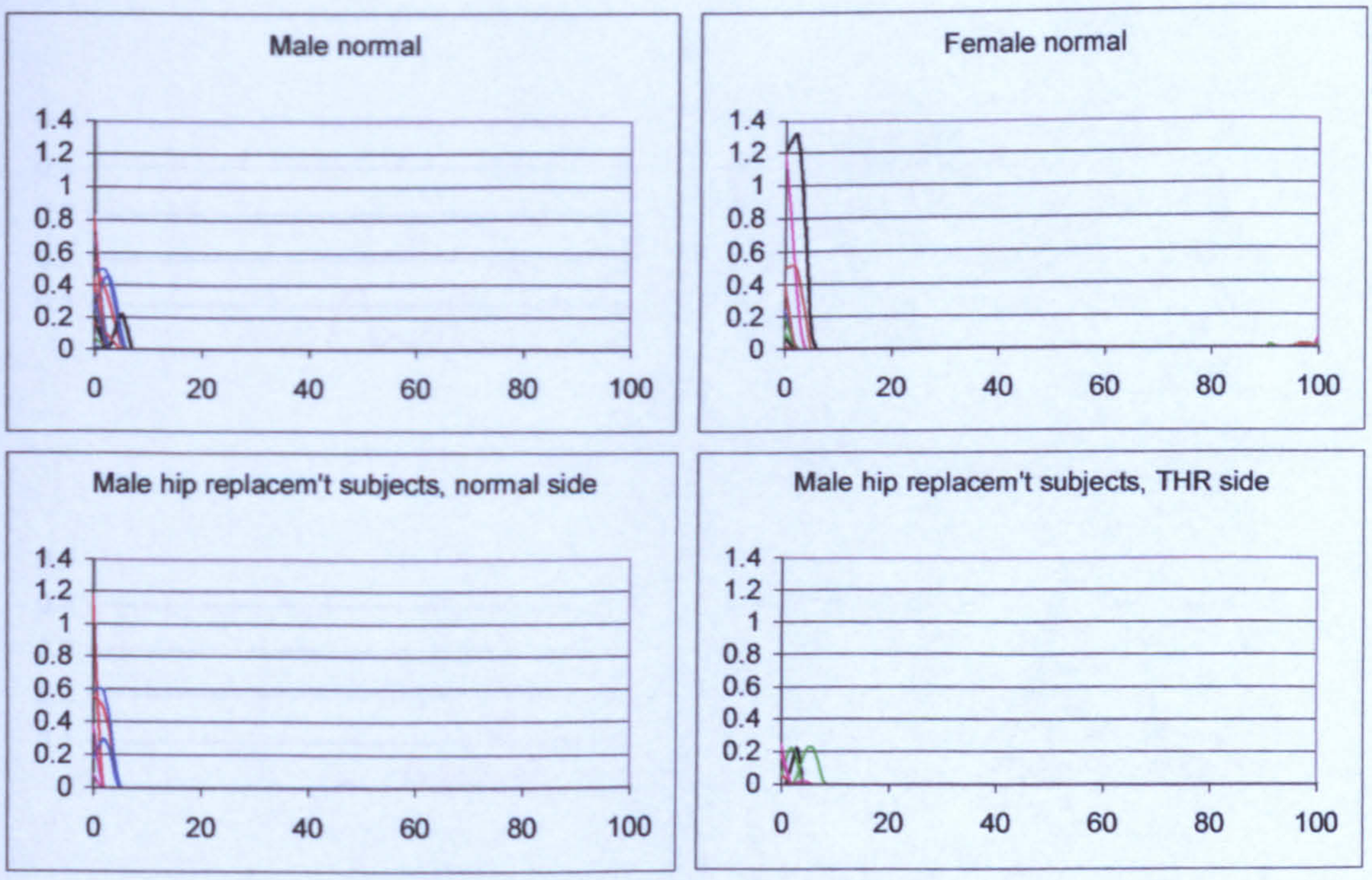

Stair ascent, knee force PCL (N/body weight) by % stance phase

Figure A-VI.5.24 Stair ascent, knee force PCL

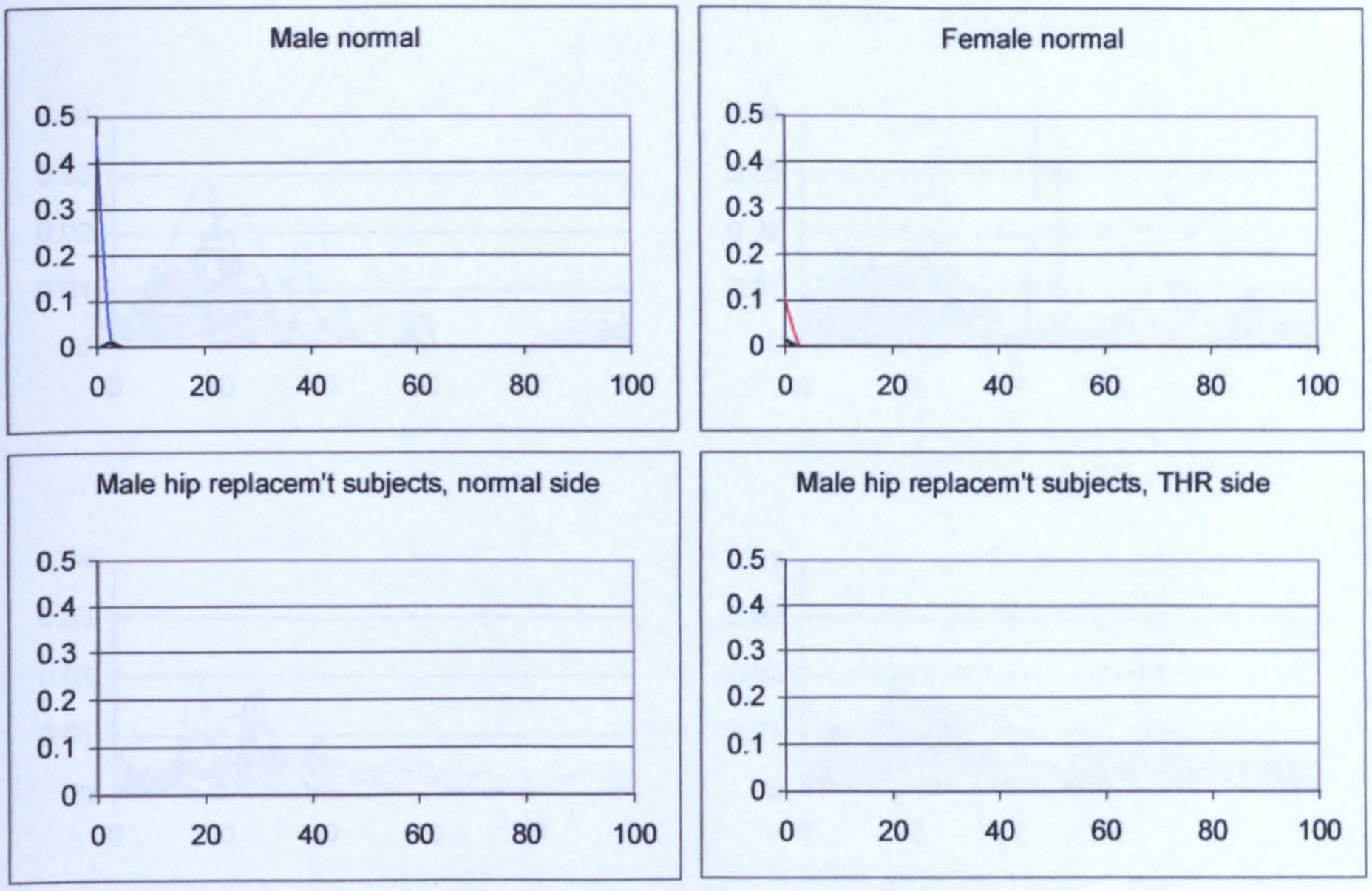

Stair ascent, knee force MCL (N/body weight) by % stance phase

Figure A-VI.5.25 Stair ascent, knee force MCL

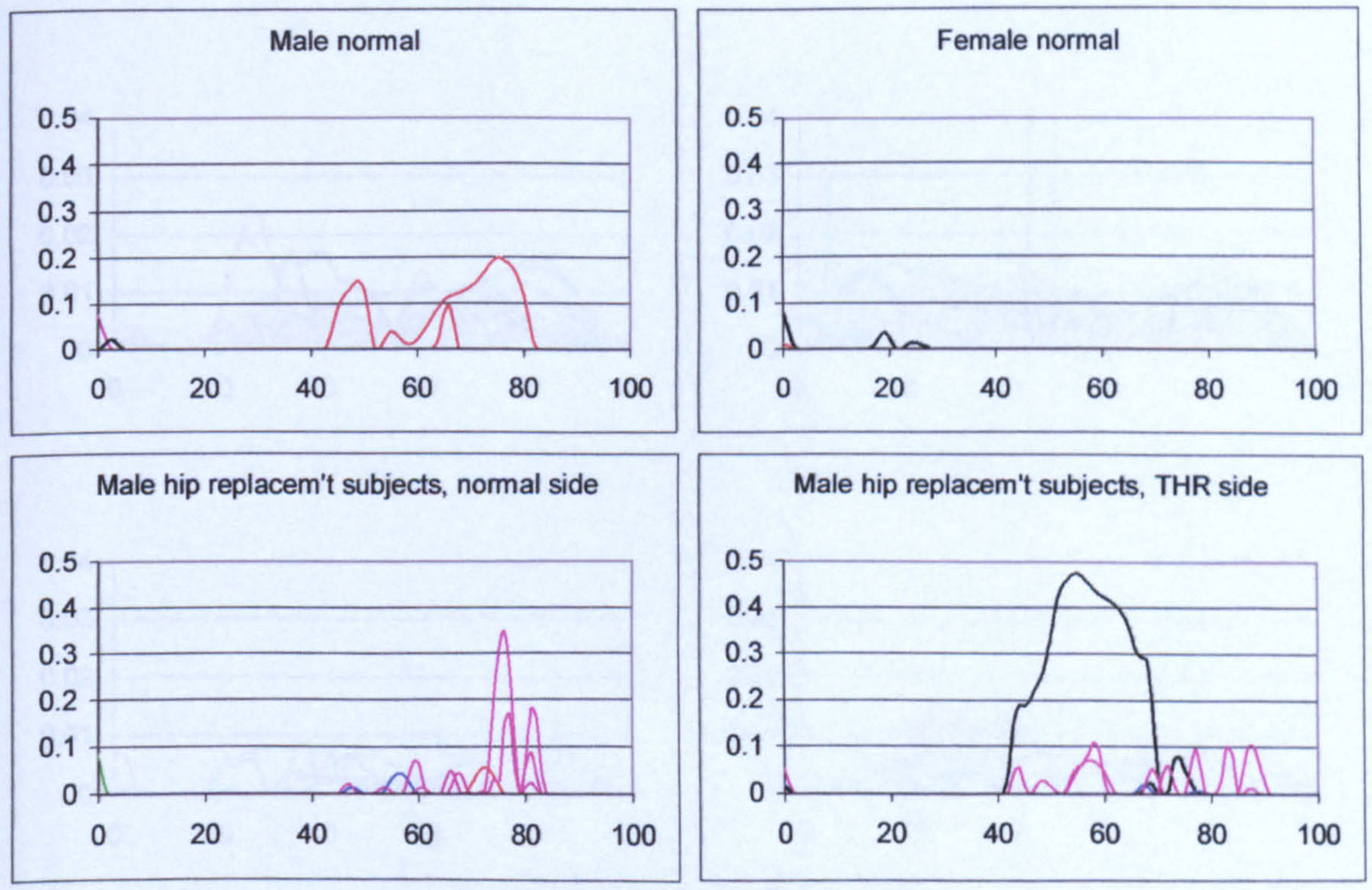

Stair ascent, knee force LCL (N/body weight) by % stance phase

Figure A-VI.5.26 Stair ascent, knee force LCL

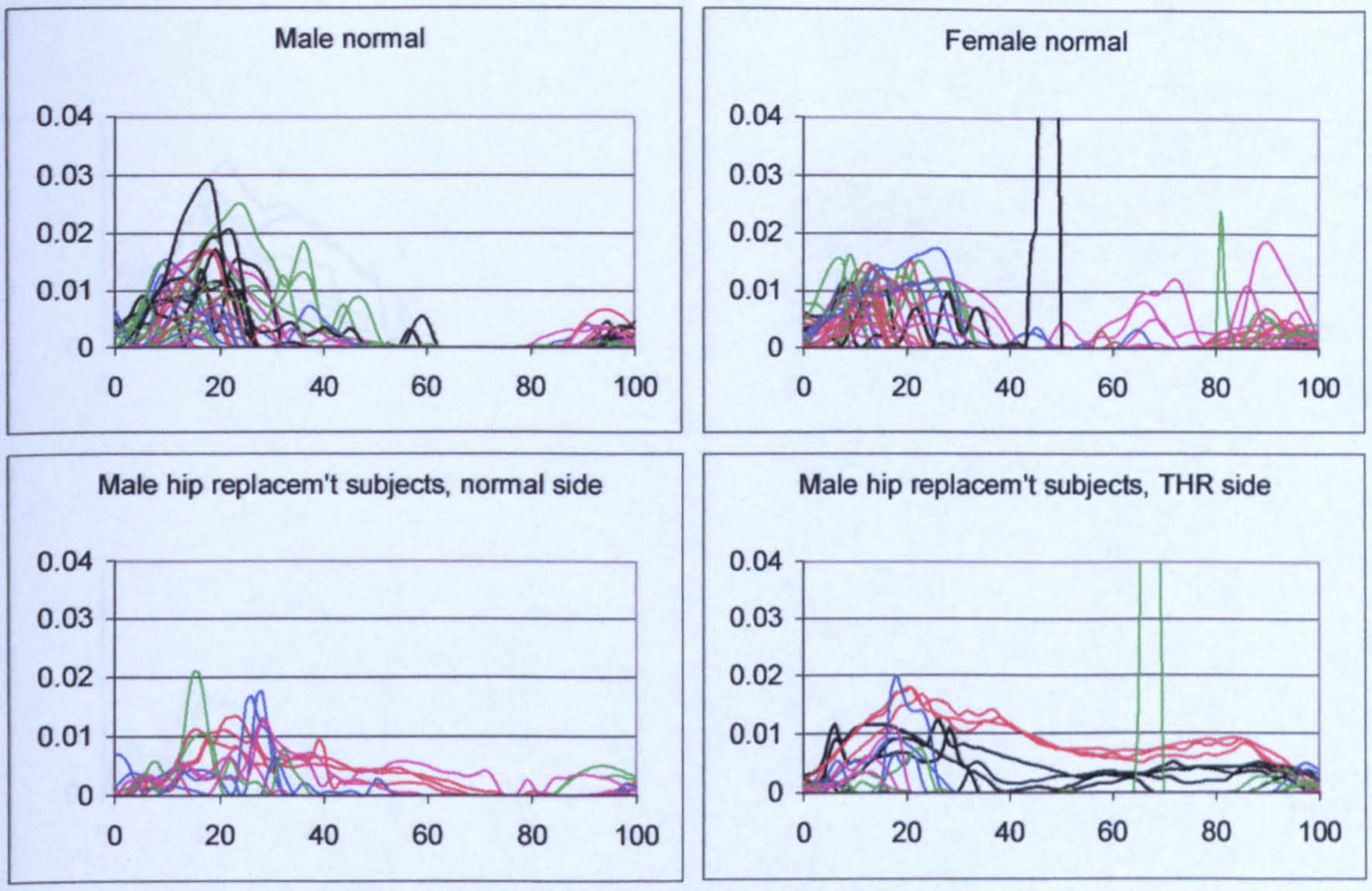

Figure A-VI.5.27 Stair ascent, knee force KJX1

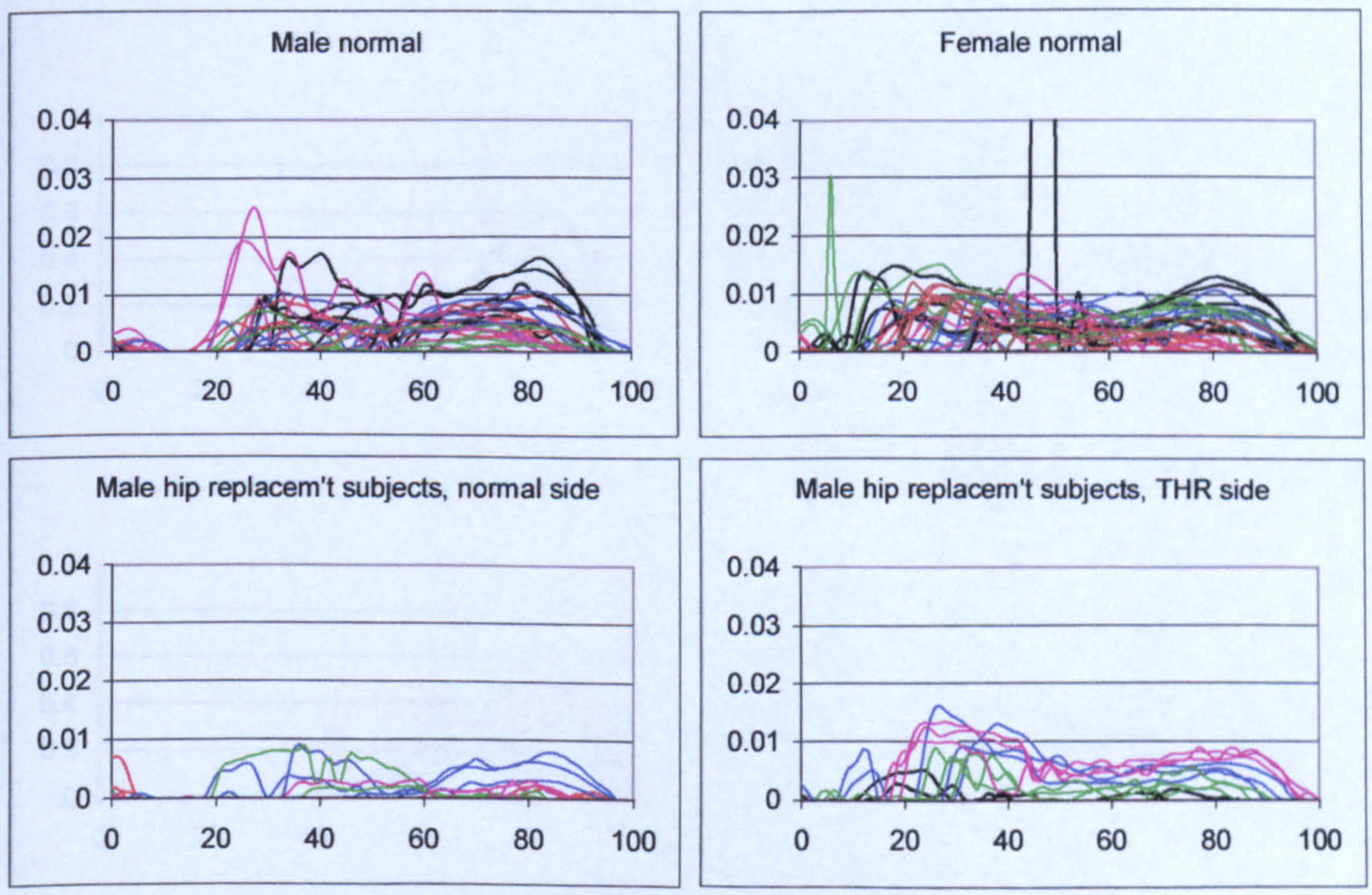

Figure A-VI.5.28 Stair ascent, knee force KJX2

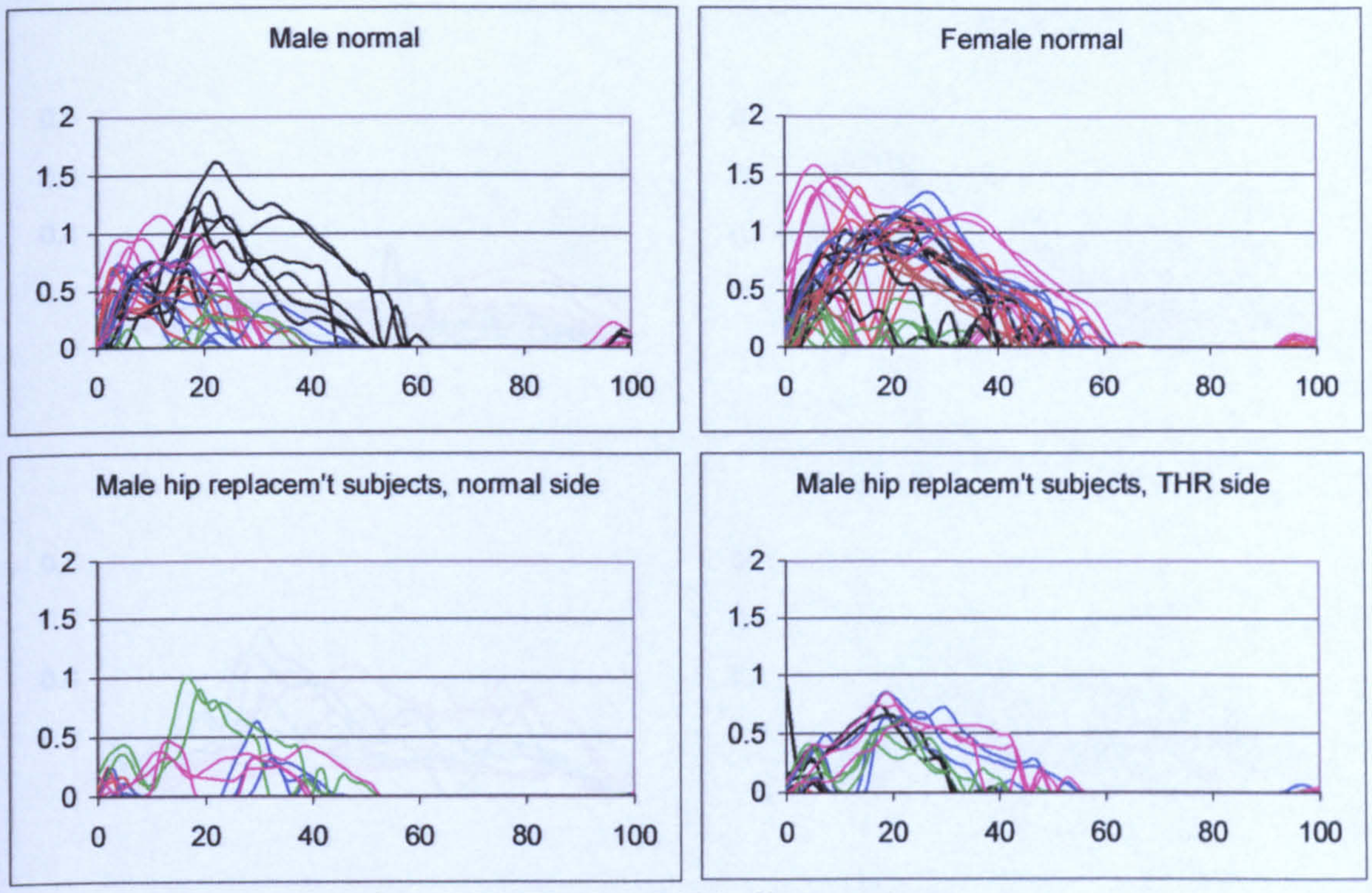

Figure A-VI.5.29 Stair ascent, knee force KJX3

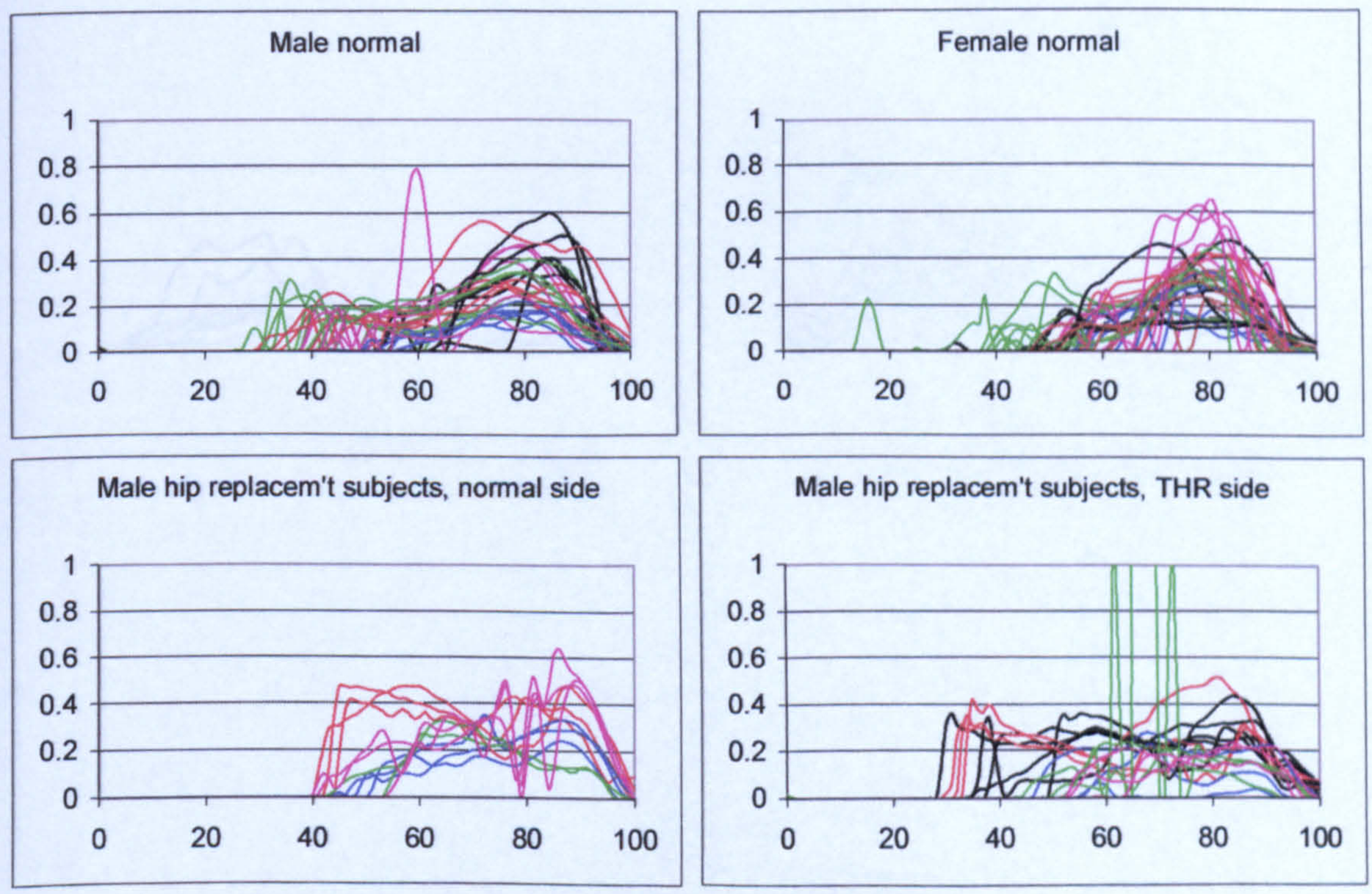

Figure A-VI.5.30 Stair ascent, knee force KJX4

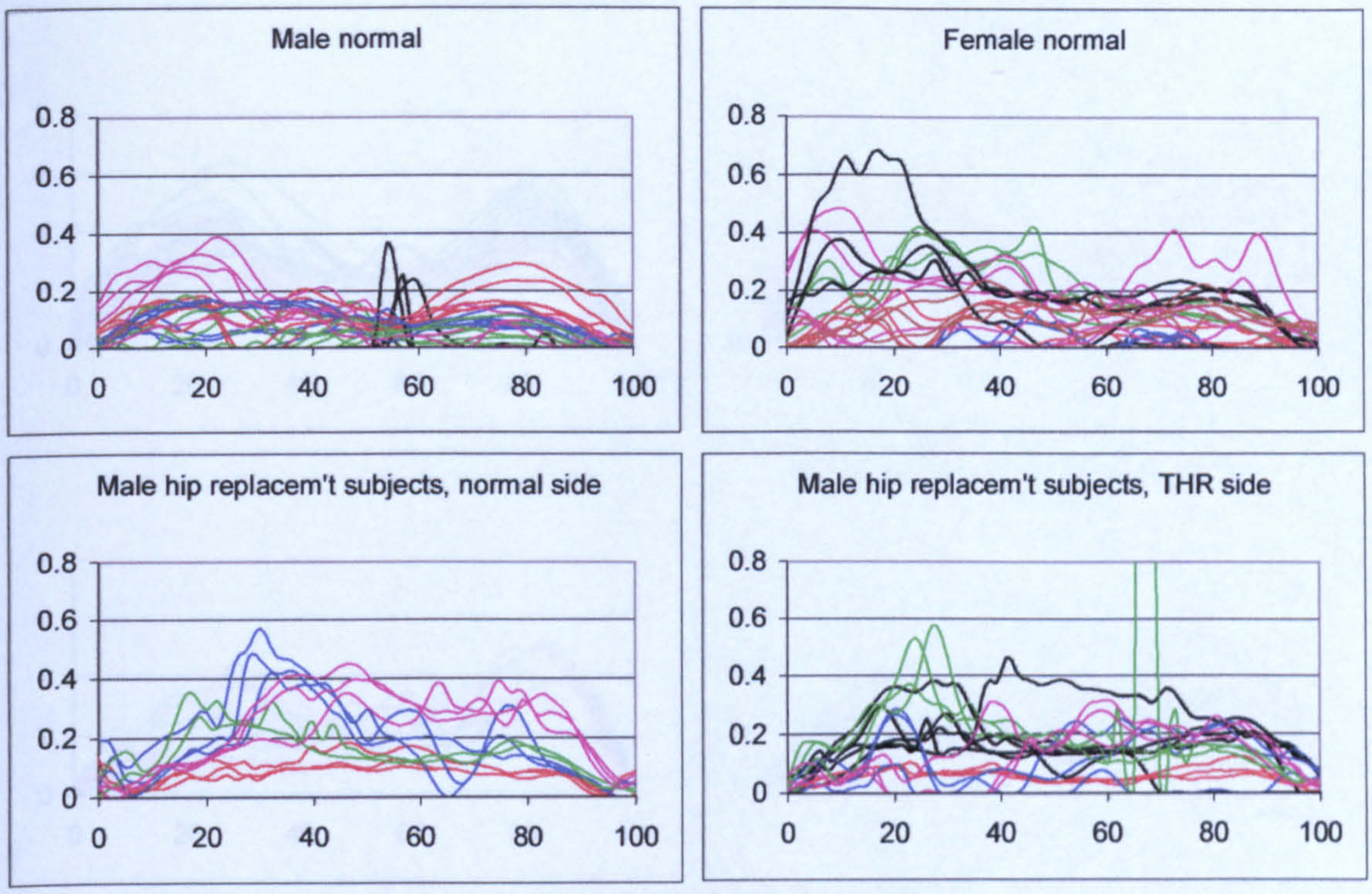

Stair ascent, knee force KJZ1 (N/body weight) by % stance phase

Figure A-VI.5.31 Stair ascent, knee force KJZ1

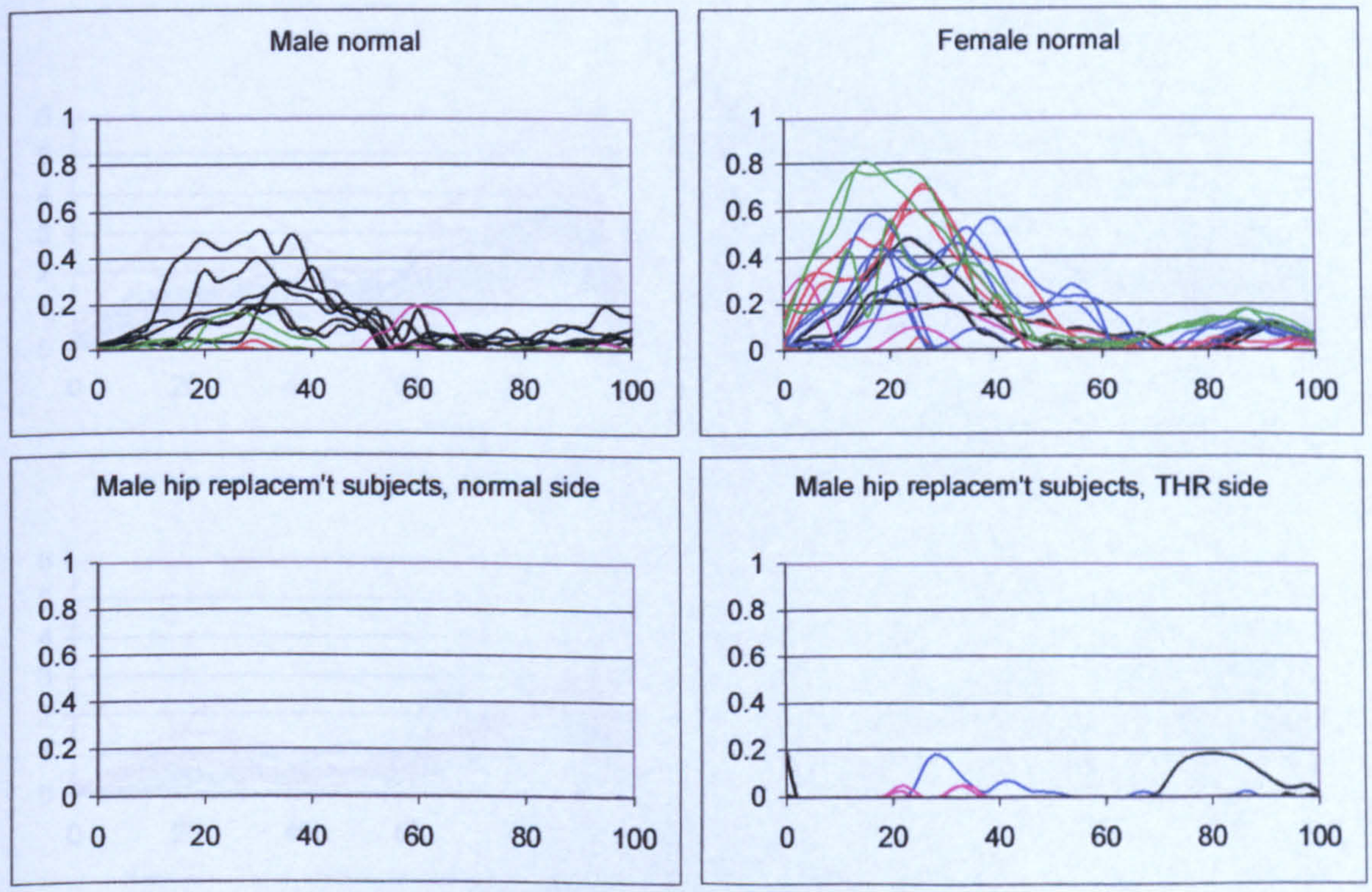

Stair ascent, knee force KJZ4 (N/body weight) by % stance phase

Figure A-VI.5.32 Stair ascent, knee force KJZ4

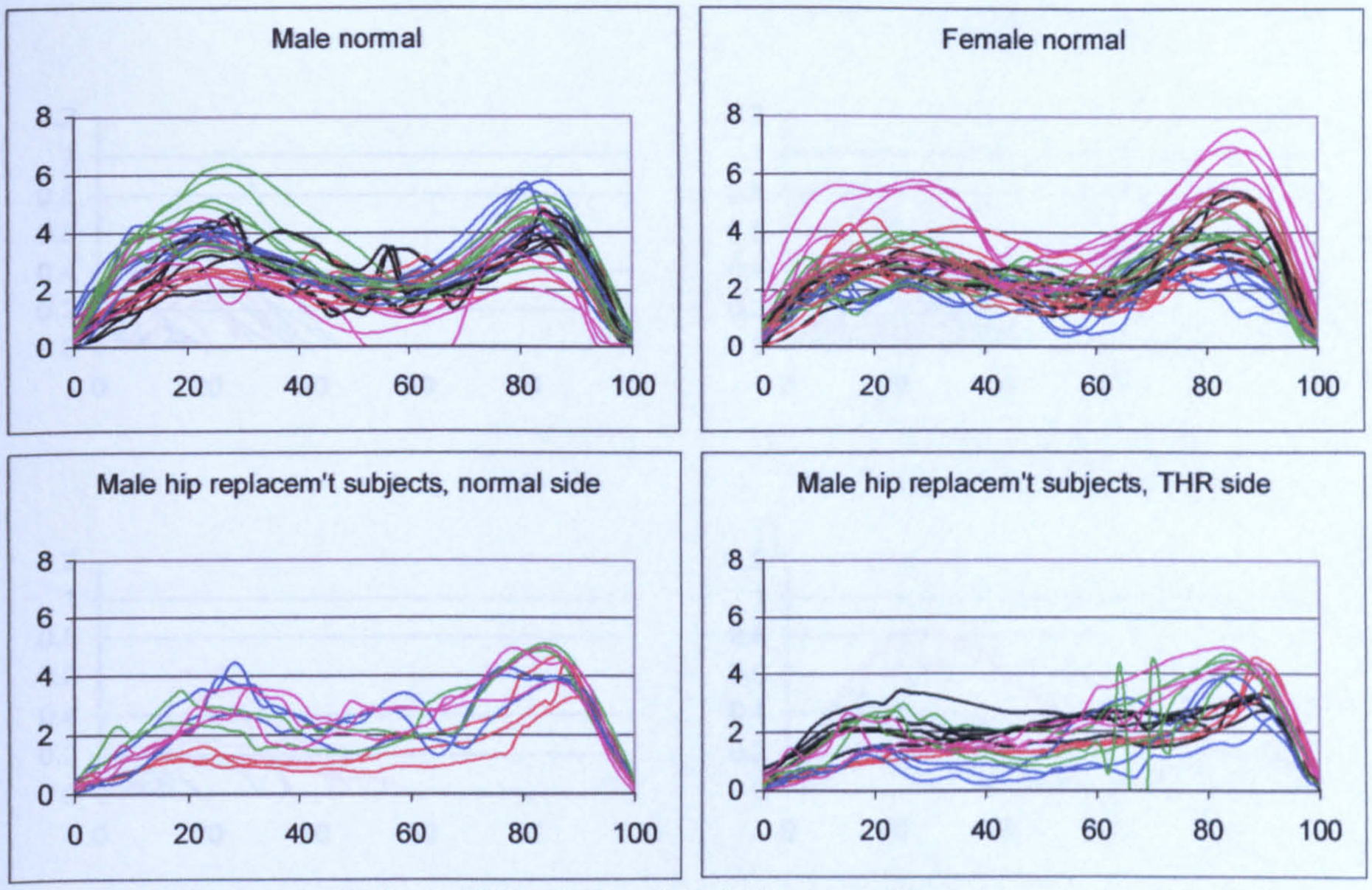

Stair ascent, ankle force AJY1 (N/body weight) by % stance phase

Figure A-VI.5.33 Stair ascent, ankle force AJY1

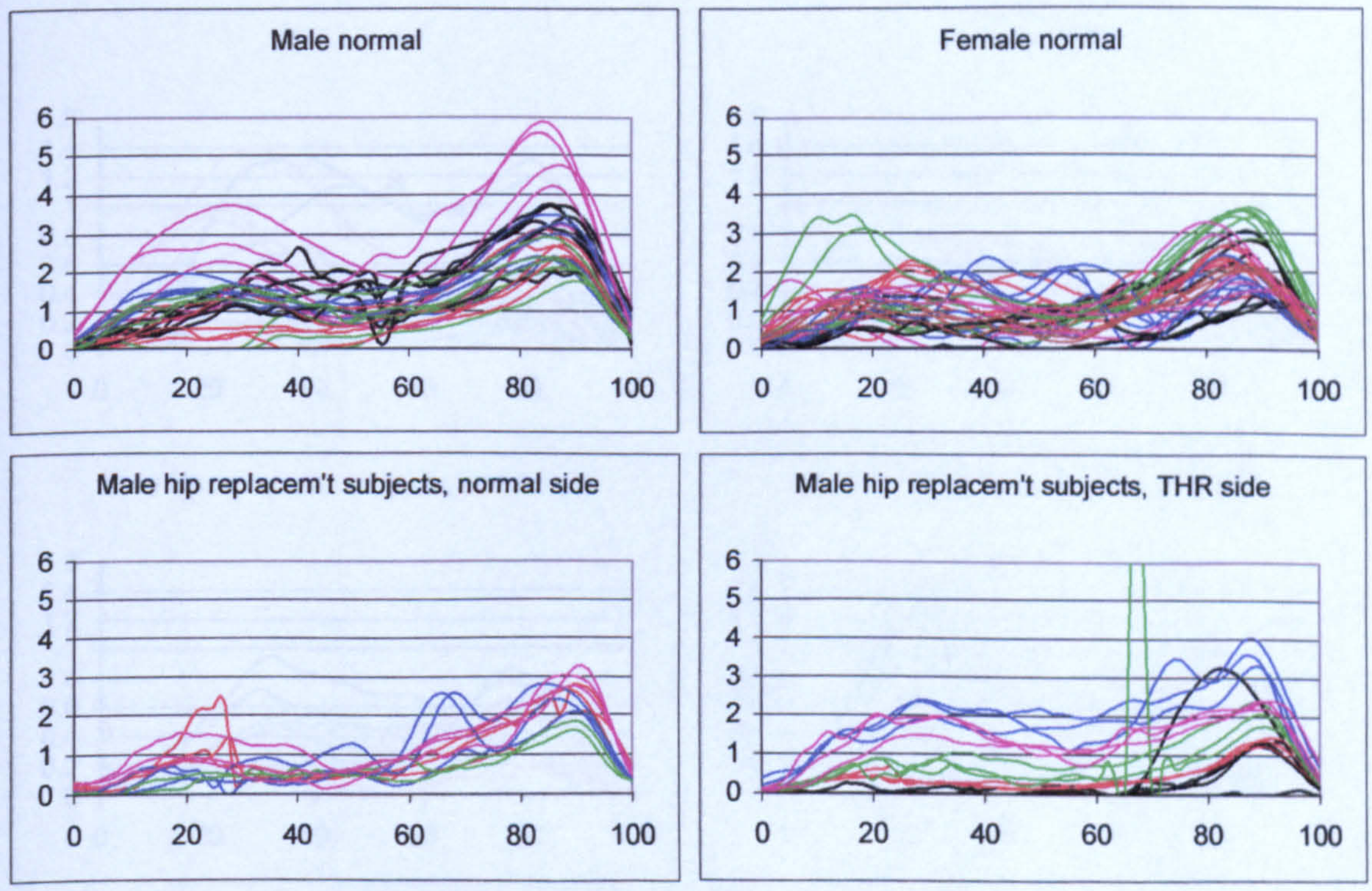

Stair ascent, ankle force AJY2 (N/body weight) by % stance phase

Figure A-VI.5.34 Stair ascent, ankle force AJY2

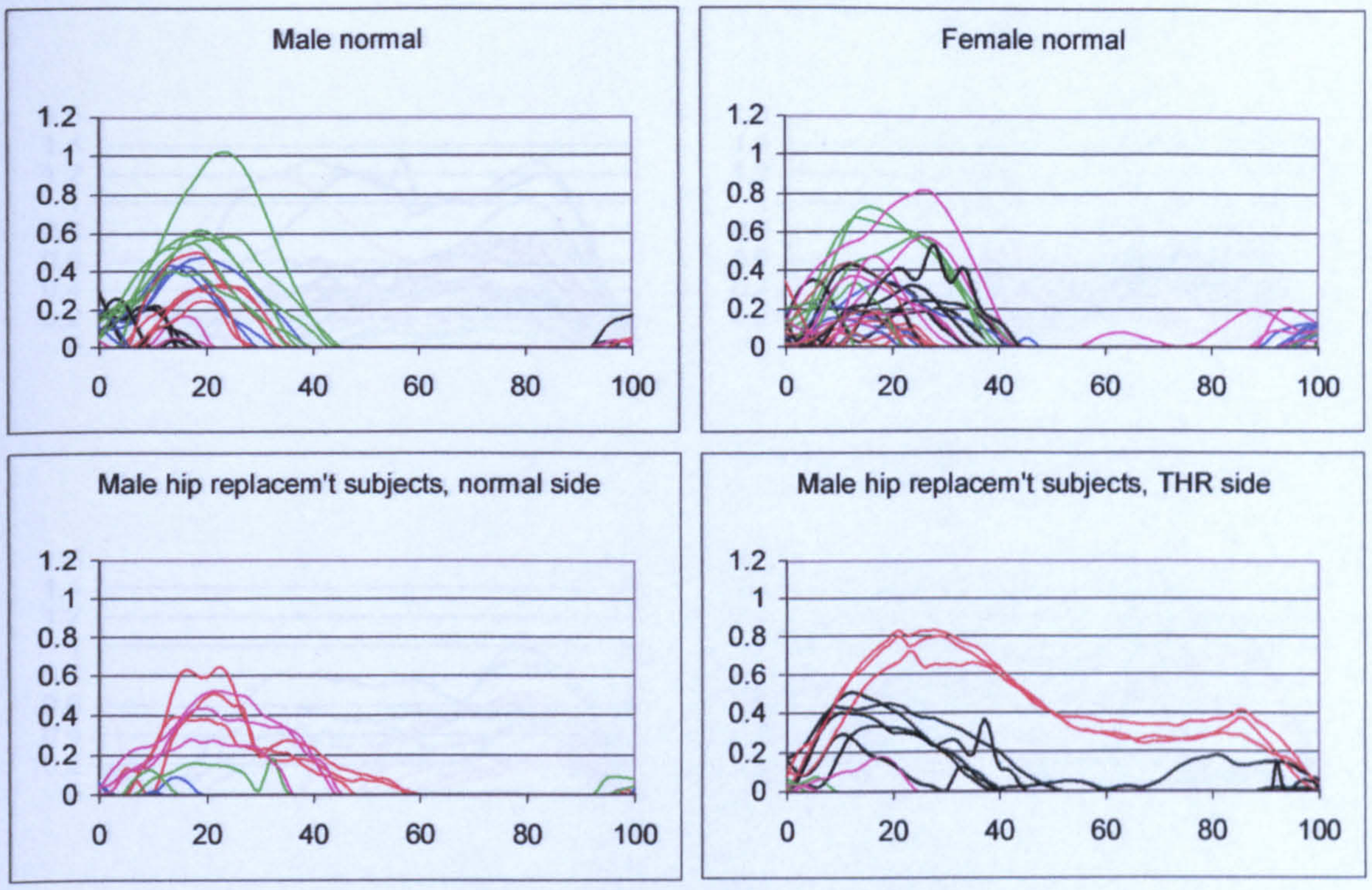

Figure A-VI.5.35 Stair ascent, ankle force AJX1

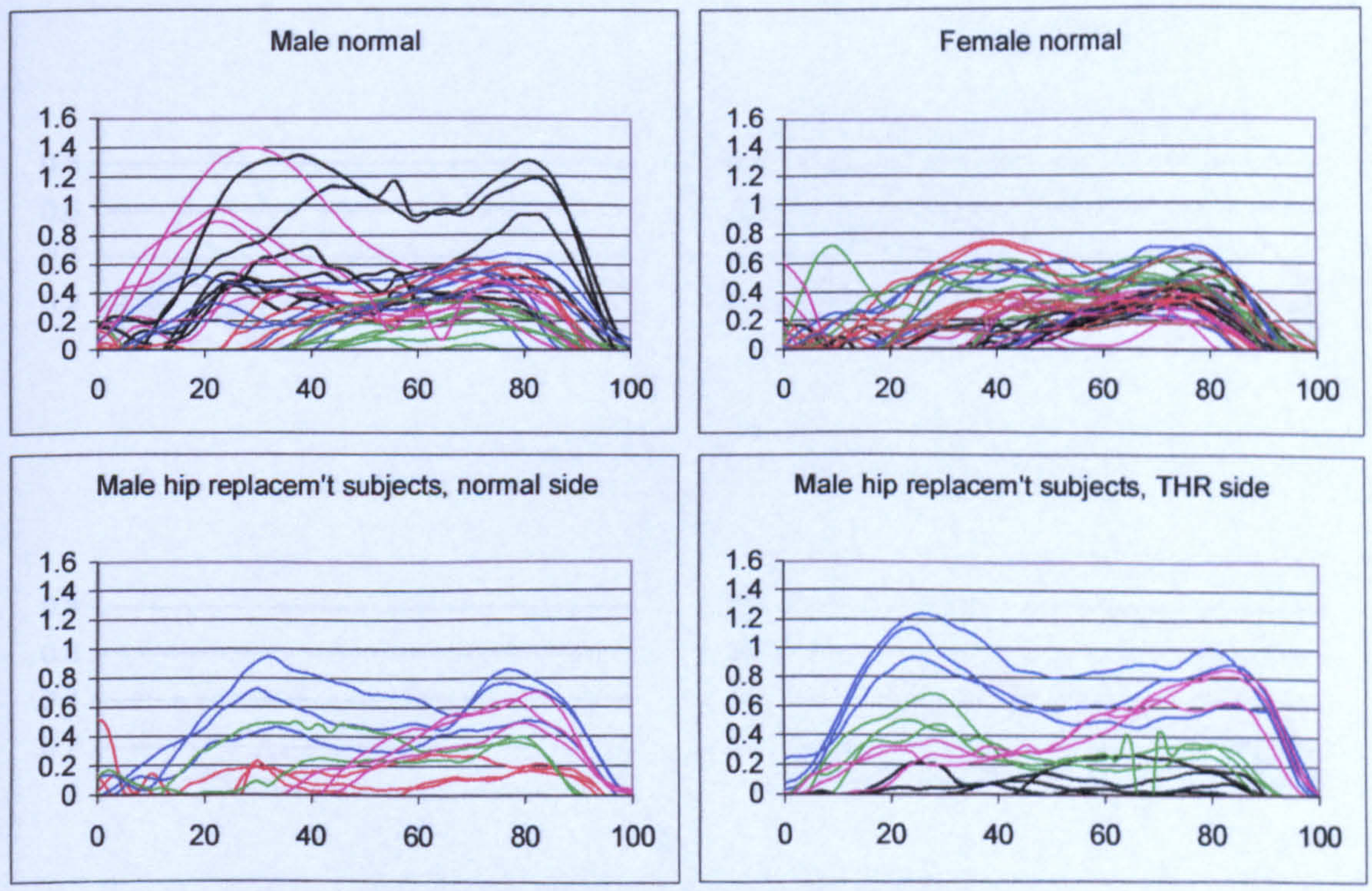

Figure A-VI.5.36 Stair ascent, ankle force AJX2

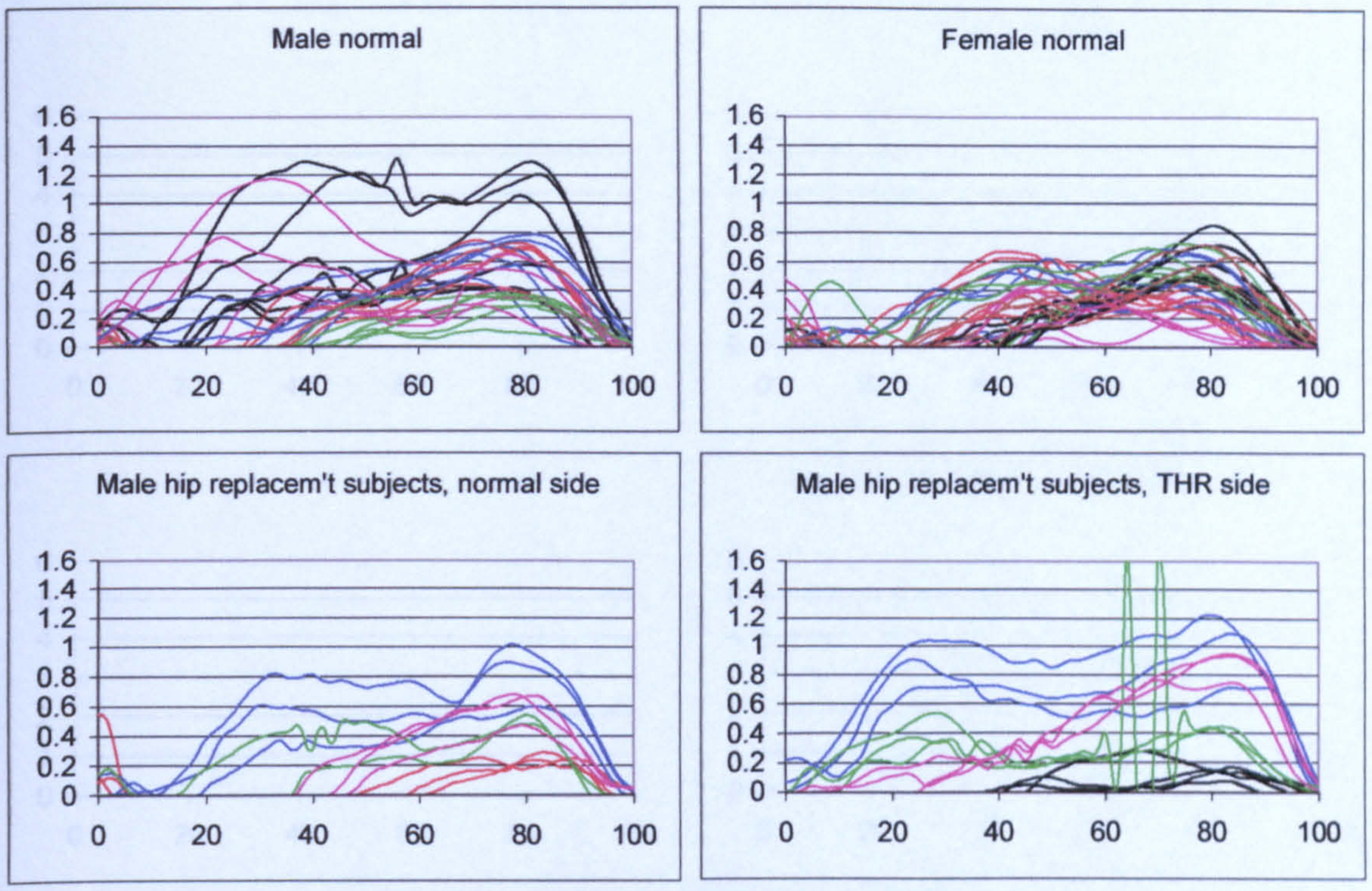

Stair ascent, ankle force AJX3 (N/body weight) by % stance phase

Figure A-VI.5.37 Stair ascent, ankle force AJX3

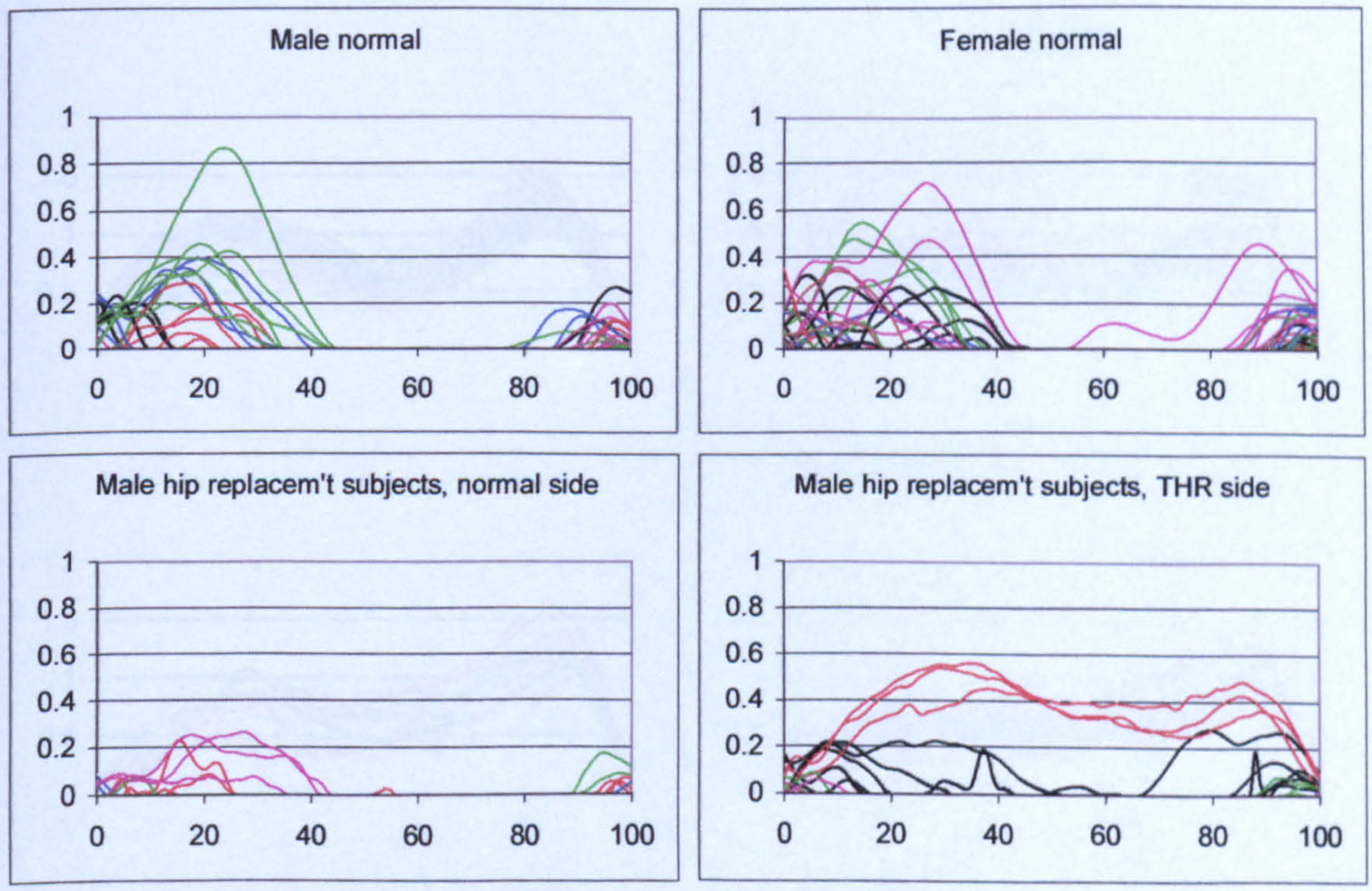

Stair ascent, ankle force AJX4 (N/body weight) by % stance phase

Figure A-VI.5.38 Stair ascent, ankle force AJX4

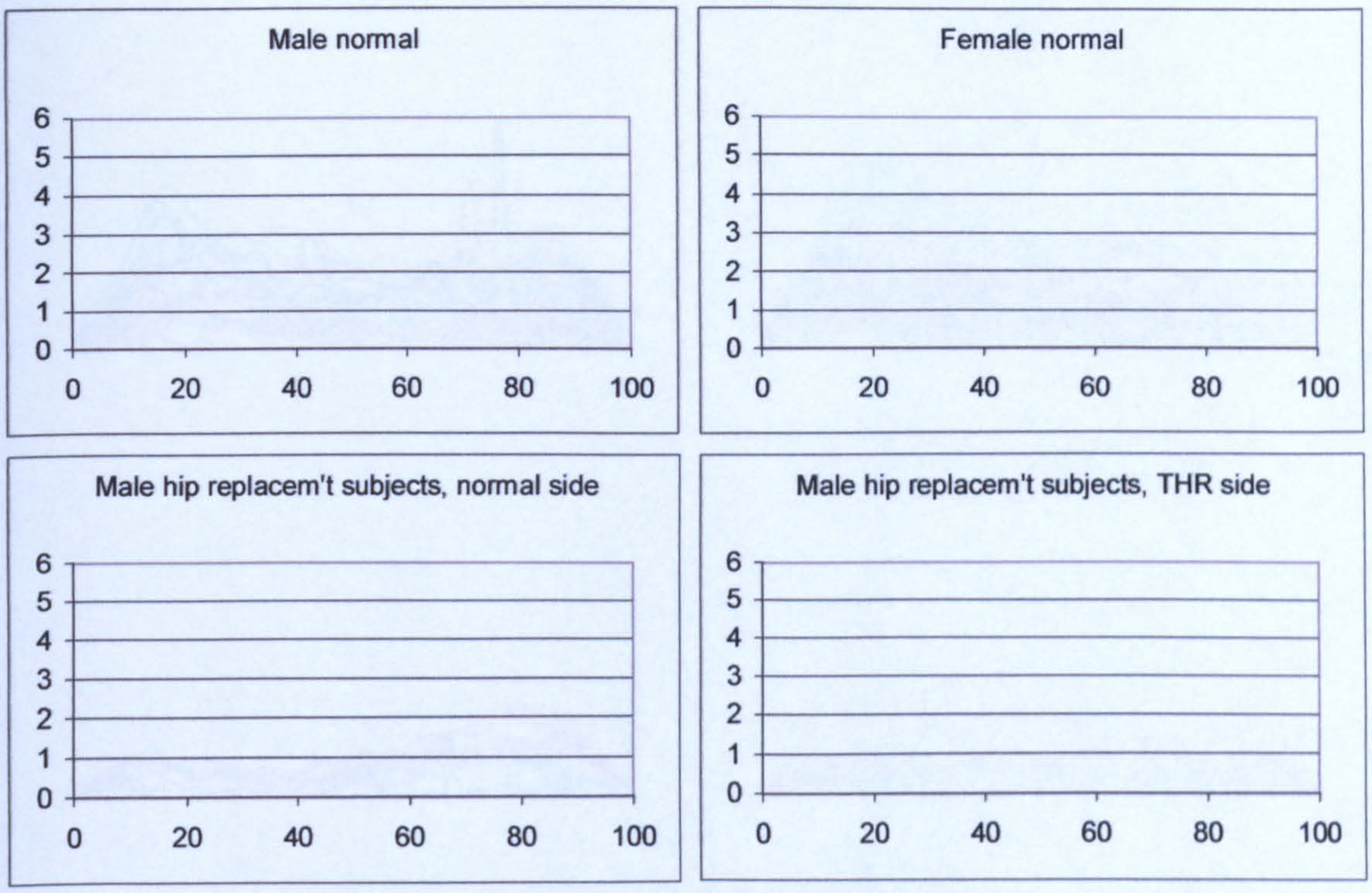

Stair ascent, ankle force AJZ1 (N/body weight) by % stance phase

Figure A-VI.5.39 Stair ascent, ankle force AJZ1

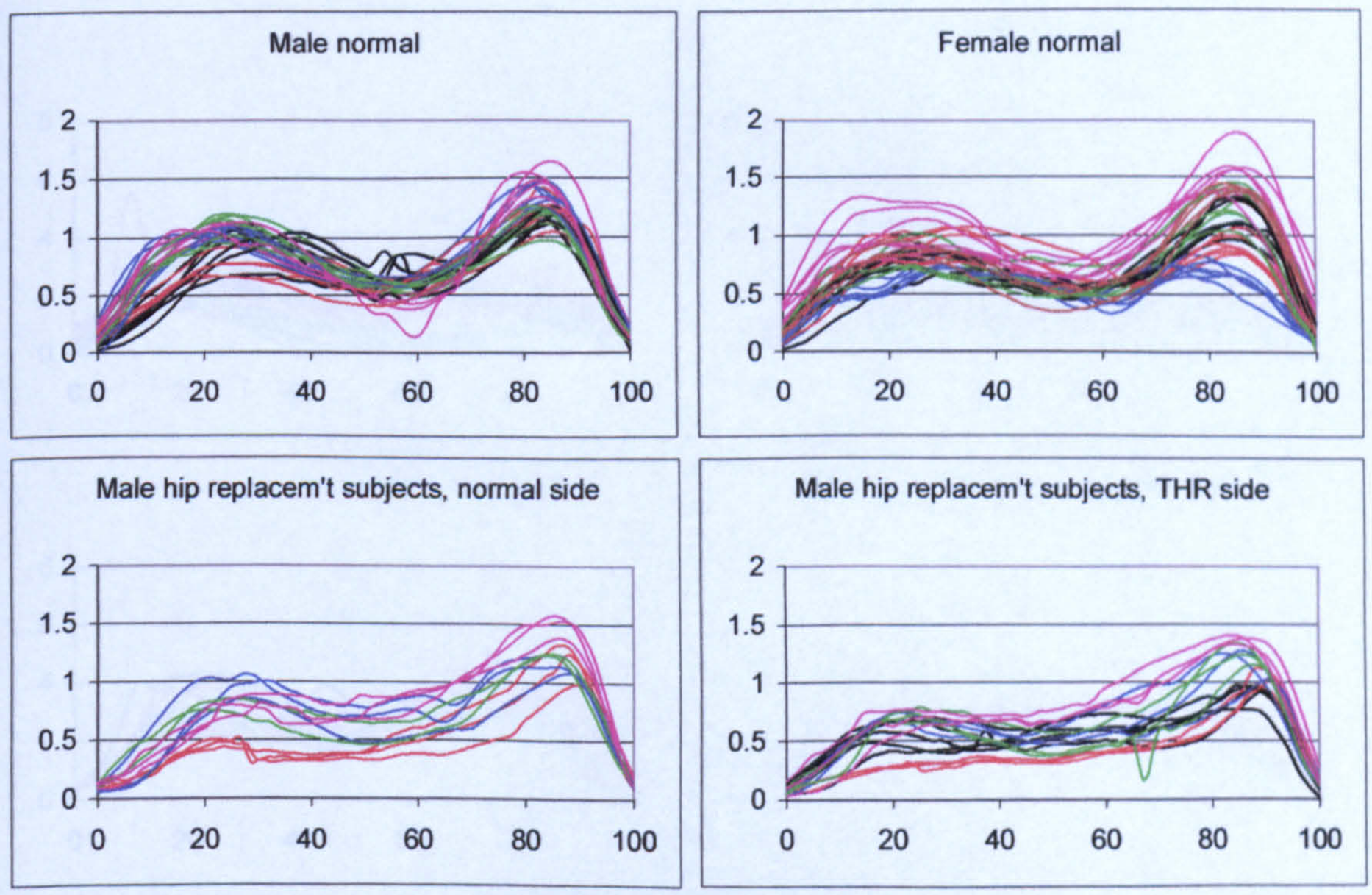

Stair ascent, ankle force AJZ2 (N/body weight) by % stance phase

Figure A-VI.5.40 Stair ascent, ankle force AJZ2

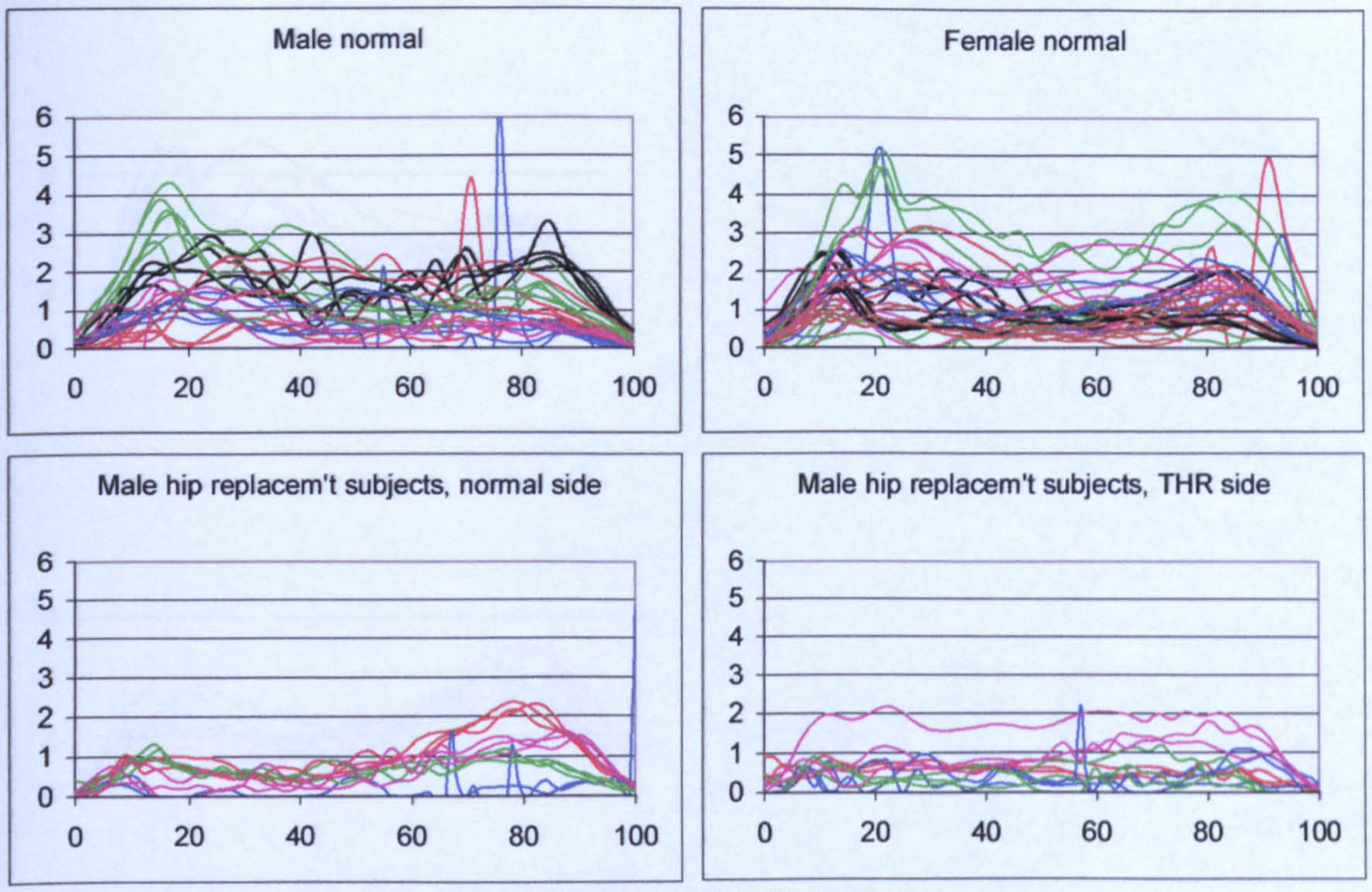

Figure A-VI.5.41 Stair descent, knee force KJY1

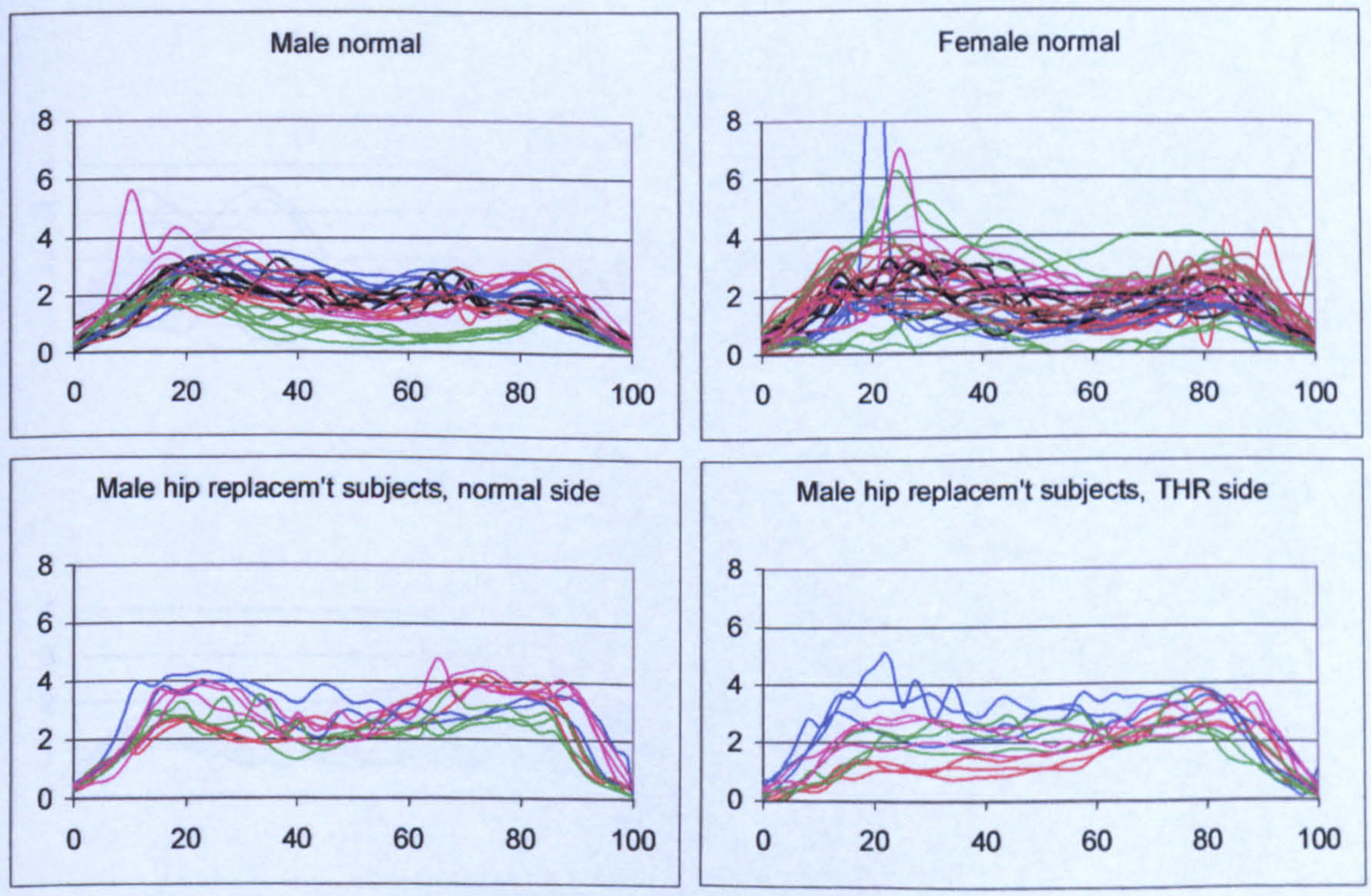

Figure A-VI.5.42 Stair descent, knee force KJY2

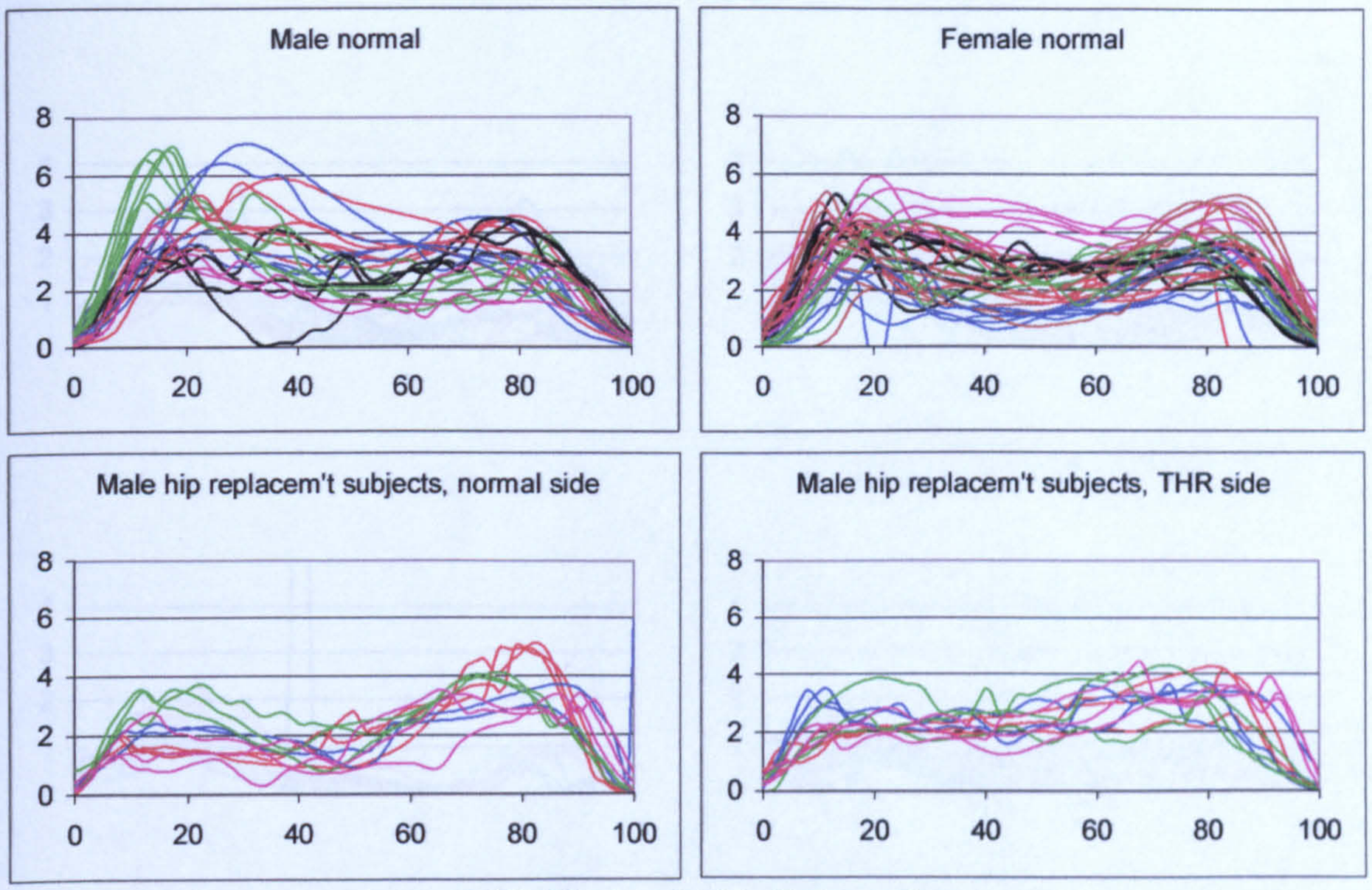

Figure A-VI.5.43 Stair descent, ankle force AJY1

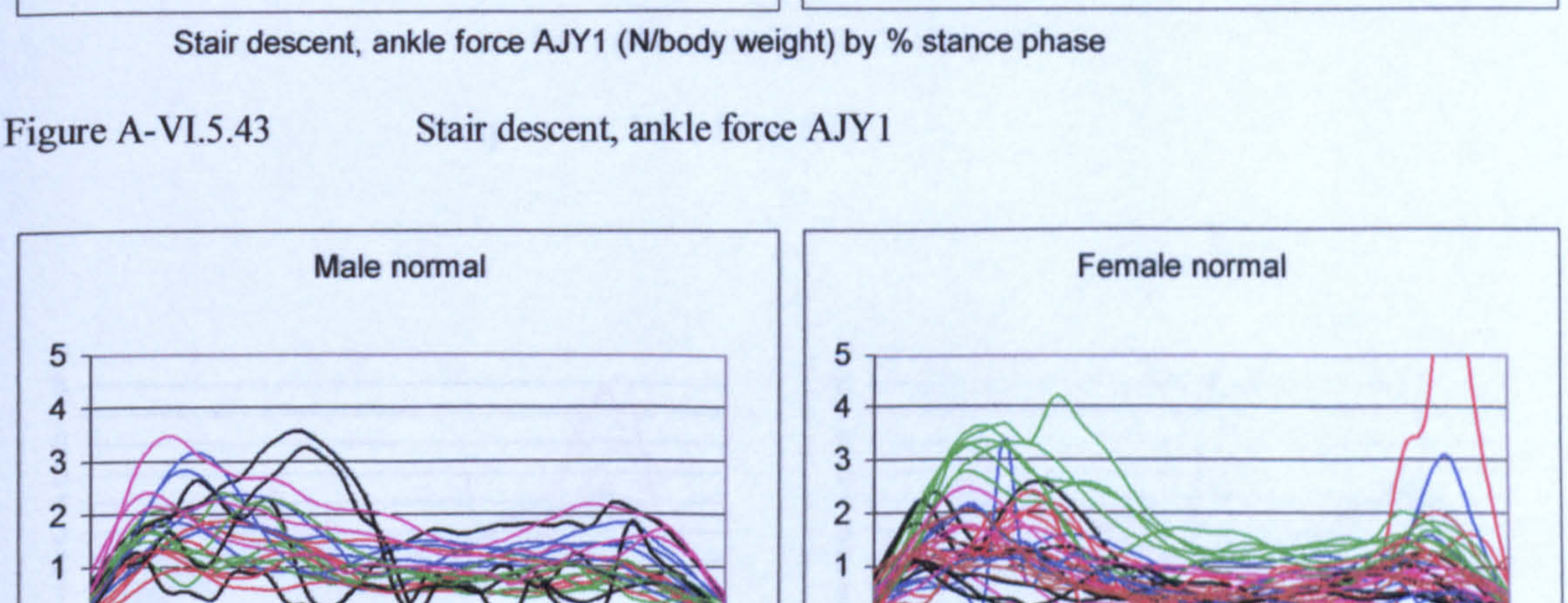

Figure A-VI.5.44 Stair descent, ankle force AJY2

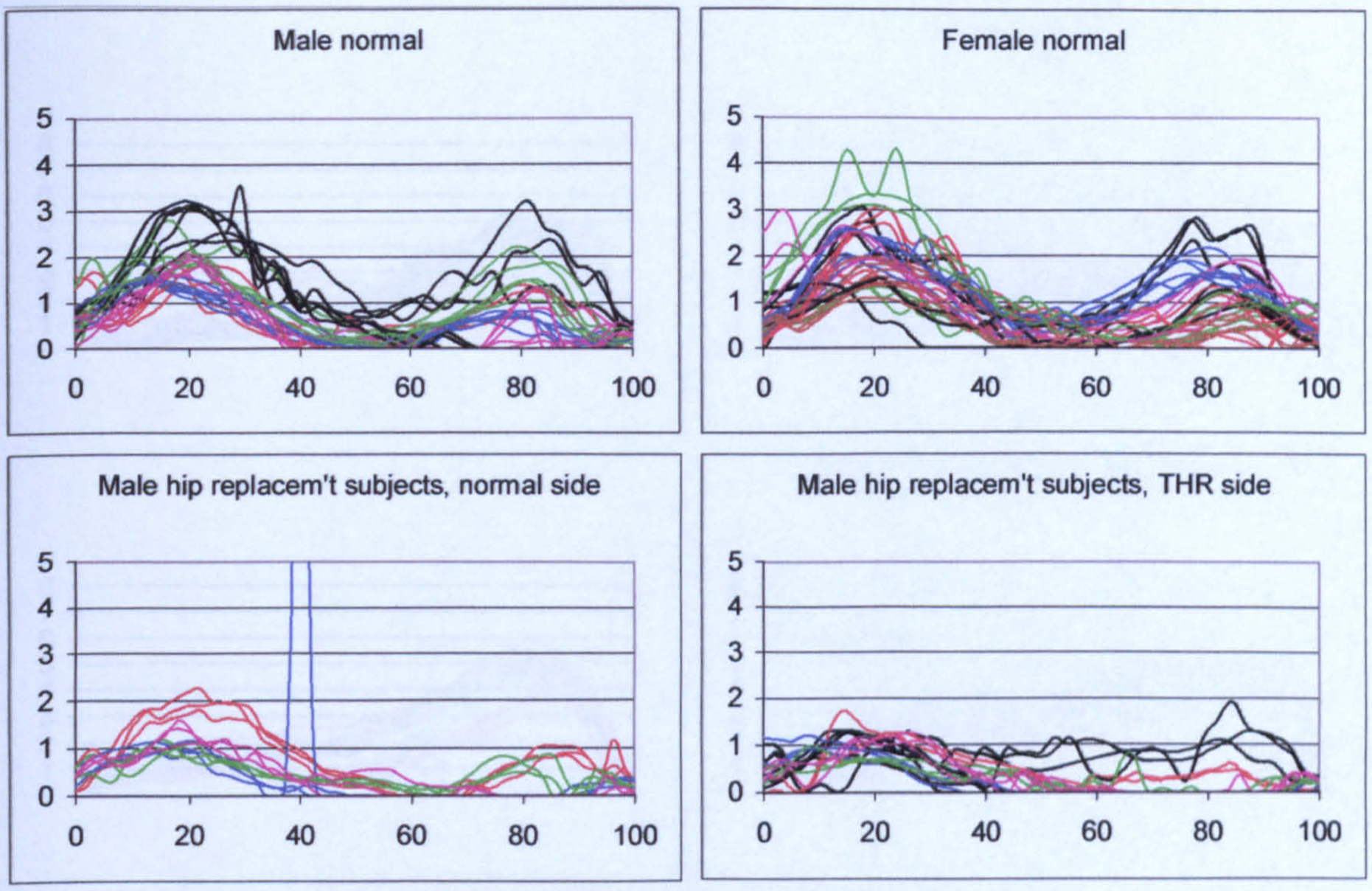

Ramp ascent, knee force KJY1 (N/body weight) by % stance phase

Figure A-VI.5.45 Ramp ascent, knee force KJY1

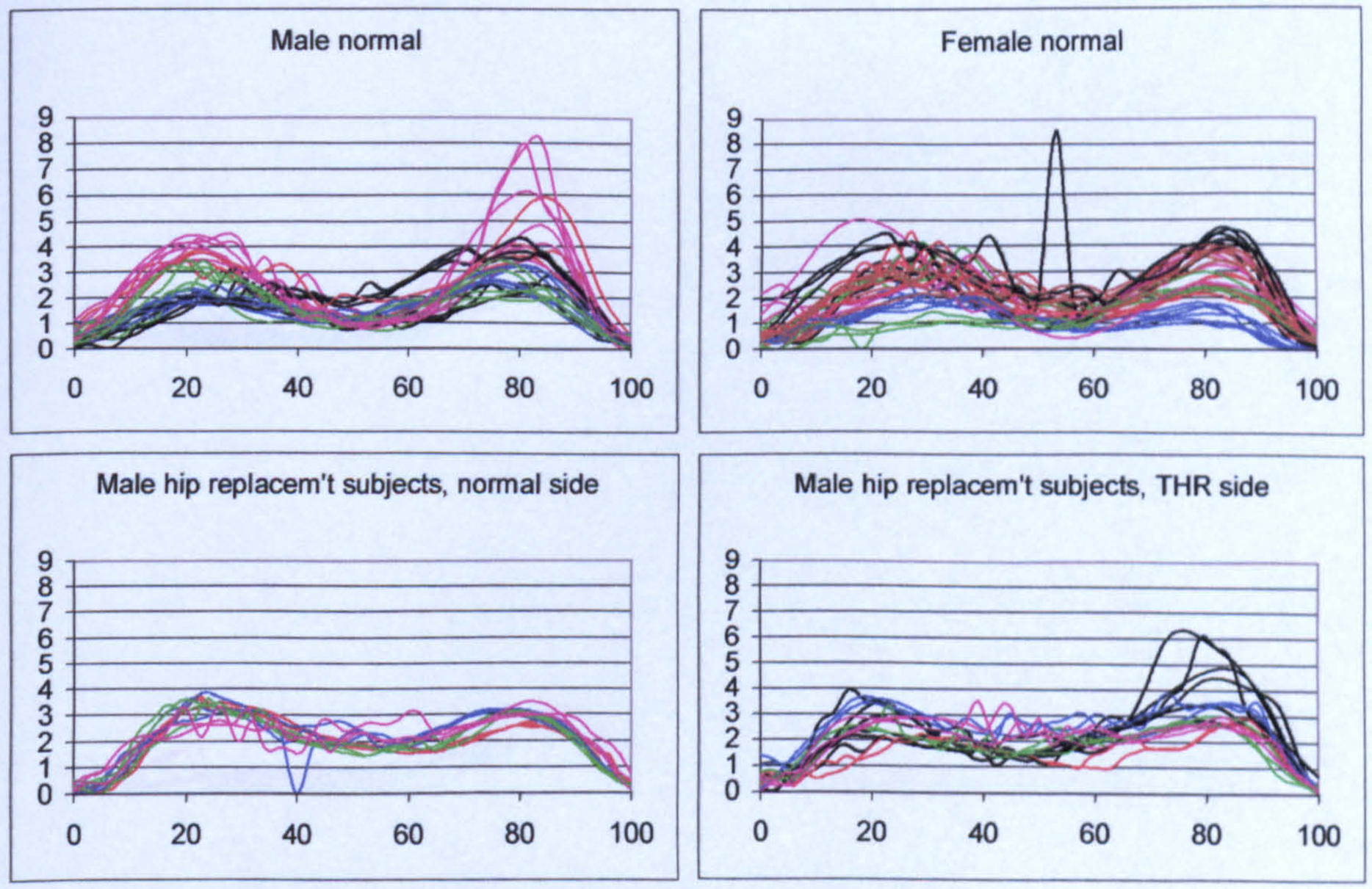

Ramp ascent, knee force KJY2 (N/body weight) by % stance phase

Figure A-VI.5.46 Ramp ascent, knee force KJY2

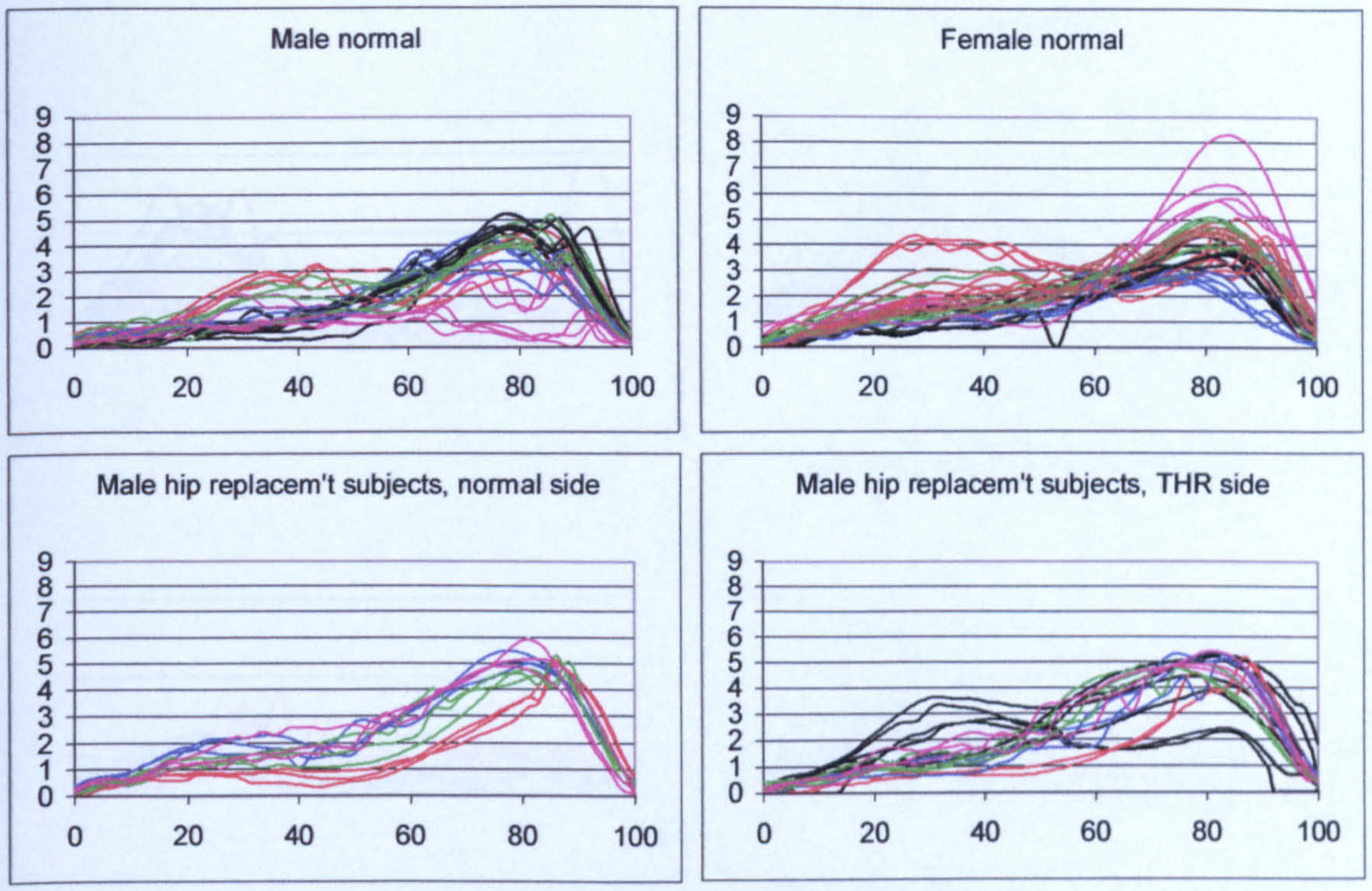

Ramp ascent, ankle force AJY1 (N/body weight) by % stance phase

Figure A-VI.5.47 Ramp ascent, ankle force AJY1

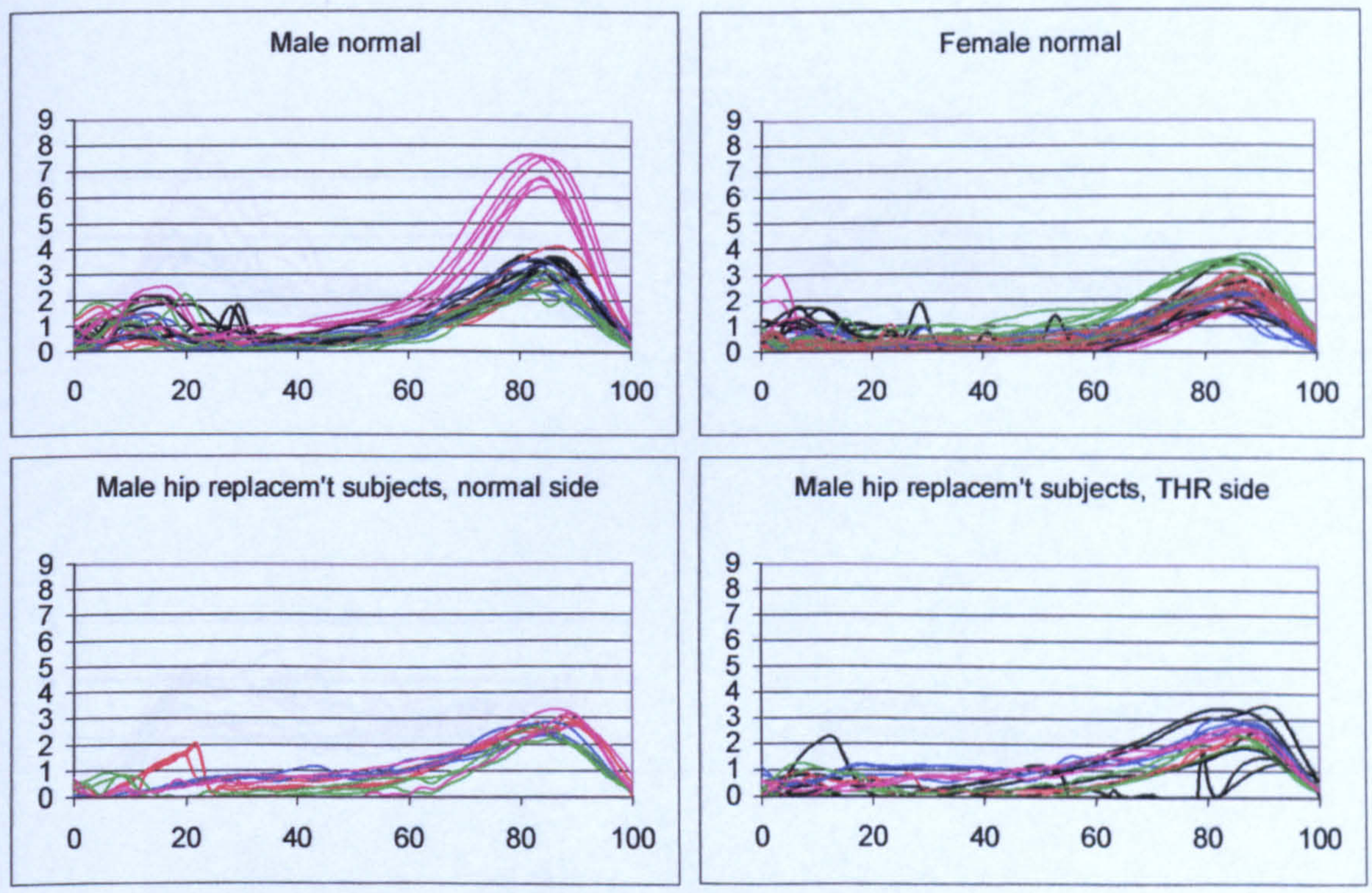

Ramp ascent, ankle force AJY2 (N/body weight) by % stance phase

Figure A-VI.5.48 Ramp ascent, ankle force AJY2

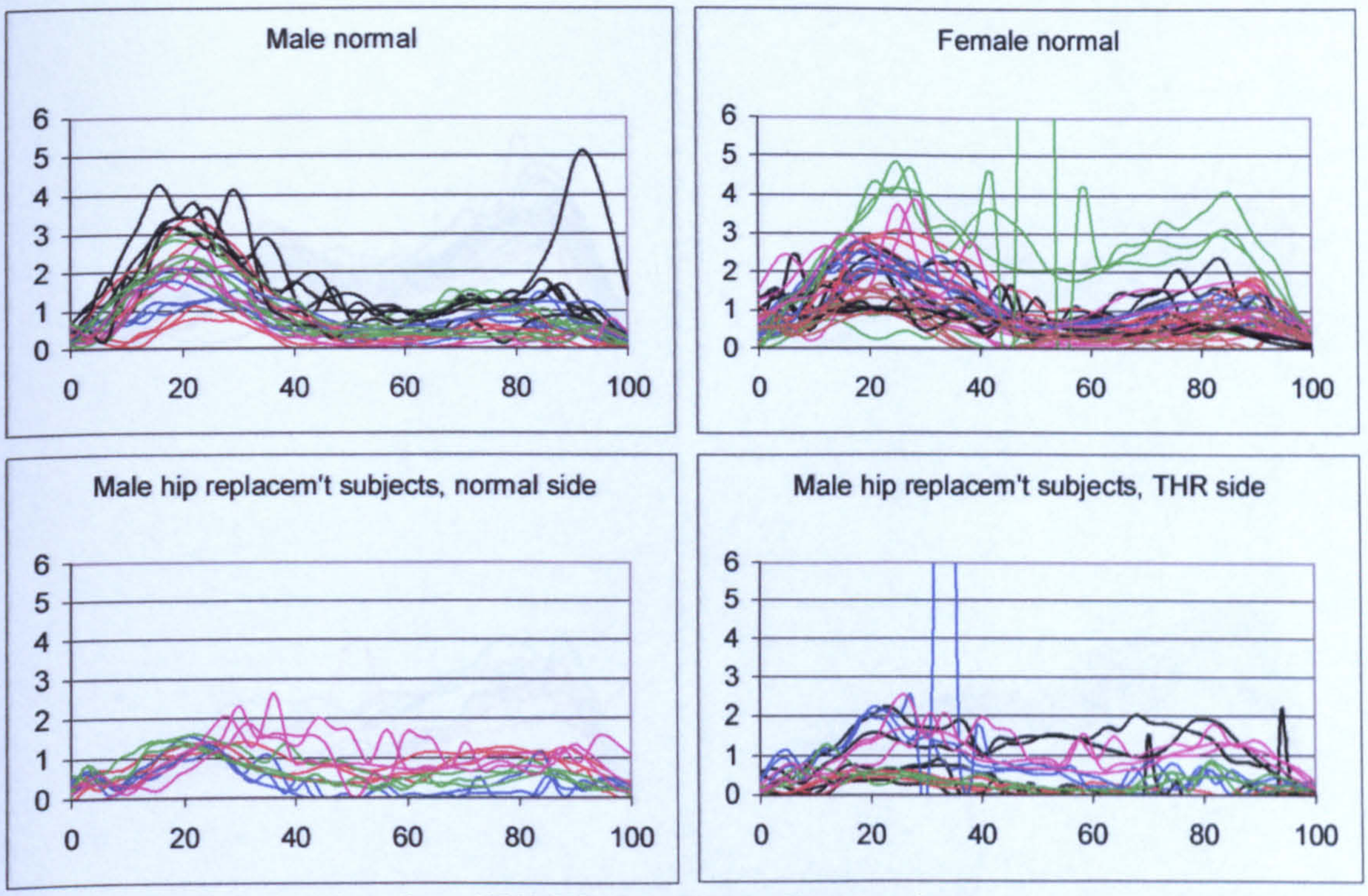

Figure A-VI.5.49 Ramp descent, knee force KJY1

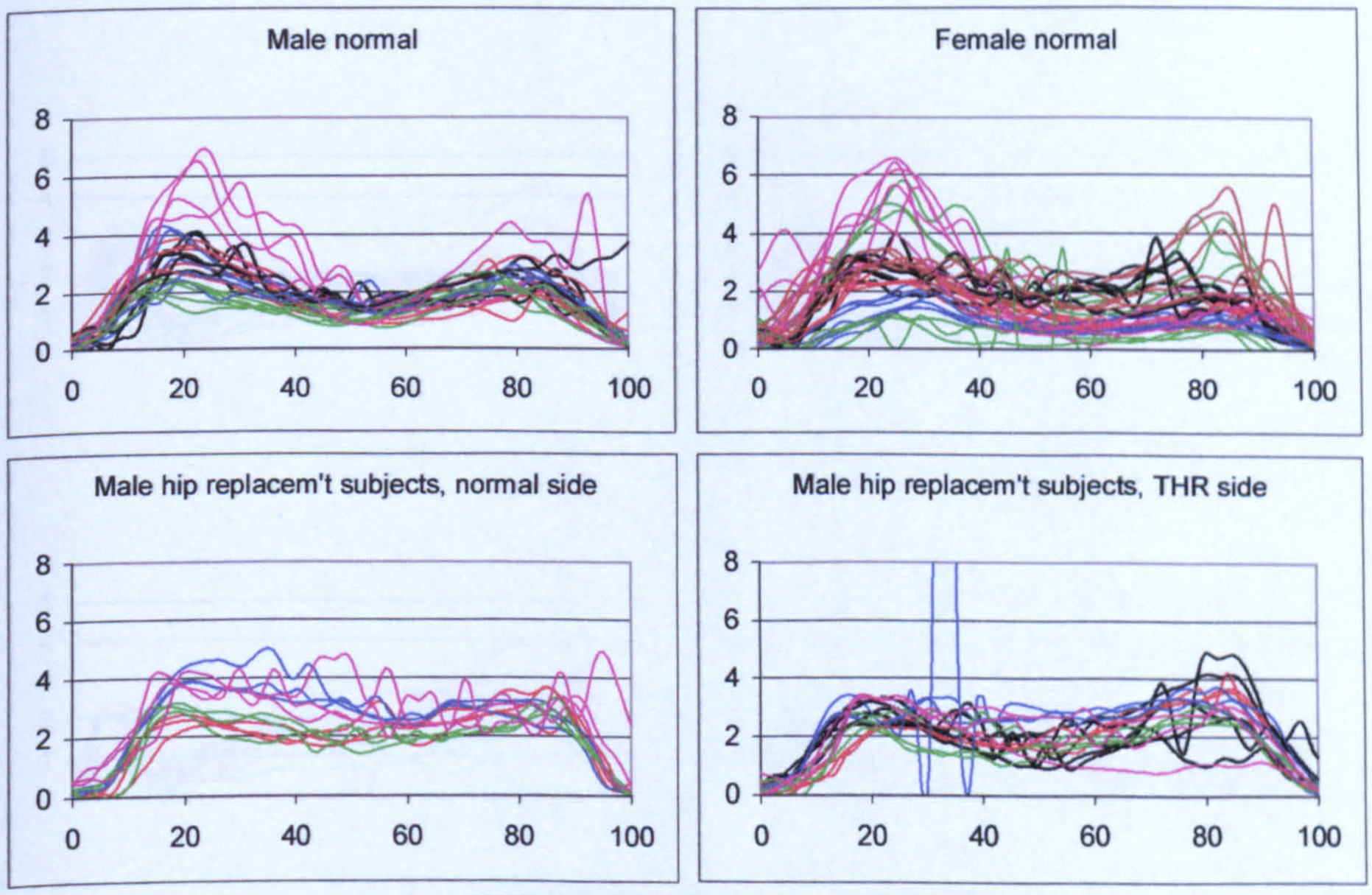

Figure A-VI.5.50 Ramp descent, knee force KJY2

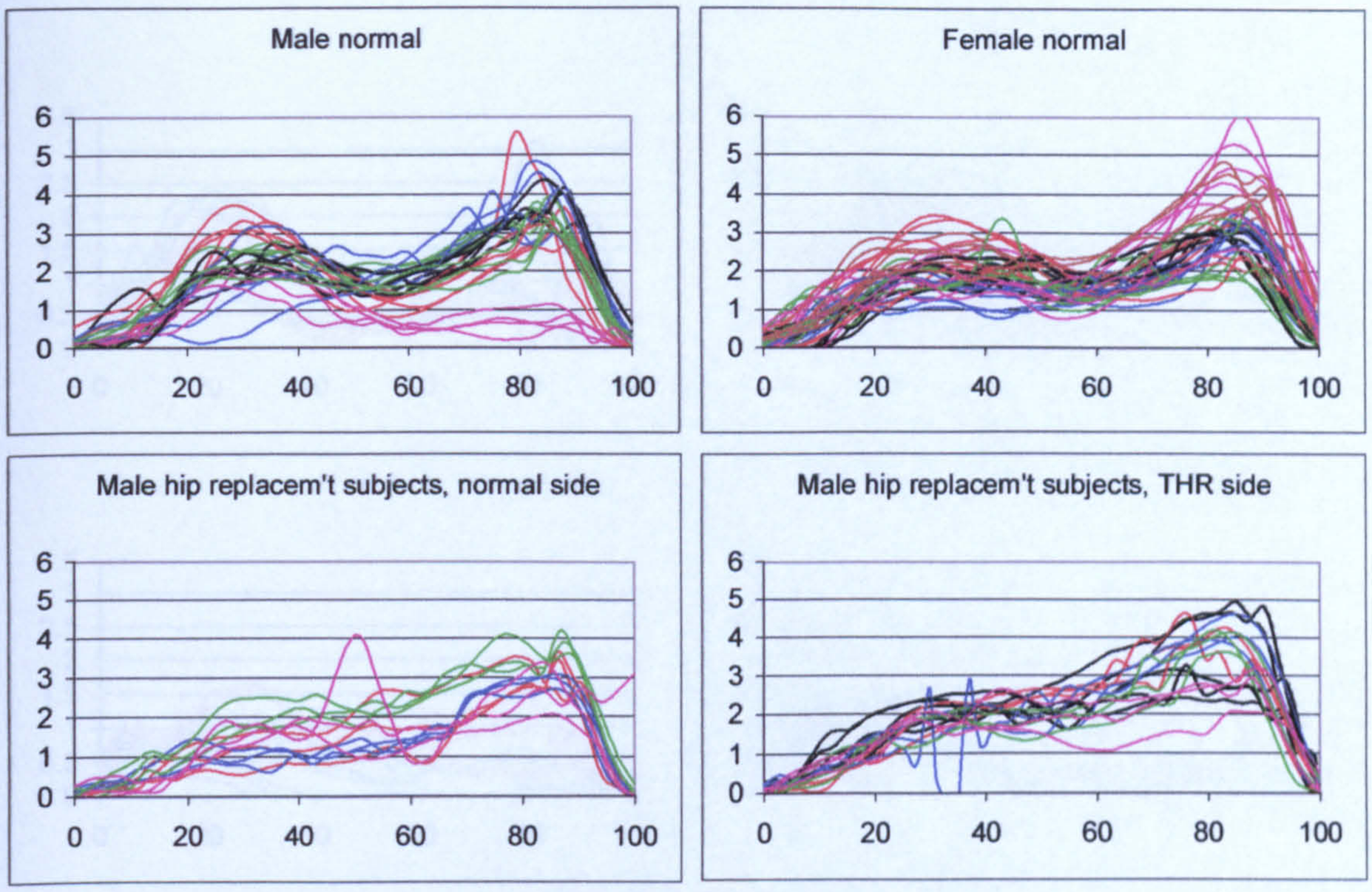

Ramp descent, ankle force AJY1 (N/body weight) by % stance phase

Figure A-VI.5.51 Ramp descent, ankle force AJY1

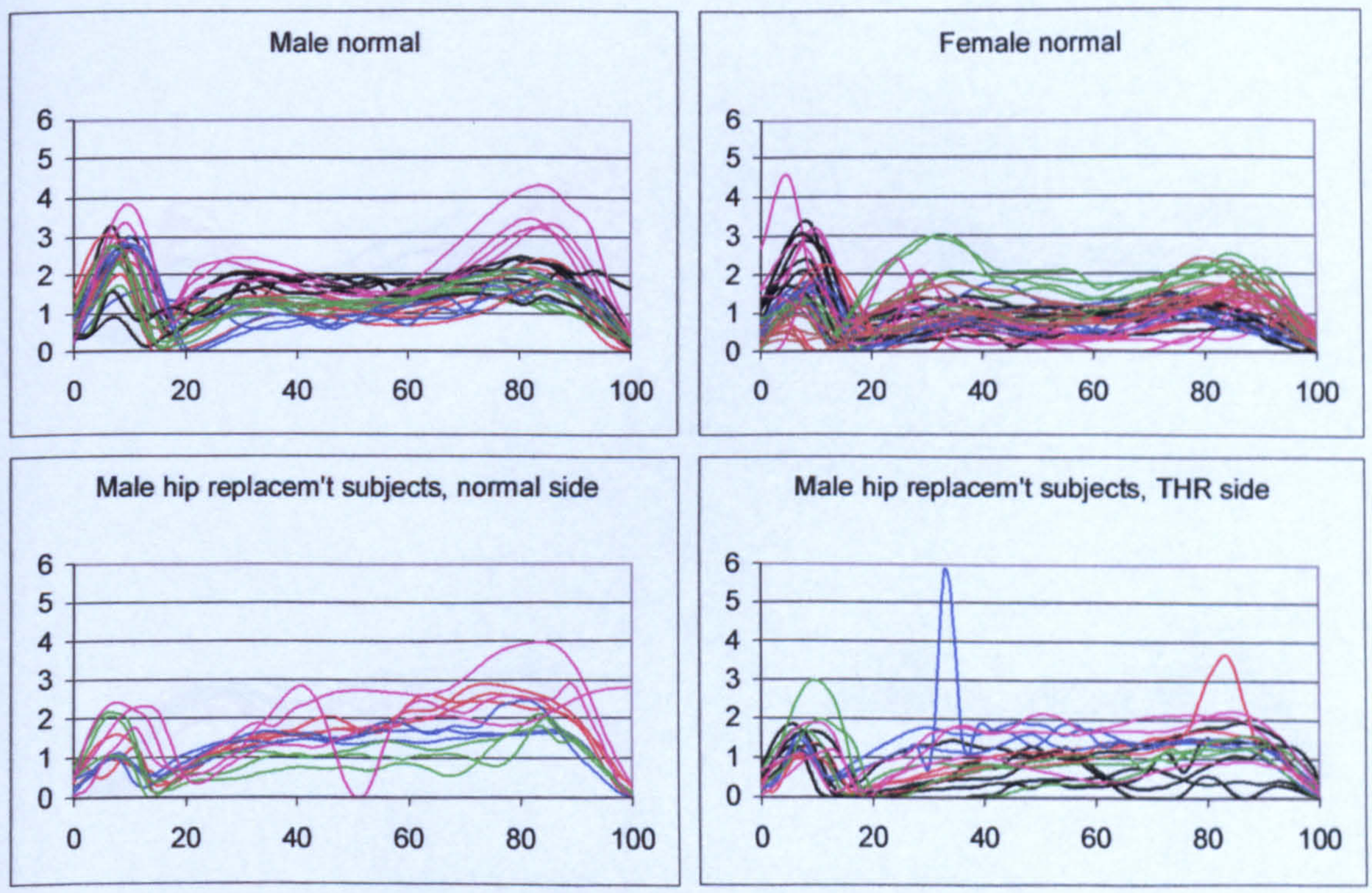

Ramp descent, ankle force AJY2 (N/body weight) by % stance phase

Figure A-VI.5.52 Ramp descent, ankle force AJY2

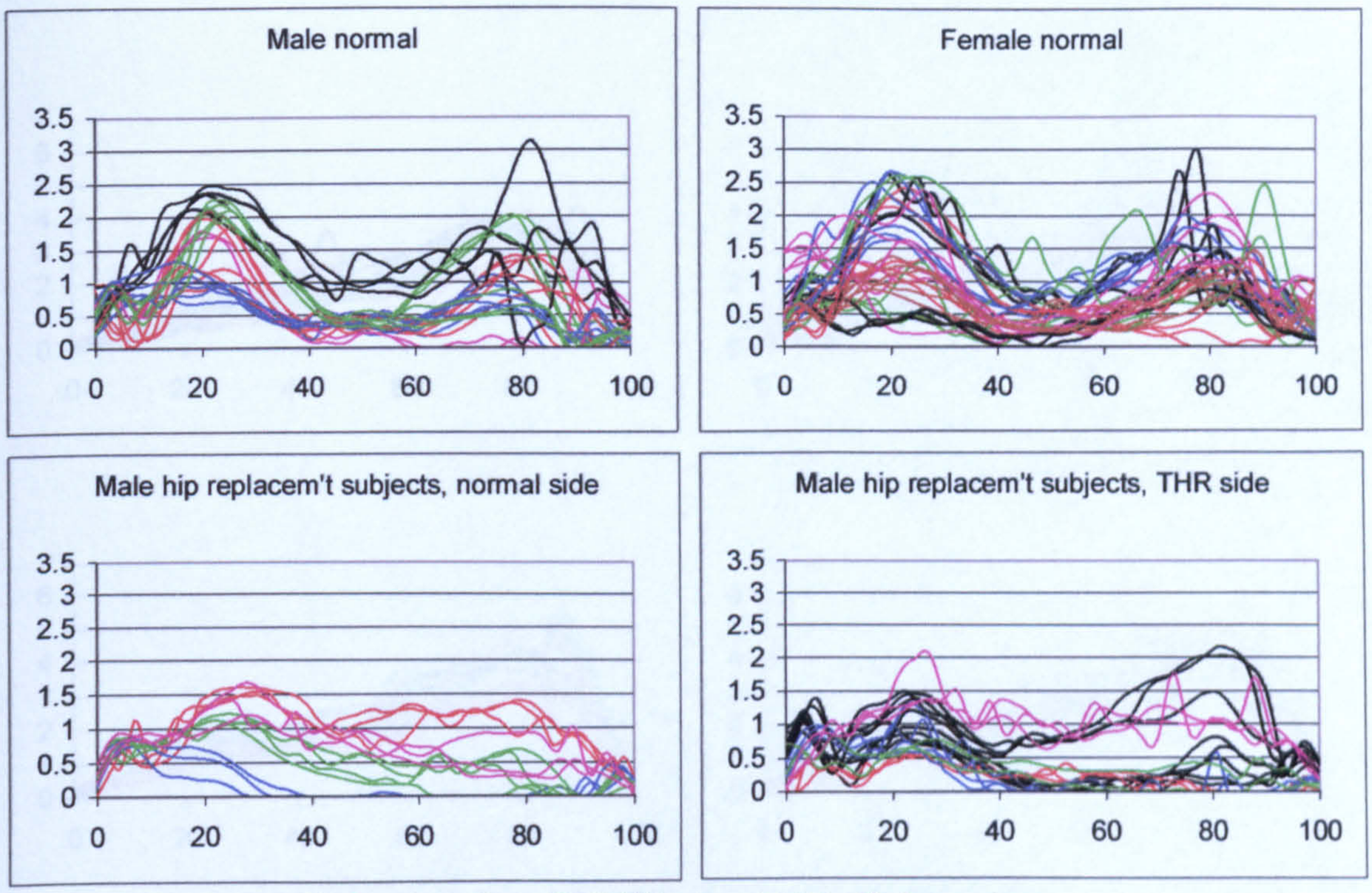

Figure A-VI.5.53 Camber foot up, knee force KJY1

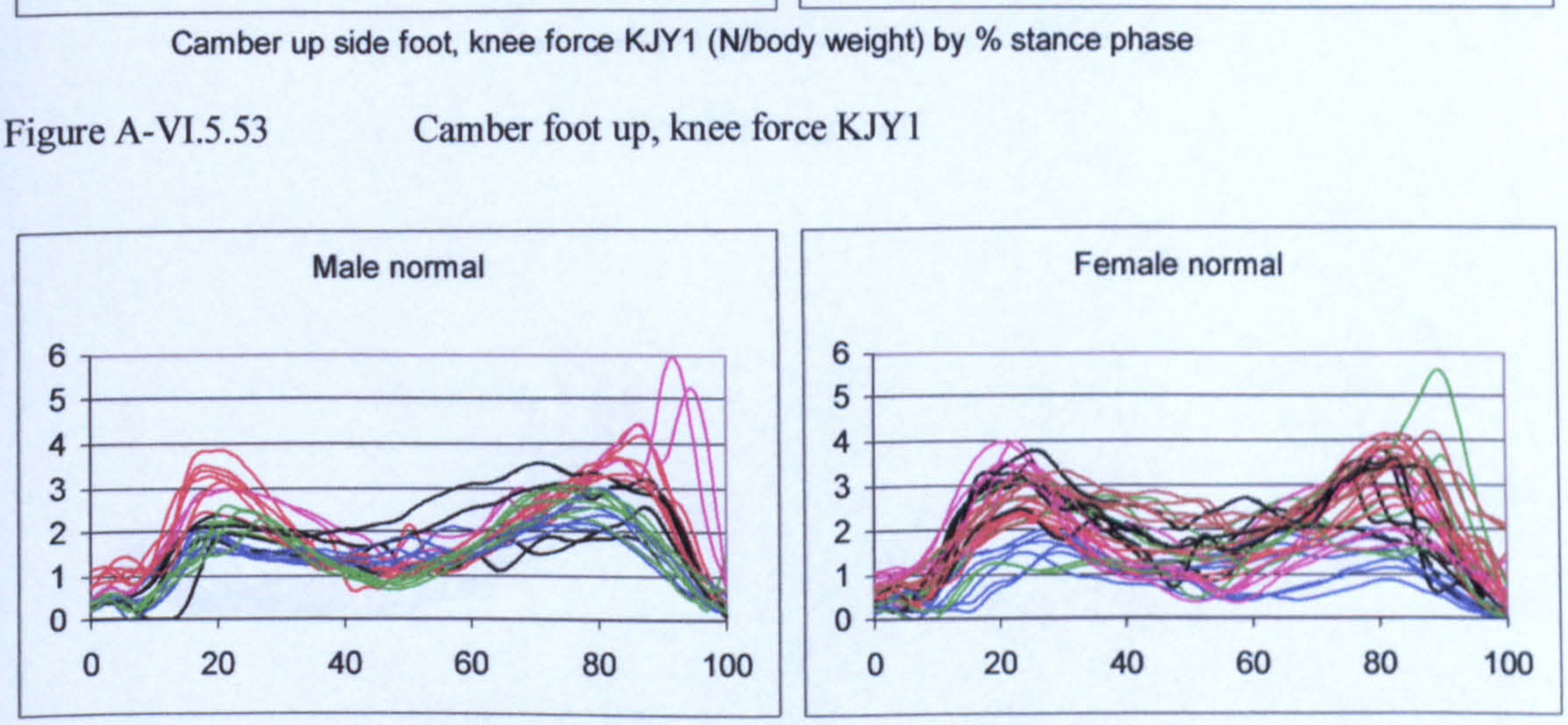

Figure A-VI.5.54 Camber foot up, knee force KJY2

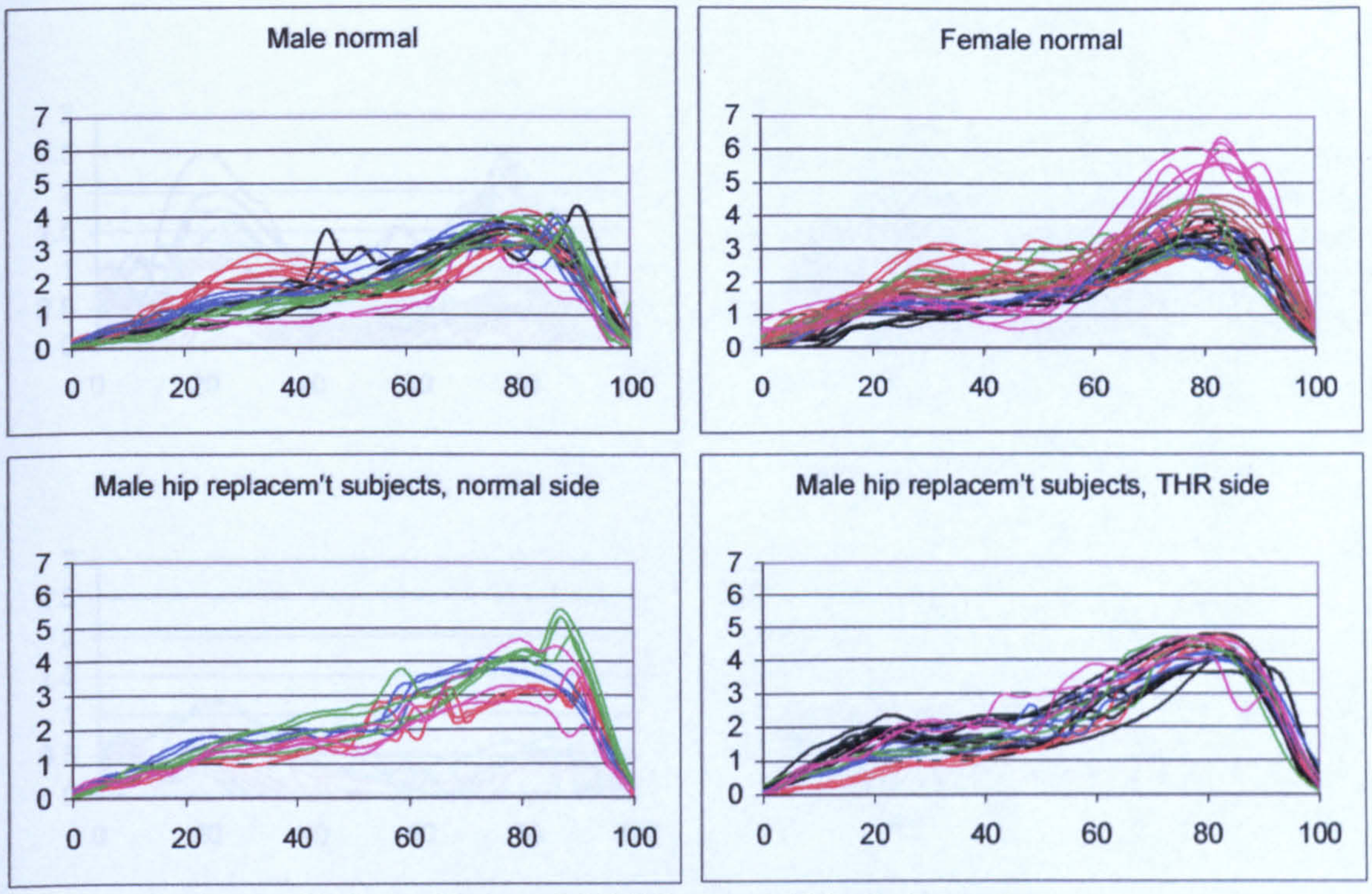

Figure A-VI.5.55 Camber foot up, ankle force AJY1

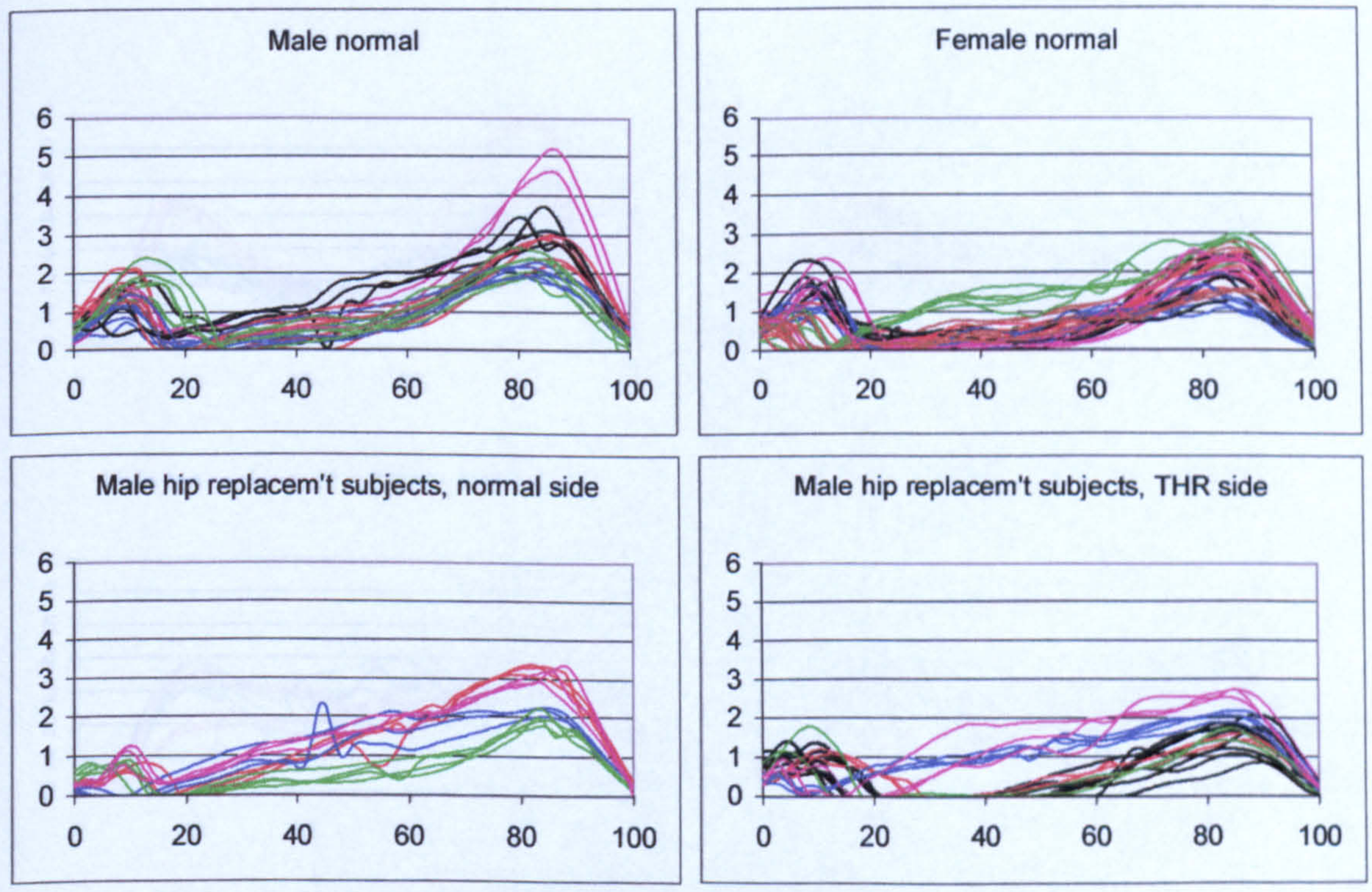

Figure A-VI.5.56 Camber foot up, ankle force AJY2

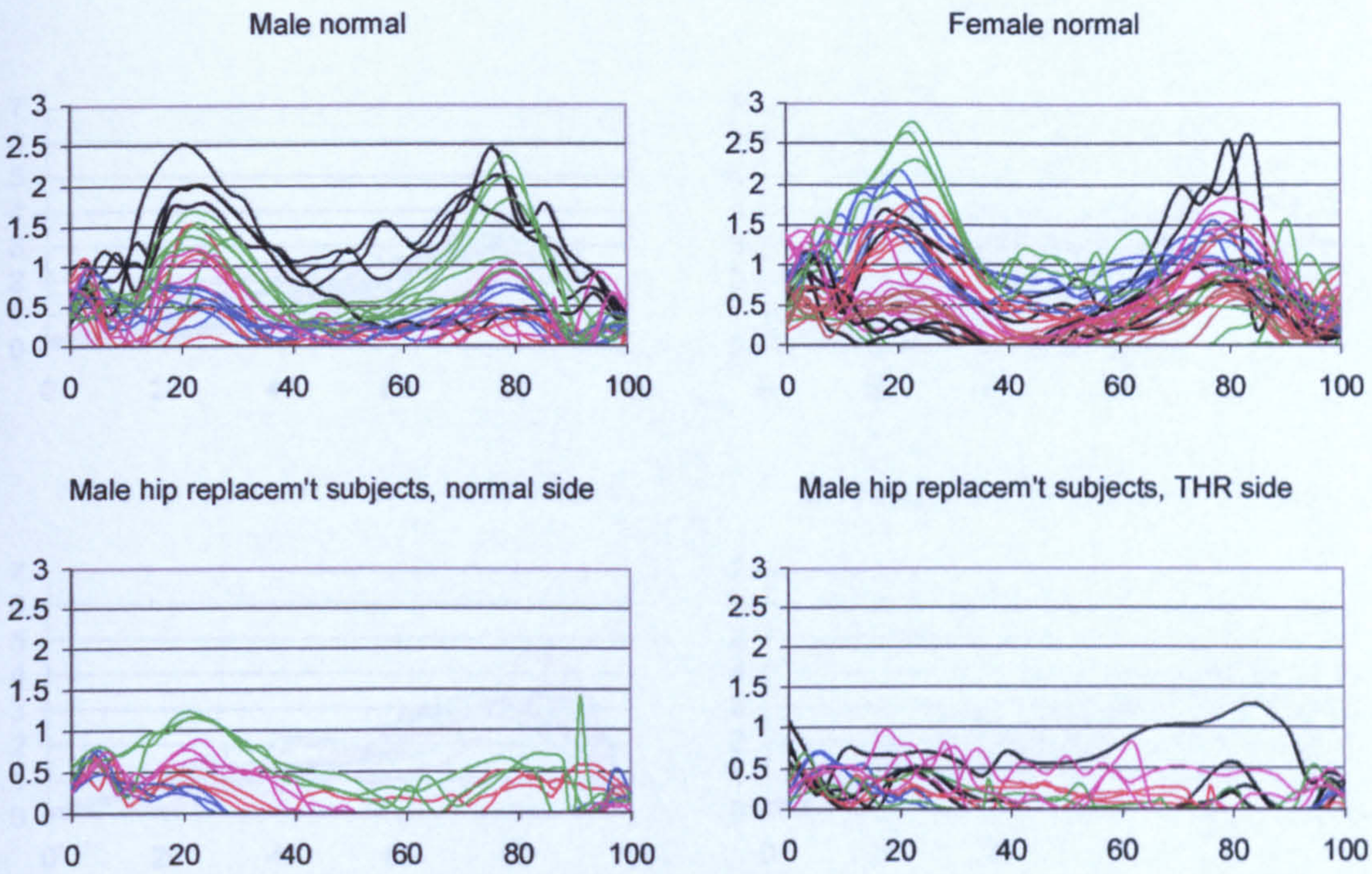

Figure A-VI.5.57 Camber foot down, knee force KJY1

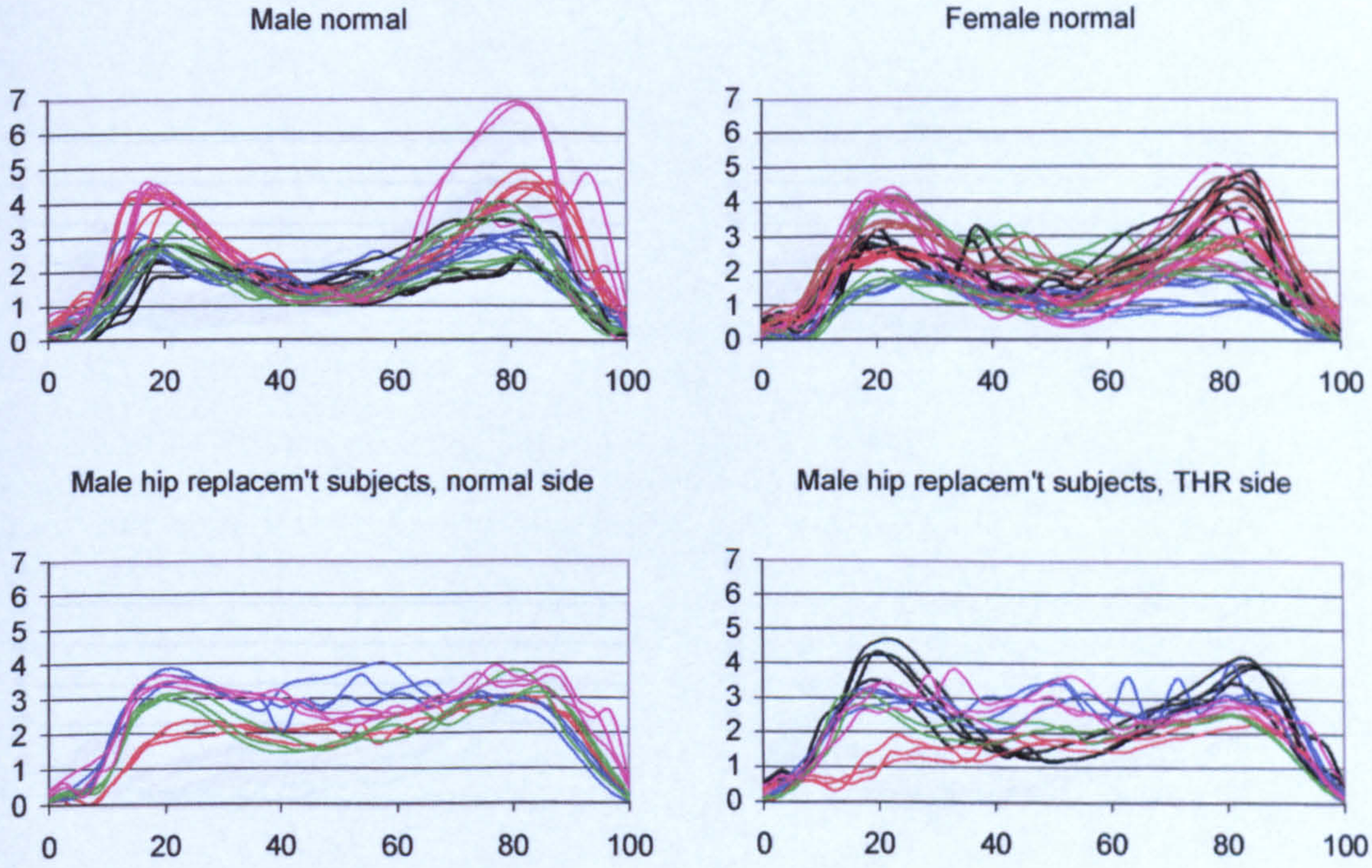

Figure A-VI.5.58 Camber foot down, knee force KJY2

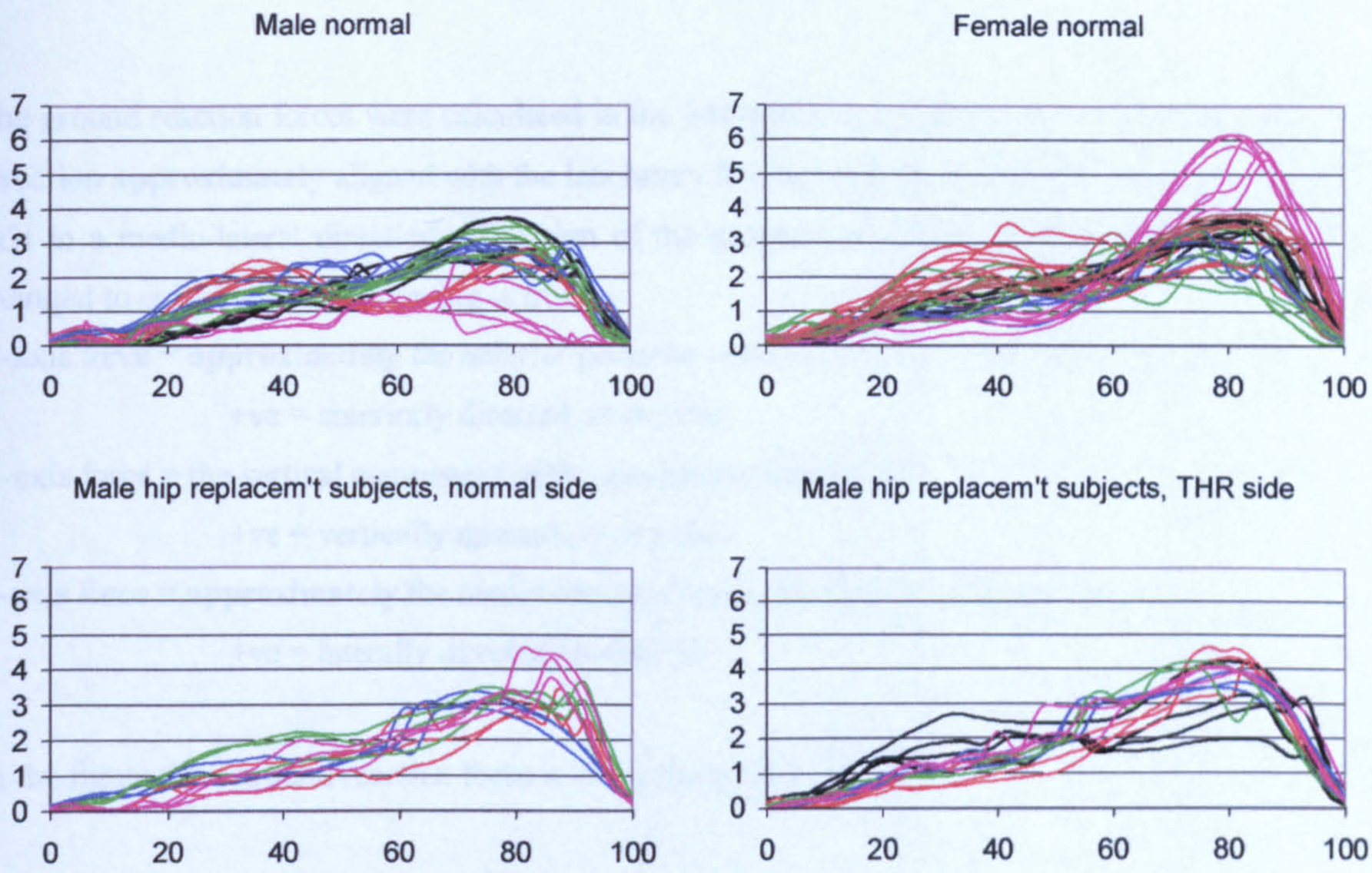

Figure A-VI.5.59 Camber foot down, ankle force AJY1

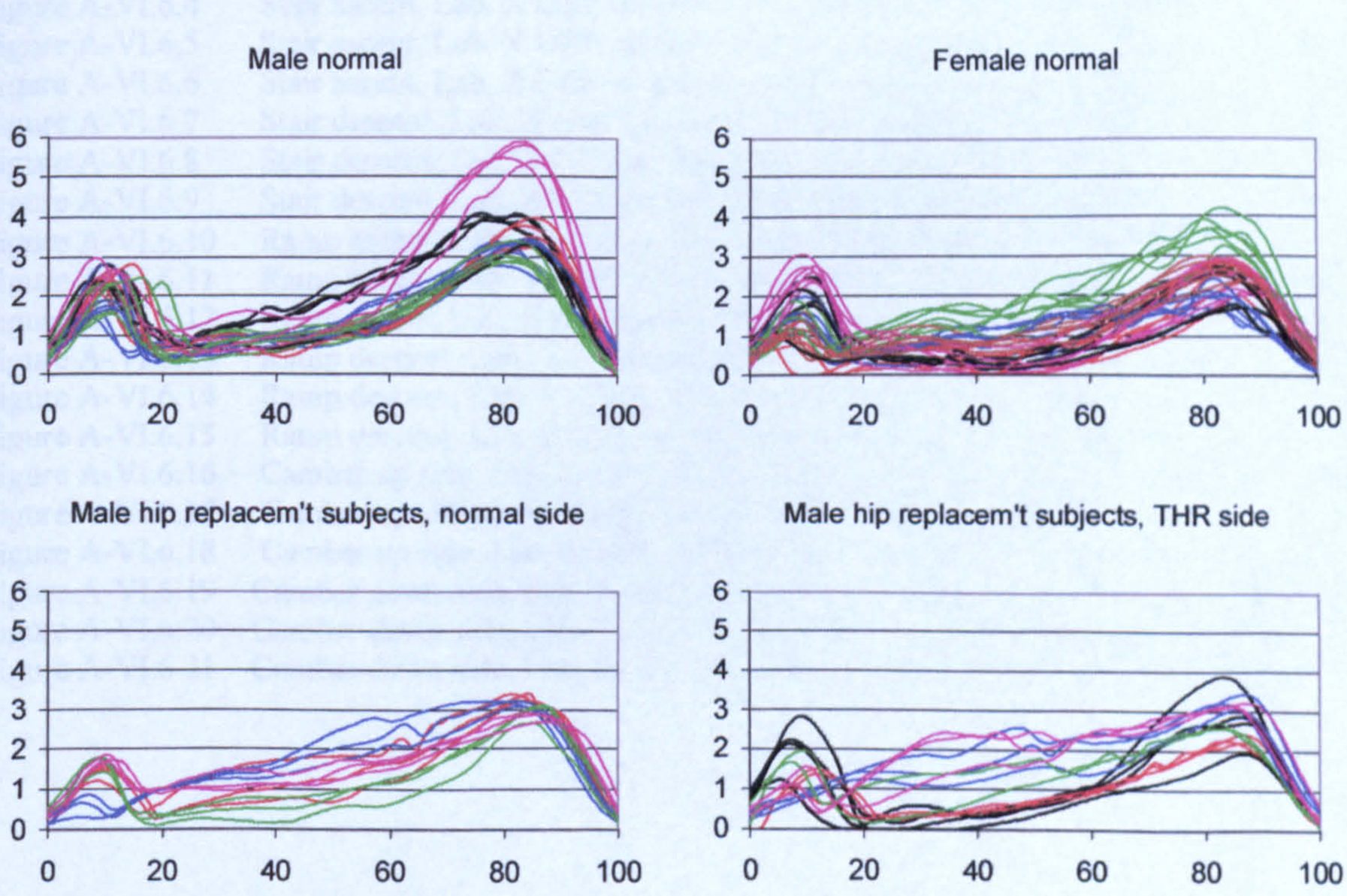

Figure A-VI.5.60 Camber foot down, ankle force AJY2

A-VI.6 Ground reaction forces

The ground reaction forces were calculated in the laboratory axis system. Activities were performed in a direction **approximately** aligned with the laboratory X-axis, with the Y-axis vertically upwards and the Z-axis in a medio-lateral direction. The sign of the ground reaction forces has, where appropriate, been changed to ensure that the following is true:

X-axis force = **approximately** the anterior posterior component of the ground reaction force

+ve = anteriorly directed on the foot

Y-axis force = the vertical component of the ground reaction force

+ve = vertically upwards on the foot

Z-axis force = **approximately** the medio-lateral component of the ground reaction force

+ve = laterally directed on the foot

In the figure titles ground reaction force is abbreviated with 'GRF'.

List of figures

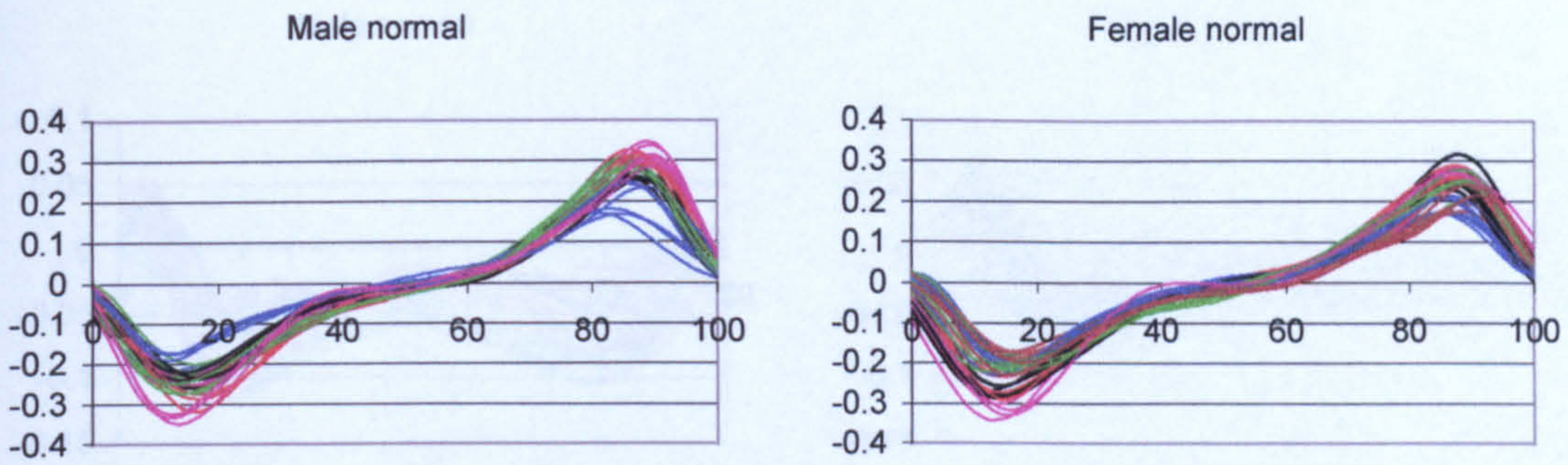

Figure A-VI.6.1 Walking, Lab. X GRF on foot (+ve = anteriorly directed on foot)

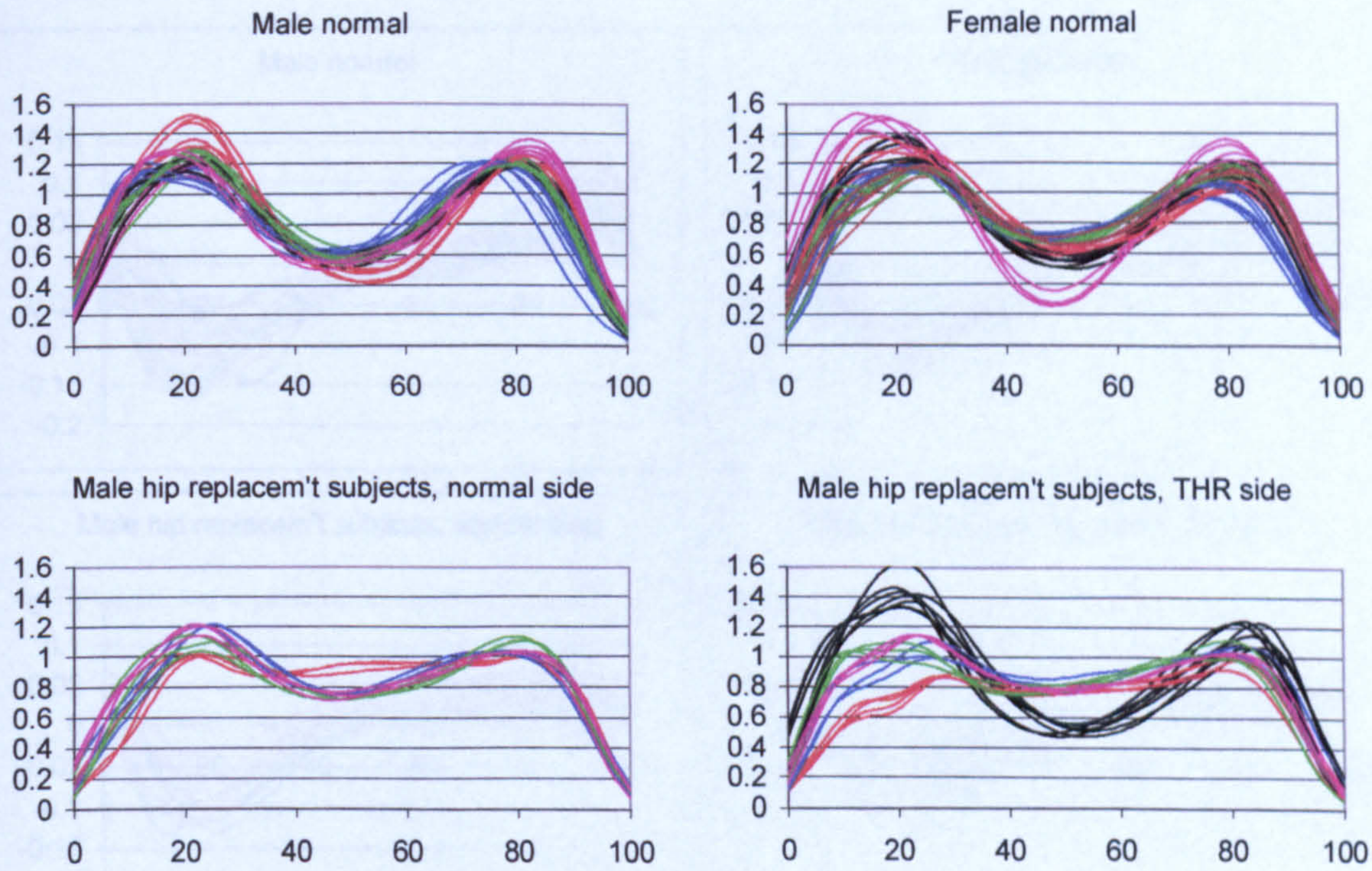

Figure A-VI.6.2 Walking, Lab. Y GRF on foot (+ve = vertically upwards)

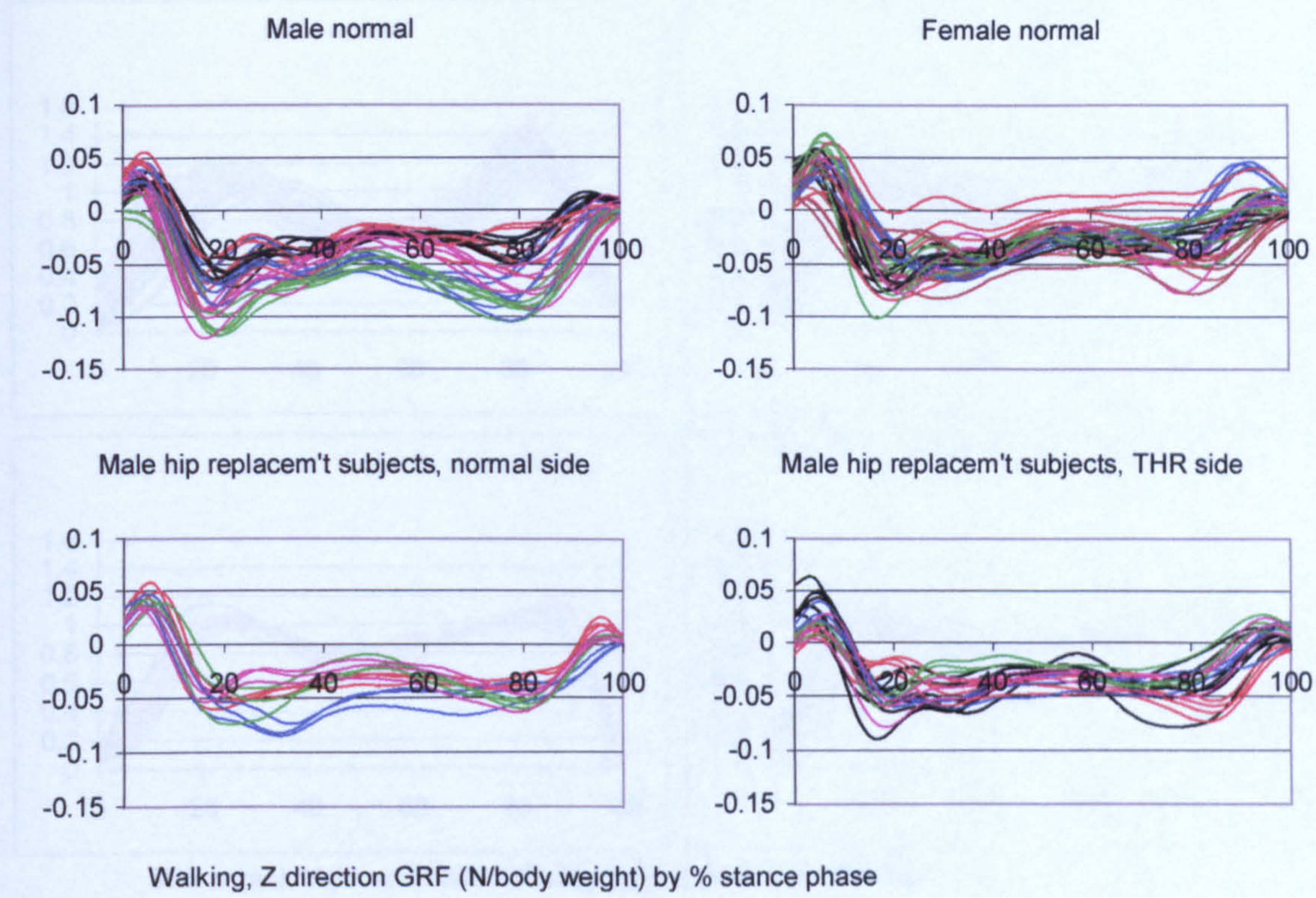

Figure A-VI.6.3 Walking, Lab. Z GRF on foot (+ve = laterally directed on foot)

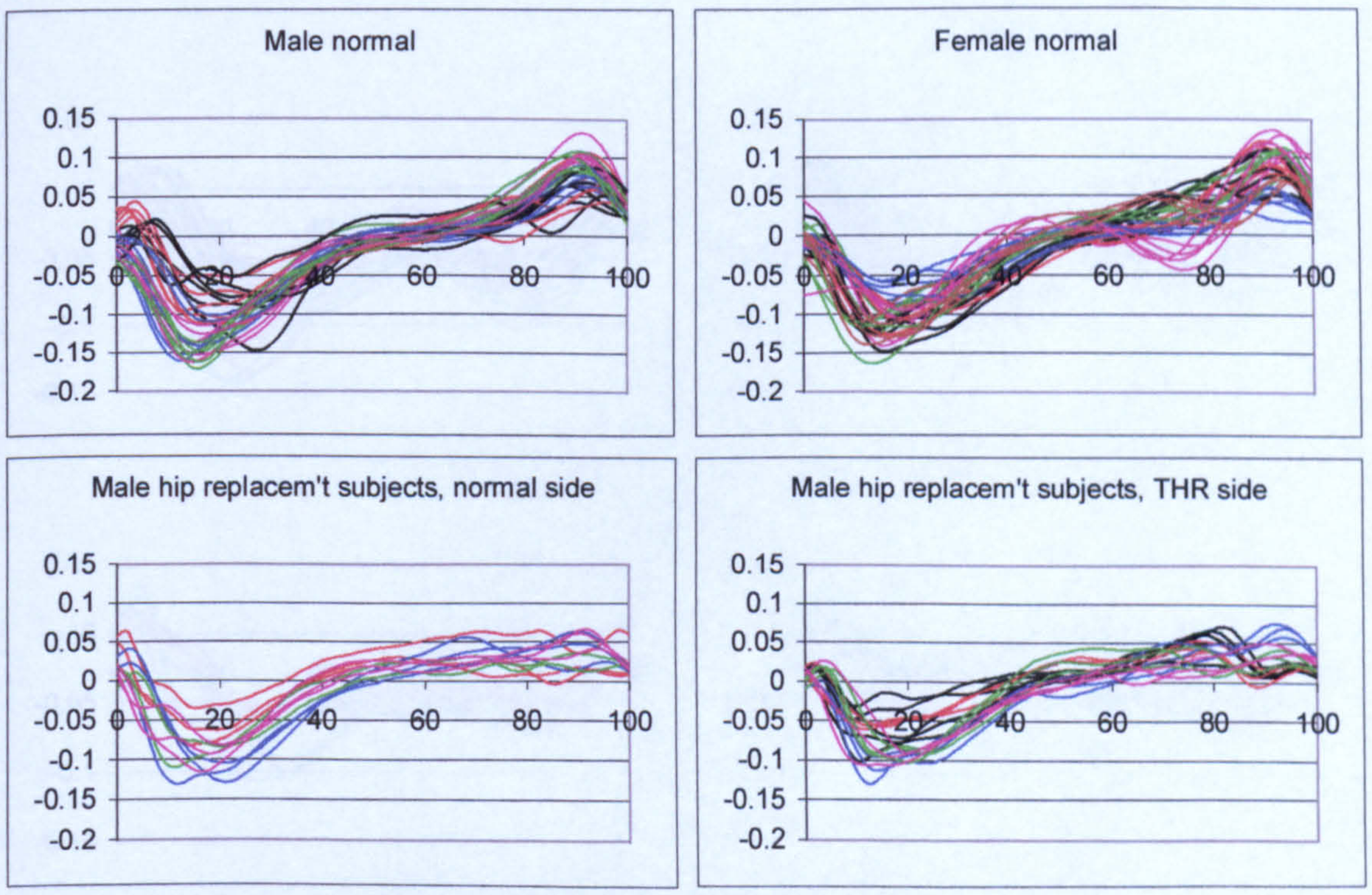

Figure A-VI.6.4 Stair ascent, Lab. X GRF on foot (+ve = anteriorly directed on foot)

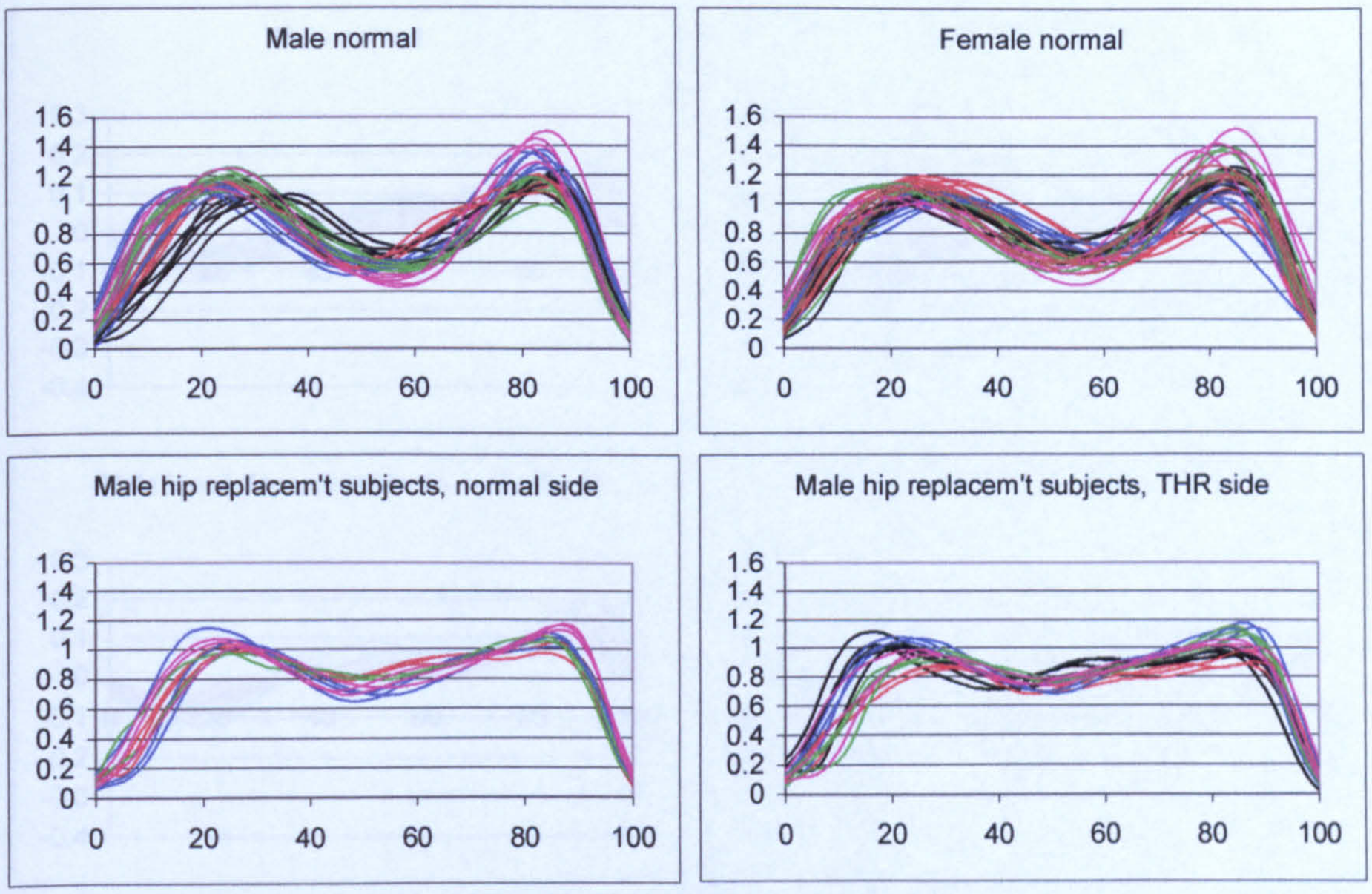

Figure A-VI.6.5 Stair ascent, Lab. Y GRF on foot (+ve = vertically upwards)

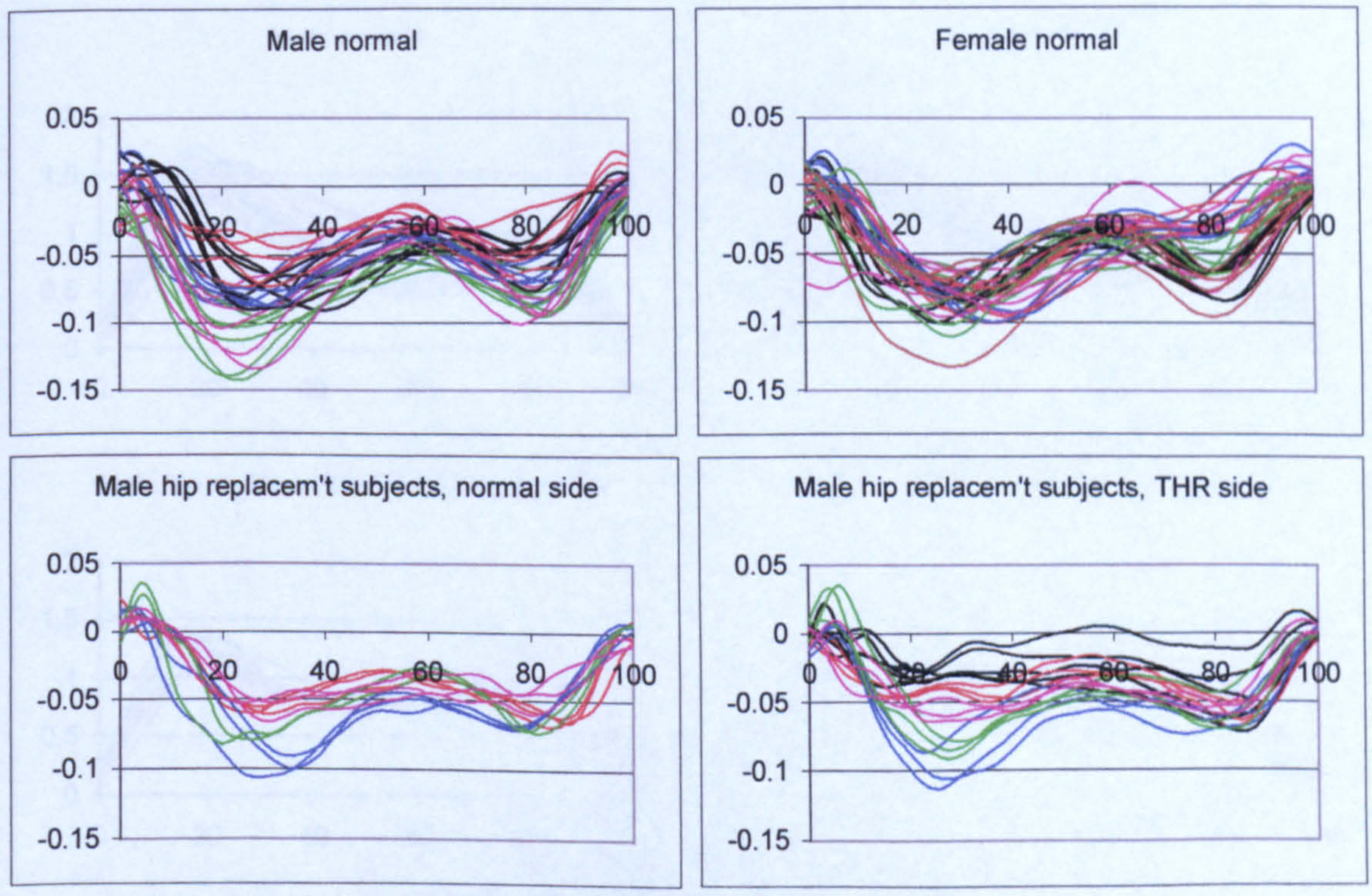

Figure A-VI.6.6 Stair ascent, Lab. Z GRF on foot (+ve = laterally directed on foot)

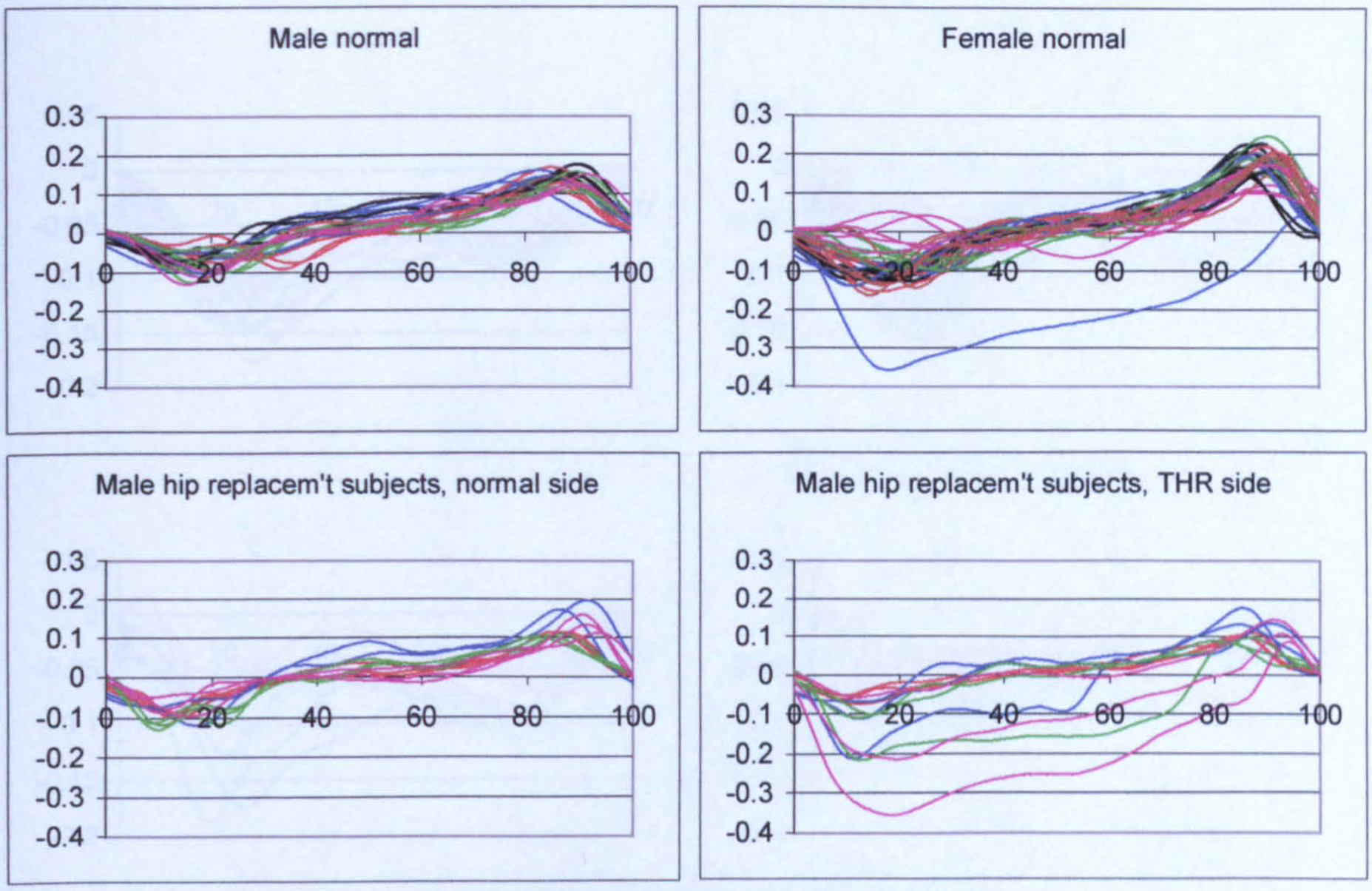

Stair descent, X direction GRF (N/body weight) by % stance phase

Figure A-VI.6.7 Stair descent, Lab. X GRF on foot (+ve = anteriorly directed on foot)

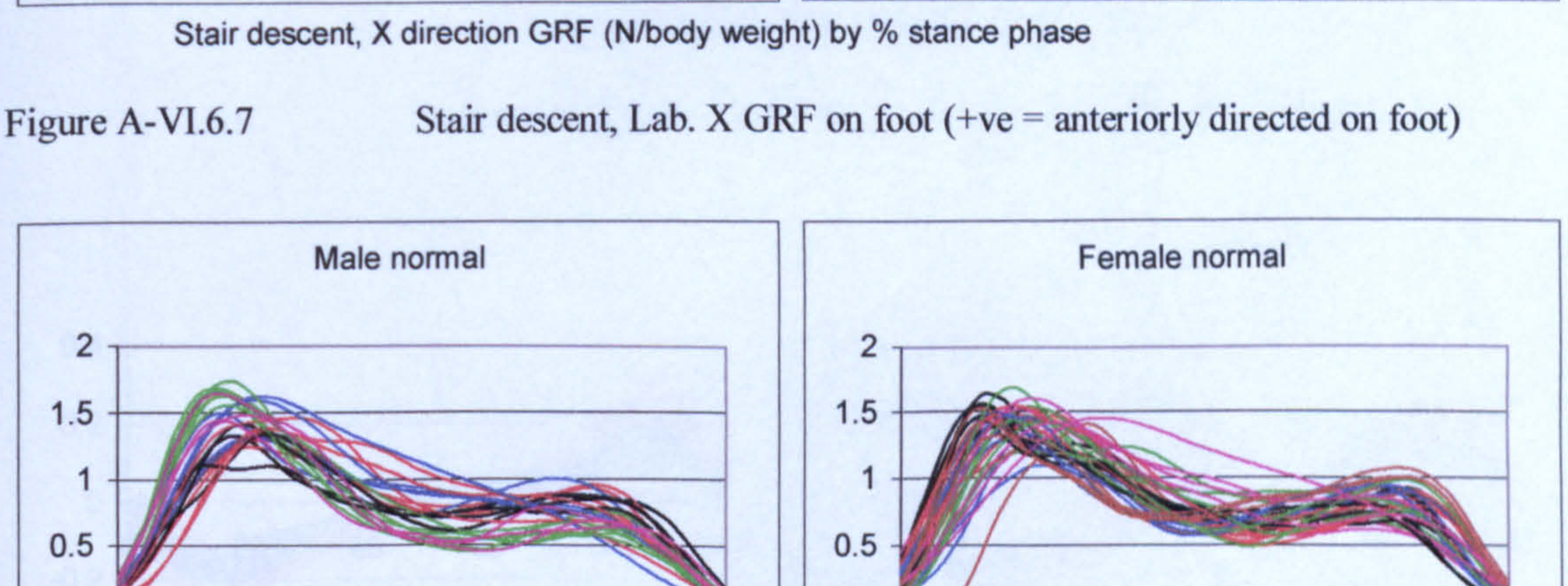

Stair descent, Y direction GRF (N/body weight) by % stance phase

Figure A-VI.6.8 Stair descent, Lab. Y GRF on foot (+ve = vertically upwards)

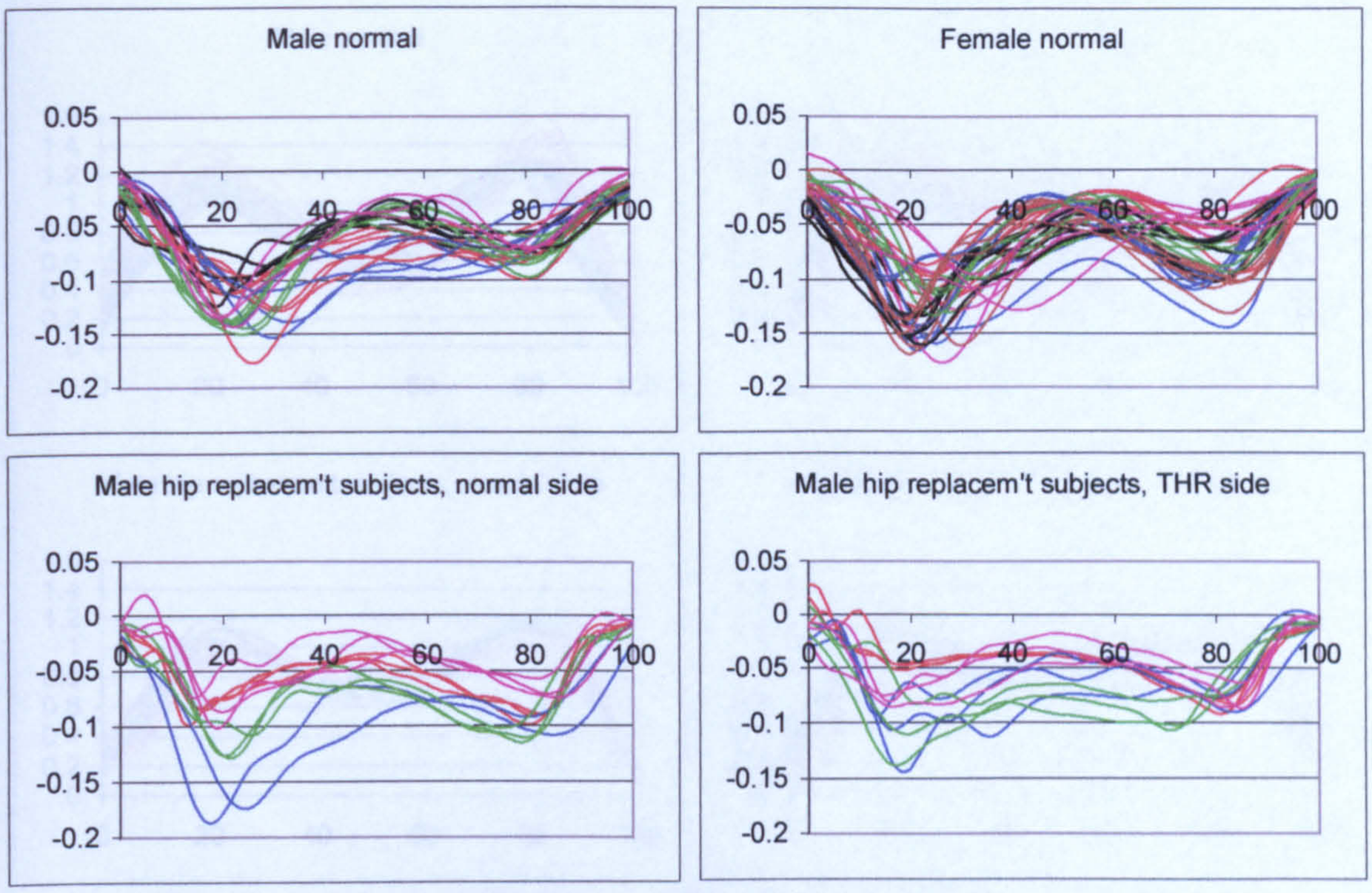

Figure A-VI.6.9 Stair descent, Lab. Z GRF on foot (+ve = laterally directed on foot)

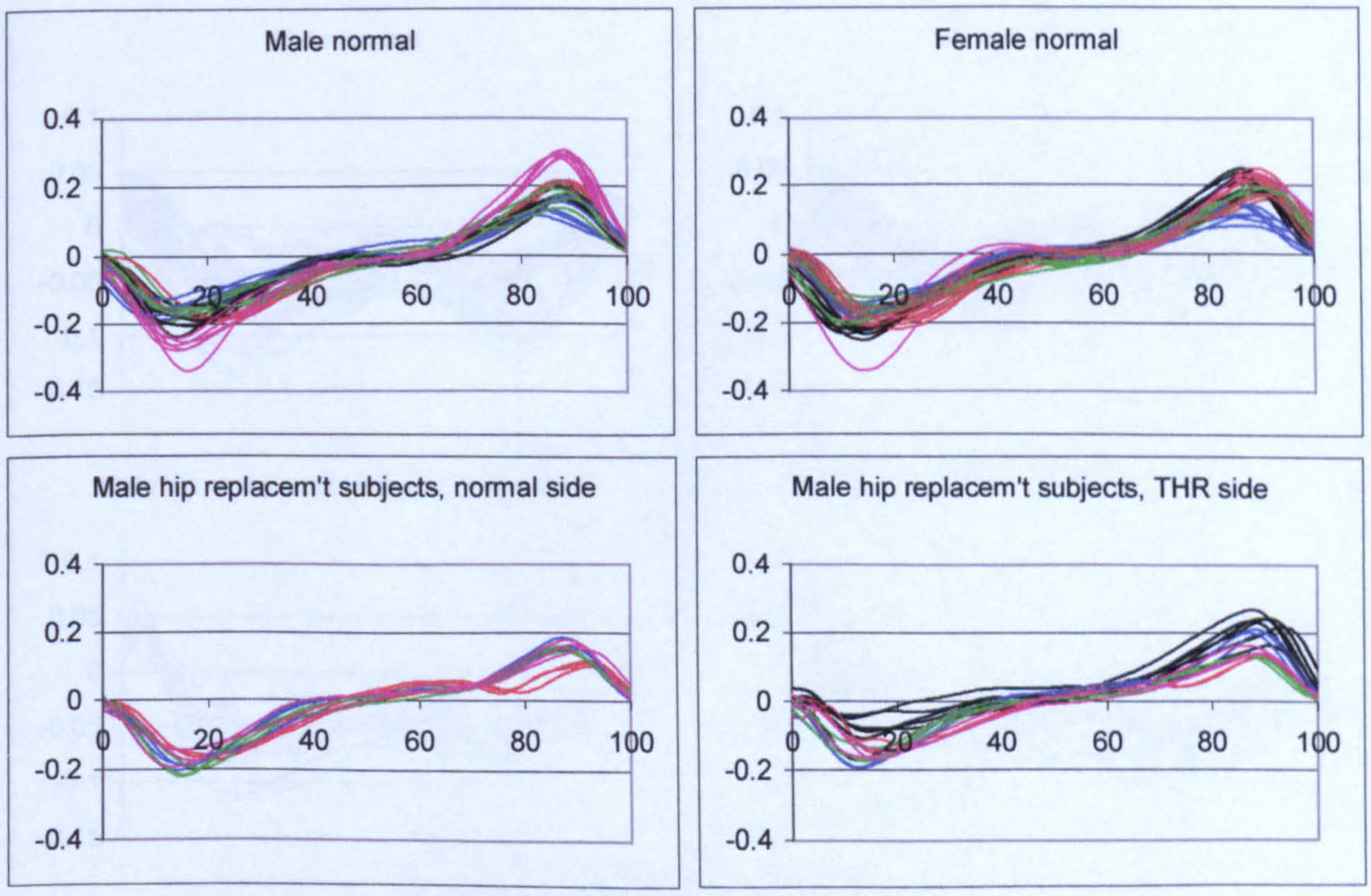

Figure A-VI.6.10 Ramp ascent, Lab. X GRF on foot (+ve = anteriorly directed on foot)

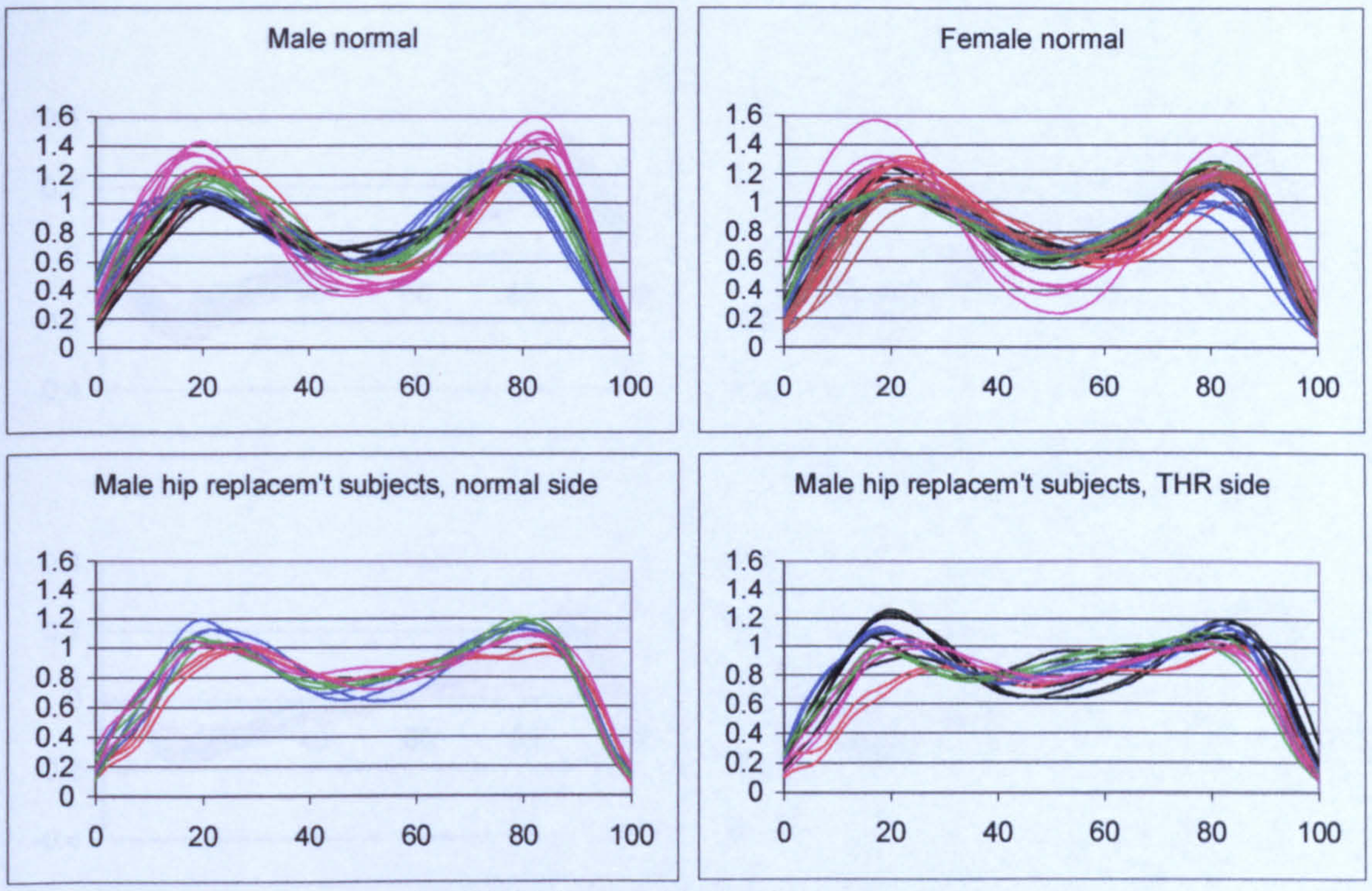

Figure A-VI.6.11 Ramp ascent, Lab. Y GRF on foot (+ve = vertically upwards)

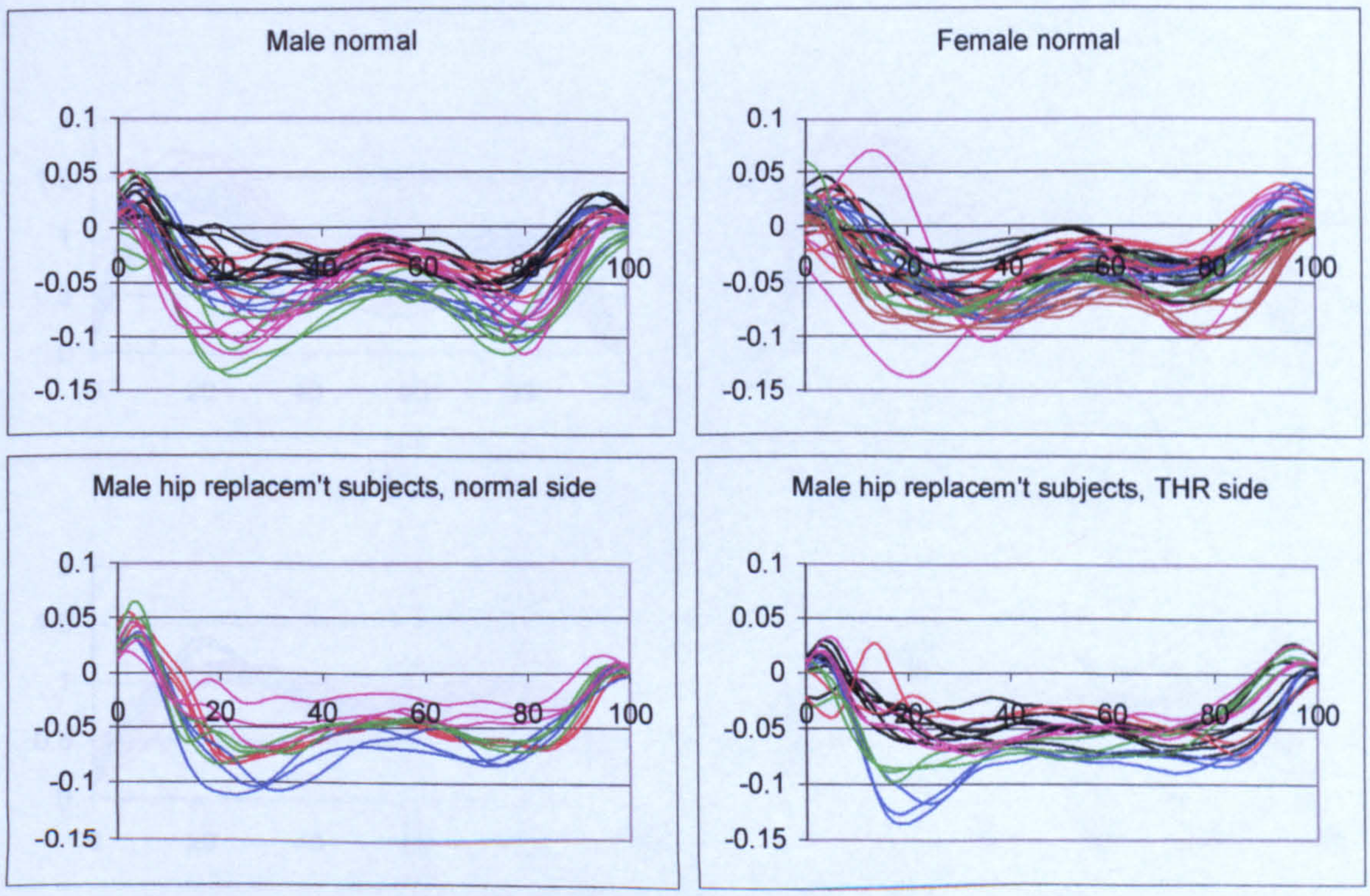

Figure A-VI.6.12 Ramp ascent, Lab. Z GRF on foot (+ve = laterally directed on foot)

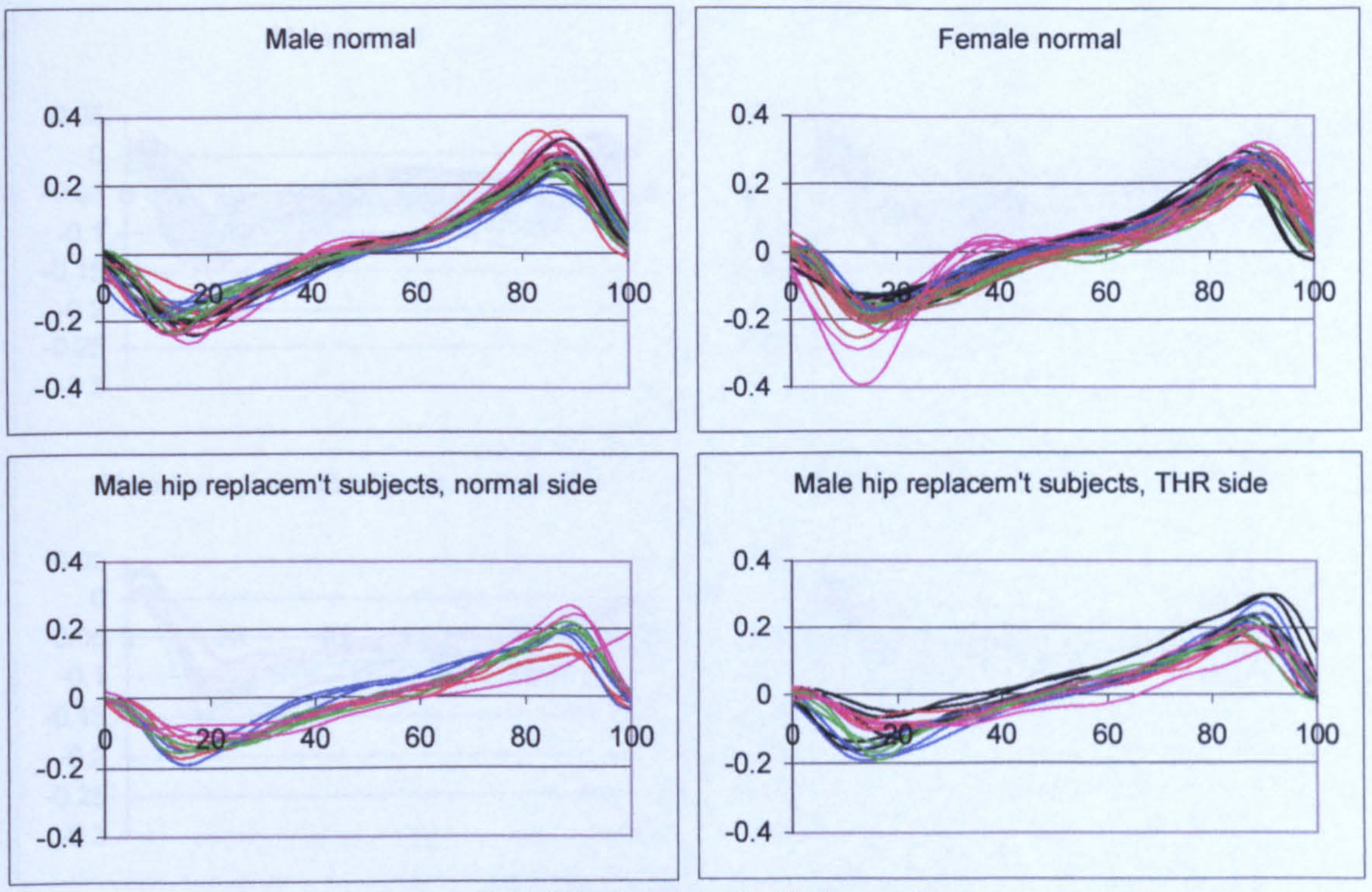

Figure A-VI.6.13 Ramp descent, Lab. X GRF on foot (+ve = anteriorly directed on foot)

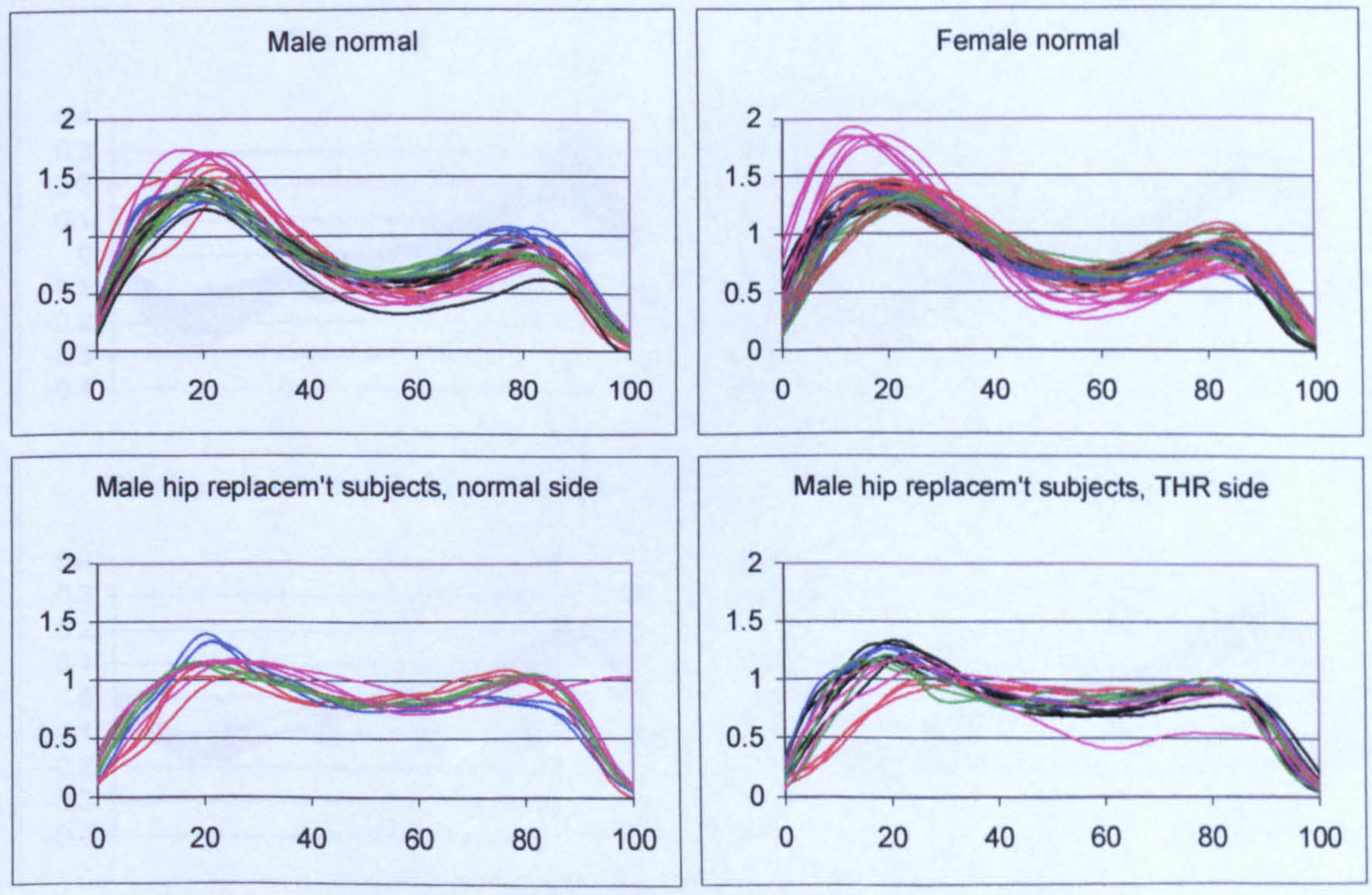

Figure A-VI.6.14 Ramp descent, Lab. Y GRF on foot (+ve = vertically upwards)

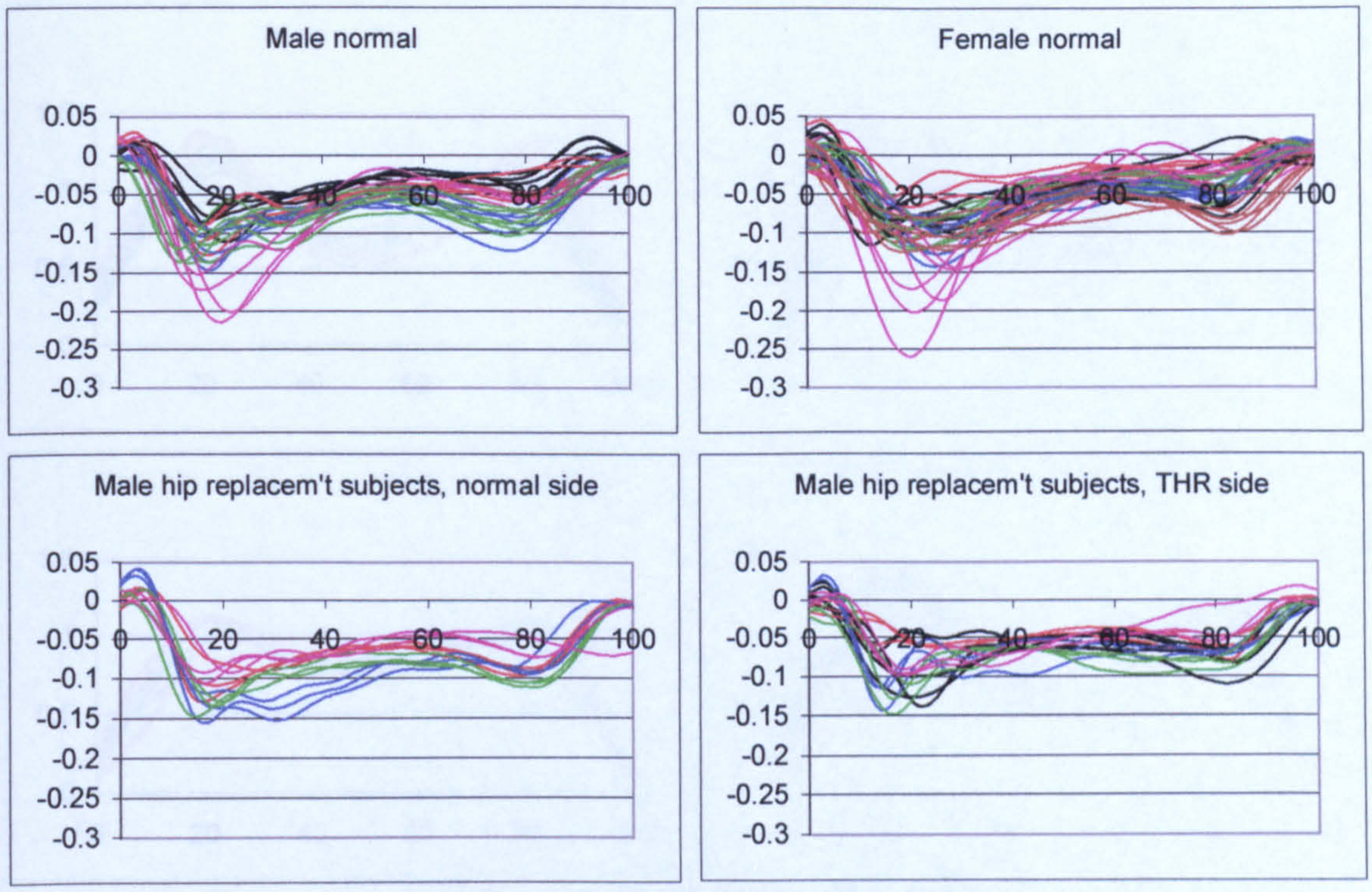

Figure A-VI.6.15 Ramp descent, Lab. Z GRF on foot (+ve = laterally directed on foot)

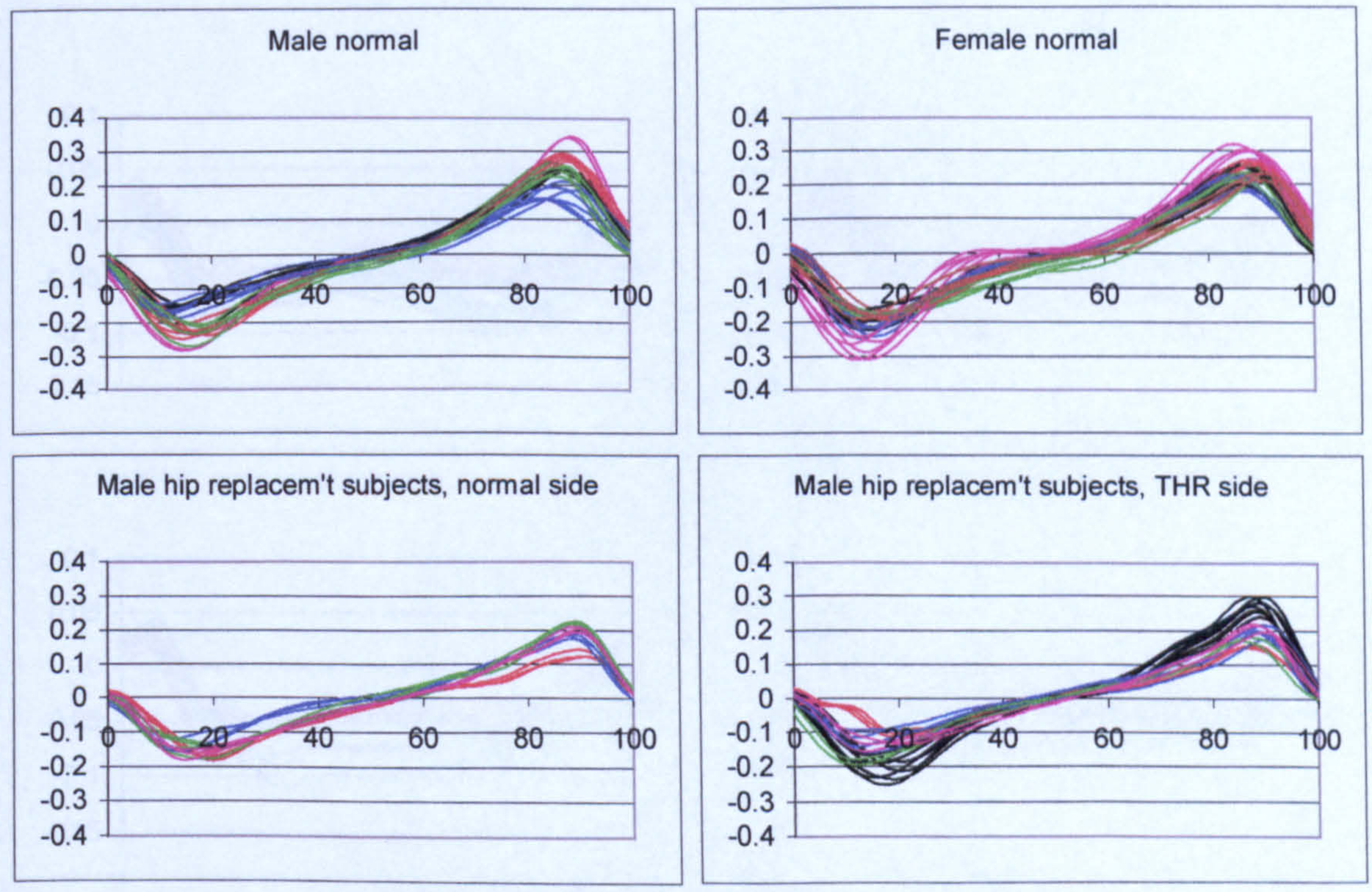

Figure A-VI.6.16 Camber up side, Lab. X GRF on foot (+ve = anteriorly directed on foot)

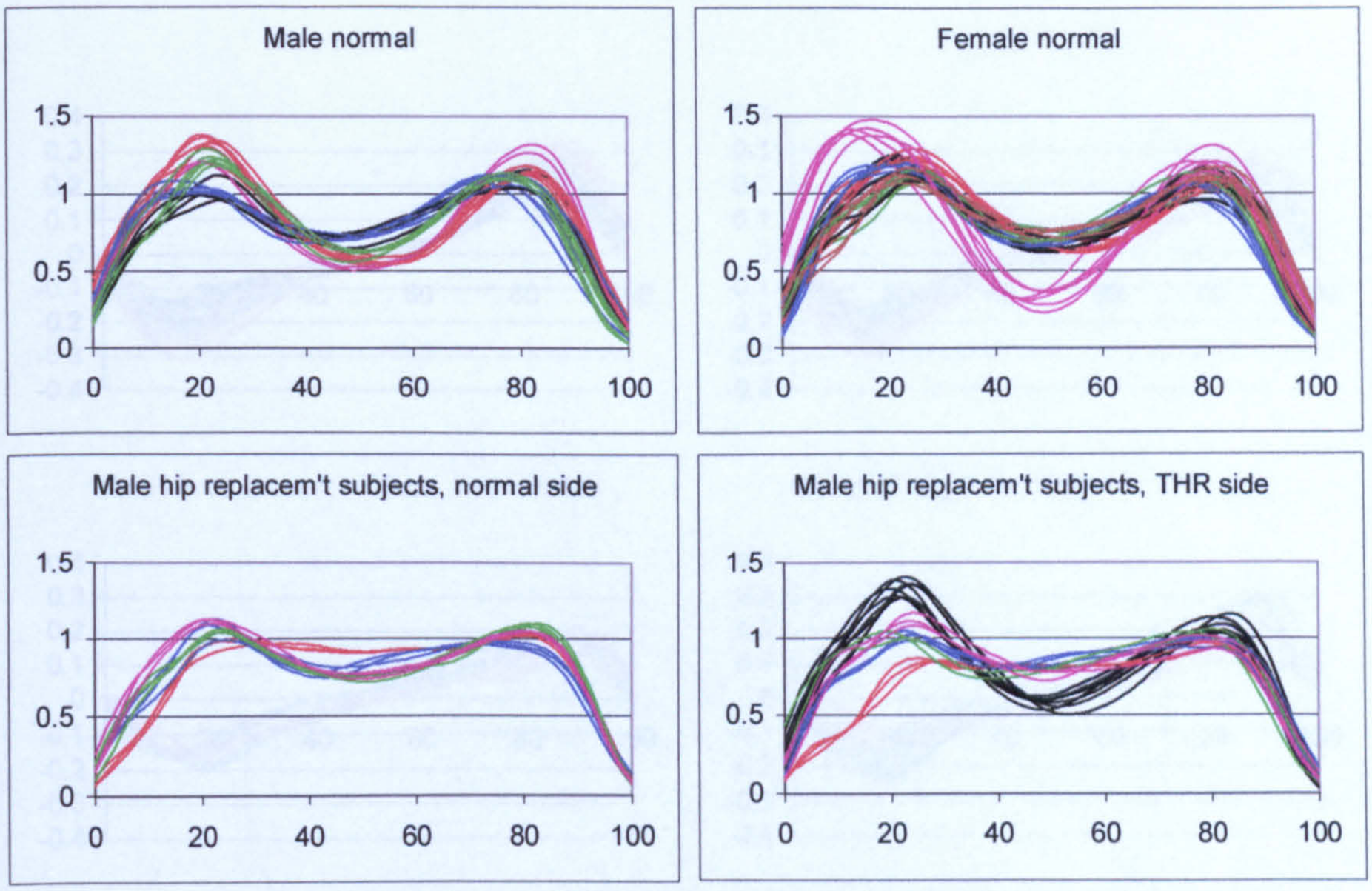

Camber up side foot, Y direction GRF (N/body weight) by % stance phase

Figure A-VI.6.17 Camber up side, Lab. Y GRF on foot (+ve = vertically upwards)

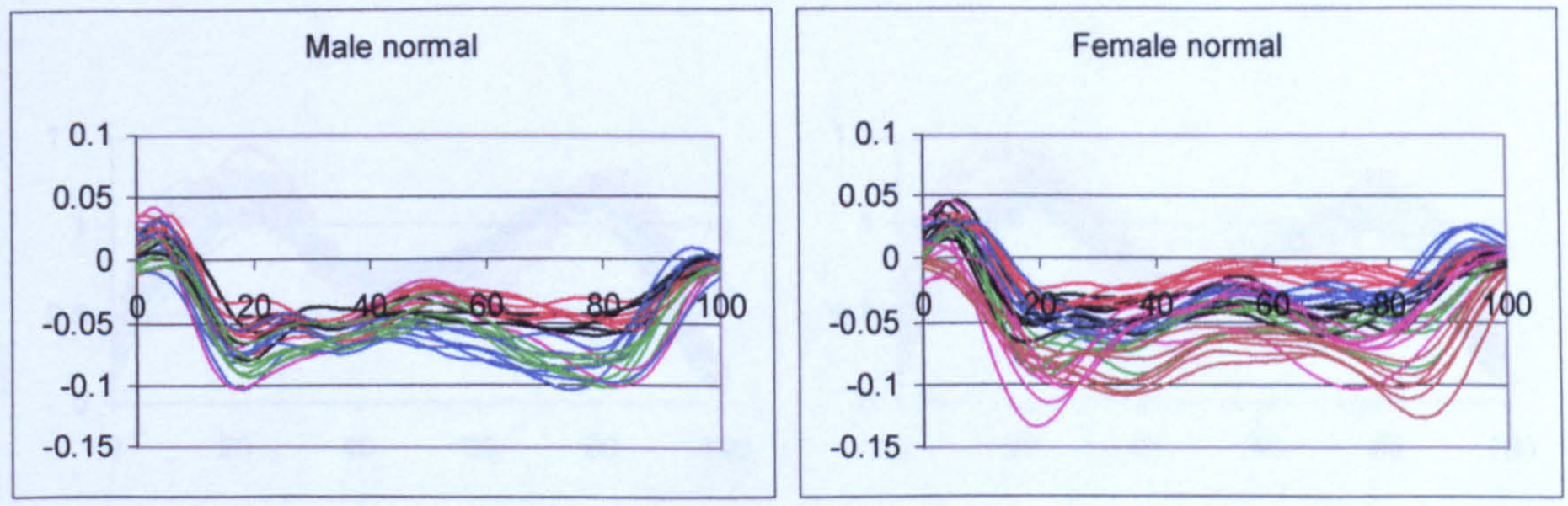

Camber up side foot, Z direction GRF (N/body weight) by % stance phase

Figure A-VI.6.18 Camber up side, Lab. Z GRF on foot (+ve = laterally directed on foot)

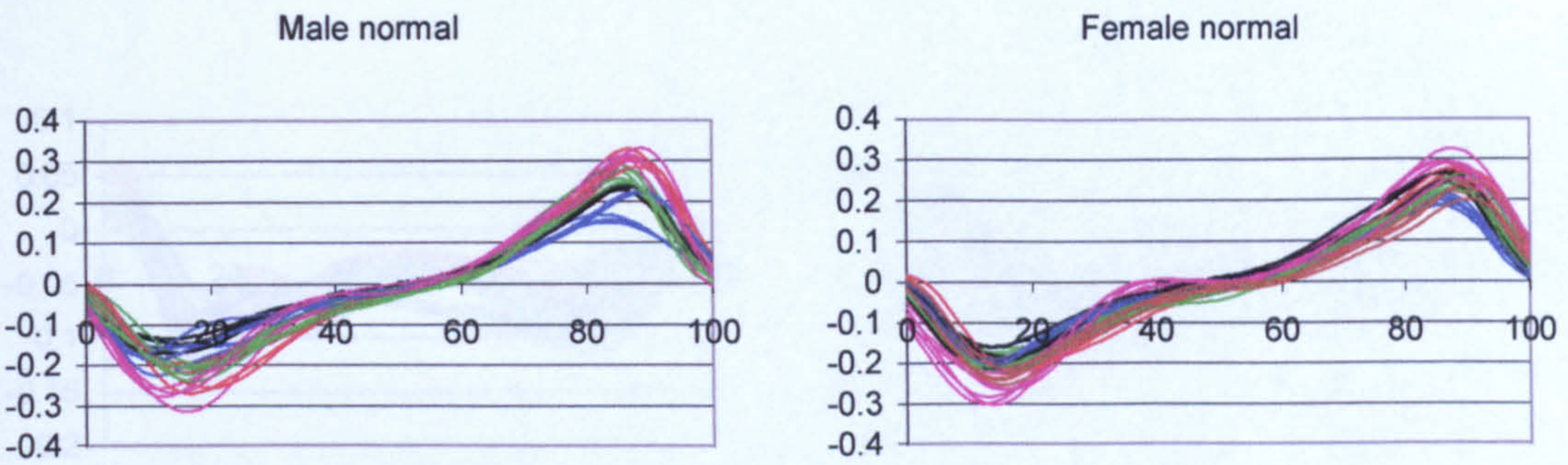

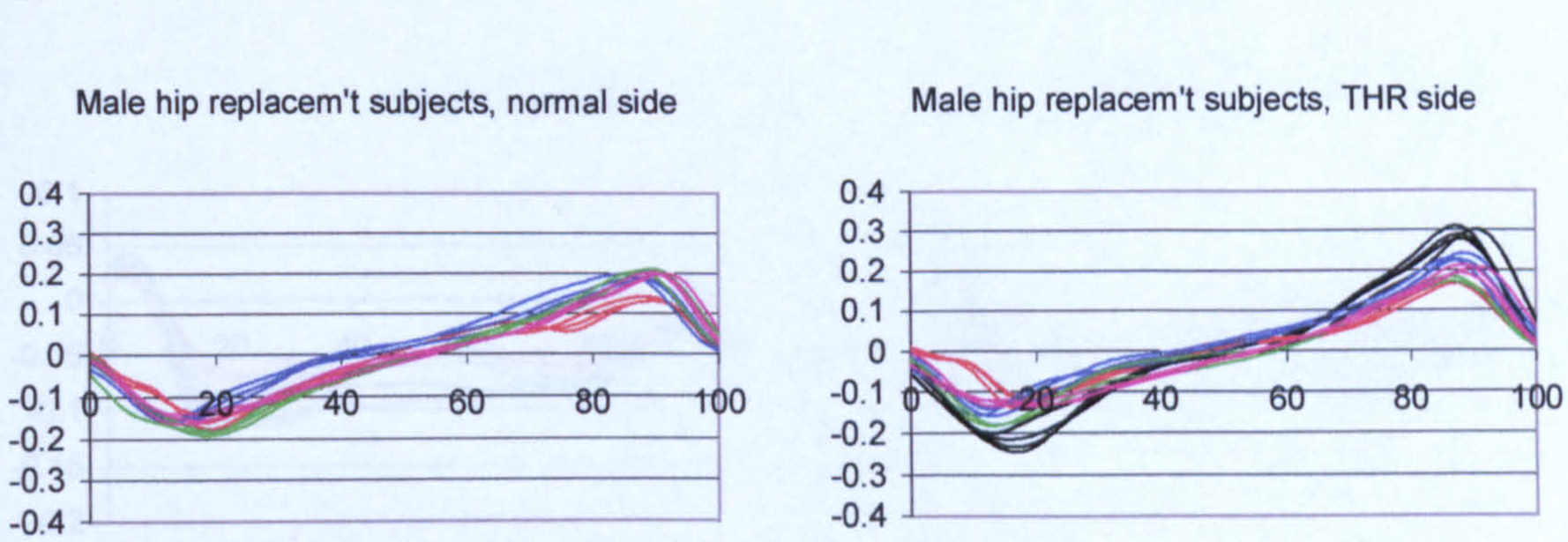

Figure A-VI.6.19 Camber down side, Lab. X GRF on foot (+ve = anteriorly directed on foot)

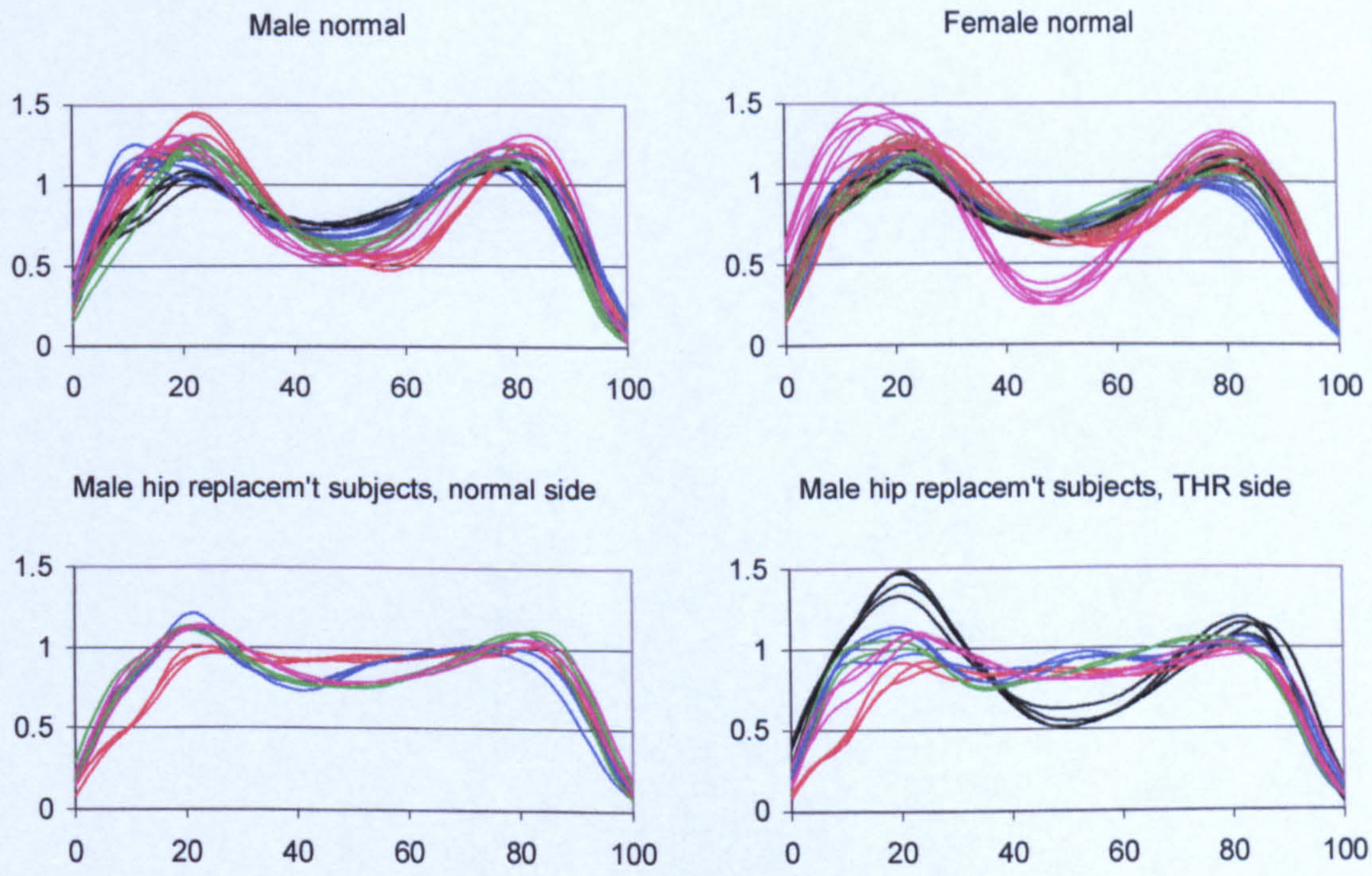

Figure A-VI.6.20 Camber down side, Lab. Y GRF on foot (+ve = vertically upwards)

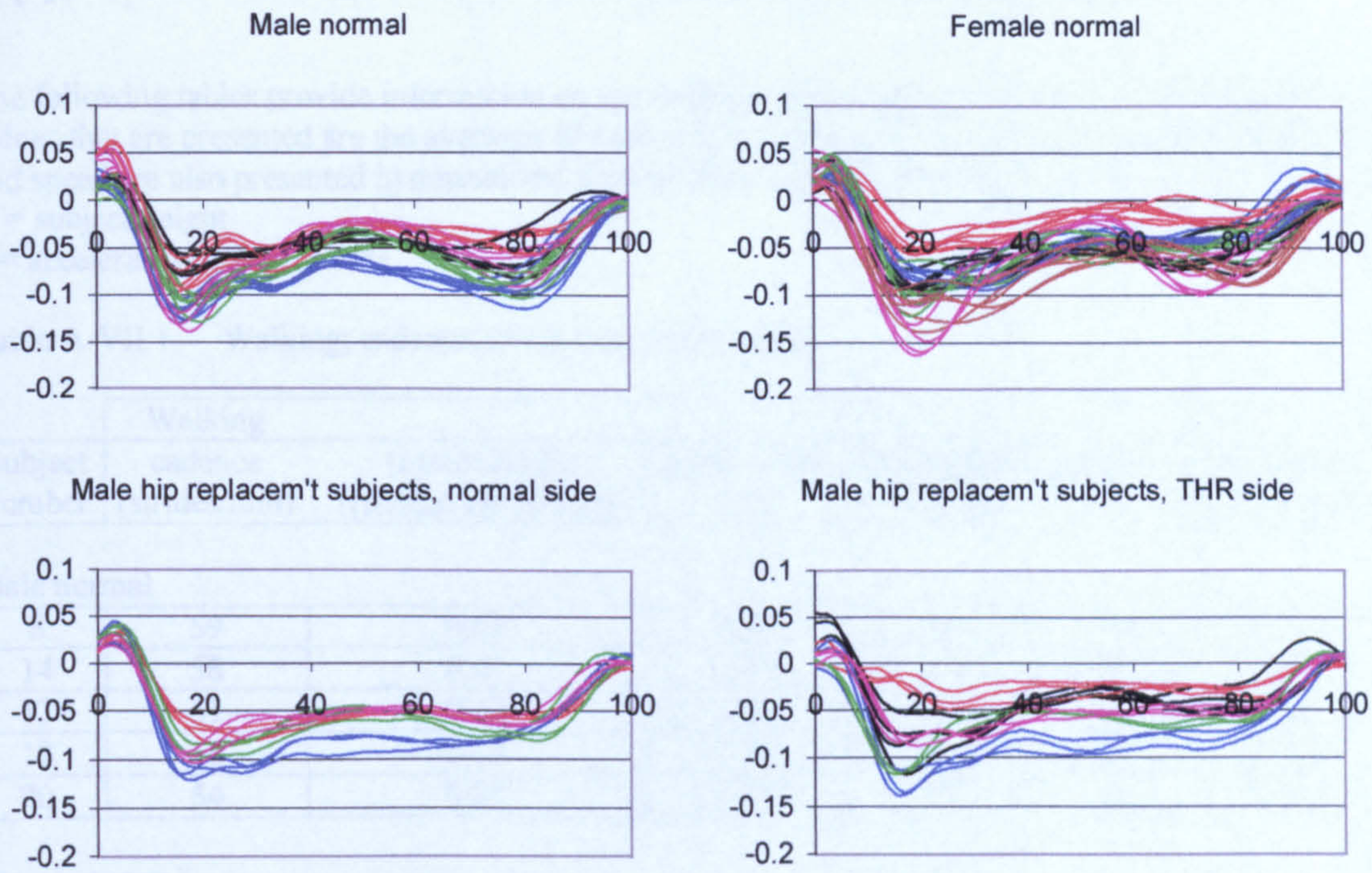

Figure A-VI.6.21 Camber down side, Lab. Z GRF on foot (+ve = laterally directed on foot)

Appendix VII Cadence, stride length and speed

The following tables provide information on the cadence, stride length and speed of the subjects. The values that are presented are the averages of each subject's trials for that activity. Cadence, stride length and speed are also presented in normalised form as dimensionless quantities.
H = subject height
g = acceleration due to gravity

Table A-VII.1 Walking; cadence, stride length and speed

	Walking					
Subject number	cadence (strides/min)	(normalised) ([strides/s]×√(H/g))	stride length (m)	(normalised) ([m]/H)	speed (m/s)	(normalised) ([m/s]/√(g×H)
Male normal						
8	59	0.41	1.67	0.97	1.63	0.40
14	58	0.41	1.85	1.03	1.77	0.42
17	61	0.42	1.48	0.88	1.50	0.37
18	56	0.40	1.78	0.97	1.65	0.39
20	54	0.39	1.88	1.03	1.69	0.40
Female normal						
15	59	0.40	1.63	0.99	1.61	0.40
19	59	0.40	1.60	0.99	1.56	0.39
33	59	0.40	1.44	0.88	1.42	0.36
34	57	0.41	1.54	0.85	1.46	0.35
35	74	0.49	1.56	1.00	1.92	0.49
36	59	0.41	1.39	0.83	1.38	0.34
Male hip replacement subjects normal side						
27	41	0.28	1.38	0.79	0.93	0.23
28	57	0.39	1.16	0.69	1.11	0.27
29	54	0.37	1.39	0.85	1.26	0.31
38	53	0.36	1.40	0.84	1.23	0.30
Male hip replacement subjects replaced side						
26	59	0.42	1.79	0.99	1.76	0.42
27	42	0.30	1.36	0.78	0.96	0.23
28	56	0.38	1.21	0.72	1.12	0.28
29	54	0.37	1.39	0.84	1.24	0.31
38	54	0.37	1.45	0.87	1.30	0.32

Table A-VII.2 Stair ascent and descent; cadence

	Stair ascent		Stair descent	
Subject number	cadence (strides/min)	(normalised) ([strides/s]×√(H/g))	cadence (strides/min)	(normalised) ([strides/s]×√(H/g))
Male normal				
8	46	0.32	52	0.36
14	47	0.33	61	0.43
17	52	0.36	69	0.48
18	52	0.38	60	0.43
20	56	0.40	56	0.40
Female normal				
15	46	0.32	55	0.37
19	58	0.39	59	0.40
33	54	0.36	56	0.38
34	57	0.41	66	0.47
35	73	0.48	89	0.59
36	47	0.32	48	0.33
Male hip replacement subjects normal side				
27	28	0.20	34	0.24
28	42	0.29	46	0.32
29	39	0.26	46	0.31
38	40	0.27	42	0.29
Male hip replacement subjects replaced side				
26	33	0.23	32	0.23
27	32	0.22	31	0.22
28	43	0.29	42	0.29
29	40	0.27	41	0.28
38	41	0.28	40	0.28

Table A-VII.3 Ramp ascent; cadence, stride length and speed

	Ramp ascent					
Subject number	cadence (strides/min)	(normalised) ([strides/s]×√(H/g))	stride length (m)	(normalised) ([m]/H)	speed (m/s)	(normalised) ([m/s]/√(g×H)
Male normal						
8	49	0.34	1.70	0.99	1.38	0.34
14	50	0.35	1.69	0.95	1.40	0.33
17	54	0.37	1.46	0.86	1.31	0.32
18	51	0.37	1.54	0.84	1.32	0.31
20	53	0.38	1.94	1.06	1.70	0.40
Female normal						
15	51	0.35	1.56	0.94	1.33	0.33
19	55	0.37	1.43	0.89	1.30	0.33
33	55	0.37	1.33	0.82	1.21	0.30
34	52	0.37	1.56	0.86	1.35	0.32
35	72	0.47	1.53	0.98	1.82	0.47
36	52	0.36	1.38	0.83	1.19	0.29
Male hip replacement subjects normal side						
27	36	0.26	1.32	0.76	0.80	0.19
28	49	0.34	1.36	0.81	1.10	0.27
29	44	0.30	1.43	0.87	1.06	0.26
38	43	0.30	1.43	0.86	1.03	0.25
Male hip replacement subjects replaced side						
26	42	0.30	1.50	0.83	1.06	0.25
27	37	0.26	1.33	0.77	0.81	0.20
28	46	0.32	1.41	0.84	1.08	0.27
29	45	0.31	1.44	0.88	1.08	0.27
38	45	0.31	1.47	0.88	1.10	0.27

Table A-VII.4 Ramp descent; cadence, stride length and speed

	Ramp descent					
Subject number	cadence (strides/min)	(normalised) ([strides/s]×√(H/g))	stride length (m)	(normalised) ([m]/H)	speed (m/s)	(normalised) ([m/s]/√(g×H)
Male normal						
8	54	0.37	1.63	0.95	1.46	0.36
14	57	0.40	1.69	0.94	1.59	0.38
17	55	0.38	1.48	0.88	1.36	0.33
18	52	0.38	1.55	0.84	1.34	0.32
20	58	0.41	1.94	1.07	1.86	0.44
Female normal						
15	53	0.36	1.50	0.91	1.32	0.33
19	59	0.40	1.41	0.88	1.39	0.35
33	61	0.42	1.33	0.81	1.36	0.34
34	60	0.43	1.37	0.76	1.36	0.32
35	76	0.50	1.62	1.04	2.05	0.53
36	56	0.39	1.34	0.80	1.25	0.31
Male hip replacement subjects normal side						
27	38	0.27	1.18	0.68	0.75	0.18
28	48	0.33	1.30	0.78	1.05	0.26
29	49	0.33	1.19	0.72	0.97	0.24
38	47	0.32	1.38	0.83	1.07	0.27
Male hip replacement subjects replaced side						
26	46	0.33	1.54	0.85	1.18	0.28
27	38	0.26	1.18	0.68	0.74	0.18
28	48	0.33	1.29	0.77	1.03	0.25
29	48	0.33	1.31	0.80	1.06	0.26
38	51	0.35	1.35	0.81	1.15	0.28

Table A-VII.5 Camber up foot; cadence, stride length and speed

	Camber up foot					
Subject number	cadence (strides/min)	(normalised) ([strides/s]×√(H/g))	stride length (m)	(normalised) ([m]/H)	speed (m/s)	(normalised) ([m/s]/√(g×H)
Male normal						
8	54	0.37	1.49	0.87	1.33	0.32
14	55	0.39	1.75	0.98	1.61	0.38
17	55	0.38	1.43	0.85	1.30	0.32
18	52	0.37	1.76	0.96	1.51	0.36
20	55	0.39	1.91	1.05	1.74	0.41
Female normal						
15	53	0.36	1.52	0.92	1.35	0.34
19	58	0.39	1.47	0.92	1.42	0.36
33	59	0.40	1.38	0.85	1.36	0.34
34	54	0.39	1.59	0.88	1.44	0.34
35	73	0.48	1.62	1.04	1.96	0.50
36	57	0.39	1.40	0.84	1.33	0.33
Male hip replacement subjects normal side						
27	36	0.26	1.38	0.79	0.83	0.20
28	48	0.33	1.32	0.79	1.06	0.26
29	50	0.34	1.41	0.86	1.17	0.29
38	51	0.35	1.41	0.85	1.19	0.30
Male hip replacement subjects replaced side						
26	53	0.38	1.71	0.94	1.51	0.36
27	34	0.24	1.39	0.80	0.80	0.19
28	49	0.34	1.28	0.76	1.05	0.26
29	50	0.34	1.41	0.86	1.17	0.29
38	52	0.36	1.38	0.83	1.20	0.30

Table A-VII.6 Camber down foot; cadence, stride length and speed

	Camber down foot					
Subject number	cadence (strides/min)	(normalised) ([strides/s]×√(H/g))	stride length (m)	(normalised) ([m]/H)	speed (m/s)	(normalised) ([m/s]/√(g×H)
Male normal						
8	51	0.35	1.54	0.90	1.30	0.32
14	56	0.40	1.74	0.97	1.63	0.39
17	53	0.37	1.55	0.92	1.35	0.33
18	53	0.38	1.74	0.94	1.53	0.36
20	56	0.40	1.85	1.02	1.73	0.41
Female normal						
15	55	0.37	1.52	0.92	1.39	0.35
19	58	0.39	1.47	0.92	1.43	0.36
33	59	0.40	1.39	0.85	1.37	0.34
34	53	0.38	1.60	0.89	1.43	0.34
35	73	0.48	1.61	1.04	1.95	0.50
36	61	0.42	1.37	0.82	1.39	0.34
Male hip replacement subjects normal side						
27	36	0.25	1.36	0.78	0.81	0.20
28	48	0.33	1.34	0.80	1.08	0.27
29	50	0.34	1.44	0.88	1.19	0.30
38	49	0.34	1.46	0.88	1.20	0.30
Male hip replacement subjects replaced side						
26	55	0.39	1.72	0.95	1.57	0.37
27	34	0.24	1.45	0.83	0.82	0.20
28	49	0.34	1.29	0.77	1.06	0.26
29	50	0.34	1.45	0.88	1.19	0.30
38	50	0.34	1.45	0.87	1.20	0.30

Appendix VI Results

This appendix has been divided into the following parts:

The results are presented in a common format. This consists of four graphs per variable. Each graph represents one of the groups; male, female, male hip replacement subject's normal side or male hip replacement subject's replaced side. There has been no attempt to allow the values of individual traces to be measured from the graphs although this is possible in some figures. Different colours have been used to define each individual. Individual's left and right sides are included without distinction. The figure below defines the colours assigned to individuals.

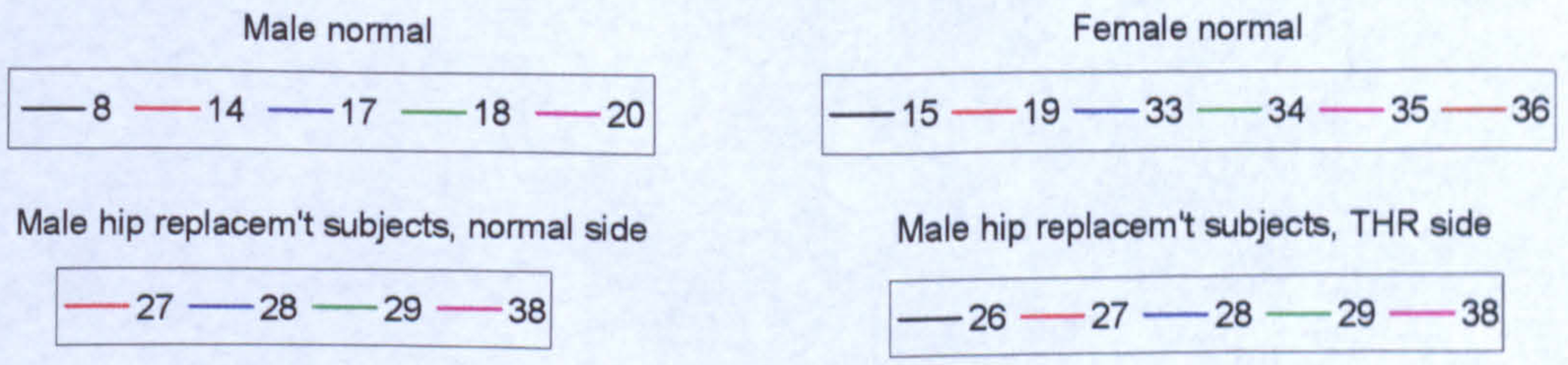

Pages and figures have been numbered by section of this Appendix. Thus all figures in section 3 are prefixed with A-VI.3 as are all page numbers.

Section A-V1.3 contains indications of muscle emg activity after University of California [1953].
The following example illustrates the levels of activity expected: